BUILDING UP MOLECULAR COMPLEXITY VIA C-H FUNCTIONALIZATION AND SKELETAL REARRANGEMENTS

Alvaro Gutiérrez Bonet

Building up molecular complexity via C—H functionalization reactions and skeletal rearrangements

Doctoral Thesis

Álvaro Gutiérrez Bonet

Advisor: Prof. Rubén Martín

Tarragona, January 2016.

Prof. Rubén Martín, Group Leader of the Institue of Chemical Research of Catalonia (ICIQ) and Research Professor of the Catalan Institution for Research and Advanced Studies (ICREA),

STATES that the present study, entitled "Building up molecular complexity via C—H functionalization reactions and skeletal rearrangements", presented by Álvaro Gutiérrez Bonet for the award of the degree of Doctor, has been carried out under my supervision at the Department Organic Chemistry of this University.

Tarragona, January 2016.

Doctoral Thesis Supervisor

Prof. Rubén Martín.

Thalassa! Thalassa!

(The Sea! The Sea!)

Xenophon, Anabasis

Table of Contents.

Acknowledgements

I would like to start by thanking Rubén, who has guided me during these four years, from the time I arrived at the Group as a Summer Fellow until I left. Thank you for trying to bring the best out of me, for continuously challenging me and teaching me how to be a good researcher. Thank you so much.

I would like to thank Ingrid as well for all her help during these four years. Also, I would like to thank Petr, Vanesa, Paula, Akira, Evan, Javier, Marino, Manuel and Daniel.

Areli, thank you so much for sharing your fumehood with me, your chemistry and for your friendship. Thank you for your help and tips on my beginning. I cannot forget Sara, it is impossible to remember those times without picturing Areli and you there. Arkaitz, I cannot add anything that you do not already know. Thank you for all your help, your support, your music… Wait! No! Not for your music! For your friendship and all your support, and, equally important, thank you for all the good moments. Thierry and Nekane, it was also great to spend time there with you both, I have laughed tons with you.

Joan, you are special! Always ready to make a bad joke while holding a paper in your hand! Always sharing your findings with me! Miriam, always yelling at me and correcting my Catalan - you did un gran treball!

Asraa, what can I say? I cannot recall how many stupid things we have done and said together, how many songs we have played on the speakers to annoy the others, how many times we have been close to crying for laughing so much. And then, if we sum up Caye to the equation… there you go! Crazy night! Caye, you were always the one who knew what was going on in my head and it was always easy to speak with you. It was really nice to have you there. Elo, it was amazing to have you on the neighboring fumehood; you know that I really like you, even your craziness, and I really enjoyed how we taught each other Spanish. Lidia, it was a pleasure to work with you and being ignored by you (once I got used to the 'modo Lidia'). I cannot forget going together to Ann Arbor and having you in our kitchen all the time.

Paco, Paco! I am so sorry for decreasing your productivity… But it was great to have you as a neighbour. You made me develop my critical vision, my passion for chemistry and my desire for keep on learning. You have taught me a lot in the lab and out of the lab; it was always fun with you. But more importantly, while you were feeding my brain, Noelia was feeding my stomach. I really appreciate it!

Toni! I hope I haven't scared you! I am sorry for increasing your grey hair and for making fun of it! Thanks for all your help in the lab, for making it so fun, for the soundtrack contests and for that awkward moment with the song 'Disintegration'. From where do I know that song? - Morgane, I am still doubting whether I should have acknowledged you or not, tu sais pourquoi! It was great to meet you as a Summer Fellow, later as a colleague, and then as a drinking partner in the evenings with Toni, Paco and… Pep who was always ready to make the more funny comments; having him at the table always meant bags of laughter. Carla… I still remember your first words! But I couldn't care less! You bring out the best of me.

Yu Liu, it was amazing meeting you! Really great! Now, every time I see a turtle I think of you and the lab-book that I threw on the floor! Viva México! Xue! We also had a lot of funny moments together and a lot of looooong talks in the evenings, I will really miss them! Masaki! I prefer not to write your nickname here. We definitely need to take one of these sugar free

gummy bears. Jeez! I have had tons of fun with you and your sick mind! Xiang-Wei, I will think of you every single time I have to use a glovebox! How much fun we have had around her!

And… Yangui! I do not even know where to start! You have serious problems bro! But it is so great to be around you! Working with Paco and you in the lab is something different, something great and awesome! I will miss you a lot.

Sarah, Melissa, Naoko, Devin and Pablo, you are great people. You made me love my stay at Ann Arbor! Illa, illa, illa!!! Seriously, it was awesome to have the chance of meeting you all. Mónica and Natalia, my Spanish connection in Ann Arbor, many thanks to you too for your friendship and help overseas.

Abraham. Thank you. You taught me a lot back in 2011 and if I am now here, it is because of you, your help, your advice and friendship. Thank you very much.

Albano, thank you for the good times and your friendship. Living with you was such an experience. Pili! Thank you for your kindness and friendship.

Marc! It has been amazing to discuss with you about my nightmares while having a coke in the deck of your garden (Bordeaux, Korean and Kiwi accent respectively). Emilie and James, merci beaucoup pour votre aide et les bons moments. Emilie, je n'ai rien dit de Thomas ici, es-tu contente?

Alice and Avni, it was really nice to have you there on my few free evenings laughing around the table. Alice, merci beaucoup pour les crêpes, les biscuits et le soutien moral. Avni, thank you for the nine glasses of water.

Jose, Nae, Mombi, Martín, Urki, Matt, Franco, Ciervo and Peña, thank you for helping me to forget about chemistry, to make me feel like I had never left Madrid. Igna, thank you so much for your stops by Tarragona and your friendship!

Muchas gracias también a toda mi familia por todo el apoyo que me han mostrado. A mis padres, por seguir cuidándome y preocupándose por mí. A mi padre, por asegurarse de que siempre tuviese un lomo en casa. A mi madre y a mi abuela por los tuppers de comida, consejos y ayuda y horas de teléfono. A Pepe, por venir incluso cojo. A Yupi por el libro de recetas de mi abuela y sus llamadas a Skype con Jaime. A Silvia y Jose por sus llamadas y ganas de que les contase a qué me dedicacaba.

A mis hermanos, Antonio, Rosa y Carmen que siempre han estado ahí con sus llamadas y visitas. ¡Al igual que mi prima Rocío! Muchas gracias por seguir cerca de mí aún estando lejos.

Samantha, gracias por todo tu cariño, apoyo, comprensión y paciencia. Durante estos cuatro años no he dejado ni un solo momento de aprender y de investigar, pero solo tú has conseguido hacerme entender el significado del papayal. ¡Has sido mi mejor descubrimiento!

Abbreviations

Boc: *tert*-Butyloxycarbonyl

BQ: *p*-Benzoquinone

CDC: Catalytic Dehydrogenative Cross-coupling

CMD: Concerted metalation-deprotonation

COD: 1,5-Cyclooctadiene

COE: Cyclooctene

Cp: Cyclopentadienyl

Cp*: 1,2,3,4,5-Pentamethylcyclopentadienyl

DCE: 1,2-Dichloroethane

DDQ: 2,3-Dichloro-5,6-dicyano-*p*-benzoquinone

DFT: Density functional theory

DG: Directing group

DMA: *N,N*-Dimethylacetamide

DMF: *N,N*-Dimethylformamide.

DMSO: Dimethyl sulfoxide

HASPO: Heteroatom-substituted secondary phosphine oxide

HOMO: Highest occupied molecular orbital

J: Coupling constant

KIE: Kinetic isotope effect

LUMO: Lowest unoccupied molecular orbital

MTBE: methyl *tert*-butyl ether

MVK: Methyl vinyl ketone

NFBS: *N*-Fluorobenzenesulfonimide

NFSI: *N*-Fluorobenzenesulfonimide

NHC: *N*-Heterocyclic Carbene

NMP: 1-Methyl-2-pyrrolidinone

NMR: Nuclear magnetic resonance.

PCC: Pyridinium chlorochromate

TBAF: Tetrabutylammonium fluoride

TBHP: *tert*-butylhydroperoxide

THF: Tetrahydrofuran

Scope of this Doctoral Thesis

During the last decades, numerous reports have been published related to C—H bond functionalization events. Despite the formidable advances realized within this field, there are still important challenges that have not been addressed.

Because of their ubiquity, the selective functionalization of a single C—H bond amongst the rest represents a major challenge of this methodology. In addition to this, their inherent low reactivity makes C—H bond functionalization difficult to achieve. For many years, chemists have been focused on a solution for these two main drawbacks. Indeed, these issues have been overcome mainly by the use of directing groups, which directly influence in selectivity and activity. However, and besides its great development and usefulness, this is not the most desirable solution as usually the installation and removal of the directing group requires adding further steps to the synthesis, thus lowering down its applicability.

During this doctoral thesis, we have focused our efforts on functionalizing C—H bonds that are surprisingly underrepresented in the literature with the aim of synthesizing rather challenging bicyclic backbones. First, we decided to functionalize aldehydic C—H bonds for the synthesis of highly valuable benzocyclobutenones. Although hydroacylation reactions are well stablished, the lack of protocols taking advantage of the functionalization of aldehydic C—H bonds is rather shocking. Secondly, we realized that despite of the several works published, the synthesis of quaternary carbons by means of C(sp^3)—H bond functionalization is still on its youth, therefore, we decided to contribute to its development by creating an useful methodology able to generate quaternary carbons while constructing interesting indanyl-type backbones.

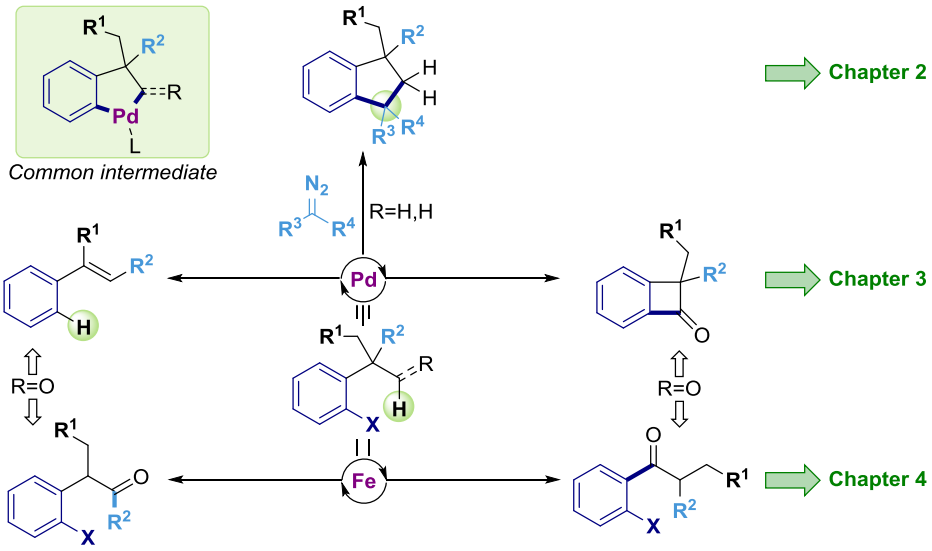

Figure 1: General Abstract of this Doctoral Thesis.

Despite our interest on C—H functionalization reactions, we could also corroborate that serendipity is Science's driving force. Indeed, we discovered a mild Fe-catalyzed skeletal rearrangement of aldehydes for an atom and step-economical synthesis of ketones. Furthermore, we observed that the selectivity of this transformation was ruled and could be switched by electronic effects.

Interestingly, benzocyclobutenone synthesis as well as the skeletal rearrangement use α-aryl aldehydes as starting materials. Even more interesting is the fact that the same type of aldehydes could be employed for the selective synthesis of trisubstituted styrenes. Therefore, four different products could be obtained from the same compound by simply changing the catalytic system, what considerably increases the synthetic value of α-aryl aldehydes.

Chapter 1. Introduction

1.1 Carbon-Hydrogen Bonds: The New Coupling Partner

Cross coupling reactions[1] (Figure 1.1) are transformations in which a nucleophile (organometallic reagent) and an electrophile (commonly an aryl/alkenyl halide or pseudohalide) are coupled by transition metal catalysis to form a new C—C(heteroatom) bond. This reactivity revolutionized the field of organic synthesis by allowing the formation of previously inaccesible C—C bonds. Not surprisingly, cross-coupling reactions have successfully been applied in natural product synthesis[2] and on industrial processes as well.[3]

Despite the obvious advantages of cross-coupling reactions, the atom-[4] and step-economy[5] is still rather problematic. As shown in Figure 1.1, stoichiometric amounts of organometallic reagents are typically required such as highly reactive Grignard reagents (Kumada-Corriu coupling), organozincates (Negishi coupling), toxic organostannanes (Stille coupling) or boronic acids and esters (Suzuki-Miyaura coupling). Additionally, these organometallic species are typically prepared from the corresponding organic halide, thus reducing the efficiency of the process.

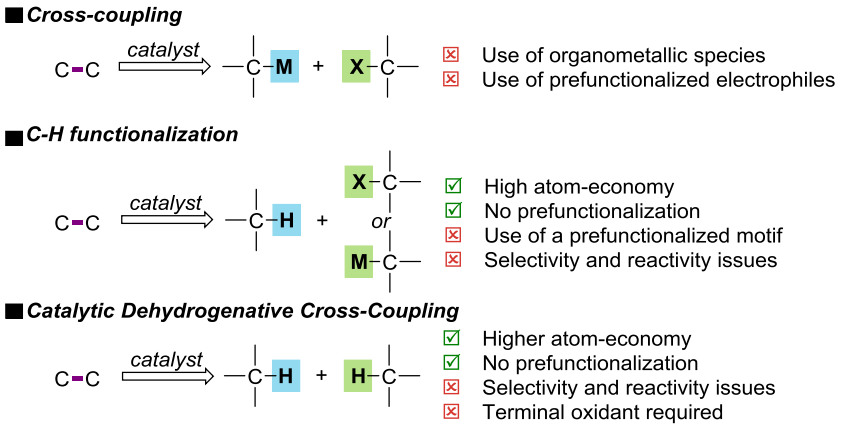

Figure 1.1. Recent strategies for the synthesis of C-C and C-heteroatom bonds.

The last decades have witnessed an exponential growth on methodologies based on C—H bond-functionalization[6,7] (Figure 1.1). Unlike classical cross-coupling reactions, C—H functionalization reactions have the advantage of replacing the nucleophile or electrophile component by the *in situ* preparation of an organometallic reagent. Such seemingly trivial modification avoids the use of prefunctionalized starting materials, thus increasing the efficiency of the process. However, numerous are the challenges derived from the utilization of C—H bonds. The two major drawbacks are the (generally) low reactivity of C—H bonds and the site-selectivity issues in the presence of similarly reactive C—H bonds.

---

[1] Seechurn, J. C. C. C.; Kitching, M. O.; Colacot, T. J.; Snieckus, V. *Angew. Chem. Int. Ed.* **2012**, *51*, 5062.
[2] Nicolau, K. C.; Bulger, P. G.; Sarlah, D. *Angew. Chem. Int. Ed.* **2005**, *44*, 4442.
[3] (a) King, A. O.; Yasuda, N. *Palladium-Catalyzed cross-coupling reactions in the synthesis of pharmaceuticals* **2004**, *6*, 205. (b) Biajoli, A. F. P.; Schwalm, C. S.; Limberger, J.; Claudino, T. S.; Monteiro, A. L. *J. Braz. Chem. Soc.* **2014**, *25*, 2186. (c) Dumrath, A.; Lübbe, C.; Beller, M. *Palladium-catalyzed cross-coupling reactions – Industrial applications* **2013**, 445.
[4] Trost, B. M. *Angew. Chem. Int. Ed.* **1995**, *34*, 259.
[5] (a) Newhouse, T.; Baran, P. S.; Hoffmann, R. W. *Chem. Soc. Rev.* **2009**, *38*, 3010. (b) Wender, P. A.; Verma, V. A.; Paxton, T. J.; Pillow, T. H. *Acc. Chem. Res.* **2008**, *41*, 40. (c) Roschangar, F.; Sheldon, R. A.; Senanayake, C. H. *Green Chem.* **2015**, *17*, 752.
[6] Goldberg, K. I.; Goldman, A. S. *Activation and functionalization of C—H bonds. ACS Symposium Series, Vol. 885.*
[7] (a) Labinger, J. A.; Bercaw, J. E. *Nature*, **2002**, *417*, 507. (b) Yamaguchi, J.; Yamaguchi, A. D.; Itami, K. *Angew. Chem. Int. Ed.* **2012**, *51*, 8960. (c) Wencel-Delord, J.; Glorius, F. *Nature Chem.* **2013**, *5*, 369.

Catalytic dehydrogenative cross-coupling (CDC)[8] strategies offer the advantage of using non-prefunctionalized starting materials (Figure 1.1), representing an added value from an atom- and step-economical standpoint. However, the low reactivity of C—H bonds and site-selectivity issues constitute considerable challenges that need to be addressed. Although only molecular hydrogen is generated as byproduct, a stoichiometric hydrogen scavenger is usually employed (oxidants or alkenes among others) thus reducing the atom-economy of the transformation.

1.2 Carbon—Hydrogen Bond Functionalization

The term C—H functionalization is nowadays widely employed in scientific literature; however, such a term is rather ambiguous and can be utilized in many different scenarios. To avoid any misinterpretation, we will use the term C—H functionalization in agreement with an organometallic standpoint,[7a] that indicates that a C—H functionalization reaction converts a C—H bond into a C—X (C ≠ H) bond via formation of an organometallic intermediate. According to such definition, C—H functionalization reactions are narrowed to transformations through an inner-sphere mechanism (Figure 1.2).

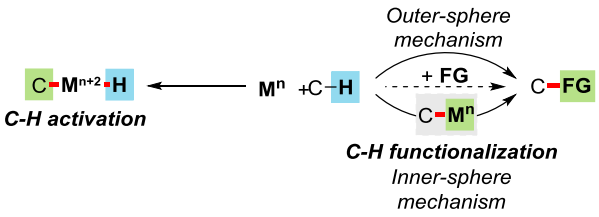

Figure 1.2. Representation of the organometallic definition of C—H bond functionalization.

When designing C—H functionalization reactions, chemists should take into consideration site-selectivity issues in the presence of other C—H bonds and the inherent low reactivity of the targeted C—H bond. An exquisite control of all these aspects will be crucial for determining not only the feasibility but also the prospective impact of such methodologies.

1.2.1 Selectivity Control[9]

The development of C—H functionalization reactions in complex organic settings represent a daunting challenge since these techniques should be able to discriminate among a variety of C—H bonds. These selectivity issues were observed by Ishii and coworkers[10] in which simple arenes were coupled with acrylates under palladium catalysis using molecular oxygen as terminal oxidant (Scheme 1.1). Specifically, the authors described that mixtures of *ortho*, *meta* and *para* functionalized products (**2a-c**) were observed when dealing with monosubstituted arenes, thus lowering down the applicability of this methodology.

[8] Yeung, C. S.; Dong, V. *Chem. Rev.* **2011**, *111*, 1215.
[9] (a) Neufeldt, S.; Sanford, M. S. *Acc. Chem. Res.* **2012**, *45*, 936. (b) Kuhl, N.; Hopkinson, M. N.; Wencel-Delord, J.; Glorius, F. *Angew. Chem. Int. Ed.* **2012**, *51*, 10236.
[10] Tani, M.; Sakaguchi, S.; Ishii, Y. *J. Org. Chem.* **2004**, *69*, 1221.

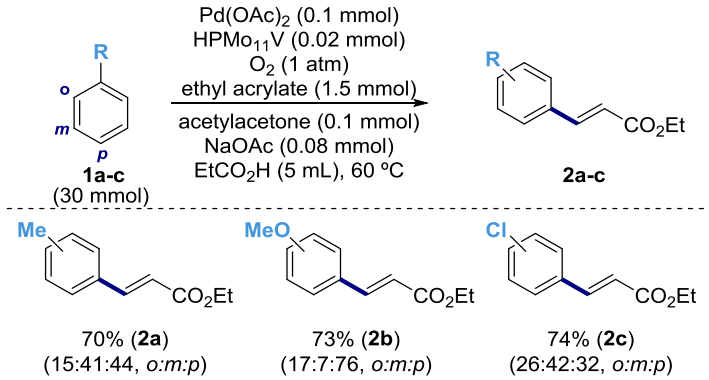

Scheme 1.1. Pd-catalyzed oxidative alkenylation of simple arenes.

An otherwise similar drawback was found by Sanford in palladium-catalyzed oxidative arylation of unbiased arenes (**4a-d**) using benzoquinone **3** as coupling partner (Scheme 1.2).[11] It is worth noting that, in some cases, high selectivities were observed when employing biased arenes via steric effects (**5a-b**)

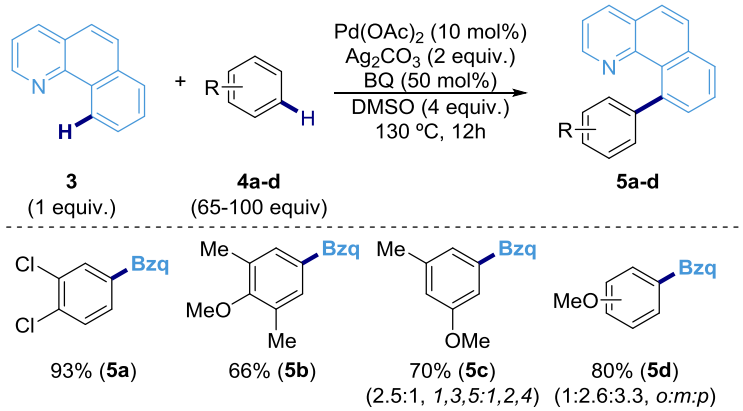

Scheme 1.2. Pd-catalyzed oxidative arylation of benzoquinoline.

Taking into account such observations, an efficient discrimination of the targeted C—H bond must be effected in the presence of other C—H bonds. Such challenge has been tackled by a number of different approaches, the most commonly employed ones being the following:

- Use of electronically biased systems.
- Use of sterically biased systems.
- Use of Directing-groups (DGs).
- Oxidative addition directed C—H functionalization.
- Catalyst controlled selectivity.

1.2.1.1 Electronic control

Aromatic C(sp^2)—H bonds have been functionalized by electrophilic aromatic substitution taking advantage of the ability of different functional groups present on the aromatic backbone to direct the functionalization at a specific reaction site in a highly realiable and predictable manner. The same concept applies when operating with metal-catalyzed transformation using catalysts in high oxidation states. Usually, this electronic control has been successfully employed in electron rich heterocyclic systems where there is a high electronic

[11] Hull, K. L.; Sanford, M. S. *J. Am. Chem. Soc.* **2007**, *129*, 11904.

differentiation among different C—H bonds over the ring (Scheme 1.3, top pathway).[12] Alternatively, high regioselectivity control can also be achieved with biased arenes (bottom pathway). Unfortunately, such selectivity control might be difficult to achieve with more complex settings due to the need for introducing a certain group at a specific reaction site, thus requiring multistep synthetic sequences.

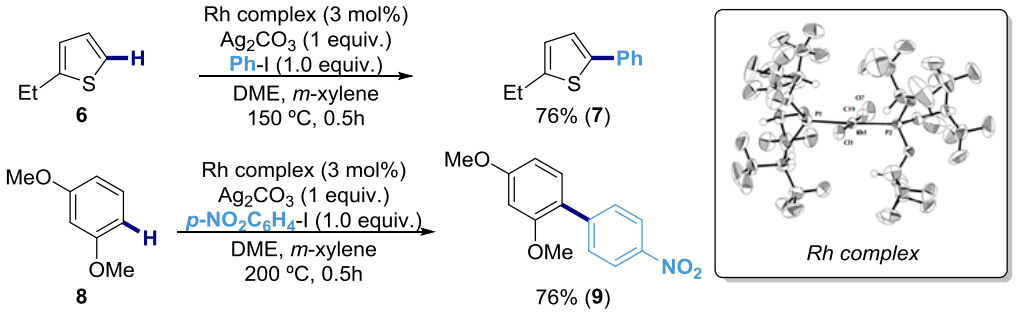

Scheme 1.3. Rhodium-catalyzed C—H bond arylation of electron-rich (hetero)arenes.

1.2.1.2 Steric control[13]

Steric interactions allow to functionalize the less sterically encumbered C—H bond. This discrimination relies only in steric repulsive interactions; therefore, when these interactions are not strong enough other factors come into play to control the selectivity. This approach has been successfully applied for the functionalization of 1,2- (**11**) and 1,3-substituted (**10**) aromatic rings (Figure 1.3). However, the selective functionalization of unsymmerically substituted 1,2-aryls (**12**) generates a mixture of 1,2,4- and 1,2,5-trisubstituted arenes (**12'**) as the metal is not able to achieve an effective differentiation among substituents at the *meta*-position.

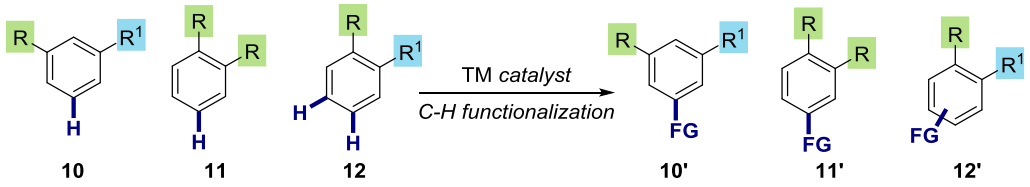

Figure 1.3. Achieving steric control in disubstituted arenes.

Apart from the above-mentioned work of Sanford[11] (Scheme 1.2) an elegant example of steric-controlled selectivity was found by Hartwig and Cheng for the rhodium-catalyzed intermolecular silylation of arenes.[14] In this work, the selectivity was dictated by steric interactions where the silyl moiety is introduced at the less sterically hindered position regardless of wether electron-rich or electron-poor substituents were present (Scheme 1.4). For example, the authors showed that the use of benzodioxole **13c**, a substrate that typically has evolved via *ortho* C—H functionalization due to the higher acidity of such C—H bonds, results in the functionalization at the *meta* position, an explanation attributed merely due to steric repulsive interactions. Equally impressive, was the observation that unsymmetrically substituted 1,2-arenes with bulky substituents (**13d-e**) operated equally well, resulting in the functionalization at the *para* position to the more sterically demanding group. The limitations

[12] Yanagisawa, S.; Sudo, T.; Noyori, R.; Itami, K. *J. Am. Chem. Soc.* **2006**, *128*, 11748.
[13] Tobisu, M.; Chatani, N. *Science*, **2014**, *343*, 850.
[14] Cheng, C.; Hartwig, J. F. *Science*, **2014**, *343*, 853.

of this system were illustrated by using **13f**, in which silylation occurs predominantly at the *orho* position of the methoxy group which is larger than the chlorine atom (cyclohexane A value = 0.55 to 0.75 and 0.53 to 0.64, respectively). The authors justified this result as a consequence of the activation of the C—H bond by the methoxy substituent close to it.

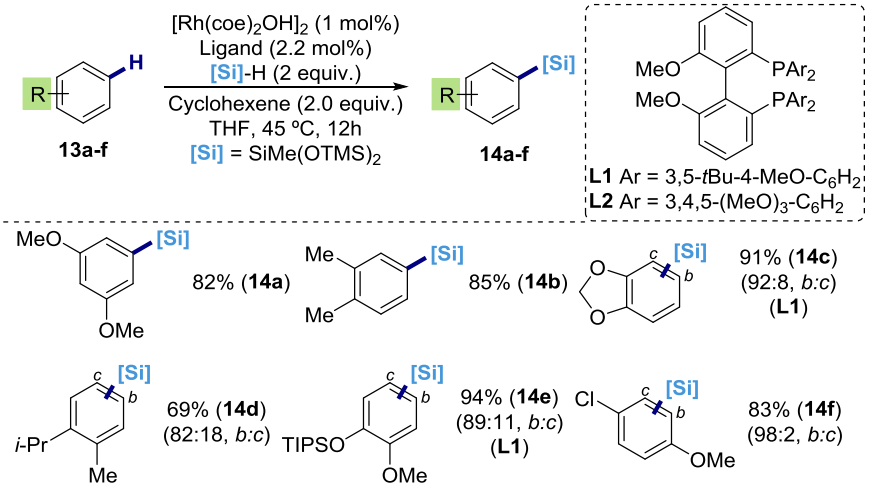

Scheme 1.4. Rhodium-catalyzed intermolecular C–H silylation of arenes.

Selectivity by steric interactions can be also achieved in non-cyclic systems as exemplified in the rhodium-catalyzed C(sp^3)—H borylation of alkanes reported by the Hartwig group.[15] In this publication, the catalytic system was selective for primary over secondary sp^3-carbons (Scheme 1.5). Interestingly, the authors observed discrimination among different primary carbons that likely arises from the substituents adjacent to the targeted C(sp^3)—H bond (**15a**). A surprising case was that the introduction of a fluorine group resulted in the exclusive formation of **16c**, a finding that suggests that steric discrimination dominates over the acidity of the targeted C(sp^3)—H.

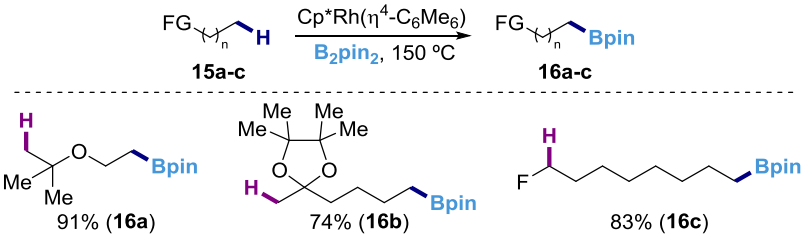

Scheme 1.5. Rh-catalyzed regiospecific C—H bond functionalization of alkanes.

1.2.1.3 Directing-Groups (DGs)[16]

The drawbacks associated to the inclusion of certain group within the aromatic or alkyl side-chain has prompted chemists to study other viable solutions to exert high degree of selectivity in the presence of molecules possessing multiple C—H bonds. In this context, the use of directing groups has gained considerable momentum in C—H bond-functionalization

[15] Lawrence, J. D.; Takahashi, M.; Bae, C.; Hartwig, J. F. *J. Am. Chem. Soc.* **2004**, *126*, 15334.

[16] (a) Chen, Z.; Wang, B.; Zhang, J.; Yu, W.; Liu, Z.; Zhang, Y. *Org. Chem. Front.* **2015**, *2*, 1107. (b) Rousseau, G.; Breit, B. *Angew. Chem. Int. Ed.* **2011**, *50*, 2450. (c) Lyons, T. W.; Sanford, M. S. *Chem. Rev.* **2010**, *110*, 1147. (d) Zhang, F.; Spring, D. R. *Chem. Soc. Rev.* **2014**, *43*, 6906. (e) Yu, J.-Q.; Giri, R.; Chen, X. *Org. Biomol. Chem.* **2006**, *4*, 4041. (e) Rouquet, G.; Chatani, N. *Angew. Chem. Int. Ed.* **2013**, *52*, 11726.

techniques, allowing to form a metallacycle via the activation of a proximal C—H bond within the organic backbone by either hydrogen bonding, covalent interactions or Lewis acid-base interactions (Figure 1.4)

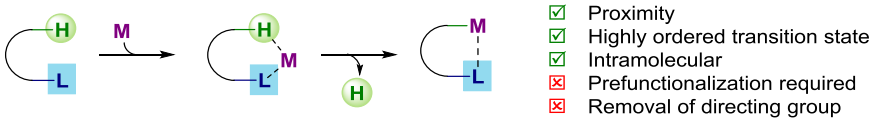

Figure 1.4.

The C—H bond-functionalization in the presence of directing groups proceeds through a highly ordered (poly)cyclic transition state that discriminates between different C—H bonds more efficiently. As the reaction is intramolecular, there is less distortion in the transition state (reduction of the activation entropy), hence resulting in a significant rate enhancement for the C—H bond cleavage step.[17]

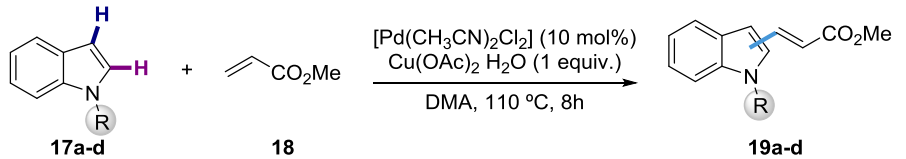

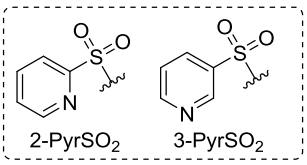

Entry	R	Yield (%)	C2:C3
1	H	66	2:98
2	Ts	45	87:13
3	2-PyrSO$_2$	75	98:2
4	3-PyrSO$_2$	27	76:24

Scheme 1.6. Directing-group selectivity control in the oxidative alkenylation of indoles.

Apart from the features highlighted above, the inclusion of directing groups allows for overriding the innate reactivity of organic molecules to trigger C—H functionalization events not apparent at first sight. For example, Carretero *et al*. demonstrated the possibility to overcome the natural propensity of indoles towards C3-alkenylation in the presence of a pyridyl sulfonyl group (2-pyrSO$_2$),[18] resulting in the predominant formation of the C2-product (Scheme 1.6, entries 1 and 3).

There are a number of pre-requisites that directing groups should ideally fulfill to promote C—H bond-functionalization reactions: (1) reversible coordination to the metal center; (2) efficient control over the selectivity and reactivity; (3) easily introduced and readily removed or transformed into functionalized entities. Directing groups can be classified into the following categories: [16b,d]

- ❖ Intrinsic directing groups
- ❖ Traditional directing groups
- ❖ Removable directing groups
- ❖ Traceless directing groups
- ❖ Reactive directing groups
- ❖ Catalytic directing groups

Intrinsic Directing Groups

[17] Albrecht, M. *Chem. Rev.* **2010**, *110*, 576.
[18] García-Rubia, A.; Arrayás, R. G.; Carretero, J. C. *Angew. Chem. Int. Ed.* **2009**, *48*, 6511.

Intrinsic directing groups refer to scaffolds already present within an organic backbone capable to successfully promote a C—H functionalization event in an efficient and selective manner. Such scenario is certainly ideal as no prefunctionalization steps are required to introduce or remove the corresponding directing group.

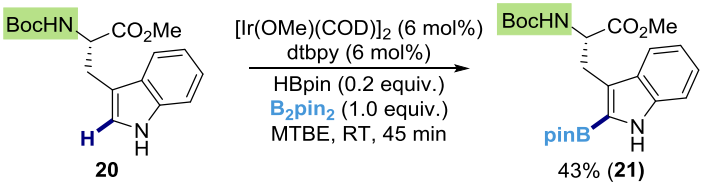

Scheme 1.7. Ir-catalyzed C—H borylation of tryptophan.

Intrinsic directing groups have been broadly employed for the derivatization of aminoacids in a straightforward fashion.[19] For example, Smith and Maleczka reported the borylation of aminoacids via iridium-catalyzed regioselective C2-borylation of NBoc-tryptophan methyl ester employing B_2pin_2 as borylating agent (Scheme 1.7) and the Boc moiety as directing group.[20]

Another example of intrinsic directing groups was reported by Wang and Yu on the total synthesis of (+)-Lithospermic acid (Scheme 1.8).[21] The authors envisioned that the carboxylic acid present in the benzofuran motif (**22**) could be employed as a directing group for the selective C—H olefination step. Although the presence of electron-rich C—H bonds as well as chiral centers might be rather problematic, the reaction proceeded with an excellent yield, showcasing the importance of late-stage functionalization en route to advanced synthetic intermediates.

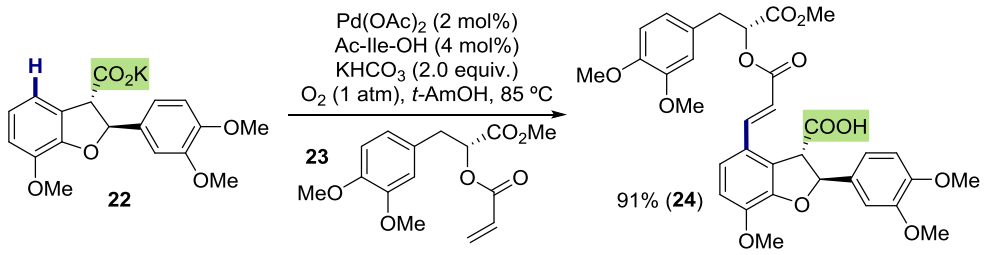

Scheme 1.8. Synthesis of Hexamethyl lithosparmate**.**

Traditional Directing Groups

Directing groups that efficiently triggers selective C—H bond-functionalization despite the difficulty on cleaving such groups fall under such category. Usually, nitrogen-containing groups such as pyridines, pyrazoles, triazoles, imines, ketones, sulfur-containing groups and phosphine oxides have been employed for such purposes (Figure 1.5).[22]

[19] Noisier, A. F. M.; Brimble, M. A. *Chem. Rev.* **2014**, *114*, 8775.
[20] Kallepalli, V. A.; Shi, F.; Paul, S.; Onyeozili, E. N.; Maleczka, R. E.; Smith, M. R. *J. Org. Chem.* **2009**, *74*, 9199.
[21] Wang, D.-H.; Yu, J.-Q. *J. Am. Chem. Soc.* **2011**, *133*, 5767.
[22] (a) Huan, Z.-H.; Ren, Z.-H.; Spinella, S. M.; Yu, S.; Liang, Y.-M.; Zhang, X. *J. Am. Chem. Soc.* **2009**, *131*, 729. (b) Desai, L. V.; Hull, K. L.; Sanford, M. S. *J. Am. Chem. Soc.* **2004**, *126*, 9542. (c) Kakiuchi, F.; Sekine, S.; Tanaka, Y.; Kamatani, A.; Sonoda, M.; Chatani, N.; Murai, S. *Bull. Chem. Soc. Jap.* **1995**, *68*, 62. (d) Wang, H.-L.; Hu, R-B.; Zhang, H.; Zhou, A.-X.; Yang, S.-D. *Org. Lett.* **2013**, *15*, 5302.

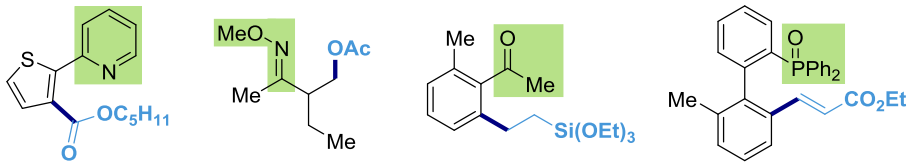

Figure 1.5. Selective C—H bond functionalization by means of directing-groups.

These directing groups can be classified according to their heteroatom as strongly-coordinating (pyridines, oxazolines, imines, etc) or weakly-coordinating groups[23] (carboxylic acids, ketones, aldehydes, etc). Additionally, such groups can be classified depending on whether the C—H bond-functionalization occurs at the *ortho* (like the previous examples), *meta* or *para*-position.[24] An elegant example of non-removable *meta* directing group was reported by Frost (Scheme 1.9) for the ruthenium-catalyzed C—H sulfonation of 2-phenylpyridines (**29**).[25] Subsequently, a similar catalytic system was employed by Ackermann for the C—H alkylation reaction.[26] Although the reaction outcome gives the *meta*-substituted product, the ruthenation takes place at the *ortho* position to the pyridine (**31**) forming a σ Ru—C bond that directs, by mesomeric and inductive effects, the sulfonation or alkylation reaction at the *para* position of the ruthenium atom (**30**).

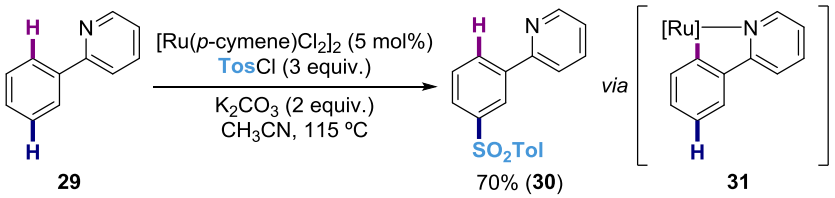

Scheme 1.9. Ru-catalyzed *meta*-sulfonation of 2-phenylpyridines.

Removable Directing Groups[16b,d]

One of the main drawbacks associated to directing groups is the need for locating a specific group at a certain position within the organic backbone. Such group might, in certain cases, not be trivial to modify or remove, thus lowering down the application of these methodologies. In order to deal with such issues, a considerable amount of effort has been directed towards the development of new directing groups that can be easily detachable or converted into other functionalities. Although the use of removable directing groups is not ideal, the synthetic route gains in efficiency.

[23] (a) de Sarkar, S.; Liu, W.; Kozhuskhov, S. I.; Ackermann, L. *Adv. Synth. Catal.* **2014**, *356*, 1461. (b) Engle, K. M.; Mei, T.-S.; Wasa, M.; Yu, J.-Q. *Acc. Chem. Res.* **2012**, *45*, 788.
[24] (a) Yang, J. *Org. Biomol. Chem.* **2015**, *13*, 1930. (b) Juliá-Hernández, F.; Simonetti, M.; Larrosa, I. *Angew. Chem. Int. Ed.* **2013**, *52*, 11458.
[25] Saidi, O.; Marafie, J.; Ledger, A. E. W.; Liu, P. M.; Mahon, M. F.; Kociok-Köhn, G.; Whittlesey, M. K.; Frost, C. G. *J. Am. Chem. Soc.* **2011**, *133*, 19298.
[26] Hofmann, N.; Ackermann, L. *J. Am. Chem. Soc.* **2013**, *135,* 5877.

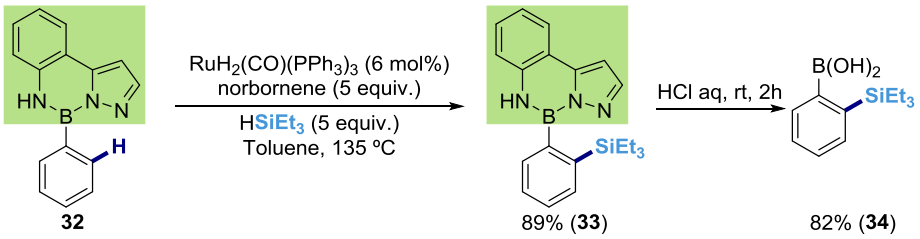

Scheme 1.10. Ru-catalyzed aromatic C—H silylation.

This strategy is nicely illustrated in the work of Suginome and Ihara (Scheme 1.10) for the ruthenium-catalyzed aromatic C—H silylation.[27] In this report, a boronic acid was in situ protected as Bpza group in the presence of $pzaH_2$ ($pzaH_2$ = 2-pyrazol-5-ylaniline). Finally, the pza group could be easily removed in the presence of aqueous HCl furnishing the free boronic acid (**34**).

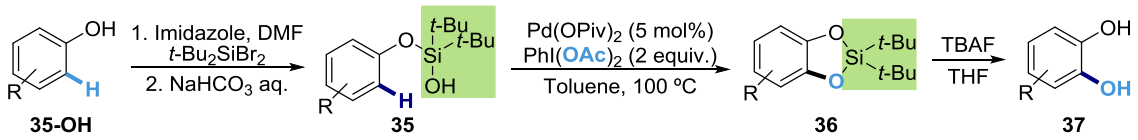

Scheme 1.11. Pt-catalyzed regioselective silylation of internal alkynes.

The Gevorgyan group reported a novel synthesis of catechols (**37**) under palladium catalysis using silanol protecting groups that were easily prepared from the corresponding phenol derivative (Scheme 1.11).[28] Such silanol **35** promotes an efficient *ortho* C—H bond-functionalization in the presence of hypervalent iodine oxidants, obtaining a silacycle **36** that could be easily converted into catechol **37** in the presence of tetrabutylammonium fluoride. Although the authors anticipated a mechanistic scenario involving palladacycles in high oxidation state, it was demonstrated by labeling experiments that the C—O reductive elimination does not involve the silanol moiety but rather the acetoxy introduced in the palladium inner coordination sphere after oxidation with the iodine(III) reagent. The acetoxylated obtained product ultimately evolves under reaction conditions to **36**. It is worth noting that in both Scheme 1.10 and 1.11, the directing group is not only easily removed, but it is also easily attached, hence increasing the value of this approach.

[27] Ihara, H.; Suginome, M. *J. Am. Chem. Soc.* **2009**, *131*, 7502.
[28] Huang, C.; Ghavtadze, N.; Chattopadhyay, B.; Gevorgyan, V. *J. Am. Chem. Soc.* **2011**, *133*, 17630.

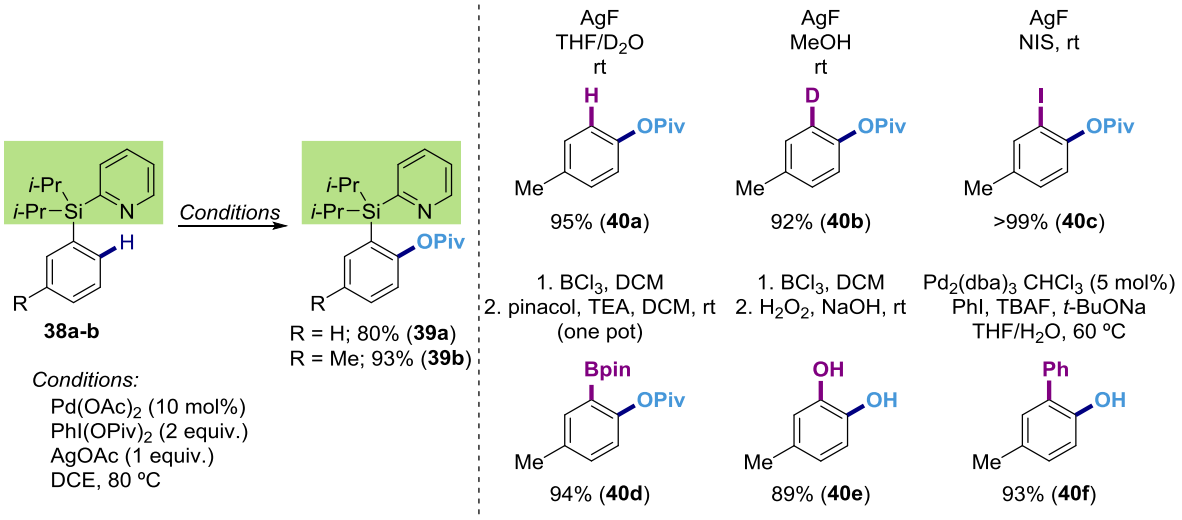

Figure 1.6. Easily modifiable/traceless Si-tethered directing group for C—H acyloxylation of arenes.

Despite the high interest in discovering new easily removable directing groups, it is also extremely important that such groups are versatile enough to be converted in other functionalities in a straightforward manner, thus significantly increasing the synthetic value and the molecular complexity. With the idea of finding an easily modifiable and effective directing group, Gevorgyan and co-workers[29] found that pyridyldiisopropylsilyl group (PyDipSi) efficiently directed the palladium-catalyzed C-H acyloxylation of arenes (Figure 1.6). Importantly, this directing group could be easily removed or converted into other versatile functionalities, such as iodide (**40c**), boronates (**40d**), alcohols (**40e**), or aromatic motifs via Hiyama-Denmark cross-coupling reaction (**40f**).

Traceless Directing Groups

A step forward in C—H bond-functionalization reactions is the employment of traceless directing groups, scaffolds that are removed during the course of the reaction after having successfully accomplished its role. Their main advantage in comparison with the previous categories is that the detachment step is avoided as it has already taken place during the course of the reaction. One of the main challenges that have to be overcome to succeed in such endeavor is to avoid the undesired elimination of the directing group before the reaction occurs.

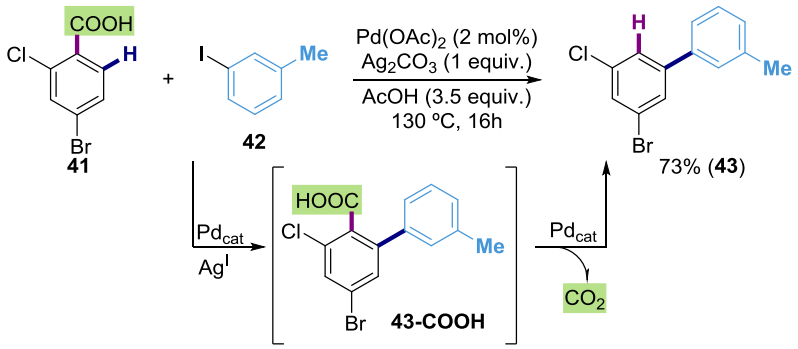

[29] Chernyak, N.; Dudnik, A. L.; Huang, C.; Gevorgyan, V. *J. Am. Chem. Soc.* **2010**, *132*, 8270.

Scheme 1.12. Carboxylic acids as traceless directing groups for the Pd-catalyzed synthesis of biaryls.

An example of such strategy was reported by Larrosa in which a carboxylic acid is used for promoting a *meta*-arylation with aryl iodides as coupling partners (Scheme 1.12).[30] The major concern while developing this transformation was the undesired formation of 1,3-bromochlorobenzene arising from the protodecarboxylation of the starting carboxylic acid **41**. Gratifyingly, selective protodecarboxylation of the biaryl intermediate **43-COOH** was achieved, an observation attributed to the presence of an *ortho* aromatic motif. Subsequently, Larrosa and co-workers expanded this methodology to the formal *meta*-arylation of phenols by *in situ* formation of salicylic acid derivatives from phenol, followed by carboxylate assisted arylation/ protodecarboxylation.[31]

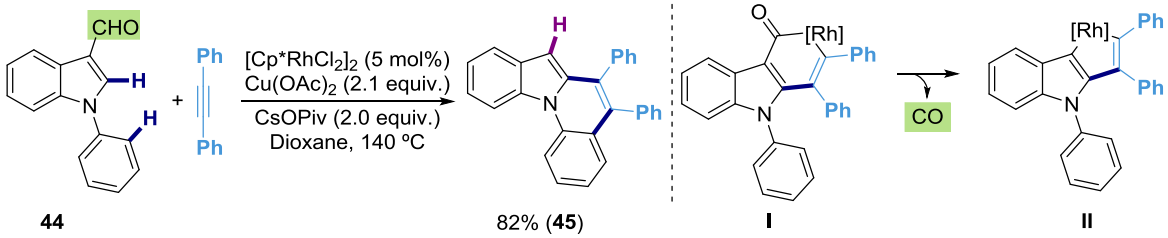

Scheme 1.13: Traceless aldehyde directed Rh-catalyzed synthesis of indolo[1,2-a]quinolones.

Another remarkable example of traceless directing group was recently published by You and Lan (Scheme 1.13).[32] This strategy was built upon the ability of aldehydes to direct functionalization followed by a decarbonylation step. Examples on the use of aldehydes as directing groups are scarce due to its poor Lewis basicity (compared to other directing groups) and its tendency to oxidation. Since carboxylic acids were successfully employed as traceless directing groups and aldehydes are particularly prone to oxidation, the authors initially speculated about the intermediacy of an *in situ* generated carboxylic acid. However, this possibility was ruled out by the authors by performing control experiments. Strikingly, no hydroacylation product was observed despite the proclivity of rhodium(I) to oxidatively insert into aldehydic C—H bonds followed by a hydrometalation event. The authors suggested that CO extrusion occured from a six-membered acyl vinyl rhodium intermediate **I**, resulting in the formation of a 5-membered rhodacylce **II**.

Reactive directing groups

In some cases, the role of the directing groups is not only limited to bind the metal center in close proximity to the targeted C—H bond, but also to react over the course of the reaction with the newly introduced functionality.

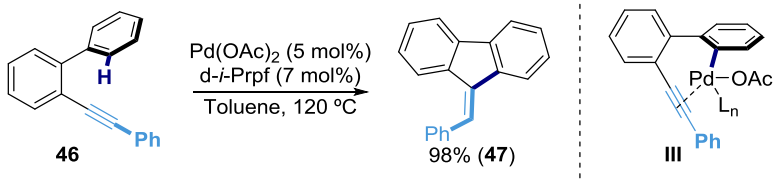

[30] Cornella, J.; Righi, M.; Larrosa, I. *Angew. Chem. Int. Ed.* **2011**, *50*, 9429.
[31] Luo, J.; Preciado, S.; Larrosa, I. *J. Am. Chem. Soc.* **2014**, *136*, 4109.
[32] Liu, X.; L, X.; Liu, H.; Guo, Q.; Lan, J.; Wang, R.; You, J. *Org. Lett.* **2015**, *17*, 2936.

Scheme 1.14. Synthesis of fluorenes via the palladium-catalyzed 5-*exo-dig* annulation of *o*-alkynyl biaryls.

This strategy was described by Chernyak and Gevorgyan[33] in which an alkyne (**46**) was employed as a formal directing group for effecting the C—H bond-functionalization en route to fluorenes (Scheme 1.14). After alkyne-directed *ortho*-palladation (**III**), a migratory insertion event occurs, forming a vinyl palladium(II) intermediate that renders product **47** after protodepalladation. Interestingly, the 5-*exo-trig* product is formed selectively while under ligand free conditions the 6-*endo-trig* product dominates.

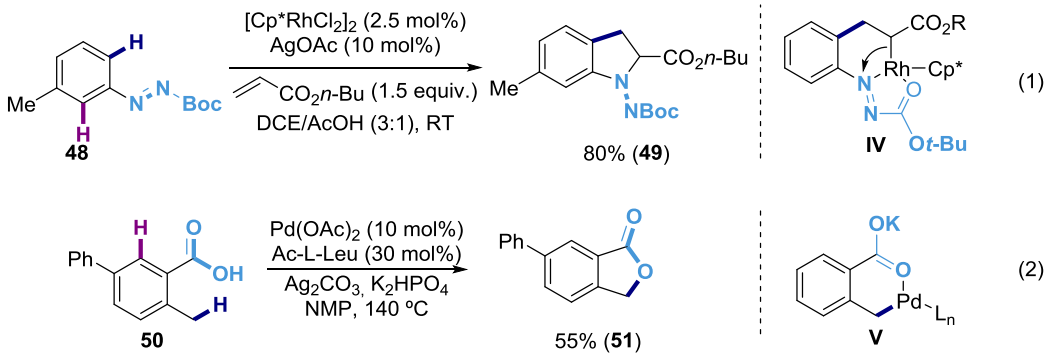

Figure 1.7. Reactive directing groups for the transition metal-catalyzed C—H bond functionalization en route to heterocycles.

As shown in Figure 1.7, eq. 1, indoline cores **49** can be prepared using cationic rhodium(I) catalysts in the presence of a Boc-diazene directing group.[34] The reaction proceeds via diazene directed C—H bond cleavage followed by a migratory insertion event to form **IV**. Then, the *ipso* carbon can promote an intramolecular attack on the electrophilic diazene carboxylate moiety forming the *N*-aminoindoline backbone. In another example (eq. 2), Martin *et al.*[35] used a weakly-coordinating carboxylic acid[23b] for the synthesis of phthalides **51**. The reaction consisted of a carboxylate directed benzylic C—H bond cleavage forming intermediate **V** that ultimately promotes a reductive elimination with the concomitant formation of palladium(0) that eventually gets oxidized by silver(I) salts.

Catalytic directing groups

We have seen in all the previous sections how chemists have faced the challenge of increasing the efficiency of the directing group strategy by attempting to simplify the synthetic operations to attach or detach the directing group. However, this is not the only manner in which efficiency can be improved. An ideal case scenario would be the employment of directing groups in a catalytic fashion. In order to do so, it is necessary to design a system where the directing group can bind the substrate covalently, resulting in a temporal directing group that will promote the metalation while transferring the auxiliary to another molecule of starting material once the reaction is performed.

[33] (a) Chernyak, N.; Gevorgyan, V. *J. Am. Chem. Soc.* **2008**, *130*, 5636. (b) Chernyak, N.; Gevorgyan, V. *Adv. Synth. Catal.* **2009**, *351*, 1101.
[34] Zhao, D.; Vásquez-Céspedes, S.; Glorius, F. *Angew. Chem. Int. Ed.* **2014**, *54*, 1657.
[35] Nóvak, P.; Correa, A.; Gallardo-Donaire, J.; Martin, R. *Angew. Chem. Int. Ed.* **2011**, *50*, 12236.

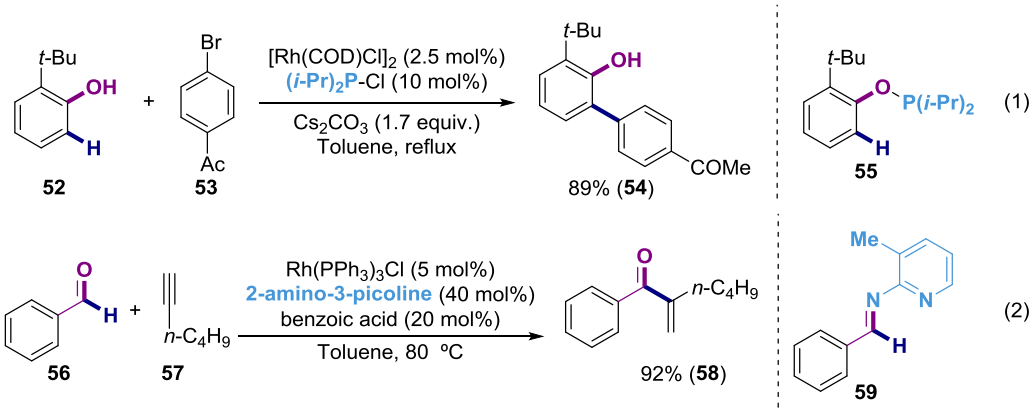

Figure 1.8. Aryl and formyl functionalization in the presence of catalytic directing groups.

To such end, Bedford, Caffyn and Prashar designed a system (Figure 1.8, eq 1) for the catalytic arylation of phenols using *in situ* formation of the directing group with $(i\text{-Pr})_2PCl$) as auxiliary.[36] The key steps of this transformation are the formation of a phosphonate that triggers a C—H bond-functionalization followed by a final transphosphination with the starting material. Most likely, the driving force for the transphosphination step is the difference in steric hindrance between the starting material and final product. In another example, Jun and coworkers used 2-amino-3-picoline and benzaldehyde **56** to *in situ* form an aldimine (**59**) (Figure 1.8, eq. 2).[37] The pyridine coordinates with the rhodium catalyst to promote the oxidative addition on the aldiminic C—H bond. Importantly, undesired decarbonylation of the aldehyde is avoided by condensation of the aldehyde with the amine. A final 1,2-addition and a reductive elimination results in an imine that is in equilibrium with the final compound **58**. This equilibrium is shifted towards the ketone as the aldehyde present in the reaction media reacts preferentially with the amine because of the higher electrophilicity of the former.

1.2.1.4 Oxidative Addition directs C—H bond functionalization

Despite the obvious advantages associated to directing groups, their utilization might not be ideal in complex settings. As shown previously, directed C—H functionalization is based on bringing the metal in close proximity to the targeted C—H bond (Figure 1.4). Such situation might eventually take place in a scenario based on an oxidative addition to a C—X bond (X = leaving group), forming a C—M bond while increasing the oxidation state of the metal in two units (Figure 1.9).

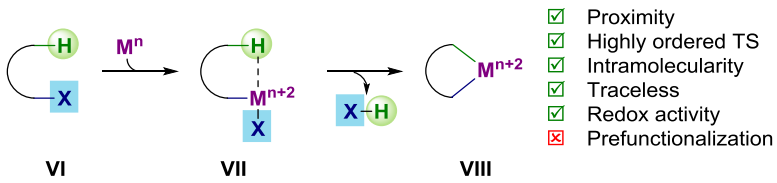

Figure 1.9. Oxidative addition-directs C—H bond metalation.

Although prefunctionalization is required, this approach does not require the use of an oxidant or directing group constituting a bonus from a synthetic standpoint.

[36] Bedford, R. B.; Betham, M.; Caffyn, A. J. M.; Charmant, J. P. H.; Lewis-Alleyne, L. C.; Long, P. D.; Polo-Cerón, D.; Prashar, S. *Chem. Commun.* **2008**, 990.
[37] Jun, C-H.; Lee, H.; Hong, J.-B.; Kwon, B.-I. *Angew. Chem. Int. Ed.* **2002**, *41*, 2146.

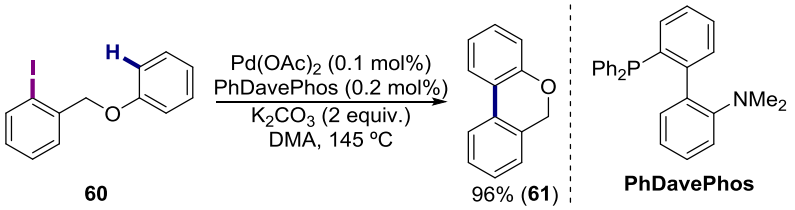

Scheme 1.15. Pd-catalyzed synthesis of biaryls via C—H bond arylation.

Fagnou and coworkers employed this strategy for the synthesis of biaryl compounds in an intramolecular fashion. The reactions are triggered by the insertion of *in situ* formed palladium(0) into the C—I bond forming an arylpalladium(II) intermediate. Subsequently, the C—H bond cleavage occurs due to the proximity to the metal center. A latter reductive elimination renders the product **61** while recovering the catalytically active palladium(0) complex (Scheme 1.15).[38]

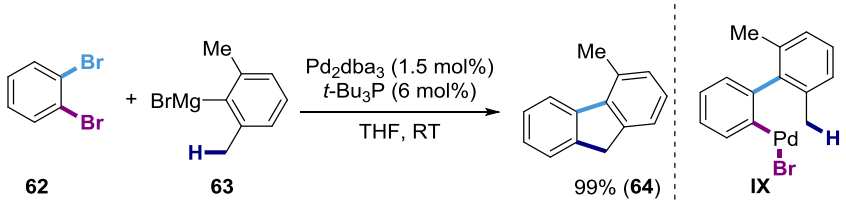

Scheme 1.16. Pd-catalyzed tandem Kumada cross-coupling/ oxidative addition directed C—H bond functionalization.

In a related work, Hu and Dong designed a tandem transformation between 1,2-dibromobenzenes (**62**) and *ortho*-alkylated aryl Grignard reagents (**63**) where a fluorene core (**64**) was obtained via Kumada cross-coupling/C—H bond functionalization (Scheme 1.16).[39] The reaction is initiated by a Kumada cross-coupling forming an *ortho*-phenylbromobenzene. The subsequent C—H bond functionalization is possible due to the oxidative addition of the palladium(0) into the C—Br bond (**IX**) that will bring together the metal center and the C—H bond to be functionalized. Interestingly, no cross-coupling reaction of **IX** with **63** occurs, most likely due to steric effects.

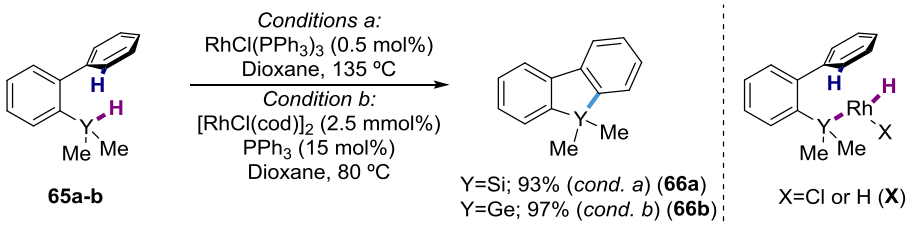

Scheme 1.17. Rh-catalyzed dehydrogenative synthesis of sila- and germafluorenes.

In a remarkable work, Takai and co-workers took advantage of the weak Si—H and Ge—H bond (**65a-b**) to use it as a formal directing group after oxidative addition (**X**).[40] A final reductive elimination of the *in situ* formed metalacycle results in sila- and germanofluorenes. Although the mechanism of the C—H bond cleavage is not clear yet, these reports represent

[38] Campeau, L.-C.; Parisien, M.; Leblanc, M.; Fagnou, K. *J. Am. Chem. Soc.* **2004**, *126*, 9186.
[39] Dong, C.-G.; Hu, Q.-S. *Angew. Chem. Int. Ed.* **2006**, *45*, 2289.
[40] (a) Urshino, T.; Yoshida, T.; Kuninobu, Y.; Takai, K. *J. Am. Chem. Soc.* **2010**, *132*, 14324. (b) Murai, M.; Matsumoto, K.; Okada, R.; Takai, K. *Org. Lett.* **2014**, *16*, 6492.

the paradigm of efficiency as rather challenging substrates are formed in one step with molecular hydrogen as the sole byproduct (Scheme 1.17).

1.2.1.5 Catalyst induced selectivity

In the previous sections, it has been shown how the substrate itself can direct the C—H bond cleavage either by tuning its stereoelectronic properties or by binding to the metal catalyst. However, these transformations are substrate-controlled, thus limiting the scope of this transformation. Alternatively, directional differentiation is within reach by modifying the stereoelectronic properties of the catalyst. As a consequence, distinction between different C—H bons can be accomplished by a fine-tuning the catalyst of choice. The catalyst-induced selectivity approach possesses great potential because of the ability to promote selective transformations but also because different products can be formed by simply changing the reactions conditions from the same starting materials.

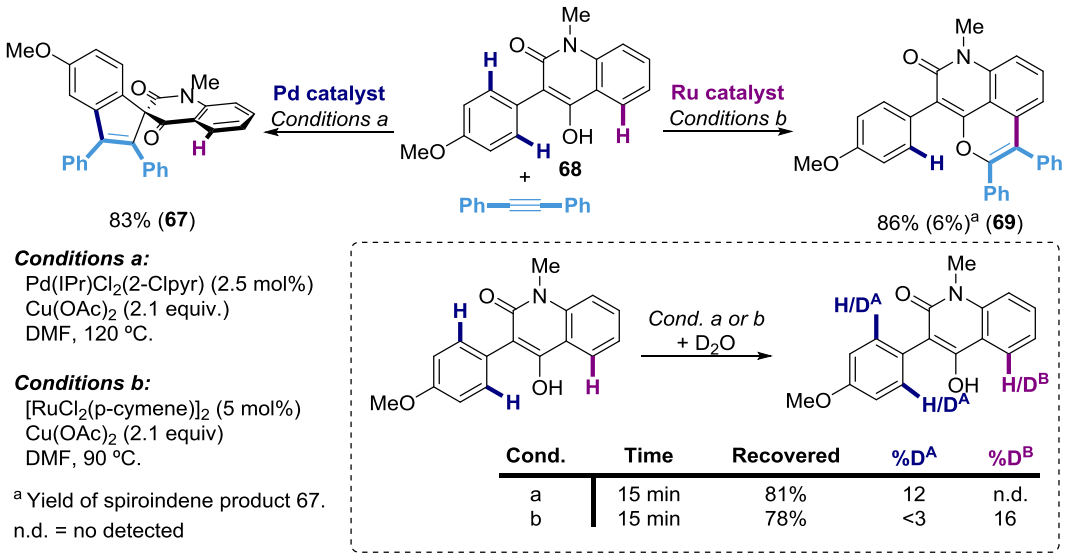

Figure 1.10. Catalyst-Controlled Divergent C–H Functionalization of Unsymmetrical 2-Aryl Cyclic 1,3-Dicarbonyl Compounds.

In a stunning report, Lam and coworkers developed a divergent C—H functionalization of unsymmetrical 2-aryl cyclic 1,3-dicarbonyl compounds (**68**) with alkynes and alkenes depending on the catalyst of choice (Figure 1.10).[41] In this regard, palladium-catalysis provides spiroindene cores **67**, whereas ruthenium-catalysis gives benzopyran derivatives **69**. To gain insight into the mechanism, the starting material **68** was submitted to the reaction conditions in the presence of deuterated water in the absence of alkyne. After 15 minutes under palladium-catalysis, only deuteration at the anisole backbone was observed. In contrast, deuteration at H^B was predominantly observed under ruthenium catalysis. Although these experiments nicely illustrate the differences in reactivity between palladium and ruthenium catalysts, the authors were unable to explain the insights behind such behavior.

[41] Dooley, J. D.; Chidipudi, S. R.; Lam, H. W. *J. Am. Chem. Soc.* **2013**, *135*, 10829

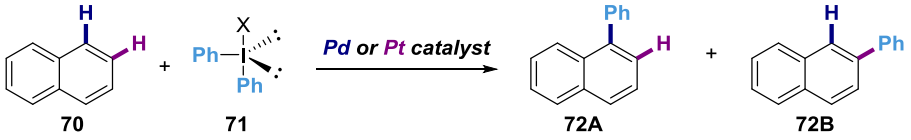

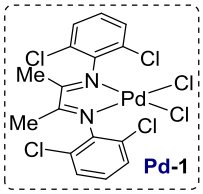

Entry	Catalyst	X	Solvent	Additive	Yield (%)	A:B
1	Na_2PdCl_4	TFA	TFE	none	65	25:1
2	Na_2PtCl_4	TFA	TFE	none	31	1:10
3	**Pd**-1	BF_4	$PhNO_2$	none	70	71:1
4	Na_2PtCl_4	TFA	None	Bu_4NOTf	65	1:35

Figure 1.11. Orthogonal regioselective C—H arylation of naphthalene.

Another attractive example was described by Sanford and co-workers regarding the C—H arylation of naphthalene (**70**) with aryl-λ^3-iodanes (**71**) under transition metal catalysis (Figure 1.11).[42] Whereas C1 is more nucleophilic, the C2 position is less sterically crowded. Based on this observation, Sanford and co-workers succeeded in developing catalytic conditions for the regioselective synthesis of 1-phenylnaphthalene **72A** under palladium-catalysis conditions (entry 1 and 4) and 2-phenylnaphthalene **72B** under platinum-catalysis conditions (entry 2 and 4). Such dichotomy is nicely explained from a mechanistic perspective. Both mechanisms are based on the same elementary steps (Figure 1.12): 1) Oxidation of M(II) to M(IV) by the iodonium salt forming an Ar—M(IV) bond (**XII**). 2) π-coordination of the highly electrophilic metal to the naphthalene (not shown). 3) Metalation via C—H bond cleavage (**XIII**) and 4) reductive elimination yielding the biaryl product. Although the mechanism is similar for both metals, while the rate-limiting step under palladium-catalysis is the oxidation to palladium(IV), the reductive elimination step is rate-determining for platinum. Because of this difference and because of the larger size of platinum, sterics will rule the regioselectivity of the transformation over electronic control in the case of platinum-catalysis, thus disfavoring the metalation in C1 (**XIV**) and favoring the platination of the more available, yet less nucleophilic, C2 position (**XV**). Indeed, when using the more sterically demanding $[Cl_4Pt(o\text{-}tol)]^{2-}$ the A:B ratio increased to >1:100, confirming the important role played by steric interactions in the selectivity. On the other hand, under palladium-catalysis, the repulsive interaction with the proton at position 8 is not big enough to overcome the benefits coming from reacting with the most nucleophilic position; consequently, 1-phenylnaphthalene is preferentially formed.

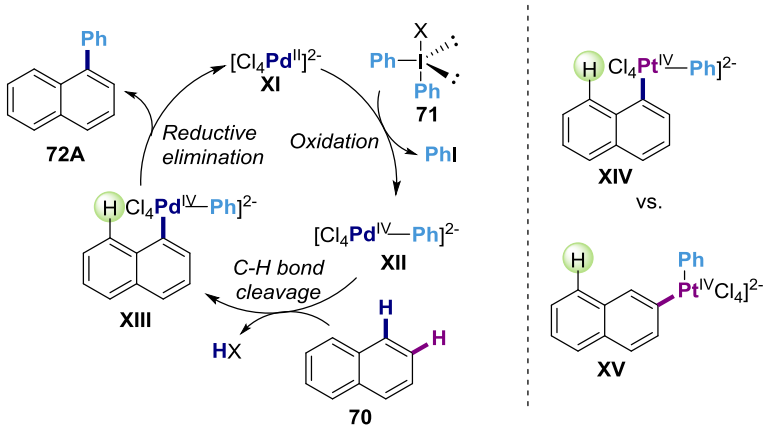

[42] (a) Wagner, A. M.; Hickman, A. J.; Sanford, M. S. *J. Am. Chem. Soc.* **2013**, *135*, 15710. (b) Hickman, A. J.; Sanford, M. S. *ACS. Catal*. **2011**, *1*, 170.

Figure 1.12. Catalytic cycle for the arylation of naphthalene with palladium or platinum catalysts.

Catalyst-control selectivity is not uniquely achieved using different metals. Since ancillary ligands are able to modulate the properties of the bonded metal, one might expect to obtain different selectivity when changing the coordination sphere of the catalyst. In 2010, Itami *et al.* developed a novel methodology for the β-arylation of thiophenes[43] that are well known for being more reactive towards α-arylation. The reactivity switch is based on a meticulous ligand selection (Figure 1.13); while the most electron-deficient phosphine (entry 1) gave the higher β/α ratio, more electron-donating phosphines reverse the regioselectivity. It is believed that highly electron-deficient phosphines promote nucleophilic attack of the thiophene to the palladium center (**XVII**), and subsequent aryl migration (**XVIII**) would be responsible for the regioselectivity observed. In analogy with Fagnou's report, α-arylation might be a consequence of a concerted-metalation mechanism as the electrophilic pathway might not be favored with palladium(II) intermediates.

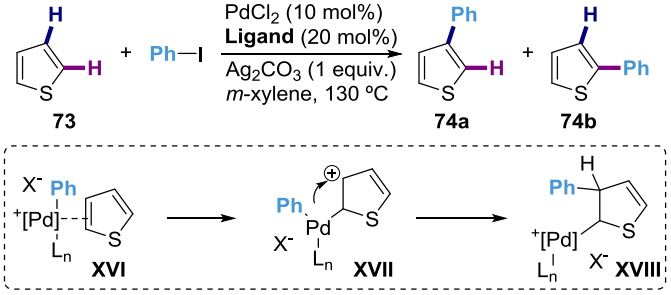

Entry	Ligand	Yield (%)	Ratio
1	$P\{OCH(CF_3)_2\}_3$	86	86:14
2	$P(OPh)_3$	14	38:62
3	$P(C_6F_5)_3$	66	31:69
4	PPh_3	75	4:96
5	PCy_3	>99	<1:99

Figure 1.13. β-selective C—H bond arylation of thiophenes with iodoarenes.

Interestingly, selective C—H bond-functionalization can be achieved by tuning other reaction parameters of the catalytic system. For example, Gaunt and co-workers reported the intermolecular alkenylation of free indoles (Figure 1.14), where the selectivity was dependent on the acidic media and the solvent.[44] For example, they observed that an acidic media was deleterious for the alkenylation at the C3 position (entries 1 *vs* 2). On the other hand, the polarity of the solvent was crucial, favoring the C3 alkenylation in the presence of *t*-BuOOBz as terminal oxidant with acetonitrile (entries 3 *vs* 4).

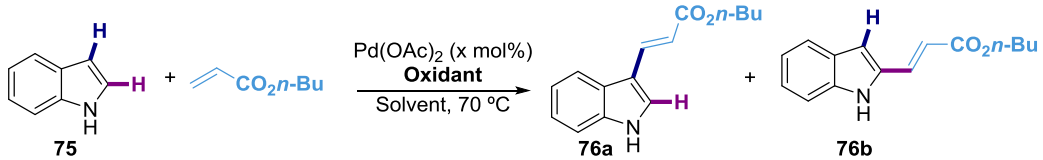

Entry	Catalyst loading (x mol%)	Oxidant (equiv.)	Solvent (v/v)	Yield (%)	Ratio
1	10	$Cu(OAc)_2$ (1.8)	DMF	54	>95:5
2	10	$Cu(OAc)_2$ (1.8)	DMF/AcOH (3:1)	54	1:1
3	20	*t*-BuOOBz (0.9)	Dioxane/AcOH (3:1)	58	1:7
4	10	*t*-BuOOBz (0.9)	CH_3CN/AcOH (3:1)	65	>95:5

[43] (a) Ueda, K.; Yanagisawa, S.; Yamaguchi, J.; Itami, K. *Angew. Chem. Int. Ed.* **2010**, *49*, 8946. For a recent mechanistic study using DFT see: (b) Tang, S.-Y.; Guo, Q.-X.; Fu, Y. *Chem. Eur. J.* **2011**, *17*, 13866.
[44] Grimster, N. P.; Gauntlett, C.; Godfrey, C. R. A.; Gaunt, M. J. *Angew. Chem. Int. Ed.* **2005**, *44*, 3125.

Figure 1.14. Solvent-controlled regioselective C—H functionalization of indoles.

Similarly, DeBoef *et al.* observed an oxidant-dependent selectivity switch for the arylation of benzofurans and indoles.[45] In the benzofuran case, a dramatical loss of selectivity arose by replacing $Cu(OAc)_2$ by AgOAc (Figure 1.15, entries 1-2). This effect was even amplified in the case of *N*-acetylindole, where a complete inversion of regioselectivity was observed (entries 3-4). Although tentatively, the authors proposed the formation of polymetallic clusters between palladium and the oxidant to be responsible of the selectivity switch.

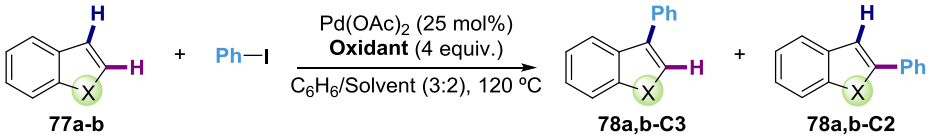

Entry	X	Oxidant	Solvent	Yield (%)	C3:C2
1	O	$Cu(OAc)_2$	AcOH	44	>99:1
2	O	AgOAc	AcOH	84	52:48
3	NAc	$Cu(OAc)_2$	Dioxane	66	80:20
4	NAc	AgOAc	Dioxane	55	22:78

Figure 1.15. Oxidant-controlled regioselectivity in the oxidative arylation of heterocycles.

1.2.2 Overcoming the inherent low reactivity

In the previous section, we have overviewed different existing approaches in order to achieve selectivity in C—H functionalization reactions. However the innate poor reactivity of C—H bonds still constitutes a tremendous challenge.

C-H	CH_3-H	$MeCH_2$-H	Me_2CH-H	Me_3C-H	*c*-H_5C_3-H			Ph-H	$PhCH_2$-H	Ph_2CH-H
DH_{298} (kcal/mol)	104.9	101.1	98.6	96.5	106.3	88.8	110.7	112.9	89.7	84.5
pK_a DMSO	56					44			43	32.2
pK_a Water	48		51	53	46	43	50	43	41	33.5

Table 1.1. Bond dissociation energies (Kcal/mol) and pK_a values of different C—H bonds.[46]

As demonstrated by their dissociation energies (DH_{298}) and pK_a values, C—H bonds are difficult to cleave, either in a homolytical or heterolytical fashion. In order to make this process thermodinamically feasible, the high cost of cleaving such a stable bond must be somehow compensated by forming a stronger C—M bond. However, C—M bonds are usually not sufficiently strong (i.e. C—Pt bond energies of 60 to 64 Kcal/mol have been estimated for neutral square-planar Pt(II) complexes) which makes the functionalization of C—H bonds difficult from a thermodynamically point of view. In spite of these difficulties, chemists have been able to achieve reactivity by following different strategies:

1.2.2.1 Intramolecular reactions

[45] Potavathri, S.; Dumas, A. S; Dwight, T. A.; Naumiec, G. R.; Hammann, J. M.; DeBoef, B. *Tetrahedron Lett.* **2008**, *49*, 2008.
[46] (a) Luo, Y-R. *Handbook of Bond Dissociation Energies in Organic Compounds*, **2002**. (b) Blanksby, S. J.; Ellison, G. B. *Acc. Chem. Res.* **2003**, *36*, 255. (c) Evans, pK_a table.

The ability of the metal catalyst to be in close proximity of a C—H reduces the enthalpic and entropic costs of the subsequent C—H bond cleavage (Figure 1.16). In this category we can find the directing group C—H bond functionalization strategy (section 1.2.1.3) as well as the oxidative addition directed strategy (section 1.2.1.4).

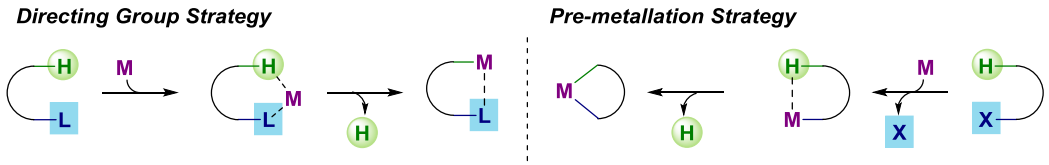

Figure 1.16. Different prior metalation strategies to the C—H bond cleavage.

Glorius et al. reported a methodology for the synthesis of dibenzofurans (**80**)[47] where the C—H bond cleavage was possible through a prematalation of the substrate (scheme 1.18). In order to achieve such palladation, the authors envisioned a scenario in which a carboxylic acid could act as a halogen-free precursor in a tandem silver(I) catalyzed decarboxylation/transmetallation. Additionally, silver also plays a crucial role as oxidant in order to ensure catalyst turnover.

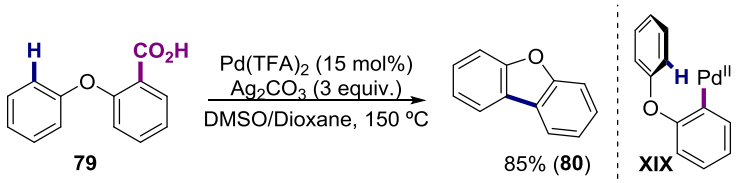

Scheme 1.18. Cooperative silver/palladium-catalyzed decarboxylative synthesis of dibenzofurans.

Similarly, Kuninobu and Takai accomplished the synthesis of dibenzophosphole oxides **82** through cleavage of a non-active C—H bond.[48] In order to promote the bond rupture, they designed a system in which the C—H bond cleavage would become intramolecular and, therefore, easier. To such end, they use secondary hydrophosphine oxides (**81**) with two purposes. Firstly, to introduce the phosphine motif into the molecule, and secondly, to use it as directing group to promote reactivity and selectivity to the transformation. The mechanism follows two different pathways; during the first turnover the palladation occurs by elimination of acetic acid (**XX**), subsequent C—H bond cleavage followed by reductive elimination forms the product along with palladium(0) that re-enters in the cycle. At this point, the metalation takes places through oxidative addition on the C—H bond (scheme 1.19).

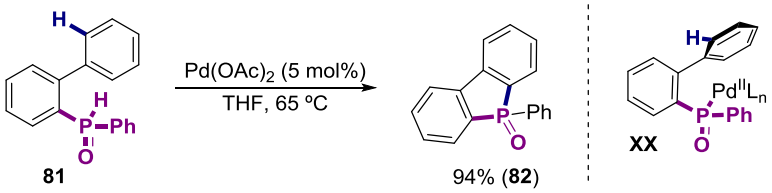

Scheme 1.19. Palladium-catalyzed oxidative synthesis of dibenzophosphole oxides.

1.2.2.2 Reactivity enhancement of C—H bonds

[47] Wang, C.; Piel, I.; Glorius, F. *J. Am. Chem. Soc.* **2009**, *131*, 4194.
[48] Kuninobu, Y.; Yoshida, T.; Takai, K. *J. Org. Chem.* **2011**, *76*, 7370.

The different reactivity of C—H bonds can be turned into a strategic advantage for designing C—H bond-functionalization techniques. For example, the higher nucleophilicity of C3 position of electron-rich aromatic ring such as benzothiophene allows for a regioselective transformation via S_EAr. On the contrary, the C2 position is more acidic, and therefore, more reactive for concerted-metalation deprotonation processes. For example, Hu and You reported the palladium-catalyzed oxidative cross-coupling of heteroarenes using an acidic heterocycle **83a-c** and a nucleophilic heterocycle **84a-b** (Figure 1.17).[49] The proposed mechanism is initiated by a S_EAr featured by the most nucleophilic substrate. At this point, there is a complete inversion of reactivity as the mechanism switches to a concerted-metallation deprotonation and therefore, the more acidic substrate becomes reactive, thus ensuring the selectivity of the process and showing how the reactivity of a C—H bond depends on the ongoing mechanism.[50]

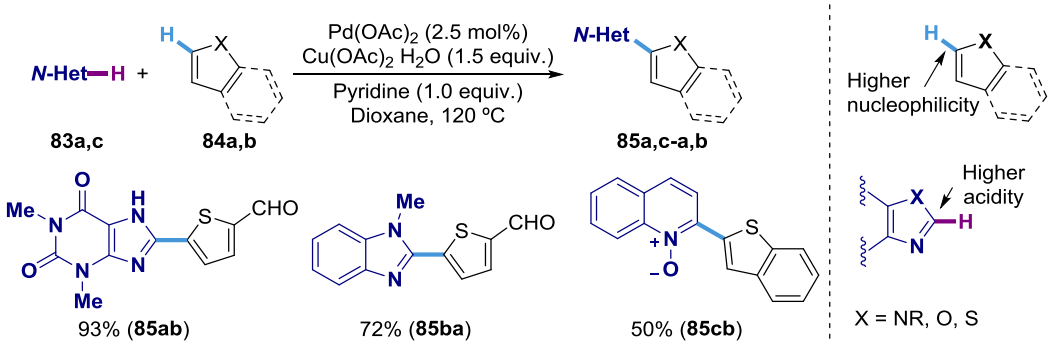

Figure 1.17. Palladium(II)-catalyzed oxidative C–H/C–H cross-coupling of heteroarenes.

Although an in depth explanation of the concerted-metallation deprotonation will be treated in Section 1.2.4.4, Figure 1.18 indicates that there is not a direct dependence between electronic effects and reactivity under a concerted metalation-deprotonation mechanism.

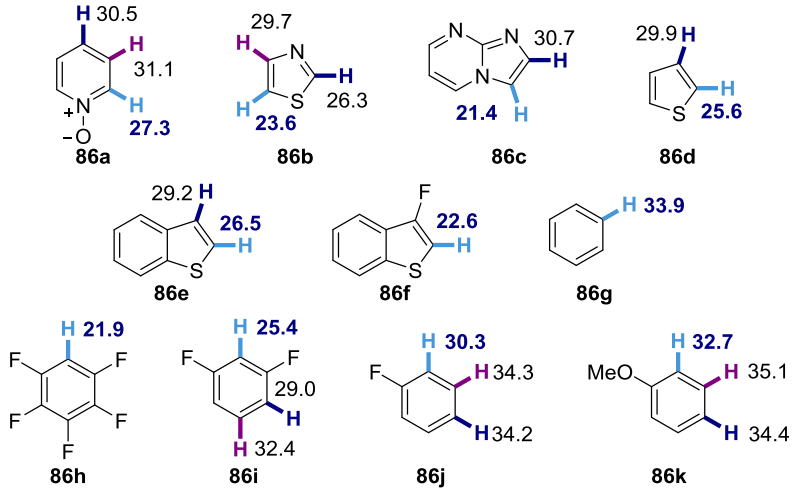

[49] Xi, P.; Yang, F.; Qin, S.; Zhao, D.; Lan, J.; Gao, G.; Hu, C.; You, J. *J. Am. Chem. Soc.* **2010**, *132*, 1822.

[50] It must be noticed that we do not agree with the author's explanation and we belive that both metalation steps are occurring through a concerted metalation-deprotonation mechanism based on the reactivity displayed by benzothiophene.

Figure 1.18. Free energy of activation ($\Delta G^{\ddagger}$ 298K, kcal/mol) for direct arylation via the CMD pathway involving an acetate ligand. Bold values represent the position that is functionalized experimentally.[51]

As shown in Figure 1.18, fluorine atoms play a key role for enhancing the reactivity of proximal C—H bonds. This is particularly the case for 3-fluorobenzothiophene (**86f**), where the C2 position is more reactive when compared to benzothiophene (**86e**). Not surprisingly, a wide number of reports have been described when using polyfluoroarenes. For example, Lafrance and Fagnou reported the intermolecular direct arylation of polyfluoroarenes **87a-c** under palladium-catalysis conditions (Figure 1.19).[52] As shown for **87b**, the most acidic C—H bond reacts preferentially, being the C—H bond between two fluorine atoms exclusively activated (position 2).

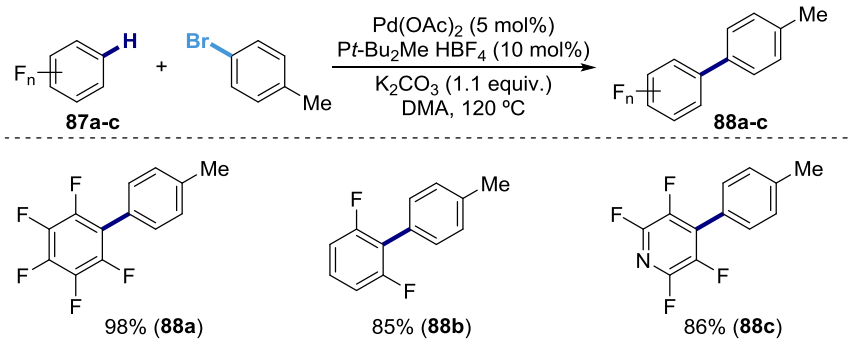

Figure 1.19. Catalytic Intermolecular Direct Arylation of Perfluorobenzenes.

A sophisticated example showing the active nature of C—H bonds in perfluoroarenes was reported by Echavarren and co-workers.[53] As shown, C—H functionalization occurs preferentially at the polyfluoroarene backbone with an excellent selectivity profile (Scheme 1.20).

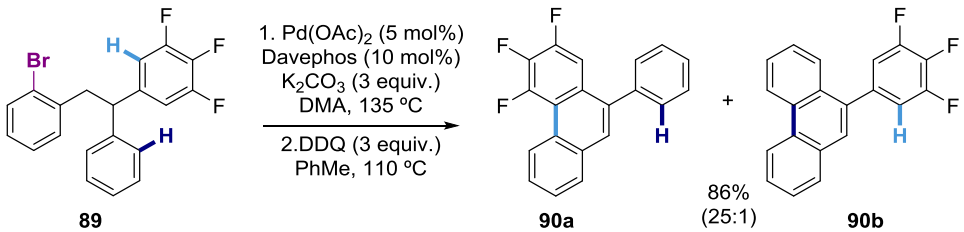

Scheme 1.20. Pd-catalyzed highly selective intramolecular C—H bond arylation.

Larrosa and co-workers, envisioned a strategy to increase the reactivity of less reactive C—H bonds. They hypothesized that the formation of the (η^6-arene)$Cr(CO)_3$ complex **91** would reduce the electron density of the arene, thus favoring the C—H cleavage through a concerted metalation-deprotonation mechanism (Figure 1.20).[54] Unfortunately, such strategy required stoichiometric amount of chromium complexes.

[51] Gorelsky, S. I. *Coord. Chem. Rev.* **2013**, *257*, 153.
[52] Lafrance, M.; Rowley, C.N.; Woo, T. K.; Fagnou, K. *J. Am. Chem. Soc.* **2006**, *128*, 8754.
[53] García-Cuadrado, D.; Braga, A. A. C.; Maseras, F.; Echavarren, A. M. *J. Am. Chem. Soc.* **2006**, *128*, 1066.
[54] (a) Ricci, P.; Krämer, K.; Cambeiro, X. C.; Larrosa, I. *J. Am. Chem. Soc.* **2013**, *135*, 13258. (b) Ricci, P.; Krämer, K.; Larrosa, I. *J. Am. Chem. Soc.* **2014**, *136*, 18082.

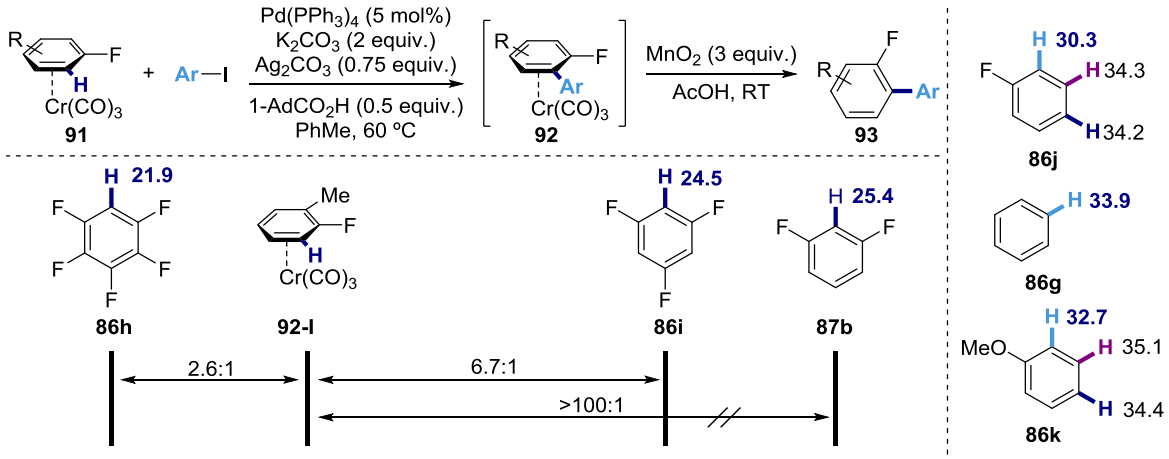

Figure 1.20. Tuning reactivity and site selectivity of simple arenes in C—H activation via arene–metal π-complexation.[55]

The authors observed that while (η^6-*o*-fluorotoluene)$Cr(CO)_3$ could perform the C—H bond-functionalization, *o*-fluorotoluene did not react under the same reaction conditions, thus confirming the importance of the 'reactivity enhancing' substituent. Competition experiments (see Figure 1.20) showed that (η^6-o-fluorotoluene)$Cr(CO)_3$ (**92-l**) presented a much higher reactivity than 1,3,5-trifluorobenzene and 1,3-difluorobenzene (**86i** and **87b** respectively) and a reactivity similar to pentafluorobenzene (**86h**), therefore demonstrating again the effect of the $Cr(CO)_3$ moiety in enhancing the reactivity. Moreover, poorly activated substrates (fluorobenzene, benzene and anisole) were also reactive through the formation of the $Cr(CO)_3$ complex with high selectivity towards the C—H bond predicted by Fagnou. DFT studies were conducted to shed light into the $Cr(CO)_3$ effect. Surprisingly, it was not an increase on the acidity of the C—H bond but rather a reduced destabilization arising from the distortion in the transition state the responsible of such reactivity enhancement (see Section 1.2.4.4). This strategy represents a novel manner to enhance the activity of C—H bonds with no need to form a covalent bond with the targeted molecule.

While in general $C(sp^3)$—H bonds are considerably less reactive than $C(sp^2)$—H bonds, care must be taken when generalizing such observation. The lower reactivity as compared to $C(sp^2)$—H bonds is a consequence of the lack of empty low-energy or filled high-energy orbitals on the vicinity of the $C(sp^3)$—H bond, hampering the interaction of the substrate with the catalyst. Consequently, the reactivity is lower that for $C(sp^2)$—H bonds, where the orbitals of the aromatic ring are available to interact with the catalyst, usually forming a π-complex prior to the C—H bond cleavage event thus enhancing the reactivity of the system. Amongst $C(sp^3)$—H bonds, cyclopropyl $C(sp^3)$—H bonds are unique as they are readily activated as compared to other $C(sp^3)$—H bonds. Such higher reactivity is believed to be related to the inherent ring strain and orbital rehybridization of the cyclopropyl ring that confers it σ-aromaticity.[56] In other words, there is an electronic cloud plane on the ring due to the delocalization of six electrons in the CCC bonds. This electronic cloud would allow an efficient

[55] Free energy of activation ($\Delta G^{\ddagger}$ 298K, kcal/mol) for direct arylation via the CMD pathway involving an acetate ligand. Bold values represent the position that is functionalized experimentally
[56] Exner, K.; Schleyer, P. R. *J. Phys. Chem. A.* **2001**, *105*, 3407.

interaction with the catalyst, bringing it into the proximity of the aimed bond what will facilitate the C(sp^3)—H cleavage.

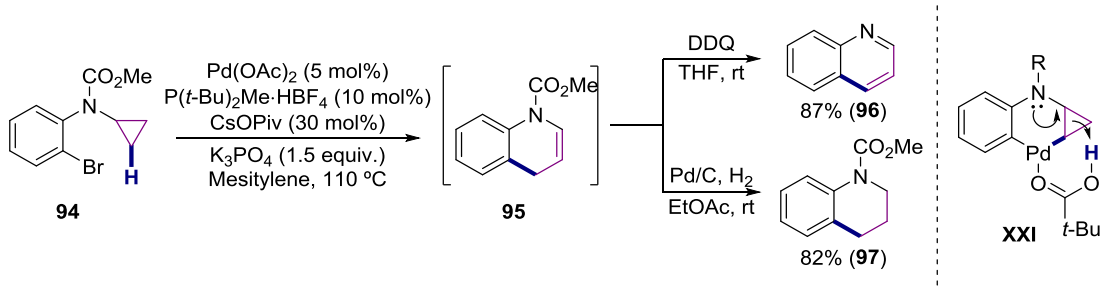

Figure 1.21. Palladium(0)-catalyzed cyclopropane C—H bond functionalization: synthesis of quinoline and tetrahydroquinoline derivatives

As shown in Figure 1.21, Rousseaux took advantage of this innately higher reactivity of cyclopropyl C—H bonds to effect the synthesis of quinolone (**96**) and tetrahydroquinoline derivatives (**97**) through palladium-catalysis.[57] The authors demonstrated that the reaction follows a mechanism consisting of (1) oxidative addition of a palladium(0) complex on to the C—Br bond, (2) concerted metalation-deprotonation forming a fused six-membered ring (**XXI**), followed by (3) ring expansion, rendering a benzofused seven-membered ring, (4) deprotonation and (5) final reductive elimination. The product presented poor stability, although it could be easily transformed to quinolone or tetrahydroquinoline under oxidative and reductive conditions respectively.

Allylic and benzylic C(sp^3)—H bonds are also activated and can trigger easily C—H bond-functionalization reactions due to the formation of rather stable allyl palladium intermediates. For example, the White's group have reported several transformations involving allylic C—H bond functionalization,[58] such as alkylation with soft nucleophiles and C—O bond-formation events (Scheme 1.21).

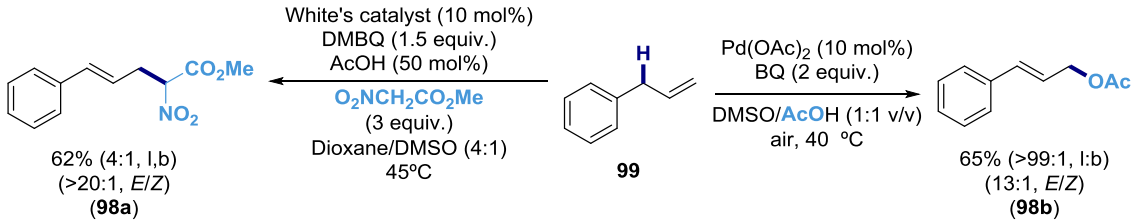

Scheme 1.21. Pd-catalyzed allylic C—H bond functionalization.

1.2.3 Mechanistic Manifolds

Although a myriad of transition metals are known to effect C—H bond-functionalization reactions, the use of palladium catalysts has dominated this field of expertise. The different

[57] Rousseaux, S.; Liégault, B.; Fagnou, K. *Chem. Sci.* **2012**, *3*, 244,
[58] Chen, M. S.; Prabagaran, N.; Labenz, N. A.; White, M. C. *J. Am. Chem. Soc.* **2005**, *127*, 6970. (b) Young, A. J.; White, M. C. *J. Am. Chem. Soc.* **2008**, *130*, 14090. (c) Chen, M. S.; White, M. C. *J. Am. Chem. Soc.* **2004**, *126*, 1346.

catalytic cycles[59] involving palladium-catalyzed C—H bond functionalization can be classified depending on the oxidation state of the palladium during the catalytic cycle:

- Pd(0)/Pd(II)
- Pd(II)/Pd(0)
- Pd(II)/Pd(IV)
- Dimeric Pd(III)/Pd(III) or Pd(II)/Pd(IV)

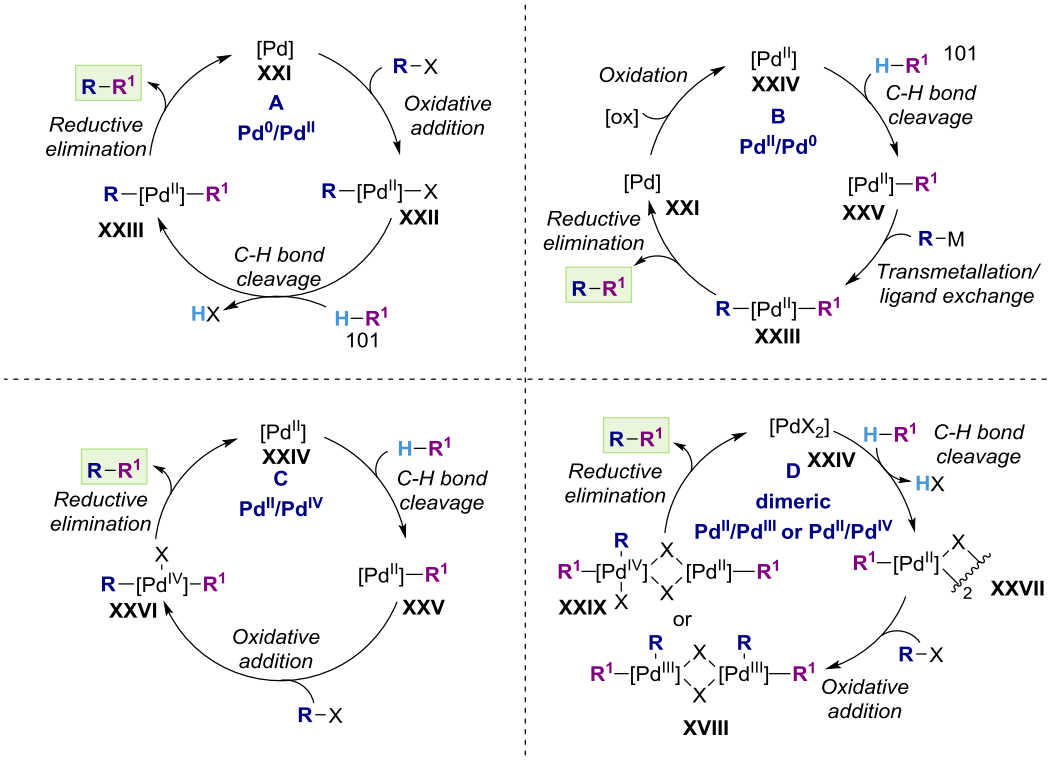

Figure 1.22. Different catalytic cycles of palladium catalyzed C—H bond functionalization reactions.

Pd(0)/Pd(II):

This type of catalytic cycle (Figure 1.22, A) is initiated by an oxidative addition of a the C—Heteroatom bond to a palladium(0) catalyst **XXI** thus forming palladium(II) species (**XXII**). Next, the C—H bond cleavage occurs giving a palladium(II) intermediate bearing two distinctive reactive ligands (**XXIII**). A final reductive elimination step will deliver the product while recovering the active palladium(0) species. Several examples of this type of catalysis have already been explained in previous sections. The main advantage of this methodology is the fact that the substrate possesses the required redox activity so that a further oxidant is not required. In general, this approach is based on the fine-tuning of the metal center by a careful ligand selection. The ligand must be able to promote oxidative addition as well as to trigger the final reductive elimination.

Pd(II)/Pd(0):

[59] This classification and the following schemes represent a very general and narrow approach towards reactivity of palladium catalysis.

This catalytic cycle (Figure 1.22, B) involves an initial C—H bond cleavage, forming an organometallic intermediate (**XXV**). At this point, transmetallation, ligand exchange, etc. introduces a second reactive ligand (**XXIII**). Finally, a reductive event such as reductive elimination or β-hydride elimination/deprotonation will deliver the final compound together with palladium(0) (**XXI**) that ultimately gets oxidized to deliver the propagating palladium(II) species.

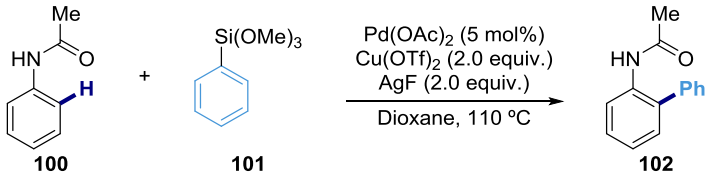

Scheme 1.22. *Ortho*-arylation of acetanilides via Pd(II)-catalyzed C—H functionalization.

An example of this type of catalysis was published by Shi and co-workers.[60] In their report, *ortho*-arylation of acetanilides (**100**) was achieved by C—H bond cleavage with a Pd(II) catalyst. The reaction commences via palladacycle formation, transmetallation with the aryl silane **101**, aided by fluoride ions and a final reductive elimination to deliver the targeted biaryl while forming palladium(0) which is oxidized by copper(II) or silver(I) salts.

Pd(II)/Pd(IV) catalytic cycles:[61]

Pd(II)/Pd(IV) catalytic cycles (Figure 1.22, C) begin with the palladation of a C—H bond by a palladium(II) catalyst (**XXV**). At this point, a strong oxidant (hypervalent iodine reagents, peracids, peroxides, F^+ oxidants) oxidizes the palladium(II) to palladium(IV). The selectivity of this oxidation is granted as the redox potential of alkyl and arylpalladium complexes (**XXV**) is significantly lower than that of simple palladium(II) salts (**XXIV**). Once the palladium(IV) is formed and a new reactive ligand is present in the complex **XXVI**, a reductive elimination will form the new C—C(heteroatom) bond with concomitant formation of the palladium(II) active catalyst. The fast palladium(II)/palladium(IV) oxidation prevents β-hydride elimination. Furthermore, challenging C—heteroatoms bond-reductive elimination will be possible because of the low barrier-energy for the metal when changing from a high oxidation state to a lower one. Other advantages are the tolerance towards C—halogen bonds (except with iodides), the no necessity of using strong bases and the stability of the catalyst towards moisture and oxygen. On the other hand, it is worth noting that most common ligands used in palladium chemistry are not stable under the oxidizing conditions of palladium(II)/palladium(IV) methodologies.

Probably, the most notorious palladium(II)/palladium(IV) work is the Catellani reaction[62] where norbornene is employed in combination with aryl iodides to perform the arylation of distal C—H bonds. In this case, aryl iodides are employed both as oxidants and as arylating reagent, whereas norbornene is responsible for directing the C—H bond-cleavage. A notable example to illustrate the potential of palladium(II)/palladium(IV) catalysis is the *meta*-C—H

[60] Yang, S.; Li, B.; Wan, X.; Shi, Z. *J. Am. Chem. Soc.* **2007**, *129*, 6066.
[61] (a) Muñiz, K. *Angew. Chem. Int. Ed.* **2009**, *48*, 9412. (b) Xu, L.-M.; Li, B.-J.; Yang, Z.; Shi, Z.-J. *Chem. Soc. Rev.* **2010**, *39*, 712. (c) Sehnal, P.; Taylor, R. J. K.; Fairlamb, I. J. S.; *Chem. Rev.* **2010**, *110*, 824.
[62] Catellani, M.; Motti, E.; della Ca', N. *Acc. Chem. Res.* **2008**, *41*, 1512.

alkylation of arenes developed by Yu and co-workers (Figure 1.23).[63] The use of alkyl iodides with β-hydrogens is feasible as β-hydrogen elimination is not as favorable as reductive elimination for palladium(IV) complexes.

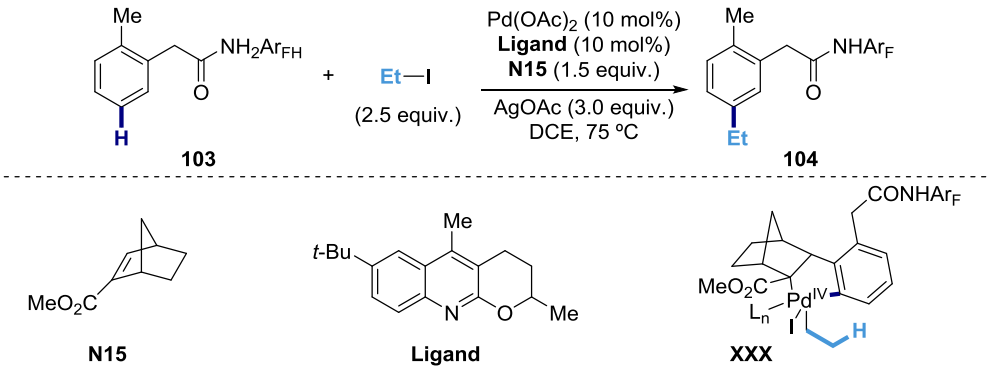

Figure 1.23. *Meta*-alkylation of C—H bonds under Pd(II)/Pd(IV) catalysis.

Dimeric Pd(II)/Pd(III) or Pd(II)/Pd(IV):

The groups of Sanford[64] and Ritter[65], have suggested that Pd(II)/Pd(IV) manifolds might follow a distinctive mechanism via the formation of Pd(III) dimers. However, the distribution of charge will depend on the proximity of both palladium atoms. Consequently, mixed-valent palladium(II)/palladium(IV) (**105**) or Pd(III)~Pd(III) (**106**) species can be formed (Figure 1.22D and 1.24).

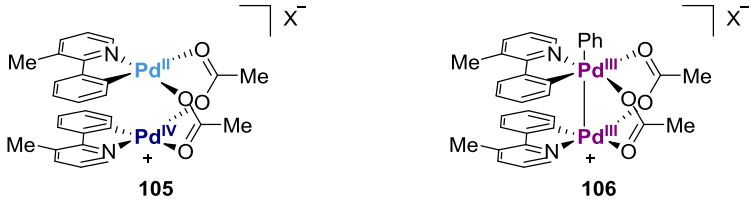

Figure 1.24. Structure of dimeric Pd(IV)/Pd(II) and Pd(III)/Pd(III) intermediates in the C—H arylation of 3-methyl-2-phenylpyridine.

1.2.4 Modes of activation for C—H bond metallation[7a,66]

C—H functionalization techniques operate with different activation modes that strongly depend on the metal catalyst of choice as well as the use of different additives. The different reaction pathways can be classified into the following categories:

- Oxidative addition
- σ-bond metathesis
- Electrophilic substitution
- Concerted metalation-deprotonation

[63] (a) Shen, P.-X.; Wang, X.-C.; Wang, P.; Zhu, R.-Y.; Yu, J.-Q. *J. Am. Chem. Soc.* **2015**, *137*, 11574. (b) Wang, X.-C.; Gong, W.; Fang, L.-Z.; Zhu, R.-Y.; Li, S.; Engle, K. M.; Yu, J.-Q. *Nature*, **2015**, *519*, 334.
[64] Deprez, N. R.; Sanford, M. S. *J. Am. Chem. Soc.* **2009**, *131*, 11234.
[65] (a) Powers, D. C.; Geibel, M. A. L.; Klein, J. E. M. N.; Ritter, T. *J. Am. Chem. Soc.* **2009**, *131*, 17050. (b) Powers, D. C.; Ritter, T. *Nat. Chem.* **2009**, *1*, 302.
[66] (a) Shilov, A. E.; Shul'pin, G. B. *Chem. Rev.* **1997**, *97*, 2879. (b) Balcells, D.; Clot, E.; Eisenstein, O. *Chem. Rev.* **2010**, *110*, 749. (c) Boutadla, Y.; Davies, D. L.; Macgregor, S. A.; Poblador-Bahamonde, A. I. *Dalton Trans.* **2009**, 5820.

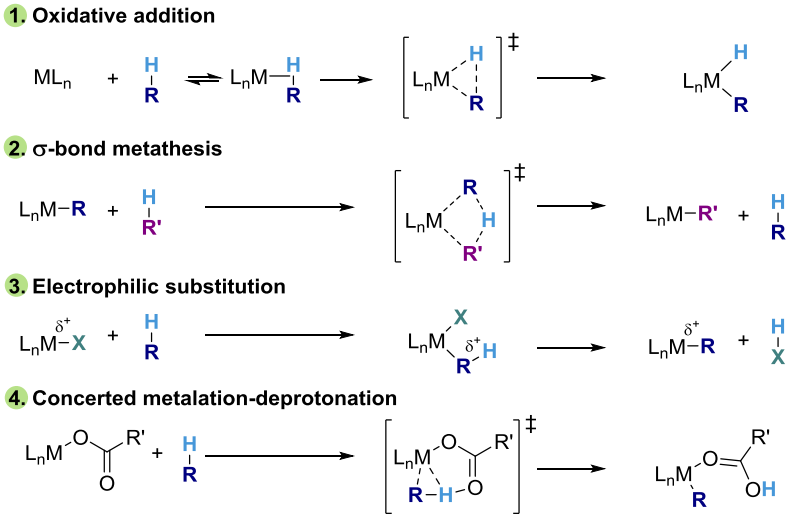

Figure 1.25. Principal proposed mechanisms for C—H bond metalation.

1.2.4.1 Oxidative Addition

Oxidative addition (Figure 1.25, eq. 1) typically takes place with electron-rich, low-valent late transitions metals (Re, Fe, Ru, Os, Rh, Ir, Pt). This can be explained because their ionization energy is lower due to the more effective electron shielding, thus favoring the oxidation of the metal center. Usually, the reactive metal complex is coordinatively unsaturated and therefore relatively unstable. During the oxidative addition two new anionic ligands enter into the metal inner sphere while its oxidation state generally increases in two units. By definition, C—H bond metalation following an oxidative addition mechanism is known as C—H bond activation as a new C—M and M—H bonds are formed.

A notable example of C—H activation was reported by Enders and co-workers ten years ago (Figure 1.26).[67] This work is the paradigm of C—H bond activation as the criteria of electron-rich and low-valent complex of late transition metals are fulfilled. Additionally, the formation of an unsaturated metal complex previous oxidative addition takes place as well. The reaction is triggered by visible light irradiation of the rhodium complex **107**. This leads to ethylene release generating a vacant site on the rhodium where the nitrogen atom of the quinoline will coordinate (**108**). As this nitrogen atom is a poor acceptor ligand whereas the metal center is rich in electron density, the bonding between the two of them will be weak allowing the oxidative insertion of the benzene C—D bond. A subsequent hydrometalation generates **110**, setting the stage for a β-hydride elimination (**111**). Final reductive elimination will deliver C_6D_5H with formation of deuterated ethylene. After several days under irradiation in the presence of benzene-d_6, the authors where able to achieve complete deuterium enrichment on ethylene and even partial deuteration on the quinolone backbone.

[67] Kohl, G.; Rudolph, R.; Pritzkow, H.; Enders, M. *Organometallic*, **2005**, *24*, 4774.

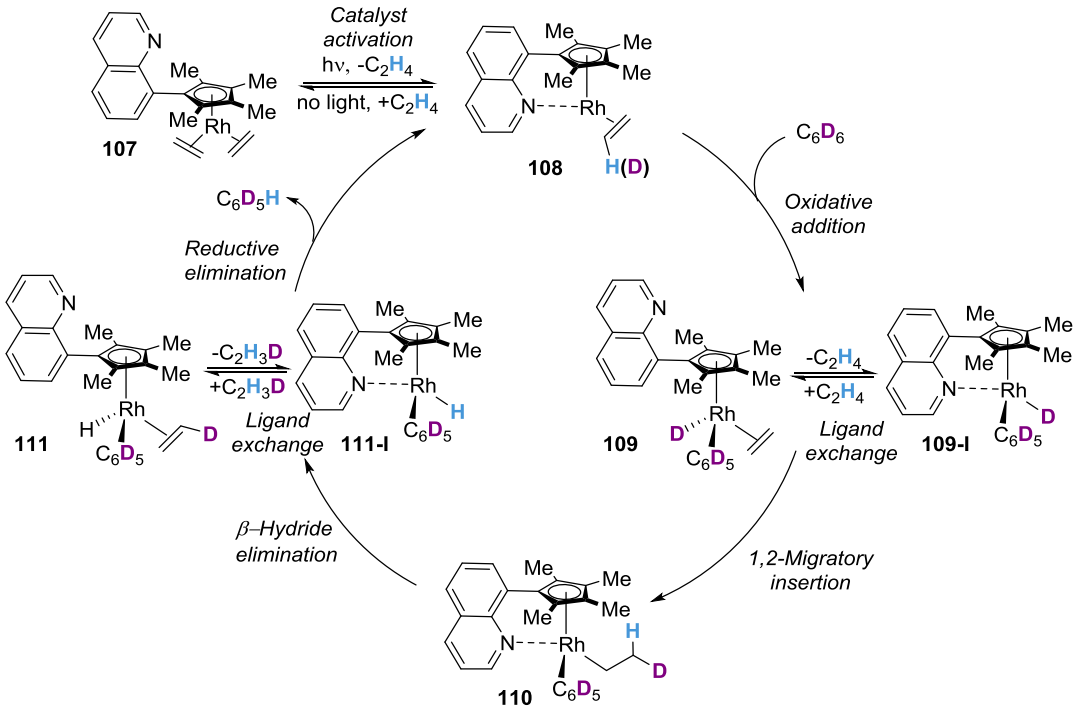

Figure 1.26. Catalytic C—H activation of benzene by rhodium(I) complex with hemilabile quinolyl-Cp* ligand.

1.2.4.2 σ-Bond Metathesis[68,69]

σ-Bond metathesis is common for early transition metals[70] with d^0 and d^0f^n configuration such as scandium, lanthanides and actinides. The reaction occurs with an alkyl or hydrido metal complex and a C—H bond (Figure 1.25, eq. 2). The transition state for this transformation is characterized as a single four-centered with a small R^1—M—R angle and no bonding between the metal and the hydrogen atom.

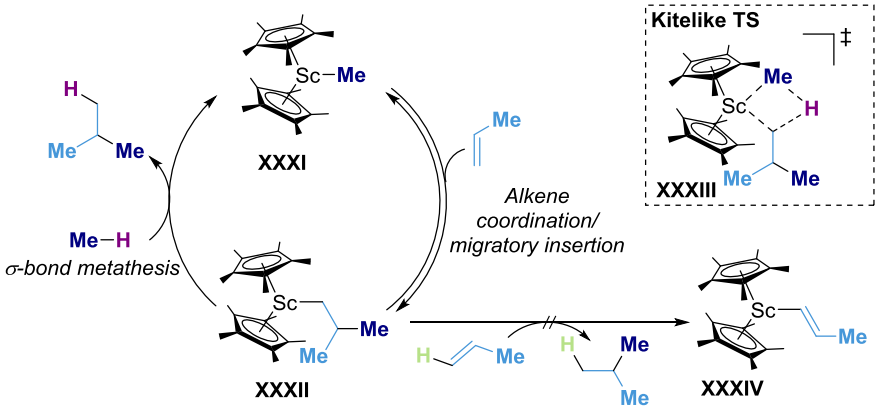

[68] (a) Waterman, R. *Organometallics* **2013**, *32*, 7249. (b) Perutz, R. N.; Sabo-Etienne, S. *Angew. Chem. Int. Ed.* **2007**, *46*, 2578.

[69] From a computational perspective, alternative mechanisms are considered for σ-bond metathesis based on computed geometric parameters. Differences lie on bond distances with the hydrogen atom and the R^1—M—R angle. However, in here we will not apply such differentiation. See: Vastine, B. A.; Hall, M.B. *J. Am. Chem. Soc.* **2007**, *129*, 12068.

[70] For an example with ruthenium see: Hartwig, J. F.; Bhandari, S.; Rablen, P. R. *J. Am. Chem. Soc.* **1994**, *116*, 1839.

Figure 1.27. Proposed catalytic cycle for hydromethylation of propene by Cp^*_2ScMe complex.

An example of σ-bond metathesis applied in a catalytic transformation was reported by Tilley and Sadow (Figure 1.27).[71] In this transformation, propene was selectively converted into isobutane in the presence of methane. The reaction proceeds by a slow alkene insertion/migratory insertion forming an isobutyl intermediate (**XXXII**) that selectively reacts with methane via σ-bond metathesis releasing isobutane and recovering the active catalyst. Interestingly, no reaction between the isobutylscandium **XXXII** and propene took place forming the corresponding vinylic complex **XXXIV**.

1.2.4.3 Electrophilic substitution

Electrophilic activation (Figure 1.25, eq. 3) takes place with electron-deficient late transition metals (usually in high oxidation states) and an electron-rich nucleophilic motif. In this transformation, the substrate attacks the electron-deficient metal creating a positive charge within the aromatic ring (Wheland intermediate). Next, a usually fast deprotonation occurs to complete the metalation while rearomatizing the aromatic motif.

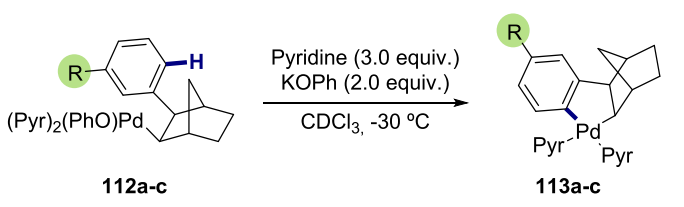

R	σ_p	Time (min)[a]
OMe	- 0.27	10
H	0.00	100
NO_2	0.78	240

[a]*Time needed to reach 50% conversion*

Figure 1.28. Palladacycle formation by electrophilic aromatic substitution, as monitored by ^1H NMR.

Catellani and Chiusoli studied the stoichiometric cyclopalladation of arenes by ^1H NMR spectroscopy.[72] They observed that the more electron-donating the substituent R is (Figure 1.28, see σ_p values on the table)[73] at the *para*-position to the targeted C—H bond, the faster the cyclopalladation event, an observation that is in agreement with a S_EAr behavior.[74]

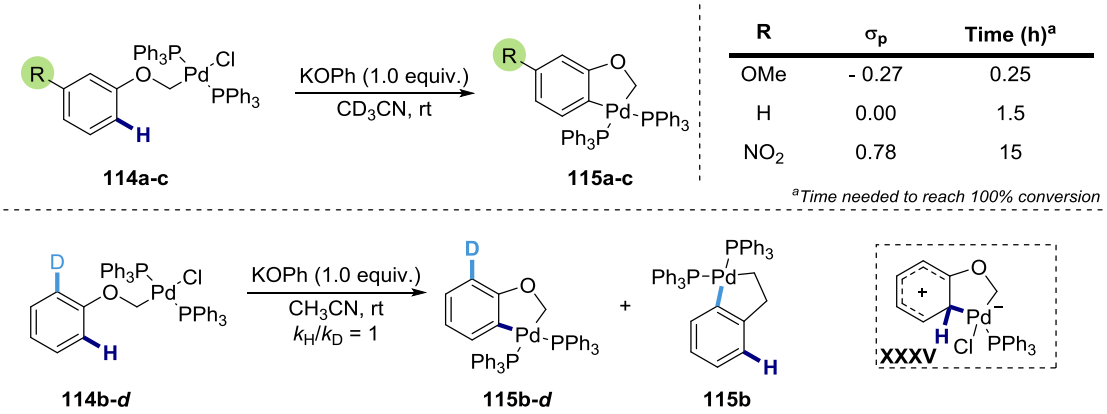

R	σ_p	Time (h)[a]
OMe	- 0.27	0.25
H	0.00	1.5
NO_2	0.78	15

[a]*Time needed to reach 100% conversion*

Figure 1.29. Mechanistic studies regarding the intramolecular C—H bond cleavage by alkylpalladium(II) complexes.

[71] Sadow, A. D.; Tilley, T. D. *J. Am. Chem. Soc.* **2003**, *125*, 7971.
[72] Catellani, M.; Chiusoli, G. P. *J. Organomet. Chem.* **1992**, *425*, 151.
[73] Hansch, C.; Leo, A.; Taft, R. W. *Chem. Rev.* **1991**, *91*, 165.
[74] Olah, G. A. *Acc. Chem. Res.* **1971**, *4*, 240.

Echavarren and co-workers employed the same approach to study the cyclopalladation step using anisole palladium(II) complex **114**.[75] They quantified the time required to reach complete conversion for substrates bearing different *para*-substituents (Figure 1.29). The observed results were similar to those obtained by Catellani and are in agreement with an electrophilic aromatic substitution pathway[74] via putative Wheland intermediate **XXXV**. Furthermore, no intramolecular kinetic isotopic effect was observed, a common feature of S_EAr,[76] reinforcing the hypothesis of an electrophilic metalation.

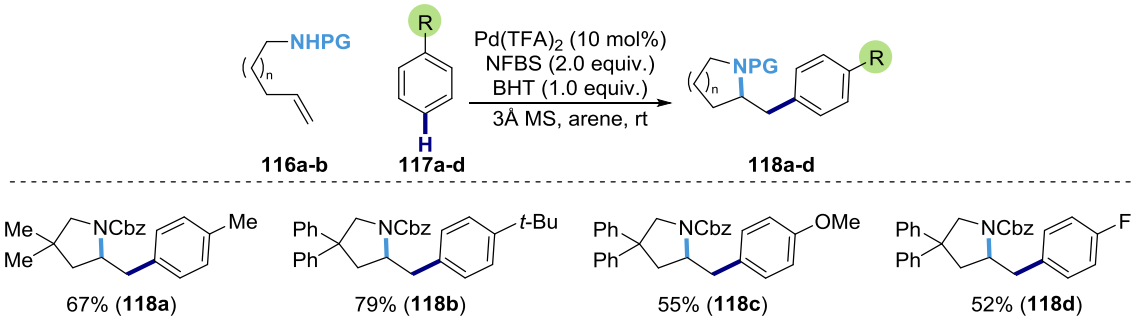

Scheme 1.23. Pd-catalyzed oxidative carboamination of alkenes via C—H bond functionalization.

Michael et al.[77] were able to perform an oxidative intramolecular amination/intermolecular arylation under palladium(II)/palladium(IV) conditions with excellent *para*-selectivity (Scheme 1.23). The authors suggested a mechanism arising from the well-known aminopalladation of alkenes. Next, the *in situ* formed alkyl palladium(II) is rapidly oxidized to palladium(IV) by NFBS. Subsequently, this highly electrophilic palladium(IV) intermediate is attacked by an electron-rich arene (**117**) following a S_EAr pathway. A final reductive elimination is responsible for delivering the product **118** along with the active catalyst. The S_EAr pathway was proposed on the basis that electron-poor arenes do not react under the reaction conditions and the observed *para*-selectivity.

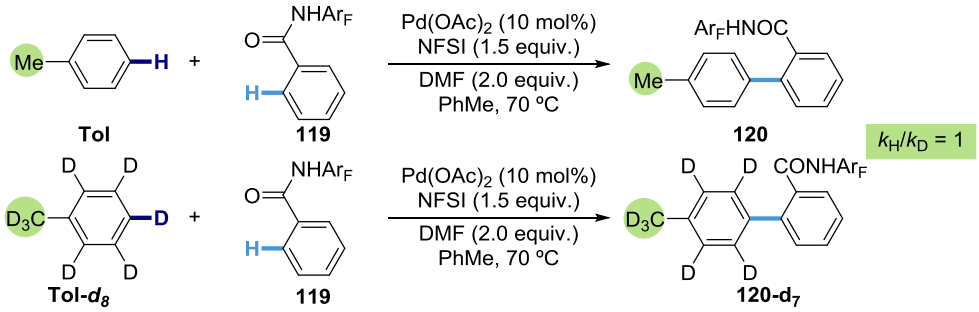

Figure 1.30. Kinetic isotopic effect on the palladium(II)-catalyzed *para*-selective C—H arylation of monosubstituted arenes.

Likewise, Yu and co-workers reported a *para*-selective oxidative arylation of arenes bearing directing groups.[78,79] Similarly to Michael's report, the arylation reaction is mediated by a

[75] Martín-Matute, B.; Mateo, C.; Cárdenas, D. J.; Echavarren, A. M. *Chem. Eur. J.* **2001**, *7*, 2341.
[76] Zollinger, H. *Adv. Phys. Org. Chem.* **1964**, *2*, 163.
[77] Rosewall, C. F.; Sibbald, P. A.; Liskin, D. V.; Michael, F. E. *J. Am. Chem. Soc.* **2009**, *131*, 9488.
[78] Wang, X.; Leow, D.; Yu, J.-Q. *J. Am. Chem. Soc.* **2011**, *133*, 13864.

highly electrophilic palladium(IV) intermediate. Next, an electrophilic arylation is suggested based on the lack of intermolecular kinetic isotopic effect when using toluene and toluene-d_8 (Figure 1.30).[76]

1.2.4.4 Concerted metalation-deprotonation (CMD)[51,80,81]

Concerted metalation-deprotonation mechanism (Figure 1.25, eq. 4) arose because some reported arylation reactions of electron-deficient substrates could not be successfully explained by most common S_EAr mechanism or others (σ-bond metathesis, oxidative addition, Heck-type palladation). Consequently, a new mechanistic scenario was necessary to explain conveniently such reactivity. C—H bond metalation under a concerted metalation-deprotonation mechanism is characterized by the presence of a bifunctional ligand bearing an additional Lewis-basic heteroatom that assists the metal in the C—H bond cleavage event.[82] The transition state for a concerted metalation-deprotonation event is characterized by the formation of agostic, three-center, two-electron interactions between the σ C—H bond and the palladium(II) atom. As a consequence of this interaction, a significant weakening of the C—H bond occurs. This weakening is somehow compensated by Pd—H and Pd—C interactions, which involve electron donation, and the simultaneous formation of the O—H bond (Figure 1.31).[83] The highly synchronous nature of the process was theoretically demonstrated by Fagnou and coworkers by DFT calculations.[84]

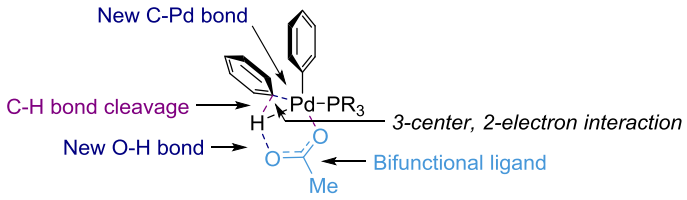

Figure 1.31. Accepted concerted metalation-deprotonation transition state

During the first studies of concerted metalation-deprotonation processes, it was not clear whether the bromide or the carbonate were acting as base (Figure 1.32). Soon, the possible role of the bromide ion (coming from the oxidative addition of palladium(0) to an Ar—Br bond) as intramolecular base (case a) was ruled out by Echavarren and Fagnou based on DFT calculations and empiric results.[52,85] Echavarren observed that the barrier for the bromide assisted deprotonation was 20 Kcal/mol higher than for the carbonate assisted process (Figure 1.32a-b).[85,85c] On the other hand, Fagnou observed a fast displacement of the bromide ligand

---

[79] For a related transformation see: Ciana, C. L.; Phipps, R. J.; Brandt, J. R.; Meyer, F.-M.; Gaunt, M. J. *Angew. Chem. Int. Ed.* **2011**, *50*, 458.

[80] (a) Lapointe, D.; Fagnou, K. *Chem. Lett.* **2010**, *39*, 1118. (b) Ackermann, L. *Chem. Rev.* **2011**, *111*, 1315. (c) Gorelsky, S. I. *Coord. Chem. Rev.* **2013**, *257*, 153. (d) Ackermann, L. *Acc. Chem. Res.* **2014**, *47*, 281.

[81] Because of its general acceptance, only CMD will be reviewed here, and no other mechanisms like ambiphilic metal-ligand activation (AMLA).

[82] Commonly, carboxylates are employed as ligands to trigger the CMD. For heteroatom-substituted secondary phosphine oxide (HASPO) ligands promoting a CMD see: Ackermann, L.; Vicente, R.; Althammer, A. *Org. Lett.* **2008**, *10*, 2299.

[83] Lafrance, M.; Gorelsky, S. I.; Fagnou, K. *J. Am. Chem. Soc.* **2007**, *129*, 14570.

[84] Gorelsky, S. I.; Lapointe, D.; Fagnou, K. *J. Org. Chem.* **2012**, *77*, 658.

[85] (a) Gorelsky, S. I.; Lapointe, D.; Fagnou, K. *J. Am. Chem. Soc.* **2008**, *130*, 10848. (b) Rousseaux, S.; Gorelsky, S. I.; Chung, B. K. W.; Fagnou, K. *J. Am. Chem. Soc.* **2010**, *132*, 10692. (c) García-Cuadrado, D.; de Mendoza, P.; Braga, A. A. C.; Maseras, F.; Echavarren, A. M. *J. Am. Chem. Soc.* **2007**, *129*, 6880.

by a carboxylate in the reaction by NMR monitoring and DFT calculations.[52,86,85b] These observations were considered sufficient to rule out a bromide-mediated deprotonation.

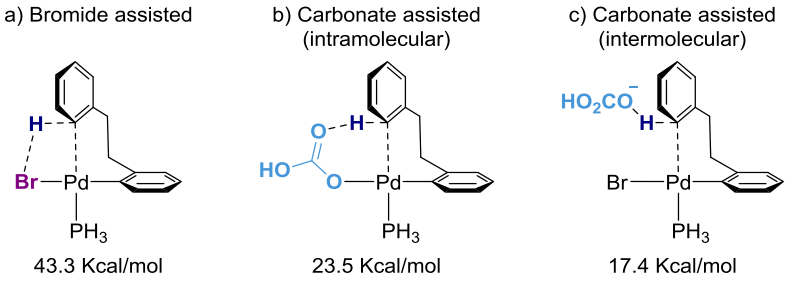

Figure 1.32. Evaluated transitions states for Echavarren and Maseras for the concerted metalation-deprotonation.[85c]

Once the role of the base was clarified, it was necessary to determine whether the deprotonation was an inner- or an outer-sphere event (cases b-c). To date, there are still discrepancies about this, as DFT studies on different systems lead to different conclusions. Echavarren and co-workers suggested an outer-sphere mechanism base on DFT calculations and experimental evidences. The empirical regioisomeric ratio was in better agreement whith DFT calculations considering an outer-sphere mechanism.[85c] Fagnou and co-workers also evaluated this possibility but they rejected it based on DFT calculations.[85a] However, in the case of using diphosphines, they could not completely rule out this possibility because of their different behavior under catalytic conditions.[87]

Based on the fact that arenes bearing electron-withdrawing groups could be arylated under these reactions conditions and in the presence of base, the acidity of the C—H bond was considered to be the determinant factor for reactivity.[52,85c] Soon, this statement was revised and clarified by Gorelsky and Fagnou. Although they agreed that Brönsted acidity could match the reactivity trend, they conclude that it was not a general influence.[85b] In order to determine the factors governing reactivity and selectivity, an activation-strain analysis was conducted.[84,85] The idea behind this analysis is quite simple: there are two main contributors to the transition state energy, an energy cost related with the distortion of the arene and the catalyst from their ground state structure to their geometry in the transition state (E_{dist}, distortion energy), and an energy gain as a consequence of the electronic interaction between the substrate and the catalyst in the transition state (E_{int}, interaction energy). See Figure 1.33.

[86] Lafrance, M.; Fagnou, K. *J. Am. Chem. Soc.* **2006**, *128*, 16496.
[87] Lafrance, M.; Lapointe, D.; Fagnou, K. *Tetrahedron*, **2008**, *64*, 6015.

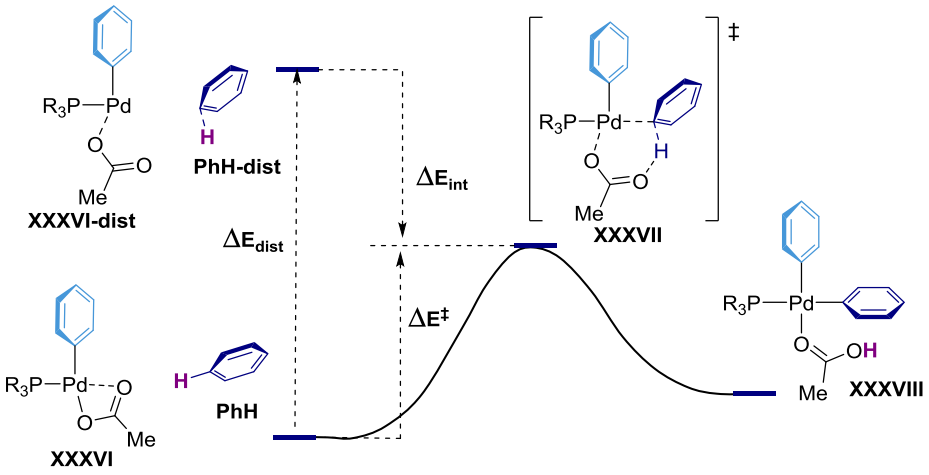

Figure 1.33. Activation-strain analysis for benzene concerted metalation-deprotonation pathway.

Depending of which one of these factors contributes the most to the regioselectivity during the C—H bond functionalization under concerted metalation-deprotonation conditions, the reactions employing (hetero)arenes can be classified in the following categories: (see Figure 1.34)

- Class I: regioselectivity is controlled by the E_{dist} of the arene. Usually, class I (hetero)arenes contain electron-withdrawing groups.
- Class II: the regioselectivity is a consequence of the E_{int}, in which the substrate catalyst interaction prevails.
- Class III: (hetero)arenes whith a concerted metalation-deprotonation event favored by a low E_{dist} and a high E_{int}.

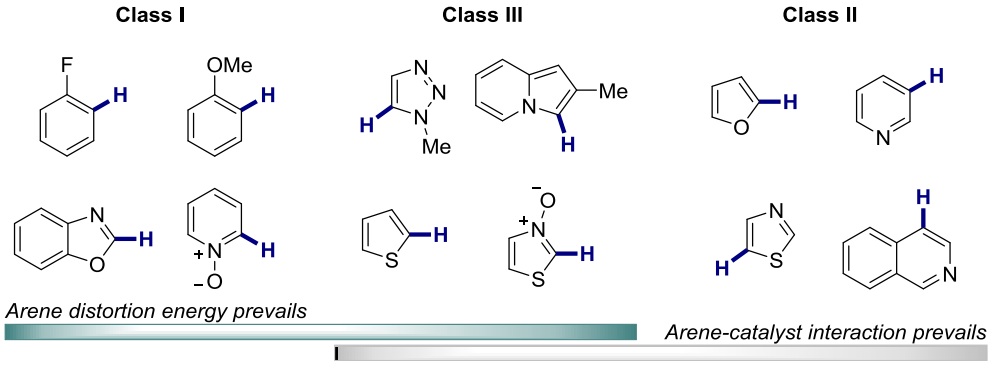

Figure 1.34: (Hetero)arene classification in terms of the governing factors determining the refioselectivity under concerted metalation-deprotonation conditions.

As the rationale behind the factors responsible of the interaction and distortion energy was not absolutely clear, DFT analysis was carried out. It was observed that the distortion energy was governed by two main factors, the energy of the out-of-plain bending and by the stretching mode of the C—H bond. It was observed that the out-of-plain bending was nearly a constant value and therefore its influence was minimum, being the stretching mode the main

factor influencing the distortion energy. Finally, it was observed that the stretching of the C—H bond is related to the acidity of the bond. On the other hand, the interaction energy has also two main features, the M—C and the O—H interaction. Concerning the M—C interaction, Fagnou and Gorelsky successfully related it to the nucleophilicity of the arene. Taken together, the regioselectivity of the C—H bond cleavage is not only explained by the nucleophilicity of the arene but also by the acidity of the C—H bond. Although the out-of-plain bending plays an important role, its value is almost constant in all the (hetero)arene spectra and therefore cannot be considered as determinant for the regioselectivity (Figure 1.35).[84]

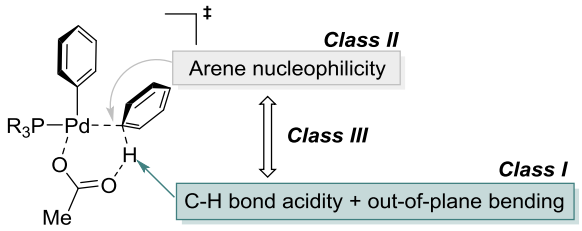

Figure 1.35. Schematic representation of the main factors controlling regioselectivity under concerted metalation-deprotonation conditions.

A breakthrough on concerted metalation-deprotonation implementation was performed by Lafrance and Fagnou when pivalic acid was used, for the first time,[83] as additive in the reaction, improving the reaction outcome considerably. They observed that most common bases used in transformations following a concerted metalation-deprotonation mechanism were barely soluble in the reaction solvent. Accordingly, the effective amount of base in the reaction media was low, which could result in bad reaction performance. Therefore, Lafrance and Fagnou envisioned that adding carboxylic acids to the reaction media lead to the in situ formation of a soluble base that would enhance the reactivity. Importantly, it was observed that the base was not only responsible for the formation of the pivalate anion. As shown in Scheme 1.36, when only base was added, the reaction yield was very low (entry 1). Likewise, cesium pivalate worked poorly, which was completely unexpected (entry 2). In contrast, the combination of base and pivalic acid resulted fundamental, obtaining 97% yield of the isolated product.

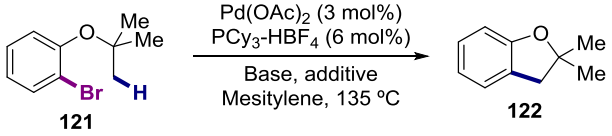

Entry	Base	Additive	Yield (%)
1	Cs_2CO_3	none	15
2	CsOPiv	none	14
3	Cs_2CO_3	PivOH (30 mol%)	97

Scheme 1.36. Pd-catalyzed intramolecular alkane arylation. Pivalic acid influence.

In light of these results, experimental as well as DFT studies were conducted in order to cast some light on the role of pivalic acid during the reaction.[85c] It was found that pivalic acid improves the reaction outcome because of several factors (Figure 1.37):

1. The higher solubility of the pivalate anion as compared to carbonate, which increases the base molarity in the reaction.
2. Its basicity, sufficient to assist the palladium(II) during the metalation event by binding the proton.
3. Its ability to displace the halide in the oxidative addition palladium(II) complex.
4. Its steric bulkiness makes it a labile ligand when κ^2-coordination is not possible.

5. Its denticity, which will affect the reaction in different factors. First, once the bromide is replaced by the pivalate (**XL**), the pivalate will adopt a κ^2-coordination removing a phosphine from the coordination sphere of the metal (**XLI**). This is of great importance, since it has been observed that the concerted metalation-deprotonation event is favored by the monophosphine complex. Additionally, this κ^2-coordination will prevent catalyst poisoning by excess of ligand, as the κ^2-pivalate coordination is more favored than the introduction of a new phosphine. Third, because of the presence of two coordinating sites, the pivalate will be able to interact with the proton of the substrate and the metal catalyst at the same time during the metalation process.[88,89]
6. It has also been demonstrated by DFT calculations that the concerted metalation-deprotonation transition state is more favorable (by a difference of 1.3 kcal/mol) for the pivalate than for the carbonate.

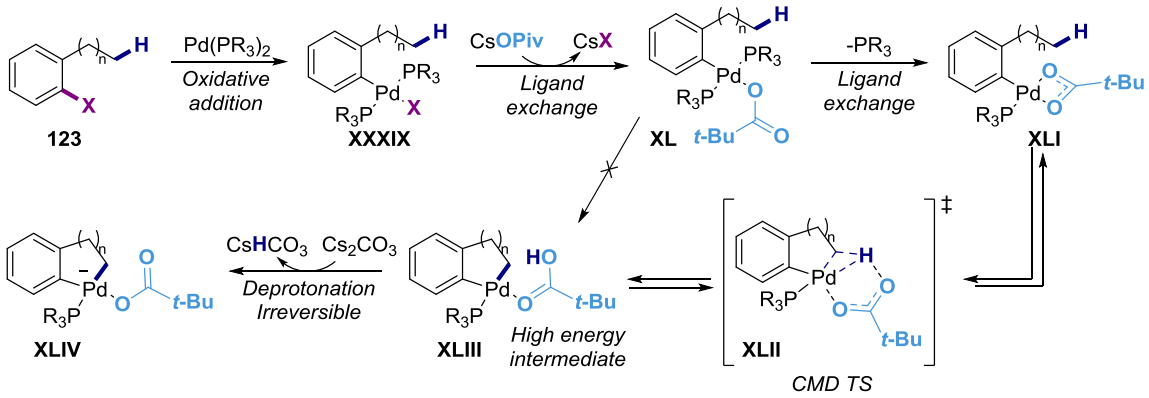

Figure 1.37. Pivalate role during the concerted metalation-deprotonation.

On the other hand, the insoluble base plays two important roles. The first and more obvious, is to deprotonate the pivalic acid generating the pivalate anion. The second one, and of great importance, is to act as a proton sink. It has been observed that after the concerted metalation-deprotonation occurs, the pivalic acid remains attached to the palladium complex intermediate (**XLIII**), hence establishing an equilibrium with **XLII**. However, if there is a base able to deprotonate the coordinated pivalic acid, the corresponding pivalate intermediate **XLIV** will be much more stable reducing the reversibility of the event. Thus, the insoluble base is of great importance for driving the reaction forward.

In a catalytic cycle, all these factors will play in concert: after oxidative addition (**XXXIX**), the halide attached to the palladium(II) will be easily exchanged by an entering pivalate anion (**XL**). Because of its denticity, the pivalate will be able to displace a phosphine ligand from the palladium inner-sphere forming a κ^2-OPiv (**XLI**). In the presence of an excess of phosphine, the

[88] Under iridium-catalysis conditions, no ligand dissociation takes place due to its high coordination number. Additionally, the carboxylate does not need to go through κ^1-coordination to effect the metalation, as there is already a vacant position on the metal center to allow the agostic interaction with the arene. For further details about concerted metalation-deprotonation under iridum-catalysis see: García-Melchor, M.; Gorelsky, S. I.; Woo, T. K. *Chem. Eur. J.* **2011**, *17*, 13847.
[89] For mechanistic studies suggesting a ligand free concerted metalation-deprotonation see: Tan, Y.; Harwig, J. F. *J. Am. Chem .Soc.* **2011**, *133*, 3308.

pivalate will be able to avoid catalyst poisoning because of this κ^2-coordination.[90] Once **XLI** is formed, the electrophilic palladium(II) will form an agostic interaction with the C—H bond, thus weakening this bond due to a charge transfer from the C—H bond to the palladium center. At the same time, one of the oxygens from the pivalate will coordinate to the hydrogen atom (**XLII**). This transition state has been demonstrated to be 1.2 Kcal/mol more stable for pivalate than for carbonate. After the metalation of the substrate (**XLIII**), the pivalic acid molecule will remain coordinated to the palladium(II). This intermediate is high in energy and could potentially reverse the reaction. At this stage, the inorganic base partakes by deprotonating the pivalic acid, thus forming intermediate **XLIV** that is considerably more stable. Although the authors suggested the carbonate to be the base responsible of this deprotonation, this deprotonation could be performed by a non-coordinated pivalate molecule (note that the coordinate pivalic acid will have a lower pK_a) forming free pivalic acid that will be subsequently deprotonated by the poorly soluble carbonate.

[90] No direct metalation from complex **XL** was found by DFT analysis.

1.3. Objectives

We decided to focus our doctoral studies on the development of new methodologies based on the functionalization of C—H bonds. The following objectives were established:

1. To study C—H bond-functionalization events of non-activated C(sp^3)—H bonds and aldehydic C(sp^2)—H bonds
2. To target the synthesis of elusive, organic backbones via C—H bond-functionalization, thus improving existing methodologies for similar means.
3. To explore the utility of other coupling partners in C—H bond-functionalization methodologies.
4. To use C—H bond-functionalization for the synthesis of quaternary carbons, a transformation that has little precendents in the literature.
5. To study the mechanism of new bond-disconnections prepared via C—H bond-functionalization, thus opening up new perspectives to be implemented in near future.

Chapter 2. Pd-catalyzed C(sp^3)—H Functionalization/Carbenoid Insertion: Quaternary Carbon Centers via Multiple C–C Bond-Formation.

2.1 Non-activated C(sp^3)—H bond: Challenges

As shown in Chapter 1, reactivity in C—H functionalization is dramatically enhanced when an interaction between the metal catalyst and the substrate is induced (i.e. directing groups, π-coordination, prior metalation). This explains the rapid functionalization of arenes and the difficult functionalization of alkanes. Alkanes are poor donors and poor acceptors of electron density. Furthermore, the C(sp^3)—H bond is, usually, non-polar and strong (see Table 1.1). From a molecular orbital perspective, the HOMO σ is low-lying, and, therefore, non-suitable for electron donation. On the other hand, the LUMO σ* is high in energy, therefore, it can hardly accept electron density. Taking into consideration all these factors, the poor coordination of alkanes to the metal catalyst makes particularly difficult to effect a C(sp^3)—H bond functionalization.[91,92]

2.2 Functionalizing non-active C(sp^3)—H bonds[16e,93]

Unquestionably, the lower bond dissociation energy for allylic, benzylic and cyclopropyl C(sp^3)—H bonds make them particularly suitable for C(sp^3)—H bond-functionalization. In the case of allylic C—H bonds,[94] the metalation is easier thanks to the presence of the adjacent olefin, which formally acts as a directing group. Importantly, the presence of an unsaturation allows the formation of a rather stable π-allyl intermediate. As for benzylic C(sp^3)—H bonds, the same principles apply; however, the loss of aromaticity forming the η^3-complex makes the reaction less favorable. As for cyclopropyl C(sp^3)—H bonds, the high reactivity is associated to the ring strain and special rehybridization on the cyclopropyl backbone (see Section 1.2.2.2). Figure 2.1 illustrates examples of functionalization of such type of C—H bonds (substrates **124a-d** and **124l**).

[91] In this manuscript, the terms "non-activated", "unactivated", "inert" and related terms associated with C(sp^3)—H bonds will refer to C(sp^3)—H bonds close to pKa ≥ 30. Therefore, C(sp^3)—H adjacent to electron-withdrawing groups will be not considered.

[92] For a review dealing with the functionalization of activated C(sp^3)—H bonds see: (a) Bellina, F.; Rossi, R. *Chem. Rev.* **2010**¸ *110*,1082. (b) Culkin, D. A.; Hartwig, J. F. *Acc. Chem. Res.* **2003**, *36*, 234. (c) Johansson, C. C. C.; Colacot, T. J. *Angew. Chem. Int. Ed.* **2010**, *49*, 676.

[93] (a) Jazzar, R.; Hitce, J.; Renaudat, A.; Sofack-Kreutzer, J.; Baudoin, O. *Chem. Eur. J.* **2010**, *16*, 2654. (b) Baudoin, O. *Chem. Soc. Rev.* **2011**, *40*, 4902. (c) Qiu, G.; Wu, J. *Org. Chem. Front.* **2015**, *2*, 169. (d) Li, H.; Li, B-J.; Shi, Z.-J. *Catal. Sci. Technol.* **2011**, *1*, 191.

[94] Liron, F.; Oble, J.; Lorion, M. M.; Poli, G. *Eur. J. Org. Chem.* **2014**, *27*, 5863.

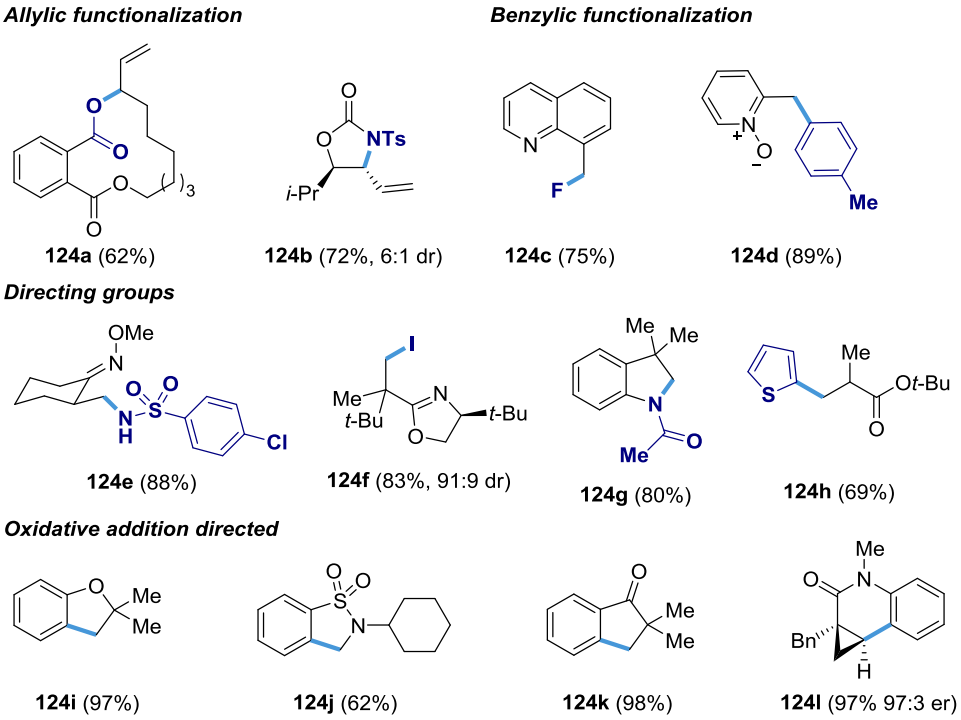

Figure 2.1. Different strategies for the palladium-catalyzed functionalization of inert C(sp^3)—H bonds.[95]

In share contrast, unactivated C(sp^3)—H bonds typically require metalation of the substrate. Amongst different strategies, the use of directing groups (**124e-h**) or oxidative addition directed strategies (**124i-l**) have been particularly effective.

2.3 Functionalization of inert C(sp^3)—H bonds for the synthesis of quaternary carbons

Despite the advances realized in C(sp^3)—H bond-functionalization, this field has virtually not include the synthesis of quaternary centers.

First of all, clarifying the definition of quaternary center is essential, as this term has been indistinctly employed in the literature. A quaternary center is a tetrasubstituted carbon where all the substituents are carbons.[96] It is also known as all-carbon quaternary carbon center, although this last terminology is redundant. If any of these substituents is a heteroatom, the term should be better called tetrasubstituted carbon (see Figure 2.2).

[95] Allylic functionalization: (a) Fraunhoffer, K. J.; Prabagaran, N.; Sirois, L. E.; White, M. C. *J. Am. Chem. Soc.* **2006**, *128*, 9032. (b) Rice, G. T.; White, M. C. *J. Am. Chem. Soc.* **2009**, *131*, 11707. Benzyl functionalization: (c) Hull, K. L.; Anani, W. Q.; Sanford, M. S. *J. Am. Chem. Soc.* **2006**, *128*, 7134. (d) Campeau, L.-C.; Schipper, D. J.; Fagnou, K. *J. Am. Chem. Soc.* **2008**, *130*, 3266. Directing groups: (e) Thu, H.-Y.; Yu, W.-Y.; Che, C.-M. *J. Am. Chem. Soc.* **2006**, *128*, 9048. (f) Giri, R.; Lan, Y.; Liu, P.; Houk, K. N.; Yu, J.-Q. *J. Am. Chem. Soc.* **2012**, *134*, 14118. (g) Neumann, J. J.; Rakshit, S.; Dröge, T.; Glorius, F. *Angew. Chem. Int. Ed.* **2009**, *48*, 6892. (h) Renaudat, A. R.; Jean-Gérard, L.; Jazzar, R.; Kefalidis, C. E.; Clot, E.; Baudoin, O. *Angew. Chem. Int. Ed.* **2010**, *49*, 7261. Oxidative addition: (i) See ref. 84. (j) See ref. 86b (k) Rousseaux, S.; Davi, M.; Sofack-Kreutzer, J.; Pierre, C.; Kefalidis, C. E.; Clot, E.; Fagnou, K.; Baudoin, O. *J. Am. Chem. Soc.* **2010**, *132*, 10706.

[96] Quasdorf, K. W.; Overman, L. E. *Nature* **2014**, *516*, 181.

There are two main approaches towards the synthesis of quaternary carbons by means of C(sp^3)—H functionalization. In the first approach (Figure 2.2, path a), the carbon coming from the C(sp^3)—H bond becomes quaternary. In the second approach, however, the carbon coming from the C(sp^3)—H bond is a substituent of the quaternary center. In the former, a tertiary carbon is functionalized; in the latter, a primary or secondary C(sp^3)—H bond is utilized.

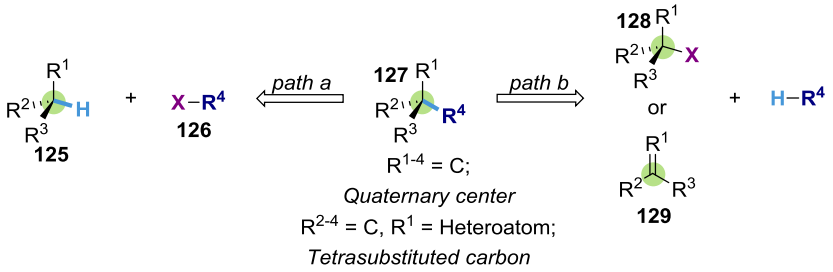

Figure 2.2. Functionalization of inert C(sp^3)—H bonds for the synthesis of quaternary carbons.

A close inspection into the literature reveals only ten examples for the synthesis of quaternary centers by means of C(sp^3)—H bond functionalization.[97] While nine of these are based on the functionalization of a methine motif (Figure 2.2, path a), only one example use a functionalized carbon to prepare a quaternary center (path b). As for the reports on methine functionalization, the substrate is rather biased and activated. For example, substrate **130**[98] is not formed via direct functionalization of the C(sp^3)—H bond, but by a Heck-type mechanism (see Figure 2.3)[99] Substrates **132-135** are formed by intramolecular arylation of the activated cyclopropyl C(sp^3)—H bond,[57,100] and **136** by an intermolecular arylation of the cyclopropyl motif using 8-aminoquinoline as bidentate directing group.[101] The authors rationalized the activation of the methine bond over the methylene of the cyclopropyl motif via the formation of a six-membered palladacycle over a seven-membered ring formation. In the intermolecular arylation, the same rationale was applied in which the [5,8]-bicyclic system was preferentially formed over the [6,9]-bicyclic system.

[97] It must be noticed that the following criteria was followed: it has to be the functionalization (from an organometallic standpoint) of a non-activated C(sp^3)—H bond for the synthesis of a quaternary center, not a tetrasubstituted carbon.
[98] Zuber, R.; Carlens, G.; Haag, R.; de Meijere, A. *Synlett*, **1996**, *6*, 542.
[99] For the preparation of substrate 19: Khusnutdinov, R. I.; Schadneva, N. A.; Malikov, A. I.; Dzhemilev, U. M. *Petroleum Chem.* **2006**, *46*, 159.
[100] (a) Ladd, C. L.; Roman, D. S.; Charette, A. B. *Org. Lett.* **2013**, *15*, 1350 (b) Saget, T.; Perez, D.; Cramer, N. *Org. Lett.* **2013**, *15*¸1354. (c) Ladd, C. L.; Roman, D. S.; Charette, A. B. *Tetrahedron*, **2013**, *69*, 4479 (d) Pedroni, J.; Saget, T.; Donets, P. A.; Cramer, N. *Chem. Sci.* **2015**, *6*, 5164. (e) Tsukano, C.; Okuno, M.; Takemoto, Y. *Chem. Lett.* **2013**, *42*, 753. For isolated examples formed unexpectedly see: (f) Saget, T.; Cramer, N. *Angew. Chem. Int. Ed.* **2012**, *51*, 12842. (g) Janody, S.; Jazzar, R.; Comte, A.; Holstein, P. M.; Vors, J-P.; Ford, M. J.; Baudoin, O. *Chem. Eur. J.* **2014**¸ *20*, 11084
[101] Hoshiya, N.; Kobayashi, T.; Arisawa, M.; Shuto, S. *Org. Lett.* **2013**, *15*, 6202.

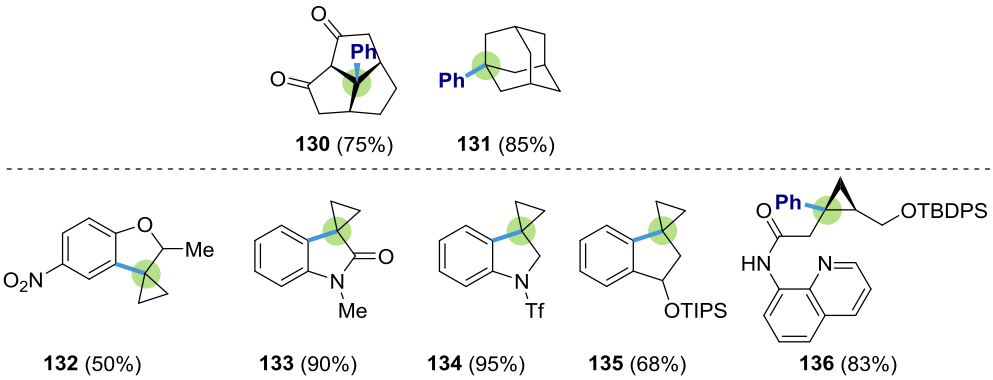

Figure 2.3. Synthesis of quaternary center via methyne functionalization

Noteworthy, Takemoto and collaborators[100e] attempted the cyclization of cyclobutyl and cyclopentyl groups (**137b**) but no product was observed, thus illustrating the higher reactivity of cyclopropyl C(sp^3)—H bonds (Figure 2.4).

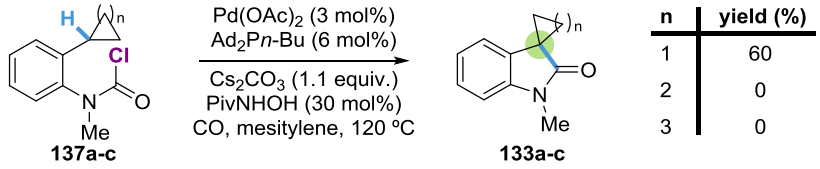

n	yield (%)
1	60
2	0
3	0

Figure 2.4 Synthesis of spirooxindoles from carbamoyl chlorides via methine C(sp^3)—H functionalization.

Early this year, Zhu and Zhou reported the synthesis of quaternary centers by dual C(sp^3)—H/ C(sp^2)—H functionalization,[102] representing the first and only report where a quaternary center was prepared following the strategy showed in Figure 2.2, path b. However, it must be noticed that this reaction is based on an activated C(sp^3)—H bond due to the presence of an α-nitrogen. Mechanistic studies conducted by the authors presented two possible mechanisms; one involving a C(sp^3)—H bond functionalization, and the other one considering the formation of a reactive iminium intermediate (Scheme 2.1).

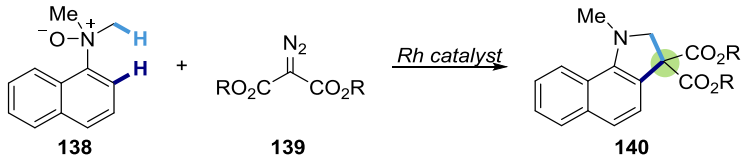

Scheme 2.1. Rhodium(III)-catalyzed regioselective annulation reaction of 1-naphthylamine *N*-oxides with diazo compounds.

2.4 Developing a new strategy for the synthesis of quaternary carbons by means of C(sp^3)—H bond functionalization.

In light of the presented results, we envisioned that a novel approach towards the synthesis of quaternary centers via inert C(sp^3)—H bond functionalization would have a great impact at the scientific community. Among the different strategies, we decided not to use an approach based on activated C(sp^3)—H bonds or directing groups. Consequently, we decided to use a

[102] Zhou, B.; Chen, Z.; Yang, Y.; Ai, W.; Tang, H.; Wu, Y.; Zhu, W.; Li, Y. *Angew. Chem. Int. Ed.* **2015**, *54*, 12121.

system triggered by an initial metalation step consisting of an oxidative addition of the metal into a C—Br bond followed by an unactivated C(sp^3)—H bond-functionalization. The presence of the C—Br bond will play a dual role, both directing the C(sp^3)—H functionalization as well as providing a redox manifold to re-oxidize the catalyst, thus avoiding the use of oxidants. Indeed, this strategy has been successfully employed in several transformations involving the use of C(sp^3)—H bonds (Figure 2.4), but none of them for preparing quaternary carbon centers.

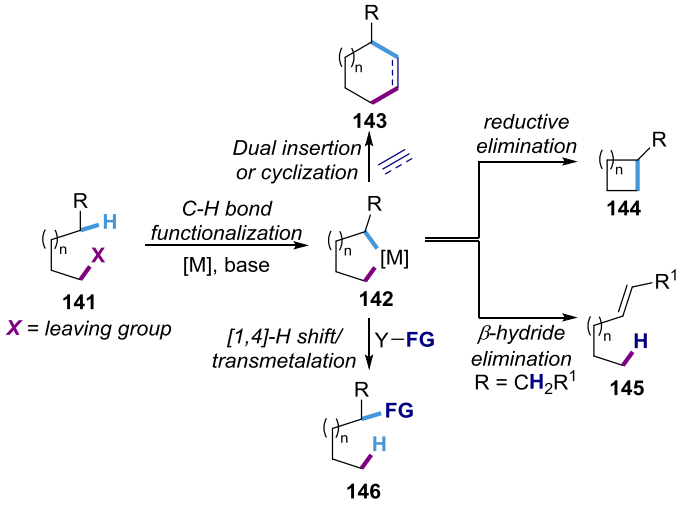

Figure 2.4 Oxidative addition directed functionalization/derivatization.

Upon metalation, four different type of reactions have been reported via **142**:

1. *Dual insertion or cyclization:* these reactions are based on the insertion of a π-system from **142** leading to cyclic systems via migratory insertion/reductive elimination. To date, there are no catalytic examples for such transformations, and only stoichiometric reactions can be find in the literature. As pictured in Figure 2.5, different products can be achieved by a dual C(sp^2)/C(sp^3) insertion reaction. For example, 1,2-dihydronaphthalenes **147b** could be prepared by addition of alkynes.[103,104] When unsymmetrical alkynes were employed, regioselectivity issues came into play. Likewise, related benzyne can be employed obtaining biphenyl structures (**147a**). Noteworthy, carbon disulfide was employed for the synthesis of dithiolactones **147c**,[105] however, the related carbon dioxide could not be used for the synthesis of lactones because of the challenging reductive elimination. Nevertheless, its combination with carbon monoxide produced cyclic anhydrides (**147e**).[106,103b] Similarly, addition of formaldehyde (either aqueous or the polymer form) was combined with carbon monoxide for the synthesis of lactones **147d** as no reductive elimination after formaldehyde insertion could be achieved.[106,103b]

[103] (a) Campora, J.; Llebaria, A.; Moreto, J. M.; Poveda, M. L.; Carmona, E. *Organometallics* **1993**, *12*, 4032. (b) Carmona, E.; Gutierrez-Puebla, E.; Marin, J. M.; Monge, A.; Paneque, M.; Poveda, M. L.; Ruiz, C. *J. Am. Chem. Soc.* **1989**, *111*, 2883.
[104] For an example with the corresponding palladacycle see: Cámpora, J.; López, J. A.; Palma, P.; del Rio, D.; Carmona, E. *Inorg. Chem.* **2001**, *40*, 4116.
[105] (a) Cámpora, J.; Carmona, E.; Gutiérrez-Puebla, E.; Poveda, M. L.; Ruíz, C. *Organometallics* **1988**, *7*, 2577. (b) Cámpora, J.; Gutiérrez, E.; Monge, A.; Palma, P.; Povedam, L.; Ruíz, C.; Carmona, E. *Organometallics* **1994**, *13*, 1728.
[106] Carmona, e.; Palma, P.; Paneque, M.; Poveda, M. L.; Gutierrez-Puebla, E.; Monge, A. *J. Am. Chem. Soc.* **1986**, *108*, 6424.

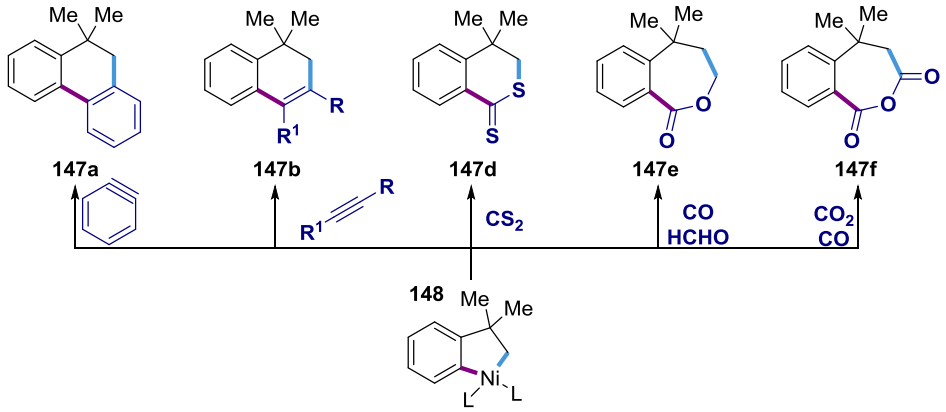

Figure 2.5. Representative examples of stoichiometric insertion reactions of C(sp^3)-nickelacycles.

Cyclization reactions involving the construction of polycyclic structures have also been reported without dealing with migratory insertion event. Dyker[107] pioneered this field based on a Pd(0)/Pd(II)/Pd(IV) catalytic cycle. For example, Dyker found the trimerization of iodoanisole (**149**)[108] by means of oxidative addition/C(sp^3)—H bond functionalization (Figure 2.6). A related reactivity was observed for the dimerization of 2-iodo-*tert*-butylbenzene (**151**).[109] The reaction was initiated by oxidative addition on the C—I bond forming the aryl palladium(II) intermediate **XLVI**. Next, cleavage of the C(sp^3)—H bond occured forming palladacycle **XLVII**. At this stage, two pathways were possible, reductive elimination to form **153** or oxidation by another molecule of **151** leading to a palladium(IV) complex (**XLVIII**). The latter was favored since **153** was never observed. After biaryl formation via reductive elimination, alkyl palladium(II) compound **XLIX** is formed. Intermediate **XLIX** reacted intramolecularly to cleave the closest C(sp^2)—H bond, forming **L** which yielded the final product after reductive elimination. The authors postulated that the presence of the sterically demanding aryl substituent in intermediate **L** facilitated the reductive elimination (in contrast with the formation of **153** from **XLVII**).

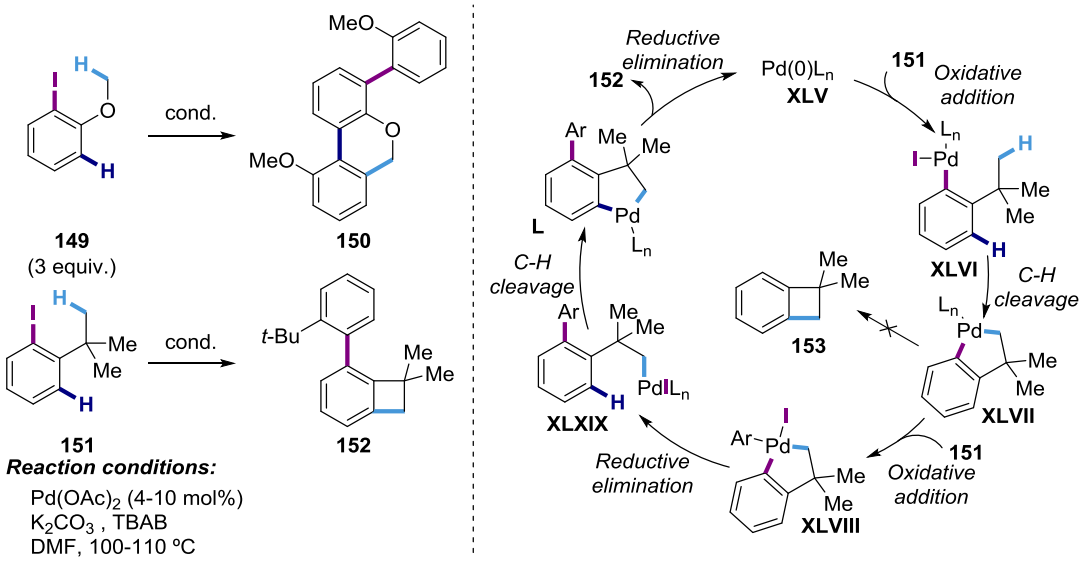

[107] Dyker, G. *J. Org. Chem.* **1993**, *58*, 6426.
[108] (a) Dyker, G. *Angew. Chem. Int. Ed.* **1992**, *31*, 1023. (b) Dyker, G. *Chem. Ber.* **1994**, *127*, 739.
[109] Dyker, G. *Angew. Chem. Int. Ed.* **1994**, *33*, 103.

Figure 2.6. Oxidative addition-directed C(sp^3)—H bond functionalization.

2. *Reductive elimination:* This second strategy consists of the synthesis of cyclic compounds via the formation of metalacycle **142** followed by a reductive elimination step (some examples have already been illustrated in Figures 2.1 and 2.3). This area was pioneered by Lafrance and Fagnou[83] for the synthesis of chromanes. Prompted by these precedents, Baudoin and coworkers were able to synthesize benzocyclobutane **153** from 2-bromo-*tert*-butylbenzene (**154a**).[110] The reaction follows a similar mechanistic pathway to that depicted in Figure 2.6, but reductive elimination from **XLVII** occurs instead of oxidative addition. The switched reactivity observed in this case is probably due to the utilization of bulky tri-*tert*-butylphosphine as ligand, which facilitates the reductive elimination event by increasing the interaction between the aryl and the alkyl ligands.

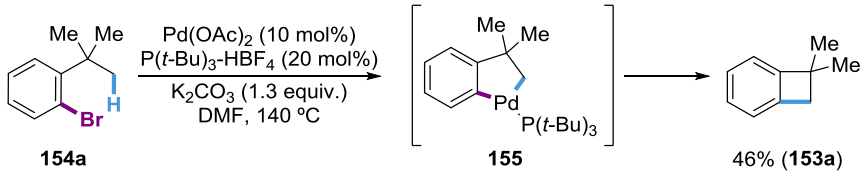

154a **155** 46% (**153a**)

Scheme 2.2. Synthesis of benzocyclobutenes by palladium-catalyzed C(sp^3)—H bond functionalization.

Subsequently, Baudoin and coworkers succeeded to expand the scope of this transformation to (hetero)aryl chlorides[111] and vinyl bromides[112] for the synthesis of bicyclic systems, achieving in some cases high diastereoisomeric ratios[113] (see Figure 2.3).

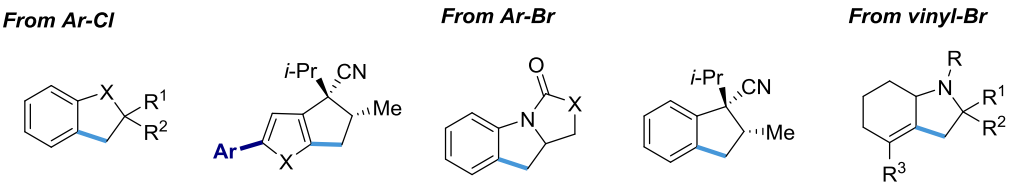

156 X = no atom, NR, O, CR_2, CO

157 X = O, S

158 X = CH_2, O, NBn

159

160

Figure 2.3. Synthesis of different bicyclic cores by means of oxidative addition-directed C(sp^3)—H bond functionalization.

In recent years, C(sp^3)—H functionalization strategies not based on the utilization of aryl halides have been reported, such as the cleavage of Si—H bonds[114] or the use of acid chlorides as substrates[115] (Scheme 2.3).

---

[110] Chaumontet, M.; Piccardi, R.; Audic, N.; Hitce, J.; Peglion, J-L.; Clot, E.; Baudoin, O. *J. Am. Chem. Soc.* **2008**, *130*, 15157.

[111] Rousseaux, S.; Davi, M.; Sofack-Kreutzer, J.; Pierre, C.; Kefalidis, C. E. ; Clot, K. ; Baudoin, O. *J. Am. Chem. Soc.* **2010**, *132*, 10706.

[112] Sofack-Kreutzer, J.; Martin, N.; Renaudat, A.; Jazzar, R.; Baudoin, O. *Angew. Chem. Int. Ed.* **2012**, *51*, 10399.

[113] (a) Martin, N.; Pierre, C.; Davi, M.; Jazzar, R.; Baudoin, O. *Chem. Eur. J.* **2012**, *18*, 4480. (b) Pierre, C. ; Baudoin, O. *Tetrahedron* **2013**, 4473. (c) Janody, S. ; Jazzar, R. ; Comte, A. ; Holstein, P. M. ; Vors, J.-P.; Ford, M. J.; Baudoin, O. *Chem. Eur. J.* **2014**, *20*, 11084.

[114] Kuninobu, Y.; Nakahara, T.; Takeshima, H.; Takai, K. *Org. Lett.* **2013**, *15*, 426.

[115] (a) Tsukano, C.; Okuno, M. Takemoto, Y. *Angew. Chem. Int. Ed.* **2012**, *51*, 2763. (b) Zhang, Q.; Yu, H.-Z.; Fu, Y. *Organometallics* **2013**, *32*, 4165. See also ref. 100e

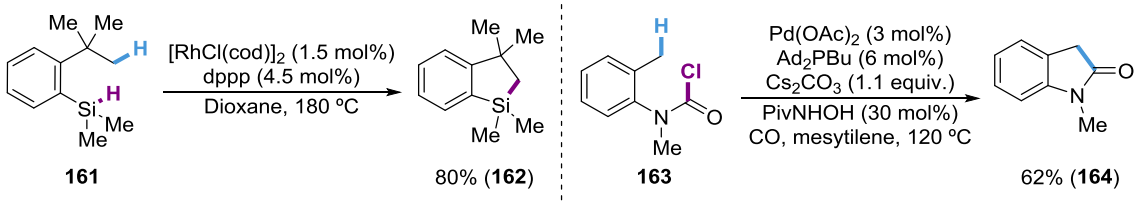

Scheme 2.3. Achieving C(sp^3)—H bond functionalization beyond arylhalides.

3. *β-Hydride elimination:* An alternative reactivity from *in situ* generated **142** would be the ability to promote β-hydride elimination to form an alkene with concomitant reduction of the arylhalide. This methodology has been successfully applied for the synthesis of natural products such as Verapamil[116] and Combretastatin A-4 analogues.[117] Additionally, the in situ formed alkene has been employed in two tandem intramolecular/intermolecular Heck reactions (Figure 2.4, eq. 2).

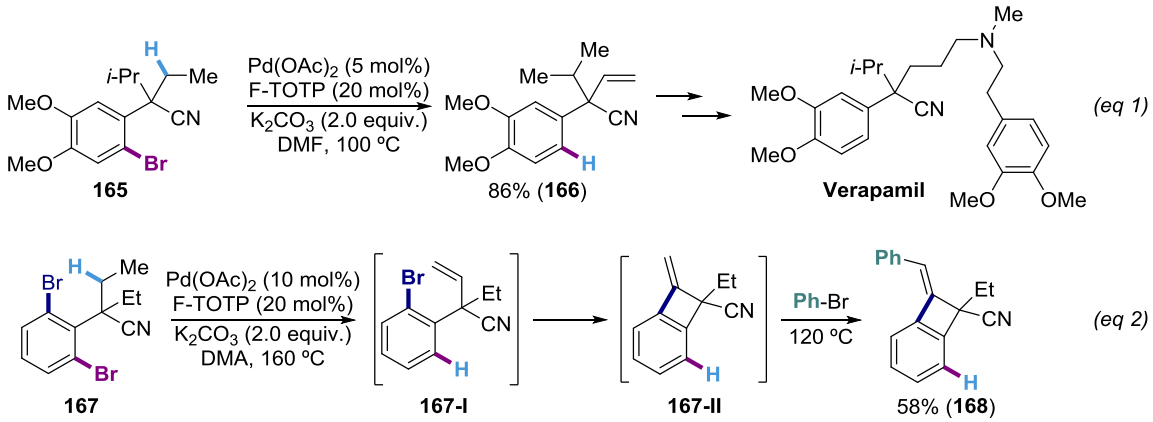

Figure 2.4. Synthesis of alkenes via β-hydride elimination from functionalized C(sp^3)—H bonds

These achievements are highly interesting as it has been previously demonstrated[83] that the functionalization of secondary C(sp^3)—H bond is a high energy process. Related to the previous works, Motti and Catellani developed a synthesis of styrene derivatives from *o*-alkylated iodoarenes.[118]

4. *[1,4]-palladium shift/transmetallation:* The corresponding metallacycles obtained from metalation formed by oxidative addition/C(sp^3)—H bond-functionalization have also been employed in subsequent cross-coupling reactions. The idea was used by Buchwald and others[119] to functionalized C(sp^3)—H bonds. While originally designed fro promoting bond-formation at the aromatic motif, it was found that **XLVIIa** was generated upon [1,4]-palladium shift, followed by transmetalation and a final reductive elimination to form **170**.

[116] Hitce, J.; Retailleau, P.;Baudoin, O. *Chem. Eur. J.* **2007**, *13*, 792.
[117] Hitce, J.; Baudoin, O. *Adv. Synth. Catal.* **2007**, *349*, 2054.
[118] Motti, E.; Catellani, M. *Adv. Synth. Catal*. **2008**, *350*, 565.
[119] (a) Barder, T. E.; Walker, S. D.; Martinelli, J. R.; Buchwald, S. *J. Am. Chem. Soc.,* **2005**, *127*, 4685. (b) Pan, J.; Su, M.; Buchwald, S. *Angew. Chem. Int. Ed*. **2011**, *50*, 8647. (c) Hoshi, T.; Honma, T.; Mori, A.; Konishi, M.; Sato, T.; Hagiwara, H.; Suzuki, T. *J. Org. Chem.*, **2013**, *78*, 11513. (d) Rahimi, A.; Pápai, I.; Madarász, Á.; Gjikaj, M.; Namyslo, J. C.; Schmidt, A. *Eur. J. Org. Chem*. **2012**, 754.

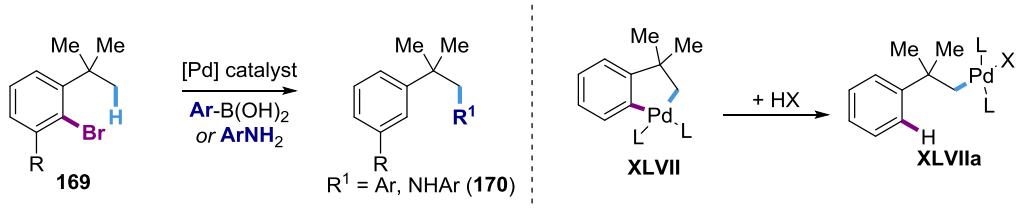

Figure 2.5. Palladium-catalyzed Intermolecular arylation/amination of unactivated C(sp^3)—H bonds.

In view of the versatility shown by the *in situ* generation of metallacycles **XLVII**, we envisioned that we could employed this strategy for installing a quaternary carbon center (Figure 2.6).

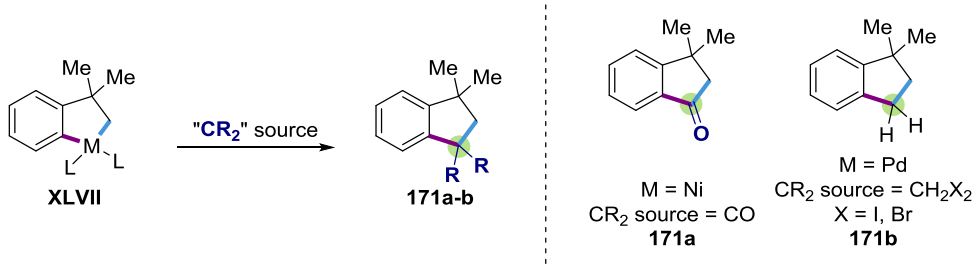

Figure 2.6. Examples of dual insertion of carbon sources into metalacycle **XLVII**.

It is worth noting that such strategy is somewhat reminiscent from the insertion of carbon atoms such as CO or CH_2X_2 into **XLVII**, but in a stoichiometric fashion.[106,103b] The mechanism of the former reaction is well known. It is initiated by coordination of carbon monoxide to the nickelacycle (**LIV**), followed by migratory insertion into the aryl—Ni bond. Finally, acyl nickel(II) complex **LV** renders the final product after reductive elimination (Figure 2.7). In the second case, dihalomethane is employed for the synthesis of indane **171b**.[120] Although two mechanisms were proposed, the authors considered an option consisting of an oxidative addition of the dihalomethane (**LI**), α-elimination forming a palladium carbenoid (**LII**), migratory insertion and a final reductive elimination.

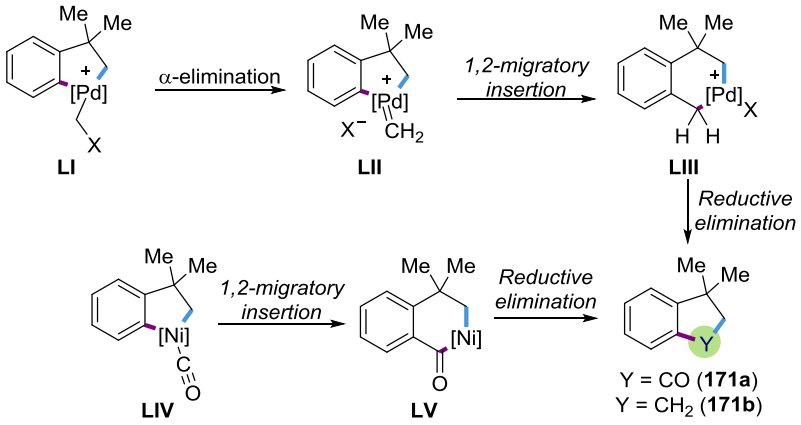

Figure 2.7. Mechanistic proposal for the stoichiometric synthesis of **171a-b**.

2.5 Cross-coupling reactions involving the intermediacy of metal-carbenoids.

[120] Cámpora, J.; Palma, P.; del Río, D.; López, J. A.; Valerga, P. *Chem. Commun.* **2004**, 1490.

Prompted by the mechanistic interpretations of Figure 2.7, we envisioned to generate a palladium-carbenoid bearing two substituents, which could potentially form a quaternary center by means of oxidative addition-directed C(sp^3)—H bond functionalization. Among all the different possibilities to produce a metal-carbenoid, we chose the decomposition of diazo-compounds **175** for two main reasons: atom-economy and availability (Figure 2.8).

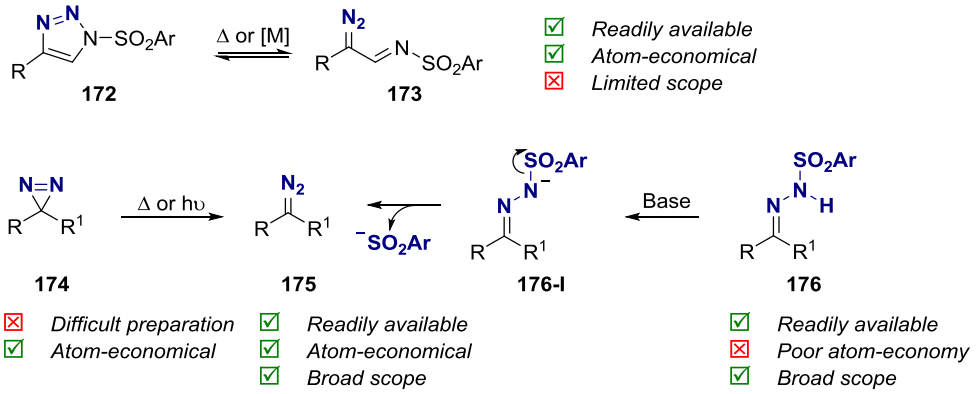

Figure 2.8. Diazo compound surrogates.

The most common precursors for the formation of metal-carbenoids are shown in Figure 2.8. 1-sulfonyl-1,2,3-triazoles (**172**)[121] can be easily prepared via Click-reaction, and, under thermal conditions or in the presence of transition metals, undergo Dimroth equilibration to form diazo compounds of type **173**. The equilibration requires the presence of a sulfonyl group, which could be detrimental for the scope of this carbenoid source. Diazirines **174**[122] are usually prepared by the oxidation of the corresponding diaziridines.[123] In the presence of light or under thermal conditions they rearrange to form diazo compounds **175**. The same products can be easily obtained by *N*-sulfonyl-hydrazones (**176**).[124] Under basic conditions, the sulfonylamine is deprotonated, generating a negative charge that will trigger the release of sulphinate anion rendering **175**.[125] Their preparation is straightforward, consisting of the condensation of sulfonylhidrazide with a carbonyl group under acidic catalytic conditions. It is woth noting that a wide number of diazo compounds (**175**) are readily available[126] and that during the formation of the metal-carbenoid[127,128] only molecular nitrogen will be generated as byproduct (Figure 2.9).

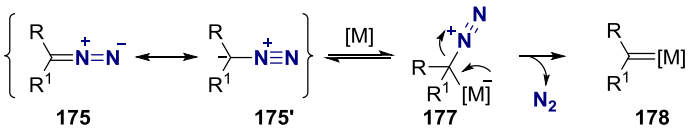

Figure 2.9. Metal-carbenoid formation via diazo compound decomposition.

[121] (a) Boyer, A. *Org. Lett.* **2014**, *16*, 5878. (b) Lindsay, V. N. G.; Viart, H. M.-F.; Sarpong, R. *J. Am. Chem. Soc.* **2015**, *137*, 8368. (c) Chuprakov, S.; Malik, J. A.; Zibinsky, M.; Fokin, V. V. *J. Am. Chem. Soc.* **2011**, *133*, 10352.
[122] Doyle, M. P.; High, K. G.; Oon, S.-M.; Osborn, A. K. *Tetrahedron Lett.* **1989**, *30*, 3049.
[123] Church, R. F. R.; Weiss, M. J. *J. Org. Chem.* **1970**, *35*, 2465.
[124] Bamford, W. R.; Stevens, T. S.; *J. Chem. Soc.* **1952**, 4735.
[125] Barluenga, J.; Valdés, C. *Angew. Chem. Int. Ed*. **2011**, *50*, 7486.
[126] Maas, G. *Angew. Chem. Int. Ed.* **2009**, *48*, 8186.
[127] Pirrung, M. C.; Morehead, A. T. *J. Am. Chem. Soc.* **1996**, *118*, 8162.
[128] Ye, F.; Qu, S.; Zhou, L.; Peng, C.; Wang, C.; Cheng, J.; Hossain, M. L.; Liu, Y.; Zhang, Y.; Wang, Z.-X.; Wang, J. *J. Am. Chem. Soc.* **2015**, *137*, 4435.

The resulting carbenoid-complexes can be classified into three main categories based upon the electronic nature of the substituents on the carbenic carbon (Figure 2.10). This carbenic atom becomes electrophilic as the lone pair of electrons is involved in the new σ M—C bond, whereas the p orbital is almost empty (π-back donation is usually low). (a) Acceptor/acceptor carbenoids containing two electron-withdrawing groups. This type of carbenes are highly electrophilic and reactive, usually leading to poor selectivities. (b) Acceptor carbenoids contain only one electron-withdrawing substituent, and are also consider rather electrophilic, and therefore highly reactive. (c) Donor/acceptor carbenoids are considerably more stable due to the stabilization of the carbenic atom by the electron-donating properties of one of the substituents (it must be noticed that electron-donating group in this classification stands for electron-releasing substituents).

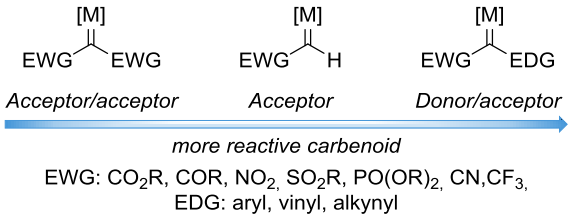

Figure 2.10. Classifications of metal-carbenoids by substituent electronics.

Metal-carbenoids are well-known for promoting C(sp^3)—H bond insertion reactions[129] through an out-sphere mechanism. Although the mechanism is not completely understood to date, it is considered to occur in a single step. Based on Hammett studies[130] and DFT[131] calculations, it has been postulated to go through a three-centered hydride transfer-like transition state in which the 2p orbital of the carbenic carbon initiates an electrophilic attack over the σ C(sp^3)—H bond (Figure 2.11). Although the reaction is concerted, it occurs in a highly asynchronous manner.[132]

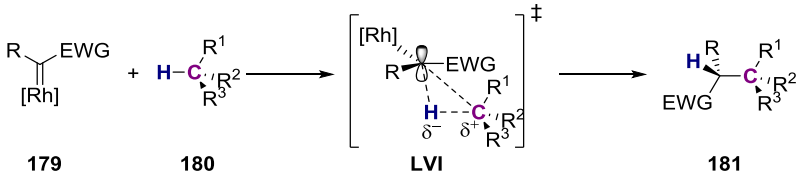

Figure 2.11. Mechanism of carbenoid C(sp^3)—H bond insertion.

Among all transition metals, rhodium is, by far, the most employed for this kind of insertions, followed by copper, iron and ruthenium.[129] Surprisingly, no catalytic C(sp^3)—H bond insertion of palladium-carbenoids have been reported to date. Recently, the insertion of nucleophilic palladium-pincer carbenoids into C(sp^3)—H bond has been published (Figure

[129] (a) Davies, H. M. L.; Morton, D. *Chem. Soc. Rev.* **2011**, *40*, 1857. (b) Davies, H. M. L.; Manning, J. R. *Nature*, **2008**, *451*, 417.(c) Davies, H. M. L.; Beckwith, R. E. J. *Chem. Rev.* **2003**, *103*, 2861. For a review concerning X-H insertion reactions see (d) Gillingham, D.; Fei, N. *Chem. Soc. Rev.* **2013**, *42*, 4918.

[130] (a)Wang, J.; Chen, B.; Bao, J. *J. Org. Chem.* **1998**, *63*, 1853. (b) Davies, H. M. L.; Jin, Q.; Ren, P.; Kovalevsky, A. Y. *J. Org. Chem.* **2002**, *67*¸4165.

[131] Nakamura, E.; Yoshikai, N.; Yamanaka, M. *J. Am. Chem. Soc.* **2002**, *124*, 7181.

[132] Importantly, as no M—C bond is formed between the catalyst and the substrate, this reaction is not consider as a C—H bond functionalization from an organometallic standpoint.

2.12).[133] However, the authors found a clear relationship between the acidity of the substrate and the reactivity. Thus, substrates with pK_a values higher than 29 did not react even upon heating (**183f**). Contrarily to rhodium-carbenoid insertion reactions, the carbenic carbon atom behaves as a nucleophile when reacting with the C—H bond and therefore, the hydrogen atom behaves like a proton instead of acting as a hydride. Importantly, care must be taken when looking at these results as these pincer complexes are better described as a nucleophilic carbon bonded to the palladium through a single σ-bond (**182b**) rather than a carbene (**182a**) as judged by X-Ray analysis, DFT calculations, and reactivity tests with other electrophiles.[134]

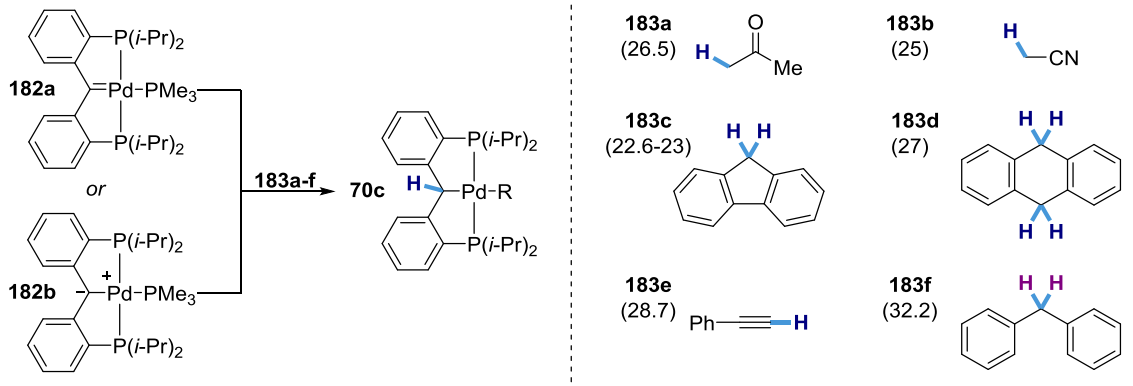

Figure 2.12. C(sp^3)—H bond insertion of a nucleophilic palladium-carbenoid (numbers in brackets indicate the pK_a of the highlighted bond).

Although C—H bond insertion of palladium-carbenoids seems difficult, the scientific community has discovered a new approach to achieve a similar reactivity than the one of rhodium-carbenoids. In this approach, the palladium-catalyst (or any other metal), reacts with the substrate to metalate the targeted bond (**185**). Afterwards, the metal catalyst reacts with the diazo compound **175** to form metal-carbenoid **186** with concomitant nitrogen extrusion. At this point, the reactive ligand R will insert into the carbenoid bond generating **187** that will form different products depending on the subsequent steps.

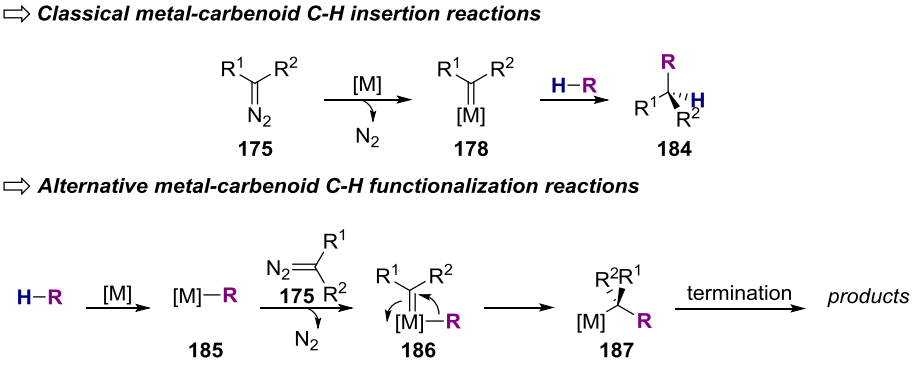

Figure 2.13. Migratory insertion, a new approach towards C—H bond functionalization based on metal-carbenoids.

[133] Comanescu, C. C.; Iluc, V. M. *Organometallics* **2015**, *34*, 4684.
[134] Comanescu, C. C.; Iluc, V. M. *Organometallics* **2014**, *33*, 6059.

Unlike the cleavage of activated C(sp^3)—H bonds or aromatic C(sp^2)—H bonds,[135] a close inspection into the literature data[125,136] indicated that there are no reactions involving the functionalization of inert C(sp^3)—H bond with metal-carbenoids. However, examples involving cleavage of activated C(sp^3)—H bonds or aromatic C(sp^2)—H bonds are known. At present, these transformations are dominated by the use of copper or rhodium catalysts, and three-different termination manners have been reported: proto-dematalation (**190**), β-hydride elimination (**191**) or C—X (X = nitrogen or oxygen) bond formation via nucleophilic attack or direct reductive elimination (**188**).

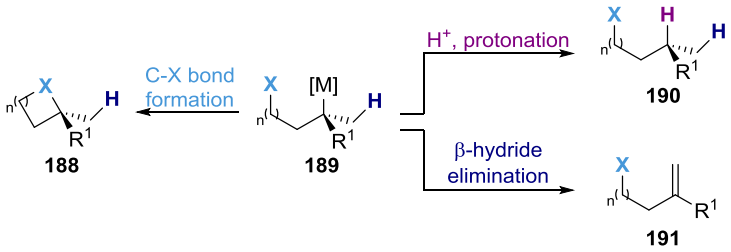

Figure 2.14. Different termination reactions reported to the date for migratory insertion complexes 68.

In Figure 2.15 are represented the most important transformations reported to date involving the functionalization of C(sp^2)—H bonds in the presence of metal-carbenoids sources. However, because of our interest on C(sp^3)—H bond functionalization, we will not discuss further the examples showed in Figure 2.15.

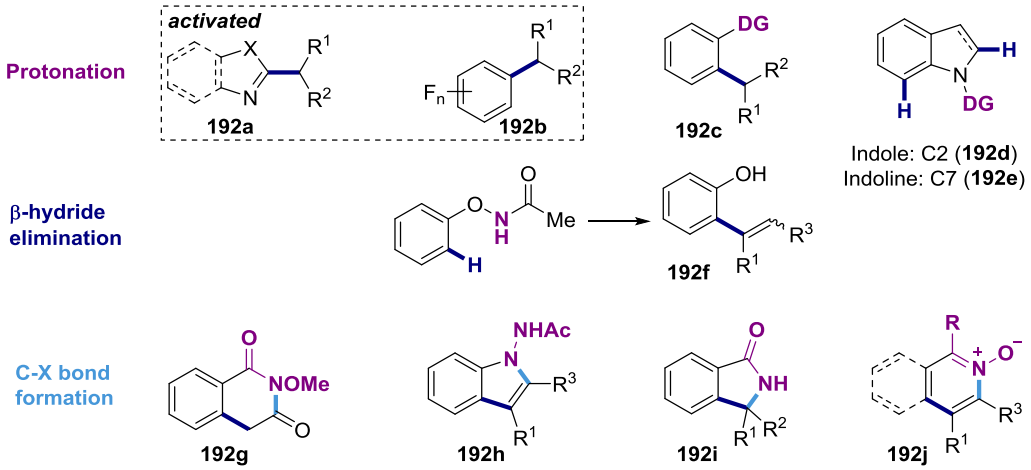

Figure 2.15. Representative examples of C(sp^2)—H bond functionalization via metal-carbenoid migratory insertion.

Regarding the functionalization of C(sp^3)—H bonds, only one example describing the cleavage of relatively activated allylic C—H bonds[137,138] has been reported with metal carbenoid (see Section 1.2.2.2). Under palladium catalysis, the authors were able to develop

[135] Hu, F.; Xia, Y.; Ma, C.; Zhang, Y.; Wang, J. *Chem. Commun.* **2015**, *51*, 7986.
[136](a) Liu, Z.; Wang, J. *J. Org. Chem.* **2013**, *78*, 10024. (b) Xia, Y.; Zhang, Y.; Wang, J. *ACS Catal.* **2013**, *3*, 2586. (c) Zhang, Y.; Wang, J. *Eur. J. Org. Chem.* **2011**, 1015.
[137] Wang, P.-S.; Lin, H.-C.; Zhou, X.-L.; Gong, L.-Z. *Org. Lett.* **2014**, *16*, 3332.
[138] For a report delaing with the functionalization of C(sp^3)—H bonds adjacent to a ketone see: Zhang, Y.; Wang, J.; Wang, J. *Synlett* **2013**, *24*, 1643.

an efficient system for the synthesis of polyene molecules.[139] The scope tolerated aryl, alkenyl andaliphatic side chains, although moderate yields were observed in the latter. The transformation is regioselective favoring the linear product due to the influence of the sulfoxide ligand, as already demonstrated by Christina White in related endeavors.[58] Interestingly, the presence of the chromium co-catalyst was crucial to achieve reactivity. The authors proposed that the coordination of chromium(III) with the diazo compound is critical to obtain the correct reaction outcome by enhancing the nucleophilicity of the carbenoid species. The mechanism is initiated by C(sp^3)—H bond functionalization followed by π-ally palladium(II) formation. Subsequently, carbenoid formation (**LVII**) mediated by the chromium co-catalyst followed by migratory insertion and β-hydride elimination delivers the targeted product and palladium(0) that is re-oxidized in the presence of benzoquinone and acetic acid.

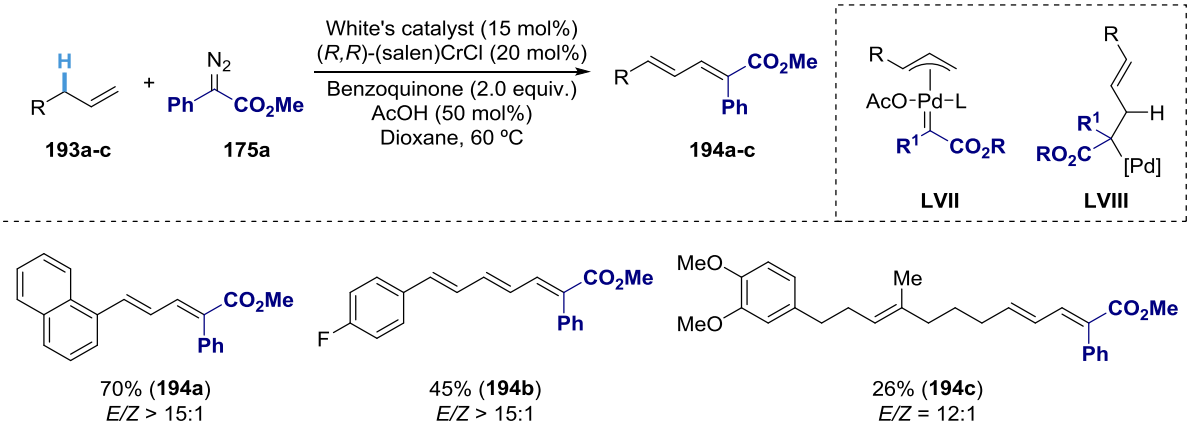

Figure 2.16. Tandem allylic C(sp^3)—H bond-functionalization/carbenoid insertion.

2.6 Pd-catalyzed C(sp^3)—H Functionalization/Carbenoid Insertion: Quaternary Carbon Centers via Multiple C–C Bond-Formation.

Taking into account all the previously considered background, we envisioned a new approach towards the synthesis of quaternary centers by means of C(sp^3)—H bond functionalization. Specially, we decided to target the synthesis of indanyl cores **195** by the combination of 2-*tert*-alkylbromoarenes (**154**) and diazo compounds (**175**) under palladium catalysis (Figure 2.17).

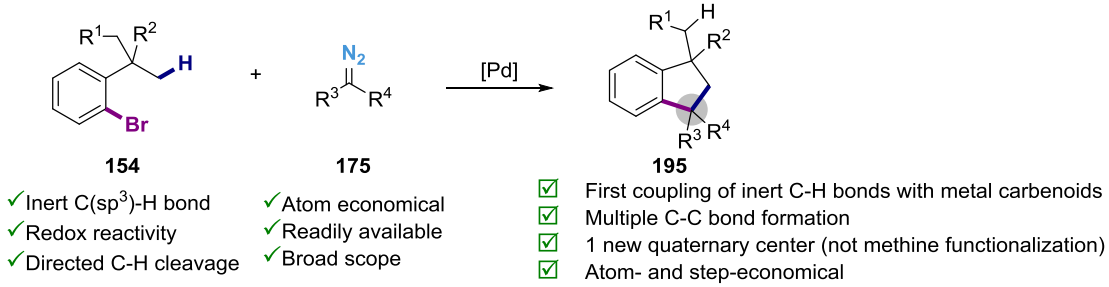

Figure 2.17. Pd-catalyzed C(sp^3)—H Functionalization/Carbenoid Insertion.

The presence of the bromoarene was expected to direct the C(sp^3)—H bond-functionalization while providing a redox manifold that would avoid the use of stoichiometric

[139] Wang, P.-S.; Lin, H.-C.; Zhou, X.-L.; Gong, L.-Z. *Org. Lett.* **2014**, *16*, 3332.

amounts of oxidant. If successful, the approach of Figure 2.17 would be the first time that a non-activated C(sp^3)—H bond is coupled with a metal-carbenoid via C—H bond functionalization. Additionally, a new quaternary center would be formed and could be potentially enantioenriched if combined with the appropriate selection of chiral ligands.

In order to face the challenges posed by this transformation, we first considered how this reaction might proceed from a mechanistic perspective. *In situ* generated palladium(0) catalyst would oxidatively add aryl bromide **154** leading to complex **LX**, setting the stage for a C(sp^3)—H cleavage to form palladacycle **XLVII**. However, complex **LX** could also lead to dehalogenated starting material (**196**) or react with diazo compound **175**, generating an arylpalladium carbenoid that might evolve via migratory insertion and protonolysis affording **197**. If the cyclometalation takes place (**XLVII**), then two competing reactions might occur, either reductive elimination en route to **153** as reported by Baudoin[110,111] or the formation of a palladium carbenoid **LXI** upon reaction with **175** with concomitant nitrogen extrusion. Then, after a [1,2]-migratory insertion event (both, aryl or alkyl migration could occur), six-membered palladacycle **LXII** or **LXII'** would be obtained. This palladacycle would finally formed the product and regenerate the active catalyst **LIX**. However, palladacycle **LXII** might be prone to protonolysis forming **197** or **197-I** in an overall reductive insertion transformation.[140]

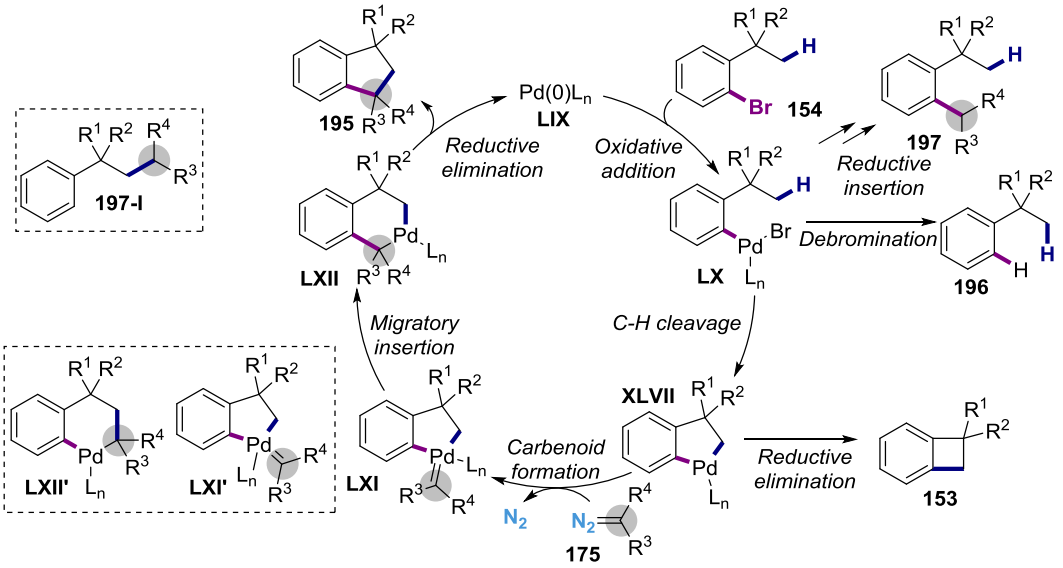

Figure 2.18. Tentative mechanistic proposal for palladium-catalyzed C(sp^3)—H functionalization/carbenoid insertion.

2.6.1 Optimization of the reaction conditions.[141]

We initiated the optimization of our protocol[142] using classical reaction conditions for arylation of C(sp^3)—H bonds,[83,110] with a palladium(II) precatalyst and a base with high

[140] (a) Xia, Y.; Hu, F.; Liu, Z.; Qu, P.; Ge, R.; Ma, C.; Zhang, Y.; Wang, J. *Org. Lett.* **2013**, *15*, 1784. (b) Zhang, Z.; Liu, Y.; Gong, M.; Zhao, X.; Zhang, Y.; Wang, J. *Angew. Chem. Int. Ed.* **2010**, *49*, 1139.

[141] Beatriz de Luis is deeply acknowledged for her contributions during the optimization of the reaction conditions.

[142] For our first optimization studies, substrate **154l** was employed, yet, its purity was not absolute. Furthermore, in the optimizations studies with this substrate, only the yield of **196l** is corrected, as the other compounds could not be isolated completely pure. Preliminary studies were conducted under

denticity to favor the concerted metalation-deprotonation step. Pivalic acid was also added due to its ability to improve the reactivity.[86]

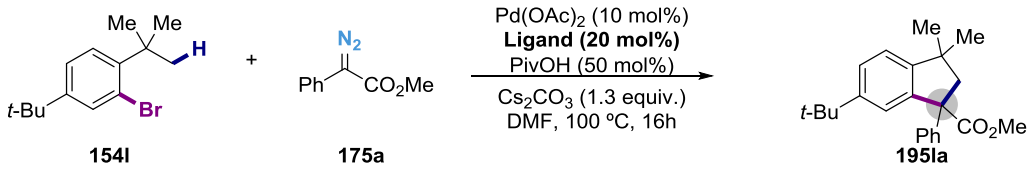

Entry	Phosphine	Conv. (%)	Yield 153l (%)	Yield 196l (%)	Yield 196l (%)	Yield 195la (%)
1	$P(t\text{-}Bu)_3 \cdot HBF_4$	>99	82	14	0	0
2	$P(t\text{-}Bu)_2Me \cdot HBF_4$	>99	14	36	20	9
3	$P(t\text{-}Bu)_2(i\text{-}Pr)$	>99	56	17	5	8
4	$P(o\text{-}tol)_3$	>99	34	2	10	35
5	$PCy_3 \cdot HBF_4$	>99	22	26	18	16
6	PCy_2Ph	>99	16	3	6	61
7	$PCyPh_2$	>99	20	7	35	30
8	DCEphos	>99	16	1	4	80
9	DPEphos	>99	30	6	33	29
10	Xantphos	0	0	0	0	0
11	Sphos	62	43	16	0	2

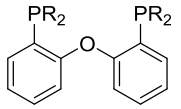

R = Cy; **DCEphos**
R = Ph; **DPEphos**

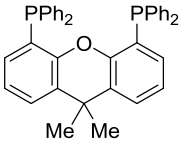

Xantphos

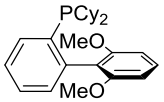

Sphos

154l (0.18 mmol), **175a** (1.5 equiv.), $Pd(OAc)_2$ (10 mol%), ligand (20 mol% monodentates, 12mol% bidentates), PivOH (50 mol%) Cs_2CO_3 (1.3 equiv.) in dry DMF (0.25M) at 100 ºC for 16h. Yield and conversion were determined by GC using *o*-xylene as internal standard.

Table 2.1. Initial optimization studies. Ligand screening.

Based on the work of Baudoin and co-workers,[110] we decided to initially use tri-*tert*-butylphosphine as ligand, hoping to form palladacycle **XLVII** (see Figure 2.18). Although no product formation was observed, benzocyclobutane **153a** was obtained in high yields along with some debrominated starting material **196l** (Table 2.1, entry 1).[143] This result can be rationalized by the bulkiness of tri-*tert*-butylphosphine that might trigger a facile reductive-elimination (see Figure 2.18).

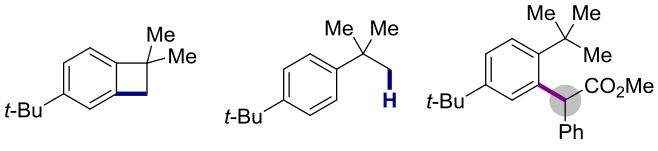

Figure 2.19. Byproducts observed during the optimization studies.

Consequently, we envisioned to employ less sterically hindered ligands to avoid the undesired reductive elimination while facilitating the formation of the palladium-carbenoid. In fact, when one *tert*-butyl moiety was exchanged by an *iso*-propyl or a methyl, lower amounts

these circumstances but soon the substrate was changed to **154a** that could be obtained completely pure.

[143] Surprisingly, in the presence of unreactive aryl bromides, diazo compound dimerization was typically observed at some extent. For the only reported dimerization of diazo compounds under palladium catalysis see: Ojha, D. P.; Prabhu, R. *J. Org. Chem.* **2013**, *78*, 12136.

of benzocyclobutane **153l** (56% and 14% for *iso*-propyl and methyl respectively) were obtained.

Interestingly, we were able to observe product **195la** for the first time (entries 2-3). The bulkier tris-*o*-tolylphosphine[144] (entry 4) gave higher yields of product while the formation of benzocyclobutane was kept in relatively low yields, thus indicating that electronic factors of the ligand also play an important role. When tricyclohexylphosphine was employed, no improvement could be achieved, whereas phenyldicyclohexylphosphine lead to product **195la** in good yields. Remarkably, diphenylcyclohexylphosphine shutted down the reactivity (entries 5-7 respectively) suggesting that subtle steric and electronic modifications were crucial for success. Accordingly, we decided to test related ligands, such as Sphos and DCEphos (entries 11 and 8 respectively). Interestingly, while Sphos[145] gave only traces amounts of product, more rigid DCEphos gave **195la** in 80% yield with low amounts of benzocyclobutane **153l**. To study whether the ligand backbone was responsible for such behavior, DPEphos (entry 9) was tested under the reaction conditions; interestingly, lower yields of product were obtained (29%), indicating that cyclohexyl substituents are of utmost importance for reactivity. However, the backbone structure was also beneficial as shown by the different reactivity of structurally related DPEphos and Xantphos (entries 9 and 10).

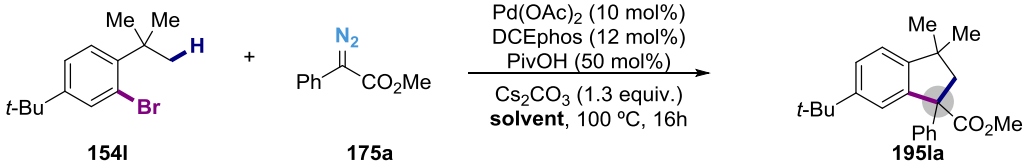

154l **175a** **195la**

Entry	Solvent	Conv. (%)	Yield 153l (%)	Yield 196l (%)	Yield 197l	Yield 195la (%)
1	DMF	>99	16	1	4	80
2	DMA	>99	27	1	2	67
3	NMP	>99	13	2	2	76
4	CH_3CN	>99	30	3	3	63
5	DMSO	>99	18	3	4	45
6	1,4-Dioxane	>99	76	11	5	3
7	DCE	58	19	8	2	2
8	Toluene	>99	75	10	3	0

154l (0.18 mmol), **175a** (1.5 equiv.), $Pd(OAc)_2$ (10 mol%), DCEphos (12mol%), PivOH (50 mol%) Cs_2CO_3 (1.3 equiv.) in dry solvent (0.25M) at 100 ºC for 16h. Yield and conversion were determined by GC using *o*-xylene as internal standard.

Table 2.2. Solvent screening.

With these results in hand, we then focused our attention on studying the effect of the solvent. As shown in Table 2.2, the best results were found for highly polar coordinating solvents (entries 1-5), whith less polar or less coordinating solvents (entries 6-7) providing traces amounts of product with non-negligible amounts of benzocyclobutane **153l**. Unfortunately, we do not have any rationale for such striking behavior.

[144] Ferguson, G.; Roberts, P. J.; Alyea, E. C.; Khan, M. *Inorg. Chem.* **1978**, *17*, 2965.
[145] Sphos was previously employed as ligand by Buchwald to promote the Suzuki-Miyaura coupling with this kind of substrates. See ref. 119a.

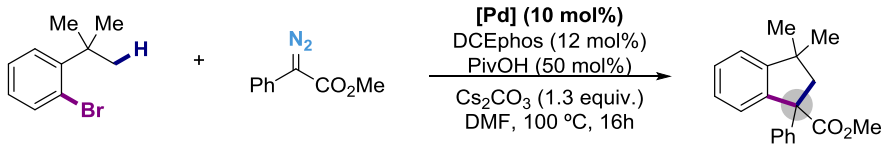

154a **175a** **195aa**

Entry	[Pd] precatalyst	Conv. (%)	Yield 153a (%)	Yield 196a (%)	Yield 197a (%)	Yield 195aa (%)
1	$Pd(OAc)_2$	>99	6	1	6	80
2	$Pd(dba)_2$	>99	8	0	3	77
3	$Pd(OPiv)_2$[a]	>99	0	0	3	83
4	$PdCl_2$	83	7	0	4	80
5	*t*-$PdCl_2(SMe_2)_2$	>99	4	0	3	87
6	$Pd(COD)Cl_2$	>99	4	1	3	80

154a (0.18 mmol), **175a** (1.5 equiv.), [Pd] (10 mol%), DCEphos (12mol%), PivOH (50 mol%) Cs_2CO_3 (1.3 equiv.) in dry DMF (0.25M) at 100 ºC for 16h. Yield and conversion were determined by GC using *o*-xylene as internal standard. [a] No PivOH was added.

Table 2.3. Effects of palladium-precatalysts in the reaction outcome.

At this stage,[146] different palladium precatalysts were employed using **154a** as the model substrate. Surprisingly, little effect was observed when comparing palladium(0) and palladium(II) precatalysts. Nonetheless, a slight improvement could be obtained with *trans*-$PdCl_2(SMe_2)_2$ (87% yield, entry 5) probably due to its better solubility compared to $PdCl_2$ (entries 4-5). Interestingly, palladium(II) pivalate (entry 3) worked equally well than other precatalysts although no pivalic acid was added to the reaction mixture.

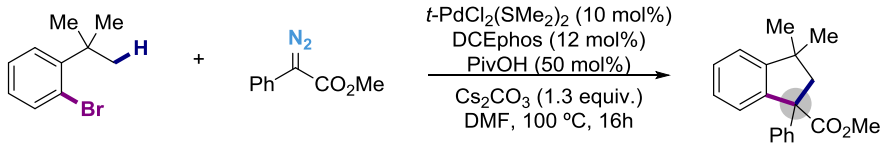

154a **175a** **195aa**

Entry	175a (x equiv.)	Conv. (%)	Yield 153a (%)	Yield 196a (%)	Yield 197a (%)	Yield 195aa (%)
1	1.00	>99	31	0	2	48
2	1.25	>99	16	0	3	68
3	1.50	>99	4	0	3	87
4	1.75	>99	0	0	3	91
5	2.00	>99	0	0	4	82

154a (0.18 mmol), **175a** (x equiv.), *t*-$PdCl_2(SMe_2)_2$ (10 mol%), DCEphos (12 mol%), PivOH (50 mol%) Cs_2CO_3 (1.3 equiv.) in dry DMF (0.25M) at 100 ºC for 16h. Yield and conversion were determined by GC using *o*-xylene as internal standard.

Table 2.4 Equivalents of diazo compound **175a**.

[146] Please, note that from now on, substrate **154a** will be used as model substrate. Additionally, from now on, all the given yields and conversions are adequately corrected.

In light of these results, we envisioned that a higher concentration of diazo compound could avoid the undesired formation of benzocyclobutane **153a**. Gratifyingly, this was indeed the case, and the higher the amount of **175a** employed, the lower benzocyclobutane was observed (Table 2.4). As shown, the best results were accomplished with 1.75 equivalents of **175a**.

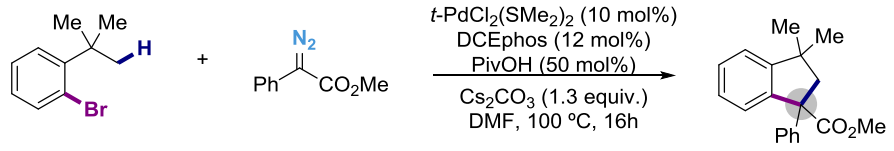

154a **175a** **195aa**

Entry	DMF (x mL)	Conv. (%)	Yield 153a (%)	Yield 196a (%)	Yield 197a (%)	Yield 195a (%)
1	0.15	>99	16	3	3	45
2	0.25	>99	11	0	4	70
3	0.50	>99	2	0	4	86
4	0.75	>99	0	0	4	88
5	1.0	>99	0	0	4	85
6	0.75 (80 ºC)	>99	0	0	0	92
7	0.75 (110 ºC)	>99	4	0	4	87
8	0.75[a]	>99	18	0	4	73

154a (0.18 mmol), **175a** (1.75 equiv.), *t*-$PdCl_2(SMe_2)_2$ (10 mol%), DCEphos (12 mol%), PivOH (50 mol%) Cs_2CO_3 (1.3 equiv.) in dry DMF (x M) at 100 ºC for 16h. Yield and conversion were determined by GC using *o*-xylene as internal standard.
[a]Diazo compound **175a** was added in two additions, (1.0 equiv. followed by 0.75 equiv. after 1 hour).

Table 2.5. Concentration and temperature screening.

The overall reaction concentration was also studied by varying the amount of DMF employed (Table 2.5). Surprisingly, the more concentrated the reaction mixture, the higher the benzocyclobutane **153a** formation, an observation that goes in contrast with the ability of intramolecular reactions to be accelerated under diluted conditions. While the reaction proceeded equally well at 80 ºC or 100 ºC (entries 6 and 4 respectively), undesired benzocyclobutane **153a** was observed at 110 ºC, although in low yields. This result could indicate that reductive elimination has a higher activation barrier than carbenoid formation (see Figure 2.18). Notably, portionwise addition of diazo compound **175a** had a deleterious effect on the reaction outcome (entry 8).

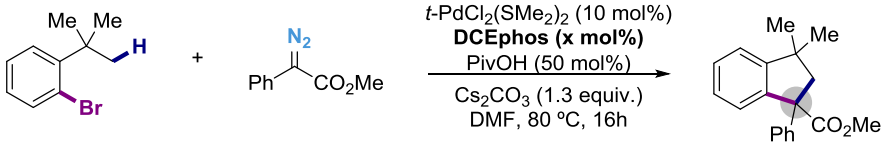

154a **175a** **195aa**

Entry	Pd:L ratio	Conv. (%)	Yield 153a (%)	Yield 196a (%)	Yield 197a (%)	Yield 195aa (%)
1	1:1	>99	3	0	4	77
2	1:1.25	>99	0	0	4	85
3	1:1.5	>99	0	0	4	91
4	1:1.75	>99	0	0	4	92
5	1:2	>99	0	0	4	89

154a (0.18 mmol), **175a**(1.75 equiv.), *t*-$PdCl_2(SMe_2)_2$ (10 mol%), DCEphos (x mol%), PivOH (50 mol%) Cs_2CO_3 (1.3 equiv.) in dry solvent (0.25 M) at 80 ºC for 16h. Yield and conversion were determined by GC using *o*-xylene as internal standard.

Table 2.6. Palladium:Ligand ratio.

The optimal ratio between the precatalyst and the ligand was next studied, as it is well-known that the amount of ligand might influence dramatically the scope of catalytic reactions. In our case, the effect was almost unnoticeable, although a slight improvement could be observed when increasing the relative amount of ligand (entries 1-5), with 1.5:1 ligand to metal ratio being optimal (entry 3).

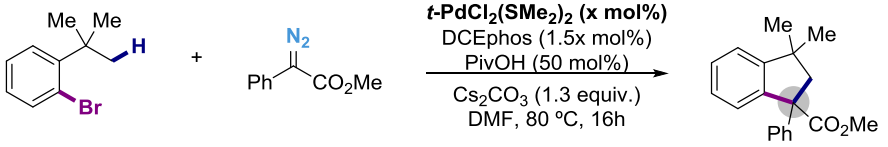

154a **175a** **195aa**

Entry	*t*-$PdCl_2(SMe_2)_2$ (x mol%)	Conv. (%)	Yield 153a (%)	Yield 196a (%)	Yield 197a (%)	Yield 195aa (%)
1	2.5	17	0	0	3	8
2	5.0	>99	0	0	4	87
3	10.0	>99	0	0	4	90

154a (0.18 mmol), **175a** (1.75 equiv.), *t*-$PdCl_2(SMe_2)_2$ (x mol%), DCEphos (1.5x mol%), PivOH (50 mol%) Cs_2CO_3 (1.3 equiv.) in dry solvent (0.25 M) at 80 ºC for 16h. Yield and conversion were determined by GC using *o*-xylene as internal standard.

Table 2.7. Catalyst loading.

Once the optimal catalyst to ligand ratio was determined, we explored the reactivity of this catalytic system under lower catalyst loading (Table 2.7). Noteworthy, the reaction worked equally well at 5 mol% (entries 2 and 3) but a significant erosion on activity was found at 2.5 mol% (entry 1).

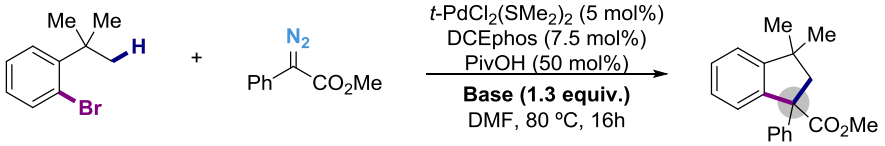

154a **175a** **195aa**

Entry	Base	Conv. (%)	Yield 153a (%)	Yield 196a (%)	Yield 197a (%)	Yield 195aa (%)
1	K_2CO_3	79	0	0	3	66
2	K_3PO_4	85	0	0	3	67
3	KOAc	35	0	0	4	9
4	CsOPiv[a]	67	0	0	3	63

154a (0.18 mmol), **175a** (1.75 equiv.), *t*-$PdCl_2(SMe_2)_2$ (5 mol%), DCEphos (7.5 mol%), PivOH (50 mol%) base (1.3 equiv.) in dry solvent (0.25 M) at 80 ºC for 16h. Yield and conversion were determined by GC using *o*-xylene as internal standard.
[a] No PivOH was added.

Table 2.8. Screening of bases.

Next, we turned our attention to the influence of the base (Table 2.8). Polydentate bases were tested since they are known to promote the concerted metalation-deprotonation step. However, none of the bases tested could improve our previously obtained result (Table 2.8, entries 1-4). In order to study the acid/base equilibrium between cesium carbonate and pivalic acid, cesium pivalate was employed under our reaction conditions; however, the reaction did not achieve the same levels of efficiency (entry 4). This behavior has already been observed by Fagnou[83,85a] and suggests that cesium carbonate might be acting as a proton sink.

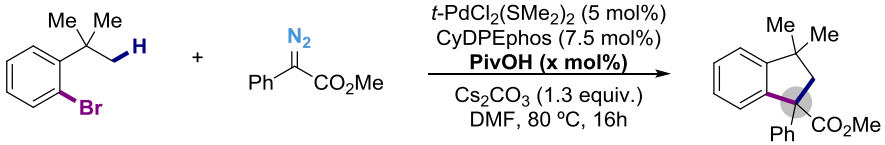

154a **175a** **195aa**

Entry	PivOH (x mol%)	Conv. (%)	Yield 153a (%)	Yield 196a (%)	Yield 197a (%)	Yield 195aa (%)
1	25	78	0	0	4	60
2	50	>99	0	0	3	93
3	75	>99	0	0	4	93
4	AdCOOH[a]	76	0	0	3	63

154a (0.18 mmol), **175a** (1.75 equiv.), *t*-$PdCl_2(SMe_2)_2$ (5 mol%), DCEphos (7.5 mol%), PivOH (x mol%) Cs_2CO_3 (1.3 equiv.) in dry solvent (0.25 M) at 80 ºC for 16h. Yield and conversion were determined by GC using *o*-xylene as internal standard.
[a] AdCOOH (50 mol%) was used instead of pivalic acid.

Table 2.9. Exploring the influence of pivalic acid.

In order to understand the important role of pivalic acid, a series of experiments were conducted to such purpose. As shown in entries 1-3, the amount of pivalic acid played a critical role en route to **195aa**, with 50 mol% of pivalic acid resulting in the best compromise in terms

of yield and conversion. A simple comparison with 1-adamantyl carboxylic acid (entry 4) clearly highlighted the superior activity of pivalic acid as promoter of this reaction.

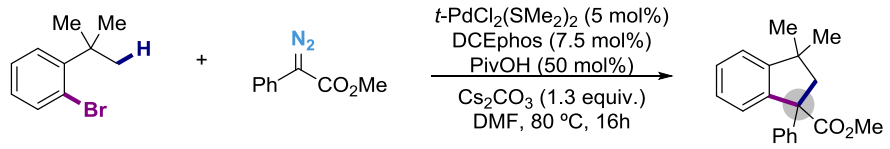

154a **175a** **195aa**

Entry	*t*-$PdCl_2(SMe_2)_2$	DCEphos	PivOH	Cs_2CO_3	Yield 195aa (%)
1	✓	✓	✓	✓	91
2	×	✓	✓	✓	0
3	✓	×	✓	✓	0
4	✓	✓	×	✓	9
5	✓	✓	✓	×	0

154a (0.18 mmol),**175a** (1.75 equiv.), *t*-$PdCl_2(SMe_2)_2$ (5 mol%), DCEphos (7.5 mol%), PivOH (50 mol%) Cs_2CO_3 (1.3 equiv.) in dry DMF (0.25 M) at 80 ºC for 16h. Yield and conversion were determined by GC using *o*-xylene as internal standard.

Table 2.10. Blank experiments.

Finally, a series of control experiments were carried out (Table 2.10). As expected, control experiments revealed that all components were essential for the reaction to occur, although, 9% of **195aa** could be observed in the absence of pivalic acid (entry 4).

It must be noticed that, during the optimization process, the formation of product **198** was constantly detected, a product arising from the insertion of the carbenoid into the O—H bond of the pivalic acid. It is worth noting that the reaction of donor/donor diazo compounds with carboxylics acids in the absence of any further reagents has been reported[147] under palladium catalysis.[148]

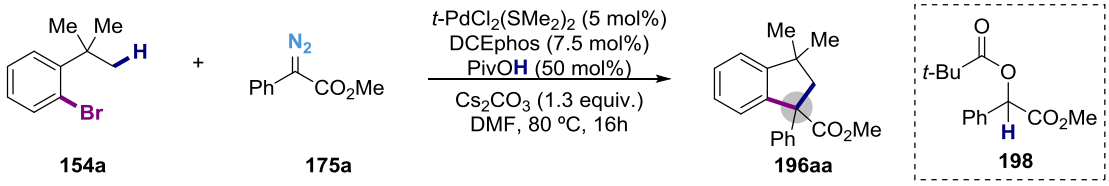

154a **175a** **196aa** **198**

Scheme 2.4. Formation of compound **198**.

2.6.2. Scope regarding the diazo compound moiety

With a robust set of reaction conditions in hand, we decided to study the preparative scope for the transformation. Our first goal focused on studying the influence of the diazo compound for preparing indane backbones from simple *ortho*-substitued **154a**.

Monosubstituted diazo compounds.

[147] Perusquía-Hernández, C.; Lara-Issasi, G. R.; Fontana-Uribe, B. A.; Cuevas-Yañez, E. *Tetrahedron Lett.* **2013**, *54*, 3302.
[148] Kitamura, M.; Kisanuki, M.; Sakata, R.; Okauchi, T. *Chem. Lett.* **2011**, *40*, 1129.

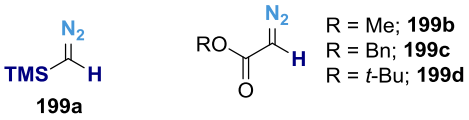

Figure 2.19. Donor/H and acceptor/H diazo compounds tested.

We first studied the performance of monosubstituted diazo compounds (Figure 2.19), as they would provide tertiary carbons (or secondary upon TMS removal) that could be easily modified, especially in the case of **199b-d**. However, no reaction was observed, recovering the starting material unaltered after 16 hours. Importantly, we observed strong bubbling upon addition of the diazo compound before heating, probably indicating the decomposition of the reagent. Noteworthy, acceptor/H as well as donor/H diazo compounds behaved equally. Based on these results, we decided to test the electronic influence of disubstitued diazo compounds.

Donor/Donor diazo compounds.

We first studied donor/donor diazo compounds to explore if the reactivity was hampered in the presence of relatively stable carbene sources. Unfortunately, substrate **200b** did not provide any product, while **200a** led to several products that could not be identified. A possible explanation for the inertness of these substrates is based on the higher nucleophilic character of the diazo compound when compared with **175**. Because of this higher nucleophilicity, the diazo compound could directly react with the precatalyst therefore avoiding the catalytic cycle initiation.

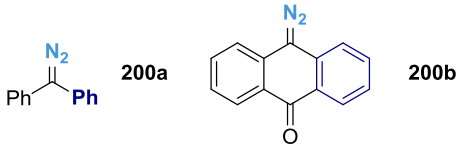

Figure 2.20. Donor/donor diazo compounds explore.

Acceptor/Acceptor diazo compounds.

After the unfortunate results obtained with donor/donor diazo compounds we decided to test diazo compounds of the opposite nature, which are acceptor/acceptor diazo compounds. Surprisingly, symmetric cyclic 1,3-dicarbonylic diazo compounds (**201a-c**) did not react, and **154a** was recovered. To study whether the cyclic structure of these compounds could be hampering the reaction, non-cyclic diazo compounds were then tested. When performing the reaction with **201e**, starting material **154a** was once again recovered. We assumed that the acidic α-protons of the ketone involved are responsible the lack of reactivity. Unfortunately, no reactivity was observed for **201f** as well. Finally, diazo malonate **201g** was submitted under the reaction conditions, furnishing low yield of **202**. However, forcing the reaction conditions (see Figure 2.21) resulted in 68% yield of isolated product **202**, an important findinding since **202** can be decarboxylated under Krapcho's conditions to form tertiary centers. Finally, it is important to highlight the different behavior of electronically similar diazo compounds **201b** and **201g**. Although tentatively, we suggested that acceptor/acceptor diazo compounds are not nucleophilic enough to react with the competent palladium complex. However, it is surprising that not even benzocyclobutane **153a** was observed. Indeed, in any case **198** was formed in the presence of non-reactive diazo compounds.

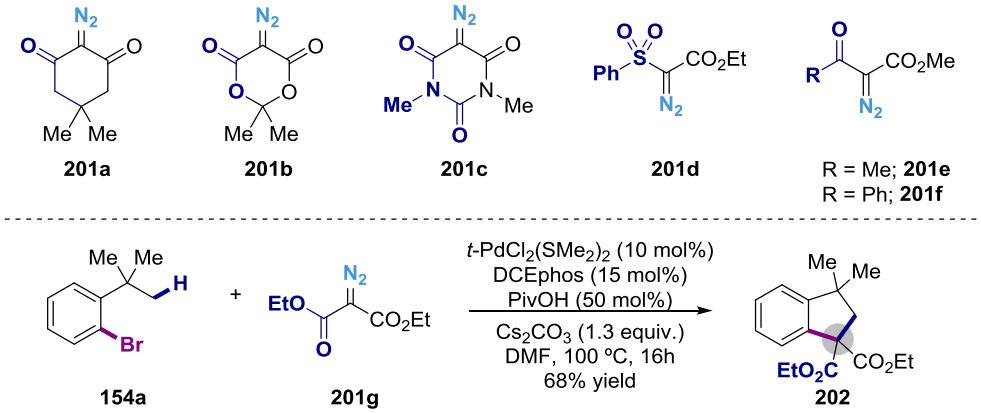

Figure 2.21. Acceptor/Acceptor diazo compounds.

Acceptor/Donor diazo compounds.

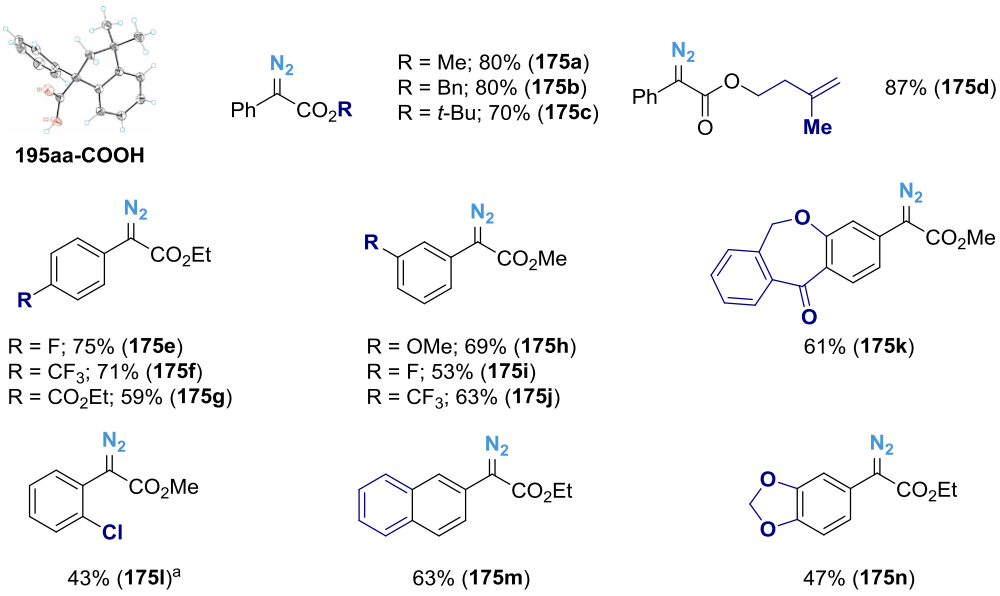

[a]*Using the reactions conditions specified in figure 2.21*

Figure 2.22. Functional group tolerance on acceptor/donor diazo compounds.

Finally, we focused our attention on the functional group tolerance of acceptor/donor diazo compounds. First of all, the influence of the ester moiety was studied (**175a-d**), and no significant impact on the general reactivity was noticed, although the sterically demanding *tert*-butyl ester **175c** gave the product in lower yield. To further confirm the structure of the product obtained, substrate **195aa** was hydrolyzed under basic conditions obtaining the carboxylic acid **195aa-COOH** which could crystalized. Interestingly, substrate **175d** bearing a pending alkene afforded the corresponding product in high yield without detecting even traces of intramolecular cyclopropanation of the alkene motif in the crude reaction mixture. Subsequently, we studied the effect of the electronic nature of the arene motif within the diazo compound. As shown with substrates **175e-j**, electron-withdrawing groups at the *para*- and *meta*- position were well accommodated, affording moderate to good yields of the final products. Noteworthy, the diazo compound derived from Isoxepac (**175k**), a nonstereoidal anti-inflammatory drug (NSID), could be employed giving good yields of the corresponding

product.[149] Other arene motifs, like benzodioxol and naphthtalene were employed with equal ease (**175m-n**) under the optimized reaction conditions. Importantly, substrate **175l**, bearing a chlorine atom at the *ortho* position provided the product in moderate yields. This substrate is rather challenging due to the possibility of promoting an oxidative addition with palladium(0).

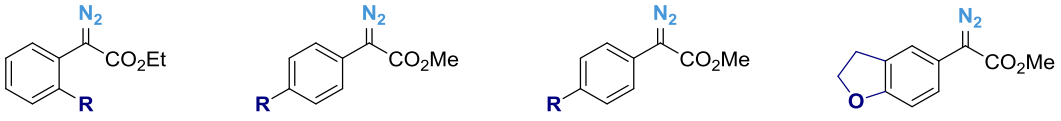

Figure 2.23. Non-reactive acceptor/donor diazo compounds. Arene substitution.

It should be noticed that some substitution patterns were not well tolerated under the reaction conditions. For example, *ortho*-substituted diazo compounds (**175o-p**) as well as strongly electron deficient arenes led to no conversion (**175q-r**). Importantly, electron-donating substituents in *para* position (**175s-u**) dramatically hampered the reactivity giving low yields of the corresponding products. These results highlights the sensitivity of the system to the electronic nature of the carbenic carbon. Moreover, the results displayed by **175q-r** are in agreement with the lack of reactivity of acceptor/acceptor diazo compounds.

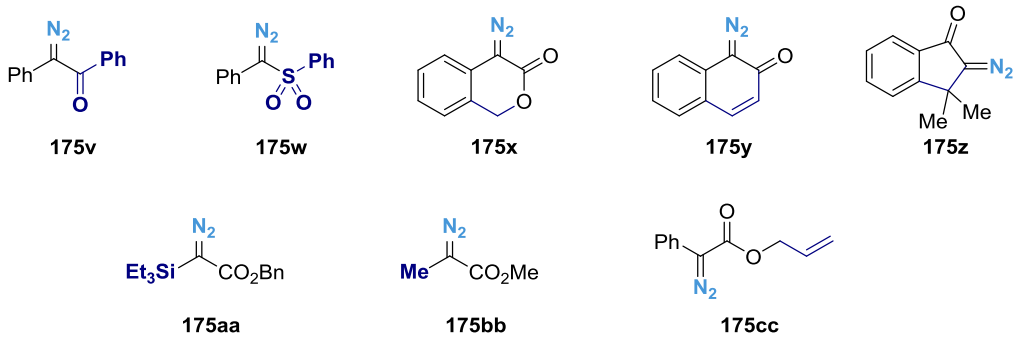

Figure 2.24. Non-reactive acceptor/donor diazo compounds.

As it can be seen in Figure 2.23, our system is currently limited to diazo compounds bearing esters as the electron-withdrawing group. Other electron-withdrawing groups were tested, but no conversion of the starting material occurred, reinforcing the notion that our system was highly sensitive to electronic effects. Noteworthy, substrate **175x**, closely related to **175a**, did not work under the standard conditions, confirming the low reactivity of cyclic diazo compounds. Substrate **175cc**, bearing an allyl unit did not react either, most probably because of preferential oxidative addition of palladium(0) over the allyl acetate rather than the aryl bromide. Finally, we decided to exchange the electron-releasing aryl with an electron-donating group (**175aa-bb**). We envisioned that **175aa** could form a tertiary center after TES removal thus behaving like a surrogate of compound **199c**. Although complete conversion was achieved in both cases, we could not identify the different products.

2.6.3 Scope regarding the aryl bromide backbone

Next, we turned our attention to disclose how the substitution onto the aryl bromide affects the overall reaction. To such end, different strategies were designed in order to prepare the starting materials (Figure 2.25).

[149] Honing, W. J.; Pelgrom, R.; Chadha, D. R. *J. Clinical. Pharmacology* **1982**, *22*, 82.

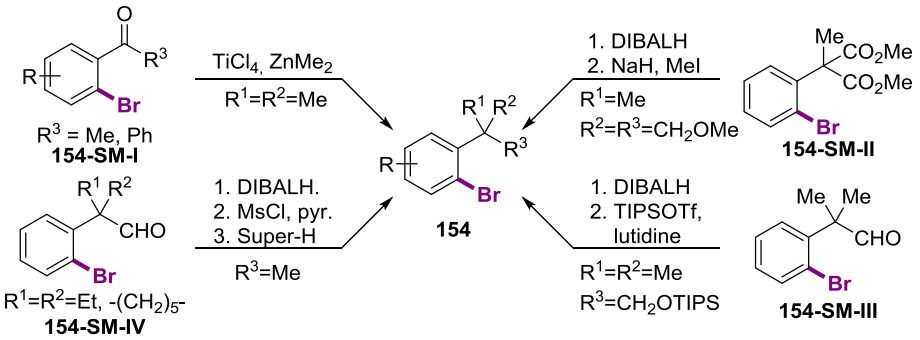

Figure 2.25. Procedure for the synthesis of aryl bromides.

Four main approaches were employed for the synthesis of **154**. Most of the substrates were prepared from the corresponding ketone **154-SM-I** in the presence of *in situ* formed $TiCl_2Me_2$ that will render the final product along with the tertiary alcohol and the corresponding styrene. Treatment of the crude reaction mixture with *m*-CPBA and purification by silica gel column allowed to obtain the products in low to moderate yields. Alternatively, substrates bearing pending ethers were prepared by reduction of the ester or aldehyde motif with DIBALH followed by hydroxyl protection. Finally, the synthesis of more challenging substrates bearing only one methyl group was achieved by reduction of the aldehyde **154-SM-IV** to the primary alcohol followed by mesyl formation wich will be reduced in the presence of Super-hydride to the corresponding methyl.

With a set of different aryl bromides on our hand we decided to test their performance under reaction conditions to study the influence exerted by the different substitution patterns. First, we carried out the reaction with the chlorinated analog **154a-Cl**, but only traces of product were detected by GC-MS. This result is indeed not surprising since the activation of aryl chloride is more difficult due to their higher C—Cl bond-dissociation energy. Next, different alkyl substituents were tested, confirming that *para* and *meta* substitution was well tolerated (substrates **195ba-ca**). On the other hand, alkyl substituents at the *ortho* position completely inhibited the reactivity, most probably because of the steric hindrance (**154i-j**). Electron-withdrawing groups at the *meta* position to the bromine atom afforded the corresponding products in high yields (**195da-fa**). This trend cannot be generalized since nitro groups (**154l**) worked poorly and amide substituents (**154k**) only provided traces amounts of product. On the other hand, electron-donating groups such as **195ga-ha** dimethylat amines or free aniline resulted in moderate to good yields. Although *para*-methoxy groups yielded the final product, it could not be obtained in a pure form (**154l**). Finally, homologated aryl bromide **154m** was tested, but no reaction took place. A plausible explanation to such behavior would be the formation of a stable palladium(II) complex after oxidative addition by coordination with the Lewis basic oxygen.

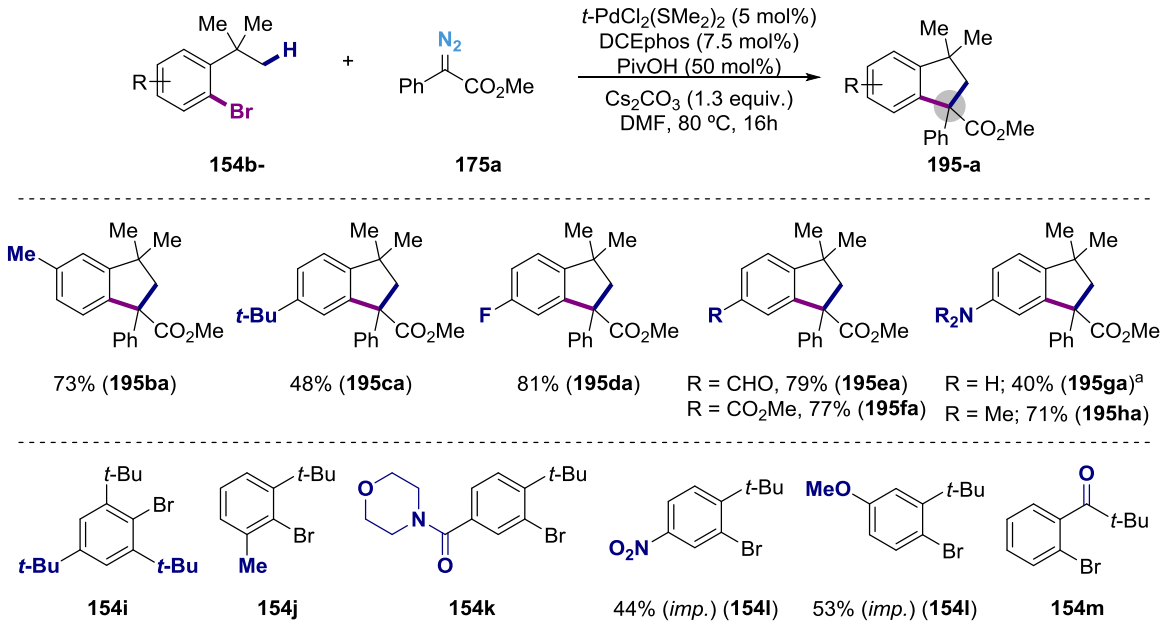

Figure 2.26. Electronic effects on the aryl bromide arene backbone.

Our next goal was to study if the reaction could occur in the presence of motifs other than *tert*-butyl groups. This approach was successful and several different groups were well accommodated (**195na-ra**). Importantly, in all cases the reaction was selective towards the primary C(sp^3)—H bond over secondary position (**195na-qa**). If multiple C(sp^3)—H bonds were present, the reaction exclusively took place at the most accessible C(sp^3)—H bond. This result is in agreement with Fagnou's observation for the synthesis of dihydrobenzofurans.[83] They calculated that the transition state for methylene activation was 5.5 Kcal/mol higher than for methyl activation (27.0 Kcal/mol). Similarly, the transition state for the formation of a homologated palladacycle was 6.1 Kcal/mol higher (see Figure 2.27).

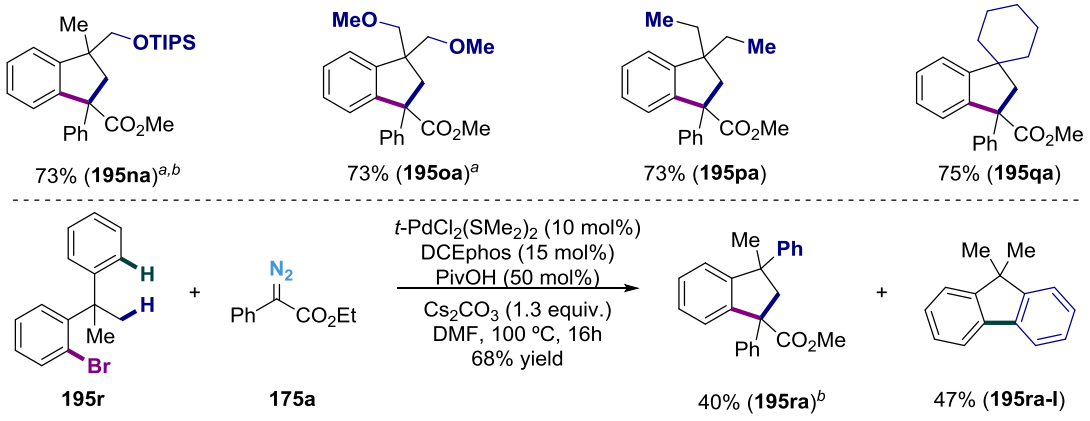

Figure 2.27. Scope beyond *tert*-butyl groups.

As expected, a mixture C(sp^2)—H and C(sp^3)—H functionalization occurred in the presence of C(sp^2)—H and C(sp^3)—H bonds (Figure 2.27, **195r**). Nevertheless, the achieved selectivity is remarkable as only arene functionalization was observed in other literature protocols.[83]

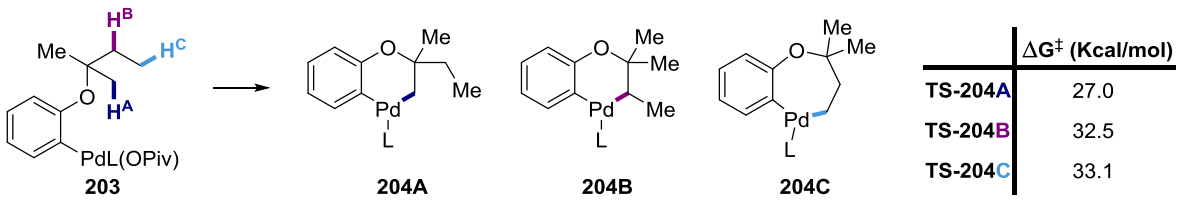

Figure 2.28. Palladium-catalyzed synthesis of dihydrobenzofurans: Regioselectivity control.

Although groups other than methyl groups were tested (Figure 2.29,**154s-u,w**) no product was obtained. In some cases, reductive insertion (**197a**) was detected as major product (**154s-t**, **154w-x**). These results indicates that after oxidative addition, the in situ formed aryl palladium(II) **LX** reacts with diazo compound **175a** preferentially over cyclometalation. **154u** gave several unidentified products, whereas no conversion was achieved for **154v**. When a functional group was introduced at the *ortho*-position (**154y-dd**), the reaction was completely shut down, and the starting material was recovered. Only substrate **154cc** led to traces of product. A plausible explanation for this lack of reactivity would be catalyst sequestration after the oxidative addition.

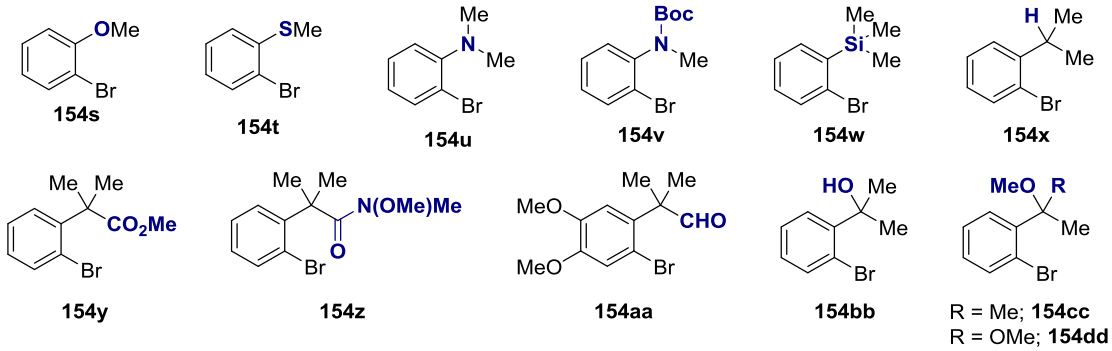

Figure 2.29. Unproductive substrates: part 1.

The selectivity of the system was examined with substrates **154ee-gg** (Figure 2.30). Substrate **154ee** gave relatively good conversions towards a mixture of products (**195eea-I** and **II**) along with **154ee-I** produced via double Heck cyclization. Unfortunately, we could not determine if the products arose via C(sp^2)—H or C(sp^3)—H functionalization, since they could isomerize under the reaction conditions. Substrate **154ff**, bearing two phenyl groups afforded quantitative yield of fluorene **154ff-I**. Finally, substrate **154gg** reacted poorly under the reaction conditions leading to low conversion and providing a mixture of products arising from non-selective functionalization (**195gga-I** and **II**).

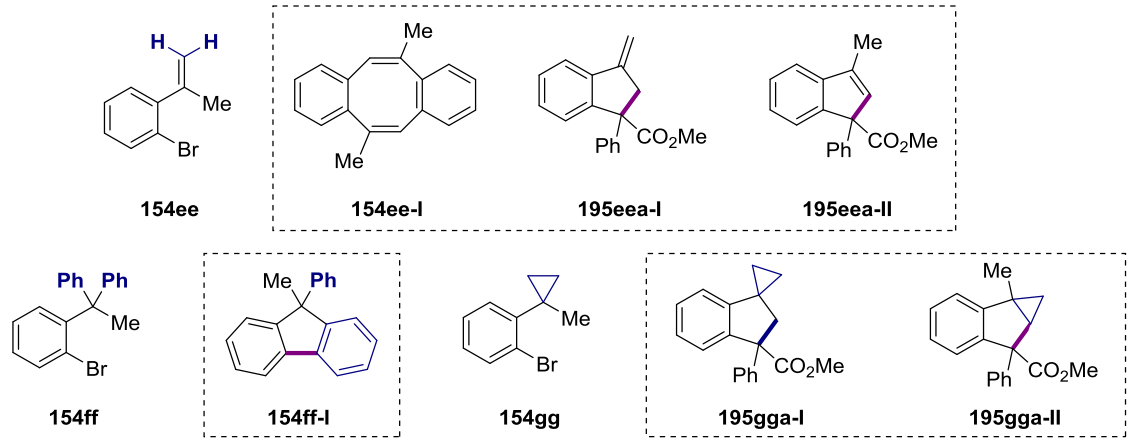

Figure 2.30. Unproductive substrates: part 2.

2.6.3 Mechanistic studies.

We postulated two distinctive mechanistic pathways, A and B (see Figure 2.31). In both cases, the reaction is initiated by oxidative addition of palladium(0) **LIX** over the aryl bromide **154**, providing intermediate **LX**, where the bromide ion has been replaced by the pivalate anion. At this point, both mechanisms diverge. In mechanism A, cyclometalation of **LX** forms **XLVII**, which would react with diazo compound **175** to form complex **LXI**. Subsequent migratory insertion of the aryl or alkyl group followed by reductive elimination would lead to the formation of product **195** together with the recovered palladium(0) catalyst. On the other hand, **LX** could first react with diazo compound **175** to form complex **LXIII**, which after aryl migration, would afford palladium complex **LXIX**. Next, cyclopalladation followed by final reductive elimination would release **195** while recovering the active catalyst.

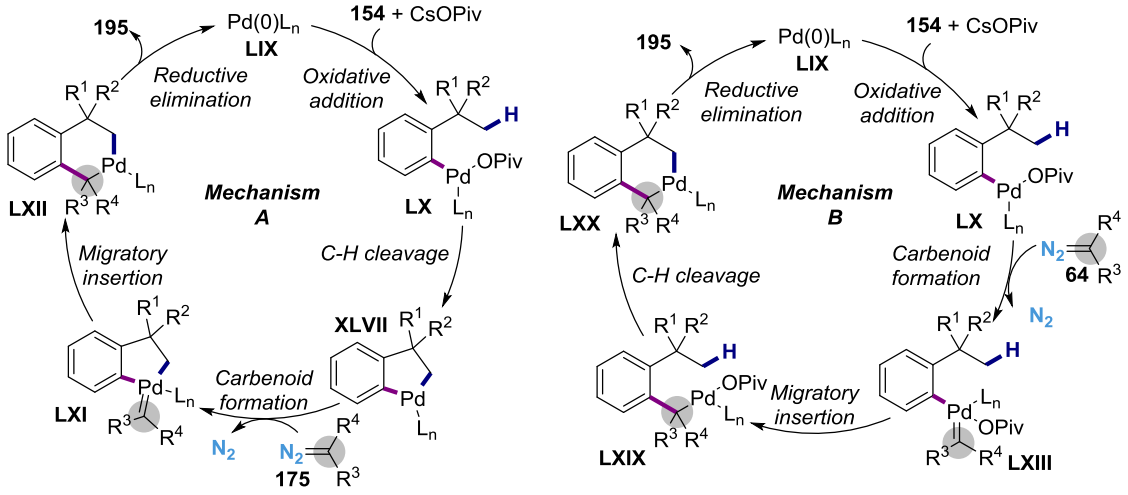

Figure .31. Considered catalytic cycles for the synthesis of indanes.

2.6.3.1 Putative activity of palladacycles-XLVII

In order to shed light onto the mechanism, we turned our attention to the isolation of some putative reaction intermediates. Therefore, the synthesis of palladacycle **XLVII** was attempted since related complexes have already been reported.[104] To such end, palladacycle **XLVII-DCEphos** and **XLVII-Phanephos**[150] were prepared from a variation of the reported

[150] Formed from (S)-Phanephos.

procedure.[151] Both complexes were synthesized since **XLVII-DCEphos** could not be fully characterized by NMR due to its poor solubility; however, **XLVII-Phanephos** was considerably more soluble and could be fully characterized.[152]

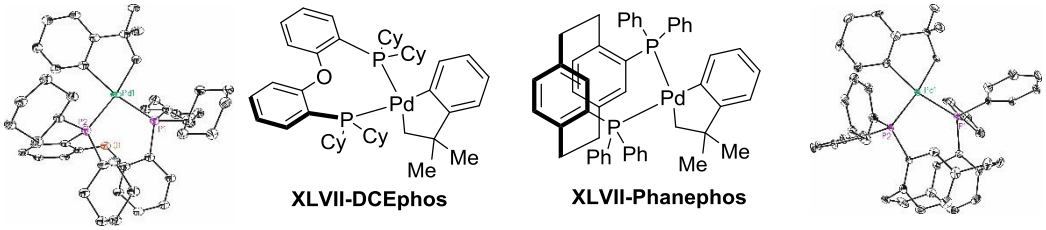

Figure 2.32. Palladacycles **XLVII-Ligand**. X-Ray structure.

Importantly, both palladacycles could be characterized by X-Ray diffraction. Both structures present a palladium atom adopting a slightly distorted square planar geometry. The bite angles $\widehat{P1PdP2}$ of both structures are almost identical whereas $\widehat{C1PdC4}$ slightly differs in 1.3º. The distance $\overline{C1C4}$ is 2.675Å and 2.578Å for DCEphos and Phanephos respectively. Interestingly, the distance between palladium and the carbon atom allowed us to determine that the *trans* influence[153] of the alkyl motif is higher than the one of the aryl ligand in all cases.

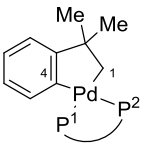

Ligand	$\widehat{C1PdC4}$ (º)	$\widehat{P1PdP2}$ (º)	$\overline{C1C4}$ (Å)	$\overline{PdP1}$ (Å)	$\overline{PdP2}$ (Å)	$\overline{PdC1}$ (Å)	$\overline{PdC4}$ (Å)
DCEphos	77.9	101.33	2.675	2.388	2.342	2.143	2.087
Phanephos	76.6	101.73	2.578	2.3944	2.3626	2.087	2.069
PMe_3	77.4	98.3	---	2.341	2.310	2.08	2.04

Table 2.12. Selected bond distances and angles for palladacycles-**XLVII-Ligand**.

Once synthesized and fully characterized, palladacycle **XLVII-Phanephos** was tested under the reaction conditions to study its possible role as a competent intermediate (Figure 2.33). Firstly, it was examined under catalytic conditions and, indeed, catalytic activity was achieved (57%) which could be improved (77%) in the presence of additional ligand, indicating that the addition of an excess of ligand prevents catalyst decomposition (see Figure 2.32). However, these results are not conclusive enough to demonstrate the intermediacy of such type of palladacycles in the reaction, as the *in situ* decomposition of the palladacycle might form other competent active catalyst. Therefore, we decided to test its activity under stoichiometric conditions.

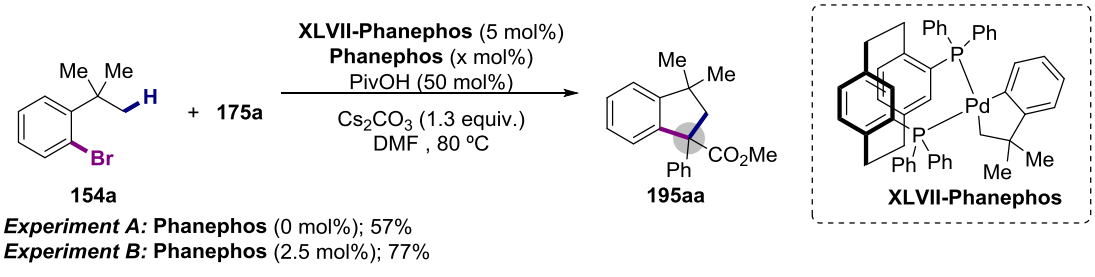

Figure 2.33. Catalytic experiments with **XLVII-Phanephos**.

[151] See the Experimental Section for further details.
[152] (S)-Phanephos behaves similarly to DCEphos under standard conditions (>99%, 83% yield).
[153] Appleton, T. G.; Clark, H. C.; Manzer, L. E. *Coord. Chem. Rev.* **1973**, *10*, 335.

Under stoichiometric conditions, two different experiments were performed. In experiment A (Figure 2.34), a solution of complex **XLVII-Phanephos** in DMF was heated at 80 ºC. Analysis of the reaction mixture by gas-chromatography showed quantitative formation of benzocyclobutane **153a** and traces of *tert*-butylbenzene (**196a**). On the other hand, in the presence of diazo compound **175a** (experiment B) the product **195aa** was obtained in quantitative yield. These two results explain the observation of benzocyclobutane **153a** during the optimization process as a consequence of direct reductive elimination from **XLVII-Phanephos**. Furthermore, the observed reduced starting material **196a** can be rationalized from the results of experiment A, although it could as well be obtained from the oxidative addition complex **LX**, most likely because of DMF. Importantly, experiment A validates Baudoin's mechanistic proposal for the synthesis of benzocyclobutanes via reductive elimination of type-**XLVII** palladacycles that was only supported by theoretical calculations.[110] The result from experiment B also indicate that pivalic acid and cesium carbonate are not playing a significant role in the catalytic cycle once palladacycle **XLVII** is formed. In fact, the formation of **195aa** from **XLVII-Phanephos** in the absence of pivalic acid is of utmost importance in order to rule out mechanism B (Figure 2.31). If pivalic acid would have been required, one might argue the protonation of the alkyl ligand on **XLVII-Phanephos** to reverse the cyclometalation leading to oxidative addition intermediate **LX**, which could then afford product **195aa** following the sequence shown in mechanism B. However, experiment B clearly indicates that **XLVII-Phanephos** is responsible for forming **195aa**.

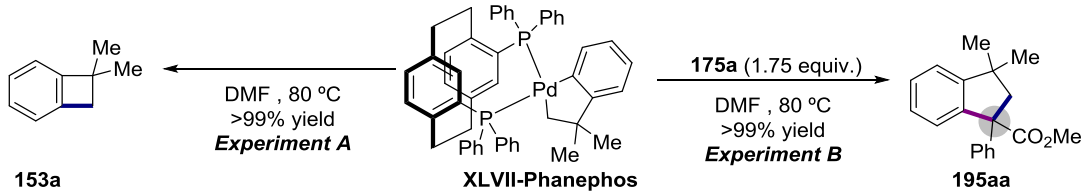

Figure 2.34. Stoichiometric experiments with **XLVII-Phanephos**.

2.6.3.2. Exploring the reversibility of the concerted metalation-deprotonation.

Next, we decided to shed light on the cyclometalation step. To such end, we prepared deuterated pivalic acid (PivOD) as it could afford indirect information concerning the reversibility of the concerted metalation-deprotonation step. We envisioned that, in a reversible concerted metalation-deprotonation scenario, hydrogen/deuterium scrambling would occur resulting in partial deuteration of the methyl and methylene positions of the product. Interestingly, deuteration was not observed in these positions, but 25% of deuterium incorporation at the *ortho* position of the *gem*-dimethyl unit was obtained (Figure 2.35). We postulated that palladacycle intermediate **XLVII** is selectively protonated in the reaction media resulting in the formation of neophyl palladium complex **LXXI-DCEphos** via formal [1,4]-palladium migration. Subsequently, this complex will form again palladacycle **XLVII** via concerted metalation-deprotonation with any of the two accessible C(sp^2)—H(D) bond.

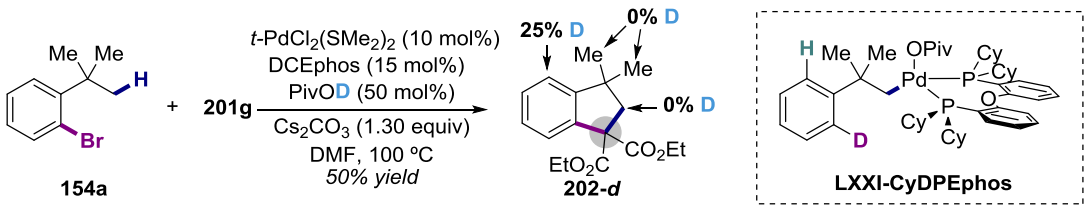

Figure 2.35. H/D scrambling experiments.

Actually, this [1,4]-palladium migration has already been reported in related works, such as the arylation or amination of *ortho-tert*-butylbromides published by Buchwald,[119] or in the work of Baudoin and co-workers[110] for the synthesis of benzocyclobutanes from aryl bromides and chlorides. In the latter case, in the presence of electron-withdrawing substituents at the *para* position of the halogen, two isomers were obtained as a consequence of the migratory event (Figure 2.36). In our case, the only substrate of the scope bearing a *para* substituent to the halogen was **154b** with a methyl. However, **154b** gave only one regioisomer as judged by NMR analysis of the crude reaction mixture. This result, however, is not totally unexpected: first, methyl substituents are relatively demanding in steric terms compared to fluorine or methoxy, which could impede the cyclometalation. Secondly, while fluorine and methoxy substituents are known to increase the acidity of the adjacent C—H bonds, methyl substituent exerts the opposite effect.

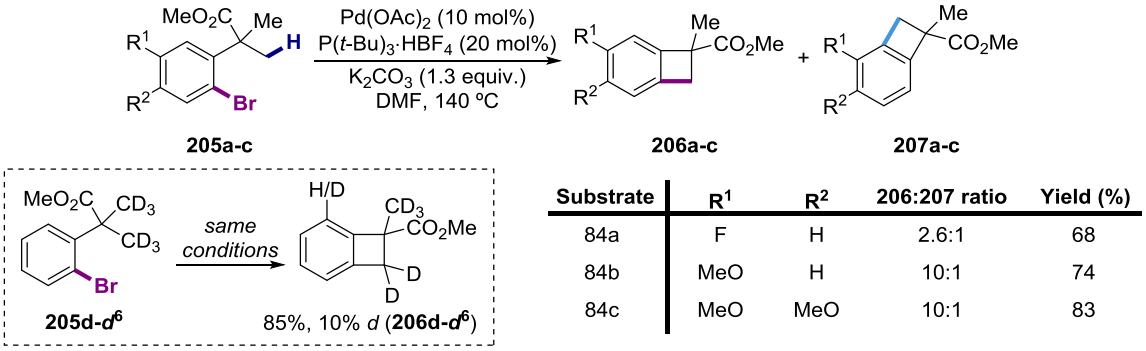

Substrate	R^1	R^2	206:207 ratio	Yield (%)
84a	F	H	2.6:1	68
84b	MeO	H	10:1	74
84c	MeO	MeO	10:1	83

Figure 2.36. [1,4]-palladium migration prevalence on the synthesis of benzocyclobutenes.

In order to further confirm the intermediacy of **LXXI-DCEphos** its synthesis was attempted. Despite all our efforts, we did not succeed in this matter. Nonetheless, related complex **LXXII** was synthesized and tested simulating the conditions during the catalytic cycle. We argued that under such conditions, **LXXI-DCEphos** would most likely be formed. Gas-chromatography analysis of the reaction crude showed quantitative formation of product **195aa**, thus implying the involvement of an intramolecular concerted metalation-deprotonation followed by carbenoid insertion (Figure 2.37). This experiment further supports our explanation for the hydrogen/deuterium scrambling experiment and, importantly, it also explains and validates Baudoin's hypothesis.[110-110]

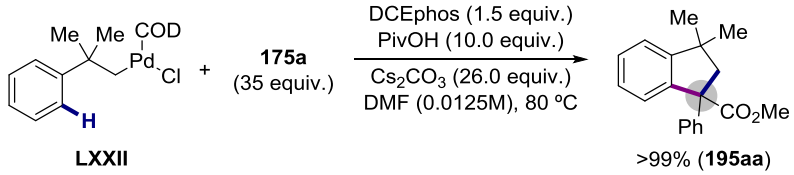

Figure 2.37. Stoichiometric experiments for the validation of [1,4]-palladium migration mechanism.

Finally, we studied the possible role of benzocyclobutane **153a** as an intermediate. Because of its high strain, the reinsertion of product **153a** into the catalytic cycle could be possible via oxidative addition of palladium(0) on the C—C bond[154] regenerating palladacycle **XLVII**. To such end, benzocyclobutane **153a** was tested under the reaction conditions (Figure 2.38).

[154] (a) Jun, C.-H. *Chem. Soc. Rev.* **2004**, *33*, 610. (b) Souillart, L.; Cramer, N. *Chem. Rev.* **2015**, *115*, 9410.

Careful examination of the crude mixture showed no product formation and starting material unaltered, thus ruling out the possibility of a reinsertion of product **153a** into the catalytic cycle. This result is not completely surprising since C—C bond activation on cyclobutanes and related molecules are restricted to activated biphenylenes and four-membered rings bearing a ketone functionality such as (benzo)cyclobutenones and (benzo)cyclobutenediones.

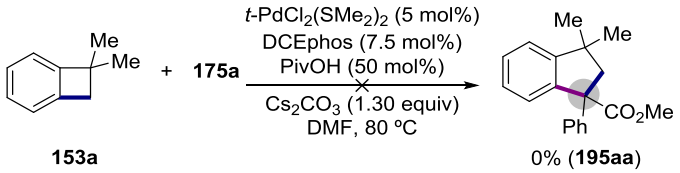

Figure 2.38. Studying the intermediacy of benzocyclobutene 46a.

2.6.4. Mechanistic rationale

Based on the previous experiments we suggested the following reaction pathway. The reaction is initiated by *in situ* reduction of palladium(II) to palladium(0)[155] in the presence of phosphine, pivalate and adventitious water, forming the corresponding phosphine oxide. This transformation has been widely studied by electrochemical methods, although mostly for $Pd(OAc)_2$ and triphenylphosphine.[156] Yet, other bidentate oxygenated ligands, such as trifluoroacetate and acetylacetonate, are also able to promote this reduction.[156] The same reactivity was reported by Hayashi[157] in the presence of bidentate BINAP forming palladium(0) with concomitant BINAP(O) formation. This report is highly interesting as it could suggest that, in our protocol, mono-oxidized DCEphos (DCEphos(O)) is the real ligand of the transformation. Indeed, recently, Blackmond and co-workers have reported the palladium/Xantphos-catalyzed C—H arylation of imidazoles, where mono-oxidized Xantphos results vital for the reactivity.[158] However, we considered unlikely the role of mono-oxidized DCEphos as ancillary ligand based on the results obtained during the optimization of the reaction (see Table 2.3). During the optimization of the palladium precatalyst, we observed that comparable yields were obtained with $Pd(OAc)_2$ and $Pd(dba)_2$ (80% and 77% respectively). The fact that palladium(0) precatalyst (where no DCEphos(O) is formed) gives a comparable yield as the palladium(II) precatalyst (reduced *in situ* with concomitant DCEphos(O) formation) could indicate that mono-oxidized DCPEphos is not playing an important role during the reaction. However, its role cannot be totally excluded.

[155] For a case where reduction to palladium(0) is promoted by a diazo compound see: Illa, O.; Rodríguez-García,; Acosta-Silva, C.; Favier, I.; Picurelli, D.; Oliva, A.; Gómez, M.; Branchadell, V.; Ortuño, R. M. Organometallics **2007**, *26*, 3306. We ruled out reduction to palladium(0) by **154a** based on the lack of the required α-hydrogens according to the reported mechanism.

[156] (a) Amatore, C.; Jutand, A. *Acc. Chem. Res.* **2000**, *33*, 314. (b) Amatore, C.; Jutand, A.; M'Barki, M. A. *Organometallics* **1992**, *11*, 3009. (c) Amatore, C.; Carré, E.; Jutand, A.; M'Barki, M. A. *Organometallics* **1995**, *14*, 1818. (d) Fors, B. P.; Krattiger, P.; Strieter, E.; Buchwald, S. L. *Org. Lett.* **2008**, *10*, 3505.

[157] Ozawa, F.; Kubo, A.; Hayashi, T. *Chem. Lett.* **1992**, *21*, 2177.

[158] Ji, Y.; Plata, R. E.; Regens, C. S.; Hay, M.; Schmidt, M.; Razler, T.; Qiu, Y.; Geng, P.; Hsiao, Y.; Rosner, T.; Eastgate, M. D.; Blackmond, D. G. *J. Am. Chem. Soc.* **2015**, *37*, 13272..

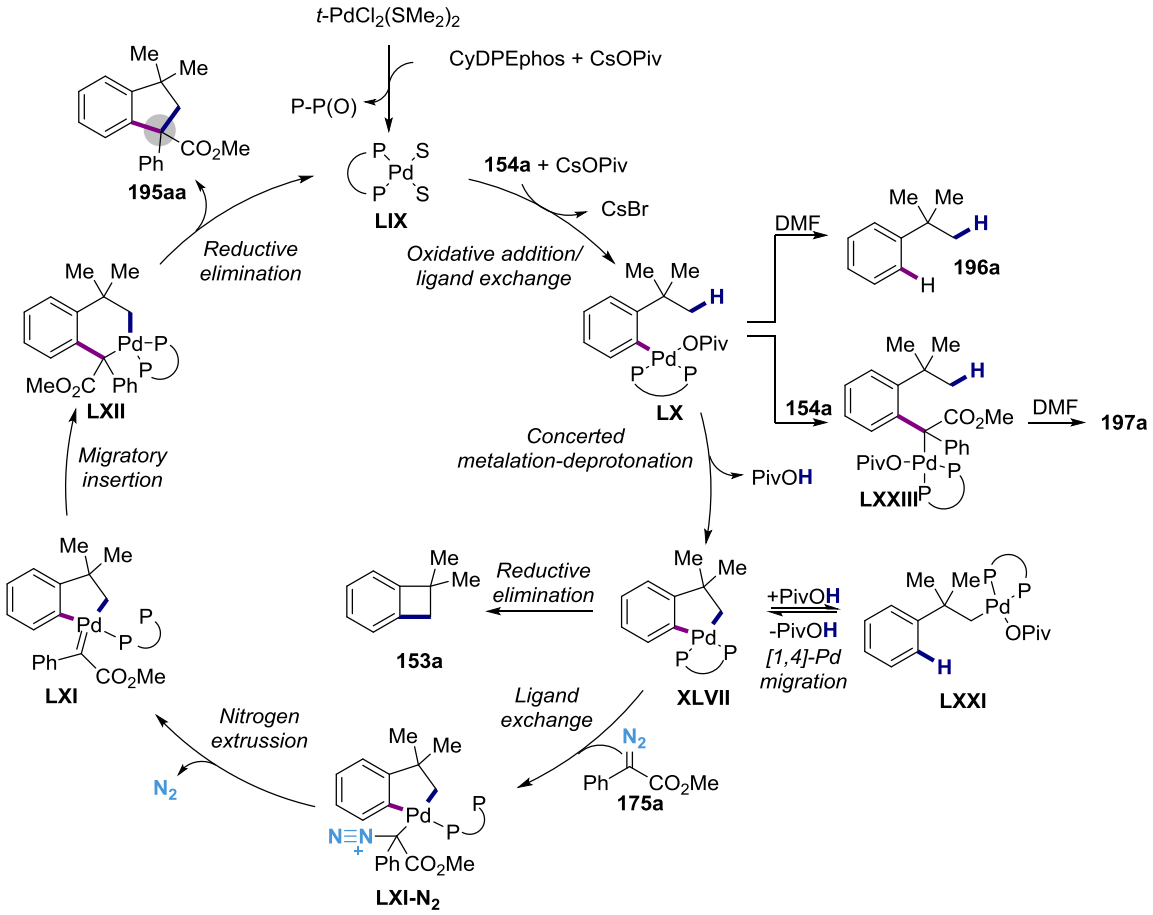

Figure 2.39. Mechanistic proposal.

Once the active species **LIX** are formed, it reacts with the aryl bromide **154a** to give the oxidative addition product that rapidly exchanges the bromide ion with pivalate.[83,85b,159] The resulting intermediate **LX** is likely responsible for the formation of debrominated starting material (**196a**). Most likely, the proton is coming from the solvent, as it has been demonstrated that aryl palladium(II) complexes are reduced under basic conditions in DMF.[160] Alternatively, intermediate **LX** can also react with diazo compound **175** which will form **LXXIII** after migratory insertion. This benzyl palladium complex will evolve towards the product of reductive insertion **197a**. The third possible outcome for intermediate **LX** is the metalation of the C(sp^3)—H bond via concerted metalation-deprotonation. Although the ongoing mechanism is not yet clear, there are two important facts: first, the pivalic acid plays a vital role in the reaction (see Table 2.10) and, consequently we propose a concerted metalation-deprotonation event. Second, the concerted metalation-deprotonation is not a reversible step as determined by the hydrogen/deuterium exchange experiment. However, the precise nature of this step is beyond our knowledge, and several possibilities might be considered as shown in Figure 2.40. It is generally accepted that the mechanism for a concerted metalation-deprotonation requires an open coordination site on the palladium center. In our particular case, with a bidentate phosphine several possibilities arise. First, we could considered a phosphine displacement trigger by a κ^1/κ^2 pivalate isomerization (**LXI** and **LXI-κ^2**). Indeed,

[159] Kefalidis, C. E.; Baudoin, O.; Clot, E. *Dalton Trans.* **2010**, *39*, 10528.
[160] De la Torre, J. A. M.; Espinet, P.; Albéniz, A. *Organometallics* **2013**, *32*, 5428.

ligand dissociation promoted by pivalate isomerization has been demonstrated in the case of monodentate phosphines by NMR analysis.[85b] Additionally, if DCEphos(O) is the true ligand for this transformation, we can postulate formation of **LXXIV** after oxidative addition, where the phosphine oxide is readily displaced by the coordinated pivalate anion via κ^1/κ^2 isomerization. Yet, one might argue that, if ligand dissociation is required, then, bidentate ligands should be inferior than monodentate phosphines, where the ligand dissociation is much faster. However this was not our case, and DCEphos proved to be considerably better than the monodentate analogue PCy_2Ph (see Table 2.1, entries 8 and 6 respectively). However, the fluxional nature of DCPEphos as a consequence of the Ar—O—Ar bond might confer certain hemilabile character to the ligand. Another possibility is the so-called ligandless concerted metalation-deprotonation event,[89] where the ligand is not playing any role and, therefore, its denticity does not become an issue (**LXXV**). Finally, it has been postulated by Maseras and Echavarren that concerted metalation-deprotonation mechanism in the presence of bidentate phosphines occurs in an intermolecular manner from a coordinatively unsaturated palladium(II) center (**LXXVI**).[161]

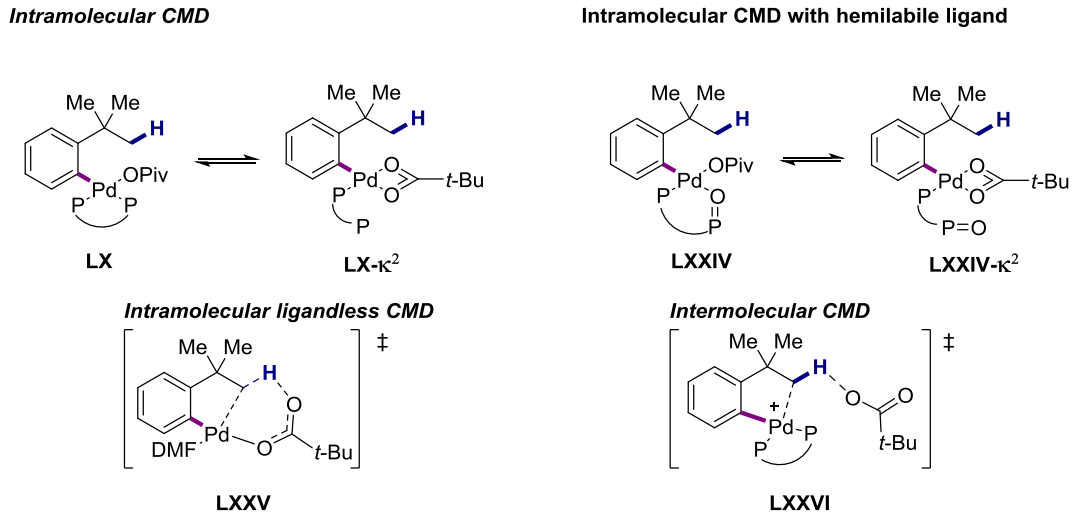

Figure 2.40. Putative relevant intermediates or transition state for the concerted metalation-deprotonation event.

Upon formation of palladacycle **XLVII**, three new possibilities arise, which has been previously demonstrated in stoichiometric reactions. First, palladacycle **XLVII** can reductively eliminate forming benzocyclobutane **153a** as reported by Baudoin[110] in catalytic reactions and by us previously in this manuscript in stoichiometric fashion (Figure 2.34, left). Importantly, we have demonstrated that benzocyclobutane formation is a dead end for our catalytic cycle (Figure 2.38). We have also proved by hydrogen/deuterium scrambling experiments (Figure 2.35) and stoichiometric reactions with compound **LXXII** (Figure 2.37) the existence of an equilibrium between palladacycle **XLVII** and its open form **LXXI**. Based on the absence of deuteration at the methyl or methylene position we concluded the irreversibility of the concerted metalation-deprotonation step, as well as a regiospecific protonation of **XLVII**. This result is in agreement with the work reported by Carmona and co-workers.[162] Furthermore, because of the hydrogen/deuterium scrambling we can conclude that the rate constant for the

[161] Pascual, S.; Mendoza, P.; Braga, A. C. C.; Maseras, F.; Echavarren, A. M. *Tetrahedron*, **2008**, *64*, 6021.
[162] Cámpora, J.; López, J. A.; Palma, P.; Valerga, P.; Spillner, E.; Carmona, E. *Angew. Chem. Int. Ed.* **1999**, 147.

equilibrium **XLVII** – **LXXI** is higher than the rate constant for the reaction with diazo compound **175**. Finally, palladacycle **XLVII** will progress towards the formation of **LXI** by nucleophilic attack of diazo compound followed by nitrogen extrusion.[163] The formation of compound **LXI** can be inferred from the results obtained when palladacycle **XLVII-Phanephos** was reacted with **175a** (Figure 2.34, right) obtaining quantitative yield of the product. The exact mechanism for **LXI** formation remains unclear for the same reason than for the concerted metalation-deprotonation. The general accepted mechanism for palladium carbenoid formation[164] involves the nucleophilic attack of the carbenic carbon from **175a** over the electrophilic palladium center, forming an intermediate of the type **LXI-N_2**, subsequently, donation of electron density form palladium will release nitrogen resulting in a Pd=C bond formation. However, in our system, the palladacycle **XLVII** is coordinatively saturated by two reactive ligands (aryl and alkyl motifs) and the two phosphines from DCEphos. There are two possibilities for this transformation. First, a dissociative mechanism where a phosphine would leave the inner coordination sphere of the palladium atom generating a vacant position, and facilitating the attack of **175**. The second alternative is an associative mechanism[165] where the nucleophilic carbenic carbon would interact with the empty and perpendicular p_Z orbital of the palladium forming a pentacoordinated intermediate which would liberate a coordinated phosphine to recover the square planar geometry. Among these two options, the last one seems more likely as the formation of a tricoordinated palladium intermediate in the presence of a chelating bidentate phosphine is highly unlikely. Furthermore, it has been reported that insertion of sulfur dioxide into palladacycles of type **XLVII** occurs via pentacoordinated palladium intermediate with a molecule of SO_2 coordinated to the palladium center (Scheme 2.5).[104]

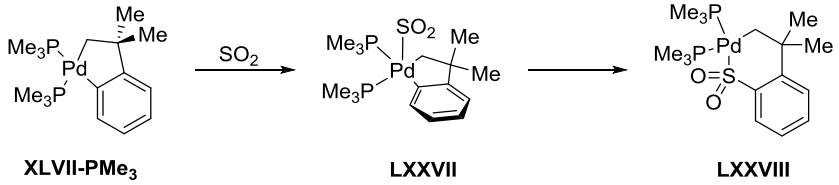

Scheme 2.5. SO_2 insertion into palladacycle **XLVII**.

The product obtained upon reaction with diazo compound will afford complex **LXI** with two possible configurations; the aryl and the phosphine in relative *cis* position to each other (**LXI-I**), or the aryl and the phosphine *trans* to each other (**LXI**). Although speculative, the higher *trans* influence[166] of the alkyl ligand might favor **LXI** preferentially. In addition, we cannot rule out an isomerization between the two products shifting the equilibrium towards the thermodynamic product.

[163] For related reported palladium-carbenoids see: (a) Oulié, P.; Nebra, N.; Saffon, N.; Maron, L.; Martin-Vaca, B.; Bourissou, D. *J. Am. Chem. Soc.* **2009**, *131*, 3493. (b) Schuster, O.; Raubenheimer, H. G. *Inorg. Chem.* **2006**, *45*, 7997. (c) Taubmann, C.; Öfele, K.; Herdtweck, E.; Herrmann, W. A. *Organometallics*, **2009**¸ *28*, 4254.

[164] (a) Straub, B. F. *J. Am. Chem. Soc.* **2002**, *124*, 14195. (b) Ye, F.; Qu, S.; Zhou, L.; Peng, C.; Wang, C.; Cheng, J.; Hossain, M. L.; Liu, Y.; Zhang, Y.; Wang, Z.-X.; Wang, J. *J. Am. Chem. Soc.* **2015**, *137*, 4435.

[165] Anderson, G. K.; Cross, R. J. *Chem. Soc. Rev.* **1980**, *9*, 185.

[166] *Trans* influence is a thermodynamic term and it does not always correlates with the kinetic *trans* effect, that is the true responsible of the selectivity. The reader is encourage to keep its skepticism about this statement.

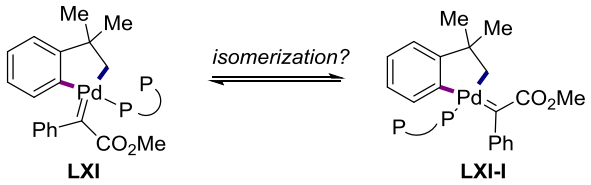

Figure 2.41. Geometrical isomers of compound **LXI**.

After generation of **LXI**, 1,2-migratory insertion occurs[164b,167] to form the six-membered palladacycle XVIII. Whether the preferred migrating group is the aryl or the alkyl substituent is uncertain and it will be highly dependent on which isomer (**LXI** or **LXI-I**) is preferentially formed as the migrating group has to be *cis* to the carbenic substituent. Based on previous results reported by Carmona (see Scheme 2.5) concerning the insertion of sulfur dioxide or alkynes into type-**XLVII** palladacycles, we fashioned a carbenoid insertion into the Pd—aryl bond rather than the Pd—alkyl bond, thus forming intermediate **LXII**.

To close the catalytic cycle, a final reductive elimination from **LXII** releases product **195aa** while recovering the active catalyst. We expect a relatively easy reductive elimination, as it is known that reductive elimination is favored between fragments with pairing electronic character,[168] therefore, in our case where two alkyl fragments of different nature are present, it might be favored. Furthermore, bidentate ligands with large bite angle also promote a more efficient reductive elimination because of a smaller $\widehat{CPdC}$ angle and a $\widehat{PPdP}$ close to linearity. However, a study of the ligand bite angle with electronically-related ligands during early optimization studies showed no evident relationship between this property and reaction yield (Figure 2.42). Although tentative, we believe that reductive elimination is not rate-determining because of the lack of relationship between the bite angle[169] and reactivity. Finally, it must be considered that this set of ligands is considerably different from electron-rich DCEphos and, consequently, the rate-limiting step can vary when using DCEphos or Xanthpos type ligands.

[167] Xia, y.; Qu, S.; Xiao, Q.; Wang, Z.-X.; Qu, P.; Chen, L.; Liu, Z.; Tian, L.; Huang, Z.; Zhang, Y.; Wang, J. *J. Am. Chem. Soc,* **2013**, *135*, 13502.
[168] (a) Hartwig, J. F. *Inorg. Chem.* **2007**, *46*, 1936. (b) Culkin, D. A.; Hartwig, J. F. *Organometallics* **2004**, *23*, 3398.
[169] (a) Birkholz, M.-N.; Freixa, Z.; van Leeuwen, P. W. N. M. *Chem. Soc. Rev.* **2009**, *38*, 1099. (b) Dierkes, P.; van Leeuwen, P. W. N. M. *J. Chem. Soc. Dalton Trans.* **1999**, 1519.

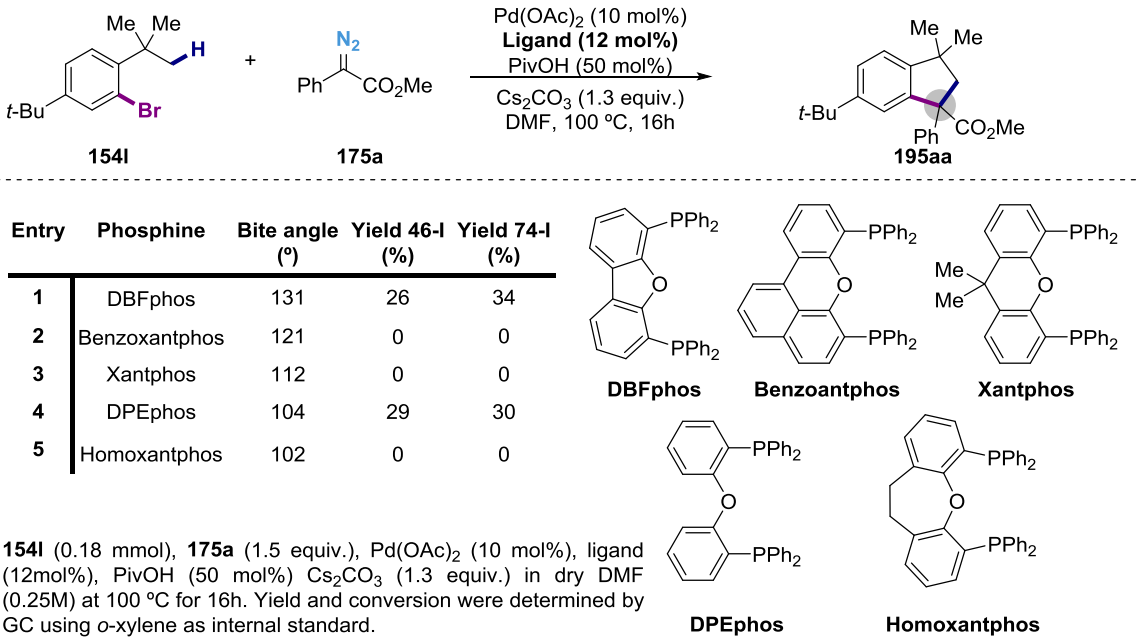

Entry	Phosphine	Bite angle (º)	Yield 46-l (%)	Yield 74-l (%)
1	DBFphos	131	26	34
2	Benzoxantphos	121	0	0
3	Xantphos	112	0	0
4	DPEphos	104	29	30
5	Homoxantphos	102	0	0

154l (0.18 mmol), **175a** (1.5 equiv.), $Pd(OAc)_2$ (10 mol%), ligand (12mol%), PivOH (50 mol%) Cs_2CO_3 (1.3 equiv.) in dry DMF (0.25M) at 100 ºC for 16h. Yield and conversion were determined by GC using *o*-xylene as internal standard.

Figure 2.42. Bite angle influence on the reaction outcome.

To conclude, it is worth noting that no enantiocontrol was achieved during this transformation in the presence of chiral phoshines. Indeed, reaction of diazo compound **175a** with palladacycle **XLVII-Phanephos**, containing (S)-Phanephos gave only racemic product 74aa. This results are in line with the lack of diastereocontrol for products **195na** and **195ra** (Figure 2.27). We suggest that the enantioselective-determining step is the migratory insertion or the carbenoid formation. The lack of enantiocontrol could therefore be explained on the basis of a loss of chirality information when the bidentate ligand becomes monodentate, as the ligand planar chirality will only manifest intensively in the chelate form. The lack of diastereocontrol can be also explained for the loss of chiral information during the concerted metalation-deprotonation, for the same reasons previously explained.

2.6.5 Conclusion

To summarize, we have developed a novel transformation that allows the synthesis of quaternary carbons by a combination of non-activated C(sp^3)—H bonds and diazo compounds. This is the first time that diazo compounds have been employed in a coupling event with unactivated C(sp^3)—H bonds. Importantly, the bivalent carbenic carbon becomes quaternary in a tandem inter/intramolecular transformation by reaction with two different carbon atoms. The transformation shows an excellent selectivity towards indane formation in lieu of benzocyclobutane formation, or reductive insertion products. The chemoselectivity profile was excellent in both diazo compounds and aryl bromides. However, limitations such as the absence of electron-donating groups in the diazo compound or the exclusivity of α-diazoesters should be taken into consideration for future aspects of this chemistry. Regarding the aryl bromide, only quaternary alkyl substituents worked under the reaction conditions thus limiting the preparative scope. Unfortunately, no diastereoselection was achieved and any attempt of enantiocontrol resulted unsuccessful.

We have achieved enough empirical evidences to propose a catalytic cycle, yet, there are still many features that remain elusive and a deeper mechanistic study would be necessary to

address all the open questions. Probably, DFT studies will be necessary to answer the most difficult questions such as the particular mechanism of the concerted metalation-deprotonation, the carbenoid formation and the migratory insertion. It is important ro mention that the reactivity found in this reaction opens up a new research line where different bivalent reagents could be used in combination with aryl bromides such as carbon and sulfur dioxide, carbon monoxide, alkynes, alkenes, isocyanides, etc. for the synthesis of molecules with added value.

Chapter 3. Palladium-catalyzed intramolecular acylation of aryl chlorides via aldehydic C(sp^2)—H bond cleavage.

3.1 Introduction.

Although the use of aldehydes for the synthesis of ketones under transition-metal catalysis has been widely explored via the well-known hydroacylation of alkenes and alkynes[170](Scheme 3.1), the synthesis of aryl ketones remains rather unexplored. This is somewhat surprising, as the use of aldehydes would avoid the use of highly toxic carbon monoxide[171] or other surrogates,[172] therefore increasing the reaction efficiency.

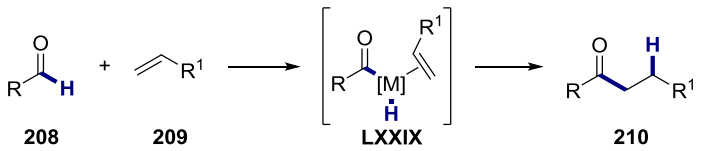

Scheme 3.1. General scheme for the intermolecular hydroacylation of alkenes

3.1. Aldehydic C(sp^2)—H bond arylation of aldehydes.

At present, there are three different approaches for converting aldehydes into aryl ketones involving the use of metal catalysts. Still, not all of these approaches can be classified as a truly aldehydic C(sp^2)—H bond functionalization event as some of them are a formal aldehydic C—H bond functionalizations and others involve outer-sphere mechanisms.[173]

3.1.1 Heck-type reactivity

Beyond any reasonable doubt, the most widely method for the oxidative functionalization of aldehydes towards the synthesis of aryl ketones is via Heck-type processes. The mechanism consists of the insertion of an *in situ* generated organometallic reagent motif across the polar C—O double bond of the aldehyde or corresponding surrogate. Subsequently, the formed alkoxy metal complex will render the product after a β-hydride elimination event. Although, this method does not go via the formation of an acyl metal complex, it will be treated in this section as formally constitutes an acyl-bond functionalization.

This strategy can be divided into three categories depending on the approach taken for the preparation of complex **LXXX**. It can be formed either by transmetallation between the transition metal catalyst (MX_2) and a more reactive organometallic compound **211** (i.e. Grignard reagents, organolithium compound, boronic acids, etc). Alternatively, complex **LXXX** can be formed by oxidative addition of the transition metal catalyst (M) over a reactive C—X bond (X = leaving group, **212**), such as aryl halides or pseudohalides or by C—H bond functionalization (**213**) allowing for a much more straightforward approach (see Figure 3.1).

[170] (a) Willis, M. C. *Chem. Rev.* **2010,** *110,* 725. (b) Leung, J. C.; Krische, M. J. *Chem. Sci.* **2012,** *3,* 2202.
[171] (a) Brennführer, A.; Neumann, H.; Beller, M. **2009**, *48*, 4114. (b) Wu, X.-F.; Neumann, H.; Beller, M. *Chem. Rev.* **2013**, *113*, 1.
[172] Gautam, P.; Bhanage, B. M. *Catal. Sci. Technol.* **2015**, *5*, 4663.
[173] For two reports proposing two alternative, yet not fully demonstrated mechanisms see: (a) Tang, B.-X.; Song, R.-J.; Wu, C.-Y.; Liu, Y.; Zhou, M.-B.; Wei, W.-T.; Deng, G.-B.; Yin, D.-L.; Li, J.-H. *J. Am. Chem. Soc.* **2010**, *132*, 8900. (b) Lee, H.; Yi, C. S. *Eur. J. Org. Chem.* **2015**, 1899.

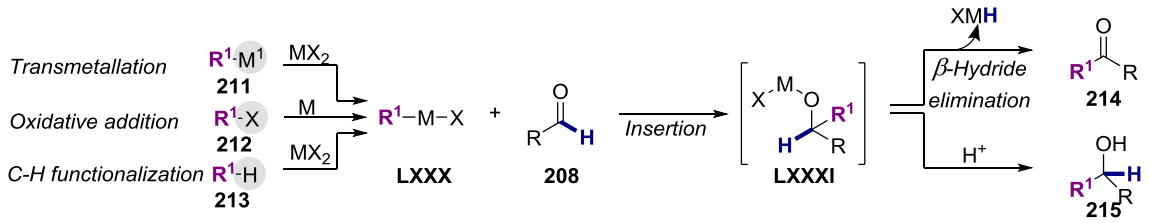

Figure 3.1. Functionalization of aldehydes for the synthesis of ketones. Heck-type mechanism.

3.1.1.a. Heck-type mechanism inititated by transmetallation.

The first report for a Heck-type mechanism was described by Hirao's group,[174] although in a stoichiometric fashion. The reaction consisted of the addition of *in situ* generated organovanadium compound **LXXXII** to an aldehyde **208**. Interestingly, work-up at -78 ºC gave the secondary alcohol **215** as the only product. However, the selectivity of the process could be reversed upon heating the complex **LXXXIII**, forming ketone **214**. This finding supported a mechanism involving a migratory insertion/β-hydride elimination sequence. Furthermore, upon heating independently prepared **LXXXIII**, ketone **214** was exclusively formed, thus corroborating the proposed mechanistic scenario.

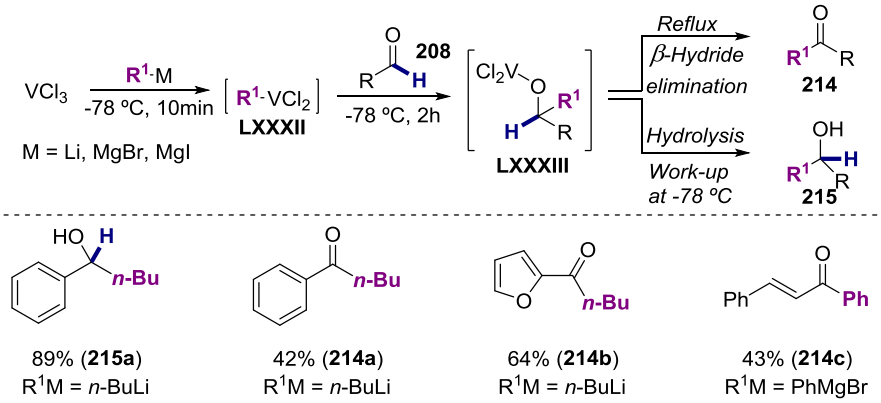

Figure 3.2. Addition of organovanadium reagents to aldehydes towards the synthesis of ketones.

Prompted by the seminal discovery of Hirao, several groups have described alternative methods using less-reactive organometallic compounds.

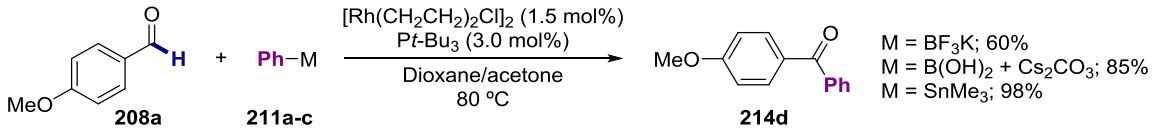

Scheme 3.2. Formal functionalization of aldehydic C-H bonds with aryl boronic acids under rhodium(I) catalysis.

[174] Hirao, T.; Misu, D.; Agawa, T. *J. Am. Chem. Soc.* **1985**, *107*, 7179.

The group of Genet described the rhodium-catalyzed oxidative functionalization of aldehydic C—H bonds with boronic acids, trifluoroborates and organostananes (**211a-c**)[175] for the synthesis of diaryl ketones (Scheme 3.2). Notably, the presence of acetone as co-solvent was mandatory to avoid undesired formation of **215** (Figure 3.3). Deuterium labelling experiments as well as reaction monitoring pointed towards a tandem mechanistic scenario. Although quantitative formation of carbinol **215** occurs as determined by analysis of the crude reaction mixture, sampling at longer reaction times showed slow decay of carbinol **215** with concomitant formation of ketone **214**. The authors proposed a mechanistic scenario initiated by transmetalation of the rhodium catalyst **LXXXIV** with the organometallic compound **211**, forming the aryl rhodium(I) complex **LXXX**. Then, upon coordination of **208** and migratory insertion, alcoxo-rhodium complex **LXXXI** is formed which will render carbinol **215** upon reaction with adventitious water.[176] Next, carbinol **215** will react with complex **LXXXIV** regenerating the alcoxo—rhodium complex **LXXXI** that after a β-hydride elimination step will yield the final product **214** along with rhodium(I) hydride (**LXXXV**). At this point, acetone will react with the rhodium(I)-hydride complex regenerating complex **LXXXIV**. The presence of acetone is of utmost importance as it is the responsible of avoiding the undesired formation of carbinol **215**,[177] as well as for obtaining good turnover-numbers.

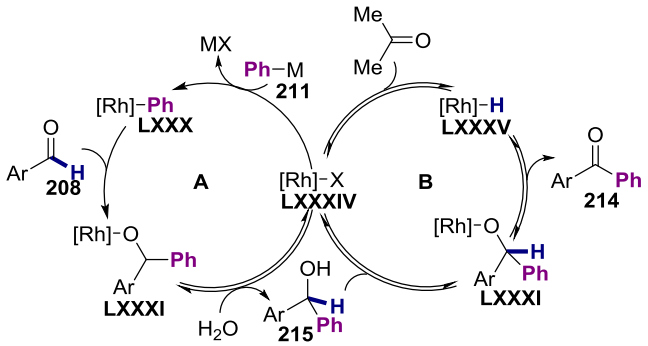

Figure 3.3. Tentative mechanism for the synthesis of ketones via rhodium-catalyzed acylation reaction.

The group of Jun reported a related reaction using aldimines as aldehyde surrogates. After ruthenium-catalyzed[178] cross-coupling with boronic acid **217**, ketamine **218** was formed which rendered the ketone **214e** upon acidic work up. The provided data was not sufficient to clearly point towards a Heck-type mechanism instead of a pyridine directed ruthenium(0) oxidative addition on the aldehydic C—H bond (Scheme 3.3).

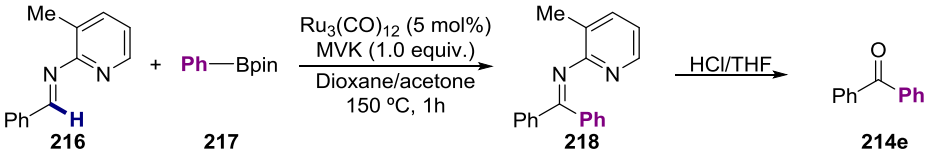

[175] (a) Pucheault, M.; Darses, S.; Genet, J.-P. *J. Am. Chem. Soc.* **2004**, *126*, 15356. (b) Mora, G.; Darses, S.; Genet, J.-P. *Adv. Synth. Catal.* **2007**, *349*, 1180. (c) Chuzel, O.; Roesch, A.; Genet, J.-P.; Darses, S. *J. Org. Chem.* **2008**, *73*, 7800.

[176] The authors propose water generationn by formation of boroxines upon boronic acid condensation, furthermore, in some cases water was employed as cosolvent.

[177] For an elegant mechanistic study see: Krug, C.; Hartwig, J. F. *J. Am. Chem. Soc.* **2002**, *124*, 1674.

[178] For a stoichiometric insertion of a ruthenium complex across an aldehydic C—O double bond see: Hartwig, J. F.; Andersen, R. A.; Bergman, R. G. *J. Am. Chem. Soc.* **1989**, *111*, 2717.

Scheme 3.3. Ruthenium-catalyzed acylation of arylboronates with aldimines.

3.1.1.b. Heck-type mechanism initiated by oxidative addition.

In contrast with section 3.1.1.a, Heck-type mechanisms can be also accomplished via the *in situ* generation of organometallic reagents by oxidative addition. Chen and co-workers described the nickel-catalyzed acylation of aryl iodides with aldehydes (Figure 3.4).[179] Although the mechanism was not studied in detail, the authors suggested a Heck-type mechanism as the most likely scenario. Few years later, a related work was published using palladium catalysts in combination with a chelating heterobidentate hemilabile ligand.[180] Surprisingly, no α-arylation of the starting aldehyde was observed (**219**) under reaction conditions being the acylation product **214f** exclusively formed (Figure 3.4). This example must be carefully considered as the only evidence towards a Heck-type mechanism is the observation of a palladium hydride by ^{1}H-NMR spectroscopy. Indeed, the authors claimed that only aldehydes with α-hydrogens are active under reactions conditions; therefore, a different mechanistic scenario could be operating.

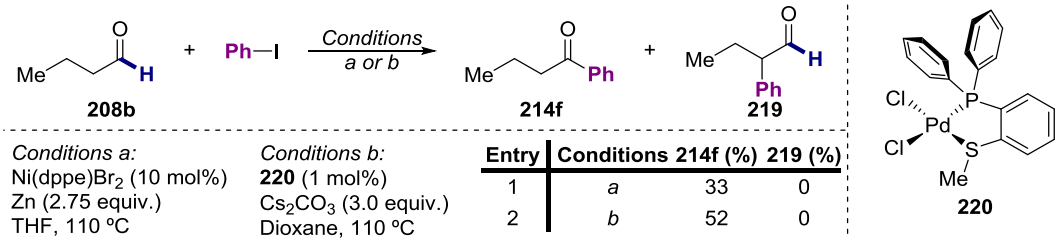

Figure 3.4. Nickel- and Palladium-catalyzed acylation of aryl iodides with aldehydes.

The palladium-catalyzed intermolecular acylation of aryl iodides with aldehydes was described by Solé.[181] Mechanistic studies based on DFT calculations suggested a Heck-type mechanism (insertion/β-hydride elimination) as the ongoing pathway. In a related work, the group of Hartwig achieved the synthesis of ketones from aldimines **221** with aryl iodides under rhodium catalysis.[182] The formed ketamine product **222** yielded the corresponding ketones upon acidic work up (scheme 3.4).

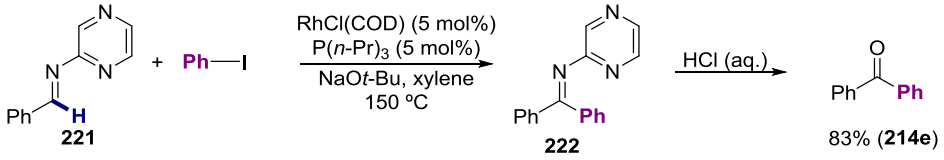

Scheme 3.4. Rhodium-catalyzed formal arylation of aldehydic C—H bonds.

In this case, more mechanistic evidences were gathered by isolation of reaction of intermediates and by studying the outcome of stoichiometric reactions (Scheme 3.5).[183] The authors were able to demonstrate the feasibility of the insertion of the aryl rhodium complex **223** across the C—N double bond of the aldimine **221a** forming the amido rhodium complex

[179] Huang, Y.-C.; Majumdar, K. K.; Cheng, C.-H. *J. Org. Chem.* **2002**, *67*, 1682.
[180] Saikia, K.; Dutta, D. K. *J. Mol. Catal. A. Chem.* **2015**, *408*, 20.
[181] Solé, D.; Mariani, F.; Fernández. I.; Sierra, M. A. *J. Org. Chem.* **2012**, *77*, 10272.
[182] Ishiyama, T.; Hartwig, J. *J. Am. Chem. Soc.* **2000**, *122*, 12043.
[183] Krug, C.; Hartwig, J. F. *J. Am. Chem. Soc.* **2004**, *126*, 2694.

224. Subsequent thermolysis gave a mixture of ketamine **222a** formed via β-hydride elimination along with the secondary amine **225**.

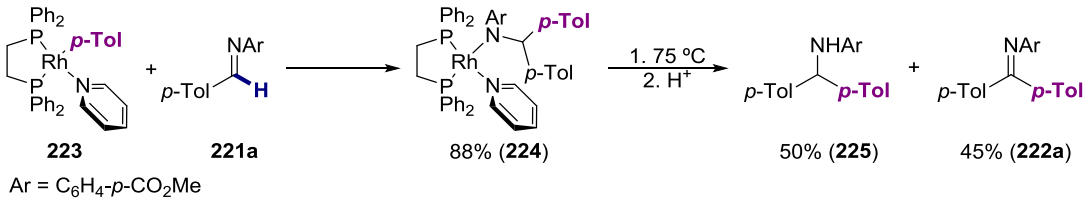

Scheme 3.5. Stoichiometric studies for the rhodium-catalyzed acylation of via formal functionalization aldehydic C—H bonds.

An elegant related transformation was reported by Xiao and co-workers.[184,185] Their strategy relies on the *in situ* formation of an enamine (**226**) by condensation of the starting aldehyde with pyrrolidine. Next, the organometallic compound formed upon oxidative addition of the metal catalyst on the aryl halide inserts across the electron-rich enamine double bond placing the aryl ligand in α-position to the heteroatom while the palladium catalyst is positioned at the β-position (**LXXXVI**). Finally, β-hydride elimination will form product **227** that will be transformed into the corresponding ketone upon hydrolysis.

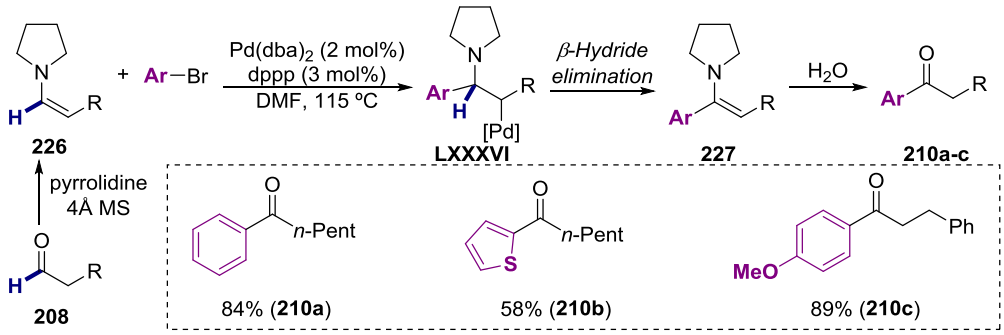

Figure 3.5. Acylation of aryl bromides via enamine intermediates.

3.1.1.c. Heck-type mechanism based on a catalytic dehydrogenative cross-coupling.

This last approach relies on metalation of the substrate (**228**) via C—H cleavage that will further react with the aldehyde in a Heck-type fashion. The advantages of this approach are obvious and have been previously reviewed in this dissertation. However, a directing group must be always present to achieve the desired reactivity, thus limiting the preparative scope of the transformation. Surprisingly, there are only a few methods in this regard. Yet, different directing groups can be employed under palladium[186] and rhodium catalysis[187] (Figure 3.6)

[184] (a) Ruan, J.; Saidi, O.; Iggo, J. A.; Xiao, J. *J. Am. Chem. Soc.* **2008**, *130*, 10510. (b) Ruan, J.; Xiao, J. *Acc. Chem. Res.* **2011**, *44*, 614 and references therein.
[185] For similar transformation reported by other groups see: (a) Adak, L.; Bhadra, S.; Ranu, B. *Tetrahedron Lett*. **2010**, *51*, 3811. (b) Zanardi, A.; Mata, J. A.; Peris, E. *Organometallics* **2009**, *28*, 1480.
[186] Jia, X.; Wang, Zhang, S.; Wang, W.; Luo, F.; Cheng, J. *Org. Lett.* **2009**, *11*, 3120.
[187] (a) Park, J.; Park, E.; Kim, A.; Lee, Y.; Chi, K.-W.; Kwak, J. H.; Jung, Y. H.; Kim, I. S. *Org. Lett.* **2011**, *13*, 4390. (b) Zhou, B.; Yang, Y.; Li, Y. *Chem. Commun.* **2012**, *48*, 5163.

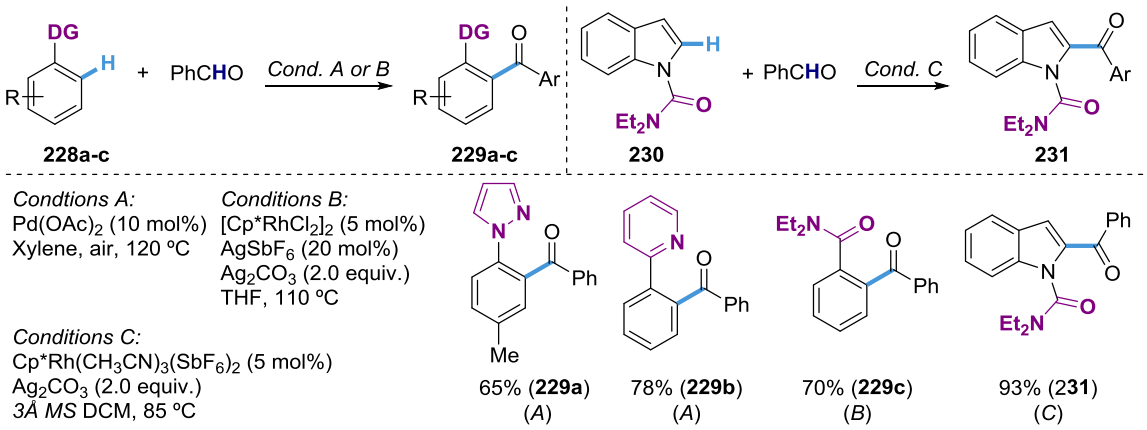

Figure 3.6. Aryl/aldehyde catalytic dehydrogenative coupling.

3.1.2. Acyl radical mediated catalyst oxidation

A second approach towards the oxidative functionalization of aldehydes is based on the formation of an acyl metal complex in high oxidation state by formation of an acyl radical.[188] This approach consists of a catalytic dehydrogenative cross-coupling between aryl compounds featuring a directing group (**228**) and an aldehyde in the presence of a peroxide that will trigger the acyl radical formation upon homolysis under thermal conditions.[189] Next, the cyclometalated intermediate **LXXXVII** will result oxidized by the previously formed acyl radical **232** forming the acyl cyclometalated intermediate **LXXXVIII** in a high oxidation state which will be prone to reductively eliminate, forming the product **229** while recovering back the active catalyst (Figure 3.7).

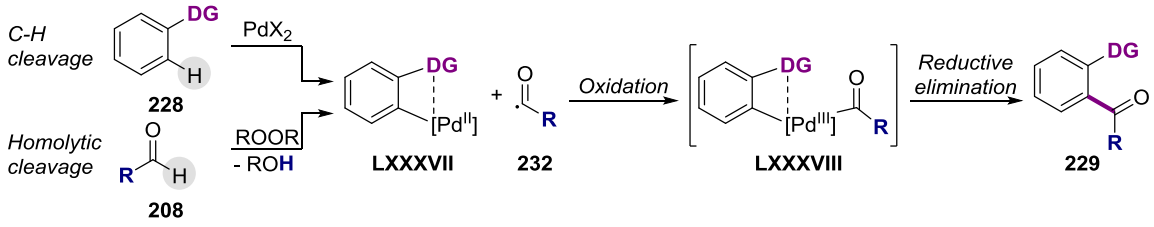

Figure 3.7. Putative mechanism for catalytic dehydrogenative cross-couplings under radical conditions.

Li and co-workers developed a palladium-catalyzed acylation of 2-phenylpryridines or benzoquinoline **228d** with aromatic and aliphatic aldehydes in the presence of *tert*-butylhydroperoxide (Scheme 3.6).[190,191] The authors proposed a mechanism similar to the one

[188] Chatgilialoglu, C.; Crich, D.; Komatsu, M.; Ryu, I. *Chem. Rev.* **1999**, *99*, 1991.
[189] It has been demonstrated that formation of acyl radicals is a rapid phenomenon in the presence of electrophilic abstracting radicals. Furthermore, the formation of acyl radicals by oxygen-centered radicals is considered as the cleanest method to generate them. See ref. 188.
[190] Baslé, O.; Bidange, J.; Shuai, Q.; Li, C.-J. *Adv. Synth. Catal.* **2010**, *352*, 1145.
[191] For related transformations see: (a) Chan, C.-W.; Zhou, Z.; Chan, A. S. C.; Yu, W.-Y. *Org. Lett.* **2010**, *12*, 3926. (b) Wu, Y.; Li, B.; Mao, F.; Li, X.; Kwong, F. Y. *Org. Lett.* **2011**, *13*, 3258. (c) Shin, Y.; Sharma, S.; Mishra, N. K.; Han, S.; Park, J.; Oh, H.; Ha, J.; Yoo, H.; Hoon, Y.; Kim, I. S. *Adv. Synth. Catal.* **2015**, *357*¸594. (d) Kianmehr, E.; Kazemi, S.; Foroumadi, A. *Tetrahedron* **2014**, *70*, 349. For a review see: (e) Pan, C.; Jia, X.; Cheng, J. *Synthesis* **2012**, *5*, 677 and references therein.

depicted in Figure 3.7 based on stoichiometric experiments with palladacycle intermediate **LXXXIX**. The authors observed that no product was obtained in the absence of *tert*-butylhydroperoxide thus suggesting the intermediacy of acyl radicals.[192]

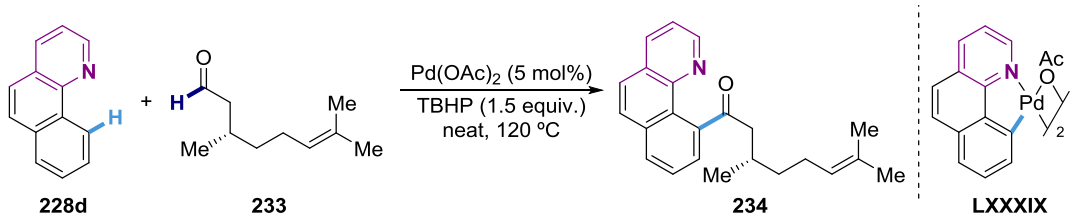

Scheme 3.6. Palladium-catalyzed catalytic dehydrogenative coupling between benzoquinone and e (*S*)-(-)-Citronellal.

3.1.3. Aldehydic C—H bond activation

The third general approach towards the functionalization of aldehydes relies on the ability of the metal catalyst to oxidatively add into the aldehydic C(sp^2)—H bond forming an acyl metal hydride intermediate. While such phenomenon is well documented, the subsequent steps should be considered with skepticism as some of these steps could be better explained through a concerted metalation deprotonation event.[193]

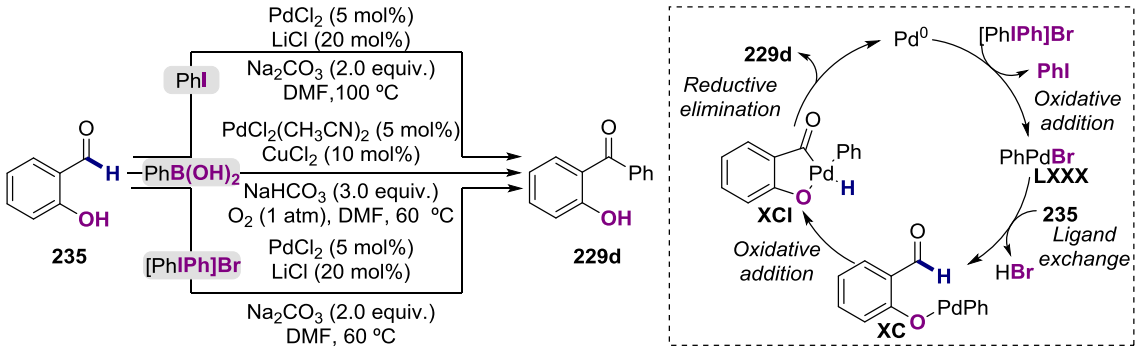

Figure 3.8. Palladium-catalyzed cross-coupling of salicylaldehydes and proposed mechanism.

Several years ago, a series of palladium-catalyzed functionalization of aldehydic C(sp^2)—H bonds with different coupling partners (iodoarenes,[194] diaryl iodonium salts[195] and boronic acids[196]) were published using salicylaldehyde **235**, where the hydroxyl motif was crucial for the reactivity due to its role as directing group. Interestingly, all of these reports employed similar reaction conditions (a soluble palladium source, a carbonate base and a highly polar and coordinating organic solvent). Mechanistically, it was proposed an initial oxidative addition of the palladium catalyst over the aldehydic C(sp^2)—H bond. When using diaryl iodonium salts, the authors postulated an oxidative addition of the palladium catalyst over the iodonium salt forming palladium complex **LXXX**. Next, ligand exchange with the phenoxide yielding complex

[192] For an alternative mechanistic proposal see: Chu, J.-H.; Chen, S.-T.; Chiang, M.-F.; Wu, M.-J. *Organometallics* **2015**, *34*, 953.
[193] The reader is encouraged to carefully consider both alternatives as the CMD proposal is a personal suggestion based on indirect literature evidences.
[194] Satoh, T.; Itaya, T.; Miura, M.; Nomura, M. *Chem. Lett.* **1996**, *25*, 823.
[195] (a) Xia, M.; Chen, Z. *Synth. Commun.* **2000**, *30*, 531. (b) Chen, D.-J.; Chen, Z.-C. *Synlett* **2000**, *8*, 1175.
[196] Weng, F.; Wang, C.; Xu, B *Tetrahedron Lett.* **2010**, *51*, 2593.

XC followed by an intramolecular oxidative addition would render palladacycle **XCI**. Finally, two subsequent reductive eliminations would produce the final product while regenerating the active catalyst (Figure 3.8, right). However, we consider this mechanistic scenario rather unlikely and we hypothesized that a concerted metalation-deprotonation pathway would be more likely based on literature precedents and the reaction conditions.

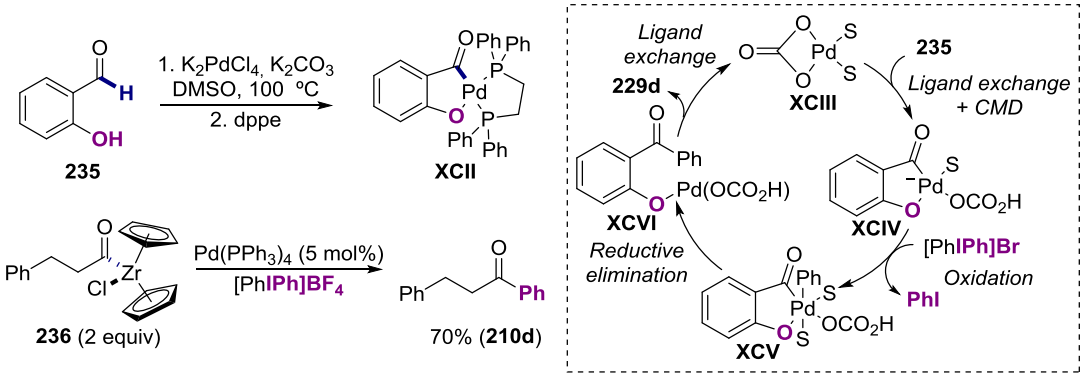

Figure 3.9. Alternative mechanistic proposal.

In our mechanistic hypothesis, we postulate a palladium(II) carbonate **XCIII** as the active catalyst (Figure 3.9, right). Then, it will coordinate the phenoxide motif of **235** introducing it into the inner coordination sphere, thus allowing the cleavage of the aldehydic C(sp^2)—H bondn while forming palladacycle **XCIV** following a concerted metalation-deprotonation event under ligandless conditions.[89] As a matter of fact, stoichiometric experiments (Figure 3.9, left) serve as validation to the previous statement as salicylaldehyde **235** in the presence of a soluble palladium source and carbonate in coordinating DMSO as solvent afforded dimeric cyclopalladated complexes featuring an acyl ligand.[197] Further treatment with a bidentate phosphine dissociates the dimer and allows the formation of palladacycle **XCII**. Subsequently, we propose the oxidation of the palladacycle **XCIV**[61] mediated by diphenyl iodonium salts forming complex **XCV** and iodobenzene concomitantly. Reductive elimination from palladium(IV) complex **XCV** will form the ketone while the palladium catalyst will remain attached to the phenoxide until it is released triggered by a κ^1/κ^2-isomerization featured by the base. This last part of the catalytic cycle is based on the reactivity displayed by acyl zircocene **236** and aryl iodonium salts under palladium catalysis,[198] where the reaction likely goes via transmetallation forming the corresponding acyl palladium(II) intermediate, followed by oxidation to palladium(IV) and a final reductive elimination forming ketone **210d** (Figure 3.9).

It is worth mentioning that there is a report where an acyl hydride metal is likely to be a competent intermediate of the transformation.[199] The transformation is based on the oxidative arylation of aldehydic C(sp^2)—H bonds from quinolone-8-carboxaldehyde **237** under cooperative ruthenium and palladium catalysis. Noteworthy, the use of 1-naphthaldehyde **239** under reaction conditions yielded naphthalene **240**, thus indicating that an acyl metal species evolves via decarbonylation in the absence of directing group. The reaction was monitorized by NMR which allowed the observation of the disappearance of the aldehydic proton while an acyl ruthenium hydride emerged. On the basis of the previous findings, the authors proposed a

[197] (a) Anklin, C. G.; Pregosin, P. S. *J. Organomet. Chem.* **1981**, *222*, 175. (b) Anklin, C. G.; Pregosin, P. S. *J. Organomet. Chem.* **1983**, *243*, 101.
[198] Kang, S.-K.; Yoon, S.-K. *J. Chem. Soc., Perkin. Trans. 1* **2002**, 459.
[199] Ko, S.; Kang, B.; Chang, S. *Angew. Chem. Int. Ed.* **2005**, *44*, 455.

mechanism involving oxidative addition of ruthenium(0) over the aldehydic C(sp^2)—H bond forming intermediate **XCVII**. Next, the *in situ* formed aryl palladium(II) complex **XCVIII** transmetalates with **XCVII** forming palladacycle **XCIX** that will yield the product after reductive elimination.

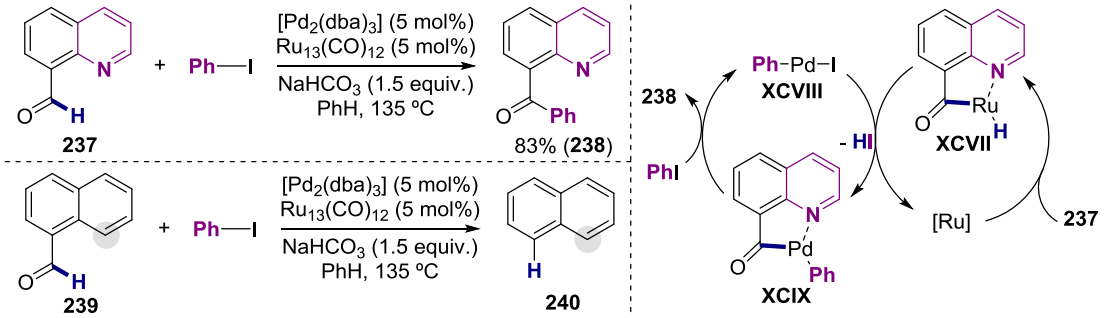

Figure 3.10. Synergistic ruthenium/palladium catalyzed arylation of aldehydes.

As previously exposed in this section, few examples involved a truly C—H bond functionalization event of aldehydic C—H bonds (Section 3.1.3). Furthermore, all these cases rely on the presence of a directing group, either for facilitating the functionalization of the aldehydic C—H bond or for avoiding decarbonylative events.

3.2. Benzocyclobutenones: A versatile scaffold in organic synthesis.

We envisioned that a novel directing group-free methodology involving an arylation of aldehydic C(sp^2)—H bonds via concerted metalation-deprotonation mechanism avoiding a decarbonylative pathway would be an important challenge in organic synthesis. Among the different alternatives, we decided to develop such methodology aiming at an efficient synthesis of benzocyclobutenone cores, rather elusive and unique synthetic scaffolds (Figure 3.11).

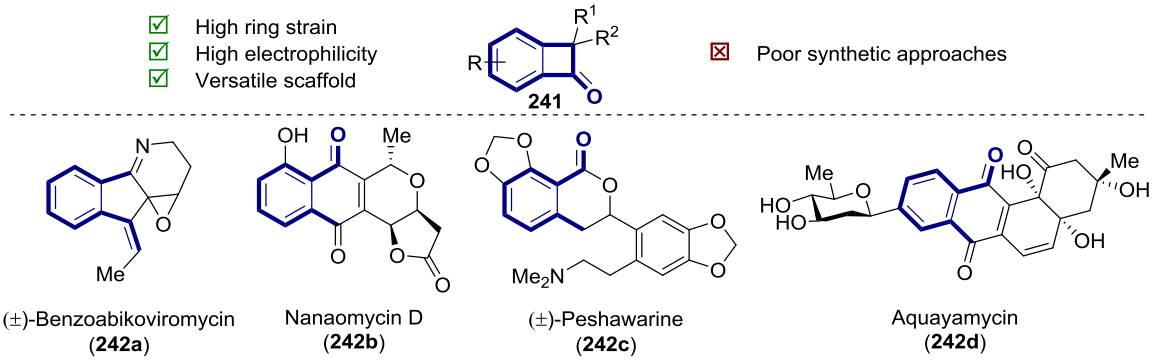

Figure 3.11. Natural products synthesized from benzocyclobutenone **241**.

Benzocyclobutenones (bicyclo[4.2.0]octa-1(6),2,4-trien-7-one, **241**) are characterized by their high reactivity[200] and versatility as synthons in organic synthesis. Indeed, several natural products have been prepared from this scaffold such as the antibiotic Benzoabikoviromycin (**242a**),[201] the antifungal Nanaomycin D (**242b**),[202] or the tyrosine hydroxylase inhibitor

[200] (a) Bellus, D.; Ernst, B. *Angew. Chem. Int. Ed.* **1988**, *27*, 797. (b) Sadana, A. K.; Saini, R. K.; Billups, W. E. *Chem. Rev*. **2003**, *103*, 1539.
[201] Mitchell, D.; Liebesind, L. S. *J. Am. Chem. Soc.* **1990**, *112*, 291.

Aquayamycin[203] (**242d**) among others.[204] Its versatility is the consequence of two main features: the high ring strain of the four-membered ring[205,206] and the high electrophilicty of the carbonyl unit. Not surprisingly, benzocyclobutenones **241** are particularly sensitive to nucleophiles and to ring opening reactions. Importantly, under thermal or photochemical conditions, benzocyclobutenones undergo conrotatory retro-4π cyclization rendering vinyl ketenes **CII** (Figure 3.12) that will be prone to form cycloaddition products **243**. Unfortunately, the formation of these vinyl ketene intermediates is rather slow and require high temperatures. However, the addition of a nucleophile results in an alcoxide intermediate **C** that rapidly generates the corresponding *ortho*-quinodimethane adducts **CI**. Following this approach, several backbones are within reach such as naphthalenes (**243a**) and tetrahydronaphthalenes (**243b**), benzo[n]annulenes (**243e**), anthraquinones (**243c**), α-tetralones (**243g**), benzodiazepines (**243d**) and isochromanones (**243f**), among others.

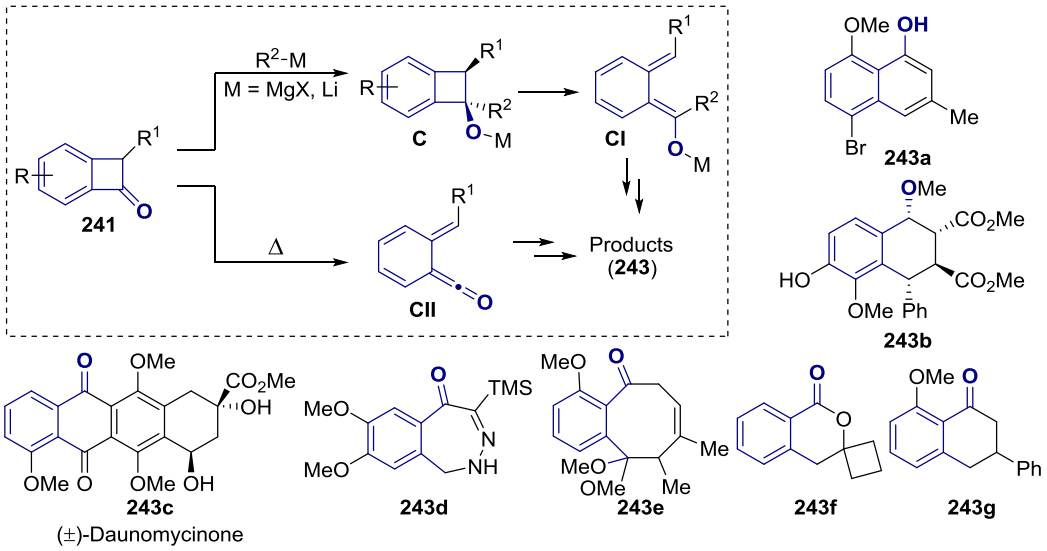

Figure 3.12. Versatility of benzocyclobutenone backbone via *ortho*-quinodimethane intermediates

Other heterocyclic backbones are within reach following more classical ring opening reactions such as phthalides (**244a**) via Bayer-Villiger oxidation[207] or indoles (**244b**)[208] and

[202] Winters, M. P.; Stranberg, M.; Moore, H. W. *J. Org. Chem.* **1994**, *59*, 7572.
[203] Matsumoto, T.; Yamaguchi, H.; Hamura, T.; Tanabe, M.; Kuriyama, Y.; Suzuki, K. *Tetrahedron Lett.* **2000**, *41*, 8383.
[204] (a) Fitzgerald, J. J.; Pagano, A. R.; Sakoda, V. M.; Olofon, R. A. *J. Org. Chem.* **1994**, *59*, 4117. (b) Takahashi, N.; Kanayama, T.; Okuyama, K.; Kataoka, H.; Fukaya, H.; Suzuki, K.; Matsumoto, T. *Chem. Asian J.* **2011**, *6*, 1752. (c) Takemura, I.; Imura, K.; Matsumoto, T.; Suzuki, K. *Org. Lett*. **2004**, *6*, 2503. (d) Ben, A.; Hsu, D. S.; Matsumoto, T.; Suzuki, K. *Tetrahedron* **2011**, *67*, 6460. (e) Michellys, P.; Maurin, P.; Toupet, L.; Pellissier, H.; Santelli, M. *J. Org. Chem.* **2001**, *66*, 115. (f) Pellisier, H.; Santelli, M. *Tetrahedron* **1996**, *52*, 9093.
[205] (a) Bach, R. D.; Dmitrenko, O. *J. Am. Chem. Soc.* **2006**, *128*, 4598. (b)Wilberg, K. B. *Angew. Chem. Int. Ed.* **1986**, *25*, 312.
[206] Mack, D. J.; Njardarson, J. T. *ACS Catal.* **2013**, *3*, 272.
[207] Rioz-Martínez, A.; de Gonzalo, G.; Pazmiño, D. E. T.; Fraaije, M. W.; Gotor, V. *Eur. J. Org. Chem.* **2009**, 2526.
[208] Adam, G.; Andrieux, J.; Plat, M. *Tetrahedron* **1985**, *41*, 399.

indolines (**244c**)[209] through a Beckmann-type rearrangement. On the other hand, indanones (**244d-e**)[210] are within range through a Grob-type fragmentation.

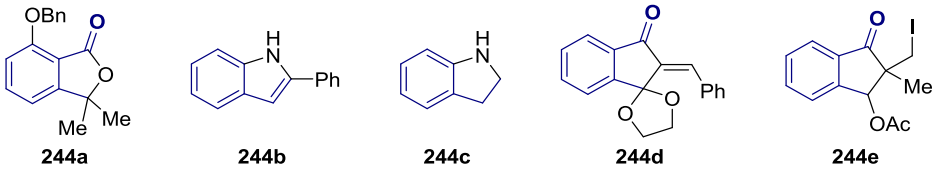

Figure 3.13. Versatility of benzocyclobutenone backbone via ring-expansion.

In addition, in the last years several reports have been published taking advantage of the inherent ring strain of benzocyclobutenones to promote ring expansion reactions by combination of a transition metal catalyst and a π-electrophile. Particularly, our group described the intermolecular insertion of dienes (**245a**) and alkynes (**245b**) into the proximal benzocyclobutenone bond under nickel catalysis.[211] The Dong group have published several reports describing the intramolecular insertion of olefins and alkynes across the proximal bond of the benzocyclobutenone core under rhodium catalysis (**245d,f**).[212] Notably, in some cases the alkene can be generated *in situ* through a β-hydride elimination event (**245c**)[213] or a decarbonylative event occurs en route to **245e**[214] (Figure 3.14).

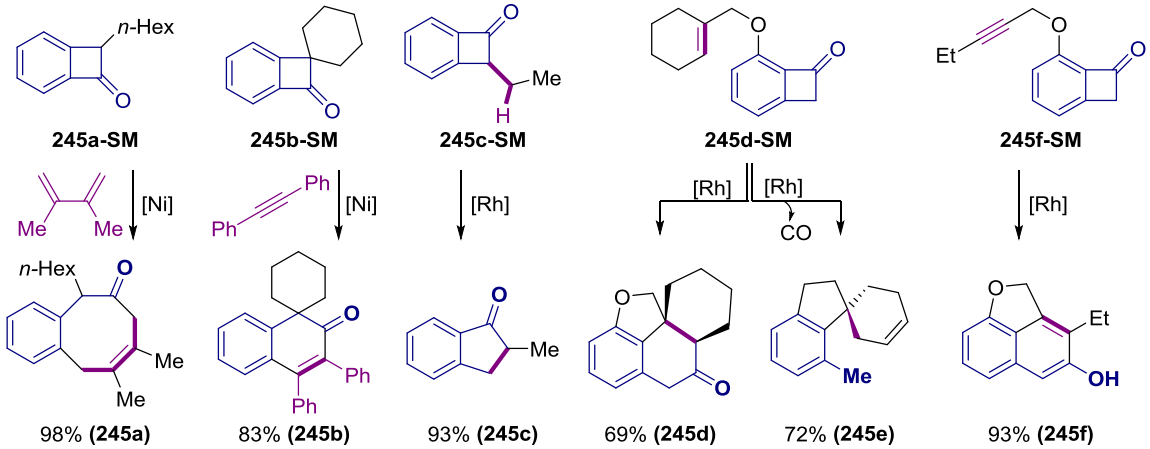

Figure 3.14. Transition metal-catalyzed ring expansion of the benzocyclobutenone core.

Despite the high versatility of benzocyclobutenones, a limited number of methods for their synthesis have been reported. Unfortunately, the available literature data indicates that the current methods are not particularly attractive. For example, non-substitued **241** could be prepared from *ortho*-toluoyl chloride **246** through flash vacuum pyrolysis; however, temperatures of 780 ºC are required and no substitution is tolerated.[215] Alternatively, the

[209] Cho, H.; Iwama, Y.; Sugimoto, K.; Mori, S.; Tokuyama, H. *J. Org. Chem.* **2010**, *75*, 627.
[210] (a) Liebeskind, L. S.; Mitchell, D.; Foster, B. S. *J. Am. Chem. Soc.* **1987**, *109*, 7908. (b) Hamura, T.; Suzuki, T.; Matsumoto, T.; Suzuki, K. *Angew. Chem. Int. Ed.* **2006**, *45*, 6294.
[211] Juliá-Hernández, F.; Ziadi, A.; Nishimura, A.; Martin, R. *Angew. Chem. Int. Ed.* **2015**, *54*, 9537.
[212] (a) Xu, T.; Ko, H. M.; Savage, N. A.; Dong, G. *J. Am. Chem. Soc.* **2012**, *134*, 20005. (b) Xu, T.; Dong, G. *Angew. Chem. Int. Ed.* **2012**, *51*, 7567.
[213] Chen, P.-H.; Sieber, J.; Senanayake, C. H.; Dong, G. *Chem. Sci.* **2015**, *6*, 5440.
[214] (a) Xu, T.; Savage, N. A.; Dong, G. *Angew. Chem. Int. Ed.* **2014**, *53*, 1891. (b) Chen, P.-H.; Xu, T.; Dong, G. *Angew. Chem. Int. Ed.* **2014**, *53*, 1674.
[215] Suzzarini, L.; Lin, J.; Wang, Z. Y. *Tetrahedorn Lett.* **1998**, *39*, 1695.

Hasegawa group reported the synthesis of benzocyclobutenones through a photochemical induced cyclization of *ortho*-alkylphenyl 1,3-diketones **248**.[216] The method requires a high-pressure mercury lamp to form the corresponding alcohol intermediates **247**. Then, after isolation, the benzocyclobutenols **247** were submitted to pyrolysis conditions (150-180 ºC) to trigger the retro-aldol reaction delivering the final benzocyclobutenone. Once again, the scope of the transformation was limited and the yields were mediocre in most cases.

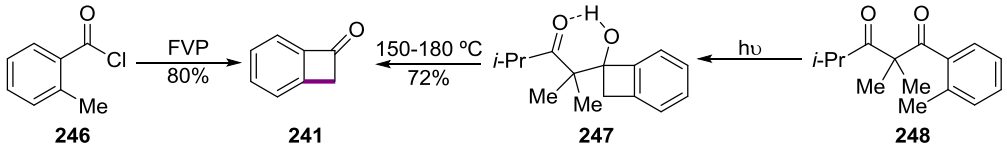

Scheme 3.7. Synthesis of benzocyclobutenones through flash-vacuum pyrolysis or through photochemical cyclization

Stille cross-coupling reactions have been used to prepare benzocyclobutenones as well (Figure 3.15). An intramolecular synthesis was achieved by *in situ* formation of the corresponding vinylstannane (**250**) that was subsequently intramolecularly coupled with the aryl bromide forming 2-benzylidenebenzocyclobutenone **241-I** under palladium catalysis (eq a).[217] An intermolecular approach was also envisioned involving the coupling of 4-chlorocyclobutenones **251** and 3-stannylcyclobutenone **252** under palladium catalysis rendering the bicyclic structure **253** that delivered the final product **241-II** after a 6π-electrocyclization through vinyl ketene intermediate (eq b).[218]

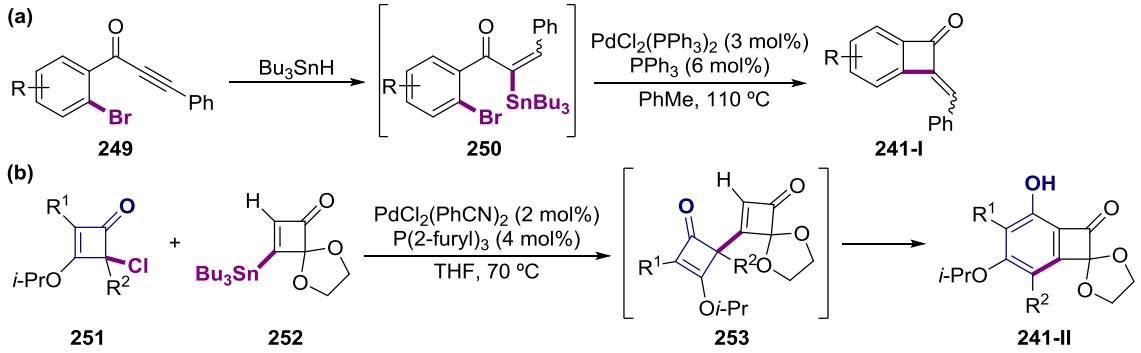

Figure 3.15. Stille cross-coupling for the synthesis of benzocyclobutenones.

The most applied synthetic methods for preparing benzocyclobutenones are probably the [2+2] cycloaddition of benzynes with enolate derivatives and tandem lithium-halogen exchange/ cyclization (Figures 3.16 and 3.17). The [2+2] cycloaddition classically involves the *in situ* preparation of benzynes **256** that often requires harsh reaction conditions[219] such as

[216] (a) Yoshioka, M.; Arai, M.; Nishizawa, K.; Hasegawa, T. *J. Chem. Soc., Chem. Commun*. **1990**, 374. (b) Yoshioka, M.; Momose, S.; Nishizawa, K.; Hasegawa, T. *J. Chem. Soc., Perkin Trans. 1* **1992**, 499. (c) Yoshioka, M.; Nishizawa, K.; Arai, M.; Hasegawa, T. *J. Chem. Soc., Perkin Trans. 1* **1991**, 541.
[217] Bradley, J. C.; Durst, T. *J. Org. Chem.* **1991**, *56*, 5459.
[218] Edwards, J. P.; Krysan, D. J.; Libeskind, L. S. *J. Org. Chem.* **1993**, *58*, 3942.
[219] For example of benzyne generation under mild reaction conditions see: (a) Bronner, S. M.; Bahnck, K. B.; Garg, N. K. *Org. Lett.* **2009**, *11*, 1007. (b) Im, G.-Y. J.; Bronner, S. M.; Goetz, A. E.; Paton, R. S.; Cheong, P. H.-Y.; Houk, K. N.; Garg, N. K. *J. Am. Chem. Soc.* **2010**, *132*, 17933.

sodium amide[220] or organolithium reagents,[221] limiting the preparative scope of the method. Furthermore, the presence of substituents on the aryl ring will give rise to the formation of regioisomeric mixtures of products **241**. Notably, some advances have been done regarding the regiocontrol of the transformation by introducing fused cyclobutanes[222] or alkyl ethers[223] (substrates **241-III** and **241-V**); however, only these two types of functionalities are able to exert an adequate regiocontrol. As for the alkene counterpart **257**, enolates, ketene acetals and ketene silyl acetals with different degree of substitution have been employed. The main drawbacks of this approach are the required prefunctionalization of the substrate to prepare the benzyne intermediate, as well as the harsh reaction conditions and the poor regioselectivity of the cycloaddition event in the absence of control elements.

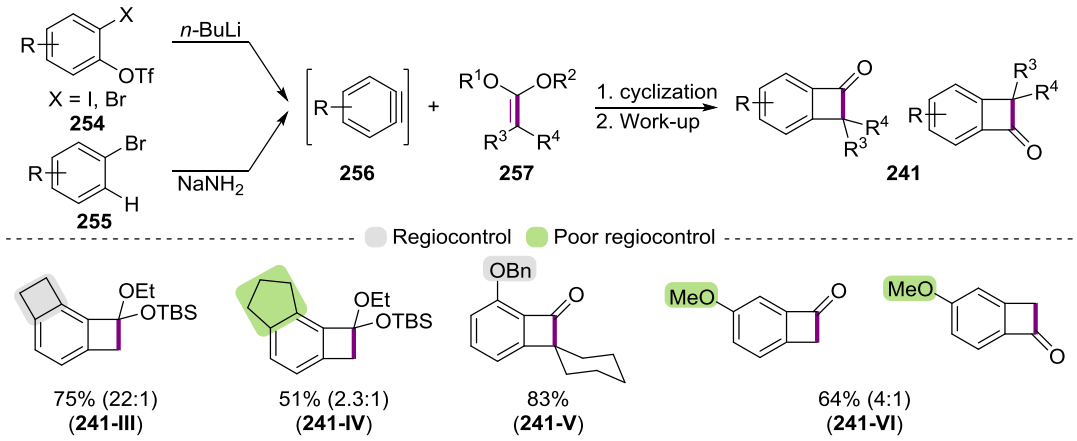

Figure 3.16. Synthesis of benzocyclobutenones via [2+2] cycloaddition.

Ahuja and Aidhen reported[224] the cyclization of Weinreb amides **258** triggered by a halogen-lithium exchange event. This reaction, because of its intramolecular nature, ensures an absolute regiocontrol, yet highly reactive *tert*-butyllithium is required, dramatically reducing the functional group tolerance and attractiveness of such approach (Figure 3.17).

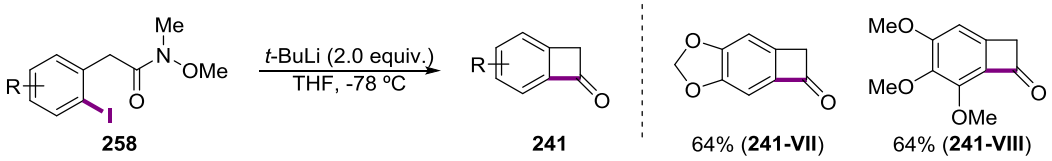

Figure 3.17. Lithium-halogen exchange promotes cyclization of Weinreb amides towards the synthesis of benzocyclobutenones.

In summary, the available synthetic methods for preparing benzocyclobutenones possess numerous drawbacks, such as poor functional group tolerance, poor yields, poor

[220] (a) Stevens, R. V.; Bisacchi, G. S. *J. Org. Chem.* **1982**, *47*, 2393 (b) Maurin, P.; Ibrahim-Ouali, M.; Santelli, M. *Tetrahedron Lett.* **2001**, *42*, 8147. (c) Mariet, N.; Ibrahim-Ouali, M.; Santelli, M. *Tetrahedron Lett.* **2002**, *43*, 5789.
[221] (a) Hosoya, T.; Hasegawa, T.; Kuriyama, Y.; Matsumoto, T.; Suzuki, K. *Synlett* **1995**, *2*, 177. (b) Chen, P.-H.; Savage, N. A.; Dong, G. *Tetrahedron* **2014.** *70*, 4135. (c)
[222] (a) Hamura, T.; Ibusuki, Y.; Sato, K.; Matsumoto, T.; Osamura, Y.; Suzuki, K. *Org. Lett.* **2003**, *5*, 3551. (b) Hamura, T.; Ibusuki, Y.; Uekusa, H.; Matsumoto, T.; Suzuki, K. *J. Am. Chem. Soc.* **2006**, *128*, 3534.
[223] (a) Hosoya, T.; Hamura, T.; Kuriyama, Y.; Miyamoto, M.; Matsumoto, T.; Suzuki, K. *Synlett* **2000**, *4*, 520. (b) Hamura, T.; Hosoya, T.; Yamaguchi, H.; Kuriyama, Y.; Tanabe, M.; Miyamoto, M.; Yasui, Y.; Matsumoto, T.; Suzuki, K. *Helv. Chim. Acta* **2002**, *85*, 3589
[224] Aidhen, I. S.; Ahuja, J. R. *Tetrahedron Lett.* **1992**, *33*, 5431.

regioselectivity, complex reactants, harsh reaction conditions, high waste generation, etc. Challenged by this observation, we decided to design a novel synthetic route that would allow an efficient synthesis of benzocyclobutenones from rather simple starting materials.

3.3 Palladium-catalyzed intramolecular oxidative acylation of aryl chlorides via aldehydic C(sp²)—H bond cleavage.[225]

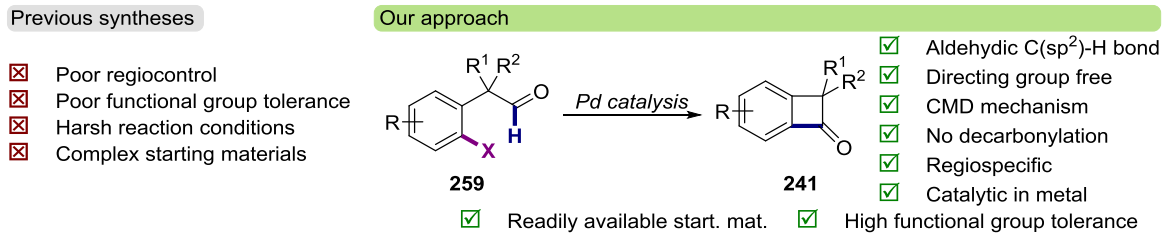

Figure 3.18. Palladium-catalyzed oxidative arylation of pending aldehydes.

We envisioned a novel synthesis of benzocyclobutenones following the strategy showed in Figure 3.18. Our strategy is based on the use of readily available α-aryl aldehydes as starting materials.[226] The aryl moiety features a halogen in *ortho* position that will be playing a dual role. First, it will direct the C—H cleavage step, and secondly, it will provide the system a redox manifold so that an oxidant will not be required. By using this halide functionality, we would avoid the use of traditional directing groups and the need for a terminal oxidant. If successful this methodology would represent a considerable step-forward for the synthesis of benzocyclobutenones as catalytic amounts of metals should be employed, no dangerous reagents would be needed, and regiospecificity will be accomplished due to its intramolecular nature.

In 2010, our group reported the successful synthesis of benzocyclobutenones **241** using aryl bromides (**259**) as starting materials under palladium catalysis[227] (see Figure 3.19, left). The reaction nicely worked using a combination of palladium(II) acetate and BINAP as ligand with cesium carbonate as base in dioxane. The method is characterized by its functional group tolerance and reliability.[228] Interestingly, no reaction occurred in the presence of aryl chloride, illustrating that the cleavage of the rather inert C—Cl bond did not compete with the productive formation of benzocyclobutenone (Figure 3.19, right).

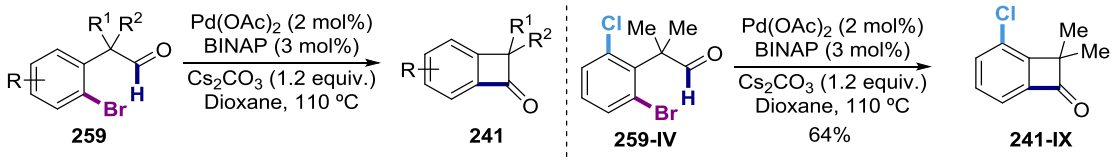

Figure 3.19. Palladium-catalyzed intramolecular acylation of aryl bromides towards the synthesis of benzocyclobutenones.

The use of aryl chlorides would be of utmost importance for several factors:

[225] Flores-Gaspar, A.; Gutiérrez-Bonet, Á.; Martin, R. *Org. Lett.* **2012**, *14*, 5234.
[226] See Experimental Section.
[227] Álvarez-Bercedo, P.; Flores-Gaspar, A.; Correa, A.; Martin, R. *J. Am. Chem. Soc.* **2010**, *132*, 466.
[228] Martin, R.; Flores-Gaspar, A. *Org. Synth.* **2013**, *45*, 563.

- Aryl chlorides are cheaper and more readily available than the corresponding aryl bromides or iodides.
- The use of aryl chlorides as coupling partner would improve the efficiency of the transformation by positively affecting the E factor[229] of the transformation (Figure 3.20).
- The stronger C—Cl bond[230]makes these substrates rather inert under traditional cross-coupling conditions.[231] If successful, this would be the first report dealing with the functionalization of aldehydic C(sp^2)—H bonds with aryl chlorides.
- Because of the relative inertness of aryl chlorides, the starting material can potentially be decorated under traditional transition metal catalysis if other halides are present within the molecule.

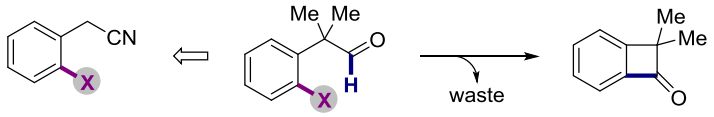

260 **259** **241**

Ar-X	mmol/€ (5g bottle)	mmol/€ (25g bottle)	E factor[a]	E factor[b] (1 equiv Cs_2CO_3)	BDE[c] (Kcal/mol)
Br	0.74	0.98	0.55	2.78	81
Cl	0.91	1.99	0.25	2.47	96

[a] This is an oversimplification, HX (1.0 equiv.) was considered as the only waste generated. [b] Cs_2CO_3 (1.0 equiv.) was introduced in the E factor ecuation as waste. [c] For the corresponding Ph-X

Figure 3.20. Advantages and challenges of using aryl chlorides instead of aryl bromides.

3.3.1 Optimization of the reaction conditions for the synthesis of benzocyclobutenones

In principle, the transformation would be initiated by oxidative addition of palladium(0) catalyst over the C—Cl bond forming an aryl palladium(II) intermediate (**CIV**). Subsequently, a ligand exchange would occur between the coordinated chloride anion and the carbonate base. The next step would be the cleavage of the aldehydic C(sp^2)—H bond forming the acyl palladacycle complex **CV**. Finally, a challenging reductive elimination would release the product with concomitant regeneration of the active catalyst. Taking a closer look into intermediate **CV**, we hypothesized a possible *ipso*-protonation of the palladacycle, in analogy to the behavior displayed by palladacycle **XLVII** (see Figure 2.39 in Chapter 2), thus a pending acyl palladium(II) intermediate could be formed (**CVI**). This compound could regenerate palladacycle **CV** after an aryl C(sp^2)—H bond cleavage, or evolve to intermediate **CVII** through a CO extrusion event. Finally, β-hydride elimination from **CVII** would deliver the styrene **261** and palladium complex **CVIII** that after a reductive elimination step would regenerate the active catalyst. Importantly, these styrenes were already observed by our group[227,232] and Larock's[233] when using aryl bromides and iodides respectively (Figure 3.21).

[229] Lipshutz, B. H.; Isley, N. A.; Fennewald, J. C.; Slack, E. D. *Angew. Chem. Int. Ed.* **2013**, *52*, 10952.
[230] Bond dissociation energies for Ph—X: Cl: 96 kcal/mol; Br: 81 kcal/mol; I: 65 kcal/mol).
[231] Please, note that the bond strength is a very basic explanation. For further details see: V. V. Grushin, H. Alper in *Activation of Unreactive Bonds and Organic Synthesis* (Ed.: S. Murai), Springer, Berlin, **1999**, p. 203.
[232] Flores-Gaspar, A.; Martin, R. *Adv. Synth. Catal.* **2011**, *353*, 1223.
[233] Kesharwani, T.; Verma, A. K.; Emrich, D.; Ward, J. A.; Larock, R. C. *Org. Lett.* **2009**, *11*, 2591.

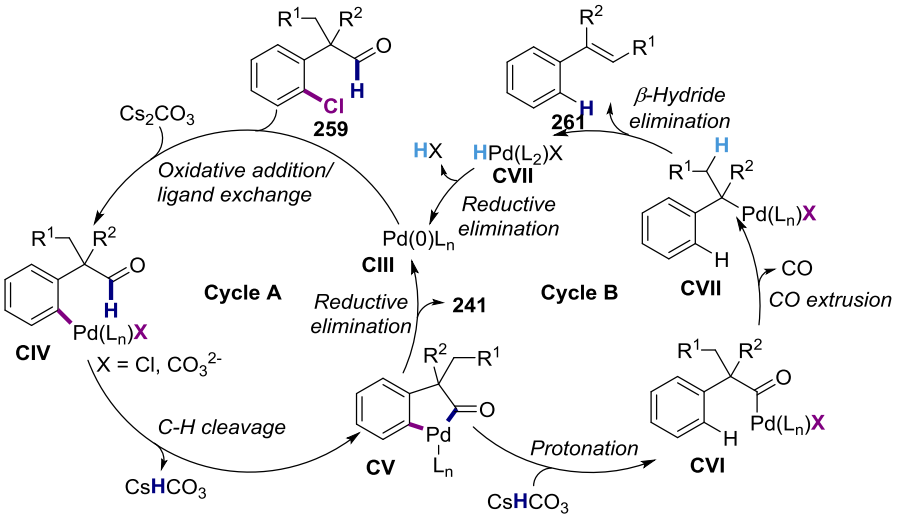

Figure 3.21. Mechanistic rational for the intramolecular acylation of aryl chlorides.

With a mechanistic rational in our hands, we identified several steps that would be particularly challenging. For example, it is generally admitted that the oxidative addition on aryl chlorides is more difficult than for aryl bromides.[234] In order to promote the oxidative addition, a strong electron-donating ligand would be required in order activate the C—Cl bond; however, in order to promote the challenging reductive elimination for the formation of a highly strained ring, electron-withdrawing ligands would be desired.[235] Additionally, a careful optimization of the reaction conditions will be needed in order to discriminate efficiently between cycle A and B once intermediate palladacycle **CV** is formed.

In order to optimize the reaction conditions, we decided to use the reported conditions for the synthesis of benzocyclobutenones **241** from aryl bromides as starting point (see Figure 3.19). An initial screening of mono- and bidentate phosphines resulted in conversions lower than 5%. Consequently, we decided to test the activity of a catalytic system based on *N*-heterocyclic carbene ligands that are known to be highly σ-electron-donating and poor π-acceptors.[236] *N*-heterocyclic carbenes could be regarded as an ideal class of ligands for our system since their electron-richness might facilitate the oxidative addition event, whether their bulkiness would easily promote the reductive elimination.

[234] (a) Grushin, V. V.; Alper, H. *Chem. Rev.* **1994**, *94*, 1047. (b) Littke, A. F.; Fu, G. C. *Angew. Chem. Int. Ed.* **2002**, *41*, 4176. (c) Bedford, R. B.; Cazin, C. S. J.; Holder, D. *Coord. Chem. Rev.* **2004**, *248*, 2283. (d) Alonso, F.; Beletskaya, I. P.; Yus, M. *Chem. Rev.* **2002**, *102*, 4009.
[235] Hartwig, J. F. *Inorg. Chem.* **2007**, *46*, 1936.
[236] (a) Kantchev, E. A. B.; O'Brien, C. J.; Organ, M. G. *Angew. Chem. Int. Ed.* **2007**, *46*, 2768. (b) Valente, C.; Calimsiz, S.; Hoi, K. H.; Mallik, D.; Sayah, M.; Organ, M. G. *Angew. Chem. Int. Ed.* **2012**, *51*, 3314. (c) Clavier, H.; Nolan, S. P. *Chem. Commun.* **2010**, *46*, 841. (d) Dröge, T.; Glorius, F. *Angew. Chem. Int. Ed.* **2010**¸*49*¸6940.

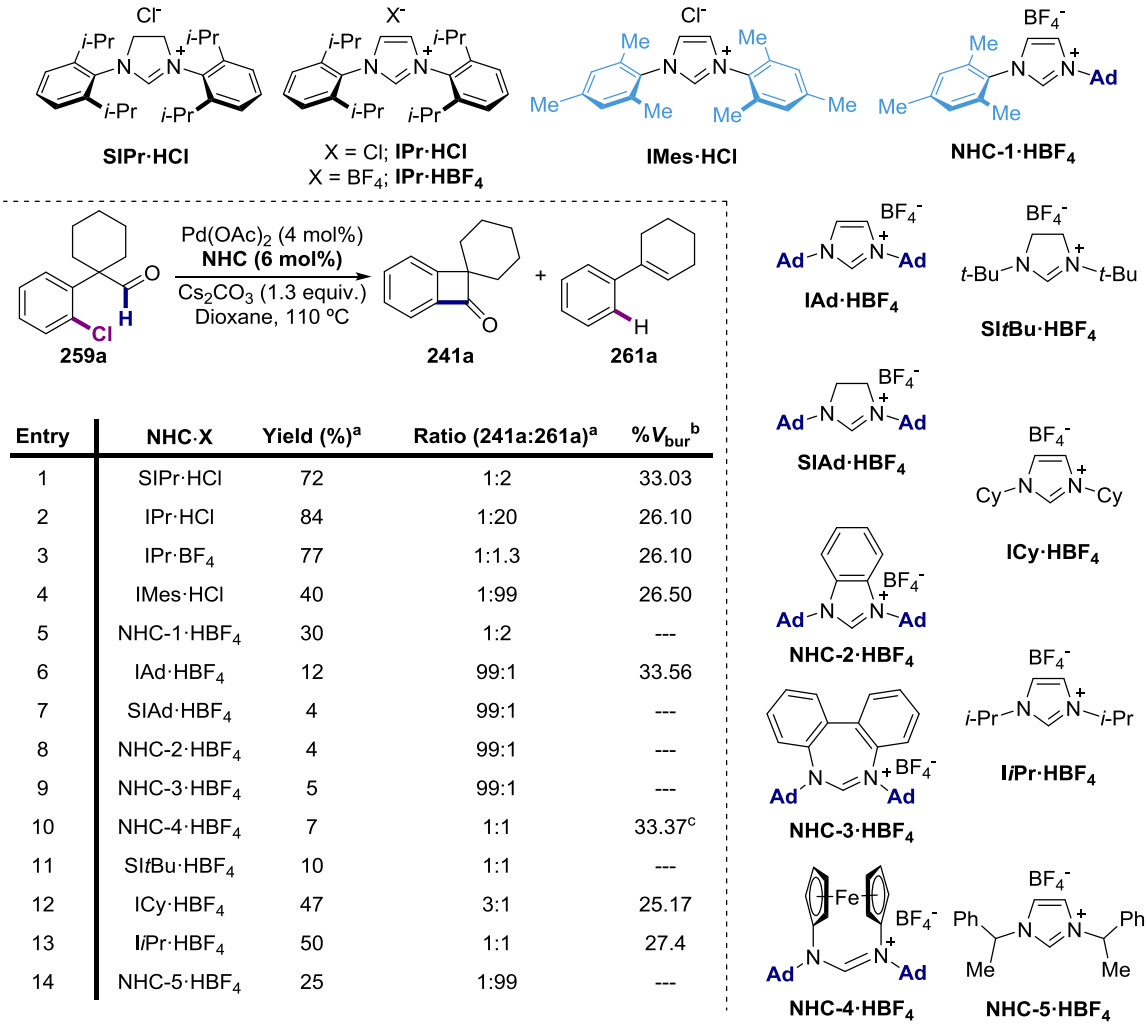

Entry	NHC·X	Yield (%)[a]	Ratio (241a:261a)[a]	%V_{bur}[b]
1	SIPr·HCl	72	1:2	33.03
2	IPr·HCl	84	1:20	26.10
3	IPr·BF_4	77	1:1.3	26.10
4	IMes·HCl	40	1:99	26.50
5	NHC-1·HBF_4	30	1:2	---
6	IAd·HBF_4	12	99:1	33.56
7	SIAd·HBF_4	4	99:1	---
8	NHC-2·HBF_4	4	99:1	---
9	NHC-3·HBF_4	5	99:1	---
10	NHC-4·HBF_4	7	1:1	33.37[c]
11	SI*t*Bu·HBF_4	10	1:1	---
12	ICy·HBF_4	47	3:1	25.17
13	I*i*Pr·HBF_4	50	1:1	27.4
14	NHC-5·HBF_4	25	1:99	---

259a (0.25 mmol), $Pd(OAc)_2$ (4 mol%), **ligand** (6 mol%), Cs_2CO_3 (1.3 equiv.), dioxane (0.25 M), 110 ºC, 14 hours. [a] Determined by GC using dodecane as internal standard. [b] For (NHC)Pd(allyl)Cl complexes at M-NHC = 2.00 Å. [c] Value for I^{t}Bu.

Table 3.1. Screening of NHC ligands for the synthesis of benzocyclobutenones.[237]

As shown in Table 3.1, the employment of NHC ligands allowed us to achieve high conversions; however, a mixture of products **241a** and **261a** was obtained. The use of arylated NHC ligands (entries 1-5) gave modest to good yields of the mixture of **241a** and **261a** in different ratios. For example, when **SIPr** was employed, a 72% yield was obtained, although with poor selectivity. Interestingly, the less electron-donating **IPr** gave higher yields and in a remarkable good selectivity towards **261a.** Strikingly, an otherwise innocent change of the counterion from chloride to tetrafluoroborate in **IPr** (entries 2-3) dramatically affected the selectivity of the process. The use of **IMes** furnished selectively styrene **261a** but in moderate yields (entry 4). When comparing the buried volume (%V_{bur}) of the different NHC ligands employed (entries 1-2,4) bearing the same counterion, we can roughly establish a relationship with the selectivity of the transformation. The less bulky the ligand is, the higher selectivity towards styrene product is observed. Consequently, we decided to make use of this observation and use bulkier NHC ligands in order to revert the selectivity. Indeed, replacement

[237] The buried volumes were taken from: Viciu, M. S.; Navarro, O.; Germaneau, R. F.; Kelly III, R. A.; Sommer, W.; Marion, N.; Stevens, E. D.; Cavallo, L.; Nolan, S. P. *Organometallics* **2004**, *23*, 1629.

of one mesityl unit by an adamantly (**NHC-1**, entry 5) dramatically reduced the selectivity observed. Furthermore, the utilization of Arduengo's carbene **IAd** (entry 6) completely reversed the reaction selectivity, giving exclusively the targeted benzocyclobutenone **241a** but in low yields. In view of this promising result, we decided to keep the steric properties of the ligand but modifying the backbone in order to achieve higher yields by tuning the electronic properties (entries 7-10). Unfortunately, more electron-donating (**SIAd**) or less electron-donating ligands (**NHC-7** and **8**) displayed poor conversions while keeping high selectivity. Finally, other alkyl substituents were tested on the NHC backbone (entries 11-13). Although high yields were obtained, low selectivites were found in all cases. Next, we decided to utilize Arduengo's carbene **IAd** (entry 6) as ligand and then we moved to explore other parameters of the reaction that might have an impact on reactivity while maintaining similar selectivity.

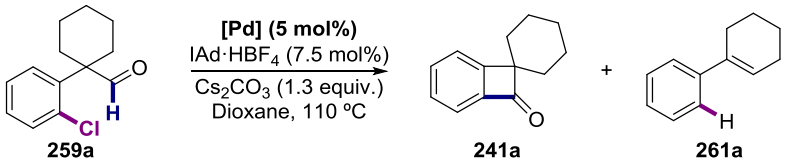

Entry	[Pd]	Conv. (%)[a]	Yield 241a (%)[a]
1	$PdCl_2$	24	20
2	*t*-$PdCl_2(SMe_2)_2$	5	3
3	$Pd(OTf)_2$	11	7
4	$Pd(dba)_2$	20	18
5	$Pd_2(dba)_3$	11	10
6	$Pd(TMEDA)Me_2$	28	24
7	Pd-1	6	6
8	Pd-2	21	18
9	Pd-3	39	34
10	Pd-3 (140 ºC)	63	60
11	Pd-4[b]	43	40

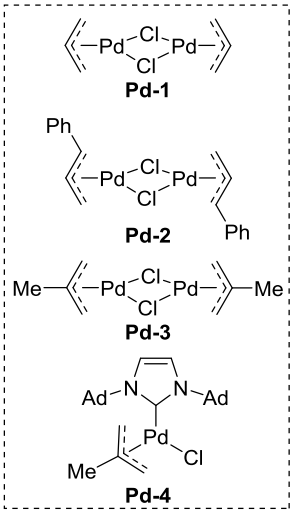

259a (0.25 mmol), [Pd] (5 mol% in Pd), **IAd·BF$_4$** (7.5 mol%), Cs_2CO_3 (1.3 equiv.), dioxane (0.25 M), 110 ºC, 14 hours. [a]Determined by GC using dodecane as internal standard.[b]Pd-4 (5 mol%). No further ligand added.

Table 3.2. Screening of palladium precatalysts for the synthesis of benzocyclobutenones.

First, different palladium(II) precatalysts were explored (Table 3.2, entries 1-3). Importantly, we observed that palladium(II) chloride showed a higher reactivity than palladium(II) acetate (Table 3.1, entry 6). More electrophilic palladium(II) sources gave lower yields (entry 3). Palladium(0) sources were tested as it could be possible that the palladium(II) is not being quantitatively reduced under reaction conditions[156] to palladium(0), a process that is known to require phosphines or amines. However, no significant improvement was observed. Based on the good performance of palladium(II) chloride, the allyl dimers (**Pd-1-3**) were tested as precatalysts. Importantly, **Pd-3** dimer was able to boost the reactivity to a 34% yield, and even a 60% yield upon heating at 140 ºC.

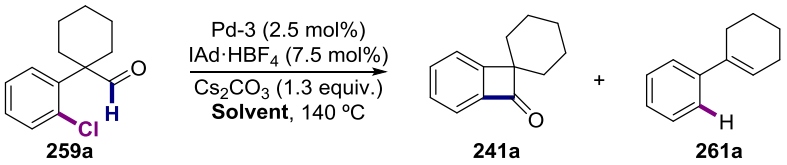

259a **241a** **261a**

Entry	Solvent	Conv. (%)[a]	Yield 241a (%)[a]
1	Dioxane	63	60
2	THF	38	33
3	Toluene	10	9
4	DMF	6	4

259a (0.25 mmol), **Pd^{-3}** (2.5 mol%), **IAd·HBF$_4$** (7.5 mol%), Cs_2CO_3 (1.3 equiv.), dioxane (0.25 M), 140 ºC, 14 hours. [a]Determined by GC using dodecane as internal standard.

Table 3.3. Screening of solvents for the synthesis of benzocyclobutenones.

Interestingly, the selectivity was seriously affected depending on the solvent utilized. For example, a 1:1 ratio of **241a** and **261a** were observed on the presence of cyclohexane, mesitylene or *tert*-butyl methyl ether. The coordinating THF reduced drastically the reactivity (entry 2), whereas stronger coordinating DMF almost gave no conversion (entry 4). Non-polar toluene resulted inadequate for the transformation obtaining only a 9% yield of the benzocyclobutenone (entry 3). Consequently, we decided to maintain dioxane as the solvent of choice.

After careful examination of the previous results, we realized that conversion and yield were always in good agreement (Tables 3.2 and 3.3) with a difference no bigger than 6%. Therefore, we hypothesized that the moderate yields obtained could be originated from a decomposition of the catalytic system or a very slow rate. Next, we decided to test the influence exerted by exogenous olefins in our catalytic system for two main reasons:[238]

- Olefins are known to stabilize low-coordinated metal species by coordinating to the naked metal center.[239]
- Electron-deficient olefins are known to enhance the rate of the reductive elimination by decreasing the electron density on the metal center through π-back donation.[240]

However, the addition of olefins could potentially jeopardize the oxidative addition step by saturating the metal center as it is known that the oxidative addition proceeds more efficiently through low-coordinated palladium(0) complexes.[156]

[238] Johnson, J. B.; Rovis, T. *Angew. Chem. Int. Ed.* **2008**, *47*, 840.
[239] Krause, J.; Cestaric, G.; Haack, K.-J.; Seevogel, K.; Storm, Pörschke, K.-R. *J. Am. Chem. Soc.* **1999**, *121*, 9807.
[240] (a) Pérez-Rodríguez, M.; Braga, A. A. C.; Garcia-Melchor, M.; Pérez-Temprano, M. H.; Casares, J. A.; Ujaque, G.; de Lera, A. R.; Álvarez, R.; Maseras, F.; Espinet, P. *J. Am. Chem. Soc.* **2009**, *131*, 3650. (b) Yamamoto, T.; Yamamoto, A.; Ikeda, S. *J. Am. Chem. Soc.* **1971**, *93*, 3350.

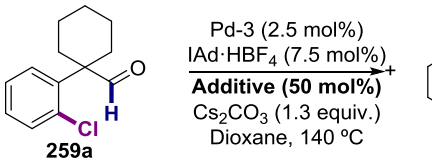

Entry	Additive	Conv. (%)[a]	Yield 241a (%)[a]
1	Alk-1	76	73
2	Alk-1[b]	82	80
3	Alk-2	56	55
4	Alk-3	76	71
5	Alk-4	53	51
6	Alk-5	62	62

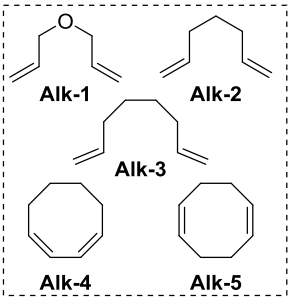

259a (0.25 mmol), **Pd-3** (2.5 mol%), **IAd·BF$_4$** (7.5 mol%), Cs_2CO_3 (1.3 equiv.), additive (50 mol%), dioxane (0.25 M), 140 ºC, 14 hours. [a]Determined by GC using dodecane as internal standard.[b]Pd:Ligand 1:2 (10 mol% NHC-5-HBF$_4$)

Table 3.4. Study of olefinic additives for the synthesis of benzocyclobutenones.

To our delight, the addition of alkene additives increased the yield of the transformation as anticipated (Table 3.4, entries 1 and 4). This result can be rationalized by the formation of a more stable 16-electron-complex (NHC)Pd^0(diene) intermediate, thus avoiding catalyst decomposition at a higher extent.[239] Importantly, 80% yield of benzocyclobutenone **241a** was observed when the palladium/ligand ratio was increased to 1:2 (entry 2). Although further efforts were done to achieve higher yields, we were not able to improve these results even further.[241]

Finally, a fast optimization for obtaining **261a** selectively was conducted observing that a judicious choice of the palladium precatalyst was critical for achieving both selectivity and reactivity towards the synthesis of styrene **261a** in the presence of **IMes** as ancillary ligand.

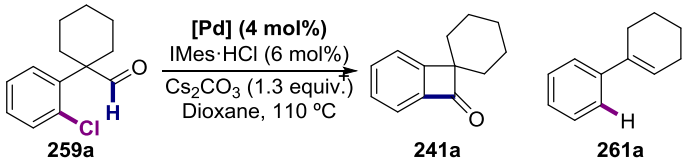

Entry	[Pd]	Conv. (%)[a]	Yield 241a (%)[a]	Yield 261a (%)[a]
1	$PdCl_2(CH_3CN)_2$	7	2	6
2	$Pd(OTf)_2$	84	29	36
3	$Pd(dba)_2$	23	2	19
4	Pd-1	38	3	34
5	Pd-2	52	3	43
6	Pd-3	>99	0	98

259a (0.25 mmol), [Pd] (4 mol% in Pd), IMes·HCl (6 mol%), Cs_2CO_3 (1.3 equiv.), dioxane (0.25 M), 110 ºC, 14 hours. [a]Determined by GC using dodecane as internal standard.[b]

Table 3.5. Palladium precatalyst screening for the synthesis of styrenes.

[241] Other bases were tested: K_2CO_3 (23% yield), NaO^{t}Bu that is well-known for promoting the formation of Pd(NHC) complexes gave 30% yield.

As shown in Table 3.5, the palladium source played an important role determining both selectivity and reactivity. Although in all the cases the selectivity was shifted towards **261a**, the use of palladium(II) triflate gave rise to nearly 1:1 ratios of products (entry 2). To our delight, the use of allyl palladium chloride dimers (entries 4-6) displayed high selectivity with chloro(2-methallyl)palladium dimer (**Pd-3**) giving quantitative yield (entry 6). With an optimal set of reaction conditions, we decided to explore the generality of the reactions en route to benzocyclobutenones **241a** or styrenes **261a**.

3.3.2. Scope for the palladium-catalyzed synthesis of benzocyclobutenones.

Before moving to explore the scope of our transformation we first prepared the differently substituted α-aryl aldehydes by a well-stablished method already employed for the synthesis of benzocyclobutenones from aryl bromides.[227] This approach consist of the alkylation of benzyl cyanides or phenyl acetates **259-SM-III** with a base and an electrophile followed by a subsequent alkylation, if required. Substrates **259-SM-IV** were then reduced with DIBALH. If necessary, substrate **259** was further transform by cross-coupling reactions or classical transformations to prepare further substrates. Alternatively, the ester could be reduced to the primary alcohol with $LiAlH_4$ followed by PCC oxidation. In some cases, the route was better performed by reaction of a Grignard or organolithium reagent with **259-SM-1** forming the tertiary alcohol, that in the presence of TMSCN and catalytic amounts on indium(III) bromide[242] gave the nitrile **259-SM-IV** which was reduced to the aldehyde in the presence of DIBALH (Figure 3.22).

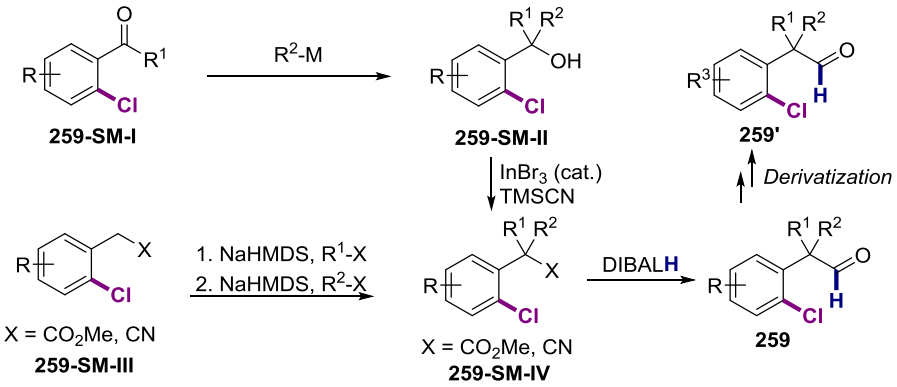

Figure 3.22. Synthesis of α-aryl aldehydes.

[242] Chen, G.; Wang, Z.; Wu, J.; Ding, K. *Org. Lett.* **2008**, *10*, 4573.

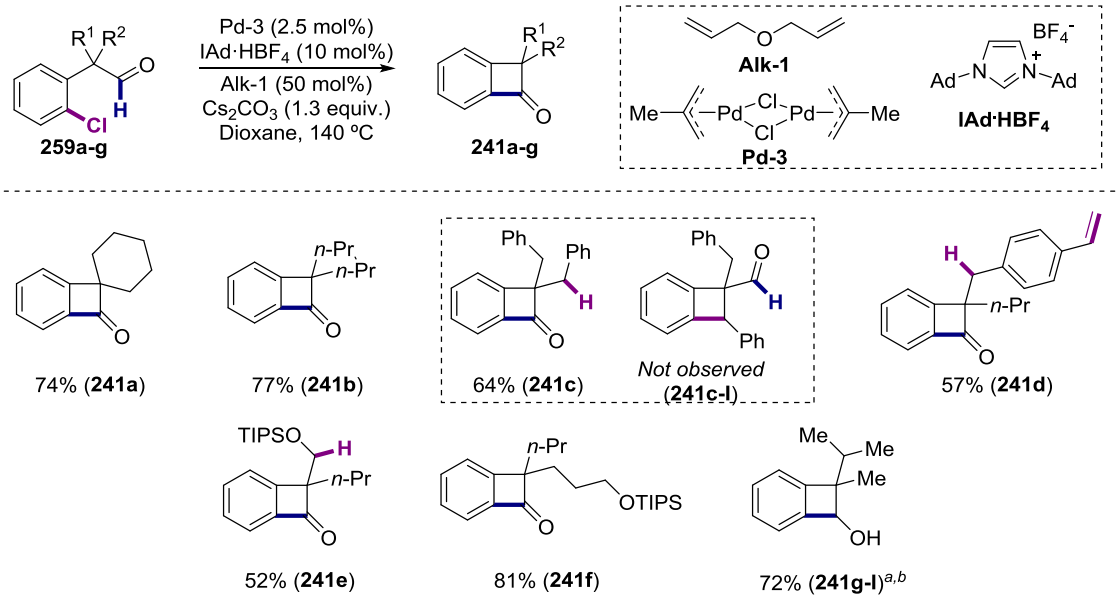

259a-g (0.5 mmol), **Pd-3** (2.5 mol%), **IAd·BF$_4$** (7.5 mol%), Cs_2CO_3 (1.3 equiv.), additive (50 mol%), dioxane (0.25 M), 140 ºC, 14 hours. [a]Isolated as the alcohol after reduction with $NaBH_4$.[b] 2.3:1 diastereoisomeric ratio.

Figure 3.23. Scope of benocyclobutenones bearing different α-substituents.

In order to explore the influence of the substituents on the reaction outcome, we decided to first study the influence exerted by the substituents placed in α-position to the aldehyde motif (Figure 3.23). Regardless of whether the α-substituents are cyclic or not, the products were obtained in good yields. **259c** featuring two benzylic positions gave rise exclusively to benzocyclobutenone and not benzocyclobutene **241c-l**, as judged by analysis of the crude reaction mixture. This results likely indicates the preferential formation of a 5-membered palladacycle over the benzylic C—H bond functionalization. Next, we explored the synthesis of benzocyclobutenones with different substitution pattern in α-position (entries **241d-g**). Again, aldehydic C(sp^2)—H bond functionalization was preferred over benzylic positions (**241d**) or activated C(sp^3)—H bonds by an adjacent oxygen atom (**241e**). Importantly, the sterically encumbered benzocyclobutenone **241g** was obtained in good yields after reduction to the alcohol because of the volatility of the corresponding benzocyclobutenone.

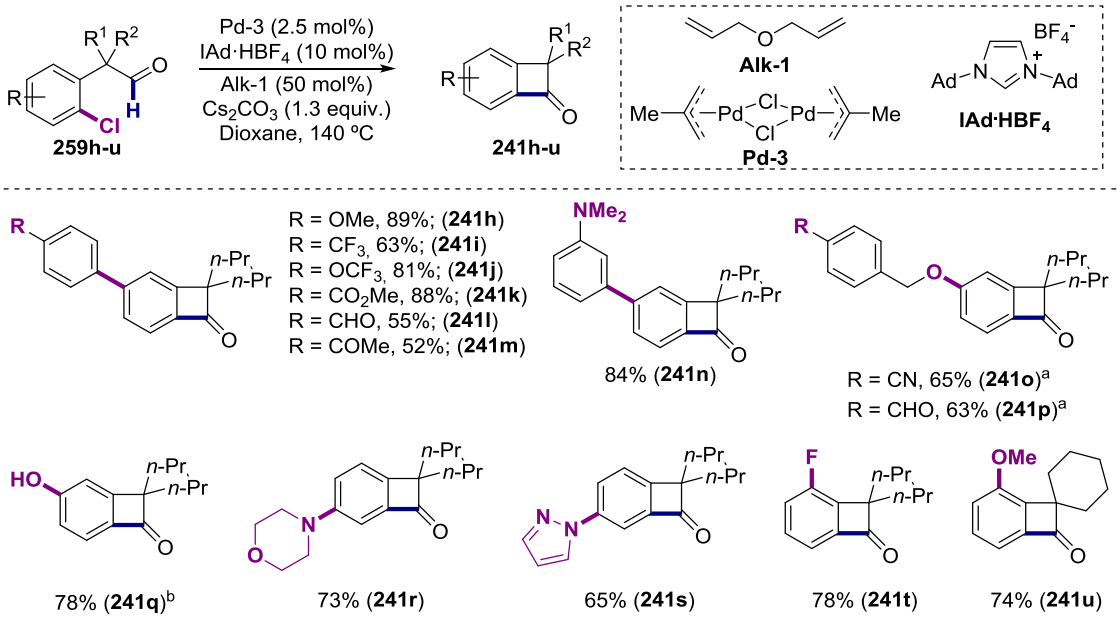

259a (0.5 mmol), **Pd-3** (2.5 mol%), **IAd·BF$_4$** (7.5 mol%), Cs_2CO_3 (1.3 equiv.), additive (50 mol%), dioxane (0.25 M), 140 ºC, 14 hours. [a] **Pd-3** (5 mol%), **IAd·HBF$_4$** (20 mol%). [b] Cs_2CO_3 (2.6 equiv.) used.

Figure 3.24. Scope of benzocyclobutenones bearing modified aryl backbones.

Next, we studied the effect exerted by modifying the electronic nature of the substituents on the aromatic motif as well as to study the functional group tolerance of the transformation. To such end, aldehydes (**259h-n**) were prepared featuring different functional groups at different positions over the aromatic ring. As shown in Figure 3.24, different functional groups were well accommodated. Importantly, no intermolecular acylation was observed in the presence of aldehydes **241l** and **241p**, even though benzaldehydes should be more reactive than phenylacetaldehydes. It is worth noting that no decarbonylation was observed in those cases. Substrates possessing acidic α-protons such as **259m** posed no problems although the corresponding product **241m** was obtained in modest yields. Surprisingly, the reaction was not affected by strong coordinating groups, such as nitriles, amines, phenoxides or heterocycles (**241n-s**). As expected, electron-withdrawing groups at the *meta* position did not inhibit the reaction, obtaining the corresponding products in good yields (**241r,t-u**). Likewise, electron-donating groups at the *para* position were also well accommodated (**241o-q**). This finding is rather surprising taking into consideration that such groups might slow down the rate of oxidative addition.

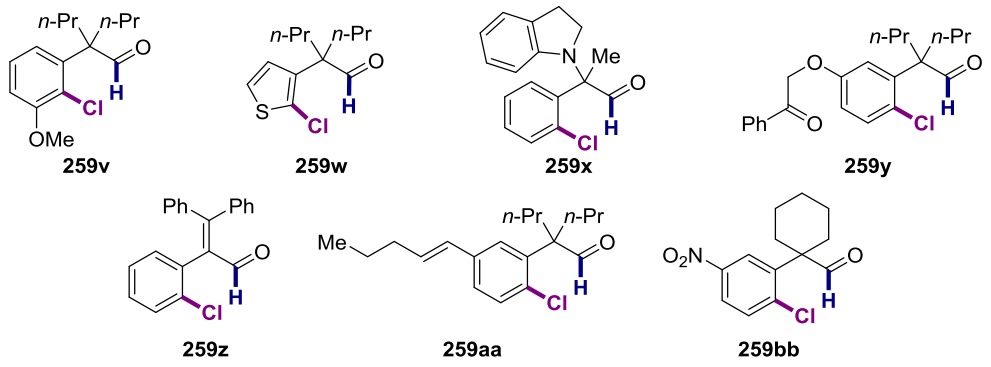

Figure 3.25. Failed substrates under palladium catalysis.

Not surprisingly, not all the substrates tested succeeded in yielding the corresponding benzocyclobutenone. In most cases no reaction took place and the starting material was recovered, although sometimes degradation of the starting material was observed (Figure 3.25). We speculate that substrates **259v-w** failed because of a challenging oxidative addition step of the palladium catalyst over an electron-rich aromatic system. Substrate **259z** resulted in decomposition and no product was observed. We argued that the product might be not formed because of a very uphill reductive elimination (a highly strained benzocyclobutenone would be formed) or because of decomposition of the final product once formed. Probably, **259bb** failed because of catalyst poisoning by coordination with the nitro group.

Interestingly, some other substrates that did not provide the benzocyclobutenone core displayed an alternative reactivity. The first time we observed such a behavior was when using the pyridine derivative **259cc**. We noticed that the presence of an electron-withdrawing group in α-position to the aldehyde motif was a common feature for the substrates showing the mentioned reactivity.[243]

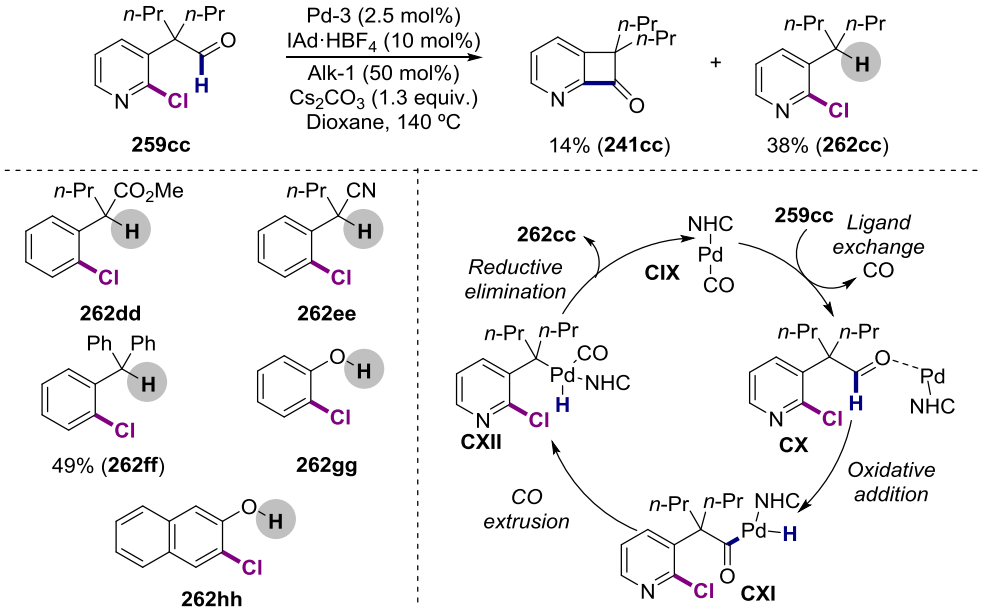

Figure 3.26. Palladium-catalyzed selective decarbonylation of phenylacetaldehydes.

The transition metal-catalyzed decarbonylation of aldehydes is a well-documented process,[244] yet examples with palladium are still rare.[245] Although no mechanistic studies has been conducted, we propose a mechanism based on coordination of the substrate to the palladium(0) catalyst followed by an oxidative addition on the aldehydic C(sp^2)—H bond. The formed acyl palladium(II) complex **CXI** will form alkyl palladium(II) complex (**CXII**) after CO extrusion. Finally, the product will be released after a reductive elimination event. Although a β-hydride elimination could be expected as well from intermediate **CXII**, we did not observed the corresponding styrene products.

[243] Only examples **262cc** and **262ff** were isolated. In any other case the products were identified by GC-MS.
[244] Garralda, M. A. *Dalton Trans.* **2009**, 3635.
[245] (a) Huang, Y.-B.; Yang, Z.; Chen, M.-Y.; Dai, J.-J.; Guo, Q.-X.; Fu, Y. *ChemSusChem* **2013**, *6*, 1348. (b) Modak, A.; Deb, A.; Patra, T.; Rana, S.; Maity, S.; Maiti, D. *Chem. Commun.* **2012**, *48*, 4253. (c) Modak, A.; Naveen, T.; Maiti, D. *Chem. Commun*. **2013**, *49*, 252.

Under rhodium catalysis,[246] the CO extrusion has been postulated as the rate limiting step based on the study of kinetic isotope effect, Hammett plots and DFT calculations. The same DFT calculations, as well as Hammett studies (+0.43 slope), have shown a buildup of negative charge on the α-carbon to the carbonyl during the rate limiting step. Based on these observations, we postulate that the observation of this reactivity in substrates bearing an electron-withdrawing group is based on a more favorable CO extrusion as the negative charge buildup in the benzylic position will be stabilized by the α-electron-withdrawing group. In the case of formates **259gg** and **259hh**, it has been demonstrated the rapid decarbonylation in the presence of carbonate bases, leading to the corresponding phenoxides.[247]

Our previous work using aryl bromides had few drawbacks, primarily the limitation to form four-membered rings and the synthesis of α,α-disubstituted benzocyclobutenones.[227] As shown in Scheme 3.8, our new protocol allowed for obtaining indanone **241ii** in high yield. Likewise, the monosubstituted benzocyclobutenone **241jj** could be prepared using an α-silylated aldehyde followed by TBAF treatment.

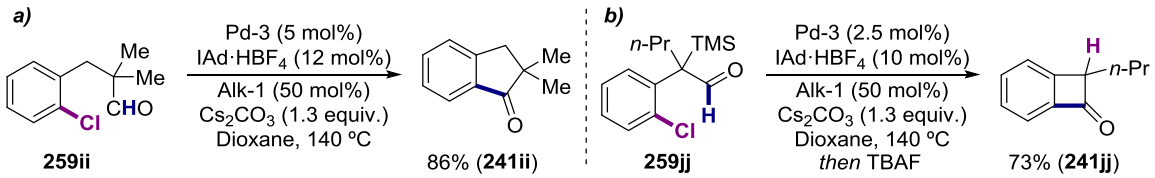

Scheme 3.8. Overcoming the previous limitations.

Finally, we decided to study the regioselectivity of our methodology by introducing potential reactive sites within the side chain to study whether our protocol is able to differentiate between bonds of related nature. First, we evaluated the regioselectivity in the presence of two different C(sp^2)—H bonds (Scheme 3.9a). While activation of the aldehydic bond would render the benzocyclobutenone **241kk**, the aromatic C(sp^2)—H bond-functionalization would form the fluorene **241kk-I**. Consequently, in this experiment not only the nature of the bond must be considered but also the relative position between the aryl chloride and the bond to be cleaved. Interestingly, regioselective formation of benzocyclobutenone **241kk** was observed with not even traces of the corresponding fluorene detected in the crude reaction mixture. It should be noticed that in the previous chapter such selectivity was not observed and functionalization of the methyl (**195ra**) and the aryl equally occurred (**195ra-I**) thus showing the higher reactivity of aldehydes in comparison with methyl motifs (Figure 2.27). When two electronically similar aryl chlorides were present within the substrate featuring a distinct relative position to the aldehyde only benzocyclobutenone **241ll** was observed, whereas indanone formation (**241ll-I**) was not observed[248] (Scheme 3.9b).

[246] Fristrup, P.; Kreis, M.; Palmelund, A.; Norrby, P.-O.; Madsen, R. *J. Am. Chem. Soc.* **2008**, *130*, 5206.
[247] (a) Bruder, M.; Smith, S. J.; Blake, A. J.; Moody, C. J. *Org. Biomol. Chem.* **2009**, *7*, 2127. (b) Chen, J.; Chen, X.; Willot, M.; Zhu, J. *Angew. Chem. Int. Ed.* **2006**, *45*, 8028. (c) Fischer, J.; Reynolds, A. J.; Sharp, L. A.; Sheerburn, M. S. *Org. Lett.* **2004**, *6*, 1345. (d) Yalfani, M. S.; Lolli, G.; Wolf, A.; Mieczko, L.; Müller, T. E.; Leitner, W. *Green. Chem.* **2013**, *15*, 1146.
[248] Some hydrodechlorination of **259ll** was observed by GC-MS, yet the dechlorinated position remains unidentified.

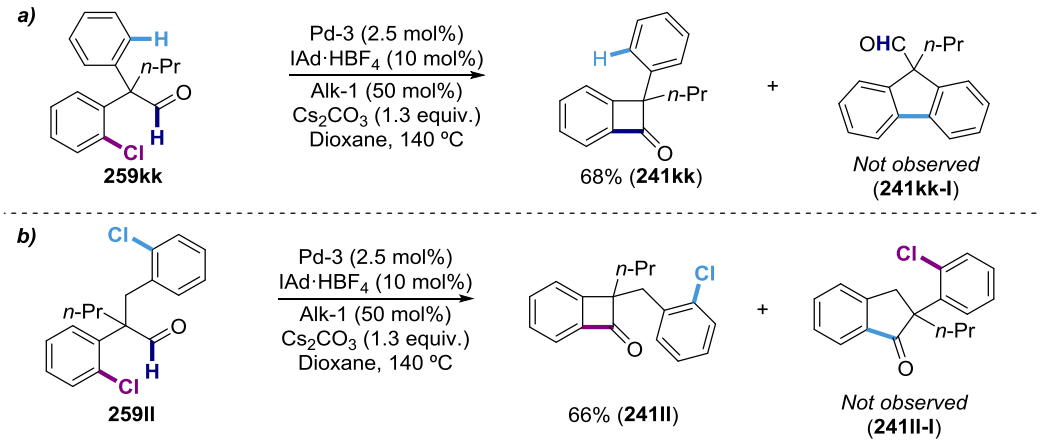

Scheme 3.9. Regioselectivity studied for the synthesis of benzocyclobutenones.

3.3.3. Scope for the palladium-catalyzed synthesis of styrenes.

In order to demonstrate the orthogonal reactivity of our system, we briefly explored the preparative scope for the synthesis of styrenes using **IMes** as ligand. However, the scope was not studied in detail since our interest was primarily focused on the synthesis of benzocyclobutenones.

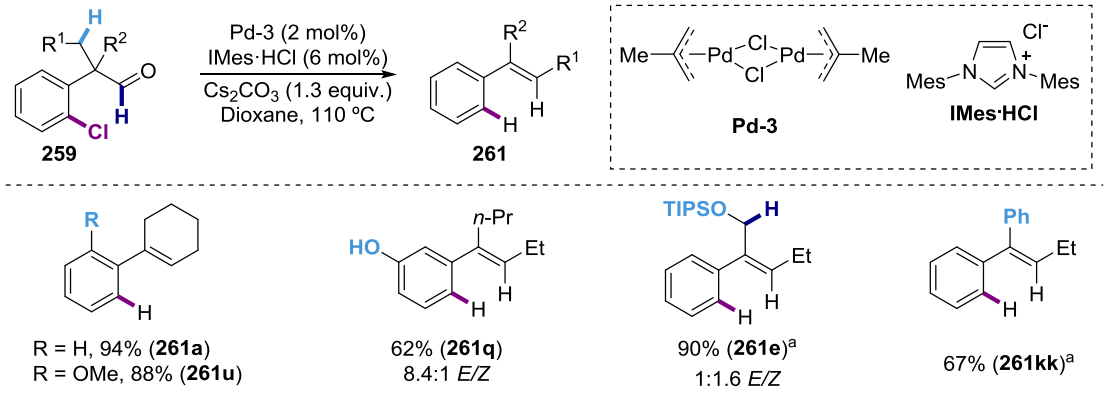

259 (0.5 mmol), **Pd-3** (2 mol%), **IMes·HCl** (6 mol%), Cs_2CO_3 (1.3 equiv.), dioxane (0.25 M), 110 ºC, 14 hours. [a] 140 ºC.

Figure 3.26. Substrate scope for the synthesis of trisubstitutedstyrenes.

As depicted in Figure 3.26, the reaction was not affected by electronic effects and *meta*-electron-withdrawing groups (**261u**) as well as *para*-electron-donating groups (**261q**) were well accommodated. Importantly, the reaction outcome was insensitive by the cyclic (**261a,u**) or acyclic nature of the α-substitutents (**261q,e,kk**). In the presence of distinct α-alkyl chains, the reaction was regioselective as evidenced by exclusive formation of **261e**.

3.3.4. Mechanistic discussion concerning the synthesis of benzocyclobutenones.

The reactivity observed for the palladium-catalyzed intramolecular acylation of aryl chlorides can be rationalized by two mechanisms (see Figure 3.28). Both pathways are initiated by oxidative addition of monocoordinated palladium(0) to the aryl—Cl bond. Then, a ligand exchange occurs between the chloride ligand and exogenous carbonate base forming **CIV**. Cycle A evolves through a concerted metalation-deprotonation mechanism rendering palladacycle **CV-CsHCO$_3$** that will form **CV** upon bicarbonate dissociation.[85] A final reductive elimination will release the benzocyclobutenone **241** with concomitant recovery of **CXIII**. On

the other hand, mechanism B will follow a different pathway; upon aldehyde coordination to the metal center, an insertion across the C—O double bond of the aldehyde could form palladium alcoxyde **CXIV**.[249] Subsequently, a β-hydride elimination followed by a final reductive elimination step would generate the final product while regenerating the active catalytic species.

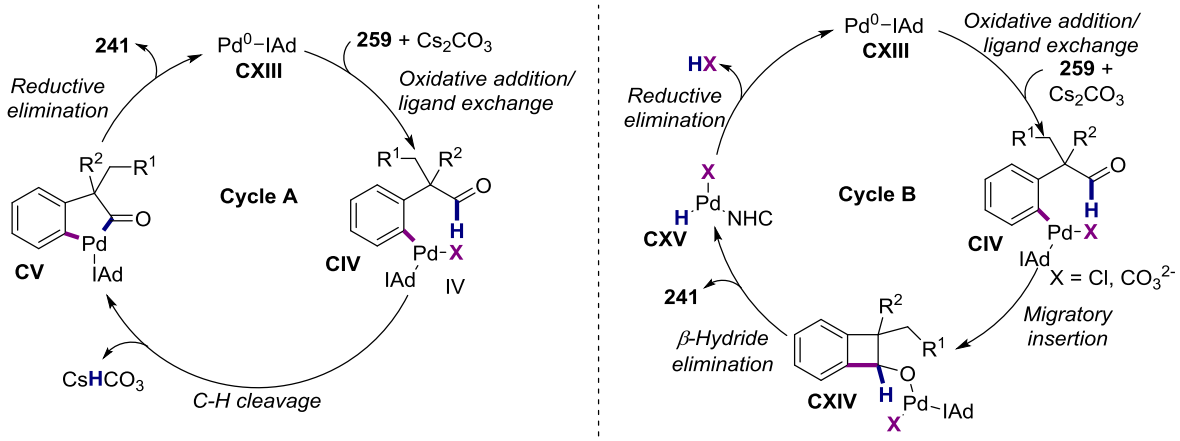

Figure 3.28. Putative mechanistic pathways for the synthesis of benzocyclobutenones.

In order to gain some insights on the mechanism, the kinetic isotope effect[250] was studied using aldehydes **259b** and **259b-*d1***. We anticipated that both mechanisms could potentially display a normal KIE if the aldehydic C—H cleavage event is the rate-determining step[80] for mechanism A or if β-hydride elimination is the rate-limiting step[251] for mechanism B. Furthermore, an inverse secondary kinetic isotope effect in B could be expected if the migratory insertion step is rate-determining as a consequence of the rehybridization of the C—H bond from sp^2 to sp^3.[252]

[249] (a) Solé, D.; Fernández, I. *Acc. Chem. Res.* **2014**, *47*, 168. (b) Fernández, I.; Solé, D.; Sierra, M. A. *J. Org. Chem.* **2011**, *76*, 1592.
[250] Simmons, E.; Hartwig, J. F. *Angew. Chem. Int. Ed.* **2012**, *51*, 3066.
[251] (a) Mueller, J. A.; Goller, C. P.; Sigman, M. S. *J. Am. Chem. Soc.* **2004**, *126*, 9724. (b) Steinhoff, B. A.; Stahl, S. S. *Org. Lett.* **2002**, *4*, 4179. (c) Blum, O.; Milstien, D. *J. Am. Chem. Soc.* **1995**, *117*, 4582. (d) Alexanian, E. J.; Hartwig, J. F. *J. Am. Chem. Soc.* **2008**, *130*, 15627.
[252] Gómez-Gallego, M.; Sierra, M. A. *Chem. Rev.* **2011**, *111*, 4857.

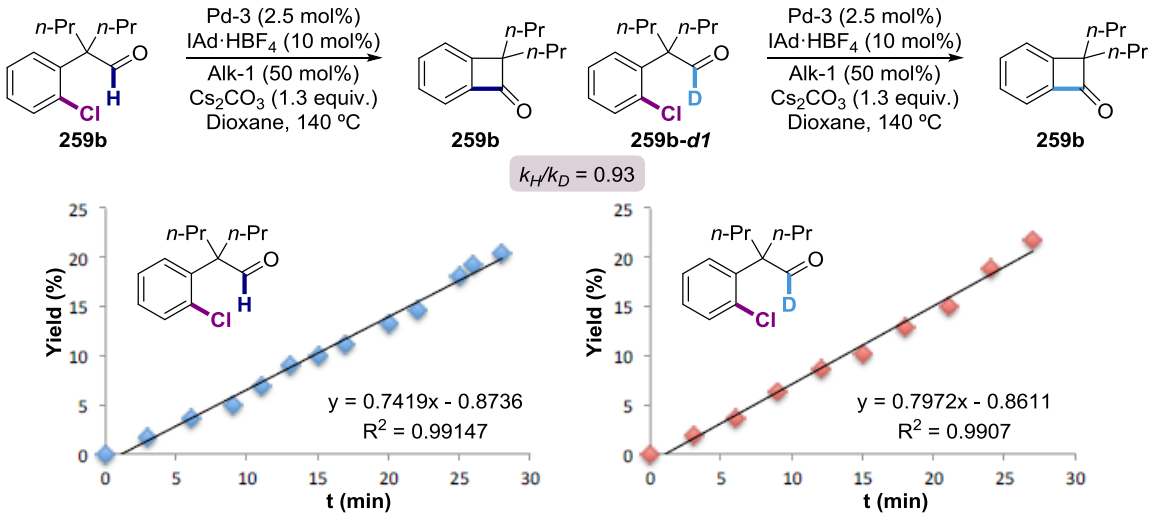

Figure 3.29. Kinetic isotope effect studies for the synthesis of benzocyclobutenones.

Kinetic isotope effect determined by measuring the initial rate constant of two independent reactions showed a kinetic isotope effect of 0.93. Although such inverse secondary kinetic isotope effect[253] might suggest a mechanism of the type B, the highly heterogeneous components might trigger a non-negligible experimental error on the measurement.

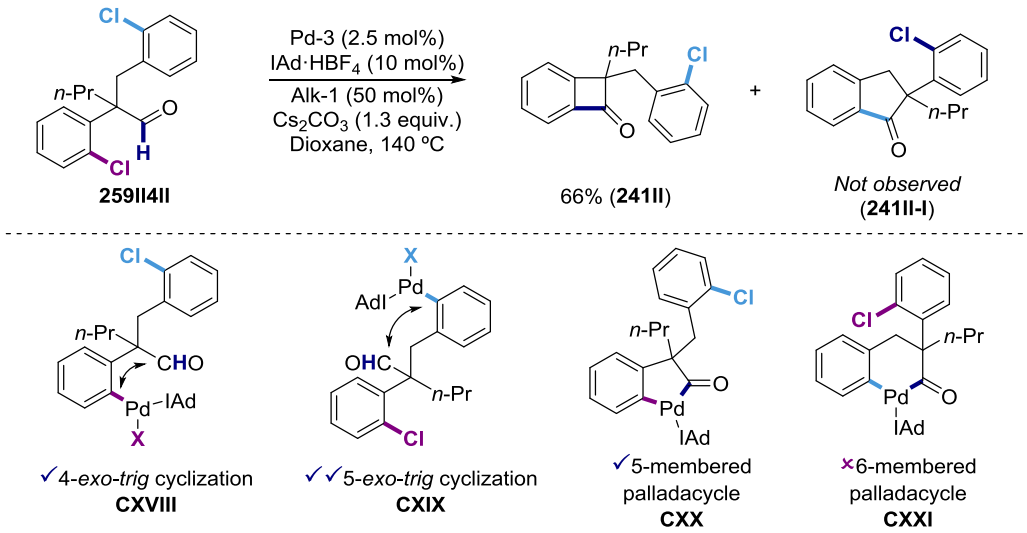

Figure 3.30. Mechanistic rational for the regioselective synthesis of benzocyclobutenones.

If mechanism B is operating and the migratory insertion is the rate-determining step, then, formation of **241ll-I** should be favored over the formation of **241ll** as the formation of five-membered rings is usually preferred over four-membered rings.[254] However, we did not observe formation of indanone **241ll-I**. Remarkably, a mechanism of type A would favor the formation of benzocyclobutenone **241ll** through formation of a more stable 5-membered palladacycle. Several are the possible explanations for the lack of indanone formation under an operating mechanism B. (1) It could be attributed to a slower cyclization event because of

[253] It could be also attributed to an equilibrium isotope effect. See ref. 252.
[254] (a) Baldwin, J. E. *J. Chem. Soc., Chem. Commun.* **1976**, *734.* (b) Gilmore, K.; Alabugin, I. V. *Chem. Rev.* **2011**, *111*, 6513.

higher freedom levels for intermediate **CXIX** than for **CXVIII**, (2) because of a higher Thorpe-Ingold effect for intermediate **CXVIII** than for intermediate **CXIX** or (3) because of a more favorable oxidative addition directed by coordination with the aldehyde. Importantly, the experiment shown in Figure 3.30 also suggests a reversible oxidative addition step for the C—Cl bond not adjacent to the aldehydic motif. Actually, the reversible oxidative addition has been demonstrate in the presence of bulky phosphines by the groups of Hartwig and Lautens.[255] However, the pre-coordination with the aldehyde might lead to a regioselective and irreversible oxidative addition.

It must be highlighted that in the previous work published by our group regarding the synthesis of benzocyclobutenones from aryl bromides,[227] a kinetic isotope effect of 2.8 was observed, indicating a possible concerted metalation-deprotonation (mechanism A) or β-hydride elimination (mechanism B) as rate-limiting steps. Because of indanone **241ii** could not be prepared from the corresponding aryl bromide, the mechanism B was considered unlikely (the 5-*exo*-*trig* cyclization should be favored under a Heck-type mechanism) therefore, mechanism A was considered to be the most likely to be operating. In the present case, the evidences are pointing towards the opposite direction, indanones are within reach (see scheme 3.8a) and an inverse secondary kinetic isotope effect is observed. However, in the absence of further available data, we cannot rule out neither mechanism A or B when using aryl chlorides as substrates.

3.3.5. Mechanistic discussion concerning the synthesis of styrenes.

Regarding the synthesis of styrenes from aryl chlorides, two mechanisms can be proposed. Both of them are initiated by an oxidative addition of the palladium(0) catalyst **CXVI** over the aryl chloride **259** generating the complex **CIV**. This is followed by a concerted metalation-deprotonation event forming palladacycle **CV**. At this point, two possibilities arise. For mechanism C, the hydrogen carbonate transfers the proton to the aryl ring in a formal [1,4]-palladium migration[256] forming a pending acyl palladium(II) complex (**CVI**). This complex will extrude CO forming the alkyl palladium complex **CVII** that, upon ligand dissociation, will be able to interact with the β-hydrogens thus triggering a β-hydride elimination step that will lead to the styrene **261** and the complex **CXV** formation. A final reductive elimination would recover the active catalyst. On the other hand, if mechanism D is operating, once the palladacycle **CV** is formed, the next step will be extrusion of CO forming a highly strained palladacycle (**CXVII**). Subsequently, β-hydride elimination will occur after ligand dissociation forming an aryl palladium(II) hydride (**CXVIII**). A final reductive elimination would yield the product and the active catalyst.

[255] (a) Roy, A. H.; Hartiwg, J. F. *Organometallics* **2004**, *23*, 1533. (b) Newman, S. G.; Lautens, M. *J. Am. Chem. Soc.* **2010**, *132*, 11416.
[256] (a) Ma, S.; Gu, Z. *Angew. Chem. Int. Ed.* **2005**, *44*, 7512. (b) Zhao, J.; Yue, D.; Campo, M. A.; Larock, R. C. *J. Am. Chem. Soc.* **2007**, *129*, 5288. (c) Campo, M. A.; Huang, Q.; Yao, T.; Tian, Q.; Larock, R. C. *J. Am. Chem. Soc.* **2003**, *125*, 11506.

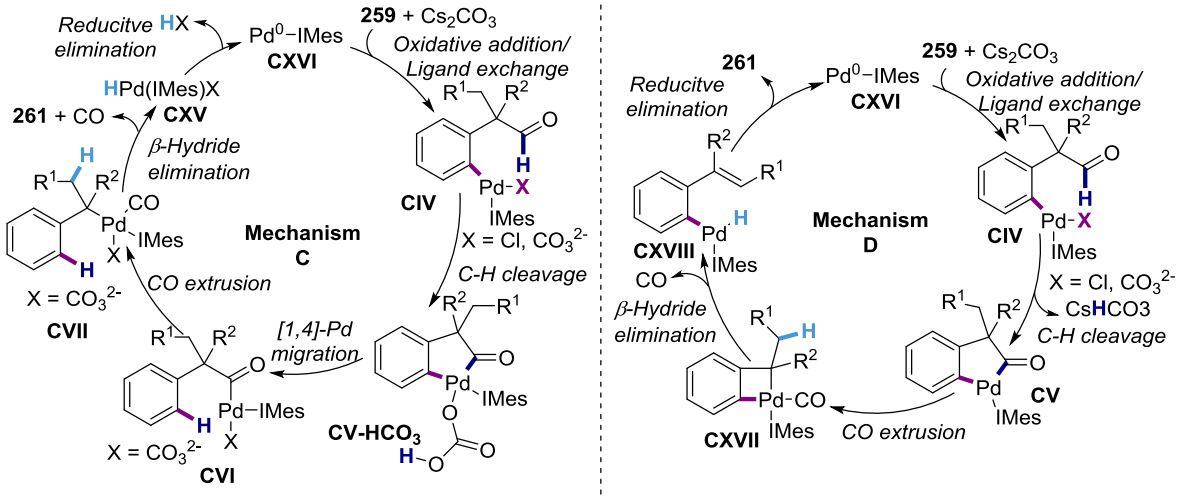

Figure 3.31. Mechanistic proposals for the synthesis of styrenes from aryl chlorides.

In order to rule out any of the two proposed mechanisms, we envisioned that submitting labelled-aldehyde **259a-*d1*** under reaction conditions could provide empirical evidence for these mechanistic hypothesis. If mechanism C is working, we might expect deuterium transfer to the arene *ipso*-position, whereas if mechanism D is operating, then, the deuterium label will be lost during the catalytic cycle. Interestingly, we observed complete deuterium transfer to the *ipso*-position thus ruling out the mechanism D (Scheme 3.10).

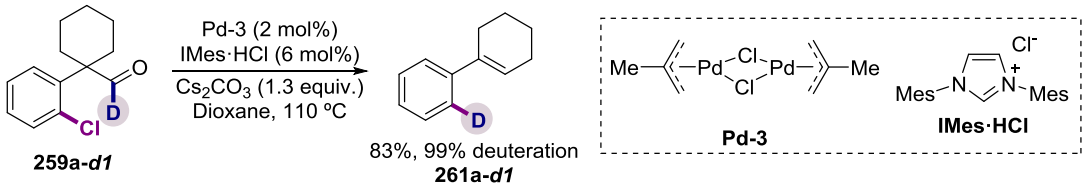

Scheme 3.10. Deuterium-labelling experiments.

Considering that mechanism C is operating, we will next explain the results observed in the scope of the transformation. It was shown in Figure 3.26 that the reaction of **259e** gave the product **261e** preferentially and not even traces of **261e-l** were detected. If mechanism C is operating, the product determining step will be the β-hydride elimination. As shown in Figure 3.32, the intermediate **CVI-259e** has the possibility to react with two different hydrogens. As it is known, the β-hydride elimination step requires, among other things, the palladium to be in *syn* position to the hydrogen which is achieved by the free rotation across the C—C bond. The formation of **261e** or **261e-l** will depend on the energy of the transition state for this step. It is known that in the transition state of the β-hydrogen elimination, there is a positive charge buildup at the *ipso* carbon (see Figure 3.32, **β-H-TS**), consequently, electron-donor R substituents will be able to stabilize the transition state, whereas electron-withdrawing R groups will do the opposite.[257] In the case of substrate **259e**, the upper path will lead to a transition state with an ethyl group adjacent to the positive buildup charge, therefore stabilizing it by inductive effect. On the other hand, the alternative pathway will lead to a transition state where an OTIPS is attached to the positive buildup and because of the

[257] (a) Sam, B.; Luong, T.; Krische, M. J. *Angew. Chem. Int. Ed.* **2015**, *54*, 5465. (b) Gellman, A. J.; Dai, Q. *J. Am. Chem. Soc.* **1993**, *115*, 722.

electron-negativity of the oxygen atom the transition state will result destabilized. On this basis, **CVI-TS** will be lower in energy than **CVI-I-TS** and therefore, **261e** will be formed preferentially.[258]

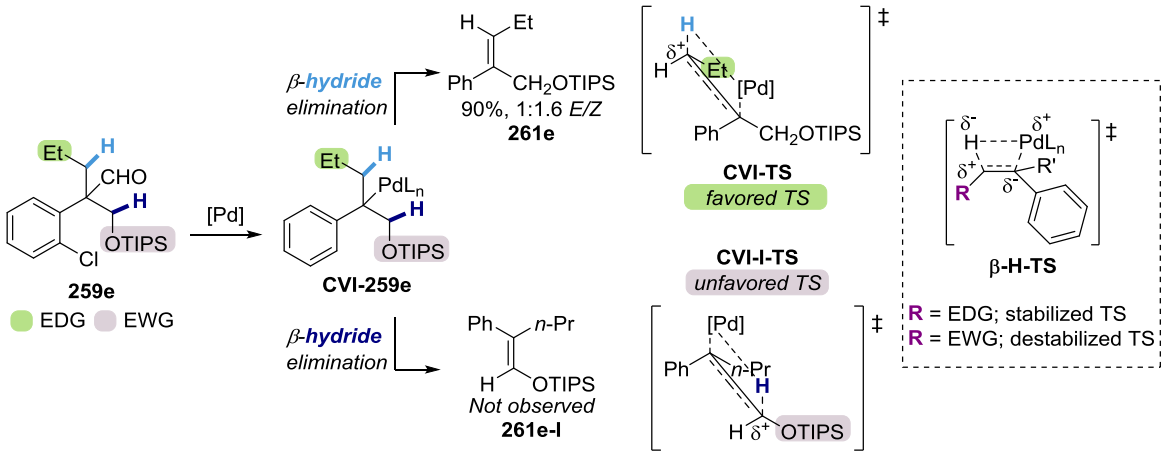

Figure 3.32. Regioselective β-hydride elimination: Transition state stabilization.

On the other hand, the stereochemical outcome of the reaction can be explained by the Curtin-Hammett principle. This principle states[259] that in situations in which two different products can be formed from two substrates involved in a fast equilibrium, the product distribution will not be determined only by the relative proportion of the reactants (determined by the equilibrium) but it will be also controlled by the difference in standard Gibbs energies ($\Delta\Delta G^{\ddagger}$) of the transition states.

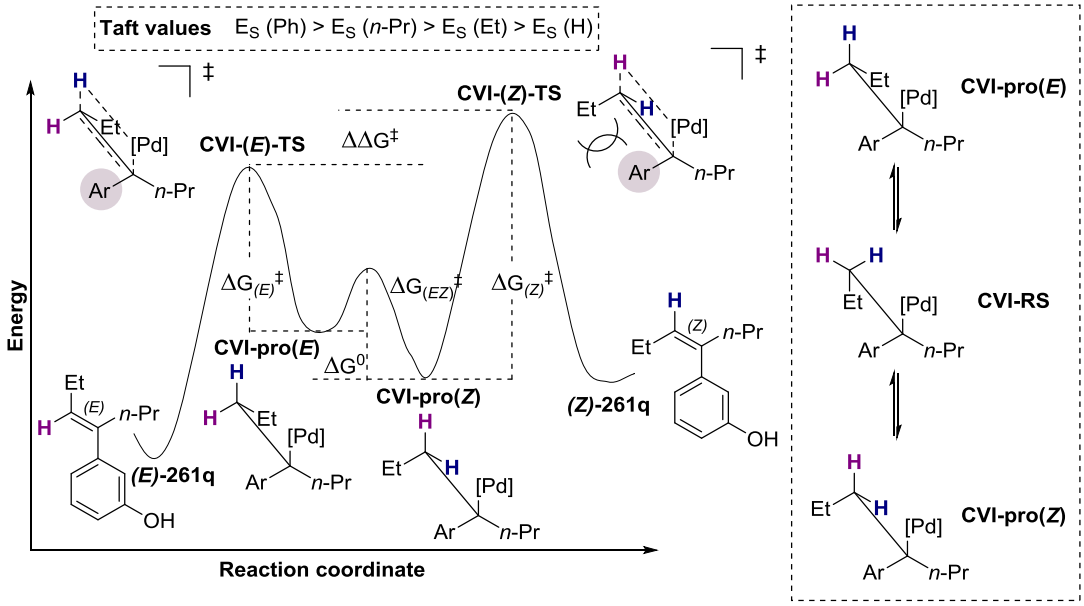

Figure 3.32. Stereoselectivity control based on the Curtin-Hammett principle.

Unlike the previous case studied where the different stability of the transition states were based mostly on electronic factors, in this case the energy of the transition state will be

[258] The explanation here is just a hypothesis and could occur that the observed styrene is formed upon isomerization in the reaction media.
[259] (a) Seeman, J. I. *Chem. Rev.* **1983**, *83*, 83. (b) Seeman, J. I. *J. Chem. Ed.* **1986**, *63*, 42.

determined by steric interactions.[260] The stereochemical control for substrate **259e** will be determined by the stability of the transition states **CVI-(*E*)-TS** and **CVI-(*Z*)-TS** since the β-hydride elimination will be the stereochemical-determining step. The two different transition states will be formed from the conformers **CVI-pro(*E*)** and **CVI-pro(*Z*)** respectively which are in fast equilibrium through intermediate **CVI-RS**. When the two possible transition state are compared, **CVI-(*Z*)-TS** will be higher in energy as the ethyl and aryl substituents are in eclipsed conformation whereas in **CVI-(E)-TS** the more bulky aryl is eclipsed with a small proton. Consequently, the formation of **(*E*)-261q** will be favored.[261,262]

3.3.6. Further comments concerning the different steps.

3.3.6.1 Catalyst activation

The two presented methodologies are based on a similar catalytic system based on the use of a palladium(II) precatalyst and an ancillary NHC ligand. The first step of the catalytic cycle has not been yet commented and occurs similarly for the synthesis of benzocyclobutenones and styrenes. It has been reported that (allyl)palladium(II) chloride dimers react with equimolecular amounts of NHC ligands in the presence of *tert*-butoxide base to form the monocoordinated palladium(0) (**CXVI**) along with allyl *tert*-butyl ether **262** and potassium chloride (Figure 3.33).[263] However, the authors claimed that other bases such as cesium carbonate, cesium fluoride and potassium phosphate or sodium acetate were unable to activate the catalyst as they could not promote a Suzuki-Miyaura cross-coupling. Nevertheless, this is a very strong statement based on indirect evidences. Indeed, Suzuki-Miyaura reaction using the aforementioned bases in combination with allylpalladium(II) chloride dimers and a NHC ligand has been reported using aryl bromides as substrates.[264] Although we cannot be certain of the mechanism for the formation of **CXVI** in the presence of carbonate base, we believe that it is indeed formed under the reactions conditions.[265]

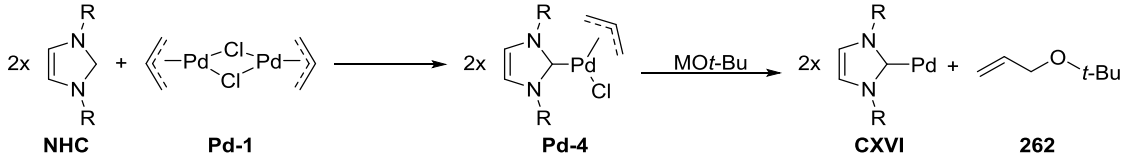

Figure 3.33. Formation of monocoordinated Pd(0) active catalysts.

The 12-electron-complex **CXVI** will be very reactive towards oxidative addition, and is expected that the use of bulky ligands such as NHC would stabilize these intermediates while avoiding decomposition pathways. This is likely due to the pocket-array of NHC ligands in comparison with the cone-array for phosphines (whereas in the phosphines the substituents

[260] Beletskaya, I. P.; Cheprakov, A. V. *Chem. Rev.* **2000**, *100*, 3009.
[261] Steric bulkiness was determined by the Taft factor: E_s (H) = 1.24 < E_s (Et) = -0.07 < E_s (*n*-Pr) = -0.36 < E_s (Ph) = -2.55. See Taft Jr. R. W.; *J. Am. Chem. Soc.* **1952**, *74*, 2729.
[262] Please, note that the energy for the reactants and products might be no correctly assigned. The picture only targets to represent the principles of the Curtin-Hammett principle and the relative energy of the TS, the other energy levels have been assigned randomly.
[263] (a) Viciu, M. S.; Germaneau, R. F.; Navarro-Fernandez, O.; Stevens, E. D.; Nolan, S. P. *Organometallics* **2002**, *21*, 5470. (b) Marion, N,; Nolan, S. P. *Acc. Chem. Res.* **2008**, *41*, 1440.
[264] Wang, A.-E.; Zhong, J.; Xie, J.-H.; Li, K.; Zhou, Q.-L. *Adv. Synth. Catal.* **2004**, *346*, 595.
[265] (a) Hruszkewycz, D. P.; Guard, L. M.; Balcells, D.; Feldamn, N.; Hazari, N.; Tilset, M. *Organometallics* **2015**, *34*, 381. (b) Melvin, P. R.; Balcells, D.; Hazari, N.; Nova, A. *Organometallics* **2015**, *5*, 5596.

are oriented away from the metal, in the NHC ligands the metal is surrounded by the ligand as the substituents of the nitrogen atoms are oriented towards the metal center)

3.3.6.3 The role of allyl ether

We have previously seen that the addition of allyl ether (**Alk-1**) exerted an important effect on the reaction outcome by increasing considerably the yield of the transformation (Table 3.4). We hypothesized, based on the good match between yield and conversion that under the reaction conditions in the absence of additive, the catalyst was slowly decomposing, thus leading to poor conversions. In fact, the addition of allyl ether was translated in high conversions and yields therefore confirming our hypothesis. The rationale behind the utilization of allyl ether relies on its ability to stabilize low-coordinated metal centers.[266] Table 3.4 shows that the yield was higher for allyl ether (**Alk-1**) than for 1,6-heptadiene (**Alk-2**). We believe that the better binding of allyl ether to the metal center is responsible of a better stabilization of the active catalyst and therefore higher conversion whereas for **Alk-2**, the binding affinity with **CXVI** is lower and therefore the stabilization is not as effective as for allyl ether.[267,238]

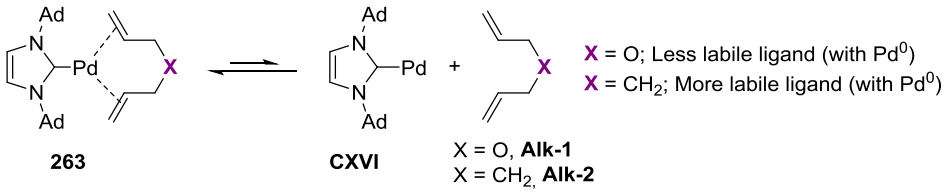

Figure 3.34. Coordination of the ligand with the active catalyst.

As we have seen before, the addition of the additive was only required for the synthesis of benzocyclobutenones, consequently, it could be thought that the additive is playing an important role in a step that is not shared with the synthesis of styrenes beyond the catalyst stabilization. However, we believe that this is not the case, and the reason why its addition is not required for the synthesis of styrenes is because the product itself is acting as a stabilizing ligand.

3.3.6.2 Oxidative addition

Oxidative addition of aryl chlorides has been demonstrated to occur by a dissociative mechanism with 12-electron species.[268] Usually, this step takes place with bulky phosphines as the dissociation of these phosphines is easier than for the less sterically demanding ones.[269] The advantage of using an allyl pallaldium(II) chloride dimer in combination with a NHC ligand and a base is that a 12 electron palladium(0) complex is rapidly formed, and therefore, the catalytic system do not have to rely on dissociation equilibriums to form the active species. In

[266] (a) Wu, J.; Faller, J. W.; Hazari, N.; Scheimer, T. J. *Organometallics* **2012**, *31*, 806. (b) Andreu, M. G.; Zapf, A.; Beller, M. *Chem. Commun.* **2000**, 2475. (c) Jackstell, R.; Andreu, M. G.; Frisch, A.; Selvakumar, K.; Zapf, A.; Klein, H.; Spannenberg, A.; Röttger, D.; Briel, O.; Karch, R.; Beller, M. *Angew. Chem. Int. Ed.* **2002**, *41*, 986. (d) Krause, J.; Cestaric, G.; Haack, K.-J.; Seevogel, K.; Storm, W.; Pörschke, K.-R. *J. Am. Chem. Soc.* **1999**, *121*, 9807.

[267] In Pd(0) centers, the binding affinity with olefins will be higher for those that are electron-deficient based on a higher π-back donation from the palladium to the olefin.

[268] Christmann, U.; Vilar, R. *Angew. Chem. Int. Ed.* **2005**, *44*, 366.

[269] (a) Alcazar-Roman, L. M; Hartwig, J. F. *J. Am. Chem. Soc.* **2001**, *123*, 12905. (b) Hamann, B. C.; Hartiwg, J. F. *J. Am. Chem. Soc.* **1998**, *120*, 7369. (c) Ahlquist, M.; Norrby, P.-O. *Organometallics* **2007**, *26*, 550.

fact, mechanistic studies have demonstrated that the dissociative oxidative addition of $Pd(NHC)_2$ on aryl chlorides is rate determining because of the ligand dissociation.[270] In addition, the oxidative addition will be also favored by the high electron-density of the palladium center given by the NHC ligand.

3.3.6.3 Reductive elimination vs. [1,4]-palladium migration

If we consider that mechanism A and C are operating for the synthesis of benzocyclobutenones and styrenes respectively, then the product determining step will take place from the intermediate **CV** or **CV-HCO$_3$** (Figure 3.35). Based on this hypothesis, we believe that the selectivity switch can be explained based on the reductive elimination rate. It is known that the reductive elimination is favored by electron-deficient ligands as the generated driving force for the reduction is larger because of a higher stability of the formed complex.[235] However, it has also been demonstrated that in the presence of bulky ligands the steric factors overcome the electronics. For example, Hartwig and Roy have demonstrated that whereas the reductive elimination with bulky and strong-donor *tert*-butylphosphine is feasible for aryl amidopalladium(II) complexes, only a 10-15% of product is obtained with cyclohexyldi(*tert*-butyl)phosphine and no reductive elimination occurs with the less donating, yet smaller, tricyclohexylphosphine.[271]

In our case, after the C—H bond-cleavage two products can be formed, **CV** and **CV-HCO$_3$**. For these complexes, the reductive elimination is only observed when **IAd** is used as ligand, which is bigger than **IMes** (see buried volumes on Figure 3.35). In addition, **IAd** is more electron donating as well, therefore, we can conclude that the reductive elimination is mostly controlled by steric factors and not by electronic factors.[272] On the other hand, in the presence of **IMes** no reductive elimination is observed, an observation that goes in line with the lower buried volume of **IMes**. Alternatively, in the presence of a smaller ligand, the *ipso*-protonation might occur at a higher rate than reductive elimination.

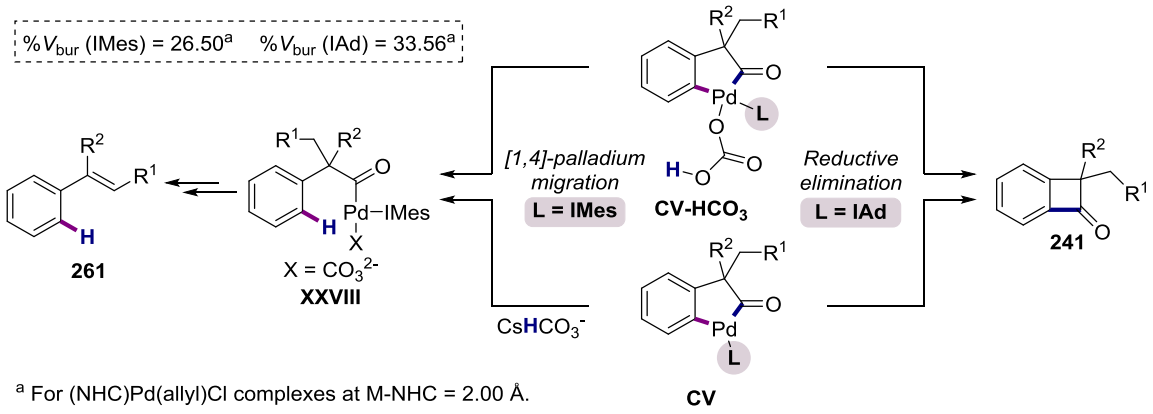

Figure 3.35. Ligand induced mechanistic switch: The importance of the bulkiness.

[270] Lewis, A. K. K.; Caddick, S.; cloke, F. G. N.; Billingham, N. C.; Hitchcock, P. B.; Leonard, J. *J. Am. Chem. Soc.* **2003**, *125*, 10066.
[271] Roy, A. H.; Hartwig, J. F. *Organometallics* **2004**, *23*, 1533.
[272] pK_a (H_2O) for the chloride salt are 26.50 and 33.56 for IMes and IAd respectively, thus indicating a higher donor character for IAd. Tollman electronic parameters cannot be evaluated as for IMes the complex formed is [Ni(IMes)$(CO)_3$] and [Ni(IAd)$(CO)_2$] for IAd showing the bulkiness of the latter ligand. See: Nelson, D. J.; Nolan, S. P. *Chem. Soc. Rev.* **2013**, 42, 6723.

Alternatively, we can conceive a scenario where the *ipso*-protonation only occurs in an intramolecular fashion from **CV-HCO$_3$**. Then, the selectivity displayed could be explained based on the fast dissociation of hydrogen carbonate form intermediate **CV-HCO$_3$** in the presence of the very bulky **IAd**, thus favoring the formation of **CV**. On the other hand, the smaller **IMes** will be able to keep the bicarbonate bound in the inner-coordination sphere of the metal and therefore the [1,4]-migration would be feasible. As a final remark, it has been demonstrated that the rate of the reductive elimination is higher for [PdL(Ar)X)] complexes than for tetracoordinated [PdL$_2$(Ar)X]. In the presence of bulky NHC ligands, the T-shape conformation is common and therefore the reductive elimination will not be as demanding as expected.[273]

3.3.7 Reversibility studies

A possibility that has not been yet considered is the intermediacy of benzocyclobutenones in the synthesis of styrenes. That is, under reaction conditions, the benzocyclobutenone **241** is formed and subsequently it is transformed to the styrene **261**. This possibility was considered in the context of the synthesis of benzocyclobutenones[227] and styrenes[232] from aryl bromides **264** as a part of an ongoing collaboration to disclose the operative mechanism for this transformation. As can be seen in Scheme 3.11, the selectivity switch from product **261** to **241** is based on the ligand choice, where the more flexible and sterically hindered dcypp is responsible for the styrene formation. We believe, that **dcypp** is more prone to dissociate one phosphorus atom in contrast to the less hindered and more rigid **BINAP**. Because of the hemilabile character of **dcypp**, the intermediate **CV-HCO$_3$** will be more likely to be formed with this ligand and therefore the [1,4]-migration will be favored.

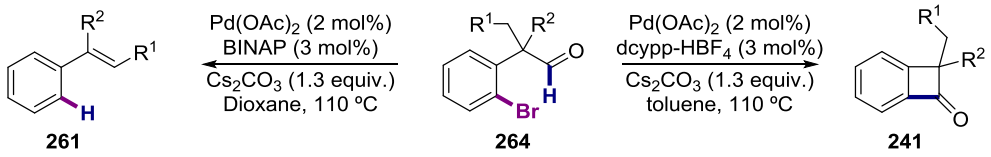

Scheme 3.11. Palladium-catalyzed synthesis of benzocyclobutenones and styrenes from aryl bromides.

In order to study the intermediacy of benzocyclobutenones **241**, substrate **241a** was submitted under styrene reaction conditions (Figure 3.36). Surprisingly, quantitative formation of styrene **261a** was observed when using PCy$_3$, a ligand with similar reactivity than **dcypp**. Indeed, it was observed that Pd(PCy$_3$)$_2$ alone was able to catalyze this transformation in quantitative yields. Does this result imply that benzocyclobutenones are intermediates in the synthesis of styrenes? As shown by deuterium-labelling experiments (Scheme 3.10), a complete deuterium transfer from the aldehydic proton to the *ipso*-position of the aromatic ring was found, thus ruling out this alternative.

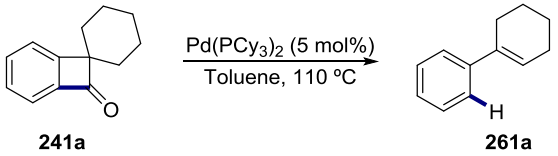

Deviation	Yield 241a (%)	Yield 261a (%)
None	0	>99
Cs_2CO_3	39	62
CO (1 atm)	0	>99
D_2O (1 equiv.)	0	>99

Figure 3.36. Reversibility studies.

[273] Yamashita, M.; Hartwig, J. F. *J. Am. Chem. Soc.* **2004**, *126*, 5344.

In order to gather some information about the ongoing mechanism, different additives were tested (Figure 3.36). The addition of cesium carbonate (1.3 equivalents) resulted deleterious for the transformation, whereas the addition of carbon monoxide and water did not hamper the reaction outcome at all. The fact that carbon monoxide was not inhibiting or hampering the transformation is surprising as mechanistically, an acyl-palladium complex must be formed at some point to extrude carbon monoxide. Finally, reaction of **241a** under palladium catalysis in the presence of deuterated methanol gave 80% yield of the *ipso*-deuterated ester **265a** (Scheme 3.36).

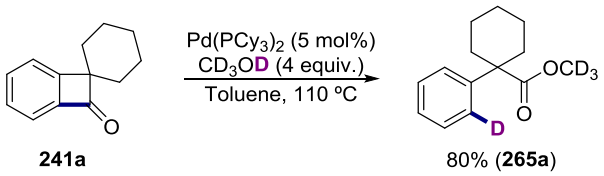

Scheme 3.36. Synthesis of esters from benzocyclobutenones. Trapping of intermediate acyl palladium complex.

Although hardly supported by empirical evidences we proposed a mechanism initiated by oxidative addition of $Pd(PCy_3)_2$ to benzocyclobutenone **241a** (Figure 3.37). Importantly, this step has been demonstrated in stoichiometric reactions with rhodium[274] and gold[275] complexes with different degrees of selectivity towards distal or proximal addition. For example, Bourissou observed only proximal addition under kinetic control but distal addition upon prolonged heating. On the other hand, Murakami observed only distal addition. They explained the observed selectivity based on steric factors. Liebeskind however, observed mixtures of distal and proximal addition with Wilkinson's catalyst. We believe that proximal activation is favored over distal oxidative addition because this C—C bond is more available in steric terms and because of the existing possibility of pre-coordination with the π-system of the aromatic ring. Indeed, the formation of ester **265a** demonstrates, indirectly, the intermediacy of acyl complex **CXIX-prox**. Although sterically disfavored, complex **CXIX-dist** would be formed as well, but in a lesser extent. Indeed, we propose an equilibrium between **CXIX-prox** and **CXIX-dist**. The formation of **CXIX-dist** from **CXIX-prox** can occur through a reductive elimination/oxidative addition[276] process or through the intermediacy of complex **CXX**, although we considered this possibility less likely because of the large ring strain of the putative palladacycle intermediate. Once distal-activation takes place, the complex will dissociate one phosphine ligand to form an unsaturated palladium-complex **CXXII** that will be able now to undergo β-hydride elimination rendering complex **CXXIII** featuring a palladium hydride. Subsequently, CO extrusion will occur forming intermediate **CXXIV**. Finally, a reductive elimination from this last intermediate will deliver the styrene along with $Pd(PCy_3)_2(CO)_n$ (n = 1 or 2).[277] On the other hand, complex **CXIX-prox** could react in the presence of alcohol to form

[274] (a) Huffman, M. A.; Liebeskind, L. S. *Organometallics* **1990**, *9*, 2194. (b) Huffman, M. A.; Liebeskind, L. S. *Organometallics* **1992**, *11*, 255. (c) Masuda, Y.; Hasegawa, M.; Yamashita, M.; Nozaki, K.; Ishida, N,; Murakami, M. **2013**, *135*, 7142.

[275] Joost, M.; Estévez, L.; Miqueu, K.; Amgoune, A.; Bourissou, D. *Angew. Chem. Int. Ed.* **2015**, *54*, 5236.

[276] This sequence of steps has been documented by Bourissou. See ref 275.

[277] Although one might believe that the presence of electron-withdrawing carbonyl ligand(s) could inhibit the catalyst turnover because of a difficult oxidative addition over **241a**, it has been demonstrated that compounds of the structure $(Xantphos)Pd(CO)_2$ are able to undergo oxidative addition over aryl iodides as long as there is no a CO atmosphere. See: (a) Miloserdov, F. M.; McMullin,

ester **265a**. Although preliminary, we suggest a mechanism involving a formal [1,4]-palladium migration by a regioselective *ipso*-protonation of the aryl-palladium complex[278] forming acyl palladium **CXXI**. Then, the ester is formed upon nucleophilic attack in an outer-sphere mechanism or by reductive elimination if methoxide is bound to the palladium center (not shown). Additionally, complex **CXIX-prox** could react by nucleophilic attack of methanol over the activated carbonyl group, subsequent reductive elimination of the generated aryl palladium complex would render the ester **254a**. Independently of the mechanism, the fact that no methyl benzoate **266a** is observed is indicative of a favored proximal addition over distal addition. It should be highlight that this transformation is one of the few examples of a palladium catalytic C—C cleavage through an oxidative addition mechanism.[154]

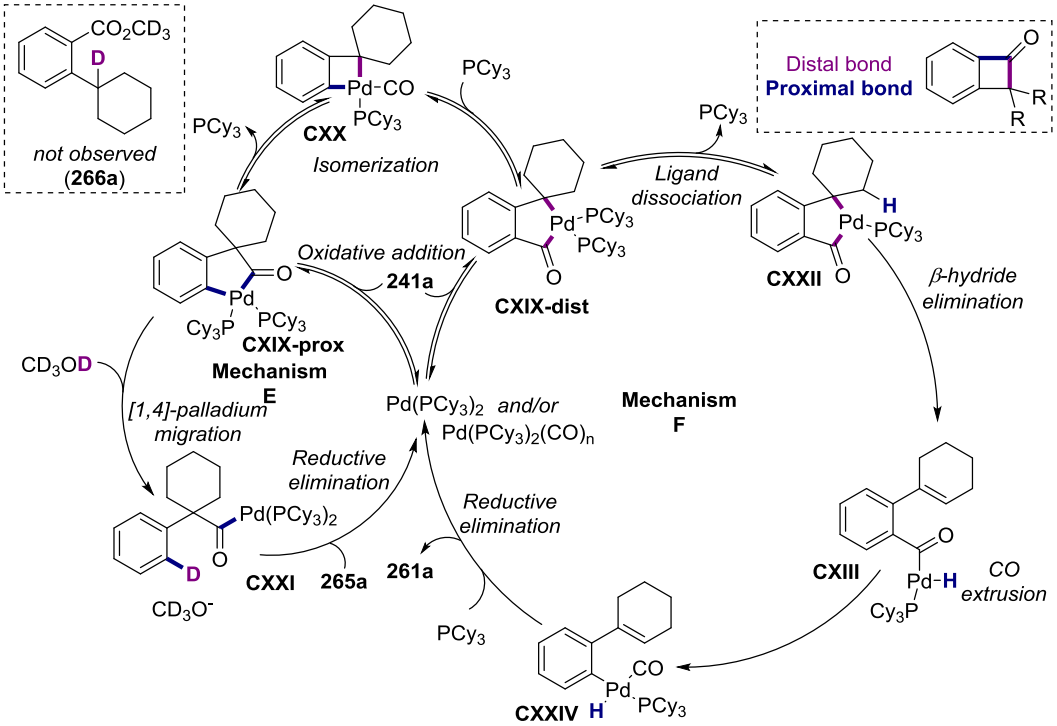

Figure 3.37. Mechanistic rationale for the synthesis of styrenes from benzocyclobutenone.

In order to gather some evidences to support the suggested mechanistic proposal, we attempted to isolate the complex **CXIX-prox**. To such end, the reaction of $Pd(PCy_3)_2$ with an equimolar amount of **241a** in benzene at room temperature was monitorized by ^{31}P NMR. After four days, a red/orange crystalline solid was obtained quantitatively along with styrene **261a**. Unfortunately, the compound obtained was not the oxidative addition complex but the palladium cluster $[Pd(PCy_3)_2(\mu\text{-}CO)_2][Pd(PCy_3)]_2(\mu\text{-}CO)$ (Figure 3.38) which showed no catalytic activity. It must be noticed that although several palladium clusters featuring carbonyl and

C. L.; Belmonte, M. M.; Benet-Buchholz, J.; Bakhmutov, V. I.; Macgregor, S. A.; Grushin, V. V. *Organometallics* **2014**, *33*, 736.

[278] For related *ipso*-protonation by *alcoholic protons* see: (a) Melero, C.; Shishilov, O. N.; Álvarez, E.; Palma, P.; Cámpora, J. *Dalton. Trans.* **2012**, *41*, 14087. (b) Chai, D. I.; Thansandote, P.; Lautens, M. *Chem. Eur. J.* **2011**, *17*, 8175. (c) Esqueda, C.; Alvarado-Monzón, J. C.; Andreu-de-Riquer, G.; Gutiérrez, A.; León-Rodríguez, L. M.; Serrano, O.; Alvarado-Rodríguez, J. G.; López, J. A. *Polyhedron* **2012**, *40*, 11.

phosphine ligands are known[279], a complex like ours, bearing one square planar and two trigonal palladium atoms has been only described once.[280]

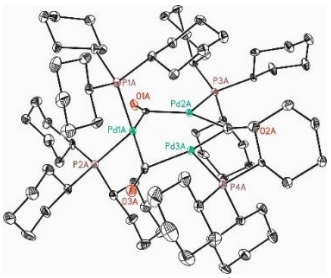

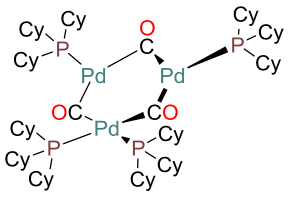

[Pd(PCy$_3$)$_2$(μ-CO)$_2$]{[Pd(PCy$_3$)]$_2$(μ-CO)}

Figure 3.38. X-Ray diagram of complex [Pd(PCy$_3$)$_2$(μ-CO)$_2$]{[Pd(PCy$_3$)]$_2$(μ-CO)}.

3.3.8 Conclusions.

In summary, in the present chapter we have been able to expand the palladium-catalyzed intramolecular acylation of aryl bromides for the synthesis of benzocyclobutenones to the more readily available and cheaper aryl chlorides. The reaction displays a good functional group tolerance and excellent site-selectivity. We have been able to overcome the previous limitations of the method based on aryl bromides by expanding the scope to the synthesis of indanones and monosubstituted benzocyclobutenones. In analogy to the reactivity manifested by aryl bromides, the judicious choice of ligands enables a mechanistic switch that render styrene derivatives.

This new method for the synthesis of benzocyclobutenones not only overcomes the limitations of our previous work using aryl bromides, but also represents the most efficient synthesis of benzocyclobutenones published to the date as the reaction is completely regioselective and good to high yields are obtained in the presence of several functional groups. More importantly, no dangerous reagents are employed and only catalytic amounts of metallic waste are generated.

In addition, we have presented a mechanistic discussion based on experimental evidences and literature precedents. Although the mechanism for the synthesis of benzocyclobutenones is not completely clear yet, the synthesis of styrenes is better understood. Furthermore, a rational explanation has been given to explain the observed selectivity in terms of the ligand's buried volume. However, further studies are required to shed light into these two mechanisms.

Finally, we have disclosed a novel palladium-catalyzed C—C cleavage event through an oxidative addition mechanism. Although not catalytically competent, the novel off-cycle complex [Pd(PCy$_3$)$_2$(μ-CO)$_2$][Pd(PCy$_3$)]$_2$(μ-CO) has been isolated and characterized by X-Ray diffraction.

---

[279] (a) Benn, R.; Jolly, P. W.; Mynott, R.; Raspel, B.; Schenker, G.; Schick, K.-P.; Schroth, G. *Organometallics,* **1985**, *4*, 1945. (b) Willocq, C.; Tinant, B.; Aubriet, F.; Carré, V.; Devillers, M.; Hermans, S. *Inorg. Chim. Acta* **2011**, *373*, 233. (c) Mednikov, E.; Dahl, L. F. *Chem. Commun.* **2013**, *49*, 1085.
[280] Bertani, R.; Cavinato, G.; Facchin, G.; Toniolo, L.; Vavasori, A. *J. Organomet. Chem.* **1994**, *466*, 273.

Chapter 4. Iron(III)-catalyzed regiodivergent [1,2]-shift of α-aryl aldehydes.

'Gold is for the mistress – silver for the maid –

Copper for the craftsman cunning at his trade.'

'Good!' said the Baron, sitting in his hall.

'But Iron – Cold Iron – is master of them all.'

Rudyard Kipling, *Rewards and Fairies*.

4.1 Unexpected results.

In the previous chapter, we have discussed the versatility of the benzocyclobutenone core and the existing methods for its synthesis. Being aware of the great potential of that backbone and the important limitations of the reported methodologies for their synthesis we envisioned a novel synthesis of benzocyclobutenone by an intramolecular acylation event via aldehydic C—H bond functionalization using aryl bromides and chlorides (see Chapter 3). A catalytic dehydrogenative cross-coupling (CDC) strategy[8] (see Scheme 4.1) starting from a non-prefunctionalized aryl motif would be highly desirable because of a dramatically higher efficiency when compared with the introduction of a halogen motif (molecular hydrogen would be the only byproduct). Furthermore, a plethora of different starting materials could be rapidly prepared from commercial sources and the formation of halogenated-waste would be avoided.

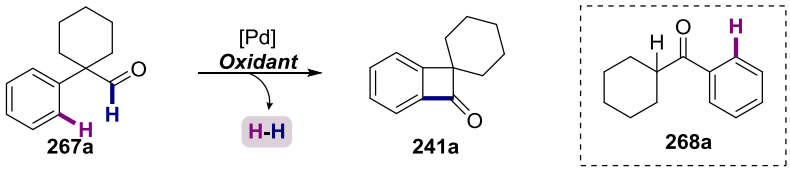

Scheme 4.1. Synthesis of benzocyclobutenones via cross dehydrogenative coupling.

Unfortunately, we never obtained benzocyclobutenone **241a** under different reaction conditions. However, when iron(III) chloride (2 equivalents) was used as stoichiometric oxidant in combination with catalytic amounts of palladium(II) acetate, a new rearranged product (**268a**, scheme 4.1) was observed in 72% isolated yield. Control experiments showed that the palladium(II) was not participating in the catalysis and that the transformation could be easily executed with just iron(III) chloride. We were puzzled about this unexpected result and we performed a thorough literature survey taking special interest in the rearrangement of aldehydes into ketones, pinacol and semi-pinacol rearrangements[281] as well as other [1,2]-migrations.[282] In this manner, a more insightful evaluation concerning the interest of this transformation will be analyzed.

4.2 Skeletal rearrangements of aldehydes into ketones.

The skeletal rearrangement of aldehydes into ketones is a transformation that has already been known for a century. This transformation is based on the activation of the carbonyl group followed by a [1,2]-migration event that will render the ketone (scheme 4.2). This reaction has a great potential in organic synthesis as ketones (one of the most versatile functional groups) can be prepared without waste generation. However, its potential relies on the ability to achieve high degrees of regioselectivity. In other words, this reaction can only be relevant if the migratory aptitude of the different substituents can be controlled and predicted.

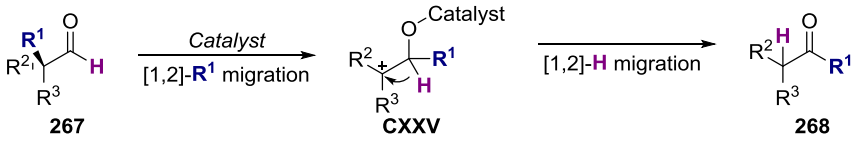

[281] Song, Z.-L.; Fan, C.-A.; Tu, Y.-Q. *Chem. Rev.* **2011**, *111*, 7523. (b) Overman, L. E.; Pennington, L. D. *J. Org. Chem.* **2003**, *68*, 7143.
[282] Crone, B.; Kirsch, S. F. *Chem. Eur. J.* **2008**, *14*, 3514.

Scheme 4.2. Skeletal rearrangement of aldehydes into ketones.

4.2.1 Skeletal rearrangement of aldehydes under strong acidic conditions

The first examples describing the rearrangement of aldehydes into ketones were published at the beginning of the last century.[283] In these reports, triphenylacetaldehyde was converted into 1,2,2-triphenylethan-1-one under hot sulfuric acid. Likewise, diphenylethylacetaldehyde was converted into a mixture of rearranged ketones under similar conditions. More recently, pivalaldehyde **269** has been converted into methyl isopropyl ketone under superacidic conditions.[284] Mechanistic studies and DFT calculations suggested the intermediacy of protosolvated carboxonium ion **CXXVI** thus explaining the necessity for the superacidic media (Scheme 4.3). Additionally, the tandem formylation/rearrangement of isoalkanes (**271**) with carbon monoxide has also been reported (Scheme 4.3, right).[285] This transformation is based on the *in situ* formation of the corresponding aldehyde followed by skeletal rearrangement.

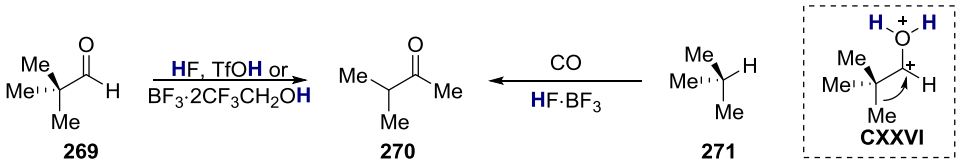

Scheme 4.3. Superacid-catalyzed synthesis of ketones via the skeletal rearrangement of aldehydes.

4.2.2. α-Ketol rearrangement (acyloin rearrangement)[286]

The α-ketol rearrangement is a type of ketogenic isomerization where an alcohol (or alcoxide or silyl ether) becomes a ketone while the migrating motif relocates to form a new alcohol. This transformation is reversible, and the more stable isomer is preferiantally formed (see scheme 4.4).

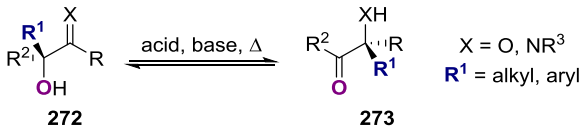

Scheme 4.4. α-Ketol rearrangement.

In substrate **272**, where R stands for hydrogen and X for oxygen (Scheme 4.4), then, an α-ketol rearrangement will render a ketone from an initial aldehyde. For example, Kuwajima reported in the late 80's the Lewis acid-promoted ring expansion of α-siloxy cycloalkanecarbaldehydes (Figure 4.1).[287] The reaction nicely worked in the presence of symmetric cyclic aldehydes (**274a-c**). However, in the presence of unsymmetrically substituted aldehydes (eq b) two distinct ketones **276-I** and **276-II** were formed (see table). This is because

[283] (a) Danilov, S.; Venus-Dalinova, E. *Berichte* **1927**, *60*, 1050. (b) Danilov, S. N; Venus-Danilova, E. D. *Zhurnal Russkogo Khimicheskogo Obshchestva* **1919**, *51*, 97. (c) Tiffeneau; Orechov *Compt. Rend.;* **1926**, *182*, 67.
[284] (a) Olah, G. A.; Mathew, T.; Marinez, E. R.; Esteves, P. M.; Etzkorn, M.; Rasul, G.; Prakash, G. K. S. *J. Am. Chem. Soc.* **2001**, *123*, 11556. (b) Prakash, G. K. S.; Mathew, T.; Marinez, E. R.; Esteves, P. M.; Rasul, G.; Olah, G. A. *J. Org. Chem.* **2006**, *71*, 3952. (c) van de Water, L. G. A.; van der Waal, J. C.; Jansen, J. C.; Machmeyer, T. *J. Catal.* **2004**, *223*, 170. (d) Olah, G. A.; Klumpp, D. A. *Acc. Chem. Res.* **2004**, *37*, 211.
[285] Olah, G. A.; Prakash, G. K. S.; Mathew, T.; Marinez, E. R. *Angew. Chem. Int. Ed.* **2000**, *39*, 2547.
[286] Paquette, L. A.; Hofferberth, J. E. *Org. React.* **2003**, *62*, 477.
[287] Matsuda, T.; Tanino, K.; Kuwijima, I. *Tetrahedron Lett.* **1989**, *30*, 4267.

of a lack of a selective [1,2]-alkyl shift event, thus leading to mixtures of products. Importantly, it was observed that the migratory aptitude could be tuned by a judicious choice of the Lewis acid (entry 2).

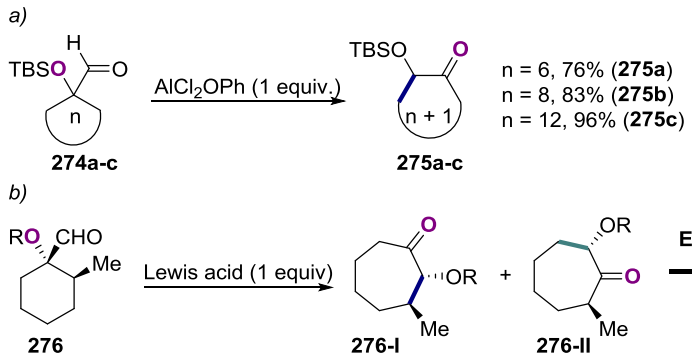

Entry	R	Yield(%) (276-I:276-II) $AlCl_2OPh$	$SnCl_4$
1	TBS	71% (2.2:1)	
2	TIPS	99% (1:1)	80% (8:1)

Figure 4.1. α-Ketol rearrangement: The regioselectivity problem.

While an important accomplishment, Kuwajima's work was limited by the poor regiocontrol. Although the regiocontrol problem disappears by using symmetrically substituted aldehydes (Scheme 4.4, $R^1 = R^2$) this hampers the application profile of such methodologies.[288] Therefore, transformations with exquisite regioselectivity control are highly desirable. In this context, Maruoka and co-workers reported the asymmetric and regioselective conversion of α-siloxy aldehydes **277** to enantioenriched acyloins **278** using catalytic amounts of a chiral aluminum Lewis acid.[289] The authors demonstrated that the migrating event can be controlled by judicious choice of the Lewis acid (Figure 4.2).[290] Particularly, strong Lewis acids favored the aryl migrations whereas the opposite scenario was found with weaker Lewis acids. Unfortunately, although several mechanistic studies were conducted, the authors did not offer any explanation to such intriguing behavior.[291]

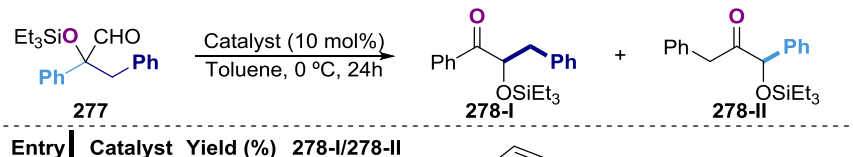

Entry	Catalyst	Yield (%)	278-I/278-II
1	$AlMe_2Cl$	91	>20:1
2	**14a**	71	5:1
3	**14b**	99	3:1
4	**14c**	99	1:1.5
5[a]	**14c**	99	<1:20

Lower Lewis acidity Higher

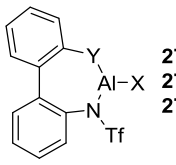

279a: Y = O, X = Me
279b: Y = NTf, X = Me
279c: Y = NTf, X = Cl

[a] Dichloromethane, -20 ºC, 12h

Figure 4.2. Influence of the Lewis acid acidity in the regioselectivity of the transformation.

4.2.3. Formal [4+3]-cycloaddition reaction: Tandem Diels-Alder/ring expansion

2-Siloxyacroleins are known to undergo [4+3]-cycloadditions with dienes in the presence of an adequate Lewis acid. Although the [4+3]-cycloaddition has traditionally been considered as the ongoing mechanism (an allyl cation is postulated as reaction intermediate)[292] recent

[288] Ooi, T.; Saito, A.; Maruoka, K. *J. Am. Chem. Soc.* **2003**, *125*, 3220.
[289] Ooi, T.; Ohmatsu, K.; Maruoka, K. *J. Am. Chem. Soc.* **2007**, *129*, 2410.
[290] Ohmatsu, K.; Tanaka, T.; Ooi, T.; Maruoka, K. *Angew. Chem. Int. Ed.* **2008**, *47*, 5203.
[291] Ohmatsu, K.; Tanaka, T.; Ooi, T. Maruoka, K. *Tetrahedron* **2009**, *65*, 7516.
[292] Harmata, M.; Rashatasakhon, P. *Tetrahedron* **2003**, *59*, 2371. And references therein.

studies point towards a tandem Diels-Alder reaction/ring expansion. This transformation was firstly reported by Sasaki and co-workers using tin(IV) chloride.[293] A year later, experiments conducted by Childs[294] with related 2-siloxyenones showed that the [4+3]-cycloaddition also occurred but the [4+2]-cycloadduct was obtained upon spontaneous retro-acyloin rearrangement. More recently, Harmata[295] and Funk[296] further developed this methodology. Importantly, in Harmata's protocol (Figure 4.3) the Lewis acid was employed in catalytic amounts whereas in Funk's protocol, equimolar amounts of Lewis acid were required. However, both cyclic as non-cyclic dienes could be employed in the latter whereas only cyclic substrates were adequate under Harmata's conditions (**281e**).

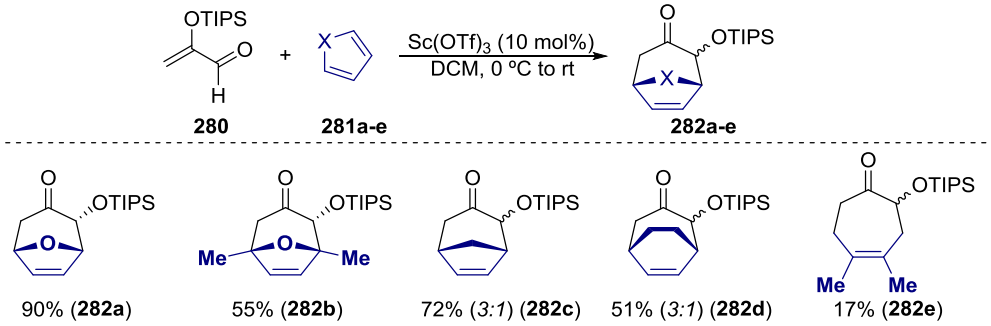

Figure 4.3. Formal [4+3]-cycloaddition of 2-(triisopropylsilyloxy)acrolein.

The importance of this methodology was proved in the total synthesis of (±)-Cortistatin J, a steroidal alkaloid that has shown cytostatic and antiproliferative activity against human vein endothelial cells (HUVECs) with high selectivity.[297] The key step of the synthesis was the formation of a seven-membered ring (**284**) by a formal [4+3]-cycloaddition using catalytic amounts of trifluoromethanesulfonic acid. Importantly, **284** was obtained in high yields as a single diastereoisomer.

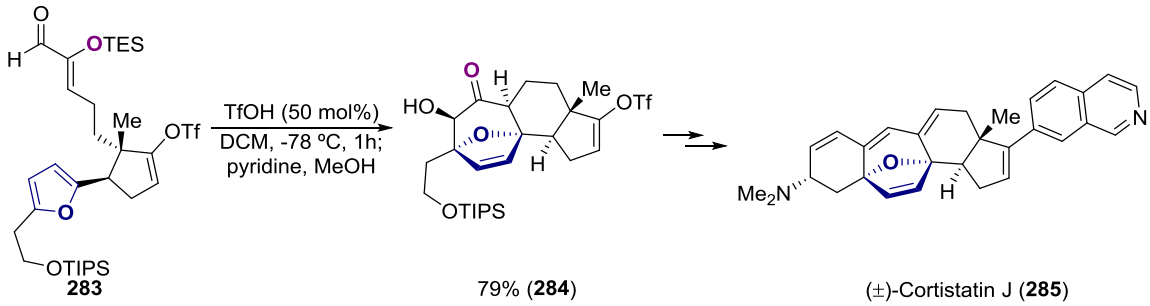

Scheme 4.5. Formal [4+3]-cycloaddition for the total synthesis of (±)-Cortistatin J.

Recently, Davies published some results that point towards a tandem Diels-Alder/ring expansion rather than a direct [4+3]-cycloaddition.[298] They first observed (Figure 4.4) that when enal **287** was reacted with cyclopentadiene in the presence of a Lewis acid at -78 ºC only

[293] Sasaki, T.; Ishibashi, Y.; Ohno, M. *Tetrahedron Lett.* **1982**, *23*, 1693.
[294] Blackburn, C.; Childs, R. F.; Kennedy, R. A. *Can. J. Chem.* **1983**, *61*, 1973.
[295] Harmata, M.; Sharma, U. *Org. Lett.* **2000**, *2*, 2703.
[296] Aungst Jr, R. A.; Funk, R. L. *Org. Lett.* **2001**, *3*, 3553.
[297] Nilson, M. G.; Funk, R. L. *J. Am. Chem. Soc.* **2011**, *133*, 12451.
[298] (a) Davies, H. M. L.; Dai, X. *J. Am. Chem. Soc.* **2004**, *126*, 2692. (b) Dai, X.; Davies, H. M. L. *Adv. Synth. Catal.* **2006**, *348*, 2449.

the Diels-Alder product was formed as a mixture of diastereoisomers **288-I** and **288-II** (entry 1). Importantly, if the reaction was allowed to warm to zero degrees (entry 2), the formal [4+3]-cycloadduct **289** was obtained as the major product along with **288-I** and **288-II**. These results suggested that cycloadduct **289** is formed via ring-expansion of the [4+2]-cycloadducts.

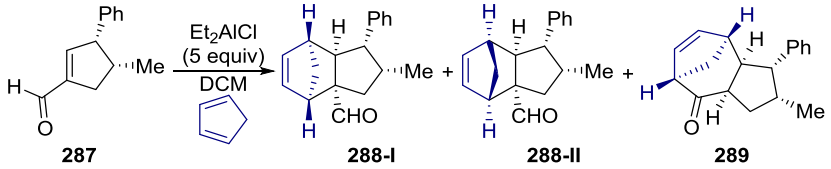

Entry	Temp (°C)	288-I:288-II:289
1	-78	84:16:0
2	-78 to 0	7:21:72

Figure 4.4. First evidences of a tandem Diels-Alder/ring expansion.

In order to gather further evidences, different [4+2]-cycloadducts were prepared and tested under Lewis acidic conditions (Figure 4.5). Notably, it was observed complete conversion towards the formation of [4+3]-cycloadducts (**291a-b**) under reactions conditions, thus suggesting the intermediacy of Diels-Alder cycloadducts. Importantly, the same behavior was observed for the expected α-siloxyketones under Harmata's conditions (**290b**),[295] implying that the same mechanism is operative, although DFT calculations suggest a step-wise cycloaddition when furan is used as diene.[299]

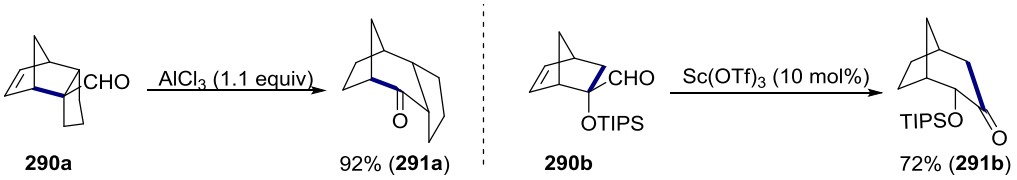

Figure 4.5. Ring expansion reaction of Diels-Alder cycloadducts.

Alternatively, [4+2]-cycloadducts might be able to undergo retro-Diels-Alder reaction under the reaction conditions to subsequently react through a [4+3]-cycloaddition. In order to rule out this possibility, two experiments were conducted (Figure 4.6). First, an enantioenriched substrate (**290c**, 85% *ee*) was reacted under reaction conditions and product **291c** was obtained without any loss in optical activity. This result suggests that no retro-Diels-alder occurs, since if this would be the case, then, erosion in enantioselectivity should be expected during the [4+3]-cycloaddition as no chiral Lewis acid is being employed. On the other hand, the reaction of deuterated aldehyde **292-*d*^{1}** gave complete deuterium transfer to the 3β-position of the [4+3]-cycloadduct **291-*d*^{1}**, demonstrating a suprafacial [1,2]-deuteride shift that will deliver the *endo*-product **291-*d*^{1}**. Finally, it should be mentioned that this mechanism is also supported by DFT calculations.[300]

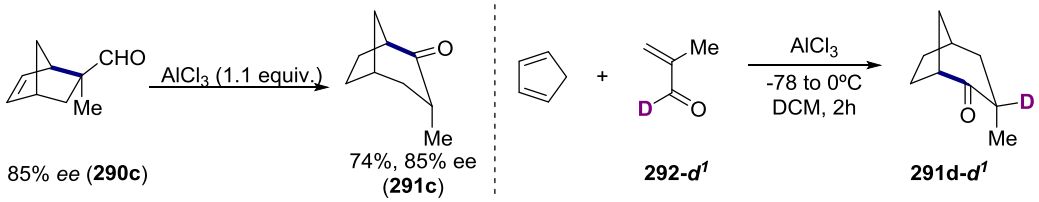

Figure 4.6. Evidence of a Diels-Alder/ring expansion tandem sequence.

[299] Sáez, J. A.; Arnó, M.; Domingo, L. R. *Org. Lett.* **2003**, *5*, 4117.
[300] Domingo, L .R.; Arnó, M.; Sáez, J. A. *J. Org. Chem.* **2009**, *74*, 5934.

4.2.4. Simple skeletal rearrangement of aldehydes under mild reaction conditions

In previous sections, we have studied the skeletal rearrangement of structurally biased aldehydes. In the case of the α-ketol rearrangement, it is mandatory the presence of a hydroxyl group at the α-position of the aldehyde, whereas in the formal [4+3]-cycloaddition reactions, the system requires a strained bicyclic system or the presence of a hydroxyl group at the α-position. In 1988, Kuwajima and co-workers reported the ring expansion of aldehydes bearing a (trimethylsilyl)methyl substituent at the α-position.[301] The presence of the silicon atom was crucial for the reactivity, most likely because of its ability to stabilize carbocations at the β-position by the so-called β-silicon effect.[302] The protocol was restricted to symmetrical carbocycles (**293a-c**) and stoichiometric amounts of Lewis acid were required (scheme 4.6).

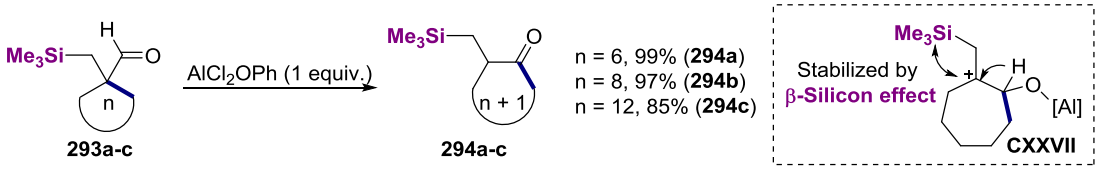

Scheme 4.6. β-Silicon effect promotes ring expansion of cyclic aldehydes.

Chatani and co-workers published in 2005 the skeletal rearrangement of aldehydes under gallium(III) chloride catalysis.[303] Although it represents an important breakthrough because more diversity was tolerated in the aldehydic skeleton, the reaction was not regioselective, and a mixture of regioisomers was usually obtained (Figure 4.7). It must be noticed that the authors observed certain electronic-control (see table) being [1,2]-methyl migration favored in the presence of electron-rich aryl motifs (entry 1 *versus* entry 3).

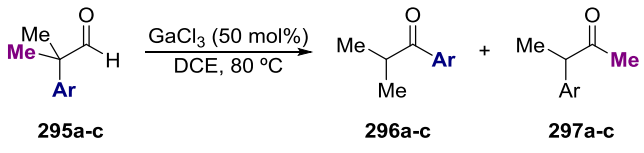

Entry	Ar	296 (%)	297 (%)
1	4-$CH_3C_6H_4$	33	50
2	C_6H_5	58	26
3	4-$CF_3C_6H_4$	57	13

Figure 4.7. Gallium-catalyzed skeletal rearrangement of aldehydes. Regioselectivity issues: electronic control.

On the other hand, the ring-size was found to exert a higher control of the migratory aptitude which is probably related to the ring strain of the starting material (Figure 4.8). For example, [1,2]-alkyl shift was exclusive found for substrate **295d** resulting in the selective formation of the ring-expansion product **297d**.

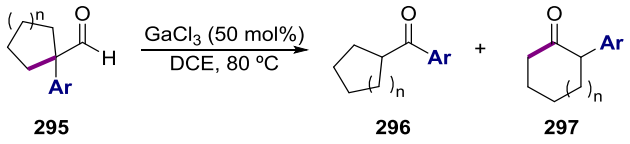

Entry	n	296 (%)	297 (%)
1	1	0	83
2	2	84	9

Figure 4.8. Gallium-catalyzed skeletal rearrangement of aldehydes. Regioselectivity issues: ring-strain control.

[301] Tanino, K.; Katoh, T.; Kuwajima, I. *Tetrahedron Lett.* **1988**, *29*, 1815.
[302] Wierschke, S. G.; Chandrasekhar, J.; Jorgensen, W. L. *J. Am. Chem. Soc.* **1985**, *107*, 1496
[303] Oshita, M.; Okazaki, T.; Ohe, K.; Chatani, N. *Org. Lett.* **2005**, *7*, 331.

In addition to the poor regioselectivity, high catalyst loadings were required (20 – 50 mol%) and no functional groups were present in the scope of the transformation limiting significantly its applicability. Interestingly, experimental evidences along with DFT calculations favored a dual activation of the aldehyde. This resembles the case of the isomerization of pivalaldehyde to form methyl isopropyl ketone under superacidic conditions,[284,285] where the intermediacy of the protosolvated carboxonium ion II was demonstrated (Scheme 4.3).

4.3. Skeletal rearrangement of epoxides: the Meinwald rearrangement

Although this rearrangement does not invoke aldehydes as substrates, the Meinwald rearrangement will be briefly discussed here as it is highly related with the skeletal rearrangement of aldehydes into ketones and because of its implications on the mechanism of the transformation that will be discussed throughout this chapter. The skeletal rearrangement of epoxides **298** into ketones **268** or aldehydes **267** is known as the Meinwald rearrangement.[304] The product distribution varies significantly depending on the substrate and the catalyst employed. Yet, an accurate control of the migratory aptitude is of utmost importance in order to develop a versatile method (Figure 4.9)

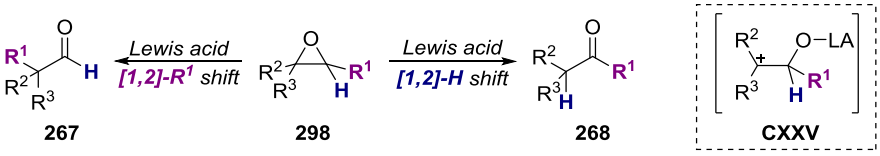

Figure 4.9. The Meinwald rearrangement.

The Meinwald rearrangement has been deeply studied and protocols covering the regiospecific [1,2]-hydride shift[305] or the [1,2]-R shift[306] are abundant. For example, in Figure 4.10 we can observe that, depending on the Lewis acid employed one migratory event over the other is favored. In this particular case, whereas an iron(III) catalyst triggers a [1,2]-hydride shift (entry 1), a chromium-based Lewis acid favores the alkyl migration (**301**) (entry 2) . Unfortunately, this behavior is not yet well understood.[307]

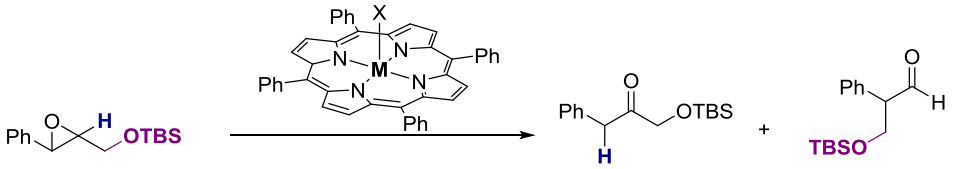

Reaction Conditions	300 (%)	301 (%)
M = Fe, X = ClO_4; Dioxane, 100 ºC	>99	0
M = Cr, X = OTf; DCE, 83 ºC	0	97

[304] (a) Meinwald, J.; Labana, S. S.; Chadha, M. S. *J. Am. Chem. Soc.* **1963**, *85*, 582. (b) Fraile, J. M.; Mayoral, J. A.; Salvatella. *J. Org. Chem.* **2014**, *79*, 5993.
[305] (a) Karamé, I.; Tommasino, M. L.; Lemaire, M. *Tetrahedron Lett.* **2003**, *44*, 7687. (b) Kulasegaram, S.; Kulawiec, R. J. *J. Org. Chem.* **1994**, *59*, 7195. (c) Anderson, A. M.; Blazek, J. M.; Garg, P.; Payne, B. J.; Mohan, R. S. *Tetrahedron Lett*. **2000**, *41*, 1527. (d) Martínez, F.; del Campo, C.; Llama, E. F. *J. Chem. Soc., Perkin Trans. 1* **2000**, 1749. (e) Ranu, B. C.; Jana, U. *J. Org. Chem*. **1998**, *63*, 8212 and references therein.
[306] (a) Hrdina, R.; Müller, C. E.; Wende, R. C.; Lippert, K. M.; Benassi, M.; Spengler, B.; Schreiner, P. R. *J. Am. Chem. Soc.* **2011**, *133*, 7624. (b) Maruoka, K.; Murase, N.; Bureau, R.; Ooi, T.; Yamamoto, H. *Tetrahedron* **1994**, *50*, 3663. (c) Maruoka, K.; Ooi, T.; Yamamoto, H. *J. Am. Chem. Soc.* **1989**, *111*, 6431. (d) Suda, K.; Nakajima, S.-I.; Satoh, Y.; Takanami, T. *Chem. Commun.* **2009**, 1255.
[307] Suda, K.; Kikkawa, T.; Nakajima, S.-I.; Takanami, T. *J. Am. Chem. Soc.* **2004**, *126*, 9554.

Figure 4.10. Meinwald rearrangement. Lewis acid-induced regioselectivity switch.

Importantly, if Figure 4.9 and 4.2 are to be compared, then, the similarities between the skeletal rearrangements of epoxides and aldehydes are evident, and the fact that the same intermediate **CXXV** is postulated should not be ignored when studying both transformations.

4.4 Iron(III)-catalyzed regiodivergent [1,2]-shift of α-aryl aldehydes.[308]

After a deep literature survey, we have observed that although the skeletal rearrangement of aldehydes to ketones is a well-known transformation and is more than 100 years old, the transformation is not well-developed yet and there is room to significant improvement by addressing the most significant drawbacks. For example, we have seen that in order to get good reactivities strong acidic conditions are needed. However, if the aldehyde is structurally biased (having an α-hydroxo substituent, a β-silicon atom or the system is highly strained) the transformation occurs smoothly in the presence of Lewis acids, albeit in almost all cases under stoichiometric amounts. To date, Chatani's protocol could be considered as the most adequate.[303] Yet, the employment of high catalyst loading, the lack of regioselectivity and the poor substrate scope are serious drawback in this methodology.

On the basis of the previous considerations, we envisioned that our findings could be of highly interest to the Community if the following objectives are fulfilled:

- Catalytic amounts of a Lewis acid as catalyst
- Mild reaction conditions
- Broad functional group tolerance
- High regioselectivity

4.4.1 Skeletal rearrangement of α-aryl aldehydes: Optimization studies

As shown in Scheme 4.1, our initial finding concerning the skeletal rearrangement of α-aryl aldehydes relied on the use of stoichiometric amounts of iron(III) chloride. Because of the unparalleled advantages of iron such as its low cost and its availability (iron is, after aluminum, the most abundant metal in the Earth's crust), low toxicity and low environmental impact, iron is, nowadays, one of the most appealing transition metal for catalysis.[309] Therefore, we decided to focus the optimization of our reaction on the utilization of an iron-catalyst although other metals such as copper, aluminum or gallium showed some degree of reactivity as well (Table 4.4).

[308] Gutiérrez -Bonet, Á.; Flores-Gaspar, A.; Martin, R. *J. Am. Chem. Soc.* **2013**, *135*, 12576.
[309] (a) Bauer, I.; Knölker, H.-H. *Chem. Rev.* **2015**, *115*, 3170. (b) Correa, A.; Mancheño, O. G.; Bolm, C. *Chem. Soc. Rev.* **2008**, *37*, 1108. (c) Sherry, B. D.; Fürstner, A. *Acc. Chem. Res.* **2008**, *41*, 1500. (d) Bolm, C.; Legros, J.; Le Paih, J.; Zani, L. *Chem. Rev.* **2004**, *104*, 6217. (e) Fürstner, A. Martin, R. *Chem. Lett.* **2005**, *34*, 624. (f) Gopalaiah, K.; *Chem. Rev.* **2013**, *113*, 3248. (g) Czaplik, W. M.; Mayer, M.; Cvengros, J.; von Wangelin, A. J. *ChemSusChem* **2009**, *2*, 396.

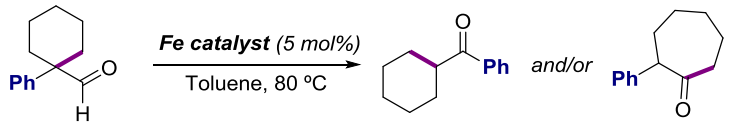

267a **268a** *[1,2]-**Aryl** shift* **302a** *[1,2]-**Alkyl** shift*

Entry	Fe cat.	268a (%)[a]	302a (%)[a]
1	FeF_3	0	*n.d.*
2	$FeCl_3 \cdot 6H_2O$	12	*n.d.*
3	$FeCl_3$	22	*n.d.*
4	$FeBr_3$	94[b]	*n.d.*
5	$Fe(acac)_3$	3	*n.d.*
6	$Fe(OTf)_3$	11	*n.d.*
7	$FeBr_2$	0	*n.d.*

[a] **267**a (0.5 mmol), Fe catalyst (5 mol%), toluene (0.25M), 80 ºC, 16h. GC yield using dodecane as internal standard. [b] Isolated yield

Table 4.1. Optimization studies for the skeletal rearrangement of α-aryl aldehydes: Fe-catalyst influence.

First, we studied the effect of different iron Lewis acids in catalytic amounts (Table 4.1). Based on literature data, we can expect the following Lewis acidity: $FeBr_3$ > $FeCl_3$ > FeF_3.[310] On the basis of this scale, we observed a direct relationship between the Lewis acidity and the yield of **268a** (entries 1,3-4); the higher Lewis acidity of the catalyst is, the higher the yield. Thus iron(III) bromide (entry 4) arose as an excellent catalyst for this transformation. Importantly, **302a** arising from a ring expansion event was never observed. The importance of the Lewis acidity was uncovered when iron(II) bromide was employed (entry 7). Iron(II) bromide is expected to have a lower Lewis acidity because of its lower oxidation state compared to iron(III) bromide,[311,310f] consequently, iron(II) bromide resulted ineffective in promoting the reactivity. Although the yield obtained with ferric bromide was excellent and no further screening would be required, we decided to briefly explore other parameters to gather further information about the factors controlling the reactivity.[312]

[310] The Lewis acidity is a very complex term to be measured as several variables are influencing. Several are the studies and methods to do so and, often, the different terms measured give opposite trends. (a) Satchell, D. P. N.; Satchell, R. S. *Chem. Rev.* **1969**, *69*, 251. (b) Heston, A. J.; Panzner, M. J.; Youngs, W. J.; Tessier, C. A. *Inorg. Chem.* **2005**, *44*, 6518. (c) Plumley, J. A.; Evanseck, J. D. *J. Phys. Chem. A.* **2009**, *113*, 5985. (d) Zhang, Y. *Inorg. Chem.* **1982**, *21*, 3889. (e) Hilt, G.; Pünner, F.; Möbus, J.; Naseri, V.; Bohn, M. A. *Eur. J. Org. Chem.* **2011**, 5962. (f) Fukuzumi, S.; Ohkubo, K. *J. Am. Chem. Soc.* **2002**, *124*, 10270. (g) Ogawa, A.; Fujimoto, H. *Inorg. Chem.* **2002**, *41*, 4888.

[311] According to reference 304f, the relative Lewis acidity is related with the λ_{max} (nm) displayed by the adduct 10-methylacridone-Lewis acid, so that the higher the λ_{max} is, the higher Lewis acidity of the metal complex will be. λ_{max} ($Fe(ClO_4)_2$) = 471 nm < λ_{max} ($Fe(ClO_4)_3$) = 478 nm.

[312] Lower temperatures as well as lower catalyst loading resulted in lack of reactivity.

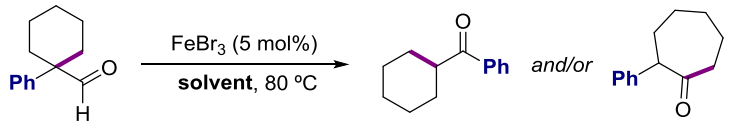

267a **268a** *[1,2]-**Aryl** shift* **302a** *[1,2]-**Alkyl** shift*

Entry	Solvent	268a (%)[a]	302a (%)[a]	DN[b]
1	Toluene	94[c]	*n.d.*	1.0
2	Toluene[d]	0	0	1.0
3	*o*-xylene	90	*n.d.*	5.0[e]
4	DCE	42	*n.d.*	0 (ref.)
5	Dioxane	0	0	14.8
6	DMF	0	0	26.6
7	*t*-BuOH	0	0	38.0

[a] **267**a (0.5 mmol), $FeBr_3$ (5 mol%), solvent (0.25M), 80 ºC, 16h. GC yield using dodecane as internal standard. [b] Gutmann's Donor Number. [c]Isolated yield. [d] Using 4Å MS. [e] The value corresponds to *m*- and *p*-xylene.

Table 4.2. Solvent effects in the skeletal rearrangement of α-aryl aldehydes [313]

Next, different solvents were tested under the otherwise optimal reaction conditions. The results obtained were confronted with the Gutmann's donor number (DN),[314] which is indicative of the nucleophilic behavior of different solvents. As we can see in Table 4.2, the use of coordinating solvents such as dioxane, DMF or *tert*-butanol (entries 5-7) resulted in no product formation, most probably by catalyst poisoning. On the other hand, the use of the non-coordinating 1,2-dichloroethane resulted in low yields towards the formation of **268a**. We believe that this is the result of a very low effective concentration of the catalyst in the reaction media. On the other hand, *o*-xylene, which is closely related to toluene, gave the expected ketone **268a** in comparable yield (entry 3). Interestingly, the nature of the solvent did not play a fundamental role on the regioselectivity of the process since ketone **302a** was never observed.

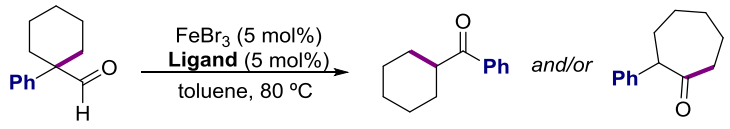

267a **268a** *[1,2]-**Aryl** shift* **302a** *[1,2]-**Alkyl** shift*

Entry	Ligand	268a (%)[a]	302a (%)[a]
1	**303a**	0	0
2	**303b**	0	0
3	**303c**	0	0

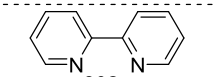

302a

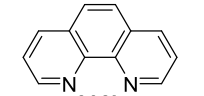

302b

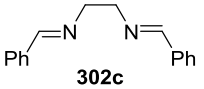

302c

[a] **267**a (0.5 mmol), $FeBr_3$ (5 mol%), ligand (5 mol%), toluene (0.25M), 80 ºC, 16h. GC yield using dodecane as internal standard.

Table 4.3. Ligand effects the skeletal rearrangement of α-aryl aldehydes

[313] For a compilation of Gutmann's Donor Number see: Marcus, Y. *Chem. Soc. Rev.* **1993**, *22*, 409.
[314] (a) Gutman, V. *Electrochimica Acta* **1976**, *21*, 661. (b) Taft, R. W.; Pienta, N. J.; Kamlet, M. J.; Arnett, E. M. *J. Org. Chem.* **1981**, *46*, 661.

Finally, the effect of different ligands in the reaction outcome was tested envisioning the possibility of making the transformation enantioselective or triggering a ligand-induced regioselectivity switch towards the formation of the ring expansion product **302a**.[309f] However, in the presence of catalytic amounts of ligand the reactivity was suppressed, probably by catalyst inhibition due to the coordination of the nitrogen atoms (DN (pyridine) = 33.1).

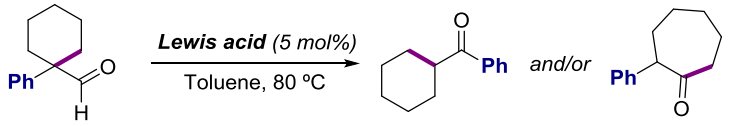

267a | **268a** *[1,2]-**Aryl** shift* | **302a** *[1,2]-**Alkyl** shift*

Entry	Lewis acid	Conv. (%)[a]	268a (%)[a]	Entry	Lewis acid	Conv (%)[a]	268a (%)[a]
1	$ZnBr_2$	15	0	11	$Sc(OTf)_2$	13	0
2	$Zn(OTf)_2$	12	0	12	$CoBr_2$	11	0
3	$PtCl_2$	5	0	13	$MnCl_2$	14	0
4	$Al(OTf)_3$	12	0	14	$CrCl_3$	16	0
5	$AlCl_3$	20	7	15	$BF_3\ OEt_2$	8	0
6	$InCl_3$	9	0	16	$Ni(OTf)_2$	8	0
7	$In(OTf)_3$	8	0	17	$NiCl_2$	10	0
8	$MgCl_2$	8	0	18	$RuCl_3\ xH_2O$	8	0
9	$Mg(OTf)_2$	13	0	19	$GaCl_3$	7	4
10	$Cu(OTf)_2$	3	6				

[a] **267**a (0.5 mmol), Lewis acid (5 mol%), toluene (0.25M), 80 ºC, 16h. GC yield and conversion were determined using dodecane as internal standard. [b] **302a** was never observed.

Table 4.4. Ruling out the active nature of the metallic traces.

Once the optimal reaction conditions were found (Table 4.1, entry 4) and being aware of the fact that metal impurities might have a significant impact on reactivity,[315] we decided to study the impurities composition of our metal catalyst in order to rule out any effect played by these entities.[316] Analysis by inductive-couple plasma (ICP) showed the presence of an array of different metallic elements (zinc, platinum, aluminum, indium, magnesium, copper, scandium, cobalt, manganese, chromium, boron, nickel and ruthenium).[317] In order to determine whether any of the metals present were acting as the real catalyst, reactions with 5 mol% of different salts of the found metals were tested. Interestingly, only aluminum(III) chloride (entry 5), copper(II) triflate (entry 10) and gallium(III) chloride (entry 19) were able to deliver the product albeit only one turnover was achieved. The result of gallium(III) chloride is highly interesting since it is known to promote this transformation in 1,2-dichloroethane at 80 ºC and 20 mol% of catalyst loading,[303] delivering **268a** in a 84% yield and **302a** in a 9% yield (Figure 4.8). To conclude, blank experiments were conducted. As expected, no reaction occurred in the absence of metal catalyst. Even after heating at 150 ºC no product consumption was observed.

4.4.2 Skeletal rearrangement of α-aryl aldehydes: [1,2]-aryl migratory event scope.

[315] Buchwald, S. L.; Bolm, C. *Angew. Chem. Int. Ed.* **2009**, *48*, 5586.
[316] In addition, different commercial sources of iron(III) bromide were tested with similar results.
[317] See Experimental Section for further details.

With the optimized conditions in hand, we decided to explore the preparative scope of the transformation.[318] We started by studying the effect of different substituents on the aryl ring while keeping the cyclohexyl motif. As shown in Figure 4.11, different halide groups were well tolerated (**268b-d**, **f-i**), and their presence at the *ortho*-position of the aryl ring (**268b-d**) did not hamper the reaction, obtaining the desired products in quantitative yields. However, in some cases, catalyst loading and temperature had to be increased. The excellent reaction performance with aryl halides is interesting as it provides an additional handle via cross-coupling reactions. Aryl ketones (**268k,l**) could also be accommodated, an observation that goes in line with the ability of ketones to not interfere with the catalytic activity.

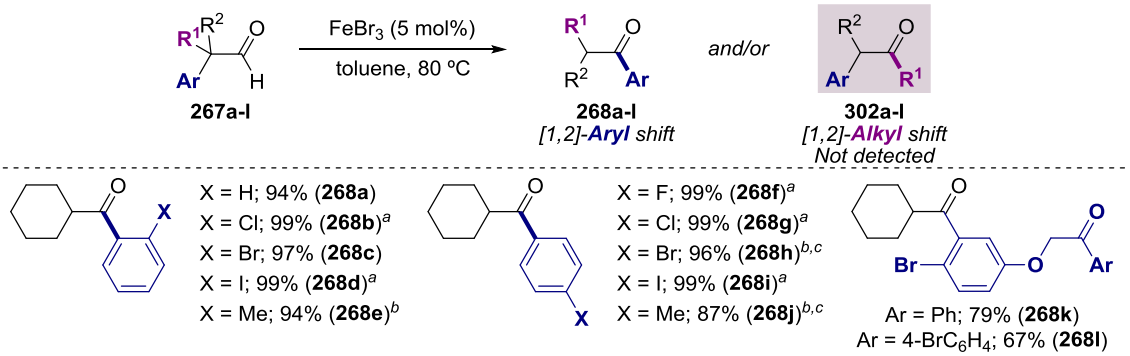

267 (0.5 mmol), $FeBr_3$ (5 mol%), toluene (0.25M), 80 ºC, 16h. Isolated yields, average of at least two independent runs. [a] $FeBr_3$ (15 mol%) at 130 ºC. [b] 110 ºC. [c] $FeBr_3$ (10 mol%).

Figure 4.11. [1,2]-Aryl shift: Different aryl substitution.

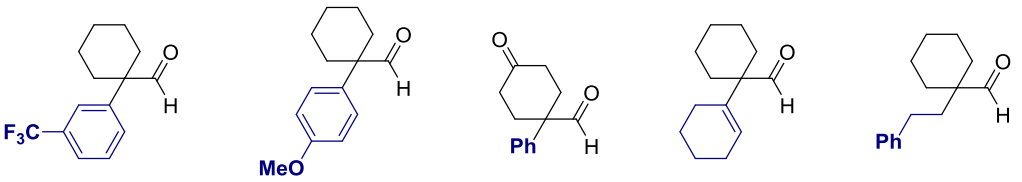

Figure 4.12. Failed substrates bearing a cyclohexyl motif.

Although trifluoromethyl group at the *meta*-position was tolerated (**267m**), no complete conversion could be achieved and the product could not be isolated in pure form. We also observed that in the presence of electron-donating groups (**267n**) the reaction failed and very poor conversions were obtained. This result will be further discussed during the mechanistic explanation. Unexpectedly, the presence of an alkyl ketone (**267o**) completely inhibited the reaction. This is surprising as phenyl ketones did not hamper the reaction, therefore, we hypothesized that dialkyl ketone is basic enough to bind the catalyst and poison it, whereas with aryl ketones, the binding is reversible. We next move to study whether the presence of the aryl motif was essential for the rearrangement to occur. In the presence of an alkene instead of an aryl ring (**267p**), very low conversions were obtained. Although full conversion was achieved with **267q** under harsh conditions ($FeBr_3$ 15 mol%, 130 ºC), a myriad on unknown byproducts were detected in the crude reaction.

[318] The synthesis of the starting material was accomplished following the similar strategy that the previously employed for the synthesis of α-aryl aldehydes. See Chapter 4.

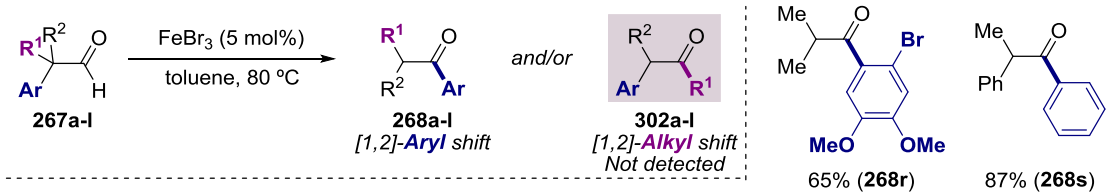

267 (0.5 mmol), $FeBr_3$ (5 mol%), toluene (0.25M), 80 ºC, 16h. Isolated yields, average of at least two independent runs.

Figure 4.12. [1,2]-Aryl shift: Beyond the cyclohexyl motif.

In light of these results, one might argue that the aldehyde-ketone rearrangement could be limited to aldehydes bearing cyclohexyl motifs. As shown in Figure 4.12, this was not the case and aldehydes possessing aliphatic substituents could also be employed, delivering the corresponding [1,2]-aryl shift exclusively.

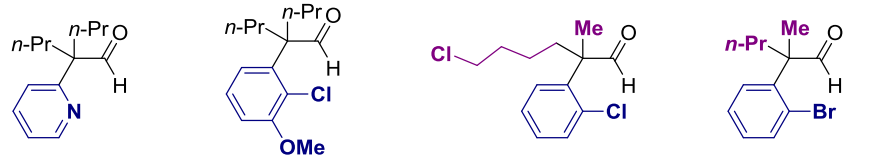

267t	267u	267v	267w
A: no reaction B: no reaction	A: no reaction B: decomposition	A: no reaction B: low conversion, unselective	A: no reaction B: low converion, unselective

Conditions A: $FeBr_3$ (5 mol%), 110 ºC ***Conditions B***: $FeBr_3$ (15 mol%), 115 ºC

Figure 4.13. Failed substrates with different alkyl substituents.

Unfortunately, the introduction of a pyridine motif (**267t**) resulted in no conversion of the starting material. Taking into consideration the reaction outcome in the presence of pyridine-based ligands (Table 4.3) this result was not surprising. We believe that the coordination of the pyridine to the catalyst forms a very stable adduct unable to promote any reactivity. Interestingly, the introduction of different alkyl motifs (**267v-w**) resulted in low conversions and unselective migratory events where all three possible regioisomers were observed by GC-MS.

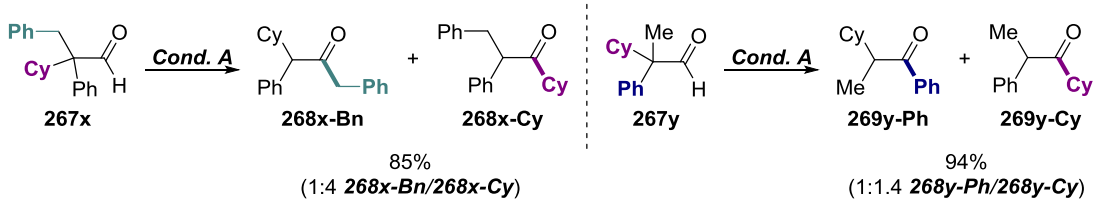

Figure 4.14. [1,2]-Shift. Migratory aptitude studies

In line with these observations, we tested other substrates bearing three different groups at the α-position to study whether the regioselectivity could be controlled or not (Figure 4.14). Surprisingly, **267x** gave a mixture of [1,2]-benzyl and [1,2]-cyclohexyl shift (**268x-Bn** and **268x-Cy**). Importantly, unlike previous examples, no aryl migration did occur. On the other hand, when aldehyde **267y** was submitted under reaction conditions migration of the phenyl and the cyclohexyl occurred, whereas the methyl group stayed at the original site (**268y-Ph** and **268y-Cy**). Therefore, we can conclude that although the reaction is not regiospecific, certain degree of regioselectivity can be achieved, and that the migratory aptitude follows the following trend: cyclohexyl>phenyl>methyl.

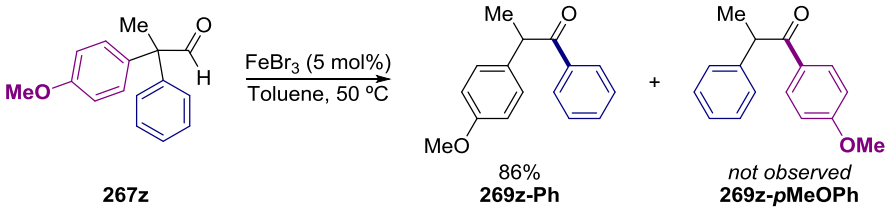

Scheme 4.7. Regiospecific [1,2]-aryl shift.

Finally, we were interested in determining whether regioselectivity could be achieved with two different aryl groups. To such end, aldehyde **267z** was tested under reaction conditions yielding **269z-Ph** as the sole product. Importantly, the reaction yielded only the product arising from the phenyl shift, with no *para*-anisole shift being observed. Therefore, we concluded that the introduction of an electron-rich group in the aryl substituent was able to ensure the regiospecificity of the process resulting in the migration of the less-electron rich arene.

4.4.3 Skeletal rearrangement of α-aryl aldehydes: [1,2]-alkyl migratory event scope.

Intrigued by the electronic effect showed in Scheme 4.7, we wondered if we could take advantage of the poorer migratory aptitude of electron-rich arenes, and promote exclusively a [1,2]-alkyl shift (Figure 4.14). Furthermore, we already observed that, with some substrates, mixtures of different migratory events were observed (Figure 4.13); therefore, if the migratory tendency of the aryl ring can be tuned, then we could have the opportunity to increase the regioselectivity of these substrates.

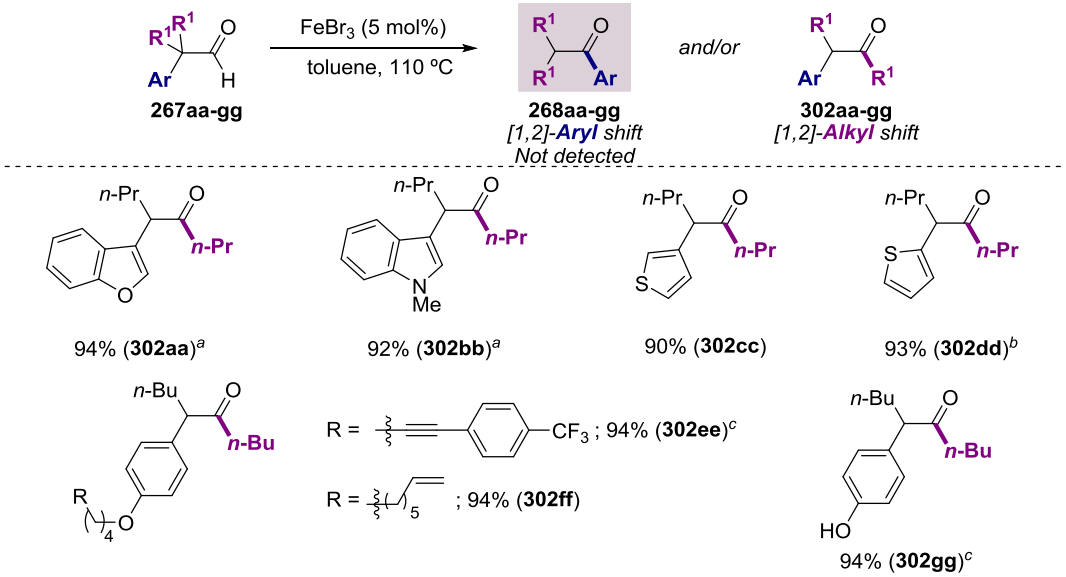

267 (0.5 mmol), $FeBr_3$ (5 mol%), toluene (0.25M), 110 ºC, 16h. Isolated yields, average of at least two independent runs. [a]T = 50 ºC. [b]1g scale. [c]T = 25 ºC.

Figure 4.15. [1,2]-Alkyl shift. Regioselectivity switch in the presence of electron-rich arenes.

We first prepared a set of α-(electron-rich)aryl aldehydes with the same two identical alkyl groups (**267aa-gg**) to study whether a regioselectivity switch could be possible under electronic control. This was indeed the case and the corresponding [1,2]-alkyl migration products were obtained in excellent yields (Figure 4.15). The reaction nicely accommodated different heteroarenes (**302aa-dd**). Importantly, no significant influence was displayed by the relative position of the heteroarene as shown by substrates **302cc** and **302dd**. Differently substituted electron-rich arenes (**302ee-ff**) were also tolerated, thus demonstrating that the

presence of π-basic motifs did not pose any problems. Remarkably, a free phenol (**302gg**) did not inhibit the reaction even though one could expect catalyst poisoning by the presence of a hydroxyl group. Although *a priori* unexpected, it has been demonstrated that anilines are much less Lewis basic than ketones towards aluminum and gallium halides, and therefore, it must be expected from phenols to be even less Lewis basic, thus explaining the lack of inhibition.[310a]

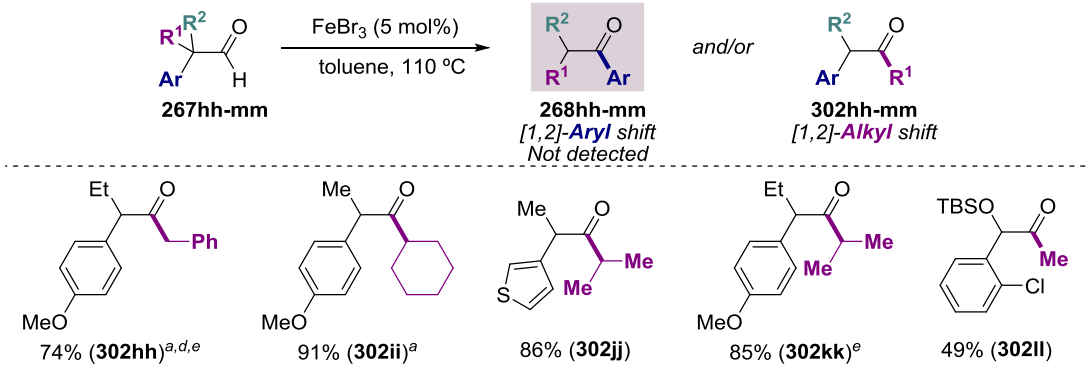

267 (0.5 mmol), $FeBr_3$ (5 mol%), toluene (0.25M), 110 ºC, 16h. Isolated yields, average of at least two independent runs. [a]T = 50 ºC. [b]1g scale. [c]T = 25 ºC. [d]5:1 regioisomeric mixture [1,2]-Bn vs [1,2]-Et migration. [e]$FeBr_3$ (10 mol%).

Figure 4.16. Evaluating the migratory aptitude on the [1,2]-alkyl shift.

Once the possibility to trigger the [1,2]-alkyl shift event selectively was demonstrated, we decided to further expand this protocol and study if, in the presence of two distinct alkyl groups, it could be possible to achieve selectivity. We first compared two primary alkyl substituents featuring different electronic nature (**267hh**). To our delight, although sterically related, a significant selectivity was achieved, being the benzyl motif preferentially migrated (**302hh**). When comparing alkyl motifs with different degree of substitution we could observe the dominant migratory aptitude of secondary carbons against primary (**267ii-kk**). The results displayed by substrates **267hh-kk** points towards a certain degree of positive buildup during the [1,2]-alkyl shift transition state which is stabilized by the adjacent phenyl ring for substrate **267hh** and by hyperconjugation in the other cases. Therefore, a very poor migratory tendency should be expected for the methyl group. However, if the proper substituents are present, methyl migration is possible as shown by the formation of **302ll**, although in low yield due to decomposition of the starting material under the reaction conditions. Remarkably, the alkyl migration is preferred in the presence of an electron-deficient aryl ring. We believe this result is related to the presence of the electron donating silyl ether, a behavior that resembles the one of acyloin rearrangement (Section 4.2.2).

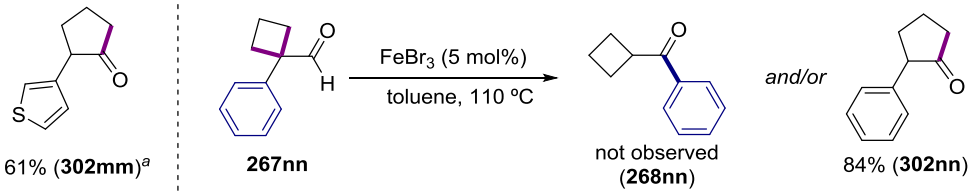

267 (0.5 mmol), $FeBr_3$ (5 mol%), toluene (0.25M), 110 ºC, 16h. Isolated yields, average of at least two independent runs. [a]T = 50 ºC.

Figure 4.17. [1,2]-Alkyl shift towards the ring expansion of cyclic substrates.

Finally, we studied the possibility to achieve a [1,2]-alkyl migration event in a cyclic substrate, thus leading to a ring expansion phenomena which, to date, has remained elusive

under the optimal reaction conditions. Specifically, we studied the ring expansion of α-cyclobutyl aryl aldehydes.[319] As shown in Figure 4.17, the ring expanded products were obtained in good to high yields. The case of substrate **267nn** is of particular interest, as, according to our previous finding, we might expect a preferential phenyl migration over the ring expansion leading to the formation of ketone **268nn**. However, only cyclopentanone **302nnn** was observed. Although this observation could be in disagreement with the previous behavior observed with cyclohexyl substituents, we might emphasized that the formation of a five-membered ring from a four-membered ring is highly favored, whereas the formation of a seven-membered ring from a six-membered ring is not favored to the same extent.

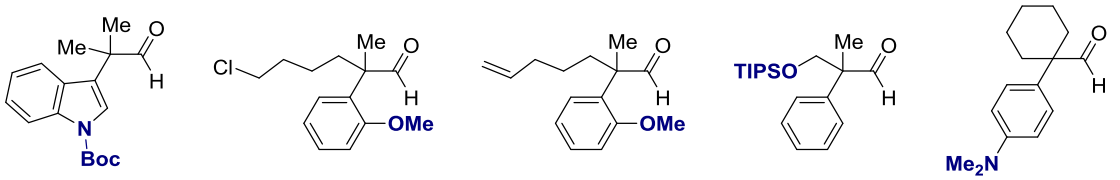

267oo **267pp** **267qq** **267rr** **267ss**

Figure 4.18. Substrates that failed to undergo [1,2]-alkyl shift.

The reaction presented a few limitations. For example, it was highly sensitive to the relative position of the electron-donor group within the aryl motif. Specifically, when such group was at the *ortho*-position (**267qq-rr**) no conversion was achieved. Although the lack of activity could be reasoned on steric basis, we do not support such assumption, since we have previously shown that *ortho*-substitution is not an issue (**268b-e**). The poor proclivity of cyclohexyl rings to undergo ring-expansion is illustrated by the lack of reactivity of **267ss**. Although one might argue a catalyst poisoning by the aniline group, this is highly unlikely, since the Lewis basicity of such motif is low as previously explained. Although indole motif is well tolerated on our protocol, aldehyde **267oo** did not react, most probably due to the presence of the Boc group that reduces de electronics over the indole core as well as the poor migratory aptitude of the methyl group. Finally, aldehyde **267rr** bearing a silyl ether further support our previous statement regarding substrate **302ll**, where we claimed that the OTBS motif was fundamental to stabilize the formed positive charge. In the case of substrate **267rr**, the silyl ether is too distant from the generated carbocation, and therefore, it will be not able to stabilize it, resulting in lack of reactivity.

On the basis of the observed results, we concluded that electron-rich arenes are able to promote regioselective [1,2]-alkyl shift, where the migration event is exquisitely controlled by preferential migration of the moiety that better stabilizes a cationic intermediate. However, in the absence of electron-rich groups, the selectivity is more problematic, and it becomes necessary to employ more biased systems (methyl substituents or cyclohexyls) to achieve good regioselectivites since in the presence of other alkyl substituents unselective migration occurs (Figures 4.13 and 4.14).

4.4.4 Mechanistic studies and proposal

Based on the previous work of Chatani,[303] and in previous works concerning the α-ketol rearrangement, the Meinwald rearrangement and others (see Sections 4.2 and 4.3), we believe that the reaction follows the mechanism depicted in Figure 4.19.

[319] α-Cyclopropyl and α-cyclopentyl aryl aldehydes led to decomposition.

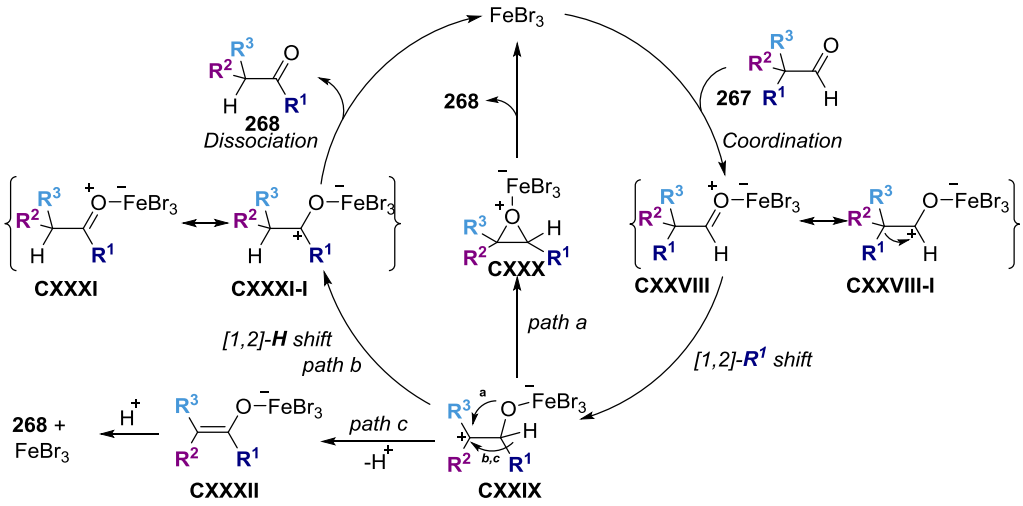

Figure 4.19. Mechanistic rational for the Fe-catalyzed skeletal rearrangement of α-aryl aldehydes.

We believe that the reaction is initiated by σ-coordination of the aldehyde **267** to the Lewis acid in the π-nodal plane, forming adduct **CXXVIII**. Subsequently, [1,2]-R^1 migration (where R^1 stands for the motif with better migratory aptitude) occurs forming intermediate **CXXIX**, which possesses a carbocation at the α-position. At this point, three different possibilities arise: path a: the oxygen atom collapses over the carbocation forming an epoxide **CXXX**, which will deliver the final product after classical Meinwald-rearrangement.[320] Alternatively, a [1,2]-hydrogen shift could occur leading to the ketone adduct **CXXXI** which, upon dissociation, will release the active catalyst. Finally, proton elimination must be considered as well leading to enolate **CXXXII**, which will yield the product after a sequential protonation/tautomerization.

In order to shed some light into the mechanism, we decided to prepare epoxide **303a**, which would be formed from aldehyde **267a** if path *a* is operating. If this is the case, then, we should expect regioselective formation of ketone **268a**, in analogy to the result displayed by **267a**. However, under our reaction conditions, we observed a mixture of aldehyde **267a**, the expected ketone **268a** and ketone **302a**, the formal ring expansion product (Figure 4.20). The product distribution, which is constant and does not depend on the temperature, does not match with the expected results. Additionally, **302a** is obtained in 47-49% yield, indicating that epoxides are not intermediates of our reaction, as this product was never detected during the optimization studies.

[320] (a) Coxon, J. M.; Maclagan, R. G. A. R.; Rauk, A.; Thorpe, A. J.; Whalen, D. *J. Am. Chem. Soc.* **1997**, *119*, 4712. (b) Fraile, J. M.; Mayoral, J. A.; Salvatella, L. *J. Org. Chem.* **2014**, *79*, 5993.

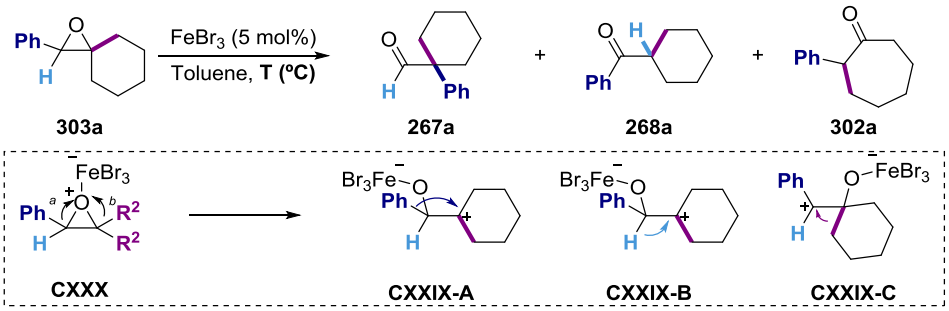

Entry	Temp (ºC)	Conv (%)	267a (%)	268a (%)	302a (%)
1	110	>99	25	28	47
2	80	>99	23	28	49
3	rt	>99	20	32	48

Figure 4.20. Studying the intermediacy of epoxides.

Next, we decided to demonstrate the intermediacy of carbocations during the catalytic cycle. To such end, we first envisioned to study the system by performing a Hammett-plot, however, because of the divergent migratory event depending on the electronic effects we ruled out this approach. Nevertheless, we decided to prepare an enantioenriched and a diastereoenriched aldehyde (Figure 4.21) and study the configuration of the obtained products. Because a mechanistic switch could be responsible for the different migratory regioselectvity, we decided to study the intermediacy of a carbocation for both cases, for the [1,2]-aryl migration (Figure 4.21, eq a) and for the [1,2]-alkyl migration event (eq b). For substrate **267tt**, if a concerted mechanism is operating, we should expect a relative *cis* configuration between the ketone and the methyl in the final product. This was not the case and formation of *trans* product was observed, thus suggesting the intermediacy of carbocations in the [1,2]-aryl shift leading to the more stable compound locating the aryl ketone at the equatorial position. Likewise, if a concerted mechanism would be operating in the case of [1,2]-alkyl migration, a enantioenriched ketone should be formed. However, **302jj** was obtained as a racemic mixture.[321]

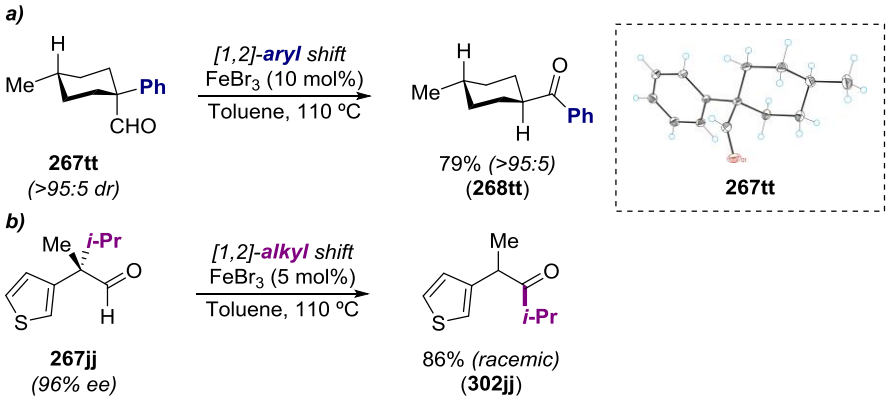

Figure 4.21. Cationic *versus* concerted mechanism.

Once we demonstrated the intermediacy of carbocations, we decided to study in depth the migratory event, in order to determine whether it occurs in an intra- or intermolecular

[321] The observed loss of chiral information could be also rationalized by proposing a concerted mechanism followed by a Lewis-acid catalyzed epimerization of the final ketone.

fashion.[322,291] To such end, we designed a cross-over experiment with two aldehydes bearing different, yet very similar, aryl and alkyl substitution. The equimolar mixture of aldehyde **267tt** and **267e** under iron(III) catalysis gave only the expected products and not even traces of the cross-over products was observed, thus indicating that the [1,2]-shift occurs faster than the diffusion of the migrating group.

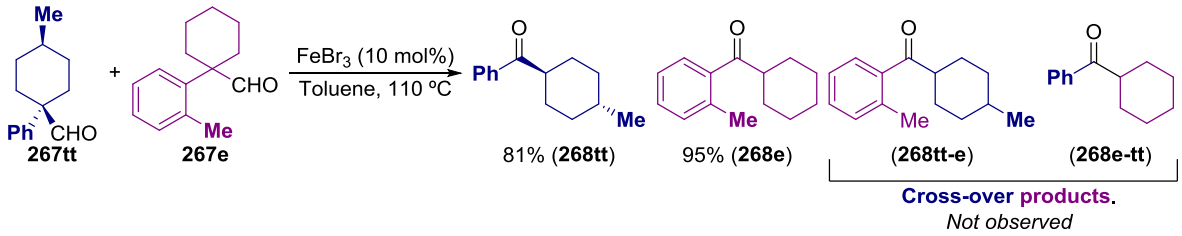

Scheme 4.8. Cross-over experiments.

In this manner, we have ruled out the possibility of a Meinwald-type mechanism and, subsequently, we have studied the nature of the [1,2]-R^1 migratory event (see Figure 4.19), which occurs in an intramolecular fashion. However, at this point we had not studied yet the [1,2]-hydrogen shift from intermediate **CXXIX**. In this regard, we envisioned studying such event indirectly by labelling the migrating hydrogen. Surprisingly, not complete deuterium transfer was observed when aldehyde **267cc-*d*^{1}** was submitted under reaction conditions (Scheme 4.9), thus suggesting that the migrating hydrogen does not come exclusively from the aldehyde but from other vicinal positions. To date, we are not able to determine whether the transformation follows path b or path c or both of them.

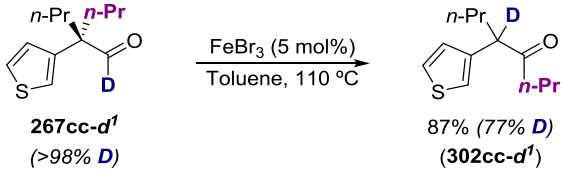

Scheme 4.9. Deuterium-labelling experiments.

A final study was conducted in order to rule out the Brønsted acid catalysis instead of iron(III) bromide, as traces of hydrobromic acid could be expected upon reaction of iron(III) bromide with water. Indeed, we have previously seen the feasibility of the skeletal rearrangement of aldehydes under superacidic conditions.[283,284,285,297] In order to rule out this hypothesis, different test reactions were conducted in the presence of catalytic amounts of acid (Figure 4.22). Interestingly, among the different acids tested, only the superacidic trifluoromethanesulfonic acid was able to give product (entry 1) although in low yields and giving mainly decomposition of the starting material. Remarkably, hydrobromic acid, was not competent as reagent. In this regard, we ruled out the Brønsted acid-catalysis, and therefore, we corroborated that this protocol was catalyzed by iron(III) bromide.

[322] Hür, D. *Hacettepe J. Biol. & Chem.* **2007**, *35*, 187.

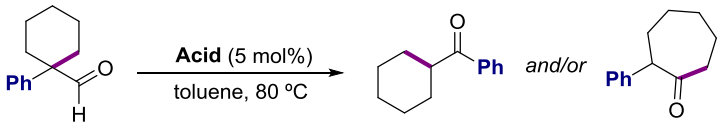

267a | 268a [1,2]-*Aryl* shift | 302a [1,2]-*Alkyl* shift

Entry	Acid	Conv. (%)	268a (%)	302a (%)
1	TfOH	>99	10	0
2	HBr	0	0	0
3	*p*TsOH·H_2O	0	0	0
4	TFA	0	0	0

Figure 4.22. Skeletal rearrangement in the presence Brønsted acids.

4.4.4.1 Regiodivergent [1,2]-shift: Its origin

Once the mechanistic pathway is relatively clear, we will proceed to explain the origin of the electronic control of the migratory event. It must be noticed that the following explanation has not been confirmed by mechanistic studies and is, therefore, speculative. Consequently, the reader is encouraged to consider carefully the following section. The observed regiodivergency can be explained in two different ways. If we consider that all the elementary steps are reversible, then the reaction will be ruled by the formation of the more stable carbocations. Therefore, in the presence of electron-rich aryl moieties, the intermediate **CXXIX** will be more stabilized than in the presence of electron-neutral or electron-poor aryl rings. Consequently, the [1,2]-alkyl migration would be favored for electron-rich rings. However, we consider such scenario unlikely since DFT calculations from the group of Chatani have demonstrated that the reaction does not involve a thermodynamic equilibrium.[303] On the other hand, if we consider a kinetic control, then, the [1,2]-shift will be determined by the differences in energy of the different transition states for the product-determining step (Figure 4.23). The product-determining step will be the [1,2]-shift, and therefore, its transition state will be the one responsible for the selectivity. If a [1,2]-aryl shift is occurring, the intermediacy of an arenium ion[323] is generally accepted. Therefore, we propose that the [1,2]-shift occurs through **TS-[1,2]-aryl** (Figure 4.23) where the carbocation is stabilized by delocalization within the aryl ring. On the other hand, if a [1,2]-alkyl shift is taking place, then, we propose a transition state of the type **TS-[1,2]-alkyl** which is related to the postulated transition state for the Bayer-Villiger oxidation.[324] In this transition state the positive charge will be splitted within the three different carbons involved in the migratory event. We believe that in general, **TS-[1,2]-alkyl** will be favored according to the experimental results, probably because no loss of aromaticity is required. Furthermore, the arene will be able to stabilize the positive charge built-up at the benzylic position, being this stabilization higher in the presence of electron-rich arenes. This will be responsible of the divergence regarding electron-rich systems. On the other hand, in the presence of electron-neutral or electron-deficient arenes we believe as well that **TS-[1,2]-alkyl** will be lower in energy as there is no loss in aromaticity. However, the difference in energy between **TS-[1,2]-alky** and **TS-[1,2]-aryl** will be lower than with electron-rich arenes because of a poorer stabilization of the benzylic position in **TS-[1,2]-alkyl**, thus

[323] (a) Ajaz, A.; McLaughlin, C.; Skraba, S. L.; Thamatam, R.; Johnson, R. P. *J. Org. Chem.* **2012**,*77*, 9487. (b) Nakamura, K.; Osamura, Y. *Tetrahedron Lett.* **1990**, *31*, 251. (c) Winstein, S.; Morse, B. K.; Grunwald, E.; Schreiber, K. C.; Corse, J. *J. Am. Chem. Soc.* **1952**, *74*, 1113. (d) Olah, G. A.; Meyer, M. W. *J. Org. Chem.* **1962**, *27*, 3682. And references therein.
[324] Grein, F.; Chen, A. C.; Edwards, D.; Crudden, C. M. *J. Org. Chem.* **2006**, *71*, 861.

explaining the lack of selective migratory events (Figures 4.13 and 4.14) in simple systems. It must be noticed that in the case of non-electron-rich arenes, selectivity was only achieved with methyl or cyclohexyl substituents which have a poor migratory aptitude. We believe that such poor migratory aptitude is the responsible for the selectivity observed. Finally, it must be noticed that whereas some electron-rich arenes were able to react even at room temperature, electron-deficient o neutral arenes required temperatures between 80 – 130 ºC, thus revealing the intermediacy of cationic transition states and the ability of electron-donating groups to stabilize them.

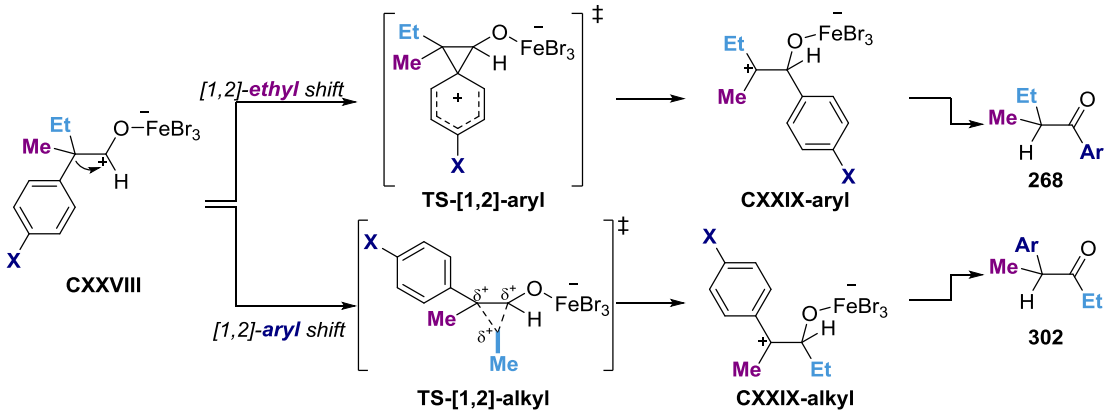

Figure 4.23. Divergence origin. Putative transition states for the migratory event.

We previously showed the better migratory aptitude of secondary carbons over primary, and benzylic motifs over alkylic (Figure 4.16). We can easily explain these results by considering **TS-[1,2]-alkyl**. In the transition state, there is a positive charge built-up on the migrating carbon, therefore, the migratory tendency will be determined by the ability to stabilize it. Among primary and secondary carbons, secondary carbons will be able to better stabilize it by hyperconjugation.[325] On the other hand, if an ethyl and a benzyl are competing, the ability of the benzyl to stabilize the positive charge built-up by means of mesomeric effect will overcome the hyperconjugation of the ethyl, and, therefore, the benzyl will migrate preferentially (Figure 4.16, **302hh**).

4.4.4.2 Final remarks concerning the reaction mechanism

Finally, we would like to draw attention on three facts. First, during all the mechanistic discussion we have considered the aldehyde to be activated by only one molecule of Lewis acid for simplicity. However, it must be noticed that we do not have evidences supporting such scenario. Actually, dual activation on the skeletal rearrangements of aldehydes has already been demonstrated by the groups of Olah[284,285] and Chatani.[303] Importantly, it has been demonstrated that in benzene solutions, iron(III) chloride adopts a dimeric structure, therefore, we cannot ignore the possibility of a dimeric iron(III) bromide in toluene that will lead to dual aldehyde activation.[326] Secondly, we have not addressed yet the reason why catalytic turnover is possible (Figure 4.24). In principle, one might anticipate that the more

[325] (a) Alabugin, I. V.; Gilmore, K. M.; Peterson, K. M. *WIREs Comput. Mol. Sci.* **2011**, *1*, 109. (b) Deasy, C. L. *Chem. Rev.* **1945**, *36*, 145.
[326] (a) Ooi, T.; Asao, N.; Maruoka, K. *Chem. Lett.* **1998**, *56*, 377 *(in Japanese)* (b) Ooi, T.; Takahashi, M.; Yamada, M.; Tayama, E.; Omoto, K.; Maruoka, K. *J. Am. Chem. Soc.* **2004**, *126*, 1150. (c) Ooit, T.; Miura, T.; Itagaki, Y.; Ichikawa, H.; Maruoka, K. *Synthesis* **2002**, *2*, 279. (d) *Pihko, P. M. Angew. Chem. Int. Ed.* **2004**, *43*, 2062.

Lewis basic ketone would coordinate with the Lewis acid stronger than with the aldehyde, and therefore, there could not be catalyst turnover. However, we believe that the steric hindrance around the carbonyl motif in the ketone (one primary carbon or an aryl motif at one side, and a secondary carbon at the other) will help to shift the equilibrium towards formation of the aldehyde adduct **267-FeBr$_3$** which, besides possessing a tertiary carbon, is less sterically encumbered as the Lewis acid can bind it in a *cis* fashion relative to the aldehydic proton, therefore avoiding the steric repulsion of the tertiary carbon.[327] During the scope of the reaction, we observed that no product was formed with **267o**. We believe that this is because two factors. First, a dialkyl ketone is way more Lewis basic than aryl ketones as previously explained. Second, because the steric hindrance around this highly directional ketone will be relatively low as only one proton will be interfering. Therefore, the Lewis acid will tightly coordinate this ketone resulting in catalyst inhibition (**2670-FeBr$_3$**).

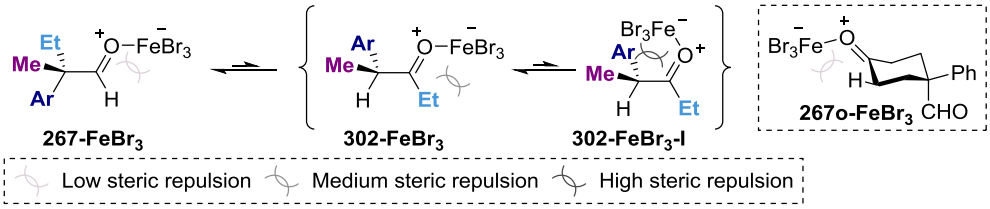

Figure 4.24. Rational behind the catalyst turnover.

Although tentative, we believe that the reason why iron(III) bromide possesses such high reactivity in this system unlike other common Lewis acid relies on the steric hindrance of the big iron atom and the bulky bromides which will ensure the catalytic turnover. The transfer of the iron(III) bromide will not necessarily imply a complete dissociation like represented in Figure 4.19 and it could occur through a pentacoordinated iron(III) intermediate **304**, in analogy to the behavior displayed by aluminum(III) bromide with 9-fluorenone.[328]

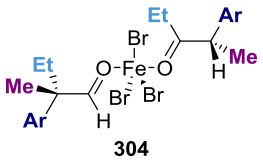

Figure 4.25. Possible intermediate for catalytic turnover.

Finally, during different poster sessions and talks concerning this last chapter, a recurrent question refers to the possibility of a radical mechanism. Although we have not conducted any mechanistic study in this regard, we consider such possibility unlikely for several reasons. Usually, reactions involving iron-catalysis and acyl radical formation[188] requires the presence of an iron(II) salt in the presence of peroxides, this mixture will lead to acyl radical formation through a Fenton-type reaction between the iron(II) and the peroxide.[329] Iron(IV)-oxo species can also promote a hydrogen atom abstraction event by being reduced to iron(III) and iron(II).[330] Finally, the non-catalyzed acyl radical formation has been demonstrated under aerobic conditions with concomitant formation of the corresponding carboxylic acids, acetals

[327] LePage, T. J.; Wiberg, K. B. *J. Am. Chem. Soc.* **1988**, *110*, 6642.
[328] Branch, C. S.; Bott, S. G.; Barron, A. R. *J. Organomet. Chem.* **2003**, *666*, 23.
[329] (a) Correa, A.; Fiser, B.; Gómez-Bengoa, E. *Chem. Commun.* **2015**, *51*, 13365. (b) Liu, W.; Li, Y.; Li, Z. *J. Am. Chem. Soc.* **2011**, *133*, 10756. (c) Lv, L.; Xi, H.; Bai, X.; Li, Z. *Org. Lett.* **2015**, *17*, 4324.
[330] Rana, S.; Dey, A.; Maiti, D. *Chem. Commun.* **2015**, *51*, 14469.

and acylation products.[331] Based on these precedents, we consider the intermediacy of radicals rather unlikely as we are using an iron(III)-catalyst, no peroxides are being used and the reaction is conducted under a strict inert atmosphere (the presence of air resulted deleterious for the transformation). Furthermore, the classical byproducts involving the intermediacy of acyl radicals, such as the carboxylic acid, the decarbonylated aldehyde, acetals, alohols, etc[332] were not observed on the reaction mixture.

4.4.5 Conclusions

To summarize, we have developed an iron(III)-catalyzed skeletal rearrangement of α-aryl aldehydes to ketones under mild reaction conditions and using an environmentally friendly iron catalyst. Although traditionally the Lewis acid-catalyzed chemistry presents a restricted substrate scope because of catalyst poisoning, we present herein a wide substrate scope were σ- and π-coordinating groups are well tolerated. Furthermore, the reaction tolerates heterocyclic motifs and can be scaled up with any erosion of the yield. More importantly, the [1,2]-shift can be easily controlled by tuning the electronic nature of the aryl motif. While [1,2]-aryl shift occurs with electron-poor or electron-neutral aryl rings, the presence of electron-rich arenes switches the selectivity towards [1,2]-alkyl migration. Furthermore, the [1,2]-alkyl shift is highly selective resulting in preferential migration of the alkyl motif which stabilizes better the positive charge generated during the transition state.

Different mechanistic studies have been conducted in order to shed light into the reaction mechanism. Although some of the elementary steps are yet not clear, we demonstrated that the reaction proceeds through carbocationic intermediates and that a Meinwald-type rearrangement of *in situ* generated epoxides can be ruled out. Additionally, we have demonstrated that there are several competing [1,2]-hydrogen shifts. Control experiments have shown that the reaction is certainly catalyzed by iron(III) and that no scrambling of the migrating groups occurred. Finally, different aspects of the mechanism have been explained in depth based on literature precedents and some empirical observations. Further studies will need to be perform in order to develop the asymmetric version of the transformation.

[331] Chudasama, V.; Fitzmaurice, R. J.; Caddick, S. *Nature. Chem.* **2010**, *2*, 592.
[332] (a) Rust, F. F.; Seubold, F. H.; Vaughan, W. E. *J. Am. Chem. Soc,* **1948**, *70*, 4253. (b) Bentrude, W. G.; Darnall, K. R. *J. Am. Chem. Soc.* **1968**, *90*, 3588. (c) Lunazzi, L.; Ingold, K. U.; Scaiano, J. C. *J. Phys. Chem.* **1983**, *87*, 529. (d) Ho, S. K. *Proceedinf of the Royal Society A* **1963**, 278. (e) Sawaki, Y.; Ogata, Y. *J. Org. Chem.* **1976**, *41*, 2340.

Chapter 5. Conclusions.

Finally, it would be appropriate to determine wether the objectives stablished at the beginning of this Doctoral Thesis have been fulfilled or not.

During the Chapter 2 and 3, several important contributions have been done:

- Two methodologies have been developed for the synthesis of rather elusive benzofused cycles. Among them, benzocyclobutenones are characterized but their importance as an intermediate in numerous organic transformations and synthesis of natural products.
- The activation of unconventional non-activated C(sp^3)—H bonds and aldehydic C(sp^2)—H bonds has been achieved allowing for novel disconnections.
- In Chapter 2, the functionalization of non-activated C(sp^3)—H bonds has been accomplished for the formation of quaternary centers, using, for the first time, diazo compounds as coupling partners.
- Importantly, several mechanistic studies have been conducted in order to support a mechanistic proposal. Particularly, the results obtained in the Chapter 2 have also important implications for other related transformations on the field.

It must be noticed that while conducting this Doctoral Thesis, a new transformation was found by serendipity. Although not considered in the initial objectives, the new methodology is highly interesting because of several reasons:

- It is the first skeletal rearrangement of α-aryl aldehydes with an absolute control over the regioselectivity of the process.
- Importantly, the reaction occurs under mild reaction conditions using highly appealing iron(III) salts as catalyst.
- We have stablished a rationale of the migratory aptitude based on empirical observations.
- Mechanistic studies have been able to explain with detail the mechanistic pathway and to explain the migratory aptitude.

Finally, it should be highlighted that with the work herein presented not only our initial objectives have been satisfactorily fulfilled but new research lines have been opened that are being currently pursued towards the development of an enantioselective version of the transformatios described in Chapters 2 and 4 as well as the employment of other coupling partners for the transformation described in Chapter 2.

Chapter 6. Experimental Procedures.

6.1. Pd-catalyzed C(sp^3)–H functionalization/carbenoid insertion: quaternary carbon stereocenters via multiple C–C Bond-Formation. Experimental procedures.

6.1.1. General considerations.

Reagents: Unless otherwise stated, all reactions were carried out under an argon atmosphere in resealable screw-cap test tubes using standard Schlenk and/or drybox techniques for the manipulation of solvents and reagent. *trans*-Dichlorobis(dimethylsulfide)palladium(II) (*t*-$PdCl_2(SMe_2)_2$) was prepared following the reported method.[333] All the diazo compounds were prepared following the reported literature protocol.[334] All other reagents were purchased from commercial sources and used as received.

Analytical Methods: ^{1}H NMR and ^{13}C NMR spectra and melting points (where applicable) are included for all new compounds. ^{1}H NMR and ^{13}C NMR spectra were recorded on a Bruker 300 MHz, a Bruker 400 MHz or a Bruker 500 MHz at 20 ºC. All ^{1}H NMR spectra are reported in parts per million (ppm) downfield of TMS and were measured relative to the signals for $CHCl_3$ (7.26 ppm). All ^{13}C NMR spectra were reported in ppm relative to residual $CHCl_3$ (77.16 ppm) and were obtained with ^{1}H decoupling. Coupling constants, *J*, are reported in hertz (Hz). In the case of diastereisomeric mixtures, a crude NMR was recorded to determine the ratio. Melting points were measured using open glass capillaries in a Büchi B540 apparatus. Infrared spectra were recorded on a Bruker Tensor 27. Mass spectra were recorded on a Waters LCT Premier spectrometer. Gas chromatographic analyses were performed on HewlettPackard 6890 gas chromatography instrument with a FID detector using 25m x 0.20 mm capillary column with cross-linked methyl siloxane as the stationary phase. Flash chromatography was performed with EM Science silica gel 60 (230- 400 mesh) and using $KMnO_4$ as TLC stain. The yields reported throughout the Chapter 2 refer to isolated yields and represent an average of at least two independent runs. The procedures described in this section are representative. Thus, the yields may differ slightly from those given in in the Chapter 2.

[333] Inorganic Synthesis, Vol. 32. Page 163.
[334] Muthusamy, S.; Sivaguru, M. *Org. Lett.*, **2014**, *16*, 4248.

6.1.2. Optimization of Reaction Conditions.

General procedure for screening reactions: A 12.0 mL test tube is charged with Pd precatalyst (5 mol%), ligand (7.5 mol%) and the additive (50 mol%). Then, the base (0.13 mmol, 1.3 equiv.) is weighed out into the glovebox. Under a positive Ar flow, **154a** (0.1 mmol, 1.0 equiv., 21.3 mg) and **175a** (0.175 mmol, 1.75 equiv., 30.8 mg) were added with a microsyringe follow by addition of the corresponding anhydrous solvent (0.4 mL, 0.25M).[335] Finally, the reaction is placed on a preheated block and stirred for 14h at the desired temperature. After this time, the reaction is cooled down to room temperature. Next, *p*-xylenes (0.1 mmol, 1.0 equiv., 12.1 µL) was added via microsyringe followed by 5 mL of EtOAc. An aliquot was filtered through a plug of silica and celite and analyzed by GC.

6.1.3. Synthesis of the starting materials

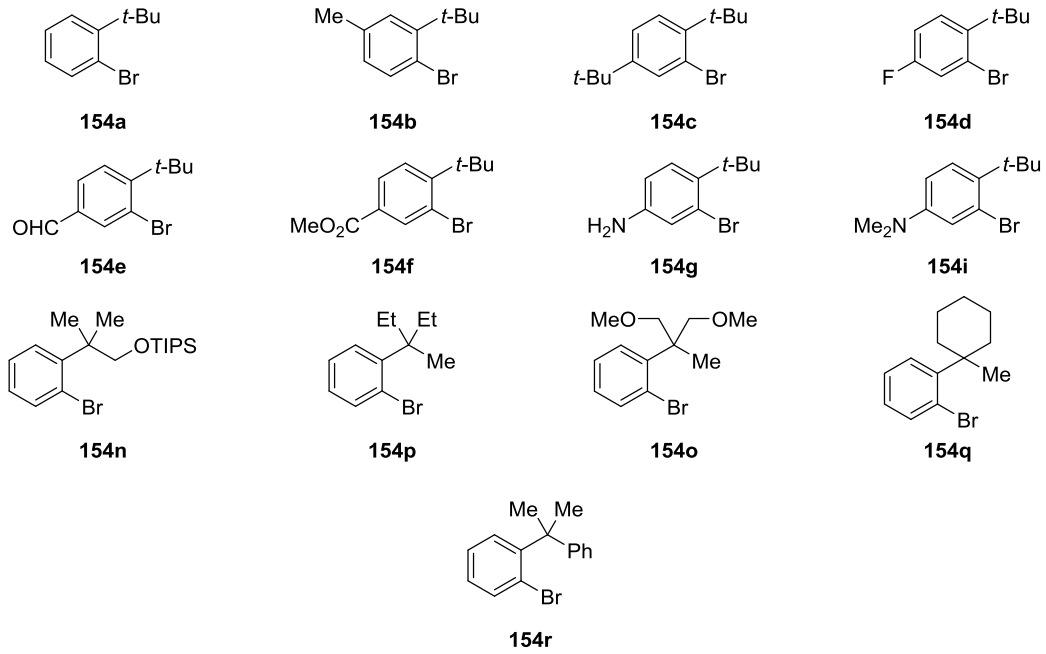

Figure 6.1.S1. Prepared starting materials

Substrates **154a**[336], **154c**[337], **154e**[338] and 154**g**[339] were prepared following literature procedures.

[335] We observed that the reaction outcome is highly dependent on the DMF quality. Bottles opened within the last 3 weeks gave comparably lower yields.
[336] Mazzanti, A.; Lunazzi, L.; Minzoni, M.; Anderson, J. E. *J. Org. Chem.* **2006**, *71*, 5474.
[337] Yap, J. S. L.; Ding, Y.; Yang, X.-Y.; Wong, J.; Li, Y.; Pullarkat, S. A.; Leung, P.-H. *Eur. J. Inorg. Chem*. **2014**, *20*, 5046
[338] Hambley, T. W.; Sternhell, S.; Tansey, C. W. *Aust. J. Chem.* **1990**, *43*, 807.
[339] Varghese, J.; Hom, R.; Sealy, J.; Aquino, J.; Probst, G.; Tung, J.; Fang, L. WO **2005**/070407 A1.

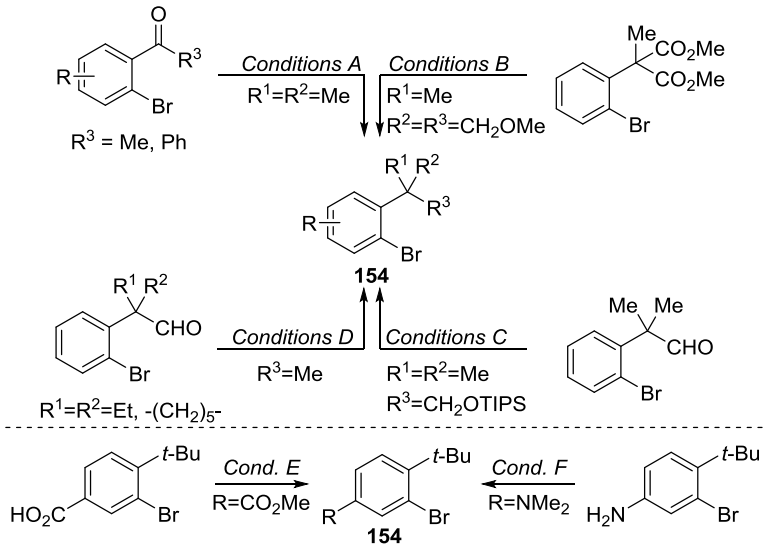

Figure 6.1.S2. General reaction conditions for preparing starting materials.

Reaction conditions *A (Figure 6.1.S2):* Over a -40 ºC solution of $TiCl_4$ (2.2 equiv.) in anhydrous DCM (0.3 M) was dropwise added Me_2Zn (2M in toluene, 2.2 equiv.) and the mixture was stirred for 15 min. Next, a solution of the aryl ketone (1.0 equiv.) in anhydrous DCM (0.6 M) was dropwise added. The reaction was stirred overnight at 0 ºC. Once completed, the reaction was poured on an ice/water bath (*exothermic reaction!*), extracted with Et_2O (x3) and washed with brine. After drying over $MgSO_4$, it was taken to dryness. Then, the crude was dissolved in DCM (0.3 equiv.) and cooled to 0 ºC. Next, *m*CPBA (3.0 equiv.) was added and the mixture was stirred overnight at rt. The crude was filtered through Celite®, washed with $NaHCO_3$, brine, dried over $MgSO_4$ and concentrated. The product was purified on silica gel chromatography with pentane 100%. (32-47% yield)

Reaction conditions *B (Figure 6.1.S2):* ***Step 1***: Over a solution of dimethyl 2-(2-bromophenyl)-2-methylmalonate[340] (1.0 equiv.) in anhydrous DCM (0.16 M) at 0 ºC was slowly added DIBALH (1.0M in Hexanes, 6.1 equiv.). The mixture was stirred overnight at rt. Once completed, it was quenched by addition of EtOAc at 0 ºC, followed by water and then HCl 2M (aq.). It was extracted with EtOAc (x3), washed with brine and dried over $MgSO_4$. The crude was used in the next step without further purification.

Step 2: Over a 0 ºC suspension of NaH (3.0 equiv.) in anhydrous DMF (0.3 M) was added the diol (1.0 equiv.) previously prepared dissolved in DMF (0.6 M). After stirring for 30 min at 0 ºC, iodomethane (4.0 equiv.) was added. The reaction was stirred overnight at rt. When finished,

[340]Chaumontet, M.; Piccardi, R.; Audic, N.; Hitce, J.; Peglion, J.-L.; Clot, E.; Baudoin, O. *J. Am. Chem. Soc.* **2008**, *130*, 15157.

the reaction was quenched with NH_4Cl (aq.), and extracted with EtOAC (x3). After washing with brine and drying over $MgSO_4$, the product was purified on silica gel column chromatography Hexanes/EtOAc 9:1 obtaining a pale yellow oil (76% yield, **154o**).

Reaction conditions *C (Figure 6.1.S2):* ***Step 1***: Over a 0 ºC solution of 2-(2-bromophenyl)-2-methylpropanal[341] (1.0 equiv.) in anhydrous MeOH (0.5 M), was added $NaBH_4$ (2.5 equiv.) portionwise. The reaction was stirred overnight at rt. When completed, EtOAc was added followed by NH_4Cl (aq.). The reaction was extracted with EtOAc (x3), washed with brine, dried over $MgSO_4$ and concentrated. The crude was used in the next step without further purification.

Step 2: Over a solution of the alcohol (1.0 equiv.) in anhydrous DCM (0.2 M) at 0 ºC, was added 2,6-lutidine (3.0 equiv.) followed by TIPSOTf (2.0 equiv.). The reaction was stirred at rt overnight. When completed, as judged by TLC, the reaction was quenched with NH_4Cl (aq.) and extracted with DCM (x3). After washing with brine and drying over $MgSO_4$, the crude was submitted to column chromatography Hexanes/EtOAc 95:5 giving a pale yellow oil (93% yield, **154n**).

Reaction conditions *D (Figure 6.1.S2):* ***Step 1***: Over a 0 ºC solution of the aldehyde[341] (1.0 equiv.) in anhydrous MeOH (0.5 M), was added $NaBH_4$ (2.5 equiv.) portionwise. The reaction was stirred overnight at rt. When completed, EtOAc was added followed by NH_4Cl (aq.). The reaction was extracted with EtOAc (x3), washed with brine, dried over $MgSO_4$ and concentrated. The crude was used in the next step without further purification.

Step 2: Over a solution of the alcohol (1.0 equiv.) and DMAP (0.2 equiv.) in anhydrous DCM (0.2 M) was added dry Et_3N (3.0 equiv.). After stirring for 30 min at 0 ºC, MsCl (2.0 equiv.) was added. The reaction was stirred overnight while warming up to rt. When completed, Et_2O was added followed by NH_4Cl (aq.). The reaction was extracted with Et_2O (x3), washed with brine, dried over $MgSO_4$ and concentrated. The crude was used in the next step without further purification.

Step 3: Over a solution of the mesylate (1.0 equiv.) in anhydrous THF (1.0 M) under N_2 atmosphere was added Super-Hydride (1M sol. in THF, 2.1 equiv.). The reaction was heated at 70 ºC overnight. When completed, the reaction was quenched by addition of NH_4Cl (aq.). The reaction was extracted with Et_2O (x3), dried over $MgSO_4$, concentrated and purified on silica gel column with pentane 100%. (53-66% yield)

[341] Álvarez-Bercedo, P.; Flores-Gaspar, A.; Correa, A.; Martin, R *J. Am. Chem. Soc.* **2010**, *132*, 466.

Reaction conditions *E (Figure 6.1.S2):* A solution of 3-bromo-4-(tert-butyl)benzoic acid[338] (1.0 equiv.) in MeOH and a few drops of H_2SO_4 was refluxed for two hours. Then, it was allowed to reach rt. The crude was concentrated, dissolved in Et_2O and washed with $NaHCO_3$ (aq.). After three extractions with Et_2O the combined organic phases were dried over $MgSO_4$, filtered and concentrated to dryness. The product was purified on silica gel column 9/1 affording the pure product as a colorless oil (88% yield, **154f**).

Reaction conditions *F (Figure 6.1.S2):* Aqueous H_2SO_4 (2.0 M, 1.8 equiv.) was added to a stirred solution of formaldehyde (37 wt.% in water, 3.0 equiv.) in THF (0.37 M). The mixture was cooled to 0 ºC and stirred for 10 min. Then, 3-bromo-4-(tert-butyl)aniline **154g**[339] (1.0 equiv.) was added dropwise within 10 min and the reaction was further stirred for 10 min at 0 ºC. Next, $NaBH_4$ (4.0 equiv.) was slowly added within 30 min while keeping the temperature at 0 ºC. The reaction was allowed to reach RT while stirring overnight. The next morning, the reaction was quenched by addition of NaOH (2 M) until pH = 12. The crude reaction mixture was extracted with Et_2O (x3), washed with brine and dried over $MgSO_4$, concentrated and purified on silica gel column Hexanes/EtOAc 98/2 obtaining a white solid (54% yield, **154h**).

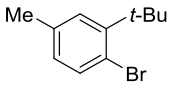

1-Bromo-2-(tert-butyl)-4-methylbenzene (154b): Following Reaction conditions A. Colorless oil. ^{1}H NMR (400 MHz, $CDCl_3$) δ 7.46 (d, *J* = 8.0 Hz, 1H), 7.24 (d, *J* = 1.9 Hz, 1H), 6.85 (ddd, *J* = 8.0, 2.2, 0.6 Hz, 1H), 2.30 (s, 3H), 1.50 (s, 9H) ppm. ^{13}C NMR (101 MHz, $CDCl_3$) δ 147.5, 137.0, 135.6, 129.0, 128.3, 119.4, 36.6, 29.9, 21.3 ppm. IR (neat, cm^{-1}): 3000, 2957, 1739, 1474, 1364, 1214, 1016, 807. HRMS *calcd for* ($C_{11}H_{15}Br$) 226.0357, *found* 226.0357.

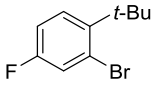

2-Bromo-1-(tert-butyl)-4-fluorobenzene (154d): Following Reaction conditions A. Colorless oil. ^{1}H NMR (500 MHz, $CDCl_3$) δ 7.40 (dd, *J* = 8.9, 6.2 Hz, 1H), 7.34 (dd, *J* = 8.4, 2.8 Hz, 1H), 6.95 (ddd, *J* = 8.9, 7.5, 2.8 Hz, 1H), 1.50 (s, 9H) ppm. ^{13}C NMR (126 MHz, $CDCl_3$) δ 160.5 (d, *J* = 248.8 Hz), 143.8 (d, *J* = 3.6 Hz), 128.9 (d, *J* = 7.9 Hz), 122.7 (d, *J* = 23.8 Hz), 122.5 (d, *J* = 8.8 Hz), 113.9 (d, *J* = 19.6 Hz), 36.4, 30.0 ppm. IR (neat, cm^{-1}): 2968, 2913, 1593, 1480, 1365, 1210, 860, 813. HRMS *calcd for* ($C_{10}H_{12}BrF$ -CH_3) 214.9866, *found* 214.9862.

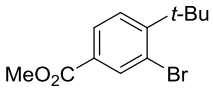

Methyl 3-bromo-4-(tert-butyl)benzoate (154f): Following Reaction conditions E. Colorless oil. ^{1}H NMR (500 MHz, $CDCl_3$) δ 8.24 (d, *J* = 1.9 Hz, 1H), 7.88 (dd, *J* = 8.3, 1.9 Hz, 1H), 7.50 (d, *J* = 8.3 Hz, 1H), 3.91 (s, 3H), 1.52 (s, 9H) ppm. ^{13}C NMR (126 MHz, $CDCl_3$) δ 165.9, 153.1, 136.9, 129.4, 128.4, 128.1, 122.6, 52.4, 37.2, 29.6 ppm. The spectroscopical data match those previously reported in the literature.[342]

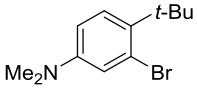

3-Bromo-4-(tert-butyl)-N,N-dimethylaniline (154h): Following Reaction conditions F. White solid. Mp: 89-90 ºC. ^{1}H NMR (500 MHz, $CDCl_3$) δ 7.30 (d, *J* = 8.8 Hz, 1H), 6.99 (d, *J* = 2.8 Hz, 1H), 6.62 (dd, *J* = 8.8, 2.8 Hz, 1H), 2.92 (s, 6H), 1.50 (s, 9H) ppm. ^{13}C NMR (126 MHz, $CDCl_3$) δ 149.5, 135.3, 128.2, 123.5, 119.5, 111.3, 40.52 35.7, 30.3 ppm. IR (neat, cm^{-1}): 3095, 2946, 1739, 1607, 1505, 1360, 1237, 797. HRMS *calcd for* ($C_{12}H_{18}BrN$+H) 256.0695, *found* 256.0687.

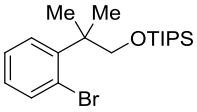

(2-(2-Bromophenyl)-2-methylpropoxy)triisopropylsilane (154n): Following Reaction conditions C. Colorless oil. ^{1}H NMR (500 MHz, $CDCl_3$) δ 7.56 (dd, *J* = 7.9, 1.4 Hz, 1H), 7.47 (dd, *J* = 8.0, 1.7 Hz, 1H), 7.23 (ddd, *J* = 8.0, 7.3, 1.5 Hz, 2H), 7.02 (ddd, *J* = 7.9, 7.3, 1.7 Hz, 1H), 4.05 (s, 2H), 1.51 (s, 6H), 1.08 – 1.02 (m, 3H), 1.02 – 0.97 (m, 18H) ppm. ^{13}C NMR (126 MHz, $CDCl_3$) δ 145.1, 135.7, 130.2, 127.7, 127.1, 122.6, 69.9, 42.6, 25.1, 18.1, 12.1 ppm. IR (neat, cm^{-1}): 2941, 2865, 1738, 1643, 1098, 1016, 881, 751. HRMS *calcd for* ($C_{19}H_{33}BrOSi$+H) 385.1557, *found* 385.1546.

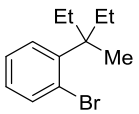

1-Bromo-2-(3-methylpentan-3-yl)benzene (154p): Following Reaction conditions D. Colorless oil. ^{1}H NMR (400 MHz, $CDCl_3$) δ 7.57 (dd, *J* = 7.9, 1.4 Hz, 1H), 7.30 (dd, *J* = 8.0, 1.7 Hz, 1H), 7.25 – 7.20 (m, 1H), 7.02 (ddd, *J* = 7.8, 7.2, 1.8 Hz, 1H), 2.48 (dq, *J* = 14.8, 7.5 Hz, 2H), 1.54 (dq, *J* =

[342]Hadida-Ruah, S. S.; Grootenhuis, P. D. J.; Miller, M. T.; Anderson, C.; Pontillo, J.; Kallel, E. A.; Numa, M. M. D.; Frieman, B. A.; McCartney, J.; Worley, J. F.; Arumugam, V.; Uy, J.; Hilgraf, N.; Bear, B. R.; WO 2012-US63153

14.9, 7.5 Hz, 2H), 1.38 (s, 3H), 0.64 (t, *J* = 7.5 Hz, 6H) ppm. ^{13}C NMR (126 MHz, $CDCl_3$) δ 144.5, 135.7, 131.0, 127.4, 127.0, 122.6, 44.2, 31.9, 25.0, 9.1 ppm. IR (neat, cm^{-1}): 2965, 2876, 1739, 1466, 1378, 1016, 748. HRMS *calcd for* ($C_{12}H_{17}Br$) 240.0514, *found* 240.0523.

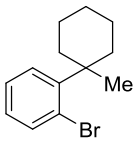

1-Bromo-2-(1-methylcyclohexyl)benzene (154q): Following Reaction conditions D. Colorless oil. ^{1}H NMR (500 MHz, $CDCl_3$) δ 7.60 (dd, *J* = 7.9, 1.4 Hz, 1H), 7.46 (dd, *J* = 8.1, 1.7 Hz, 1H), 7.29 – 7.23 (m, 1H), 7.04 – 6.98 (m, 1H), 2.30 – 2.22 (m, 2H), 1.90 – 1.81 (m, 2H), 1.65 – 1.55 (m, 2H), 1.56 – 1.47 (m, 3H), 1.45 (s, 3H), 1.43 – 1.37 (m, 1H) ppm. ^{13}C NMR (126 MHz, $CDCl_3$) δ 147.3, 136.4, 129.3, 127.3, 127.3, 122.8, 39.9, 37.0, 26.4, 25.0, 22.9 ppm. IR (neat, cm^{-1}): 2923, 2854, 1739, 1466, 1422, 1013, 749. HRMS *calcd for* ($C_{13}H_{17}Br$-CH_3) 237.0273, *found* 237.0273.

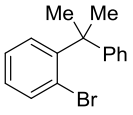

1-Bromo-2-(2-phenylpropan-2-yl)benzene (154r): Following Reaction conditions A. White solid. Mp: 34-35 ºC. ^{1}H NMR (400 MHz, $CDCl_3$) δ 7.66 (dd, *J* = 7.9, 1.6 Hz, 1H), 7.51 (dd, *J* = 7.9, 1.4 Hz, 1H), 7.38 – 7.33 (m, 1H), 7.28 – 7.23 (m, 2H), 7.20 – 7.12 (m, 3H), 7.12 – 7.07 (m, 1H), 1.77 (s, 6H) ppm. ^{13}C NMR (101 MHz, $CDCl_3$) δ 149.8, 147.7, 135.7, 128.4, 128.2, 128.0, 127.3, 126.4, 125.5, 124.3, 45.0, 30.4 ppm. IR (neat, cm^{-1}): 2995, 2970, 2874, 1739, 1465, 1426, 1363, 1017, 759. HRMS *calcd for* ($C_{15}H_{15}Br$-CH_3) 259.0117, *found* 259.01115.

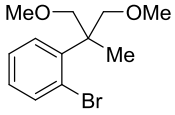

1-Bromo-2-(1,3-dimethoxy-2-methylpropan-2-yl)benzene (154o): Following Reaction conditions B. Yellow oil. ^{1}H NMR (400 MHz, $CDCl_3$) δ 7.57 (dd, *J* = 7.9, 1.4 Hz, 1H), 7.39 (dd, *J* = 8.0, 1.7 Hz, 1H), 7.27 (ddd, *J* = 7.3, 6.5, 1.5 Hz, 1H), 7.05 (ddd, *J* = 7.9, 7.3, 1.7 Hz, 1H), 3.90 (d, *J* = 9.3 Hz, 2H), 3.79 (d, *J* = 9.3 Hz, 2H), 3.35 (s, 6H), 1.54 (s, 3H) ppm. ^{13}C NMR (101 MHz, $CDCl_3$) δ 142.0, 135.9, 130.5, 128.1, 127.5, 122.4, 76.3, 59.4, 45.8, 20.4 ppm. IR (neat, cm^{-1}): 2978, 2921, 2810, 1469, 1099, 1014, 753. HRMS *calcd for* ($C_{12}H_{17}BrO_2$+Na) 295.0304, *found* 295.0308.

6.1.4. Preparative scope[343]

General Procedure A (GP-A): A 12.0 mL test tube is charged with *trans*-$PdCl_2(SMe_2)_2$ (7.5 mg, 0.025 mmol, 5 mol%), DCEphos (21.1 mg, 0.0375 mmol, 7.5 mol%), PivOH (25.5 mg, 0.25 mmol, 50 mol%) and the corresponding aryl bromide (0.5 mmol) and diazo compound (0.875 mmol, 1.75 equiv.) if solids. Then, Cs_2CO_3 (211.8 mg, 0.65 mmol, 1.3 equiv.) is weighed out into the glovebox. Next, anhydrous DMF (2.0 mL, 0.25M) is added by syringe. If the aryl bromide or the diazocompound are not solids, then these reagents are added at this stage as a stock solution in DMF. The reaction is then placed on an 80 ºC preheated block and stirred for 16h at this temperature. After this time, the reaction is cooled down to room temperature, diluted with diethyl ether (10 mL) and transfer to a separation funnel. Brine is added (40 mL) and the reaction is extracted 3 times with Et_2O (30 mL) and washed once with brine (40 mL). The combined organic phases are dried with $MgSO_4$, filtered and concentrated under vacuum. The crude reaction mixture is purified on silica gel column chromatography on a Hexanes/Ethyl acetate mixtures.

General Procedure B (GP-B): A 12.0 mL test tube is charged with *trans*-$PdCl_2(SMe_2)_2$ (15.1 mg, 0.05 mmol, 10 mol%), DCEphos (42.2 mg, 0.075 mmol, 15 mol%), PivOH (25.5 mg, 0.25 mmol, 50 mol%) and the corresponding aryl bromide (0.5 mmol) and diazo compound (0.875 mmol, 1.75 equiv.) if solids. Then, Cs_2CO_3 (211.8 mg, 0.65 mmol, 1.3 equiv.) is weighed into the glovebox. Next, anhydrous DMF (2.0 mL, 0.25M) is added by syringe. If the aryl bromide or the diazo compound are not solids, then these reagents are added at this stage as a stock solution in DMF. The reaction is then placed on a 100 ºC preheated block and stirred for 16h at this temperature. After this time, the reaction is cooled down to room temperature, diluted with diethyl ether (10 mL) and transfer to a separation funnel. Brine is added (40 mL) and the reaction is extracted 3 times with Et_2O (30 mL) and washed once with brine (40 mL). The combined organic phases are dried with $MgSO_4$, filtered and concentrated under vacuum. The crude reaction mixture is purified on silica gel column chromatography on a Hexanes/Ethyl acetate mixtures.

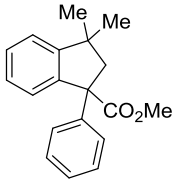

[343] The TLC plates were stained with Hanessian's stain observing the product as a blue spot. Usually, the product spot is the first one that appears when heating. $KMnO_4$ stain was used in the case of substrate **202**.

Methyl 3,3-dimethyl-1-phenyl-2,3-dihydro-1H-indene-1-carboxylate (195aa): Prepared following GP-A using **154a** (0.5 mmol 106.6 mg) and **175a** (0.875 mmol, 154.1 mg). The product was purified on 98/2 Hexanes: ethyl acetate, obtaining a white solid (112.5 mg, 80% yield). Mp: 61–62 ºC. ^{1}H NMR (400 MHz, $CDCl_3$) δ 7.48 (d, *J* = 7.7 Hz, 1H), 7.38 – 7.33 (m, 1H), 7.32 – 7.16 (m, 5H), 7.14 – 7.10 (m, 2H), 3.72 (s, 3H), 3.21 (d, *J* = 13.4 Hz, 1H), 2.22 (d, *J* = 13.4 Hz, 1H), 1.32 (s, 3H), 1.14 (s, 3H) ppm. ^{13}C NMR (101 MHz, $CDCl_3$) δ 175.2, 153.4, 145.7, 141.3, 128.6, 128.5, 127.8, 126.9, 126.8, 126.7, 122.7, 63.3, 54.6, 52.7, 43.0, 30.2, 30.1 ppm. IR (neat, cm^{-1}): 2954, 2862 1723, 1435, 1228. 1207, 752, 699. HRMS *calcd for* ($C_{19}H_{20}O_{2+}Na$) 303.1356, *found* 303.1354.

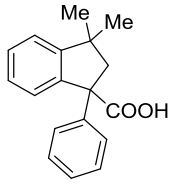

3,3-Dimethyl-1-phenyl-2,3-dihydro-1H-indene-1-carboxylic acid (195aa-COOH): A solution of **195aa** (47.1 mg, 0.17 mmol) and KOH (85%, 10.0 equiv.) in EtOH (0.15M) was refluxed overnight. When completed, HCl 2M (aq.) was added until pH = 1, the product was extracted with ethyl acetate, washed with brine and dried over $MgSO_4$. The product was purified on silica gel column chromatography 2/1 Hexanes: ethyl acetate obtaining a white solid (38.0 mg, 84% yield). A sample for X-Ray was obtained by slow evaporation of a solution of compound **74aa-COOH** in DCM. Mp: 138-140 ºC. ^{1}H NMR (400 MHz, $CDCl_3$) δ 7.57 – 7.53 (m, 1H), 7.36 (tt, *J* = 3.9, 1.9 Hz, 1H), 7.32 – 7.25 (m, 3H), 7.25 – 7.21 (m, 2H), 7.20 – 7.17 (m, 2H), 3.15 (d, *J* = 13.4 Hz, 1H), 2.25 (d, *J* = 13.4 Hz, 1H), 1.33 (s, 3H), 1.10 (s, 3H) ppm. ^{13}C NMR (101 MHz, $CDCl_3$) δ 180.1, 153.4, 144.8, 140.6, 128.8, 128.6, 127.8, 127.0, 127.0, 126.9, 122.8, 63.0, 54.2, 43.1, 30.3, 30.2 ppm. IR (neat, cm^{-1}): 3064, 2956, 2863, 1689, 1478, 1297, 1275, 948, 767. ESI *calcd. for* ($C_{18}H_{18}O_2$-CO_2-H) 221.1, *found* 221.1.

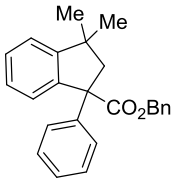

Benzyl 3,3-dimethyl-1-phenyl-2,3-dihydro-1H-indene-1-carboxylate (194ab): Prepared following GP-A using **154a** (0.5 mmol 106.6 mg) and **175b** (0.875 mmol, 220.7 mg). The product was purified on 10/1 Hexanes: ethyl acetate, obtaining a yellow oil (138.0 mg, 77% yield). ^{1}H NMR (400 MHz, $CDCl_3$) δ 7.48 (d, *J* = 7.6 Hz, 1H), 7.37 – 7.15 (m, 11H), 7.12 – 7.08 (m, 2H), 5.19 (d, *J* = 12.6 Hz, 1H), 5.13 (d, *J* = 12.5 Hz, 1H), 3.21 (d, *J* = 13.4 Hz, 1H), 2.23 (d, *J* = 13.4 Hz, 1H), 1.29 (s, 3H), 1.14 (s, 3H) ppm. ^{13}C NMR (101 MHz, $CDCl_3$) δ 174.4, 153.4, 145.5, 141.2, 136.0, 128.6, 128.5, 128.4, 128.1, 128.0, 127.9, 126.9, 126.7, 126.6, 122.7, 67.1, 63.3, 54.5,

43.0, 30.3, 30.2 ppm. IR (neat, cm^{-1}): 3030, 2955, 2864, 1728, 1448, 1212, 1135, 695. HRMS *calcd for* ($C_{25}H_{24}O_{2+}Na$) 379.1669, *found* 379.1675.

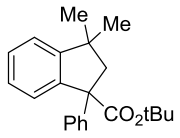

tert-Butyl 3,3-dimethyl-1-phenyl-2,3-dihydro-1H-indene-1-carboxylate (195ac): Prepared following GP-A using **154a** (0.5 mmol 106.6 mg) and **175c** (0.875 mmol, 191.0 mg). The product was purified on 100/1 Hexanes: ethyl acetate, obtaining a colorless oil (128.0 mg, 79% yield). ^{1}H NMR (500 MHz, $CDCl_3$) δ 7.46 (d, *J* = 7.7 Hz, 1H), 7.33 (td, *J* = 7.4, 1.2 Hz, 1H), 7.28 – 7.24 (m, 3H), 7.22 – 7.18 (m, 2H), 7.15 – 7.12 (m, 2H), 3.13 (d, *J* = 13.3 Hz, 1H), 2.16 (d, *J* = 13.3 Hz, 1H), 1.40 (s, 9H), 1.31 (s, *J* = 4.6 Hz, 3H), 1.13 (s, 3H) ppm. ^{13}C NMR (126 MHz, $CDCl_3$) δ 173.6, 153.3, 146.3, 142.0, 128.3, 128.3, 127.8, 126.8, 126.5, 126.4, 122.5, 81.2, 63.9, 54.5, 42.8, 30.3, 30.1, 28.0 ppm. IR (neat, cm^{-1}): 2969, 2864, 1721, 1449, 1366, 1239, 1157, 698. HRMS *calcd for* ($C_{22}H_{26}O_{2+}Na$) 345.1825, *found* 345.1817.

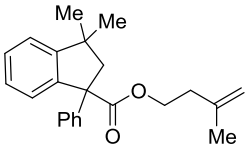

3-Methylbut-3-en-1-yl 3,3-dimethyl-1-phenyl-2,3-dihydro-1H-indene-1-carboxylate (195ad): Prepared following GP-A using **154a** (0.5 mmol 106.6 mg) and **175d** (0.875 mmol, 201.5 mg). The product was purified on 100/1 Hexanes: ethyl acetate, obtaining a yellow solid that melts at rt (143.4 mg, 86% yield). ^{1}H NMR (500 MHz, $CDCl_3$) δ 7.49 (d, *J* = 7.3 Hz, 1H), 7.36 – 7.31 (m, 1H), 7.29 – 7.24 (m, 3H), 7.23 – 7.19 (m, 2H), 7.15 – 7.10 (m, 2H), 4.70 (s, *J* = 14.3 Hz, 1H), 4.59 (s, 1H), 4.23 (t, *J* = 6.8 Hz, 2H), 3.19 (d, *J* = 13.4 Hz, 1H), 2.32 – 2.24 (m, 2H), 2.21 (d, *J* = 13.3 Hz, 1H), 1.64 (d, *J* = 4.6 Hz, 3H), 1.31 (s, 3H), 1.13 (s, 3H) ppm. ^{13}C NMR (126 MHz, $CDCl_3$) δ 174.6, 153.4, 145.7, 141.6, 141.3, 128.5, 128.4, 127.9, 126.9, 126.7, 126.6, 122.6, 112.5, 63.8, 63.3, 54.5, 42.9, 36.7, 30.3, 30.2, 22.4 ppm. IR (neat, cm^{-1}): 2957, 2864, 1726, 1477, 1215, 760, 699. HRMS *calcd for* ($C_{23}H_{26}O_2$+Na) 357.1826, *found* 357.1825.

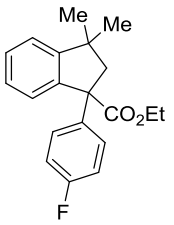

Ethyl 1-(4-fluorophenyl)-3,3-dimethyl-2,3-dihydro-1H-indene-1-carboxylate (195ae): Prepared following GP-A using **154a** (0.5 mmol 106.6 mg) and **175e** (0.875 mmol, 182.2 mg). The product was purified on 95/5 Hexanes: ethyl acetate, obtaining a colorless oil (109.5 mg, 70% yield) ^{1}H NMR (500 MHz, $CDCl_3$) δ 7.49 – 7.46 (m, 1H), 7.35 (td, *J* = 7.4, 1.2 Hz, 1H), 7.30 – 7.26 (m, 1H), 7.23 – 7.20 (m, 1H), 7.11 – 7.07 (m, 2H), 6.97 – 6.92 (m, 2H), 4.17 (q, *J* = 7.1 Hz, 2H), 3.18 (d, *J* = 13.3 Hz, 1H), 2.17 (d, *J* = 13.3 Hz, 1H), 1.31 (s, 3H), 1.20 (t, *J* = 7.1 Hz, 3H), 1.11 (s, 3H) ppm. ^{13}C NMR (126 MHz, $CDCl_3$) δ 174.4, 161.6 (d, *J* = 245.4 Hz), 153.3, 141.6 (d, *J* = 3.2 Hz), 141.3, 128.7, 128.5 (d, *J* = 7.9 Hz), 127.6, 126.8, 122.8, 115.2 (d, *J* = 21.3 Hz), 62.6, 61.6, 54.5, 42.9, 30.3, 30.2, 14.2 ppm. IR (neat, cm^{-1}): 2958, 2865, 1726, 1507, 1218, 1162, 832, 761. HRMS *calcd for* ($C_{20}H_{21}O_2$+Na) 335.1418, *found* 335.1418.

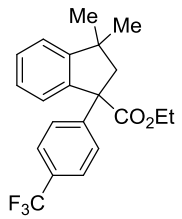

Ethyl 3,3-dimethyl-1-(4-(trifluoromethyl)phenyl)-2,3-dihydro-1H-indene-1-carboxylate (195af): Prepared following GP-A using **154a** (0.5 mmol 106.6 mg) and **175f** (0.875 mmol, 225.9 mg). The product was purified on 95/5 Hexanes: ethyl acetate, obtaining a colorless oil (118.0 mg, 65% yield). ^{1}H NMR (400 MHz, $CDCl_3$) δ 7.53 (d, *J* = 8.3 Hz, 2H), 7.47 (dd, *J* = 7.6, 0.6 Hz, 1H), 7.38 (td, *J* = 7.4, 1.2 Hz, 1H), 7.30 (td, *J* = 7.5, 1.3 Hz, 1H), 7.27 – 7.23 (m, 3H), 4.20 (q, *J* = 7.1 Hz, 2H), 3.24 (d, *J* = 13.4 Hz, 1H), 2.17 (d, *J* = 13.4 Hz, 1H), 1.34 (s, 3H), 1.22 (t, *J* = 7.1 Hz, 3H), 1.13 (s, 3H) ppm. ^{13}C NMR (101 MHz, $CDCl_3$) δ 174.0, 153.5, 149.9, 149.8, 140.6, 129.0 (q, *J* = 32.4 Hz), 128.9, 127.5, 127.3, 127.0, 125.4 (q, *J* = 3.8 Hz), 124.3 (q, *J* = 271.8 Hz), 63.3, 61.8, 54.4, 43.1, 30.4, 30.2, 14.1 ppm. IR (neat, cm^{-1}): 2962, 2856, 1706, 1527, 1222, 1160, 841, 759. HRMS *calcd for* ($C_{21}H_{21}F_3O_2$+Na) 385.1386, *found* 385.1382.

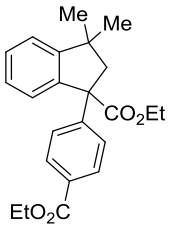

Ethyl 1-(4-(ethoxycarbonyl)phenyl)-3,3-dimethyl-2,3-dihydro-1H-indene-1-carboxylate (195ag): Prepared following GP-A using **154a** (0.5 mmol 106.6 mg) and **175g** (0.875 mmol, 229.5 mg). The product was purified on 9/1 Hexanes: : ethyl acetate, obtaining a colorless oil (108.9 mg, 59% yield) ^{1}H NMR (400 MHz, $CDCl_3$) δ 7.96 – 7.92 (m, 2H), 7.51 – 7.44 (m, 1H), 7.37

(td, *J* = 7.4, 1.3 Hz, 1H), 7.29 (td, *J* = 7.5, 1.3 Hz, 1H), 7.23 (dd, *J* = 7.6, 0.6 Hz, 1H), 7.19 (d, *J* = 8.7 Hz, 2H), 4.36 (q, *J* = 7.1 Hz, 2H), 4.18 (q, *J* = 7.1 Hz, 2H), 3.23 (d, *J* = 13.4 Hz, 1H), 2.18 (d, *J* = 13.4 Hz, 1H), 1.37 (t, *J* = 7.1 Hz, 3H), 1.33 (s, 3H), 1.20 (t, *J* = 7.1 Hz, 3H), 1.11 (s, 3H) ppm. ^{13}C NMR (101 MHz, $CDCl_3$) δ 173.9, 166.3, 153.3, 150.8, 140.6, 129.6, 128.8, 128.6, 127.4, 126.8, 122.7, 63.3, 61.5, 60.9, 54.2, 43.0, 30.2, 30.1, 14.3, 14.0 ppm. IR (neat, cm^{-1}): 2958, 2866, 1716, 1271, 1218, 1103, 761. HRMS *calcd for* ($C_{23}H_{26}O_4$+Na) 389.1723, *found* 389.1725.

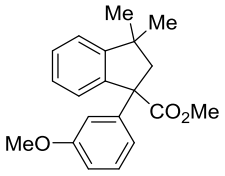

Methyl 1-(3-methoxyphenyl)-3,3-dimethyl-2,3-dihydro-1H-indene-1-carboxylate (195ah): Prepared following GP-A using **154a** (0.5 mmol 106.6 mg) and **175h** (0.875 mmol, 180.4 mg). The product was purified on 98/2 Hexanes: ethyl acetate, obtaining a colorless oil (110.9 mg, 71% yield). ^{1}H NMR (500 MHz, $CDCl_3$) δ 7.50 (d, *J* = 7.6 Hz, 1H), 7.34 (td, *J* = 7.4, 1.2 Hz, 1H), 7.29 – 7.25 (m, 1H), 7.21 (d, *J* = 7.6 Hz, 1H), 7.20 (t, *J* = 8.0 Hz, 1H), 6.76 (ddd, *J* = 8.2, 2.5, 0.7 Hz, 1H), 6.71 (ddd, *J* = 7.8, 1.7, 0.8 Hz, 1H), 6.68 – 6.66 (m, 1H), 3.74 (s, 3H), 3.71 (s, 3H), 3.19 (d, *J* = 13.4 Hz, 1H), 2.21 (d, *J* = 13.4 Hz, 1H), 1.31 (s, 3H), 1.14 (s, 3H) ppm. ^{13}C NMR (126 MHz, $CDCl_3$) δ 175.0, 159.7, 153.4, 147.3, 141.0, 129.5, 128.6, 127.7, 126.8, 122.7, 119.3, 113.3, 111.5, 63.3, 55.3, 54.4, 52.8, 42.9, 30.3, 30.2 ppm. IR (neat, cm^{-1}): 2952, 1729, 1581, 1431, 1219, 1050, 761. HRMS *calcd for* ($C_{20}H_{22}O_3$+Na) 333.1461, *found* 333.1452.

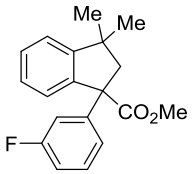

Methyl 1-(3-fluorophenyl)-3,3-dimethyl-2,3-dihydro-1H-indene-1-carboxylate (195ai): Prepared following GP-A using **154a** (0.5 mmol 106.6 mg) and **175i** (0.875 mmol, 169.9 mg). The product was purified on 95/5 Hexanes: ethyl acetate, obtaining a white solid (36.8 mg, 49% yield). Mp: 51-52 ºC. ^{1}H NMR (400 MHz, $CDCl_3$) δ 7.50 – 7.46 (m, 1H), 7.36 (td, *J* = 7.4, 1.3 Hz, 1H), 7.29 (td, *J* = 7.5, 1.3 Hz, 1H), 7.25 – 7.20 (m, 2H), 6.94 – 6.88 (m, 2H), 6.86 – 6.81 (m, 1H), 3.71 (s, *J* = 5.3 Hz, 3H), 3.20 (d, *J* = 13.4 Hz, 1H), 2.20 (d, *J* = 13.4 Hz, 1H), 1.32 (s, *J* = 21.6 Hz, 3H), 1.13 (s, 3H) ppm. ^{13}C NMR (75 MHz, $CDCl_3$) δ 174.6, 162.9 (d, *J* = 245.7 Hz), 153.4, 148.2 (d, *J* = 7.0 Hz), 140.6 (s), 129.9 (d, *J* = 8.3 Hz), 128.8, 127.5 (s), 126.9, 122.8, 122.6 (d, *J* = 2.8 Hz), 114.1 (d, *J* = 22.6 Hz), 113.7 (d, *J* = 21.1 Hz), 63.1 (d, *J* = 1.6 Hz), 54.4, 52.9, 43.0, 30.3,

30.1 ppm. IR (neat, cm^{-1}): 2957, 2864, 1724, 1585, 1434, 1223, 1159, 1063, 766. HRMS *calcd for* ($C_{19}H_{19}FO_2$+H) 299.1442, *found* 299.1440.

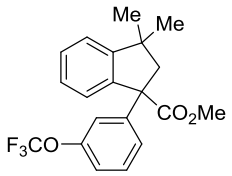

Methyl 3,3-dimethyl-1-(3-(trifluoromethoxy)phenyl)-2,3-dihydro-1H-indene-1-carboxylate (195aj): Prepared following GP-A using **154a** (0.5 mmol 106.6 mg) and **175j** (0.875 mmol, 227.6 mg). The product was purified on 95/5 Hexanes: ethyl acetate, obtaining a colorless oil (51.8 mg, 51.8% yield). ^{1}H NMR (500 MHz, $CDCl_3$) δ 7.47 (dd, *J* = 7.7, 0.6 Hz, 1H), 7.38 (td, *J* = 7.4, 1.2 Hz, 1H), 7.33 – 7.30 (m, 1H), 7.30 – 7.28 (m, 1H), 7.26 – 7.22 (m, *J* = 7.6 Hz, 1H), 7.11 – 7.06 (m, 2H), 6.99 – 6.97 (m, 1H), 3.73 (s, 3H), 3.22 (d, *J* = 13.4 Hz, 1H), 2.19 (d, *J* = 13.4 Hz, 1H), 1.33 (s, 3H), 1.13 (s, 3H) ppm. ^{13}C NMR (75 MHz, $CDCl_3$) δ 174.4, 153.3, 149.3 (q, *J* = 1.8 Hz), 147.9, 140.3, 129.6, 128.8, 127.3, 126.9, 125.2, 122.8, 120.4(q, *J* = 257.1 Hz), 119.7, 118.9, 63.0, 54.3, 52.7, 42.9, 30.1, 30.0 ppm. IR (neat, cm^{-1}): 3070, 2956, 2866, 1732, 1479, 1252, 1210, 1155, 761, 699. HRMS *calcd for* ($C_{20}H_{19}F_3O_3$+Na) 387.1178, *found* 387.1175.

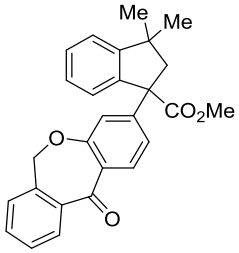

Methyl 3,3-dimethyl-1-(11-oxo-6,11-dihydrodibenzo[b,e]oxepin-3-yl)-2,3-dihydro-1H-indene-1-carboxylate (195ak): Prepared following GP-A using **154a** (0.5 mmol 106.6 mg) and **175k** (0.875 mmol, 269.8 mg). The product was purified on 7/1 Hexanes: ethyl acetate, obtaining a yellow solid (133.4 mg, 65% yield). Mp: 54-56 ºC. ^{1}H NMR (400 MHz, $CDCl_3$) δ 8.08 (d, *J* = 2.6 Hz, 1H), 7.90 (dd, *J* = 7.7, 1.2 Hz, 1H), 7.57 (td, *J* = 7.4, 1.4 Hz, 1H), 7.53 – 7.45 (m, 2H), 7.43 – 7.30 (m, 3H), 7.30 – 7.22 (m, 2H), 6.99 (d, *J* = 8.6 Hz, 1H), 5.20 (s, 2H), 3.76 (s, 3H), 3.23 (d, *J* = 13.4 Hz, 1H), 2.29 (d, *J* = 13.4 Hz, 1H), 1.36 (s, 3H), 1.16 (s, 3H) ppm. ^{13}C NMR (101 MHz, $CDCl_3$) δ 190.7, 174.8, 160.0, 153.0, 141.0, 140.5, 139.1, 135.5, 134.0, 132.7, 129.9, 129.5, 129.2, 128.7, 127.7, 127.3, 126.9, 124.9, 122.7, 120.8, 73.6, 62.4, 54.2, 52.7, 42.9, 30.1, 30.0 ppm. IR (neat, cm^{-1}): 3065, 2953, 2864, 1727, 1647, 1483, 1297, 1219, 759. HRMS *calcd for* ($C_{27}H_{24}O_4$+Na) 435.1567, *found* 435.1566.

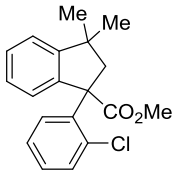

Methyl 1-(2-chlorophenyl)-3,3-dimethyl-2,3-dihydro-1H-indene-1-carboxylate (195al): Prepared following GP-B using **154a** (0.5 mmol 106.6 mg) and **175l** (0.875 mmol, 184.3 mg). The product was purified on 95/5 Hexanes:ethyl acetate, obtaining a colorless oil (72.4 mg, 46% yield). ^{1}H NMR (400 MHz, $CDCl_3$) δ 7.42 (td, *J* = 7.4, 1.4 Hz, 2H), 7.39 – 7.36 (m, 1H), 7.33 (dd, *J* = 7.1, 1.2 Hz, 1H), 7.29 (d, *J* = 8.2 Hz, 1H), 7.21 (td, *J* = 7.6, 1.7 Hz, 1H), 7.10 (td, *J* = 7.6, 1.4 Hz, 1H), 6.82 (dd, *J* = 7.9, 1.6 Hz, 1H), 3.76 (s, 3H), 3.51 (d, *J* = 13.8 Hz, 1H), 2.26 (d, *J* = 13.8 Hz, 1H), 1.47 (s, *J* = 9.6 Hz, 3H), 1.05 (s, 3H) ppm. ^{13}C NMR (101 MHz, $CDCl_3$) δ 174.5, 153.9, 144.0, 140.7, 133.7, 130.4, 129.3, 129.2, 128.2, 127.1, 126.4, 126.2, 123.5, 63.2, 53.0, 51.7, 43.5, 31.3, 30.1 ppm. IR (neat, cm^{-1}): 3067, 2952, 1736, 1431, 1218, 1120, 754. HRMS *calcd for* ($C_{19}H_{19}O_2Cl$+Na) 337.0966, *found* 337.0963.

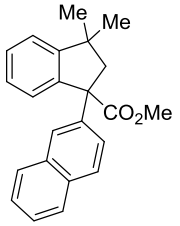

Methyl 3,3-dimethyl-1-(naphthalen-2-yl)-2,3-dihydro-1H-indene-1-carboxylate (195am): Prepared following GP-A using **154a** (0.5 mmol 106.6 mg) and **175m** (0.875 mmol, 198.0 mg). The product was purified on 98/2 Hexanes: ethyl acetate, obtaining a colorless oil (111.0 mg, 67% yield). ^{1}H NMR (400 MHz, $CDCl_3$) δ 7.85 – 7.79 (m, 2H), 7.74 (dq, J = 6.5, 3.1 Hz, 1H), 7.58 (d, J = 7.7 Hz, 1H), 7.55 – 7.52 (m, 1H), 7.49 – 7.44 (m, 2H), 7.42 (dd, J = 7.4, 1.2 Hz, 1H), 7.38 – 7.27 (m, 3H), 3.76 (s, 3H), 3.33 (d, J = 13.4 Hz, 1H), 2.35 (d, J = 13.4 Hz, 1H), 1.39 (s, 3H), 1.17 (s, 3H) ppm. ^{13}C NMR (101 MHz, $CDCl_3$) δ 175.1, 153.5, 143.0, 141.1, 133.3, 132.3, 128.7, 128.4, 128.2, 127.8, 127.6, 126.9, 126.3, 126.0, 125.4, 125.2, 122.8, 63.5, 54.3, 52.8, 43.1, 30.4, 30.3 ppm. IR (neat, cm^{-1}): 2952, 2863, 1728, 1449, 1220, 746, 475. HRMS *calcd for* ($C_{23}H_{22}O_2$+Na) 353.1512, *found* 353.1506.

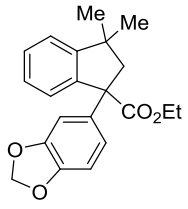

Ethyl 1-(benzo[d][1,3]dioxol-5-yl)-3,3-dimethyl-2,3-dihydro-1H-indene-1-carboxylate (195an): Prepared following GP-A using **154a** (0.5 mmol 106.6 mg) and **175n** (0.875 mmol, 204.9 mg). The product was purified on 95/5 Hexanes: ethyl acetate, obtaining a colorless oil (73.9 mg, 44% yield). ^{1}H NMR (500 MHz, $CDCl_3$) δ 7.54 – 7.50 (m, 1H), 7.34 (td, *J* = 7.4, 1.2 Hz, 1H), 7.27 (dt, *J* = 7.4, 1.3 Hz, 1H), 7.22 – 7.19 (m, 1H), 6.69 (d, *J* = 8.1 Hz, 1H), 6.64 (d, *J* = 1.9 Hz, 1H), 6.58 (dd, *J* = 8.2, 1.9 Hz, 1H), 5.92 (dd, *J* = 3.2, 1.4 Hz, 2H), 4.18 (qd, *J* = 7.1, 1.0 Hz, 2H), 3.15 (d, *J* = 13.3 Hz, 1H), 2.18 (d, *J* = 13.3 Hz, 1H), 1.31 (s, 3H), 1.22 (t, *J* = 7.1 Hz, 3H), 1.13 (s, 3H) ppm. ^{13}C NMR (126 MHz, $CDCl_3$) δ 174.6, 153.3, 147.8, 146.3, 141.4, 139.8, 128.5, 127.7, 126.7, 122.7, 120.1, 108.0, 107.7, 101.2, 62.9, 61.5, 54.5, 42.8, 30.3, 30.2, 14.2 ppm. IR (neat, cm^{-1}): 2956, 2865, 1724, 1486, 1216, 1037, 934. HRMS *calcd for* ($C_{21}H_{22}O_4$+Na) 361.1410, *found* 361.1410.

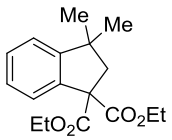

Diethyl 3,3-dimethyl-2,3-dihydro-1H-indene-1,1-dicarboxylate (202): Prepared following GP-B using **154a** (0.5 mmol 106.6 mg) and **201g** (0.875 mmol, 162.9 mg). The product was purified on 9/1 Hexanes: ethyl acetate, obtaining a colorless oil (99.1 mg, 68% yield) ^{1}H NMR (400 MHz, $CDCl_3$) δ 7.53 – 7.49 (m, 1H), 7.32 (td, *J* = 7.4, 1.3 Hz, 1H), 7.25 (td, *J* = 7.5, 1.3 Hz, 1H), 7.19 – 7.13 (m, 1H), 4.27 – 4.17 (m, 4H), 2.66 (s, 2H), 1.31 (s, 6H), 1.27 (t, *J* = 7.1 Hz, 6H) ppm. ^{13}C NMR (126 MHz, $CDCl_3$) δ 171.1, 152.7, 137.7, 128.9, 126.8, 126.7, 122.4, 64.5, 61.7, 48.3, 43.1, 30.1, 14.0 ppm. IR (neat, cm^{-1}): 2960, 2867, 1730, 1230, 1209, 1139, 1020, 759. HRMS *calcd for* ($C_{17}H_{22}O_4$+Na) 313.1410, *found* 313.1399.

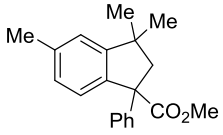

Methyl 3,3,5-trimethyl-1-phenyl-2,3-dihydro-1H-indene-1-carboxylate (194ba): Prepared following GP-A using **154b** (0.5 mmol 113.6 mg) and **175a** (0.875 mmol, 154.2 mg). The product was purified on 95/5 Hexanes: ethyl acetate, obtaining a colorless oil (111.8 mg, 76% yield). ^{1}H NMR (400 MHz, $CDCl_3$) δ 7.38 (d, *J* = 7.9 Hz, 1H), 7.32 – 7.26 (m, 2H), 7.26 – 7.21 (m, 1H), 7.17 – 7.11 (m, 3H), 7.04 (s, 1H), 3.72 (s, 3H), 3.22 (d, *J* = 13.4 Hz, 1H), 2.43 (s, 3H), 2.22 (d, *J* = 13.4 Hz, 1H), 1.33 (s, 3H), 1.14 (s, 3H) ppm. ^{13}C NMR (101 MHz, $CDCl_3$) δ 175.1, 153.4, 145.6, 138.2, 128.3 (2C), 127.7, 127.3, 126.7, 126.5, 123.1, 62.8, 54.7, 52.5, 42.7, 30.1, 30.0, 21.5

ppm. IR (neat, cm^{-1}): 2952, 2865, 1730, 1447, 1219, 1119, 698. HRMS *calcd for* ($C_{20}H_{22}O_2$+Na) 317.1512, *found* 317.1510.

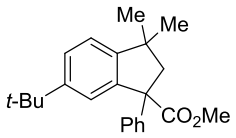

Methyl 6-(tert-butyl)-3,3-dimethyl-1-phenyl-2,3-dihydro-1H-indene-1-carboxylate (194ca): Prepared following GP-A but at 70 ºC using **154c** (0.5 mmol 134.6 mg) and **175a** (0.875 mmol, 154.2 mg). The product was purified on 95/5 Hexanes: ethyl acetate, obtaining a colorless oil (101.1 mg, 60% yield). ^{1}H NMR (400 MHz, $CDCl_3$) δ 7.55 (d, *J* = 1.9 Hz, 1H), 7.41 (dd, *J* = 8.0, 1.9 Hz, 1H), 7.33 – 7.28 (m, 2H), 7.27 – 7.21 (m, 1H), 7.18 – 7.12 (m, 3H), 3.73 (s, 3H), 3.23 (d, *J* = 13.3 Hz, 1H), 2.21 (d, *J* = 13.3 Hz, 1H), 1.36 (s, 9H), 1.34 (s, 3H), 1.12 (s, 3H) ppm. ^{13}C NMR (101 MHz, $CDCl_3$) δ 175.1, 150.4, 149.7, 145.7, 140.7, 128.3, 126.7, 126.5, 125.5, 124.5, 121.9, 63.3, 54.7, 52.5, 42.4, 34.7, 31.6, 30.2, 30.1 ppm. IR (neat, cm^{-1}):2953, 2865, 1731, 1492, 1363, 1220, 1121, 698. HRMS *calcd for* ($C_{23}H_{28}O_2$+Na) 359.1982, *found* 359.1975.

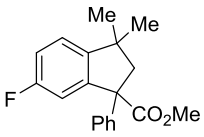

Methyl 6-fluoro-3,3-dimethyl-1-phenyl-2,3-dihydro-1H-indene-1-carboxylate (195da): Prepared following GP-A using **154d** (0.5 mmol 115.6 mg) and **175a** (0.875 mmol, 154.2 mg). The product was purified on 95/5 Hexanes: ethyl acetate, obtaining a colorless oil (124.5 mg, 83% yield). ^{1}H NMR (500 MHz, $CDCl_3$) δ 7.34 – 7.29 (m, 2H), 7.28 – 7.24 (m, 1H), 7.21 – 7.12 (m, 4H), 7.06 (td, *J* = 8.6, 2.5 Hz, 1H), 3.75 (s, 3H), 3.24 (d, *J* = 13.4 Hz, 1H), 2.27 (d, *J* = 13.4 Hz, 1H), 1.32 (s, 3H), 1.15 (s, 3H) ppm. ^{13}C NMR (101 MHz, $CDCl_3$) δ 174.5, 162.0 (d, *J* = 243.0 Hz), 148.8 (d, *J* = 2.4 Hz), 144.9, 143.1 (d, *J* = 7.9 Hz), 128.5, 126.8, 126.5, 123.5 (d, *J* = 8.8 Hz), 115.7 (d, *J* = 22.6 Hz), 114.3 (d, *J* = 22.8 Hz), 62.9 (d, *J* = 1.8 Hz), 54.7, 52.7, 42.3, 30.2, 30.1 ppm. IR (neat, cm^{-1}): 2954, 2866, 1731, 1485, 1222, 820, 698. HRMS *calcd for* ($C_{19}H_{19}O_2F$+Na) 321.1261, *found* 321.1258.

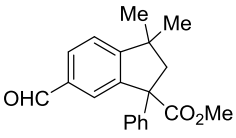

Methyl 6-formyl-3,3-dimethyl-1-phenyl-2,3-dihydro-1H-indene-1-carboxylate (195ea): Prepared following GP-A using **154e** (0.5 mmol 120.6 mg) and **175a** (0.875 mmol, 154.2 mg). The product was purified on 7/1 Hexanes: ethyl acetate, obtaining a white solid (128.6 mg,

83% yield). Mp: 82-83 ºC. ^{1}H NMR (400 MHz, $CDCl_3$) δ 10.04 (s, 1H), 8.01 (d, *J* = 1.2 Hz, 1H), 7.92 (dd, *J* = 7.9, 1.5 Hz, 1H), 7.39 (d, *J* = 7.9 Hz, 1H), 7.36 – 7.22 (m, 3H), 7.14 – 7.10 (m, 2H), 3.77 (s, 3H), 3.27 (d, *J* = 13.5 Hz, 1H), 2.32 (d, *J* = 13.5 Hz, 1H), 1.35 (s, 3H), 1.21 (s, 3H) ppm. ^{13}C NMR (126 MHz, $CDCl_3$) δ 192.0, 174.4, 160.3, 144.5, 142.6, 135.9, 130.0, 129.9, 128.6, 127.0, 126.5, 123.3, 62.8, 54.3, 52.9, 43.2, 29.8, 29.7 ppm. IR (neat, cm^{-1}): 2951, 2861, 2755, 1728, 1689, 1601, 1427, 1219, 1067, 701 ppm. HRMS *calcd for* ($C_{20}H_{20}O_3$+Na) 331.1305, *found* 331.1301.

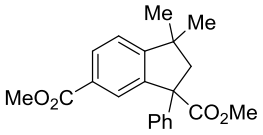

Dimethyl 3,3-dimethyl-1-phenyl-2,3-dihydro-1H-indene-1,6-dicarboxylate (195fa): Prepared following GP-A using **154f** (0.5 mmol 135.6 mg) and **175a** (0.875 mmol, 154.2 mg). The product was purified on 7/1 Hexanes: ethyl acetate, obtaining a colorless oil (136.7 mg, 81% yield). ^{1}H NMR (500 MHz, $CDCl_3$) δ 8.17 (d, *J* = 1.5 Hz, 1H), 8.07 (dd, *J* = 8.0, 1.6 Hz, 1H), 7.34 – 7.29 (m, 3H), 7.28 – 7.23 (m, 1H), 7.14 – 7.11 (m, 2H), 3.92 (s, 3H), 3.76 (s, 3H), 3.26 (d, *J* = 13.4 Hz, 1H), 2.28 (d, *J* = 13.4 Hz, 1H), 1.34 (s, 3H), 1.19 (s, 3H) ppm. ^{13}C NMR (101 MHz, $CDCl_3$) δ 174.6, 167.1, 158.6, 144.8, 141.7, 130.1, 129.2, 129.1, 128.5, 126.8, 126.5, 122.6, 62.9, 54.5, 52.8, 52.1, 43.0, 29.8, 29.7 ppm. IR (neat, cm^{-1}): 2953, 2866, 1720, 1434, 1287, 1223, 1103, 772, 698. HRMS *calcd for* ($C_{21}H_{22}O_4$+Na) 361.1410, *found* 361.1412.

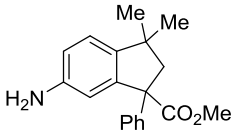

Methyl 6-amino-3,3-dimethyl-1-phenyl-2,3-dihydro-1H-indene-1-carboxylate (195ga): Prepared following GP-B using **154g** (0.5 mmol 114.1 mg) and **175a** (0.875 mmol, 154.2 mg). The product was purified on 2/1 Hexanes: ethyl acetate, obtaining a brown solid (58.2 mg, 39% yield). MP: 110-112 ºC. ^{1}H NMR (500 MHz, $CDCl_3$) δ 7.27 (t, *J* = 7.4 Hz, 2H), 7.21 (t, *J* = 7.3 Hz, 1H), 7.16 – 7.11 (m, 2H), 7.00 (d, *J* = 8.1 Hz, 1H), 6.79 (d, *J* = 2.2 Hz, 1H), 6.70 (dd, *J* = 8.1, 2.3 Hz, 1H), 3.72 (s, 3H), 3.63 (s, 2H), 3.17 (d, *J* = 13.3 Hz, 1H), 2.17 (d, *J* = 13.3 Hz, 1H), 1.27 (s, 3H), 1.08 (s, 3H) ppm. ^{13}C NMR (126 MHz, $CDCl_3$) δ 175.2, 145.8, 145.3, 143.9, 142.4, 128.4, 126.9, 126.7, 123.2, 116.2, 113.9, 63.3, 55.0, 52.7, 42.3, 30.4, 30.4 ppm. IR (neat, cm^{-1}): 3458, 3373, 2950, 1718, 1606, 1495, 1223, 821. HRMS *calcd for* ($C_{19}H_{21}NO_2$+H) 296.1645, *found* 296.1645.

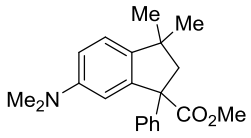

Methyl 6-(dimethylamino)-3,3-dimethyl-1-phenyl-2,3-dihydro-1H-indene-1-carboxylate (195ha): Prepared following GP-A using **154h** (0.5 mmol 128.1 mg) and **175a** (0.875 mmol, 154.2 mg). The product was purified on 7/1 Hexanes: ethyl acetate, obtaining a yellow solid (130.0 mg, 80% yield). MP: 89-90 ºC. 1H NMR (500 MHz, CDCl3) δ 7.30 – 7.24 (m, 2H), 7.21 (ddd, J = 7.3, 3.8, 1.3 Hz, 1H), 7.17 – 7.13 (m, 2H), 7.08 (d, J = 8.4 Hz, 1H), 6.86 (d, J = 2.5 Hz, 1H), 6.80 (dd, J = 8.4, 2.5 Hz, 1H), 3.72 (s, 3H), 3.19 (d, J = 13.3 Hz, 1H), 2.93 (s, 6H), 2.16 (d, J = 13.3 Hz, 1H), 1.29 (d, J = 3.3 Hz, 3H), 1.08 (s, 3H) ppm. 13C NMR (126 MHz, CDCl3) δ 175.3, 150.2, 146.1, 142.2, 142.1, 128.4, 127.0, 126.6, 122.9, 113.9, 111.8, 63.6, 55.2, 52.7, 42.2, 41.4, 30.5, 30.4 ppm. IR (neat, cm-1): 2950, 2862, 1729, 1609, 1501, 1219, 699. HRMS *calcd for* ($C_{21}H_{25}NO_2$+H) 324.1958, *found* 324.1943.

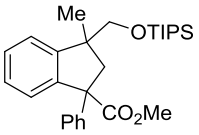

(1:1 Mixture of diastereoisomers)

Methyl 3-methyl-1-phenyl-3-(((triisopropylsilyl)oxy)methyl)-2,3-dihydro-1H-indene-1-carboxylate (195na): Prepared following GP-B using **154n** (0.5 mmol 192.7 mg) and **175a** (0.875 mmol, 154.2 mg). The two diastereoisomers were independently isolated on 9/1 Hexanes: ethyl acetate, obtaining as white solids (Diast. 1: 72.5 mg, 32% yield. Diast. 2: 96.5mg, 43% yield. Combined yields: 75%). Diast.1: Mp: 57-59 ºC. ^{1}H NMR (500 MHz, $CDCl_3$) δ 7.47 – 7.44 (m, 1H), 7.33 – 7.30 (m, 2H), 7.30 – 7.28 (m, 1H), 7.27 (t, J = 1.8 Hz, 1H), 7.26 – 7.25 (m, 1H), 7.23 – 7.19 (m, 1H), 7.10 (dt, J = 8.5, 2.5 Hz, 2H), 3.70 (s, 3H), 3.67 (s, 2H), 3.41 (d, J = 13.8 Hz, 1H), 2.05 (d, J = 13.8 Hz, 1H), 1.23 (s, 3H), 1.13 – 1.07 (m, 3H), 1.06 – 1.02 (m, 18H) ppm. ^{13}C NMR (126 MHz, $CDCl_3$) δ 175.1, 150.1, 146.3, 142.4, 128.5, 128.1, 127.7, 127.2, 126.7, 126.6, 124.2, 71.3, 63.4, 52.7, 50.1, 48.9, 25.1, 18.2, 12.2 ppm. Diast. 2: Mp: 69-70 ºC. ^{1}H NMR (500 MHz, $CDCl_3$) δ 7.57 – 7.51 (m, 1H), 7.36 – 7.28 (m, 3H), 7.27 – 7.22 (m, 2H), 7.22 – 7.17 (m, 1H), 7.14 – 7.09 (m, 2H), 3.72 (s, 3H), 3.39 (s, 2H), 3.05 (d, J = 13.6 Hz, 1H), 2.54 (d, J = 13.6 Hz, 1H), 1.37 (s, 3H), 1.04 – 0.84 (m, 21H) ppm. ^{13}C NMR (126 MHz, $CDCl_3$) δ 175.3, 150.0, 145.6, 142.2, 128.4, 128.2, 127.6, 127.1, 127.0, 126.7, 124.3, 70.6, 63.1, 52.7, 49.1, 49.0, 24.8, 18.1, 18.0, 12.0 ppm. Diast. 1 IR (neat, cm^{-1}): 2938, 2862, 1726, 1455, 1229, 1091, 1062, 883, 687.

Diast.2 IR (neat, cm^{-1}): 2941, 2864, 1725, 1236, 1092, 1066, 765, 688. HRMS *calcd for* ($C_{28}H_{40}NaO_3Si$) 475.2639, *found* 475.2633.

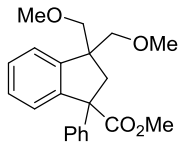

Methyl 3,3-bis(methoxymethyl)-1-phenyl-2,3-dihydro-1H-indene-1-carboxylate (195oa): Prepared following GP-B using **154o** (0.5 mmol 136.6 mg) and **175a** (0.875 mmol, 154.2 mg). The product was purified on 9/1 Hexanes: ethyl acetate, obtaining yellow oil (78.4 mg, 46% yield). ^{1}H NMR (500 MHz, $CDCl_3$) δ 7.52 – 7.48 (m, 1H), 7.44 – 7.39 (m, 1H), 7.36 – 7.30 (m, 2H), 7.30 – 7.25 (m, 2H), 7.24 – 7.20 (m, 1H), 7.14 – 7.09 (m, 2H), 3.72 (s, 3H), 3.56 – 3.47 (m, 2H), 3.40 – 3.36 (m, 1H), 3.36 – 3.34 (m, 3H), 3.31 – 3.25 (m, 2H), 3.21 – 3.18 (m, 3H), 2.29 – 2.23 (m, 1H) ppm. ^{13}C NMR (126 MHz, $CDCl_3$) δ 175.0, 146.8, 145.8, 143.0, 128.5, 128.2, 127.9, 127.8, 126.8 (2C), 125.0, 76.4, 76.2, 63.4, 59.5, 59.4, 52.7, 52.1, 45.6 ppm. IR (neat, cm^{-1}): 2925, 2886, 1729, 1447, 1219, 1099, 758,699. HRMS *calcd for* ($C_{21}H_{24}O_4$+Na) 363.1567, *found* 363.1555.

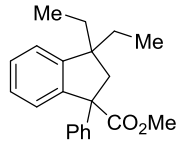

Methyl 3,3-diethyl-1-phenyl-2,3-dihydro-1H-indene-1-carboxylate (195pa): Prepared following GP-A using **154p** (0.5 mmol 120.6 mg) and **175a** (0.875 mmol, 154.2 mg). The product was purified on 95/5 Hexanes: ethyl acetate, obtaining a colorless oil (102.4 mg, 66% yield). ^{1}H NMR (500 MHz, $CDCl_3$) δ 7.48 (dd, *J* = 7.5, 0.5 Hz, 1H), 7.33 (td, *J* = 7.4, 1.2 Hz, 1H), 7.31 – 7.25 (m, 3H), 7.24 – 7.20 (m, 1H), 7.15 (d, *J* = 7.7 Hz, 1H), 7.11 (d, *J* = 7.2 Hz, 2H), 3.71 (s, 3H), 3.26 (d, *J* = 13.8 Hz, 1H), 2.14 (d, *J* = 13.8 Hz, 1H), 1.69 – 1.60 (m, 2H), 1.50 (dq, *J* = 13.9, 7.1 Hz, 2H), 0.86 (t, *J* = 7.4 Hz, 3H), 0.67 (t, *J* = 7.4 Hz, 3H) ppm. ^{13}C NMR (126 MHz, $CDCl_3$) δ 175.4, 151.1, 146.3, 142.4, 128.5, 128.1, 128.0, 126.7 (2C), 126.7, 124.0, 63.4, 52.7, 50.6, 49.0, 32.4, 31.3, 9.1, 9.0 ppm. IR (neat, cm^{-1}): 3063, 2964, 1729, 1446, 1214, 756, 698. HRMS *calcd for* ($C_{21}H_{24}O_2$+Na) 331.1669, *found* 331.1666.

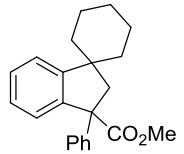

Methyl 3'-phenyl-2',3'-dihydrospiro[cyclohexane-1,1'-indene]-3'-carboxylate (195qa): Prepared following GP-A using **154q** (0.5 mmol 126.6 mg) and **175a** (0.875 mmol, 154.2 mg). The product was purified on 9/1 Hexanes: ethyl acetate, obtaining a colorless oil (121.8 mg,

76% yield). ^{1}H NMR (400 MHz, $CDCl_3$) δ 7.49 (dd, *J* = 7.6, 0.6 Hz, 1H), 7.37 (td, *J* = 7.4, 1.3 Hz, 1H), 7.33 – 7.27 (m, 4H), 7.26 – 7.23 (m, 1H), 7.16 – 7.11 (m, 2H), 3.73 (s, 3H), 3.36 (d, *J* = 13.6 Hz, 1H), 2.20 (d, *J* = 13.6 Hz, 1H), 1.77 – 1.71 (m, 1H), 1.69 – 1.53 (m, 6H), 1.42 – 1.25 (m, 3H) ppm. ^{13}C NMR (101 MHz, $CDCl_3$) δ 175.3, 153.7, 146.1, 141.6, 128.5, 128.4, 127.9, 127.0, 126.7, 126.6, 123.0, 63.5, 52.7, 49.4, 47.3, 39.0, 38.5, 26.0, 23.6, 23.3 ppm. IR (neat, cm^{-1}): 3062, 2924, 2850, 1729, 1433, 1218, 756, 298. HRMS *calcd for* ($C_{22}H_{24}O_2$+Na) 343.1669, *found* 343.1668.

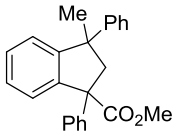

(1:1 Mixture of diastereoisomers)

Methyl 3-methyl-1,3-diphenyl-2,3-dihydro-1H-indene-1-carboxylate (195ra): Prepared following GP-B using **154r** (0.5 mmol 137.6 mg) and **175a** (0.875 mmol, 154.2 mg). The product was purified on 9/1 Hexanes: ethyl acetate, obtaining a colorless oil (69.8 mg, 41% yield). Both diastereoisomers were isolated together in a 1:1 ratio. ^{1}H NMR (500 MHz, $CDCl_3$) δ 7.58 – 7.54 (m, 1H), 7.48 (d, *J* = 7.3 Hz, 1H), 7.42 – 7.06 (m, 26H), 3.75 (s, 3H), 3.63 (d, *J* = 13.3 Hz, 1H), 3.49 (d, *J* = 13.7 Hz, 1H), 3.46 (s, 3H), 2.66 (d, *J* = 13.7 Hz, 1H), 2.56 (d, *J* = 13.3 Hz, 1H), 1.72 (s, 3H), 1.60 (s, 3H) ppm. ^{13}C NMR (126 MHz, $CDCl_3$) δ 175.1, 174.2, 152.5, 151.2, 149.1, 148.9, 144.8, 144.7, 143.2, 142.2, 128.6, 128.5, 128.4, 128.3, 128.1, 128.0, 127.9, 127.8, 127.3, 127.1, 127.0, 126.9, 126.8, 126.6 (2C), 126.5, 126.0, 125.9, 125.0, 124.9, 63.8, 63.4, 57.7, 57.0, 52.9, 52.4, 51.2, 51.1, 28.9 (2C) ppm. IR (neat, cm^{-1}): 2971, 2958, 1757, 1734, 1216, 1136, 1048, 696. HRMS *calcd for* ($C_{24}H_{22}O_2$+Na) 365.1512, *found* 365.1505.

6.1.5. Mechanistic Studies

→ Isotope-labelling studies.

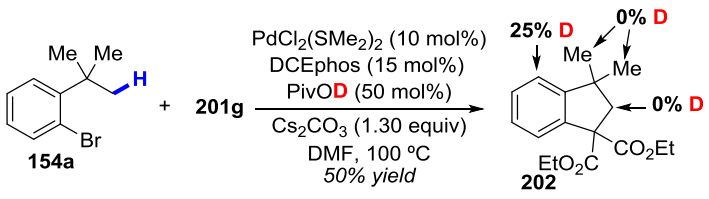

A 12.0 mL test tube is charged with *trans*-$PdCl_2(SMe_2)_2$ (10 mol%, 15.1 mg), DCEphos (15 mol%, 42.2 mg), PivOD[344] (50 mol%, 25.8 mg) and **201g** (0.875 mmol, 162.9 mg). Then, Cs_2CO_3 (1.3 equiv. 211.8 mg) is weighed into the glovebox. Next, a solution of **154a** (0.5 mmol, 106.6 mg)

[344] Prepared following the reported method. Duan, P.; Lan, X.; Chen, Y.; Qian, S.-S.; Li, J. J.; Lu, L.; Chen, B.; Hong, M.; Zhao, J. *Chem. Commun.* **2014**, *50*, 12135.

in anhydrous DMF (2.0 mL) was added by syringe. Finally, the reaction was placed on a 100 ºC preheated block and stirred for 16h at this temperature. After this time, the reaction was cooled down to room temperature, diluted with diethyl ether (10 mL) and transfer to a separation funnel. Brine was added (40 mL) and the reaction was extracted 3 times with Et_2O (30 mL) and washed once with brine (40 mL). The combined organic phases were dried with $MgSO_4$, filtered and concentrated under vacuum. Finally, the reaction crude was purified on silica gel column chromatography on a Hexanes/Ethyl acetate 9/1 obtaining the pure product **202** (73.3 mg, 50% yield). 25% deuteration at the *ortho*-position[345] was observed by ^{1}H NMR.

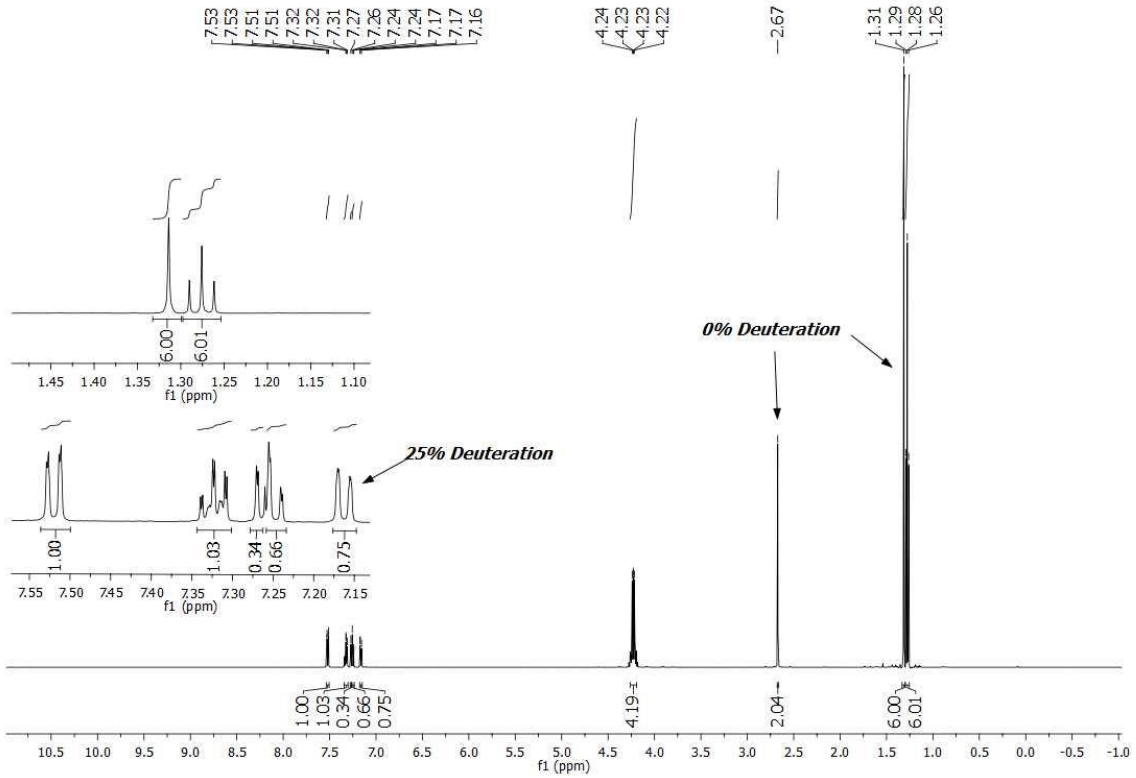

→ Intermediacy of Benzocyclobutanes via C–C cleavage.

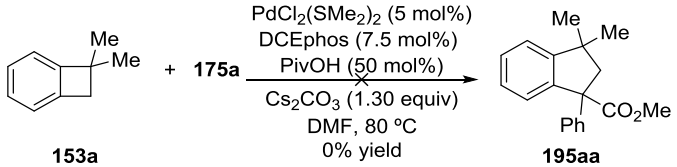

A 12.0 mL test tube is charged with *trans*-$PdCl_2(SMe_2)_2$ (5 mol%, 7.1 mg), DCEphos (15 mol%, 21.1 mg), PivOH (50 mol%, 25.5 mg) and 7,7-dimethylbicyclo[4.2.0]octa-1,3,5-triene **153a**[340] (0.5 mmol, 66.1 mg, 1.0 equiv.). Then, Cs_2CO_3 (1.3 equiv. 211.8 mg) is weighed into the glovebox. Next, a solution of **175a** (0.875 mmol, 154.1 mg) in anhydrous DMF (2.0 mL) was

[345] Identified by NOESY, and a combination of HMQC and HMBC experiments.

added by syringe. Finally, the reaction was placed on an 80 ºC preheated block and stirred for 14h at this temperature. After this time, the reaction was cooled down to room temperature. Next, o-xylene (0.5 mmol, 1.0 equiv., 61.7 µL) was added as internal standard via microsyringe followed by 10 mL of EtOAc. An aliquot was filtered through a plug of silica and Celite® and analyzed by GC, obtaining 0% conversion of **153a** and 0% yield of **195aa** as judged by GC.

→ Synthesis of Pd complexes **XLVII-DCEphos** and **XLVII-Phanephos**[346] and study of their catalytic activity.

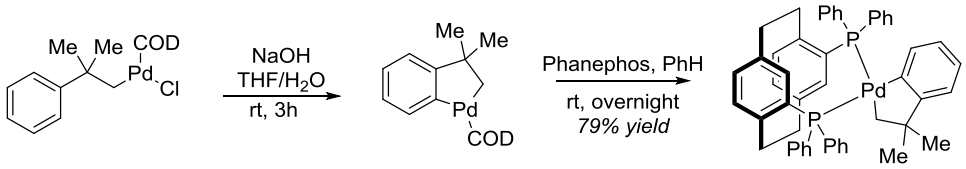

LXXII **XLVII-COD** **XLVII-Phanephos**

Synthesis of LXXII: Prepared following the method reported by Cámpora.[347,348]

Synthesis of Palladacycle XLVII-Phanephos:

A solution of (S)-Phanephos (1.0 equiv.) in anhydrous benzene (0.04M) under inert atmosphere was added into a Schlenk tube under inert atmosphere containing palladacycle **LXXII** (1.0 equiv.), obtaining immediately a pale yellow clear solution. After stirring at rt for 30 min. a white solid precipitated out, and the suspension was stirred overnight at rt. Next, the white solid was filtered and washed with cold benzene and pentane. The white solid obtained was dried under high vacuum (79% yield). A sample suitable for X-Ray analysis was obtained by layering pentane over a solution of **6** in DCM. Mp: 131 ºC (dec.) ^{1}H NMR (500 MHz, $CDCl_3$) δ 8.28 – 8.20 (m, 4H), 7.73 – 7.63 (m, 4H), 7.57 – 7.48 (m, 3H), 7.46 – 7.35 (m, 5H), 7.34 – 7.27 (m, 3H), 7.23 (td, *J* = 7.3, 1.2 Hz, 1H), 7.14 (td, *J* = 7.7, 1.5 Hz, 2H), 6.97 – 6.91 (m, 1H), 6.85 (td, *J* = 7.3, 0.9 Hz, 1H), 6.71 – 6.65 (m, 1H), 6.43 – 6.36 (m, 1H), 6.36 – 6.32 (m, 2H), 6.32 – 6.27 (m, 2H), 2.58 (ddd, *J* = 24.2, 14.9, 7.0 Hz, 4H), 2.50 – 2.38 (m, 3H), 2.18 (td, *J* = 11.9, 6.9 Hz, 1H), 2.10 (ddd, *J* = 13.8, 9.1, 2.9 Hz, 1H), 2.07 – 2.01 (m, 1H), 1.49 (s, 3H), 1.22 (s, 3H) ppm. ^{13}C NMR (126 MHz, $CDCl_3$) δ 166.9 (t, *J* = 3.0 Hz), 166.9 (dd, *J* = 111.8, 13.8 Hz), 142.7, 142.0, 139.6 (d, *J* = 1.5 Hz), 139.5, 139.4, 139.2 (d, *J* = 6.2 Hz), 139.2 (d, *J* = 4.1 Hz), 138.3 (dd, *J* = 26.0, 2.5 Hz), 137.9 (dd, *J* = 22.5, 1.3 Hz), 137.7 (d, *J* = 13.0 Hz), 137.2 – 136.8 (m), 136.7 (d, *J* = 3.1 Hz), 136.6 – 136.4 (m), 136.2 (d, *J* = 5.0 Hz), 136.0 (d, *J* = 5.3 Hz), 135.9 (d, *J* = 12.1 Hz), 135.2 (d, *J* = 30.5 Hz), 133.8 (d, *J* = 22.6 Hz), 133.1 (dd, *J* = 7.8, 1.7 Hz), 132.4 (dd, *J* = 8.8, 5.9 Hz), 131.1 – 130.8

[346] During all this work (S)-Phanephos was used.
[347] Cámpora, J.; López, J. A.; Palma, P.; del Rio, D.; Carmona, E. *Inorg. Chem*. **2001**, *40*, 4116.
[348] Better results were obtained when the Grignard reagent was freshly-prepared instead of using commercially available sources. See: Griffiths, D. C.; Young, G. B. *Organometallics*, **1989**, *8*, 875.

(m), 130.9, 129.3 (dd, *J* = 10.0, 1.6 Hz), 128.6 (d, *J* = 10.0 Hz), 128.2 (d, *J* = 10.1 Hz), 128.1 (d, *J* = 8.2 Hz), 128.1 – 127.9 (m), 127.8 (d, *J* = 9.1 Hz), 127.7 (d, *J* = 9.2 Hz), 123.5 (dd, *J* = 8.5, 1.4 Hz), 123.2, 121.8 (d, *J* = 2.9 Hz), 57.8 (dd, *J* = 83.1, 7.7 Hz), 51.4 (t, *J* = 5.5 Hz), 35.6, 35.3, 32.7, 32.5, 32.4, 32.2 ppm. ^{31}P NMR (202 MHz, $CDCl_3$) δ 36.79 (d, *J* = 20.5 Hz), 32.08 (d, *J* = 20.4 Hz). IR (neat, cm^{-1}): 3030, 2943, 2850, 1739, 1434, 1366, 1217, 747, 694. HRMS *calcd for* ($C_{50}H_{47}P_2{}^{106}Pd$) 815.2182, *found* 815.2177.

→ Stoichiometric Experiments with **LXXII**

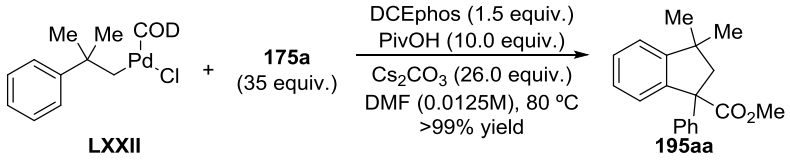

A schlenk tube was charged with **LXXII** (19.2 mg, 0.05 mmol, 1.0 equiv.), DCEphos (42.2 mg, 0.075 mmol, 1.5 equiv.) and PivOH (51.1 mg, 0.5 mmol, 10 equiv.). Next, Cs_2CO_3 (423.6 mg, 1.3 mmol, 26 equiv.) was added in the glovebox. Finally, a solution of **175a** (308.3 mg, 1.75 mmol, 35 equiv.) in anhydrous DMF (4 mL, 0.0125M) was added by syringe under inert atmosphere, and the mixture was heated at 80 ºC overnight. The reaction was then cooled to rt and *o*-xylene (6.2 µL, 0.05 mmol, 1.0 equiv.) was added as internal standard. After filtration through a plug of Celite®, the reaction was analyzed by GC, observing **195aa** in essentially quantitative yield (99%).

→ Stoichiometric Experiments **XLVII-Phanephos**

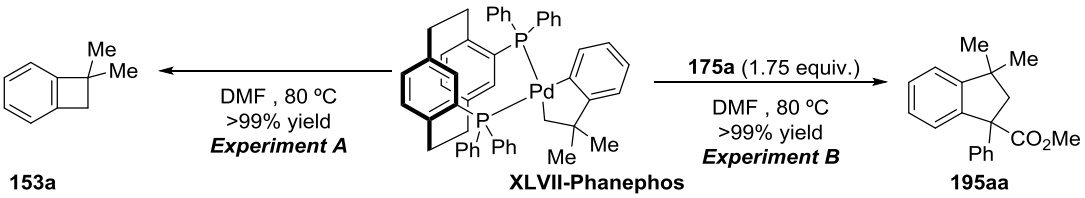

Experiment A: A solution of **XLVII-Phanephos** (40.7 mg, 0.05 mmol, 1.0 equiv.) in anhydrous DMF (0.5 mL) was heated at 80 ºC under inert atmosphere overnight. GC analysis using o-xylene as internal standard (6.2 µL, 0.05 mmol, 1.0 equiv.) showed quantitative formation of **153a** (>99% yield).

Experiment B: A solution of **XLVII-Phanephos** (40.7 mg, 0.05 mmol, 1.0 equiv.) and **175a** (15.4 mg, 0.0875 mmol, 1.0 equiv.) in anhydrous DMF (0.5 mL) was heated at 80 ºC under inert atmosphere overnight. GC analysis using o-xylene as internal standard (6.2 µL, 0.05 mmol, 1.0 equiv.) showed quantitative formation of **195aa** (>99% yield).

→ Catalytic Experiments with XLVII-Phanephos.

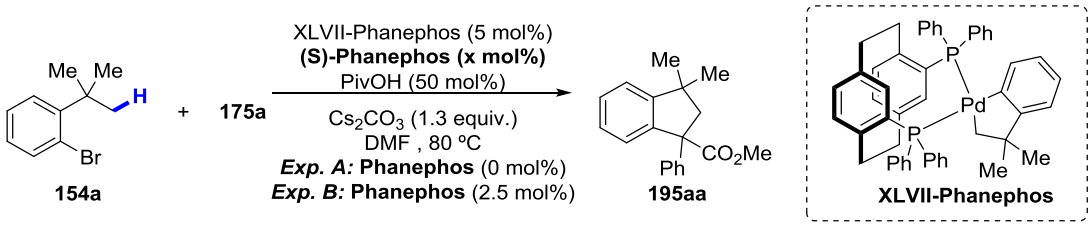

→ ***Experiment A***: Following **GP-A** but using **XLVII-Phanephos** (20.4 mg, 0.025 mmol, 5 mol%) instead of $PdCl_2(SMe_2)_2$ with no additional ligand. GC analysis using o-xylene as internal standard (61.7 µL, 0.5 mmol, 1 equiv.) showed that the product **195aa** was obtained in 57% yield.

→ ***Experiment B***: Following **GP-A** but using **XLVII-Phanephos** (20.4 mg, 0.025 mmol, 5 mol%) instead of $PdCl_2(SMe_2)_2$ and additional (S)-Phanephos (7.2 mg, 0.0125 mmol, 2.5 mol%) instead of DCEphos. GC analysis using o-xylene as internal standard (61.7 µL, 0.5 mmol, 1 equiv.) showed that the product **195aa** was obtained in 77% yield.

6.1.6. X-Ray crystallographic data (195aa-COOH, 6 and Pd-metallacycle containing XLVII-Phanpephos, XLVII-Phanephos)

Table 1. Crystal data and structure refinement for **195aa-COOH**.

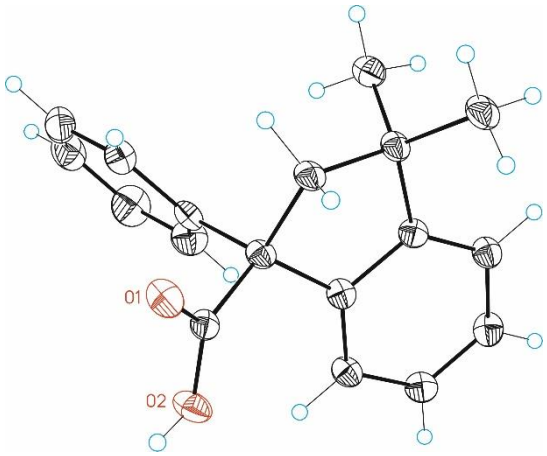

Identification code	mo_AGB15080-b_0m	
Empirical formula	C18 H18 O2	
Formula weight	266.32	
Temperature	100(2) K	
Wavelength	0.71073 Å	
Crystal system	Triclinic	
Space group	P-1	
Unit cell dimensions	a = 8.2724(6)Å	α = 99.3703(19)°.

	b = 8.3263(5)Å	β = 98.059(2)°.
	c = 12.4647(8)Å	γ = 119.5564(18)°.
Volume	712.13(8) $Å^3$	
Z	2	
Density (calculated)	1.242 Mg/m^3	
Absorption coefficient	0.080 mm^{-1}	
F(000)	284	
Crystal size	0.30 x 0.20 x 0.10 mm^3	
Theta range for data collection	1.713 to 25.445°.	
Index ranges	-10<=h<=8,-7<=k<=10,-14<=l<=15	
Reflections collected	6017	
Independent reflections	2550[R(int) = 0.0464]	
Completeness to theta =25.445°	97.0%	
Absorption correction	Empirical	
Max. and min. transmission	0.992 and 0.642	
Refinement method	Full-matrix least-squares on F^2	
Data / restraints / parameters	2550/ 0/ 184	
Goodness-of-fit on F^2	1.115	
Final R indices [I>2sigma(I)]	R1 = 0.0598, wR2 = 0.1705	
R indices (all data)	R1 = 0.0646, wR2 = 0.1743	
Largest diff. peak and hole	0.317 and -0.265 $e.Å^{-3}$	

Table 2. Bond lengths [Å] and angles [°] for **195aa-COOH**.

Bond lengths----	
C1-O1	1.251(3)
C1-O2	1.285(3)
C1-C2	1.521(3)
C2-C3	1.522(3)
C2-C11	1.554(3)
C2-C10	1.555(3)
C3-C4	1.393(3)
C3-C8	1.399(3)
C4-C5	1.394(3)
C5-C6	1.389(3)
C6-C7	1.392(3)
C7-C8	1.389(3)
C8-C9	1.515(3)
C9-C18	1.533(3)
C9-C17	1.535(3)
C9-C10	1.544(3)
C11-C12	1.387(4)
C11-C16	1.398(4)
C12-C13	1.387(4)
C13-C14	1.380(4)
C14-C15	1.385(4)
C15-C16	1.382(4)
Angles----------	
O1-C1-O2	123.3(2)
O1-C1-C2	119.2(2)
O2-C1-C2	117.31(19)
C1-C2-C3	115.35(18)
C1-C2-C11	103.55(17)
C3-C2-C11	113.18(18)
C1-C2-C10	111.03(18)
C3-C2-C10	101.49(18)
C11-C2-C10	112.60(18)
C4-C3-C8	120.2(2)
C4-C3-C2	129.8(2)

C8-C3-C2	109.96(19)
C3-C4-C5	119.0(2)
C6-C5-C4	120.7(2)
C5-C6-C7	120.4(2)
C8-C7-C6	119.2(2)
C7-C8-C3	120.5(2)
C7-C8-C9	127.6(2)
C3-C8-C9	111.8(2)
C8-C9-C18	112.77(19)
C8-C9-C17	110.76(19)
C18-C9-C17	108.83(19)
C8-C9-C10	101.44(18)
C18-C9-C10	111.44(19)
C17-C9-C10	111.50(19)
C9-C10-C2	106.53(18)
C12-C11-C16	118.1(2)
C12-C11-C2	122.3(2)
C16-C11-C2	119.6(2)
C11-C12-C13	120.8(3)
C14-C13-C12	120.5(3)
C13-C14-C15	119.3(2)
C16-C15-C14	120.3(3)
C15-C16-C11	121.0(2)

Table 3. Torsion angles [°] for **195aa-COOH**.

O1-C1-C2-C3	144.0(2)
O2-C1-C2-C3	-40.2(3)
O1-C1-C2-C11	-91.8(2)
O2-C1-C2-C11	84.0(2)
O1-C1-C2-C10	29.3(3)
O2-C1-C2-C10	-155.0(2)
C1-C2-C3-C4	42.8(3)
C11-C2-C3-C4	-76.2(3)
C10-C2-C3-C4	162.9(2)
C1-C2-C3-C8	-139.6(2)
C11-C2-C3-C8	101.3(2)
C10-C2-C3-C8	-19.6(2)
C8-C3-C4-C5	-0.4(3)
C2-C3-C4-C5	177.0(2)
C3-C4-C5-C6	-0.8(3)
C4-C5-C6-C7	1.2(4)
C5-C6-C7-C8	-0.3(3)
C6-C7-C8-C3	-0.9(3)
C6-C7-C8-C9	180.0(2)
C4-C3-C8-C7	1.2(3)
C2-C3-C8-C7	-176.6(2)
C4-C3-C8-C9	-179.55(19)
C2-C3-C8-C9	2.6(3)
C7-C8-C9-C18	-45.9(3)
C3-C8-C9-C18	135.0(2)
C7-C8-C9-C17	76.3(3)
C3-C8-C9-C17	-102.8(2)
C7-C8-C9-C10	-165.2(2)
C3-C8-C9-C10	15.7(2)
C8-C9-C10-C2	-27.5(2)
C18-C9-C10-C2	-147.70(19)
C17-C9-C10-C2	90.5(2)
C1-C2-C10-C9	152.10(18)
C3-C2-C10-C9	29.0(2)
C11-C2-C10-C9	-92.3(2)
C1-C2-C11-C12	-108.5(2)

C3-C2-C11-C12	17.1(3)
C10-C2-C11-C12	131.5(2)
C1-C2-C11-C16	69.8(2)
C3-C2-C11-C16	-164.6(2)
C10-C2-C11-C16	-50.2(3)
C16-C11-C12-C13	1.1(4)
C2-C11-C12-C13	179.5(2)
C11-C12-C13-C14	-0.3(4)
C12-C13-C14-C15	-0.3(4)
C13-C14-C15-C16	0.0(4)
C14-C15-C16-C11	0.9(4)
C12-C11-C16-C15	-1.4(3)
C2-C11-C16-C15	-179.8(2)

Table 1. Crystal data and structure refinement for **XLVII-Phanephos**.

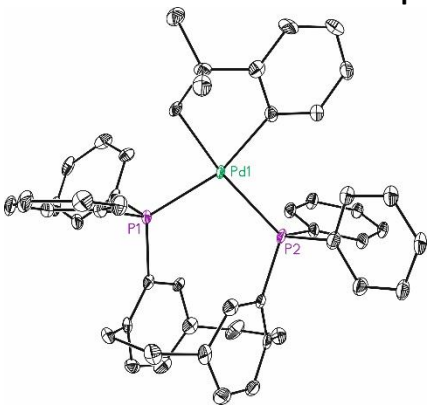

Identification code	mo_AGB16_032_0m	
Empirical formula	C50 H46 P2 Pd	
Formula weight	815.21	
Temperature	100(2) K	
Wavelength	0.71073 Å	
Crystal system	Monoclinic	
Space group	P2(1)	
Unit cell dimensions	a = 10.3194(8)Å	α = 90°.
	b = 8.9387(8)Å	β = 90.850(3)°.
	c = 20.8179(14)Å	γ = 90°.
Volume	1920.1(3) $Å^3$	
Z	2	
Density (calculated)	1.410 Mg/m^3	

Absorption coefficient	0.602 mm^{-1}
F(000)	844
Crystal size	0.45 x 0.01 x 0.01 mm^3
Theta range for data collection	0.978 to 28.425°.
Index ranges	-13<=h<=9,-11<=k<=11,-21<=l<=27
Reflections collected	19991
Independent reflections	9103[R(int) = 0.0719]
Completeness to theta =28.425°	98.0%
Absorption correction	Multi-scan
Max. and min. transmission	0.994 and 0.729
Refinement method	Full-matrix least-squares on F^2
Data / restraints / parameters	9103/ 332/ 588
Goodness-of-fit on F^2	1.021
Final R indices [I>2sigma(I)]	R1 = 0.0599, wR2 = 0.1111
R indices (all data)	R1 = 0.0907, wR2 = 0.1222
Flack parameter	x =-0.05(3)
Largest diff. peak and hole	1.432 and -0.960 e.$Å^{-3}$

Table 2. Bond lengths [Å] and angles [°] for **XLVII-Phanephos**.

Bond lengths----	
Pd1-C4	2.069(8)
Pd1-C1	2.087(7)
Pd1-P1	2.3626(19)
Pd1-P2	2.3944(19)
P1-C11	1.831(7)
P1-C17	1.845(8)
P1-C23	1.854(8)
P2-C45	1.827(9)
P2-C29	1.847(8)
P2-C39'	1.850(7)
P2-C45'	1.851(13)
P2-C39	1.854(6)
C1-C2	1.548(11)
C2-C9	1.504(12)
C2-C3	1.519(11)
C2-C10	1.536(11)
C3-C8	1.380(11)
C3-C4	1.407(12)
C4-C5	1.410(10)
C5-C6	1.404(11)
C6-C7	1.371(13)
C7-C8	1.405(12)
C11-C16	1.399(9)
C11-C12	1.401(11)
C12-C13	1.385(11)
C13-C14	1.406(11)
C14-C15	1.364(13)
C15-C16	1.387(13)
C17-C22	1.393(11)
C17-C18	1.400(11)
C18-C19	1.376(11)
C19-C20	1.390(12)
C20-C21	1.376(12)
C21-C22	1.386(11)
C23-C24	1.394(11)

C23-C28	1.398(11)
C24-C25	1.387(11)
C25-C26	1.410(11)
C25-C37	1.505(11)
C26-C27	1.375(13)
C27-C28	1.408(12)
C28-C35	1.535(11)
C29-C30	1.398(11)
C29-C34	1.406(12)
C30-C31	1.405(11)
C31-C32	1.391(12)
C31-C36	1.499(11)
C32-C33	1.374(12)
C33-C34	1.405(11)
C34-C38	1.517(12)
C35-C36	1.577(12)
C37-C38	1.592(12)
C39-C40	1.391(11)
C39-C44	1.394(7)
C40-C41	1.399(12)
C41-C42	1.375(12)
C42-C43	1.365(13)
C43-C44	1.391(12)
C39'-C40'	1.392(12)
C39'-C44'	1.393(6)
C40'-C41'	1.400(12)
C41'-C42'	1.375(12)
C42'-C43'	1.365(13)
C43'-C44'	1.391(12)
C45-C46	1.387(12)
C45-C50	1.409(11)
C46-C47	1.370(13)
C47-C48	1.392(13)
C48-C49	1.389(5)
C49-C50	1.389(13)
C45'-C46'	1.388(12)
C45'-C50'	1.410(11)
C46'-C47'	1.370(14)

C47'-C48'	1.392(14)
C48'-C49'	1.390(6)
C49'-C50'	1.389(14)

Angles----------

C4-Pd1-C1	76.6(3)
C4-Pd1-P1	162.1(2)
C1-Pd1-P1	87.1(2)
C4-Pd1-P2	95.3(2)
C1-Pd1-P2	169.4(2)
P1-Pd1-P2	101.73(7)
C11-P1-C17	104.4(3)
C11-P1-C23	108.4(3)
C17-P1-C23	96.1(3)
C11-P1-Pd1	112.1(2)
C17-P1-Pd1	112.8(3)
C23-P1-Pd1	121.0(2)
C45-P2-C29	108.9(13)
C29-P2-C39'	99.1(17)
C29-P2-C45'	112(3)
C39'-P2-C45'	104(3)
C45-P2-C39	103.5(14)
C29-P2-C39	95.6(8)
C45-P2-Pd1	111.8(9)
C29-P2-Pd1	117.7(2)
C39'-P2-Pd1	114.7(13)
C45'-P2-Pd1	108(2)
C39-P2-Pd1	117.4(6)
C2-C1-Pd1	109.6(5)
C9-C2-C3	111.3(7)
C9-C2-C10	108.8(7)
C3-C2-C10	112.4(7)
C9-C2-C1	111.9(7)
C3-C2-C1	103.5(6)
C10-C2-C1	108.9(7)
C8-C3-C4	121.4(8)
C8-C3-C2	123.2(8)
C4-C3-C2	115.3(7)

C3-C4-C5	116.7(7)
C3-C4-Pd1	115.4(5)
C5-C4-Pd1	127.9(6)
C6-C5-C4	121.0(8)
C7-C6-C5	121.6(8)
C6-C7-C8	117.8(8)
C3-C8-C7	121.5(8)
C16-C11-C12	119.3(8)
C16-C11-P1	123.6(7)
C12-C11-P1	117.1(5)
C13-C12-C11	120.0(7)
C12-C13-C14	120.2(8)
C15-C14-C13	119.4(8)
C14-C15-C16	121.4(8)
C15-C16-C11	119.7(10)
C22-C17-C18	117.5(7)
C22-C17-P1	120.8(6)
C18-C17-P1	121.7(6)
C19-C18-C17	121.8(8)
C18-C19-C20	119.7(8)
C21-C20-C19	119.3(7)
C20-C21-C22	120.9(8)
C21-C22-C17	120.6(8)
C24-C23-C28	119.6(7)
C24-C23-P1	108.6(6)
C28-C23-P1	131.8(6)
C25-C24-C23	123.4(7)
C24-C25-C26	115.3(8)
C24-C25-C37	120.3(7)
C26-C25-C37	122.5(7)
C27-C26-C25	120.3(9)
C26-C27-C28	122.6(8)
C23-C28-C27	116.0(8)
C23-C28-C35	125.9(7)
C27-C28-C35	116.8(7)
C30-C29-C34	119.6(7)
C30-C29-P2	108.3(6)
C34-C29-P2	132.0(6)

C29-C30-C31	122.1(8)
C32-C31-C30	116.2(8)
C32-C31-C36	123.2(8)
C30-C31-C36	119.2(8)
C33-C32-C31	120.4(8)
C32-C33-C34	122.7(8)
C33-C34-C29	115.9(8)
C33-C34-C38	117.3(8)
C29-C34-C38	125.7(7)
C28-C35-C36	113.8(6)
C31-C36-C35	112.1(8)
C25-C37-C38	112.1(7)
C34-C38-C37	113.5(6)
C40-C39-C44	117.6(7)
C40-C39-P2	118.4(10)
C44-C39-P2	123.9(10)
C39-C40-C41	120.1(8)
C42-C41-C40	120.5(9)
C43-C42-C41	120.3(8)
C42-C43-C44	119.2(9)
C43-C44-C39	122.0(8)
C40'-C39'-C44'	117.5(9)
C40'-C39'-P2	125(2)
C44'-C39'-P2	116(2)
C39'-C40'-C41'	119.9(8)
C42'-C41'-C40'	120.5(9)
C43'-C42'-C41'	120.4(9)
C42'-C43'-C44'	119.1(9)
C43'-C44'-C39'	121.8(9)
C46-C45-C50	119.5(8)
C46-C45-P2	118.7(11)
C50-C45-P2	121.4(13)
C47-C46-C45	121.8(9)
C46-C47-C48	118.9(9)
C49-C48-C47	120.4(9)
C50-C49-C48	120.7(8)
C49-C50-C45	118.6(9)
C46'-C45'-C50'	119.1(10)

C46'-C45'-P2	114(2)
C50'-C45'-P2	127(2)
C47'-C46'-C45'	121.8(11)
C46'-C47'-C48'	118.9(12)
C49'-C48'-C47'	120.3(11)
C50'-C49'-C48'	120.6(10)
C49'-C50'-C45'	119.0(11)

Table 3. Torsion angles [°] for **XLVII-Phanephos**.

Pd1-C1-C2-C9	-74.2(7)
Pd1-C1-C2-C3	45.7(7)
Pd1-C1-C2-C10	165.4(5)
C9-C2-C3-C8	-88.8(10)
C10-C2-C3-C8	33.6(12)
C1-C2-C3-C8	150.9(8)
C9-C2-C3-C4	93.0(9)
C10-C2-C3-C4	-144.7(8)
C1-C2-C3-C4	-27.3(9)
C8-C3-C4-C5	-2.6(12)
C2-C3-C4-C5	175.6(7)
C8-C3-C4-Pd1	178.7(6)
C2-C3-C4-Pd1	-3.0(9)
C3-C4-C5-C6	0.1(12)
Pd1-C4-C5-C6	178.6(6)
C4-C5-C6-C7	2.4(13)
C5-C6-C7-C8	-2.3(14)
C4-C3-C8-C7	2.7(13)
C2-C3-C8-C7	-175.4(8)
C6-C7-C8-C3	-0.2(14)
C17-P1-C11-C16	24.1(7)
C23-P1-C11-C16	-77.5(7)
Pd1-P1-C11-C16	146.4(6)
C17-P1-C11-C12	-156.9(6)
C23-P1-C11-C12	101.5(6)
Pd1-P1-C11-C12	-34.5(7)
C16-C11-C12-C13	1.0(12)
P1-C11-C12-C13	-178.1(6)
C11-C12-C13-C14	-0.1(13)
C12-C13-C14-C15	-0.5(13)
C13-C14-C15-C16	0.3(13)
C14-C15-C16-C11	0.6(12)
C12-C11-C16-C15	-1.2(11)
P1-C11-C16-C15	177.8(6)
C11-P1-C17-C22	109.6(6)
C23-P1-C17-C22	-139.6(6)

Pd1-P1-C17-C22	-12.3(7)
C11-P1-C17-C18	-69.2(7)
C23-P1-C17-C18	41.6(7)
Pd1-P1-C17-C18	168.9(6)
C22-C17-C18-C19	0.2(12)
P1-C17-C18-C19	179.0(6)
C17-C18-C19-C20	-1.7(12)
C18-C19-C20-C21	2.9(12)
C19-C20-C21-C22	-2.6(12)
C20-C21-C22-C17	1.1(12)
C18-C17-C22-C21	0.1(11)
P1-C17-C22-C21	-178.7(6)
C11-P1-C23-C24	176.7(5)
C17-P1-C23-C24	69.3(5)
Pd1-P1-C23-C24	-51.9(6)
C11-P1-C23-C28	-7.6(8)
C17-P1-C23-C28	-115.0(7)
Pd1-P1-C23-C28	123.8(6)
C28-C23-C24-C25	-1.2(11)
P1-C23-C24-C25	175.1(6)
C23-C24-C25-C26	14.2(11)
C23-C24-C25-C37	-150.5(7)
C24-C25-C26-C27	-13.6(11)
C37-C25-C26-C27	150.8(8)
C25-C26-C27-C28	0.4(12)
C24-C23-C28-C27	-12.2(10)
P1-C23-C28-C27	172.5(6)
C24-C23-C28-C35	153.9(7)
P1-C23-C28-C35	-21.5(11)
C26-C27-C28-C23	12.8(11)
C26-C27-C28-C35	-154.6(7)
C45-P2-C29-C30	-176.4(9)
C39'-P2-C29-C30	76(2)
C45'-P2-C29-C30	-174.5(17)
C39-P2-C29-C30	77.2(11)
Pd1-P2-C29-C30	-47.9(6)
C45-P2-C29-C34	1.2(11)
C39'-P2-C29-C34	-106(2)

C45'-P2-C29-C34	3.1(18)
C39-P2-C29-C34	-105.2(12)
Pd1-P2-C29-C34	129.7(7)
C34-C29-C30-C31	-2.7(11)
P2-C29-C30-C31	175.3(6)
C29-C30-C31-C32	15.6(11)
C29-C30-C31-C36	-151.0(8)
C30-C31-C32-C33	-13.4(11)
C36-C31-C32-C33	152.6(8)
C31-C32-C33-C34	-1.6(13)
C32-C33-C34-C29	14.6(11)
C32-C33-C34-C38	-154.2(8)
C30-C29-C34-C33	-12.2(11)
P2-C29-C34-C33	170.4(6)
C30-C29-C34-C38	155.6(7)
P2-C29-C34-C38	-21.8(12)
C23-C28-C35-C36	-83.4(10)
C27-C28-C35-C36	82.6(9)
C32-C31-C36-C35	-87.6(10)
C30-C31-C36-C35	78.0(11)
C28-C35-C36-C31	2.1(11)
C24-C25-C37-C38	74.1(9)
C26-C25-C37-C38	-89.5(10)
C33-C34-C38-C37	81.5(9)
C29-C34-C38-C37	-86.1(9)
C25-C37-C38-C34	4.4(10)
C45-P2-C39-C40	101(3)
C29-P2-C39-C40	-148(2)
C39'-P2-C39-C40	17(50)
C45'-P2-C39-C40	97(4)
Pd1-P2-C39-C40	-23(3)
C45-P2-C39-C44	-84(3)
C29-P2-C39-C44	27(3)
C39'-P2-C39-C44	-167(54)
C45'-P2-C39-C44	-87(4)
Pd1-P2-C39-C44	153(2)
C44-C39-C40-C41	5(4)
P2-C39-C40-C41	-179(2)

C39-C40-C41-C42	-2(4)
C40-C41-C42-C43	-4(3)
C41-C42-C43-C44	6(2)
C42-C43-C44-C39	-2(2)
C40-C39-C44-C43	-3(4)
P2-C39-C44-C43	-178.6(17)
C45-P2-C39'-C40'	97(6)
C29-P2-C39'-C40'	-151(6)
C45'-P2-C39'-C40'	93(6)
C39-P2-C39'-C40'	-165(56)
Pd1-P2-C39'-C40'	-25(7)
C45-P2-C39'-C44'	-72(5)
C29-P2-C39'-C44'	40(5)
C45'-P2-C39'-C44'	-75(5)
C39-P2-C39'-C44'	26(47)
Pd1-P2-C39'-C44'	167(4)
C44'-C39'-C40'-C41'	-7(8)
P2-C39'-C40'-C41'	-175(5)
C39'-C40'-C41'-C42'	-1(8)
C40'-C41'-C42'-C43'	6(6)
C41'-C42'-C43'-C44'	-2(5)
C42'-C43'-C44'-C39'	-6(5)
C40'-C39'-C44'-C43'	10(7)
P2-C39'-C44'-C43'	180(3)
C29-P2-C45-C46	102(3)
C39'-P2-C45-C46	-153(3)
C45'-P2-C45-C46	-50(47)
C39-P2-C45-C46	-157(3)
Pd1-P2-C45-C46	-30(3)
C29-P2-C45-C50	-85(3)
C39'-P2-C45-C50	20(3)
C45'-P2-C45-C50	124(51)
C39-P2-C45-C50	16(3)
Pd1-P2-C45-C50	143(2)
C50-C45-C46-C47	-1(5)
P2-C45-C46-C47	172(2)
C45-C46-C47-C48	0(4)
C46-C47-C48-C49	0(3)

C47-C48-C49-C50	1(3)
C48-C49-C50-C45	-1(3)
C46-C45-C50-C49	2(4)
P2-C45-C50-C49	-172(2)
C45-P2-C45'-C46'	128(54)
C29-P2-C45'-C46'	99(6)
C39'-P2-C45'-C46'	-155(6)
C39-P2-C45'-C46'	-158(5)
Pd1-P2-C45'-C46'	-32(7)
C45-P2-C45'-C50'	-54(44)
C29-P2-C45'-C50'	-83(7)
C39'-P2-C45'-C50'	23(8)
C39-P2-C45'-C50'	19(8)
Pd1-P2-C45'-C50'	145(6)
C50'-C45'-C46'-C47'	4(10)
P2-C45'-C46'-C47'	-178(5)
C45'-C46'-C47'-C48'	-7(8)
C46'-C47'-C48'-C49'	6(6)
C47'-C48'-C49'-C50'	-3(6)
C48'-C49'-C50'-C45'	0(7)
C46'-C45'-C50'-C49'	-1(10)
P2-C45'-C50'-C49'	-179(6)

Table 1. Crystal data and structure refinement for **XLVII-DCEphos**.

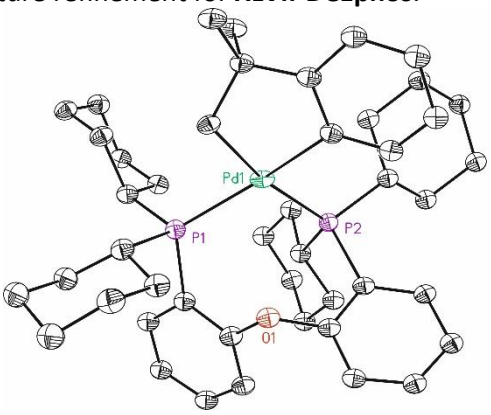

Identification code	mo_AGB12_080B_0m
Empirical formula	C46 H64 O P2 Pd
Formula weight	801.31
Temperature	100(2) K

Wavelength	0.71073 Å	
Crystal system	Triclinic	
Space group	P-1	
Unit cell dimensions	a = 9.5950(18)Å	α= 86.505(7)°.
	b = 9.6214(19)Å	β = 83.992(7)°.
	c = 21.763(5)Å	γ = 87.351(8)°.
Volume	1992.7(7) $Å^3$	
Z	2	
Density (calculated)	1.335 Mg/m^3	
Absorption coefficient	0.580 mm^{-1}	
F(000)	848	
Crystal size	0.12 x 0.06 x 0.02 mm^3	
Theta range for data collection	0.942 to 23.446°.	
Index ranges	-10<=h<=10,-10<=k<=10,-24<=l<=24	
Reflections collected	23732	
Independent reflections	5589[R(int) = 0.1971]	
Completeness to theta =23.446°	95.3%	
Absorption correction	Multi-scan	
Max. and min. transmission	0.988 and 0.638	
Refinement method	Full-matrix least-squares on F^2	
Data / restraints / parameters	5589/ 770/ 453	
Goodness-of-fit on F^2	1.516	
Final R indices [I>2sigma(I)]	R1 = 0.1332, wR2 = 0.2918	
R indices (all data)	R1 = 0.2081, wR2 = 0.3162	
Largest diff. peak and hole	4.517 and -2.908 $e.Å^{-3}$	

Table 2. Bond lengths [Å] and angles [°] for **XLVII-DCEphos**.

Bond lengths----	
Pd1-C4	2.087(17)
Pd1-C1	2.143(15)
Pd1-P1	2.342(5)
Pd1-P2	2.388(4)
P1-C17	1.842(16)
P1-C23	1.850(17)
P1-C11	1.875(15)
P2-C35	1.822(16)
P2-C29	1.864(16)
P2-C41	1.878(16)
O1-C30	1.384(18)
O1-C28	1.431(19)
C1-C2	1.48(2)
C2-C3	1.46(2)
C2-C9	1.55(2)
C2-C10	1.59(2)
C3-C4	1.41(2)
C3-C8	1.44(2)
C4-C5	1.35(2)
C5-C6	1.36(2)
C6-C7	1.40(2)
C7-C8	1.36(2)
C11-C12	1.44(2)
C11-C16	1.52(2)
C12-C13	1.54(2)
C13-C14	1.56(2)
C14-C15	1.48(2)
C15-C16	1.52(2)
C17-C18	1.54(2)
C17-C22	1.55(2)
C18-C19	1.52(2)
C19-C20	1.51(2)
C20-C21	1.52(2)
C21-C22	1.52(2)
C23-C28	1.38(2)

C23-C24	1.44(2)
C24-C25	1.37(2)
C25-C26	1.36(2)
C26-C27	1.39(2)
C27-C28	1.35(2)
C29-C30	1.37(2)
C29-C34	1.40(2)
C30-C31	1.38(2)
C31-C32	1.32(2)
C32-C33	1.35(2)
C33-C34	1.39(2)
C35-C36	1.54(2)
C35-C40	1.55(2)
C36-C37	1.55(2)
C37-C38	1.53(2)
C38-C39	1.51(2)
C39-C40	1.53(2)
C41-C46	1.55(2)
C41-C42	1.54(2)
C42-C43	1.54(2)
C43-C44	1.50(2)
C44-C45	1.49(2)
C45-C46	1.56(2)

Angles----------

C4-Pd1-C1	77.9(6)
C4-Pd1-P1	161.9(4)
C1-Pd1-P1	88.0(5)
C4-Pd1-P2	93.4(4)
C1-Pd1-P2	170.4(5)
P1-Pd1-P2	101.33(16)
C17-P1-C23	102.2(8)
C17-P1-C11	102.8(7)
C23-P1-C11	100.0(8)
C17-P1-Pd1	118.6(6)
C23-P1-Pd1	117.5(5)
C11-P1-Pd1	113.1(6)
C35-P2-C29	104.0(7)

C35-P2-C41	106.3(7)
C29-P2-C41	103.1(7)
C35-P2-Pd1	115.4(6)
C29-P2-Pd1	105.9(5)
C41-P2-Pd1	120.3(5)
C30-O1-C28	121.1(12)
C2-C1-Pd1	106.4(10)
C3-C2-C1	107.0(14)
C3-C2-C9	113.5(14)
C1-C2-C9	110.4(13)
C3-C2-C10	109.4(12)
C1-C2-C10	109.6(14)
C9-C2-C10	106.9(13)
C4-C3-C8	117.9(15)
C4-C3-C2	118.7(15)
C8-C3-C2	123.1(15)
C5-C4-C3	118.7(16)
C5-C4-Pd1	130.1(13)
C3-C4-Pd1	110.8(11)
C4-C5-C6	124.7(17)
C5-C6-C7	117.5(16)
C8-C7-C6	120.9(17)
C7-C8-C3	120.1(16)
C12-C11-C16	112.5(14)
C12-C11-P1	117.0(12)
C16-C11-P1	110.6(10)
C11-C12-C13	115.7(14)
C12-C13-C14	107.9(13)
C15-C14-C13	110.5(14)
C14-C15-C16	112.4(15)
C11-C16-C15	110.5(13)
C18-C17-C22	109.1(13)
C18-C17-P1	111.4(11)
C22-C17-P1	112.6(11)
C19-C18-C17	111.0(13)
C20-C19-C18	112.2(14)
C19-C20-C21	109.0(14)
C22-C21-C20	112.7(13)

C21-C22-C17	111.5(14)
C28-C23-C24	115.7(15)
C28-C23-P1	120.2(13)
C24-C23-P1	124.1(12)
C25-C24-C23	119.6(15)
C26-C25-C24	120.5(16)
C25-C26-C27	122.2(17)
C28-C27-C26	116.4(16)
C27-C28-C23	125.5(16)
C27-C28-O1	119.1(14)
C23-C28-O1	115.2(14)
C30-C29-C34	116.6(14)
C30-C29-P2	119.4(12)
C34-C29-P2	123.8(12)
C29-C30-O1	118.9(14)
C29-C30-C31	122.1(15)
O1-C30-C31	118.5(14)
C32-C31-C30	118.3(16)
C31-C32-C33	123.8(16)
C32-C33-C34	117.9(15)
C33-C34-C29	121.2(15)
C36-C35-C40	108.3(12)
C36-C35-P2	111.8(10)
C40-C35-P2	119.9(12)
C37-C36-C35	110.5(13)
C38-C37-C36	113.4(14)
C39-C38-C37	110.3(13)
C38-C39-C40	112.3(13)
C39-C40-C35	109.2(14)
C46-C41-C42	110.8(13)
C46-C41-P2	111.4(11)
C42-C41-P2	116.3(11)
C41-C42-C43	110.8(13)
C44-C43-C42	111.9(14)
C45-C44-C43	112.9(13)
C44-C45-C46	113.2(14)
C41-C46-C45	108.2(14)

Table 3. Torsion angles [°] for **XLVII-DCEphos**.

Pd1-C1-C2-C3	-44.8(14)
Pd1-C1-C2-C9	-168.8(10)
Pd1-C1-C2-C10	73.7(13)
C1-C2-C3-C4	28.9(19)
C9-C2-C3-C4	151.0(15)
C10-C2-C3-C4	-89.7(18)
C1-C2-C3-C8	-145.0(15)
C9-C2-C3-C8	-23(2)
C10-C2-C3-C8	96.4(18)
C8-C3-C4-C5	3(2)
C2-C3-C4-C5	-171.3(14)
C8-C3-C4-Pd1	177.1(11)
C2-C3-C4-Pd1	2.8(18)
C3-C4-C5-C6	-1(2)
Pd1-C4-C5-C6	-173.4(12)
C4-C5-C6-C7	-4(2)
C5-C6-C7-C8	5(2)
C6-C7-C8-C3	-3(2)
C4-C3-C8-C7	-1(2)
C2-C3-C8-C7	172.8(15)
C17-P1-C11-C12	48.2(15)
C23-P1-C11-C12	-57.0(14)
Pd1-P1-C11-C12	177.3(11)
C17-P1-C11-C16	178.7(13)
C23-P1-C11-C16	73.5(14)
Pd1-P1-C11-C16	-52.2(14)
C16-C11-C12-C13	53(2)
P1-C11-C12-C13	-177.8(12)
C11-C12-C13-C14	-53(2)
C12-C13-C14-C15	54.8(19)
C13-C14-C15-C16	-58.7(19)
C12-C11-C16-C15	-51(2)
P1-C11-C16-C15	176.0(12)
C14-C15-C16-C11	55(2)
C23-P1-C17-C18	-68.9(13)
C11-P1-C17-C18	-172.3(12)

Pd1-P1-C17-C18	62.1(13)
C23-P1-C17-C22	168.1(11)
C11-P1-C17-C22	64.7(13)
Pd1-P1-C17-C22	-60.9(12)
C22-C17-C18-C19	-55.2(19)
P1-C17-C18-C19	179.8(12)
C17-C18-C19-C20	58.4(19)
C18-C19-C20-C21	-57.2(18)
C19-C20-C21-C22	56.2(19)
C20-C21-C22-C17	-56(2)
C18-C17-C22-C21	54.3(18)
P1-C17-C22-C21	178.5(11)
C17-P1-C23-C28	160.6(13)
C11-P1-C23-C28	-93.8(13)
Pd1-P1-C23-C28	28.9(14)
C17-P1-C23-C24	-16.3(15)
C11-P1-C23-C24	89.3(14)
Pd1-P1-C23-C24	-148.0(11)
C28-C23-C24-C25	-2(2)
P1-C23-C24-C25	175.2(12)
C23-C24-C25-C26	0(2)
C24-C25-C26-C27	2(2)
C25-C26-C27-C28	-2(2)
C26-C27-C28-C23	0(2)
C26-C27-C28-O1	176.8(13)
C24-C23-C28-C27	2(2)
P1-C23-C28-C27	-175.6(13)
C24-C23-C28-O1	-175.1(13)
P1-C23-C28-O1	7.7(19)
C30-O1-C28-C27	36(2)
C30-O1-C28-C23	-147.1(14)
C35-P2-C29-C30	171.7(13)
C41-P2-C29-C30	-77.5(14)
Pd1-P2-C29-C30	49.7(14)
C35-P2-C29-C34	-3.7(16)
C41-P2-C29-C34	107.1(14)
Pd1-P2-C29-C34	-125.8(13)
C34-C29-C30-O1	171.6(13)

P2-C29-C30-O1	-4(2)
C34-C29-C30-C31	0(2)
P2-C29-C30-C31	-176.1(12)
C28-O1-C30-C29	90.4(18)
C28-O1-C30-C31	-97.5(17)
C29-C30-C31-C32	1(2)
O1-C30-C31-C32	-170.7(14)
C30-C31-C32-C33	-2(3)
C31-C32-C33-C34	3(3)
C32-C33-C34-C29	-2(2)
C30-C29-C34-C33	1(2)
P2-C29-C34-C33	176.1(12)
C29-P2-C35-C36	-163.2(11)
C41-P2-C35-C36	88.4(12)
Pd1-P2-C35-C36	-47.7(13)
C29-P2-C35-C40	68.5(14)
C41-P2-C35-C40	-39.9(14)
Pd1-P2-C35-C40	-176.0(10)
C40-C35-C36-C37	-57.9(17)
P2-C35-C36-C37	167.9(11)
C35-C36-C37-C38	54.5(18)
C36-C37-C38-C39	-51.6(18)
C37-C38-C39-C40	54.8(18)
C38-C39-C40-C35	-60.5(17)
C36-C35-C40-C39	60.9(17)
P2-C35-C40-C39	-169.2(11)
C35-P2-C41-C46	-51.1(12)
C29-P2-C41-C46	-160.1(11)
Pd1-P2-C41-C46	82.4(11)
C35-P2-C41-C42	77.2(13)
C29-P2-C41-C42	-31.9(14)
Pd1-P2-C41-C42	-149.3(10)
C46-C41-C42-C43	-57.1(18)
P2-C41-C42-C43	174.4(11)
C41-C42-C43-C44	53.5(18)
C42-C43-C44-C45	-52.3(19)
C43-C44-C45-C46	54.5(19)
C42-C41-C46-C45	57.0(17)

P2-C41-C46-C45	-171.8(10)
C44-C45-C46-C41	-56.1(17)

6.1.7. ^{1}H and ^{13}C NMR Spectra.

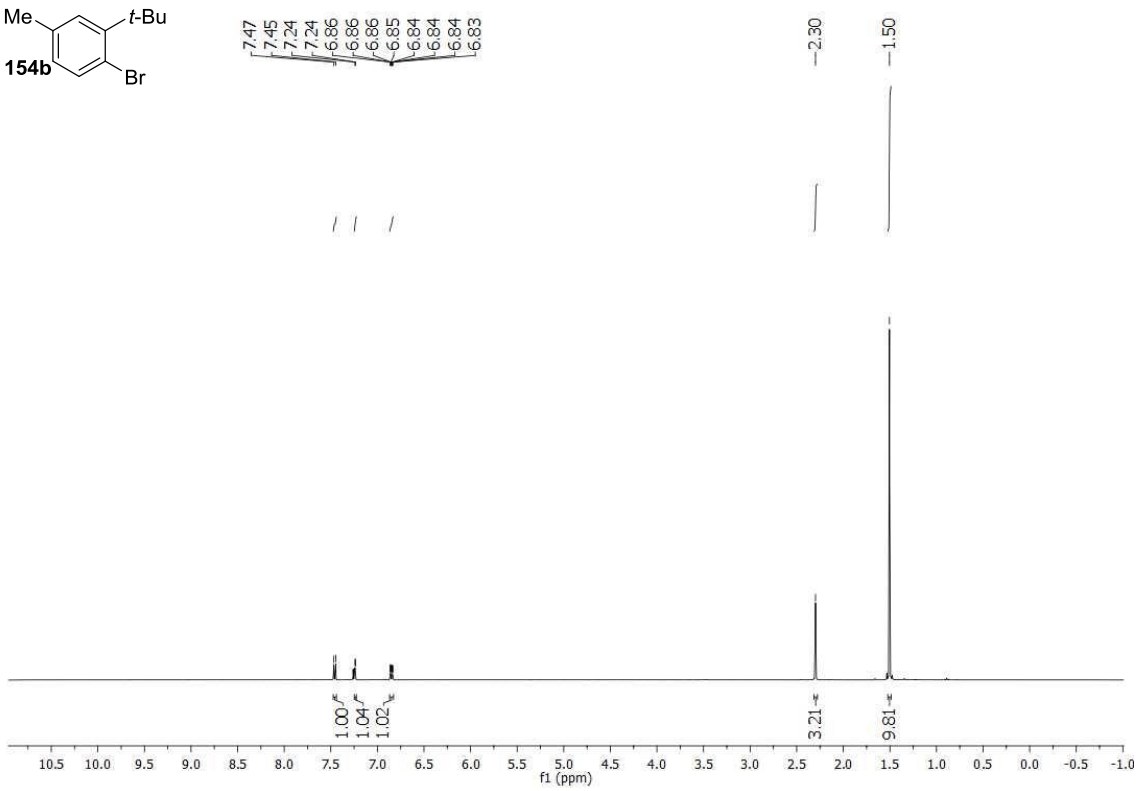
Me
t-Bu
154b
Br
7.47
7.45
7.24
7.24
6.86
6.86
6.86
6.85
6.84
6.84
6.84
6.83
2.30
1.50
1.00
1.04
1.02
3.21
9.81
f1 (ppm)

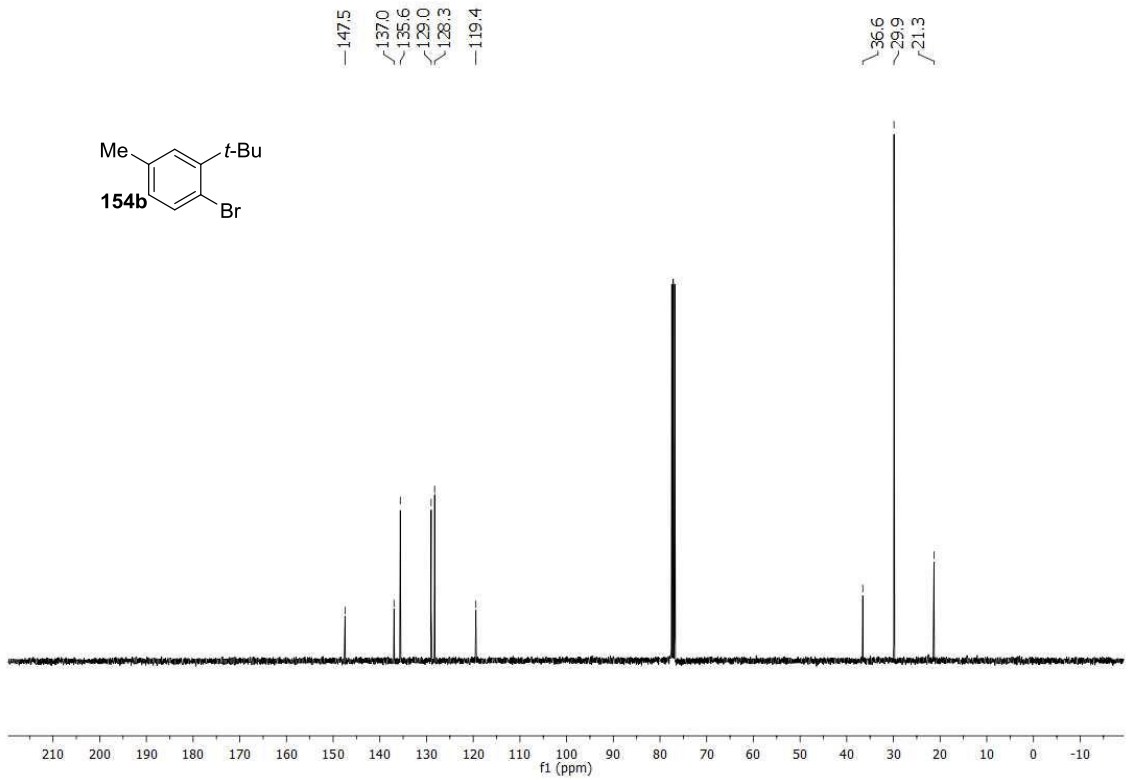
147.5
137.0
135.6
129.0
128.3
119.4
36.6
29.9
21.3
Me
t-Bu
154b
Br
f1 (ppm)

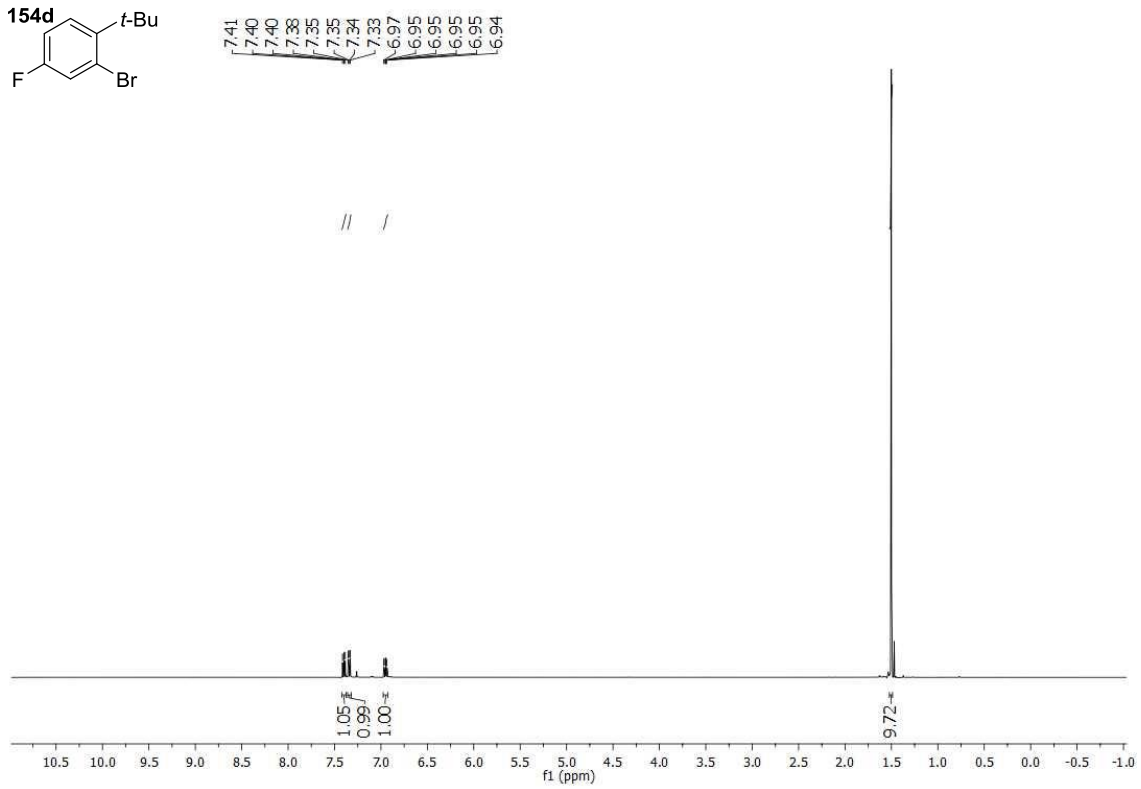
154d
t-Bu
F
Br
7.41
7.40
7.40
7.38
7.35
7.35
7.34
7.33
6.97
6.95
6.95
6.95
6.95
6.94
1.05
0.99
1.00
9.72
f1 (ppm)

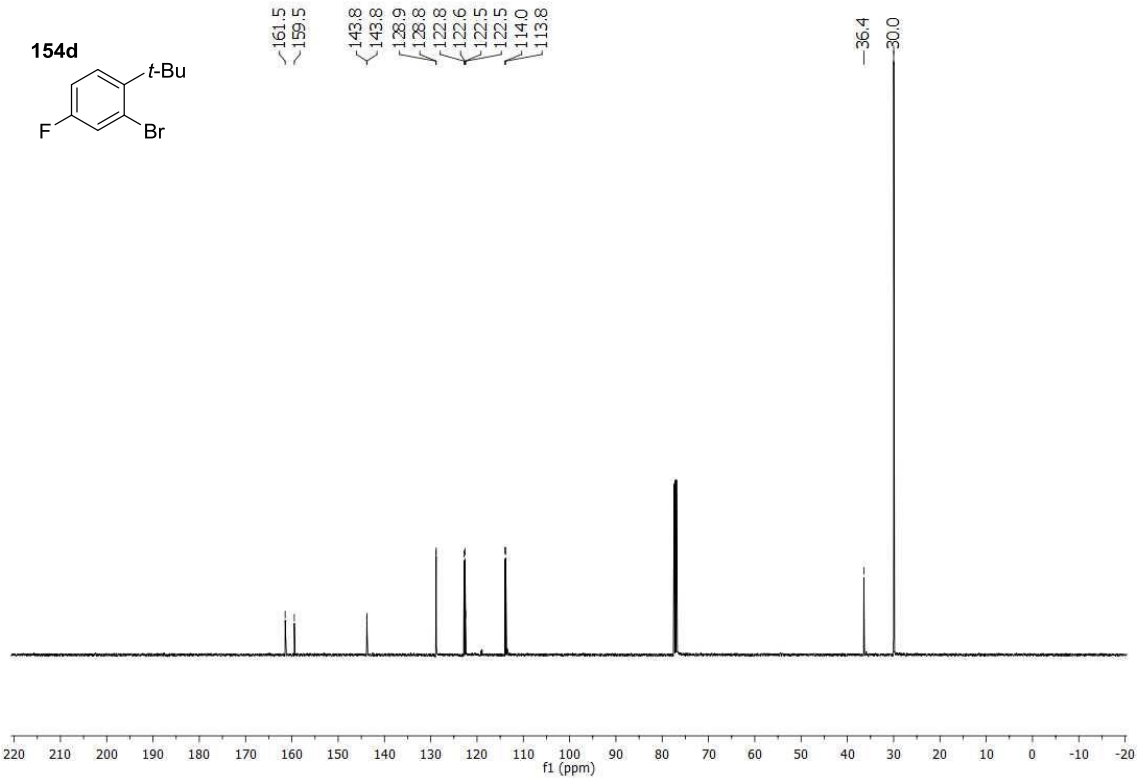
154d
t-Bu
F
Br
161.5
159.5
143.8
143.8
128.9
128.8
122.8
122.6
122.5
122.5
114.0
113.8
36.4
30.0
f1 (ppm)

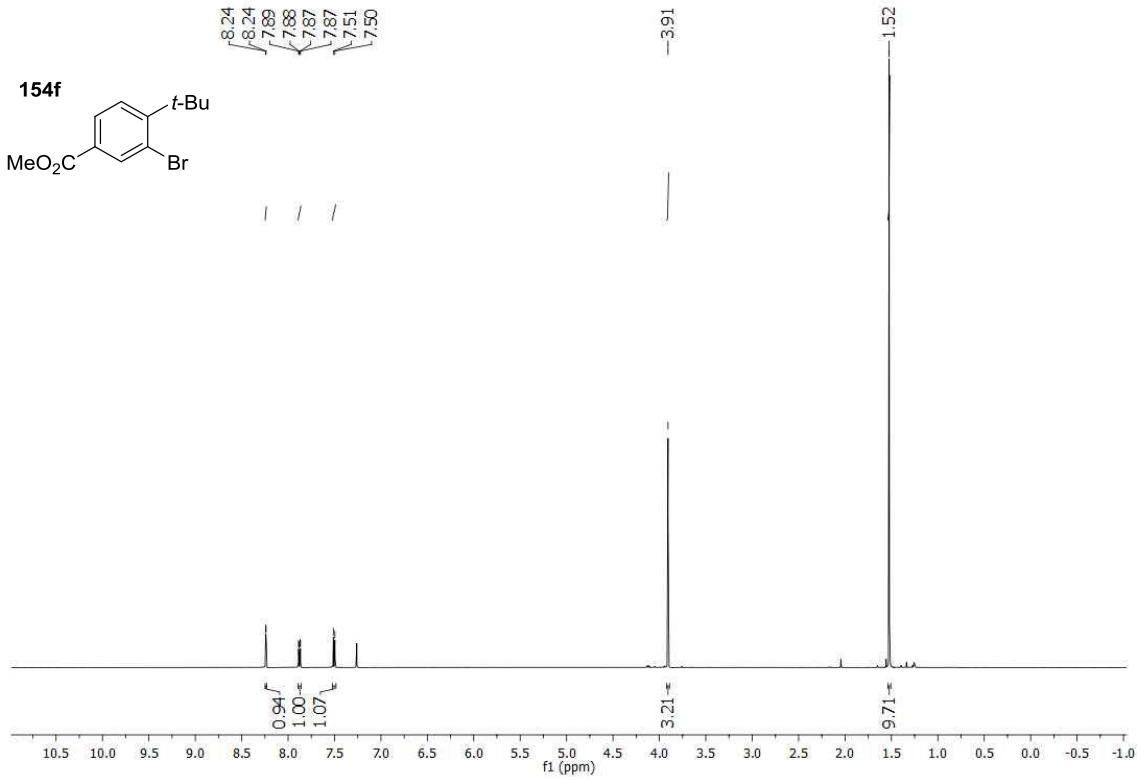
154f
t-Bu
MeO2C
Br
8.24
8.24
7.89
7.88
7.87
7.87
7.51
7.50
3.91
1.52
0.94
1.00
1.07
3.21
9.71
f1 (ppm)

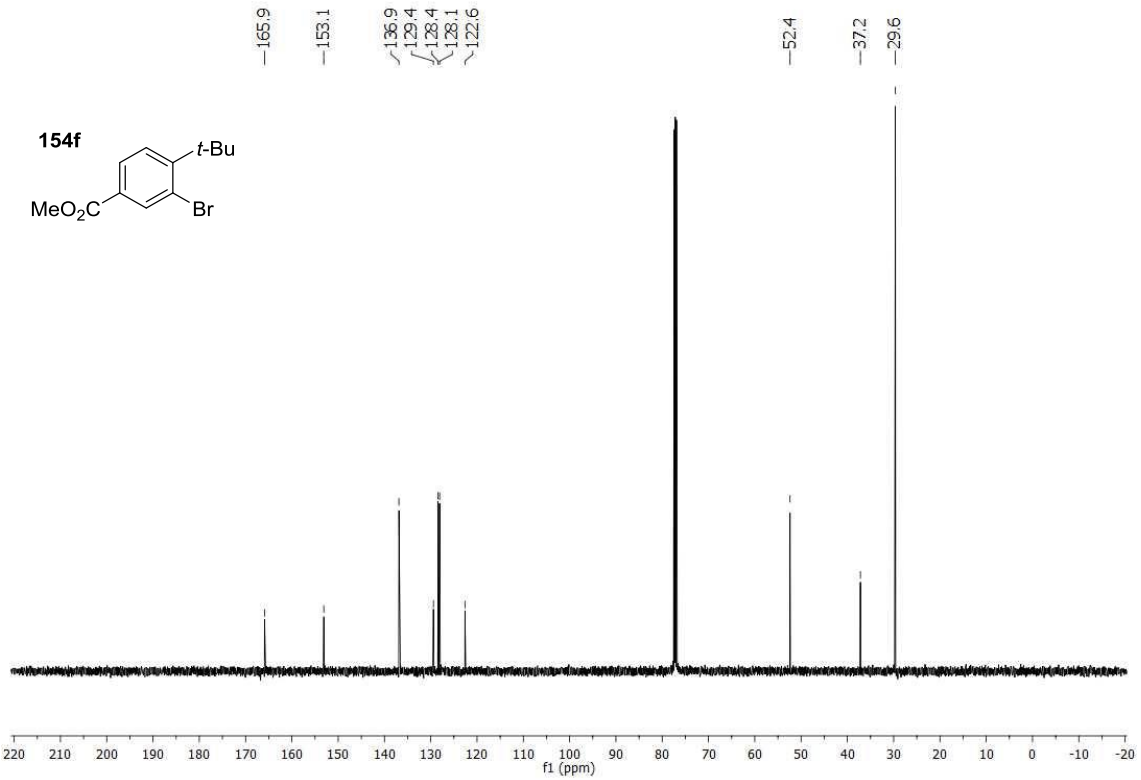
154f
t-Bu
MeO2C
Br
165.9
153.1
136.9
129.4
128.4
128.1
122.6
52.4
37.2
29.6
f1 (ppm)

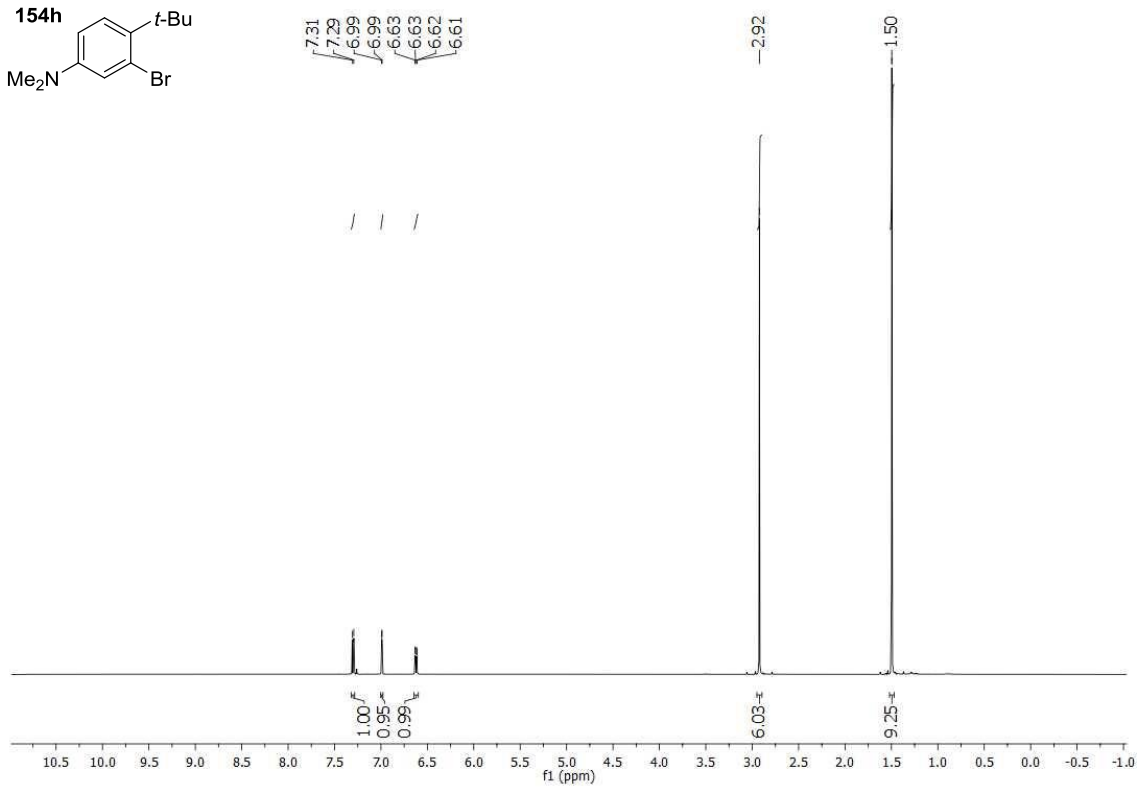
154h
t-Bu
Me2N
Br
7.31
7.29
6.99
6.99
6.63
6.63
6.62
6.61
2.92
1.50
1.00
0.95
0.99
6.03
9.25
f1 (ppm)

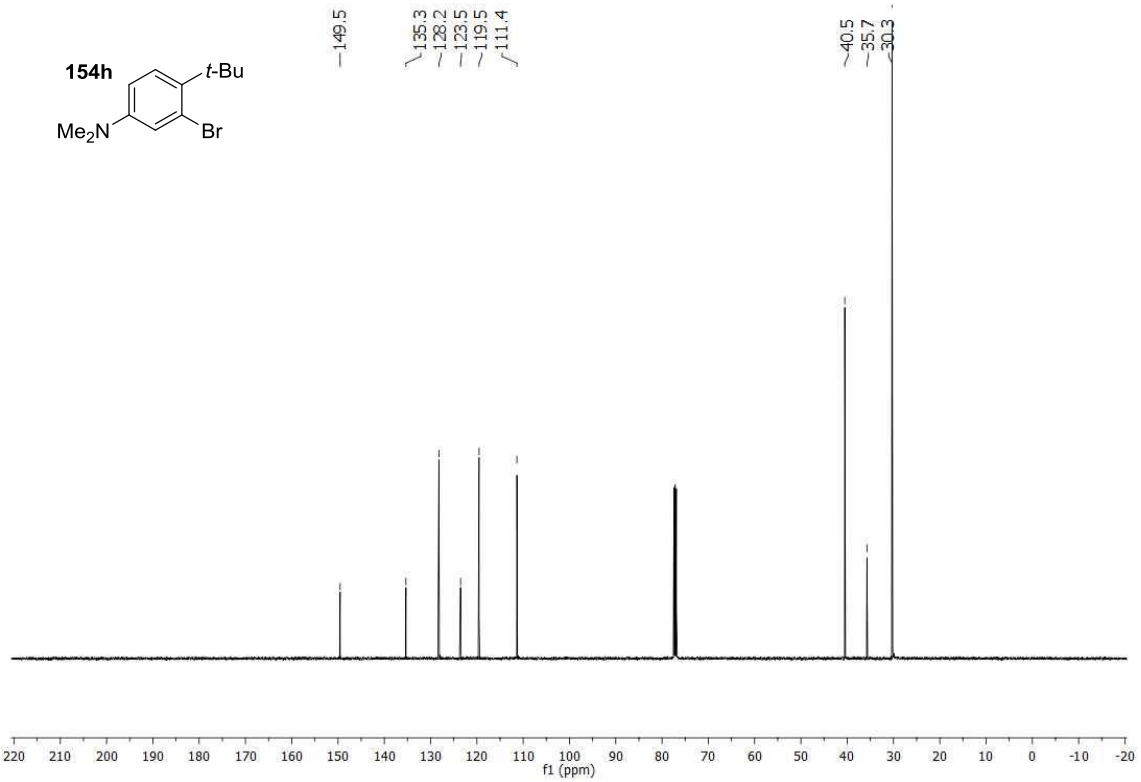
154h
t-Bu
Me2N
Br
149.5
135.3
128.2
123.5
119.5
111.4
40.5
35.7
30.3
f1 (ppm)

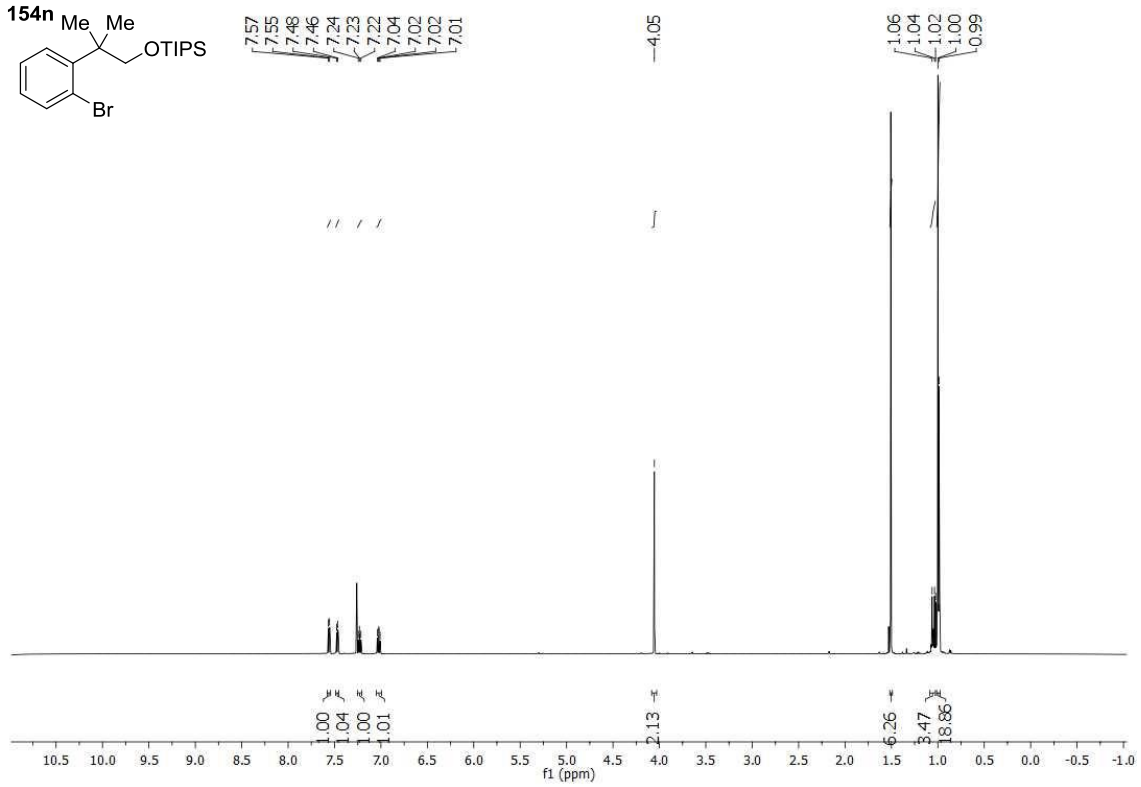
154n
Me
Me
OTIPS
Br
7.57
7.55
7.48
7.46
7.24
7.23
7.22
7.04
7.02
7.02
7.01
4.05
1.06
1.04
1.02
1.00
0.99
1.00
1.04
1.00
1.01
2.13
6.26
3.47
18.86
f1 (ppm)

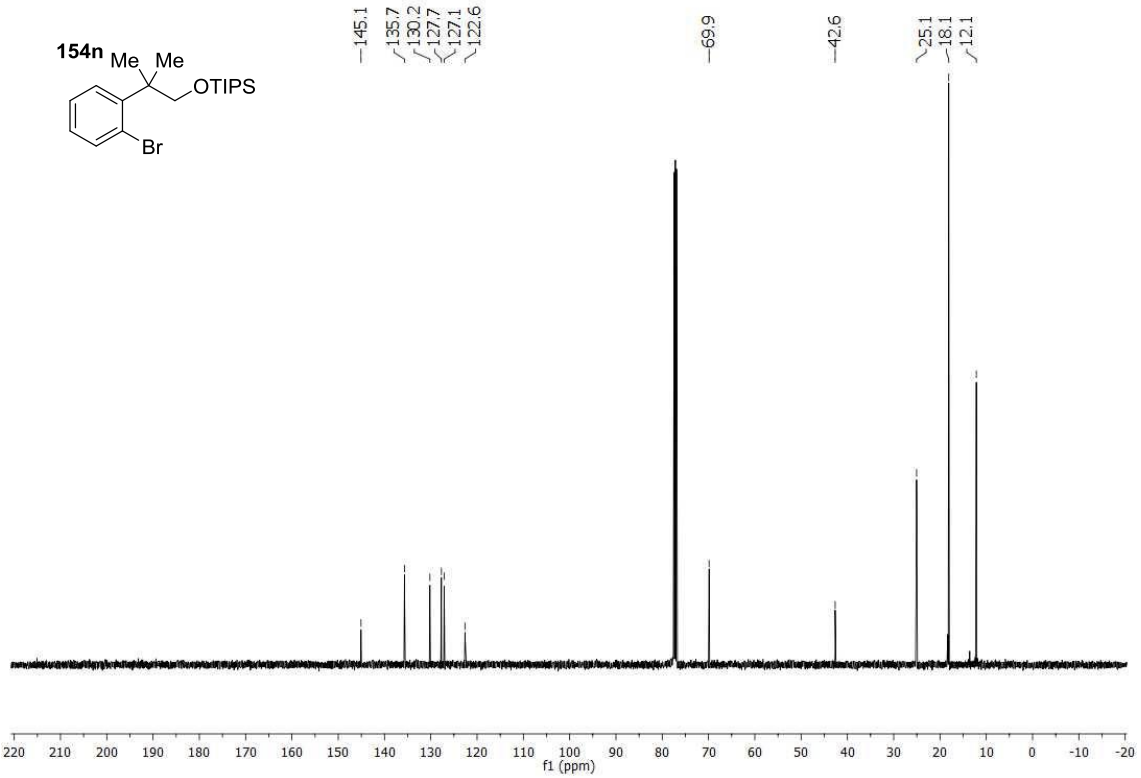
154n
Me
Me
OTIPS
Br
145.1
135.7
130.2
127.7
127.1
122.6
69.9
42.6
25.1
18.1
12.1
f1 (ppm)

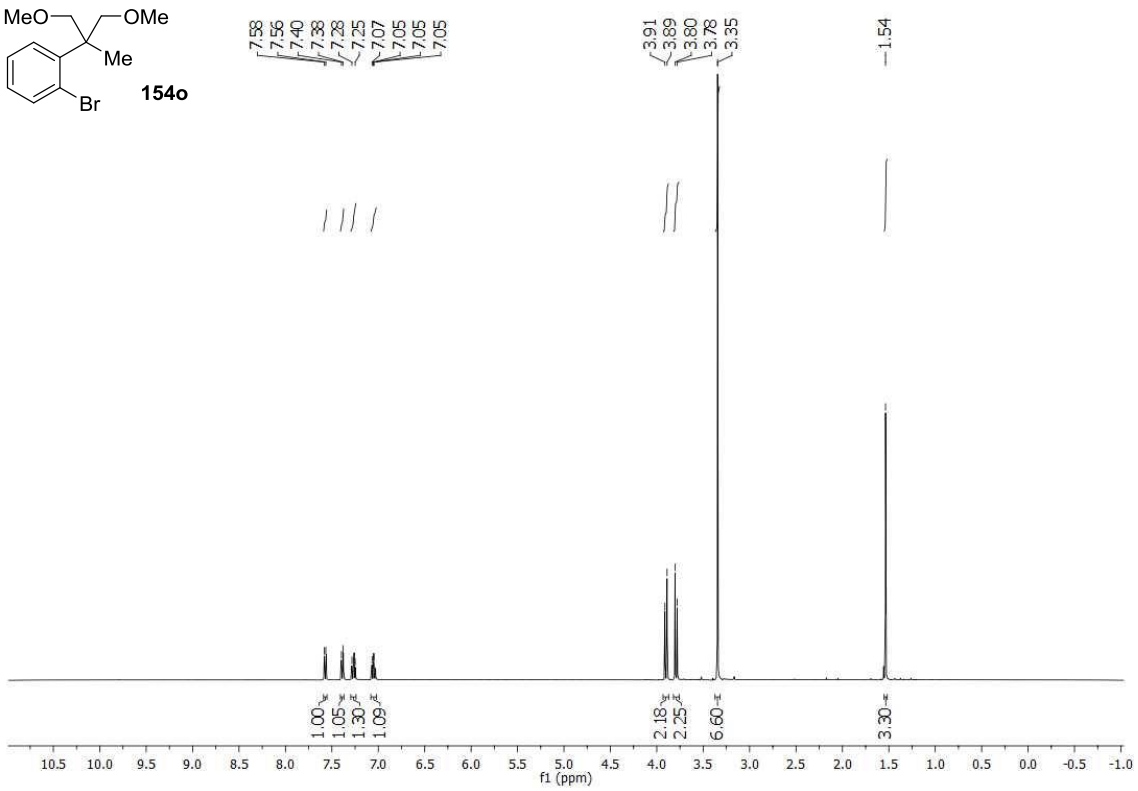
MeO
OMe
Me
Br
154o
7.58
7.56
7.40
7.38
7.28
7.25
7.07
7.05
7.05
7.05
3.91
3.89
3.80
3.78
3.35
1.54
1.00
1.05
1.30
1.09
2.18
2.25
6.60
3.30
f1 (ppm)

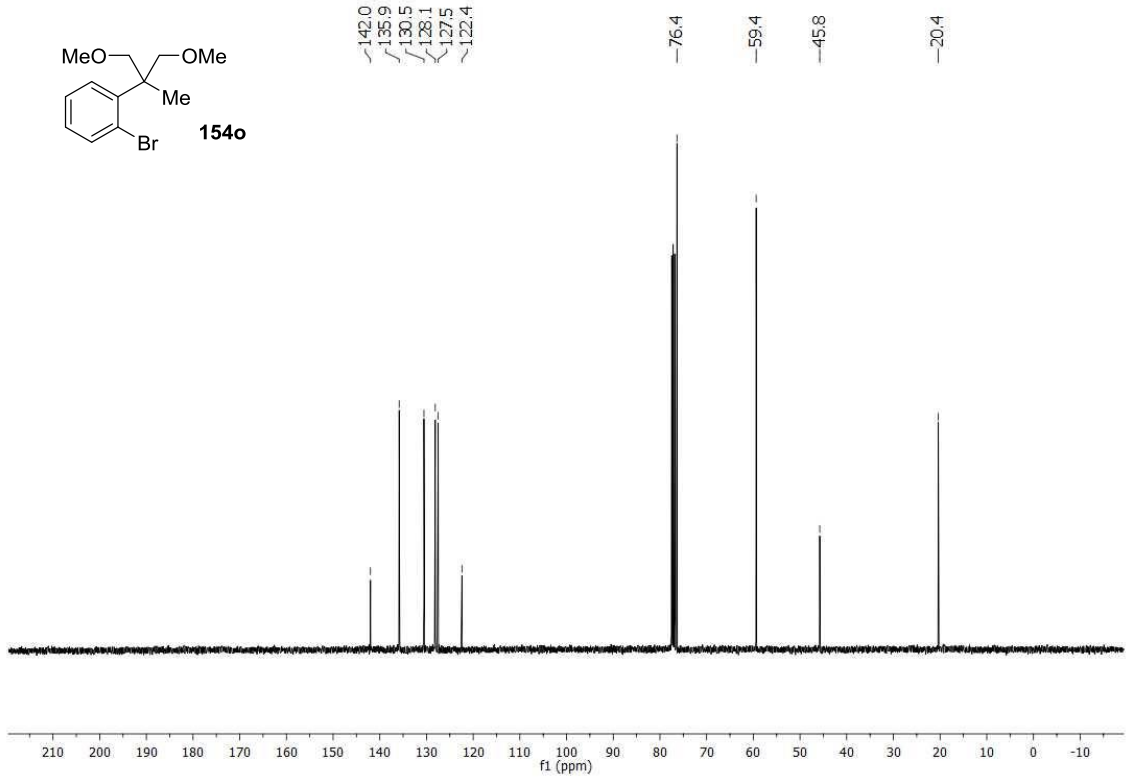
MeO
OMe
Me
Br
154o
142.0
135.9
130.5
128.1
127.5
122.4
76.4
59.4
45.8
20.4
f1 (ppm)

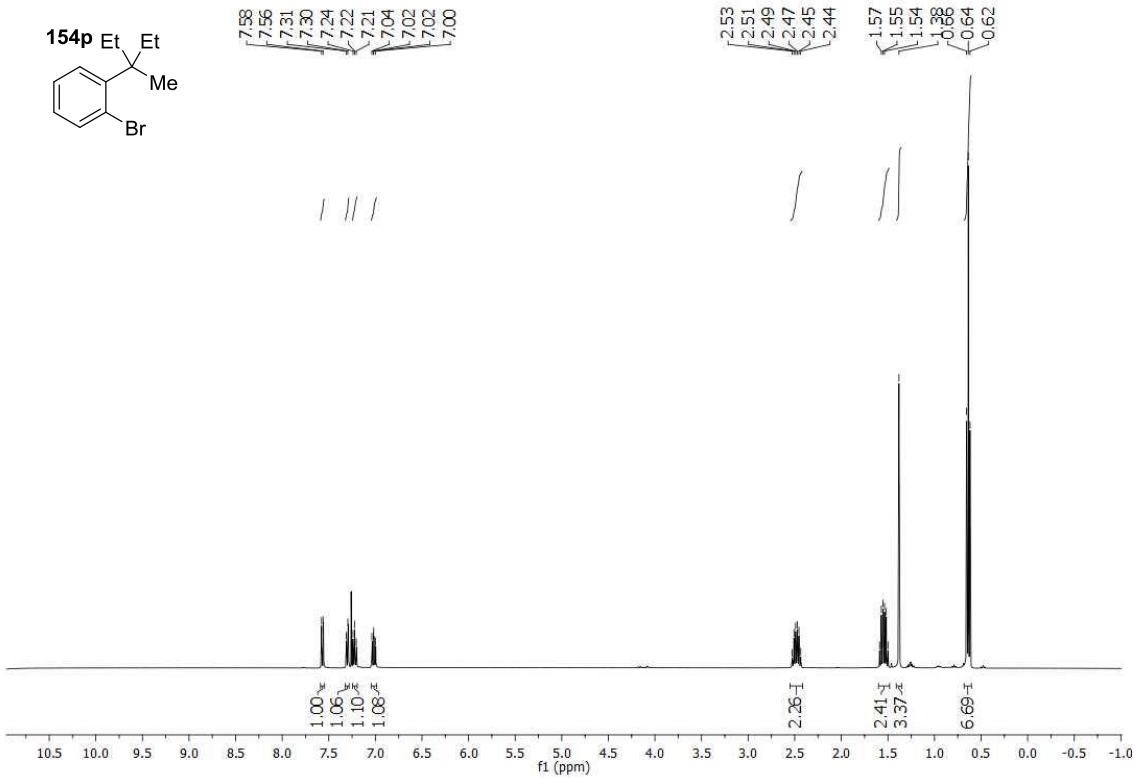
154p
Et
Et
Me
Br
7.58
7.56
7.31
7.30
7.24
7.22
7.21
7.04
7.02
7.02
7.00
2.53
2.51
2.49
2.47
2.45
2.44
1.57
1.55
1.54
1.38
0.66
0.64
0.62
1.00
1.06
1.10
1.08
2.26
2.41
3.37
6.69
f1 (ppm)

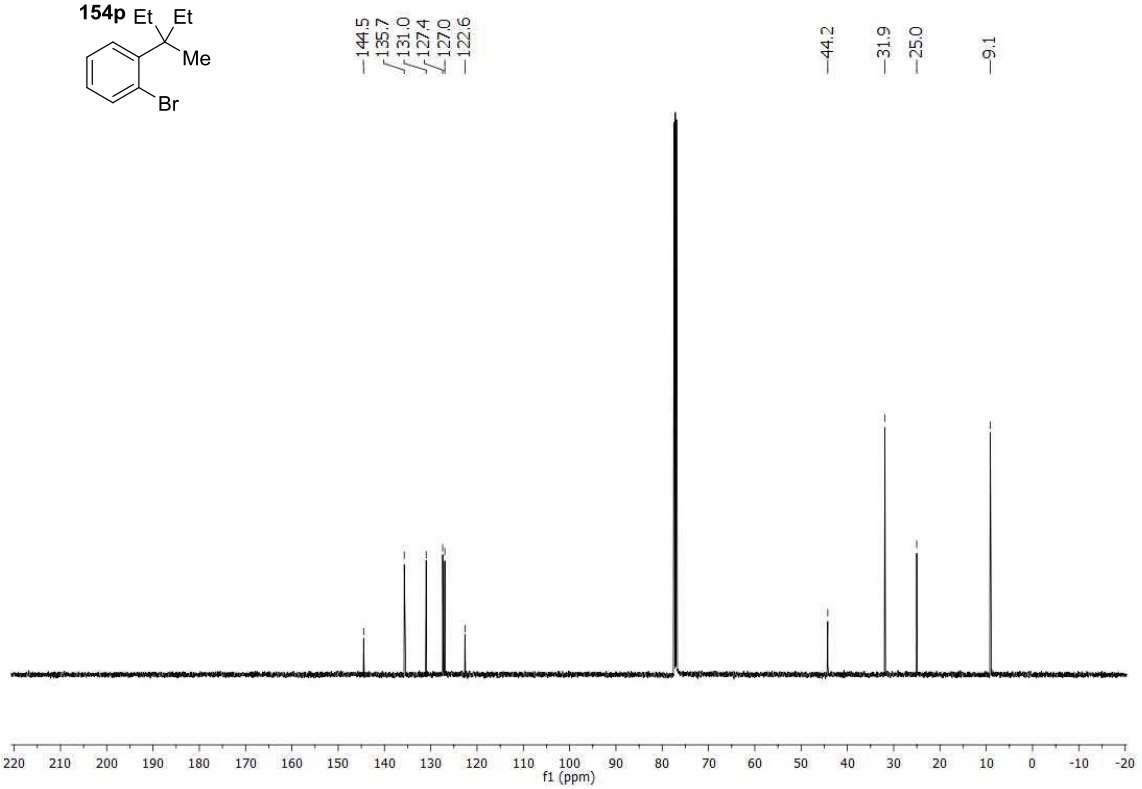
154p
Et
Et
Me
Br
144.5
135.7
131.0
127.4
127.0
122.6
44.2
31.9
25.0
9.1
f1 (ppm)

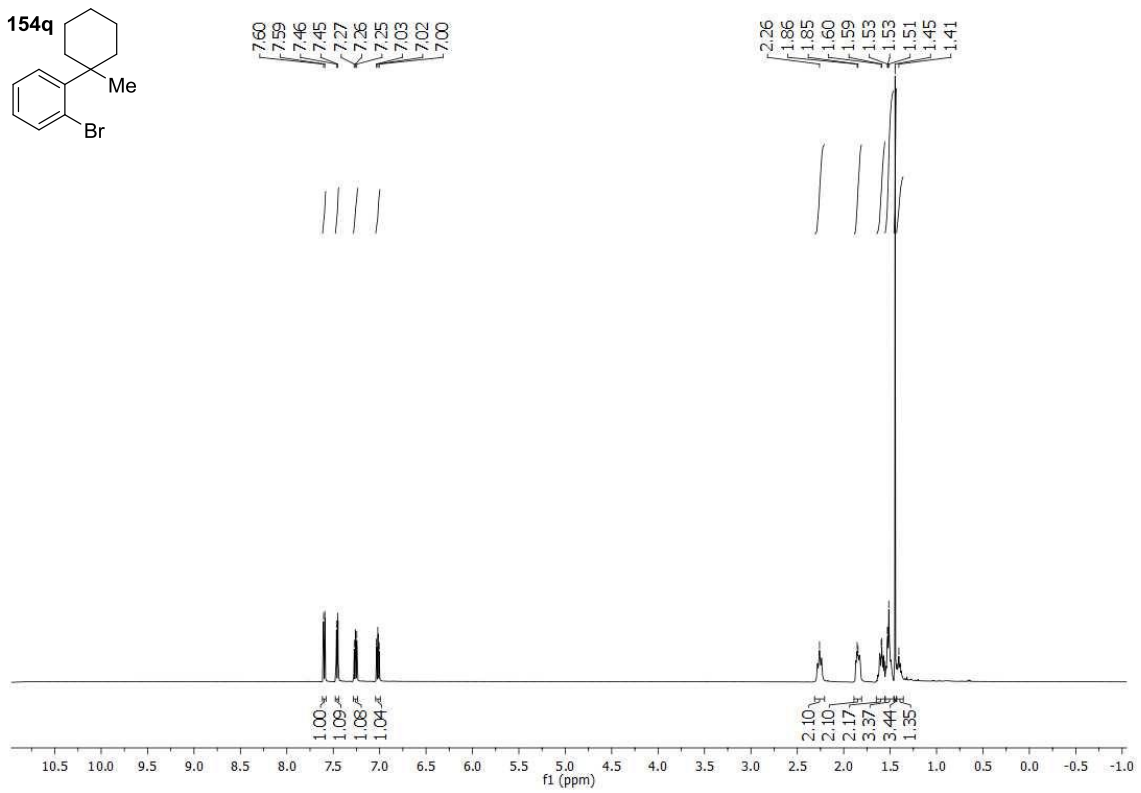
154q
Me
Br
7.60
7.59
7.46
7.45
7.27
7.26
7.25
7.03
7.02
7.00
2.26
1.86
1.85
1.60
1.59
1.53
1.53
1.51
1.45
1.41
1.00
1.09
1.08
1.04
2.10
2.10
2.17
3.37
3.44
1.35
f1 (ppm)

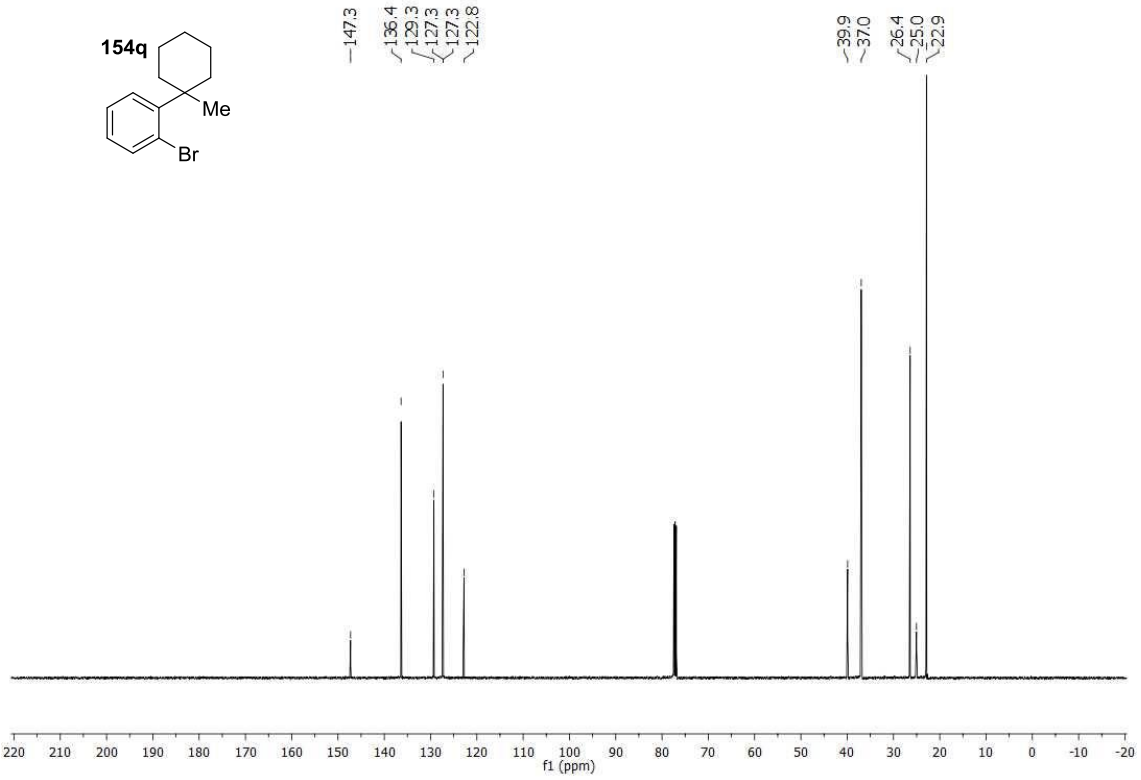
154q
Me
Br
147.3
136.4
129.3
127.3
127.3
122.8
39.9
37.0
26.4
25.0
22.9
f1 (ppm)

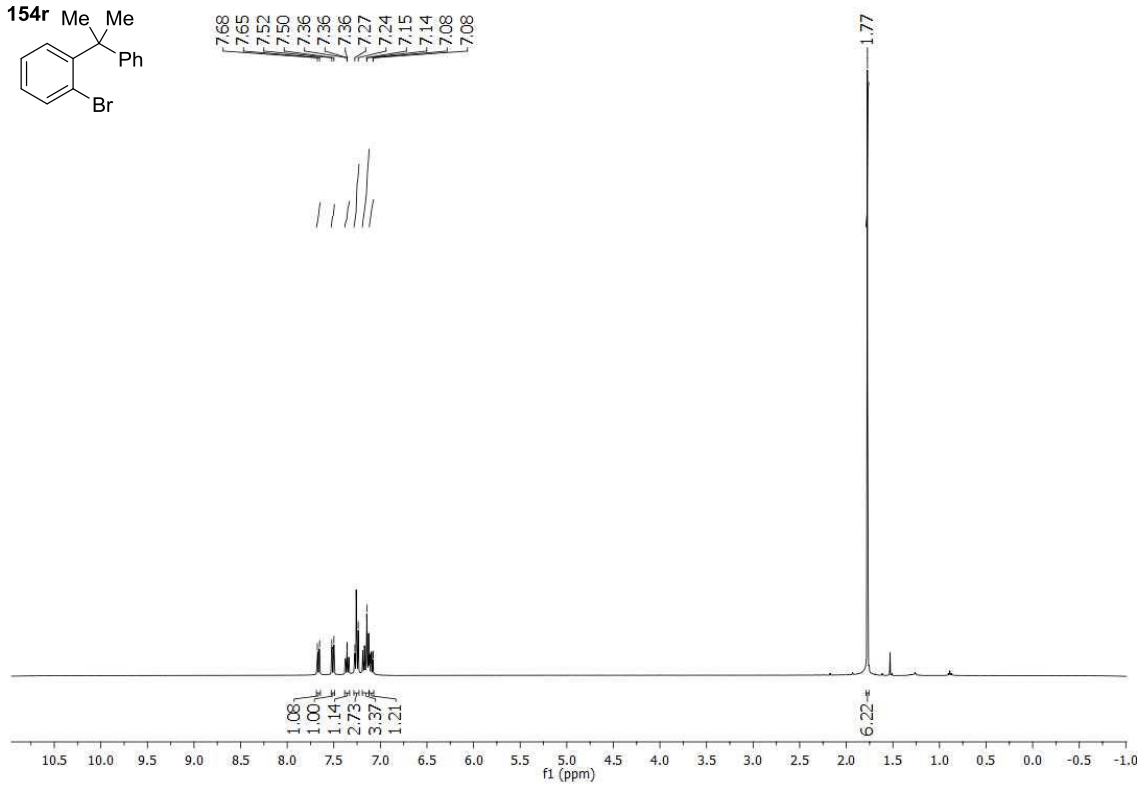
154r
Me
Me
Ph
Br
7.68
7.65
7.52
7.50
7.36
7.36
7.36
7.27
7.24
7.15
7.14
7.08
7.08
1.77
1.08
1.00
1.14
2.73
3.37
1.21
6.22
f1 (ppm)

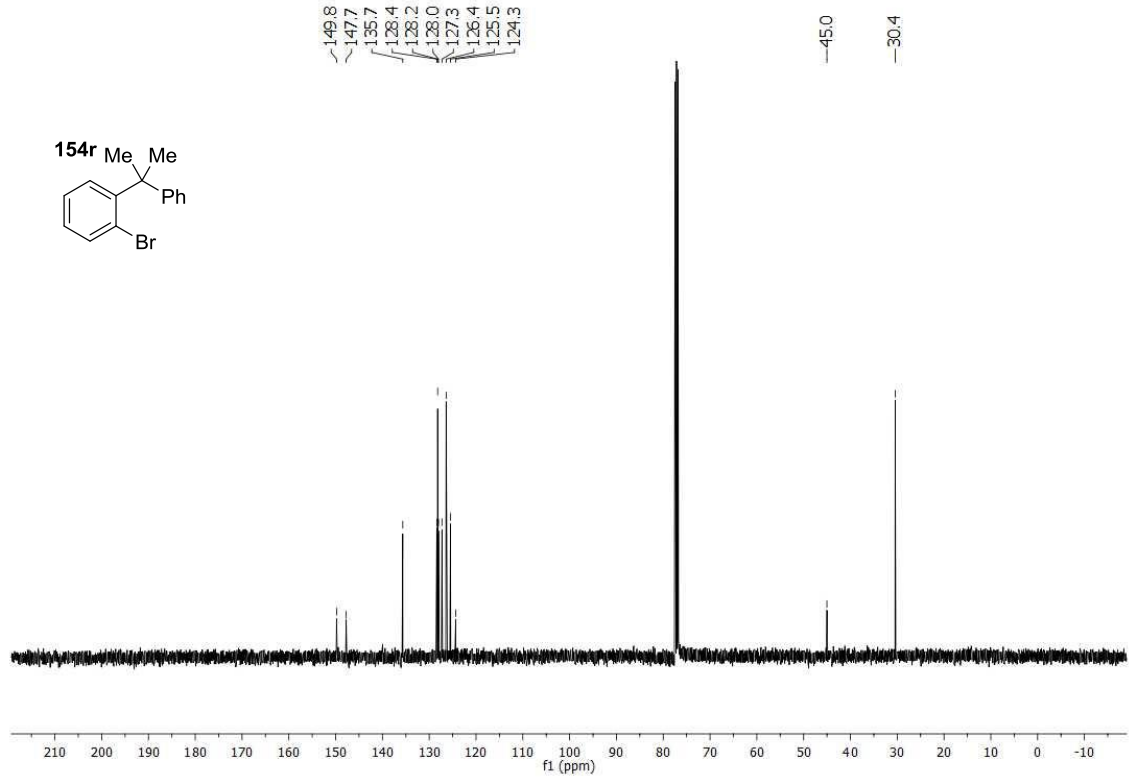
154r
Me
Me
Ph
Br
149.8
147.7
135.7
128.4
128.2
128.0
127.3
126.4
125.5
124.3
45.0
30.4
f1 (ppm)

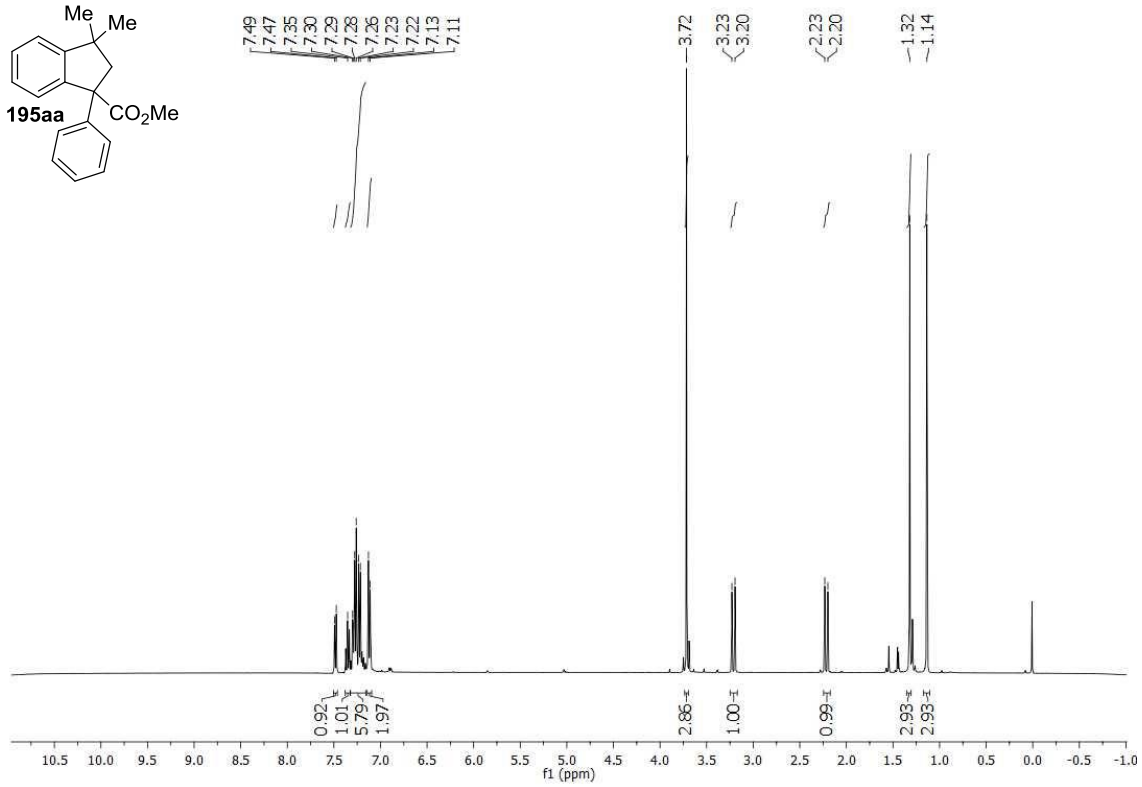
Me
Me
195aa
CO2Me
7.49
7.47
7.35
7.30
7.29
7.28
7.26
7.23
7.22
7.13
7.11
3.72
3.23
3.20
2.23
2.20
1.32
1.14
0.92
1.01
5.79
1.97
2.86
1.00
0.99
2.93
2.93
f1 (ppm)

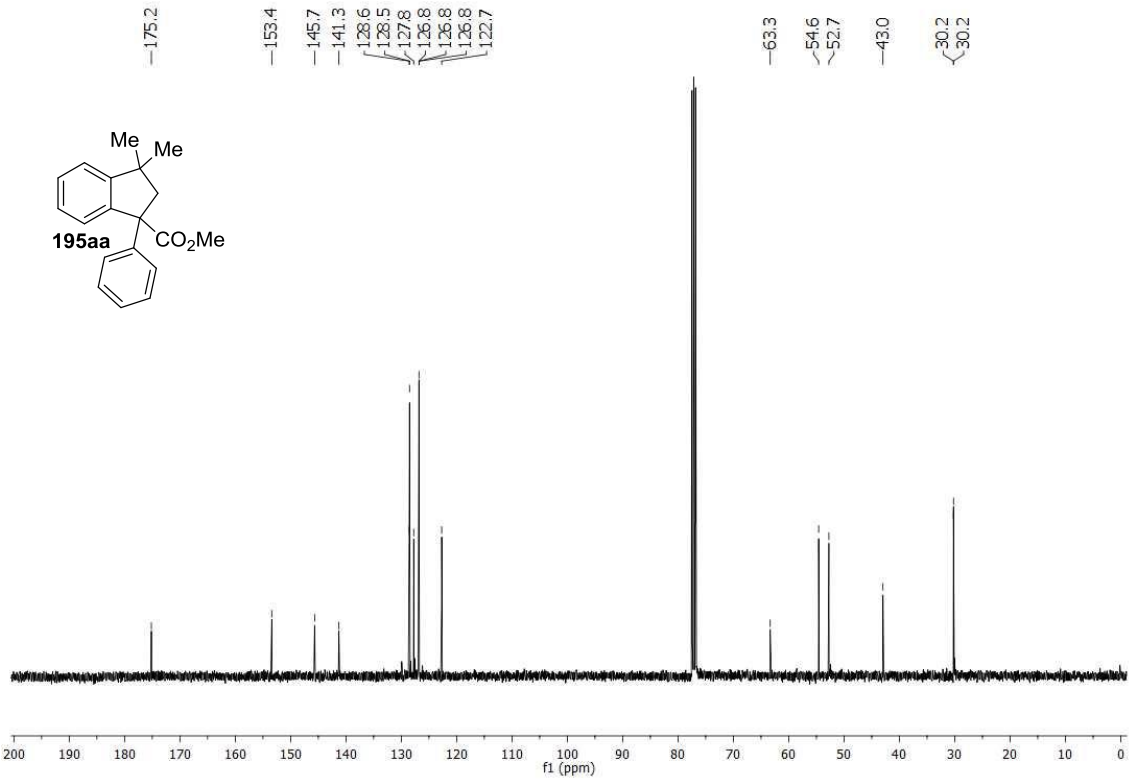
175.2
153.4
145.7
141.3
128.6
128.5
127.8
126.8
126.8
126.8
122.7
63.3
54.6
52.7
43.0
30.2
30.2
Me
Me
195aa
CO2Me
f1 (ppm)

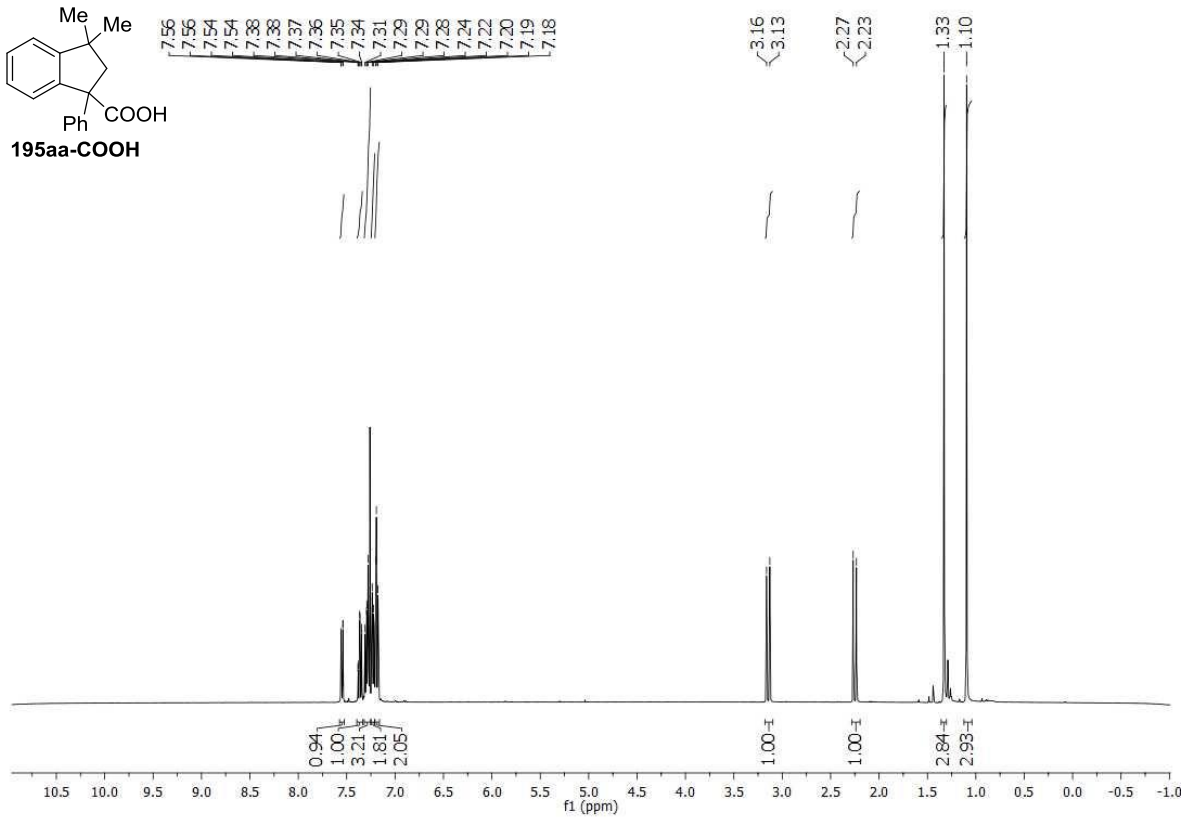
Me
Me
Ph
COOH
195aa-COOH
7.56
7.55
7.54
7.54
7.38
7.38
7.37
7.36
7.35
7.34
7.31
7.29
7.29
7.28
7.24
7.22
7.20
7.19
7.18
3.16
3.13
2.27
2.23
1.33
1.10
0.94
1.00
3.21
1.81
2.05
1.00
1.00
2.84
2.93
f1 (ppm)

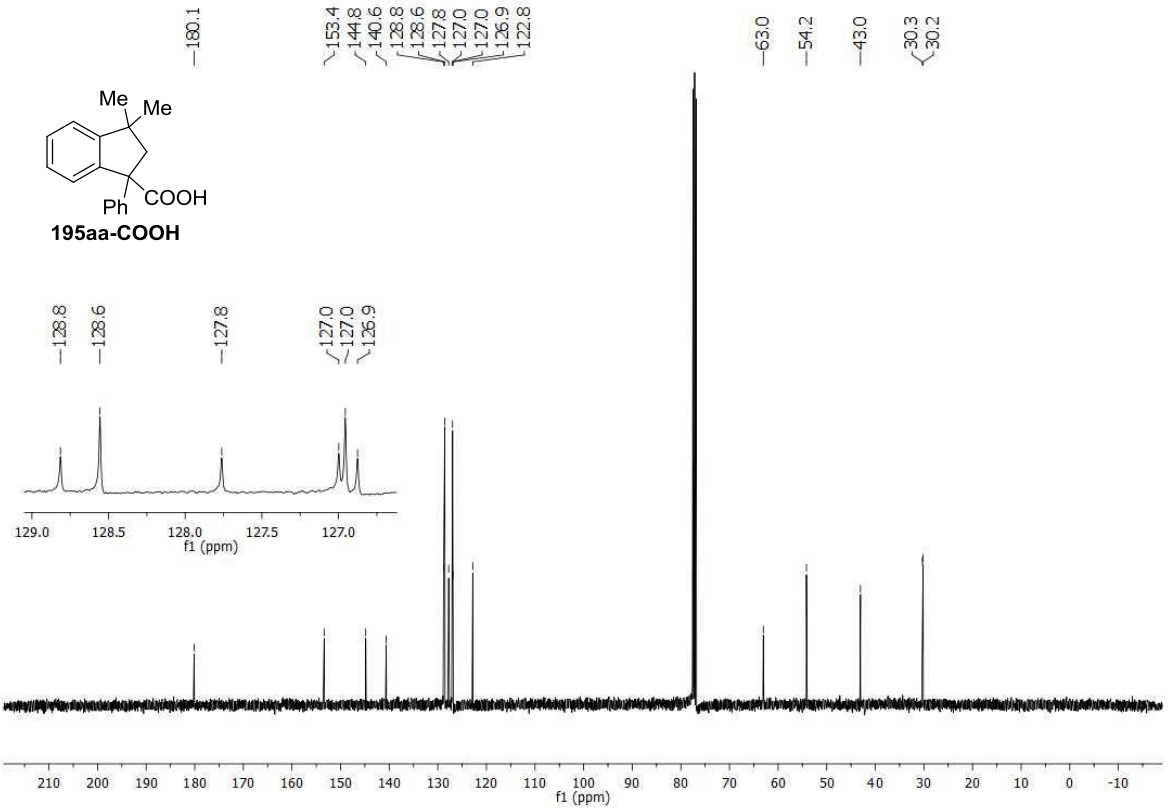
180.1
153.4
144.8
140.6
128.8
128.6
127.8
127.0
127.0
126.9
122.8
63.0
54.2
43.0
30.3
30.2
Me
Me
Ph
COOH
195aa-COOH
128.8
128.6
127.8
127.0
127.0
126.9
f1 (ppm)

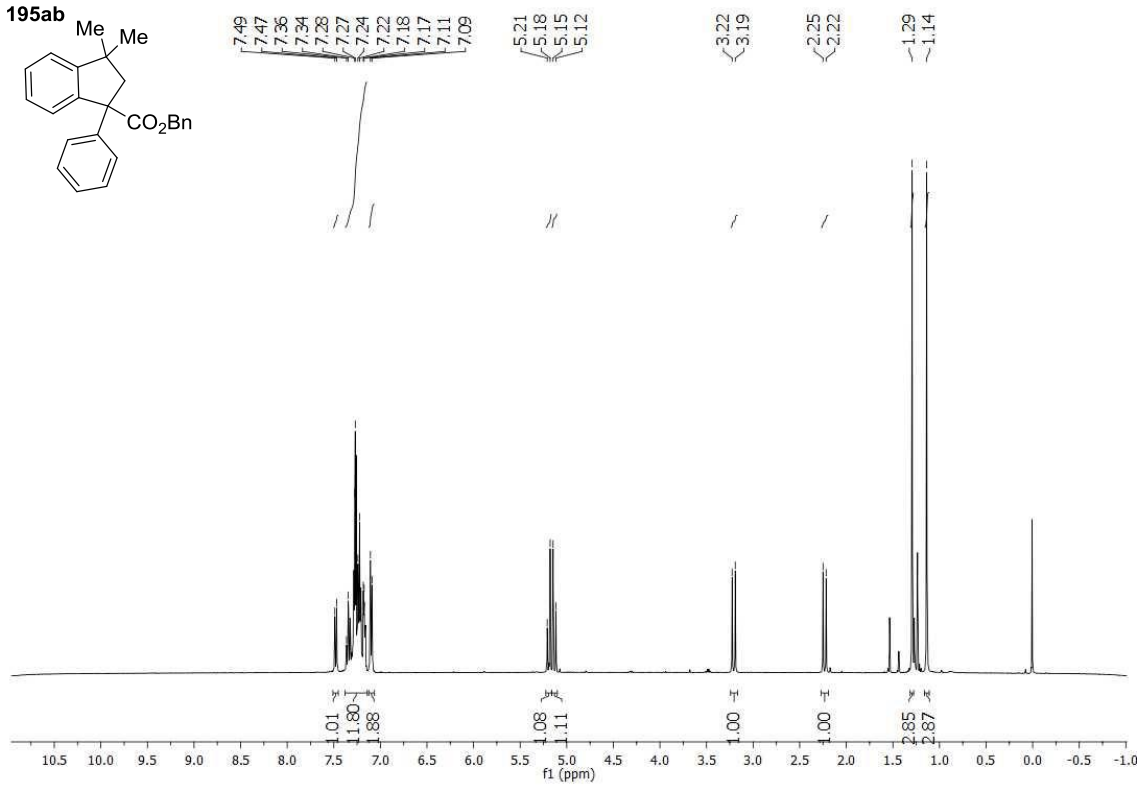
195ab
Me
Me
CO2Bn
7.49
7.47
7.36
7.34
7.28
7.27
7.24
7.22
7.18
7.17
7.11
7.09
5.21
5.18
5.15
5.12
3.22
3.19
2.25
2.22
1.29
1.14
1.01
11.80
1.88
1.08
1.11
1.00
1.00
2.85
2.87
f1 (ppm)

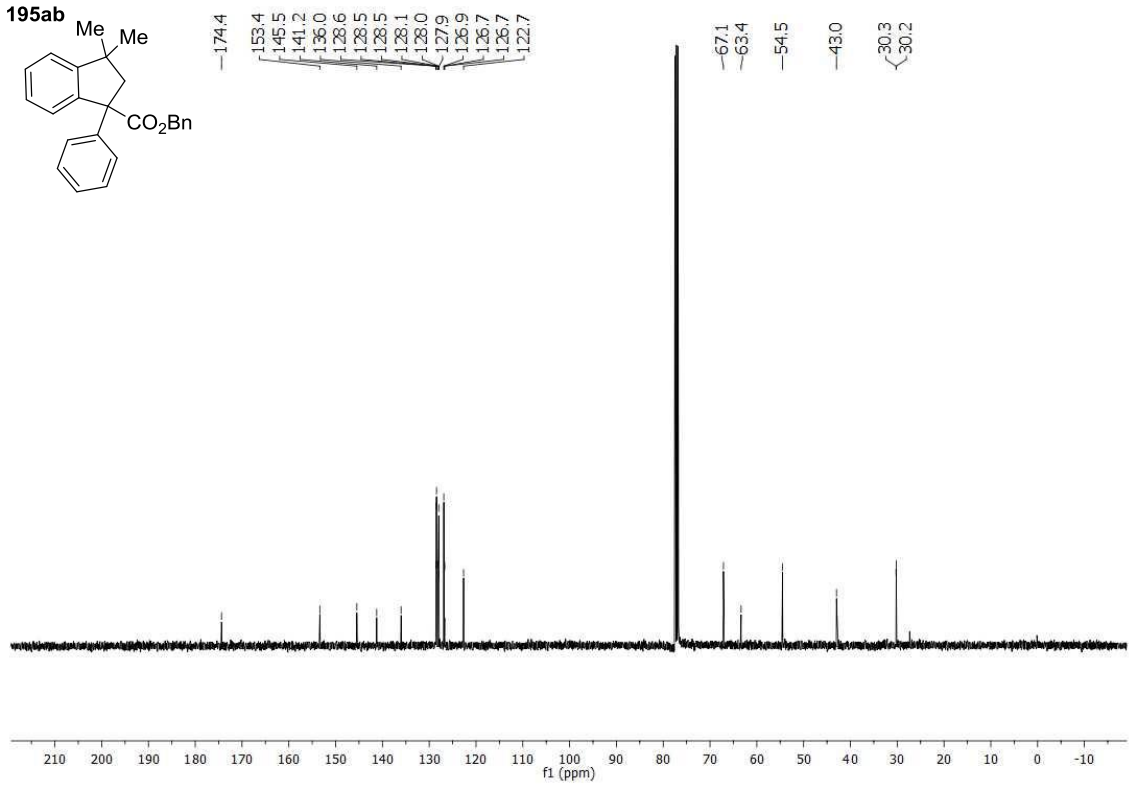
195ab
Me
Me
CO2Bn
174.4
153.4
145.5
141.2
136.0
128.6
128.5
128.5
128.1
128.0
127.9
126.9
126.7
126.7
122.7
67.1
63.4
54.5
43.0
30.3
30.2
f1 (ppm)

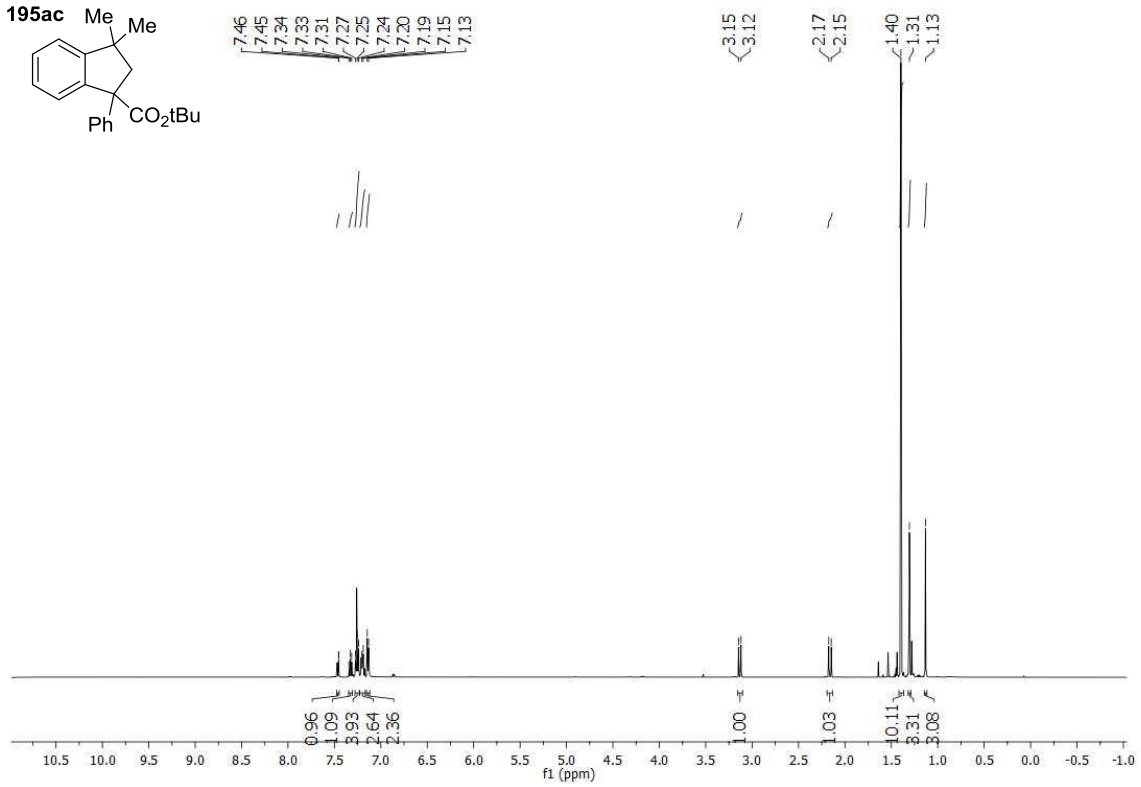
195ac
Me
Me
Ph
CO2tBu
7.46
7.45
7.34
7.33
7.31
7.27
7.25
7.24
7.20
7.19
7.15
7.13
3.15
3.12
2.17
2.15
1.40
1.31
1.13
0.96
1.09
3.93
2.64
2.36
1.00
1.03
10.11
3.31
3.08
f1 (ppm)

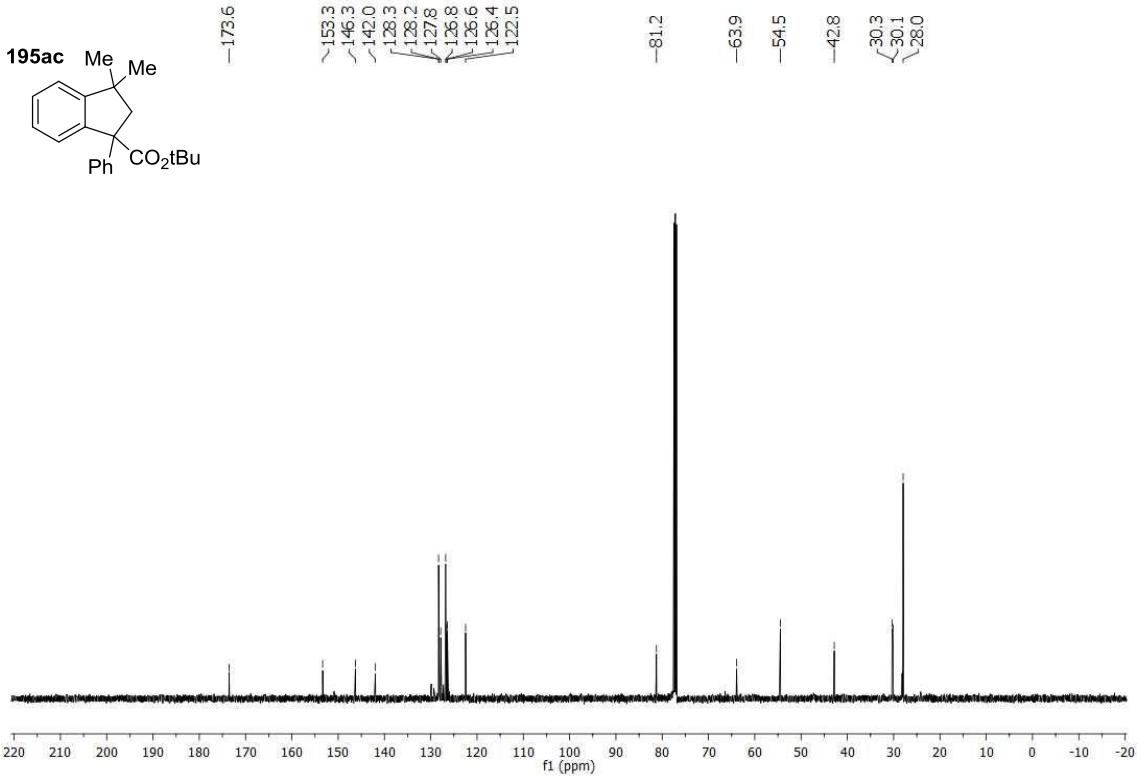
195ac
Me
Me
Ph
CO2tBu
173.6
153.3
146.3
142.0
128.3
128.2
127.8
126.8
126.6
126.4
122.5
81.2
63.9
54.5
42.8
30.3
30.1
28.0
f1 (ppm)

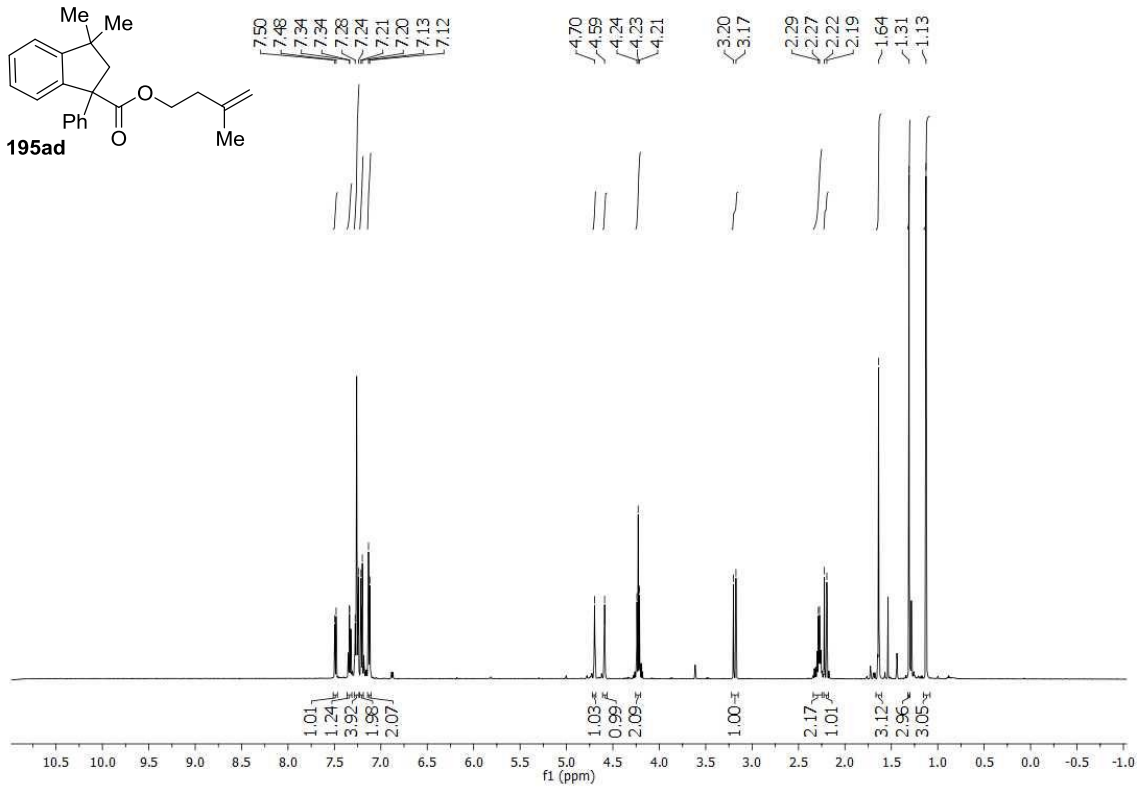
Me
Me
Ph
O
O
Me
195ad
7.50
7.48
7.34
7.34
7.28
7.24
7.21
7.20
7.13
7.12
4.70
4.59
4.24
4.23
4.21
3.20
3.17
2.29
2.27
2.22
2.19
1.64
1.31
1.13
1.01
1.24
3.92
1.98
2.07
1.03
0.99
2.09
1.00
2.17
1.01
3.12
2.96
3.05
f1 (ppm)

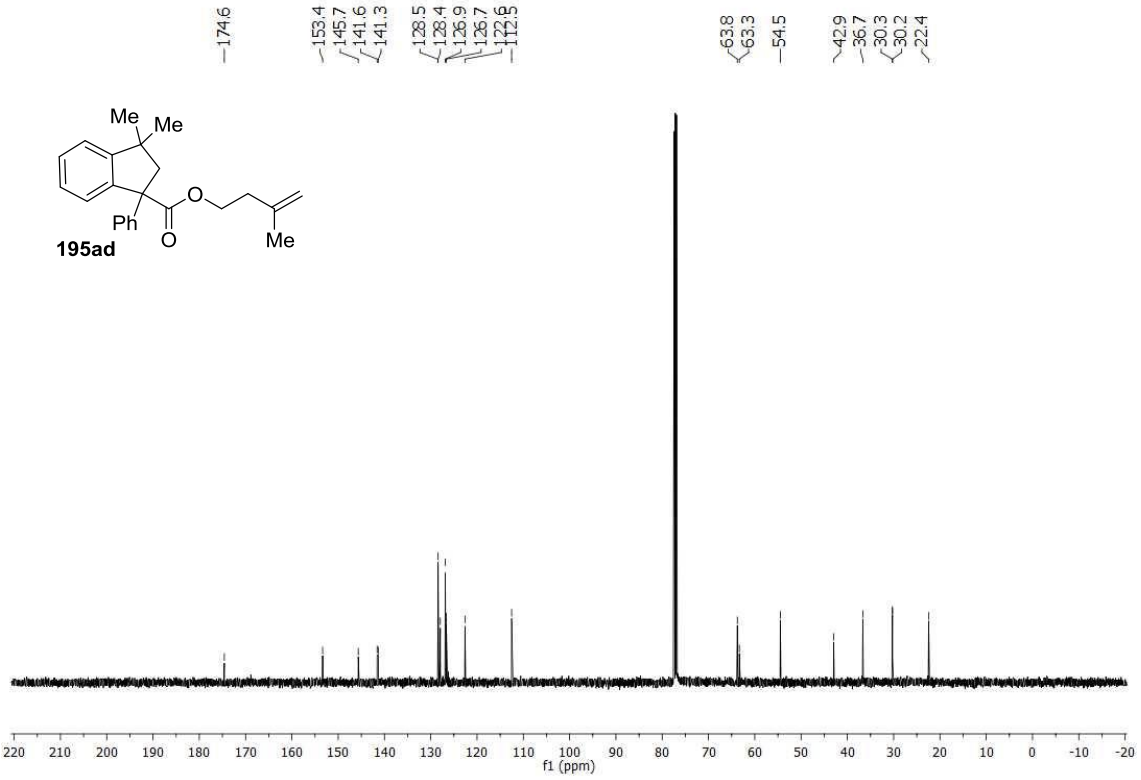
174.6
153.4
145.7
141.6
141.3
128.5
128.4
126.9
126.7
122.6
112.5
63.8
63.3
54.5
42.9
36.7
30.3
30.2
22.4
Me
Me
Ph
O
O
Me
195ad
f1 (ppm)

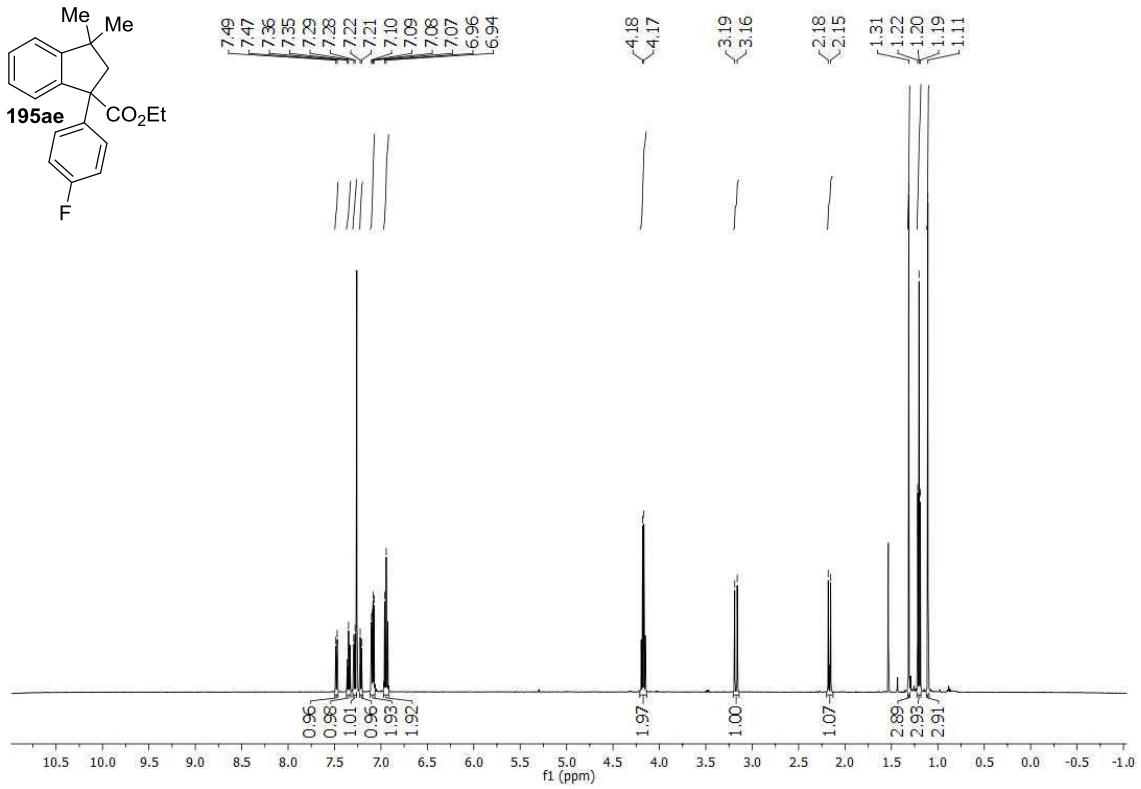
Me
Me
195ae
CO2Et
F
7.49
7.47
7.36
7.35
7.29
7.28
7.22
7.21
7.10
7.09
7.08
7.07
6.96
6.94
4.18
4.17
3.19
3.16
2.18
2.15
1.31
1.22
1.20
1.19
1.11
0.96
0.98
1.01
0.96
1.93
1.92
1.97
1.00
1.07
2.89
2.93
2.91
f1 (ppm)

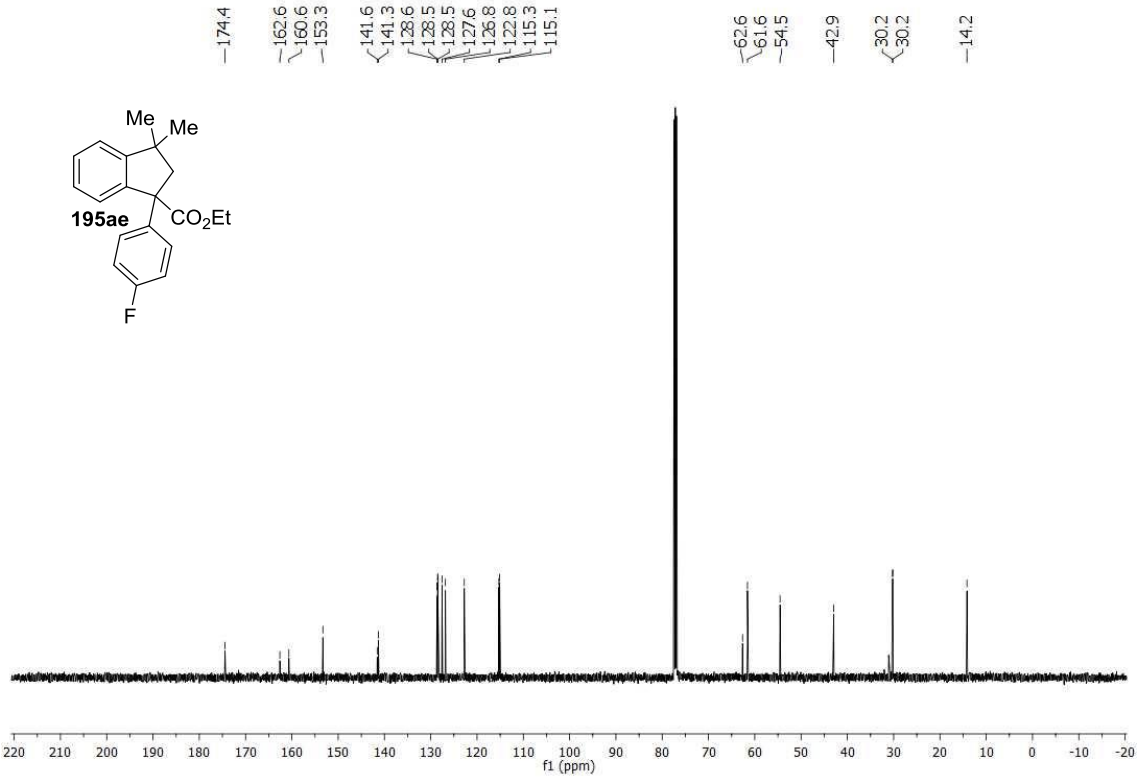
174.4
162.6
160.6
153.3
141.6
141.3
128.6
128.5
128.5
127.6
126.8
122.8
115.3
115.1
62.6
61.6
54.5
42.9
30.2
30.2
14.2
Me
Me
195ae
CO2Et
F
f1 (ppm)

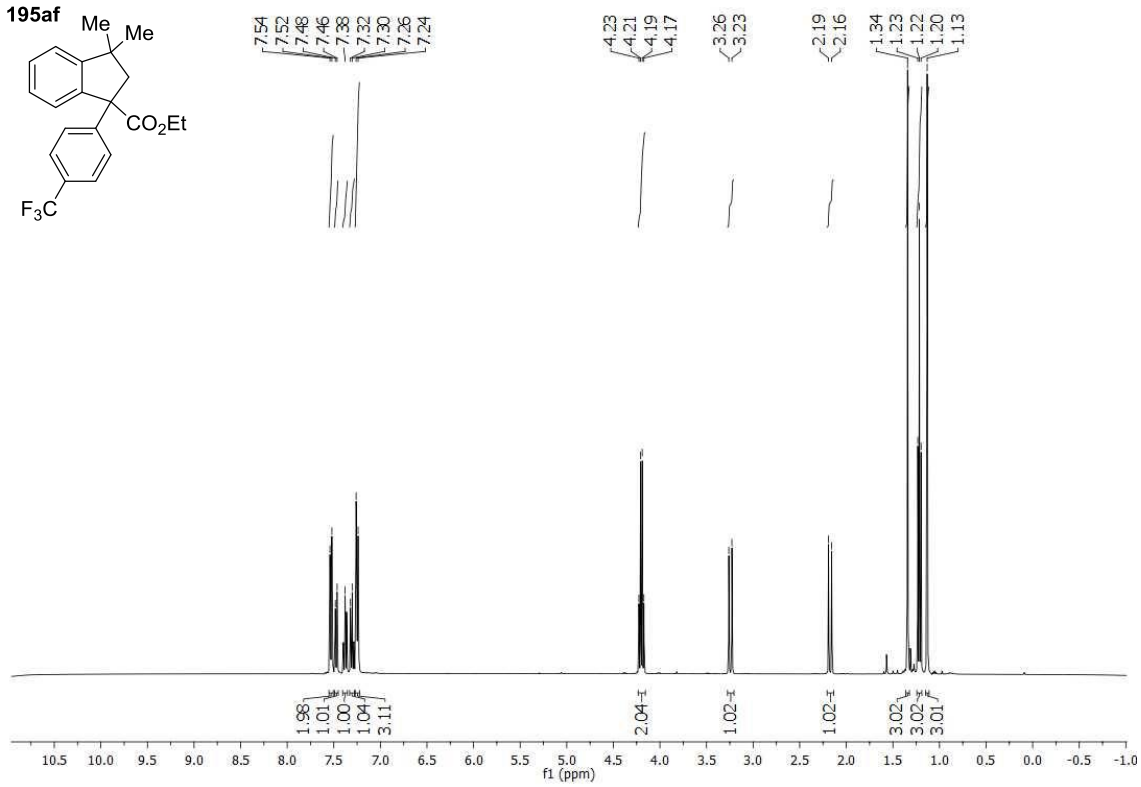
195af
Me
Me
CO2Et
F3C
7.54
7.52
7.48
7.46
7.38
7.32
7.30
7.26
7.24
4.23
4.21
4.19
4.17
3.26
3.23
2.19
2.16
1.34
1.23
1.22
1.20
1.13
1.98
1.01
1.00
1.04
3.11
2.04
1.02
1.02
3.02
3.02
3.01
f1 (ppm)

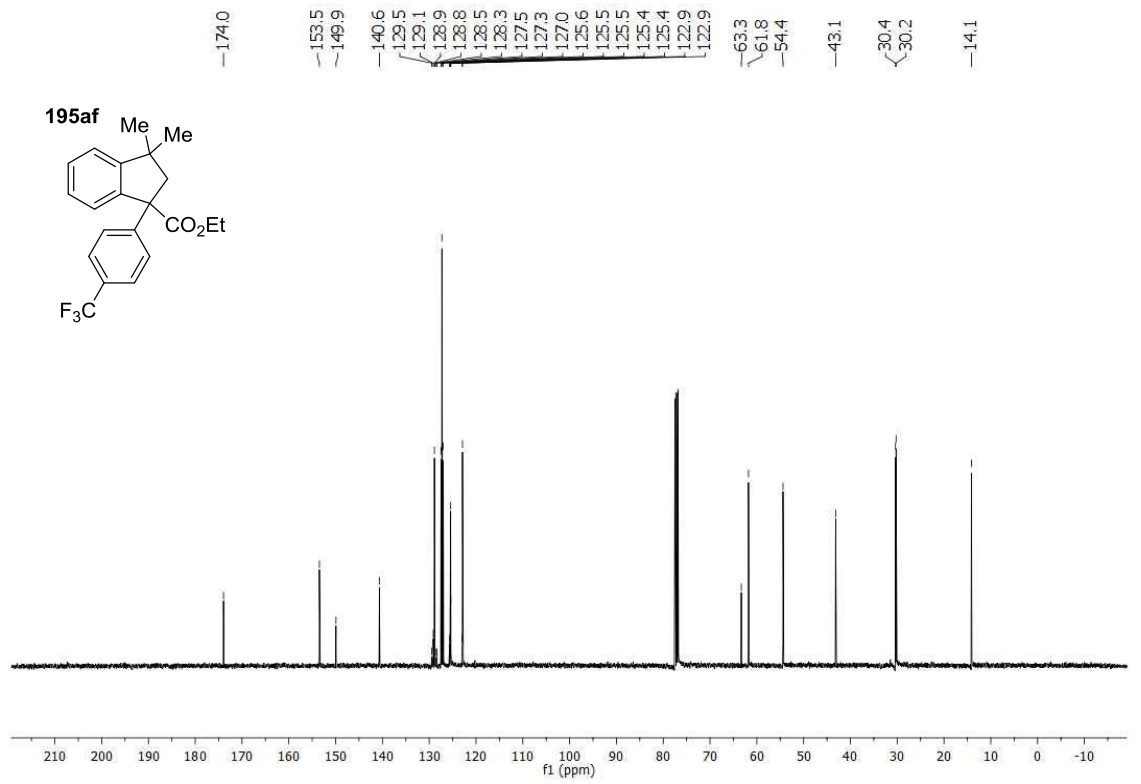
195af
Me
Me
CO2Et
F3C
174.0
153.5
149.9
140.6
129.5
129.1
128.9
128.8
128.5
128.3
127.5
127.3
127.0
125.6
125.5
125.5
125.4
125.4
122.9
122.9
63.3
61.8
54.4
43.1
30.4
30.2
14.1
f1 (ppm)

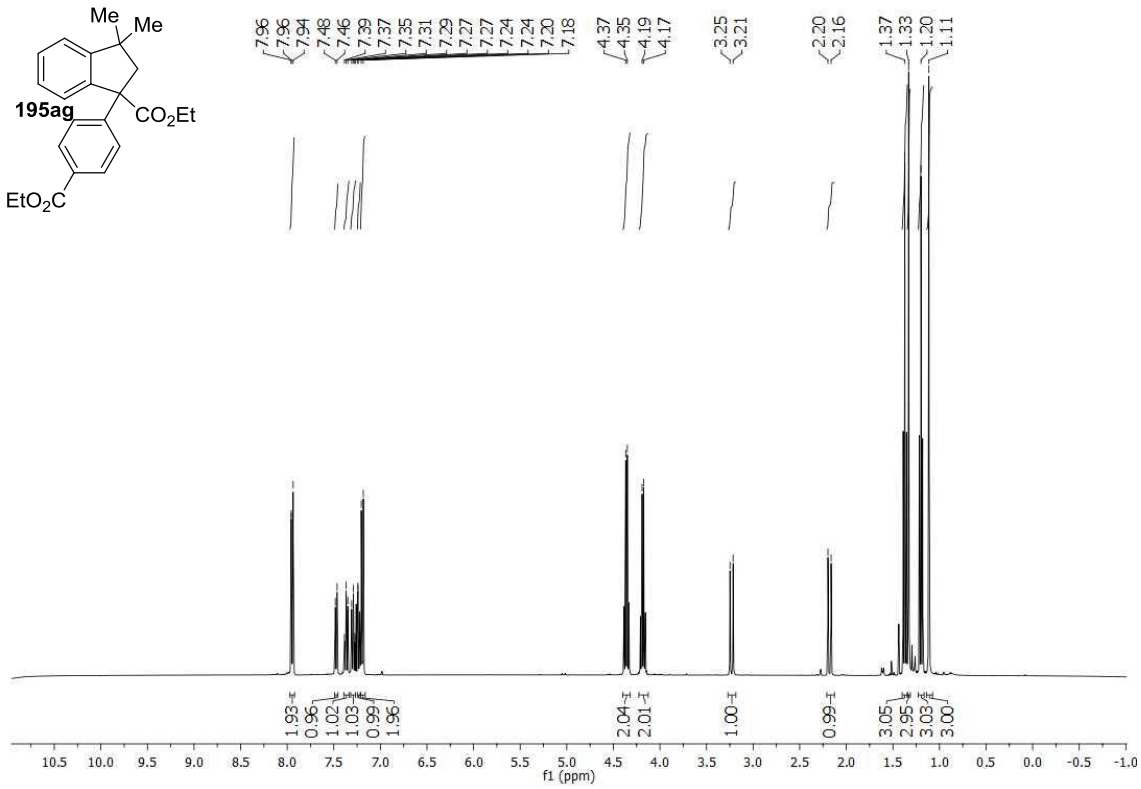
Me
Me
195ag
CO2Et
EtO2C
7.96
7.96
7.94
7.48
7.46
7.39
7.37
7.35
7.31
7.29
7.27
7.27
7.24
7.24
7.20
7.18
4.37
4.35
4.19
4.17
3.25
3.21
2.20
2.16
1.37
1.33
1.20
1.11
1.93
0.96
1.02
1.03
0.99
1.96
2.04
2.01
1.00
0.99
3.05
2.95
3.03
3.00
f1 (ppm)

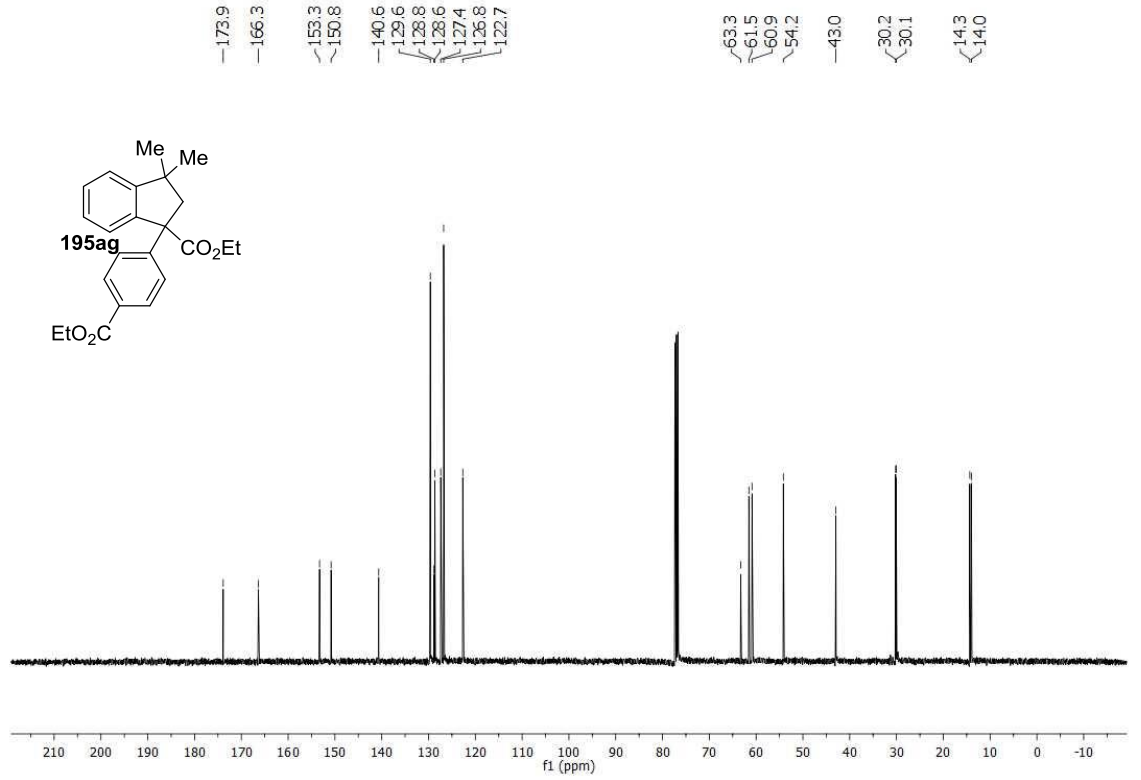
173.9
166.3
153.3
150.8
140.6
129.6
128.8
128.6
127.4
126.8
122.7
63.3
61.5
60.9
54.2
43.0
30.2
30.1
14.3
14.0
Me
Me
195ag
CO2Et
EtO2C
f1 (ppm)

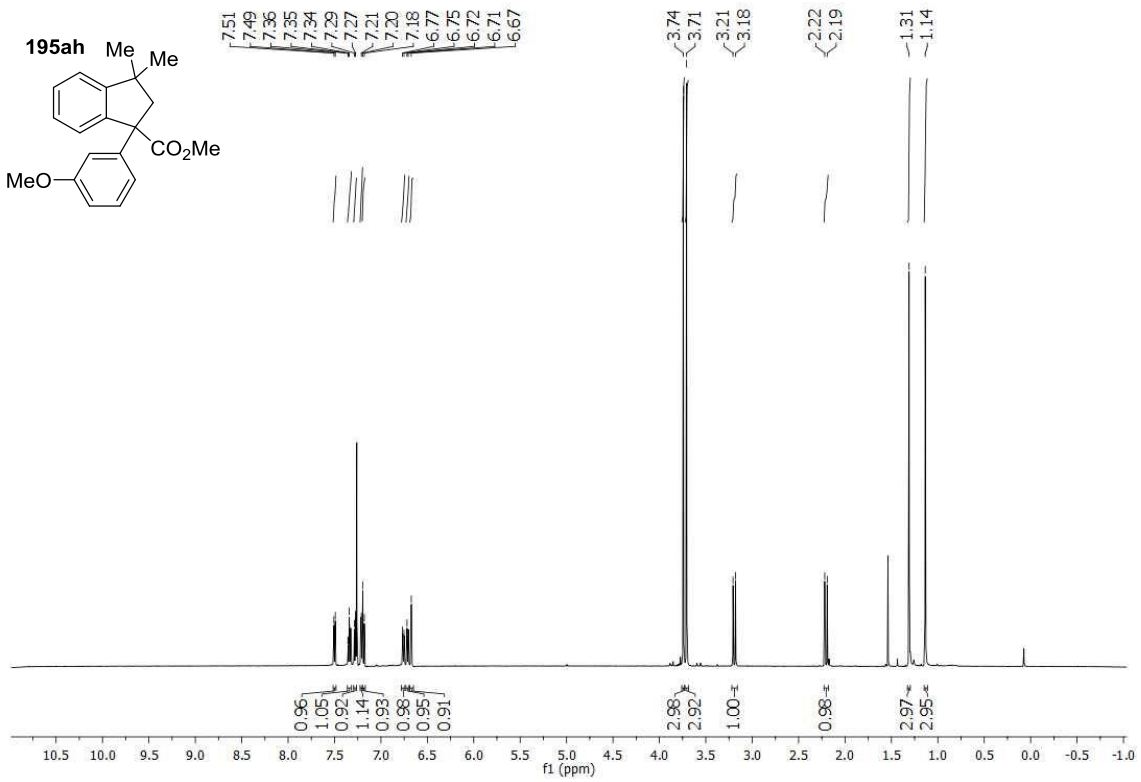
195ah
Me
Me
CO2Me
MeO
7.51
7.49
7.36
7.35
7.34
7.29
7.27
7.21
7.20
7.18
6.77
6.75
6.72
6.71
6.67
3.74
3.71
3.21
3.18
2.22
2.19
1.31
1.14
0.96
1.05
0.92
1.14
0.93
0.88
0.95
0.91
2.98
2.92
1.00
0.98
2.97
2.95
f1 (ppm)

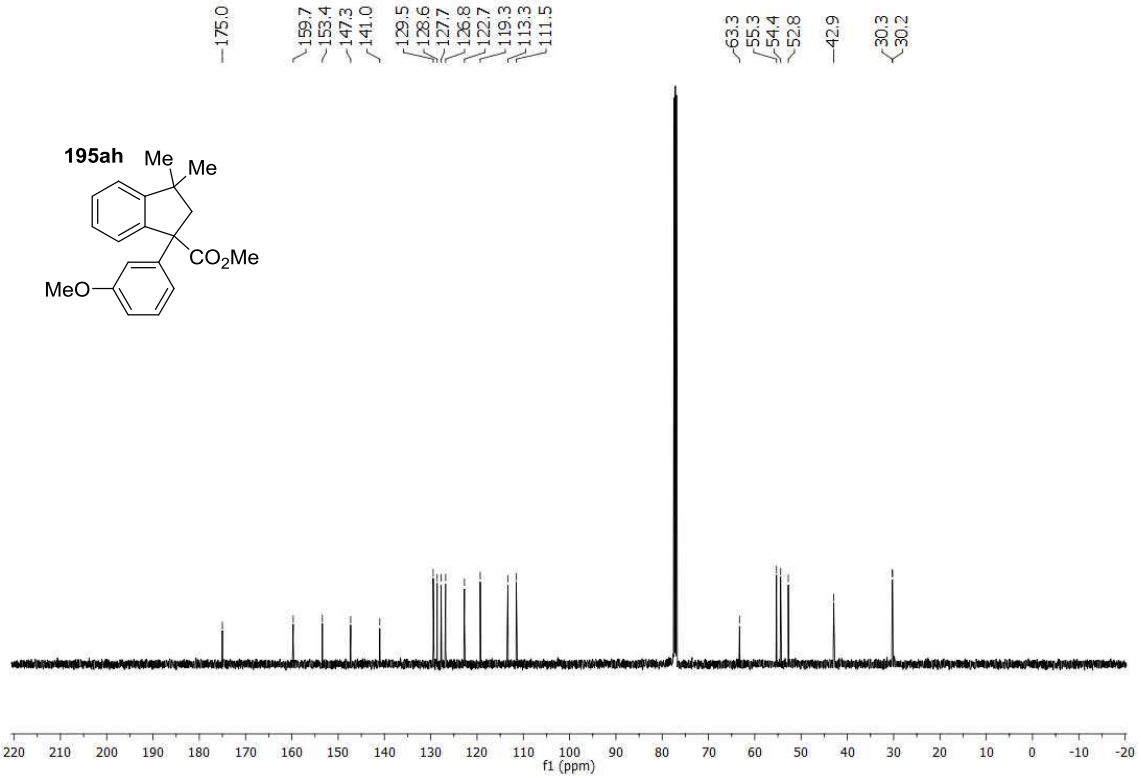
195ah
Me
Me
CO2Me
MeO
175.0
159.7
153.4
147.3
141.0
129.5
128.6
127.7
126.8
122.7
119.3
113.3
111.5
63.3
55.3
54.4
52.8
42.9
30.3
30.2
f1 (ppm)

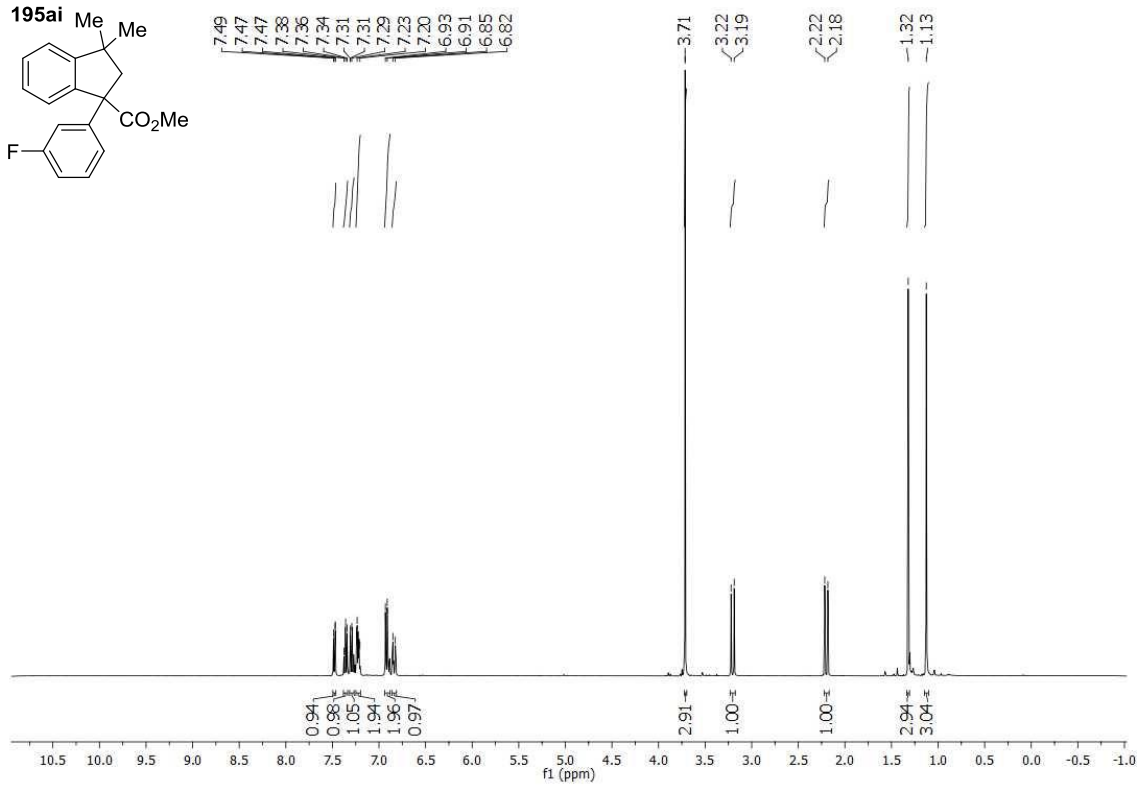
195ai
Me
Me
CO2Me
F
7.49
7.47
7.47
7.38
7.36
7.34
7.31
7.31
7.29
7.23
7.20
6.93
6.91
6.85
6.82
3.71
3.22
3.19
2.22
2.18
1.32
1.13
0.94
0.98
1.05
1.94
1.96
0.97
2.91
1.00
1.00
2.94
3.04
f1 (ppm)

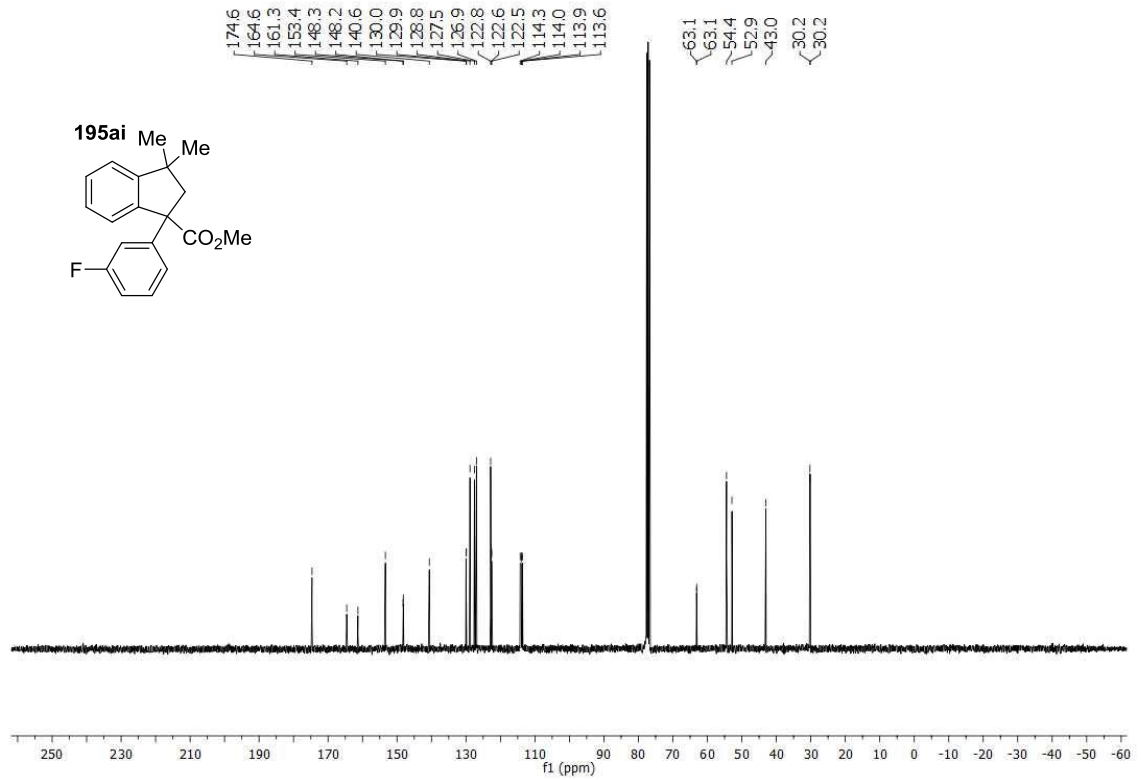
195ai
Me
Me
CO2Me
F
174.6
164.6
161.3
153.4
148.3
148.2
140.6
130.0
129.9
128.8
127.5
126.9
122.8
122.6
122.5
114.3
114.0
113.9
113.6
63.1
63.1
54.4
52.9
43.0
30.2
30.2
f1 (ppm)

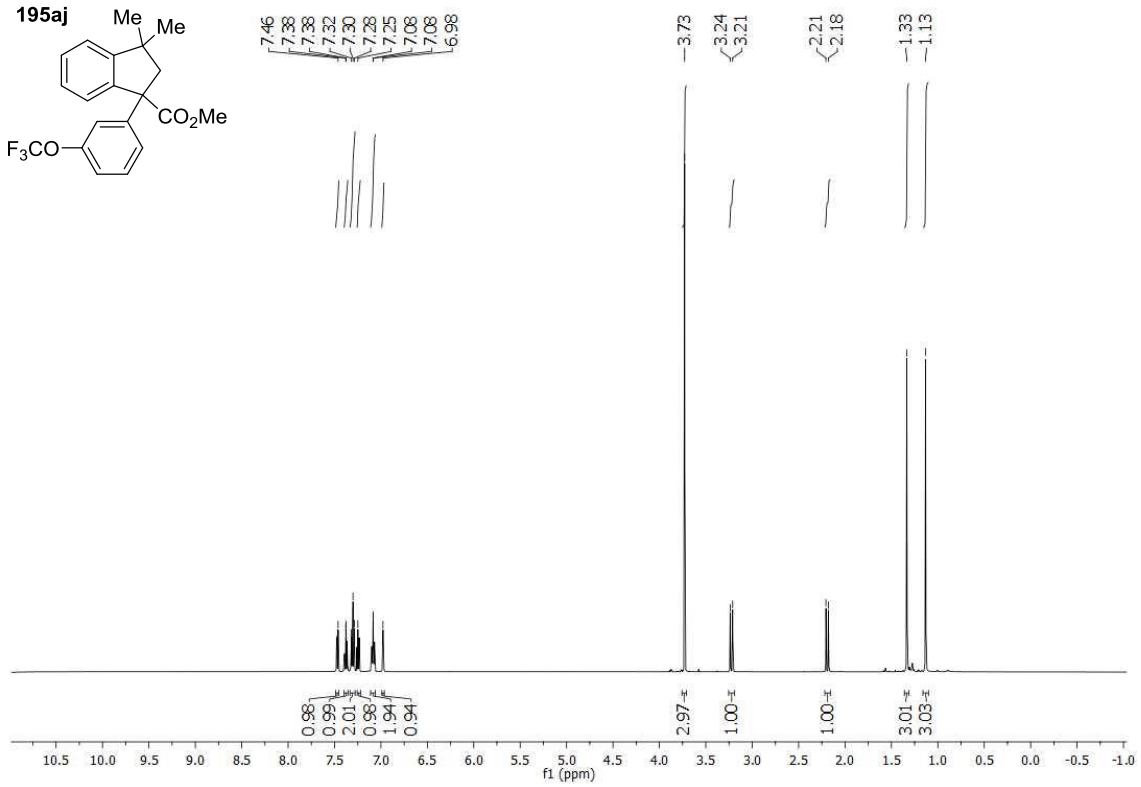
195aj
Me
Me
CO2Me
F3CO
7.46
7.38
7.38
7.32
7.30
7.28
7.25
7.08
7.08
6.98
3.73
3.24
3.21
2.21
2.18
1.33
1.13
0.98
0.99
2.01
0.98
1.94
0.94
2.97
1.00
1.00
3.01
3.03
f1 (ppm)

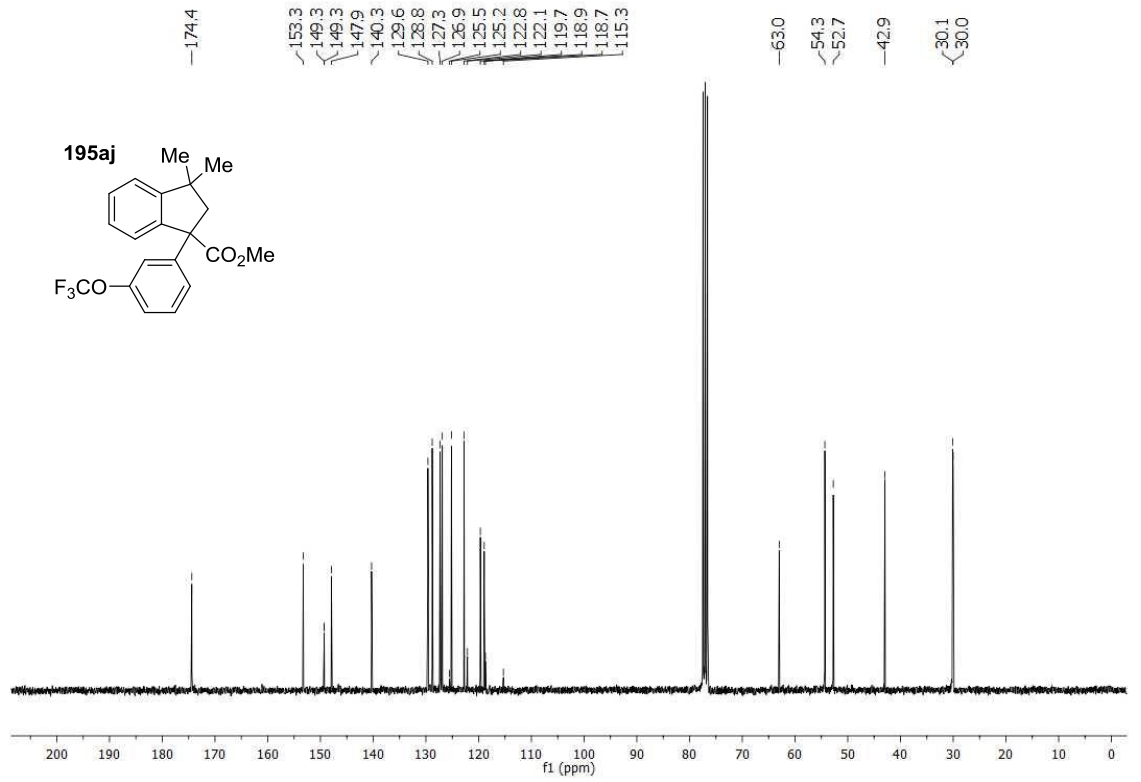
195aj
Me
Me
CO2Me
F3CO
174.4
153.3
149.3
149.3
147.9
140.3
129.6
128.8
127.3
126.9
125.5
125.2
122.8
122.1
119.7
118.9
118.7
115.3
63.0
54.3
52.7
42.9
30.1
30.0
f1 (ppm)

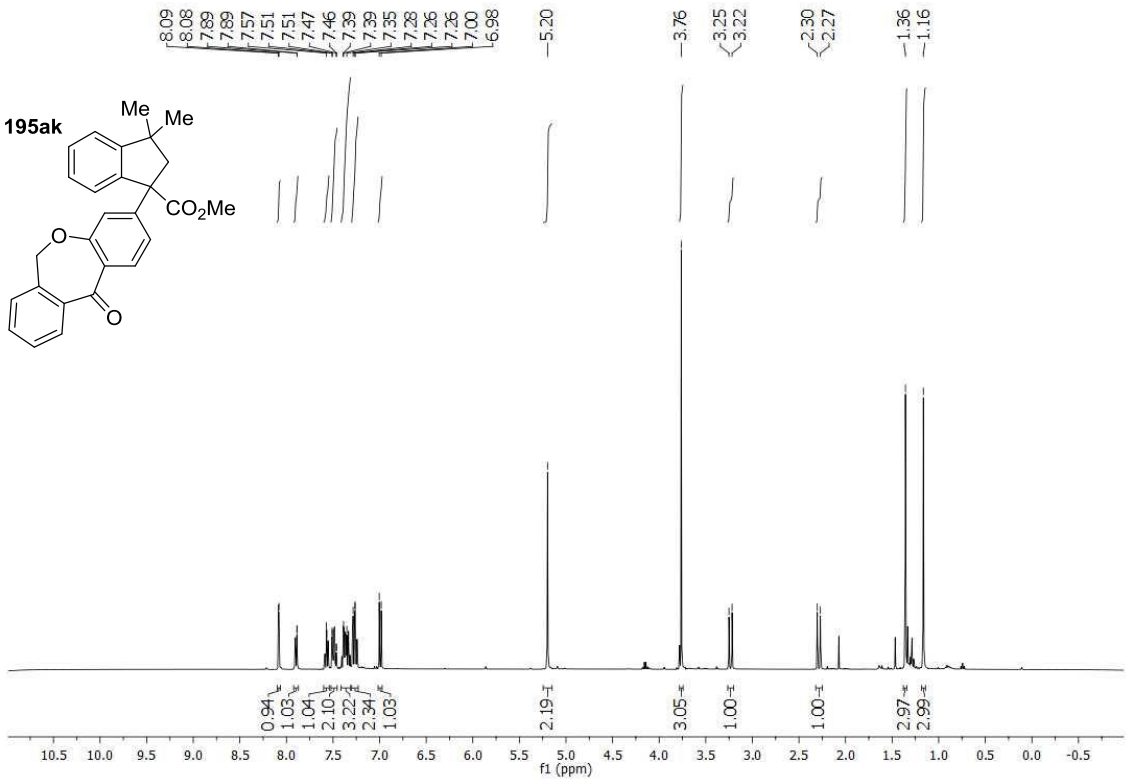
195ak
Me
Me
CO2Me
O
O
8.09
8.08
7.89
7.89
7.57
7.51
7.51
7.47
7.46
7.39
7.39
7.35
7.28
7.26
7.26
7.00
6.98
5.20
3.76
3.25
3.22
2.30
2.27
1.36
1.16
0.94
1.03
1.04
2.10
3.22
2.34
1.03
2.19
3.05
1.00
1.00
2.97
2.99
f1 (ppm)

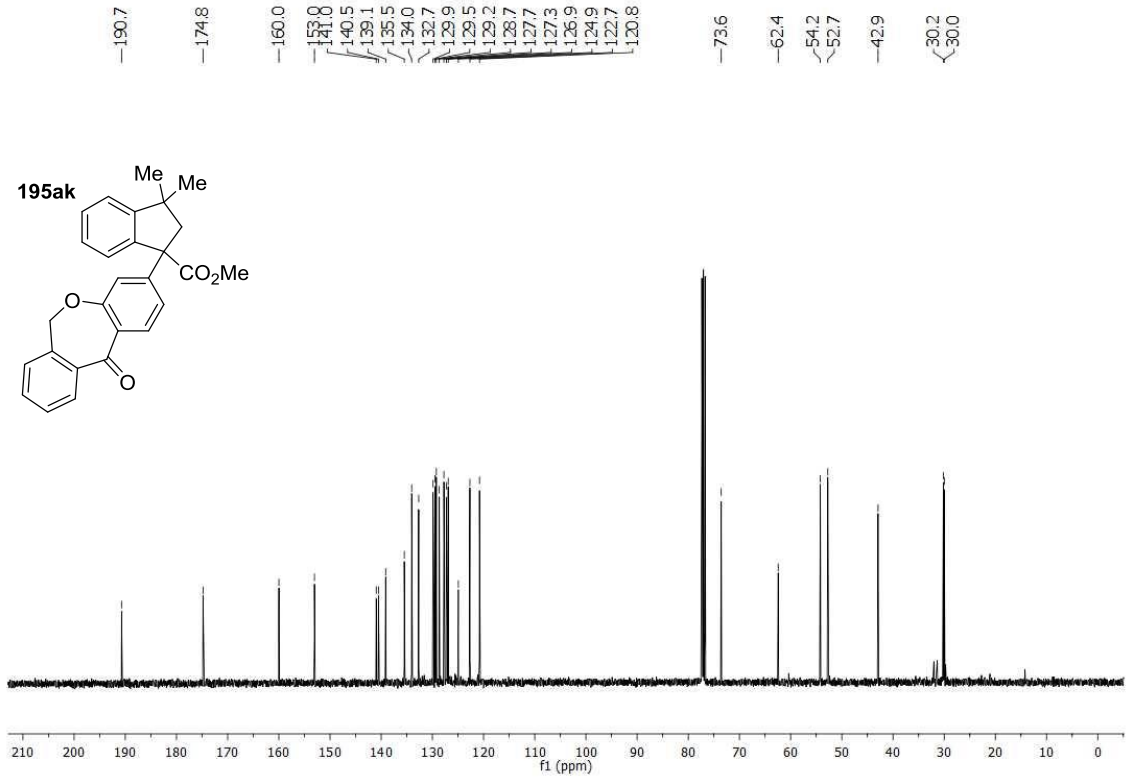
195ak
Me
Me
CO2Me
O
O
190.7
174.8
160.0
153.0
141.0
140.5
139.1
135.5
134.0
132.7
129.9
129.5
129.2
128.7
127.7
127.3
126.9
124.9
122.7
120.8
73.6
62.4
54.2
52.7
42.9
30.2
30.0
f1 (ppm)

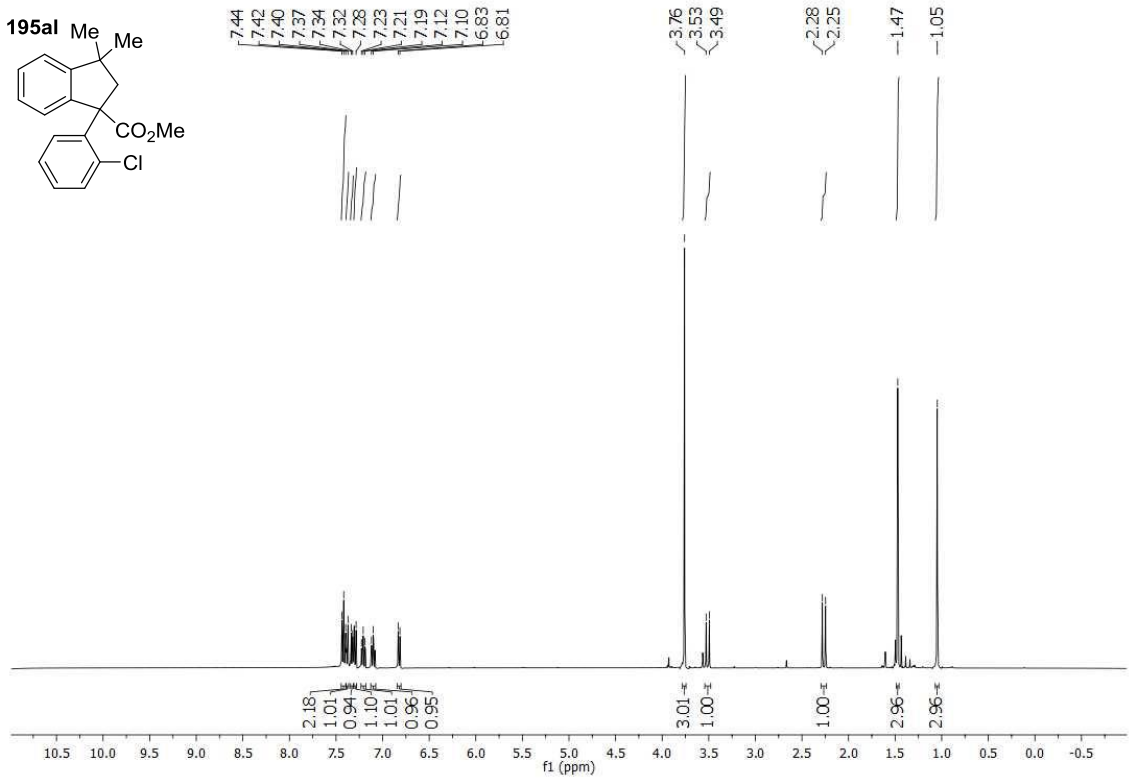
195al
Me
Me
CO2Me
Cl
7.44
7.42
7.40
7.37
7.34
7.32
7.28
7.23
7.21
7.19
7.12
7.10
6.83
6.81
3.76
3.53
3.49
2.28
2.25
1.47
1.05
2.18
1.01
0.94
1.10
1.01
0.96
0.95
3.01
1.00
1.00
2.96
2.96
f1 (ppm)

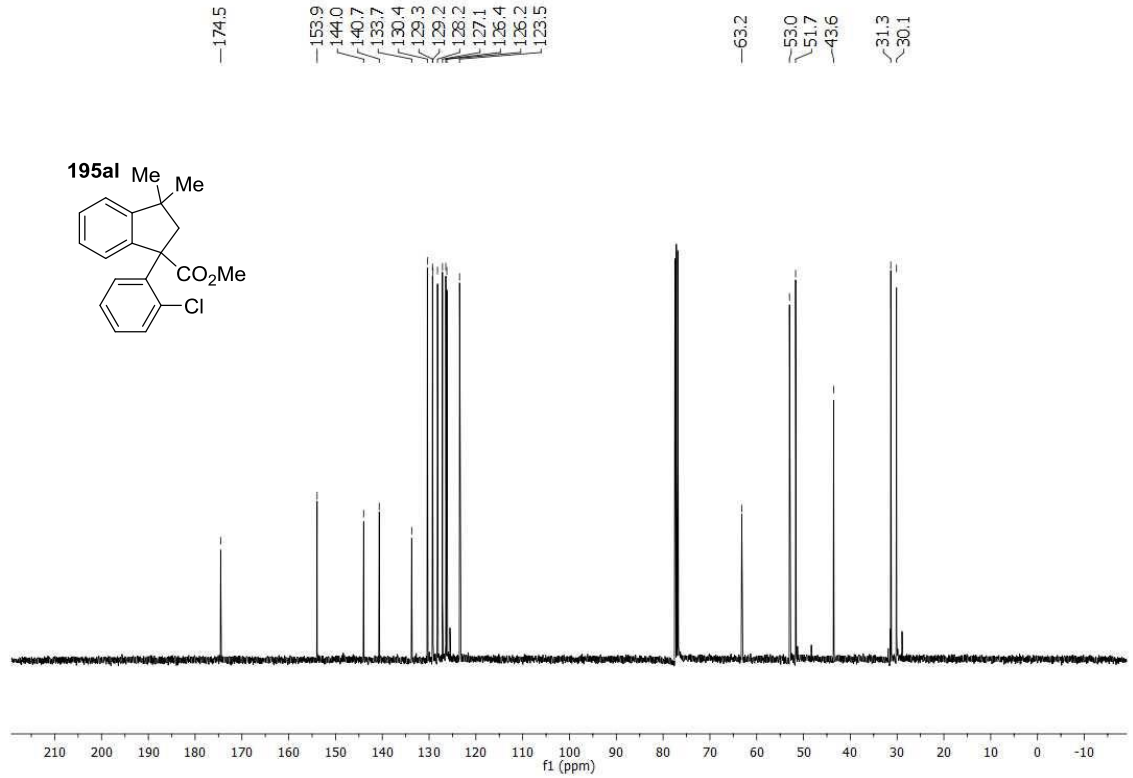
195al
Me
Me
CO2Me
Cl
174.5
153.9
144.0
140.7
133.7
130.4
129.3
129.2
128.2
127.1
126.4
126.2
123.5
63.2
53.0
51.7
43.6
31.3
30.1
f1 (ppm)

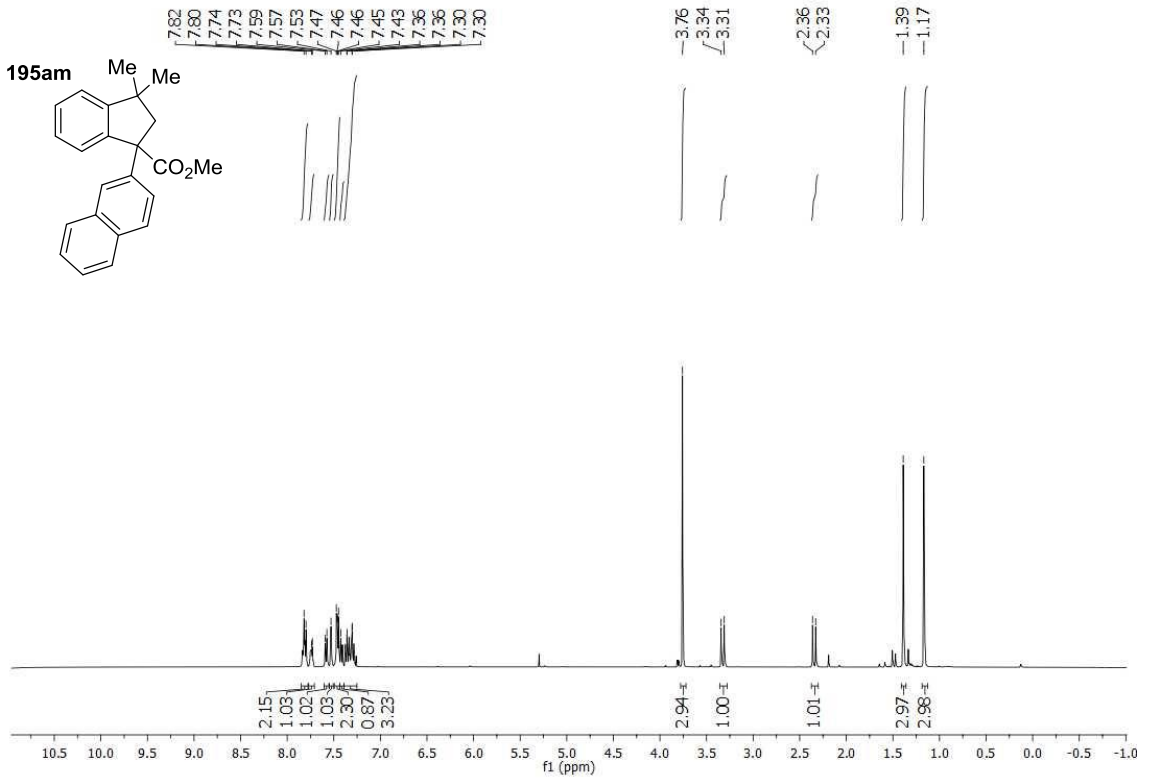
195am
Me
Me
CO2Me
7.82
7.80
7.74
7.73
7.59
7.57
7.53
7.47
7.46
7.46
7.45
7.43
7.36
7.36
7.30
7.30
3.76
3.34
3.31
2.36
2.33
1.39
1.17
2.15
1.03
1.02
1.03
2.30
0.87
3.23
2.94
1.00
1.01
2.97
2.98
f1 (ppm)

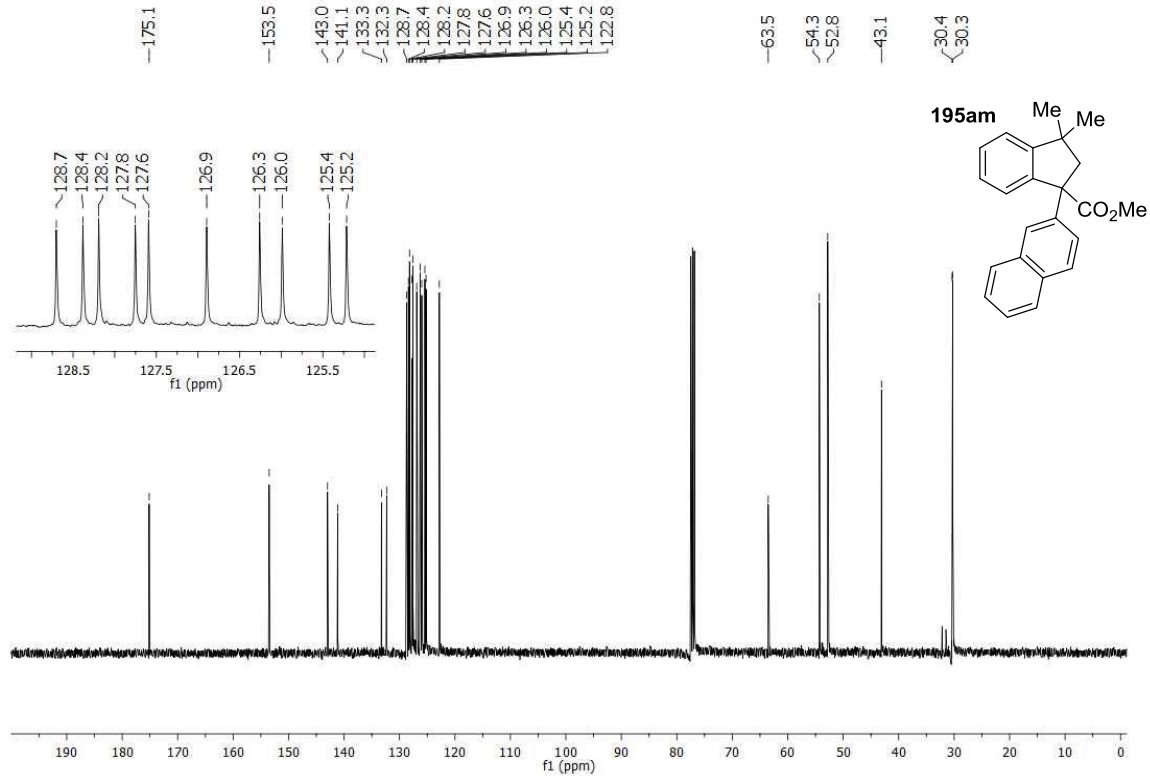
175.1
153.5
143.0
141.1
133.3
132.3
128.7
128.4
128.2
127.8
127.6
126.9
126.3
126.0
125.4
125.2
122.8
63.5
54.3
52.8
43.1
30.4
30.3
195am
Me
Me
CO2Me
f1 (ppm)

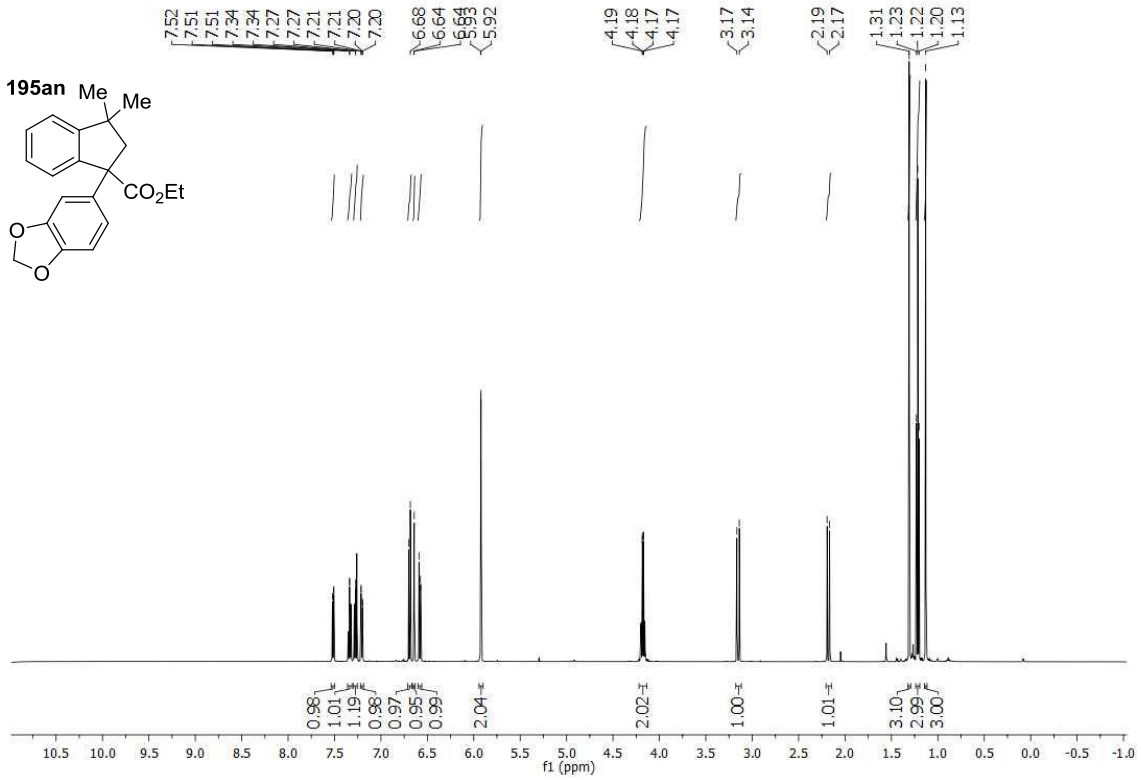
195an
Me
Me
CO2Et
O
O
7.52
7.51
7.51
7.34
7.34
7.27
7.27
7.21
7.21
7.20
7.20
6.68
6.64
6.64
5.93
5.92
4.19
4.18
4.17
4.17
3.17
3.14
2.19
2.17
1.31
1.23
1.22
1.20
1.13
0.98
1.01
1.19
0.98
0.97
0.95
0.99
2.04
2.02
1.00
1.01
3.10
2.99
3.00
f1 (ppm)

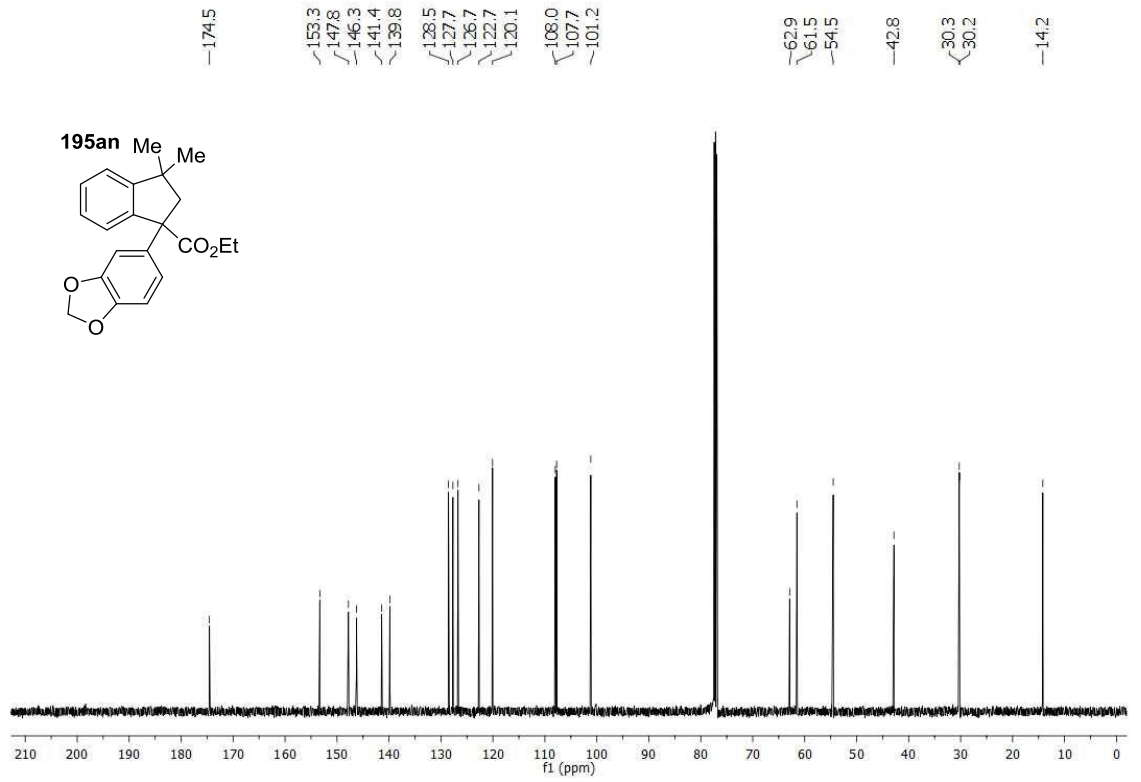
195an
Me
Me
CO2Et
O
O
174.5
153.3
147.8
146.3
141.4
139.8
128.5
127.7
126.7
122.7
120.1
108.0
107.7
101.2
62.9
61.5
54.5
42.8
30.3
30.2
14.2
f1 (ppm)

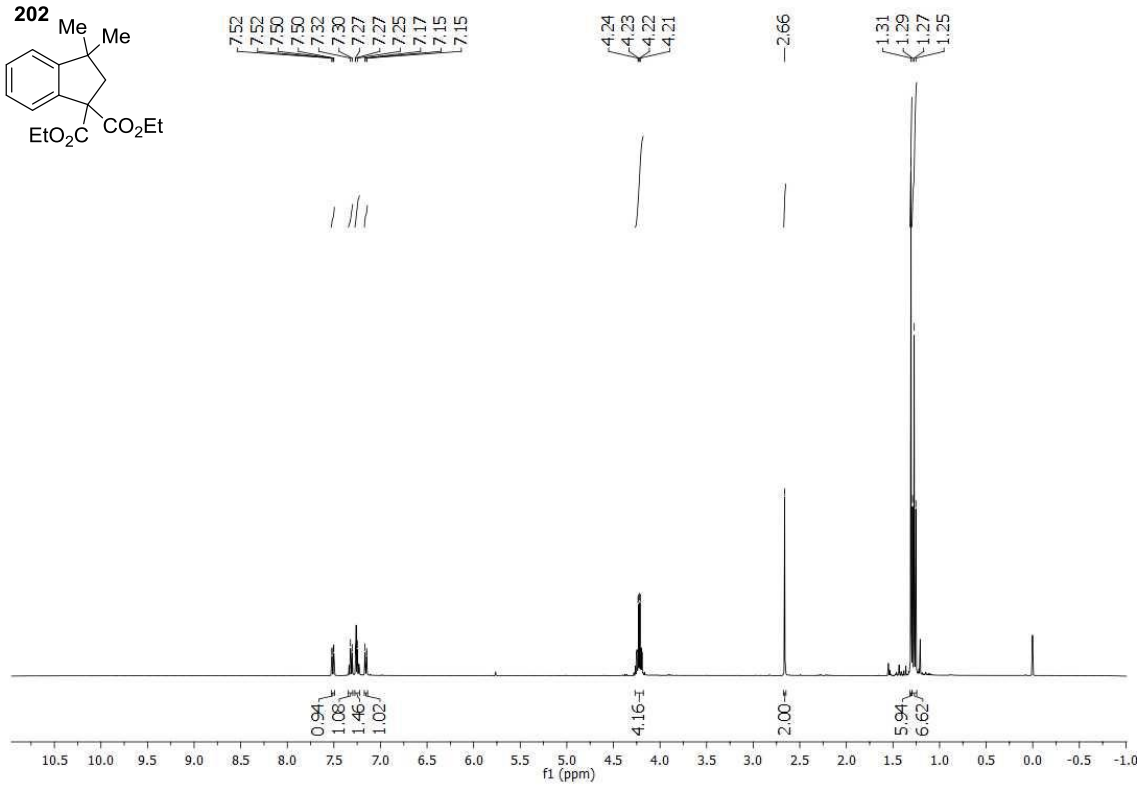
202
Me
Me
EtO2C
CO2Et
7.52
7.52
7.50
7.50
7.32
7.30
7.27
7.27
7.25
7.17
7.15
7.15
4.24
4.23
4.22
4.21
2.66
1.31
1.29
1.27
1.25
0.94
1.08
1.46
1.02
4.16
2.00
5.94
6.62
f1 (ppm)

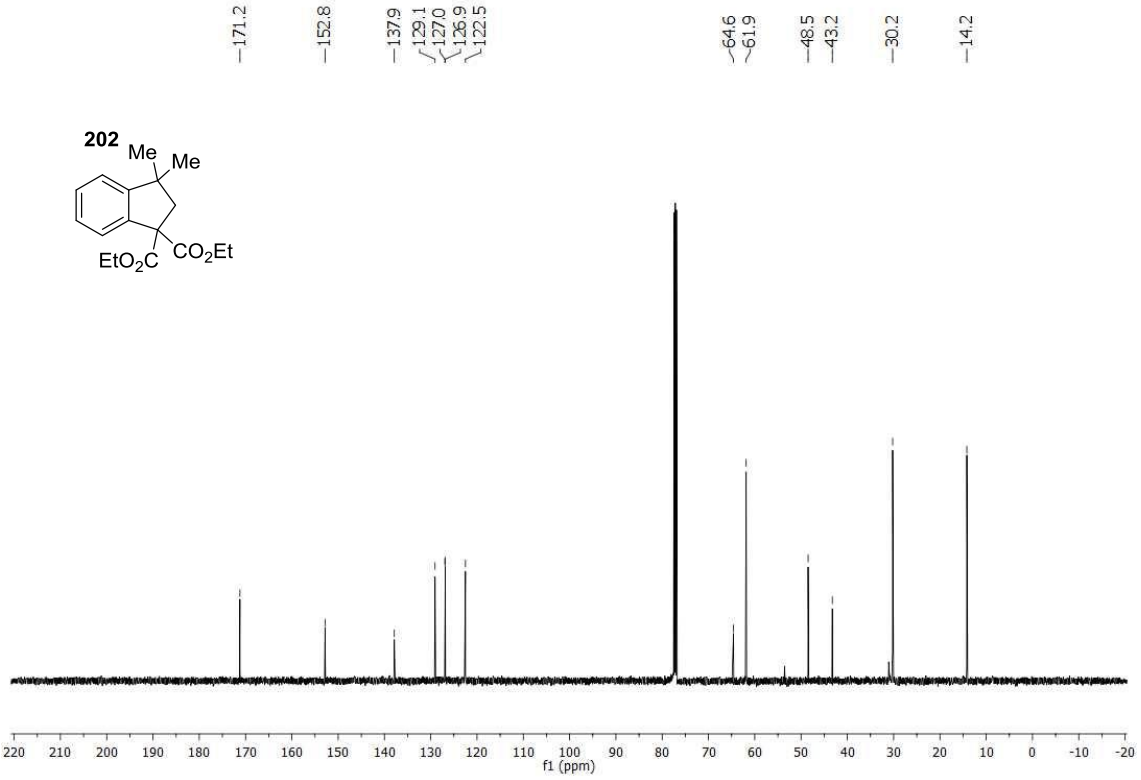
171.2
152.8
137.9
129.1
127.0
126.9
122.5
64.6
61.9
48.5
43.2
30.2
14.2
202
Me
Me
EtO2C
CO2Et
f1 (ppm)

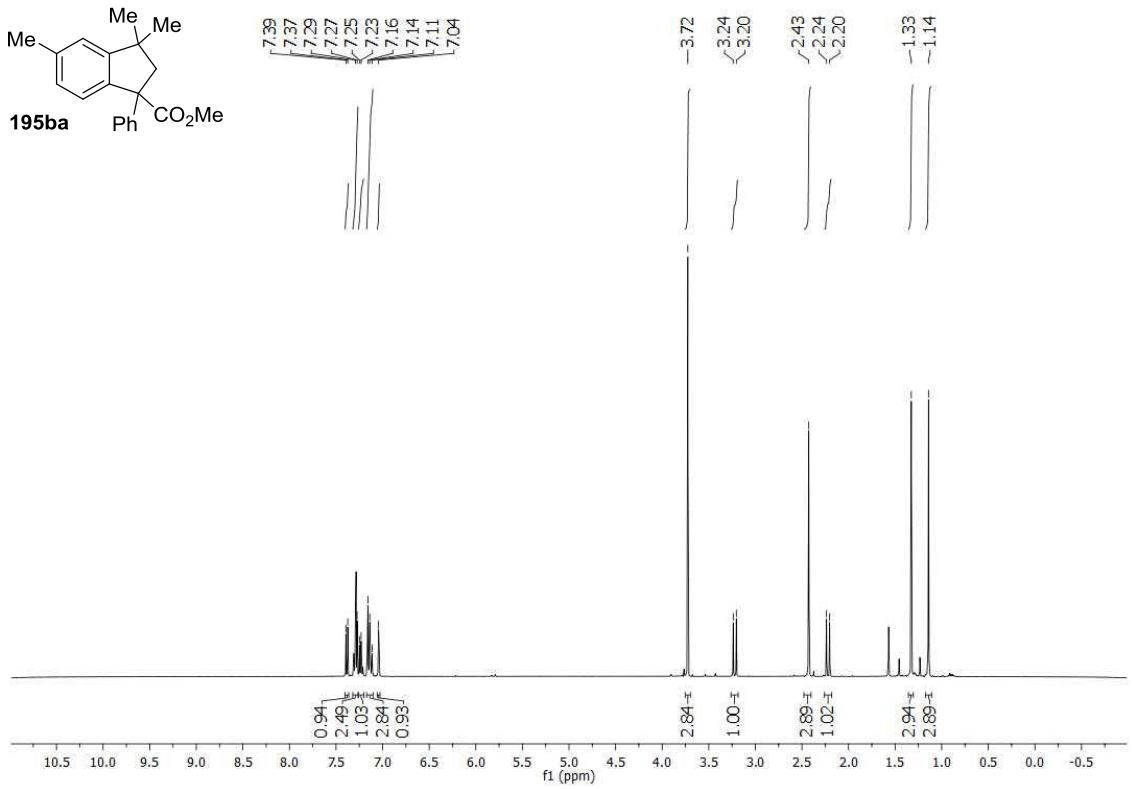
Me
Me
Me
Ph
CO2Me
195ba
7.39
7.37
7.29
7.27
7.25
7.23
7.16
7.14
7.11
7.04
3.72
3.24
3.20
2.43
2.24
2.20
1.33
1.14
0.94
2.49
1.03
2.84
0.93
2.84
1.00
2.89
1.02
2.94
2.89
f1 (ppm)

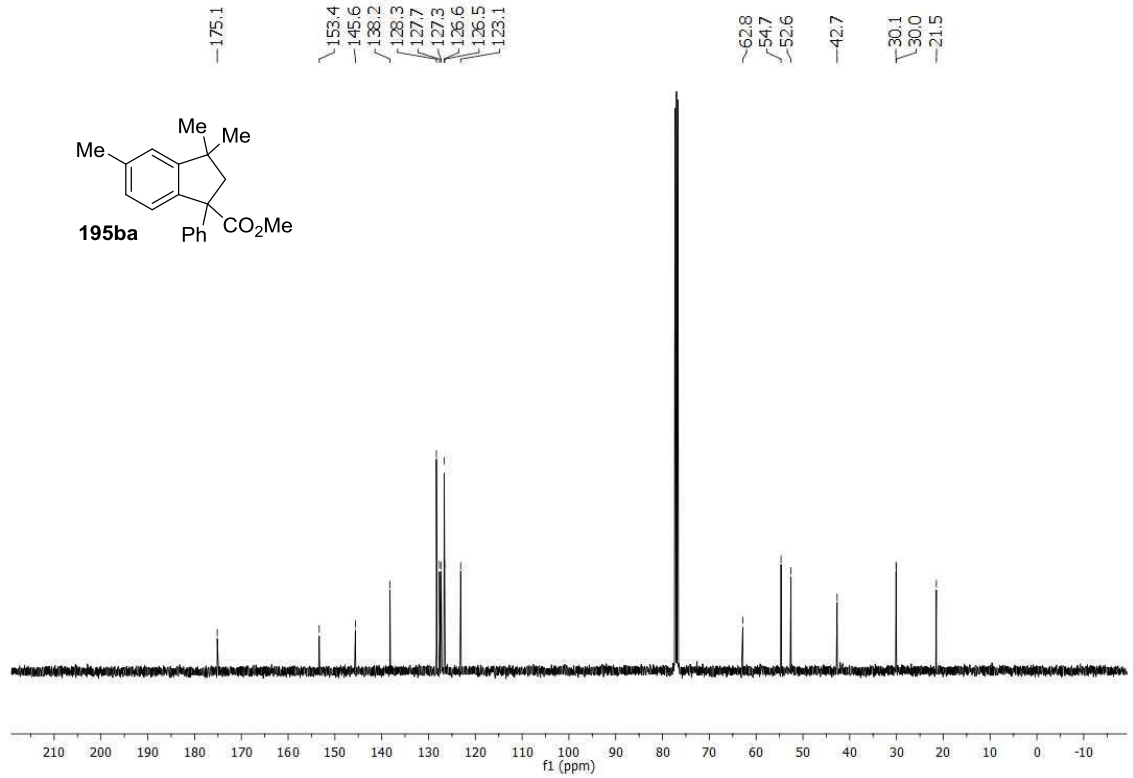
175.1
153.4
145.6
138.2
128.3
127.7
127.3
126.6
126.5
123.1
62.8
54.7
52.6
42.7
30.1
30.0
21.5
Me
Me
Me
Ph
CO2Me
195ba
f1 (ppm)

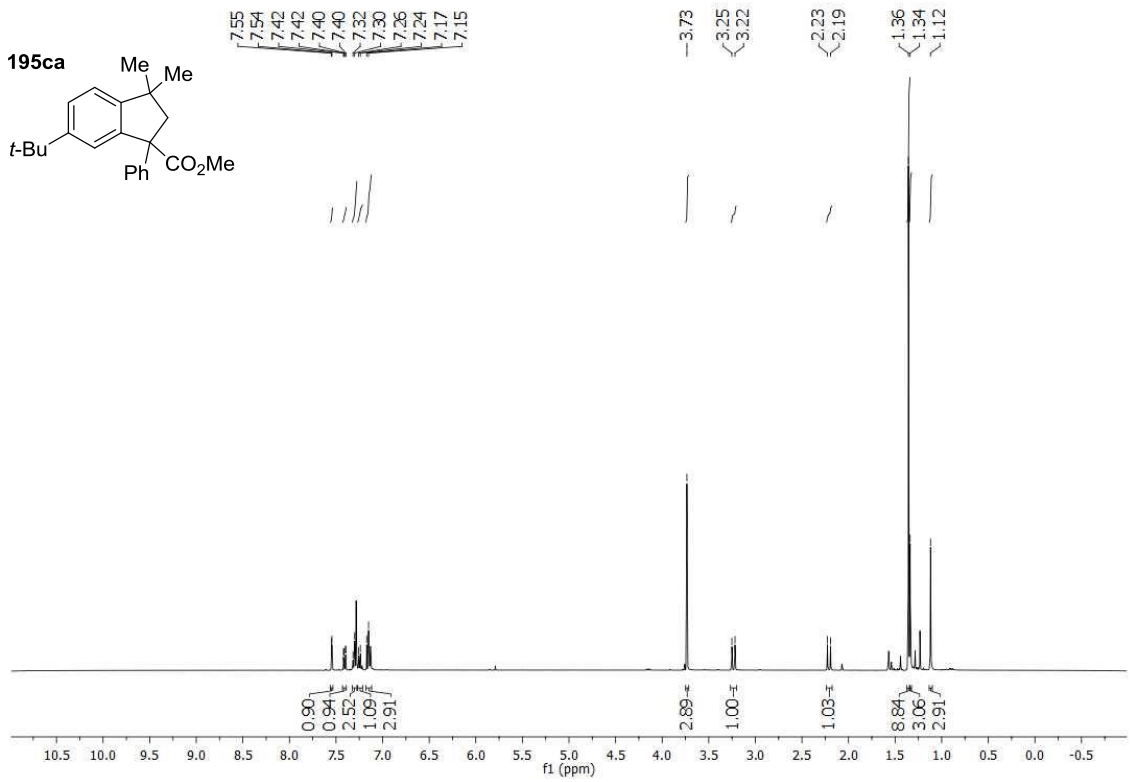
195ca
Me
Me
t-Bu
Ph
CO2Me
7.55
7.54
7.42
7.42
7.40
7.40
7.32
7.30
7.26
7.24
7.17
7.15
3.73
3.25
3.22
2.23
2.19
1.36
1.34
1.12
0.90
0.94
2.52
1.09
2.91
2.89
1.00
1.03
8.84
3.06
2.91
f1 (ppm)

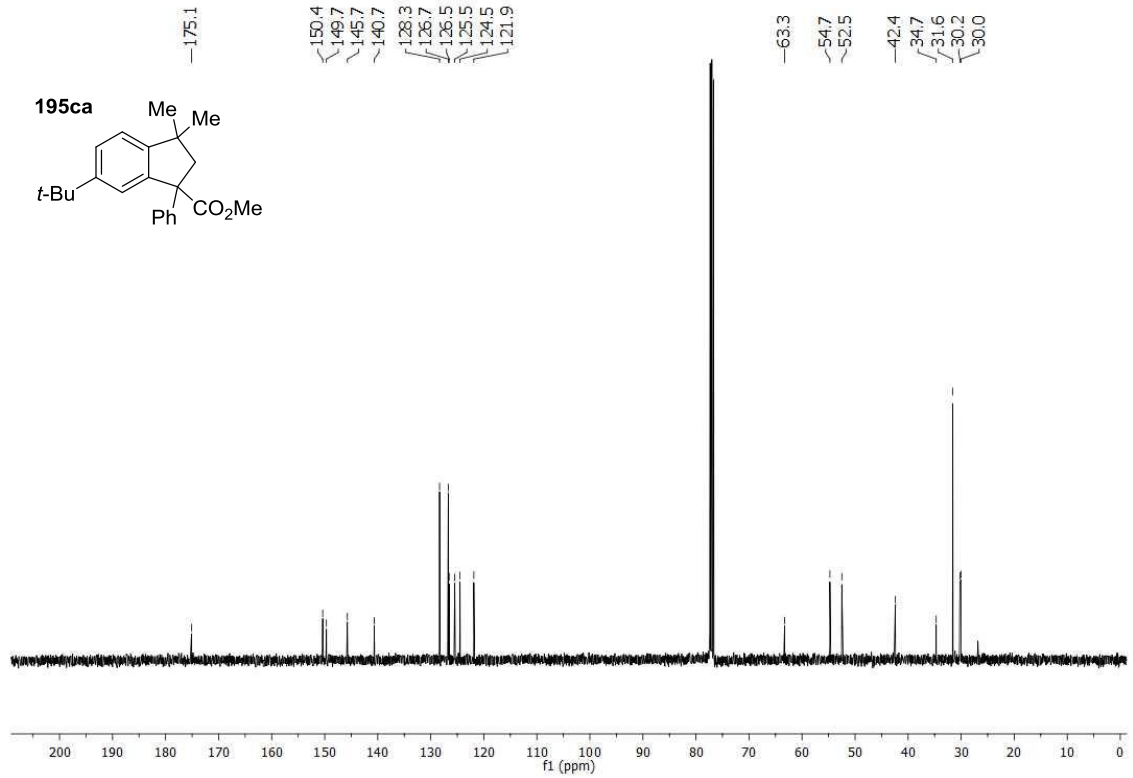
195ca
Me
Me
t-Bu
Ph
CO2Me
175.1
150.4
149.7
145.7
140.7
128.3
126.7
126.5
125.5
124.5
121.9
63.3
54.7
52.5
42.4
34.7
31.6
30.2
30.0
f1 (ppm)

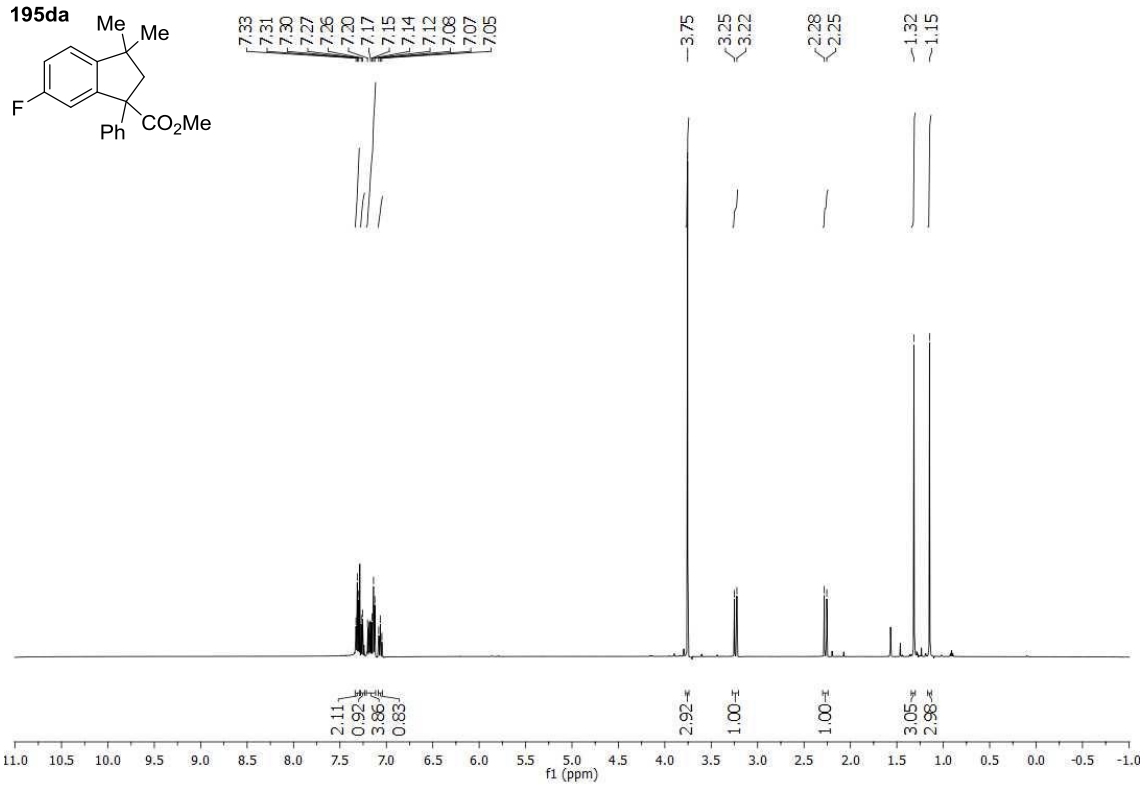
195da
Me
Me
F
Ph
CO2Me
7.33
7.31
7.30
7.27
7.26
7.20
7.17
7.15
7.14
7.12
7.08
7.07
7.05
3.75
3.25
3.22
2.28
2.25
1.32
1.15
2.11
0.92
3.86
0.83
2.92
1.00
1.00
3.05
2.98
f1 (ppm)

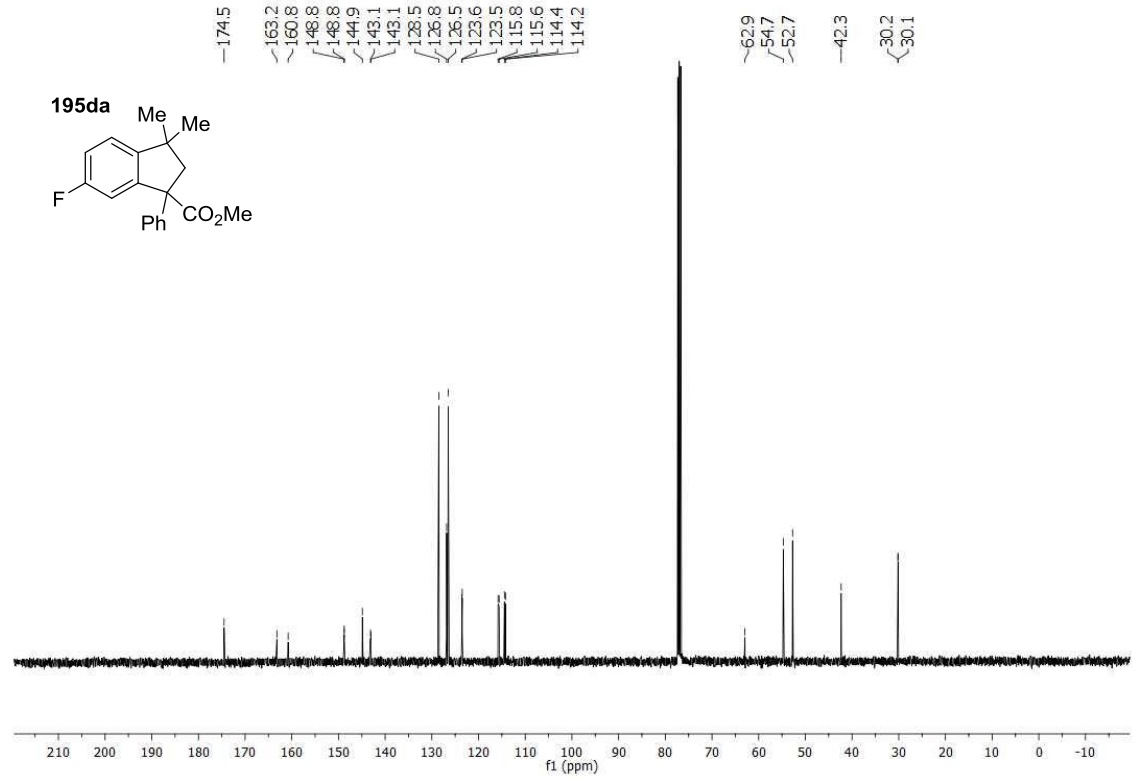
195da
Me
Me
F
Ph
CO2Me
174.5
163.2
160.8
148.8
148.8
144.9
143.1
143.1
128.5
126.8
126.5
123.6
123.5
115.8
115.6
114.4
114.2
62.9
54.7
52.7
42.3
30.2
30.1
f1 (ppm)

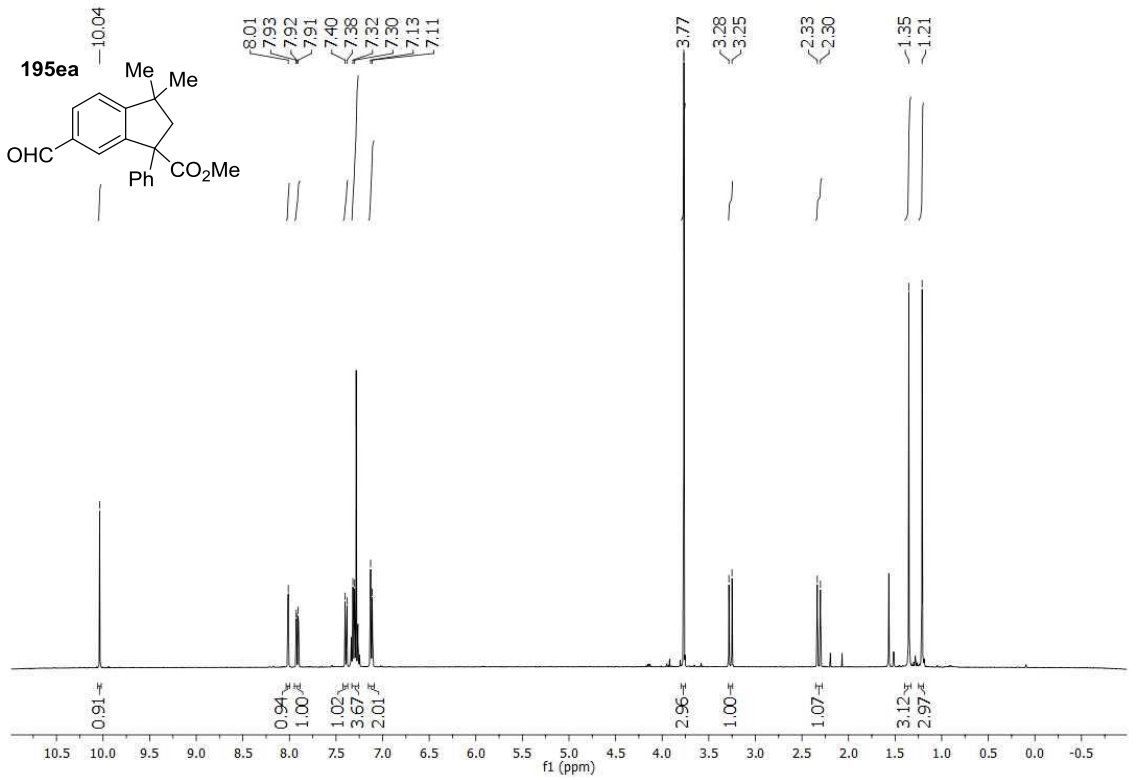
195ea
Me
Me
OHC
Ph
CO2Me
10.04
8.01
7.93
7.92
7.91
7.40
7.38
7.32
7.30
7.13
7.11
3.77
3.28
3.25
2.33
2.30
1.35
1.21
0.91
0.94
1.00
1.02
3.67
2.01
2.96
1.00
1.07
3.12
2.97
f1 (ppm)

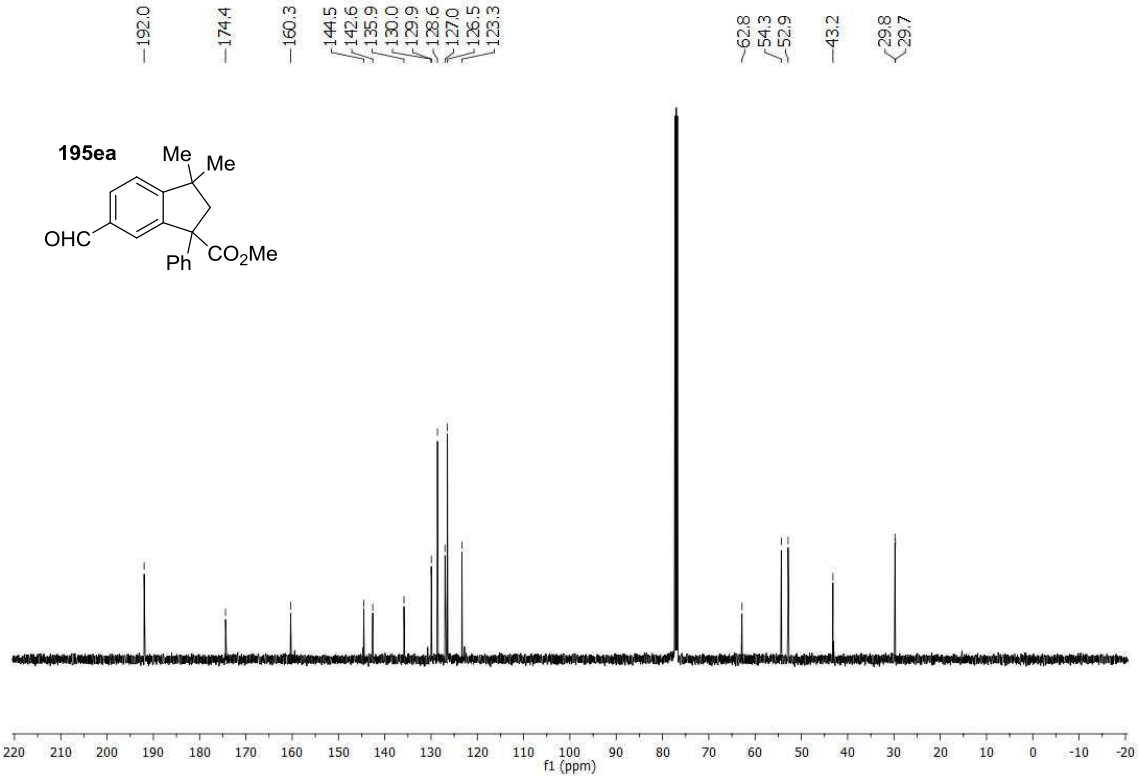
195ea
Me
Me
OHC
Ph
CO2Me
192.0
174.4
160.3
144.5
142.6
135.9
130.0
129.9
128.6
127.0
126.5
123.3
62.8
54.3
52.9
43.2
29.8
29.7
f1 (ppm)

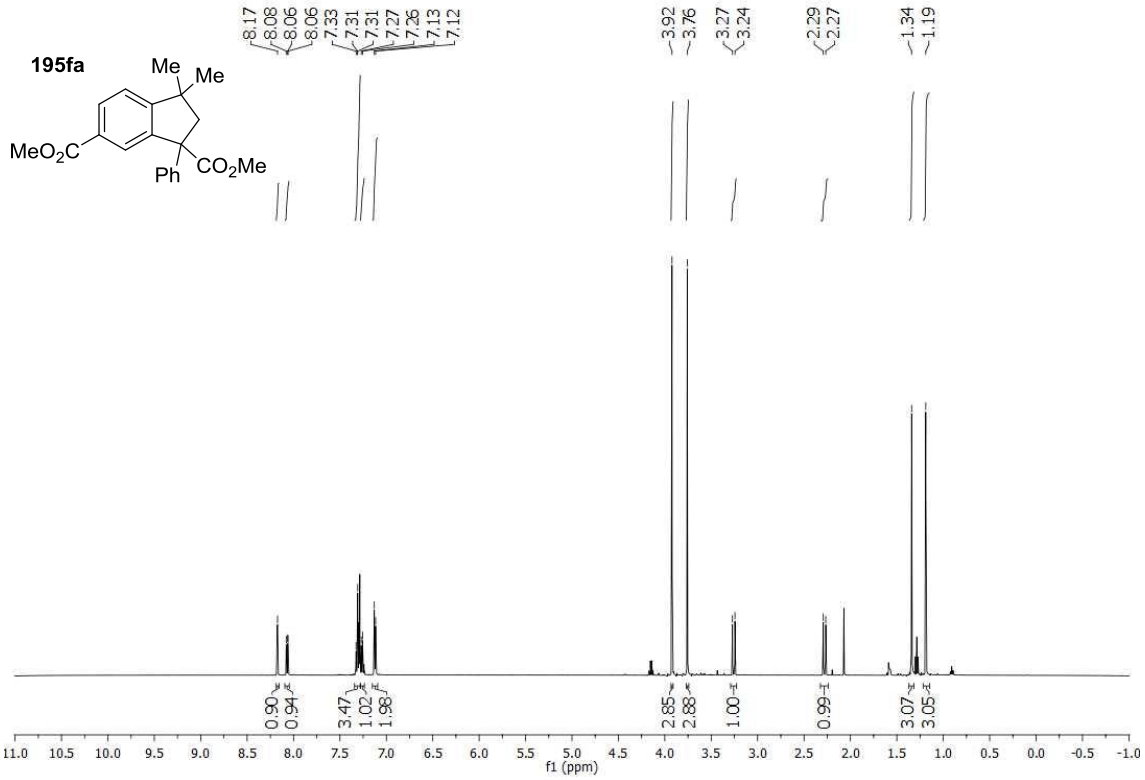
195fa
Me
Me
MeO2C
Ph
CO2Me
8.17
8.08
8.06
8.06
7.33
7.31
7.31
7.27
7.26
7.13
7.12
3.92
3.76
3.27
3.24
2.29
2.27
1.34
1.19
0.90
0.94
3.47
1.02
1.98
2.85
2.88
1.00
0.99
3.07
3.05
f1 (ppm)

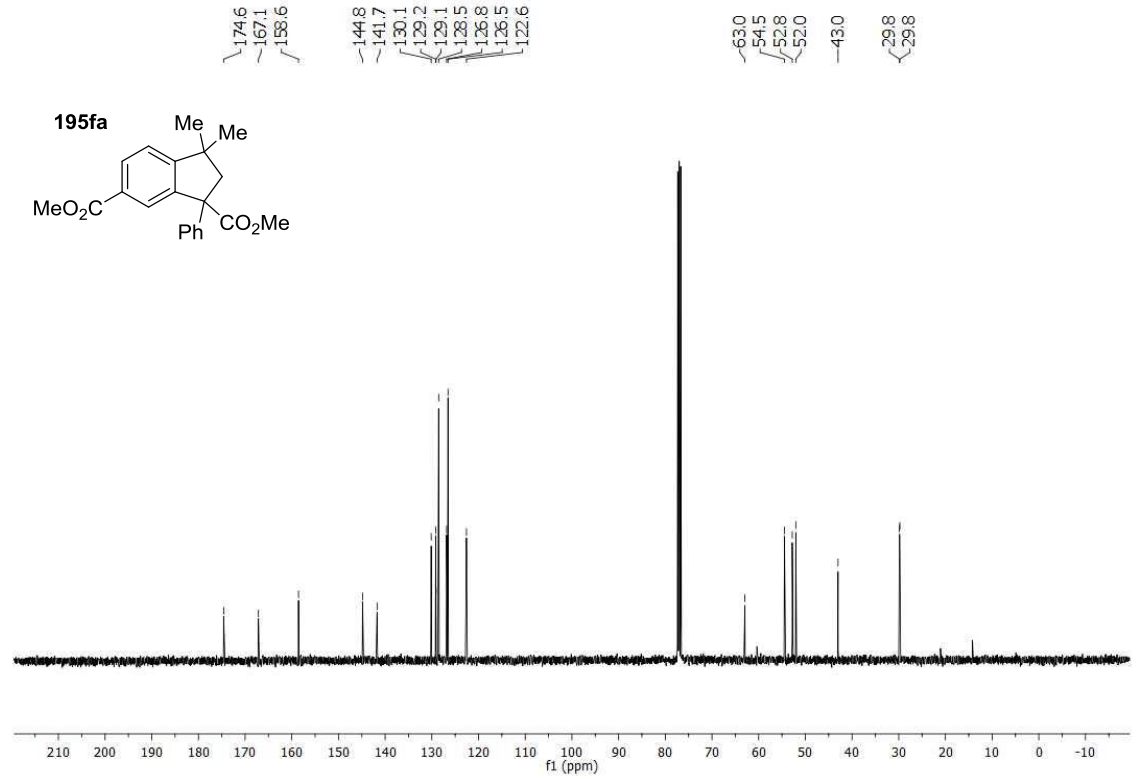
195fa
Me
Me
MeO2C
Ph
CO2Me
174.6
167.1
158.6
144.8
141.7
130.1
129.2
129.1
128.5
126.8
126.5
122.6
63.0
54.5
52.8
52.0
43.0
29.8
29.8
f1 (ppm)

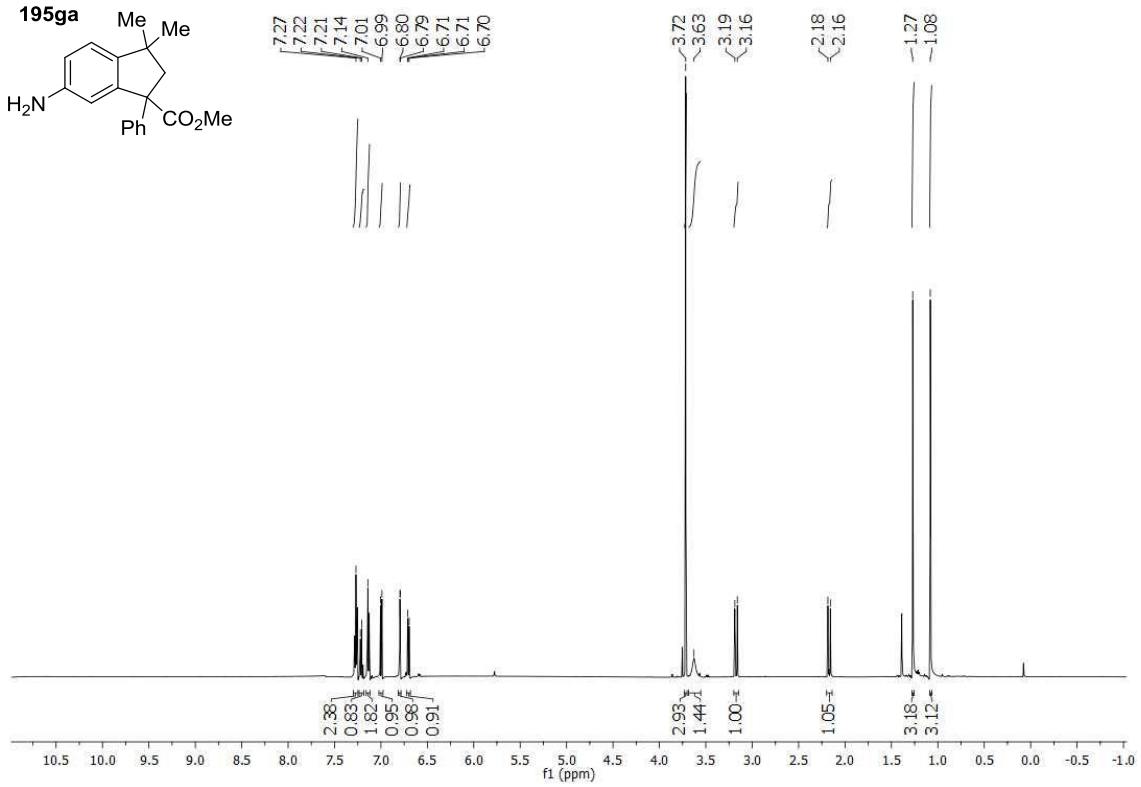
195ga
Me
Me
H2N
Ph
CO2Me
7.27
7.22
7.21
7.14
7.01
6.99
6.80
6.79
6.71
6.71
6.70
3.72
3.63
3.19
3.16
2.18
2.16
1.27
1.08
2.38
0.83
1.82
0.95
0.98
0.91
2.93
1.44
1.00
1.05
3.18
3.12
f1 (ppm)

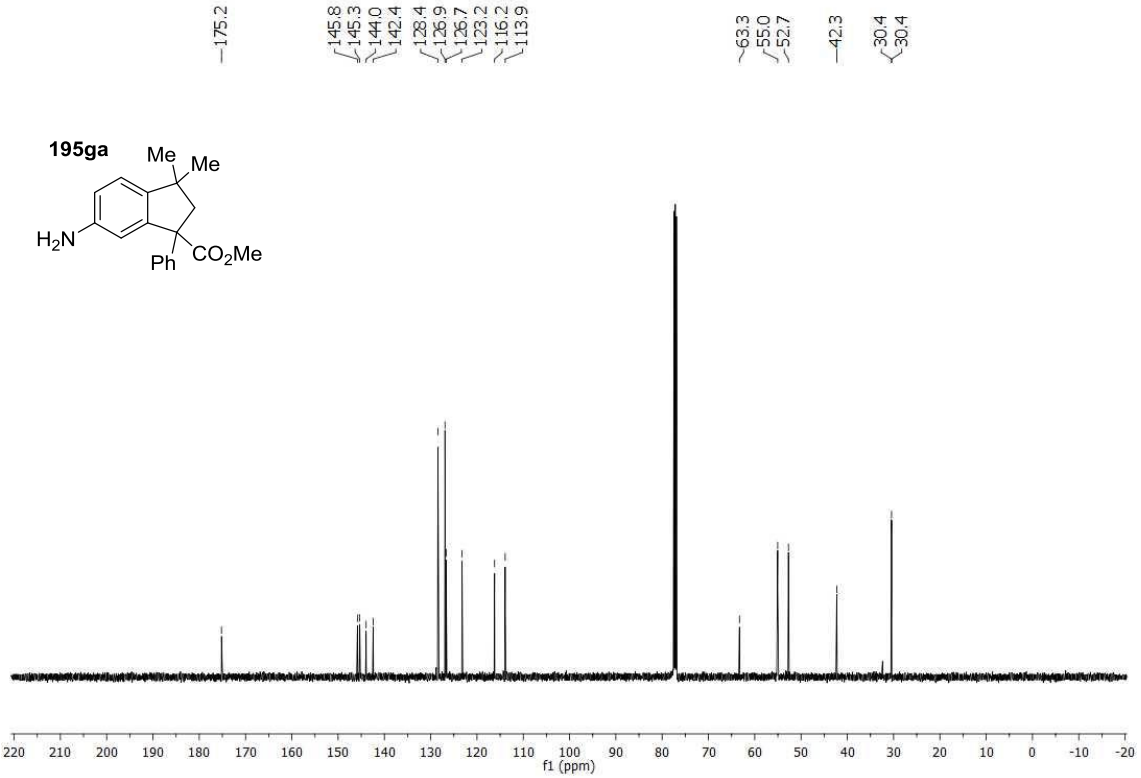
195ga
Me
Me
H2N
Ph
CO2Me
175.2
145.8
145.3
144.0
142.4
128.4
126.9
126.7
123.2
116.2
113.9
63.3
55.0
52.7
42.3
30.4
30.4
f1 (ppm)

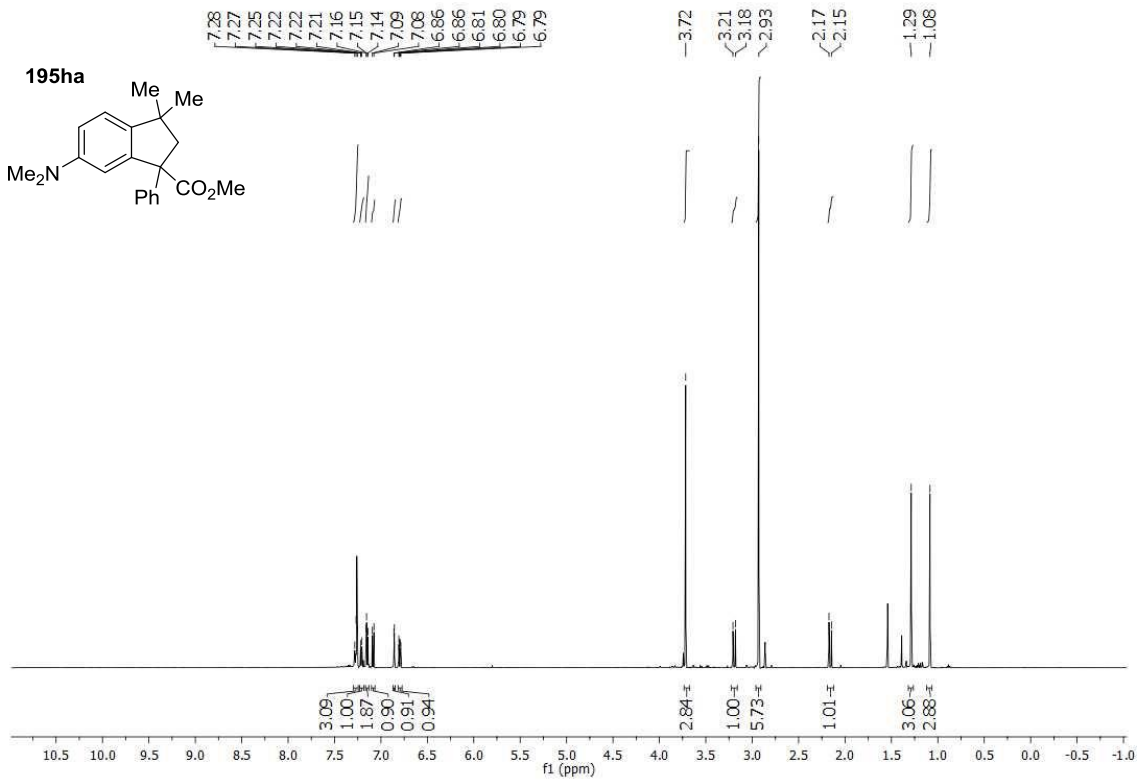
195ha
Me
Me
Me2N
Ph
CO2Me
7.28
7.27
7.25
7.22
7.22
7.21
7.16
7.15
7.14
7.09
7.08
6.86
6.86
6.81
6.80
6.79
6.79
3.72
3.21
3.18
2.93
2.17
2.15
1.29
1.08
3.09
1.00
1.87
0.90
0.91
0.94
2.84
1.00
5.73
1.01
3.06
2.88
f1 (ppm)

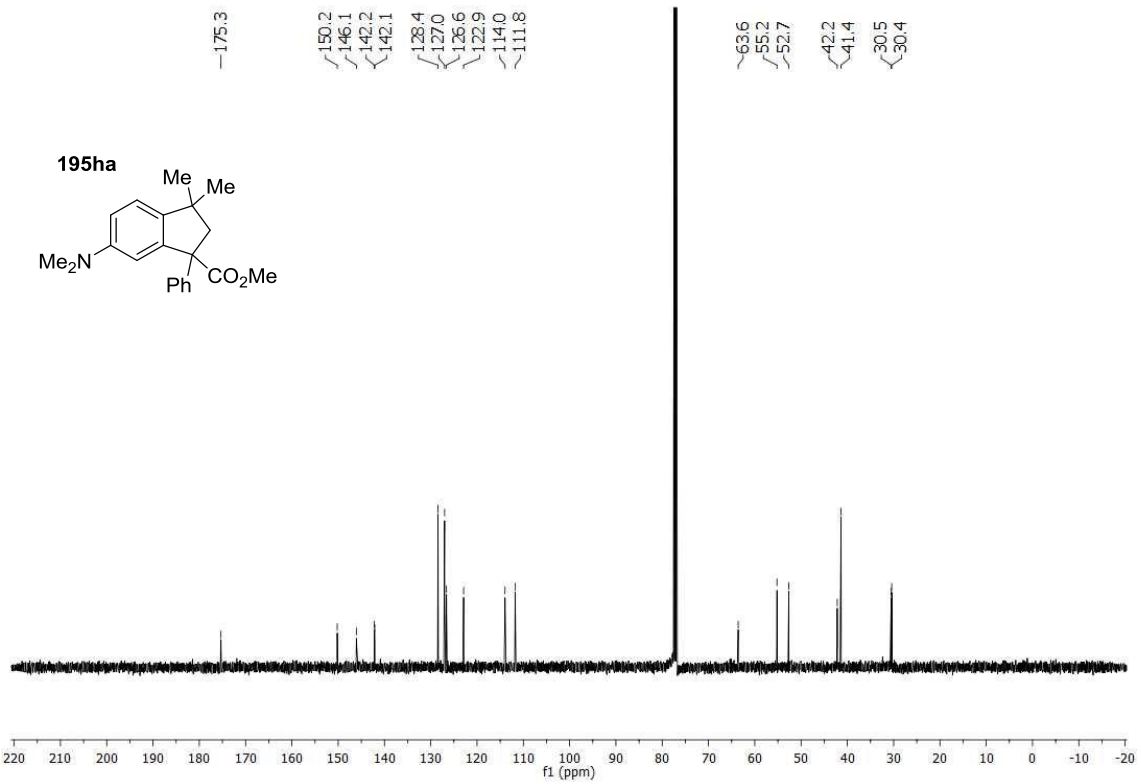
195ha
Me
Me
Me2N
Ph
CO2Me
175.3
150.2
146.1
142.2
142.1
128.4
127.0
126.6
122.9
114.0
111.8
63.6
55.2
52.7
42.2
41.4
30.5
30.4
f1 (ppm)

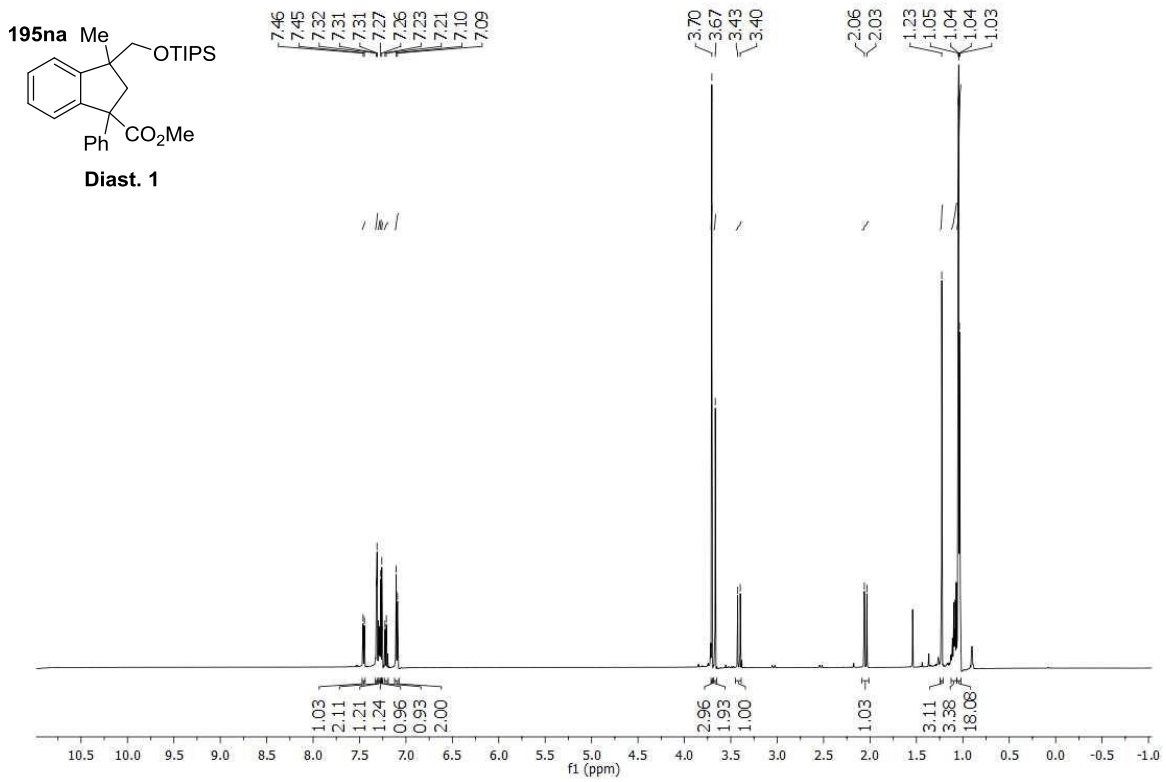
195na
Me
OTIPS
Ph
CO2Me
Diast. 1
7.46
7.45
7.32
7.31
7.31
7.27
7.26
7.23
7.21
7.10
7.09
3.70
3.67
3.43
3.40
2.06
2.03
1.23
1.05
1.04
1.04
1.03
1.03
2.11
1.21
1.24
0.96
0.93
2.00
2.96
1.93
1.00
1.03
3.11
3.38
18.08
f1 (ppm)

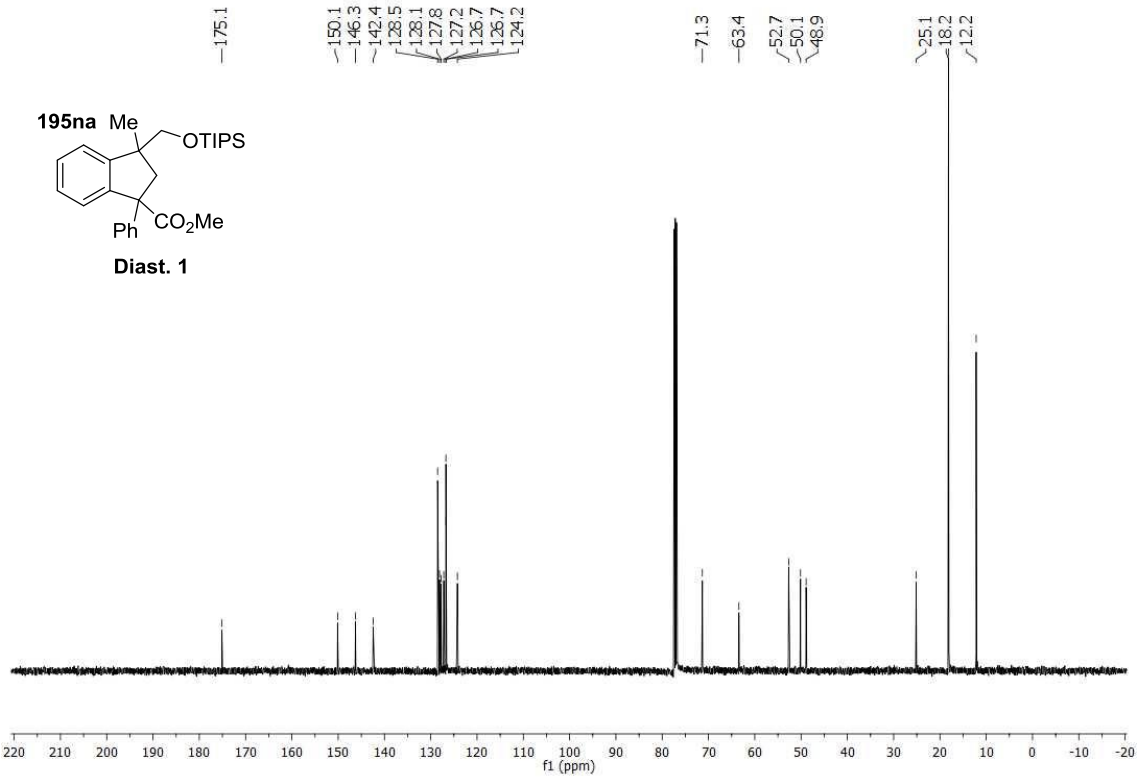
195na
Me
OTIPS
Ph
CO2Me
Diast. 1
175.1
150.1
146.3
142.4
128.5
128.1
127.8
127.2
126.7
126.7
124.2
71.3
63.4
52.7
50.1
48.9
25.1
18.2
12.2
f1 (ppm)

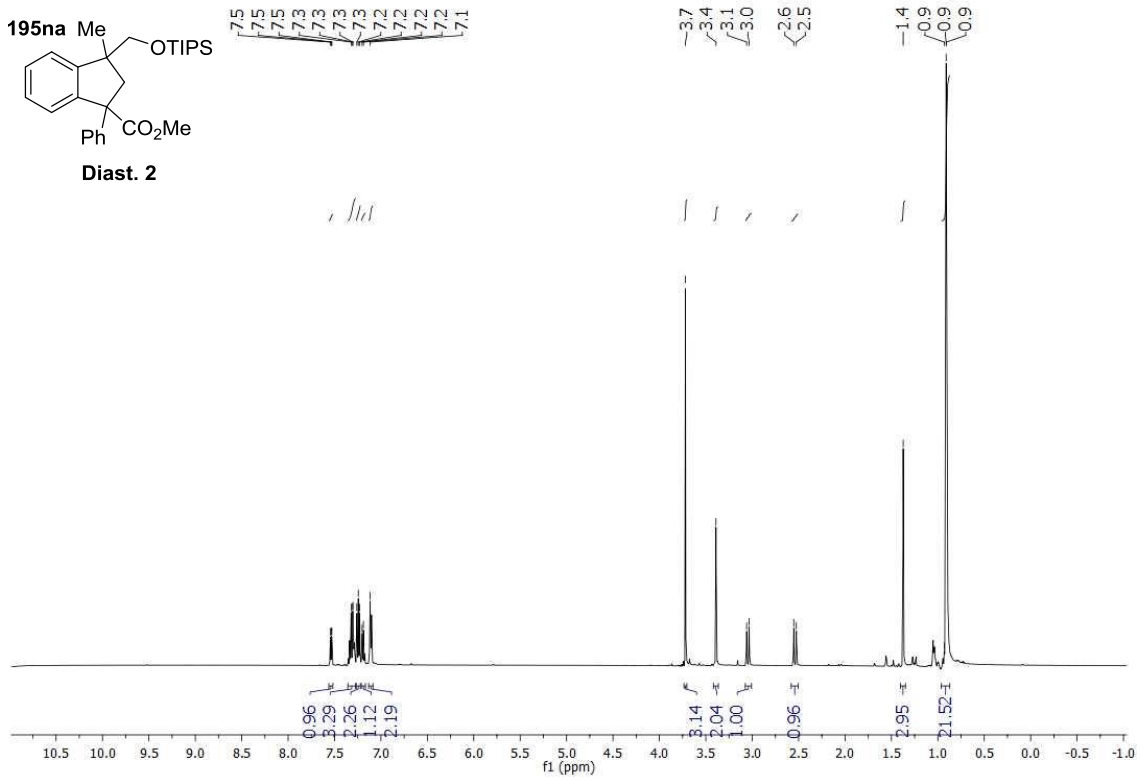
195na
Me
OTIPS
Ph
CO2Me
Diast. 2
7.5
7.5
7.5
7.3
7.3
7.3
7.3
7.2
7.2
7.2
7.2
7.1
3.7
3.4
3.1
3.0
2.6
2.5
1.4
0.9
0.9
0.9
0.96
3.29
2.26
1.12
2.19
3.14
2.04
1.00
0.96
2.95
21.52
f1 (ppm)

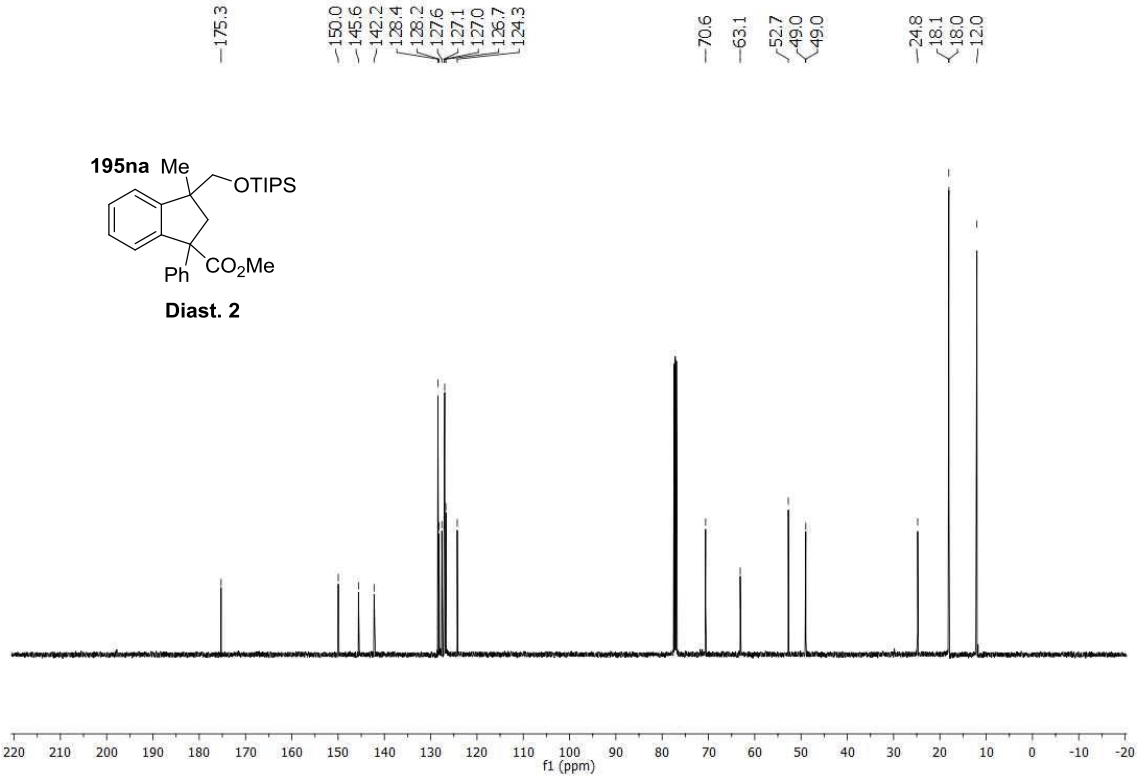
175.3
150.0
145.6
142.2
128.4
128.2
127.6
127.1
127.0
126.7
124.3
70.6
63.1
52.7
49.0
49.0
24.8
18.1
18.0
12.0
195na
Me
OTIPS
Ph
CO2Me
Diast. 2
f1 (ppm)

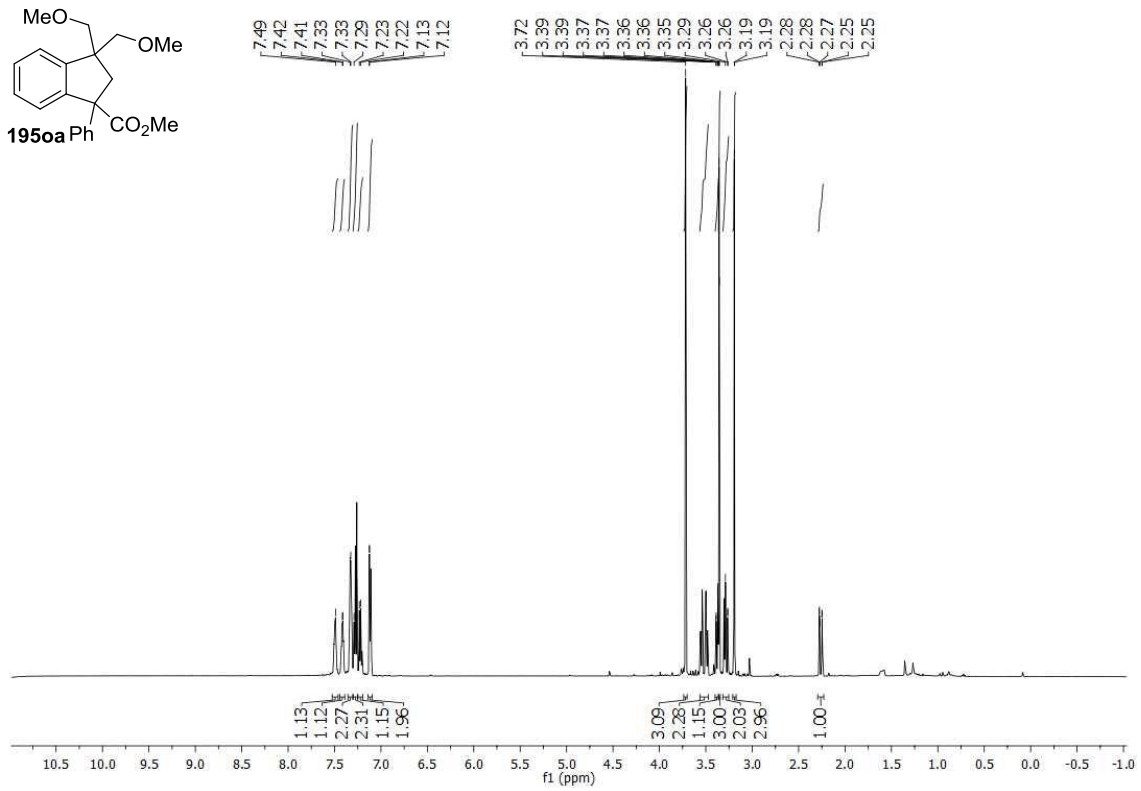
MeO
OMe
CO2Me
195oa Ph
7.49
7.42
7.41
7.33
7.33
7.29
7.23
7.22
7.13
7.12
3.72
3.39
3.39
3.37
3.37
3.36
3.36
3.35
3.29
3.26
3.26
3.19
3.19
2.28
2.28
2.27
2.25
2.25
1.13
1.12
2.27
2.31
1.15
1.96
3.09
2.28
1.15
3.00
2.03
2.96
1.00
f1 (ppm)

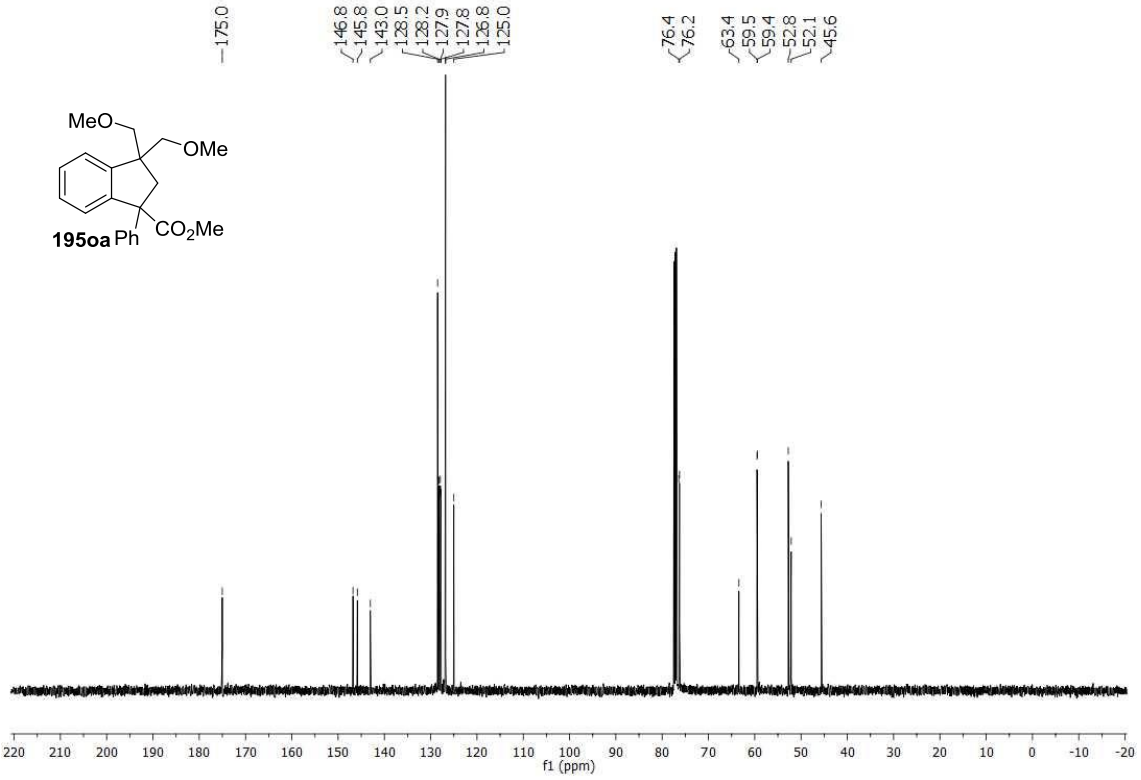
175.0
146.8
145.8
143.0
128.5
128.2
127.9
127.8
126.8
125.0
76.4
76.2
63.4
59.5
59.4
52.8
52.1
45.6
MeO
OMe
CO2Me
195oa Ph
f1 (ppm)

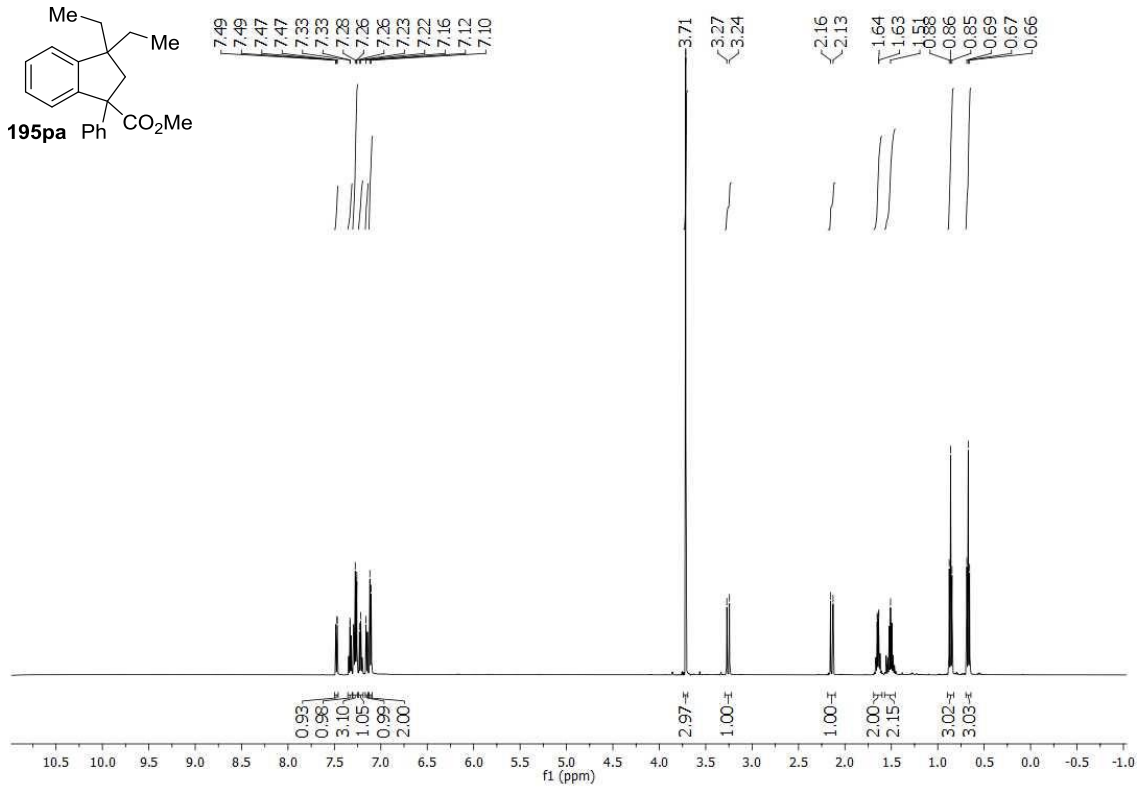
Me
Me
CO2Me
195pa Ph
7.49
7.49
7.47
7.47
7.33
7.33
7.28
7.26
7.26
7.23
7.22
7.16
7.12
7.10
3.71
3.27
3.24
2.16
2.13
1.64
1.63
1.51
0.88
0.86
0.85
0.69
0.67
0.66
0.93
0.98
3.10
1.05
0.99
2.00
2.97
1.00
1.00
2.00
2.15
3.02
3.03
f1 (ppm)

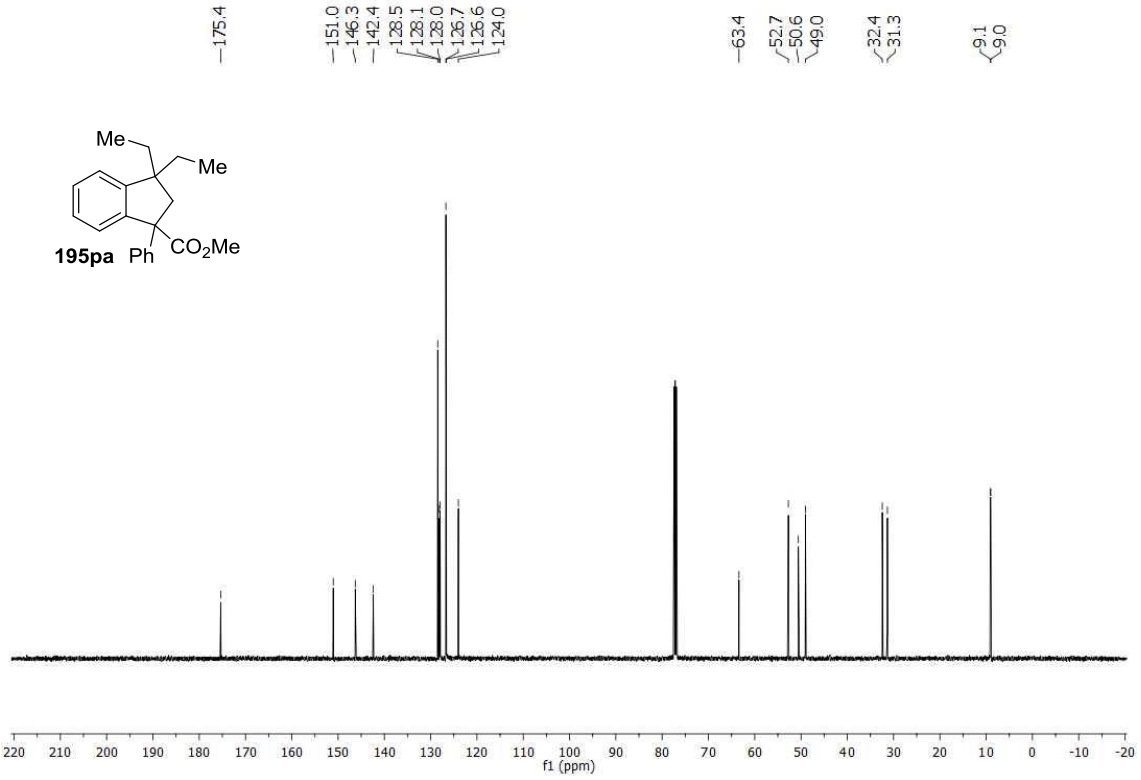
175.4
151.0
146.3
142.4
128.5
128.1
128.0
126.7
126.6
124.0
63.4
52.7
50.6
49.0
32.4
31.3
9.1
9.0
Me
Me
CO2Me
195pa Ph
f1 (ppm)

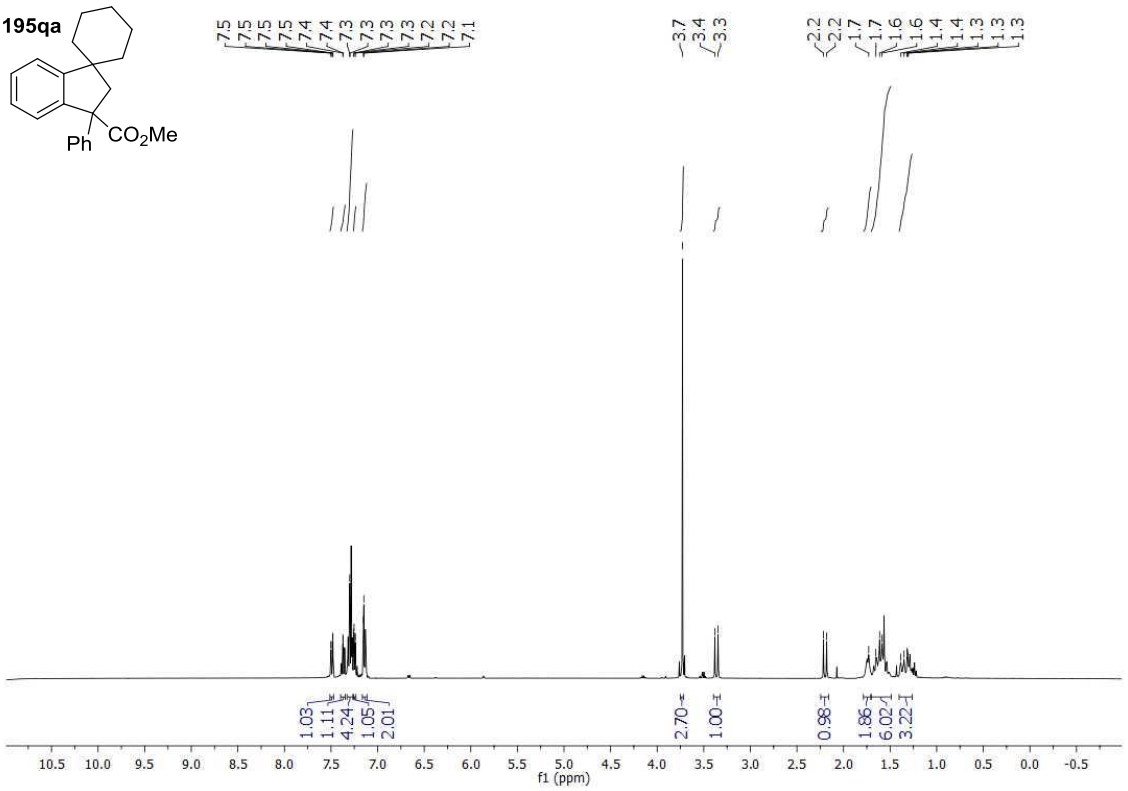
195qa
Ph
CO2Me
7.5
7.5
7.5
7.5
7.4
7.4
7.3
7.3
7.3
7.3
7.2
7.2
7.1
3.7
3.4
3.3
2.2
2.2
1.7
1.7
1.6
1.6
1.4
1.4
1.3
1.3
1.3
1.03
1.11
4.24
1.05
2.01
2.70
1.00
0.98
1.86
6.02
3.22
f1 (ppm)

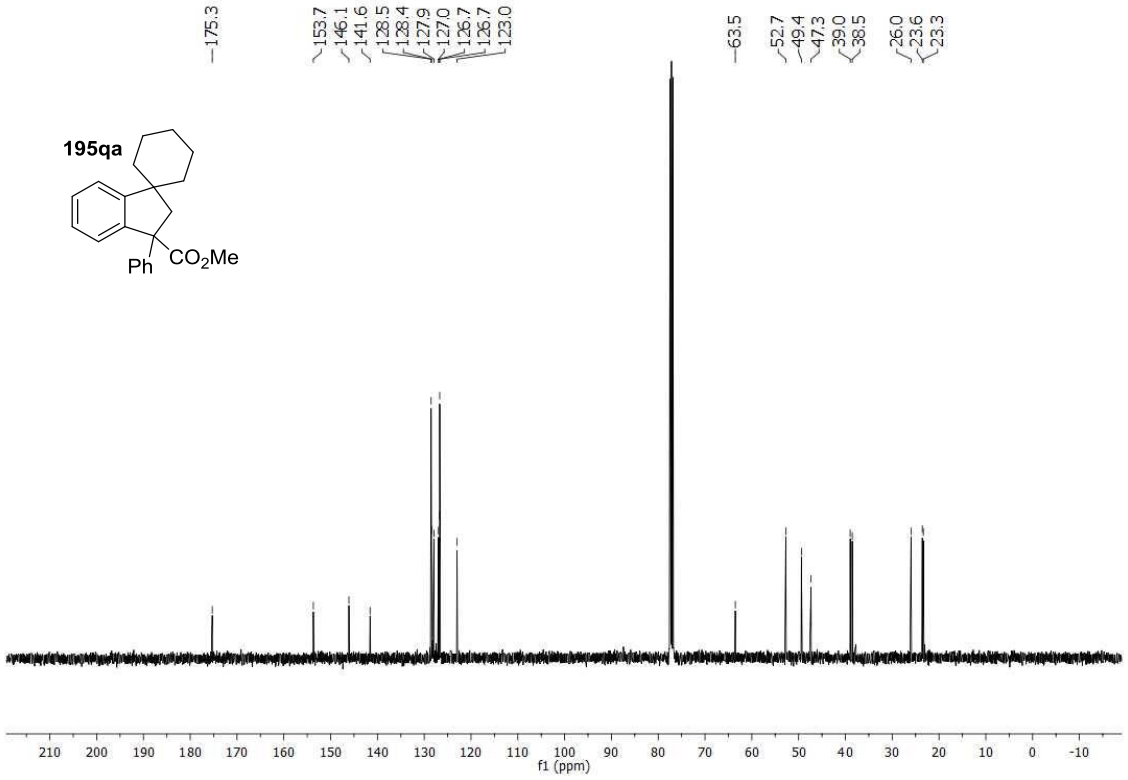
195qa
Ph
CO2Me
175.3
153.7
146.1
141.6
128.5
128.4
127.9
127.0
126.7
126.7
123.0
63.5
52.7
49.4
47.3
39.0
38.5
26.0
23.6
23.3
f1 (ppm)

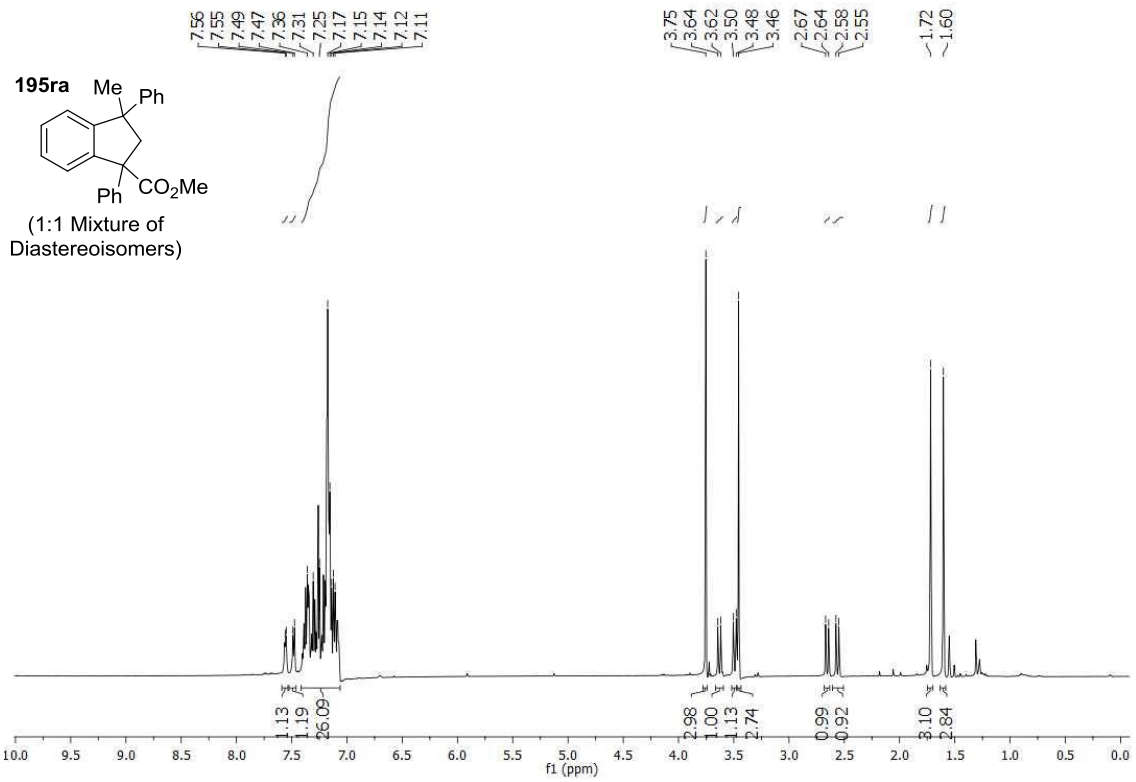
195ra
Me
Ph
Ph
CO2Me
(1:1 Mixture of Diastereoisomers)
7.56
7.55
7.49
7.47
7.36
7.31
7.25
7.17
7.15
7.14
7.12
7.11
3.75
3.64
3.62
3.50
3.48
3.46
2.67
2.64
2.58
2.55
1.72
1.60
1.13
1.19
26.09
2.98
1.00
1.13
2.74
0.99
0.92
3.10
2.84
f1 (ppm)

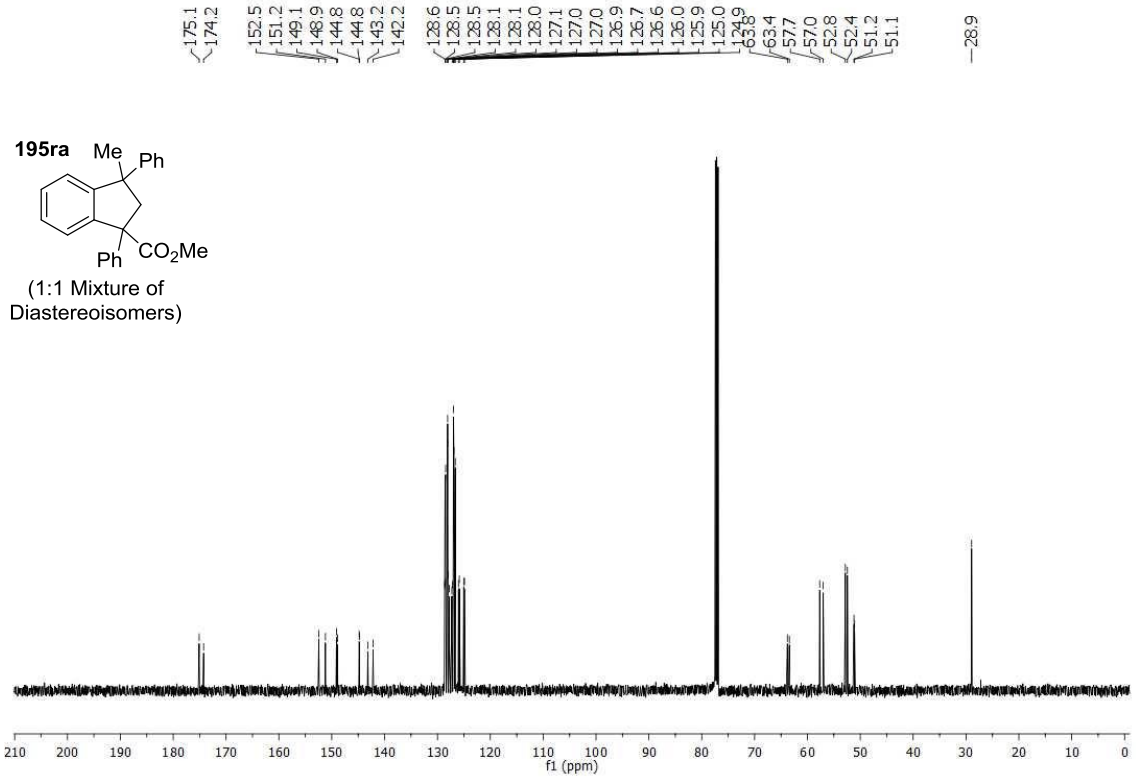
195ra
Me
Ph
Ph
CO2Me
(1:1 Mixture of Diastereoisomers)
175.1
174.2
152.5
151.2
149.1
148.9
144.8
144.8
143.2
142.2
128.6
128.5
128.5
128.1
128.1
128.0
127.1
127.0
127.0
126.9
126.7
126.6
126.0
125.9
125.0
124.9
63.8
63.4
57.7
57.0
52.8
52.4
51.2
51.1
28.9
f1 (ppm)

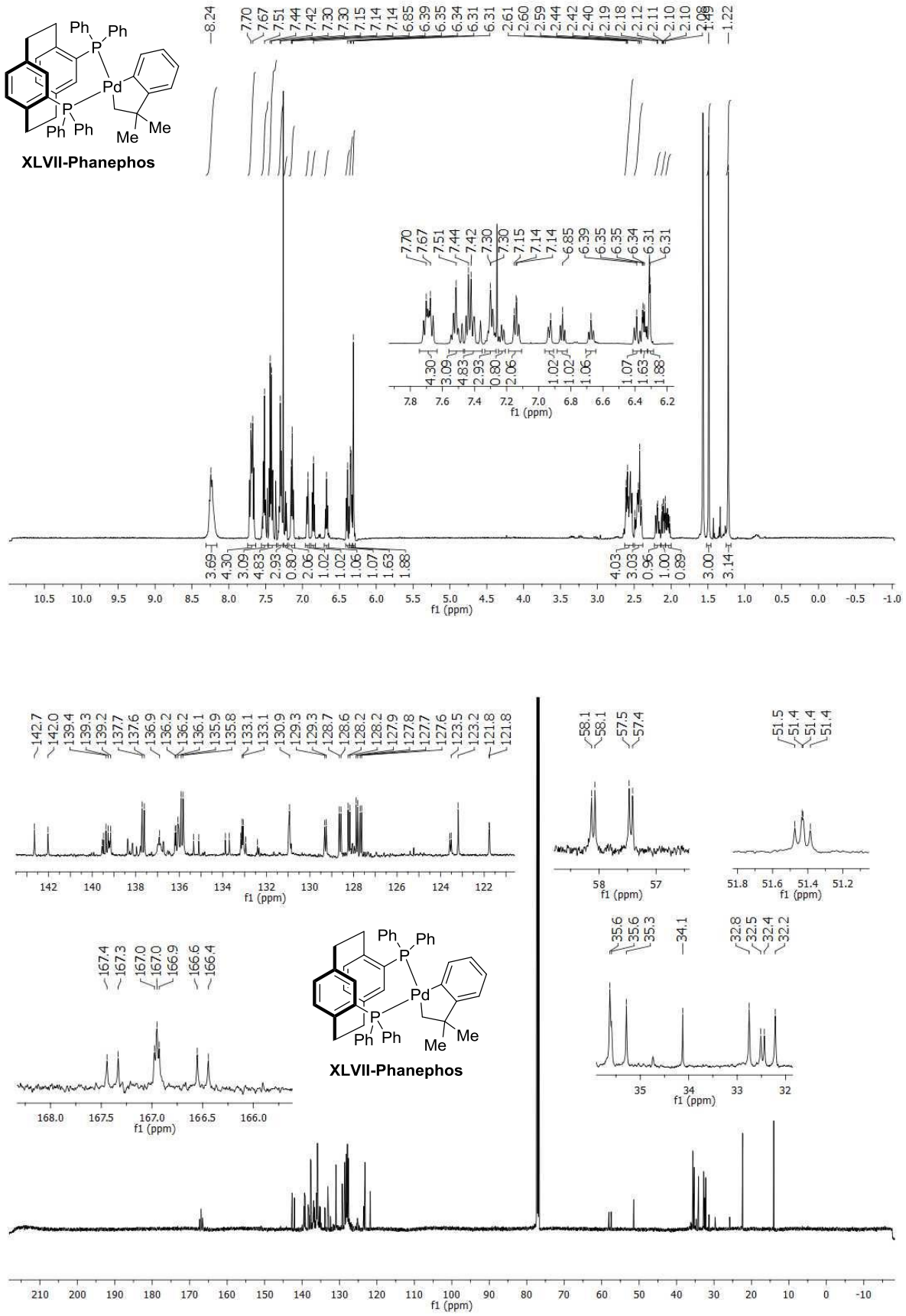
XLVII-Phanephos
f1 (ppm)
XLVII-Phanephos
f1 (ppm)

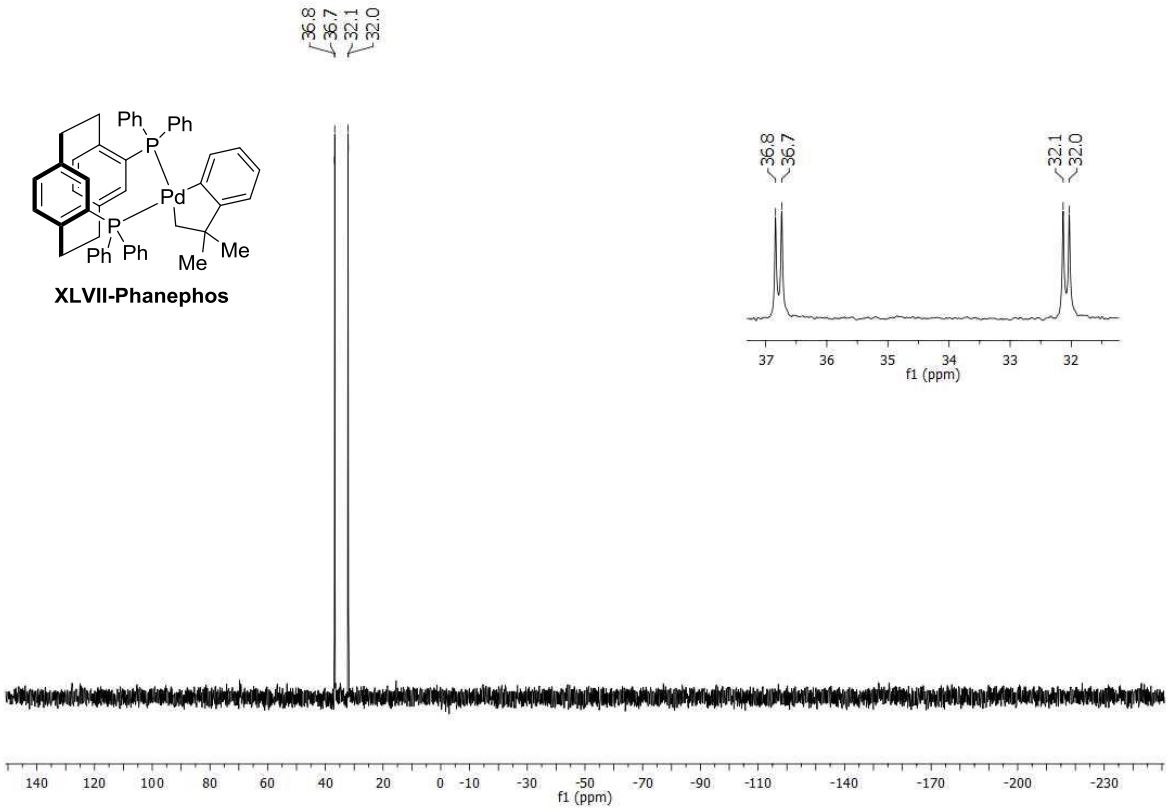

XLVII-Phanephos

6.2. NHC-Dichotomy in Pd-catalyzed Acylation of Aryl Chlorides via C-H bond-functionalization. Experimental Procedures.

6.2.1. General Considerations

Reagents. All reactions were set up in the air (with no use of a glovebox) and carried out under an argon atmosphere in resealable screw-cap test tubes. Palladium sources were purchased in Strem Chemicals, $Pd(OAc)_2$ was a gift from Johnson Matthey. IMes·Cl was purchased by Strem Chemicals; IAd·BF_4 was prepared in bulk according to the methodology described by Glorius.[349] Powdered Cs_2CO_3 was purchased from Alfa Aesar. The bulk of Cs_2CO_3 was stored under nitrogen in a vacuum atmosphere glovebox. Small portions (~ 5 g) were removed from the glovebox in glass vials, stored in the air in a desiccator filled with anhydrous calcium sulfate, and weighed in the air. Anhydrous 1,4-dioxane was purchased from Aldrich in Sure/Seal™ bottles. The corresponding α-aryl aldehydes were prepared according to the known reported procedure.[227,232] All other reagents were purchased from commercial sources and used as received. Flash chromatography was performed with EM Science silica gel 60 (230-400 mesh).

Analytical methods. ^{1}H NMR and ^{13}C NMR spectra and melting points (where applicable) are included for all compounds. ^{1}H and ^{13}C NMR spectra were recorded on a Bruker 400 MHz at 20 ^{o}C. All ^{1}H NMR spectra are reported in parts per million (ppm) downfield of TMS and were measured relative to the signals for $CHCl_3$ (7.26 ppm). All ^{13}C NMR spectra were reported in ppm relative to residual $CHCl_3$ (77 ppm) and were obtained with ^{1}H decoupling. Coupling constants, *J*, are reported in hertz. Melting points were measured using open glass capillaries in a Büchi B540 apparatus. Gas chromatographic analyses were performed on Hewlett-Packard 6890 gas chromatography instrument with a FID detector.

The yields reported in the Chapter 3 refer to isolated yields and represent an average of at least two independent runs. The procedures described in this section are representative. Thus, the yields may differ slightly from those given in the Chapter 3.

6.2.2. Optimization details

General procedure for screening reaction (Tables 3.1 to 3.5): A 12.0 mL test tube is charged with Pd precatalyst, ligand, and the substrate **259a** (0.2 mmol, 1.0 equiv., 44.5 mg). Then, the base is weighed out into the glovebox. Under a positive Ar flow the corresponding anhydrous solvent was added (0.8 mL, 0.25M) followed by addition of the additive with a microsyringe (50 mol%). Finally, the reaction is placed on a preheated block and stirred for 16h at the desired temperature. After this time, the reaction is cooled down to room temperature. Next,

[349] Richter, H., Schwertfeger, H., Schereiner, P. R., Fröhlich, r., Glorius, F. *Synlett* **2009**, 2, 193.

dodecane (0.2 mmol) was added via microsyringe followed by 5 mL of EtOAc. An aliquot was filtered through a plug of silica and Celite® and analyzed by GC.

6.2.3. Synthesis of the starting materials

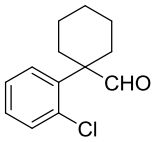

1-(2-chlorophenyl)cyclohexanecarbaldehyde (259a). Column chromatography: silica gel, hexanes:EtOAc 9:1. 1H NMR (400 MHz, $CDCl_3$) δ 9.83 (s, 1H), 7.50 (dd, J = 7.9, 1.7 Hz, 1H), 7.38 (dd, *J* = 7.8, 1.5 Hz, 1H), 7.31 (td, *J* = 7.6, 1.6 Hz, 1H), 7.26–7.21 (m, 1H), 2.38–2.26 (m, 2H), 2.00–1.89 (m, 2H), 1.79–1.60 (m, 5H), 1.49–1.36 (m, 1H) ppm. ^{13}C NMR (101 MHz, $CDCl_3$) δ 203.9, 140.7, 133.5, 131.2, 128.9, 128.6, 127.0, 53.9, 31.2, 25.5, 22.4 ppm. IR (neat, cm^{-1}): 2931, 2857, 1722, 1469, 1450, 1067, 1033, 753, 734, 705, 459. HRMS calcd for ($C_{13}H_{15}ClO$+H): 223.0890, found 223.0890

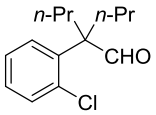

2-(2-chlorophenyl)-2-propylpentanal (259b). Column chromatography: silica gel, hexanes:EtOAc 9:1. ^{1}H NMR (400 MHz, $CDCl_3$) δ 9.77 (s, 1H), 7.41–7.34 (m, 2H), 7.31 (td, *J* = 7.6, 1.6 Hz, 1H), 7.27–7.22 (m, 1H), 2.06–1.88 (m, 4H), 1.29–1.13 (m, 2H), 1.13–0.97 (m, 2H), 0.89 (t, *J* = 7.2 Hz, 6H) ppm. ^{13}C NMR (101 MHz, $CDCl_3$) δ 203.9, 138.4, 133.8, 131.1, 129.7, 128.6, 126.8, 57.5, 34.5, 16.8, 14.6 ppm. IR (neat, cm^{-1}): 2958, 2872, 1721, 1467, 1047, 753, 727. HRMS calcd for ($C_{14}H_{18}ClO$+H): 239.1203, found 239.1196.

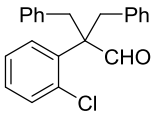

2-benzyl-2-(2-chlorophenyl)-3-phenylpropanal (259c). Column chromatography: silica gel, hexanes:EtOAc 95:5. Yellow solid (mp = 97ºC). ^{1}H NMR (300 MHz, $CDCl_3$) δ 9.93 (s, 1H), 7.46 (dd, *J* = 8.0, 1.4 Hz, 1H), 7.33–7.24 (m, 1H), 7.24–7.09 (m, 8H), 7.01–6.88 (m, 3H), 3.41 (d, *J* = 2.9 Hz, 4H) ppm. ^{13}C NMR (75 MHz, $CDCl_3$) δ 204.3, 135.8, 131.1, 130.8, 129.1, 128.0, 126.6, 126.5, 58.8, 40.2 ppm. IR (neat, cm^{-1}): 2821, 1717, 1469, 1060, 1033, 768, 699, 528. HRMS calcd for ($C_{22}H_{19}ClO$+Na): 357.1022, found 357.1007.

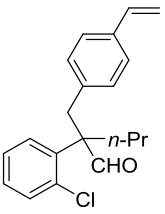

2-(2-chlorophenyl)-2-(4-vinylbenzyl)ventanal (259d). Column chromatography: silica gel, hexanes:EtOAc 12:1. Colorless liquid; ^{1}H NMR (300 MHz, $CDCl_3$) δ 9.99 (s, 1H), 7.67 (m, 1H), 7.21 (m, 2H), 7.14 (d, *J* = 8.1 Hz, 2H), 6.93 (m, 1H), 6.67 (d, *J* = 11.1 Hz, 1H), 6.59 (d, *J* = 8.1 Hz, 2H), 5.68 (d, *J* = 17.7 Hz, 1H), 5.18 (d, *J* = 17.7 Hz, 1H), 3.52 (d, *J* = 13.8 Hz, 1H), 3.32 (d, *J* = 13.8 Hz, 1H), 1.86 (t, *J* = 8.7 Hz, 2H), 1.37 (m, 2H), 0.92 (t, *J* = 7.2 Hz, 3H) ppm. ^{13}C NMR (75 MHz, $CDCl_3$) δ 204.1, 138.9, 136.5, 136.1, 135.6, 134.6, 131.0, 130.7, 129.2, 127.2, 125.5, 123.9, 113.3, 59.0, 37.8, 36.4, 16.9, 14.7 ppm. IR (neat, cm^{-1}): 3056, 2976, 2861, 1713, 1646, 1541, 1487, 1390, 1194, 978. HRMS calcd for ($C_{20}H_{21}ClO$+Na): 335.1179, found 335.1183.

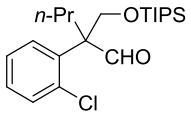

2-(2-chlorophenyl)-2-((triisopropylsilyloxy)methyl)ventanal (259e). Column chromatography: silica gel, hexanes:EtOAC 95:5. Colorless oil; ^{1}H NMR (400 MHz, $CDCl_3$) δ 9.87 (s, 1H), 7.38 (td, *J* = 7.7, 1.8 Hz, 2H), 7.30 (td, *J* = 7.6, 1.8 Hz, 1H), 7.27 - 7.23 (m, 1H), 4.37 (d, *J* = 9.7 Hz, 1H), 4.22 (d, *J* = 9.7 Hz, 1H), 2.22 (ddd, *J* = 13.9, 12.4, 4.8 Hz, 1H), 2.05 (ddd, *J* = 13.9, 12.3, 4.5 Hz, 1H), 1.28 - 0.95 (m, 12H), 0.91 (t, *J* = 7.2 Hz, 4H). ^{13}C NMR (75 MHz, $CDCl_3$) δ 204.4, 137.3, 133.7, 130.9, 130.5, 128.8, 126.8, 65.4, 59.6, 32.8, 18.0, 18.0, 17.2, 14.8, 12.0 ppm. IR (neat, cm^{-1}): 2962, 2866, 1721, 1465, 1102, 1043, 881, 747, 456. HRMS *calcd* for ($C_{21}H_{35}ClO_2Si$+Na): 405.1993, *found* 405.1988.

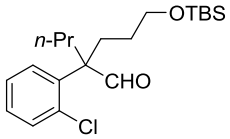

5-(*tert*-butyldimethylsilyloxy)-2-(2-chlorophenyl)-2-propylpentanal (259f). Column chromatography: silica gel, hexanes:EtOAC 9:1. Colorless oil; ^{1}H NMR (300 MHz, $CDCl_3$) δ 9.78 (s, 1H), 7.45 - 7.36 (m, 2H), 7.33 (dd, *J* = 7.3, 1.7 Hz, 1H), 7.30 - 7.25 (m, 2H), 3.56 (t, *J* = 6.2 Hz, 2H), 2.17 - 1.88 (m, 4H), 1.51 - 1.36 (m, 1H), 1.32 - 1.16 (m, 2H), 1.14 - 1.00 (m, 1H), 0.94 - 0.83 (m, 12H), 0.03 (s, 6H) ppm. ^{13}C NMR (75 MHz, $CDCl_3$) δ 204.0, 138.4, 133.9, 131.3, 130.0, 128.8, 127.0, 63.1, 57.2, 34.6, 28.6, 27.0, 26.1, 18.4, 16.9, 14.8, -5.2 ppm. IR (neat, cm^{-1}): 2956, 2930, 2857, 1472, 1254, 1099, 1040, 832, 774. HRMS *calcd* for ($C_{20}H_{33}ClO_2Si$+H): 369.2017, *found* 369.2005.

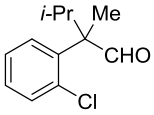

2-(2-chlorophenyl)-2,3-dimethylbutanal (259g). Column chromatography: silica gel, hexanes:EtOAc 12:1. Colorless oil; ^{1}H NMR (300 MHz, $CDCl_3$) δ 10.03 (s, 1H), 7.48 - 7.42 (m,

2H), 7.40 - 7.33 (m, 1H), 7.31 (d, *J* = 7.5 Hz, 1H), 2.94 (hept, *J* = 6.9 Hz, 1H), 1.45 (s, 3H), 1.17 (d, *J* = 6.9 Hz, 3H), 0.80 (d, *J* = 6.8 Hz, 3H) ppm. ^{13}C NMR (75 MHz, $CDCl_3$) δ 203.5, 140.2, 133.3, 131.1, 129.7, 128.6, 126.9, 56.8, 30.8, 18.6, 18.2, 17.0 ppm. IR (neat, cm^{-1}): 2967, 2877, 2816, 1720, 1469, 1430, 1043, 754, 471. HRMS *calcd* for ($C_{12}H_{15}ClO$+H): 211.0890, *found* 211.0893.

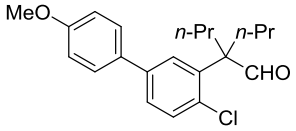

2-(4-chloro-4'-methoxy-[1,1'-biphenyl]-3-yl)-2-propylpentanal (259h). Column chromatography: silica gel, hexanes:EtOAc 2:1. White solid (mp=67.5ºC). ^{1}H NMR (300 MHz, $CDCl_3$) δ 9.81 (s, 1H), 7.50 (dd, *J* = 6.6, 2.1 Hz, 3H), 7.43 (s, 2H), 7.02 (d, *J* = 8.7 Hz, 2H), 3.88 (s, 3H), 2.17–1.88 (m, 4H), 1.35–1.19 (m, 2H), 1.17–1.02 (m, 2H), 0.92 (t, *J* = 7.1 Hz, 6H) ppm. ^{13}C NMR (101 MHz, $CDCl_3$) δ 203.9, 159.5, 139.6, 138.6, 132.7, 132.2, 131.4, 128.2, 128.1, 126.9, 114.4, 57.6, 55.4, 34.5, 16.9, 14.7 ppm. IR (neat, cm^{-1}): 2955, 2870, 1720, 1605, 1514, 1463, 1441, 1248, 1179, 1038, 817, 746, 487, 448. HRMS calcd for ($C_{21}H_{25}ClO_2$+Na): 367.1441, found 367.1433.

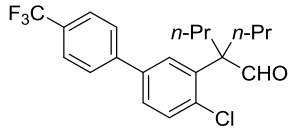

2-(4-chloro-4'-(trifluoromethyl)-[1,1'-biphenyl]-3-yl)-2-propylpentanal (259i). Column chromatography: silica gel, hexanes:EtOAc 9:1. White solid (mp=74.6ºC). ^{1}H NMR (300 MHz, $CDCl_3$) δ 9.82 (s, 1H), 7.71 (dd, *J* = 21.8, 8.3 Hz, 4H), 7.58–7.46 (m, 3H), 2.26–1.91 (m, 4H), 1.38–1.04 (m, 4H), 0.93 (t, *J* = 7.2 Hz, 6H) ppm. ^{13}C NMR (101 MHz, $CDCl_3$) δ 203.5, 143.7, 139.2, 138.6, 133.9, 131.7, 128.7, 127.4, 126.0, 124.1, 57.6, 34.4, 16.9, 14.6 ppm. IR (neat, cm^{-1}): 2965, 2875, 1719, 1615, 1465, 1321, 1160, 1109, 1069, 1014, 844, 817, 744, 677, 625, 486. HRMS calcd for ($C_{21}H_{22}OClF_3$+H): 383.1390, *found* 383.1389.

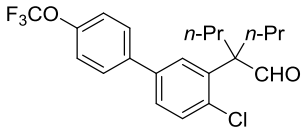

2-(4-chloro-4'-(trifluoromethoxy)-[1,1'-biphenyl]-3-yl)-2-propylpentanal (259j). Column chromatography: silica gel, hexanes:EtOAc 9:1. Yellow pale solid (mp=50.5ºC). ^{1}H NMR (300 MHz, $CDCl_3$) δ 9.82 (s, 1H), 7.58 (d, *J* = 8.7 Hz, 2H), 7.54–7.40 (m, 3H), 7.34 (d, *J* = 8.1 Hz, 2H), 2.21–1.86 (m, 4H), 1.35–1.01 (m, 4H), 0.93 (t, *J* = 7.2 Hz, 6H) ppm. ^{13}C NMR (101 MHz, $CDCl_3$) δ 203.6, 149.0 (d, $^3J_{C\text{-}F}$ = 1.8 Hz), 139.1, 138.9, 138.7, 133.3, 131.6, 128.5, 127.3, 121.4, 120.5 (d, $^1J_{C\text{-}F}$ = 257.4 Hz), 57.6, 34.4, 16.9, 14.7 ppm. IR (neat, cm^{-1}): 2960, 2872, 1720, 1511, 1466,

1250, 1206, 1153, 1051, 1016, 922, 853, 809, 739, 739, 654. HRMS calcd for ($C_{21}H_{22}ClF_3O_2$+Na): 421.1158, found 421.1148.

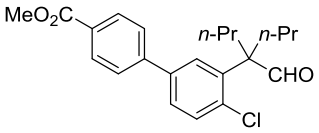

Methyl 4'-chloro-3'-(4-formylheptan-4-yl)-[1,1'-biphenyl]-4-carboxylate (259k). Column chromatography: silica gel, hexanes:EtOAc 2:1. White solid (mp=101.8ºC). ^{1}H NMR (300 MHz, $CDCl_3$) δ 9.8 (s, 1H), 8.23–8.06 (m, 2H), 7.63 (d, *J* = 8.4 Hz, 2H), 7.59–7.53 (m, 1H), 7.49 (d, *J* = 1.3 Hz, 2H), 3.96 (s, 3H), 2.17–1.90 (m, 4H), 1.38–1.01 (m, 4H), 0.92 (t, *J* = 7.2 Hz, 6H) ppm. ^{13}C NMR (75 MHz, $CDCl_3$) δ 203.6, 166.8, 144.5, 139.1, 138.8, 133.8, 131.6, 130.3, 129.4, 128.6, 127.4, 127.1, 57.6, 52.2, 34.4, 16.9, 14.7 ppm. IR (neat, cm^{-1}): 2961, 2872, 1711, 1608, 1432, 1285, 1189, 1109, 1050, 1034, 1016, 973, 865, 830, 768, 653, 474. HRMS calcd for ($C_{22}H_{25}ClO_3$+Na): 395.1390, *found* 395.1402.

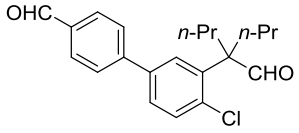

4'-chloro-3'-(4-formylheptan-4-yl)biphenyl-4-carbaldehyde (259l). Column chromatography: silica gel, hexanes:EtOAc 2:1. Yellow solid (mp = 74.5ºC). ^{1}H NMR (500 MHz, $CDCl_3$) δ 10.09 (s, 1H), 9.82 (s, 1H), 8.00 (d, *J* = 8.3 Hz, 2H), 7.73 (d, *J* = 8.2 Hz, 2H), 7.58 (s, 1H), 7.51 (d, *J* = 1.1 Hz, 2H), 2.13–1.97 (m, 4H), 1.32–1.20 (m, 2H), 1.19–1.04 (m, 2H), 0.93 (t, *J* = 7.3 Hz, 6H) ppm. ^{13}C NMR (126 MHz, $CDCl_3$) δ 203.5, 191.7, 146.0, 139.3, 138.6, 135.6, 134.1, 131.8, 130.4, 128.7, 127.7, 127.5, 57.6, 34.4, 16.9, 14.7 ppm. IR (neat, cm^{-1}): 2958, 2870, 1720, 1683, 1604, 1461, 1358, 1264, 1049, 960, 844, 739, 654, 617, 469. HRMS calcd for ($C_{21}H_{23}ClO_2$+H): 343.1465, *found* 343.1469.

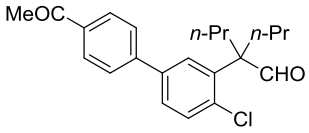

2-(4-chloro-4'-ethanoylbiphenyl-3-yl)-2-propylpentanal (259m). Column chromatography: silica gel, hexanes:EtOAc 9:1. White solid (mp=89.5ºC). ^{1}H NMR (500 MHz, $CDCl_3$) δ 9.81 (s, 1H), 8.07 (d, *J* = 8.4 Hz, 2H), 7.66 (d, *J* = 8.5 Hz, 2H), 7.57 (s, 1H), 7.50 (s, 2H), 2.66 (s, 3H), 2.17–1.92 (m, 4H), 1.34–1.21 (m, 2H), 1.21–1.04 (m, 2H), 0.93 (t, *J* = 7.3 Hz, 6H) ppm. ^{13}C NMR (126 MHz, $CDCl_3$) δ 203.6, 197.5, 144.6, 139.2, 138.7, 136.3, 133.9, 131.7, 129.1, 128.6, 127.4, 127.3, 57.6, 34.4, 26.7, 16.9, 14.7 ppm. IR (neat, cm^{-1}): 2957, 2870, 1720, 1683, 1604, 1462,

1377, 1264, 1049, 960, 813, 739, 617, 589, 469. HRMS calcd for ($C_{22}H_{25}ClO_2$+H): 357.1621, *found* 357.1607.

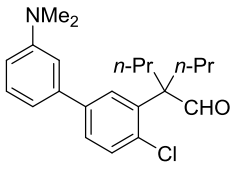

2-(4-chloro-3'-(dimethylamino)-[1,1'-biphenyl]-3-yl)-2-propylpentanal (259n). Column chromatography: silica gel, hexanes:EtOAc 2:1. Yellow pale solid (113.5ºC). ^{1}H NMR (300 MHz, $CDCl_3$) δ 9.83 (s, 1H), 7.55 (d, *J* = 1.9 Hz, 1H), 7.52–7.42 (m, 2H), 7.35 (t, *J* = 7.9, 7.9 Hz, 1H), 6.93–6.84 (m, 2H), 6.79 (ddd, *J* = 8.3, 2.7, 0.9 Hz, 1H), 3.03 (s, 6H), 2.04 (dd, *J* = 11.0, 5.9 Hz, 4H), 1.35–1.23 (m, 2H), 1.18–1.02 (m, 2H), 0.91 (t, *J* = 7.2 Hz, 6H) ppm. ^{13}C NMR (75 MHz, $CDCl_3$) δ 204.1, 151.0, 141.2, 141.1, 138.4, 132.6, 131.2, 129.6, 128.8, 127.4, 115.6, 111.9, 111.3, 57.6, 40.6, 34.7, 16.9, 14.7 ppm. IR (neat, cm^{-1}): 3130, 2957, 2871, 1722, 1600, 1498, 1465, 1354, 1215, 1141, 1040, 993, 822, 773, 696, 527. HRMS calcd for ($C_{22}H_{28}ClNO$+H): 358.1938, *found* 358.1925.

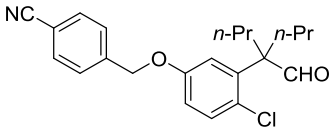

4-((4-chloro-3-(4-formylheptan-4-yl)phenoxy)methyl)benzaldehyde (259o). Column chromatography: silica gel, hexanes:EtOAc 2:1. White solid (mp=102.7ºC). ^{1}H NMR (400 MHz, $CDCl_3$) δ 9.75 (s, 1H), 7.72 (d, *J* = 8.4 Hz, 2H), 7.62–7.53 (m, 2H), 7.35–7.21 (m, 1H), 6.97 (d, *J* = 3.0 Hz, 1H), 6.85 (dd, *J* = 8.7, 3.0 Hz, 1H), 5.15 (s, 2H), 2.05–1.82 (m, 4H), 1.24–1.13 (m, 2H), 1.11–0.99 (m, 2H), 0.90 (t, *J* = 7.2 Hz, 6H) ppm. ^{13}C NMR (101 MHz, $CDCl_3$) δ 203.5, 156.8, 141.8, 140.0, 132.5, 131.8, 127.6, 125.8, 118.5, 117.5, 113.9, 112.0, 69.3, 57.5, 34.3, 16.7, 14.6 ppm. IR (neat, cm^{-1}): 2955, 2870, 2223, 1716, 1592, 1455, 1295, 1234, 1181, 1116, 1034, 845, 809, 666, 546, 481. HRMS calcd for ($C_{22}H_{24}ClNO_2$+H): 370.1574, *found* 370.1581.

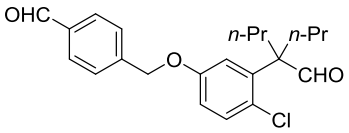

4-((4-chloro-3-(4-formylheptan-4-yl)phenoxy)methyl)benzaldehyde (259p). Column chromatography: silica gel, hexanes:EtOAc 2:1. Yellow oil. ^{1}H NMR (400 MHz, $CDCl_3$) δ 10.05 (s, 1H), 9.74 (s, 1H), 8.02–7.88 (m, 2H), 7.62 (d, *J* = 8.0 Hz, 2H), 7.30 (d, *J* = 8.7 Hz, 1H), 6.97 (d, *J* = 3.0 Hz, 1H), 6.85 (dd, *J* = 8.7, 3.0 Hz, 1H), 5.17 (s, 2H), 2.08–1.80 (m, 4H), 1.27–1.10 (m, 2H), 1.10–0.94 (m, 2H), 0.88 (t, *J* = 7.2 Hz, 6H) ppm. ^{13}C NMR (101 MHz, $CDCl_3$) δ 203.6, 191.7,

157.0, 143.3, 139.9, 136.2, 131.8, 130.1, 127.6, 117.5, 114.0, 69.7, 57.5, 34.3, 16.7, 14.7 ppm. IR (neat, cm^{-1}): 2952, 2870, 1716, 1688, 1592, 1678, 1481, 1456, 1376, 1298, 1238, 1031, 985, 808, 781 515, HRMS calcd for ($C_{22}H_{25}ClO_3$+Na): 395.1390, *found* 395.1398.

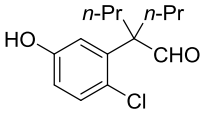

2-(2-chloro-5-hydroxyphenyl)-2-propylpentanal (259q). Column chromatography: silica gel, hexanes:EtOAc 2:1. White solid (mp=83ºC). ^{1}H NMR (300 MHz, $CDCl_3$) δ 9.75 (s, 1H), 7.34–7.12 (m, 1H), 6.89 (d, *J* = 2.8 Hz, 1H), 6.75 (dd, *J* = 8.6, 2.8 Hz, 1H), 5.39 (s, 1H), 1.96 (pd, *J* = 14.0, 5.0 Hz, 4H), 1.37–0.96 (m, 4H), 0.90 (t, *J* = 7.2 Hz, 6H) ppm. ^{13}C NMR (75 MHz, $CDCl_3$) δ 204.4, 154.5, 139.8, 131.8, 124.9, 117.0, 115.6, 57.4, 34.3, 16.7, 14.6 ppm. IR (neat, cm^{-1}): 3341, 2960, 1705, 1574, 1464, 1281, 1227, 1181, 988, 811, 745, 649, 476. HRMS calcd for ($C_{14}H_{19}O_2Cl$+Na): 277.0971, found 277.0984.

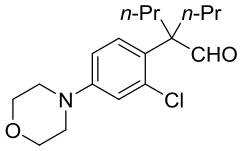

2-(2-chloro-4-morpholinophenyl)-2-propylpentanal (259r). Column chromatography: silica gel, hexanes:EtOAc 9:1. Yellow solid (mp=90.7ºC). ^{1}H NMR (300 MHz, $CDCl_3$) δ 9.73 (s, 1H), 7.24 (d, *J* = 8.8 Hz, 1H), 6.90 (d, *J* = 2.7 Hz, 1H), 6.83 (dd, *J* = 8.8, 2.7 Hz, 1H), 3.9–3.78 (m, 4H), 3.25–3.08 (m, 4H), 2.07–1.83 (m, 4H), 1.26–0.99 (m, 4H), 0.89 (t, *J* = 7.1 Hz, 6H) ppm. ^{13}C NMR (101 MHz, $CDCl_3$) δ 204.4, 150.9, 134.5, 130.1, 128.8, 117.2, 113.4, 66.7, 56.8, 48.4, 34.5, 16.8, 14.7 ppm. IR (neat, cm^{-1}): 2955, 2870, 1719, 1602, 1494, 1447, 1382, 1234, 1118, 1039, 947, 815, 745, 648, 609, 514 ppm. HRMS calcd for ($C_{18}H_{26}ClNO_2$): 324.1730, found 324.1733.

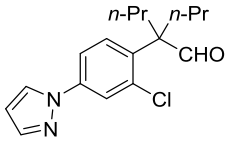

2-(2-chloro-4-(1*H*-pyrazol-1-yl)phenyl)-2-propylpentanal (259s). Column chromatography: silica gel, hexanes:EtOAc 9:1. White solid (mp=77.5ºC); ^{1}H NMR (300 MHz, $CDCl_3$) δ 9.77 (s, 1H), 7.93 (d, *J* = 2.6 Hz, 1H), 7.79 (d, *J* = 2.4 Hz, 1H), 7.74 (d, *J* = 1.8 Hz, 1H), 7.65 (dd, *J* = 8.6, 2.4 Hz, 1H), 7.44 (d, *J* = 8.7 Hz, 1H), 6.50 (t, *J* = 2.2, 2.2 Hz, 1H), 2.11–1.89 (m, 4H), 1.32–0.97 (m, 4H), 0.91 (t, *J* = 7.1 Hz, 6H) ppm. ^{13}C NMR (75 MHz, $CDCl_3$) δ 203.5, 141.6, 139.9, 136.3, 134.6, 130.6, 126.6, 121.4, 117.0, 108.2, 57.3, 34.5, 16.8, 14.6 ppm. IR (neat, cm^{-1}): 2956, 2870, 1749,

1603, 1476, 1449, 1377, 1260, 1228, 1121, 921, 896, 823, 557. HRMS calcd for ($C_{17}H_{21}ClN_2O$+Na): 327.1240, *found* 327.1248.

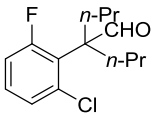

2-(2-chloro-6-fluorophenyl)-2-propylpentanal (259t). Column chromatography: silica gel, hexanes:EtOAc 95:5. Yellow pale oil. ^{1}H NMR (500 MHz, $CDCl_3$) δ 9.92 (d, $^5J_{H-F}$ = 4.9 Hz, 1H), 7.26–7.19 (m, 2H), 7.09–6.97 (m, 1H), 2.23–2.12 (m, 2H), 1.96–1.82 (m, 2H), 1.37–1.13 (m, 4H), 0.89 (t, *J* = 7.3 Hz, 6H).^{13}C NMR (126 MHz, $CDCl_3$) δ 202.2, 162.5 (d, $^1J_{C-F}$ = 249.9 Hz), 134.8 (d, $^3J_{C-F}$ = 7.6 Hz), 129.0 (d, $^3J_{C-F}$ = 11.0 Hz), 127.5 (d, $^4J_{C-F}$ = 3.0 Hz), 126.4 (d, $^2J_{C-F}$ = 14.7 Hz), 115.6 (d, $^2J_{C-F}$ = 26.9 Hz), 58.3 (d, $^3J_{C-F}$ = 4.2 Hz), 37.3, 17.7, 14.6 ppm. IR (neat, cm^{-1}): 3433, 2960, 2872, 1723, 1598, 1565, 1438, 1233, 878, 783 ppm. HRMS calcd for ($C_{14}H_{18}ClOF$+H): 257.1108, found 257.1108.

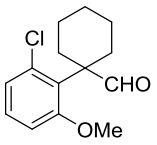

1-(2-chloro-6-methoxyphenyl)cyclohexanecarbaldehyde (259u). Column chromatography: silica gel, hexanes:EtOAc 9:1. Colorless oil. ^{1}H NMR (400 MHz, $CDCl_3$) δ 9.63 (s, 1H), 7.12 (t, *J* = 8.1 Hz, 1H), 7.04 (dd, *J* = 8.0, 1.4 Hz, 1H), 6.82 (dd, *J* = 8.1, 1.4 Hz, 1H), 3.73 (s, 3H), 2.68 (d, *J* = 4.4 Hz, 2H), 2.03 (dd, *J* = 9.1, 7.7 Hz, 2H), 1.75–1.63 (m, 3H), 1.57–1.44 (m, 2H), 1.43–1.30 (m, 1H) ppm. ^{13}C NMR (101 MHz, $CDCl_3$) δ ^{13}C NMR (101 MHz, $CDCl_3$) δ 199.9, 157.9, 134.4, 131.3, 128.3, 126.2, 112.4, 56.6, 52.9, 28.5, 24.5, 22.5 ppm. IR (neat, cm^{-1}): 2920, 2853, 2708, 1718, 1693, 1585, 1565, 1448, 1425, 1246, 1010, 980, 951, 839, 732, 693. HRMS calcd for ($C_{14}H_{17}ClO_2$+H): 253.0995, *found* 253.0989.

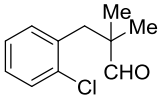

3-(2-chlorophenyl)-2,2-dimethylpropanal[350] (259ii). Column chromatography: silica gel, hexanes:EtOAc 9:1. Colorless oil. ^{1}H NMR (300 MHz, $CDCl_3$) δ 9.61 (s, 1H), 7.37 - 7.31 (m, 1H), 7.19 - 7.12 (m, 3H), 3.00 (s, 2H), 1.10 (s, 6H) ppm. ^{13}C NMR (75 MHz, $CDCl_3$) δ 205.2, 135.1, 134.8, 132.3, 129.8, 128.1, 126.6, 47.7, 39.4, 21.5 ppm.

[350] Quan, L. G.; Lamrani, M. Yamamoto, Y. *J. Am. Chem. Soc.* **2000,** *122, 4827.*

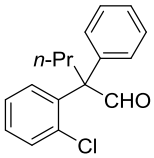

2-(2-chlorophenyl)-2-phenylpentanal (259kk). Column chromatography: silica gel, hexanes:EtOAc 10:1. Colorless oil. ^{1}H NMR (300 MHz, $CDCl_3$) δ 10.07 (s, 1H), 7.62 (dd, *J* = 7.8, 1.5 Hz, 1H), 7.28 (m, 8H), 2.49 (m, 2H), 1.13 (m, 2H), 0.98 (t, *J* = 6.9 Hz, 3H) ppm. ^{13}C NMR (75 MHz, $CDCl_3$) δ 197.6, 140.9, 138.9, 135.0, 133.5, 131.9, 128.9, 128.6, 128.4, 127.1, 127.0, 64.4, 34.6, 18.4, 14.5 ppm. IR (neat, cm^{-1}): 3090, 2941, 1727, 1632, 1503, 1395, 1312, 1184, 1096, 972, 809, 770. Anal Calcd for $C_{17}H_{17}ClO$: C, 74.86; H, 6.28. Found: C, 75.07; H, 6.15.

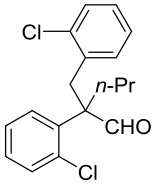

259ll

2-(2-chlorobenzyl)-2-(2-chlorophenyl)ventanal (259ll). Column chromatography: silica gel, hexanes:EtOAc 12:1. Colorless oil. ^{1}H NMR (300 MHz, $CDCl_3$) δ 10.06 (s, 1H), 7.66 (dd, *J* = 6.9, 2.4 Hz, 1H), 7.22 (m, 3H), 7.08 (td, *J* = 7.5, 1.8 Hz, 1H), 6.95 (m, 2H), 6.51 (dd, *J* = 7.5, 1.5 Hz, 1H), 3.71 (d, *J* = 13.8 Hz, 1H), 3.51 (d, *J* = 13.8 Hz, 1H), 1.98 (m, 2H), 1.34 (m, 2H), 0.91 (t, *J* = 7.2 Hz, 3H) ppm. ^{13}C NMR (75 MHz, $CDCl_3$) δ 203.7, 138.6, 135.5, 134.6, 134.5, 133.7, 132.8, 130.9, 129.5, 129.2, 127.8, 127.2, 125.8, 59.4, 36.7, 35.3, 17.1, 14.8 ppm. IR (neat, cm^{-1}): 3054, 2931, 1719, 1672, 1489, 1351, 1278, 1160, 981, 829.

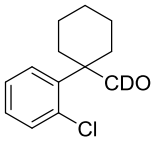

1-(2-chlorophenyl)cyclohexanecarbaldehyde-D_1 (259a-*d*^{1}): Column chromatography: silica gel, hexanes:EtOAc 9:1. Yellow oil. ^{1}H NMR (300 MHz, $CDCl_3$) δ 7.49 (dd, *J* = 7.7, 1.7 Hz, 1H), 7.35 (td, *J* = 7.2, 1.6 Hz, 1H), 7.28 (dd, *J* = 7.7, 1.6 Hz, 1H), 7.22 (td, *J* = 7.4, 1.6 Hz, 1H), 2.31 (dt, *J* = 13.3, 4.2 Hz, 2H), 1.93 (ddd, *J* = 13.3, 8.9, 3.4 Hz, 2H), 1.77 - 1.60 (m, 5H), 1.49 - 1.36 (m, 1H) ppm. ^{13}C NMR (75 MHz, $CDCl_3$) δ 203.7 (t, *J* = 26.7 Hz), 140.8, 133.5, 131.3, 129.0, 128.7, 127.2, 53.9 (t, *J* = 3.2 Hz), 31.3, 25.6, 22.5 ppm. IR (neat, cm^{-1}): 2932, 2855, 2048, 1704, 1450, 1063, 774, 628, 514. HRMS *calcd* for ($C_{13}H_{14}DClO$+H): 224.0952, *found* 224.0954.

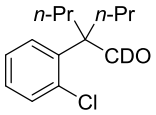

2-(2-chlorophenyl)-2-propylpentanal-D_1 (259b-*d*[1]): Column chromatography: silica gel, hexanes:EtOAc 9:1. Colorless oil. ^{1}H NMR (300 MHz, $CDCl_3$) δ 7.43 - 7.35 (m, 2H), 7.35 - 7.28 (m, 1H), 7.26 (dd, *J* = 7.5, 2.0 Hz, 1H), 2.10 - 1.88 (m, 4H), 1.32 - 1.14 (m, 2H), 1.13 - 0.98 (m, 2H), 0.89 (t, *J* = 7.1 Hz, 3H) ppm. ^{13}C NMR (75 MHz, $CDCl_3$) δ 203.7 (t, *J* = 26.8 Hz), 138.6, 133.9, 131.2, 129.8, 128.8, 126.9, 57.4 (t, *J* = 2.9 Hz), 34.7, 16.9, 14.8. IR (neat, cm^{-1}): 2959, 2873, 2064, 1714, 1467, 1041, 753. HRMS *calcd* for ($C_{14}H_{18}DClO$+H): 240.1265, *found* 240.1268.

6.2.4. Pd-catalyzed intramolecular acylation of aryl chlorides.

General procedure A for the synthesis of benzocyclobutenones via Pd-catalyzed intramolecular acylation of aryl chlorides. An oven-dried screw-cap test tube containing a stirring bar was charged with **Pd-3** (4.9 mg, 2.5 mol%), **IAd·HBF$_4$** (21.2 mg, 10 mol%), Cs_2CO_3 (209 mg, 0.65 mmol) and the aryl chloride (0.50 mmol), if a solid. The test tube was evacuated and back-filled with dry argon (this sequence was repeated three times). The aryl chloride (if liquid) and dioxane (2 mL) were then added by syringe followed by allyl ether **Alk-1** (31 µL,0.25 mmol,50 mol%) with a microsyringe. The mixture was then stirred in a pre-heated oil bath (140 ^{o}C) for 16 h. The mixture was then allowed to warm to room temperature, diluted with ethyl acetate (5 mL) and filtered through a Celite® plug, eluting with additional ethyl acetate (10 mL). The filtrate was concentrated and purified by column chromatography on silica gel (eluting with hexanes/ethyl acetate mixtures).

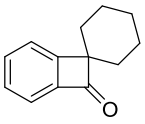

2H-spiro[cyclobutabenzene-1,1'-cyclohexan]-2-one (241a). Following general procedure, 1-(2-chlorophenyl)cyclohexanecarbaldehyde **259a**, (111 mg, 0.50 mmol) was used. Column chromatography: silica gel, hexanes:EtOAc 9:1. Yellow oil; yield: 68.8 mg (75% yield). The spectroscopical data correspond to tose previously reported in the literature.[2] ^{1}H NMR (400 MHz, $CDCl_3$) δ 7.56 (d, *J* = 7.3 Hz,1H), 7.50 (t, *J* = 7.2 Hz, 1H), 7.45–7.36 (m, 2H), 1.98–1.86 (m, 2H), 1.86–1.74 (m, 4H), 1.62 (dt, *J* = 16.9, 8.3 Hz, 3H), 1.56–1.45 (m, 1H) ppm. ^{13}C NMR (101 MHz, $CDCl_3$) δ 196.7, 162.4, 144.8, 134.8, 129.0, 122.6, 121.3, 70.8, 32.6, 25.7, 23.6 ppm.

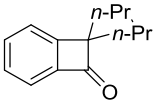

2,2-dipropylcyclobutabenzen-1(2H)-one (241b). Following general procedure 2-(2-chlorophenyl)-2-propylpentanal **259b**, (119 mg, 0.50 mmol) was used. Column chromatography: silica gel, hexanes:EtOAc 9:1. Yellow oil; yield: 76.9 mg (76% yield). The spectroscopical data correspond to tose previously reported in the literature.[2] ^{1}H NMR (400 MHz, $CDCl_3$) δ 7.52–7.47 (m, 1H), 7.43 (ddd, *J* = 4.5, 2.8, 1.1 Hz, 1H), 7.39 (dd, *J* = 7.1, 1.0 Hz, 1H), 7.35 (dt, *J* = 7.5, 1.1 Hz, 1H), 1.77 (ddd, *J* = 8.2, 6.4, 2.2 Hz, 4H), 1.35–1.12 (m, 4H), 0.86 (t, *J* = 7.3 Hz, 6H) ppm. ^{13}C NMR (101 MHz, $CDCl_3$) δ 197.0, 160.4, 145.9, 134.8, 128.9, 122.9, 120.7, 73.9, 37.1, 18.9, 14.5 ppm.

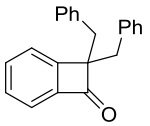

8,8-dibenzylbicyclo[4.2.0]octa-1,3,5-trien-7-one (241c). Following general procedure 2-benzyl-2-(2-chlorophenyl)-3-phenylpropanal **259c**, (167 mg, 0.50 mmol) was used. Column chromatography: silica gel, hexanes. Yellow pale solid (mp=89ºC); yield: 98.5 mg (66% yield).^{1}H NMR (300 MHz, $CDCl_3$) δ 7.39 (d, *J* = 7.1 Hz, 1H), 7.27 (dd, *J* = 7.3, 2.6 Hz, 2H), 7.22–7.10 (m, 7H), 7.09–6.99 (m, 4H), 3.19 (q, *J* = 13.7 Hz, 4H) ppm. ^{13}C NMR (75 MHz, $CDCl_3$) δ 194.7, 158.1, 145.9, 137.1, 134.6, 130.1, 129.2, 128.5, 128.0, 126.3, 124.4, 120.8, 75.4, 41.3 ppm. IR (neat, cm^{-1}): 3028, 1747, 1581, 1494, 1453, 1265, 1142, 1079, 913, 760, 735, 700, 519. HRMS calcd for ($C_{22}H_{18}O$+Na): 321.1255, found 321.1260.

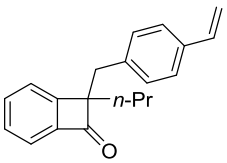

2-propyl-2-(4-vinylbenzyl)cyclobutabenzen-1(2*H*)-one (241d). Following general procedure 2-(2-chlorophenyl)-2-(4-vinylbenzyl)ventanal **259d** (157 mg, 0.50 mmol) was used. Column chromatography: silica gel, hexanes. Yellow pale solid (mp=89ºC); yield: 79 mg (57% yield).^{1}H NMR (300 MHz, $CDCl_3$) δ 7.35 (m, 6H), 7.05 (d, *J* = 8.1 Hz, 2H), 6.65 (dd, *J* = 17.7, 10.8 Hz, 1H), 5.67 (d, *J* = 17.7 Hz, 1H), 5.18 (d, *J* = 17.7 Hz, 1H), 3.11 (s, 2H), 1.81 (m, 2H), 1.28 (m, 2H), 0.87 (t, *J* = 7.5 Hz, 3H) ppm. ^{13}C NMR (75 MHz, $CDCl_3$) δ 195.9, 159.3, 145.8, 137.0, 136.5, 135.6, 134.8, 130.2, 129.2, 125.8, 123.7, 120.9, 113.2, 74.5, 41.2, 36.7, 19.0, 14.4 ppm. IR (neat, cm^{-1}): 3028, 1751, 1618, 1566, 1387, 1295, 1092, 1011, 885, 704. HRMS calcd for ($C_{20}H_{20}O$+Na): 299.1412, found 299.1419.

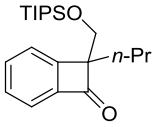

2-Propyl-2-((triisopropylsilyloxy)methyl)cyclobutabenzen-1(2*H*)-one (241e). Following general procedure, 2-(2-chlorophenyl)-2-(((triisopropylsilyl)oxy)methyl)pentanal **259e** (191.5 mg, 0.50 mmol) was used. Column chromatography: silica gel, hexanes/ethyl acetate 98/2. Colorless oil; yield: 90 mg (52% yield). ^{1}H NMR (300 MHz, $CDCl_3$) δ 7.53 - 7.48 (m, 2H), 7.45 - 7.38 (m, 1H), 7.38 - 7.34 (m, 1H), 4.05 (d, *J* = 10.0 Hz, 1H), 3.98 (d, *J* = 10.0 Hz, 1H), 1.79 (dd, *J* = 9.6, 7.2 Hz, 1H), 1.36-1.23 (m, 3H), 1.08-0.84 (m, 23H) ppm. ^{13}C NMR (75 MHz, $CDCl_3$) δ 195.1, 158.8, 147.2, 134.9, 129.2, 123.46, 120.4, 76.3, 65.6, 33.8, 19.1, 18.0, 17.9, 14.7, 12.0 ppm. IR (neat, cm^{-1}): 2941, 2865, 1757, 1461, 1113, 1068, 881, 755, 680. HRMS *calcd* for ($C_{21}H_{34}O_2Si$+Na): 369.2226, *found* 369.2218.

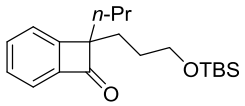

2-(3-(*tert*-butyldimethylsilyloxy)propyl)-2-propylcyclobutabenzen-1(2*H*)-one (241f). Following general procedure 5-(*tert*-butyldimethylsilyloxy)-2-(2-chlorophenyl)-2-propylpentanal **159f** (184 mg, 0.50 mmol) was used. Column chromatography: silica gel, hexanes/ethyl acetate 18:1. Colorless liquid; yield: 133 mg (81% yield). The spectroscopical data correspond to those previously reported in the literature.[2] ^{1}H NMR (300 MHz, $CDCl_3$) δ 7.46 (m, 4H), 3.60 (t, *J* = 6.6 Hz, 2H), 1.87 (m, 4H), 1.50 (m, 2H), 1.29 (m, 2H), 0.91 (t, *J* = 6.6 Hz, 3H), 0.88 (s, 9H), 0.04 (s, 3H), 0.03 (s, 3H) ppm. ^{13}C NMR (75 MHz, $CDCl_3$) δ 196.9, 160.6, 146.2, 135.3, 129.3, 123.3, 121.1, 73.8, 63.5, 37.3, 31.4, 29.1, 26.2, 19.2, 18.5, 14.7, -5.5 ppm.

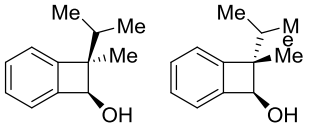

241g-I-diast1 **241g-I-diast2**

2-Isopropyl-2-methylcyclobutabenzen-1(2*H*)-one (241g-I). Following general procedure, 2-(2-chlorophenyl)-2,3-dimethylbutanal **259g** (105.4 mg, 0.50 mmol) was used. The benzocyclobutenone was dissolved under argon atmosphere in methanol (5 mL) and cooled to 0ºC. Then, $NaBH_4$ was added (5.0 mmol, 10.0 equiv.) and the reaction was stirred at rt for 12 h. The crude was then quenched by addition of water, followed by addition of HCl 2M. After extractions with ethyl acetate (3 x 5 mL) and brine (3 x 5 mL) it was dried over magnesium sulfate, filtered and concentrated. A mixture of diastereoisomers in a 2.3:1 ratio (Diast. 1: Diast. 2) was obtained as judged by NMR of the crude reaction. After purification on silica gel chromatography column (9:1 hexanes/ethyl acetate) a white solid was obtained (63.1 mg, 72%, two steps). **241g-I-diast2** (determined by NOESY experiments) could be obtained pure in a few fractions allowing for its independent characterization: mp = 51.4 – 52.6. ^{1}H NMR (300

MHz, $CDCl_3$) δ 7.33 - 7.24 (m, 3H), 7.18 - 7.13 (m, 1H), 4.82 (d, *J* = 8.9 Hz, 1H), 2.15 (d, *J* = 9.6 Hz, 1H), 1.99 (hept, *J* = 6.8 Hz, 1H), 1.26 (s, 3H), 1.09 (dd, *J* = 8.2, 6.7 Hz, 6H) ppm. ^{13}C NMR (75 MHz, $CDCl_3$) δ 152.4, 144.5, 129.3, 127.8, 123.5, 122.6, 80.5, 58.6, 31.5, 18.5, 18.1, 17.2 ppm. IR (neat, cm^{-1}): 3231, 2954, 2870, 1454, 1193, 1056, 740, 477. HRMS *calcd* for ($C_{12}H_{16}O$-OH): 159.1174, *found* 159.1179.

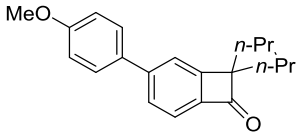

3-(4-Methoxyphenyl)-8,8-dipropylbicyclo[4.2.0]octa-1,3,5-trien-7-one (241h).

Following general procedure 2-(4-chloro-4'-methoxy-[1,1'-biphenyl]-3-yl)-2-propylpentanal **259h** (172.4 mg, 0.50 mmol) was used. Column chromatography: silica gel, hexanes:EtOAc 9:1. Colorless oil; yield: 135.7 mg (88% yield). ^{1}H NMR (300 MHz, $CDCl_3$) δ 7.60 (t, *J* = 7.3 Hz, 4H), 7.40 (d, *J* = 8.5 Hz, 1H), 7.02 (d, *J* = 8.8 Hz, 2H), 3.88 (s, 3H), 1.87–1.76 (m, 4H), 1.42–1.21 (m, 4H), 0.90 (t, *J* = 7.3 Hz, 6H) ppm. ^{13}C NMR (75 MHz, $CDCl_3$) δ 196.3, 160.9, 160.0, 147.8, 143.9, 133.0, 128.7, 128.2, 121.1, 120.7, 114.4, 73.4, 55.3, 37.1, 18.9, 14.5 ppm. IR (neat, cm^{-1}): 2956, 2871, 1749, 1587, 1456, 1094, 887, 835, 758, 695. HRMS calcd for ($C_{21}H_{24}O_2$+H): 309.1855, found 309.1867.

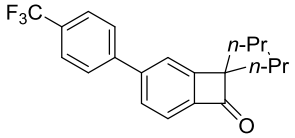

8,8-Dipropyl-3-(4-(trifluoromethyl)phenyl)bicyclo[4.2.0]octa-1,3,5-trien-7-one (241i).

Following general procedure 2-(4-chloro-4'-(trifluoromethyl)-[1,1'-biphenyl]-3-yl)-2-propylpentanal **259i** (191 mg, 0.50 mmol) was used. Column chromatography: silica gel, hexanes:EtOAc 9:1. Colorless oil; yield: 104 mg (60% yield). ^{1}H NMR (300 MHz, $CDCl_3$) δ 7.80–7.70 (m, 4H), 7.71–7.62 (m, 2H), 7.47 (d, *J* = 8.3 Hz, 1H), 1.94–1.75 (m, 4H), 1.43–1.18 (m, 4H), 0.91 (t, *J* = 7.3 Hz, 6H) ppm. ^{13}C NMR (101 MHz, $CDCl_3$) 196.2, 161.1, 146.6, 145.5, 135.5, 128.8, 128.0, 125.9 (d, $^2J_{C\text{-}F}$ = 3.8 Hz), 124.1 (d, $^1J_{C\text{-}F}$ = 272.2 Hz), 122.4, 121.7, 121.3, 73.9, 37.1, 19.0, 14.5 ppm. IR (neat, cm^{-1}): 2959, 2873, 1752, 1590, 1465, 1322, 1165, 1123, 1068, 1012, 851, 825, 615. HRMS calcd for ($C_{21}H_{21}F_3O$+Na): 369.1442, *found* 369.1430.

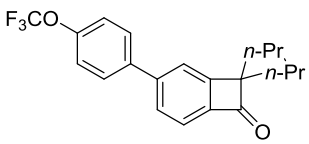

8,8-Dipropyl-3-(4-(trifluoromethoxy)phenyl)bicyclo[4.2.0]octa-1,3,5-trien-7-one (241j). Following general procedure 2-(4-chloro-4'-(trifluoromethoxy)-[1,1'-biphenyl]-3-yl)-2-propylpentanal **259j**, (199 mg, 0.50 mmol) was used. Column chromatography: silica gel, hexanes:EtOAc 9:1. Colorless oil; yield: 141.3 mg (78% yield). ^{1}H NMR (300 MHz, $CDCl_3$) δ 7.69–7.57 (m, 4H), 7.45 (d, *J* = 8.4 Hz, 1H), 7.38–7.30 (m, 2H), 1.94–1.72 (m, 4H), 1.46–1.17 (m, 4H), 0.90 (t, *J* = 7.3 Hz, 6H) ppm. ^{13}C NMR (101 MHz, $CDCl_3$) δ 196.2, 161.1, 149.4 (d, $^{3}J_{C\text{-}F}$ = 1.8 Hz), 146.7, 145.0, 139.4, 129.0, 128.6, 121.5, 121.3, 121.3, 120.5 (d, $^{1}J_{C\text{-}F}$ = 257.6 Hz), 73.8, 37.1, 19.0, 14.5 ppm. IR (neat, cm^{-1}): 2959, 2931, 1750, 1590, 1512, 1458, 1253, 1207, 1159, 1010, 923, 827, 677. HRMS calcd for ($C_{21}H_{21}F_3O_2$+Na): 385.1391, *found* 385.1379.

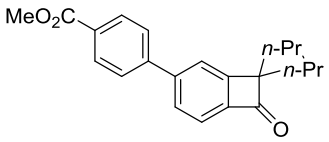

Methyl 4-(7-oxo-8,8-dipropylbicyclo[4.2.0]octa-1,3,5-trien-3-yl)benzoate (241k). Following general procedure methyl 4'-chloro-3'-(4-formylheptan-4-yl)-[1,1'-biphenyl]-4-carboxylate **259k**, (186 mg, 0.50 mmol) was used. Column chromatography: silica gel, hexanes:EtOAc 9:1. Colorless oil; yield: 141.3 mg (84% yield). ^{1}H NMR (300 MHz, $CDCl_3$) δ 8.21–8.07 (m, 4H), 7.79 (d, *J* = 7.8 Hz, 1H), 7.60 (t, *J* = 7.6 Hz, 1H), 7.44 (d, *J* = 7.2 Hz, 1H), 3.96 (s, 3H), 1.90–1.74 (m, 4H), 1.35–1.24 (m, 4H), 0.90 (t, *J* = 7.3 Hz, 6H) ppm. ^{13}C NMR (75 MHz, $CDCl_3$) δ 195.8, 166.8, 161.0, 142.9, 139.7, 135.4, 135.1, 130.3, 130.2, 127.5, 126.4, 122.3, 73.0, 52.2, 37.1, 18.9, 14.5 ppm. IR (neat, cm^{-1}):2954, 2927, 2869, 1751, 1726, 1556, 1435, 1274, 1187, 1099, 1010, 811, 794, 697. HRMS calcd for ($C_{22}H_{24}O_3$+Na): 359.1623, *found* 359.1625.

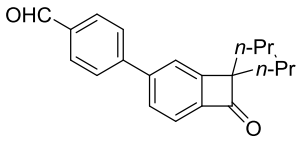

4-(1-Oxo-2,2-dipropyl-1,2-dihydrocyclobutabenzen-4-yl)benzaldehyde (241l). Following general procedure 4'-chloro-3'-(4-formylheptan-4-yl)biphenyl-4-carbaldehyde **259l** (171.4 mg, 0.50 mmol) was used. Column chromatography: silica gel, hexanes:EtOAc 9:1. Colorless oil; yield: 84.3 mg (55% yield). ^{1}H NMR (300 MHz, $CDCl_3$) δ 10.08 (s, 1H), 7.99 (d, *J* = 8.2 Hz, 2H), 7.79 (d, *J* = 8.2 Hz, 2H), 7.67 (d, *J* = 6.6 Hz, 2H), 7.45 (d, *J* = 8.4 Hz, 1H), 1.91–1.75 (m, 4H), 1.42–1.19 (m, 4H), 0.88 (t, *J* = 7.3 Hz, 6H) ppm. ^{13}C NMR (75 MHz, $CDCl_3$) δ 196.1, 191.6, 161.0, 146.5, 146.5, 145.6, 135.8, 130.2, 128.8, 128.2, 121.7, 121.2, 73.8, 37.0, 18.9, 14.4 ppm. IR (neat, cm^{-1}): 2958, 2870, 1720, 1683, 1604, 1461, 1358, 1264, 1049, 813, 739, 617, 589. HRMS calcd for ($C_{21}H_{22}O_2$+H): 307.1674, found 307.1685.

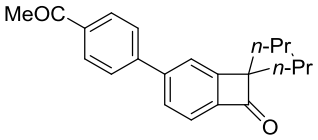

4-(4-Ethanoylphenyl)-2,2-dipropylcyclobutabenzen-1(2H)-one (241m). Following general procedure 2-(4-chloro-4'-ethanoylbiphenyl-3-yl)-2-propylpentanal **259m**, (178 mg, 0.50 mmol) was used. Column chromatography: silica gel, hexanes:EtOAc 9:1. Colorless oil; yield: 93 mg (58% yield). ^{1}H NMR (400 MHz, $CDCl_3$) δ 8.12–8.06 (m, 2H), 7.77–7.72 (m, 2H), 7.68 (dd, *J* = 4.4, 2.3 Hz, 2H), 7.47 (dd, *J* = 8.3, 0.5 Hz, 1H), 2.68 (s, 3H), 1.84 (td, *J* = 6.6, 1.4 Hz, 4H), 1.40–1.26 (m, 4H), 0.91 (t, *J* = 7.3 Hz, 6H) ppm. ^{13}C NMR (101 MHz, $CDCl_3$) δ 197.5, 196.2, 161.0, 146.8, 145.5, 145.2, 136.7, 129.0, 128.8, 127.8, 121.6, 121.3, 73.8, 37.1, 26.7, 19.0, 14.5 ppm. IR (neat, cm^{-1}): 2957, 2933, 1720, 1683, 1604, 1462, 1377, 1264, 1049, 1016, 813, 739, 617, 589. HRMS calcd for ($C_{22}H_{24}O_2$+Na): 343.1674, found 343.1657.

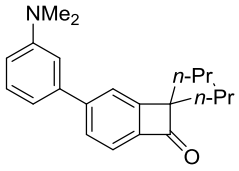

3-(3-(Dimethylamino)phenyl)-8,8-dipropylbicyclo[4.2.0]octa-1,3,5-trien-7-one (241n). Following general procedure 2-(4-chloro-3'-(dimethylamino)-[1,1'-biphenyl]-3-yl)-2-propylpentanal **259n** (179 mg, 0.50 mmol) was used. Column chromatography: silica gel, hexanes:EtOAc 9:1. Colorless oil; yield: 130.2 mg (81% yield). ^{1}H NMR (300 MHz, $CDCl_3$) δ 7.69–7.58 (m, 2H), 7.44–7.30 (m, 2H), 7.02–6.88 (m, 2H), 6.83–6.76 (m, 1H), 3.04 (s, 6H), 1.88–1.76 (m, 4H), 1.39–1.22 (m, 4H), 0.90 (t, *J* = 7.3 Hz, 6H) ppm. ^{13}C NMR (75 MHz, $CDCl_3$) δ 196.5, 160.8, 151.0, 149.4, 144.4, 141.8, 129.6, 128.9, 121.5, 120.9, 116.0, 112.5, 111.5, 73.5, 40.7, 37.1, 19.0, 14.5 ppm. IR (neat, cm^{-1}): 2955, 2928, 2870, 1748, 1585, 1499, 1456, 1353, 1164, 1113, 1094, 1060, 879, 773, 691. HRMS calcd for ($C_{22}H_{27}NO$+H): 322.2147, *found* 322.2156.

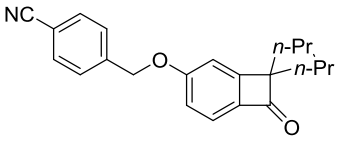

4-(((7-Oxo-8,8-dipropylbicyclo[4.2.0]octa-1,3,5-trien-3-yl)oxy)methyl) benzonitrile (241o). Following general procedure 4-((4-chloro-3-(4-formylheptan-4-yl)phenoxy)methyl)benzaldehyde **259o**, (185 mg, 0.50 mmol) was used. Column chromatography: silica gel, hexanes:EtOAc 9:1. Colorless oil; yield: 113.4 mg (68% yield); The spectroscopical data correspond to tose previously reported in the literature.[1] ^{1}H NMR (300 MHz, $CDCl_3$) δ 7.65 (d, *J* = 8.3 Hz, 2H), 7.55 (d, *J* = 8.3 Hz, 2H), 7.46 (dd, *J* = 8.2, 7.2 Hz, 1H), 6.98

(d, *J* = 7.0 Hz, 1H), 6.92 (d, *J* = 8.3 Hz, 1H), 5.53 (s, 2H), 1.81–1.68 (m, 4H), 1.33–1.11 (m, 4H), 0.85 (t, *J* = 7.3 Hz, 6H) ppm. ^{13}C NMR (75 MHz, $CDCl_3$) δ 192.7, 160.0, 151.7, 142.1, 137.8, 132.2, 130.4, 127.7, 118.7, 116.6, 114.9, 111.6, 72.6, 72.4, 37.0, 18.7, 14.5 ppm.

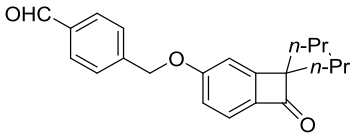

4-((1-Oxo-2,2-dipropyl-1,2-dihydrocyclobutabenzen-4-yloxy)methyl) benzaldehyde (241p). Following general procedure 4-((4-chloro-3-(4-formylheptan-4-yl)phenoxy)methyl)benzaldehyde **259p**, (186 mg, 0.50 mmol) was used. Column chromatography: silica gel, hexanes:EtOAc 2:1. Colorless oil; yield: 107.6 mg (64% yield). ^{1}H NMR (300 MHz, $CDCl_3$) δ 10.02 (s, 1H), 7.89 (d, *J* = 8.2 Hz, 2H), 7.62 (d, *J* = 8.0 Hz, 2H), 7.46 (dd, *J* = 8.2, 7.2 Hz, 1H), 6.96 (dd, *J* = 13.8, 7.7 Hz, 2H), 5.56 (s, 2H), 1.84–1.66 (m, 4H), 1.32–1.13 (m, 4H), 0.85 (t, *J* = 7.3 Hz, 6H) ppm. ^{13}C NMR (75 MHz, $CDCl_3$) δ 192.8, 191.9, 160.0, 151.9, 143.6, 137.7, 135.9, 130.5, 129.8, 127.7, 116.6, 114.8, 72.9, 72.6, 37.1, 18.8, 14.5 ppm. IR (neat, cm^{-1}): 2957, 1753, 1701, 1597, 1571, 1471, 1269, 1207, 1123, 1046, 1013, 780. HRMS calcd for ($C_{22}H_{24}O_3$+H): 337.1804, found 337.1794.

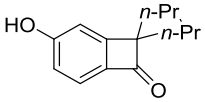

4-Hydroxy-2,2-dipropylcyclobutabenzen-1(2H)-one. (241q). Following general procedure 2-(2-chloro-5-hydroxyphenyl)-2-propylpentanal **259q**, (127 mg, 0.50 mmol) and Cs_2CO_3 (418 mg, 1.3 mmol) were used. Column chromatography: silica gel, hexanes:EtOAc 2:1. Colorless oil; yield: 85 mg (78% yield). The spectroscopical data correspond to those previously reported in the literature. ^{1}H NMR (400 MHz, $CDCl_3$) δ 7.27 (dd, *J* = 8.2, 0.9 Hz, 1H), 7.00–6.90 (m, 2H), 1.76 (td, *J* = 7.1, 2.9 Hz, 4H), 1.38–1.17 (m, 4H), 0.87 (t, *J* = 7.3 Hz, 6H) ppm. ^{13}C NMR (75 MHz, $CDCl_3$) δ 196.0, 163.0, 162.6, 136.9, 123.4, 118.2, 109.3, 72.3, 37.1, 18.9, 14.5 ppm.

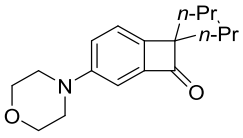

4-Morpholino-8,8-dipropylbicyclo[4.2.0]octa-1,3,5-trien-7-one (241r). Following general procedure 2-(2-chloro-4-morpholinophenyl)-2-propylpentanal **259r** (163 mg, 0.50 mmol) was used. Column chromatography: silica gel, hexanes:EtOAc 9:1. Colorless oil; yield: 103.5 mg (73% yield). ^{1}H NMR (300 MHz, $CDCl_3$) δ 7.35 (d, *J* = 8.1 Hz, 1H), 7.14 (dd, *J* = 8.2, 2.2 Hz, 1H), 6.84 (d, *J* = 1.5 Hz, 1H), 3.91–3.79 (m, 4H), 3.22–3.07 (m, 4H), 1.85–1.62 (m, 4H), 1.35–1.12 (m, 4H), 0.86 (t, *J* = 7.3 Hz, 6H) ppm. ^{13}C NMR (75 MHz, $CDCl_3$) δ 196.9, 152.8, 152.4, 146.9, 124.3,

123.5, 106.2, 72.9, 66.8, 49.7, 37.3, 19.0, 14.5 ppm. IR (neat, cm^{-1}): 2956, 2870, 1749, 1603, 1476, 1449, 1377, 1476, 1449, 1260, 1228, 1121, 896, 557. HRMS calcd for ($C_{18}H_{25}NO_2$+H): 288.1964, *found* 288.1957.

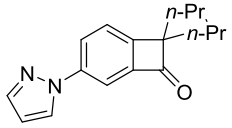

8,8-Dipropyl-4-(1*H*-pyrazol-1-yl)bicyclo[4.2.0]octa-1,3,5-trien-7-one (241s). Following general procedure 2-(2-chloro-4-(1*H*-pyrazol-1-yl)phenyl)-2-propylpentanal **259s**, (152.4 mg, 0.50 mmol) was used. Column chromatography: silica gel, hexanes:EtOAc 9:1. Colorless oil; yield: 88.6 mg (65% yield). ^{1}H NMR (300 MHz, $CDCl_3$) δ 7.96 (dd, *J* = 8.0, 1.9 Hz, 1H), 7.91 (d, *J* = 2.5 Hz, 1H), 7.73 (d, *J* = 1.8 Hz, 1H), 7.61–7.58 (m, 1H), 7.53 (dd, *J* = 8.0, 1.0 Hz, 1H), 6.51–6.46 (m, 1H), 1.85–1.74 (m, 4H), 1.37–1.14 (m, 4H), 0.88 (t, *J* = 7.2 Hz, 6H) ppm. ^{13}C NMR (75 MHz, $CDCl_3$) δ 195.9 , 158.2, 146.9, 141.5, 141.3, 126.9, 126.7, 124.0, 110.8, 108.1, 73.8, 37.1, 18.9, 14.5 ppm. IR (neat, cm^{-1}): 2957, 2872, 1755, 1520, 1477, 1391, 1334, 1142, 1044, 1020, 946, 835, 744, 611, 549. HRMS calcd for ($C_{17}H_{20}N_2O$+H): 269.1654, found 269.1641.

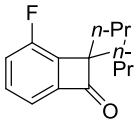

2-Fluoro-8,8-dipropylbicyclo[4.2.0]octa-1,3,5-trien-7-one (241t). Following general procedure 2-(2-chloro-6-fluorophenyl)-2-propylpentanal **259t**, (128 mg, 0.50 mmol) was used. Column chromatography: silica gel, hexanes:EtOAc 9:1. Yellow pale oil; yield: 84.8 mg (77% yield). ^{1}H NMR (400 MHz, $CDCl_3$) δ 7.40 (ddd, *J* = 8.2, 7.4, 4.1 Hz, 1H), 7.23–7.12 (m, 2H), 1.87–1.77 (m, 4H), 1.33–1.19 (m, 4H), 0.88 (t, *J* = 7.3 Hz, 6H) ppm. ^{13}C NMR (101 MHz, $CDCl_3$) δ 195.2 (d, $^4J_{C\text{-}F}$ = 2.2 Hz), 158.0 (d, $^1J_{C\text{-}F}$ = 255.6 Hz), 148.8 (d, $^3J_{C\text{-}F}$ = 7.1 Hz), 144.2 (d, $^2J_{C\text{-}F}$ = 19.0 Hz), 131.2 (d, $^3J_{C\text{-}F}$ = 5.1 Hz), 121.7 (d, $^2J_{C\text{-}F}$ = 21.3 Hz), 116.8 (d, $^4J_{C\text{-}F}$ = 4.6 Hz), 75.2 (d, $^3J_{C\text{-}F}$ = 2.4 Hz), 36.8, 19.2, 14.6, 14.4 ppm. IR (neat, cm^{-1}): 2959, 1768, 1590, 1476, 1240, 1207, 1018, 967, 805. HRMS calcd for ($C_{14}H_{17}FO$+H): 221,1342, found 221,1334.

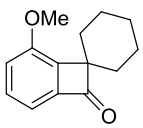

5-Methoxyspiro[bicyclo[4.2.0]octa[1,3,5]triene-7,1'-cyclohexan]-8-one (241u).

Following general procedure 1-(2-chloro-6-methoxyphenyl)cyclohexanecarbonitrile **259u**, (126 mg, 0.50 mmol) was used. Column chromatography: silica gel, hexanes:EtOAc 9:1. Colorless oil; yield: 81 mg (75% yield). ^{1}H NMR (400 MHz, $CDCl_3$) δ 7.35 (dd, *J* = 8.0, 7.5 Hz, 1H), 6.97 (dd, *J* = 7.8, 2.1 Hz, 2H), 3.89 (s, 3H), 1.99–1.86 (m, 4H), 1.85–1.69 (m, 4H), 1.57 (dd, *J* = 11.6, 5.7 Hz,

2H) ppm. ^{13}C NMR (101 MHz, $CDCl_3$) δ 196.8, 155.3, 149.4, 146.1, 130.6, 116.7, 113.2, 71.0, 55.4, 32.8, 25.7, 23.7 ppm. IR (neat, cm^{-1}): 2929, 2854, 1719, 1586, 1565, 1485, 1447, 1249, 1012, 794, 732. HRMS calcd for ($C_{14}H_{16}O_2$+H): 217.1229, *found* 217.1219.

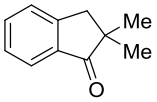

2,2-Dimethyl-2,3-dihydro-1*H*-inden-1-one (241ii). Following general procedure 3-(2-chlorophenyl)-2,2-dimethylpropanal **259ii** (158 mg, 0.50 mmol) was used. Column chromatography: silica gel, 9:1 hexanes/ethyl acetate. Yellow oil; yield: 66.6 mg (83% yield). The spectroscopical data correspond to those previously reported in the literature.[3] ^{1}H NMR (300 MHz, $CDCl_3$) δ 7.77 (d, *J* = 7.6 Hz, 1H), 7.60 (t, *J* = 7.3 Hz, 1H), 7.43 (d, *J* = 7.8 Hz, 1H), 7.38 (t, *J* = 7.6 Hz, 1H), 3.01 (s, 2H), 1.24 (s, 6H) ppm. ^{13}C NMR (75 MHz, $CDCl_3$) δ 211.5, 152.3, 135.5, 134.9, 127.5, 126.8, 124.6, 45.6, 43.0, 25.4 ppm.

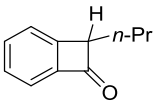

8-Propylbicyclo[4.2.0]octa-1,3,5-trien-7-one (241jj). Following general procedure 2-(2-chlorophenyl)-2-(trimethylsilyl)pentanal (**259jj**) (134 mg, 0.50 mmol) was used. Once the reaction was finished as judged by TLC (13 h), TBAF (2 mL, 2 mmol, 1M in THF) was added and the reaction was stirred for an additional 2 h. Filtration through Celite® and evaporation of the solvent afforded a crude that was purified by flash column chromatography in silica gel (hexanes/ethyl acetate 16:1). Colorless liquid; yield: 58 mg (73% yield). ^{1}H NMR (300 MHz, $CDCl_3$) δ 7.51 (m, 2H), 7.41 (m, 1H), 7.35 (td, *J* = 7.5, 1.2 Hz, 1H), 4.23 (t, *J* = 7.2 Hz), 1.87 (m, 1H), 1.73 (m, 1H), 1.51 (m, 2H), 0.97 (t, *J* = 7.2 Hz, 3H) ppm. ^{13}C NMR (75 MHz, $CDCl_3$) δ 192.9, 156.5, 146.6, 134.9, 128.9, 123.3, 120.7, 64.8, 32.4, 20.6, 13.9 ppm. IR (neat, cm^{-1}): 2958, 2872, 1757, 1581, 1461, 1142, 768, 753, 738. HRMS calcd for ($C_{11}H_{12}O$): 160.0888, found 160.0891

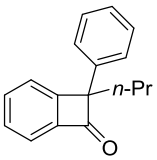

241kk

2-Phenyl-2-propylcyclobutabenzen-1(2*H*)-one (241kk). Following general procedure 2-(2-chlorophenyl)-2-phenylpentanal **259kk** (158 mg, 0.50 mmol) was used. Column chromatography: silica gel, hexanes:EtOAc 10:1. Colorless oil; yield: 80.1 mg (68% yield). ^{1}H NMR (300 MHz, $CDCl_3$) δ 7.79 (d, *J* = 6.3 Hz, 1H), 7.64 (td, *J* = 7.2, 1.5 Hz, 1H), 7.47 (m, 4H), 7.34 (t, *J* = 6.0 Hz, 2H), 7.25 (d, *J* = 7.2 Hz, 1H), 2.14 (m, 2H), 1.28 (m, 2H), 0.88 (t, *J* = 6.8 Hz, 3H)

ppm. ^{13}C NMR (75 MHz, $CDCl_3$) δ 193.2, 158.5, 145.7, IR (neat, cm^{-1}): 2997, 2891, 1751, 1511, 1424, 1340, 1298, 1110, 984, 911, 823. HRMS calcd for ($C_{17}H_{16}O$+H): 237.1279, found 237.1281.

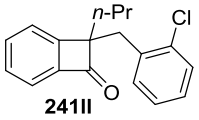

241ll

8-(2-Chlorobenzyl)-8-propylbicyclo[4.2.0]octa-1,3,5-trien-7-one. (241ll): Following general procedure 2-(2-chlorobenzyl)-2-(2-chlorophenyl)pentanal **259ll**, (152.4 mg, 0.50 mmol) was used. Column chromatography: silica gel, hexanes:EtOAc 12:1. Colorless oil; yield: 93 mg (66% yield). ^{1}H NMR (300 MHz, $CDCl_3$) δ 7.50–7.36 (m, 2H), 7.35–7.26 (m, 1H), 7.25–7.13 (m, 3H), 7.10–6.98 (m, 2H), 3.43 (d, J = 13.9 Hz, 1H), 3.26 (d, J = 13.9 Hz, 1H), 2.01–1.79 (m, 2H), 1.41–1.13 (m, 2H), 0.89 (t, J = 7.2, 7.2 Hz, 3H). ^{13}C NMR (75 MHz, $CDCl_3$) δ 195.66, 158.76, 145.88, 135.57, 134.68, 134.34, 131.72, 129.32, 129.15, 127.73, 126.37, 124.12, 120.38, 74.66, 37.51, 37.38, 18.95, 14.40. IR (neat, cm^{-1}): 2957, 2929, 1749, 1581, 1461, 1440, 1274, 1051, 1037, 890, 752, 680, 536, 514. HRMS calcd for ($C_{18}H_{17}ClO$+Na): 307.0866, *found* 307.0876.

6.2.5. Pd-catalyzed synthesis of styrenes via C-H bond-functionalization

General procedure B for the synthesis of α-aryl styrenes. An oven-dried screw-cap test tube containing a stirring bar was charged with **Pd-3** (3.9 mg, 2.0 mol%), **IMes·HCl** (10.2 mg, 6.0 mol%), Cs_2CO_3 (209 mg, 0.65 mmol) and the aryl chloride (0.50 mmol), if a solid. The test tube was evacuated and back-filled with dry argon (this sequence was repeated three times). The aryl chloride (if liquid) and dioxane (2 mL) were then added by syringe. The mixture was then placed in a pre-heated oil bath (110 °C) for 16 h. The mixture was then allowed to warm to room temperature, diluted with ethyl acetate (5 mL) and filtered through a Celite® plug, eluting with additional ethyl acetate (10 mL). The filtrate was concentrated and purified by column chromatography on silica gel (eluting with hexanes/ethyl acetate mixtures).

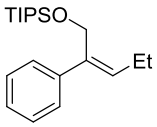

(*Z*)-Triisopropyl((2-phenylpent-2-en-1-yl)oxy)silane (261e). Following the general procedure, 2-(2-chlorophenyl)-2-(((triisopropylsilyl)oxy)methyl)pentanal **259e** (191.5 mg, 0.5 mmol) was used. Column chromatography: silica gel, hexanes/ethyl acetate 9:1. Colorless oil; yield: 144.1 mg (90% yield, 1:1.6 *E:Z*).[351] The next data corresponds to the mayor isomer *E*: ^{1}H NMR (300 MHz, $CDCl_3$) δ 7.48 (d, *J* = 7.5 Hz, 1H), 7.39 - 7.25 (m, 2H), 7.21 (t, *J* = 6.5 Hz, 1H), 5.81 (t, *J* = 7.3

Hz, 1H), 4.67 (s, 2H), 2.32 (p, *J* = 7.4 Hz, 2H), 1.24 - 0.84 (m, 25H) ppm. ^{13}C NMR (75 MHz, $CDCl_3$) δ 142.3, 139.3, 138.6, 133.2, 128.9, 128.0, 126.8, 126.6, 60.8, 21.9, 18.2, 14.6, 12.2 ppm. IR (neat, cm^{-1}):2942, 2866, 1459, 1064, 1014, 881, 755, 681, 657. HRMS *calcd* for ($C_{20}H_{34}OSi$+H): 319.2457, *found* 319.2472.

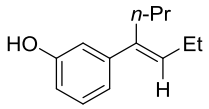

(*E*)-3-(Hept-3-en-4-yl)phenol (261q). Following general procedure 2-(2-chloro-5-hydroxyphenyl)-2-propylpentanal **259q**, (127 mg, 0.50 mmol) and Cs_2CO_3 (418 mg, 1.3 mmol) were used. Column chromatography: silica gel, hexanes:EtOAc 9:1. Colorless oil; yield: 59 mg (62% yield, 8.4:1 (*E:Z)*). The spectroscopical data correspond to those previously reported in the literature.[2] ^{1}H NMR (400 MHz, $CDCl_3$) δ 7.28–7.18 (m, 2H), 7.12–7.06 (m, 1H), 7.06–6.99 (m, 1H), 5.54 (s, 1H), 2.51–2.45 (m, 2H), 2.25 (p, *J* = 7.5 Hz, 2H), 1.35 (dt, *J* = 14.9, 7.4 Hz, 2H), 1.09 (t, *J* = 7.5 Hz, 3H), 0.89 (t, *J* = 7.3 Hz, 3H) ppm. ^{13}C NMR (101 MHz, $CDCl_3$) 158.77, 135.50, 133.66, 130.66, 127.93, 123.72, 115.49, 40.58, 32.39, 21.53, 14.28, 13.81. (*NMR shifts correspond to the major E isomer*).[351]

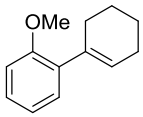

1-Cyclohexenyl-2-methoxybenzene (261u). Following general procedure 1-(2-chloro-6-methoxyphenyl)cyclohexanecarbonitrile **259u**, (126 mg, 0.50 mmol) was used. Column chromatography: silica gel, hexanes:EtOAc 9:1. Colorless oil; yield: 75.3 mg (80% yield). The spectroscopical data correspond to tose previously reported in the literature.[352] ^{1}H NMR (400 MHz, $CDCl_3$) δ 7.27 (ddd, *J* = 8.2, 7.4, 1.8 Hz, 1H), 7.22–7.17 (m, 1H), 6.97 (td, *J* = 7.4, 1.1 Hz, 1H), 6.92 (dd, *J* = 8.2, 0.9 Hz, 1H), 5.83 (tt, *J* = 3.7, 1.7 Hz, 1H), 3.87 (s, 3H), 2.53–2.37 (m, 2H), 2.32–2.20 (m, 2H), 1.87–1.69 (m, 4H) ppm. ^{13}C NMR (101 MHz, $CDCl_3$) δ 156.7 , 137.5, 133.8, 129.5, 127.7, 126.1, 120.5, 110.7, 67.1, 55.4, 28.8, 25.7, 23.1, 22.2 ppm.

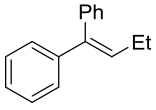

But-1-ene-1,1-diyldibenzene (261kk). Following the general procedure, 2-(2-chlorophenyl)-2-phenylpentanal **259kk** (136.4 mg, 0.50 mmol) was used at 140 ºC. Column chromatography:

[351] Diastereoselectivity was determined by NOESY experiments
[352] Flores-Gaspar, A.; Martin, R. *Adv. Synth. Catal.* **2011**, *353*, 1223

silica gel, hexanes/ethyl acetate 9:1. Colorless oil; yield: 63.1 mg (61% yield). The spectroscopical data correspond to those previously reported in the literature.[353] ^{1}H NMR (300 MHz, $CDCl_3$) δ 7.45 - 7.32 (m, 3H), 7.30 - 7.20 (m, 7H), 6.11 (t, *J* = 7.5 Hz, 1H), 2.16 (p, *J* = 7.5 Hz, 2H), 1.08 (t, *J* = 7.5 Hz, 3H) ppm. ^{13}C NMR (75 MHz, $CDCl_3$) δ 143.0, 141.1, 140.4, 131.9, 130.0, 128.3, 128.2, 127.4, 127.0, 126.9, 23.4, 14.7 ppm.

6.2.6. Mechanistic considerations

*Preparation of a **259b**/dodecane/**Pd-3**/allyl ether solution*: In the glovebox, a volumetric flash was charged with 952 µL dodecane (4.19 mmol), 1.0 g **259b** (4.19 mmol), 42 mg **Pd-3** (0.105 mmol, 2.5 mol%) and 256 µL allyl ether (2.095 mmol, 50 mol%). Then, anhydrous dioxane was added until the final volume was exactly 5 mL (0.84M in dodecane, 0.84 M in **259b**, 0.021M in **Pd-3** and 0.42M in allyl ether).

A series of oven-dried screw-cap test tubes containing a stirring bar were charged in the glovebox with **IAd·HBF$_4$** (11.0 mg, 10.0 mol%) and Cs_2CO_3 (106 mg, 0.325 mmol). Then, 300 µL of the above volumetric flask solution (0.25 mmol **259b**, 0.25 mmol dodecane, 2.5 mol% **5** and 50 mol% allyl ether) and dioxane (1 mL) were then added by syringe. In all experiments, the concentrations of the different species were the same. The test tubes were then placed in a pre-heated oil bath (140 °C) and a single GC sample / test tube was measured at different reaction times, thus plotting the corrected GC yield of benzocyclobutenone **241b** *versus* time at conversions not higher than 22%. The same sets of experiments were made when utilizing **259b-D$_1$** as substrate.

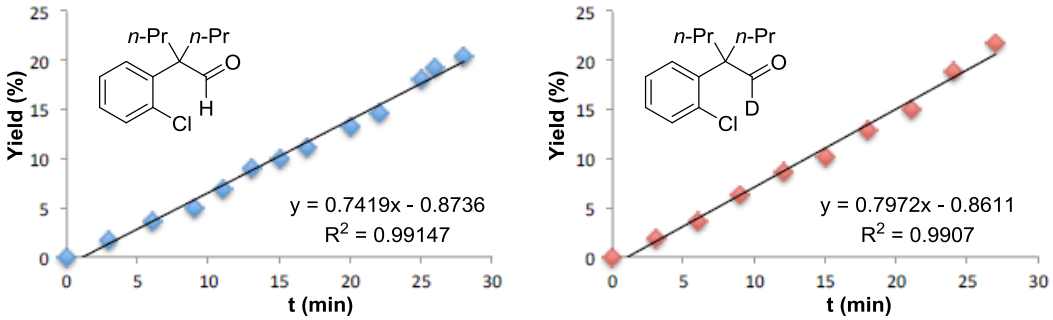

Kinetic isotope effect from calculated initial rates for **259b** and **259-*d*^{1}** was k_H/k_D = 0.93

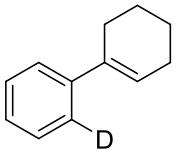

[353] Wang, T.; Hu, Y.; Zhang, S. *Org. Biomol. Chem.* **2010**, *8*, 2312.

Cyclohex-1-en-1-ylbenzene (261a-*d*[1]). Following general procedure B, 1-(2-chlorophenyl)-cyclohexanecarbaldehyde-D **259-*d*[1]** (112 mg, 0.50 mmol) was used. Column chromatography: silica gel (20:1 hexanes/Ethyl acetate). Yellow oil; 68 mg (86% yield). ^{1}H NMR (400 MHz, CDCl3) δ 7.45-7.41 (m, 1H), 7.38-7.32 (m, 2H), 7.29-7.22 (m, 1H), 6.19-6.14 (m, 1H), 2.46 (ddd, J = 8.2, 4.1, 2.2 Hz, 2H), 2.33-2.20 (m, 2H), 1.90-1.77 (m, 2H), 1.77-1.66 (m, 2H). ^{13}C-NMR (100 MHz, $CDCl_3$) δ 142.6, 136.5, 128.1, 128.0, 126.5, 124.9, 124.7, 124.6 (t, *J* = 23.9 Hz), 27.4, 25.9, 23.0, 22.2. IR (neat, cm^{-1}): 3058, 3022, 2927, 2859, 2834, 1469, 1437, 1134, 1050, 921, 769, 738, 627. HRMS *calc.* for [$C_{12}H_{13}D$] 159.1158, *found* 159.1166.

6.2.7. X-Ray crystallographic data {[Pd(PCy$_3$)$_2$(μ-CO)$_2$][Pd(PCy$_3$)]$_2$(μ-CO)}

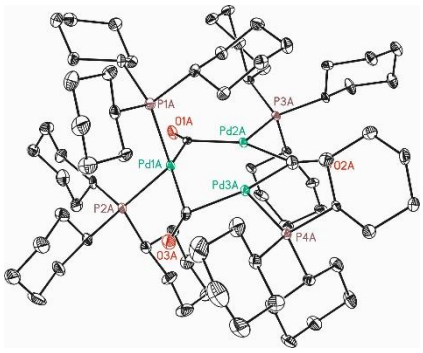

Table 1. Crystal data and structure refinement for {[Pd(PCy$_3$)$_2$(μ-CO)$_2$][Pd(PCy$_3$)]$_2$(μ-CO)}

Identification code	AGB10_033_0m	
Empirical formula	C81 H137.67 O3 P4 Pd3	
Formula weight	1602.66	
Temperature	100(2) K	
Wavelength	0.71073 Å	
Crystal system	Triclinic	
Space group	P1	
Unit cell dimensions	a = 13.2442(8) Å	α = 79.7250(10) °.
	b = 13.5171(9) Å	β = 87.1980(10) °.
	c = 35.486(2) Å	γ = 70.4870(10) °.
Volume	5891.5(6) Å^3	
Z	3	
Density (calculated)	1.355 Mg/m^3	
Absorption coefficient	0.806 mm^{-1}	
F(000)	2537	
Crystal size	0.40 x 0.20 x 0.18 mm^3	
Theta range for data collection	1.17 to 32.47 °.	
Index ranges	-19 <=h<=19 ,-20 <=k<=18 ,-53 <=l<=53	

Reflections collected	104218
Independent reflections	56804 [R(int) = 0.0330]
Completeness to theta =32.47 °	91.0%
Absorption correction	Empirical
Max. and min. transmission	0.8685 and 0.7386
Refinement method	Full-matrix least-squares on F^2
Data / restraints / parameters	56804 / 141 / 2512
Goodness-of-fit on F^2	1.017
Final R indices [I>2sigma(I)]	R1 = 0.0625 , wR2 = 0.1604
R indices (all data)	R1 = 0.0673 , wR2 = 0.1659
Flack parameter	x =0.244(15)
Largest diff. peak and hole	4.584 and -2.669 e.$Å^{-3}$

Table 2. Bond lengths [Å] and angles [°] for {[$Pd(PCy_3)_2(\mu\text{-}CO)_2$][$Pd(PCy_3)$]$_2(\mu\text{-}CO)$}

Bond lengths----	
Pd1A-C1A	2.101(5)
Pd1A-C3A	2.112(6)
Pd1A-P2A	2.4071(14)
Pd1A-P1A	2.4771(17)
Pd1A-Pd2A	2.7473(5)
Pd1A-Pd3A	2.7511(5)
Pd2A-C1A	2.048(5)
Pd2A-C2A	2.060(6)
Pd2A-P3A	2.3109(13)
Pd2A-Pd3A	2.6408(5)
Pd3A-C3A	2.045(5)
Pd3A-C2A	2.059(6)
Pd3A-P4A	2.3209(14)
P1A-C10A	1.879(6)
P1A-C4A	1.885(6)
P1A-C16A	1.886(6)
P2A-C28A	1.858(6)
P2A-C34A	1.864(7)
P2A-C22A	1.867(5)
P3A-C52A	1.851(5)
P3A-C40A	1.855(6)
P3A-C46A	1.857(5)
P4A-C64A	1.849(5)
P4A-C58A	1.855(6)
P4A-C70A	1.862(6)
O1A-C1A	1.162(7)
O2A-C2A	1.158(7)
O3A-C3A	1.163(7)
C4A-C5A	1.536(8)
C4A-C9A	1.541(8)
C5A-C6A	1.540(9)
C6A-C7A	1.534(10)
C7A-C8A	1.526(9)
C8A-C9A	1.538(9)
C10A-C11A	1.528(9)

C10A-C15A	1.537(8)
C11A-C12A	1.527(9)
C12A-C13A	1.528(11)
C13A-C14A	1.520(12)
C14A-C15A	1.523(9)
C16A-C17A	1.516(8)
C16A-C21A	1.534(8)
C17A-C18A	1.557(8)
C18A-C19A	1.514(9)
C19A-C20A	1.539(9)
C20A-C21A	1.532(8)
C22A-C27A	1.519(10)
C22A-C23A	1.533(9)
C23A-C24A	1.503(10)
C24A-C25A	1.543(12)
C25A-C26A	1.531(11)
C26A-C27A	1.540(8)
C28A-C33A	1.530(9)
C28A-C29A	1.549(9)
C29A-C30A	1.540(9)
C30A-C31A	1.515(11)
C31A-C32A	1.527(9)
C32A-C33A	1.531(8)
C34A-C39A	1.540(8)
C34A-C35A	1.542(9)
C35A-C36A	1.538(11)
C36A-C37A	1.514(10)
C37A-C38A	1.523(10)
C38A-C39A	1.525(10)
C40A-C45A	1.536(7)
C40A-C41A	1.540(8)
C41A-C42A	1.530(10)
C42A-C43A	1.525(9)
C43A-C44A	1.519(10)
C44A-C45A	1.540(10)
C46A-C51A	1.530(8)
C46A-C47A	1.538(8)
C47A-C48A	1.524(8)

C48A-C49A	1.534(9)
C49A-C50A	1.522(10)
C50A-C51A	1.533(8)
C52A-C53A	1.532(9)
C52A-C57A	1.543(7)
C53A-C54A	1.521(8)
C54A-C55A	1.533(9)
C55A-C56A	1.517(10)
C56A-C57A	1.532(8)
C58A-C59A	1.525(10)
C58A-C63A	1.528(8)
C59A-C60A	1.534(10)
C60A-C61A	1.538(13)
C61A-C62A	1.506(14)
C62A-C63A	1.543(9)
C64A-C69A	1.531(7)
C64A-C65A	1.532(9)
C65A-C66A	1.533(9)
C66A-C67A	1.517(9)
C67A-C68A	1.525(10)
C68A-C69A	1.536(8)
C70A-C71A	1.541(8)
C70A-C75A	1.551(7)
C71A-C72A	1.513(10)
C72A-C73A	1.523(9)
C73A-C74A	1.511(9)
C74A-C75A	1.542(10)
Pd1B-C3B	2.098(5)
Pd1B-C1B	2.098(5)
Pd1B-P1B	2.4110(14)
Pd1B-P2B	2.4802(16)
Pd1B-Pd3B	2.7507(5)
Pd1B-Pd2B	2.7553(6)
Pd2B-C1B	2.039(5)
Pd2B-C2B	2.070(5)
Pd2B-P3B	2.3317(14)
Pd2B-Pd3B	2.6481(5)
Pd3B-C3B	2.047(5)

Pd3B-C2B	2.052(6)
Pd3B-P4B	2.3210(13)
P1B-C16B	1.855(7)
P1B-C4B	1.856(5)
P1B-C10B	1.866(6)
P2B-C28B	1.872(6)
P2B-C34B	1.872(5)
P2B-C22B	1.887(6)
P3B-C52B	1.852(7)
P3B-C40B	1.852(6)
P3B-C46B	1.860(6)
P4B-C58B	1.853(6)
P4B-C70B	1.854(5)
P4B-C64B	1.863(6)
O1B-C1B	1.175(6)
O2B-C2B	1.150(8)
O3B-C3B	1.176(7)
C4B-C5B	1.532(9)
C4B-C9B	1.540(8)
C5B-C6B	1.524(8)
C6B-C7B	1.520(10)
C7B-C8B	1.520(13)
C8B-C9B	1.537(10)
C10B-C11B	1.526(10)
C10B-C15B	1.549(9)
C11B-C12B	1.524(9)
C12B-C13B	1.534(11)
C13B-C14B	1.503(12)
C14B-C15B	1.533(10)
C16B-C21B	1.525(8)
C16B-C17B	1.544(8)
C17B-C18B	1.520(10)
C18B-C19B	1.542(10)
C19B-C20B	1.518(9)
C20B-C21B	1.514(10)
C22B-C23B	1.533(8)
C22B-C27B	1.556(8)
C23B-C24B	1.542(8)

C24B-C25B	1.518(9)
C25B-C26B	1.516(9)
C26B-C27B	1.533(8)
C28B-C29B	1.536(8)
C28B-C33B	1.541(9)
C29B-C30B	1.538(8)
C30B-C31B	1.521(10)
C31B-C32B	1.525(8)
C32B-C33B	1.530(8)
C34B-C39B	1.541(7)
C34B-C35B	1.547(7)
C35B-C36B	1.546(7)
C36B-C37B	1.525(8)
C37B-C38B	1.546(8)
C38B-C39B	1.533(8)
C40B-C45B	1.525(10)
C40B-C41B	1.540(8)
C41B-C42B	1.546(10)
C42B-C43B	1.519(13)
C43B-C44B	1.543(10)
C44B-C45B	1.515(9)
C46B-C51B	1.509(9)
C46B-C47B	1.543(8)
C47B-C48B	1.524(9)
C48B-C49B	1.525(10)
C49B-C50B	1.534(9)
C50B-C51B	1.526(8)
C52B-C57B	1.539(8)
C52B-C53B	1.542(9)
C53B-C54B	1.528(10)
C54B-C55B	1.544(10)
C55B-C56B	1.528(10)
C56B-C57B	1.536(10)
C58B-C63B	1.525(8)
C58B-C59B	1.537(7)
C59B-C60B	1.520(9)
C60B-C61B	1.540(10)
C61B-C62B	1.524(9)

C62B-C63B	1.524(10)
C64B-C65B	1.522(9)
C64B-C69B	1.542(8)
C65B-C66B	1.541(8)
C66B-C67B	1.524(9)
C67B-C68B	1.520(10)
C68B-C69B	1.533(9)
C70B-C71B	1.518(8)
C70B-C75B	1.543(8)
C71B-C72B	1.545(8)
C72B-C73B	1.525(8)
C73B-C74B	1.520(9)
C74B-C75B	1.536(8)
Pd1C-C3C	2.077(5)
Pd1C-C1C	2.094(5)
Pd1C-P2C	2.3945(17)
Pd1C-P1C	2.4611(15)
Pd1C-Pd3C	2.7369(6)
Pd1C-Pd2C	2.7402(6)
Pd2C-C2C	2.049(6)
Pd2C-C1C	2.055(6)
Pd2C-P3C	2.3249(14)
Pd2C-Pd3C	2.6598(5)
Pd3C-C2C	2.064(6)
Pd3C-C3C	2.069(6)
Pd3C-P4C	2.3155(15)
P1C-C4C	1.860(7)
P1C-C10C	1.886(6)
P1C-C16C	1.889(6)
P2C-C22C	1.868(6)
P2C-C34C	1.869(6)
P2C-C28C	1.872(6)
P3C-C52C	1.858(6)
P3C-C40C	1.871(6)
P3C-C46C	1.885(7)
P4C-C58C	1.862(6)
P4C-C64C	1.868(7)
P4C-C70C	1.890(7)

O1C-C1C	1.176(7)
O2C-C2C	1.160(8)
O3C-C3C	1.145(8)
C4C-C5C	1.532(8)
C4C-C9C	1.537(8)
C5C-C6C	1.525(10)
C6C-C7C	1.539(10)
C7C-C8C	1.528(9)
C8C-C9C	1.535(9)
C10C-C15C	1.525(9)
C10C-C11C	1.550(9)
C11C-C12C	1.533(9)
C12C-C13C	1.521(11)
C13C-C14C	1.515(10)
C14C-C15C	1.541(8)
C16C-C17C	1.517(9)
C16C-C21C	1.533(8)
C17C-C18C	1.528(9)
C18C-C19C	1.521(10)
C19C-C20C	1.526(11)
C20C-C21C	1.525(8)
C22C-C23C	1.518(9)
C22C-C27C	1.538(8)
C23C-C24C	1.540(8)
C24C-C25C	1.523(8)
C25C-C26C	1.526(10)
C26C-C27C	1.536(8)
C28C-C33C	1.534(8)
C28C-C29C	1.542(10)
C29C-C30C	1.542(9)
C30C-C31C	1.521(9)
C31C-C32C	1.532(11)
C32C-C33C	1.524(8)
C34C-C39C	1.533(9)
C34C-C35C	1.542(8)
C35C-C36C	1.544(9)
C36C-C37C	1.529(12)
C37C-C38C	1.526(10)

C38C-C39C	1.541(9)
C40C-C45C	1.541(8)
C40C-C41C	1.553(9)
C41C-C42C	1.485(8)
C42C-C43C	1.521(10)
C43C-C44C	1.521(11)
C44C-C45C	1.528(8)
C46C-C47C	1.525(8)
C46C-C51C	1.526(10)
C47C-C48C	1.518(10)
C48C-C49C	1.533(11)
C49C-C50C	1.519(10)
C50C-C51C	1.515(11)
C52C-C53C	1.531(8)
C52C-C57C	1.546(8)
C53C-C54C	1.534(9)
C54C-C55C	1.529(9)
C55C-C56C	1.533(9)
C56C-C57C	1.535(9)
C58C-C63C	1.534(10)
C58C-C59C	1.539(9)
C59C-C60C	1.514(9)
C60C-C61C	1.551(11)
C61C-C62C	1.516(10)
C62C-C63C	1.545(9)
C64C-C69C	1.536(8)
C64C-C65C	1.538(8)
C65C-C66C	1.517(10)
C66C-C67C	1.533(10)
C67C-C68C	1.543(10)
C68C-C69C	1.534(11)
C70C-C75C	1.495(10)
C70C-C71C	1.569(9)
C71C-C72C	1.551(10)
C72C-C73C	1.476(11)
C73C-C74C	1.510(10)
C74C-C75C	1.547(11)
C1S-C6S	1.388(13)

C1S-C2S	1.403(13)
C2S-C3S	1.378(15)
C3S-C4S	1.370(14)
C4S-C5S	1.378(13)
C5S-C6S	1.367(15)
C1T-C6T	1.351(15)
C1T-C2T	1.431(16)
C2T-C3T	1.356(14)
C3T-C4T	1.395(13)
C4T-C5T	1.349(14)
C5T-C6T	1.378(14)
C1U-C6U	1.36(2)
C1U-C2U	1.37(2)
C2U-C3U	1.403(18)
C3U-C4U	1.369(19)
C4U-C5U	1.393(16)
C5U-C6U	1.381(15)
C1U'-C6U'	1.37(2)
C1U'-C2U'	1.37(2)
C2U'-C3U'	1.403(18)
C3U'-C4U'	1.370(19)
C4U'-C5U'	1.394(16)
C5U'-C6U'	1.382(15)

Angles----------

C1A-Pd1A-C3A	143.5(2)
C1A-Pd1A-P2A	92.20(15)
C3A-Pd1A-P2A	91.34(16)
C1A-Pd1A-P1A	102.95(16)
C3A-Pd1A-P1A	105.63(17)
P2A-Pd1A-P1A	122.32(5)
C1A-Pd1A-Pd2A	47.71(14)
C3A-Pd1A-Pd2A	103.70(15)
P2A-Pd1A-Pd2A	127.18(4)
P1A-Pd1A-Pd2A	102.04(4)
C1A-Pd1A-Pd3A	103.85(14)
C3A-Pd1A-Pd3A	47.51(15)
P2A-Pd1A-Pd3A	126.47(4)

P1A-Pd1A-Pd3A	103.46(4)
Pd2A-Pd1A-Pd3A	57.407(13)
C1A-Pd2A-C2A	158.7(2)
C1A-Pd2A-P3A	99.84(15)
C2A-Pd2A-P3A	99.25(17)
C1A-Pd2A-Pd3A	109.35(14)
C2A-Pd2A-Pd3A	50.09(16)
P3A-Pd2A-Pd3A	148.26(4)
C1A-Pd2A-Pd1A	49.38(14)
C2A-Pd2A-Pd1A	111.28(16)
P3A-Pd2A-Pd1A	149.19(4)
Pd3A-Pd2A-Pd1A	61.367(14)
C3A-Pd3A-C2A	158.9(2)
C3A-Pd3A-P4A	101.07(16)
C2A-Pd3A-P4A	98.10(17)
C3A-Pd3A-Pd2A	109.49(16)
C2A-Pd3A-Pd2A	50.16(16)
P4A-Pd3A-Pd2A	147.54(4)
C3A-Pd3A-Pd1A	49.62(16)
C2A-Pd3A-Pd1A	111.20(16)
P4A-Pd3A-Pd1A	150.60(4)
Pd2A-Pd3A-Pd1A	61.225(13)
C10A-P1A-C4A	101.1(3)
C10A-P1A-C16A	101.5(3)
C4A-P1A-C16A	97.2(2)
C10A-P1A-Pd1A	117.2(2)
C4A-P1A-Pd1A	120.2(2)
C16A-P1A-Pd1A	116.2(2)
C28A-P2A-C34A	101.8(3)
C28A-P2A-C22A	109.6(3)
C34A-P2A-C22A	100.2(3)
C28A-P2A-Pd1A	114.71(19)
C34A-P2A-Pd1A	113.04(19)
C22A-P2A-Pd1A	115.8(2)
C52A-P3A-C40A	103.6(3)
C52A-P3A-C46A	110.7(2)
C40A-P3A-C46A	101.5(3)
C52A-P3A-Pd2A	114.63(18)

C40A-P3A-Pd2A	112.31(17)
C46A-P3A-Pd2A	113.01(17)
C64A-P4A-C58A	111.0(3)
C64A-P4A-C70A	102.6(3)
C58A-P4A-C70A	102.7(3)
C64A-P4A-Pd3A	112.31(17)
C58A-P4A-Pd3A	113.77(19)
C70A-P4A-Pd3A	113.44(17)
O1A-C1A-Pd2A	138.9(4)
O1A-C1A-Pd1A	138.0(4)
Pd2A-C1A-Pd1A	82.91(19)
O2A-C2A-Pd3A	140.5(5)
O2A-C2A-Pd2A	139.8(5)
Pd3A-C2A-Pd2A	79.7(2)
O3A-C3A-Pd3A	139.3(5)
O3A-C3A-Pd1A	137.5(5)
Pd3A-C3A-Pd1A	82.9(2)
C5A-C4A-C9A	107.9(5)
C5A-C4A-P1A	111.4(4)
C9A-C4A-P1A	117.2(4)
C4A-C5A-C6A	110.7(5)
C7A-C6A-C5A	111.1(5)
C8A-C7A-C6A	111.3(5)
C7A-C8A-C9A	111.6(6)
C8A-C9A-C4A	110.6(5)
C11A-C10A-C15A	109.9(5)
C11A-C10A-P1A	116.9(4)
C15A-C10A-P1A	113.5(4)
C12A-C11A-C10A	111.3(5)
C11A-C12A-C13A	110.2(6)
C14A-C13A-C12A	111.3(6)
C13A-C14A-C15A	111.6(6)
C14A-C15A-C10A	109.9(5)
C17A-C16A-C21A	110.5(5)
C17A-C16A-P1A	113.7(4)
C21A-C16A-P1A	111.9(4)
C16A-C17A-C18A	111.0(5)
C19A-C18A-C17A	110.8(5)

C18A-C19A-C20A	110.4(5)
C21A-C20A-C19A	111.8(5)
C20A-C21A-C16A	112.0(5)
C27A-C22A-C23A	109.0(5)
C27A-C22A-P2A	113.9(4)
C23A-C22A-P2A	118.3(5)
C24A-C23A-C22A	111.6(7)
C23A-C24A-C25A	111.9(6)
C26A-C25A-C24A	111.9(6)
C25A-C26A-C27A	109.7(6)
C22A-C27A-C26A	110.1(5)
C33A-C28A-C29A	109.3(5)
C33A-C28A-P2A	112.1(4)
C29A-C28A-P2A	120.5(5)
C30A-C29A-C28A	109.7(6)
C31A-C30A-C29A	111.8(6)
C30A-C31A-C32A	112.3(5)
C31A-C32A-C33A	111.4(6)
C28A-C33A-C32A	110.9(5)
C39A-C34A-C35A	108.1(5)
C39A-C34A-P2A	113.0(4)
C35A-C34A-P2A	113.0(5)
C36A-C35A-C34A	111.2(6)
C37A-C36A-C35A	110.9(6)
C36A-C37A-C38A	112.1(7)
C37A-C38A-C39A	111.6(6)
C38A-C39A-C34A	111.0(5)
C45A-C40A-C41A	109.8(5)
C45A-C40A-P3A	111.9(4)
C41A-C40A-P3A	110.8(4)
C42A-C41A-C40A	110.6(5)
C43A-C42A-C41A	111.8(6)
C44A-C43A-C42A	110.4(5)
C43A-C44A-C45A	112.3(5)
C40A-C45A-C44A	110.3(5)
C51A-C46A-C47A	110.5(5)
C51A-C46A-P3A	118.0(4)
C47A-C46A-P3A	114.2(4)

C48A-C47A-C46A	110.2(5)
C47A-C48A-C49A	111.1(5)
C50A-C49A-C48A	110.7(5)
C49A-C50A-C51A	110.6(6)
C46A-C51A-C50A	109.8(5)
C53A-C52A-C57A	109.7(4)
C53A-C52A-P3A	113.1(4)
C57A-C52A-P3A	117.5(4)
C54A-C53A-C52A	111.7(5)
C53A-C54A-C55A	110.4(5)
C56A-C55A-C54A	111.8(5)
C55A-C56A-C57A	111.2(5)
C56A-C57A-C52A	111.3(5)
C59A-C58A-C63A	110.4(5)
C59A-C58A-P4A	111.5(4)
C63A-C58A-P4A	119.3(4)
C58A-C59A-C60A	110.4(6)
C59A-C60A-C61A	110.5(7)
C62A-C61A-C60A	112.3(7)
C61A-C62A-C63A	111.8(6)
C58A-C63A-C62A	110.2(6)
C69A-C64A-C65A	110.5(5)
C69A-C64A-P4A	118.3(4)
C65A-C64A-P4A	112.4(4)
C64A-C65A-C66A	110.7(5)
C67A-C66A-C65A	111.5(5)
C66A-C67A-C68A	111.0(5)
C67A-C68A-C69A	111.4(5)
C64A-C69A-C68A	110.4(4)
C71A-C70A-C75A	110.2(5)
C71A-C70A-P4A	111.9(4)
C75A-C70A-P4A	108.7(4)
C72A-C71A-C70A	112.3(5)
C71A-C72A-C73A	111.7(6)
C74A-C73A-C72A	110.0(6)
C73A-C74A-C75A	111.4(5)
C74A-C75A-C70A	110.7(5)
C3B-Pd1B-C1B	144.9(2)

C3B-Pd1B-P1B	91.34(15)
C1B-Pd1B-P1B	92.64(15)
C3B-Pd1B-P2B	102.88(18)
C1B-Pd1B-P2B	103.79(17)
P1B-Pd1B-P2B	123.52(5)
C3B-Pd1B-Pd3B	47.63(15)
C1B-Pd1B-Pd3B	103.84(15)
P1B-Pd1B-Pd3B	125.12(4)
P2B-Pd1B-Pd3B	102.93(3)
C3B-Pd1B-Pd2B	104.08(15)
C1B-Pd1B-Pd2B	47.34(14)
P1B-Pd1B-Pd2B	125.70(4)
P2B-Pd1B-Pd2B	103.48(3)
Pd3B-Pd1B-Pd2B	57.496(14)
C1B-Pd2B-C2B	157.4(2)
C1B-Pd2B-P3B	100.85(15)
C2B-Pd2B-P3B	99.37(16)
C1B-Pd2B-Pd3B	109.24(14)
C2B-Pd2B-Pd3B	49.72(15)
P3B-Pd2B-Pd3B	149.00(4)
C1B-Pd2B-Pd1B	49.17(14)
C2B-Pd2B-Pd1B	110.88(15)
P3B-Pd2B-Pd1B	149.72(4)
Pd3B-Pd2B-Pd1B	61.165(14)
C3B-Pd3B-C2B	158.1(2)
C3B-Pd3B-P4B	99.50(15)
C2B-Pd3B-P4B	99.49(15)
C3B-Pd3B-Pd2B	109.42(14)
C2B-Pd3B-Pd2B	50.32(15)
P4B-Pd3B-Pd2B	149.49(4)
C3B-Pd3B-Pd1B	49.23(15)
C2B-Pd3B-Pd1B	111.65(15)
P4B-Pd3B-Pd1B	148.63(4)
Pd2B-Pd3B-Pd1B	61.339(14)
C16B-P1B-C4B	100.3(3)
C16B-P1B-C10B	102.7(3)
C4B-P1B-C10B	108.7(3)
C16B-P1B-Pd1B	112.23(18)

C4B-P1B-Pd1B	116.05(19)
C10B-P1B-Pd1B	115.02(19)
C28B-P2B-C34B	101.6(2)
C28B-P2B-C22B	100.7(3)
C34B-P2B-C22B	96.9(2)
C28B-P2B-Pd1B	118.34(19)
C34B-P2B-Pd1B	116.2(2)
C22B-P2B-Pd1B	119.5(2)
C52B-P3B-C40B	103.8(3)
C52B-P3B-C46B	104.1(3)
C40B-P3B-C46B	109.8(3)
C52B-P3B-Pd2B	112.75(18)
C40B-P3B-Pd2B	114.1(2)
C46B-P3B-Pd2B	111.71(17)
C58B-P4B-C70B	101.3(3)
C58B-P4B-C64B	102.9(3)
C70B-P4B-C64B	110.7(2)
C58B-P4B-Pd3B	112.24(16)
C70B-P4B-Pd3B	112.96(18)
C64B-P4B-Pd3B	115.45(18)
O1B-C1B-Pd2B	139.2(4)
O1B-C1B-Pd1B	136.6(4)
Pd2B-C1B-Pd1B	83.50(18)
O2B-C2B-Pd3B	141.0(4)
O2B-C2B-Pd2B	139.0(4)
Pd3B-C2B-Pd2B	80.0(2)
O3B-C3B-Pd3B	139.0(4)
O3B-C3B-Pd1B	137.5(4)
Pd3B-C3B-Pd1B	83.15(19)
C5B-C4B-C9B	108.8(5)
C5B-C4B-P1B	113.4(4)
C9B-C4B-P1B	118.4(4)
C6B-C5B-C4B	111.7(5)
C7B-C6B-C5B	110.5(6)
C8B-C7B-C6B	110.9(6)
C7B-C8B-C9B	112.3(7)
C8B-C9B-C4B	109.9(6)
C11B-C10B-C15B	108.7(5)

C11B-C10B-P1B	112.9(4)
C15B-C10B-P1B	120.3(5)
C12B-C11B-C10B	111.6(6)
C11B-C12B-C13B	111.4(6)
C14B-C13B-C12B	110.6(6)
C13B-C14B-C15B	113.0(6)
C14B-C15B-C10B	109.0(6)
C21B-C16B-C17B	108.3(5)
C21B-C16B-P1B	113.7(4)
C17B-C16B-P1B	112.2(4)
C18B-C17B-C16B	111.3(5)
C17B-C18B-C19B	110.9(6)
C20B-C19B-C18B	111.0(6)
C21B-C20B-C19B	112.0(6)
C20B-C21B-C16B	113.1(5)
C23B-C22B-C27B	108.3(4)
C23B-C22B-P2B	117.4(4)
C27B-C22B-P2B	111.7(4)
C22B-C23B-C24B	110.8(5)
C25B-C24B-C23B	112.0(6)
C26B-C25B-C24B	112.4(5)
C25B-C26B-C27B	111.8(5)
C26B-C27B-C22B	109.8(5)
C29B-C28B-C33B	109.5(4)
C29B-C28B-P2B	115.2(4)
C33B-C28B-P2B	116.0(4)
C28B-C29B-C30B	111.5(5)
C31B-C30B-C29B	111.3(5)
C30B-C31B-C32B	111.9(5)
C31B-C32B-C33B	111.1(5)
C32B-C33B-C28B	111.1(5)
C39B-C34B-C35B	109.5(4)
C39B-C34B-P2B	113.6(4)
C35B-C34B-P2B	112.1(4)
C36B-C35B-C34B	111.2(4)
C37B-C36B-C35B	111.6(4)
C36B-C37B-C38B	109.8(5)
C39B-C38B-C37B	111.8(5)

C38B-C39B-C34B	110.8(4)
C45B-C40B-C41B	109.6(5)
C45B-C40B-P3B	112.2(4)
C41B-C40B-P3B	119.8(5)
C40B-C41B-C42B	109.8(6)
C43B-C42B-C41B	111.8(6)
C42B-C43B-C44B	111.5(7)
C45B-C44B-C43B	110.5(6)
C44B-C45B-C40B	112.7(6)
C51B-C46B-C47B	110.7(5)
C51B-C46B-P3B	112.1(4)
C47B-C46B-P3B	117.7(4)
C48B-C47B-C46B	109.8(5)
C47B-C48B-C49B	111.9(6)
C48B-C49B-C50B	109.9(5)
C51B-C50B-C49B	111.0(5)
C46B-C51B-C50B	111.4(5)
C57B-C52B-C53B	110.6(5)
C57B-C52B-P3B	109.7(4)
C53B-C52B-P3B	111.0(4)
C54B-C53B-C52B	112.8(5)
C53B-C54B-C55B	110.4(6)
C56B-C55B-C54B	109.2(5)
C55B-C56B-C57B	112.4(5)
C56B-C57B-C52B	111.2(6)
C63B-C58B-C59B	110.1(5)
C63B-C58B-P4B	112.2(4)
C59B-C58B-P4B	112.3(4)
C60B-C59B-C58B	111.5(5)
C59B-C60B-C61B	112.2(5)
C62B-C61B-C60B	111.3(5)
C61B-C62B-C63B	111.2(5)
C62B-C63B-C58B	112.2(5)
C65B-C64B-C69B	109.9(5)
C65B-C64B-P4B	112.4(4)
C69B-C64B-P4B	117.6(4)
C64B-C65B-C66B	111.2(5)
C67B-C66B-C65B	111.2(5)

C68B-C67B-C66B	111.2(5)
C67B-C68B-C69B	112.4(5)
C68B-C69B-C64B	111.1(5)
C71B-C70B-C75B	110.5(5)
C71B-C70B-P4B	113.9(4)
C75B-C70B-P4B	117.3(4)
C70B-C71B-C72B	110.4(5)
C73B-C72B-C71B	111.3(5)
C74B-C73B-C72B	111.0(5)
C73B-C74B-C75B	110.3(6)
C74B-C75B-C70B	110.0(5)
C3C-Pd1C-C1C	152.3(2)
C3C-Pd1C-P2C	93.39(19)
C1C-Pd1C-P2C	93.17(19)
C3C-Pd1C-P1C	93.22(17)
C1C-Pd1C-P1C	104.90(15)
P2C-Pd1C-P1C	124.85(5)
C3C-Pd1C-Pd3C	48.57(18)
C1C-Pd1C-Pd3C	104.90(17)
P2C-Pd1C-Pd3C	116.34(4)
P1C-Pd1C-Pd3C	108.56(4)
C3C-Pd1C-Pd2C	106.64(18)
C1C-Pd1C-Pd2C	48.05(18)
P2C-Pd1C-Pd2C	121.84(4)
P1C-Pd1C-Pd2C	108.21(4)
Pd3C-Pd1C-Pd2C	58.107(15)
C2C-Pd2C-C1C	158.5(2)
C2C-Pd2C-P3C	100.77(18)
C1C-Pd2C-P3C	99.88(15)
C2C-Pd2C-Pd3C	49.97(18)
C1C-Pd2C-Pd3C	108.81(15)
P3C-Pd2C-Pd3C	150.26(4)
C2C-Pd2C-Pd1C	110.47(17)
C1C-Pd2C-Pd1C	49.27(15)
P3C-Pd2C-Pd1C	148.73(4)
Pd3C-Pd2C-Pd1C	60.884(14)
C2C-Pd3C-C3C	157.7(2)
C2C-Pd3C-P4C	96.63(16)

C3C-Pd3C-P4C	105.11(15)
C2C-Pd3C-Pd2C	49.47(16)
C3C-Pd3C-Pd2C	109.80(15)
P4C-Pd3C-Pd2C	144.54(4)
C2C-Pd3C-Pd1C	110.10(16)
C3C-Pd3C-Pd1C	48.83(15)
P4C-Pd3C-Pd1C	152.94(4)
Pd2C-Pd3C-Pd1C	61.009(14)
C4C-P1C-C10C	101.3(3)
C4C-P1C-C16C	103.9(3)
C10C-P1C-C16C	103.5(3)
C4C-P1C-Pd1C	111.69(18)
C10C-P1C-Pd1C	116.00(19)
C16C-P1C-Pd1C	118.5(2)
C22C-P2C-C34C	100.2(3)
C22C-P2C-C28C	110.4(3)
C34C-P2C-C28C	102.6(3)
C22C-P2C-Pd1C	116.0(2)
C34C-P2C-Pd1C	114.5(2)
C28C-P2C-Pd1C	111.9(2)
C52C-P3C-C40C	103.3(3)
C52C-P3C-C46C	102.4(3)
C40C-P3C-C46C	105.4(3)
C52C-P3C-Pd2C	112.40(19)
C40C-P3C-Pd2C	113.42(19)
C46C-P3C-Pd2C	118.4(2)
C58C-P4C-C64C	104.5(3)
C58C-P4C-C70C	104.6(3)
C64C-P4C-C70C	107.5(3)
C58C-P4C-Pd3C	119.80(19)
C64C-P4C-Pd3C	113.06(17)
C70C-P4C-Pd3C	106.5(3)
O1C-C1C-Pd2C	139.5(5)
O1C-C1C-Pd1C	137.1(5)
Pd2C-C1C-Pd1C	82.7(2)
O2C-C2C-Pd2C	139.4(5)
O2C-C2C-Pd3C	139.9(5)
Pd2C-C2C-Pd3C	80.6(2)

O3C-C3C-Pd3C	141.5(5)
O3C-C3C-Pd1C	135.7(5)
Pd3C-C3C-Pd1C	82.6(2)
C5C-C4C-C9C	109.4(5)
C5C-C4C-P1C	115.3(4)
C9C-C4C-P1C	111.5(4)
C6C-C5C-C4C	110.6(5)
C5C-C6C-C7C	111.6(5)
C8C-C7C-C6C	109.9(6)
C7C-C8C-C9C	111.4(5)
C8C-C9C-C4C	110.4(5)
C15C-C10C-C11C	107.9(5)
C15C-C10C-P1C	113.6(4)
C11C-C10C-P1C	119.3(5)
C12C-C11C-C10C	109.9(5)
C13C-C12C-C11C	111.6(5)
C14C-C13C-C12C	111.6(5)
C13C-C14C-C15C	110.3(6)
C10C-C15C-C14C	111.3(5)
C17C-C16C-C21C	111.4(5)
C17C-C16C-P1C	115.9(4)
C21C-C16C-P1C	112.2(4)
C16C-C17C-C18C	111.9(6)
C19C-C18C-C17C	111.6(6)
C18C-C19C-C20C	110.1(6)
C21C-C20C-C19C	111.6(6)
C20C-C21C-C16C	110.8(5)
C23C-C22C-C27C	111.8(5)
C23C-C22C-P2C	119.2(4)
C27C-C22C-P2C	111.3(4)
C22C-C23C-C24C	110.6(5)
C25C-C24C-C23C	111.9(5)
C24C-C25C-C26C	110.3(5)
C25C-C26C-C27C	110.9(6)
C26C-C27C-C22C	110.3(5)
C33C-C28C-C29C	109.2(5)
C33C-C28C-P2C	111.7(4)
C29C-C28C-P2C	119.8(4)

C28C-C29C-C30C	109.4(5)
C31C-C30C-C29C	112.3(5)
C30C-C31C-C32C	112.0(6)
C33C-C32C-C31C	111.0(5)
C32C-C33C-C28C	110.8(5)
C39C-C34C-C35C	109.3(5)
C39C-C34C-P2C	110.7(5)
C35C-C34C-P2C	112.5(4)
C34C-C35C-C36C	110.3(5)
C37C-C36C-C35C	109.7(6)
C38C-C37C-C36C	111.7(7)
C37C-C38C-C39C	110.6(6)
C34C-C39C-C38C	111.2(6)
C45C-C40C-C41C	109.9(5)
C45C-C40C-P3C	110.4(4)
C41C-C40C-P3C	113.3(4)
C42C-C41C-C40C	111.5(5)
C41C-C42C-C43C	115.1(6)
C42C-C43C-C44C	110.5(6)
C43C-C44C-C45C	112.2(6)
C44C-C45C-C40C	110.4(5)
C47C-C46C-C51C	109.2(6)
C47C-C46C-P3C	109.8(4)
C51C-C46C-P3C	116.2(5)
C48C-C47C-C46C	113.1(6)
C47C-C48C-C49C	109.7(6)
C50C-C49C-C48C	110.7(6)
C51C-C50C-C49C	111.3(6)
C50C-C51C-C46C	112.1(6)
C53C-C52C-C57C	109.1(4)
C53C-C52C-P3C	111.0(4)
C57C-C52C-P3C	117.2(4)
C52C-C53C-C54C	110.5(5)
C55C-C54C-C53C	110.3(5)
C54C-C55C-C56C	111.6(5)
C55C-C56C-C57C	111.9(5)
C56C-C57C-C52C	109.8(5)
C63C-C58C-C59C	111.6(5)

C63C-C58C-P4C	110.7(4)
C59C-C58C-P4C	109.8(4)
C60C-C59C-C58C	112.6(5)
C59C-C60C-C61C	112.2(6)
C62C-C61C-C60C	109.9(6)
C61C-C62C-C63C	110.7(5)
C58C-C63C-C62C	112.3(6)
C69C-C64C-C65C	109.5(5)
C69C-C64C-P4C	117.0(4)
C65C-C64C-P4C	110.4(4)
C66C-C65C-C64C	111.2(5)
C65C-C66C-C67C	111.0(6)
C66C-C67C-C68C	108.9(6)
C69C-C68C-C67C	110.8(6)
C68C-C69C-C64C	111.1(5)
C75C-C70C-C71C	110.5(6)
C75C-C70C-P4C	116.6(6)
C71C-C70C-P4C	111.8(4)
C72C-C71C-C70C	110.7(6)
C73C-C72C-C71C	112.0(6)
C72C-C73C-C74C	112.6(7)
C73C-C74C-C75C	110.5(7)
C70C-C75C-C74C	111.1(7)
C6S-C1S-C2S	119.5(10)
C3S-C2S-C1S	119.4(8)
C4S-C3S-C2S	120.1(8)
C3S-C4S-C5S	120.8(10)
C6S-C5S-C4S	120.0(9)
C5S-C6S-C1S	120.2(8)
C6T-C1T-C2T	118.5(8)
C3T-C2T-C1T	119.6(8)
C2T-C3T-C4T	119.8(10)
C5T-C4T-C3T	120.5(9)
C4T-C5T-C6T	119.9(8)
C1T-C6T-C5T	121.5(10)
C6U-C1U-C2U	119.4(14)
C1U-C2U-C3U	119.8(13)
C4U-C3U-C2U	120.6(14)

C3U-C4U-C5U	118.6(13)
C6U-C5U-C4U	119.6(13)
C1U-C6U-C5U	121.1(15)
C6U'-C1U'-C2U'	118.8(14)
C1U'-C2U'-C3U'	120.2(13)
C4U'-C3U'-C2U'	120.3(15)
C3U'-C4U'-C5U'	118.5(14)
C6U'-C5U'-C4U'	119.4(14)
C1U'-C6U'-C5U'	120.7(15)

Table 3. Torsion angles [°] for {[$Pd(PCy_3)_2(\mu\text{-}CO)_2$][$Pd(PCy_3)$]$_2(\mu\text{-}CO)$}

C3A-Pd1A-Pd2A-C1A	153.8(3)
P2A-Pd1A-Pd2A-C1A	51.3(2)
P1A-Pd1A-Pd2A-C1A	-96.6(2)
Pd3A-Pd1A-Pd2A-C1A	165.0(2)
C1A-Pd1A-Pd2A-C2A	-169.4(3)
C3A-Pd1A-Pd2A-C2A	-15.6(3)
P2A-Pd1A-Pd2A-C2A	-118.0(2)
P1A-Pd1A-Pd2A-C2A	94.0(2)
Pd3A-Pd1A-Pd2A-C2A	-4.4(2)
C1A-Pd1A-Pd2A-P3A	2.5(2)
C3A-Pd1A-Pd2A-P3A	156.28(19)
P2A-Pd1A-Pd2A-P3A	53.86(10)
P1A-Pd1A-Pd2A-P3A	-94.12(9)
Pd3A-Pd1A-Pd2A-P3A	167.48(8)
C1A-Pd1A-Pd2A-Pd3A	-165.0(2)
C3A-Pd1A-Pd2A-Pd3A	-11.20(17)
P2A-Pd1A-Pd2A-Pd3A	-113.62(5)
P1A-Pd1A-Pd2A-Pd3A	98.40(4)
C1A-Pd2A-Pd3A-C3A	-0.1(3)
C2A-Pd2A-Pd3A-C3A	-173.4(3)
P3A-Pd2A-Pd3A-C3A	-155.9(2)
Pd1A-Pd2A-Pd3A-C3A	11.94(19)
C1A-Pd2A-Pd3A-C2A	173.3(3)
P3A-Pd2A-Pd3A-C2A	17.6(3)
Pd1A-Pd2A-Pd3A-C2A	-174.6(3)
C1A-Pd2A-Pd3A-P4A	159.3(2)
C2A-Pd2A-Pd3A-P4A	-14.1(3)
P3A-Pd2A-Pd3A-P4A	3.49(12)
Pd1A-Pd2A-Pd3A-P4A	171.31(8)
C1A-Pd2A-Pd3A-Pd1A	-12.05(18)
C2A-Pd2A-Pd3A-Pd1A	174.6(3)
P3A-Pd2A-Pd3A-Pd1A	-167.82(8)
C1A-Pd1A-Pd3A-C3A	-153.8(3)
P2A-Pd1A-Pd3A-C3A	-50.4(2)
P1A-Pd1A-Pd3A-C3A	99.0(2)
Pd2A-Pd1A-Pd3A-C3A	-165.2(2)

C1A-Pd1A-Pd3A-C2A	15.8(3)
C3A-Pd1A-Pd3A-C2A	169.6(3)
P2A-Pd1A-Pd3A-C2A	119.2(2)
P1A-Pd1A-Pd3A-C2A	-91.4(2)
Pd2A-Pd1A-Pd3A-C2A	4.4(2)
C1A-Pd1A-Pd3A-P4A	-159.09(18)
C3A-Pd1A-Pd3A-P4A	-5.3(2)
P2A-Pd1A-Pd3A-P4A	-55.70(10)
P1A-Pd1A-Pd3A-P4A	93.68(10)
Pd2A-Pd1A-Pd3A-P4A	-170.49(9)
C1A-Pd1A-Pd3A-Pd2A	11.41(16)
C3A-Pd1A-Pd3A-Pd2A	165.2(2)
P2A-Pd1A-Pd3A-Pd2A	114.79(5)
P1A-Pd1A-Pd3A-Pd2A	-95.83(4)
C1A-Pd1A-P1A-C10A	162.2(3)
C3A-Pd1A-P1A-C10A	-40.7(3)
P2A-Pd1A-P1A-C10A	61.2(2)
Pd2A-Pd1A-P1A-C10A	-148.8(2)
Pd3A-Pd1A-P1A-C10A	-89.9(2)
C1A-Pd1A-P1A-C4A	38.9(2)
C3A-Pd1A-P1A-C4A	-164.0(2)
P2A-Pd1A-P1A-C4A	-62.1(2)
Pd2A-Pd1A-P1A-C4A	87.9(2)
Pd3A-Pd1A-P1A-C4A	146.9(2)
C1A-Pd1A-P1A-C16A	-77.6(2)
C3A-Pd1A-P1A-C16A	79.4(2)
P2A-Pd1A-P1A-C16A	-178.70(19)
Pd2A-Pd1A-P1A-C16A	-28.70(19)
Pd3A-Pd1A-P1A-C16A	30.29(19)
C1A-Pd1A-P2A-C28A	-44.0(3)
C3A-Pd1A-P2A-C28A	172.3(3)
P1A-Pd1A-P2A-C28A	62.8(2)
Pd2A-Pd1A-P2A-C28A	-79.4(2)
Pd3A-Pd1A-P2A-C28A	-153.1(2)
C1A-Pd1A-P2A-C34A	72.0(3)
C3A-Pd1A-P2A-C34A	-71.6(3)
P1A-Pd1A-P2A-C34A	178.9(2)
Pd2A-Pd1A-P2A-C34A	36.7(2)

Pd3A-Pd1A-P2A-C34A	-37.0(2)
C1A-Pd1A-P2A-C22A	-173.2(3)
C3A-Pd1A-P2A-C22A	43.1(3)
P1A-Pd1A-P2A-C22A	-66.4(2)
Pd2A-Pd1A-P2A-C22A	151.5(2)
Pd3A-Pd1A-P2A-C22A	77.8(2)
C1A-Pd2A-P3A-C52A	33.2(3)
C2A-Pd2A-P3A-C52A	-156.4(3)
Pd3A-Pd2A-P3A-C52A	-169.94(19)
Pd1A-Pd2A-P3A-C52A	31.3(2)
C1A-Pd2A-P3A-C40A	-84.7(3)
C2A-Pd2A-P3A-C40A	85.8(3)
Pd3A-Pd2A-P3A-C40A	72.2(2)
Pd1A-Pd2A-P3A-C40A	-86.6(2)
C1A-Pd2A-P3A-C46A	161.3(3)
C2A-Pd2A-P3A-C46A	-28.3(3)
Pd3A-Pd2A-P3A-C46A	-41.9(2)
Pd1A-Pd2A-P3A-C46A	159.3(2)
C3A-Pd3A-P4A-C64A	-148.7(3)
C2A-Pd3A-P4A-C64A	40.2(3)
Pd2A-Pd3A-P4A-C64A	51.0(2)
Pd1A-Pd3A-P4A-C64A	-144.6(2)
C3A-Pd3A-P4A-C58A	-21.5(3)
C2A-Pd3A-P4A-C58A	167.4(3)
Pd2A-Pd3A-P4A-C58A	178.2(2)
Pd1A-Pd3A-P4A-C58A	-17.4(3)
C3A-Pd3A-P4A-C70A	95.5(3)
C2A-Pd3A-P4A-C70A	-75.6(3)
Pd2A-Pd3A-P4A-C70A	-64.8(2)
Pd1A-Pd3A-P4A-C70A	99.6(2)
C2A-Pd2A-C1A-O1A	-147.8(7)
P3A-Pd2A-C1A-O1A	5.3(8)
Pd3A-Pd2A-C1A-O1A	-162.0(7)
Pd1A-Pd2A-C1A-O1A	-176.0(9)
C2A-Pd2A-C1A-Pd1A	28.2(8)
P3A-Pd2A-C1A-Pd1A	-178.69(12)
Pd3A-Pd2A-C1A-Pd1A	14.0(2)
C3A-Pd1A-C1A-O1A	129.8(7)

P2A-Pd1A-C1A-O1A	34.5(7)
P1A-Pd1A-C1A-O1A	-89.4(7)
Pd2A-Pd1A-C1A-O1A	176.0(9)
Pd3A-Pd1A-C1A-O1A	163.0(7)
C3A-Pd1A-C1A-Pd2A	-46.3(4)
P2A-Pd1A-C1A-Pd2A	-141.49(15)
P1A-Pd1A-C1A-Pd2A	94.60(15)
Pd3A-Pd1A-C1A-Pd2A	-13.02(18)
C3A-Pd3A-C2A-O2A	-161.2(8)
P4A-Pd3A-C2A-O2A	-6.2(10)
Pd2A-Pd3A-C2A-O2A	-178.6(11)
Pd1A-Pd3A-C2A-O2A	176.3(9)
C3A-Pd3A-C2A-Pd2A	17.4(8)
P4A-Pd3A-C2A-Pd2A	172.43(14)
Pd1A-Pd3A-C2A-Pd2A	-5.0(2)
C1A-Pd2A-C2A-O2A	161.1(7)
P3A-Pd2A-C2A-O2A	7.9(9)
Pd3A-Pd2A-C2A-O2A	178.7(11)
Pd1A-Pd2A-C2A-O2A	-176.3(9)
C1A-Pd2A-C2A-Pd3A	-17.6(8)
P3A-Pd2A-C2A-Pd3A	-170.75(14)
Pd1A-Pd2A-C2A-Pd3A	5.1(2)
C2A-Pd3A-C3A-O3A	146.6(8)
P4A-Pd3A-C3A-O3A	-8.2(8)
Pd2A-Pd3A-C3A-O3A	160.7(7)
Pd1A-Pd3A-C3A-O3A	174.4(9)
C2A-Pd3A-C3A-Pd1A	-27.9(8)
P4A-Pd3A-C3A-Pd1A	177.34(12)
Pd2A-Pd3A-C3A-Pd1A	-13.8(2)
C1A-Pd1A-C3A-O3A	-128.4(7)
P2A-Pd1A-C3A-O3A	-32.9(8)
P1A-Pd1A-C3A-O3A	91.3(8)
Pd2A-Pd1A-C3A-O3A	-161.8(7)
Pd3A-Pd1A-C3A-O3A	-174.6(9)
C1A-Pd1A-C3A-Pd3A	46.2(4)
P2A-Pd1A-C3A-Pd3A	141.71(16)
P1A-Pd1A-C3A-Pd3A	-94.10(16)
Pd2A-Pd1A-C3A-Pd3A	12.82(19)

C10A-P1A-C4A-C5A	-156.3(4)
C16A-P1A-C4A-C5A	100.5(4)
Pd1A-P1A-C4A-C5A	-25.5(4)
C10A-P1A-C4A-C9A	-31.3(5)
C16A-P1A-C4A-C9A	-134.5(5)
Pd1A-P1A-C4A-C9A	99.4(5)
C9A-C4A-C5A-C6A	60.6(6)
P1A-C4A-C5A-C6A	-169.4(4)
C4A-C5A-C6A-C7A	-57.9(7)
C5A-C6A-C7A-C8A	53.4(7)
C6A-C7A-C8A-C9A	-53.3(7)
C7A-C8A-C9A-C4A	57.4(7)
C5A-C4A-C9A-C8A	-60.1(7)
P1A-C4A-C9A-C8A	173.1(4)
C4A-P1A-C10A-C11A	-62.3(5)
C16A-P1A-C10A-C11A	37.4(5)
Pd1A-P1A-C10A-C11A	165.1(4)
C4A-P1A-C10A-C15A	168.1(4)
C16A-P1A-C10A-C15A	-92.1(5)
Pd1A-P1A-C10A-C15A	35.6(5)
C15A-C10A-C11A-C12A	-58.2(7)
P1A-C10A-C11A-C12A	170.6(4)
C10A-C11A-C12A-C13A	56.7(7)
C11A-C12A-C13A-C14A	-55.3(8)
C12A-C13A-C14A-C15A	56.4(8)
C13A-C14A-C15A-C10A	-57.2(8)
C11A-C10A-C15A-C14A	57.6(7)
P1A-C10A-C15A-C14A	-169.4(5)
C10A-P1A-C16A-C17A	65.2(5)
C4A-P1A-C16A-C17A	168.2(5)
Pd1A-P1A-C16A-C17A	-63.0(5)
C10A-P1A-C16A-C21A	-168.7(4)
C4A-P1A-C16A-C21A	-65.8(5)
Pd1A-P1A-C16A-C21A	63.0(5)
C21A-C16A-C17A-C18A	56.2(7)
P1A-C16A-C17A-C18A	-177.0(4)
C16A-C17A-C18A-C19A	-58.1(7)
C17A-C18A-C19A-C20A	56.4(7)

C18A-C19A-C20A-C21A	-54.9(8)
C19A-C20A-C21A-C16A	54.0(8)
C17A-C16A-C21A-C20A	-54.6(7)
P1A-C16A-C21A-C20A	177.6(4)
C28A-P2A-C22A-C27A	-77.4(5)
C34A-P2A-C22A-C27A	176.2(5)
Pd1A-P2A-C22A-C27A	54.3(5)
C28A-P2A-C22A-C23A	52.6(6)
C34A-P2A-C22A-C23A	-53.9(6)
Pd1A-P2A-C22A-C23A	-175.8(5)
C27A-C22A-C23A-C24A	-58.8(8)
P2A-C22A-C23A-C24A	169.0(6)
C22A-C23A-C24A-C25A	54.0(10)
C23A-C24A-C25A-C26A	-52.0(11)
C24A-C25A-C26A-C27A	54.1(9)
C23A-C22A-C27A-C26A	61.3(7)
P2A-C22A-C27A-C26A	-164.2(5)
C25A-C26A-C27A-C22A	-59.5(8)
C34A-P2A-C28A-C33A	163.4(4)
C22A-P2A-C28A-C33A	58.0(5)
Pd1A-P2A-C28A-C33A	-74.2(4)
C34A-P2A-C28A-C29A	32.7(5)
C22A-P2A-C28A-C29A	-72.8(6)
Pd1A-P2A-C28A-C29A	155.1(4)
C33A-C28A-C29A-C30A	59.1(7)
P2A-C28A-C29A-C30A	-168.9(5)
C28A-C29A-C30A-C31A	-56.6(7)
C29A-C30A-C31A-C32A	53.6(7)
C30A-C31A-C32A-C33A	-52.8(7)
C29A-C28A-C33A-C32A	-59.3(6)
P2A-C28A-C33A-C32A	164.4(4)
C31A-C32A-C33A-C28A	56.0(7)
C28A-P2A-C34A-C39A	63.9(5)
C22A-P2A-C34A-C39A	176.5(4)
Pd1A-P2A-C34A-C39A	-59.7(4)
C28A-P2A-C34A-C35A	-173.0(4)
C22A-P2A-C34A-C35A	-60.4(5)
Pd1A-P2A-C34A-C35A	63.5(5)

C39A-C34A-C35A-C36A	-59.0(7)
P2A-C34A-C35A-C36A	175.2(5)
C34A-C35A-C36A-C37A	57.1(9)
C35A-C36A-C37A-C38A	-53.6(10)
C36A-C37A-C38A-C39A	53.8(9)
C37A-C38A-C39A-C34A	-56.7(8)
C35A-C34A-C39A-C38A	58.7(7)
P2A-C34A-C39A-C38A	-175.5(4)
C52A-P3A-C40A-C45A	-61.9(4)
C46A-P3A-C40A-C45A	-176.7(4)
Pd2A-P3A-C40A-C45A	62.3(4)
C52A-P3A-C40A-C41A	175.3(4)
C46A-P3A-C40A-C41A	60.5(4)
Pd2A-P3A-C40A-C41A	-60.5(4)
C45A-C40A-C41A-C42A	57.6(6)
P3A-C40A-C41A-C42A	-178.3(4)
C40A-C41A-C42A-C43A	-57.2(7)
C41A-C42A-C43A-C44A	55.1(7)
C42A-C43A-C44A-C45A	-54.8(7)
C41A-C40A-C45A-C44A	-56.9(6)
P3A-C40A-C45A-C44A	179.7(4)
C43A-C44A-C45A-C40A	56.4(6)
C52A-P3A-C46A-C51A	-59.8(6)
C40A-P3A-C46A-C51A	49.7(5)
Pd2A-P3A-C46A-C51A	170.1(4)
C52A-P3A-C46A-C47A	72.6(4)
C40A-P3A-C46A-C47A	-178.0(4)
Pd2A-P3A-C46A-C47A	-57.5(4)
C51A-C46A-C47A-C48A	-57.7(6)
P3A-C46A-C47A-C48A	166.4(4)
C46A-C47A-C48A-C49A	56.4(7)
C47A-C48A-C49A-C50A	-56.4(7)
C48A-C49A-C50A-C51A	57.2(7)
C47A-C46A-C51A-C50A	58.5(7)
P3A-C46A-C51A-C50A	-167.5(5)
C49A-C50A-C51A-C46A	-58.3(7)
C40A-P3A-C52A-C53A	-174.1(4)
C46A-P3A-C52A-C53A	-66.0(5)

Pd2A-P3A-C52A-C53A	63.2(4)
C40A-P3A-C52A-C57A	-44.7(5)
C46A-P3A-C52A-C57A	63.3(5)
Pd2A-P3A-C52A-C57A	-167.4(4)
C57A-C52A-C53A-C54A	57.0(6)
P3A-C52A-C53A-C54A	-169.8(4)
C52A-C53A-C54A-C55A	-56.9(6)
C53A-C54A-C55A-C56A	55.6(7)
C54A-C55A-C56A-C57A	-55.1(7)
C55A-C56A-C57A-C52A	55.4(7)
C53A-C52A-C57A-C56A	-55.8(6)
P3A-C52A-C57A-C56A	173.3(4)
C64A-P4A-C58A-C59A	62.9(5)
C70A-P4A-C58A-C59A	172.0(4)
Pd3A-P4A-C58A-C59A	-65.0(4)
C64A-P4A-C58A-C63A	-67.7(6)
C70A-P4A-C58A-C63A	41.4(5)
Pd3A-P4A-C58A-C63A	164.5(4)
C63A-C58A-C59A-C60A	-59.5(7)
P4A-C58A-C59A-C60A	165.5(5)
C58A-C59A-C60A-C61A	56.7(9)
C59A-C60A-C61A-C62A	-54.1(10)
C60A-C61A-C62A-C63A	53.4(9)
C59A-C58A-C63A-C62A	58.0(7)
P4A-C58A-C63A-C62A	-171.0(5)
C61A-C62A-C63A-C58A	-55.1(8)
C58A-P4A-C64A-C69A	48.8(6)
C70A-P4A-C64A-C69A	-60.4(5)
Pd3A-P4A-C64A-C69A	177.5(4)
C58A-P4A-C64A-C65A	-81.8(5)
C70A-P4A-C64A-C65A	169.0(4)
Pd3A-P4A-C64A-C65A	46.9(4)
C69A-C64A-C65A-C66A	56.9(6)
P4A-C64A-C65A-C66A	-168.6(4)
C64A-C65A-C66A-C67A	-56.3(8)
C65A-C66A-C67A-C68A	55.5(8)
C66A-C67A-C68A-C69A	-55.6(7)
C65A-C64A-C69A-C68A	-56.9(7)

P4A-C64A-C69A-C68A	171.6(5)
C67A-C68A-C69A-C64A	56.4(7)
C64A-P4A-C70A-C71A	-61.0(4)
C58A-P4A-C70A-C71A	-176.3(4)
Pd3A-P4A-C70A-C71A	60.4(4)
C64A-P4A-C70A-C75A	177.2(4)
C58A-P4A-C70A-C75A	61.8(4)
Pd3A-P4A-C70A-C75A	-61.4(4)
C75A-C70A-C71A-C72A	-53.5(7)
P4A-C70A-C71A-C72A	-174.6(5)
C70A-C71A-C72A-C73A	55.8(8)
C71A-C72A-C73A-C74A	-57.4(8)
C72A-C73A-C74A-C75A	58.2(8)
C73A-C74A-C75A-C70A	-57.1(7)
C71A-C70A-C75A-C74A	53.5(7)
P4A-C70A-C75A-C74A	176.5(4)
C3B-Pd1B-Pd2B-C1B	156.3(3)
P1B-Pd1B-Pd2B-C1B	54.2(2)
P2B-Pd1B-Pd2B-C1B	-96.5(2)
Pd3B-Pd1B-Pd2B-C1B	166.6(2)
C3B-Pd1B-Pd2B-C2B	-11.3(3)
C1B-Pd1B-Pd2B-C2B	-167.6(3)
P1B-Pd1B-Pd2B-C2B	-113.4(2)
P2B-Pd1B-Pd2B-C2B	96.0(2)
Pd3B-Pd1B-Pd2B-C2B	-0.9(2)
C3B-Pd1B-Pd2B-P3B	165.67(19)
C1B-Pd1B-Pd2B-P3B	9.4(2)
P1B-Pd1B-Pd2B-P3B	63.55(10)
P2B-Pd1B-Pd2B-P3B	-87.09(9)
Pd3B-Pd1B-Pd2B-P3B	176.01(9)
C3B-Pd1B-Pd2B-Pd3B	-10.35(17)
C1B-Pd1B-Pd2B-Pd3B	-166.6(2)
P1B-Pd1B-Pd2B-Pd3B	-112.46(5)
P2B-Pd1B-Pd2B-Pd3B	96.90(3)
C1B-Pd2B-Pd3B-C3B	0.2(3)
C2B-Pd2B-Pd3B-C3B	-170.2(3)
P3B-Pd2B-Pd3B-C3B	-165.2(2)
Pd1B-Pd2B-Pd3B-C3B	10.91(19)

C1B-Pd2B-Pd3B-C2B	170.5(3)
P3B-Pd2B-Pd3B-C2B	5.0(3)
Pd1B-Pd2B-Pd3B-C2B	-178.9(2)
C1B-Pd2B-Pd3B-P4B	160.9(2)
C2B-Pd2B-Pd3B-P4B	-9.6(3)
P3B-Pd2B-Pd3B-P4B	-4.56(13)
Pd1B-Pd2B-Pd3B-P4B	171.53(8)
C1B-Pd2B-Pd3B-Pd1B	-10.67(18)
C2B-Pd2B-Pd3B-Pd1B	178.9(2)
P3B-Pd2B-Pd3B-Pd1B	-176.09(9)
C1B-Pd1B-Pd3B-C3B	-156.3(3)
P1B-Pd1B-Pd3B-C3B	-52.9(2)
P2B-Pd1B-Pd3B-C3B	95.7(2)
Pd2B-Pd1B-Pd3B-C3B	-166.4(2)
C3B-Pd1B-Pd3B-C2B	167.3(3)
C1B-Pd1B-Pd3B-C2B	11.0(3)
P1B-Pd1B-Pd3B-C2B	114.4(2)
P2B-Pd1B-Pd3B-C2B	-97.0(2)
Pd2B-Pd1B-Pd3B-C2B	0.9(2)
C3B-Pd1B-Pd3B-P4B	-5.4(2)
C1B-Pd1B-Pd3B-P4B	-161.67(18)
P1B-Pd1B-Pd3B-P4B	-58.30(10)
P2B-Pd1B-Pd3B-P4B	90.37(9)
Pd2B-Pd1B-Pd3B-P4B	-171.74(8)
C3B-Pd1B-Pd3B-Pd2B	166.4(2)
C1B-Pd1B-Pd3B-Pd2B	10.08(17)
P1B-Pd1B-Pd3B-Pd2B	113.45(5)
P2B-Pd1B-Pd3B-Pd2B	-97.89(4)
C3B-Pd1B-P1B-C16B	-71.7(3)
C1B-Pd1B-P1B-C16B	73.4(3)
P2B-Pd1B-P1B-C16B	-178.10(19)
Pd3B-Pd1B-P1B-C16B	-35.5(2)
Pd2B-Pd1B-P1B-C16B	36.8(2)
C3B-Pd1B-P1B-C4B	173.8(3)
C1B-Pd1B-P1B-C4B	-41.1(3)
P2B-Pd1B-P1B-C4B	67.3(2)
Pd3B-Pd1B-P1B-C4B	-150.1(2)
Pd2B-Pd1B-P1B-C4B	-77.8(2)

C3B-Pd1B-P1B-C10B	45.3(3)
C1B-Pd1B-P1B-C10B	-169.6(3)
P2B-Pd1B-P1B-C10B	-61.2(2)
Pd3B-Pd1B-P1B-C10B	81.4(2)
Pd2B-Pd1B-P1B-C10B	153.7(2)
C3B-Pd1B-P2B-C28B	-161.4(2)
C1B-Pd1B-P2B-C28B	41.7(2)
P1B-Pd1B-P2B-C28B	-61.0(2)
Pd3B-Pd1B-P2B-C28B	149.69(19)
Pd2B-Pd1B-P2B-C28B	90.48(19)
C3B-Pd1B-P2B-C34B	77.3(2)
C1B-Pd1B-P2B-C34B	-79.6(2)
P1B-Pd1B-P2B-C34B	177.70(18)
Pd3B-Pd1B-P2B-C34B	28.38(18)
Pd2B-Pd1B-P2B-C34B	-30.82(18)
C3B-Pd1B-P2B-C22B	-38.2(2)
C1B-Pd1B-P2B-C22B	164.8(2)
P1B-Pd1B-P2B-C22B	62.1(2)
Pd3B-Pd1B-P2B-C22B	-87.2(2)
Pd2B-Pd1B-P2B-C22B	-146.4(2)
C1B-Pd2B-P3B-C52B	-90.5(3)
C2B-Pd2B-P3B-C52B	79.3(3)
Pd3B-Pd2B-P3B-C52B	75.5(2)
Pd1B-Pd2B-P3B-C52B	-97.8(2)
C1B-Pd2B-P3B-C40B	27.5(3)
C2B-Pd2B-P3B-C40B	-162.6(3)
Pd3B-Pd2B-P3B-C40B	-166.5(2)
Pd1B-Pd2B-P3B-C40B	20.3(3)
C1B-Pd2B-P3B-C46B	152.7(3)
C2B-Pd2B-P3B-C46B	-37.4(3)
Pd3B-Pd2B-P3B-C46B	-41.3(3)
Pd1B-Pd2B-P3B-C46B	145.5(2)
C3B-Pd3B-P4B-C58B	85.5(3)
C2B-Pd3B-P4B-C58B	-83.4(3)
Pd2B-Pd3B-P4B-C58B	-76.0(2)
Pd1B-Pd3B-P4B-C58B	89.7(2)
C3B-Pd3B-P4B-C70B	-160.7(3)
C2B-Pd3B-P4B-C70B	30.3(3)

Pd2B-Pd3B-P4B-C70B	37.8(2)
Pd1B-Pd3B-P4B-C70B	-156.6(2)
C3B-Pd3B-P4B-C64B	-31.9(3)
C2B-Pd3B-P4B-C64B	159.1(3)
Pd2B-Pd3B-P4B-C64B	166.57(19)
Pd1B-Pd3B-P4B-C64B	-27.8(2)
C2B-Pd2B-C1B-O1B	-139.3(7)
P3B-Pd2B-C1B-O1B	13.9(8)
Pd3B-Pd2B-C1B-O1B	-158.5(7)
Pd1B-Pd2B-C1B-O1B	-170.9(9)
C2B-Pd2B-C1B-Pd1B	31.6(7)
P3B-Pd2B-C1B-Pd1B	-175.21(12)
Pd3B-Pd2B-C1B-Pd1B	12.4(2)
C3B-Pd1B-C1B-O1B	128.6(7)
P1B-Pd1B-C1B-O1B	32.5(7)
P2B-Pd1B-C1B-O1B	-92.9(7)
Pd3B-Pd1B-C1B-O1B	159.7(7)
Pd2B-Pd1B-C1B-O1B	171.3(8)
C3B-Pd1B-C1B-Pd2B	-42.7(4)
P1B-Pd1B-C1B-Pd2B	-138.76(15)
P2B-Pd1B-C1B-Pd2B	95.75(16)
Pd3B-Pd1B-C1B-Pd2B	-11.58(19)
C3B-Pd3B-C2B-O2B	-151.6(7)
P4B-Pd3B-C2B-O2B	-2.0(9)
Pd2B-Pd3B-C2B-O2B	-177.0(10)
Pd1B-Pd3B-C2B-O2B	-178.1(8)
C3B-Pd3B-C2B-Pd2B	25.4(8)
P4B-Pd3B-C2B-Pd2B	175.07(13)
Pd1B-Pd3B-C2B-Pd2B	-1.1(2)
C1B-Pd2B-C2B-O2B	153.1(7)
P3B-Pd2B-C2B-O2B	-0.2(9)
Pd3B-Pd2B-C2B-O2B	177.1(10)
Pd1B-Pd2B-C2B-O2B	178.2(8)
C1B-Pd2B-C2B-Pd3B	-24.0(7)
P3B-Pd2B-C2B-Pd3B	-177.37(13)
Pd1B-Pd2B-C2B-Pd3B	1.1(2)
C2B-Pd3B-C3B-O3B	140.7(7)
P4B-Pd3B-C3B-O3B	-8.9(8)

Pd2B-Pd3B-C3B-O3B	161.2(7)
Pd1B-Pd3B-C3B-O3B	173.9(9)
C2B-Pd3B-C3B-Pd1B	-33.2(8)
P4B-Pd3B-C3B-Pd1B	177.16(13)
Pd2B-Pd3B-C3B-Pd1B	-12.7(2)
C1B-Pd1B-C3B-O3B	-131.3(7)
P1B-Pd1B-C3B-O3B	-34.8(7)
P2B-Pd1B-C3B-O3B	90.1(7)
Pd3B-Pd1B-C3B-O3B	-174.1(9)
Pd2B-Pd1B-C3B-O3B	-162.2(7)
C1B-Pd1B-C3B-Pd3B	42.8(4)
P1B-Pd1B-C3B-Pd3B	139.25(16)
P2B-Pd1B-C3B-Pd3B	-95.86(16)
Pd2B-Pd1B-C3B-Pd3B	11.8(2)
C16B-P1B-C4B-C5B	-176.9(4)
C10B-P1B-C4B-C5B	75.7(5)
Pd1B-P1B-C4B-C5B	-55.8(5)
C16B-P1B-C4B-C9B	53.8(6)
C10B-P1B-C4B-C9B	-53.5(6)
Pd1B-P1B-C4B-C9B	174.9(5)
C9B-C4B-C5B-C6B	-59.1(7)
P1B-C4B-C5B-C6B	166.9(5)
C4B-C5B-C6B-C7B	58.0(8)
C5B-C6B-C7B-C8B	-54.9(10)
C6B-C7B-C8B-C9B	55.2(10)
C7B-C8B-C9B-C4B	-56.7(10)
C5B-C4B-C9B-C8B	57.3(9)
P1B-C4B-C9B-C8B	-171.3(6)
C16B-P1B-C10B-C11B	-164.6(4)
C4B-P1B-C10B-C11B	-58.9(5)
Pd1B-P1B-C10B-C11B	73.1(4)
C16B-P1B-C10B-C15B	-34.1(5)
C4B-P1B-C10B-C15B	71.6(6)
Pd1B-P1B-C10B-C15B	-156.3(4)
C15B-C10B-C11B-C12B	59.2(6)
P1B-C10B-C11B-C12B	-164.7(4)
C10B-C11B-C12B-C13B	-56.6(7)
C11B-C12B-C13B-C14B	53.1(8)

C12B-C13B-C14B-C15B	-55.0(8)
C13B-C14B-C15B-C10B	58.2(8)
C11B-C10B-C15B-C14B	-58.6(7)
P1B-C10B-C15B-C14B	169.1(5)
C4B-P1B-C16B-C21B	62.6(4)
C10B-P1B-C16B-C21B	174.7(4)
Pd1B-P1B-C16B-C21B	-61.2(4)
C4B-P1B-C16B-C17B	-174.1(4)
C10B-P1B-C16B-C17B	-62.0(4)
Pd1B-P1B-C16B-C17B	62.1(4)
C21B-C16B-C17B-C18B	-57.8(6)
P1B-C16B-C17B-C18B	175.9(4)
C16B-C17B-C18B-C19B	58.0(7)
C17B-C18B-C19B-C20B	-54.6(8)
C18B-C19B-C20B-C21B	52.7(9)
C19B-C20B-C21B-C16B	-55.1(8)
C17B-C16B-C21B-C20B	56.3(6)
P1B-C16B-C21B-C20B	-178.3(4)
C28B-P2B-C22B-C23B	31.1(5)
C34B-P2B-C22B-C23B	134.3(5)
Pd1B-P2B-C22B-C23B	-100.3(5)
C28B-P2B-C22B-C27B	157.0(4)
C34B-P2B-C22B-C27B	-99.8(4)
Pd1B-P2B-C22B-C27B	25.6(4)
C27B-C22B-C23B-C24B	59.4(7)
P2B-C22B-C23B-C24B	-173.0(4)
C22B-C23B-C24B-C25B	-55.5(7)
C23B-C24B-C25B-C26B	51.5(7)
C24B-C25B-C26B-C27B	-53.0(7)
C25B-C26B-C27B-C22B	57.5(6)
C23B-C22B-C27B-C26B	-60.3(6)
P2B-C22B-C27B-C26B	168.9(4)
C34B-P2B-C28B-C29B	92.0(4)
C22B-P2B-C28B-C29B	-168.6(4)
Pd1B-P2B-C28B-C29B	-36.5(4)
C34B-P2B-C28B-C33B	-37.8(5)
C22B-P2B-C28B-C33B	61.5(4)
Pd1B-P2B-C28B-C33B	-166.4(3)

C33B-C28B-C29B-C30B	-56.5(6)
P2B-C28B-C29B-C30B	170.6(4)
C28B-C29B-C30B-C31B	55.3(7)
C29B-C30B-C31B-C32B	-54.1(7)
C30B-C31B-C32B-C33B	55.0(7)
C31B-C32B-C33B-C28B	-56.8(6)
C29B-C28B-C33B-C32B	57.3(6)
P2B-C28B-C33B-C32B	-170.2(4)
C28B-P2B-C34B-C39B	-66.6(5)
C22B-P2B-C34B-C39B	-169.0(4)
Pd1B-P2B-C34B-C39B	63.3(5)
C28B-P2B-C34B-C35B	168.6(4)
C22B-P2B-C34B-C35B	66.1(4)
Pd1B-P2B-C34B-C35B	-61.6(4)
C39B-C34B-C35B-C36B	56.5(6)
P2B-C34B-C35B-C36B	-176.4(4)
C34B-C35B-C36B-C37B	-56.8(7)
C35B-C36B-C37B-C38B	55.4(7)
C36B-C37B-C38B-C39B	-56.3(7)
C37B-C38B-C39B-C34B	57.7(7)
C35B-C34B-C39B-C38B	-57.0(7)
P2B-C34B-C39B-C38B	176.8(4)
C52B-P3B-C40B-C45B	-176.1(4)
C46B-P3B-C40B-C45B	-65.4(5)
Pd2B-P3B-C40B-C45B	60.8(5)
C52B-P3B-C40B-C41B	-45.5(6)
C46B-P3B-C40B-C41B	65.2(6)
Pd2B-P3B-C40B-C41B	-168.5(4)
C45B-C40B-C41B-C42B	-57.2(8)
P3B-C40B-C41B-C42B	171.0(5)
C40B-C41B-C42B-C43B	56.8(8)
C41B-C42B-C43B-C44B	-54.8(9)
C42B-C43B-C44B-C45B	53.4(10)
C43B-C44B-C45B-C40B	-55.8(9)
C41B-C40B-C45B-C44B	58.2(8)
P3B-C40B-C45B-C44B	-166.1(5)
C52B-P3B-C46B-C51B	-169.5(4)
C40B-P3B-C46B-C51B	79.9(5)

Pd2B-P3B-C46B-C51B	-47.6(5)
C52B-P3B-C46B-C47B	60.3(6)
C40B-P3B-C46B-C47B	-50.2(6)
Pd2B-P3B-C46B-C47B	-177.7(5)
C51B-C46B-C47B-C48B	56.6(8)
P3B-C46B-C47B-C48B	-172.7(5)
C46B-C47B-C48B-C49B	-57.0(8)
C47B-C48B-C49B-C50B	56.6(8)
C48B-C49B-C50B-C51B	-55.6(8)
C47B-C46B-C51B-C50B	-56.9(7)
P3B-C46B-C51B-C50B	169.4(5)
C49B-C50B-C51B-C46B	56.7(8)
C40B-P3B-C52B-C57B	-63.8(4)
C46B-P3B-C52B-C57B	-178.7(4)
Pd2B-P3B-C52B-C57B	60.1(4)
C40B-P3B-C52B-C53B	173.7(4)
C46B-P3B-C52B-C53B	58.9(4)
Pd2B-P3B-C52B-C53B	-62.4(4)
C57B-C52B-C53B-C54B	53.8(7)
P3B-C52B-C53B-C54B	175.8(5)
C52B-C53B-C54B-C55B	-56.8(7)
C53B-C54B-C55B-C56B	57.5(7)
C54B-C55B-C56B-C57B	-58.0(7)
C55B-C56B-C57B-C52B	56.0(7)
C53B-C52B-C57B-C56B	-52.2(7)
P3B-C52B-C57B-C56B	-175.0(4)
C70B-P4B-C58B-C63B	-58.5(4)
C64B-P4B-C58B-C63B	-173.0(4)
Pd3B-P4B-C58B-C63B	62.2(4)
C70B-P4B-C58B-C59B	176.9(4)
C64B-P4B-C58B-C59B	62.3(4)
Pd3B-P4B-C58B-C59B	-62.4(4)
C63B-C58B-C59B-C60B	55.3(6)
P4B-C58B-C59B-C60B	-178.9(4)
C58B-C59B-C60B-C61B	-54.4(6)
C59B-C60B-C61B-C62B	53.3(7)
C60B-C61B-C62B-C63B	-53.5(7)
C61B-C62B-C63B-C58B	56.1(7)

C59B-C58B-C63B-C62B	-56.4(7)
P4B-C58B-C63B-C62B	177.7(4)
C58B-P4B-C64B-C65B	172.0(4)
C70B-P4B-C64B-C65B	64.5(5)
Pd3B-P4B-C64B-C65B	-65.4(4)
C58B-P4B-C64B-C69B	42.8(5)
C70B-P4B-C64B-C69B	-64.7(5)
Pd3B-P4B-C64B-C69B	165.4(4)
C69B-C64B-C65B-C66B	-57.3(6)
P4B-C64B-C65B-C66B	169.6(4)
C64B-C65B-C66B-C67B	57.1(7)
C65B-C66B-C67B-C68B	-54.4(7)
C66B-C67B-C68B-C69B	53.8(7)
C67B-C68B-C69B-C64B	-54.7(6)
C65B-C64B-C69B-C68B	56.0(6)
P4B-C64B-C69B-C68B	-173.7(4)
C58B-P4B-C70B-C71B	177.1(4)
C64B-P4B-C70B-C71B	-74.4(5)
Pd3B-P4B-C70B-C71B	56.8(4)
C58B-P4B-C70B-C75B	-51.6(5)
C64B-P4B-C70B-C75B	57.0(6)
Pd3B-P4B-C70B-C75B	-171.8(4)
C75B-C70B-C71B-C72B	56.8(7)
P4B-C70B-C71B-C72B	-168.7(4)
C70B-C71B-C72B-C73B	-55.6(7)
C71B-C72B-C73B-C74B	56.0(7)
C72B-C73B-C74B-C75B	-57.4(7)
C73B-C74B-C75B-C70B	58.4(7)
C71B-C70B-C75B-C74B	-58.6(7)
P4B-C70B-C75B-C74B	168.6(5)
C3C-Pd1C-Pd2C-C2C	-4.6(3)
C1C-Pd1C-Pd2C-C2C	-171.5(3)
P2C-Pd1C-Pd2C-C2C	-109.6(2)
P1C-Pd1C-Pd2C-C2C	94.6(2)
Pd3C-Pd1C-Pd2C-C2C	-6.4(2)
C3C-Pd1C-Pd2C-C1C	166.9(3)
P2C-Pd1C-Pd2C-C1C	61.9(2)
P1C-Pd1C-Pd2C-C1C	-93.9(2)

Pd3C-Pd1C-Pd2C-C1C	165.1(2)
C3C-Pd1C-Pd2C-P3C	177.8(2)
C1C-Pd1C-Pd2C-P3C	11.0(2)
P2C-Pd1C-Pd2C-P3C	72.87(9)
P1C-Pd1C-Pd2C-P3C	-82.96(9)
Pd3C-Pd1C-Pd2C-P3C	176.09(8)
C3C-Pd1C-Pd2C-Pd3C	1.74(18)
C1C-Pd1C-Pd2C-Pd3C	-165.1(2)
P2C-Pd1C-Pd2C-Pd3C	-103.22(4)
P1C-Pd1C-Pd2C-Pd3C	100.95(4)
C1C-Pd2C-Pd3C-C2C	176.0(3)
P3C-Pd2C-Pd3C-C2C	11.9(2)
Pd1C-Pd2C-Pd3C-C2C	-172.2(2)
C2C-Pd2C-Pd3C-C3C	170.4(3)
C1C-Pd2C-Pd3C-C3C	-13.6(3)
P3C-Pd2C-Pd3C-C3C	-177.7(2)
Pd1C-Pd2C-Pd3C-C3C	-1.78(19)
C2C-Pd2C-Pd3C-P4C	-20.1(2)
C1C-Pd2C-Pd3C-P4C	155.84(18)
P3C-Pd2C-Pd3C-P4C	-8.22(12)
Pd1C-Pd2C-Pd3C-P4C	167.69(8)
C2C-Pd2C-Pd3C-Pd1C	172.2(2)
C1C-Pd2C-Pd3C-Pd1C	-11.85(17)
P3C-Pd2C-Pd3C-Pd1C	-175.91(9)
C3C-Pd1C-Pd3C-C2C	-171.4(3)
C1C-Pd1C-Pd3C-C2C	17.7(3)
P2C-Pd1C-Pd3C-C2C	119.0(2)
P1C-Pd1C-Pd3C-C2C	-94.0(2)
Pd2C-Pd1C-Pd3C-C2C	6.3(2)
C1C-Pd1C-Pd3C-C3C	-170.8(3)
P2C-Pd1C-Pd3C-C3C	-69.6(2)
P1C-Pd1C-Pd3C-C3C	77.4(2)
Pd2C-Pd1C-Pd3C-C3C	177.8(2)
C3C-Pd1C-Pd3C-P4C	18.0(3)
C1C-Pd1C-Pd3C-P4C	-152.8(2)
P2C-Pd1C-Pd3C-P4C	-51.57(10)
P1C-Pd1C-Pd3C-P4C	95.44(10)
Pd2C-Pd1C-Pd3C-P4C	-164.23(10)

C3C-Pd1C-Pd3C-Pd2C	-177.8(2)
C1C-Pd1C-Pd3C-Pd2C	11.38(17)
P2C-Pd1C-Pd3C-Pd2C	112.66(4)
P1C-Pd1C-Pd3C-Pd2C	-100.33(4)
C3C-Pd1C-P1C-C4C	79.8(3)
C1C-Pd1C-P1C-C4C	-79.1(3)
P2C-Pd1C-P1C-C4C	176.16(19)
Pd3C-Pd1C-P1C-C4C	32.64(19)
Pd2C-Pd1C-P1C-C4C	-28.92(19)
C3C-Pd1C-P1C-C10C	-35.6(3)
C1C-Pd1C-P1C-C10C	165.6(3)
P2C-Pd1C-P1C-C10C	60.8(2)
Pd3C-Pd1C-P1C-C10C	-82.7(2)
Pd2C-Pd1C-P1C-C10C	-144.3(2)
C3C-Pd1C-P1C-C16C	-159.6(3)
C1C-Pd1C-P1C-C16C	41.5(3)
P2C-Pd1C-P1C-C16C	-63.2(3)
Pd3C-Pd1C-P1C-C16C	153.2(3)
Pd2C-Pd1C-P1C-C16C	91.7(3)
C3C-Pd1C-P2C-C22C	27.1(3)
C1C-Pd1C-P2C-C22C	-179.8(2)
P1C-Pd1C-P2C-C22C	-69.2(2)
Pd3C-Pd1C-P2C-C22C	71.9(2)
Pd2C-Pd1C-P2C-C22C	139.12(19)
C3C-Pd1C-P2C-C34C	-88.9(3)
C1C-Pd1C-P2C-C34C	64.2(3)
P1C-Pd1C-P2C-C34C	174.8(2)
Pd3C-Pd1C-P2C-C34C	-44.1(2)
Pd2C-Pd1C-P2C-C34C	23.1(2)
C3C-Pd1C-P2C-C28C	154.9(3)
C1C-Pd1C-P2C-C28C	-52.0(2)
P1C-Pd1C-P2C-C28C	58.6(2)
Pd3C-Pd1C-P2C-C28C	-160.4(2)
Pd2C-Pd1C-P2C-C28C	-93.1(2)
C2C-Pd2C-P3C-C52C	-166.7(3)
C1C-Pd2C-P3C-C52C	19.3(3)
Pd3C-Pd2C-P3C-C52C	-176.0(2)
Pd1C-Pd2C-P3C-C52C	10.9(2)

C2C-Pd2C-P3C-C40C	76.6(3)
C1C-Pd2C-P3C-C40C	-97.4(3)
Pd3C-Pd2C-P3C-C40C	67.3(3)
Pd1C-Pd2C-P3C-C40C	-105.8(2)
C2C-Pd2C-P3C-C46C	-47.6(3)
C1C-Pd2C-P3C-C46C	138.4(3)
Pd3C-Pd2C-P3C-C46C	-56.9(3)
Pd1C-Pd2C-P3C-C46C	130.0(2)
C2C-Pd3C-P4C-C58C	166.6(3)
C3C-Pd3C-P4C-C58C	-8.4(3)
Pd2C-Pd3C-P4C-C58C	-178.2(2)
Pd1C-Pd3C-P4C-C58C	-22.4(3)
C2C-Pd3C-P4C-C64C	42.7(3)
C3C-Pd3C-P4C-C64C	-132.3(3)
Pd2C-Pd3C-P4C-C64C	57.9(2)
Pd1C-Pd3C-P4C-C64C	-146.3(2)
C2C-Pd3C-P4C-C70C	-75.2(3)
C3C-Pd3C-P4C-C70C	109.8(3)
Pd2C-Pd3C-P4C-C70C	-59.9(2)
Pd1C-Pd3C-P4C-C70C	95.9(2)
C2C-Pd2C-C1C-O1C	-148.7(7)
P3C-Pd2C-C1C-O1C	14.9(8)
Pd3C-Pd2C-C1C-O1C	-157.1(7)
Pd1C-Pd2C-C1C-O1C	-170.8(8)
C2C-Pd2C-C1C-Pd1C	22.1(7)
P3C-Pd2C-C1C-Pd1C	-174.26(12)
Pd3C-Pd2C-C1C-Pd1C	13.69(19)
C3C-Pd1C-C1C-O1C	143.4(6)
P2C-Pd1C-C1C-O1C	39.9(7)
P1C-Pd1C-C1C-O1C	-87.5(7)
Pd3C-Pd1C-C1C-O1C	158.2(6)
Pd2C-Pd1C-C1C-O1C	171.3(8)
C3C-Pd1C-C1C-Pd2C	-27.9(6)
P2C-Pd1C-C1C-Pd2C	-131.35(14)
P1C-Pd1C-C1C-Pd2C	101.28(14)
Pd3C-Pd1C-C1C-Pd2C	-13.02(18)
C1C-Pd2C-C2C-O2C	173.4(7)
P3C-Pd2C-C2C-O2C	9.9(9)

Pd3C-Pd2C-C2C-O2C	-176.1(10)
Pd1C-Pd2C-C2C-O2C	-168.8(8)
C1C-Pd2C-C2C-Pd3C	-10.4(7)
P3C-Pd2C-C2C-Pd3C	-174.02(12)
Pd1C-Pd2C-C2C-Pd3C	7.3(2)
C3C-Pd3C-C2C-O2C	151.6(8)
P4C-Pd3C-C2C-O2C	-15.5(9)
Pd2C-Pd3C-C2C-O2C	176.1(10)
Pd1C-Pd3C-C2C-O2C	168.8(8)
C3C-Pd3C-C2C-Pd2C	-24.5(8)
P4C-Pd3C-C2C-Pd2C	168.40(14)
Pd1C-Pd3C-C2C-Pd2C	-7.3(2)
C2C-Pd3C-C3C-O3C	-153.5(7)
P4C-Pd3C-C3C-O3C	13.3(9)
Pd2C-Pd3C-C3C-O3C	-173.0(8)
Pd1C-Pd3C-C3C-O3C	-175.1(10)
C2C-Pd3C-C3C-Pd1C	21.6(8)
P4C-Pd3C-C3C-Pd1C	-171.63(12)
Pd2C-Pd3C-C3C-Pd1C	2.1(2)
C1C-Pd1C-C3C-O3C	-165.1(6)
P2C-Pd1C-C3C-O3C	-61.7(8)
P1C-Pd1C-C3C-O3C	63.5(8)
Pd3C-Pd1C-C3C-O3C	175.6(9)
Pd2C-Pd1C-C3C-O3C	173.6(7)
C1C-Pd1C-C3C-Pd3C	19.3(6)
P2C-Pd1C-C3C-Pd3C	122.73(15)
P1C-Pd1C-C3C-Pd3C	-112.06(16)
Pd2C-Pd1C-C3C-Pd3C	-2.0(2)
C10C-P1C-C4C-C5C	-169.6(4)
C16C-P1C-C4C-C5C	-62.5(4)
Pd1C-P1C-C4C-C5C	66.3(4)
C10C-P1C-C4C-C9C	64.9(4)
C16C-P1C-C4C-C9C	172.0(4)
Pd1C-P1C-C4C-C9C	-59.2(4)
C9C-C4C-C5C-C6C	-58.5(6)
P1C-C4C-C5C-C6C	174.8(4)
C4C-C5C-C6C-C7C	57.7(7)
C5C-C6C-C7C-C8C	-55.4(7)

C6C-C7C-C8C-C9C	55.4(7)
C7C-C8C-C9C-C4C	-57.9(7)
C5C-C4C-C9C-C8C	58.5(6)
P1C-C4C-C9C-C8C	-172.7(4)
C4C-P1C-C10C-C15C	152.6(4)
C16C-P1C-C10C-C15C	45.2(5)
Pd1C-P1C-C10C-C15C	-86.3(4)
C4C-P1C-C10C-C11C	23.7(5)
C16C-P1C-C10C-C11C	-83.7(5)
Pd1C-P1C-C10C-C11C	144.8(4)
C15C-C10C-C11C-C12C	59.5(6)
P1C-C10C-C11C-C12C	-169.0(4)
C10C-C11C-C12C-C13C	-57.7(7)
C11C-C12C-C13C-C14C	55.1(7)
C12C-C13C-C14C-C15C	-54.2(7)
C11C-C10C-C15C-C14C	-60.3(6)
P1C-C10C-C15C-C14C	165.1(4)
C13C-C14C-C15C-C10C	58.2(6)
C4C-P1C-C16C-C17C	-35.1(6)
C10C-P1C-C16C-C17C	70.3(6)
Pd1C-P1C-C16C-C17C	-159.7(4)
C4C-P1C-C16C-C21C	94.5(5)
C10C-P1C-C16C-C21C	-160.1(5)
Pd1C-P1C-C16C-C21C	-30.1(6)
C21C-C16C-C17C-C18C	53.6(8)
P1C-C16C-C17C-C18C	-176.4(5)
C16C-C17C-C18C-C19C	-54.8(9)
C17C-C18C-C19C-C20C	55.7(9)
C18C-C19C-C20C-C21C	-57.0(8)
C19C-C20C-C21C-C16C	56.4(8)
C17C-C16C-C21C-C20C	-54.3(8)
P1C-C16C-C21C-C20C	173.9(5)
C34C-P2C-C22C-C23C	-45.3(5)
C28C-P2C-C22C-C23C	62.3(5)
Pd1C-P2C-C22C-C23C	-169.2(4)
C34C-P2C-C22C-C27C	-177.7(5)
C28C-P2C-C22C-C27C	-70.1(5)
Pd1C-P2C-C22C-C27C	58.5(5)

C27C-C22C-C23C-C24C	-54.6(6)
P2C-C22C-C23C-C24C	173.3(4)
C22C-C23C-C24C-C25C	55.2(7)
C23C-C24C-C25C-C26C	-56.5(8)
C24C-C25C-C26C-C27C	57.3(7)
C25C-C26C-C27C-C22C	-56.9(7)
C23C-C22C-C27C-C26C	55.9(7)
P2C-C22C-C27C-C26C	-168.2(5)
C22C-P2C-C28C-C33C	70.7(5)
C34C-P2C-C28C-C33C	176.7(5)
Pd1C-P2C-C28C-C33C	-60.1(5)
C22C-P2C-C28C-C29C	-58.9(5)
C34C-P2C-C28C-C29C	47.1(5)
Pd1C-P2C-C28C-C29C	170.4(4)
C33C-C28C-C29C-C30C	59.2(7)
P2C-C28C-C29C-C30C	-170.1(5)
C28C-C29C-C30C-C31C	-56.1(8)
C29C-C30C-C31C-C32C	53.0(8)
C30C-C31C-C32C-C33C	-52.8(8)
C31C-C32C-C33C-C28C	57.0(8)
C29C-C28C-C33C-C32C	-60.6(7)
P2C-C28C-C33C-C32C	164.5(5)
C22C-P2C-C34C-C39C	-61.1(5)
C28C-P2C-C34C-C39C	-174.8(5)
Pd1C-P2C-C34C-C39C	63.7(5)
C22C-P2C-C34C-C35C	176.3(5)
C28C-P2C-C34C-C35C	62.6(6)
Pd1C-P2C-C34C-C35C	-58.9(5)
C39C-C34C-C35C-C36C	59.3(8)
P2C-C34C-C35C-C36C	-177.3(6)
C34C-C35C-C36C-C37C	-58.8(9)
C35C-C36C-C37C-C38C	57.0(10)
C36C-C37C-C38C-C39C	-55.6(11)
C35C-C34C-C39C-C38C	-57.9(8)
P2C-C34C-C39C-C38C	177.6(5)
C37C-C38C-C39C-C34C	56.1(10)
C52C-P3C-C40C-C45C	-169.4(5)
C46C-P3C-C40C-C45C	83.6(5)

Pd2C-P3C-C40C-C45C	-47.4(5)
C52C-P3C-C40C-C41C	-45.6(5)
C46C-P3C-C40C-C41C	-152.7(4)
Pd2C-P3C-C40C-C41C	76.3(4)
C45C-C40C-C41C-C42C	-54.0(7)
P3C-C40C-C41C-C42C	-177.9(4)
C40C-C41C-C42C-C43C	52.5(8)
C41C-C42C-C43C-C44C	-51.6(8)
C42C-C43C-C44C-C45C	53.3(7)
C43C-C44C-C45C-C40C	-57.6(7)
C41C-C40C-C45C-C44C	56.6(7)
P3C-C40C-C45C-C44C	-177.7(5)
C52C-P3C-C46C-C47C	90.7(5)
C40C-P3C-C46C-C47C	-161.5(4)
Pd2C-P3C-C46C-C47C	-33.5(5)
C52C-P3C-C46C-C51C	-144.7(5)
C40C-P3C-C46C-C51C	-37.0(6)
Pd2C-P3C-C46C-C51C	91.1(5)
C51C-C46C-C47C-C48C	55.6(8)
P3C-C46C-C47C-C48C	-175.8(5)
C46C-C47C-C48C-C49C	-56.7(8)
C47C-C48C-C49C-C50C	55.8(8)
C48C-C49C-C50C-C51C	-56.4(8)
C49C-C50C-C51C-C46C	56.4(8)
C47C-C46C-C51C-C50C	-54.6(8)
P3C-C46C-C51C-C50C	-179.5(5)
C40C-P3C-C52C-C53C	179.5(5)
C46C-P3C-C52C-C53C	-71.2(5)
Pd2C-P3C-C52C-C53C	56.9(5)
C40C-P3C-C52C-C57C	-54.2(5)
C46C-P3C-C52C-C57C	55.1(5)
Pd2C-P3C-C52C-C57C	-176.8(4)
C57C-C52C-C53C-C54C	61.0(7)
P3C-C52C-C53C-C54C	-168.4(4)
C52C-C53C-C54C-C55C	-58.8(7)
C53C-C54C-C55C-C56C	54.6(8)
C54C-C55C-C56C-C57C	-54.0(8)
C55C-C56C-C57C-C52C	55.8(7)

C53C-C52C-C57C-C56C	-58.9(7)
P3C-C52C-C57C-C56C	173.9(4)
C64C-P4C-C58C-C63C	-166.0(4)
C70C-P4C-C58C-C63C	-53.1(5)
Pd3C-P4C-C58C-C63C	66.1(4)
C64C-P4C-C58C-C59C	70.3(5)
C70C-P4C-C58C-C59C	-176.8(5)
Pd3C-P4C-C58C-C59C	-57.6(5)
C63C-C58C-C59C-C60C	50.5(7)
P4C-C58C-C59C-C60C	173.7(5)
C58C-C59C-C60C-C61C	-53.3(8)
C59C-C60C-C61C-C62C	56.9(8)
C60C-C61C-C62C-C63C	-57.5(8)
C59C-C58C-C63C-C62C	-51.8(6)
P4C-C58C-C63C-C62C	-174.4(4)
C61C-C62C-C63C-C58C	56.2(7)
C58C-P4C-C64C-C69C	32.3(5)
C70C-P4C-C64C-C69C	-78.5(5)
Pd3C-P4C-C64C-C69C	164.2(4)
C58C-P4C-C64C-C65C	-93.8(4)
C70C-P4C-C64C-C65C	155.4(4)
Pd3C-P4C-C64C-C65C	38.1(5)
C69C-C64C-C65C-C66C	56.8(7)
P4C-C64C-C65C-C66C	-173.0(4)
C64C-C65C-C66C-C67C	-58.9(7)
C65C-C66C-C67C-C68C	58.3(8)
C66C-C67C-C68C-C69C	-57.6(8)
C67C-C68C-C69C-C64C	57.7(8)
C65C-C64C-C69C-C68C	-56.2(7)
P4C-C64C-C69C-C68C	177.3(5)
C58C-P4C-C70C-C75C	-55.2(6)
C64C-P4C-C70C-C75C	55.6(6)
Pd3C-P4C-C70C-C75C	177.0(5)
C58C-P4C-C70C-C71C	176.4(5)
C64C-P4C-C70C-C71C	-72.9(6)
Pd3C-P4C-C70C-C71C	48.6(6)
C75C-C70C-C71C-C72C	53.9(9)
P4C-C70C-C71C-C72C	-174.5(6)

C70C-C71C-C72C-C73C	-52.8(9)
C71C-C72C-C73C-C74C	55.0(10)
C72C-C73C-C74C-C75C	-56.5(10)
C71C-C70C-C75C-C74C	-56.4(9)
P4C-C70C-C75C-C74C	174.6(6)
C73C-C74C-C75C-C70C	57.5(10)
C6S-C1S-C2S-C3S	0.0(10)
C1S-C2S-C3S-C4S	0.0(10)
C2S-C3S-C4S-C5S	-0.1(11)
C3S-C4S-C5S-C6S	0.1(11)
C4S-C5S-C6S-C1S	-0.1(11)
C2S-C1S-C6S-C5S	0.1(11)
C6T-C1T-C2T-C3T	0.8(13)
C1T-C2T-C3T-C4T	1.7(14)
C2T-C3T-C4T-C5T	-3.1(14)
C3T-C4T-C5T-C6T	2.1(14)
C2T-C1T-C6T-C5T	-1.9(15)
C4T-C5T-C6T-C1T	0.5(15)
C6U-C1U-C2U-C3U	-2(3)
C1U-C2U-C3U-C4U	1(2)
C2U-C3U-C4U-C5U	5(3)
C3U-C4U-C5U-C6U	-11(4)
C2U-C1U-C6U-C5U	-3(3)
C4U-C5U-C6U-C1U	10(4)
C6U'-C1U'-C2U'-C3U'	0(3)
C1U'-C2U'-C3U'-C4U'	-4(3)
C2U'-C3U'-C4U'-C5U'	-3(4)
C3U'-C4U'-C5U'-C6U'	13(5)
C2U'-C1U'-C6U'-C5U'	11(3)
C4U'-C5U'-C6U'-C1U'	-18(5)

6.2.8. ^{1}H NMR and ^{13}C NMR spectra

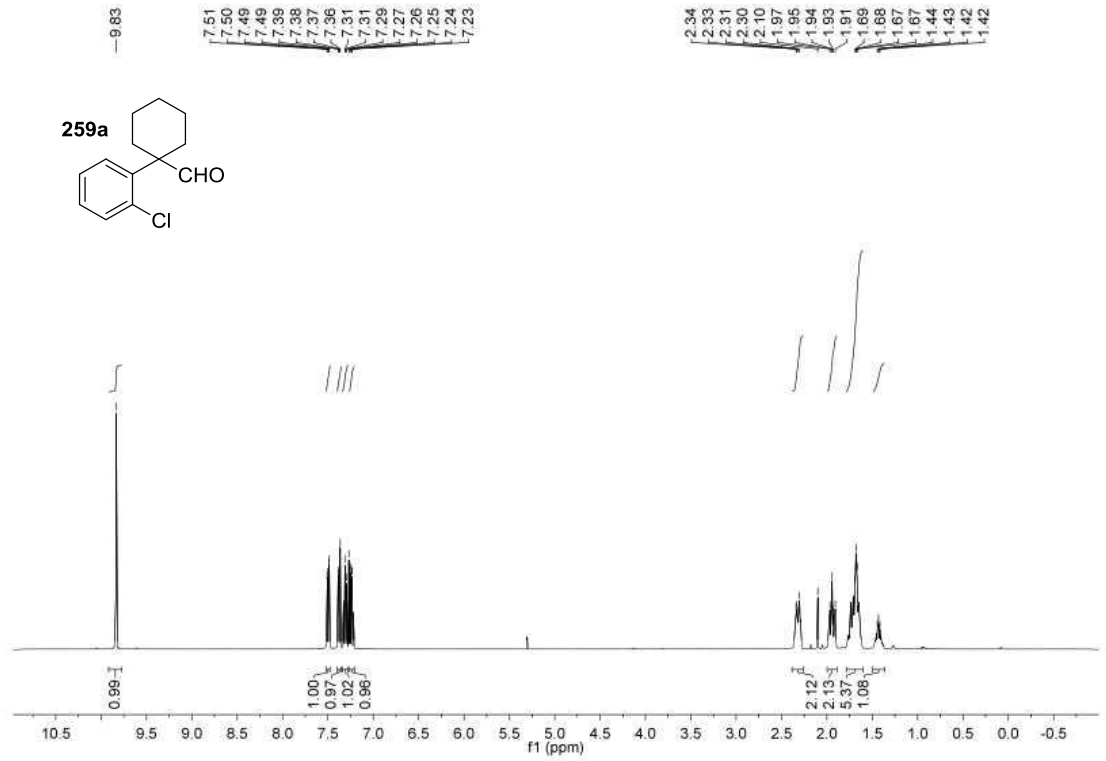

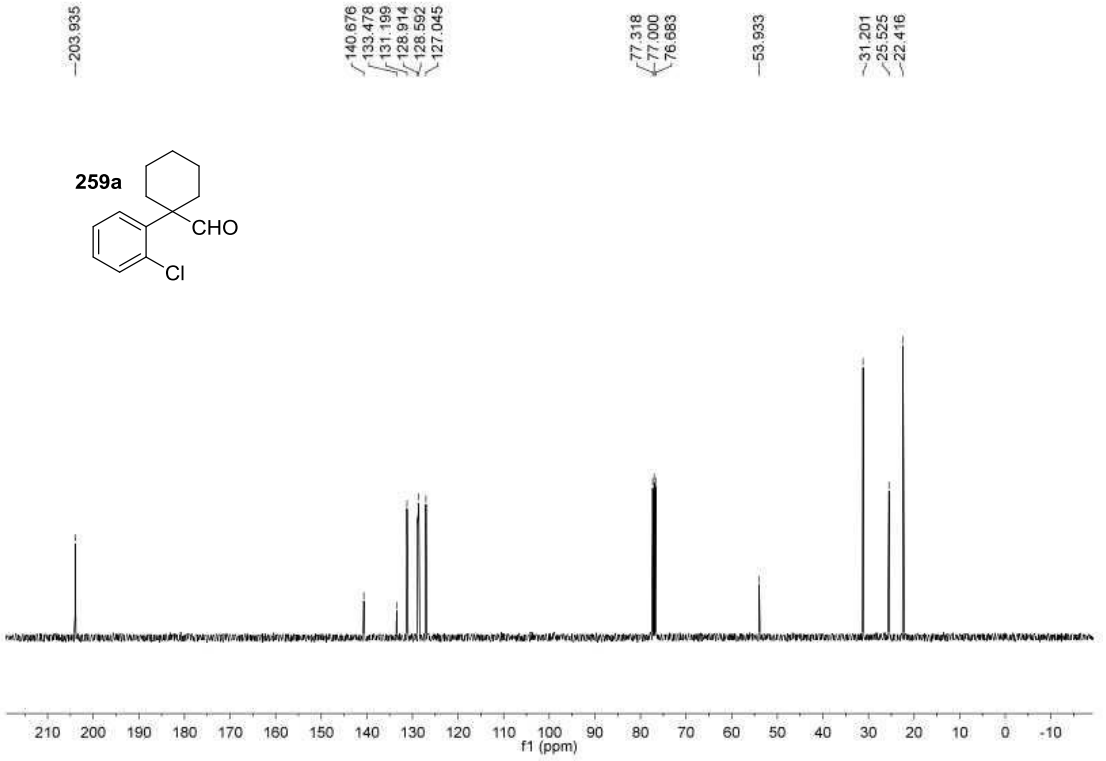

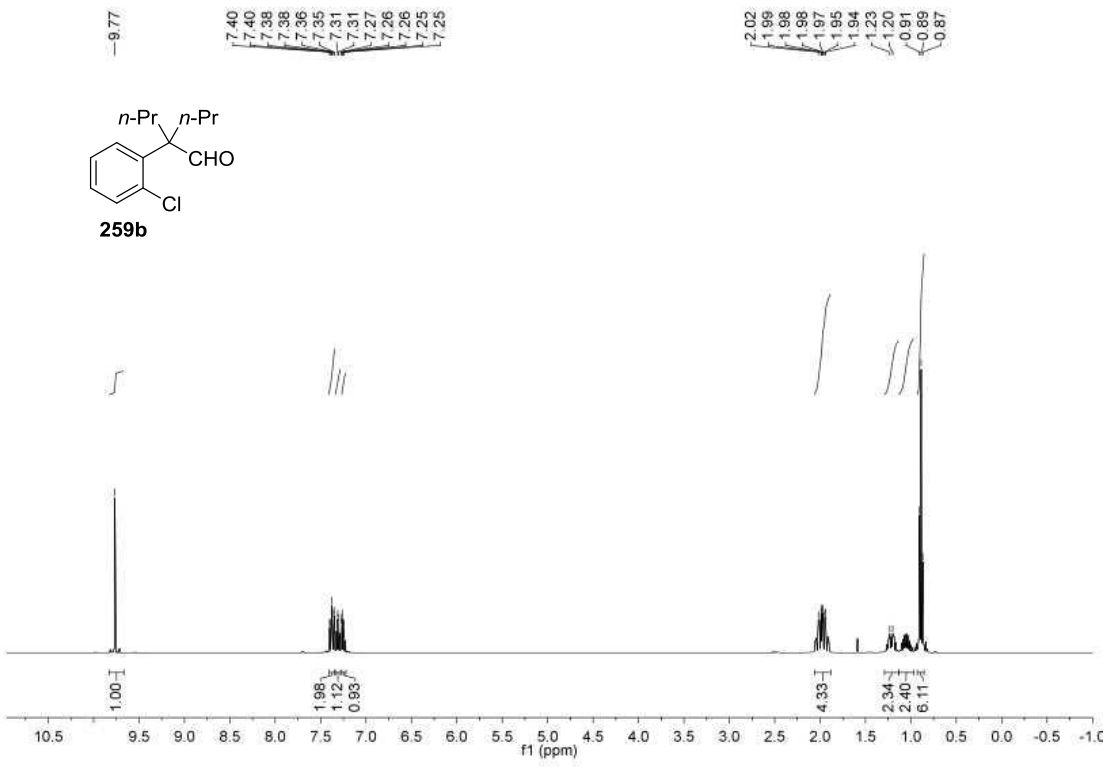
9.77
7.40
7.40
7.38
7.38
7.36
7.35
7.31
7.31
7.27
7.26
7.26
7.25
7.25
2.02
1.99
1.98
1.98
1.97
1.95
1.94
1.23
1.20
0.91
0.89
0.87
n-Pr
n-Pr
CHO
Cl
259b
1.00
1.98
1.12
0.93
4.33
2.34
2.40
6.11
f1 (ppm)

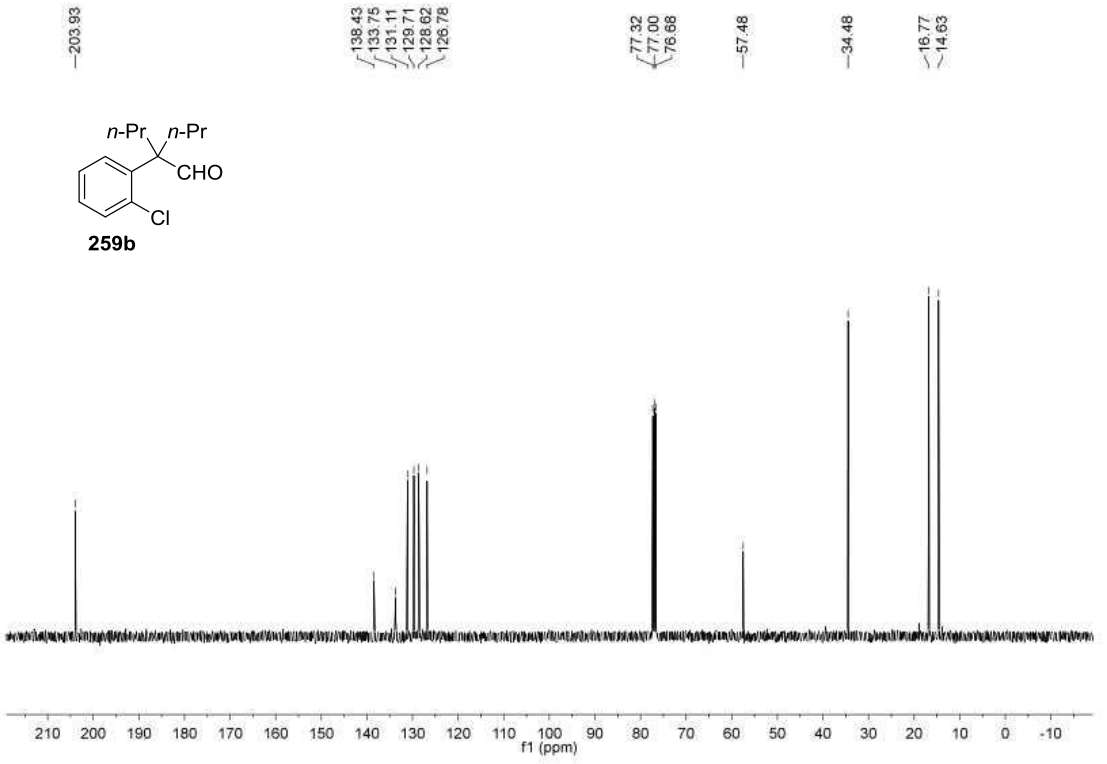
203.93
138.43
133.75
131.11
129.71
128.62
126.78
77.32
77.00
76.68
57.48
34.48
16.77
14.63
n-Pr
n-Pr
CHO
Cl
259b
f1 (ppm)

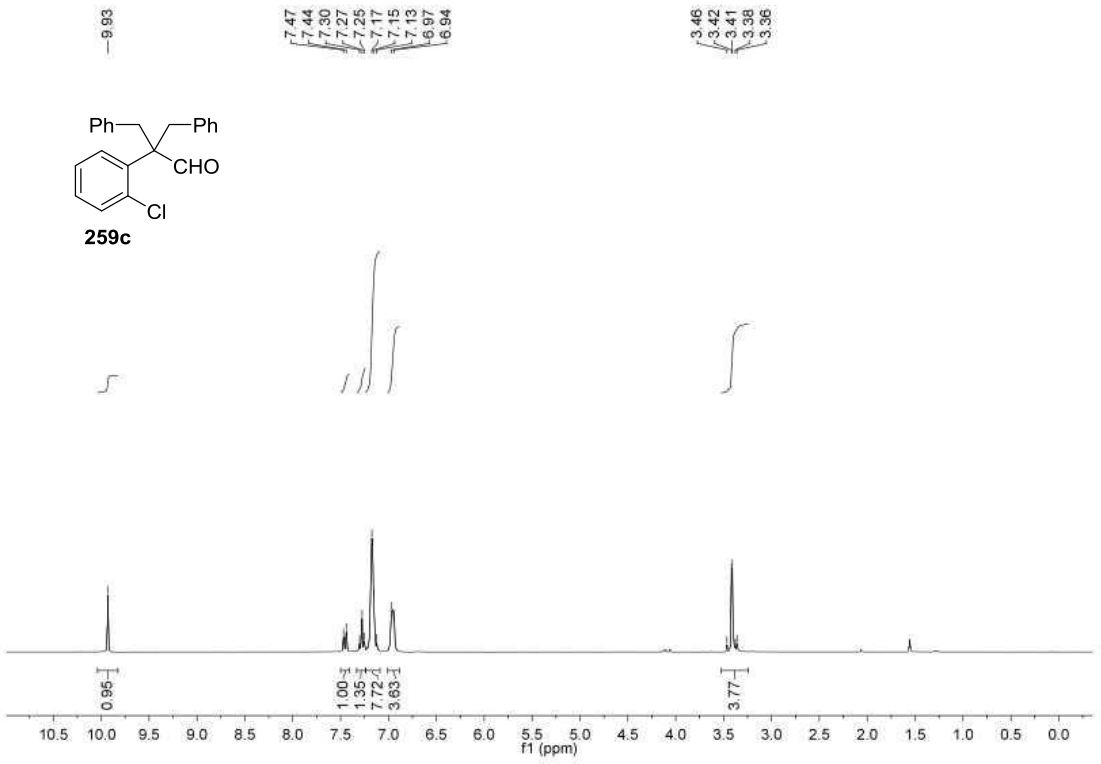
9.93
7.47
7.44
7.30
7.27
7.25
7.17
7.15
7.13
6.97
6.94
3.46
3.42
3.41
3.38
3.36
Ph
Ph
CHO
Cl
0.95
1.00
1.35
7.72
3.63
3.77
f1 (ppm)

259c

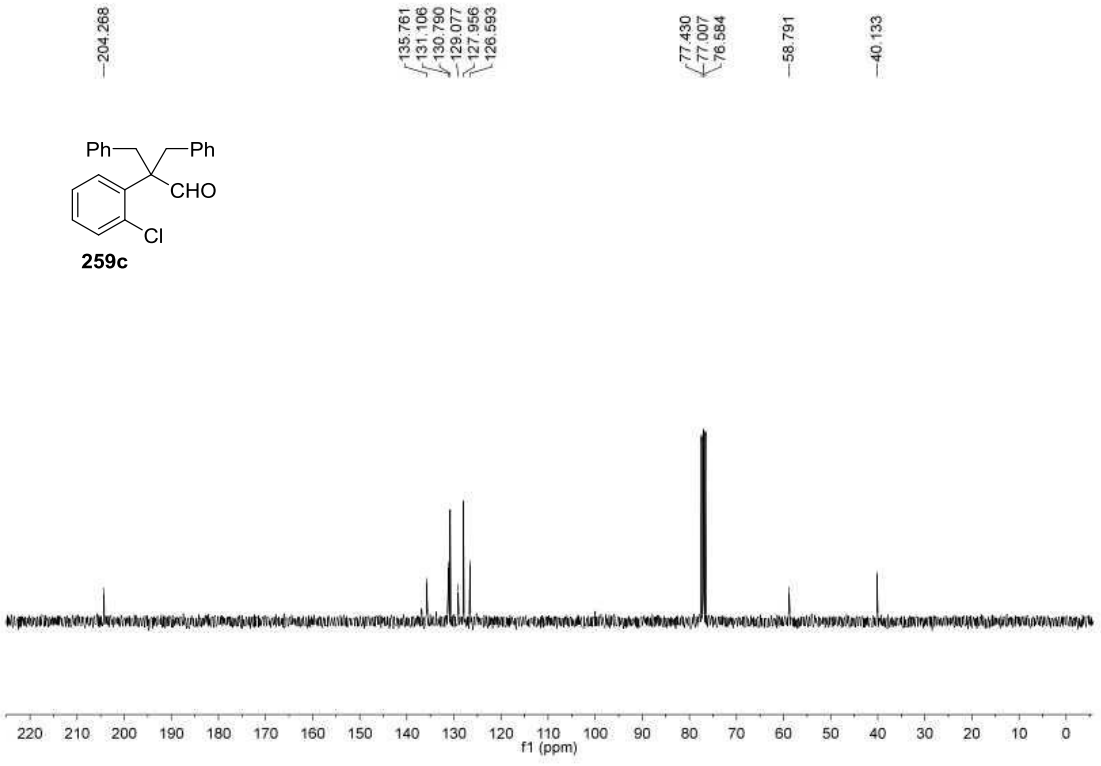
204.268
135.761
131.106
130.790
129.077
127.956
126.593
77.430
77.007
76.584
58.791
40.133
Ph
Ph
CHO
Cl
f1 (ppm)

259c

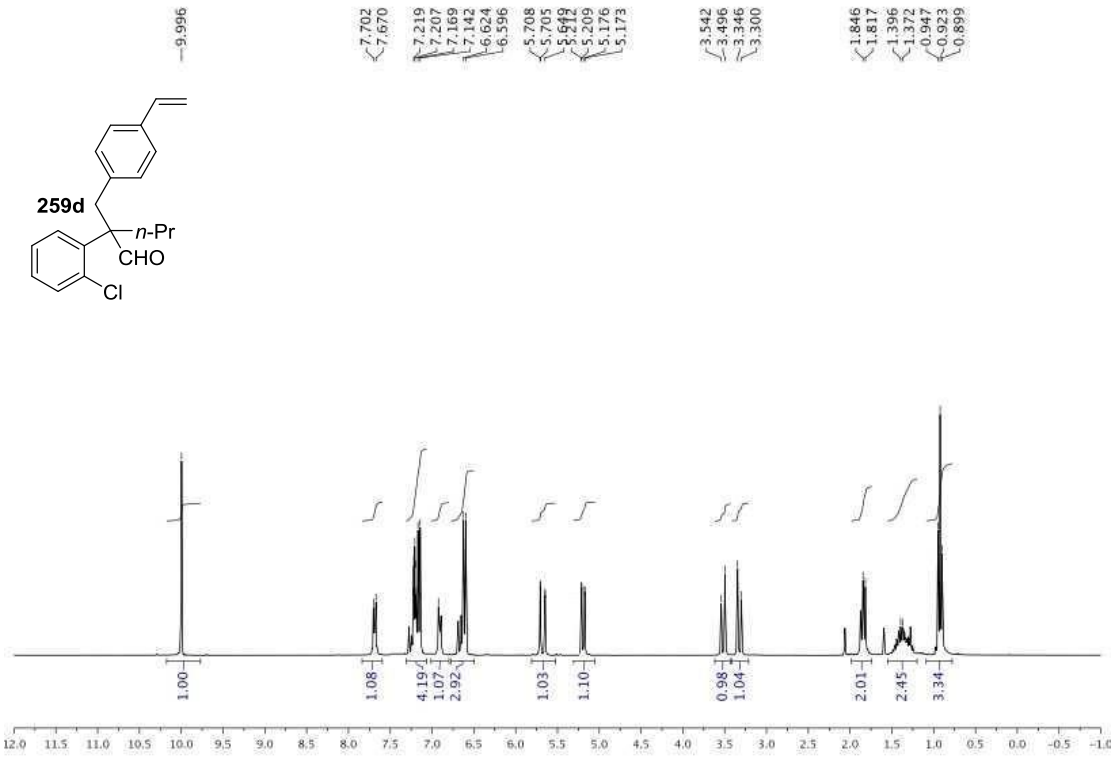
9.996
7.702
7.670
7.219
7.207
7.169
7.142
6.624
6.596
5.708
5.705
5.209
5.176
5.173
3.542
3.496
3.346
3.300
1.846
1.817
1.396
1.372
0.947
0.923
0.899
259d
n-Pr
CHO
Cl
1.00
1.08
4.19
1.07
2.92
1.03
1.10
0.98
1.04
2.01
2.45
3.34

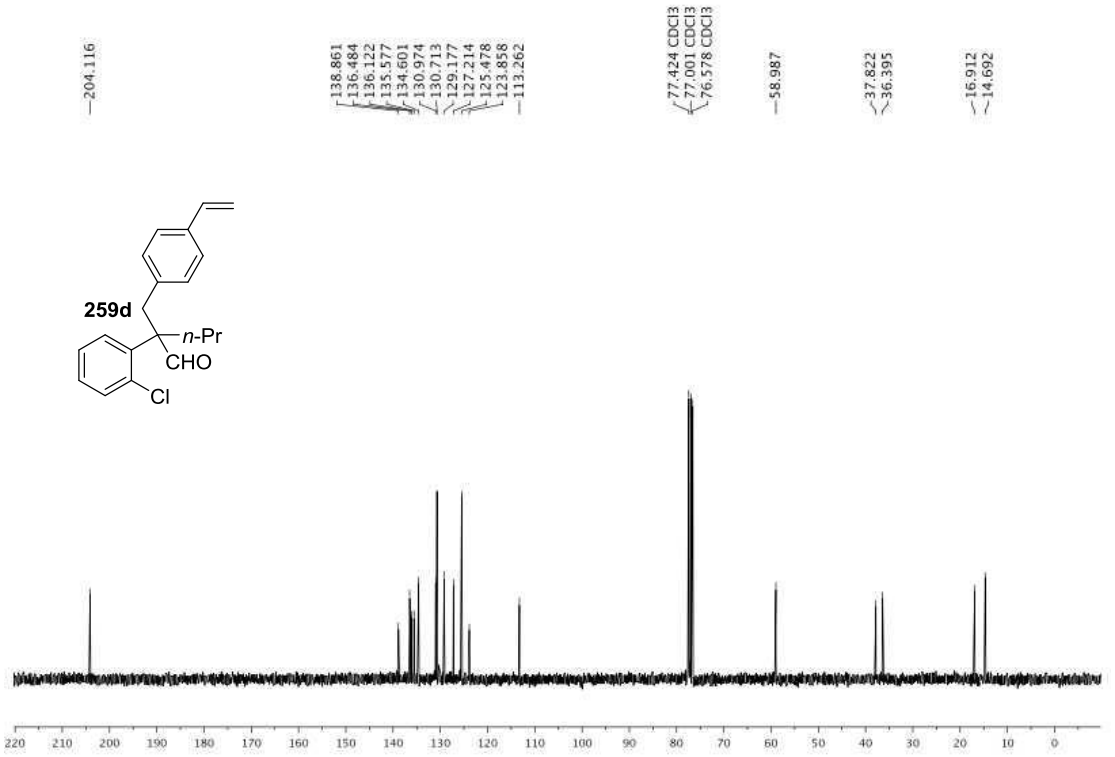
204.116
138.861
136.484
136.122
135.577
134.601
130.974
130.713
129.177
127.214
125.478
123.858
113.262
77.424 CDCl3
77.001 CDCl3
76.578 CDCl3
58.987
37.822
36.395
16.912
14.692
259d
n-Pr
CHO
Cl

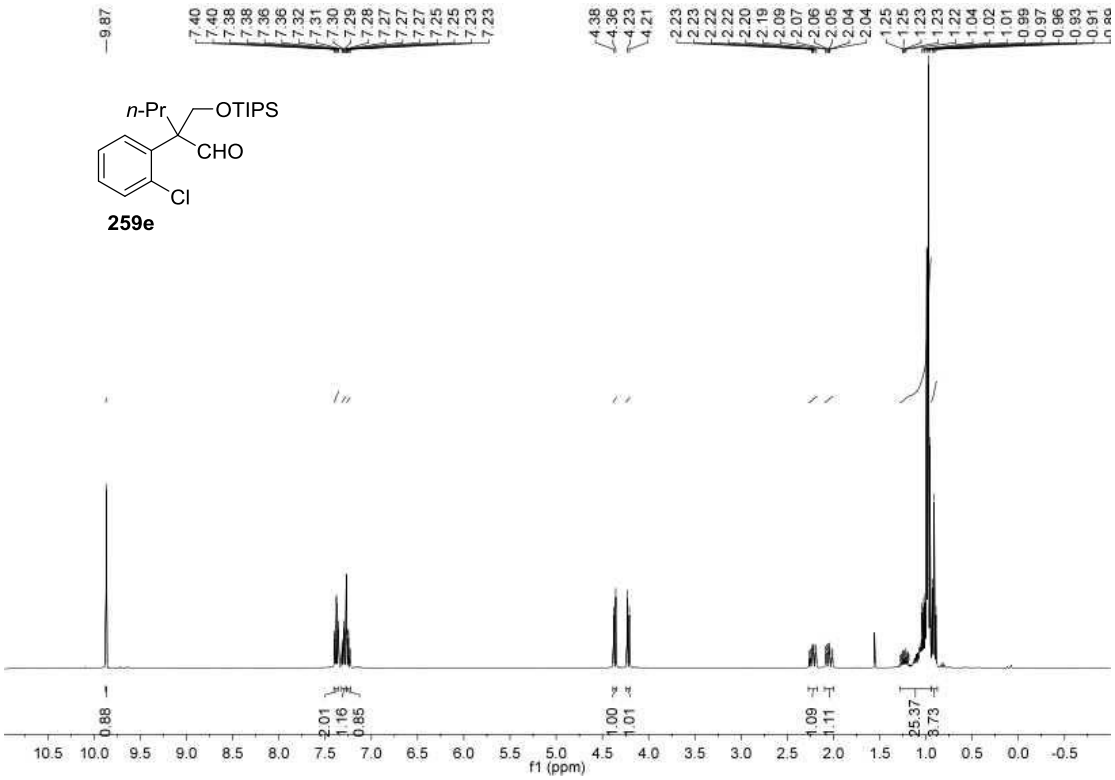
9.87
7.40
7.40
7.38
7.38
7.36
7.36
7.32
7.31
7.30
7.29
7.28
7.27
7.27
7.27
7.25
7.25
7.23
7.23
4.38
4.36
4.23
4.21
2.23
2.23
2.22
2.22
2.20
2.19
2.09
2.07
2.06
2.05
2.04
2.04
1.25
1.25
1.23
1.23
1.22
1.04
1.02
1.01
1.01
0.99
0.97
0.96
0.93
0.91
n-Pr
OTIPS
CHO
Cl
259e
0.88
2.01
1.16
0.85
1.00
1.01
1.09
1.11
25.37
3.73
10.5 10.0 9.5 9.0 8.5 8.0 7.5 7.0 6.5 6.0 5.5 5.0 4.5 4.0 3.5 3.0 2.5 2.0 1.5 1.0 0.5 0.0 -0.5
f1 (ppm)

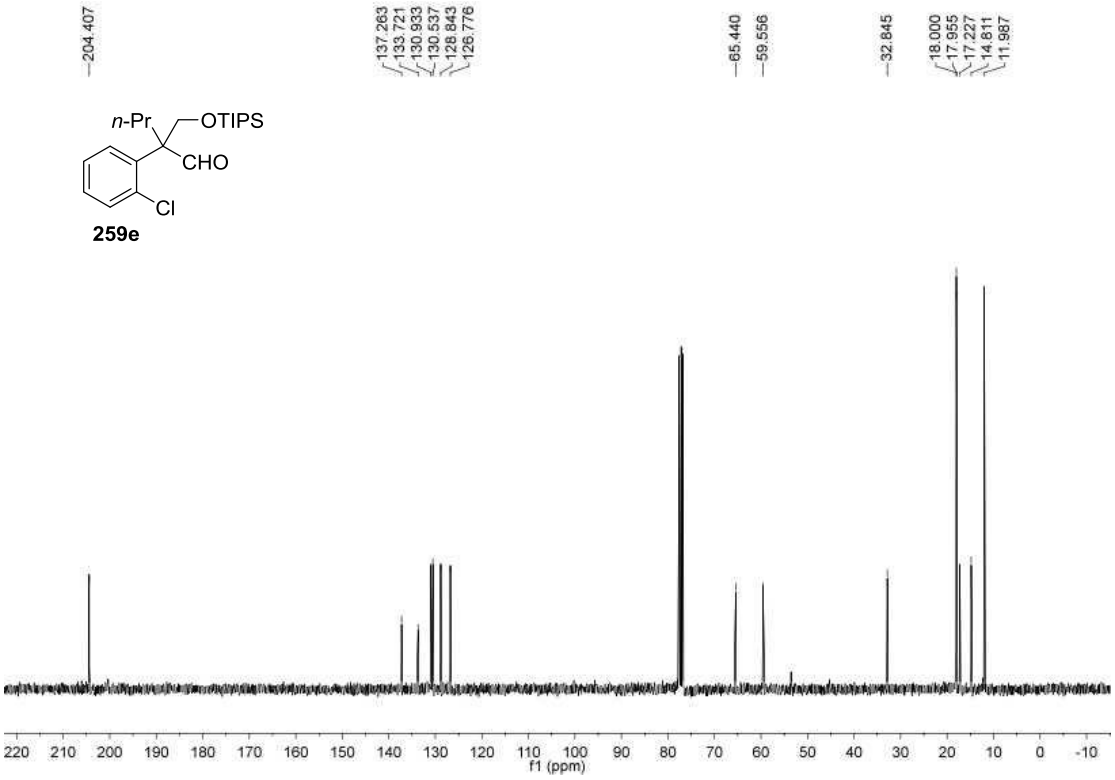
204.407
137.263
133.721
130.933
130.537
128.843
126.776
65.440
59.556
32.845
18.000
17.955
17.227
14.811
11.987
n-Pr
OTIPS
CHO
Cl
259e
220 210 200 190 180 170 160 150 140 130 120 110 100 90 80 70 60 50 40 30 20 10 0 -10
f1 (ppm)

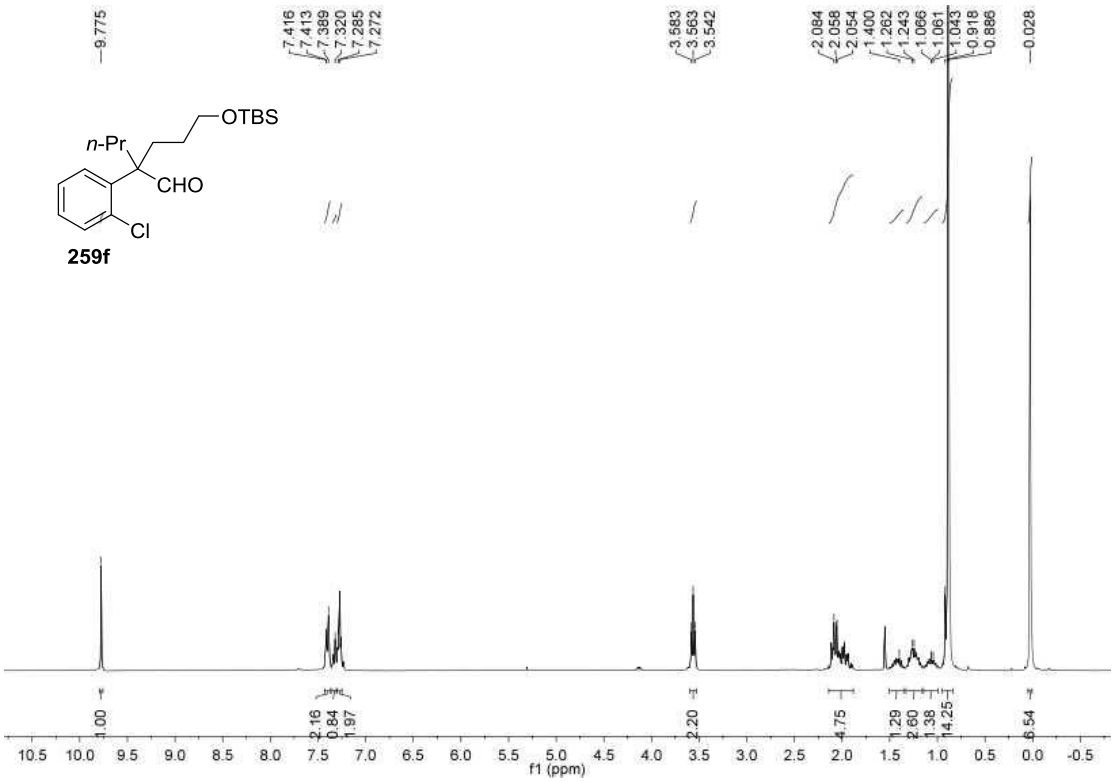
9.775
7.416
7.413
7.389
7.320
7.285
7.272
3.583
3.563
3.542
2.084
2.058
2.054
1.400
1.262
1.243
1.066
1.061
1.043
0.918
0.886
0.028
OTBS
n-Pr
CHO
Cl
259f
1.00
2.16
0.84
1.97
2.20
4.75
1.29
2.60
1.38
14.25
6.54
f1 (ppm)

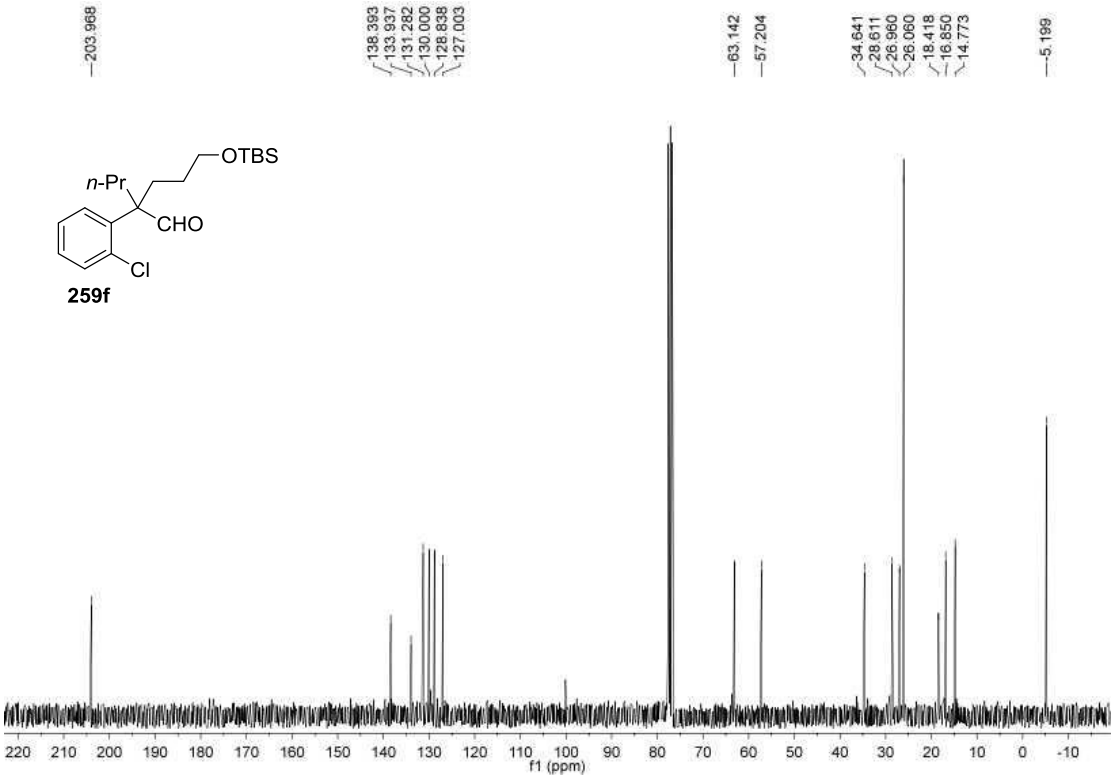
203.968
138.393
133.937
131.282
130.000
128.838
127.003
63.142
57.204
34.641
28.611
26.960
26.060
18.418
16.850
14.773
5.199
OTBS
n-Pr
CHO
Cl
259f
f1 (ppm)

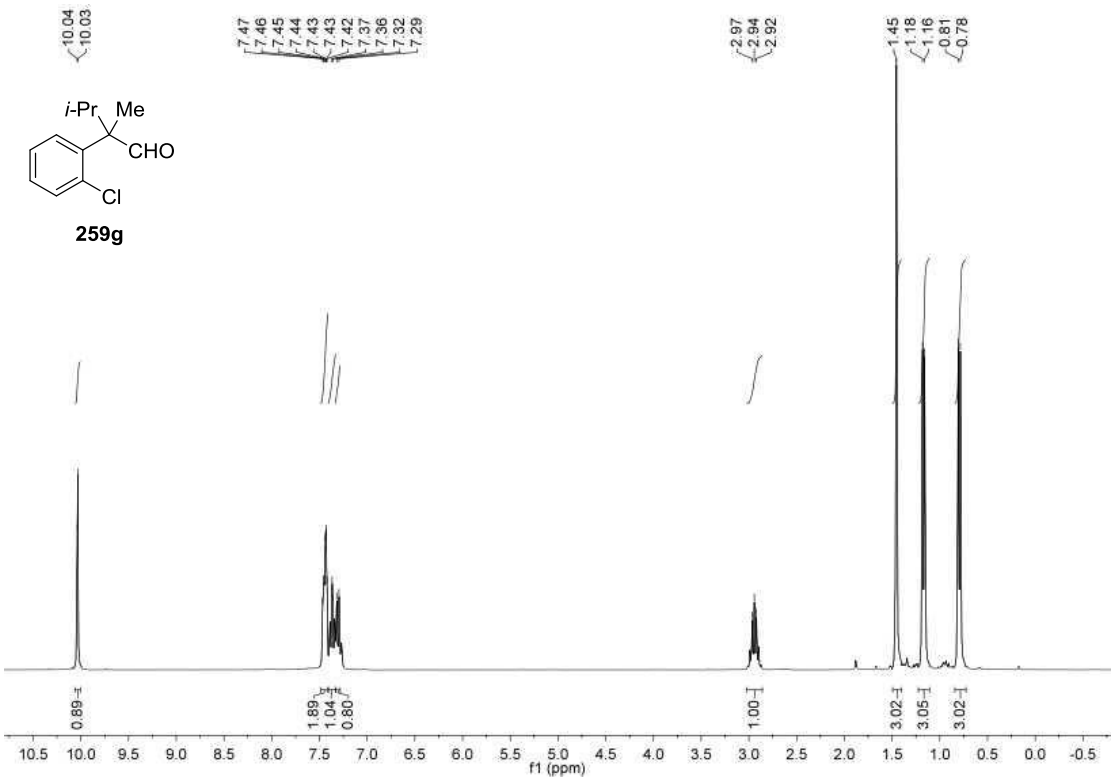
10.04
10.03
7.47
7.46
7.45
7.44
7.43
7.43
7.42
7.37
7.36
7.32
7.29
2.97
2.94
2.92
1.45
1.18
1.16
0.81
0.78
i-Pr
Me
CHO
Cl
0.89
1.89
1.04
0.80
1.00
3.02
3.05
3.02
f1 (ppm)

259g

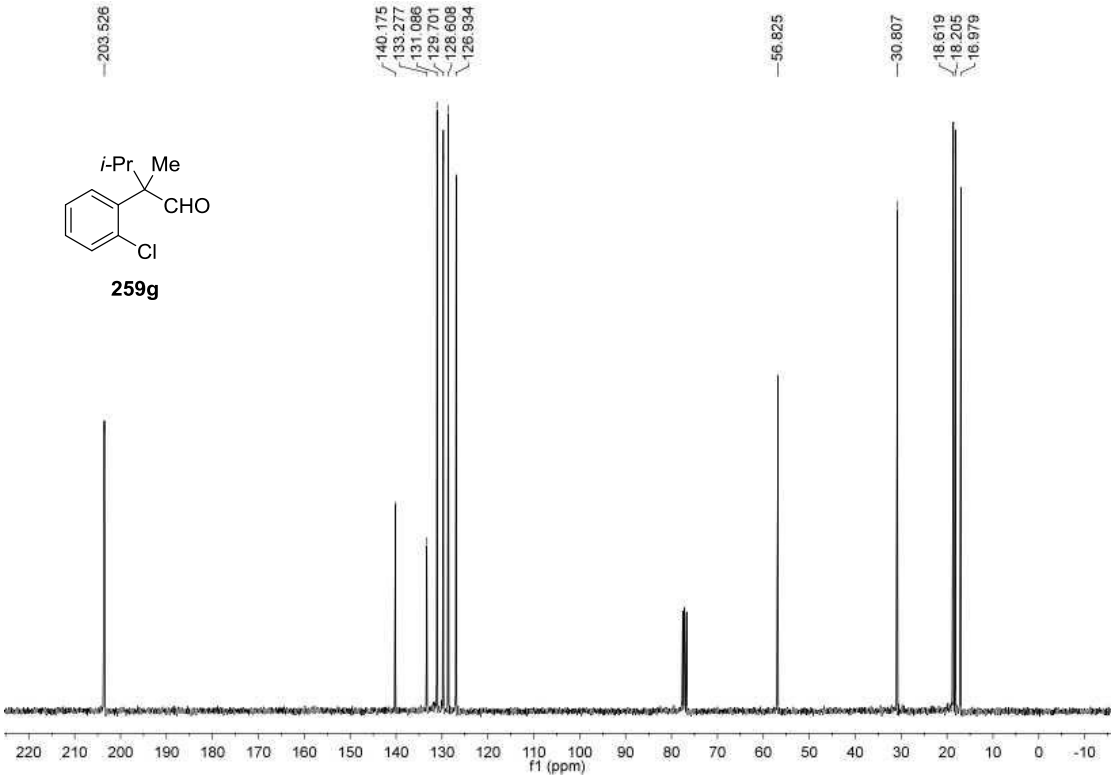
203.526
140.175
133.277
131.086
129.701
128.608
126.934
56.825
30.807
18.619
18.205
16.979
i-Pr
Me
CHO
Cl
f1 (ppm)

259g

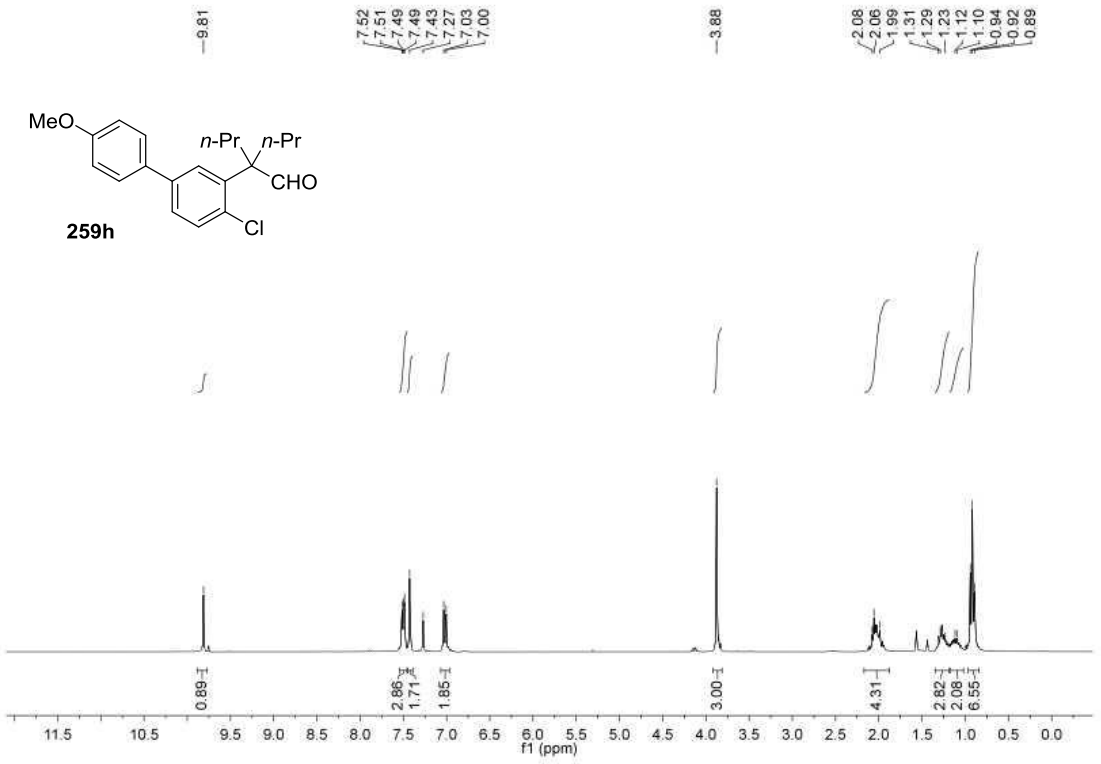
9.81
7.52
7.51
7.49
7.49
7.43
7.27
7.03
7.00
3.88
2.08
2.06
1.99
1.31
1.29
1.23
1.12
1.10
0.94
0.92
0.89
MeO
n-Pr
n-Pr
CHO
Cl
259h
0.89
2.86
1.71
1.85
3.00
4.31
2.82
2.08
6.55
f1 (ppm)

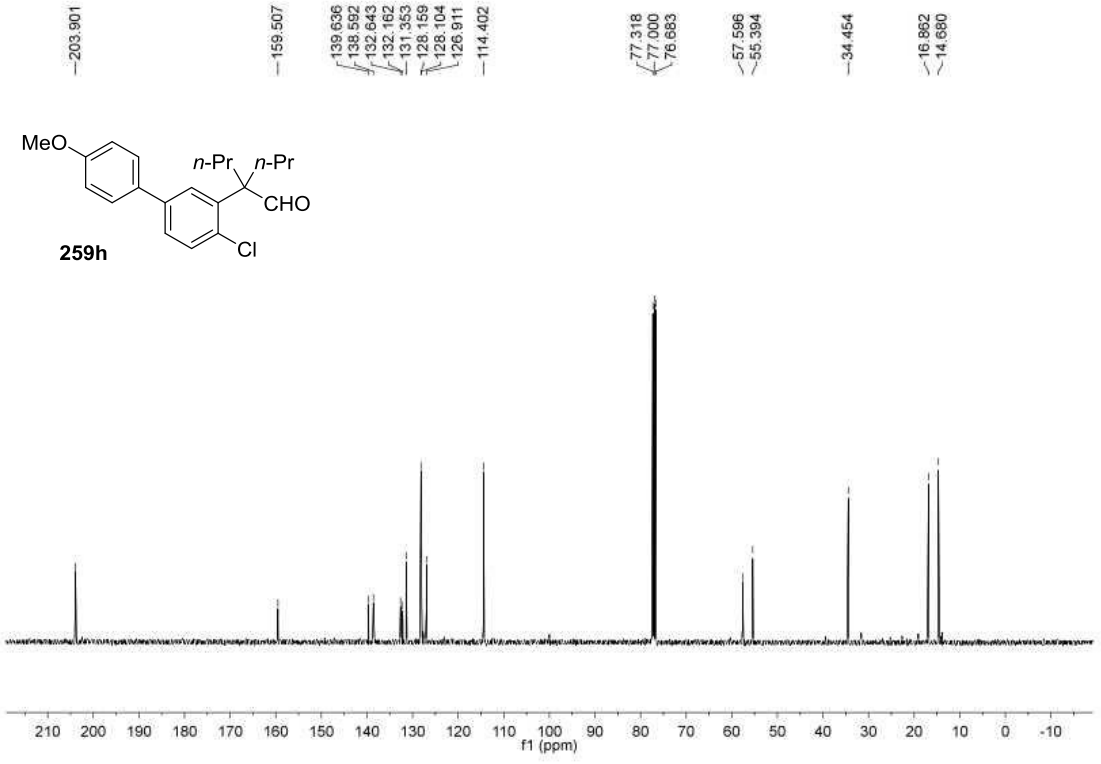
203.901
159.507
139.636
138.592
132.643
132.162
131.353
128.159
128.104
126.911
114.402
77.318
77.000
76.683
57.596
55.394
34.454
16.862
14.680
MeO
n-Pr
n-Pr
CHO
Cl
259h
f1 (ppm)

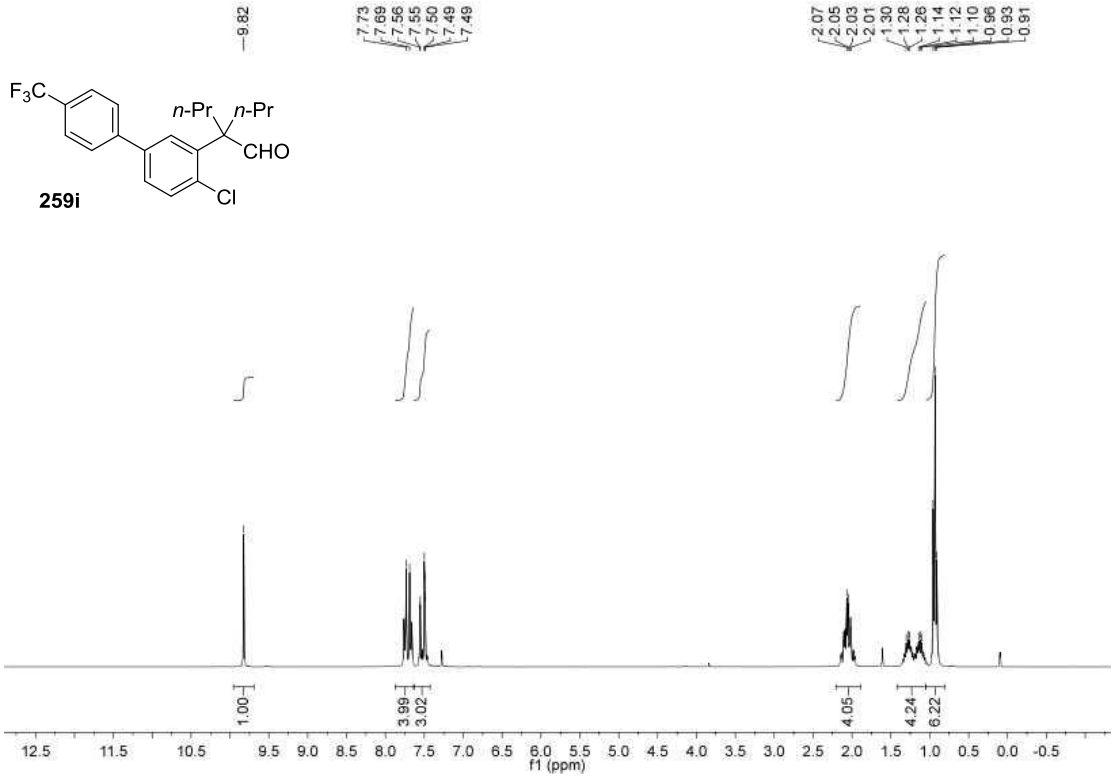
9.82
7.73
7.69
7.56
7.55
7.50
7.49
7.49
2.07
2.05
2.03
2.01
1.30
1.28
1.26
1.14
1.12
1.10
0.96
0.93
0.91
F3C
n-Pr
n-Pr
CHO
Cl
259i
1.00
3.99
3.02
4.05
4.24
6.22
f1 (ppm)

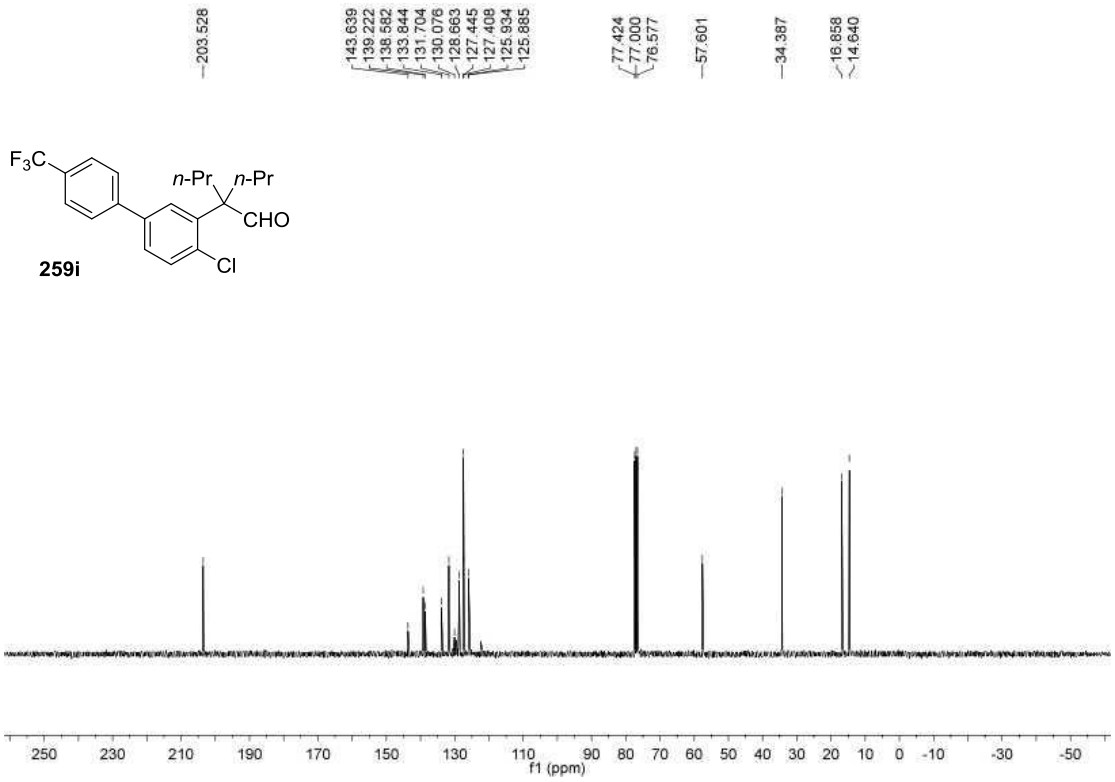
203.528
143.639
139.222
138.582
133.844
131.704
130.076
128.663
127.445
127.409
125.934
125.885
77.424
77.000
76.577
57.601
34.387
16.858
14.640
F3C
n-Pr
n-Pr
CHO
Cl
259i
f1 (ppm)

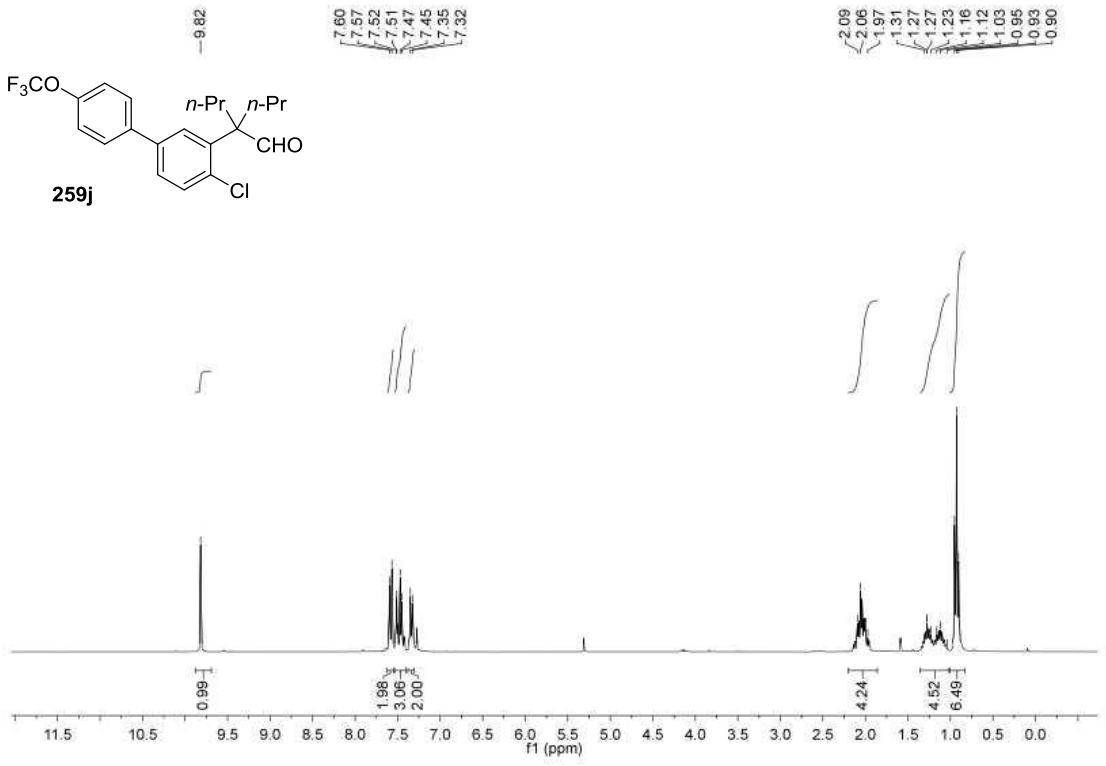
9.82
7.60
7.57
7.52
7.51
7.47
7.45
7.35
7.32
2.09
2.06
1.97
1.31
1.27
1.27
1.23
1.16
1.12
1.03
0.95
0.93
0.90
F3CO
n-Pr
n-Pr
CHO
Cl
259j
0.99
1.98
3.06
2.00
4.24
4.52
6.49
f1 (ppm)

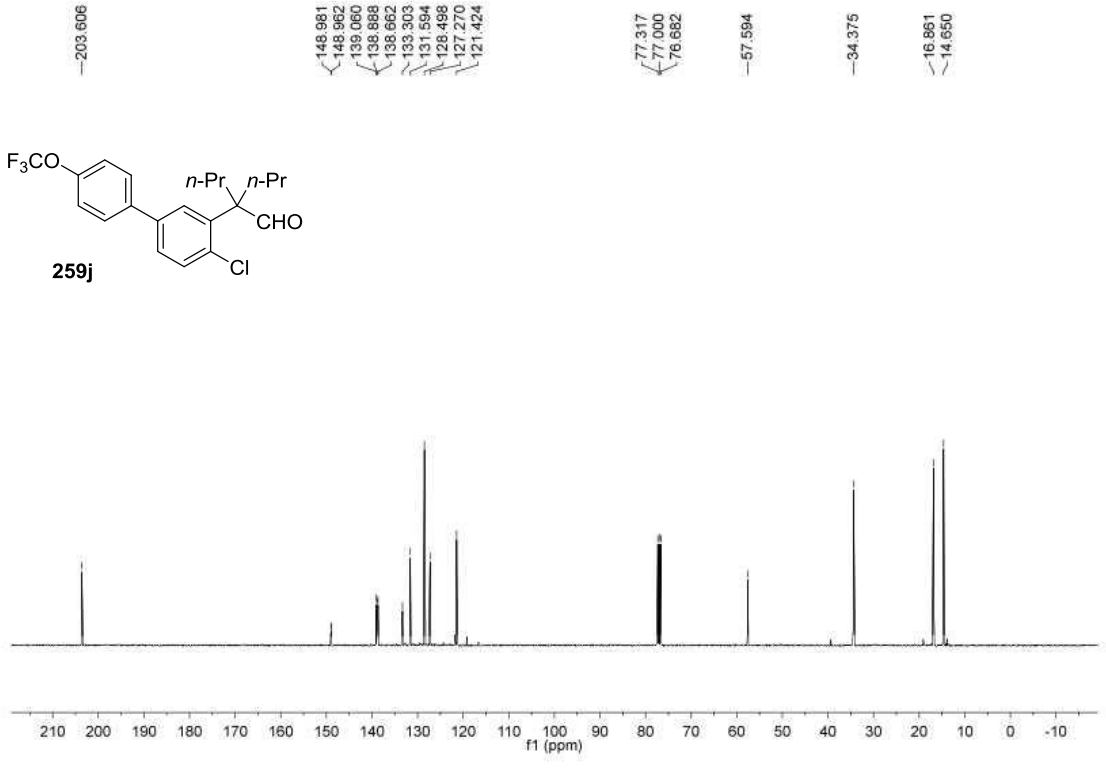
203.606
148.981
148.962
139.060
138.888
138.662
133.303
131.594
128.498
127.270
121.424
77.317
77.000
76.682
57.594
34.375
16.861
14.650
F3CO
n-Pr
n-Pr
CHO
Cl
259j
f1 (ppm)

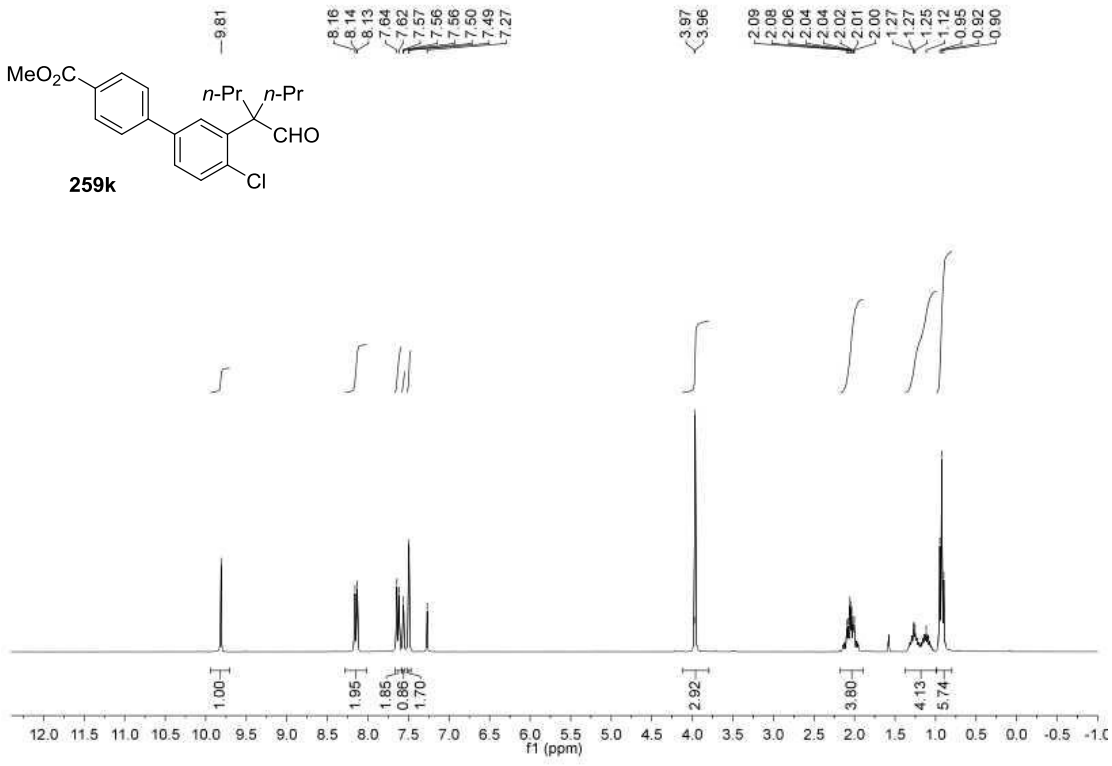
9.81
8.16
8.14
8.13
7.64
7.62
7.57
7.56
7.56
7.50
7.49
7.27
3.97
3.96
2.09
2.08
2.06
2.04
2.04
2.02
2.01
2.00
1.27
1.27
1.25
1.12
0.95
0.92
0.90
MeO2C
n-Pr
n-Pr
CHO
Cl
259k
1.00
1.95
1.85
0.86
1.70
2.92
3.80
4.13
5.74
f1 (ppm)

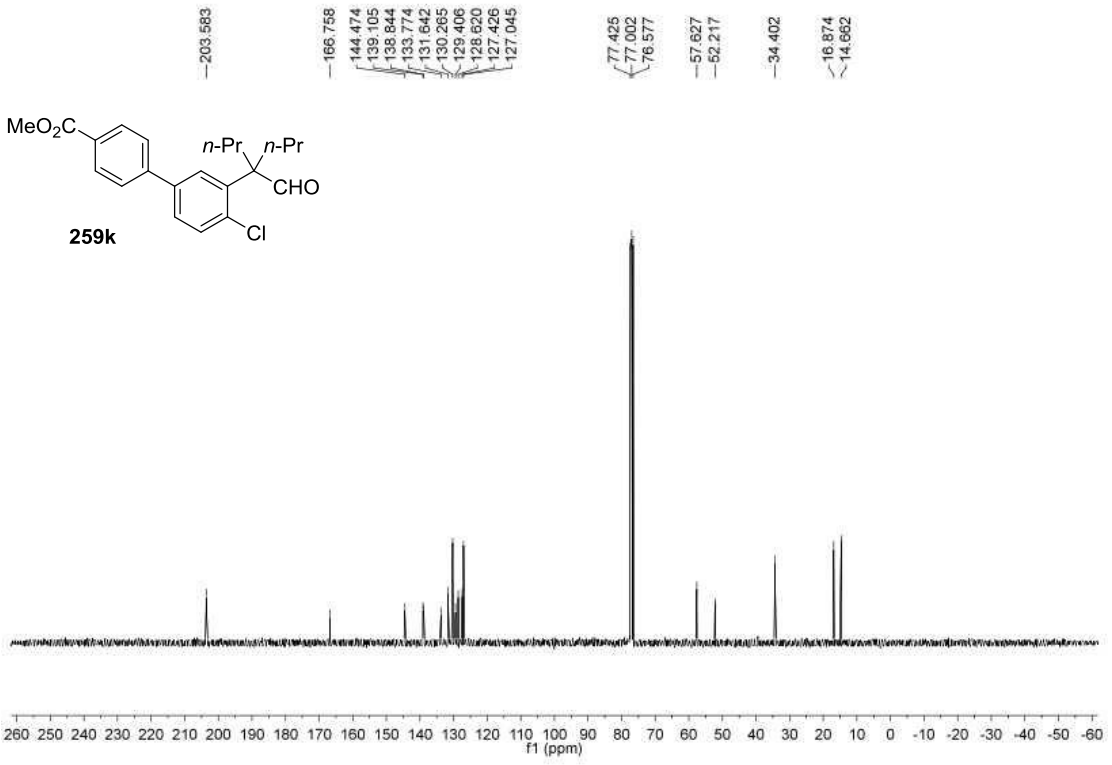
203.583
166.758
144.474
139.105
138.844
133.774
131.642
130.265
129.406
128.620
127.426
127.045
77.425
77.002
76.577
57.627
52.217
34.402
18.874
14.662
MeO2C
n-Pr
n-Pr
CHO
Cl
259k
f1 (ppm)

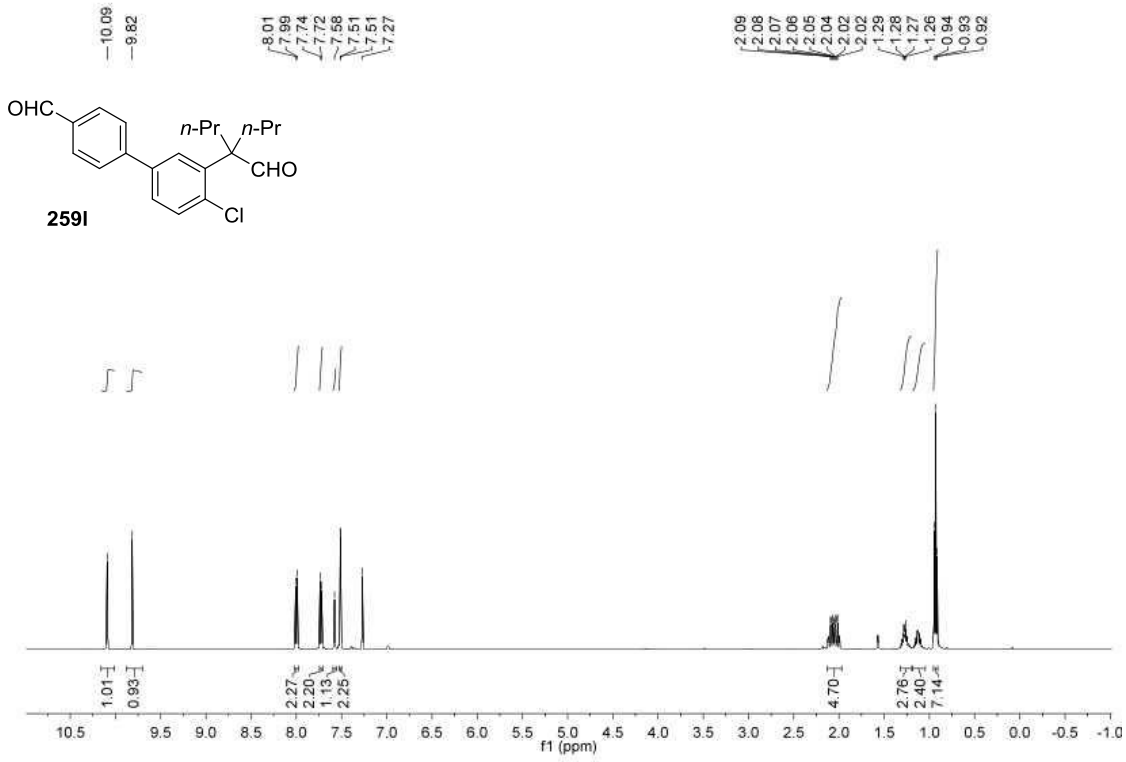
10.09
9.82
8.01
7.99
7.74
7.72
7.58
7.51
7.51
7.27
2.09
2.08
2.07
2.06
2.05
2.04
2.02
2.02
1.29
1.28
1.27
1.26
0.94
0.93
0.92
OHC
n-Pr
n-Pr
CHO
Cl
259l
1.01
0.93
2.27
2.20
1.13
2.25
4.70
2.76
2.40
7.14
f1 (ppm)

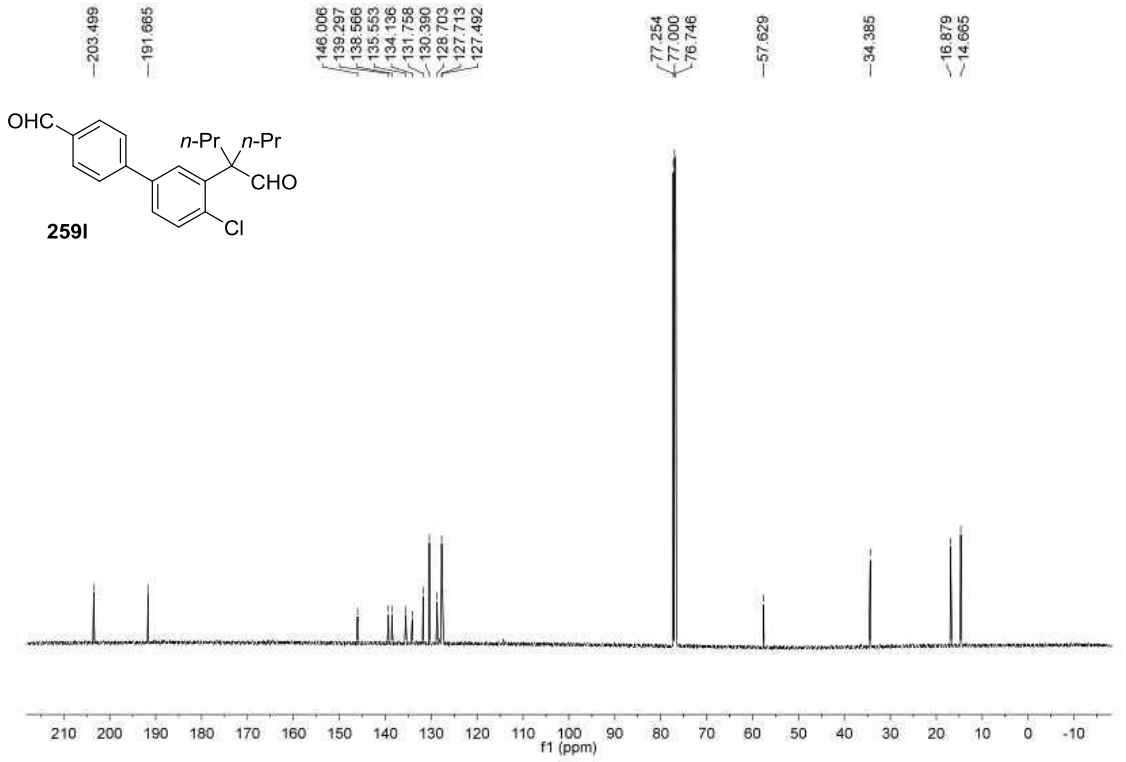
203.499
191.665
146.006
139.297
138.566
135.553
134.136
131.758
130.390
128.703
127.713
127.492
77.254
77.000
76.746
57.629
34.385
16.879
14.665
OHC
n-Pr
n-Pr
CHO
Cl
259l
f1 (ppm)

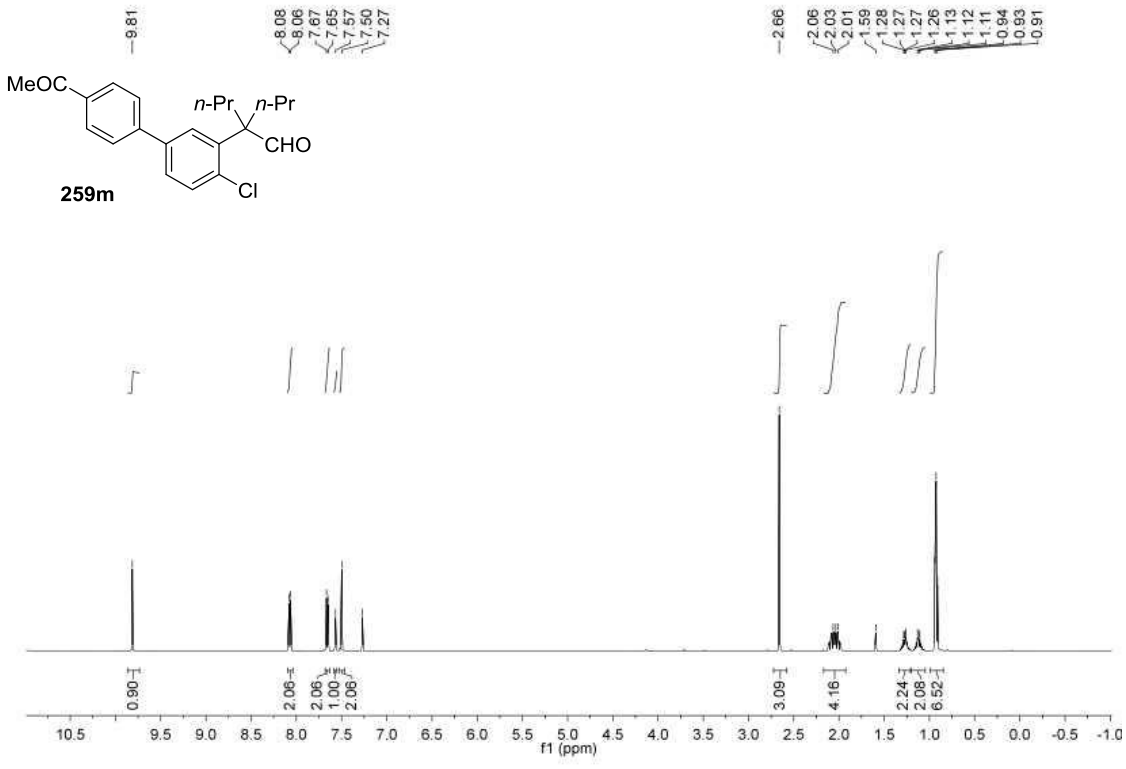
MeOC
n-Pr
n-Pr
CHO
Cl
259m
f1 (ppm)

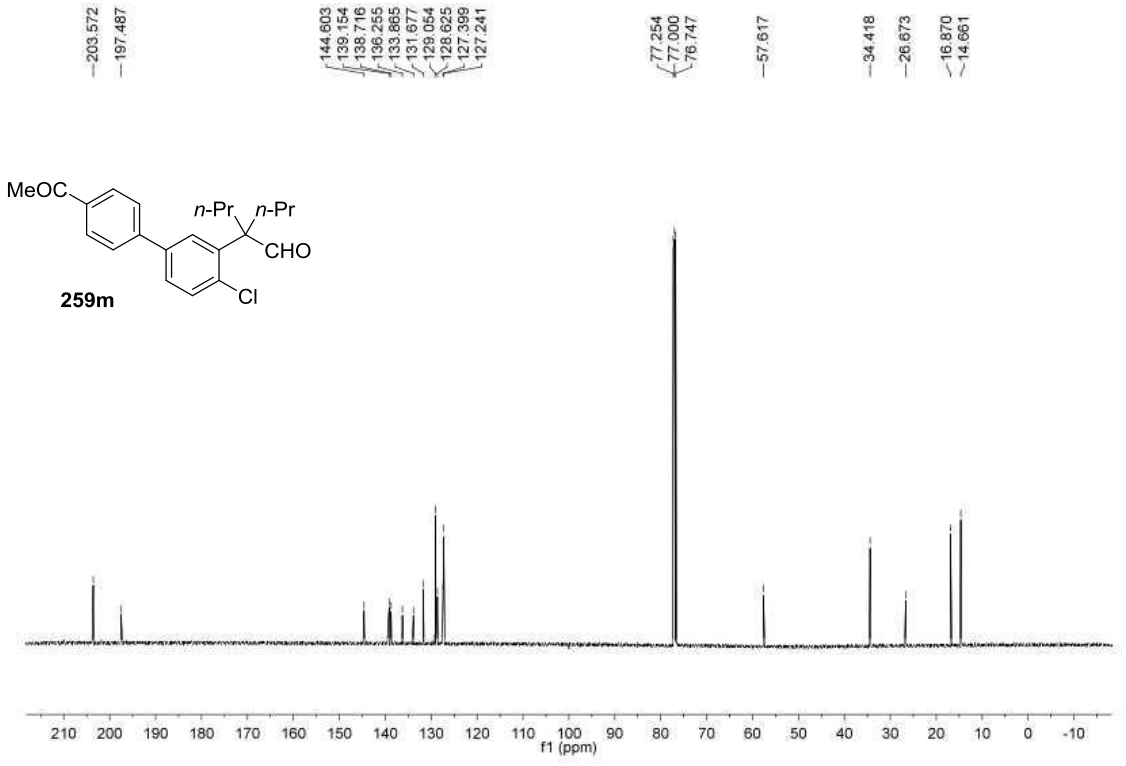
MeOC
n-Pr
n-Pr
CHO
Cl
259m
f1 (ppm)

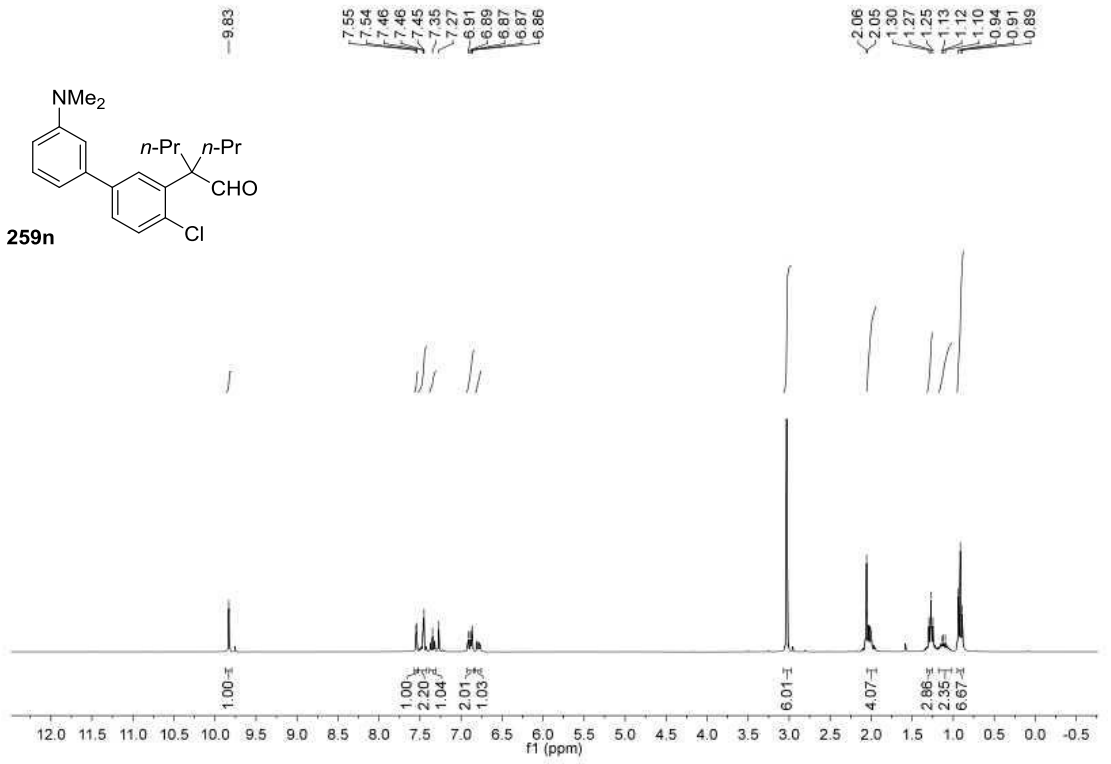
9.83
7.55
7.54
7.46
7.46
7.45
7.35
7.27
6.91
6.89
6.87
6.87
6.86
2.06
2.05
1.30
1.27
1.25
1.13
1.12
1.10
0.94
0.91
0.89
NMe2
n-Pr
n-Pr
CHO
Cl
259n
1.00
2.20
1.04
2.01
1.03
6.01
4.07
2.86
2.35
6.67
f1 (ppm)

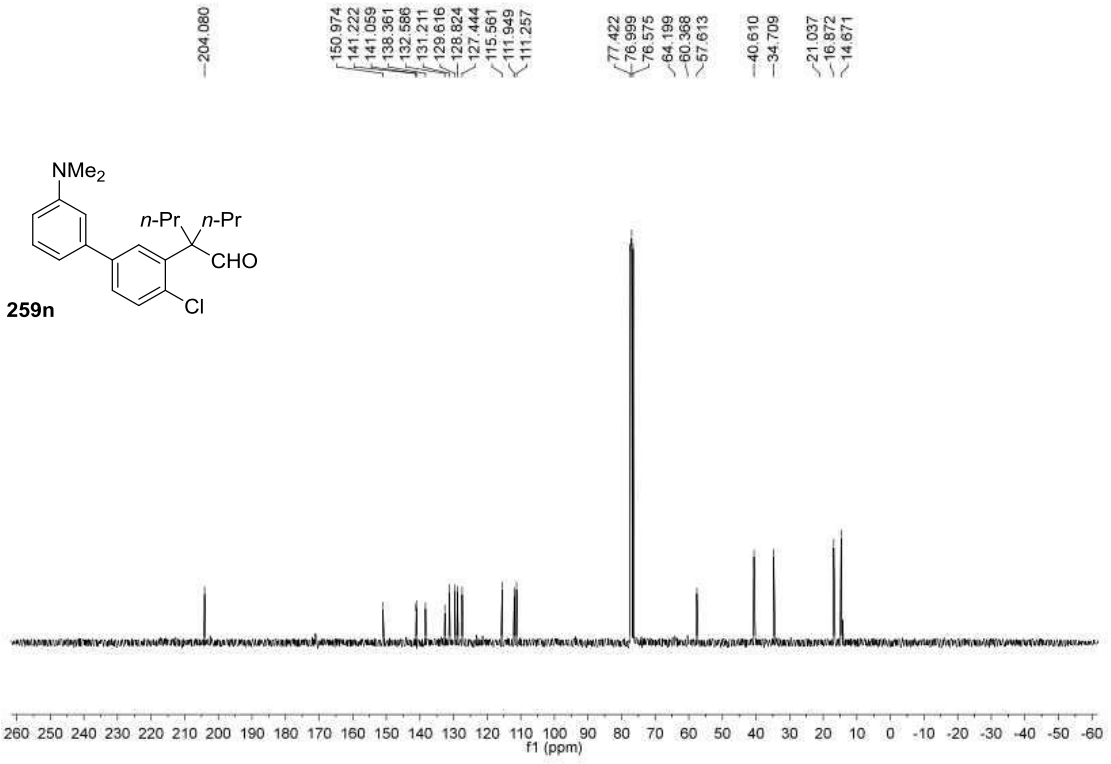
204.080
150.974
141.222
141.059
138.361
132.586
131.211
129.616
128.824
127.444
115.561
111.949
111.257
77.422
76.999
76.575
64.199
60.368
57.613
40.610
34.709
21.037
16.872
14.671
NMe2
n-Pr
n-Pr
CHO
Cl
259n
f1 (ppm)

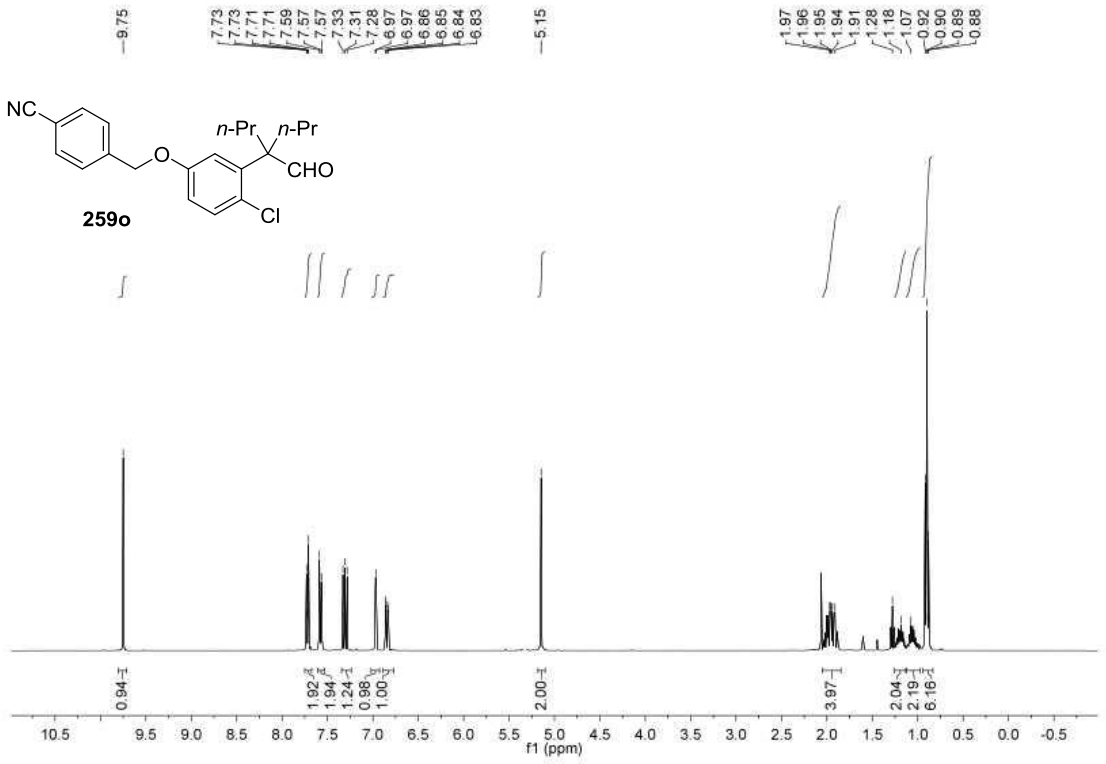
9.75
7.73
7.73
7.71
7.71
7.59
7.57
7.57
7.33
7.31
7.28
6.97
6.97
6.86
6.85
6.84
6.83
5.15
1.97
1.96
1.95
1.94
1.91
1.28
1.18
1.07
0.92
0.90
0.89
0.88
NC
O
n-Pr
n-Pr
CHO
Cl
259o
0.94
1.92
1.94
1.24
0.98
1.00
2.00
3.97
2.04
2.19
6.16
10.5
9.5
9.0
8.5
8.0
7.5
7.0
6.5
6.0
5.5
5.0
4.5
4.0
3.5
3.0
2.5
2.0
1.5
1.0
0.5
0.0
-0.5
f1 (ppm)

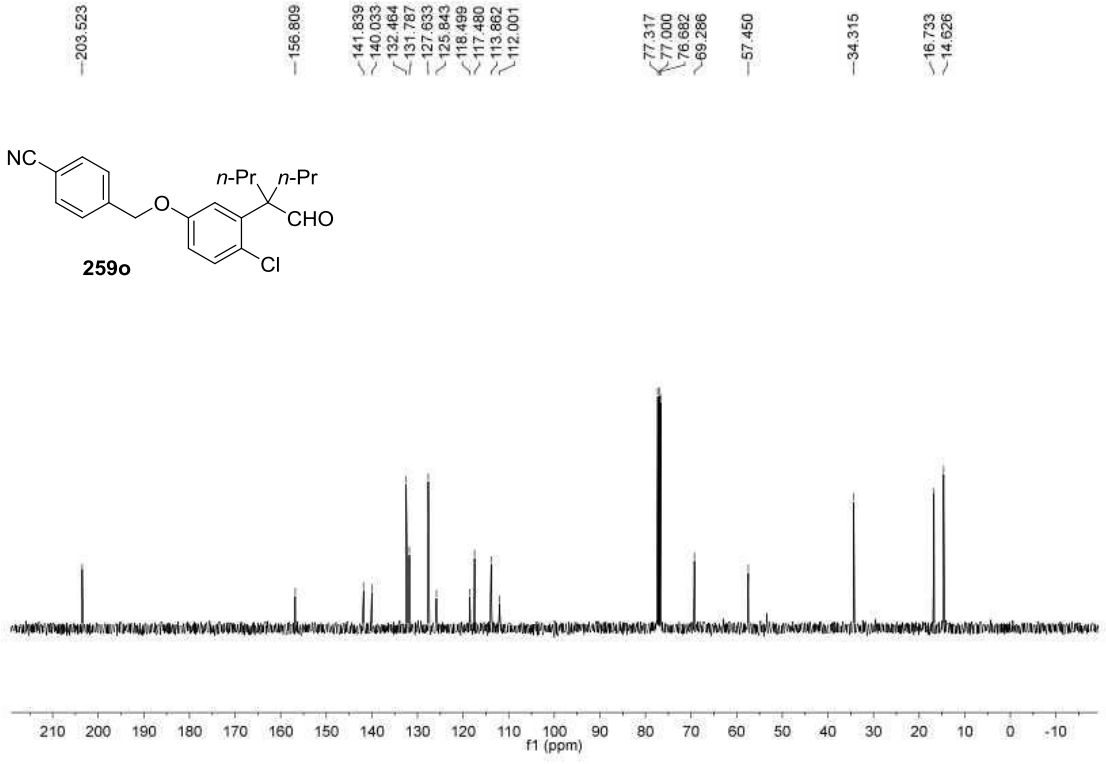
203.523
156.809
141.839
140.033
132.464
131.787
127.633
125.843
118.499
117.480
113.862
112.001
77.317
77.000
76.682
69.286
57.450
34.315
16.733
14.626
NC
O
n-Pr
n-Pr
CHO
Cl
259o
210
200
190
180
170
160
150
140
130
120
110
100
90
80
70
60
50
40
30
20
10
0
-10
f1 (ppm)

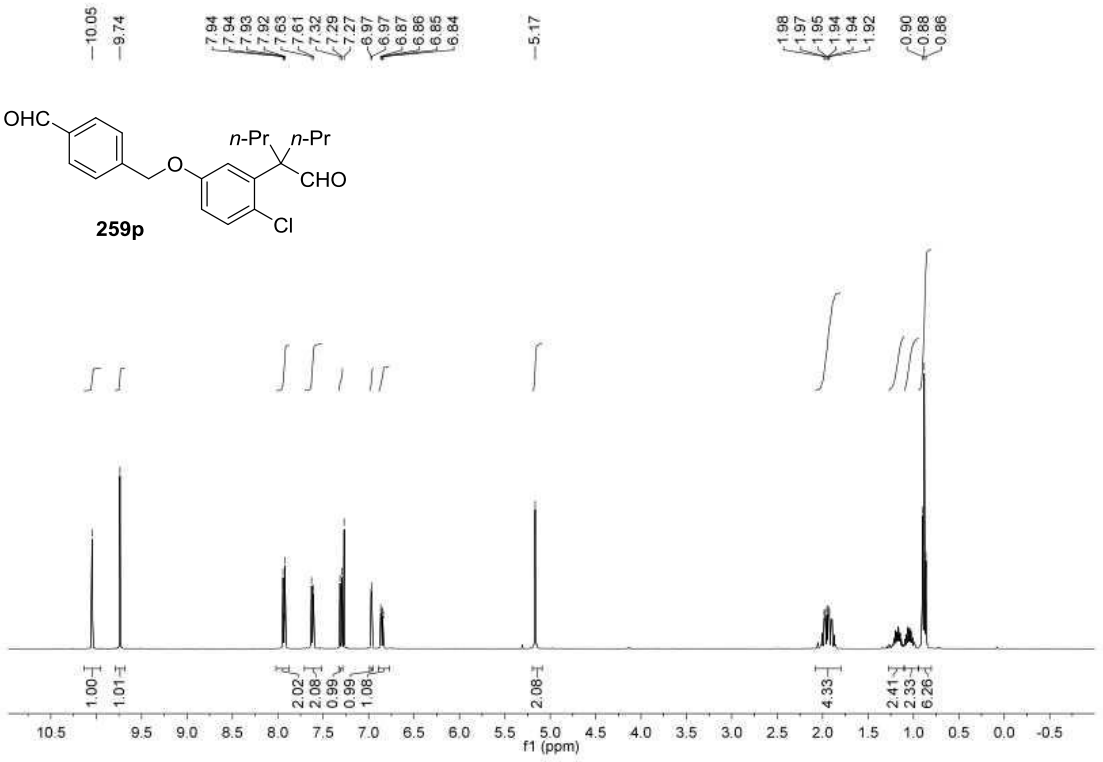
10.05
9.74
7.94
7.94
7.93
7.92
7.63
7.61
7.32
7.29
7.27
6.97
6.87
6.86
6.85
6.84
5.17
1.98
1.97
1.95
1.94
1.94
1.92
0.90
0.88
0.86
OHC
n-Pr
n-Pr
O
CHO
Cl
259p
1.00
1.01
2.02
2.08
0.99
0.99
1.08
2.08
4.33
2.41
2.33
6.26
f1 (ppm)

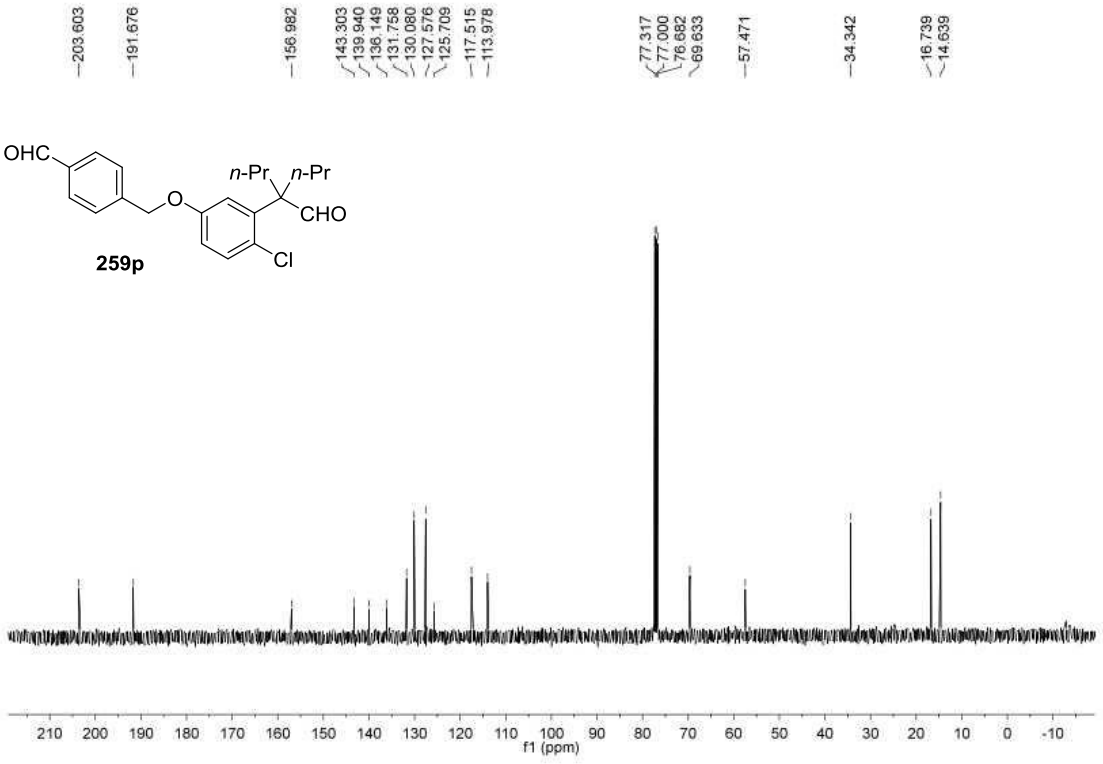
203.603
191.676
156.982
143.303
139.940
136.149
131.758
130.080
127.576
125.709
117.515
113.978
77.317
77.000
76.682
69.633
57.471
34.342
16.739
14.639
OHC
n-Pr
n-Pr
O
CHO
Cl
259p
f1 (ppm)

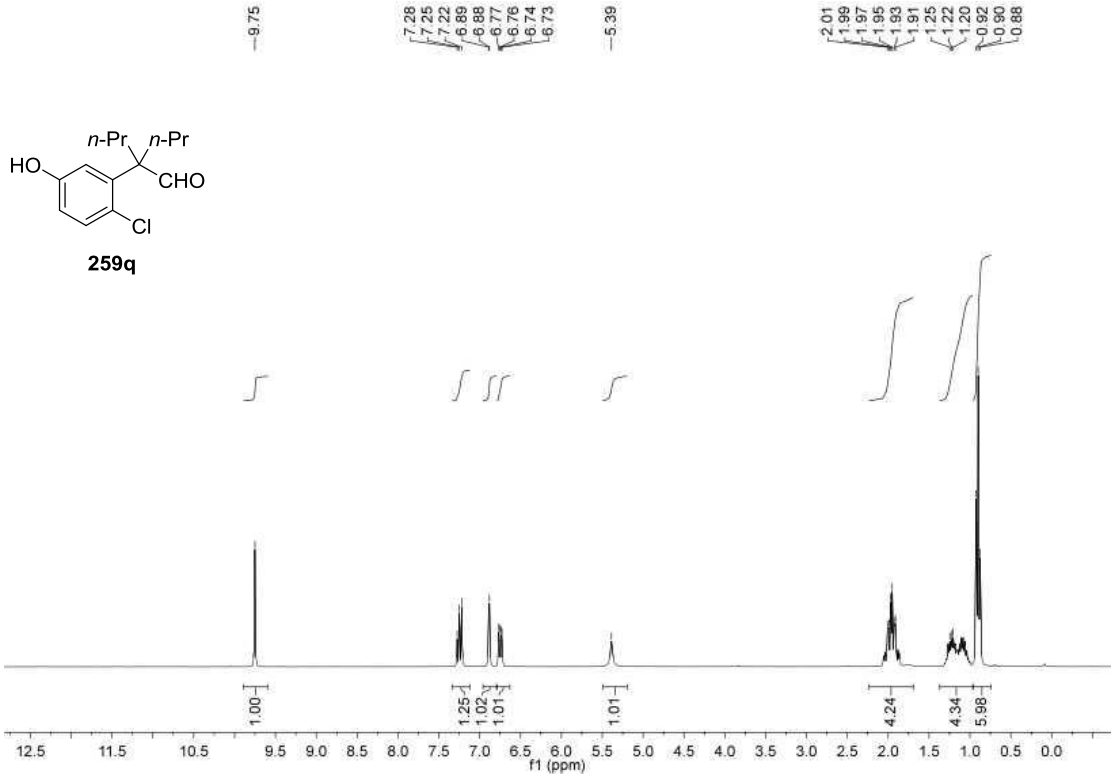
9.75
7.28
7.25
7.22
6.89
6.88
6.77
6.76
6.74
6.73
5.39
2.01
1.99
1.97
1.95
1.93
1.91
1.25
1.22
1.20
0.92
0.90
0.88
n-Pr
n-Pr
HO
CHO
Cl
1.00
1.25
1.02
1.01
1.01
4.24
4.34
5.98
f1 (ppm)

259q

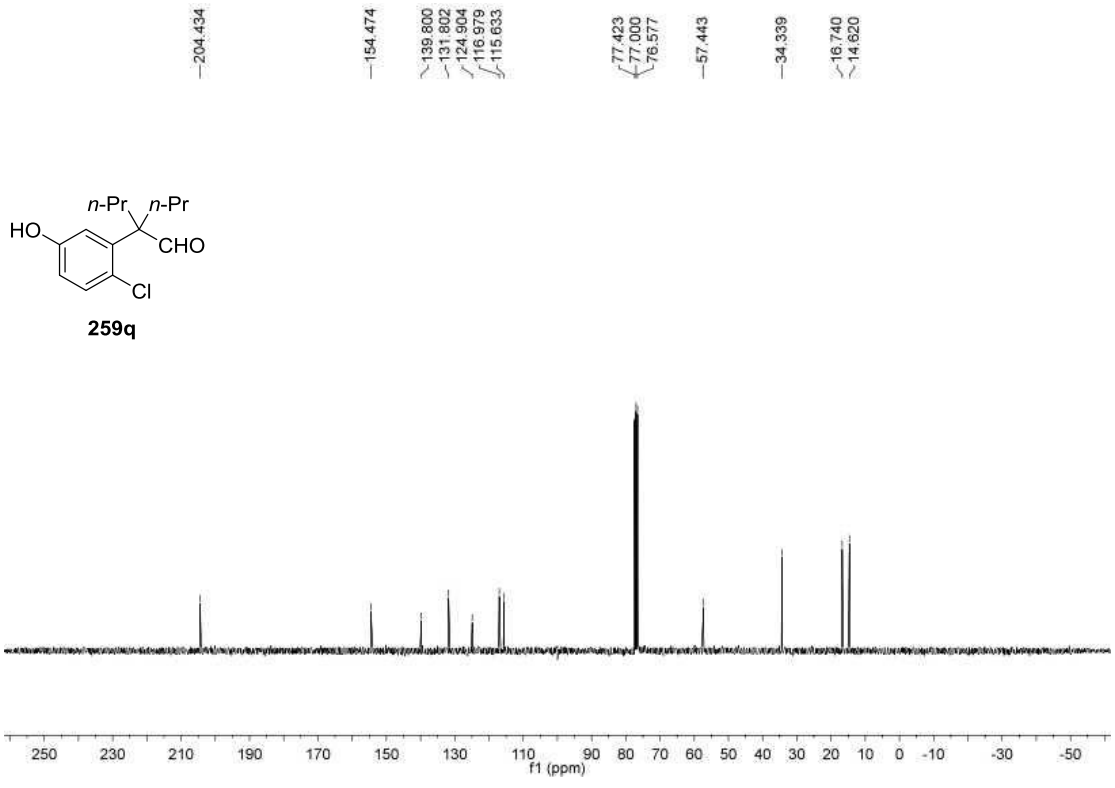
204.434
154.474
139.800
131.802
124.904
116.979
115.633
77.423
77.000
76.577
57.443
34.339
16.740
14.620
n-Pr
n-Pr
HO
CHO
Cl
f1 (ppm)

259q

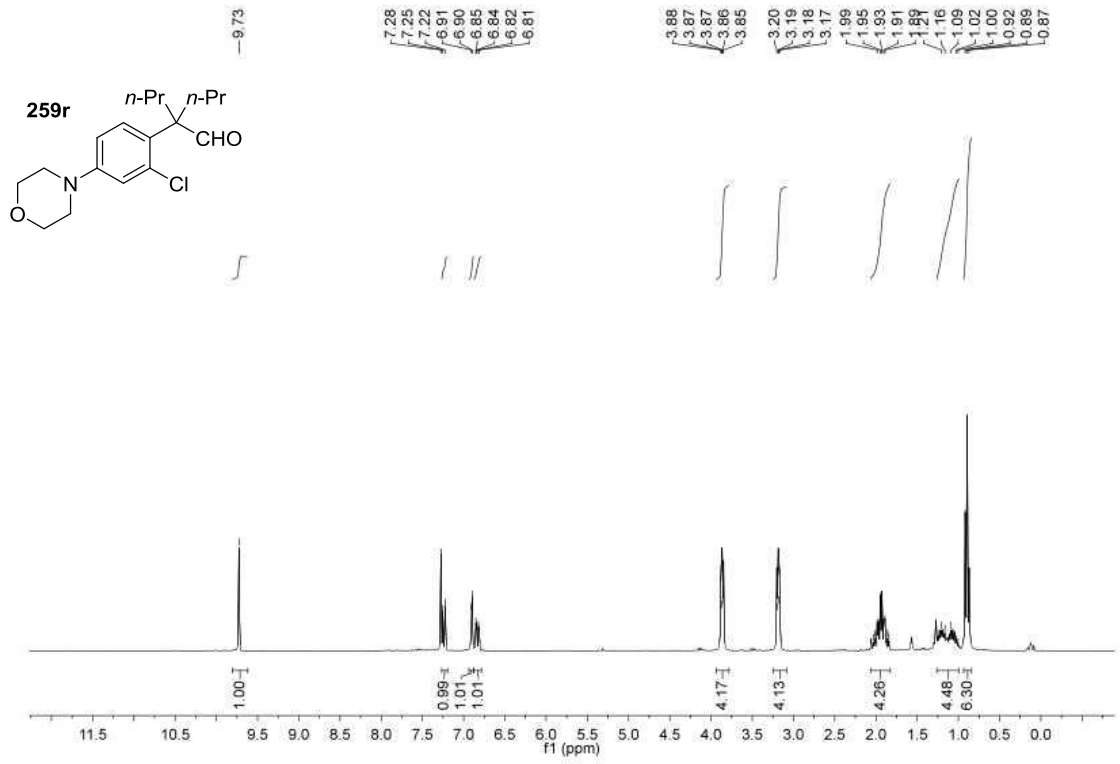
259r
n-Pr
n-Pr
CHO
Cl
N
O
9.73
7.28
7.25
7.22
6.91
6.90
6.85
6.84
6.82
6.81
3.88
3.87
3.87
3.86
3.85
3.20
3.19
3.18
3.17
1.99
1.95
1.93
1.91
1.16
1.09
1.02
1.00
0.92
0.89
0.87
1.00
0.99
1.01
1.01
4.17
4.13
4.26
4.48
6.30
f1 (ppm)

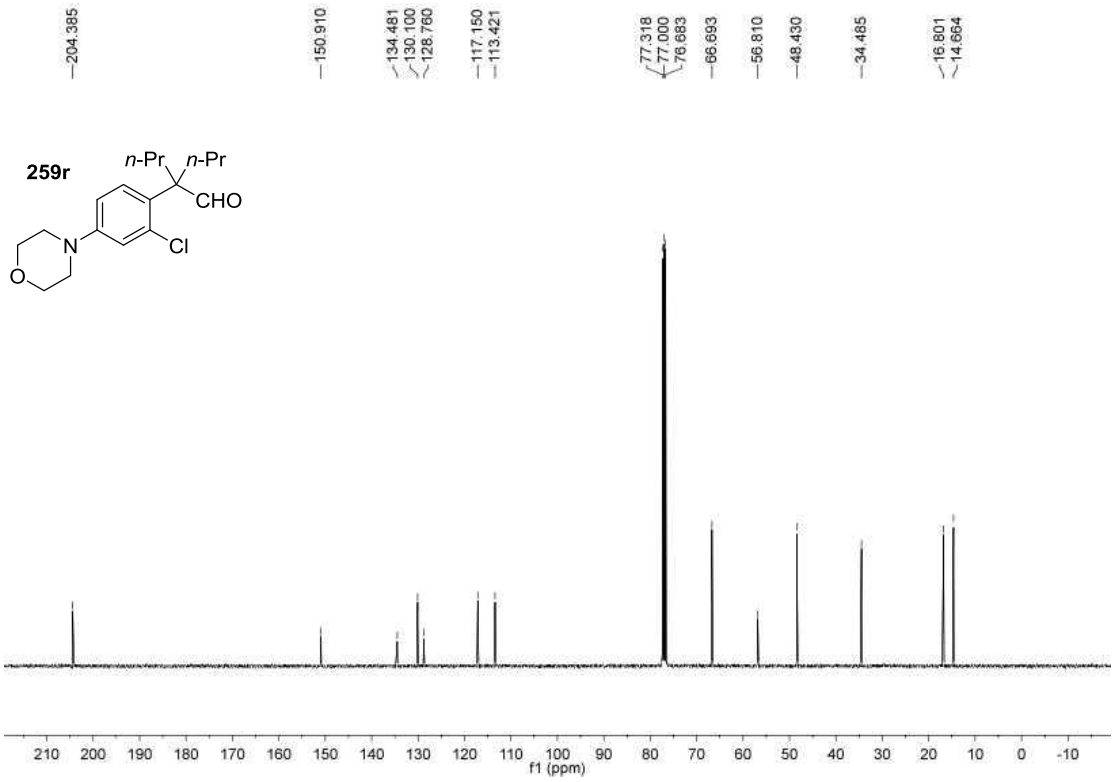
259r
n-Pr
n-Pr
CHO
Cl
N
O
204.385
150.910
134.481
130.100
128.760
117.150
113.421
77.318
77.000
76.683
66.693
56.810
48.430
34.485
16.801
14.664
f1 (ppm)

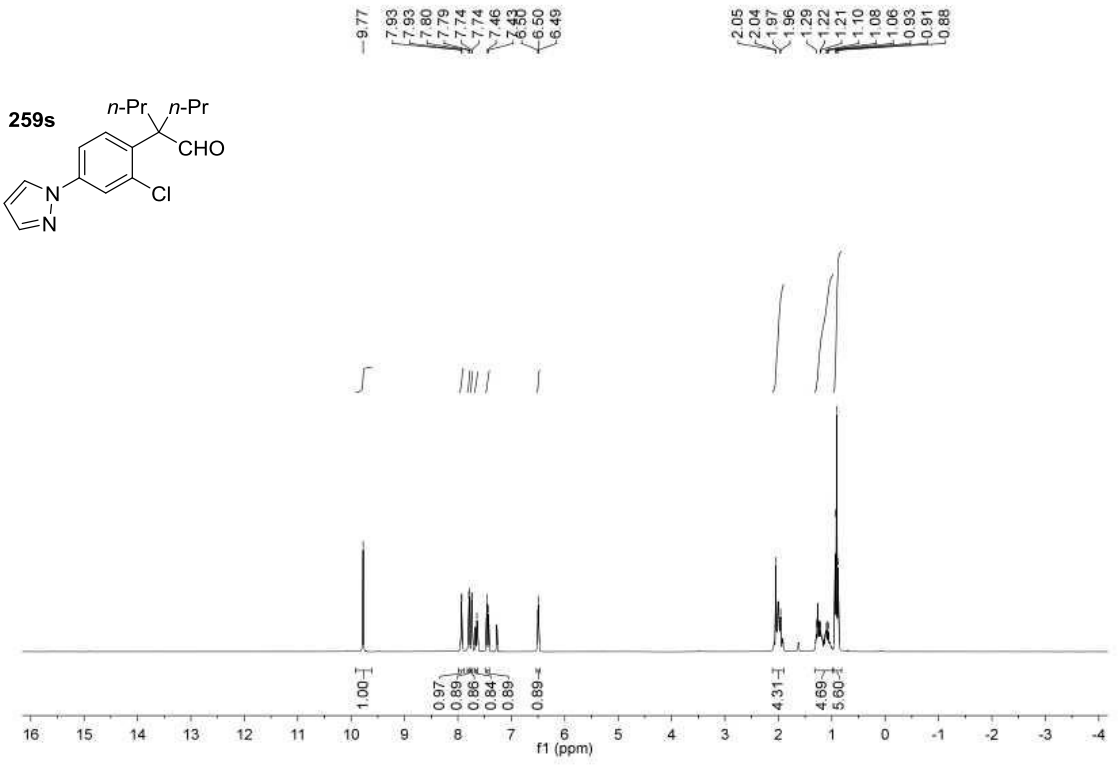
9.77
7.93
7.93
7.80
7.79
7.74
7.74
7.46
7.43
6.50
6.49
2.05
2.04
1.97
1.96
1.29
1.22
1.21
1.10
1.08
1.06
0.93
0.91
0.88
259s
n-Pr
n-Pr
CHO
Cl
N
N
1.00
0.97
0.89
0.86
0.84
0.89
0.89
4.31
4.69
5.60
f1 (ppm)

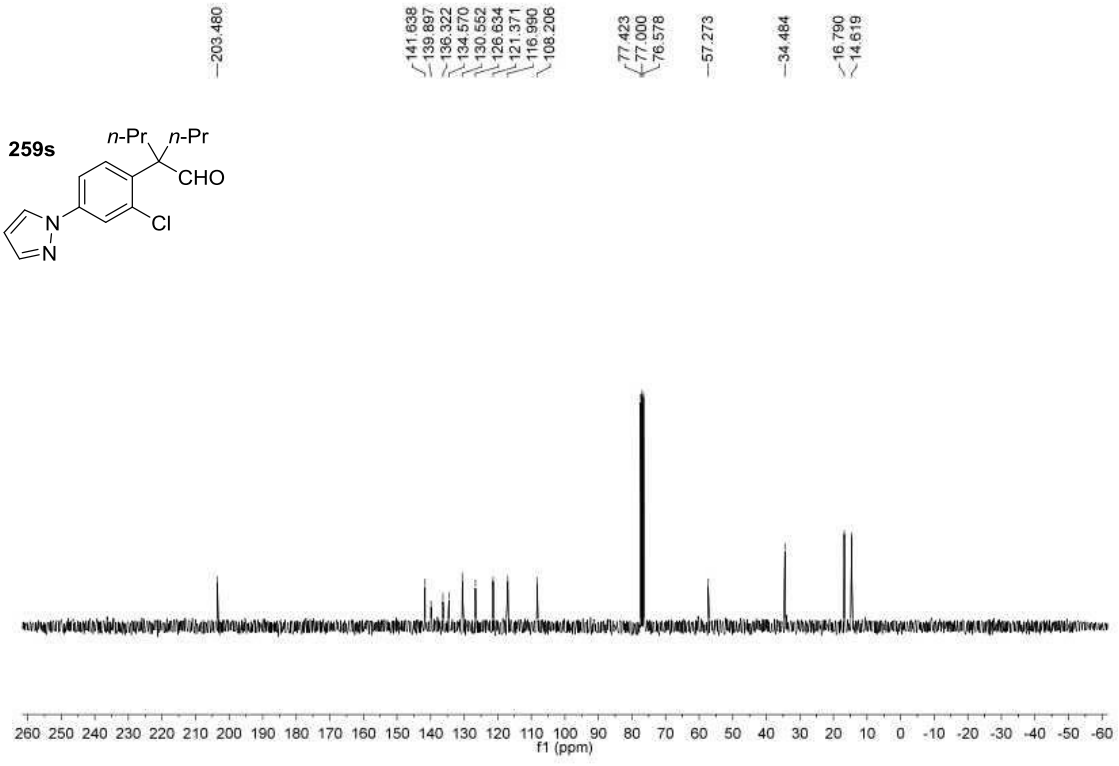
203.480
141.638
139.897
136.322
134.570
130.552
126.634
121.371
116.990
108.206
77.423
77.000
76.578
57.273
34.484
16.790
14.619
259s
n-Pr
n-Pr
CHO
Cl
N
N
f1 (ppm)

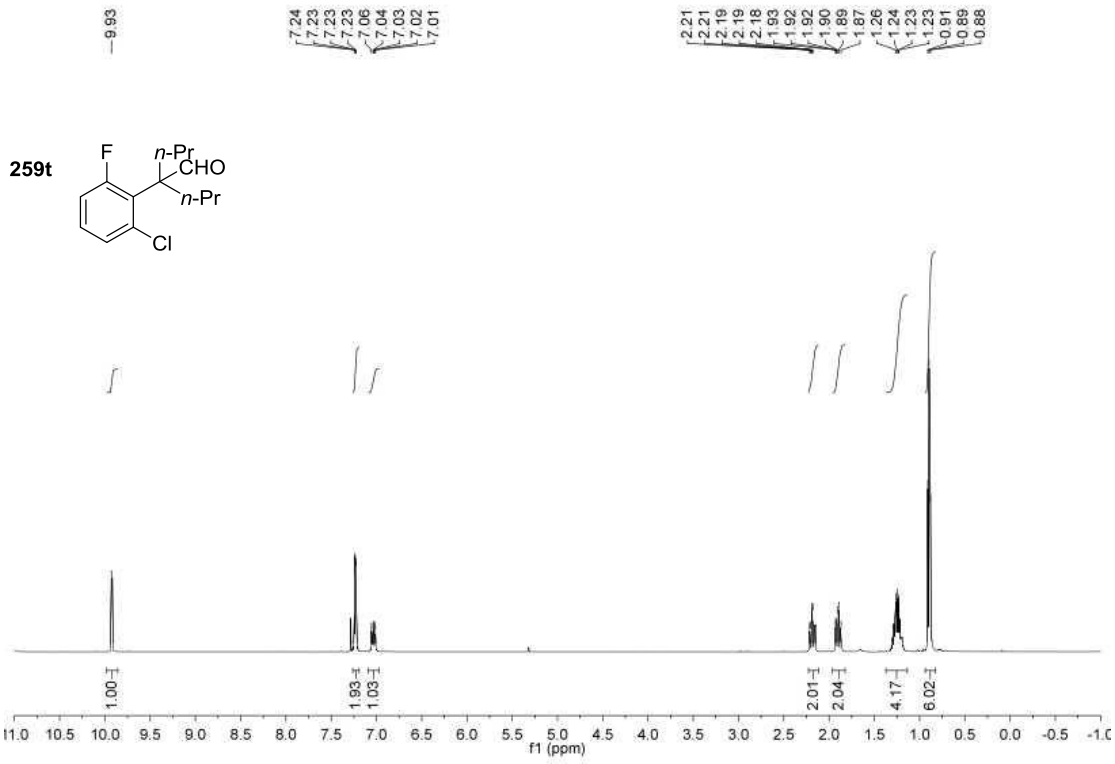
9.93
7.24
7.23
7.23
7.23
7.06
7.04
7.03
7.02
7.01
2.21
2.21
2.19
2.19
2.18
1.93
1.92
1.92
1.90
1.89
1.87
1.26
1.24
1.23
1.23
0.91
0.89
0.88
259t
F
n-Pr
CHO
n-Pr
Cl
1.00
1.93
1.03
2.01
2.04
4.17
6.02
f1 (ppm)

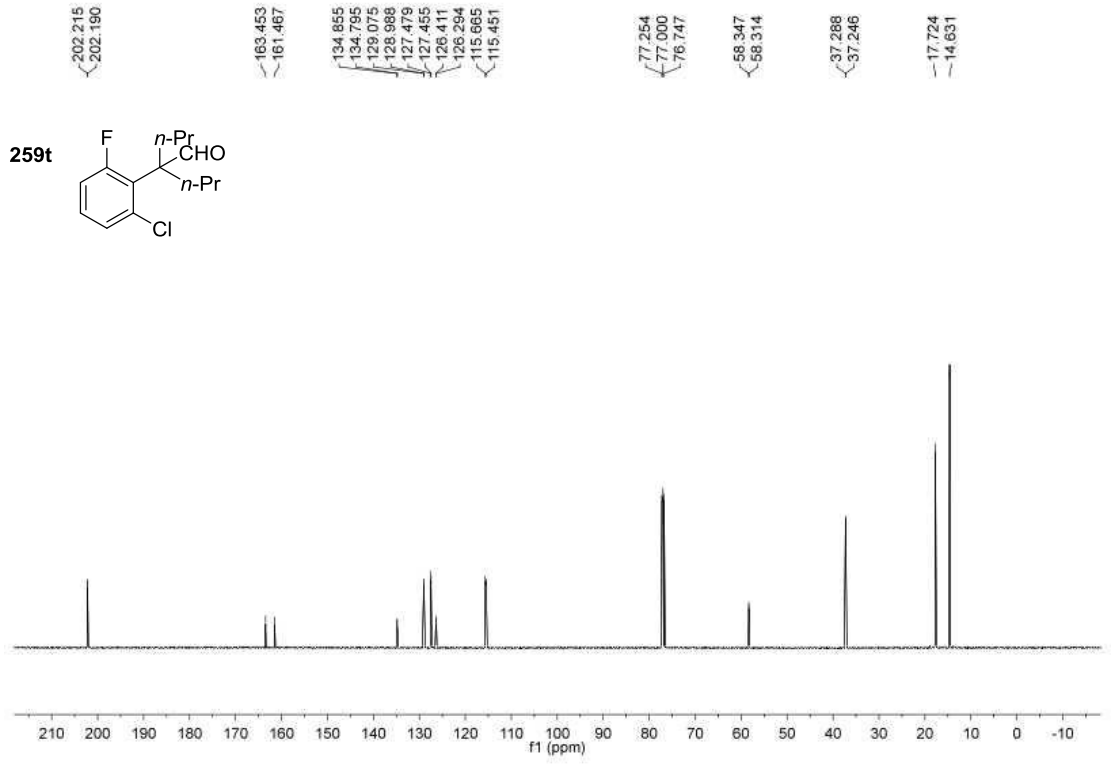
202.215
202.190
163.453
161.467
134.855
134.795
129.075
128.988
127.479
127.455
126.411
126.294
115.665
115.451
77.254
77.000
76.747
58.347
58.314
37.288
37.246
17.724
14.631
259t
F
n-Pr
CHO
n-Pr
Cl
f1 (ppm)

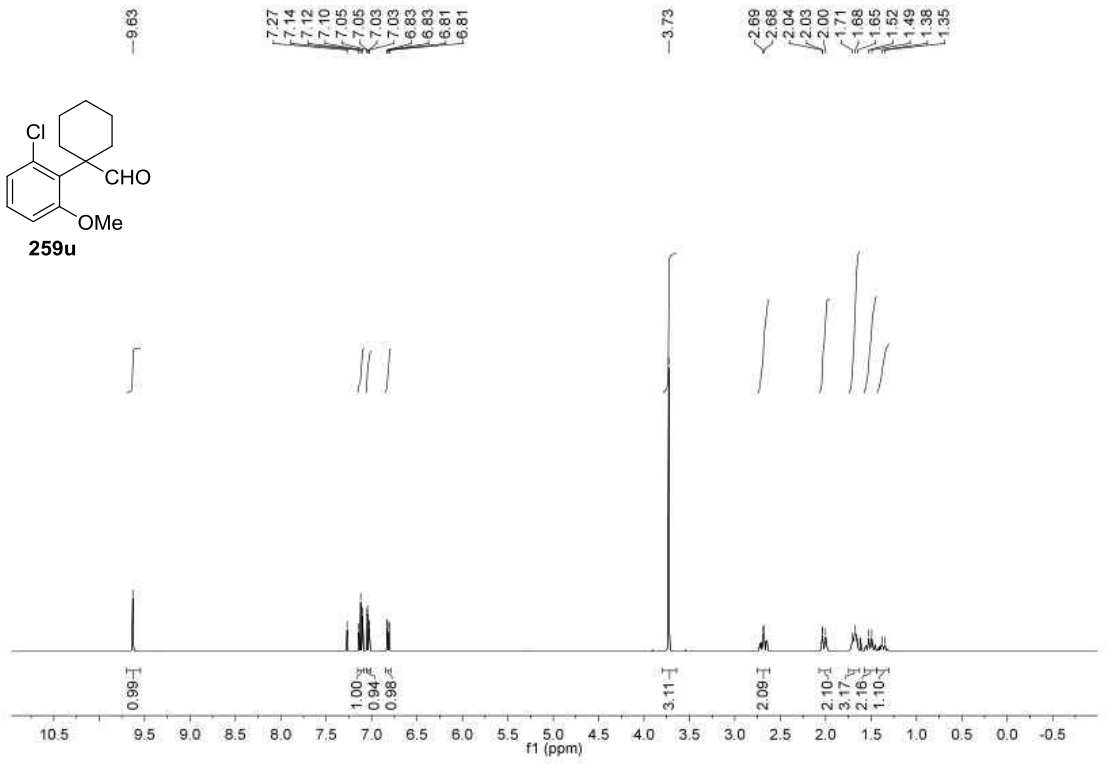
9.63
7.27
7.14
7.12
7.10
7.05
7.05
7.03
7.03
6.83
6.83
6.81
6.81
3.73
2.69
2.68
2.04
2.03
2.00
1.71
1.68
1.65
1.52
1.49
1.38
1.35
Cl
CHO
OMe
259u
0.99
1.00
0.94
0.98
3.11
2.09
2.10
3.17
2.16
1.10
f1 (ppm)

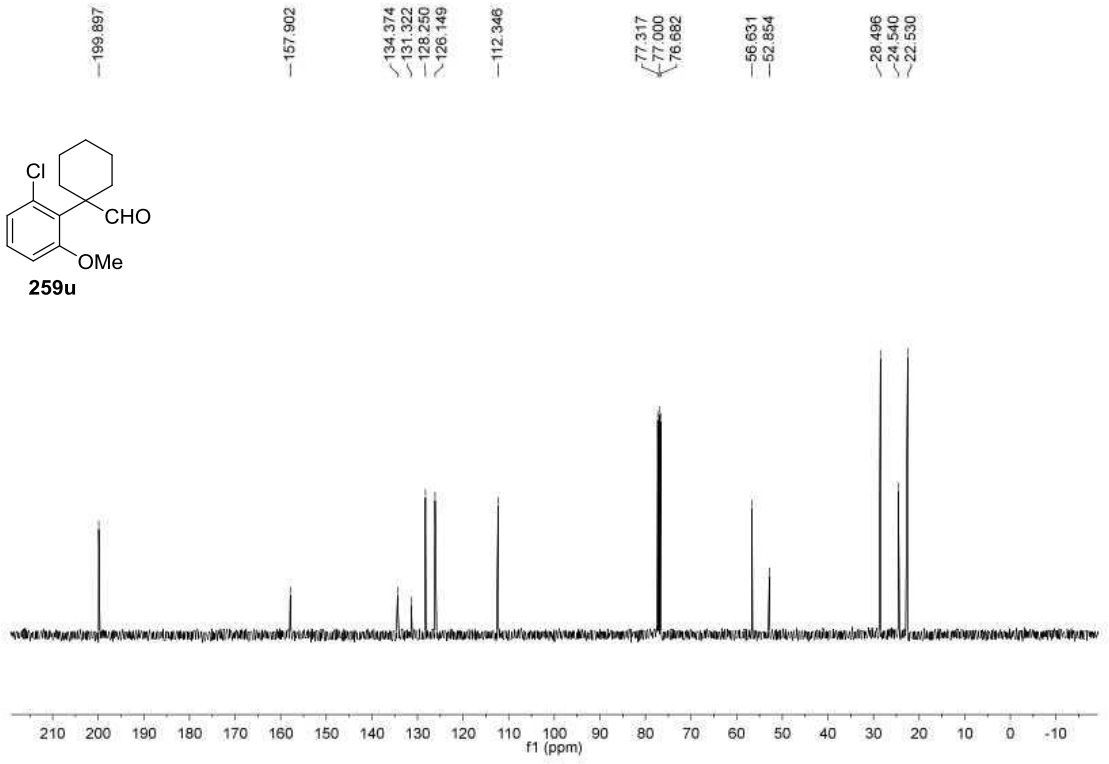
199.897
157.902
134.374
131.322
128.250
126.149
112.346
77.317
77.000
76.682
56.631
52.854
28.496
24.540
22.530
Cl
CHO
OMe
259u
f1 (ppm)

259ii

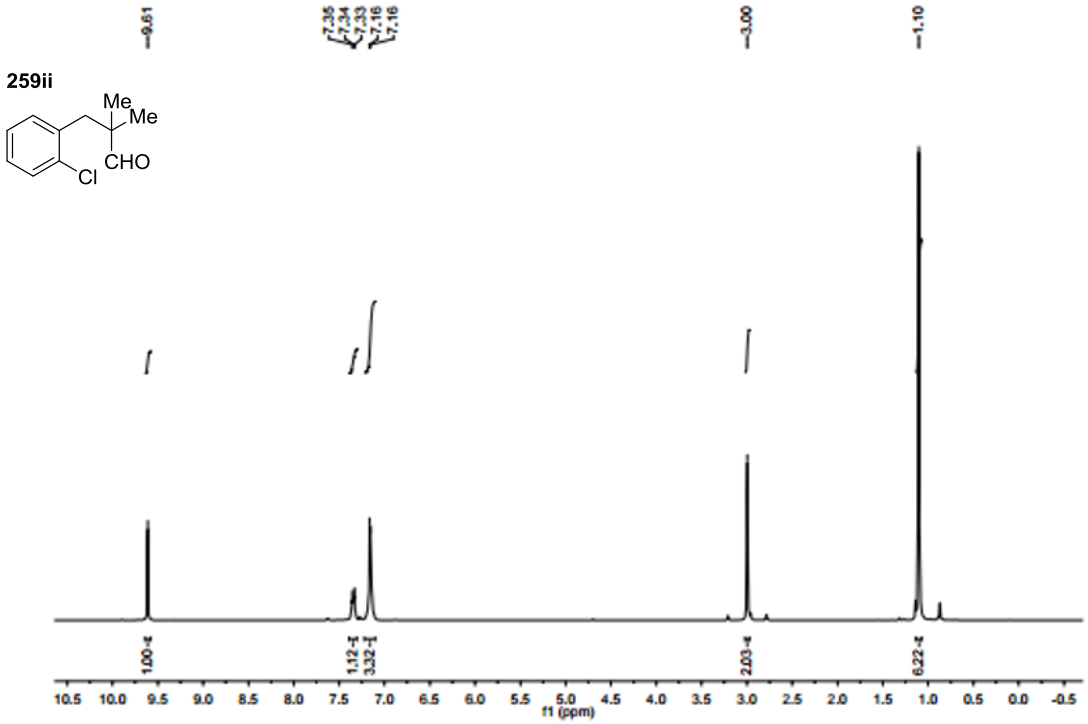
9.61
7.35
7.34
7.33
7.16
7.16
3.00
1.10
1.00
1.12
3.32
2.03
6.22
f1 (ppm)

259ii

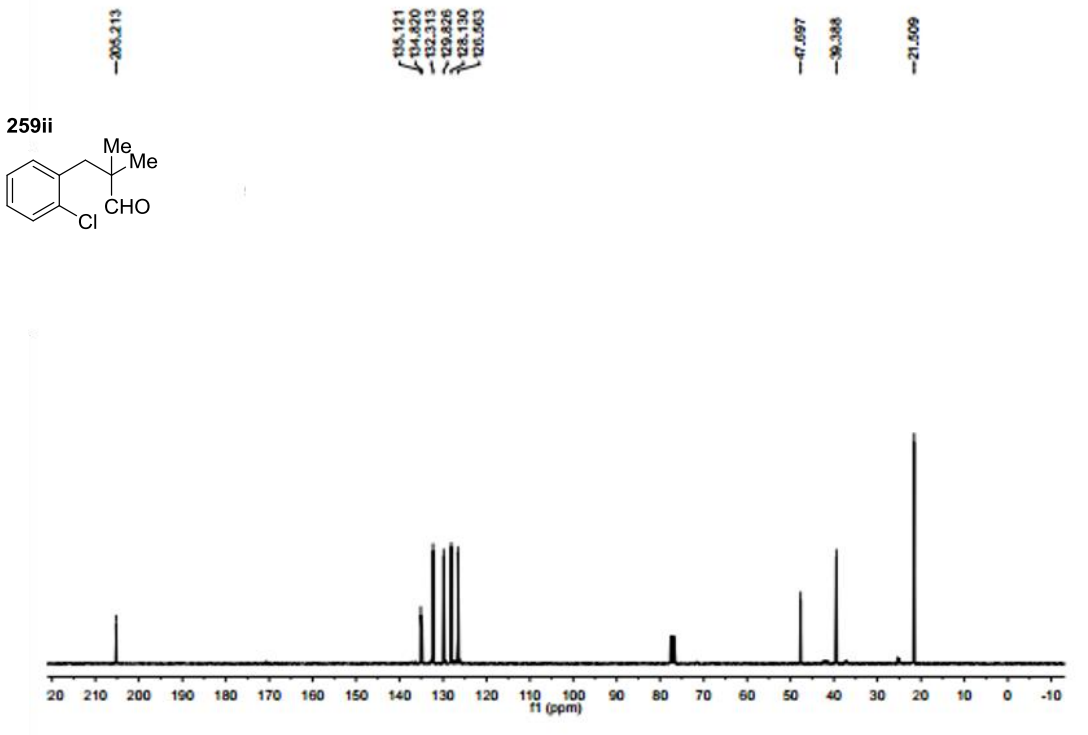
206.213
135.121
134.820
132.313
129.826
128.130
126.563
47.697
39.388
21.509
f1 (ppm)

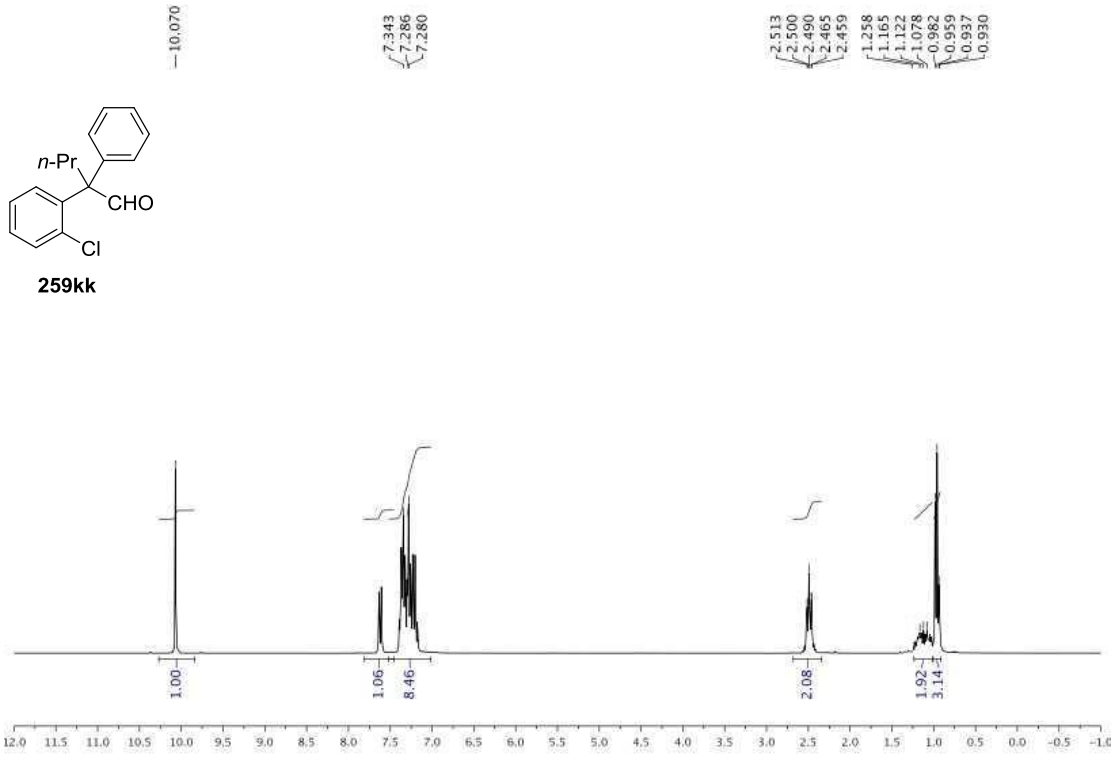
10.070
7.343
7.286
7.280
2.513
2.500
2.490
2.465
2.459
1.258
1.165
1.122
1.078
0.982
0.959
0.937
0.930
n-Pr
CHO
Cl
1.00
1.06
8.46
2.08
1.92
3.14

259kk

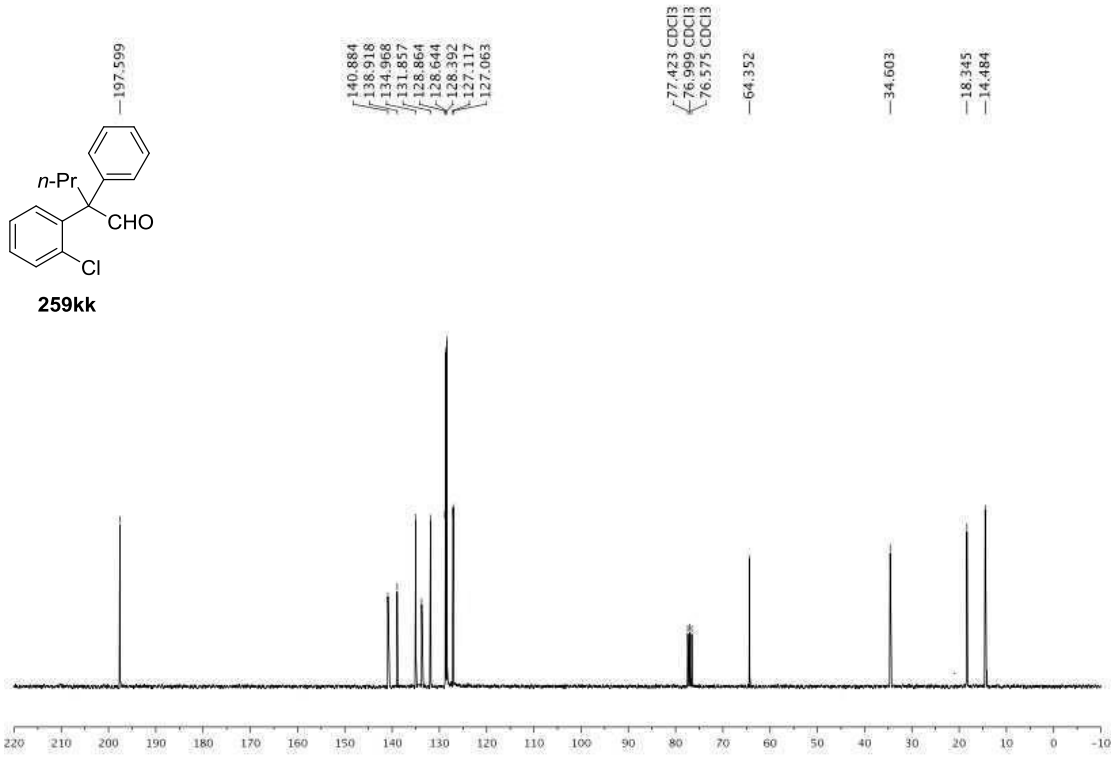
197.599
140.884
138.918
134.968
131.857
128.864
128.644
128.392
127.117
127.063
77.423 CDCl3
76.999 CDCl3
76.575 CDCl3
64.352
34.603
18.345
14.484
n-Pr
CHO
Cl

259kk

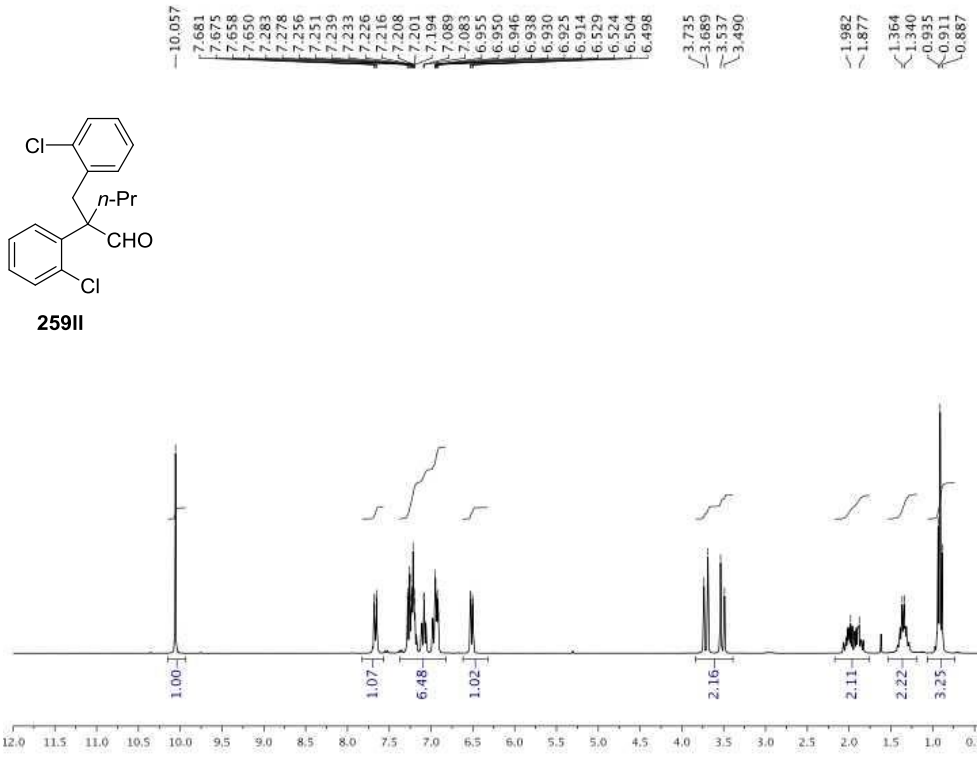
10.057
7.681
7.675
7.658
7.650
7.283
7.278
7.256
7.251
7.239
7.233
7.226
7.216
7.208
7.201
7.194
7.089
7.083
6.955
6.950
6.946
6.938
6.930
6.925
6.914
6.529
6.524
6.504
6.498
3.735
3.689
3.537
3.490
1.982
1.877
1.364
1.340
0.935
0.911
0.887
Cl
n-Pr
CHO
Cl
1.00
1.07
6.48
1.02
2.16
2.11
2.22
3.25

259ll

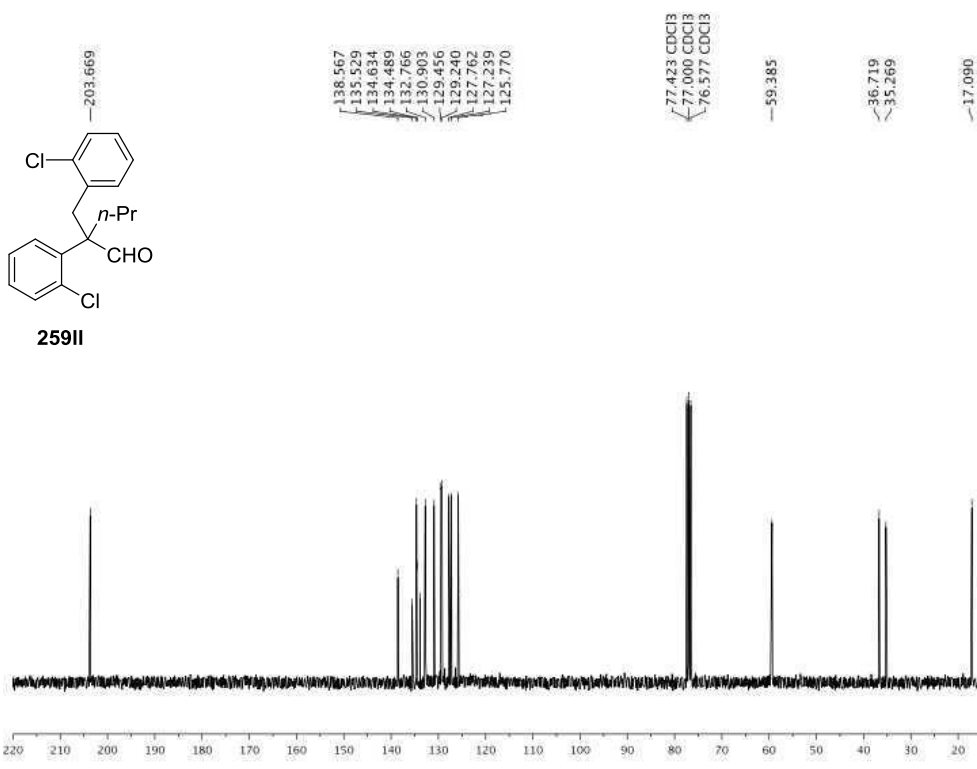
203.669
138.567
135.529
134.634
134.489
132.766
130.903
129.456
129.240
127.762
127.239
125.770
77.423 CDCl3
77.000 CDCl3
76.577 CDCl3
59.385
36.719
35.269
17.090
14.751
Cl
n-Pr
CHO
Cl

259ll

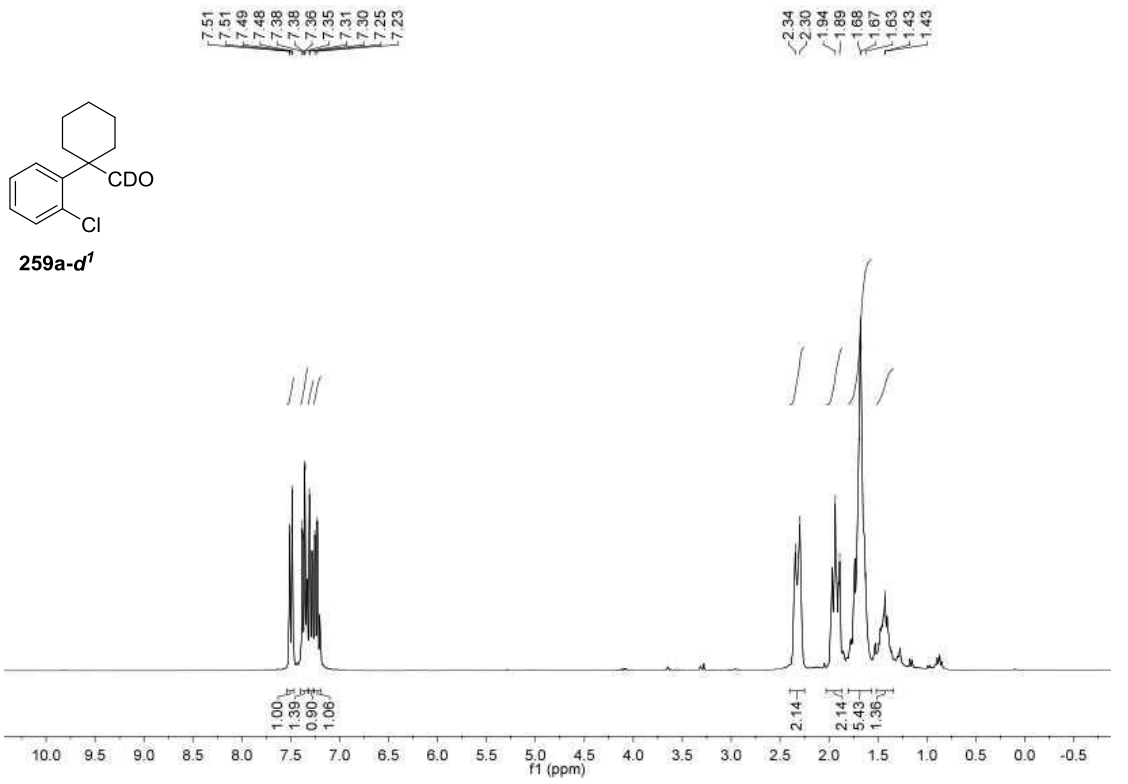

259a-*d*[1]

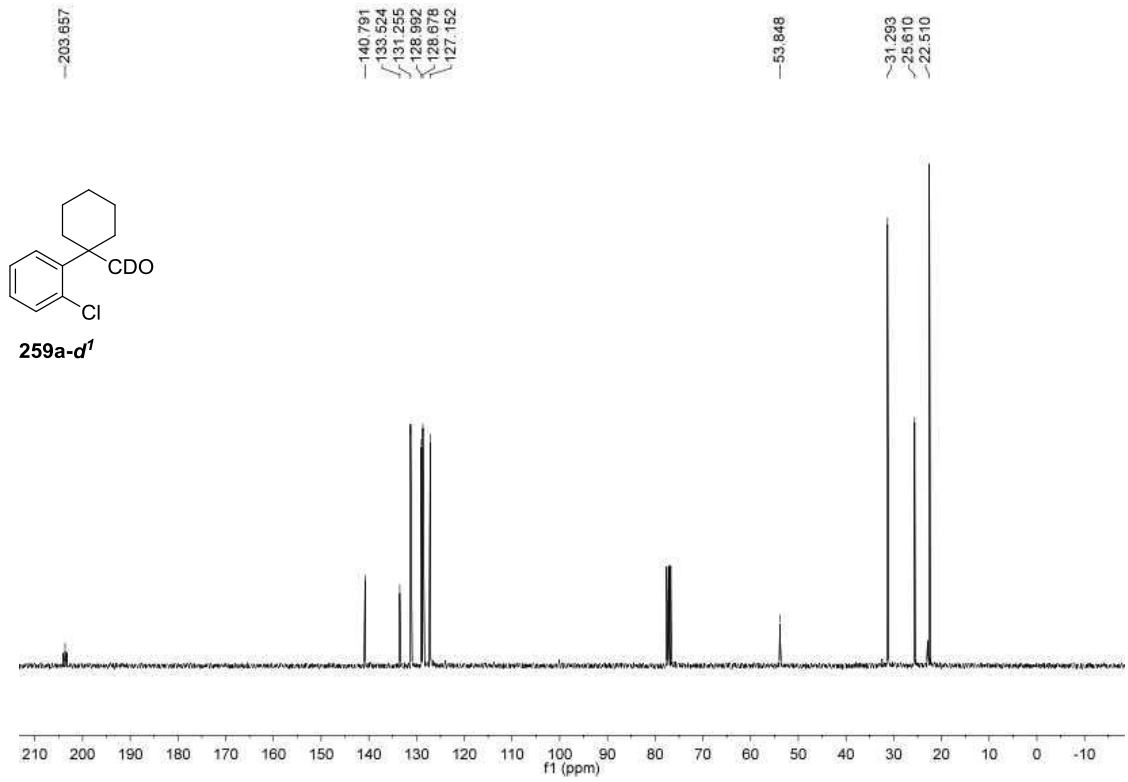

259a-*d*[1]

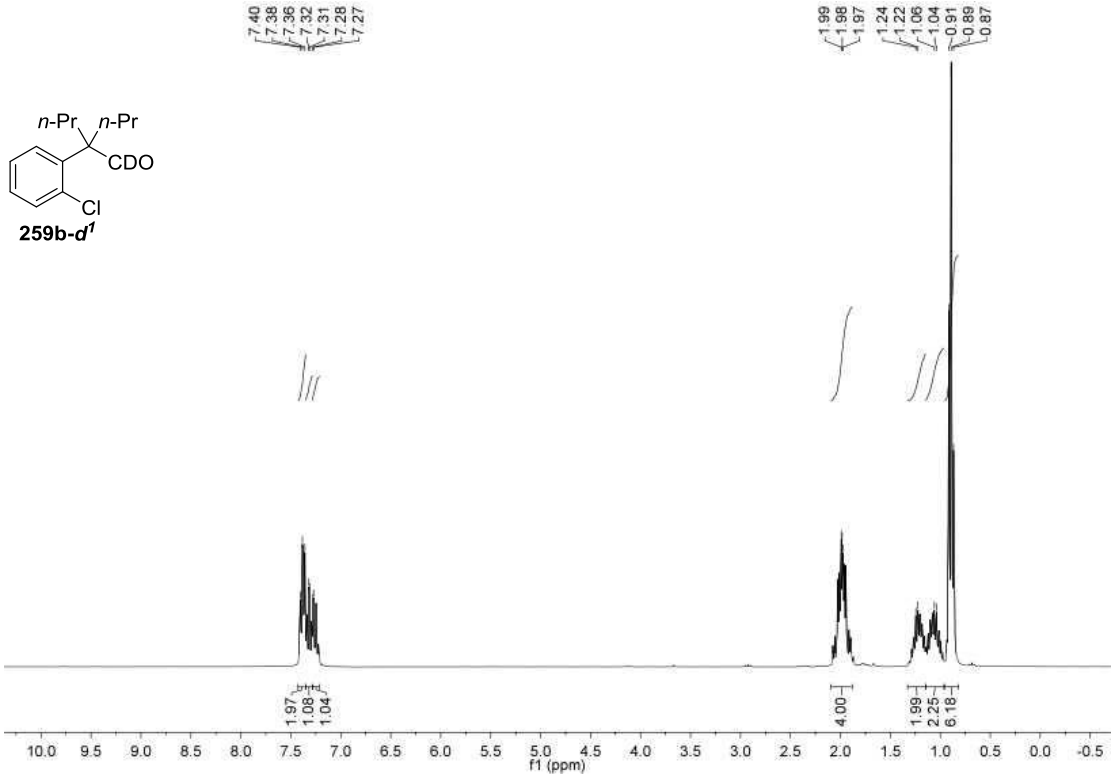
7.40
7.38
7.36
7.32
7.31
7.28
7.27
1.99
1.98
1.97
1.24
1.22
1.06
1.04
0.91
0.89
0.87
n-Pr
n-Pr
CDO
Cl
259b-d1
1.97
1.08
1.04
4.00
1.99
2.25
6.18
f1 (ppm)

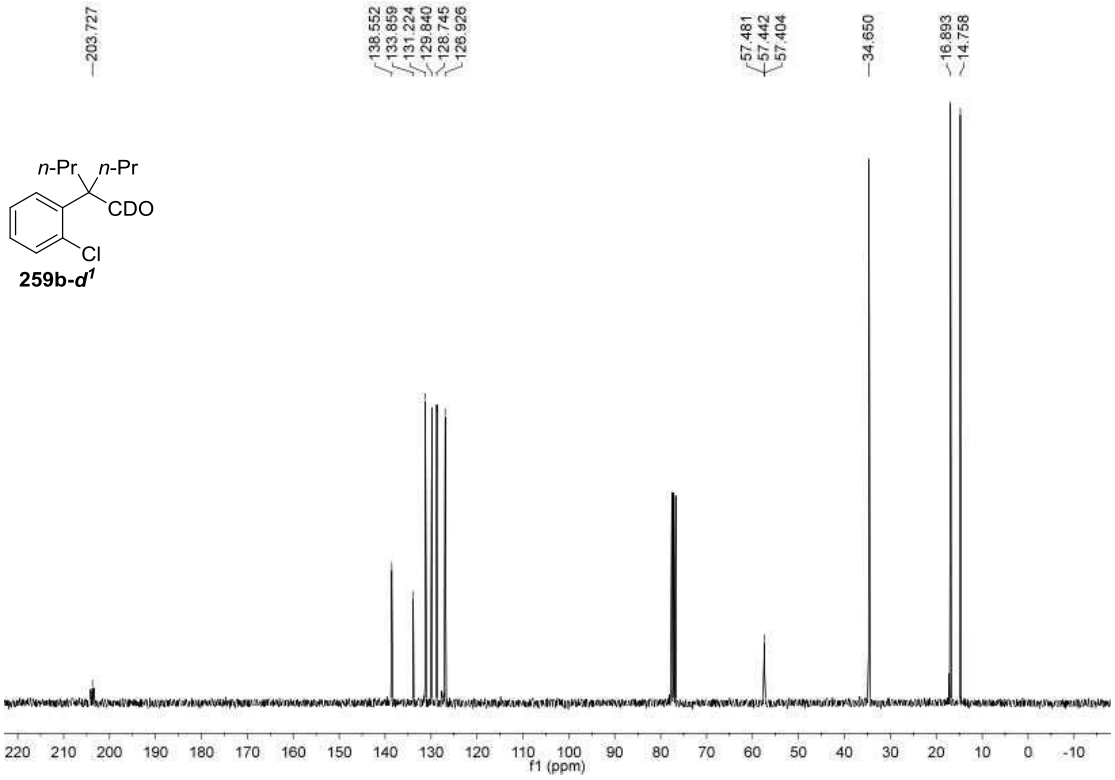
203.727
138.552
133.859
131.224
129.840
128.745
126.926
57.481
57.442
57.404
34.650
16.893
14.758
n-Pr
n-Pr
CDO
Cl
259b-d1
f1 (ppm)

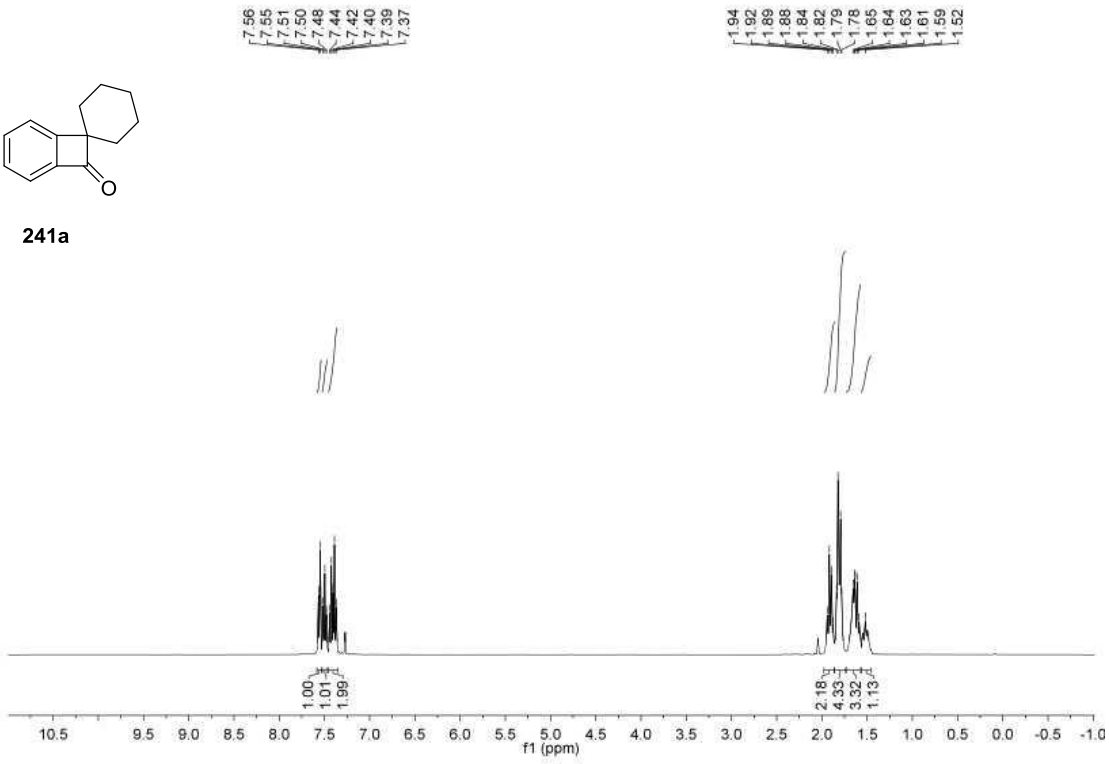
7.56
7.55
7.51
7.50
7.48
7.44
7.42
7.40
7.39
7.37
1.94
1.92
1.89
1.88
1.84
1.82
1.79
1.78
1.65
1.64
1.63
1.61
1.59
1.52
O
1.00
1.01
1.99
2.18
4.33
3.32
1.13
f1 (ppm)

241a

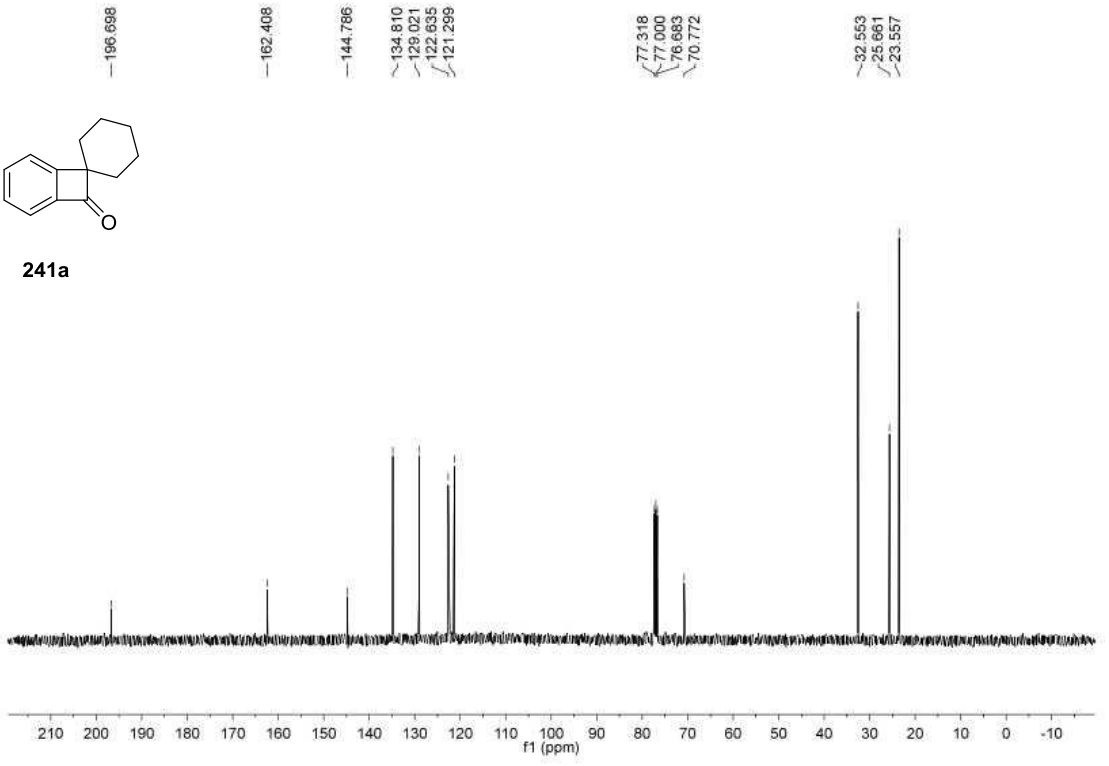
196.698
162.408
144.786
134.810
129.021
122.635
121.299
77.318
77.000
76.683
70.772
32.553
25.661
23.557
O
f1 (ppm)

241a

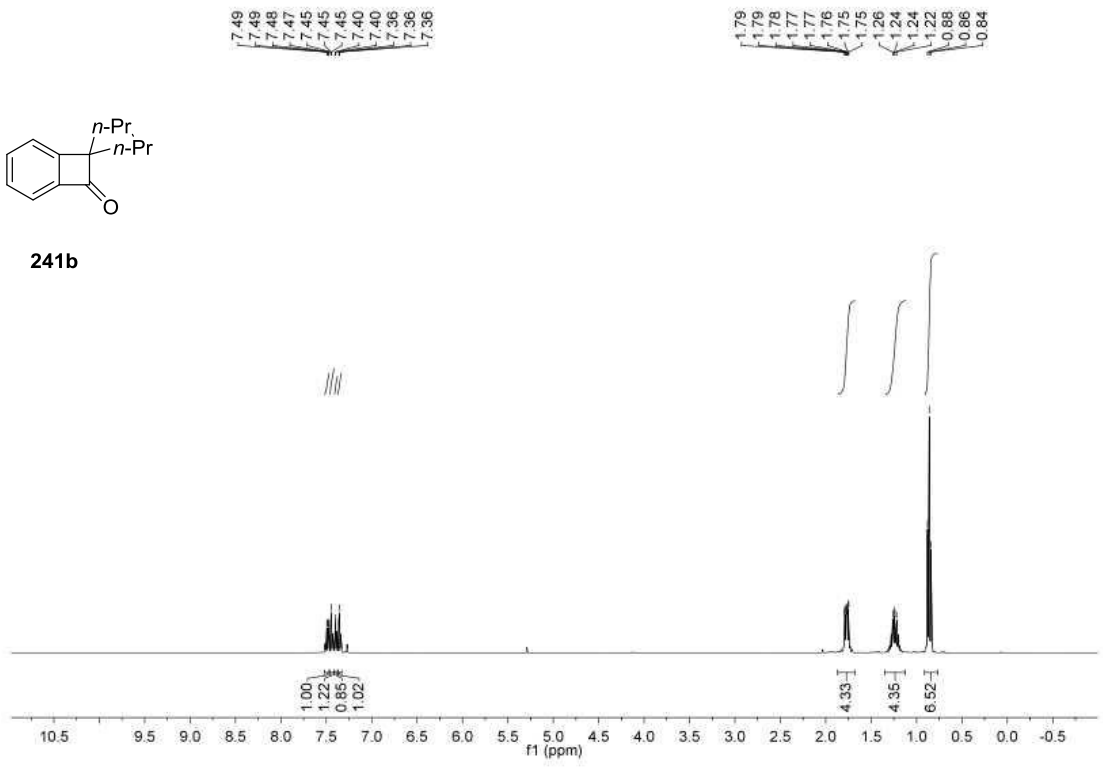
7.49
7.49
7.48
7.47
7.45
7.45
7.45
7.40
7.40
7.36
7.36
7.36
1.79
1.79
1.78
1.77
1.77
1.76
1.75
1.75
1.26
1.24
1.24
1.22
0.88
0.86
0.84
n-Pr
n-Pr
O
241b
1.00
1.22
0.85
1.02
4.33
4.35
6.52
f1 (ppm)

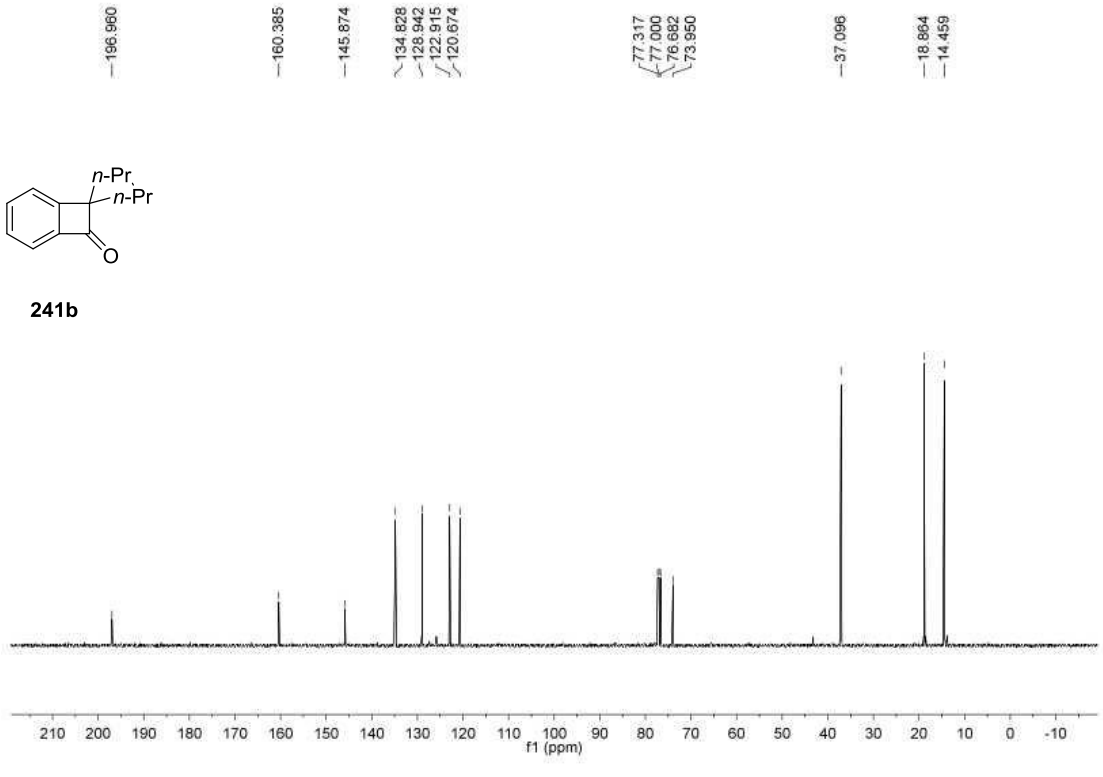
196.960
160.385
145.874
134.828
128.942
122.915
120.674
77.317
77.000
76.682
73.950
37.096
18.864
14.459
n-Pr
n-Pr
O
241b
f1 (ppm)

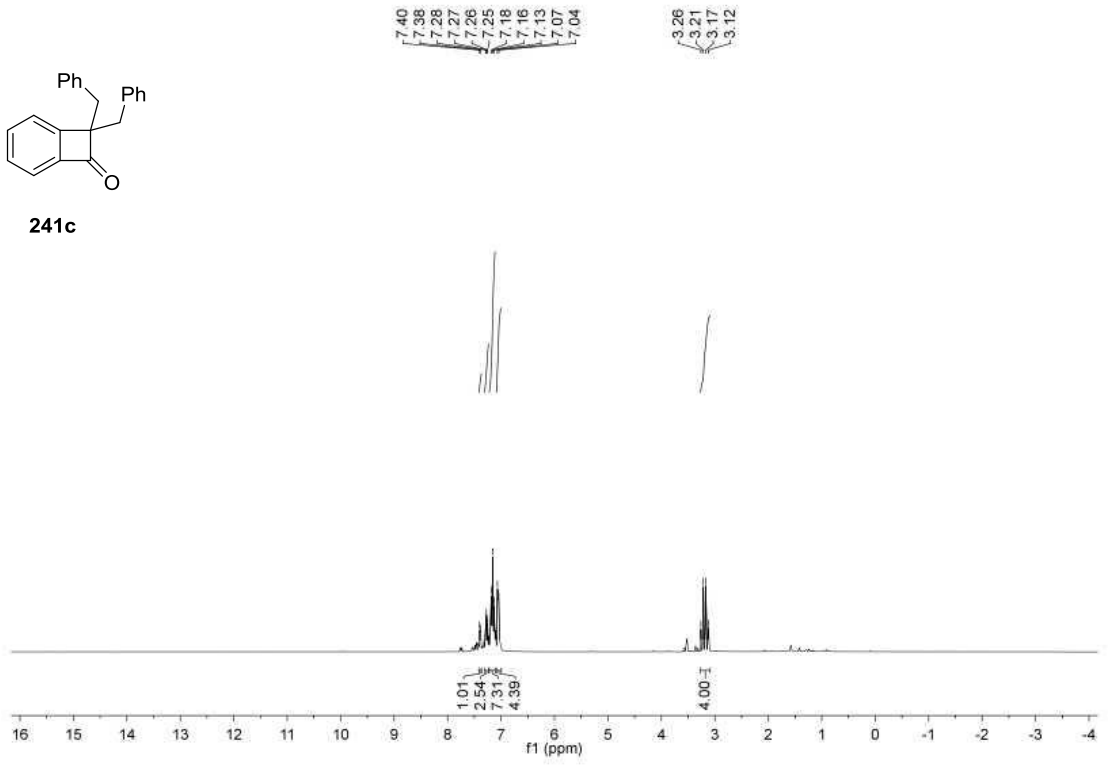
7.40
7.38
7.28
7.27
7.26
7.25
7.18
7.16
7.13
7.07
7.04
3.26
3.21
3.17
3.12
Ph
Ph
O
1.01
2.54
7.31
4.39
4.00
f1 (ppm)

241c

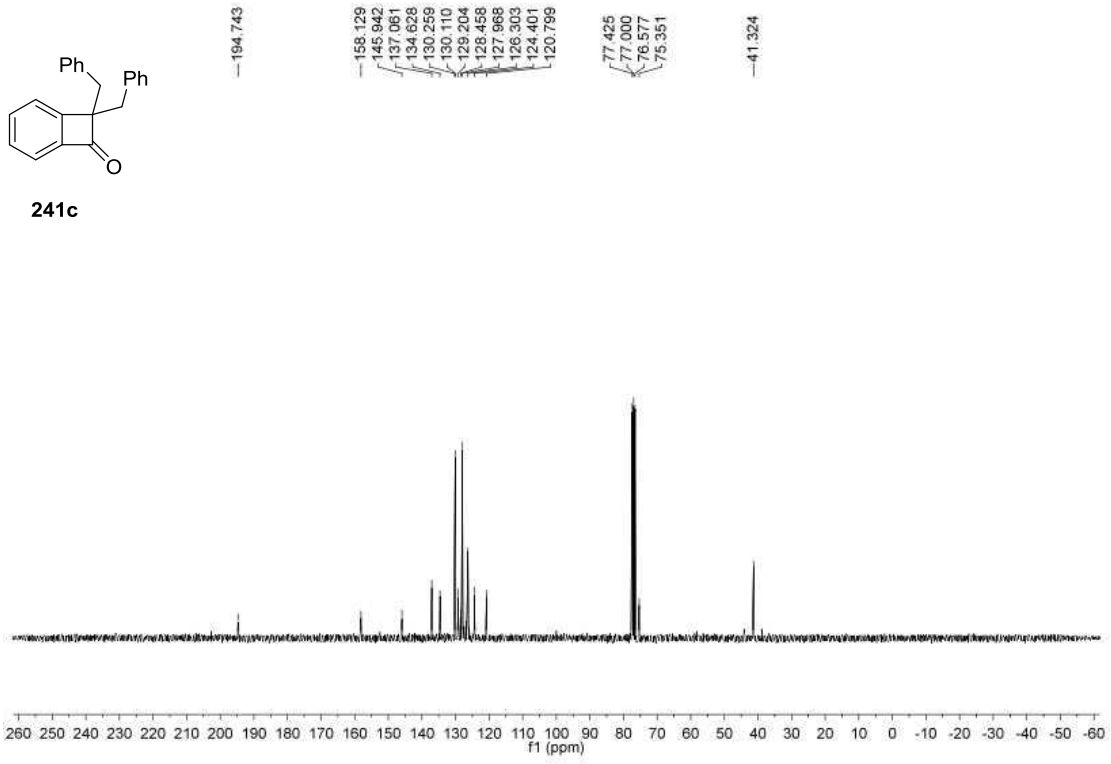
194.743
158.129
145.942
137.061
134.628
130.259
130.110
129.204
128.458
127.968
126.303
124.401
120.799
77.425
77.000
76.577
75.351
41.324
Ph
Ph
O
f1 (ppm)

241c


7.484
7.481
7.469
7.467
7.397
7.384
7.382
7.369
7.367
7.356
7.354
7.352
7.339
7.315
7.313
7.311
7.298
7.286
7.282
7.273
7.269
7.066
7.062
7.054
7.050
6.670
6.948
6.938
5.728
5.694
5.224
5.222
5.202
5.200
3.123
1.853
1.843
1.808
1.794
1.784
1.293
1.196
0.889
0.875
0.860

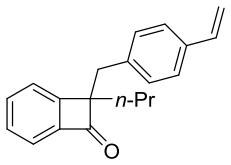
n-Pr
O

241d

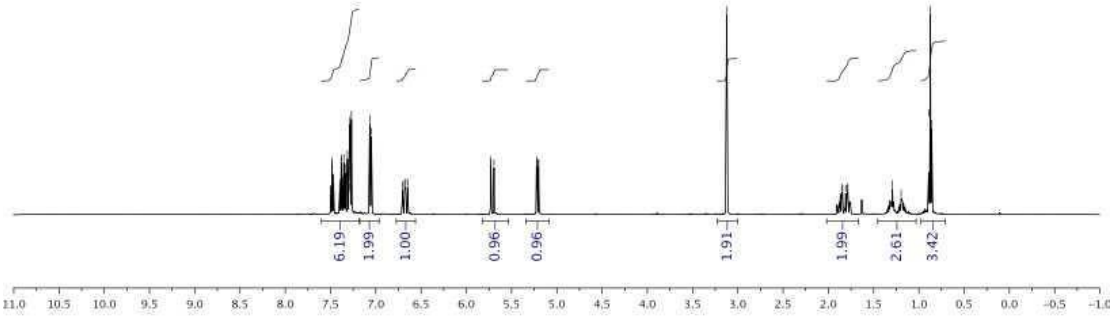
6.19
1.99
1.00
0.96
0.96
1.91
1.99
2.61
3.42
11.0
10.5
10.0
9.5
9.0
8.5
8.0
7.5
7.0
6.5
6.0
5.5
5.0
4.5
4.0
3.5
3.0
2.5
2.0
1.5
1.0
0.5
0.0
-0.5


195.875
159.333
145.831
136.525
134.808
130.187
129.188
125.836
123.691
120.867
113.268
77.253 CDCl3
76.999 CDCl3
76.744 CDCl3
74.482
41.166
36.662
19.038
14.413

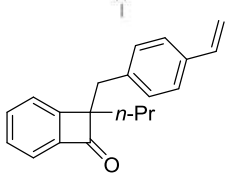
n-Pr
O

241d

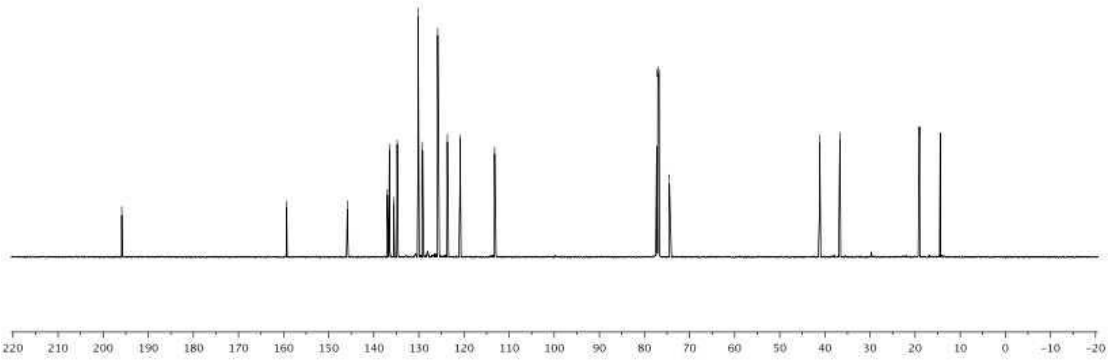
220
210
200
190
180
170
160
150
140
130
120
110
100
90
80
70
60
50
40
30
20
10
0
-10
-20

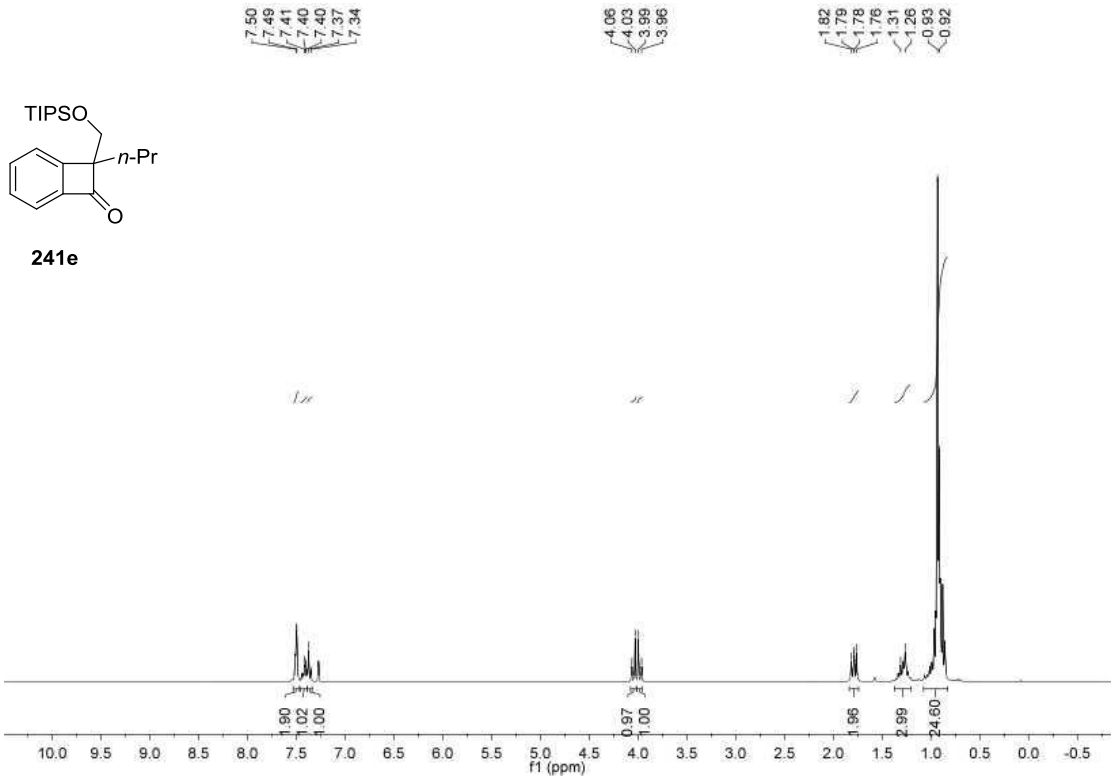
7.50
7.49
7.41
7.40
7.40
7.37
7.34
4.06
4.03
3.99
3.96
1.82
1.79
1.78
1.76
1.31
1.26
0.93
0.92
TIPSO
n-Pr
O
241e
1.90
1.02
1.00
0.97
1.00
1.96
2.99
24.60
f1 (ppm)

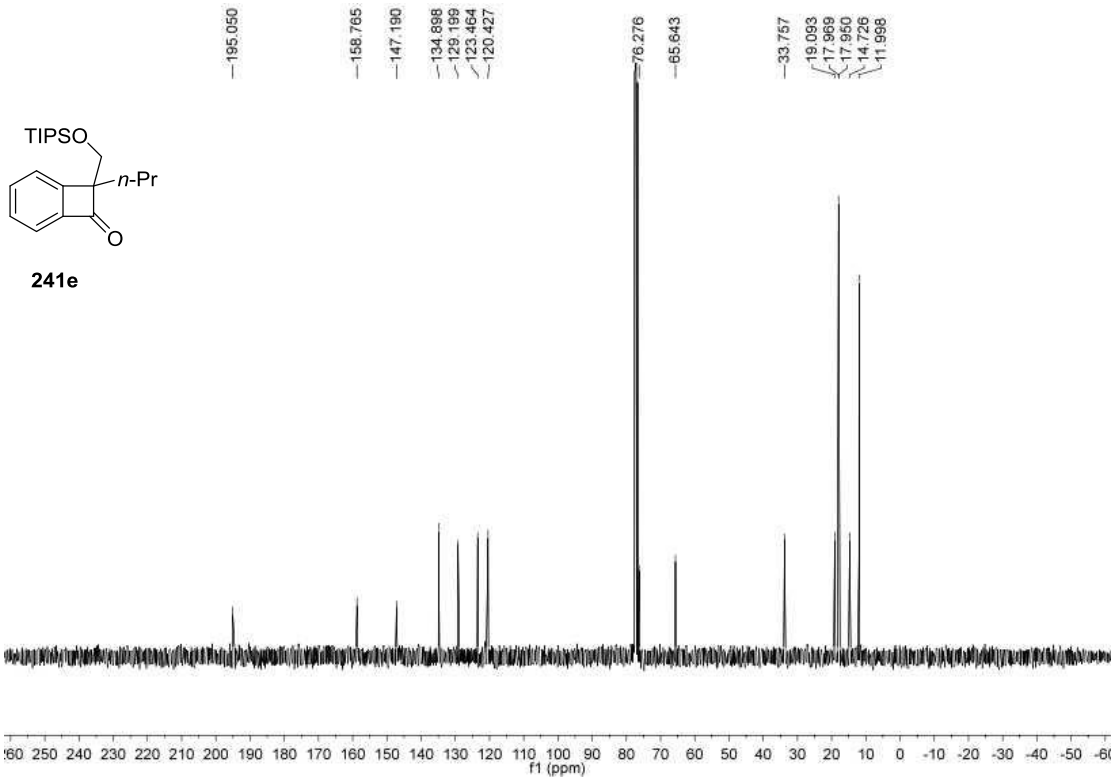
195.050
158.785
147.190
134.898
129.199
123.464
120.427
76.276
65.643
33.757
19.093
17.969
17.950
14.726
11.998
TIPSO
n-Pr
O
241e
f1 (ppm)

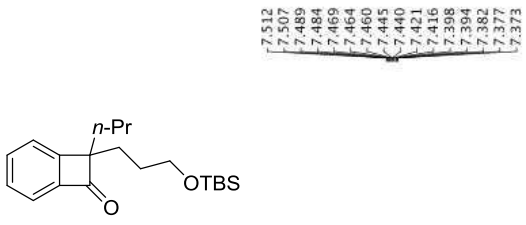
n-Pr
OTBS
O

241f

7.512
7.507
7.489
7.484
7.469
7.464
7.460
7.445
7.440
7.421
7.416
7.398
7.394
7.382
7.377
7.373
3.555
3.533
1.852
1.847
1.824
1.819
1.804
1.800
1.786
1.765
1.487
0.875
0.868
0.013
0.007
3.99
2.00
4.10
4.58
12.16
5.84

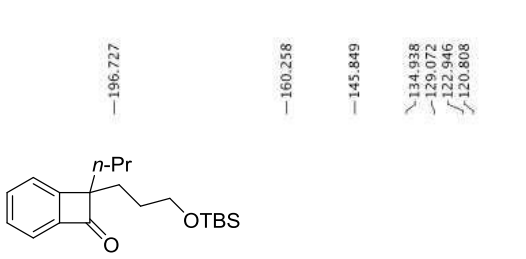
n-Pr
OTBS
O

241f

196.727
160.258
145.849
134.938
129.072
122.946
120.808
77.424 CDCl3
77.000 CDCl3
76.576 CDCl3
73.514
63.188
37.077
31.104
28.792
25.905
25.881
18.881
18.280
14.474
-5.345

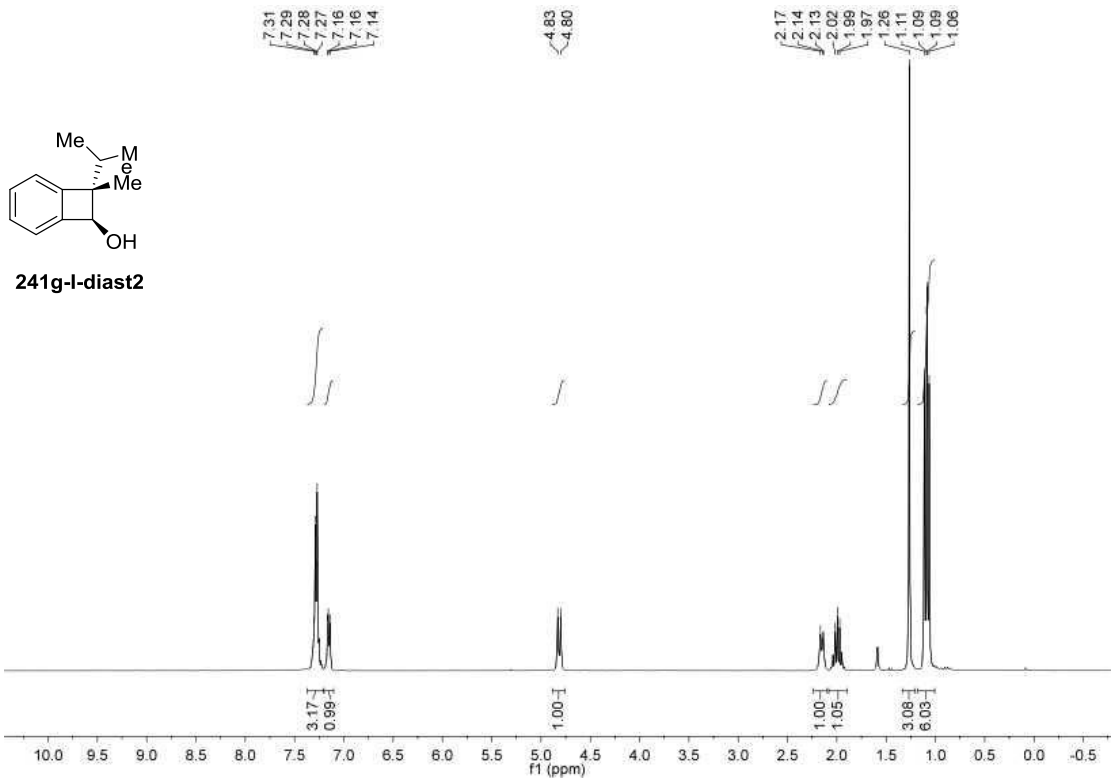
7.31
7.29
7.28
7.27
7.16
7.16
7.14
4.83
4.80
2.17
2.14
2.13
2.02
1.99
1.97
1.26
1.11
1.09
1.09
1.06
Me
Me
Me
OH
241g-l-diast2
3.17
0.99
1.00
1.00
1.05
3.08
6.03
f1 (ppm)

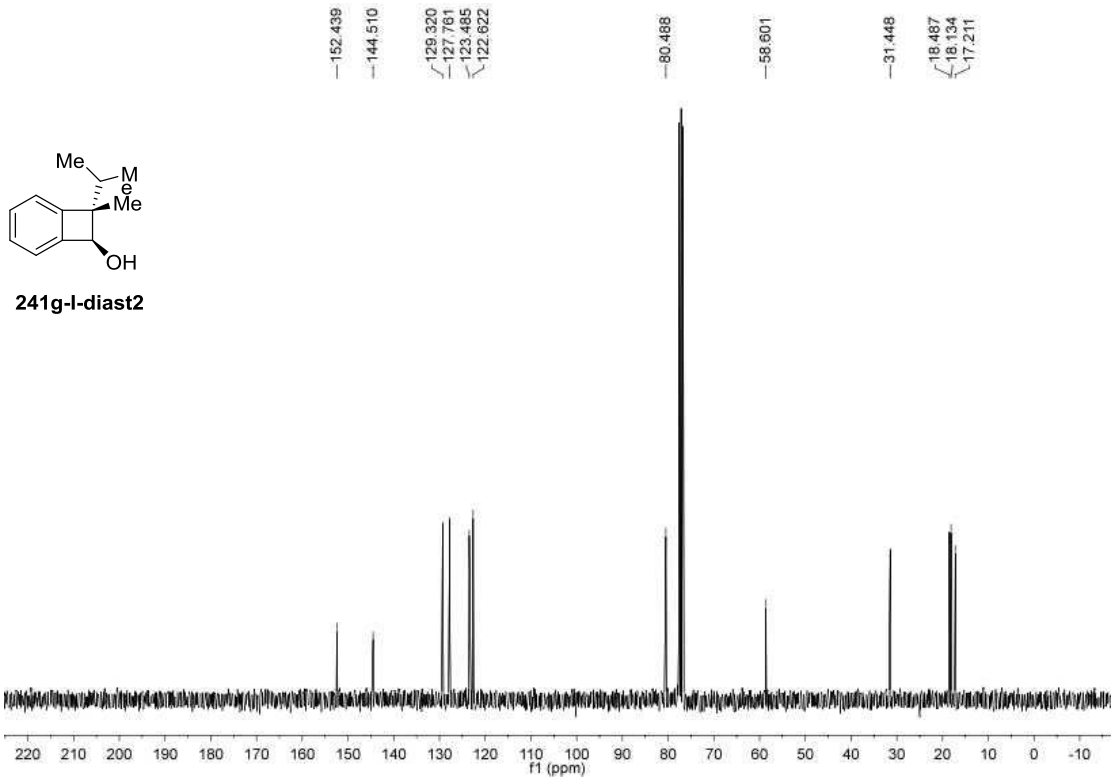
152.439
144.510
129.320
127.761
123.485
122.622
80.488
58.601
31.448
18.487
18.134
17.211
Me
Me
Me
OH
241g-l-diast2
f1 (ppm)

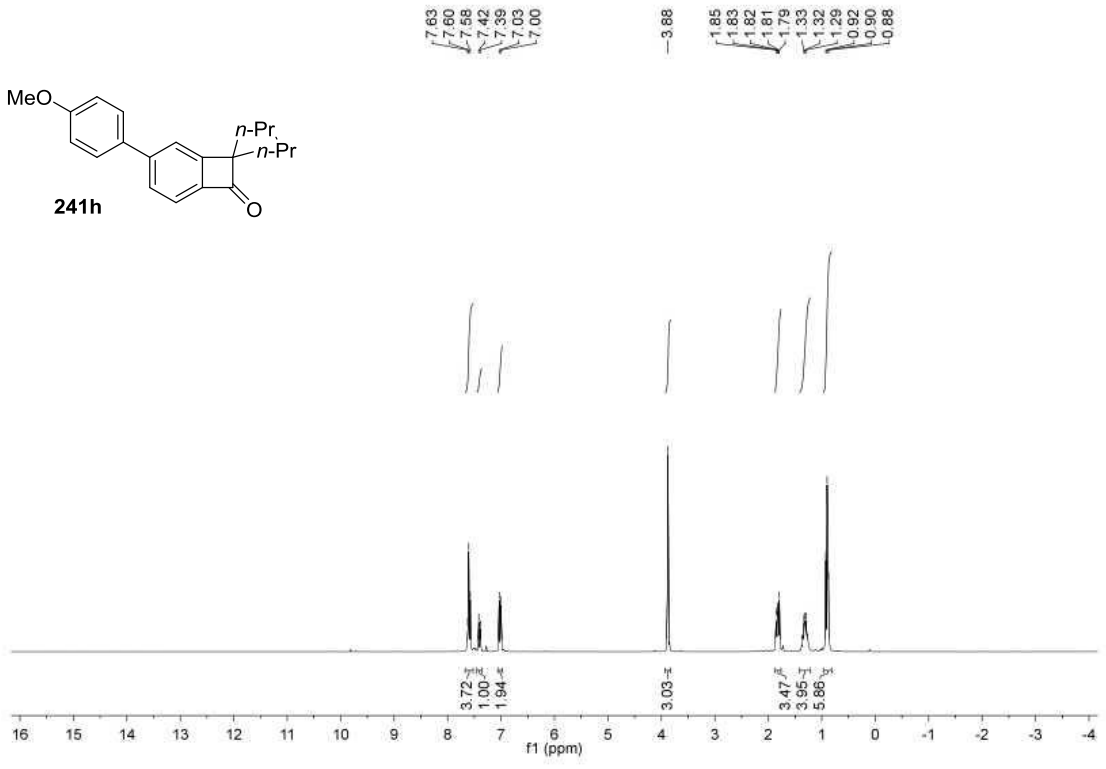
7.63
7.60
7.58
7.42
7.39
7.03
7.00
3.88
1.85
1.83
1.82
1.81
1.79
1.33
1.32
1.29
0.92
0.90
0.88
MeO
n-Pr
n-Pr
O
241h
3.72
1.00
1.94
3.03
3.47
3.95
5.88
f1 (ppm)

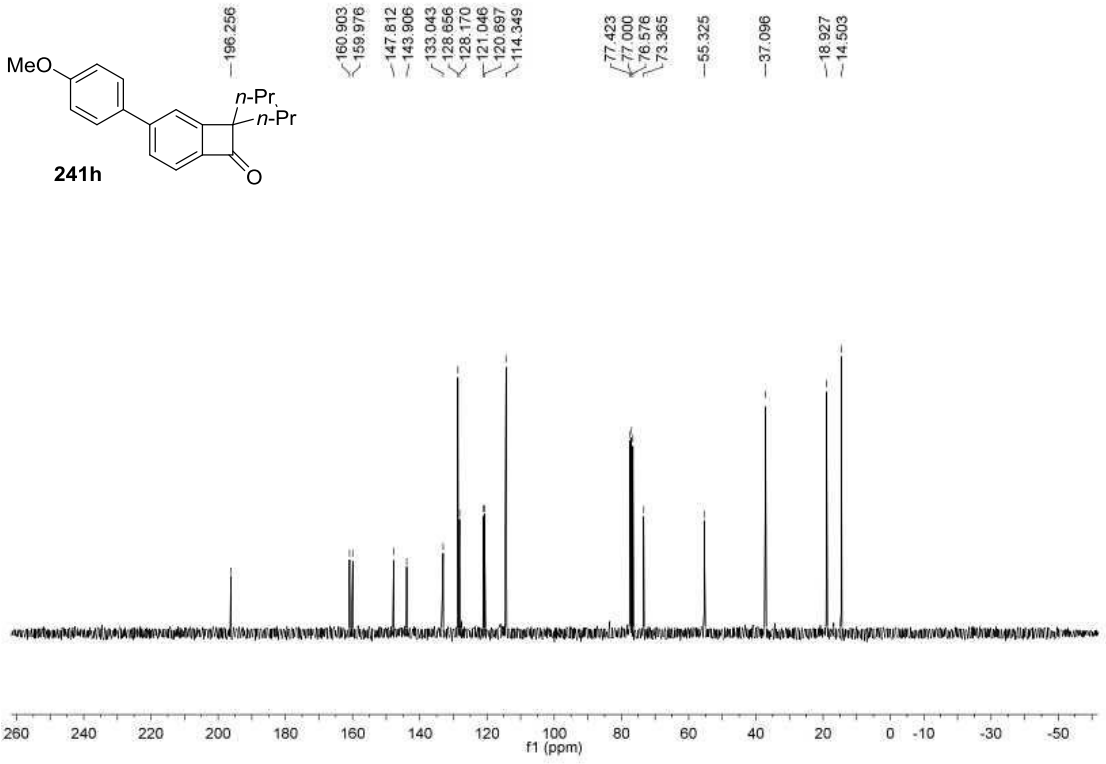
196.256
160.903
159.976
147.812
143.906
133.043
128.656
128.170
121.046
120.697
114.349
77.423
77.000
76.578
73.365
55.325
37.096
18.927
14.503
MeO
n-Pr
n-Pr
O
241h
f1 (ppm)

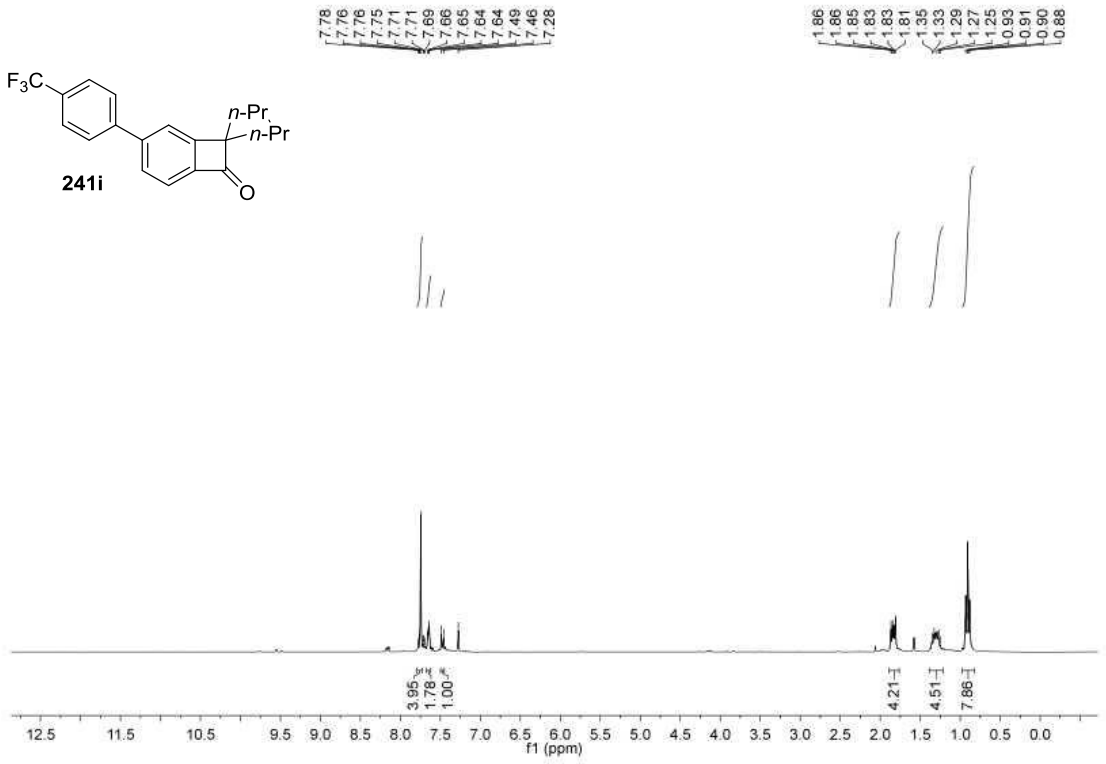
7.78
7.76
7.76
7.75
7.71
7.71
7.69
7.66
7.65
7.64
7.64
7.49
7.46
7.28
1.86
1.86
1.85
1.83
1.83
1.81
1.35
1.33
1.29
1.27
1.25
0.93
0.91
0.90
0.88
F3C
n-Pr
n-Pr
O
241i
3.95
1.78
1.00
4.21
4.51
7.86
f1 (ppm)

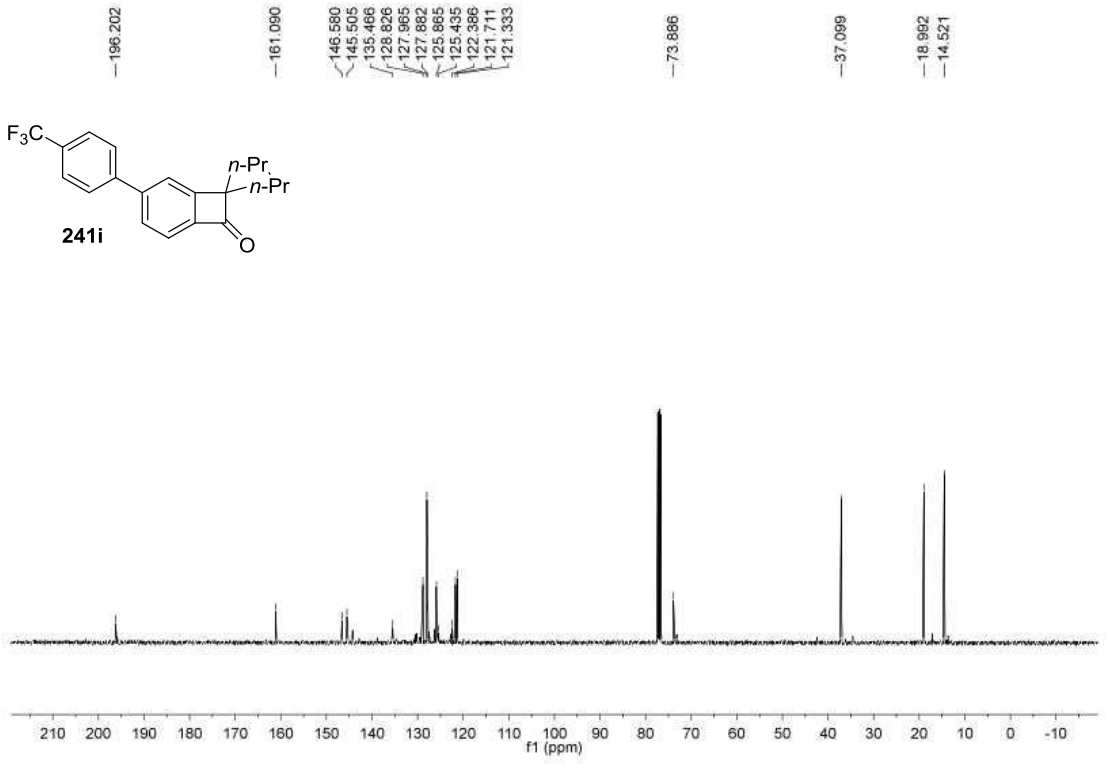
196.202
161.090
146.580
145.505
135.466
128.826
127.965
127.882
125.865
125.435
122.386
121.711
121.333
73.886
37.099
18.992
14.521
F3C
n-Pr
n-Pr
O
241i
f1 (ppm)

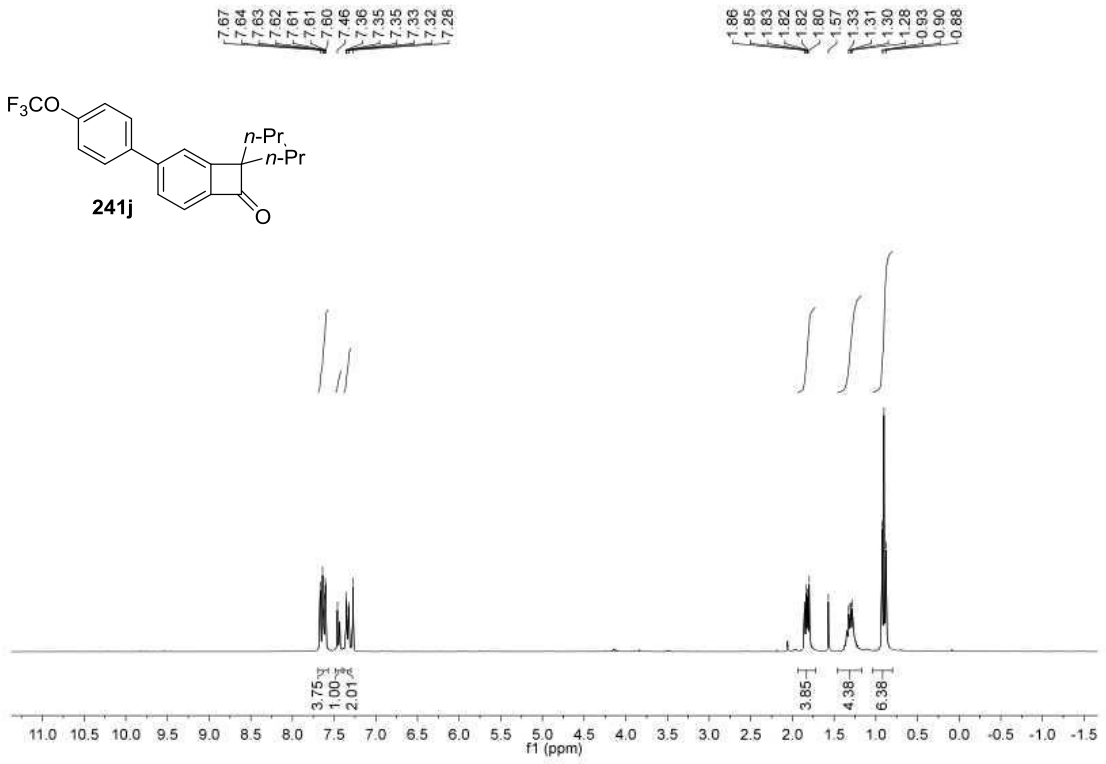
7.67
7.64
7.63
7.62
7.61
7.61
7.60
7.46
7.36
7.35
7.35
7.33
7.32
7.28
1.86
1.85
1.83
1.82
1.82
1.80
1.57
1.33
1.31
1.30
1.28
0.93
0.90
0.88
F3CO
n-Pr
n-Pr
O
241j
3.75
1.00
2.01
3.85
4.38
6.38
f1 (ppm)

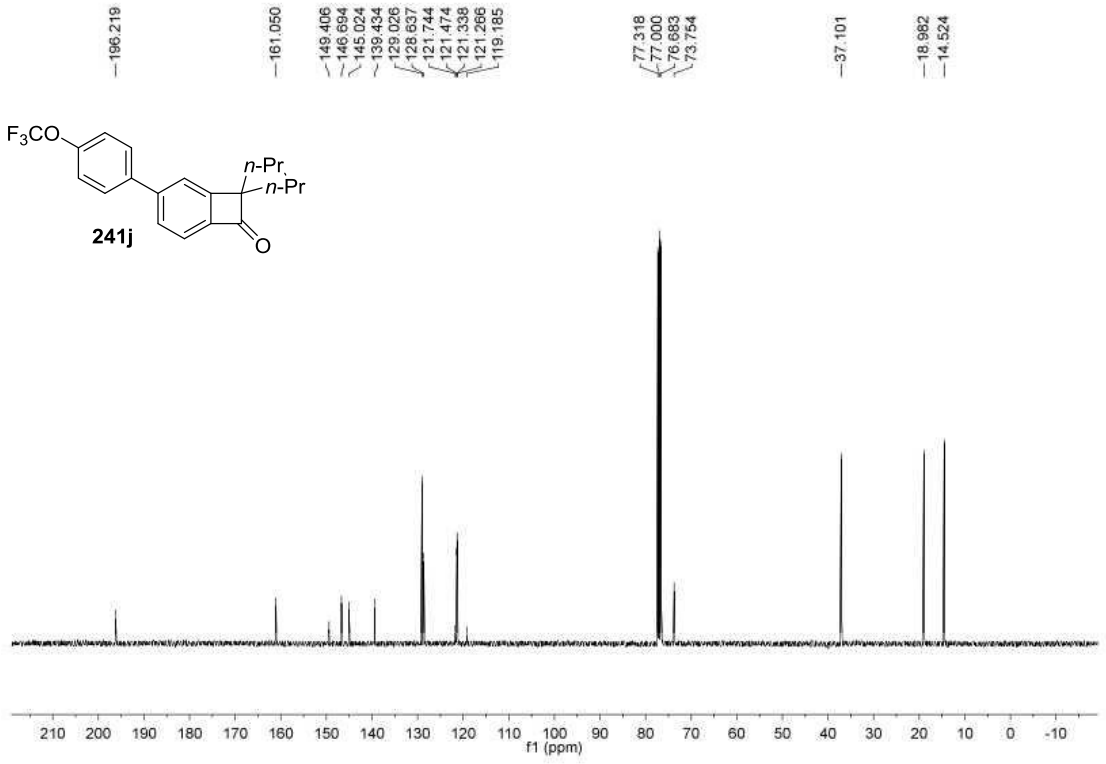
196.219
161.050
149.406
146.694
145.024
139.434
129.026
128.637
121.744
121.474
121.338
121.266
119.185
77.318
77.000
76.683
73.754
37.101
18.982
14.524
F3CO
n-Pr
n-Pr
O
241j
f1 (ppm)

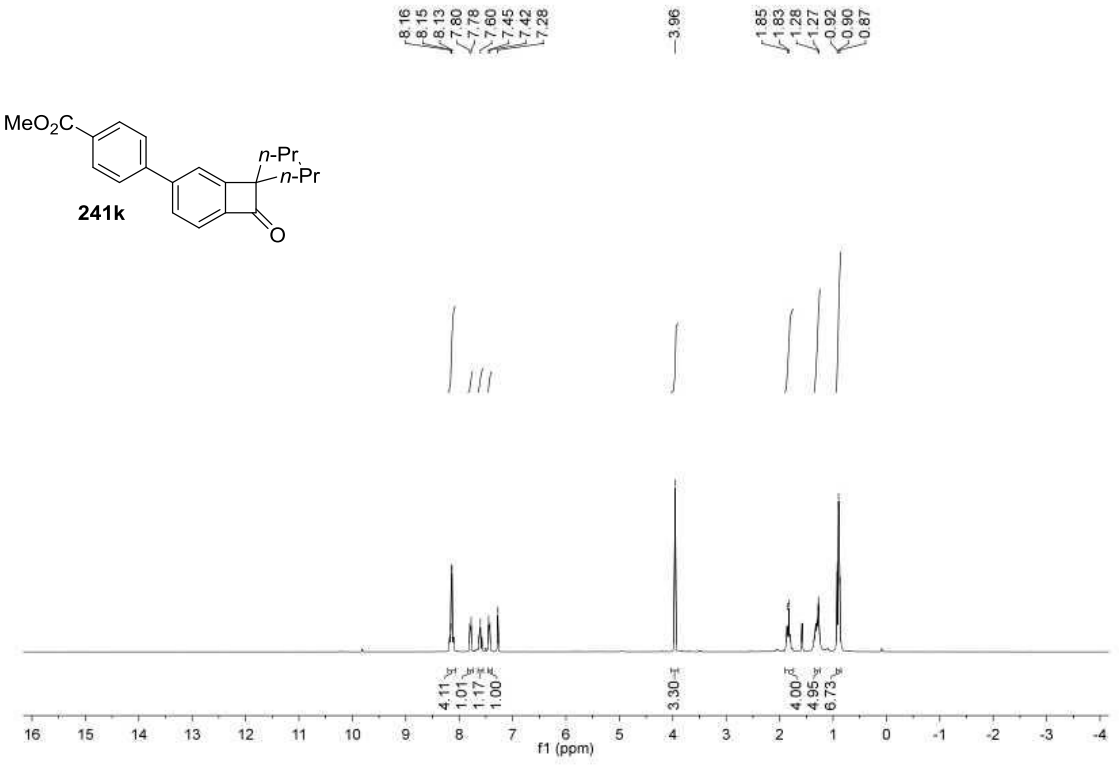
8.16
8.15
8.13
7.80
7.78
7.60
7.45
7.42
7.28
3.96
1.85
1.83
1.28
1.27
0.92
0.90
0.87
MeO2C
n-Pr
n-Pr
241k
O
4.11
1.01
1.17
1.00
3.30
4.00
4.95
6.73
f1 (ppm)

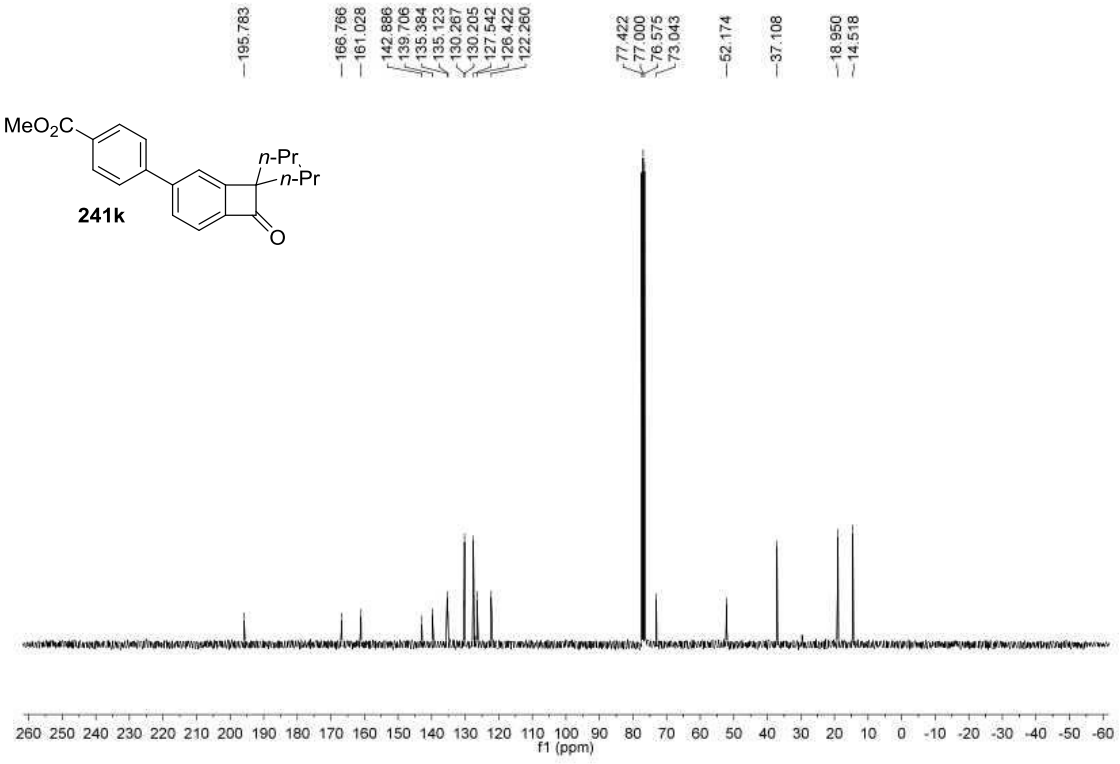
195.783
166.766
161.028
142.886
139.706
135.384
135.123
130.267
130.205
127.542
126.422
122.260
77.422
77.000
76.575
73.043
52.174
37.108
18.950
14.518
MeO2C
n-Pr
n-Pr
241k
O
f1 (ppm)

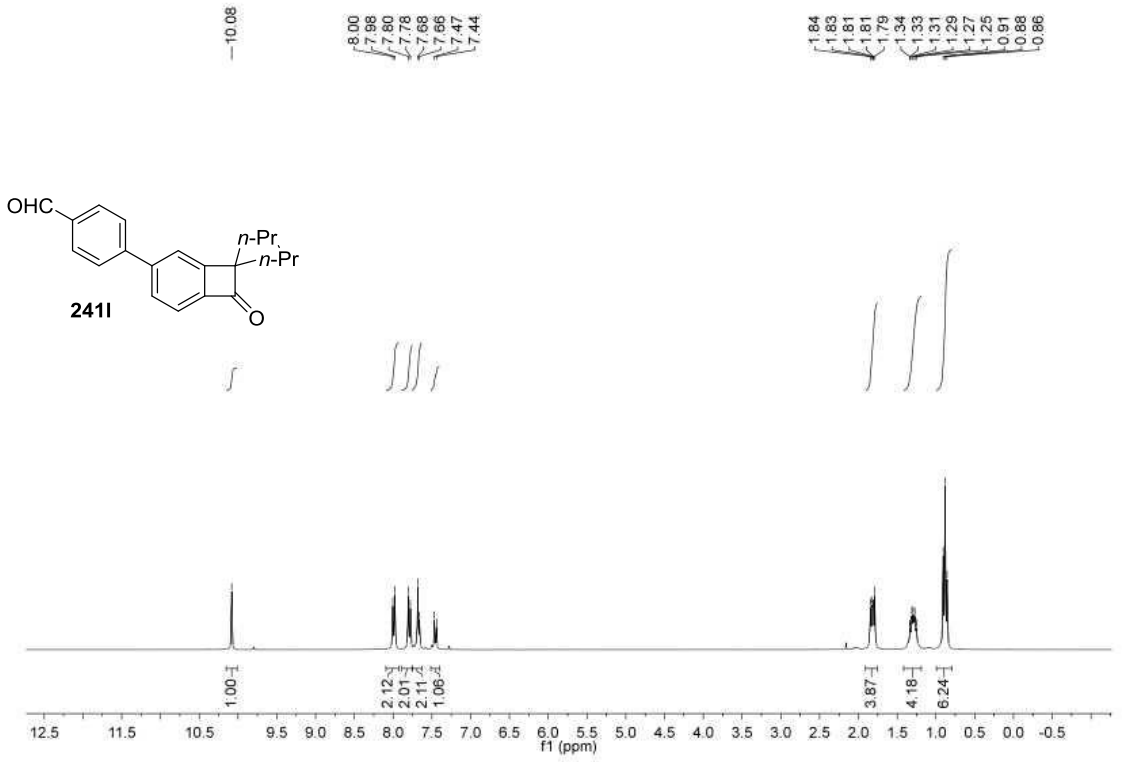
10.08
8.00
7.98
7.80
7.78
7.68
7.66
7.47
7.44
1.84
1.83
1.81
1.81
1.79
1.34
1.33
1.31
1.29
1.27
1.25
0.91
0.88
0.86
OHC
n-Pr
n-Pr
O
241l
1.00
2.12
2.01
2.11
1.06
3.87
4.18
6.24
f1 (ppm)

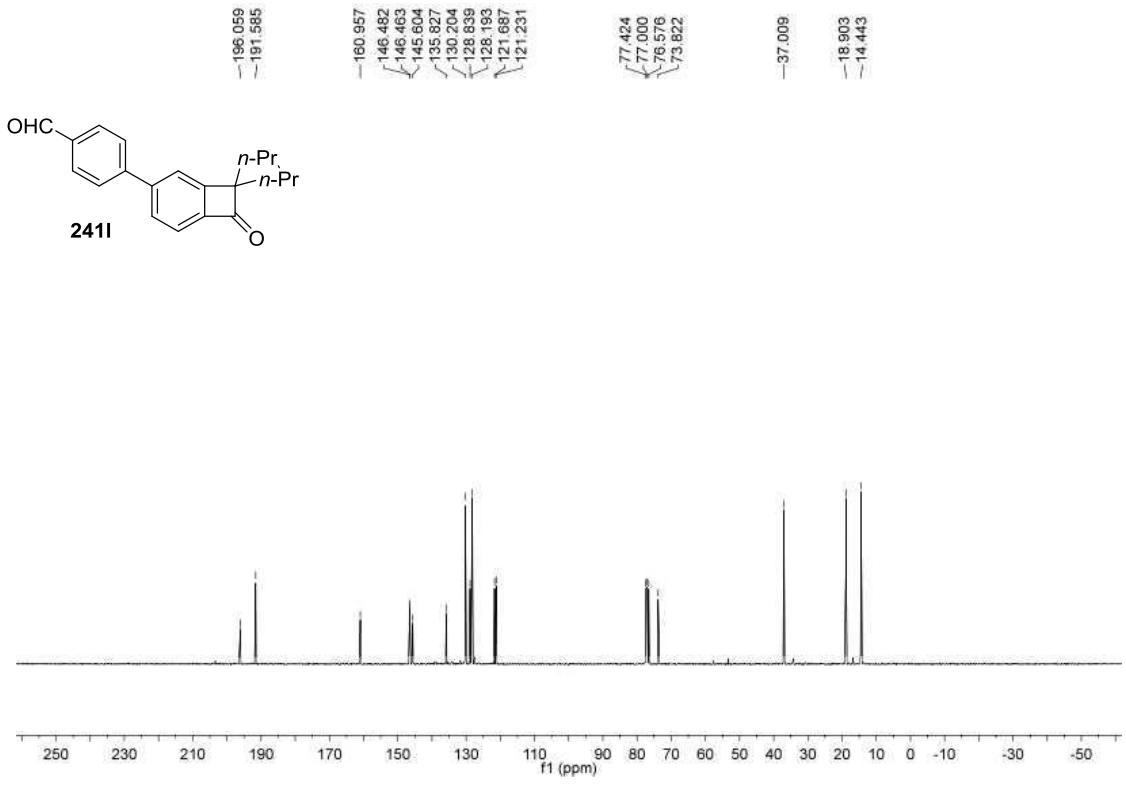
196.059
191.585
160.957
146.482
146.463
145.604
135.827
130.204
128.839
128.193
121.687
121.231
77.424
77.000
76.576
73.822
37.009
18.903
14.443
OHC
n-Pr
n-Pr
O
241l
f1 (ppm)

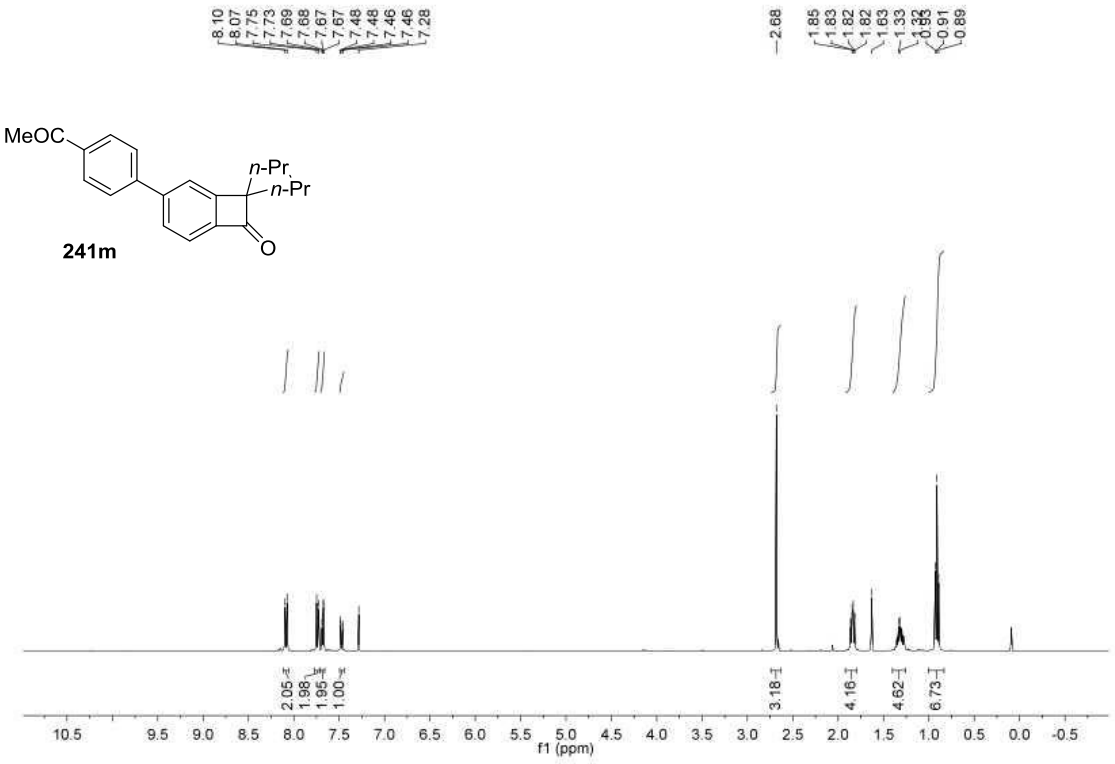
8.10
8.07
7.75
7.73
7.69
7.68
7.67
7.67
7.48
7.48
7.46
7.46
7.28
2.68
1.85
1.83
1.82
1.82
1.63
1.33
1.32
0.93
0.91
0.89
MeOC
n-Pr
n-Pr
O
241m
2.05
1.98
1.95
1.00
3.18
4.16
4.62
6.73
f1 (ppm)

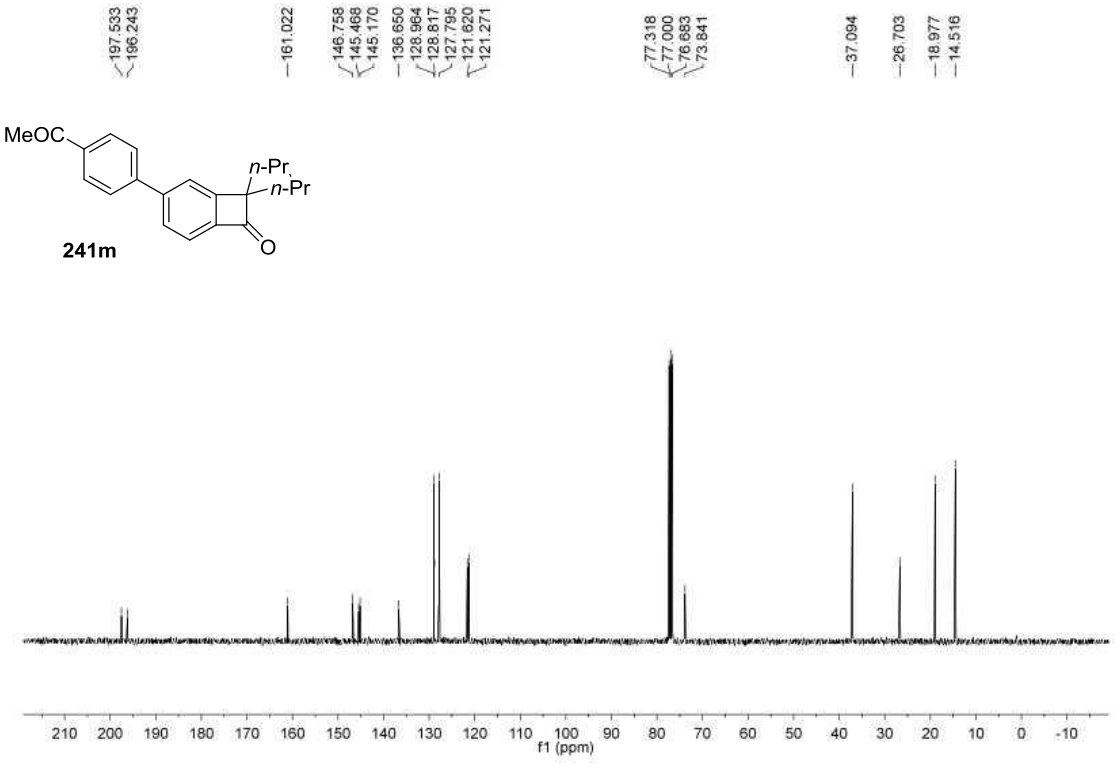
197.533
196.243
161.022
146.758
145.468
145.170
136.650
128.964
128.817
127.795
121.620
121.271
77.318
77.000
76.683
73.841
37.094
26.703
18.977
14.516
MeOC
n-Pr
n-Pr
O
241m
f1 (ppm)

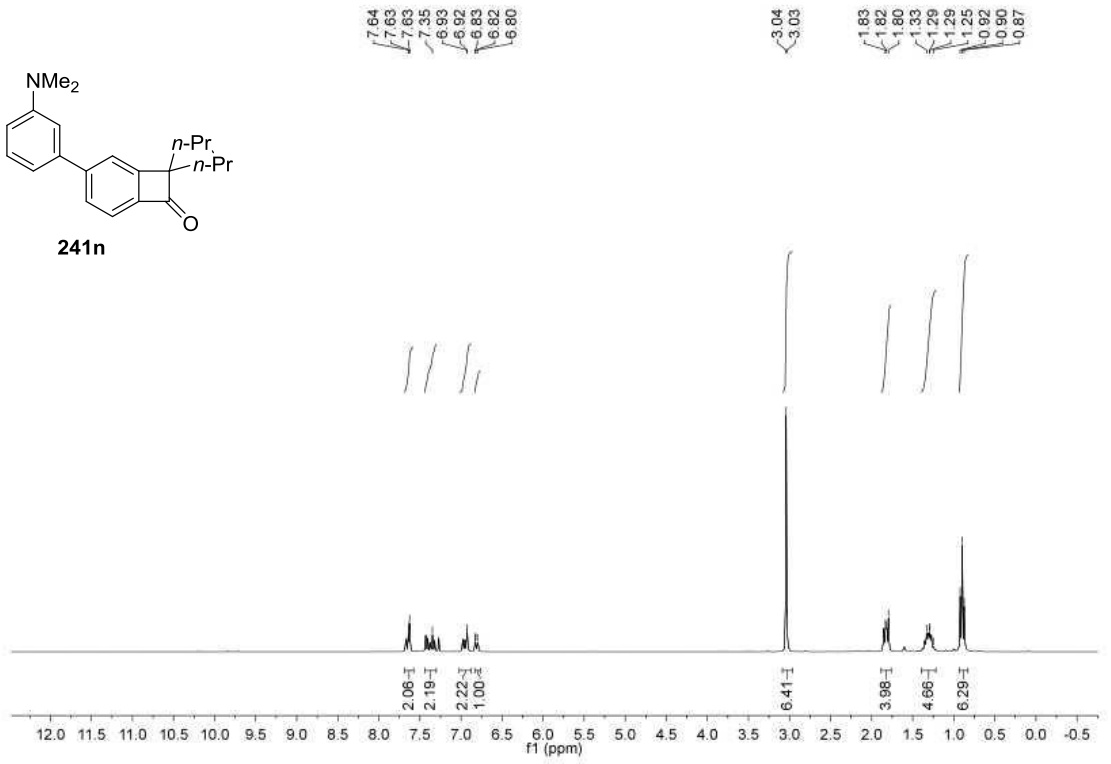
NMe2
n-Pr
n-Pr
O
241n
7.64
7.63
7.63
7.35
6.93
6.92
6.83
6.82
6.80
3.04
3.03
1.83
1.82
1.80
1.33
1.29
1.29
1.25
0.92
0.90
0.87
2.06
2.19
2.22
1.00
6.41
3.98
4.66
6.29
f1 (ppm)

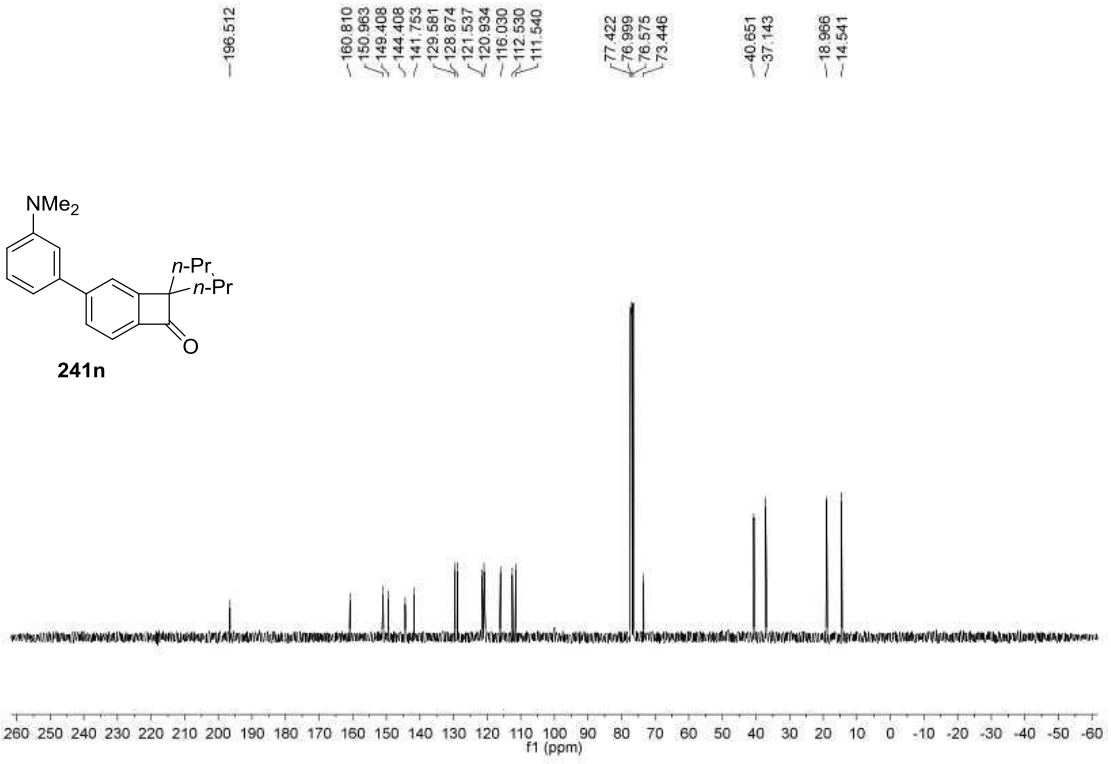
196.512
160.810
150.963
149.408
144.408
141.753
129.581
128.874
121.537
120.934
116.030
112.530
111.540
77.422
76.999
76.575
73.446
40.651
37.143
18.966
14.541
NMe2
n-Pr
n-Pr
O
241n
f1 (ppm)

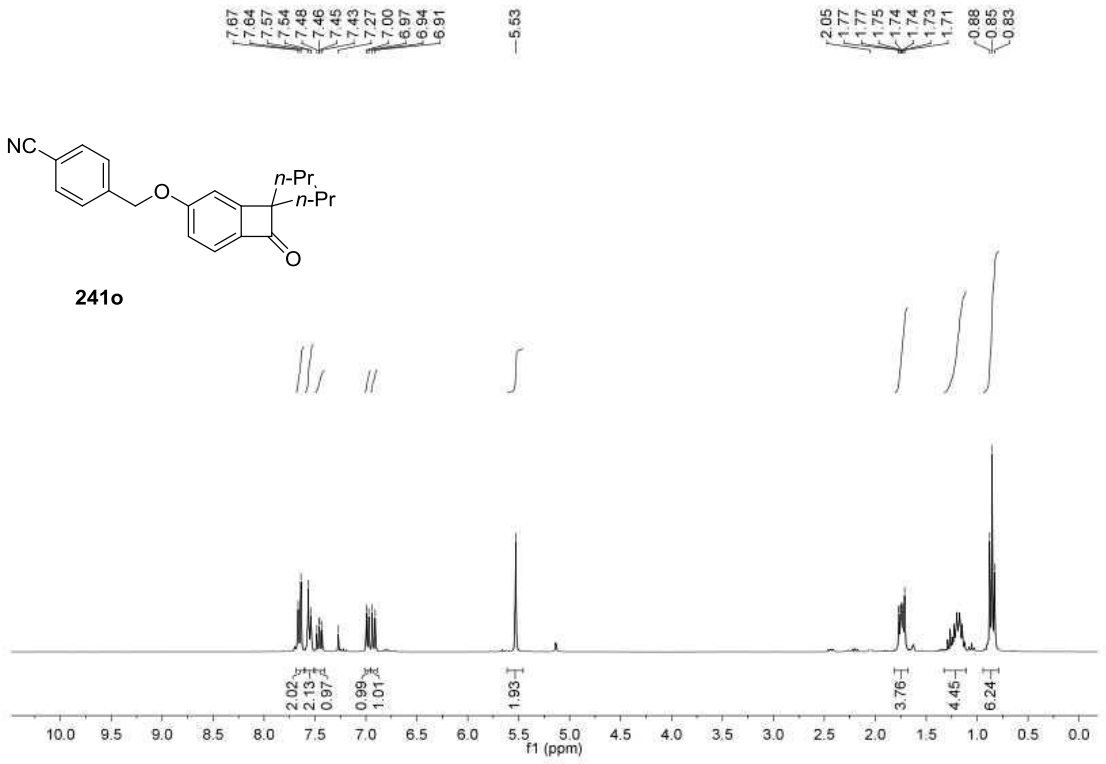
7.67
7.64
7.57
7.54
7.48
7.46
7.45
7.43
7.27
7.00
6.97
6.94
6.91
5.53
2.05
1.77
1.77
1.75
1.74
1.74
1.73
1.71
0.88
0.85
0.83
NC
n-Pr
n-Pr
O
O
2.02
2.13
0.97
0.99
1.01
1.93
3.76
4.45
6.24
f1 (ppm)

241o

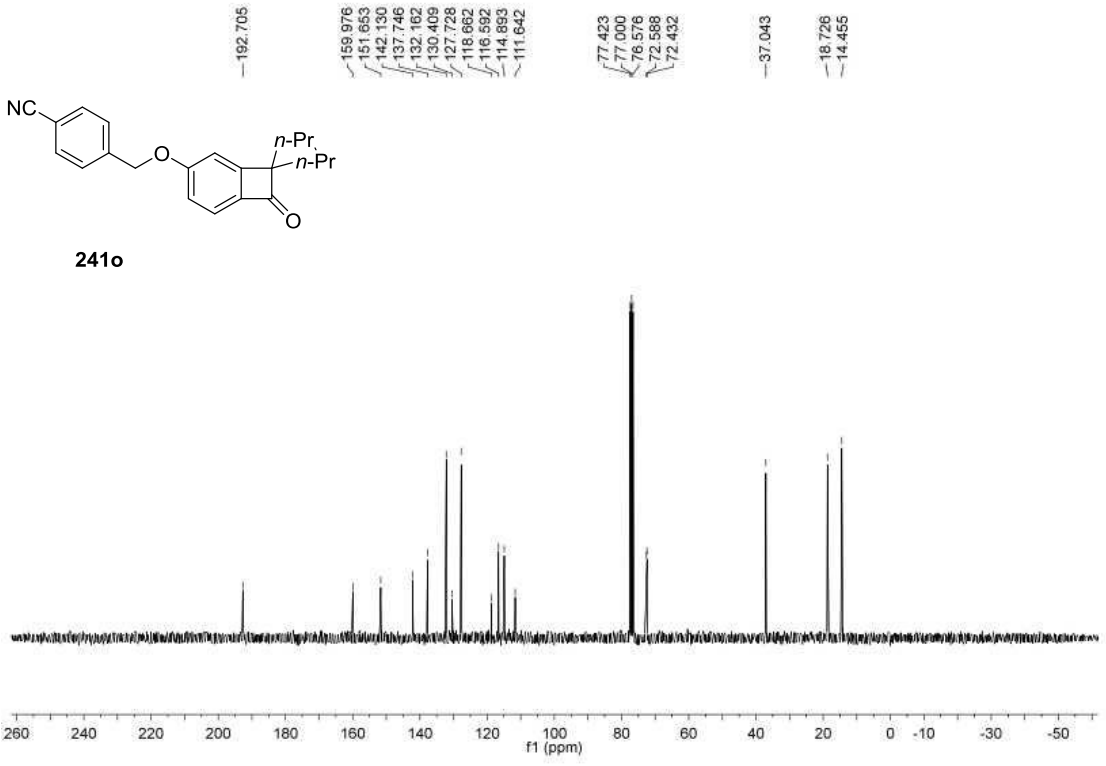
192.705
159.976
151.653
142.130
137.746
132.162
130.409
127.728
118.662
116.592
114.893
111.642
77.423
77.000
76.576
72.588
72.432
37.043
18.726
14.455
NC
n-Pr
n-Pr
O
O
f1 (ppm)

241o

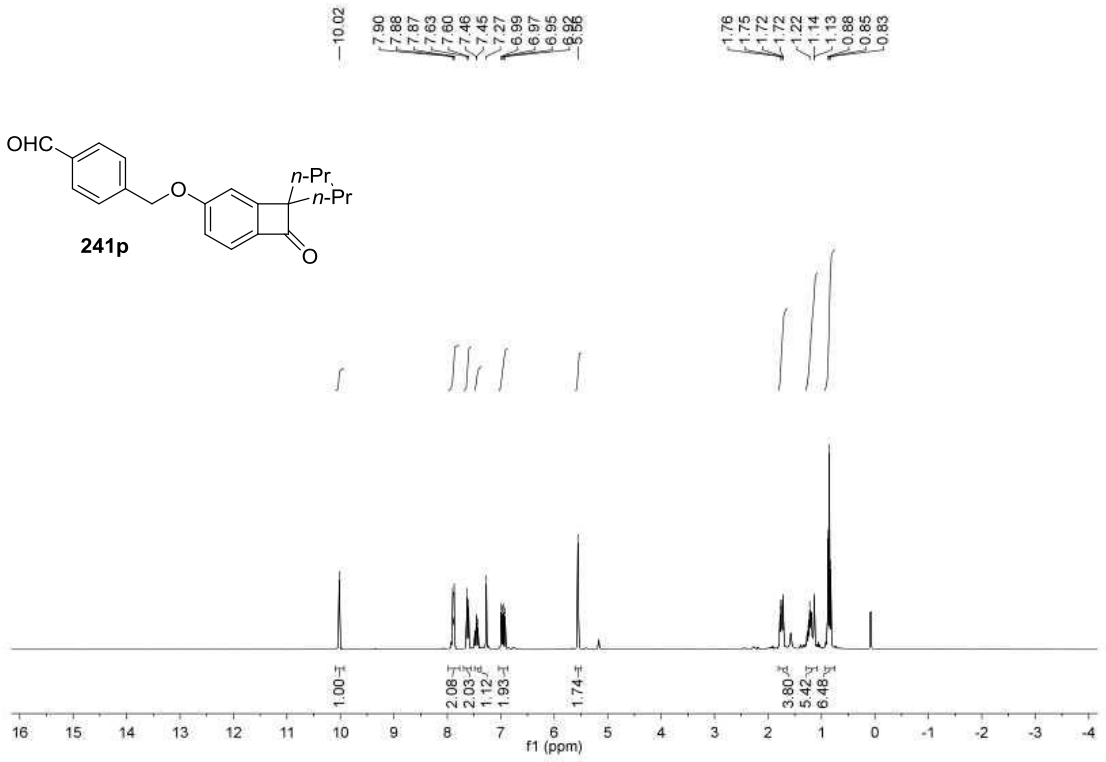
OHC
n-Pr
n-Pr
O
O
241p
10.02
7.90
7.88
7.87
7.63
7.60
7.46
7.45
7.27
6.99
6.97
6.95
6.92
6.88
1.76
1.75
1.72
1.72
1.22
1.14
1.13
0.88
0.85
0.83
1.00
2.08
2.03
1.12
1.93
1.74
3.80
5.42
6.48
f1 (ppm)

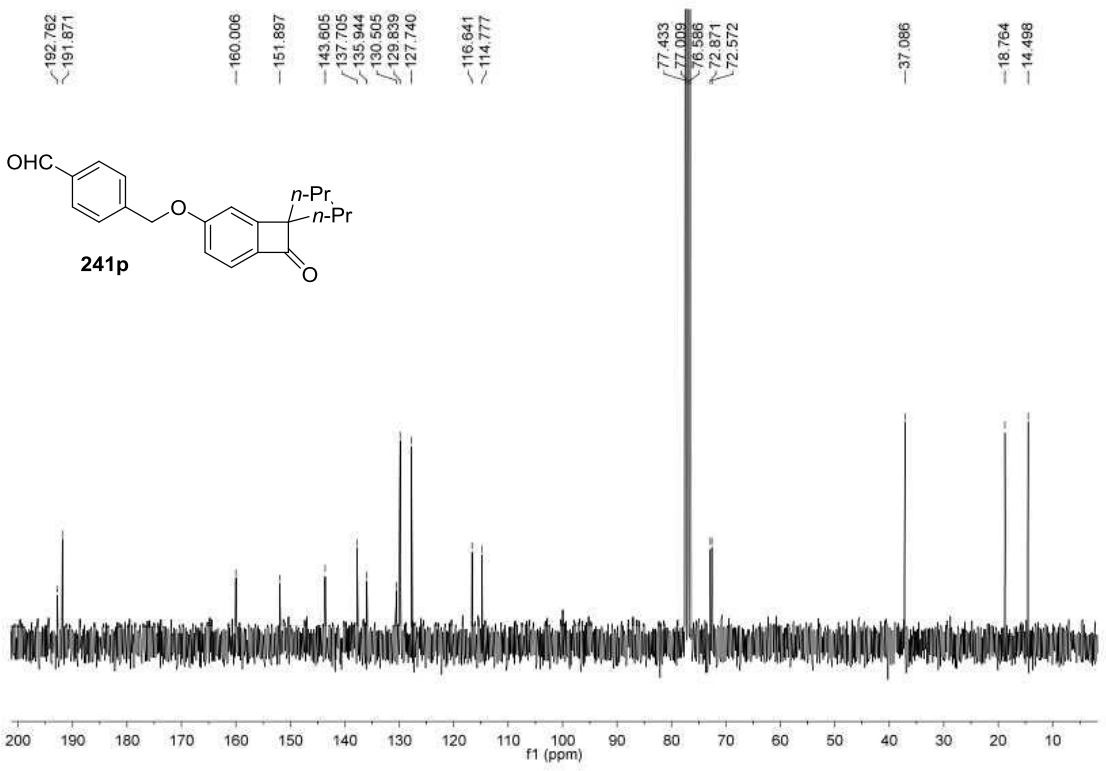
OHC
n-Pr
n-Pr
O
O
241p
192.762
191.871
160.006
151.897
143.605
137.705
135.944
130.505
129.839
127.740
116.641
114.777
77.433
77.009
76.586
72.871
72.572
37.086
18.764
14.498
f1 (ppm)

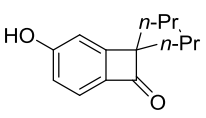
HO
n-Pr
n-Pr
O

241q

7.28
7.28
7.26
7.26
6.96
6.94
6.93
6.93
6.93
1.79
1.78
1.77
1.75
1.74
1.74
1.26
1.25
1.23
0.89
0.87
0.85
1.17
2.00
3.98
4.66
6.37
f1 (ppm)

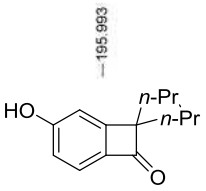
HO
n-Pr
n-Pr
O

241q

195.993
163.017
162.639
136.925
123.436
118.234
109.323
77.435
77.012
76.589
72.282
37.047
18.886
14.508
f1 (ppm)

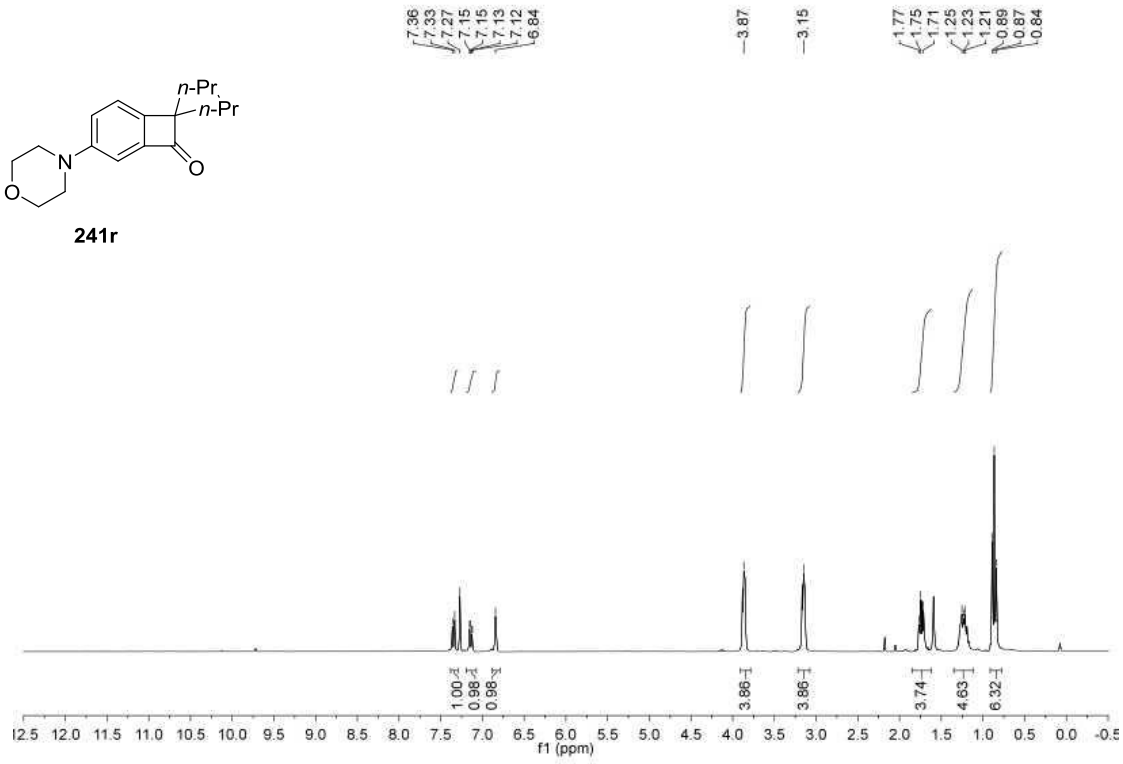
7.36
7.33
7.27
7.15
7.15
7.13
7.12
6.84
3.87
3.15
1.77
1.75
1.71
1.25
1.23
1.21
0.89
0.87
0.84
n-Pr
n-Pr
N
O
O
1.00
0.98
0.98
3.86
3.86
3.74
4.63
6.32
f1 (ppm)

241r

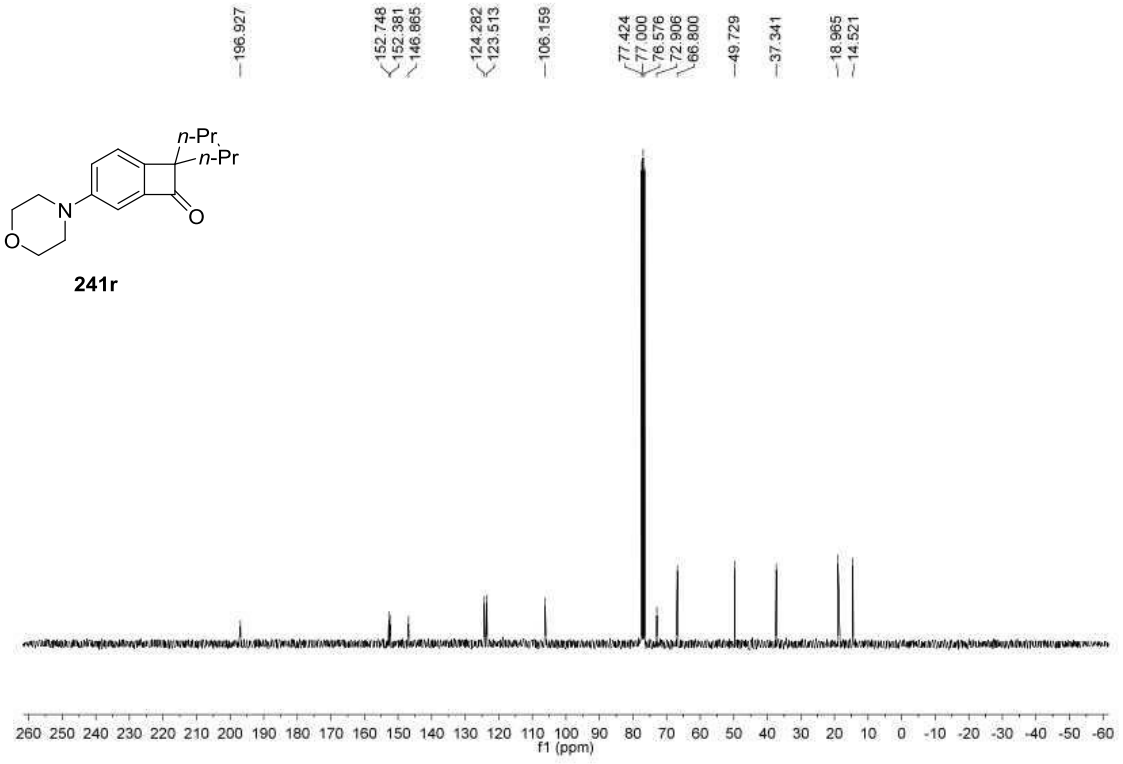
196.927
152.748
152.381
146.865
124.282
123.513
106.159
77.424
77.000
76.576
72.906
66.800
49.729
37.341
18.965
14.521
n-Pr
n-Pr
N
O
O
f1 (ppm)

241r

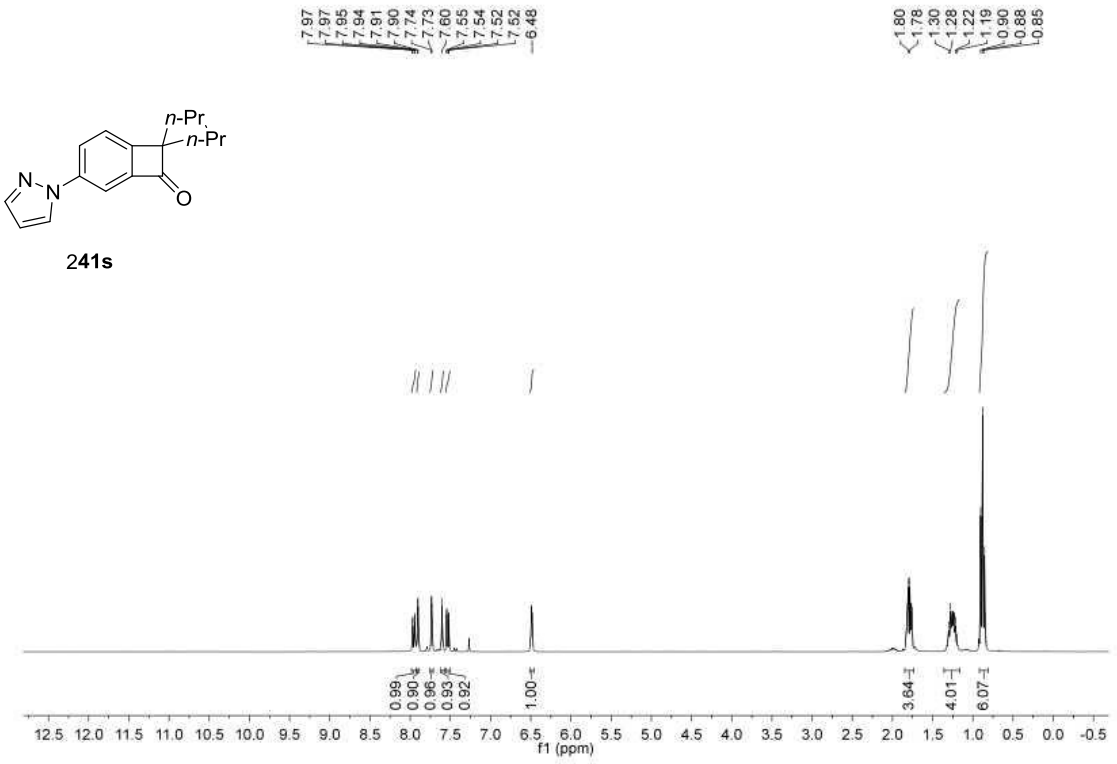
7.97
7.97
7.95
7.94
7.91
7.90
7.74
7.73
7.60
7.55
7.54
7.52
7.52
6.48
1.80
1.78
1.30
1.28
1.22
1.19
0.90
0.88
0.85
n-Pr
n-Pr
N
N
O
0.99
0.90
0.96
0.93
0.92
1.00
3.64
4.01
6.07
f1 (ppm)

241s

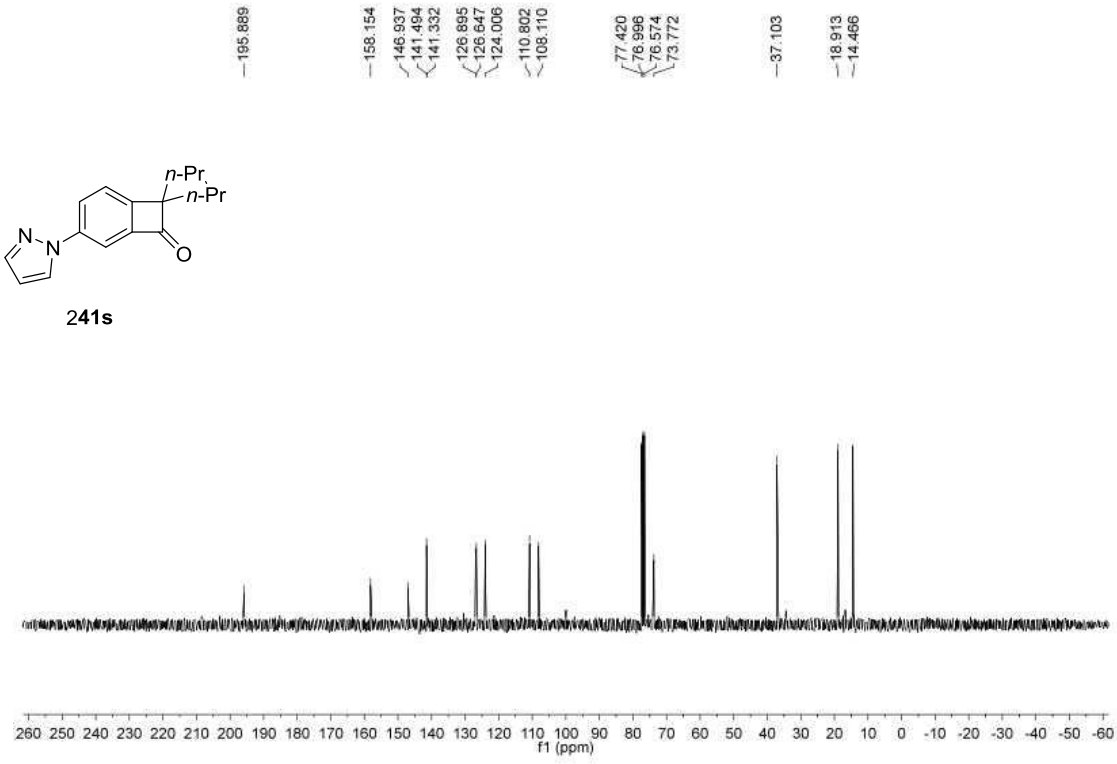
195.889
158.154
146.937
141.494
141.332
126.895
126.647
124.006
110.802
108.110
77.420
76.996
76.574
73.772
37.103
18.913
14.466
n-Pr
n-Pr
N
N
O
f1 (ppm)

241s

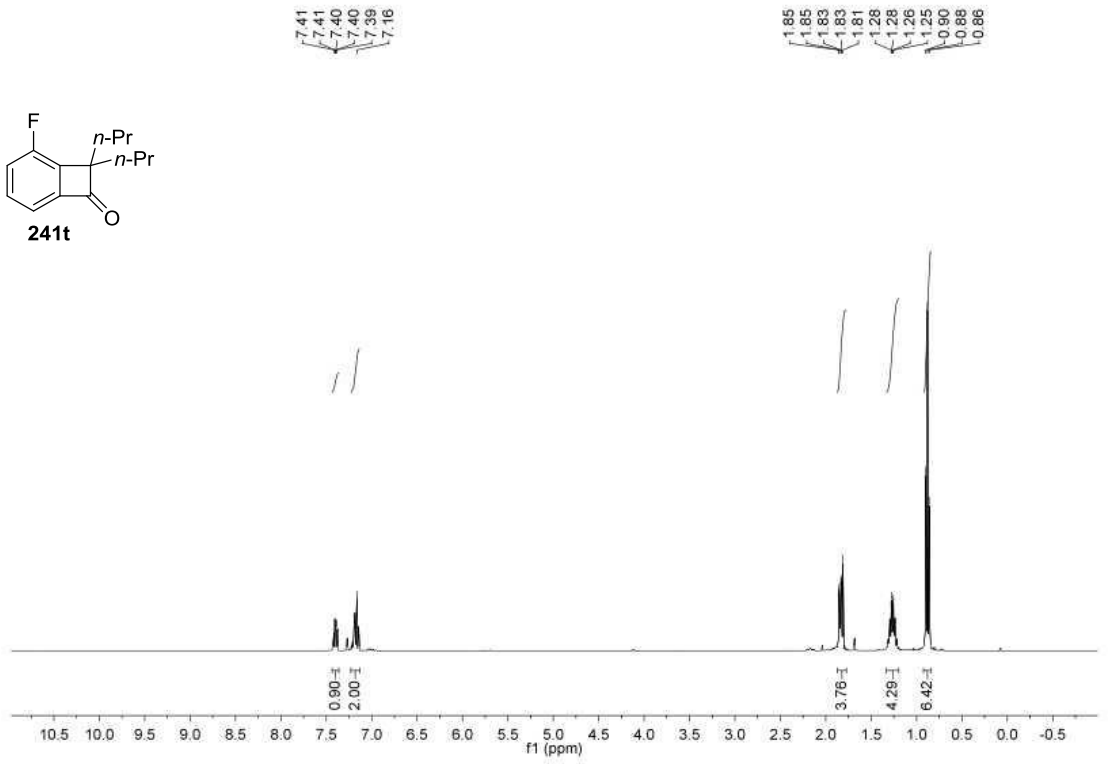
7.41
7.41
7.40
7.40
7.39
7.16
1.85
1.85
1.83
1.83
1.81
1.28
1.28
1.26
1.25
0.90
0.88
0.86
F
n-Pr
n-Pr
O
241t
0.90
2.00
3.76
4.29
6.42
f1 (ppm)

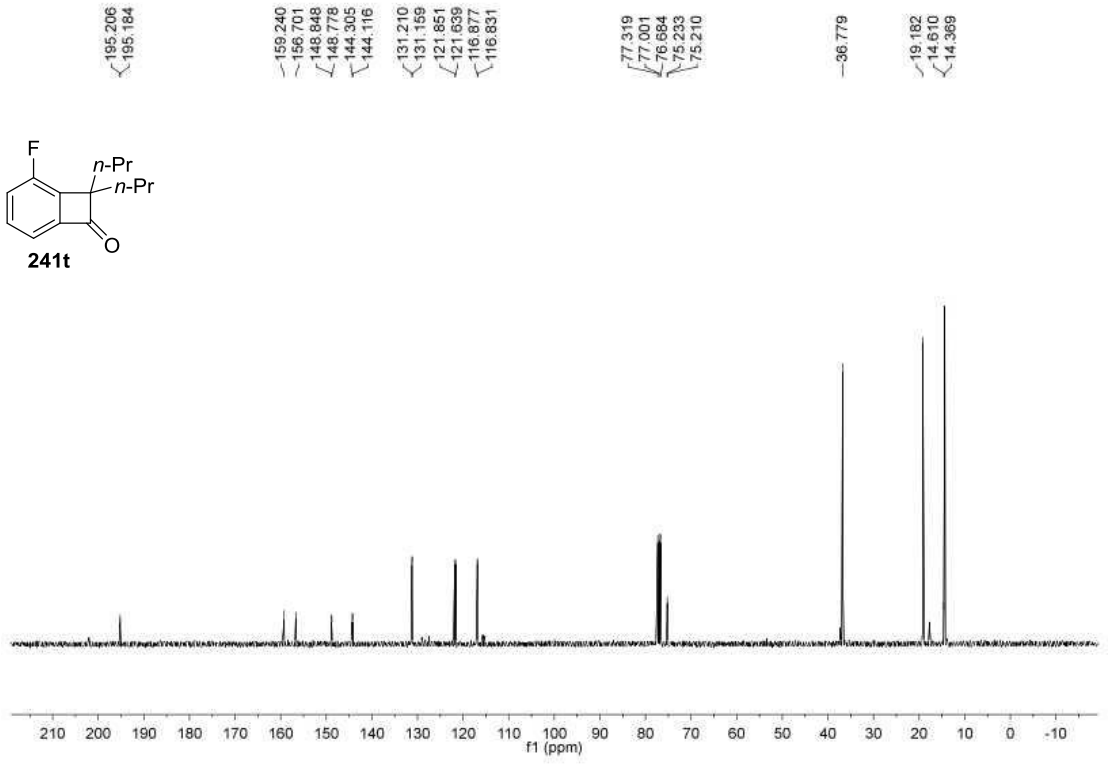
195.206
195.184
159.240
156.701
148.848
148.778
144.305
144.116
131.210
131.159
121.851
121.639
116.877
116.831
77.319
77.001
76.684
75.233
75.210
36.779
19.182
14.610
14.369
F
n-Pr
n-Pr
O
241t
f1 (ppm)

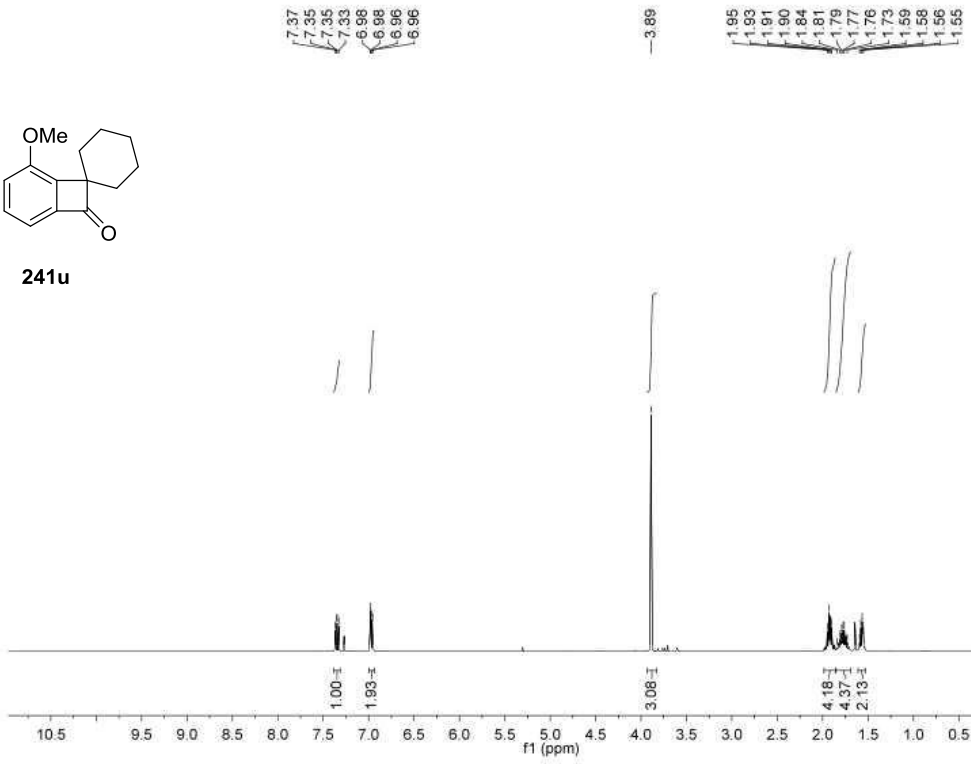
7.37
7.35
7.35
7.33
6.98
6.98
6.96
6.96
3.89
1.95
1.93
1.91
1.90
1.84
1.81
1.79
1.77
1.76
1.73
1.59
1.58
1.56
1.55
OMe
O
1.00
1.93
3.08
4.18
4.37
2.13
f1 (ppm)

241u

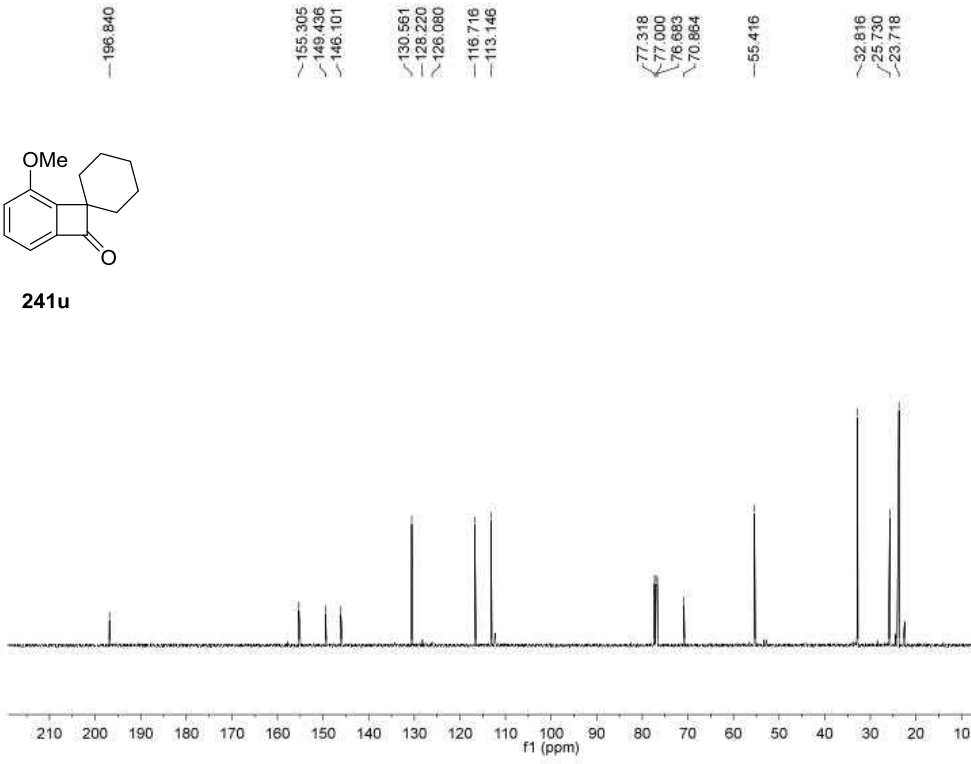
196.840
155.305
149.436
146.101
130.561
128.220
126.080
116.716
113.146
77.318
77.000
76.683
70.864
55.416
32.816
25.730
23.718
OMe
O
f1 (ppm)

241u

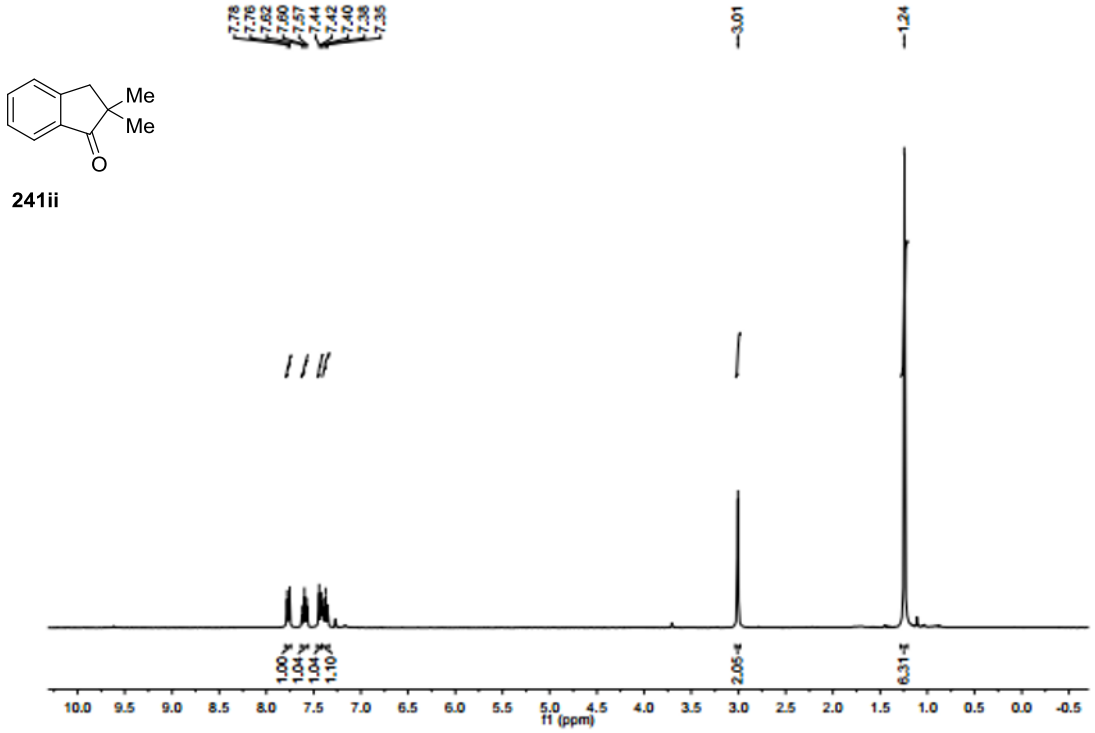
7.78
7.76
7.62
7.60
7.57
7.44
7.42
7.40
7.38
7.35
3.01
1.24
Me
Me
O
1.00
1.04
1.04
1.10
2.05
6.31
f1 (ppm)

241ii

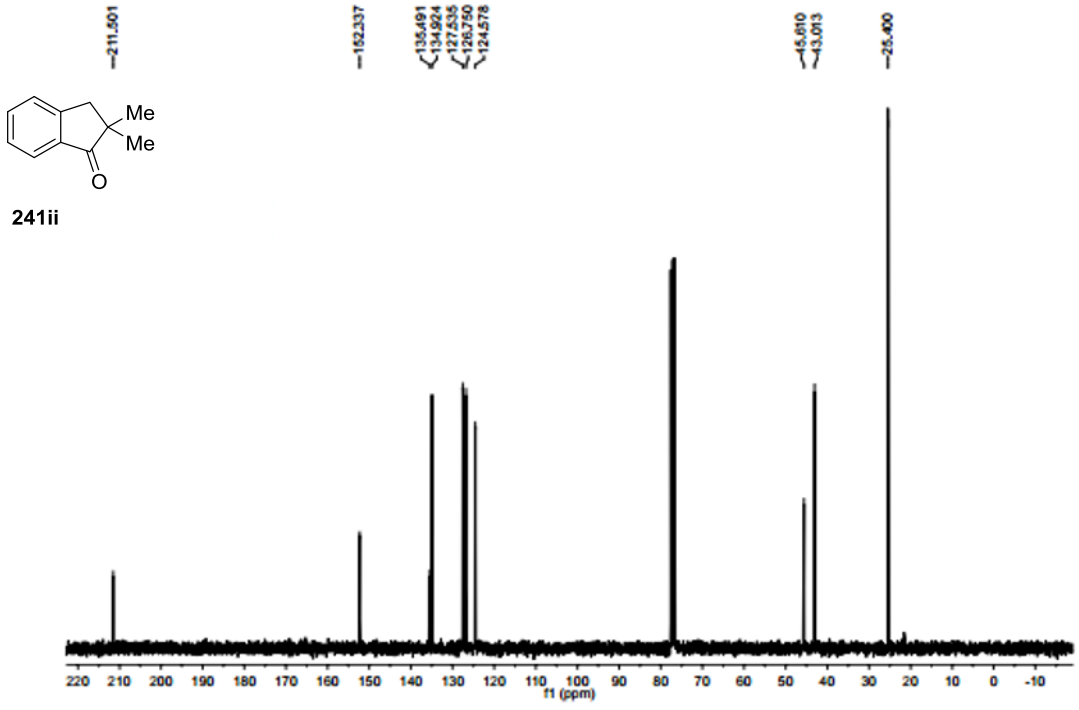
211.501
152.337
135.491
134.924
127.535
126.750
124.578
45.610
43.013
25.400
Me
Me
O
f1 (ppm)

241ii

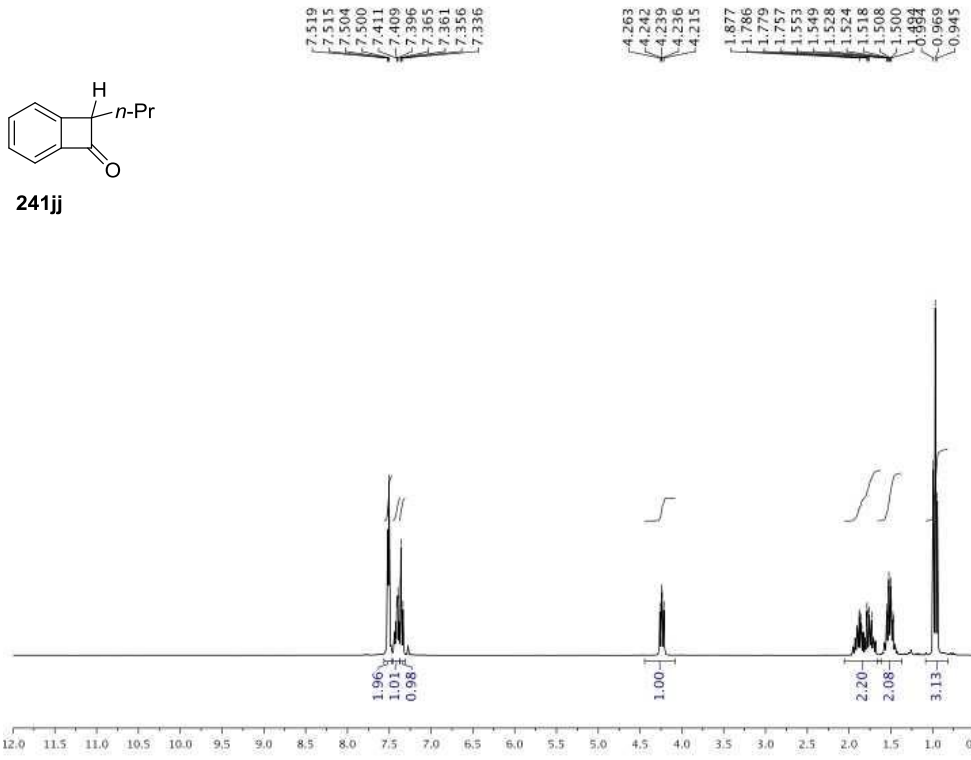
7.519
7.515
7.504
7.500
7.411
7.409
7.396
7.365
7.361
7.356
7.336
4.263
4.242
4.239
4.236
4.215
1.877
1.786
1.779
1.757
1.553
1.549
1.528
1.524
1.518
1.508
1.500
0.969
0.945
H
n-Pr
O
1.96
1.01
0.98
1.00
2.20
2.08
3.13

241jj

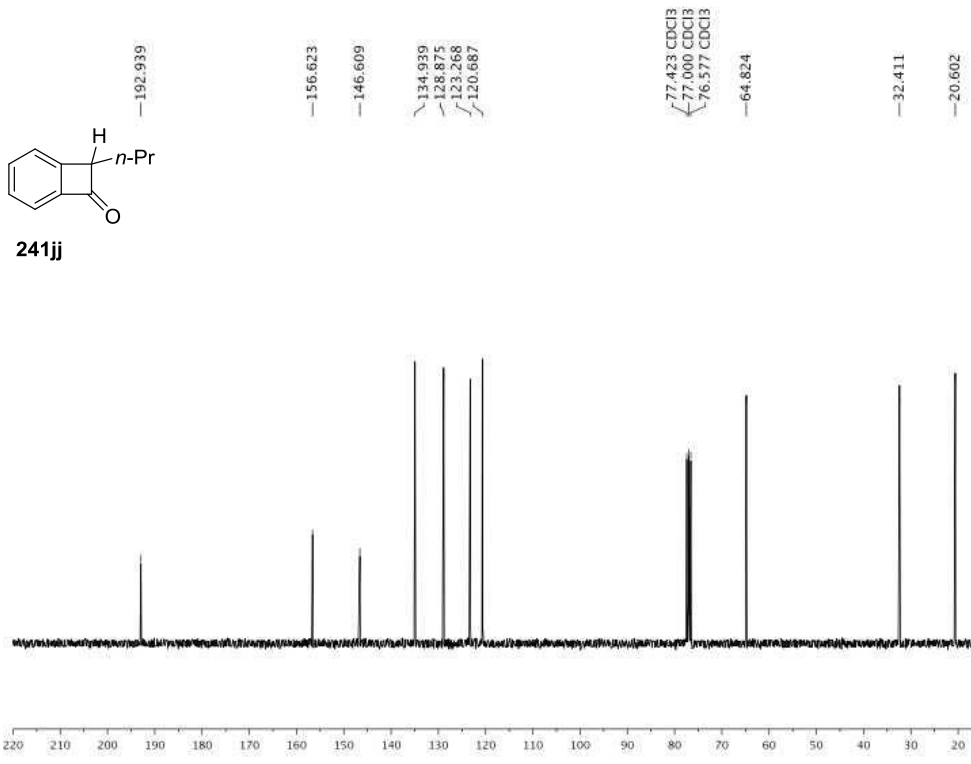
192.939
156.623
146.609
134.939
128.875
123.268
120.687
77.423 CDCl3
77.000 CDCl3
76.577 CDCl3
64.824
32.411
20.602
13.948
H
n-Pr
O

241jj

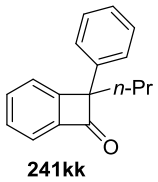
n-Pr
O

241kk

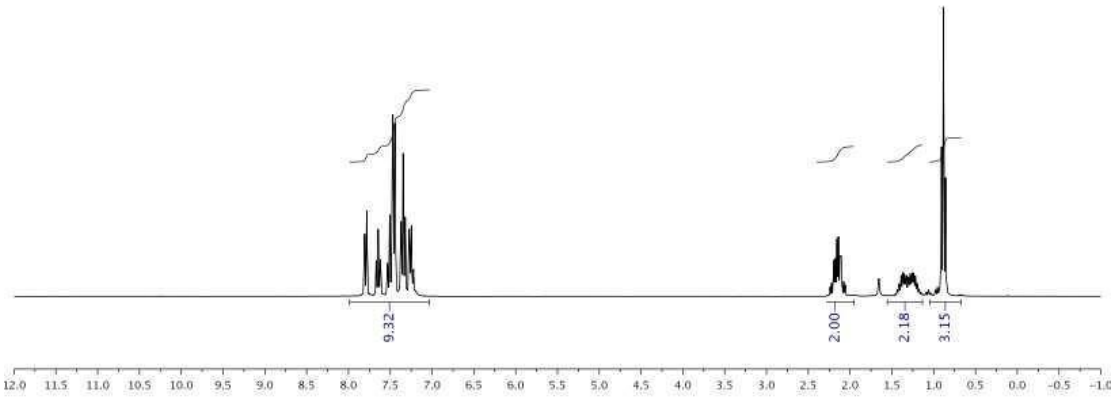
9.32
2.00
2.18
3.15


193.192
158.521
145.699
140.434
135.302
129.504
128.354
126.708
126.000
124.130
121.646
77.682
77.399 CDCl3
76.978 CDCl3
76.556 CDCl3
40.025
18.908
14.188

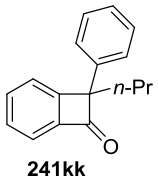
n-Pr
O

241kk

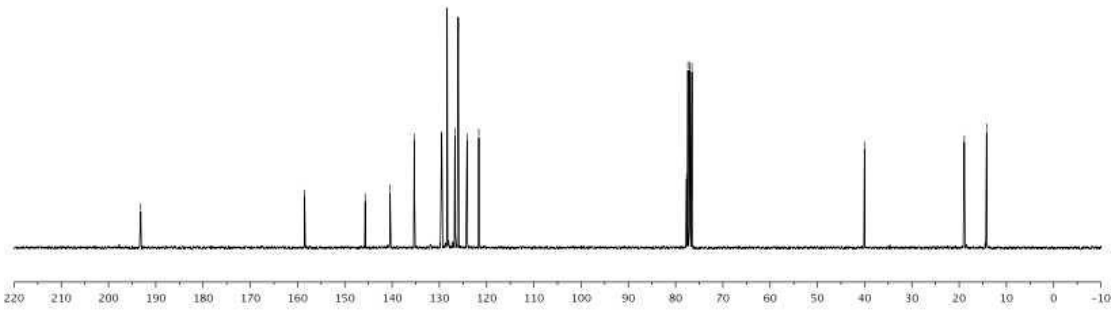

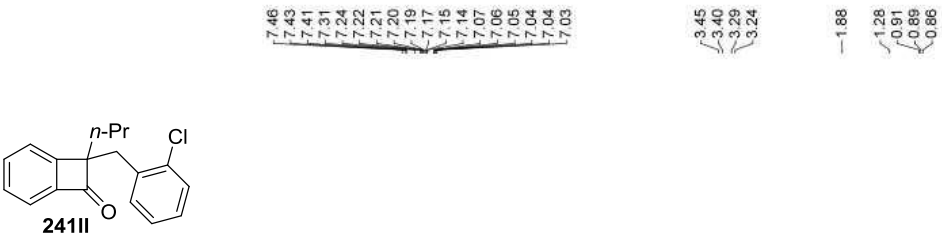
7.46
7.43
7.41
7.31
7.24
7.22
7.21
7.20
7.19
7.17
7.15
7.14
7.07
7.06
7.05
7.04
7.04
7.03
3.45
3.40
3.29
3.24
1.88
1.28
0.91
0.89
0.86

n-Pr
Cl
O

241ll

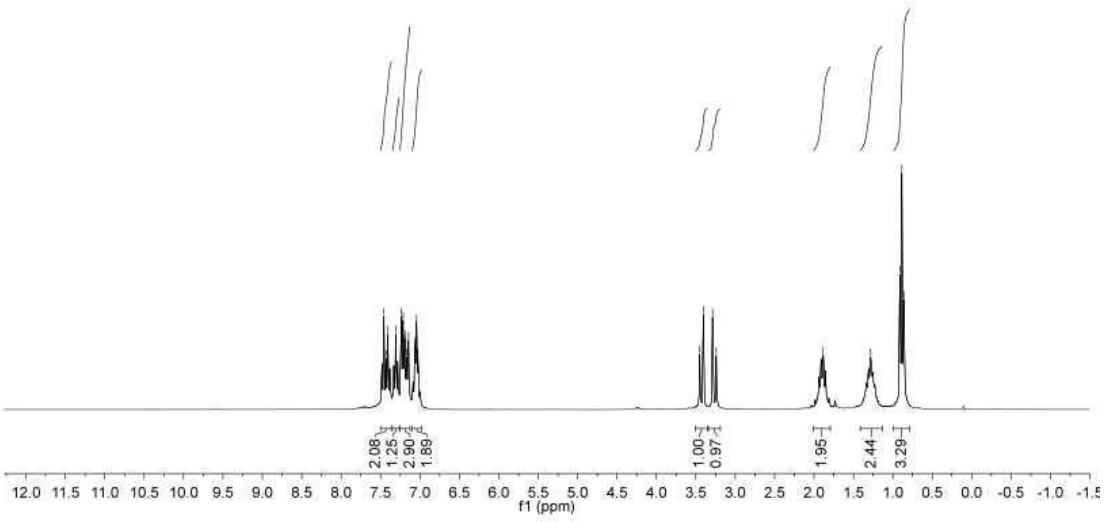
2.08
1.25
2.90
1.89
1.00
0.97
1.95
2.44
3.29
12.0 11.5 11.0 10.5 10.0 9.5 9.0 8.5 8.0 7.5 7.0 6.5 6.0 5.5 5.0 4.5 4.0 3.5 3.0 2.5 2.0 1.5 1.0 0.5 0.0 -0.5 -1.0
f1 (ppm)


195.664
158.764
145.879
135.574
134.681
134.343
131.715
129.316
129.148
127.733
126.372
124.117
120.379
77.423
77.000
76.577
74.659
37.505
37.376
18.955
14.396

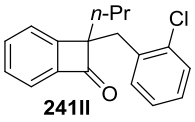
n-Pr
Cl
O

241ll

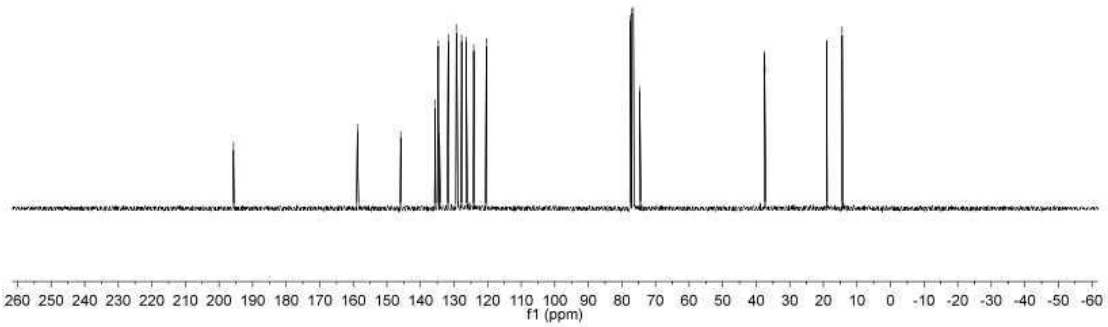
260 250 240 230 220 210 200 190 180 170 160 150 140 130 120 110 100 90 80 70 60 50 40 30 20 10 0 -10 -20 -30 -40 -50 -60
f1 (ppm)

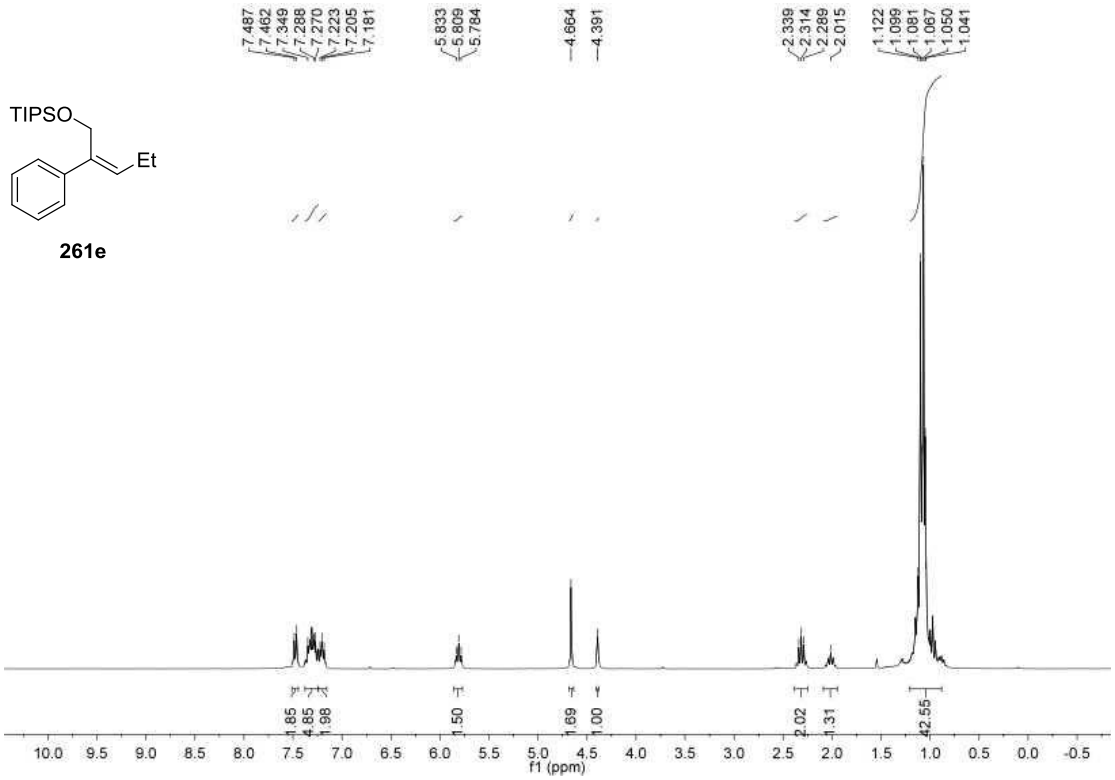
TIPSO
Et
261e
7.487
7.462
7.349
7.288
7.270
7.223
7.205
7.181
5.833
5.809
5.784
4.664
4.391
2.339
2.314
2.289
2.015
1.122
1.099
1.081
1.067
1.050
1.041
1.85
4.85
1.98
1.50
1.69
1.00
2.02
1.31
12.55
f1 (ppm)

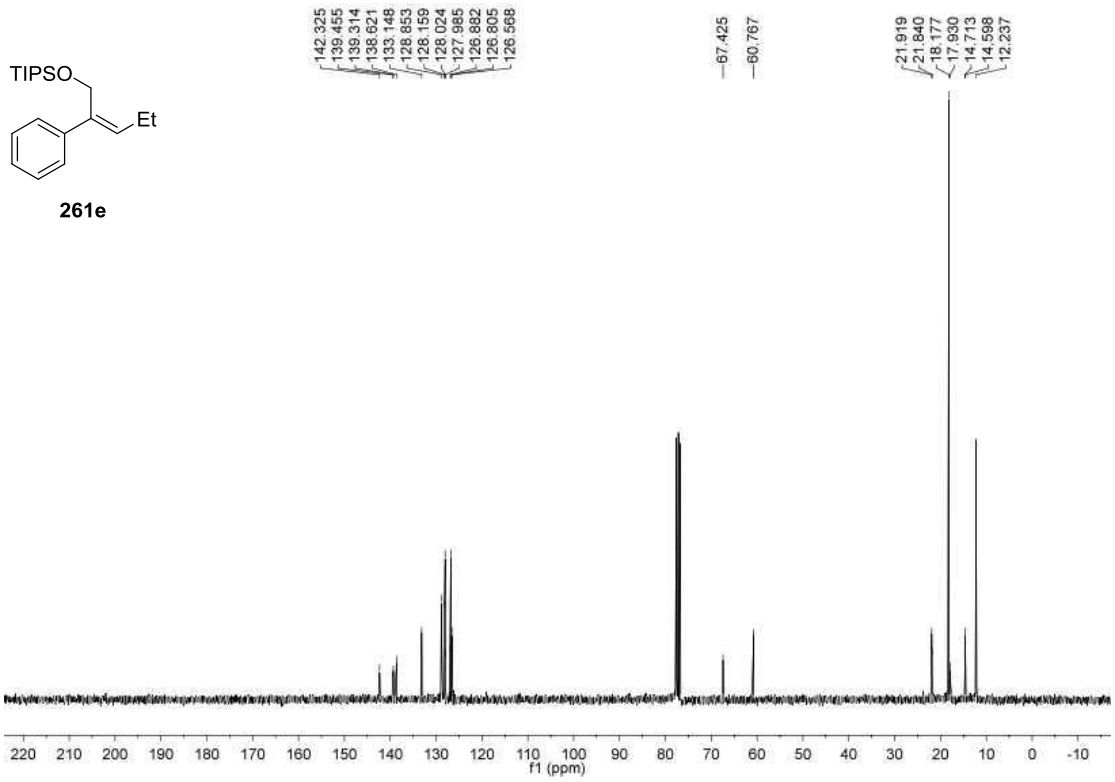
TIPSO
Et
261e
142.325
139.455
139.314
138.621
133.148
128.853
128.159
128.024
127.985
126.882
126.805
126.568
67.425
60.767
21.919
21.840
18.177
17.930
14.713
14.598
12.237
f1 (ppm)

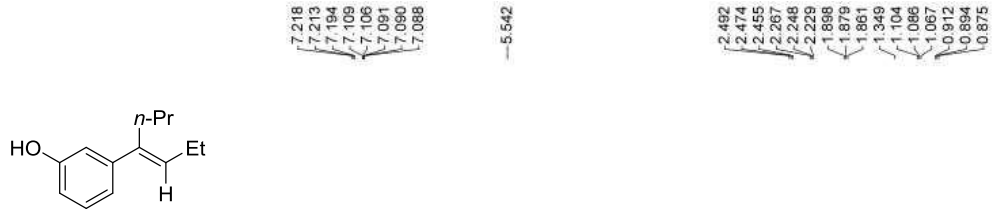
7.218
7.213
7.194
7.109
7.106
7.091
7.090
7.088
5.542
2.492
2.474
2.455
2.267
2.248
2.229
1.898
1.879
1.861
1.349
1.104
1.086
1.067
0.912
0.894
0.875

n-Pr
HO
Et
H

261q

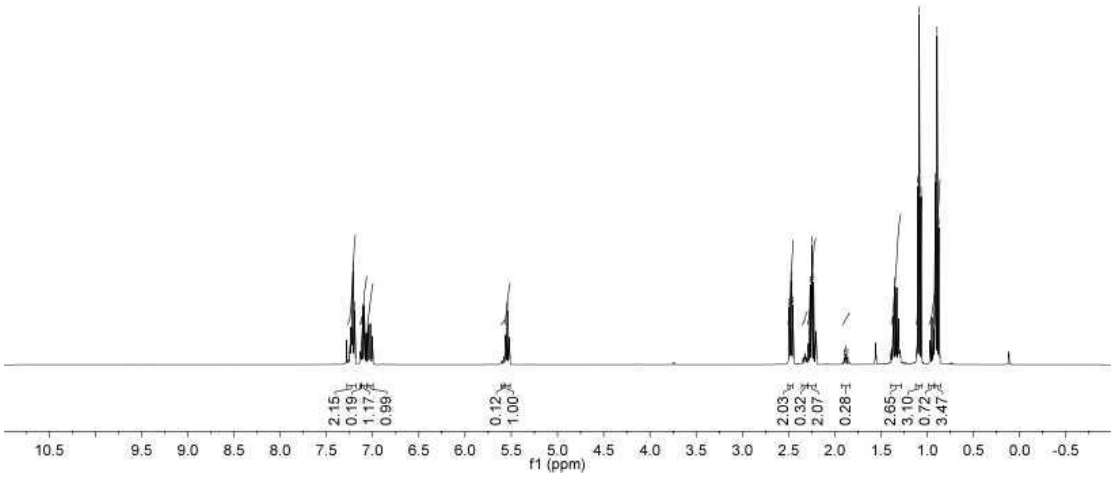
2.15
0.19
1.17
0.99
0.12
1.00
2.03
0.32
2.07
0.28
2.65
3.10
0.72
3.47
10.5
9.5
9.0
8.5
8.0
7.5
7.0
6.5
6.0
5.5
5.0
4.5
4.0
3.5
3.0
2.5
2.0
1.5
1.0
0.5
0.0
-0.5
f1 (ppm)


161.211
158.789
135.501
133.664
133.650
131.782
130.656
130.610
127.934
127.853
123.718
115.261
77.316
76.999
76.681
40.578
32.390
32.361
22.497
21.531
21.507
21.126
14.284
14.176
13.805
13.579

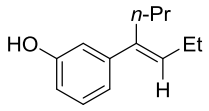
n-Pr
HO
Et
H

261q

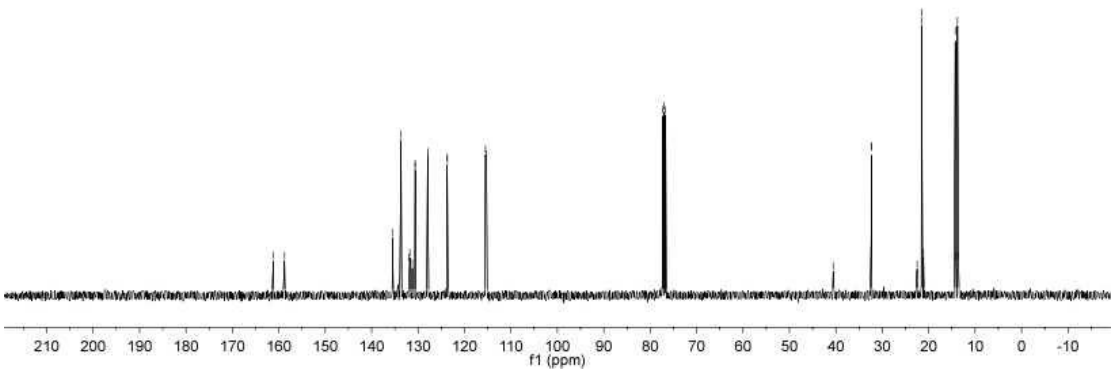
210
200
190
180
170
160
150
140
130
120
110
100
90
80
70
60
50
40
30
20
10
0
-10
f1 (ppm)

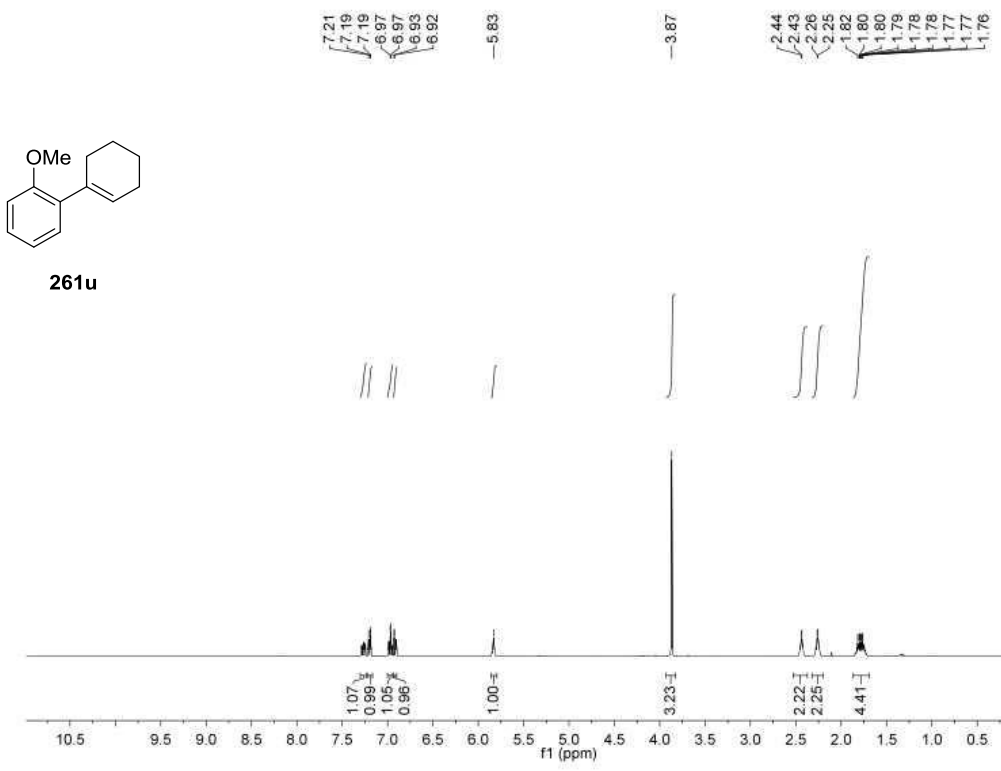
7.21
7.19
7.19
6.97
6.97
6.93
6.92
5.83
3.87
2.44
2.43
2.26
2.25
1.82
1.80
1.80
1.79
1.78
1.78
1.77
1.77
1.76
OMe
261u
1.07
0.99
1.05
0.96
1.00
3.23
2.22
2.25
4.41
f1 (ppm)

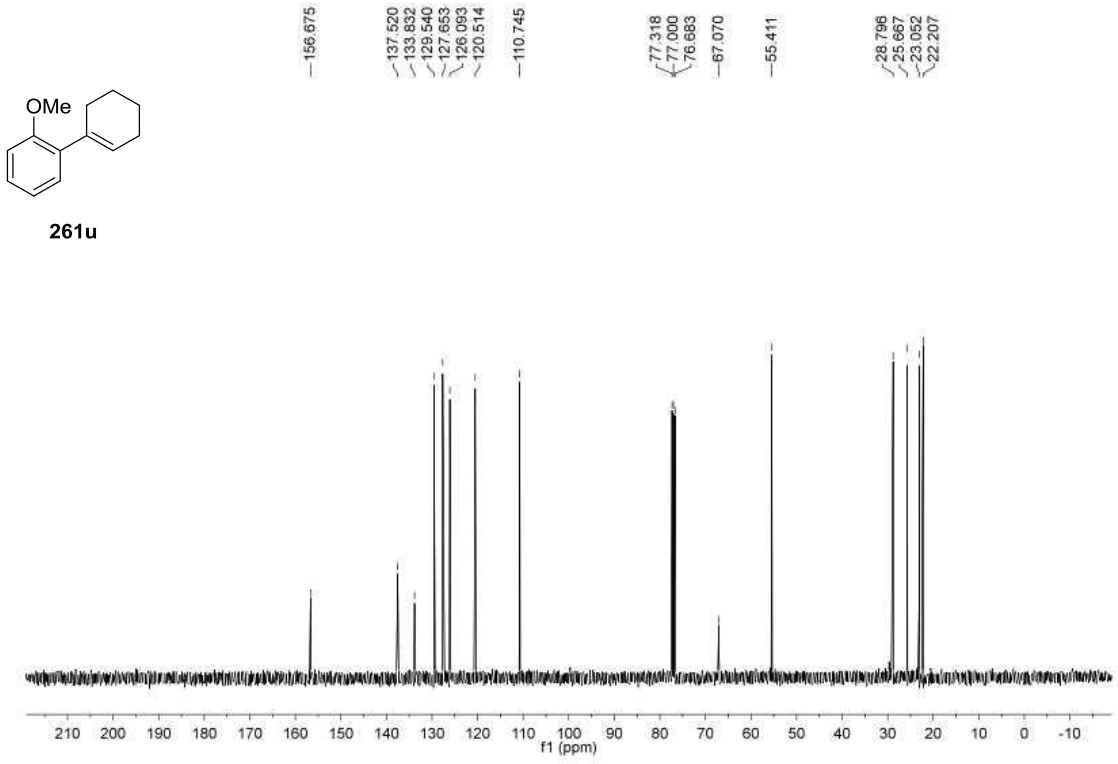
156.675
137.520
133.832
129.540
127.653
126.093
120.514
110.745
77.318
77.000
76.683
67.070
55.411
28.796
25.667
23.052
22.207
OMe
261u
f1 (ppm)

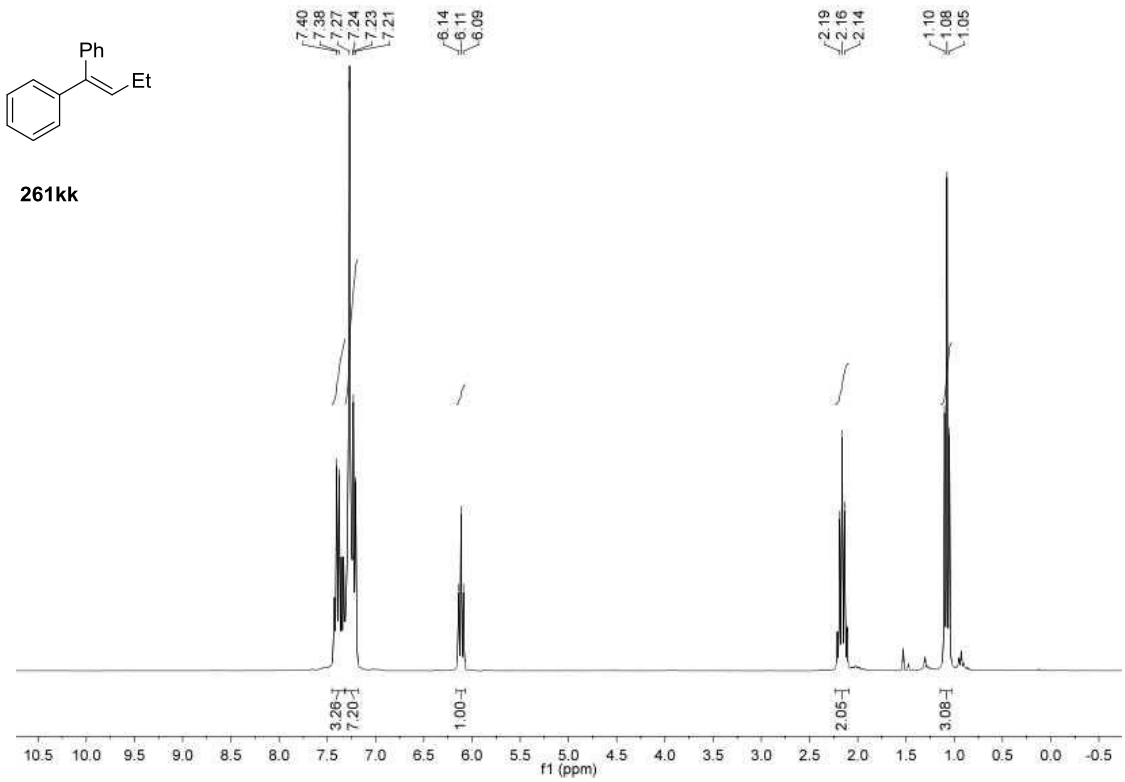
Ph
Et
261kk
7.40
7.38
7.27
7.24
7.23
7.21
6.14
6.11
6.09
2.19
2.16
2.14
1.10
1.08
1.05
3.26
7.20
1.00
2.05
3.08
f1 (ppm)

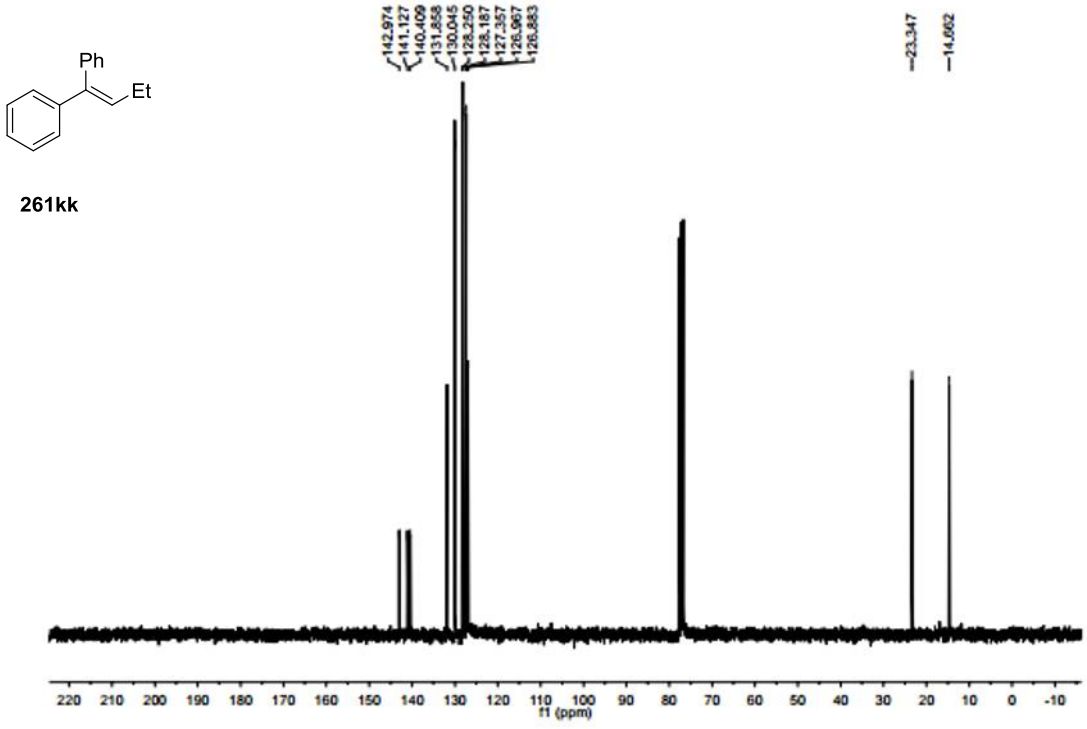
Ph
Et
261kk
142.974
141.127
140.409
131.858
130.045
128.250
128.187
127.357
126.967
126.883
23.347
14.662
f1 (ppm)

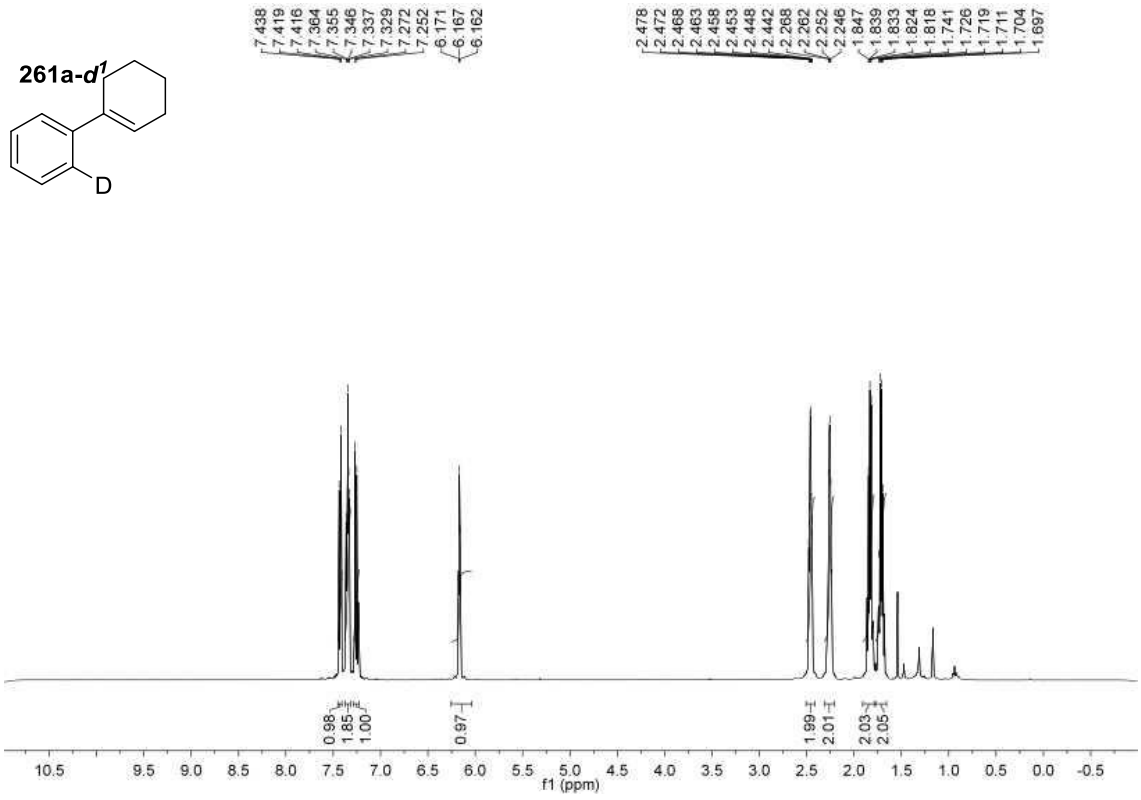
261a-d1
D
7.438
7.419
7.416
7.364
7.355
7.346
7.337
7.329
7.272
7.252
6.171
6.167
6.162
2.478
2.472
2.468
2.463
2.458
2.453
2.448
2.442
2.268
2.262
2.252
2.246
1.847
1.839
1.833
1.824
1.818
1.741
1.726
1.719
1.711
1.704
1.697
0.98
1.85
1.00
0.97
1.99
2.01
2.03
2.05
f1 (ppm)

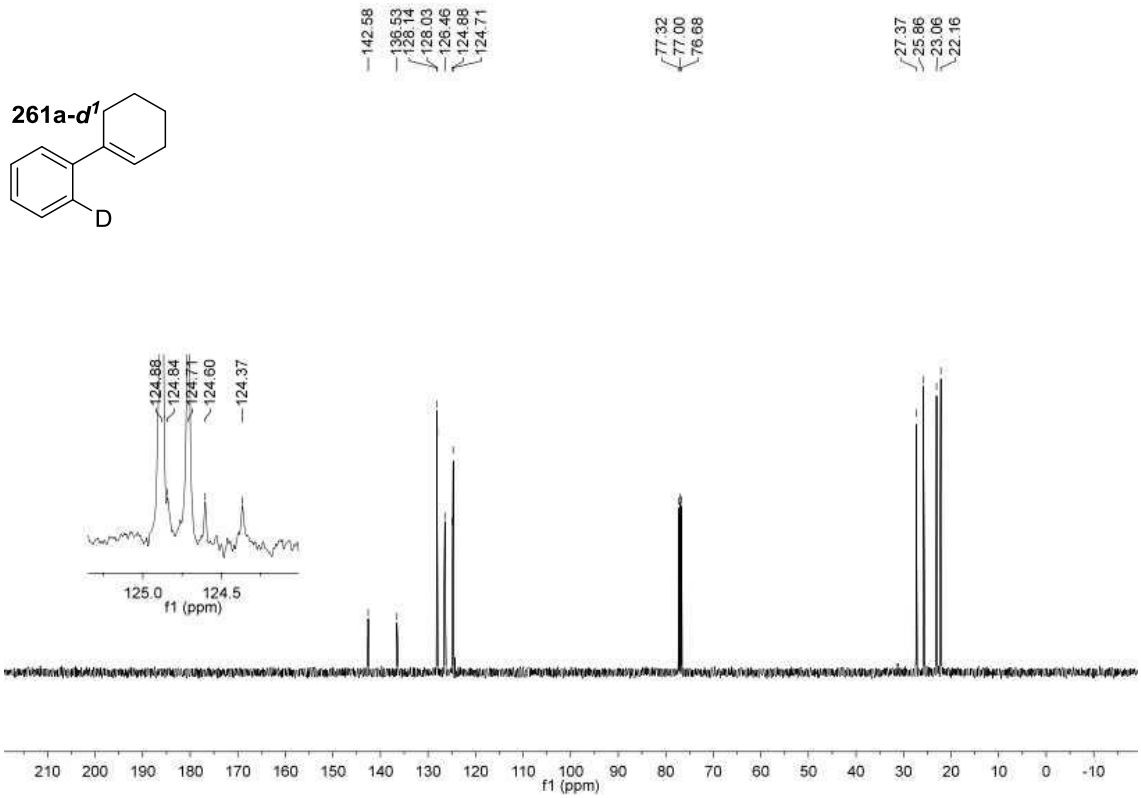
261a-d1
D
142.58
136.53
128.14
128.03
126.46
124.88
124.71
77.32
77.00
76.68
27.37
25.86
23.06
22.16
124.88
124.84
124.71
124.60
124.37
125.0
124.5
f1 (ppm)
f1 (ppm)

6.3. Fe-catalyzed Regiodivergent [1,2]-Shift of α-Aryl Aldehydes: Experimental Procedures

6.3.1. General considerations.

Reagents. Unless otherwise stated, all reactions were carried out under inert atmospheres in resalable screw-cap test tubes using standard Schlenk techniques for the manipulation of solvents and reagents. Anhydrous toluene and $FeBr_3$ (98% purity) were purchased from Sigma Aldrich. All chemicals were used as received. All other reagents were purchased from commercial sources and used also as received.

Analytical methods. ^{1}H NMR and ^{13}C NMR spectra and melting points (where applicable) are included for all compounds. ^{1}H NMR and ^{13}C NMR spectra were recorded on a Bruker 300 MHz, a Bruker 400 MHz and a Bruker 500 MHz at 20 ºC. All ^{1}H NMR spectra are reported in parts per million (ppm) downfield of TMS and were measured relative to the signals for $CHCl_3$ (7.27 ppm). All ^{13}C NMR spectra were reported in ppm relative to residual $CHCl_3$ (77.0 ppm) and were obtained with ^{1}H decoupling. Coupling constants, *J*, are reported in hertz (Hz). Melting points were measured using open glass capillaries in a Büchi B540 apparatus. Infrared spectra were recorded on a Bruker Tensor 27. Mass spectra were recorded on a Waters LCT Premier spectrometer. Gas chromatographic analyses were performed on Hewlett-Packard 6890 gas chromatography instrument with a FID detector using 25m x 0.20 mm capillary column with cross-linked methyl siloxane as the stationary phase. High Pressure Liquid Chromatographic (HPLC) analyses performed on Agilent Technologies Model 1260 Infinity HPLC chromatography instrument equipped with Agilent Eclipse Plus C18 (3.5 um, 4.6 x 100 mm) column and UV/Vis detector.

High Pressure Liquid Chromatographic (HPLC) analyses for **267jj** were performed on Agilent Technologies 1200 Series HPLC chromatography instrument equipped with a DAD detector. Daicel Chiralpack IC 250 x 4.6mm, 5mm and. Preparative High Pressure Liquid Chromatographic (Prep. HPLC) were performed on Waters HPLC equipped with a Binary Gradient Module 2545, a sample manager 2767, and UV/Vis detector 2489 equipped with Daicel Chiralpack IC 250 x 10mm, 5mm. Analytical Separation conditions: Chiralpack IC 250x4.6mm, 5mm, Hexane/TBME 95:5. 1 mL/min, sample concentration 1mg/mL in DCM, injection volume 5µL. Semi- preparative Separation conditions: Chiralpack IC 250x10mm, 5mm. Hexane/TBME 95:5. 5 mL/min, sample concentration 50mg/mL in Hexane/MTBE 95:5, injection volume 200µL. Gas Cromatography (GC) of **302jj** was performed on a Agilent 6890N GC equipped with a Agilent 5973 Inert Mass Selective detector. Separation conditions: Column

HP-CHIRAL-20B, 30m x 0.25mm, 0.25µm; isotherm 70ºC, 1.5mL/min, injection volume 1µL, split 5:1

Atomic absortion analysis was measured in an ICP-OED Spectro Arcos at the "Servei de Recursos Científics i Tècnics de la URV" in Tarragona, Spain.

Flash chromatography was performed with EM Science silica gel 60 (230-400 mesh) and using $KMnO_4$ as TLC stain. The yields reported in the Chapter 4 refer to isolated yields and represent an average of at least two independent runs. The procedures described in this section are representative. Thus, the yields may differ slightly from those given in the Chapter 4.

6.3.2. Optimization details

General procedure: A screw-cap vial charged with **267a** (0.25 mmol), Lewis acid (5 mol%) and toluene (1.0 mL) was heated at the desired temperature. After stirring for 16 h, the reaction mixture was allowed to reach room temperature and dodecane (57 µL, 0.25 mmol) was added as internal standard. After dilution with ethyl acetate, an aliquot of each reaction was analysed by GC. See Tables 5.1 to 5.4.

6.3.3. Atomic Absortion of a sample of $FeBr_3$ (Aldrich)

Sample preparation: 200.0 mg of $FeBr_3$ were stirred with 1.0 mL of HNO_3 at room temperature for 1h. Then, the solution was diluted until 100.0 mL with miliQ water.

Element	Conc (ppb)	rsd
Al	946,7	0,97
Cr	641,8	0,14
B	523,1	0,48
Ru	154,2	4,8
Mn	129,3	2,28
Mg	86,5	31,44
Zn	72,3	0,15
Mg	65,9	5,85
Ti	36,5	13,23
Pt	15,6	4,18
Cu	11,3	31,34
Co	6,5	6,7

Table 6.3.S1. Most abundants metallic traces present in an $FeBr_3$ Sigma-Aldrich sample.

SPECTRO

Printing Date: 30/01/2013 11:10:59
Current User: Operator

Method Name: Semiquant 2 Creation Date: 2011-05-18 12:07:51
Method Autor: Operator Last Change: 2013-01-30 11:01:30

Sample Name: FeBr3 Sample Type: Unknown Sample

Measure Date: 2013-01-30 11: Recalc. Date: State: Measured Quality: Total Dilution: 1.000000

Sample Identification

Sample Name
FeBr3

	Ag 328.068	Al 167.078	Ar 404.442	As 189.042	Au 242.795	B 249.773	Ba 455.404
Conc 1	3.622[ppb]	937.651[ppb]	2974620	6.586[ppb]	<-27.975[ppb]	523.012[ppb]	168.337[ppb]
Conc 2	2.878[ppb]	956.006[ppb]	2969040	<-3.215[ppb]	<-25.905[ppb]	525.675[ppb]	167.578[ppb]
Conc 3	2.475[ppb]	946.563[ppb]	2956230	<0.502[ppb]	<-25.899[ppb]	520.697[ppb]	166.199[ppb]
Conc MinRange	*0.407[ppb]*	*0.334[ppb]*	---	*3.238[ppb]*	*1.063[ppb]*	*6.248[ppb]*	*0.165[ppb]*
Conc Mean	**2.992[ppb]**	**946.740[ppb]**	**2966630**	**<1.291[ppb]**	**<-26.593[ppb]**	**523.128[ppb]**	**167.371[ppb]**
Conc MaxRange	*600.000[ppb]*	*2400.00[ppb]*	---	*2400.00[ppb]*	*2400.00[ppb]*	*2400.00[ppb]*	*2400.00[ppb]*
Conc RSD	***19.450***	***0.970***	---	***383.254***	***4.501***	***0.476***	***0.648***
Conc SD	***0.582[ppb]***	***9.179[ppb]***	***9428.90***	***<4.948[ppb]***	***<1.197[ppb]***	***2.491[ppb]***	***1.084[ppb]***
Reported	---	---	---	---	---	---	---

	Be 313.042	Ca 396.847	Cd 214.438	Co 228.616	Cr 267.716	Cu 324.754	Dy 353.170
Conc 1	1.898[ppb]	284.807[ppb]	9.935[ppb]	6.024[ppb]	641.313[ppb]	15.382[ppb]	<-164.757[ppb]
Conc 2	0.363[ppb]	284.233[ppb]	10.250[ppb]	6.887[ppb]	642.843[ppb]	9.782[ppb]	<-169.768[ppb]
Conc 3	0.147[ppb]	294.574[ppb]	10.228[ppb]	6.540[ppb]	641.185[ppb]	8.806[ppb]	<-165.544[ppb]
Conc MinRange	*0.089[ppb]*	*0.724[ppb]*	*0.418[ppb]*	*0.631[ppb]*	*0.593[ppb]*	*2.306[ppb]*	*2.655[ppb]*
Conc Mean	**0.803[ppb]**	**287.871[ppb]**	**10.137[ppb]**	**6.483[ppb]**	**641.780[ppb]**	**11.323[ppb]**	**<-166.690[ppb]**
Conc MaxRange	*2400.00[ppb]*	*2400.00[ppb]*	*2400.00[ppb]*	*2400.00[ppb]*	*2400.00[ppb]*	*2400.00[ppb]*	*2400.00[ppb]*
Conc RSD	***118.930***	***2.019***	***1.737***	***6.699***	***0.144***	***31.341***	***1.617***
Conc SD	***0.955[ppb]***	***5.812[ppb]***	***0.176[ppb]***	***0.434[ppb]***	***0.923[ppb]***	***3.549[ppb]***	***<2.695[ppb]***
Reported	---	---	---	---	---	---	---

	Er 326.478	Eu 420.505	Fe 259.941	Gd 342.247	Ge 164.919	Hf 264.141	Hg 194.227
Conc 1	13.787[ppb]	4.587[ppb]	>339748[ppb]	74.966[ppb]	<-4.352[ppb]	6.343[ppb]	6.968[ppb]
Conc 2	12.862[ppb]	<-0.651[ppb]	>340070[ppb]	78.616[ppb]	14.398[ppb]	4.490[ppb]	5.728[ppb]
Conc 3	11.994[ppb]	<-1.425[ppb]	>334857[ppb]	75.902[ppb]	23.285[ppb]	7.726[ppb]	8.190[ppb]
Conc MinRange	*4.995[ppb]*	*1.702[ppb]*	*1.432[ppb]*	*3.286[ppb]*	*2.207[ppb]*	*0.295[ppb]*	*1.396[ppb]*
Conc Mean	**12.881[ppb]**	**<0.837[ppb]**	**>338225[ppb]**	**76.495[ppb]**	**<11.110[ppb]**	**6.187[ppb]**	**6.962[ppb]**
Conc MaxRange	*2400.00[ppb]*	*2400.00[ppb]*	*2400.00[ppb]*	*2400.00[ppb]*	*2400.00[ppb]*	*2400.00[ppb]*	*2400.00[ppb]*
Conc RSD	***6.960***	***390.787***	***0.864***	***2.478***	***126.991***	***26.245***	***17.683***
Conc SD	***0.897[ppb]***	***<3.270[ppb]***	***>2921.21[ppb]***	***1.896[ppb]***	***<14.109[ppb]***	***1.624[ppb]***	***1.231[ppb]***
Reported	---	---	---	---	---	---	---

	Ho 345.600	In 325.609	Ir 212.681	Ir 224.268	La 408.672	Lu 261.542	Mg 279.079
Conc 1	<-3.732[ppb]	<-70.025[ppb]	<-19.238[ppb]	<-51.600[ppb]	11.537[ppb]	7.678[ppb]	61.446[ppb]
Conc 2	<-1.035[ppb]	<-76.649[ppb]	<-20.417[ppb]	<-54.604[ppb]	10.808[ppb]	7.465[ppb]	67.575[ppb]
Conc 3	<-1.513[ppb]	<-70.446[ppb]	<-25.259[ppb]	<-53.625[ppb]	11.339[ppb]	7.357[ppb]	68.559[ppb]
Conc MinRange	*2.018[ppb]*	*19.629[ppb]*	*2.240[ppb]*	*3.306[ppb]*	*3.058[ppb]*	*0.040[ppb]*	*2.300[ppb]*
Conc Mean	**<-2.093[ppb]**	**<-72.373[ppb]**	**<-21.638[ppb]**	**<-53.277[ppb]**	**11.228[ppb]**	**7.500[ppb]**	**65.860[ppb]**
Conc MaxRange	*2400.00[ppb]*	*2400.00[ppb]*	*2400.00[ppb]*	*2400.00[ppb]*	*2400.00[ppb]*	*2400.00[ppb]*	*2400.00[ppb]*
Conc RSD	***68.759***	***5.124***	***14.747***	***2.875***	***3.356***	***2.178***	***5.852***
Conc SD	***<1.439[ppb]***	***<3.708[ppb]***	***<3.191[ppb]***	***<1.532[ppb]***	***0.377[ppb]***	***0.163[ppb]***	***3.854[ppb]***
Reported	---	---	---	---	---	---	---

Smart Analyzer Vision 4.02.0831 - 1 - Spectro Analytical Intruments GmbH

SPECTRO

Printing Date: 30/01/2013 11:10:59
Current User: Operator

Method Name: Semiquant 2
Method Autor: Operator

Creation Date: 2011-05-18 12:07:51
Last Change: 2013-01-30 11:01:30

	Mg 279.553	Mn 257.611	Mo 202.095	Nb 295.088	Nd 401.225	Ni 231.604	Os 225.585
Conc 1	117.725[ppb]	129.412[ppb]	10.025[ppb]	<-20.834[ppb]	<-4.091[ppb]	334.628[ppb]	158.955[ppb]
Conc 2	68.378[ppb]	126.359[ppb]	4.607[ppb]	<-15.910[ppb]	<-2.255[ppb]	329.102[ppb]	158.948[ppb]
Conc 3	73.288[ppb]	132.246[ppb]	3.455[ppb]	<-18.038[ppb]	<-8.593[ppb]	328.059[ppb]	157.334[ppb]
Conc MinRange	0.073[ppb]	0.137[ppb]	3.087[ppb]	3.548[ppb]	3.726[ppb]	2.128[ppb]	0.720[ppb]
Conc Mean	86.464[ppb]	129.339[ppb]	6.029[ppb]	<-18.261[ppb]	<-4.980[ppb]	330.596[ppb]	158.412[ppb]
Conc MaxRange	2400.00[ppb]	2400.00[ppb]	2400.00[ppb]	2400.00[ppb]	2400.00[ppb]	2400.00[ppb]	2400.00[ppb]
Conc RSD	31.440	2.276	58.186	13.525	65.488	1.068	0.590
Conc SD	27.184[ppb]	2.944[ppb]	3.508[ppb]	<2.470[ppb]	<3.261[ppb]	3.530[ppb]	0.934[ppb]
Reported	---	---	---	---	---	---	---

	P 177.495	Pb 220.353	Pd 324.270	Pd 340.458	Pr 411.846	Pt 177.708	Re 221.426
Conc 1	146.442[ppb]	52.699[ppb]	<-427.049[ppb]	<-31.119[ppb]	1499.38[ppb]	16.163[ppb]	<-43.205[ppb]
Conc 2	136.212[ppb]	49.384[ppb]	<-429.060[ppb]	<-26.803[ppb]	1519.81[ppb]	15.769[ppb]	<-47.538[ppb]
Conc 3	134.239[ppb]	47.114[ppb]	<-436.693[ppb]	<-23.355[ppb]	1515.76[ppb]	14.889[ppb]	<-47.804[ppb]
Conc MinRange	2.407[ppb]	5.413[ppb]	3.076[ppb]	3.980[ppb]	27.405[ppb]	8.319[ppb]	1.849[ppb]
Conc Mean	138.964[ppb]	49.732[ppb]	<-430.934[ppb]	<-27.092[ppb]	1511.65[ppb]	15.607[ppb]	<-46.182[ppb]
Conc MaxRange	12000.0[ppb]	2400.00[ppb]	2400.00[ppb]	2400.00[ppb]	2400.00[ppb]	2400.00[ppb]	2400.00[ppb]
Conc RSD	4.714	5.648	1.181	14.358	0.716	4.179	5.590
Conc SD	6.551[ppb]	2.809[ppb]	<5.088[ppb]	<3.890[ppb]	10.817[ppb]	0.652[ppb]	<2.582[ppb]
Reported	---	---	---	---	---	---	---

	Rh 343.489	Ru 240.272	Sb 206.833	Se 196.090	Si 251.612	Sm 359.260	Sn 189.991
Conc 1	<-17.599[ppb]	158.401[ppb]	1188.45[ppb]	<-1420.01[ppb]	>9633.43[ppb]	14.484[ppb]	<-81.823[ppb]
Conc 2	<-14.156[ppb]	158.595[ppb]	1204.10[ppb]	<-1434.41[ppb]	85.556[ppb]	12.501[ppb]	<-80.725[ppb]
Conc 3	<-18.753[ppb]	145.673[ppb]	1228.66[ppb]	<-1434.93[ppb]	1692.58[ppb]	17.107[ppb]	<-76.677[ppb]
Conc MinRange	12.271[ppb]	2.544[ppb]	6.295[ppb]	3.525[ppb]	27.452[ppb]	6.365[ppb]	0.591[ppb]
Conc Mean	<-16.836[ppb]	154.223[ppb]	1207.07[ppb]	<-1429.78[ppb]	>3803.86[ppb]	14.698[ppb]	<-79.742[ppb]
Conc MaxRange	2400.00[ppb]	2400.00[ppb]	2400.00[ppb]	2400.00[ppb]	2400.00[ppb]	2400.00[ppb]	2400.00[ppb]
Conc RSD	14.207	4.802	1.679	0.592	134.392	15.718	3.398
Conc SD	<2.392[ppb]	7.405[ppb]	20.269[ppb]	<8.468[ppb]	>5112.10[ppb]	2.310[ppb]	<2.710[ppb]
Reported	---	---	---	---	---	---	---

	Sr 407.771	Ta 240.063	Tb 350.920	Te 170.000	Th 401.913	Ti 334.941	Tl 190.864
Conc 1	3.687[ppb]	<-55.703[ppb]	<-5.668[ppb]	<-270.513[ppb]	<-10.592[ppb]	37.874[ppb]	<-24.184[ppb]
Conc 2	2.612[ppb]	<-147.174[ppb]	<-6.936[ppb]	<-241.252[ppb]	<-5.771[ppb]	40.478[ppb]	<-23.218[ppb]
Conc 3	2.461[ppb]	<-149.697[ppb]	<-8.072[ppb]	<-284.236[ppb]	<-11.304[ppb]	31.124[ppb]	<-22.713[ppb]
Conc MinRange	0.082[ppb]	4.640[ppb]	1.874[ppb]	2.120[ppb]	18.565[ppb]	0.697[ppb]	6.009[ppb]
Conc Mean	2.920[ppb]	<-117.525[ppb]	<-6.892[ppb]	<-265.334[ppb]	<-9.222[ppb]	36.492[ppb]	<-23.372[ppb]
Conc MaxRange	2400.00[ppb]	2400.00[ppb]	2400.00[ppb]	2400.00[ppb]	2400.00[ppb]	2400.00[ppb]	2400.00[ppb]
Conc RSD	22.901	45.568	17.452	8.275	32.634	13.230	3.200
Conc SD	0.669[ppb]	<53.554[ppb]	<1.203[ppb]	<21.955[ppb]	<3.010[ppb]	4.828[ppb]	<0.748[ppb]
Reported	---	---	---	---	---	---	---

	Tm 313.126	U 385.958	V 292.464	Y 371.030	Yb 328.937	Zn 213.856	Ga 417.206
Conc 1	<-19.218[ppb]	1962.37[ppb]	<-26.589[ppb]	6.976[ppb]	3.854[ppb]	72.320[ppb]	8699.61
Conc 2	<-19.920[ppb]	1949.17[ppb]	<-33.056[ppb]	1.662[ppb]	3.992[ppb]	72.397[ppb]	8624.50
Conc 3	<-19.982[ppb]	1969.97[ppb]	<-33.501[ppb]	0.611[ppb]	4.031[ppb]	72.178[ppb]	8688.53
Conc MinRange	0.750[ppb]	41.234[ppb]	1.442[ppb]	0.505[ppb]	0.183[ppb]	0.495[ppb]	---
Conc Mean	<-19.707[ppb]	1960.50[ppb]	<-31.048[ppb]	3.083[ppb]	3.958[ppb]	72.298[ppb]	8670.88
Conc MaxRange	2400.00[ppb]	2400.00[ppb]	2400.00[ppb]	2400.00[ppb]	2400.00[ppb]	2400.00[ppb]	---
Conc RSD	2.154	0.537	12.460	110.675	2.357	0.154	---
Conc SD	<0.424[ppb]	10.525[ppb]	<3.869[ppb]	3.412[ppb]	0.093[ppb]	0.111[ppb]	40.546

Smart Analyzer Vision 4.02.0831 - 2 - Spectro Analytical Intruments GmbH

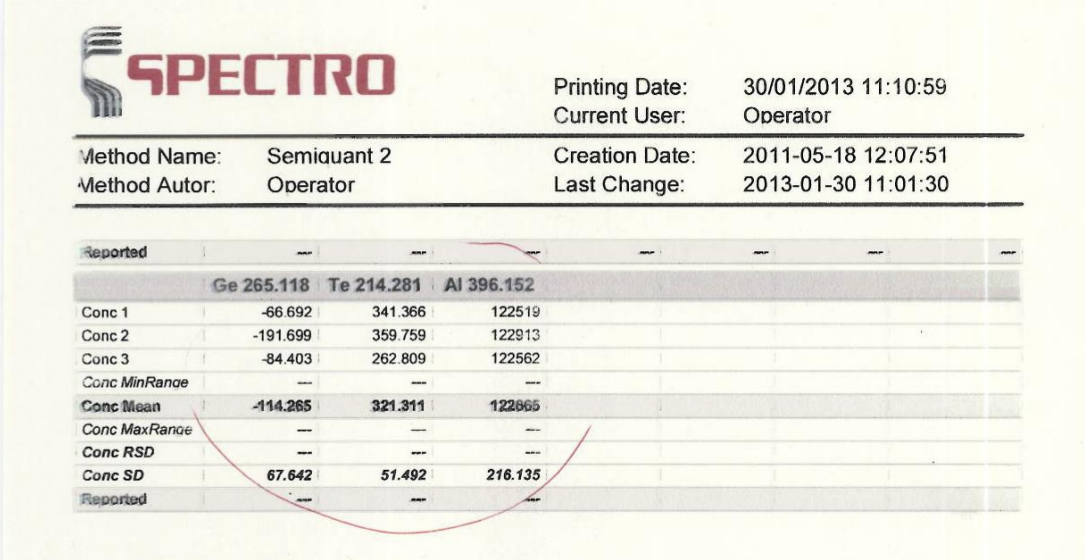

SPECTRO

Printing Date:	30/01/2013 11:10:59		
Current User:	Operator		
Method Name:	Semiquant 2	Creation Date:	2011-05-18 12:07:51
Method Autor:	Operator	Last Change:	2013-01-30 11:01:30

Reported	---	---	---
	Ge 265.118	Te 214.281	Al 396.152
Conc 1	-66.692	341.366	122519
Conc 2	-191.699	359.759	122913
Conc 3	-84.403	262.809	122562
Conc MinRange	---	---	---
Conc Mean	**-114.265**	**321.311**	**122865**
Conc MaxRange	---	---	---
Conc RSD	---	---	---
Conc SD	***67.642***	***51.492***	***216.135***
Reported	---	---	---

Figure 6.3.S1. Results from Atomic Absorption Spectroscopy.

Note: The metal elements marked in red were residual signals. Therefore, they were not taken into consideration.

6.3.4. Synthesis and characterization of α-arylaldehydes.

1. **267a**,[354] **267b**,[225] **267c**,[227] **267d**,[232] **267e**, **267f**, **267g**, **267h**, **267i**, **267j**, **267m** and **267n** were prepared from commercially available phenylacetonitrile derivative in essentially one step and with only one purification via alkylation with NaHMDS followed by treatment with the corresponding organic halide; the crude reaction mixture was then treated without purification with DIBAL-H, affording the desired starting α-arylaldehydes.
2. **267z**[355] was prepared in one step from the Pd-catalyzed α- arylation of 2-phenylpropanal with 4-bromoanisole following the methodology described by Buchwald (*Angew. Chem. Int. Ed.* **2007**, *46*, 7236 & *Org. Lett*. **2008**, *10*, 4561).
3. **267k** and **267l** were prepared from commercially available 2-(2-bromo-5-methoxyphenyl)acetonitrile following the literature procedure.[227] The reaction sequence included only two purifications by chromatography and it was initiated by alkylation of the phenylacetonitrile derivative with NaHMDS and 1,5-dibromopentane and the crude mixture was treated without purification with BBr_3 in DCM at 0 ºC. Subsequently, the crude alcohol was treated with DIBALH and the purified aldehyde was further treated with the corresponding alkylating agent to furnish **267k** or **267l**.

[354] Wang, Z.; Li, M.; Zhang, W.; Jia, J.; Wang, F. Xue, S. *Tetrahedron. Lett.* **2011**, *52*, 5968.
[355] Ranu, B. C.; Jana, U. J. *J. Org. Chem.* **1998**, *63*, 8212.

4. **267aa**, **267b**, **267cc**, **267dd**, **267gg**, **267hh**, **267ii**, **267jj**, **267kk**, **267mm** and **267nn** were prepared prepared from commercially available phenylacetonitrile derivative in essentially one step and with only one purification via alkylation with NaHMDS followed by treatment with the corresponding organic halide (in the case of dealing with **267hh**, **267ii**, **267jj** and **267kk**, the alkylation was done in a sequential manner after TLC judged no starting material left without any purification); the crude reaction mixture was then treated without purification with DIBAL-H, affording the desired starting α-arylaldehydes.
5. **267ee** and **267ff** were prepared in essentially two steps with only two purifications in a sequence that started with the alkylation of 4-methoxyphenylacetonitrile with NaHMDS and *n*-butyliodide followed by treatment of the crude mixture with BBr_3 in DCM. The corresponding purified alcohol was reduced with DIBALH and the crude mixture was treated without purification with the corresponding organic halide in K_2CO_3/DMF.
6. **267ll** was prepared from the corresponding cyanohydrine followed by alkylation and treatment of the crude with DIBALH.

6.3.5. Characterization of α-aryl aldehydes

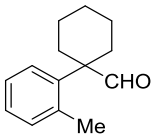

1-(*o*-tolyl)cyclohexanecarbaldehyde (267e): Colorless oil. ^{1}H NMR (300 MHz, Chloroform-*d*) δ 9.45 (s, 1H), 7.46 (d, *J* = 7.5 Hz, 1H), 7.31-7.14 (m, 3H), 2.32 (s, 3H), 2.30-2.23 (m, 2H), 1.95-1.83 (m, 2H), 1.74-1.61 (m, 5H), 1.47-1.31 (m, 1H) ppm. ^{13}C NMR (75 MHz, Chloroform-*d*) δ 203.1, 138.9, 137.4, 132.8, 127.6, 127.4, 126.5, 54.9, 31.1, 25.8, 22.6, 21.7 ppm. IR (neat, cm^{-1}): 2928, 1720, 1451, 756, 731, 459. HRMS *calcd.* for ($C_{14}H_{18}O$+Na): 225,1250, *found* 225,1256.

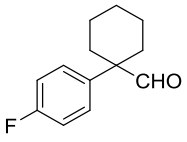

1-(4-fluorophenyl)cyclohexanecarbaldehyde (267f): Yellow solid in the fridge that melts at room temperature. ^{1}H NMR (300 MHz, Chloroform-*d*) δ 9.34 (s, 1H), 7.35-7.22 (m, 2H), 7.12-6.97 (m, 2H), 2.35-2.23 (m, 2H), 1.88-1.73 (m, 2H), 1.73-1.54 (m, 3H), 1.57-1.38 (m, 2H), 1.38-1.23 (m, 1H) ppm. ^{13}C NMR (75 MHz, Chloroform-*d*) δ 202.1, 162.0 (d, *J* = 246.7 Hz), 135.6 (d, *J*

= 3.3 Hz), 128.9 (d, *J* = 8.0 Hz), 115.7 (d, *J* = 21.2 Hz), 53.9, 31.5, 25.6, 22.8 ppm. IR (neat, cm^{-1}): 2933, 1721, 1508, 1232, 829, 533. HRMS *calcd.* for ($C_{13}H_{15}FO$+Na): 229,0999, *found* 229,1001.

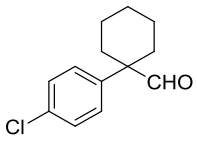

1-(4-chlorophenyl)cyclohexanecarbaldehyde (267g): White solid. Mp: 38-40 ºC. ^{1}H NMR (300 MHz, Chloroform-*d*) δ 9.35 (s, 1H), 7.34 (d, *J* = 8.7 Hz, 2H), 7.25 (d, *J* = 8.7 Hz, 2H), 2.34-2.19 (m, 2H), 1.90-1.74 (m, 2H), 1.71-1.58 (m, 3H), 1.54-1.41 (m, 2H), 1.37-1.28 (m, 1H) ppm. ^{13}C NMR (75 MHz, Chloroform-*d*) δ 202.1, 138.4, 133.4, 129.1, 128.7, 54.1, 31.4, 25.6, 22.8 ppm. IR (neat, cm^{-1}): 2932, 2858, 1720, 1491, 1094, 724, 521. HRMS *calcd.* for ($C_{13}H_{15}ClO$+H): 223.0884, *found* 223.0886.

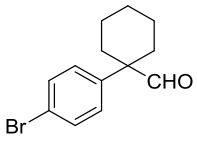

1-(4-bromophenyl)cyclohexanecarbaldehyde (267h): White solid. Mp: 46-47 ºC. ^{1}H NMR (300 MHz, Chloroform-*d*) δ 9.35 (s, 1H), 7.49 (d, *J* = 8.6 Hz, 2H), 7.19 (d, *J* = 8.6 Hz, 2H), 2.26 (dd, *J* = 13.2, 5.2 Hz, 2H), 1.89-1.74 (m, 2H), 1.72-1.47 (m, 3H), 1.56-1.39 (m, 2H), 1.39-1.23 (m, 1H) ppm. ^{13}C NMR (75 MHz, Chloroform-*d*) δ 201,9, 138.9, 132.1, 129.0, 121.5, 54.2, 31.3, 25.6, 22.8 ppm. IR (neat, cm^{-1}): 2921, 2850, 1716, 1450, 1003, 820, 526. HRMS *calcd.* for ($C_{13}H_{15}BrO$+Na): 289,0198, *found* 289,0199.

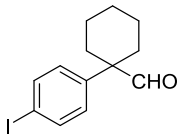

1-(4-iodophenyl)cyclohexanecarbaldehyde (267i): Orange solid in the fridge that melts at room temperature. ^{1}H NMR (300 MHz, Chloroform-*d*) δ 9.35 (s, 1H), 7.70 (d, *J* = 8.8 Hz, 2H), 7.07 (d, *J* = 8.8 Hz, 2H), 2.32-2.22 (m, 2H), 1.89-1.75 (m, 2H), 1.71-1.58 (m, 4H), 1.51-1.46 (m, 1H), 1.34 (s, 1H) ppm. ^{13}C NMR (75 MHz, Chloroform-*d*) δ 202.0, 139.7, 138.1, 129.3, 93.2, 54.3, 31.3, 25.6, 22.8 ppm. IR (neat, cm^{-1}): 2930, 1721, 1485, 1002, 811, 137, 520. HRMS *calcd.* for ($C_{13}H_{15}IO$+H): 315.0240, *found* 315.0241.

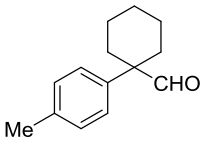

1-(*p*-tolyl)cyclohexanecarbaldehyde (267j): Colorless oil. ^{1}H NMR (300 MHz, Chloroform-*d*) δ 9.37 (s, 1H), 7.24 (d, *J* = 8.4 Hz, 2H), 7.20 (d, *J* = 8.5 Hz, 2H), 2.35 (s, 3H), 2.34-2.25 (m, 2H), 1.92-1.77 (m, 2H), 1.76-1.57 (m, 3H), 1.58-1.43 (m, 2H), 1.41-1.27 (m, 1H). ^{13}C NMR (75 MHz, Chloroform-*d*) δ 202.4, 137,0, 136.7, 129.7, 127.1, 54.1, 31.4, 25.8, 22.9, 21.0 ppm.

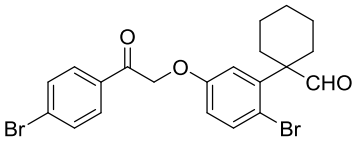

1-(2-bromo-5-(2-(4-bromophenyl)-2-oxoethoxy)phenyl)cyclohexanecarbaldehyde (267l): Yellow solid. Mp: 128-130 ºC. ^{1}H NMR (300 MHz, Chloroform-*d*) δ 9.92 (s, 1H), 7.88 (d, *J* = 8.5 Hz, 2H), 7.67 (d, *J* = 8.8 Hz, 2H), 7.46 (d, *J* = 8.7 Hz, 1H), 7.13 (d, *J* = 3.1 Hz, 1H), 5.25-5.17 (m, 2H), 6.67 (dd, *J* = 8.7, 3.0 Hz, 1H), 2.40-2.24 (m, 2H), 2.01-1.85 (m, 2H), 1.77-1.59 (m, 5H), 1.43 (s, 1H) ppm. ^{13}C NMR (75 MHz, Chloroform-*d*) δ 204.2, 193.5, 157.5, 144.3, 135.6, 133.2, 132.4, 129.8, 129.6, 118.1, 115.0, 114.0, 71.1, 54.8, 31.7, 25.6, 22.5 ppm. IR (neat, cm^{-1}): 2933, 1740, 1693, 1583, 1216, 969, 809, 452. HRMS *calcd.* for ($C_{21}H_{20}Br_2O_3$+H): 478.9852, *found* 478.9862.

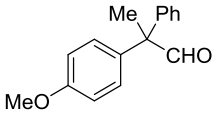

2-(4-methoxyphenyl)-2-phenylpropanal (267z): Colorless oil. ^{1}H NMR (300 MHz, Chloroform-*d*) δ 9.89 (s, 1H), 7.42-7.29 (m, 3H), 7.19 (d, *J* = 6.8 Hz, 2H), 7.13 (d, *J* = 8.8 Hz, 2H), 6.92 (d, *J* = 8.8 Hz, 2H), 3.83 (s, 3H), 1.77 (s, 3H) ppm. ^{13}C NMR (75 MHz, Chloroform-*d*) δ 199.7, 158.9, 142.5, 133.5, 129.5, 128.9, 128.2, 127.3, 114.3, 59.3, 55.4, 22.9 ppm. IR (neat, cm^{-1}): 2980, 2836, 1720, 1510, 1249, 1028, 699, 541. HRMS *calcd.* for ($C_{16}H_{16}O_2$+Na): 263,1055, *found* 263,1043.

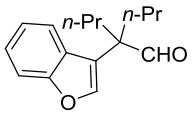

2-(benzofuran-3-yl)-2-propylpentanal (267aa): Colorless oil. ^{1}H NMR (300 MHz, Chloroform-*d*) δ 9.51 (s, 1H), 7.68 (s, 1H), 7.54 (d, *J* = 8.2 Hz, 1H), 7.51 (d, *J* = 8.9 Hz, 1H), 7.37-7.25 (m, 1H), 7.28-7.16 (m, 1H), 2.11-1.92 (m, 4H), 1.25-1.10 (m, 4H), 0.91 (t, *J* = 7.2 Hz, 6H). ^{13}C NMR (75 MHz, Chloroform-*d*) δ 202.5, 155.7, 143.4, 126.3, 124.6, 122.8, 120.9, 119.1, 111.9, 53.9, 33.81, 17.4, 14.6 ppm. IR (neat, cm^{-1}): 2958, 1726, 1453, 1105, 858, 743, 423. HRMS *calcd.* for ($C_{16}H_{20}O_2$+Na): 267,1356, *found* 267,1360.

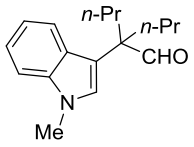

2-(1-methyl-1*H*-indol-3-yl)-2-propylpentanal (267bb): White solid. Mp: 58-60 ºC.^{1}H NMR (400 MHz, Chloroform-*d*) δ 9.43 (s, 1H), 7.56 (d, *J* = 8.1 Hz, 1H), 7.32 (dd, *J* = 8.2, 0.8 Hz, 1H), 7.24 (ddd, *J* = 8.2, 7.1, 1.0 Hz, 1H), 7.08 (ddd, *J* = 8.1, 7.0, 1.1 Hz, 1H), 7.03 (s, 1H), 3.80 (s, 3H), 2.14-2.01 (m, 2H), 2.01-1.89 (m, 2H), 1.25-1.10 (m, 4H), 0.91 (t, *J* = 7.3 Hz, 6H) ppm. ^{13}C NMR (75 MHz, Chloroform-*d*) δ 203.0, 137.6, 128.0, 126.5, 121.8, 120.4, 119.4, 112.7, 109.5, 54.2, 33.4, 33.0, 17.3, 14.8 ppm. IR (neat, cm^{-1}): 2953, 1707, 1463, 1374, 1242, 1149, 737, 432. HRMS *calcd.* for ($C_{17}H_{23}NO$+H): 258,1852, *found* 258,1842.

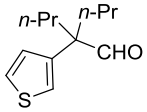

2-propyl-2-(thiophen-3-yl)pentanal (267cc): Yellow oil. ^{1}H NMR (300 MHz, Chloroform-*d*) δ 9.44 (s, 1H), 7.32 (dd, *J* = 5.0, 2.9 Hz, 1H), 7.14 (dd, *J* = 2.9, 1.4 Hz, 1H), 6.95 (dd, *J* = 5.0, 1.4 Hz, 1H), 1.92-1.85 (m, 4H), 1.22-1.08 (m, 4H), 0.91 (t, *J* = 7.2 Hz, 6H) ppm. ^{13}C NMR (75 MHz, Chloroform-*d*) δ 202.3, 140.8, 126.7, 126.0, 122.2, 56.1, 35.1, 17.3, 14.7 ppm. IR (neat, cm^{-1}): 2957, 2872, 1723, 1461, 856, 778, 655. HRMS *calcd.* for ($C_{12}H_{18}OS$+Na): 233,0971, *found* 233,0971.

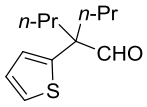

2-propyl-2-(thiophen-2-yl)pentanal (267dd): Colorless oil. ^{1}H NMR (300 MHz, Chloroform-*d*) δ 9.44 (s, 1H), 7.30 (dd, *J* = 5.2, 1.2 Hz, 1H), 7.04 (dd, *J* = 5.1, 3.6 Hz, 1H), 6.92 (dd, *J* = 3.5, 1.2 Hz, 1H), 2.04-1.85 (m, 4H), 1.34-1.10 (m, 4H), 0.95 (t, *J* = 7.2 Hz, 6H) ppm. ^{13}C NMR (75 MHz, Chloroform-*d*) δ 200.6, 144.2, 127.2, 125.3, 125.1, 56.3, 36.1, 17.3, 14.7 ppm. IR (neat, cm^{-1}): 2956, 1712, 1460, 852, 693. HRMS *calcd.* for ($C_{12}H_{18}OS$+Na): 233,0974, *found* 233,0971.

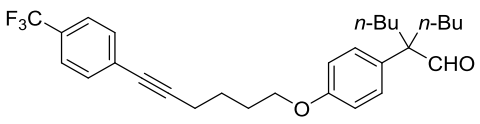

2-butyl-2-(4-((6-(4-(trifluoromethyl)phenyl)hex-5-yn-1-yl)oxy)phenyl)hexanal (267ee): Colorless oil. ^{1}H NMR (300 MHz, Chloroform-*d*) δ 9.41 (s, 1H), 7.55 (d, *J* = 8.4 Hz, 2H), 7.49 (d, *J* = 8.4 Hz, 2H), 7.14 (d, *J* = 8.8 Hz, 2H), 6.91 (d, *J* = 8.8 Hz, 2H), 4.03 (t, *J* = 6.1 Hz, 2H), 2.53 (t, *J* =

6.9 Hz, 2H), 2.04-1.90 (m, 2H), 1.95-1.77 (m, 6H), 1.41-1.23 (m, 4H), 1.16-0.99 (m, 4H), 0.88 (t, *J* = 7.3 Hz, 6H) ppm. ^{13}C NMR (75 MHz, Chloroform-*d*) δ 203.2, 158.1, 131.9, 131.3, 128.8, 125.3 (d, *J* = 3.8 Hz), 114.7, 92.7, 80.1, 67.4, 56.8, 31.8, 28.6, 26.1, 25.3, 23.5, 19.3, 14.1 ppm. IR (neat, cm^{-1}): 2934, 1721, 1611, 1511, 1320, 1165, 1066, 841, 523. HRMS *calcd.* for ($C_{29}H_{35}F_3O_2$+Na): 495,2481, *found* 495,2479.

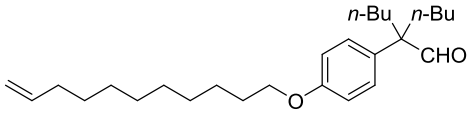

2-butyl-2-(4-(undec-10-en-1-yloxy)phenyl)hexanal (267ff): Yellow oil. ^{1}H NMR (300 MHz, Chloroform-*d*) δ 9.41 (s, 1H), 7.13 (d, *J* = 8.8 Hz, 2H), 6.90 (d, *J* = 8.8 Hz, 2H), 5.82 (ddt, *J* = 16.9, 10.2, 6.7 Hz, 1H), 5.00 (dq, *J* = 17.4, 1.8 Hz, 1H), 4.94 (ddd, *J* = 9.0, 2.2, 1.1 Hz, 1H), 3.95 (t, *J* = 6.5 Hz, 2H), 2.11-2.00 (m, 2H), 1.95-1.82 (m, 4H), 1.83-1.73 (m, 2H), 1.32 (dd, *J* = 5.2, 2.5 Hz, 16H), 1.16-0.99 (m, 4H), 0.88 (t, *J* = 7.3 Hz, 6H) ppm. ^{13}C NMR (75 MHz, Chloroform-*d*) δ 203.3, 158.3, 139.3, 131.0, 128.78, 114.7, 114.3, 68.1, 56.8, 33.9, 31.8, 29.7, 29.6, 29.5, 29.4, 29.3, 29.1, 26.2, 26.0, 23.5, 14.1 ppm. IR (neat, cm^{-1}): 2926, 2856, 1723, 1609, 1511, 1465, 1249, 827, 522. HRMS *calcd.* for ($C_{27}H_{44}O_2$+Na): 423,3221, *found* 423,3234.

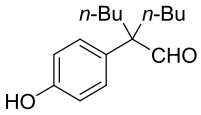

2-butyl-2-(4-hydroxyphenyl)hexanal (267gg): White solid. Mp: 58-61 ºC. ^{1}H NMR (300 MHz, Chloroform-*d*) δ 9.41 (s, 1H), 7.10 (d, *J* = 8.7 Hz, 2H), 6.84 (d, *J* = 8.7 Hz, 2H), 4.92 (s, 1H), 1.94-1.82 (m, 4H), 1.41-1.22 (m, 4H), 1.15-0.98 (m, 4H), 0.88 (t, *J* = 7.3 Hz, 6H) ppm. ^{13}C NMR (75 MHz, Chloroform-*d*) δ 203.4, 154.8, 131.4, 129.0, 115.7, 56.8, 31.8, 26.0, 23.4, 14.1 ppm. IR (neat, cm^{-1}): 3348, 2952, 2589, 1692, 1512, 1244, 825, 552. HRMS *calcd.* for ($C_{16}H_{24}O_2$-H): 247,1704, *found* 247,1707.

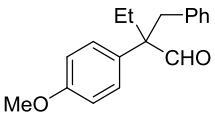

2-benzyl-2-(4-methoxyphenyl)butanal (267hh): White solid. Mp: 53-54 ºC. ^{1}H NMR (300 MHz, Chloroform-*d*) δ 9.59 (s, 1H), 7.19-7.09 (m, 3H), 7.03 (d, *J* = 8.8 Hz, 2H), 6.90 (d, *J* = 8.8 Hz, 2H), 6.78 (dd, *J* = 6.7, 2.7 Hz, 2H), 3.83 (s, 3H), 3.24 (d, *J* = 13.9 Hz, 1H), 3.14 (d, *J* = 13.9 Hz, 1H), 1.89 (qd, *J* = 7.4, 2.5 Hz, 2H), 0.93 (t, *J* = 7.5 Hz, 3H) ppm. ^{13}C NMR (75 MHz, Chloroform-*d*) δ 202.7, 158.9, 137.0, 130.4, 130.3, 129.3, 128.0, 126.4, 114.2, 58.5, 55.4, 38.8, 24.0, 8.8 ppm. IR (neat,

cm^{-1}): 2960, 2932, 1715, 1508, 1246, 1032, 702, 544. HRMS *calcd.* for ($C_{18}H_{20}O_2$ +H): 269.1536, *found* 269.1547.

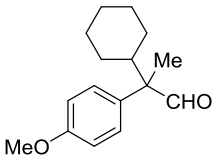

2-cyclohexyl-2-(4-methoxyphenyl)propanal (267ii): Colorless oil. ^{1}H NMR (300 MHz, Chloroform-*d*) δ 9.53 (s, 1H), 7.21 (d, *J* = 8.8 Hz, 2H), 6.91 (d, *J* = 8.8 Hz, 2H), 3.81 (s, 3H), 2.13 (tt, *J* = 11.6, 2.6 Hz, 1H), 1.83-1.72 (m, 1H), 1.72-1.60 (m, 3H), 1.38 (s, 3H), 1.34-1.25 (m, 2H), 1.23-1.00 (m, 3H), 0.96-0.77 (m, 1H) ppm. ^{13}C NMR (75 MHz, Chloroform-*d*) δ 202.9, 158.6, 131.4, 128.6, 114.2, 56.6, 55.3, 43.2, 28.8, 27.3, 27.0, 27.0, 26.7, 14.1 ppm. IR (neat, cm^{-1}): 2926, 2852, 1719, 1510, 1249, 1031, 827, 539. HRMS *calcd.* for ($C_{16}H_{22}O_2$+Na): 269,1512, *found* 269,1516.

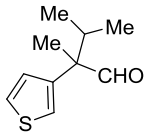

2,3-dimethyl-2-(thiophen-3-yl)butanal (267jj): Colorless oil. ^{1}H NMR (300 MHz, Chloroform-*d*) δ 9.54 (s, 1H), 7.35 (dd, *J* = 5.0, 2.9 Hz, 1H), 7.14-7.07 (m, 1H), 7.06 (d, *J* = 5.4 Hz, 1H), 2.51 (hept, *J* = 6.8 Hz, 1H), 1.38 (s, 3H), 0.92 (d, *J* = 6.8 Hz, 3H), 0.76 (d, *J* = 6.9 Hz, 3H) ppm. ^{13}C NMR (75 MHz, Chloroform-*d*) δ 202.0, 141.3, 126.5, 126.2, 122.1, 56.1, 32.6, 17.9, 17.2, 13.3 ppm. IR (neat, cm^{-1}): 2964, 1721, 1368, 779, 645. HRMS *calcd.* for ($C_{10}H_{14}OS$+Na): 205,0658, *found* 205,0660.

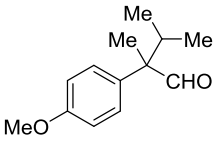

2-ethyl-2-(4-methoxyphenyl)-3-methylbutanal (267kk): Colorless oil. ^{1}H NMR (300 MHz, Chloroform-*d*) δ 9.74 (s, 1H), 7.08 (d, *J* = 8.8 Hz, 2H), 6.93 (d, *J* = 8.8 Hz, 2H), 3.83 (s, 3H), 2.38 (hept, *J* = 6.9 Hz, 1H), 2.09-1.81 (m, 2H), 0.87 (d, *J* = 7.0 Hz, 3H), 0.82-0.73 (m, 6H) ppm. ^{13}C NMR (75 MHz, Chloroform-*d*) δ 205.1, 158.5, 130.0, 129.8, 113.8, 60.5, 55.4, 30.9, 25.5, 18.7, 17.6, 8.6 ppm. IR (neat, cm^{-1}): 2964, 1720, 1512, 1429, 1034, 826, 561. HRMS *calcd.* for ($C_{14}H_{20}O_2$ +H): 221.1536, *found* 221.1535.

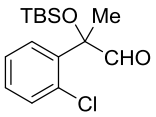

2-((*tert*-butyldimethylsilyl)oxy)-2-(2-chlorophenyl)propanal (267ll): Colorless oil. ^{1}H NMR (300 MHz, Chloroform-*d*) δ 9.73 (s, 1H), 7.69 (dd, *J* = 7.6, 1.8 Hz, 1H), 7.39-7.22 (m, 3H), 1.71 (s, 3H), 0.95 (s, 9H), 0.09 (s, 3H), -0.04 (s, 3H) ppm. ^{13}C NMR (75 MHz, Chloroform-*d*) δ 140.4, 132.1, 130.7, 129.8, 1284, 127.0, 80.5, 25.9, 22.8, 18.5, -2.3, -2.8 ppm. IR (neat, cm^{-1}): 2930, 1737, 1468, 1144, 830, 776, 464. HRMS *calcd.* for ($C_{15}H_{23}ClO_2Si$-CHO): 269.1123, *found* 269.1123.

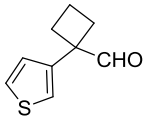

1-(thiophen-3-yl)cyclobutanecarbaldehyde (267mm): Colorless oil. ^{1}H NMR (300 MHz, Chloroform-*d*) δ 9.57 (s, 1H), 7.35 (dd, *J* = 5.0, 2.9 Hz, 1H), 7.09 (dd, *J* = 2.9, 1.4 Hz, 1H), 6.94 (dd, *J* = 5.0, 1.4 Hz, 1H), 2.78-2.63 (m, 2H), 2.43-2.27 (m, 2H), 2.07-1.90 (m, 2H) ppm. ^{13}C NMR (75 MHz, Chloroform-*d*) δ 199.1, 141.9, 126.8, 126.2, 121.3, 54.6, 28.8, 16.0 ppm. IR (neat, cm^{-1}): 2944, 1714, 864, 775, 646. HRMS *calcd.* for ($C_9H_{10}OS$): 167,0525, *found* 167,0529.

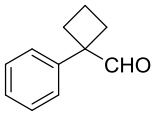

1-phenylcyclobutanecarbaldehyde (267nn): Column chromatography: silica gel, hexanes/EtOAc 98:2. Colorless oil. ^{1}H NMR (300 MHz, Chloroform-d) δ 9.56 (s, 1H), 7.44-7.37 (m, 2H), 7.33-7.26 (m, 1H), 7.21-7.16 (m, 2H), 2.83-2.72 (m, 2H), 2.50-2.37 (m, 2H), 2.11-1.87 (m, 2H) ppm. ^{13}C NMR (75 MHz, Chloroform-d) δ 199.5, 141.0, 128.9, 127.1, 126.5, 57.7, 28.4, 15.9 ppm. IR (neat, cm-1): 2942, 2796, 2705, 1711, 758, 698, 524. HRMS calcd. for (C11H12O+H): 161,0961, found 161,0961.

6.3.6. General Procedure for the Fe-catalyzed [1,2]-shift.

General Procedure: A screw-cap sealed tube was charged with the corresponding α-arylaldehyde **267** (0.5 mmol) and $FeBr_3$ (5-15 mol%) which was stored into the glove box. Then, anhydrous toluene was added (2 mL, 0.25M) under inert atmosphere and the reaction was stirred for 16 h at the indicated temperature. The reaction was then allowed to reach room temperature, diluted with ethyl acetate, concentrated under vacuum and purified by silica gel column chromatography (hexanes/ethyl acetate).

Fe-catalyzed [1,2]-aryl shift.

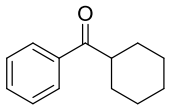

Cyclohexyl phenyl ketone (268a): Following general procedure, **267a** (94,1 mg, 0.5 mmol) with $FeBr_3$ (7.4 mg, 5.0 mol%) in 2.0 mL of toluene was heated at 80 ºC for 14h. Column chromatography: silica gel, hexanes/EtOAc 10:1. White solid; yield: 88.3 mg, 94% yield. White solid. Mp: 54-55 ºC. ^{1}H NMR (400 MHz, Chloroform-*d*) δ 7.98-7.90 (m, 2H), 7.57-7.48 (m, 1H), 7.44 (td, *J* = 6.8, 1.5 Hz, 2H), 3.26 (tt, *J* = 11.4, 3.3 Hz, 1H), 1.93-1.79 (m, 4H), 1.78-1.68 (m, 1H), 1.57-1.33 (m, 4H), 1.32-1.20 (m, 1H) ppm. ^{13}C NMR (101 MHz, Chloroform-*d*) δ 203.8, 136.4, 132.7, 128.6, 128.3, 45.6, 29.5, 26.0, 25.9 ppm. The spectroscopic data are in accordance with those previously reported in the literature [356]

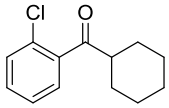

(2-chlorophenyl)(cyclohexyl)methanone (268b): Following general procedure, **267b** (111,4 mg, 0.5 mmol) with $FeBr_3$ (22.2 mg, 15.0 mol%) in 2.0 mL of toluene was heated at 130 ºC for 14h. Column chromatography: silica gel, hexanes/EtOAc 95:5. Yellow oil; yield: 110.3 mg, 99% yield. ^{1}H NMR (400 MHz, Chloroform-*d*) δ 7.40 (ddd, *J* = 7.8, 1.3, 0.7 Hz, 1H), 7.37-7.32 (m, 1H), 7.32-7.27 (m, 2H), 3.05 (tt, *J* = 11.2, 3.5 Hz, 1H), 1.97-1.87 (m, 2H), 1.86-1.76 (m, 2H), 1.72-1.62 (m, 1H), 1.45 (qd, *J* = 12.7, 3.0 Hz, 2H), 1.38-1.17 (m, 3H) ppm. ^{13}C NMR (101 MHz, Chloroform-*d*) δ 207.5, 140.1, 131.1, 130.6, 130.3, 128.4, 126.8, 50.1, 28.5, 26.0, 25.8 ppm. The spectroscopic data are in accordance with those previously reported in the literature.[357]

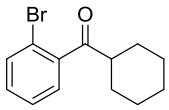

(2-bromophenyl)(cyclohexyl)methanone (268c): Following general procedure, **267c** (133.6 mg, 0.5 mmol) with $FeBr_3$ (7.4 mg, 5.0 mol%) in 2.0 mL of toluene was heated at 80 ºC for 14h. Column chromatography: silica gel, hexanes/EtOAc 10:1. Colorless oil; yield: 128.3 mg, 96% yield. ^{1}H NMR (400 MHz, Chloroform-*d*) δ 7.60-7.56 (m, 1H), 7.34 (td, *J* = 7.4, 1.2 Hz, 1H), 7.31-7.21 (m, 2H), 3.03 (tt, *J* = 11.3, 3.5 Hz, 1H), 1.98-1.88 (m, 2H), 1.86-1.76 (m, 2H), 1.72-1.63 (m, 1H), 1.53-1.38 (m, 2H), 1.38-1.18 (m, 3H) ppm. ^{13}C NMR (101 MHz, Chloroform-*d*) δ 207.9,

[356] Verho, O.; Dilenstam, M. D. V.; Karkas, M. D.; Johnston, E. V.; Akermark, T.; Bäckvall, J. –E.; Akermark, B. *Chem. Eur. J.* **2012**, *18*, 16947
[357] Yoshida, H.; Mimura, Y.; Ohshita, J.; Kunai, A. *Chem. Comm.* **2007**, 2405.

142.2, 133.4, 131.0, 128.1, 127.7, 118.7, 49.9, 28.4, 25.9, 25.7 ppm. The spectroscopic data are in accordance with those previously reported in the literature.[358]

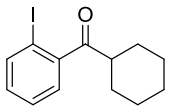

(2-iodophenyl)(cyclohexyl)methanone (268d): Following general procedure, **267d** (157.1 mg, 0.5 mmol) with $FeBr_3$ (22.2 mg, 15.0 mol%) in 2.0 mL of toluene was heated at 130 ºC for 14h. Column chromatography: silica gel, hexanes/EtOAc 95:5. Yellow oil; yield: 155.7 mg, 99% yield. ^{1}H NMR (400 MHz, Chloroform-*d*) δ 7.88 (dd, *J* = 7.9, 1.1 Hz, 1H), 7.38 (td, *J* = 7.5, 1.1 Hz, 1H), 7.25 (dd, *J* = 7.6, 1.7 Hz, 1H), 7.10 (ddd, *J* = 8.0, 7.4, 1.7 Hz, 1H), 3.01 (tt, *J* = 11.3, 3.5 Hz, 1H), 1.98-1.89 (m, 2H), 1.87-1.77 (m, 2H), 1.73-1.65 (m, 1H), 1.55-1.40 (m, 2H), 1.38-1.19 (m, 3H) ppm. ^{13}C NMR (101 MHz, Chloroform-*d*) δ 208.6, 145.6, 140.2, 131.1, 127.9, 127.6, 91.4, 49.5, 28.6, 25.9, 25.8 ppm. The spectroscopic data are in accordance with those previously reported in the literature.[359]

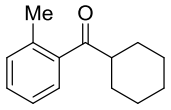

Cyclohexyl(*o*-tolyl)methanone (268e): Following general procedure, **267e** (101.2 mg, 0.5 mmol) with $FeBr_3$ (7.4 mg, 5.0 mol%) in 2.0 mL of toluene was heated at 110 ºC for 14h. Column chromatography: silica gel, hexanes/EtOAc 98:2. Colorless oil; yield: 95.1 mg, 94% yield. ^{1}H NMR (300 MHz, Chloroform-*d*) δ 7.53-7.48 (m, 1H), 7.40-7.29 (m, 1H), 7.29-7.21 (m, 2H), 3.05 (tt, *J* = 11.3, 3.2 Hz, 1H), 2.43 (s, 3H), 1.94-1.78 (m, 4H), 1.76-1.67 (m, 1H), 1.54-1.19 (m, 5H) ppm. ^{13}C NMR (75 MHz, Chloroform-*d*) δ 208.9, 139.1, 137.3, 131.6, 130.5, 127.4, 125.6, 49.1, 28.9, 26.1, 25.9, 20.8 ppm. IR (neat, cm^{-1}): 2927, 2853, 1682, 1449, 1245, 969, 729, 655. HRMS *calcd.* for ($C_{14}H_{18}O$+H): 203.1430, *found* 203.1427.

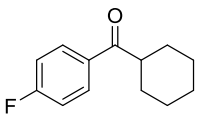

Cyclohexyl(4-fluorophenyl)methanone (268f): Following general procedure, **267f** (103.1 mg, 0.5 mmol) with $FeBr_3$ (22.2 mg, 15.0 mol%) in 2.0 mL of toluene was heated at 130 ºC for 14h. Column chromatography: silica gel, hexanes/EtOAc 98:2. Yellow oil; yield: 102.0 mg, 99% yield.

[358] Korn, T. J.; Schade, M. A.; Cheemala, M. N.; Wirth, S.; Guevara, S. A.; Cahiez, G.; Knochel, P. *Synthesis*, **2006**, 3547.
[359] Majid, T. N.; Knochel, P. *Tetrahedron Lett.* **1990,** *31*, 4413.

^{1}H NMR (400 MHz, Chloroform-*d*) δ 8.02-7.92 (m, 2H), 7.18-7.07 (m, 2H), 3.22 (tt, *J* = 11.4, 3.2 Hz, 1H), 1.93-1.79 (m, 4H), 1.79-1.69 (m, 1H), 1.58-1.20 (m, 5H) ppm. ^{13}C NMR (101 MHz, Chloroform-*d*) δ 202.3, 165.7 (d, *J* = 254.2 Hz), 132.8 (d, *J* = 3.0 Hz), 130.9 (d, *J* = 9.2 Hz), 115.7 (d, *J* = 21.8 Hz), 45.7, 29.5, 26.0, 25.9 ppm. IR (neat, cm^{-1}): 2929, 2854, 1680, 1596, 1506, 1230, 1205, 1154, 842, 600. HRMS *calcd.* for ($C_{13}H_{15}FO$+Na): 229.0009, *found* 229.1005.

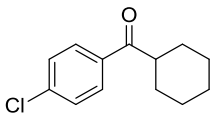

(4-chlorophenyl)(cyclohexyl)methanone (268g): Following general procedure, **267g** (111.4 mg, 0.5 mmol) with $FeBr_3$ (22.2 mg, 15.0 mol%) in 2.0 mL of toluene was heated at 130 ºC for 14h. Column chromatography: silica gel, hexanes/EtOAc 98:2. White sticky oil; yield: 110.3 mg, 99% yield. ^{1}H NMR (400 MHz, Chloroform-*d*) δ 7.93-7.84 (m, 2H), 7.48-7.39 (m, 2H), 3.21 (tt, *J* = 11.3, 3.2 Hz, 1H), 1.93-1.81 (m, 4H), 1.80-1.69 (m, 1H), 1.57-1.20 (m, 5H) ppm. ^{13}C NMR (101 MHz, Chloroform-*d*) δ 202.7, 139.2, 134.8, 129.8, 129.0, 45.8, 29.5, 26.0, 25.9 ppm. The spectroscopic data are in accordance with those previously reported in the literature.[360]

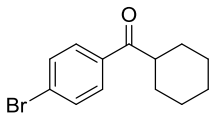

(4-bromophenyl)(cyclohexyl)methanone (268h): Following general procedure, **267h** (66.8 mg, 0.25 mmol) with $FeBr_3$ (7.4 mg, 10.0 mol%) in 1.0 mL of toluene was heated at 110 ºC for 20h. Column chromatography: silica gel, hexanes/EtOAc 98:2. Yellow solid; yield: 64.0 mg, 96% yield. Mp: 73-75 ºC. ^{1}H NMR (300 MHz, Chloroform-*d*) δ 7.81 (d, *J* = 8.5 Hz, 2H), 7.60 (d, *J* = 8.5 Hz, 2H), 3.20 (tt, *J* = 11.1, 2.9 Hz, 1H), 1.94-1.80 (m, 4H), 1.79-1.71 (m, 1H), 1.55-1.23 (m, 5H) ppm. ^{13}C NMR (75 MHz, Chloroform-*d*) δ 202.8, 135.0, 131.9, 129.8, 127.8, 45.6, 29.3, 25.9, 25.8 ppm. ^{13}C NMR (75 MHz, Chloroform-*d*) δ 202.9, 135.2, 132.0, 130.0, 127.9, 45.8, 29.5, 26.0, 25.9 ppm. IR (neat, cm^{-1}): 2923, 2852, 1677, 1581, 972, 832, 736, 462. HRMS *calcd.* for ($C_{13}H_{15}BrO$+Na): 289.0198, *found* 289.0186.

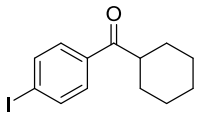

Cyclohexyl(4-iodophenyl)methanone (268i): Following general procedure, **267i** (157.1 mg, 0.5 mmol) with $FeBr_3$ (22.2 mg, 15.0 mol%) in 2.0 mL of toluene was heated at 130 ºC for 14h.

[360] Kondo, T.; Akazome, M.; Tsuji, Y.; Watanabe, Y. *J. Org. Chem.* **1990**, *55*, 1286.

Column chromatography: silica gel, hexanes/EtOAc 98:2. Yellow solid; yield: 154.9 mg, 99% yield. Mp: 67-69 ºC. ^{1}H NMR (400 MHz, Chloroform-*d*) δ 7.82 (d, *J* = 8.6 Hz, 2H), 7.65 (d, *J* = 8.5 Hz, 2H), 3.19 (tt, *J* = 11.3, 3.2 Hz, 1H), 1.92-1.80 (m, 4H), 1.79-1.69 (m, 1H), 1.56-1.23 (m, 5H) ppm. ^{13}C NMR (101 MHz, Chloroform-*d*) δ 203.2, 138.0, 135.7, 129.9, 100.7, 45.7, 29.5, 26.0, 25.9 ppm. IR (neat, cm^{-1}): 2921, 2848, 1676, 1204, 1004, 972, 781, 457. HRMS *calcd.* for ($C_{13}H_{15}IO$+Na): 337.0060, *found* 337.0067.

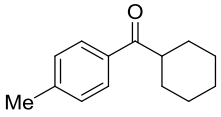

Cyclohexyl(*p*-tolyl)methanone (268j): Following general procedure, **267j** (49.2 mg, 0.25 mmol) with $FeBr_3$ (7.4 mg, 10.0 mol%) in 1.0 mL of toluene was heated at 110 ºC for 20h. Column chromatography: silica gel, hexanes/EtOAc 98:2. Yellow solid; yield: 42.8 mg, 96% yield. Mp: 55-56 ºC (*lit.* 58-60 ºC). ^{1}H NMR (300 MHz, Chloroform-*d*) δ 7.86 (d, *J* = 8.2 Hz, 2H), 7.26 (d, *J* = 7.9 Hz, 2H), 3.25 (tt, *J* = 11.2, 3.1 Hz, 1H), 2.42 (s, 3H), 1.94-1.80 (m, 4H), 1.79-1.70 (m, 1H), 1.56-1.23 (m, 5H) ppm. ^{13}C NMR (75 MHz, Chloroform-*d*) δ 203.7, 143.6, 134.0, 129.4, 128.5, 45.7, 29.6, 26.1, 26.1, 21.7 ppm. The spectroscopic data are in accordance with those previously reported in the literature.[360]

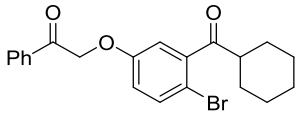

2-(4-bromo-3-(cyclohexanecarbonyl)phenoxy)-1-phenylethanone (268k): Following general procedure, **267k** (200.6 mg, 0.5 mmol) with $FeBr_3$ (7.4 mg, 5.0 mol%) in 2.0 mL of toluene was heated at 80 ºC for 14h. Column chromatography: silica gel, hexanes/EtOAc 4:1. Yellow sticky oil; yield: 158.4 mg, 79% yield. ^{1}H NMR (400 MHz,) δ 7.97 (dd, *J* = 8.4, 1.2 Hz, 2H), 7.68-7.59 (m, 1H), 7.51 (t, *J* = 7.8 Hz, 2H), 7.49-7.41 (m, 1H), 6.88-6.80 (m, 2H), 5.28 (s, 2H), 3.00 (tt, *J* = 11.3, 3.4 Hz, 1H), 1.95-1.88 (m, 2H), 1.84-1.75 (m, 2H), 1.71-1.63 (m, 1H), 1.49-1.34 (m, 2H), 1.34-1.17 (m, 3H) ppm. ^{13}C NMR (101 MHz, Chloroform-*d*) δ 207.6, 193.7, 157.3, 143.1, 134.4, 134.4, 134.3, 117.5, 115.1, 110.1, 71.0, 49.9, 28.5, 25.9, 25.7 ppm. IR (neat, cm^{-1}): 2928, 1695, 1448, 1219, 966, 688. Anal. Calcd for $C_{21}H_{21}BrO_3$: C, 62.85; H, 5.27. Found: C, 62.57; H, 5.03.

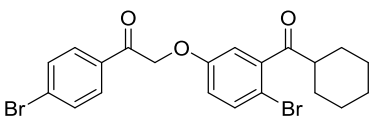

2-(4-bromo-3-(cyclohexanecarbonyl)phenoxy)-1-(4-bromophenyl)ethanone (268l): Following general procedure, **267l** (240.1 mg, 0.5 mmol) with $FeBr_3$ (7.4 mg, 5.0 mol%) in 2.0 mL of

toluene was heated at 80 ºC for 14h. Column chromatography: silica gel, hexanes/EtOAc 4:1. Brown solid; yield: 160.4 mg, 67% yield. Mp: 118-120 ºC. ^{1}H NMR (400 MHz, Chloroform-*d*) δ 7.84 (d, *J* = 8.5 Hz, 2H), 7.64 (d, *J* = 8.5 Hz, 2H), 7.49-7.41 (m, 1H), 6.87-6.79 (m, 2H), 5.22 (s, 2H), 3.00 (tt, *J* = 11.2, 3.4 Hz, 1H), 1.96-1.86 (m, 2H), 1.84-1.75 (m, 2H), 1.72-1.64 (m, 1H), 1.49-1.34 (m, 2H), 1.36-1.20 (m, 3H) ppm. ^{13}C NMR (101 MHz, Chloroform-*d*) δ 207.5, 193.0, 157.1, 143.1, 134.4, 133.1, 132.4, 129.7, 129.6, 117.5, 115.0, 110.2, 71.0, 49.9, 28.5, 25.9, 25.7 ppm. IR (neat, cm^{-1}): 2922, 1693, 1586, 1221, 973, 808, 598, 453. Anal. Calcd for $C_{21}H_{20}Br_2O_3$: C, 52.53; H, 4.20. Found: C, 52.77; H, 4.02.

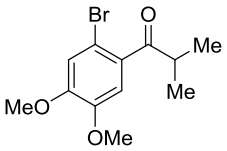

1-(2-bromo-4,5-dimethoxyphenyl)-2-methylpropan-1-one (268r): Following general procedure, **267r** (143.6 mg, 0.5 mmol) with $FeBr_3$ (7.4 mg, 5.0 mol%) in 2.0 mL of toluene was heated at 80 ºC for 14h. Column chromatography: silica gel, hexanes/EtOAc 4:1. Yellow oil; yield: 93.6 mg, 65% yield. ^{1}H NMR (400 MHz,) δ 7.04 (s, 1H), 6.88 (s, 1H), 3.91 (s, 3H), 3.88 (s, 3H), 3.47 (hept, *J* = 6.9 Hz, 1H), 1.19 (d, *J* = 6.9 Hz, 6H) ppm. ^{13}C NMR (101 MHz,) δ 207.9, 151.0, 148.4, 133.6, 116.2, 111.9, 110.5, 56.4, 56.3, 39.7, 18.6 ppm.

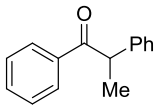

1,2-diphenylpropan-1-one (268s): Following general procedure, **267s** (105.1 mg, 0.5 mmol) with $FeBr_3$ (7.4 mg, 5.0 mol%) in 2.0 mL of toluene was heated at 80 ºC for 14h. Column chromatography: silica gel, hexanes/EtOAc 98:2. White solid; yield: 92.0 mg, 87% yield. Mp: 44-46 ºC. (*lit.* 48.3-48.9 ºC)[361] ^{1}H NMR (400 MHz,) δ 7.98 (dd, *J* = 8.4, 1.4 Hz, 2H), 7.53-7.44 (m, 1H), 7.39 (t, *J* = 7.6 Hz, 2H), 7.31 (d, *J* = 4.4 Hz, 4H), 7.27-7.17 (m, 1H), 4.71 (q, *J* = 6.9 Hz, 1H), 1.56 (d, *J* = 6.9 Hz, 3H) ppm. ^{13}C NMR (101 MHz,) δ 200.4, 141.6, 136.0, 132.9, 129.1, 128.9, 128.6, 127.9, 127.0, 48.0, 19.6 ppm. The spectroscopic data are in accordance with those previously reported in the literature.[362]

[361] Cao, C.; Wang, L.; Cai, Z.; Zhang, L.; Guo, J.; Pang, G.; Shi, Y. *Eur. J. Org. Chem.* **2011**, 1570.
[362] Kulasekharan, R.; Maddipatla, M. V. S. N.; Parthasarathy, A.; Ramamurthy, V. *J. Org. Chem***. 2013,** *78,* 942.

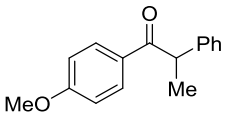

2-(4-methoxyphenyl)-1-phenylpropan-1-one (269z-Ph): Following general procedure, **1p** (120.2 mg, 0.5 mmol) with $FeBr_3$ (7.4 mg, 5.0 mol%) in 2.0 mL of toluene was heated at 50 ºC for 14h. Column chromatography: silica gel, hexanes/EtOAc 95:5. Colorless oil; yield: 102.9 mg, 86% yield. ^{1}H NMR (300 MHz, Chloroform-*d*) δ 8.01-7.91 (m, 2H), 7.48 (t, *J* = 7.3 Hz, 1H), 7.39 (t, *J* = 7.4 Hz, 2H), 7.22 (d, *J* = 8.7 Hz, 2H), 6.84 (d, *J* = 8.7 Hz, 2H), 4.66 (q, *J* = 6.8 Hz, 1H), 3.76 (s, 3H), 1.52 (d, *J* = 6.9 Hz, 3H) ppm. ^{13}C NMR (75 MHz, Chloroform-*d*) δ 200.7, 158.6, 136.7, 133.6, 132.8, 128.9, 128.9, 128.6, 114.5, 55.3, 47.1, 19.6 ppm. The spectroscopic data are in agreement with those previously reported in the literature.[363]

Fe-catalyzed [1,2]-alkyl shift.

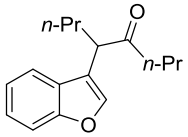

5-(benzofuran-3-yl)octan-4-one (302aa): Following general procedure, **267aa** (120.9 mg, 0.5 mmol) with $FeBr_3$ (7.4 mg, 5.0 mol%) in 2.0 mL of toluene was heated at 50 ºC for 14h. Column chromatography: silica gel, hexanes/EtOAc 98:2. Yellow oil; yield: 113.2 mg, 94% yield. ^{1}H NMR (300 MHz, Chloroform-*d*) δ 7.58 (d, *J* = 6.9 Hz, 1H), 7.55 (s, 1H), 7.49 (d, *J* = 7.9 Hz, 1H), 7.31 (td, *J* = 7.8, 1.5 Hz, 1H), 7.25 (td, *J* = 7.5, 1.0 Hz, 1H), 3.83 (t, *J* = 7.4 Hz, 1H), 2.43 (td, *J* = 7.2, 1.6 Hz, 2H), 2.15-1.99 (m, 1H), 1.93-1.74 (m, 1H), 1.67-1.46 (m, 2H), 1.41-1.22 (m, 2H), 0.93 (t, *J* = 7.3 Hz, 3H), 0.82 (d, *J* = 14.8 Hz, 3H) ppm. ^{13}C NMR (75 MHz, Chloroform-*d*) δ 210.2, 155.6, 142.4, 127.1, 124.6, 122.8, 120.2, 118.5, 111.7, 48.7, 43.2, 33.0, 20.9, 17.3, 14.1, 13.7 ppm. IR (neat, cm^{-1}): 2959, 1712, 1452, 1097, 743, 423. HRMS *calcd.* for ($C_{16}H_{20}O_2$+Na): 267.1356, *found* 267.1356.

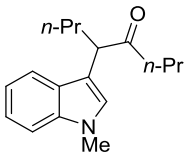

5-(1-methyl-1*H*-indol-3-yl)octan-4-one (302bb): Following general procedure, **267bb** (129.0 mg, 0.5 mmol) with $FeBr_3$ (7.4 mg, 5.0 mol%) in 2.0 mL of toluene was heated at 50 ºC for 14h. Column chromatography: silica gel, hexanes/EtOAc 98:2. Yellow oil; yield: 119.8 mg, 93% yield.

[363] Cheon, C. H.; Kanno, O.; Toste, F. D. *J. Am. Chem. Soc*. **2011**, *133*, 13248.

^{1}H NMR (300 MHz, Chloroform-*d*) δ 7.65 (d, *J* = 8.0 Hz, 1H), 7.33 (d, *J* = 8.1 Hz, 1H), 7.33-7.21 (m, 1H), 7.22-7.10 (m, 1H), 6.95 (s, 1H), 3.94 (t, *J* = 7.4 Hz, 1H), 3.79 (s, 3H), 2.48-2.38 (m, 2H), 2.18-2.03 (m, 1H), 1.90-1.74 (m, 1H), 1.66-1.46 (m, 2H), 1.41-1.25 (m, 2H), 0.95 (t, *J* = 7.3 Hz, 3H), 0.83 (t, *J* = 7.4 Hz, 3H) ppm. ^{13}C NMR (75 MHz, Chloroform-*d*) δ 211.5, 137.2, 127.5, 127.0, 121.9, 119.3, 119.2, 112.7, 109.4, 49.6, 43.3, 34.1, 32.9, 21.1, 17.4, 14.2, 13.8 ppm. IR (neat, cm^{-1}): 2957, 1706, 1466, 1329, 736, 427. HRMS *calcd.* for ($C_{17}H_{23}NO$+Na): 280.1672, *found* 280.1675.

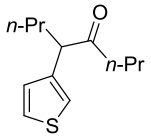

5-(thiophen-3-yl)octan-4-one (302cc): Following general procedure, **267cc** (103.9 mg, 0.5 mmol) with $FeBr_3$ (7.4 mg, 5.0 mol%) in 2.0 mL of toluene was heated at 110 ºC for 14h. Column chromatography: silica gel, hexanes/EtOAc 98:2. Yellow oil; yield: 93.8 mg, 90% yield. ^{1}H NMR (300 MHz, Chloroform-*d*) δ 7.33-7.25 (m, 1H), 7.10-7.06 (m, 1H), 6.96 (dd, *J* = 4.9, 1.2 Hz, 1H), 3.79 (t, *J* = 7.5 Hz, 1H), 2.46-2.27 (m, 2H), 2.07-1.91 (m, 1H), 1.76-1.62 (m, 1H), 1.61-1.46 (m, 2H), 1.31-1.17 (m, 2H), 0.90 (t, *J* = 7.3 Hz, 3H), 0.82 (t, *J* = 7.4 Hz, 3H) ppm. ^{13}C NMR (75 MHz, Chloroform-*d*) δ 210.4, 139.7, 127.3, 126.0, 121.9, 54.1, 43.5, 34.2, 20.8, 17.2, 14.0, 13.7 ppm. IR (neat, cm^{-1}): 2958, 1710, 1460, 1035, 767, 654. HRMS *calcd.* for ($C_{12}H_{18}OS$+Na): 233.0971, *found* 233.0969.

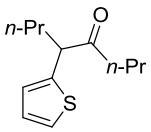

5-(thiophen-2-yl)octan-4-one (302dd): Following general procedure, **267dd** (1.00 g, 4.75 mmol) with $FeBr_3$ (70.3 mg, 5.0 mol%) in 19.0 mL of toluene was heated at 110 ºC for 14h in a Schlenk. Column chromatography: silica gel, hexanes/EtOAc 98:2. Brown oil; yield: 928.8 mg, 93% yield. ^{1}H NMR (300 MHz, Chloroform-*d*) δ 7.20 (d, *J* = 4.7 Hz, 1H), 6.96 (dd, *J* = 5.0, 3.5 Hz, 1H), 6.88 (d, *J* = 3.1 Hz, 1H), 3.92 (t, *J* = 7.5 Hz, 1H), 2.53-2.34 (m, 2H), 2.08-1.93 (m, 1H), 1.82-1.68 (m, 1H), 1.65-1.46 (m, 2H), 1.38-1.18 (m, 2H), 0.91 (d, *J* = 14.6 Hz, 3H), 0.84 (t, *J* = 7.4 Hz, 3H) ppm. ^{13}C NMR (75 MHz, Chloroform-*d*) δ 209.5, 141.9, 127.0, 125.4, 124.7, 53.6, 43.2, 35.5, 20.8, 17.3, 14.0, 13.7 ppm. IR (neat, cm^{-1}): 2959, 1712, 1460, 1033, 694. HRMS *calcd.* for ($C_{12}H_{18}OS$+Na): 233.0971, *found* 233.0969.

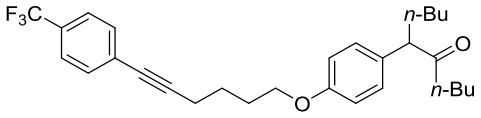

6-(4-((6-(4-(trifluoromethyl)phenyl)hex-5-yn-1-yl)oxy)phenyl)decan-5-one (302ee): Following general procedure, **267ee** (228.7 mg, 0.5 mmol) with $FeBr_3$ (7.4 mg, 5.0 mol%) in 2.0 mL of toluene was stirred at room temperature for 14h.. Column chromatography: silica gel, hexanes/EtOAc 98:2. Yellow oil; yield: 226.5 mg, 99% yield. ^{1}H NMR (300 MHz, Chloroform-*d*) δ 7.55 (d, *J* = 8.2 Hz, 2H), 7.48 (d, *J* = 8.2 Hz, 2H), 7.12 (d, *J* = 8.3 Hz, 2H), 6.86 (d, *J* = 8.3 Hz, 2H), 4.01 (t, *J* = 6.0 Hz, 2H), 3.55 (t, *J* = 7.4 Hz, 1H), 2.53 (t, *J* = 6.8 Hz, 2H), 2.41-2.29 (m, 2H), 2.04-1.92 (m, 3H), 1.88-1.76 (m, 2H), 1.72-1.59 (m, 1H), 1.53-1.42 (m, 2H), 1.38-1.09 (m, 6H), 0.93-0.76 (m, 6H) ppm. ^{13}C NMR (101 MHz, Chloroform-*d*) δ 211.2, 158.2, 131.9, 131.5, 129.4, 127.9, 125.3 (q, *J* = 3.7 Hz), 114.8, 92.7, 80.1, 67.4, 58.3, 41.6, 32.1, 29.9, 28.7, 26.1, 25.3, 22.8, 22.4, 19.4, 14.1, 13.9 ppm. IR (neat, cm^{-1}): 2932, 1711, 1509, 1321, 1124, 1066, 841, 597. HRMS *calcd.* for ($C_{29}H_{35}F_3O_2$+Na): 473.2662, *found* 473.2671.

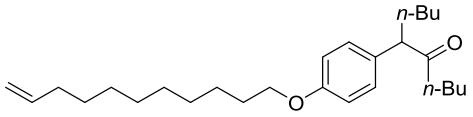

6-(4-(undec-10-en-1-yloxy)phenyl)decan-5-one (302ff): Following general procedure, **267ff** (199.5 mg, 0.5 mmol) with $FeBr_3$ (7.4 mg, 5.0 mol%) in 2.0 mL of toluene was heated at 110 ºC for 14h. Column chromatography: silica gel, hexanes/EtOAc 98:2. Yellow oil; yield: 189.8 mg, 95% yield**.** ^{1}H NMR (400 MHz, Chloroform-*d*) δ 7.11 (d, *J* = 8.6 Hz, 2H), 6.84 (d, *J* = 8.6 Hz, 2H), 5.82 (ddt, *J* = 17.0, 10.2, 6.7 Hz, 1H), 5.03-4.97 (m, 1H), 4.94 (ddt, *J* = 10.2, 2.3, 1.2 Hz, 1H), 3.93 (t, *J* = 6.6 Hz, 2H), 3.54 (t, *J* = 7.4 Hz, 1H), 2.39-2.29 (m, 2H), 2.09-1.94 (m, 3H), 1.82-1.73 (m, 2H), 1.71-1.60 (m, 1H), 1.53-1.28 (m, 16H), 1.16 (s, 4H), 0.89-0.79 (m, 6H) ppm. ^{13}C NMR (75 MHz, Chloroform-*d*) δ 211.3, 158.4, 139.3, 131.3, 129.3, 114.8, 114.3, 68.1, 58.3, 41.6, 33.9, 32.0, 29.9, 29.7, 29.6, 29.5, 29.4, 29.3, 29.1, 26.2, 26.1, 22.8, 22.4, 14.1, 13.9 ppm. IR (neat, cm^{-1}): 2926, 2855, 1712, 1509, 1245, 826, 561. HRMS *calcd.* for ($C_{27}H_{44}O_2$+H): 401.3414, *found* 401.3412.

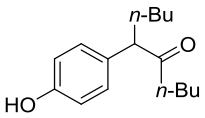

6-(4-hydroxyphenyl)decan-5-one (302gg): Following general procedure, **267gg** (118.9 mg, 0.5 mmol) with $FeBr_3$ (7.4 mg, 5.0 mol%) in 2.0 mL of toluene was stirred at room temperature for 14h. Column chromatography: silica gel, hexanes/EtOAc 9:1. Pink solid; yield: 113.9 mg, 96%

yield**.** Mp: 50-51 ºC. ^{1}H NMR (300 MHz, Chloroform-*d*) δ 7.08 (d, *J* = 8.5 Hz, 2H), 6.80 (d, *J* = 8.5 Hz, 2H), 5.00 (s, 1H), 3.55 (t, *J* = 7.5 Hz, 1H), 2.39-2.32 (m, 2H), 2.05-1.92 (m, 1H), 1.72-1.59 (m, 1H), 1.54-1.41 (m, 2H), 1.36-1.08 (m, 6H), 0.92-0.77 (m, 6H) ppm. ^{13}C NMR (75 MHz, Chloroform-*d*) δ 212.6, 155.1, 131.1, 129.5, 115.9, 58.3, 41.6, 31.9, 29.8, 26.1, 22.7, 22.3, 14.0, 13.9 ppm.

IR (neat, cm^{-1}): 3318, 2944, 2859, 1692, 1511, 1226, 819, 559. HRMS *calcd.* for ($C_{16}H_{24}O_2$+Na): 271.1669, *found* 271.1671.

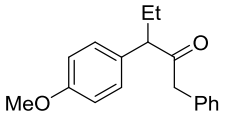

3-(4-methoxyphenyl)-1-phenylpentan-2-one (302hh): Following general procedure, **267hh** (65.3 mg, 0.25 mmol) with $FeBr_3$ (7.4 mg, 10.0 mol%) in 2.0 mL of toluene was heated at 50 ºC for 14h. Column chromatography: silica gel, hexanes/EtOAc 98:2. Colorless oil; yield: 49.7 mg, 76% yield (^{1}H NMR of the crude reaction mixture showed a 5:1 mixture of regioisomers favoring the [1,2]-Bn shift over the [1,2]-Et shift). The NMR signals given are for the major regioisomer ([1,2]-Bn shift): ^{1}H NMR (300 MHz, Chloroform-*d*) δ 7.32-7.24 (m, 3H), 7.14-7.09 (m, 2H), 7.09-7.03 (m, 2H), 6.88 (d, *J* = 8.6 Hz, 2H), 3.82 (s, 3H), 3.63 (s, 2H), 3.57 (t, *J* = 7.4 Hz, 1H), 2.11-1.90 (m, 1H), 1.75-1.60 (m, 1H), 0.75 (t, *J* = 7.4 Hz, 3H) ppm. ^{13}C NMR (75 MHz, Chloroform-*d*) δ 208.0, 159.0, 134.4, 130.8, 129.7, 129.6, 128.7, 127.0, 114.4, 59.0, 55.4, 48.8, 25.4, 12.1 ppm. IR (neat, cm^{-1}): 2961, 1710, 1509, 1247, 1031, 826, 699, 544. HRMS *calcd.* for ($C_{18}H_{20}O_2$+H): 269.1536, *found* 269.1547.

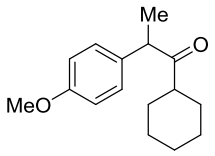

1-cyclohexyl-2-(4-methoxyphenyl)propan-1-one (302ii): Following general procedure, **267ii** (123.0 mg, 0.5 mmol) with $FeBr_3$ (7.4 mg, 5.0 mol%) in 2.0 mL of toluene was heated at 110 ºC for 14h. Column chromatography: silica gel, hexanes/EtOAc 95:5. Yellow oil; yield: 110.2 mg, 90% yield. ^{1}H NMR (300 MHz, Chloroform-*d*) δ 7.13 (d, *J* = 8.6 Hz, 2H), 6.86 (d, *J* = 8.7 Hz, 2H), 3.90-3.83 (m, 1H), 3.80 (s, 3H), 2.48-2.35 (m, 1H), 1.90-1.58 (m, 4H), 1.52-1.38 (m, 1H), 1.34 (d, *J* = 6.9 Hz, 3H), 1.30-1.10 (m, 5H) ppm. ^{13}C NMR (75 MHz, Chloroform-*d*) δ 214.2, 158.7, 132.9, 129.1, 114.3, 55.4, 50.4, 49.4, 29.6, 28.5, 26.1, 25.9, 25.5, 18.3 ppm. IR (neat, cm^{-1}): 2928, 1705, 1510, 1245, 1033, 834, 553. HRMS *calcd.* for ($C_{16}H_{22}O_2$+Na): 269.1512, *found* 269.1513.

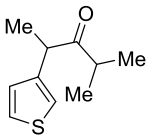

2-methyl-4-(thiophen-3-yl)pentan-3-one (302jj): Following general procedure, **267jj** (78.0 mg, 0.5 mmol) with $FeBr_3$ (7.4 mg, 5.0 mol%) in 2.0 mL of toluene was heated at 110 ºC for 14h. Column chromatography: silica gel, hexanes/EtOAc 98:2. Yellow oil; yield: 78.0 mg, 87% yield. ^{1}H NMR (300 MHz, Chloroform-*d*) δ 7.30-7.27 (m, 1H), 7.12-7.04 (m, 1H), 6.97 (d, *J* = 5.0 Hz, 1H), 4.07 (q, *J* = 6.9 Hz, 1H), 2.75 (hept, *J* = 6.9 Hz, 1H), 1.39 (d, *J* = 7.0 Hz, 3H), 1.08 (d, *J* = 7.1 Hz, 3H), 0.97 (d, *J* = 6.7 Hz, 3H) ppm. ^{13}C NMR (75 MHz, Chloroform-*d*) δ 214.5, 141.1, 127.3, 126.1, 121.6, 46.5, 39.1, 19.2, 18.5, 18.0 ppm. IR (neat, cm^{-1}): 2969, 1710, 1464, 1015, 751, 660. HRMS *calcd.* for ($C_{10}H_{14}OS$+Na): 205.0658, *found* 205.0657.

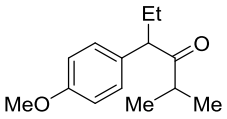

4-(4-methoxyphenyl)-2-methylhexan-3-one (302kk): Following general procedure, **267kk** (110.2 mg, 0.5 mmol) with $FeBr_3$ (14.8 mg, 10.0 mol%) in 2.0 mL of toluene was heated at 110 ºC for 14h. Column chromatography: silica gel, hexanes/EtOAc 98:2. Yellow oil; yield: 98.0 mg, 89% yield. ^{1}H NMR (300 MHz, Chloroform-*d*) δ 7.13 (d, *J* = 8.7 Hz, 2H), 6.85 (d, *J* = 8.6 Hz, 2H), 3.79 (s, 3H), 3.63 (t, *J* = 7.4 Hz, 1H), 2.65 (hept, *J* = 6.9 Hz, 1H), 2.12-1.91 (m, 1H), 1.75-1.54 (m, 1H), 1.07 (d, *J* = 7.0 Hz, 3H), 0.91 (d, *J* = 6.7 Hz, 3H), 0.81 (t, *J* = 7.4 Hz, 3H) ppm. ^{13}C NMR (75 MHz, Chloroform-*d*) δ 214.6, 158.8, 131.3, 129.5, 114.2, 58.2, 55.4, 39.9, 26.1, 19.0, 18.3, 12.3 ppm. IR (neat, cm^{-1}): 2964, 1708, 1510, 1249, 1178, 1033, 822, 551. HRMS *calcd.* for ($C_{14}H_{20}O_2$ +H): 221.1536, *found* 221.1536.

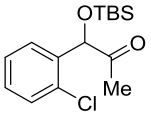

1-((*tert*-butyldimethylsilyl)oxy)-1-(2-chlorophenyl)propan-2-one (302ll): Following general procedure, **267ll** (74.7 mg, 0.5 mmol) with $FeBr_3$ (7.4 mg, 5.0 mol%) in 2.0 mL of toluene was heated at 110 ºC for 14h. Column chromatography: silica gel, hexanes/EtOAc 98:2. Yellow oil; yield: 38.1 mg, 87% yield. ^{1}H NMR (300 MHz, Chloroform-*d*) δ 7.53 (dd, *J* = 7.5, 1.9 Hz, 1H), 7.42-7.24 (m, 1H), 7.33-7.22 (m, 2H), 5.49 (s, 1H), 2.17 (s, 3H), 0.93 (s, 9H), 0.12 (s, 3H), -0.04 (s, 3H) ppm. ^{13}C NMR (75 MHz, Chloroform-*d*) δ 206.4, 137.3, 132.9, 129.7, 129.5, 128.7, 127.2,

25.8, 25.4, 18.3, -4.9, -5.0 ppm. IR (neat, cm^{-1}): 2930, 1725, 1469, 1095, 836, 750, 574. HRMS *calcd.* for ($C_{15}H_{23}ClO_2Si$+Na): 321.1048, *found* 321.1058.

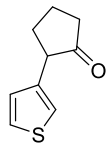

2-(thiophen-3-yl)cyclopentanone (302mm): Following general procedure, **267mm** (82.4 mg, 0.5 mmol) with $FeBr_3$ (7.4 mg, 5.0 mol%) in 2.0 mL of toluene was heated at 110 ºC for 14h. Column chromatography: silica gel, hexanes/EtOAc 95:5. Orange sticky oil; yield: 49.8 mg, 60% yield. ^{1}H NMR (300 MHz, Chloroform-*d*) δ 7.31 (dd, *J* = 5.0, 3.0 Hz, 1H), 7.13 (dt, *J* = 2.9, 1.1 Hz, 1H), 7.06 (dd, *J* = 4.9, 1.2 Hz, 1H), 3.46-3.37 (m, 1H), 2.58-2.39 (m, 2H), 2.36-2.24 (m, 1H), 2.14 (s, 2H), 2.01-1.85 (m, 1H) ppm. ^{13}C NMR (75 MHz, Chloroform-*d*) δ 217.2, 138.2, 127.3, 125.8, 121.3, 50.4, 38.1, 31.2, 21.0 ppm. IR (neat, cm^{-1}): 2963, 1666, 1505, 1399, 1278, 1164, 864, 751, 629. HRMS *calcd.* for ($C_9H_{10}OS$+Na): 189.0345, *found* 189.0345.

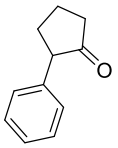

2-phenylcyclopentanone (302nn): Following general procedure, **267nn** (80.1 mg, 0.5 mmol) with $FeBr_3$ (7.4 mg, 5.0 mol%) in 2.0 mL of toluene was heated at 110 ºC for 16 h. Column chromatography: silica gel, hexanes/EtOAc 9:1. White solid in the fridge that melts at room temperature; yield 61.7 mg, 77% yield. Mp: (lit. 33-34 ºC) ^{1}H NMR (300 MHz, Chloroform-d) δ 7.40-7.33 (m, 2H), 7.31-7.26 (m, 1H), 7.26-7.20 (m, 2H), 3.35 (dd, J = 10.6, 8.9 Hz, 1H), 2.59-2.44 (m, 2H), 2.39-2.28 (m, 1H), 2.26-2.09 (m, 2H), 2.04-1.88 (m, 1H) ppm. ^{13}C NMR (75 MHz, Chloroform-d) δ 218.1, 138.5, 128.6, 128.2, 126.9, 55.4, 38.5, 31.8, 20.9 ppm. The spectroscopic data are in accordance with those previously reported in the literature[364]

6.3.7. Mechanistic studies:

Brønsted acids as catalysts:

[364] Kimura, M.; Kobayashi, K.; Yamamoto, Y.; Sawaki, Y. *Tetrahderon* **1996**, *52*, 4303.

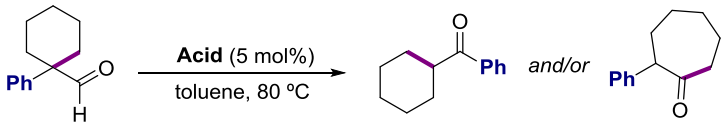

267a 268a 302a

Entry	Acid	Conv. (%)	268a (%)	302a (%)
1	TfOH	>99	10	0
2	HBr	0	0	0
3	*p*TsOH·H_2O	0	0	0
4	TFA	0	0	0

A mixture of **267a** (94.1 mg, 0.5 mmol) with the corresponding acid (5 mol%) in 2.0 mL of toluene was heated at 80 ºC. After stirring for 16 h the reaction was diluted with ethyl acetate. Next, dodecane (114 μL, 0.5 mmol) was added as internal standard and an aliquot from the reaction was analyzed by GC.

Note: only when using TfOH, **268a** was observed but only in 10% yield. The GC analysis of the crude material showed that the aldehyde was decomposed under the reaction conditions.

*Intermediacy of **303a** in the Fe-catalyzed [1,2]-shift:*

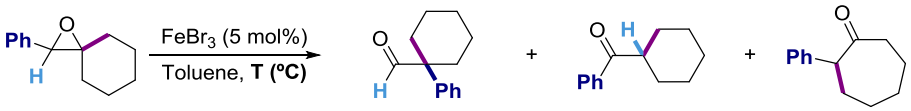

303a 267a 268a 302a

Entry	Temp (ºC)	Conv (%)	267a (%)	268a (%)	302a (%)
1	110	>99	25	28	47
2	80	>99	23	28	49
3	rt	>99	20	32	48

A mixture of **303a** (94.1 mg, 0.5 mmol) with $FeBr_3$ (7.4 mg, 5.0 mol%) in 2.0 mL of toluene was heated at the indicated temperature for 14h. Dodecane was then added as internal standard (114 μL, 0.5 mmol). After addition of 5.0 mL of ethyl acetate the mixture was filtered through a path of Celite® and analyzed by GC chromatography.

Deuterium-labelling experiments:

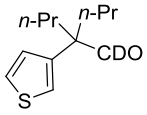

2-propyl-2-(thiophen-3-yl)pentanal d_1 (267cc-*d*[1]): Colorless oil. ^{1}H NMR (300 MHz, Chloroform-*d*) δ 7.29 (dd, *J* = 5.2, 1.2 Hz, 1H), 7.03 (dd, *J* = 5.1, 3.6 Hz, 1H), 6.90 (dd, *J* = 3.6, 1.2 Hz, 1H), 2.02-1.84 (m, 4H), 1.31-1.11 (m, 4H), 0.94 (t, *J* = 7.2 Hz, 6H) ppm. ^{13}C NMR (75 MHz,

Chloroform-*d*) δ 200.3 (t, *J* = 26.8 Hz), 144.1, 127.1, 125.2, 125.0, 56.0 (d, *J* = 3.1 Hz), 35.9, 17.2, 14.5 ppm. IR (neat, cm^{-1}): 2958, 1711, 1462, 851, 695. HRMS *calcd.* for ($C_{12}H_{17}DOS$): 212,1214, *found* 212,1212.

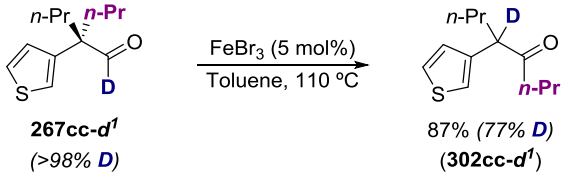

267cc-*d*[1] (*>98% D*) → 87% (*77% D*) (**302cc-*d*[1]**)

5-(thiophen-3-yl)octan-4-one d_1 (302cc-*d*[1]): A mixture of **267cc-D[1]** (52.2 mg, 0.25 mmol) with $FeBr_3$ (3.7 mg, 5.0 mol%) in 1.0 mL of toluene was heated at 110 ºC for 14h. Column chromatography: silica gel, hexanes/EtOAc 98:2 afforded the title compound (45.4 mg, 70% yield +17% **302cc**). ^{1}H NMR (300 MHz, Chloroform-*d*) (7.21 (dd, *J* = 5.2, 1.2 Hz, 1H), 6.97 (dd, *J* = 5.1, 3.5 Hz, 1H), 6.89 (dd, *J* = 3.5, 1.1 Hz, 1H), 2.57-2.32 (m, 2H), 2.02 (dt, *J* = 21.9, 7.2 Hz, 1H), 1.82-1.68 (m, 1H), 1.66-1.46 (m, 2H), 1.38-1.19 (m, 2H), 0.92 (t, *J* = 7.3 Hz, 3H), 0.85 (t, *J* = 7.4 Hz, 3H) ppm.^{13}C NMR (75 MHz, Chloroform-*d*) δ 209.6, 141.9, 127.0, 125.4 (d, *J* = 2.5 Hz), 124.6, 53.6, 43.2, 35.4 (d, *J* = 5.9 Hz), 20.8 (d, *J* = 2.2 Hz), 17.3, 14.0, 13.7 ppm. IR (neat, cm^{-1}): 2959, 1711, 1460, 695. Nominal mass *calcd.* for ($C_{12}H_{17}DOS$+H) 211,1141, *found* 212.1211.

Reaction of an enantioenriched substrate:

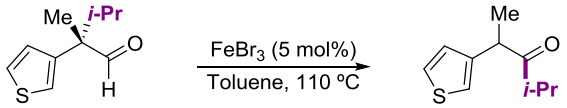

267jj (*96% ee*) → 86% (*racemic*) (**302jj**)

Enantioenriched aldehyde **267jj** (96% ee) was prepared by preparative HPLC from the racemic **302jj** sample. Separation conditions: Chiralpack IC 250x4.6mm, 5μm. Hexanes/TBME 95:5. 1 mL/min.

Sample Info : Chiralpack IC 250x4.6mm, 5µm
Hex / TBME 95:5
1 mL/min

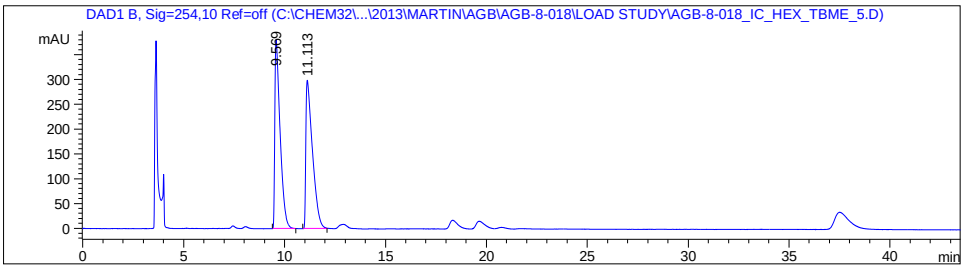

Area Percent Report

Sorted By : Signal
Multiplier : 1.0000
Dilution : 1.0000
Use Multiplier & Dilution Factor with ISTDs

Signal 1: DAD1 B, Sig=254,10 Ref=off

Peak #	RetTime [min]	Type	Width [min]	Area [mAU*s]	Height [mAU]	Area %
1	9.569	BV	0.2641	6910.18506	380.16760	50.3130
2	11.113	VV	0.3221	6824.21631	299.20459	49.6870
Totals :				1.37344e4	679.37219	

Figure 6.3.S2. Racemic mixture of aldehyde **267jj**

```
Sample Info     : Chiralpack IC 250x4.6mm, 5µm
                  Hex / MTBE 95:5
                  1 mL/min
                  Sample: 1.7mg/mL (DCM)
```

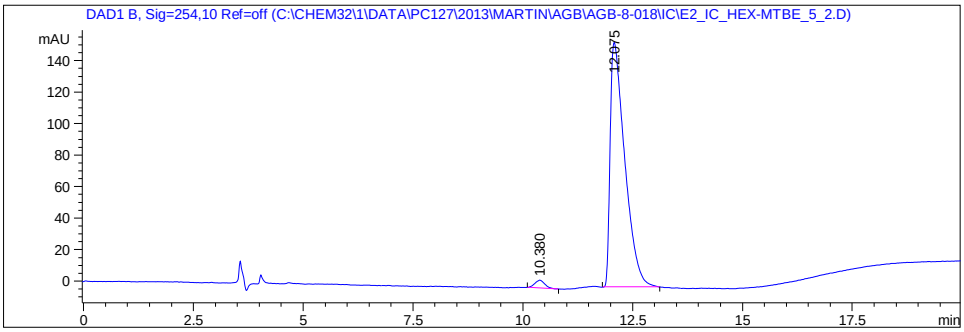


```
=====================================================================
                        Area Percent Report
=====================================================================

Sorted By             :      Signal
Multiplier            :      1.0000
Dilution              :      1.0000
Use Multiplier & Dilution Factor with ISTDs


Signal 1: DAD1 B, Sig=254,10 Ref=off

Peak RetTime Type  Width     Area      Height     Area
  #   [min]        [min]   [mAU*s]     [mAU]       %
----|-------|----|-------|----------|----------|--------|
   1  10.380 BB    0.2030   77.12367    4.97155   2.0939
   2  12.075 BB    0.3388 3606.09814  155.37273  97.9061

Totals :                  3683.22182  160.34428
```

Figure 6.3.S3. Enantioenriched aldehyde **267jj**

After running the Fe-catalyzed [1,2]-shift rearrangement, the crude product **302jj** was analyzed by GC with a chiral stationary phase. A racemic mixture was obtained, thus suggesting the intermediacy of cationic species within the catalytic cycle.

Sample AGB-8-018-Ketone
Column HP-CHIRAL-20B, 30m x 0.25mm, 0.25µm
Tª injector: 240ºC
1.5mL/min
Split 10:1 (1µL)
Isoterma 70ºC
Modo SCAN

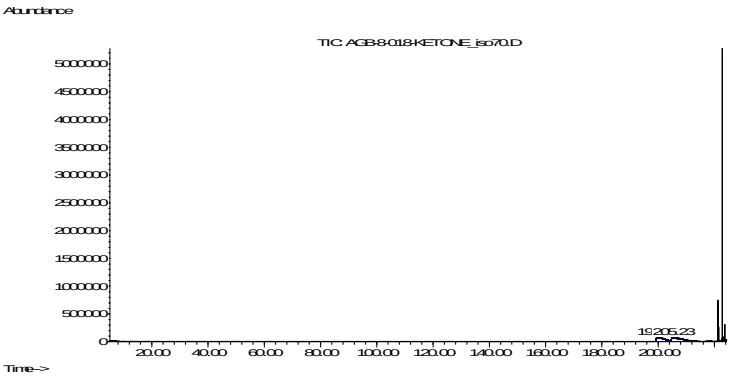

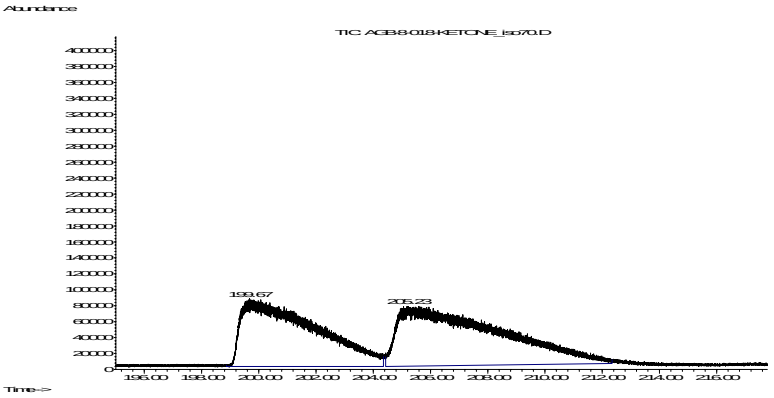

peak #	R.T. min	first scan	max scan	last scan	PK TY	peak height	corr. area	corr. % max.	% of total
1	199.674	125199	125718	128742	M6	85469	148305526	82.77%	45.287%
2	205.228	128791	129306	133903	M6	76477	179176841	100.00%	54.713%

Sum of corrected areas: 327482367

Figure 6.3.S4. Racemic mixture of ketone **302jj**

Sample AGB-8-089E2
Column HP-CHIRAL-20B, 30m x 0.25mm, 0.25µm
Tª injector: 240ºC
1.5mL/min
Split 5:1 (1µL)
Isoterma 70ºC
Modo SCAN

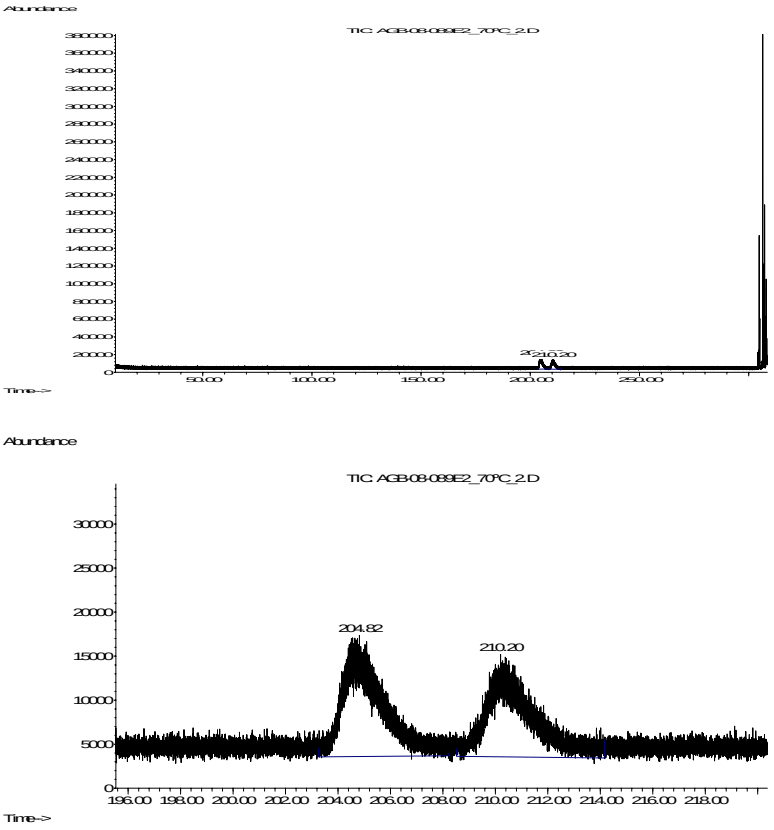

peak #	R.T. min	first scan	max scan	last scan	PK TY	peak height	corr. area	corr. % max.	% of total
1	204.816	124807	125810	128001	M	13918	12905474	100.00%	51.454%
2	210.198	128201	129287	131843	M	11746	12175927	94.35%	48.546%

Figure 6.3.S5. Product obtained from the reaction of **267jj** (96% ee).

Note: Although the retention times obtained from the racemic ketone and the product from the reaction of **267jj** (96% ee) are slightly different, GC-MS analysis showed that both are the expected **302jj.**

Cationic versus concerted mechanism:

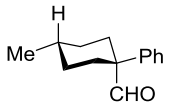

(1*s*,4*s*)-4-methyl-1-phenylcyclohexanecarbaldehyde (267tt): White solid in the fridge that melts at room temperature. ^{1}H NMR (400 MHz, Chloroform-*d*) δ 9.40 (d, *J* = 1.1 Hz, 1H), 7.42-7.26 (m, 5H), 2.62-2.53 (m, 2H), 1.82-1.66 (m, 4H), 1.48-1.34 (m, 1H), 1.20-1.06 (m, 2H), 0.94 (d, *J* = 6.5 Hz, 3H) ppm. ^{13}C NMR (101 MHz, Chloroform-*d*) δ 202.7, 140.6, 128.9, 127.4, 126.9, 54.1, 32.0, 31.9, 31.8, 22.4 ppm. IR (neat, cm^{-1}): 2923, 1448, 968, 757, 697, 556. HRMS *calcd.* for ($C_{14}H_{18}O$-CHO): 173,1325, *found* 173,1326.

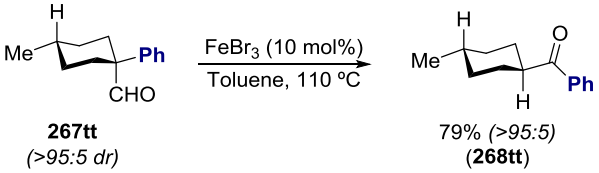

267tt
(>95:5 dr)

79% *(>95:5)*
(**268tt**)

((1*r*,4*r*)-4-methylcyclohexyl)(phenyl)methanone (268tt): A mixture of **267tt** (100.8 mg, 0.5 mmol) with $FeBr_3$ (14.8 mg, 10 mol%) in 2.0 mL of toluene was heated at 110 ºC for 14h. Column chromatography: silica gel, hexanes/EtOAc 98:2 afforded the title compound (80.9 mg, 80% yield) as a yellow sticky oil. ^{1}H NMR (300 MHz, Chloroform-*d*) δ 7.99-7.92 (m, 2H), 7.60-7.51 (m, 1H), 7.50-7.44 (m, 2H), 3.21 (tt, *J* = 11.9, 3.2 Hz, 1H), 1.99-1.78 (m, 3H), 1.76-1.36 (m, 4H), 1.10 (d, *J* = 3.0 Hz, 2H), 0.94 (d, *J* = 6.5 Hz, 3H) ppm. ^{13}C NMR (75 MHz, Chloroform-*d*) δ 204.1, 136.5, 132.8, 128.7, 128.3, 45.6, 34.7, 32.3, 29.5, 22.7 ppm. IR (neat, cm^{-1}): 2927, 2855, 1673, 1446, 1203, 947, 694. HRMS *calcd.* for ($C_{14}H_{18}O$+Na): 225.1250, *found* 225.1255. The configuration of the α-carbon was unambiguously determined by ^{1}H NMR as judged by the *J* values of the corresponding proton ($^{3}J_{ax,ax}$ is very characteristic and goes from 8 to 13 Hz, which is in agreement with the α-proton of this molecule: δ 3.21 ppm (tt, *J* = 11.9, 3.2 Hz, 1H)).[365]

Crossover experiment:

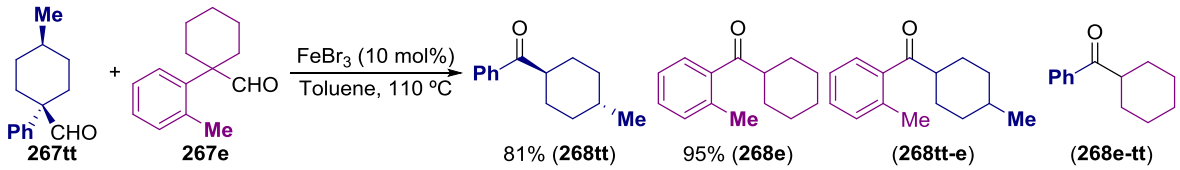

267tt **267e** 81% (**268tt**) 95% (**268e**) (**268tt-e**) (**268e-tt**)

An equimolar mixture of **267tt** (50.6 mg, 0.25 mmol) and **267e** (50.6 mg, 0.25 mmol) in toluene (2.0 mL) was stirred at 110 ºC in the presence of $FeBr_3$ (14.8 mg, 10 mol%). After 14h, the

[365] Determinación estructural de compuestos orgánicos; Pretsch, E.; Bülhman, P.; Affolter, C.; Martínez, R.; Masson,: Barcelona, 2005.

reaction was cooled to room temperature. Finally, dodecane (57 μL, 0.25 mmol) was added as internal standard and an aliquot was analyzed by HPLC. HPLC analysis showed **268tt** (81% yield) and **268e** (95% yield) as the only products of the reaction. Crossover products (**268tt-e** and **268e-tt**) were not observed thus indicating that the [1,2]-shift occurs faster than the diffusion of the migrating group.

6.3.8. X-Ray structure of 267tt:

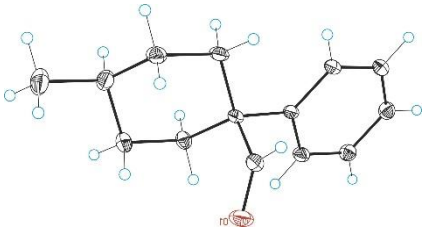

Empirical formula	C14 H18 O	
Formula weight	202.28	
Temperature	100(2) K	
Wavelength	0.71073 Å	
Crystal system	Monoclinic	
Space group	C2/c	
Unit cell dimensions	a = 18.7389(14) Å	α = 90.00 °.
	b = 6.0768(4) Å	β = 112.912(2) °.
	c = 21.6910(17) Å	γ = 90.00 °.
Volume	2275.1(3) $Å^3$	
Z	8	
Density (calculated)	1.181 Mg/m^3	
Absorption coefficient	0.072 mm^{-1}	
F(000)	880	
Crystal size	0.20 x 0.10 x 0.10 mm^3	
Theta range for data collection	2.04 to 33.70 °.	

Index ranges	-29 <=h<=28 ,-9 <=k<=9 ,-32 <=l<=33
Reflections collected	20316
Independent reflections	4227 [R(int) = 0.0358]
Completeness to theta =33.70 °	93.0%
Absorption correction	Empirical
Max. and min. transmission	0.9928 and 0.9857
Refinement method	Full-matrix least-squares on F^2
Data / restraints / parameters	4227 / 0 / 137
Goodness-of-fit on F^2	1.128
Final R indices [I>2sigma(I)]	R1 = 0.0498 , wR2 = 0.1392
R indices (all data)	R1 = 0.0537 , wR2 = 0.1421
Largest diff. peak and hole	0.625 and -0.322 e.$Å^{-3}$

Table 2. Bond lengths [Å] and angles:

Bond lengths----

O1-C14	1.2069(12)
C1-C6	1.4003(12)
C1-C2	1.4012(12)
C1-C7	1.5365(12)
C2-C3	1.3890(13)
C3-C4	1.3921(14)
C4-C5	1.3904(14)
C5-C6	1.3952(13)
C7-C14	1.5271(13)
C7-C12	1.5376(12)

C7-C8	1.5384(12)
C8-C9	1.5280(13)
C9-C10	1.5262(15)
C10-C11	1.5243(14)
C10-C13	1.5246(14)
C11-C12	1.5281(13)

Angles----------

C6-C1-C2	117.96(8)
C6-C1-C7	122.07(8)
C2-C1-C7	119.81(8)
C3-C2-C1	121.18(9)
C2-C3-C4	120.28(9)
C5-C4-C3	119.35(9)
C4-C5-C6	120.33(9)
C5-C6-C1	120.90(8)
C14-C7-C1	102.78(7)
C14-C7-C12	111.06(7)
C1-C7-C12	112.25(7)
C14-C7-C8	108.14(7)
C1-C7-C8	111.94(7)
C12-C7-C8	110.37(7)
C9-C8-C7	112.46(7)
C10-C9-C8	112.39(8)
C11-C10-C13	111.59(9)

C11-C10-C9	109.33(8)
C13-C10-C9	111.49(9)
C10-C11-C12	112.48(8)
C11-C12-C7	112.92(7)
O1-C14-C7	125.37(9)

Table 3. Torsion angles [°]

C6-C1-C2-C3	0.54(13)
C7-C1-C2-C3	175.97(8)
C1-C2-C3-C4	-0.38(14)
C2-C3-C4-C5	-0.05(14)
C3-C4-C5-C6	0.30(14)
C4-C5-C6-C1	-0.12(14)
C2-C1-C6-C5	-0.29(13)
C7-C1-C6-C5	-175.61(8)
C6-C1-C7-C14	94.70(9)
C2-C1-C7-C14	-80.53(9)
C6-C1-C7-C12	-145.89(8)
C2-C1-C7-C12	38.88(11)
C6-C1-C7-C8	-21.12(12)
C2-C1-C7-C8	163.64(8)
C14-C7-C8-C9	70.08(10)
C1-C7-C8-C9	-177.40(8)
C12-C7-C8-C9	-51.59(10)

C7-C8-C9-C10	55.65(11)
C8-C9-C10-C11	-56.28(11)
C8-C9-C10-C13	179.86(9)
C13-C10-C11-C12	179.44(8)
C9-C10-C11-C12	55.64(11)
C10-C11-C12-C7	-54.62(11)
C14-C7-C12-C11	-68.76(10)
C1-C7-C12-C11	176.80(7)
C8-C7-C12-C11	51.17(10)
C1-C7-C14-O1	101.12(11)
C12-C7-C14-O1	-19.11(13)
C8-C7-C14-O1	-140.35(10)

6.3.9. ^{1}H and ^{13}C NMR spectra

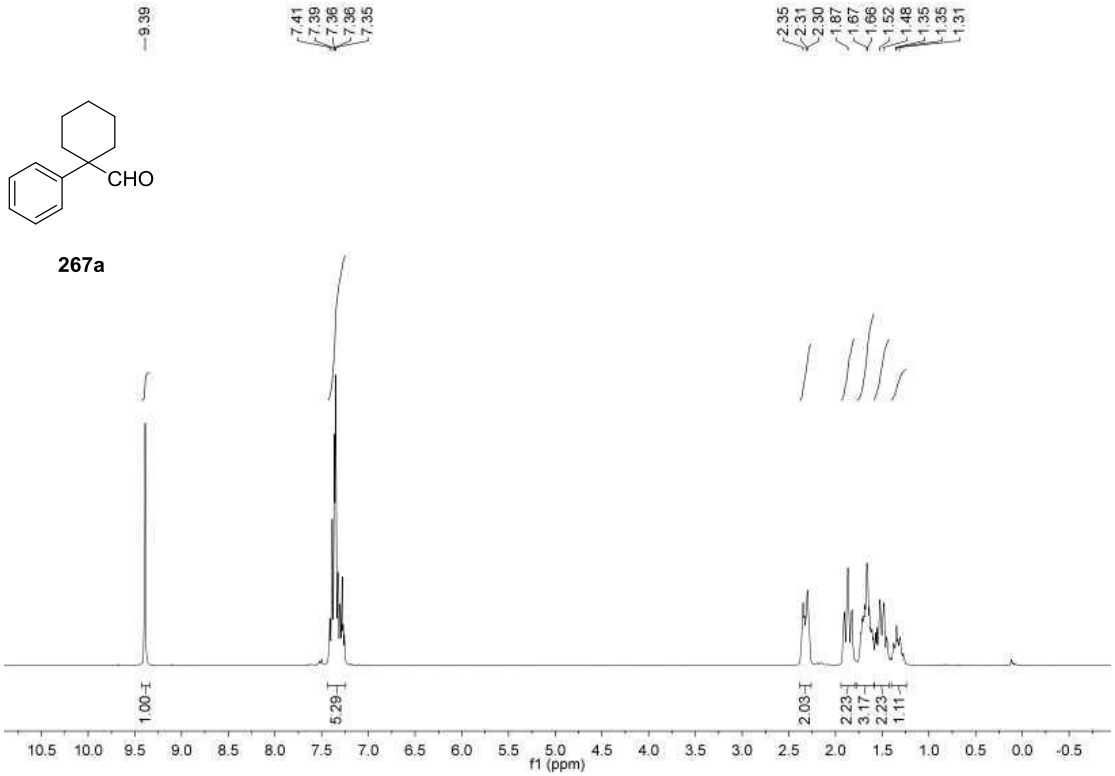

267a

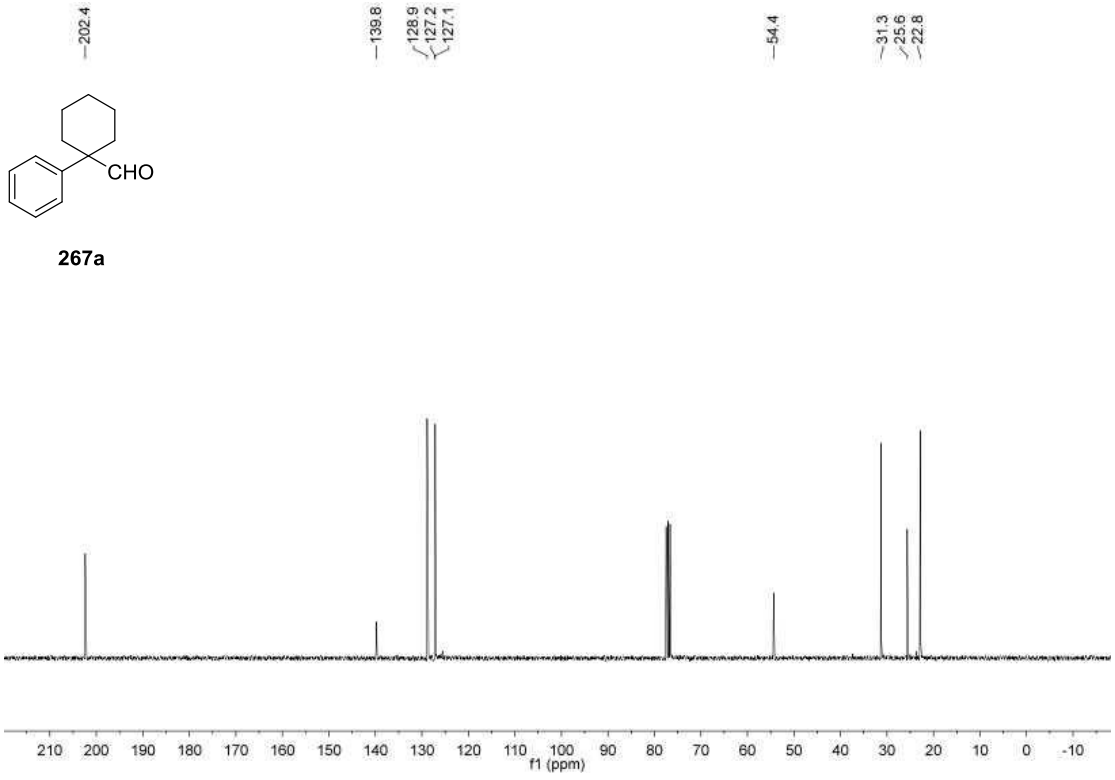

267a

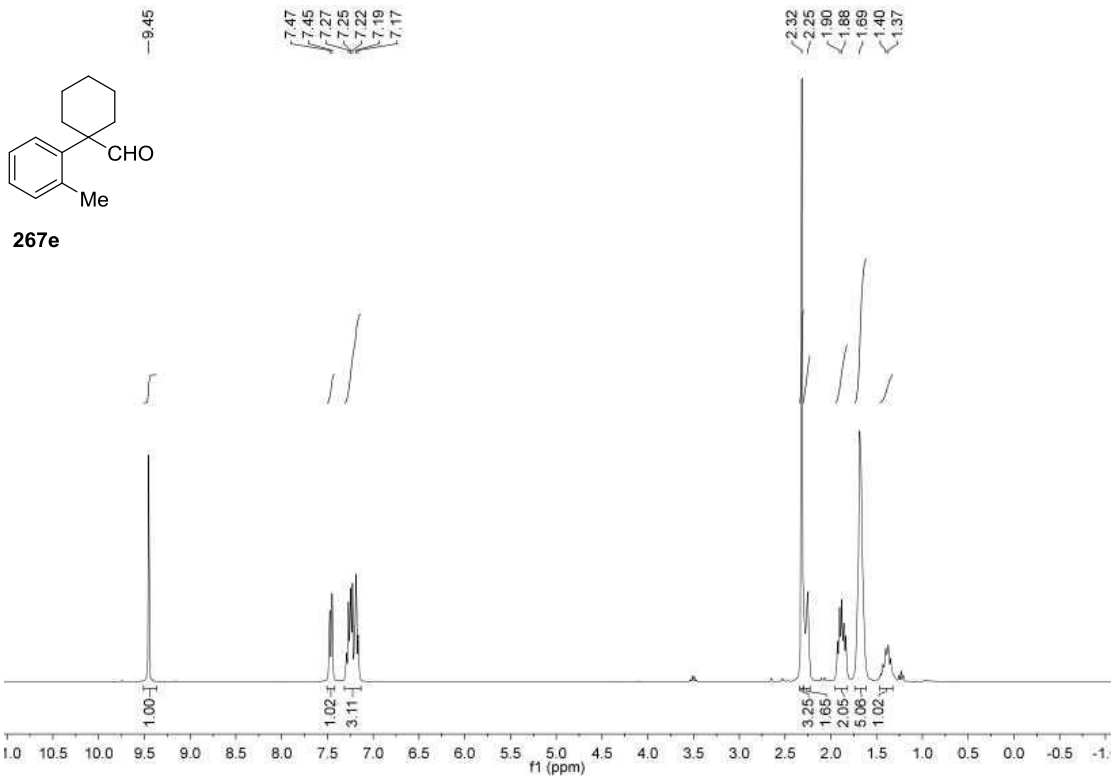
9.45
7.47
7.45
7.27
7.25
7.22
7.19
7.17
2.32
2.25
1.90
1.88
1.69
1.40
1.37
CHO
Me
267e
1.00
1.02
3.11
3.25
1.65
2.05
5.06
1.02
f1 (ppm)

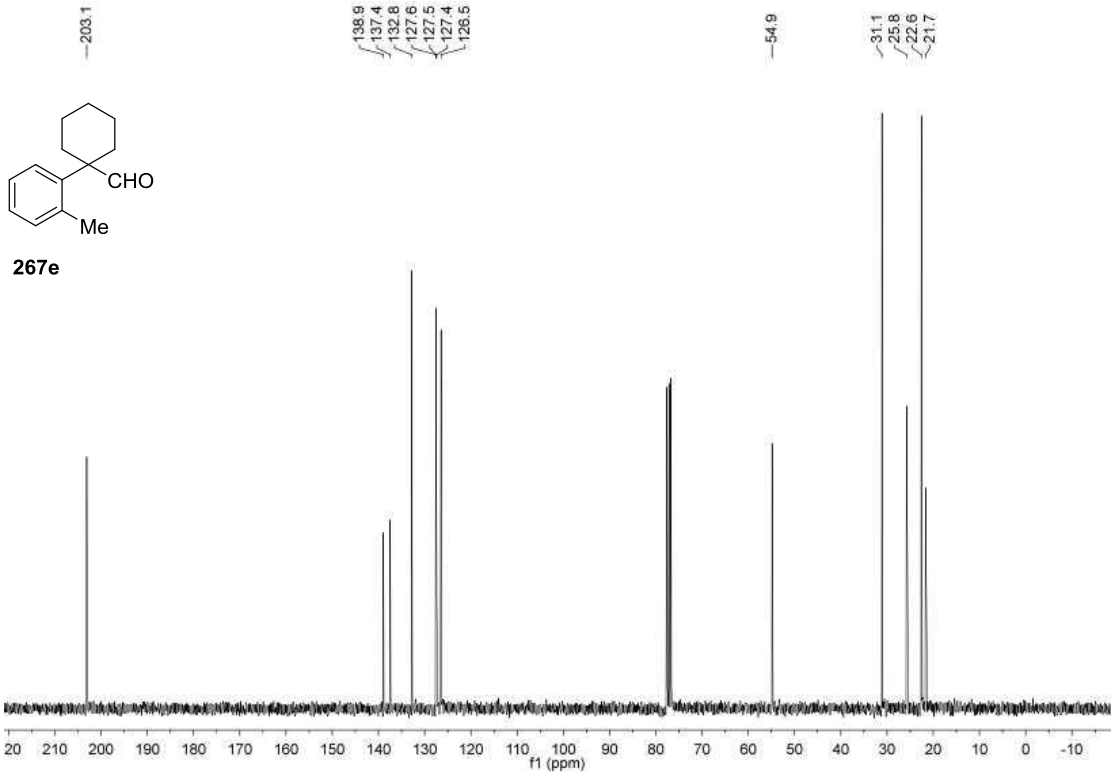
203.1
138.9
137.4
132.8
127.6
127.5
127.4
126.5
54.9
31.1
25.8
22.6
21.7
CHO
Me
267e
f1 (ppm)

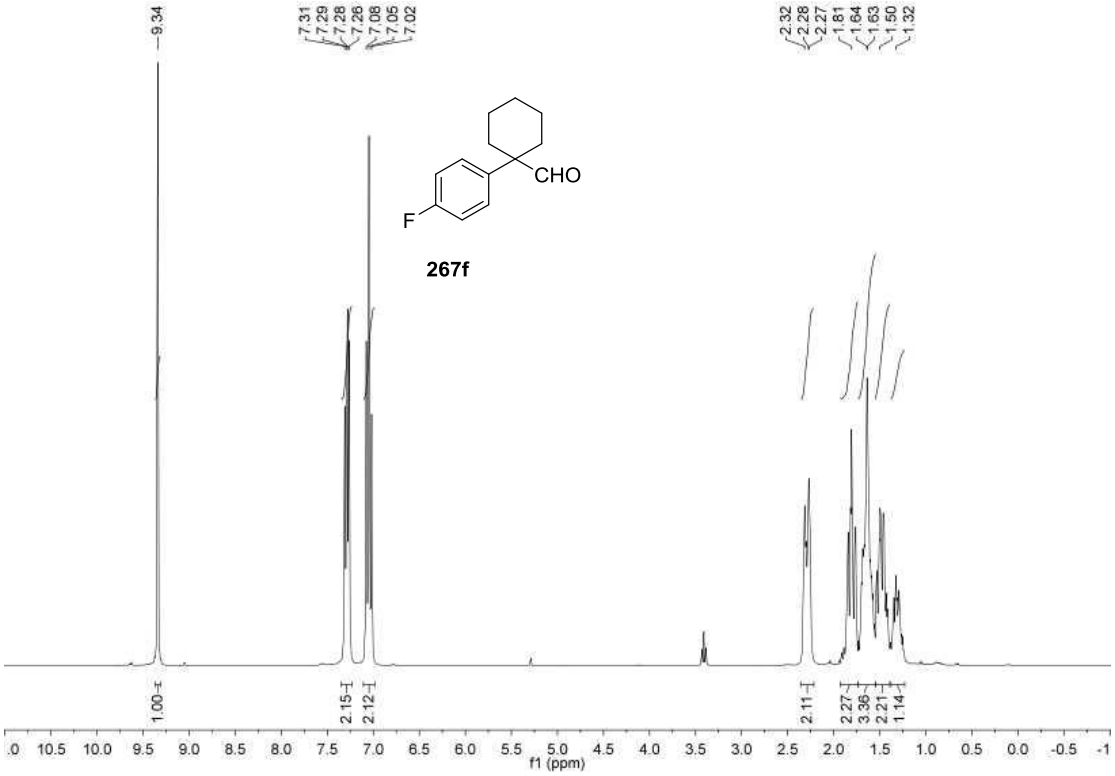
9.34
7.31
7.29
7.28
7.26
7.08
7.05
7.02
2.32
2.28
2.27
1.81
1.64
1.63
1.50
1.32
CHO
F
267f
1.00
2.15
2.12
2.11
2.27
3.36
2.21
1.14
f1 (ppm)

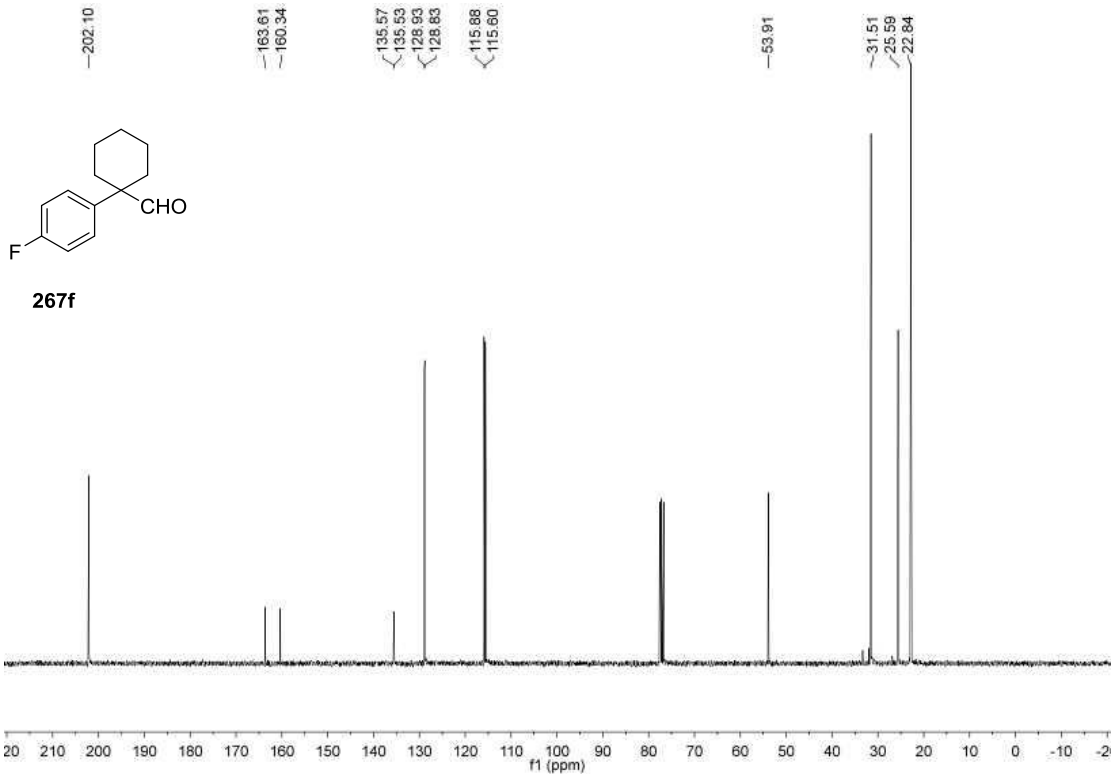
202.10
163.61
160.34
135.57
135.53
128.93
128.83
115.88
115.60
53.91
31.51
25.59
22.84
CHO
F
267f
f1 (ppm)

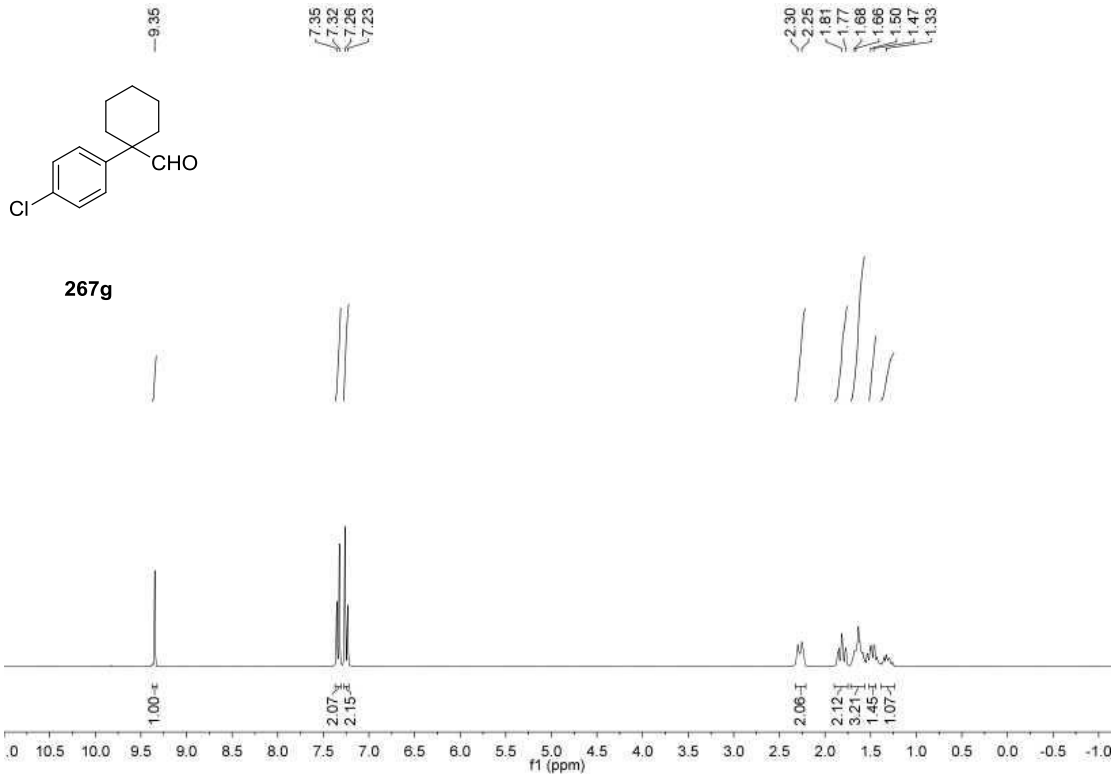
9.35
7.35
7.32
7.26
7.23
2.30
2.25
1.81
1.77
1.68
1.66
1.50
1.47
1.33
CHO
Cl
1.00
2.07
2.15
2.06
2.12
3.21
1.45
1.07
f1 (ppm)

267g

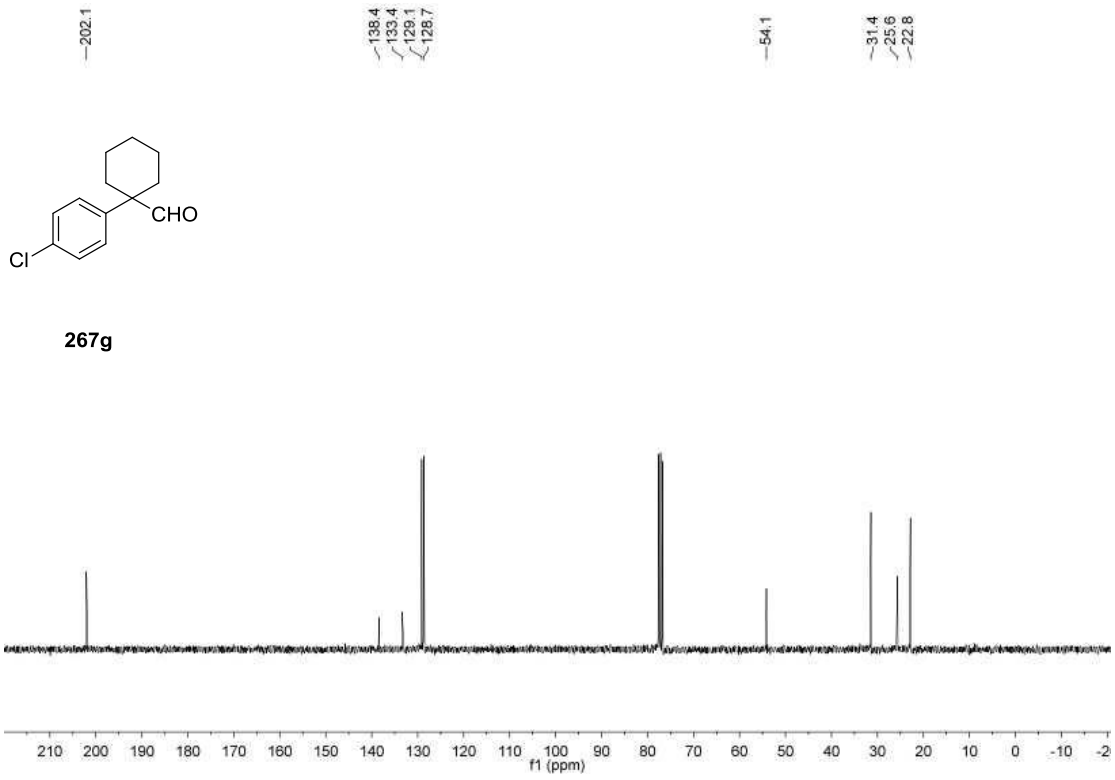
202.1
138.4
133.4
129.1
128.7
54.1
31.4
25.6
22.8
CHO
Cl
f1 (ppm)

267g

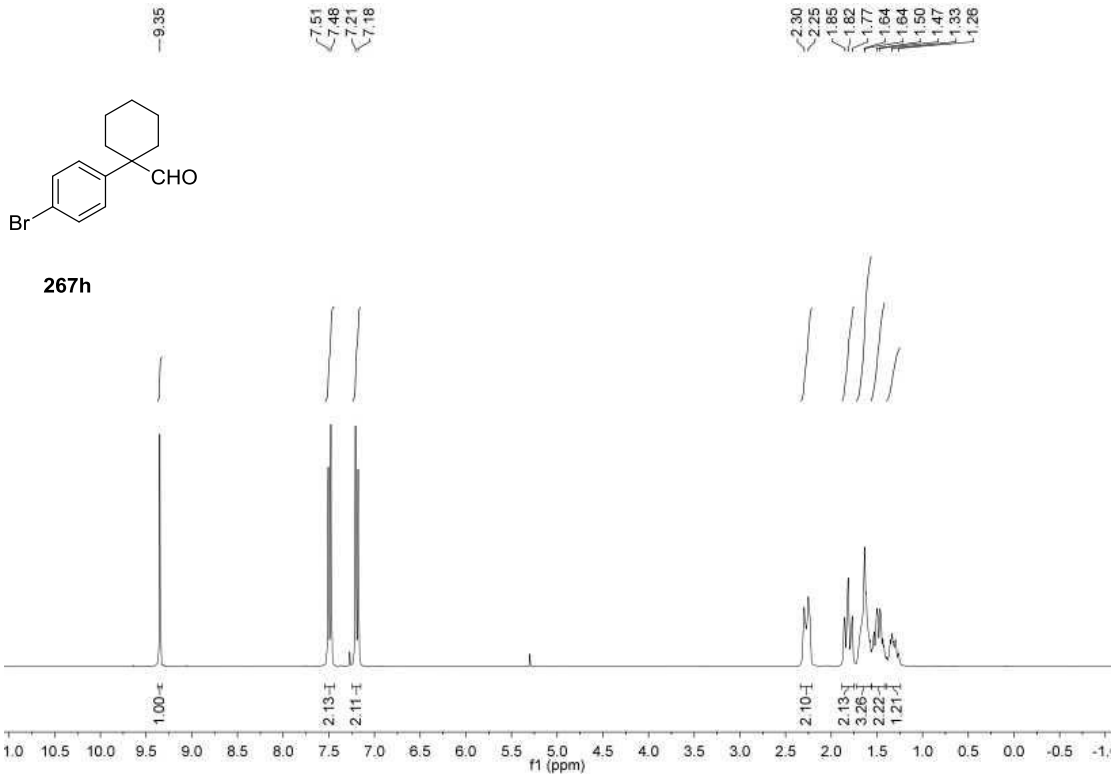
9.35
7.51
7.48
7.21
7.18
2.30
2.25
1.85
1.82
1.77
1.64
1.64
1.50
1.47
1.33
1.26
CHO
Br
267h
1.00
2.13
2.11
2.10
2.13
3.26
2.22
1.21
f1 (ppm)

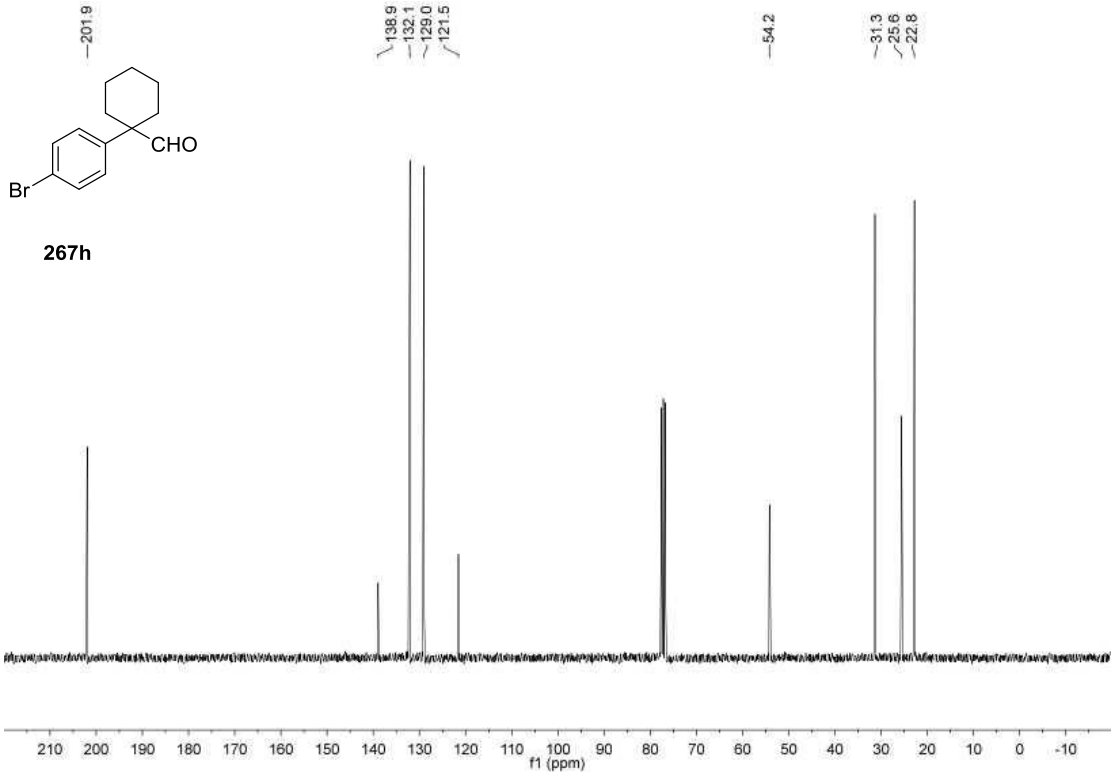
201.9
138.9
132.1
129.0
121.5
54.2
31.3
25.6
22.8
CHO
Br
267h
f1 (ppm)

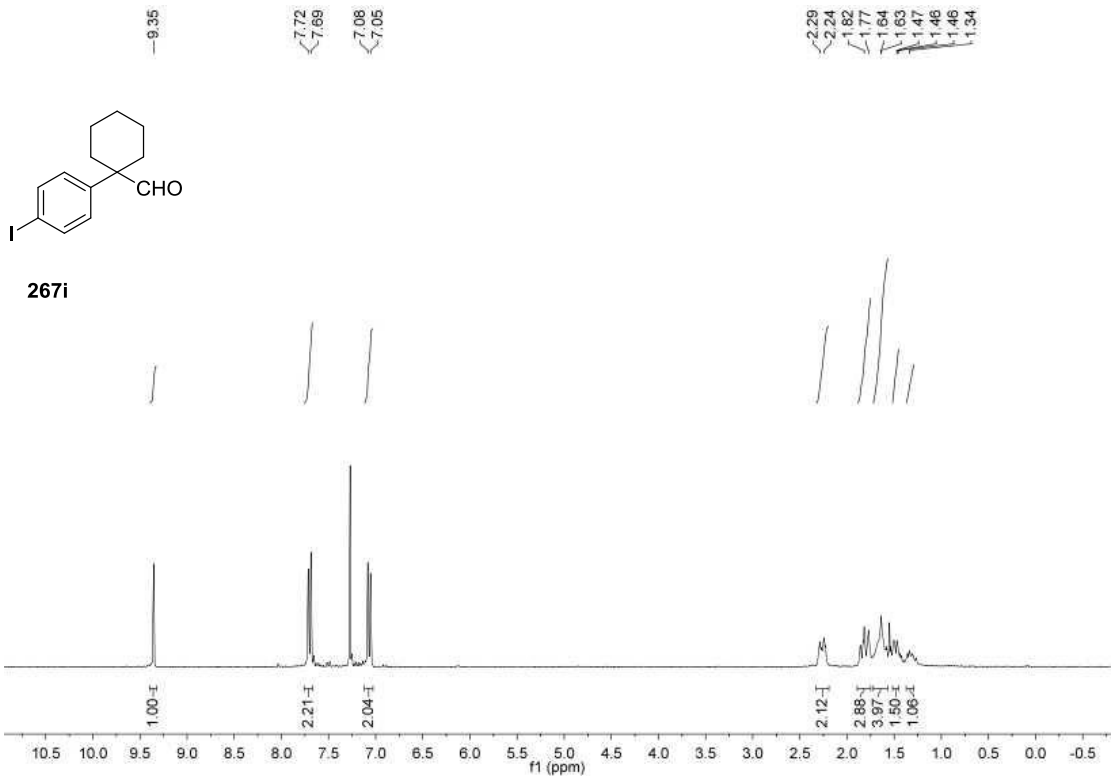
9.35
7.72
7.69
7.08
7.05
2.29
2.24
1.82
1.77
1.64
1.63
1.47
1.46
1.46
1.34
CHO
I
1.00
2.21
2.04
2.12
2.88
3.97
1.50
1.06
f1 (ppm)

267i

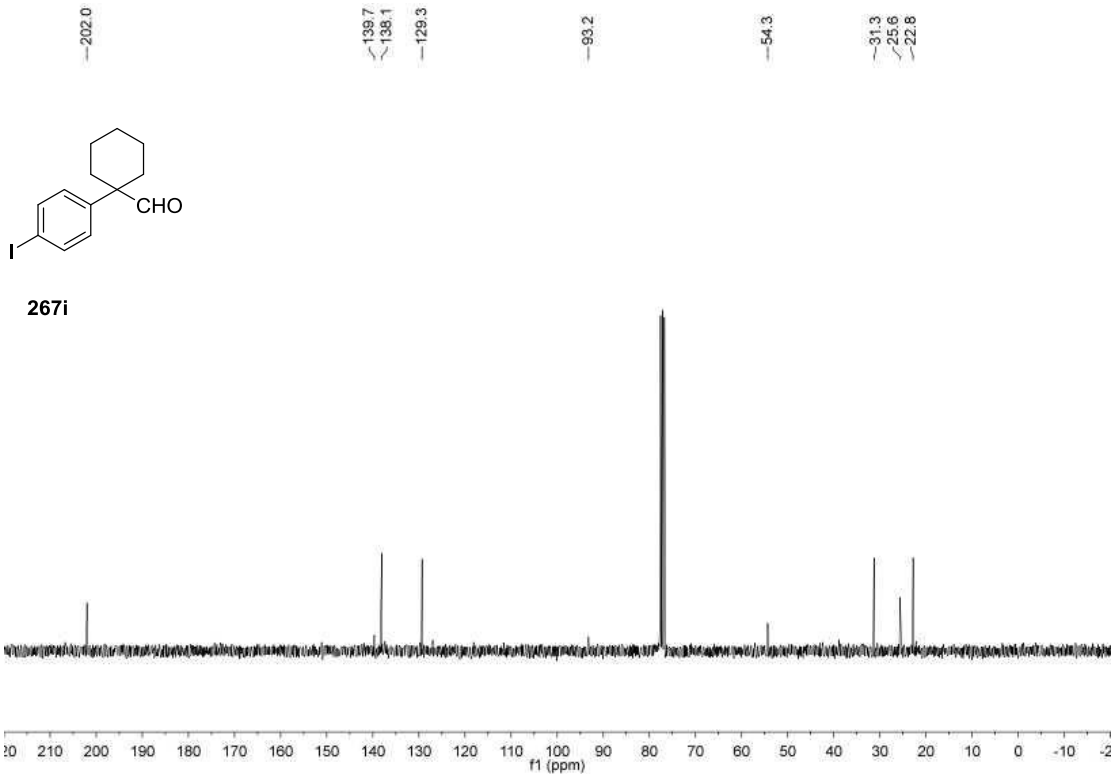
202.0
139.7
138.1
129.3
93.2
54.3
31.3
25.6
22.8
CHO
I
f1 (ppm)

267i

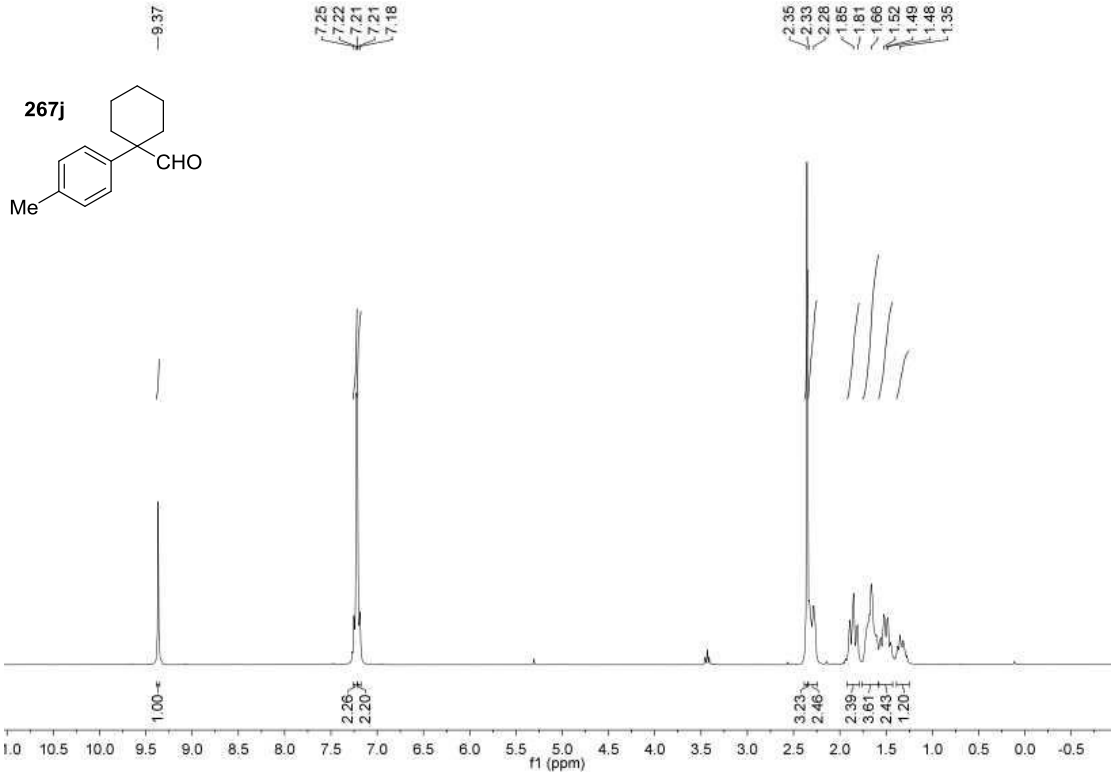
9.37
7.25
7.22
7.21
7.21
7.18
2.35
2.33
2.28
1.85
1.81
1.66
1.52
1.49
1.48
1.35
267j
CHO
Me
1.00
2.26
2.20
3.23
2.46
2.39
3.61
2.43
1.20
f1 (ppm)

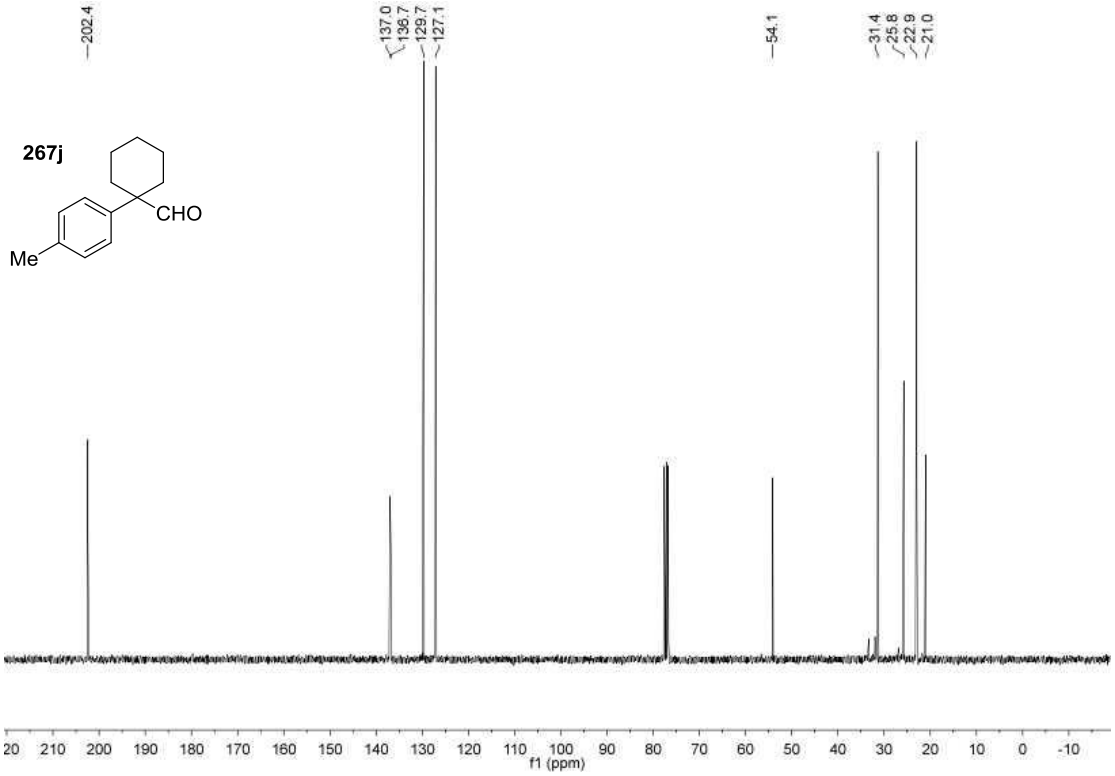
202.4
137.0
136.7
129.7
127.1
54.1
31.4
25.8
22.9
21.0
267j
CHO
Me
f1 (ppm)

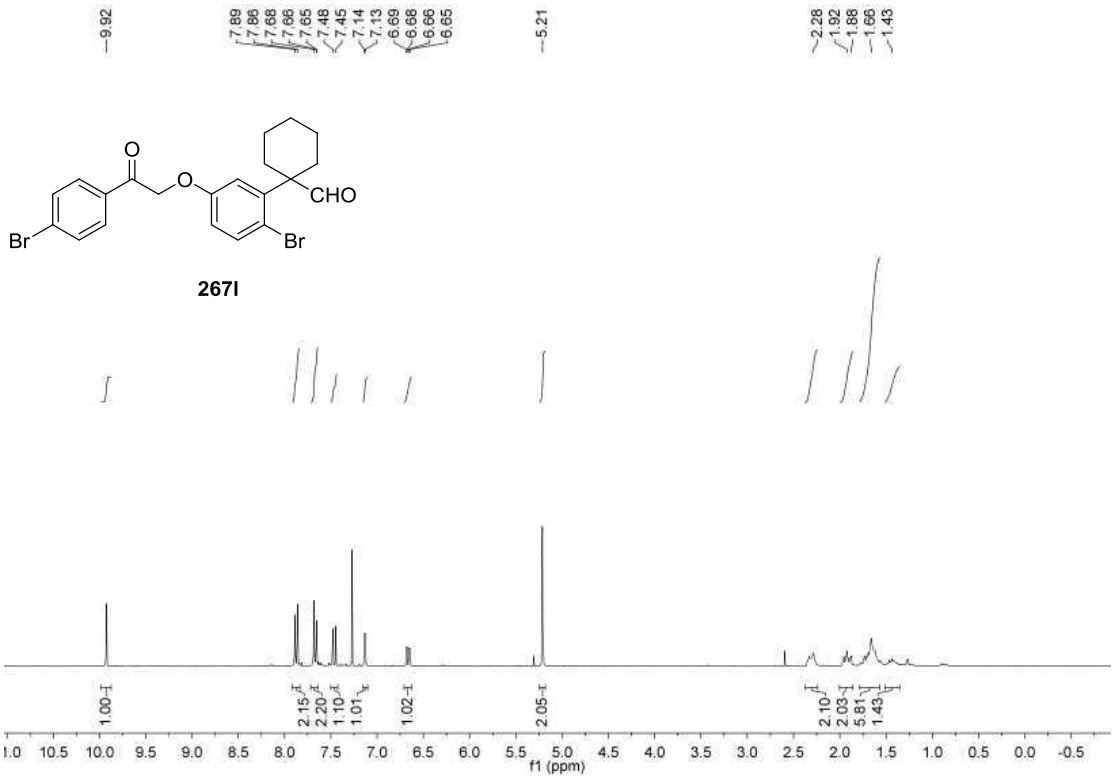
9.92
7.89
7.86
7.68
7.66
7.65
7.48
7.45
7.14
7.13
6.69
6.68
6.66
6.65
5.21
2.28
1.92
1.88
1.66
1.43
O
O
CHO
Br
Br
1.00
2.15
2.20
1.10
1.01
1.02
2.05
2.10
2.03
5.81
1.43
f1 (ppm)

267l

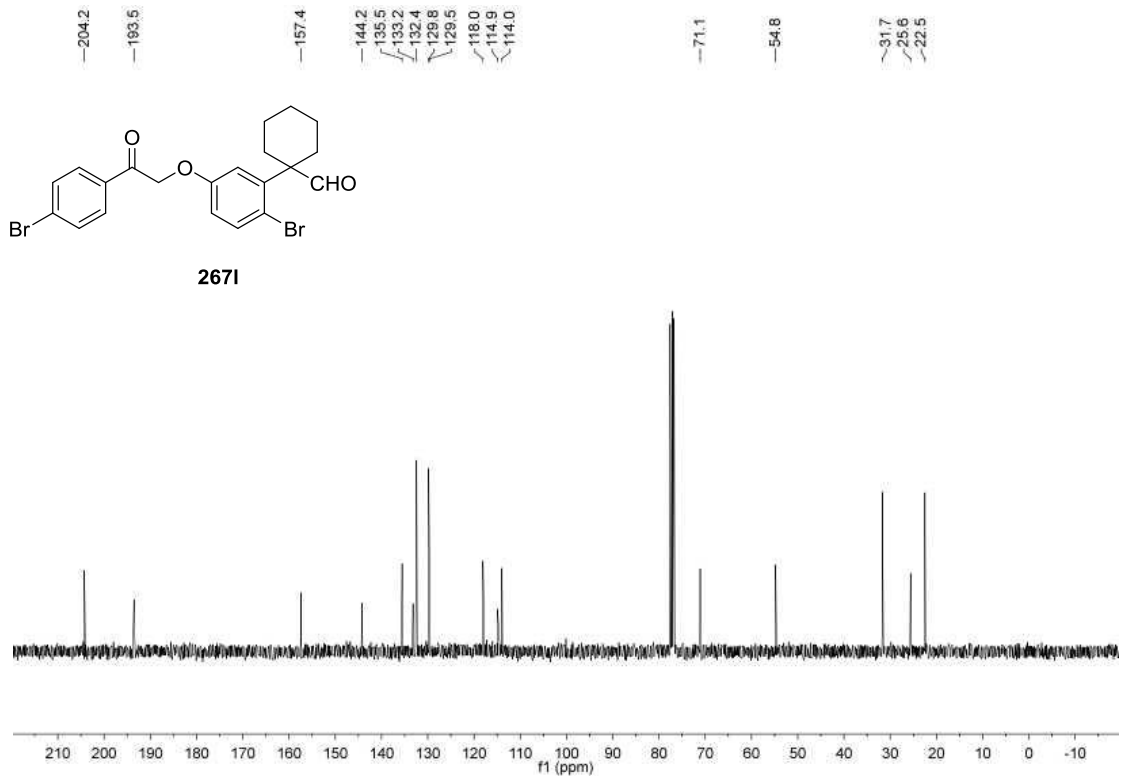
204.2
193.5
157.4
144.2
135.5
133.2
132.4
129.8
129.5
118.0
114.9
114.0
71.1
54.8
31.7
25.6
22.5
O
O
CHO
Br
Br
f1 (ppm)

267l

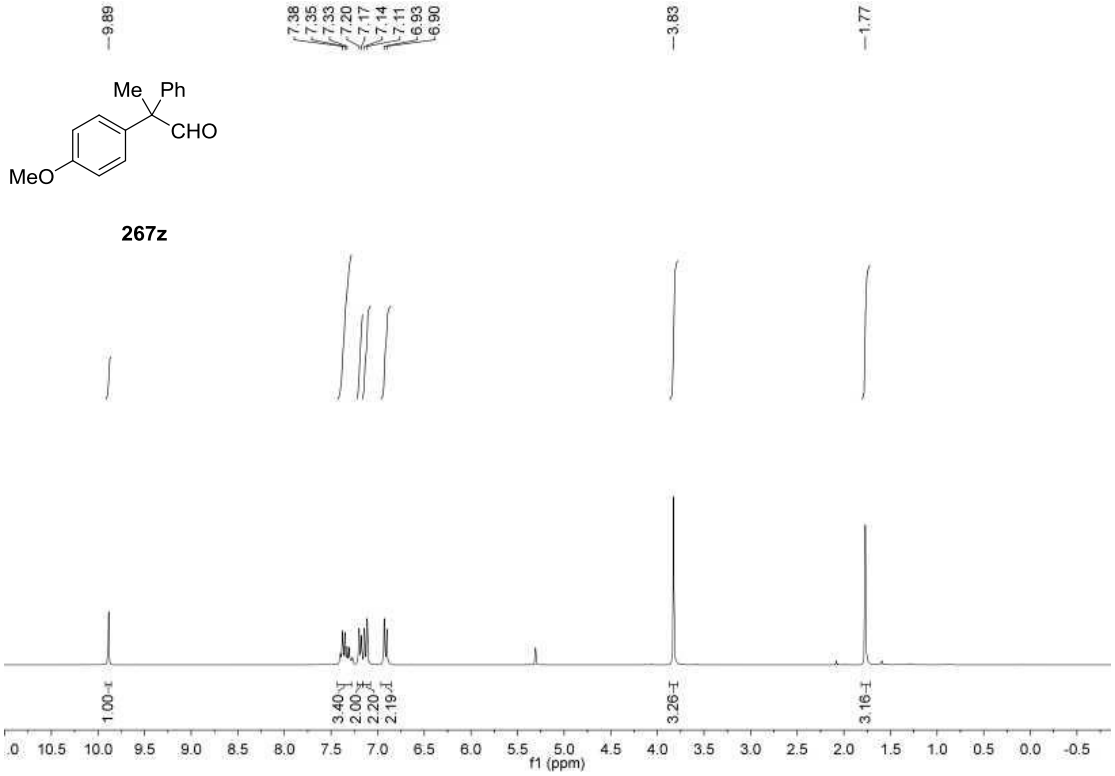
9.89
7.38
7.35
7.33
7.20
7.17
7.14
7.11
6.93
6.90
3.83
1.77
Me
Ph
CHO
MeO
1.00
3.40
2.00
2.20
2.19
3.26
3.16
f1 (ppm)

267z

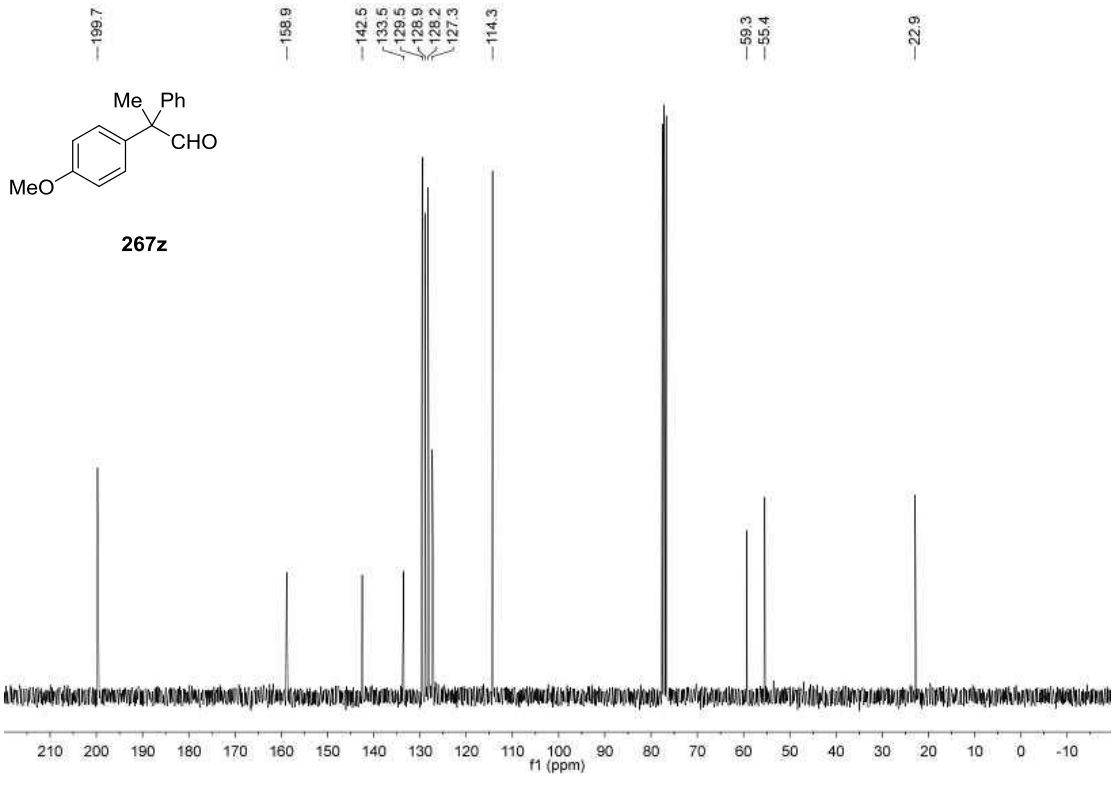
199.7
158.9
142.5
133.5
129.5
128.9
128.2
127.3
114.3
59.3
55.4
22.9
Me
Ph
CHO
MeO
f1 (ppm)

267z

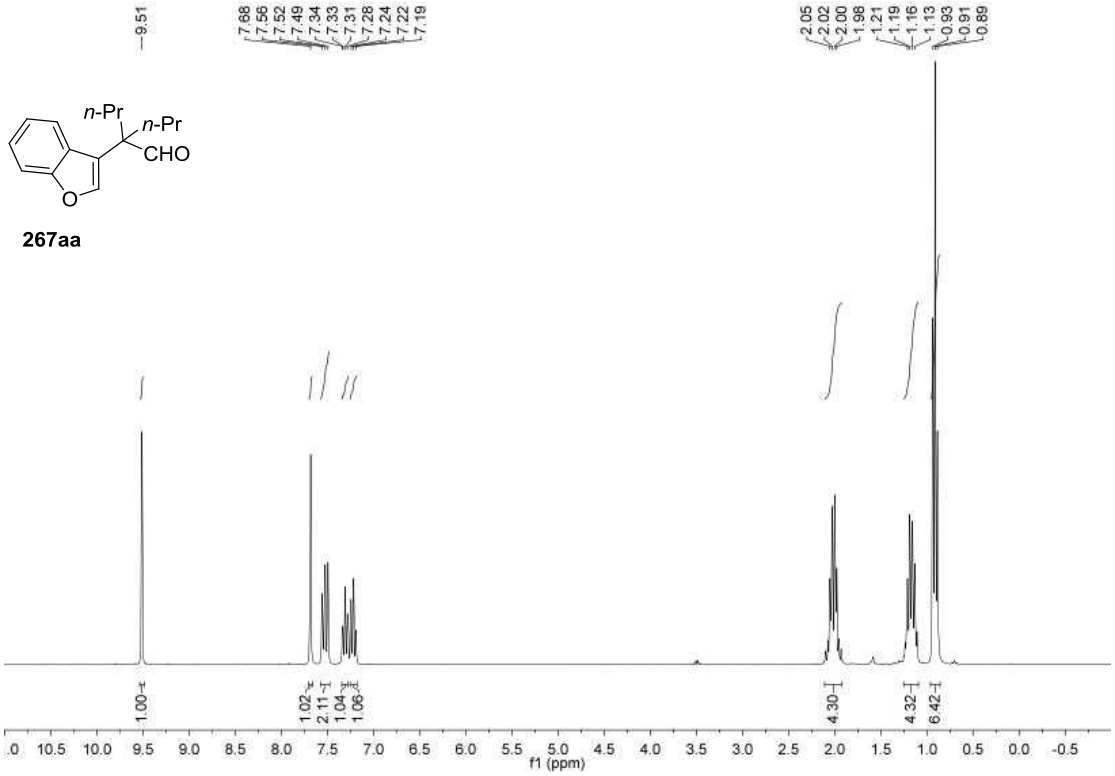
9.51
7.68
7.56
7.52
7.49
7.34
7.33
7.31
7.28
7.24
7.22
7.19
2.05
2.02
2.00
1.98
1.21
1.19
1.16
1.13
0.93
0.91
0.89
n-Pr
n-Pr
CHO
O
1.00
1.02
2.11
1.04
1.06
4.30
4.32
6.42
f1 (ppm)

267aa

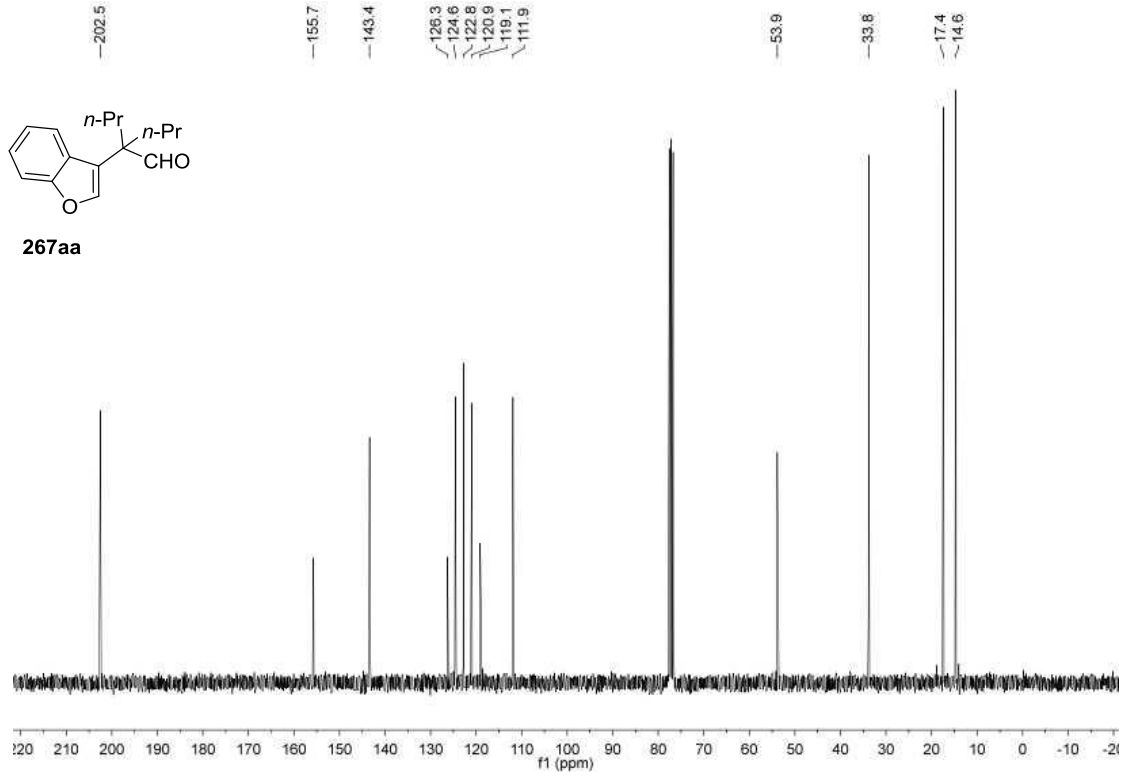
202.5
155.7
143.4
126.3
124.6
122.8
120.9
119.1
111.9
53.9
33.8
17.4
14.6
n-Pr
n-Pr
CHO
O
f1 (ppm)

267aa

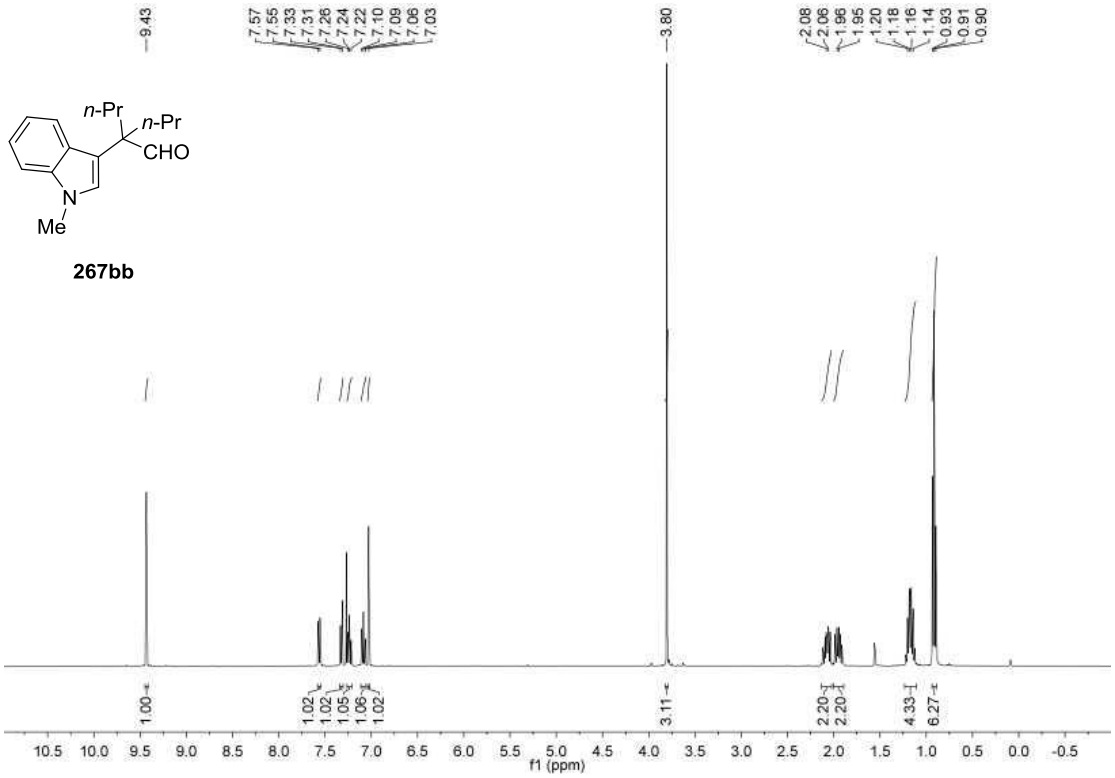
9.43
7.57
7.55
7.33
7.31
7.26
7.24
7.22
7.10
7.09
7.06
7.03
3.80
2.08
2.06
1.96
1.95
1.20
1.18
1.16
1.14
0.93
0.91
0.90
n-Pr
n-Pr
CHO
N
Me
1.00
1.02
1.02
1.05
1.06
1.02
3.11
2.20
2.20
4.33
6.27
f1 (ppm)

267bb

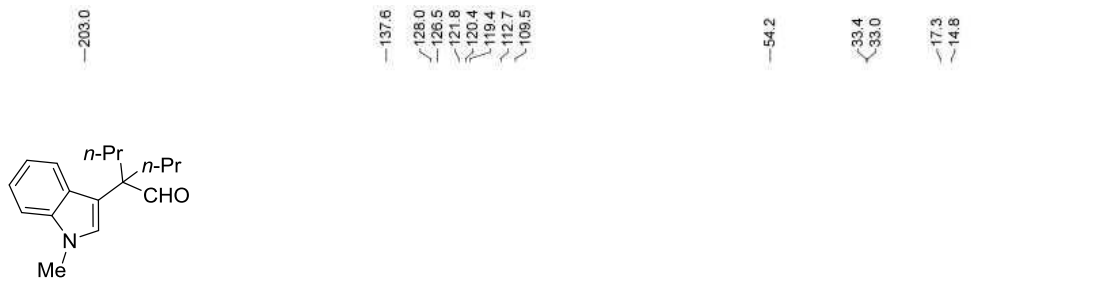
203.0
137.6
128.0
126.5
121.8
120.4
119.4
112.7
109.5
54.2
33.4
33.0
17.3
14.8

n-Pr
n-Pr
CHO
N
Me

267bb

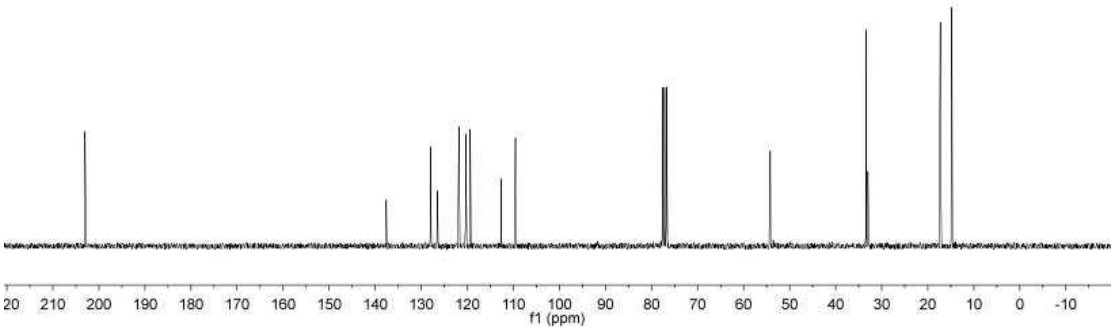
f1 (ppm)

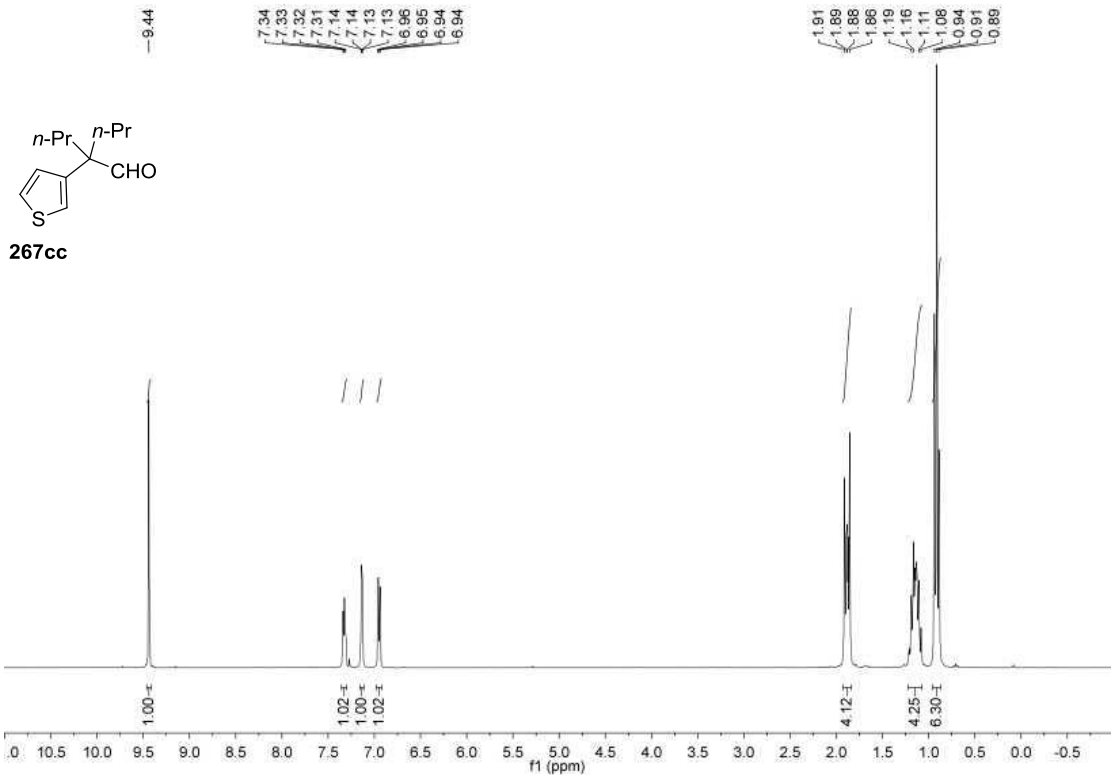
9.44
7.34
7.33
7.32
7.31
7.14
7.14
7.13
7.13
6.96
6.95
6.94
6.94
1.91
1.89
1.88
1.86
1.19
1.16
1.11
1.08
0.94
0.91
0.89
n-Pr
n-Pr
CHO
S
267cc
1.00
1.02
1.00
1.02
4.12
4.25
6.30
f1 (ppm)

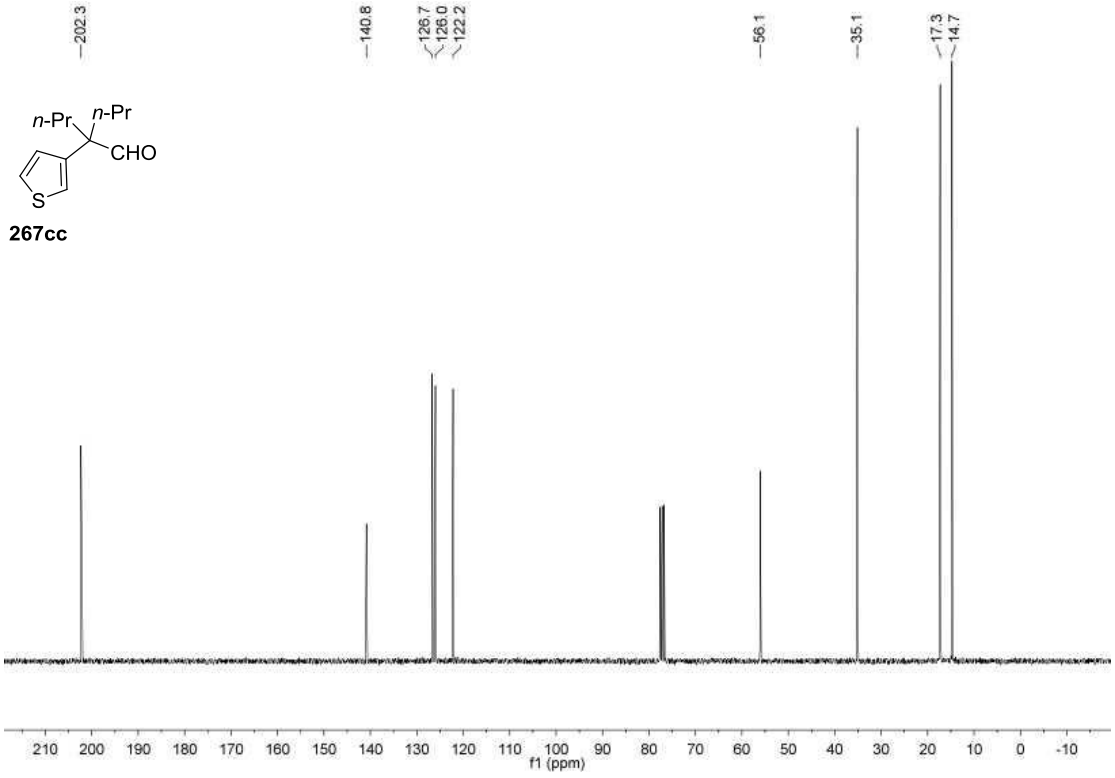
202.3
140.8
126.7
126.0
122.2
56.1
35.1
17.3
14.7
n-Pr
n-Pr
CHO
S
267cc
f1 (ppm)

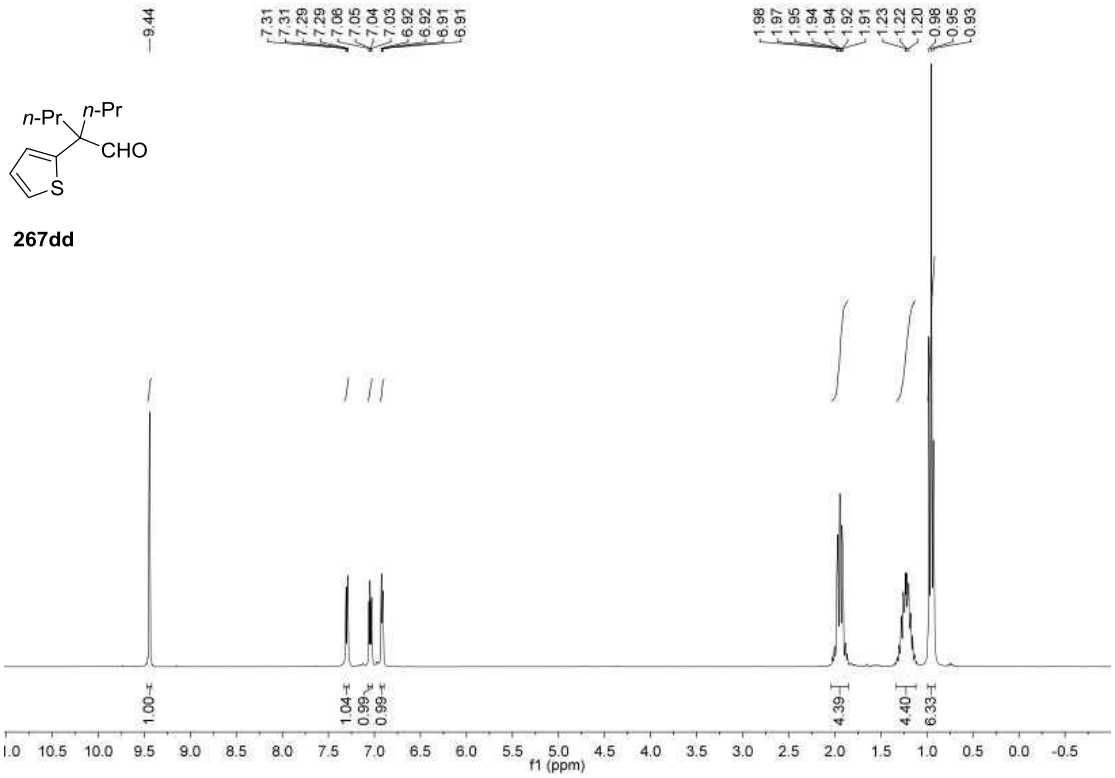
9.44
7.31
7.31
7.29
7.29
7.06
7.05
7.04
7.03
6.92
6.92
6.91
6.91
1.98
1.97
1.95
1.94
1.94
1.92
1.91
1.23
1.22
1.20
0.98
0.95
0.93
n-Pr
n-Pr
CHO
S
1.00
1.04
0.99
0.99
4.39
4.40
6.33
f1 (ppm)

267dd

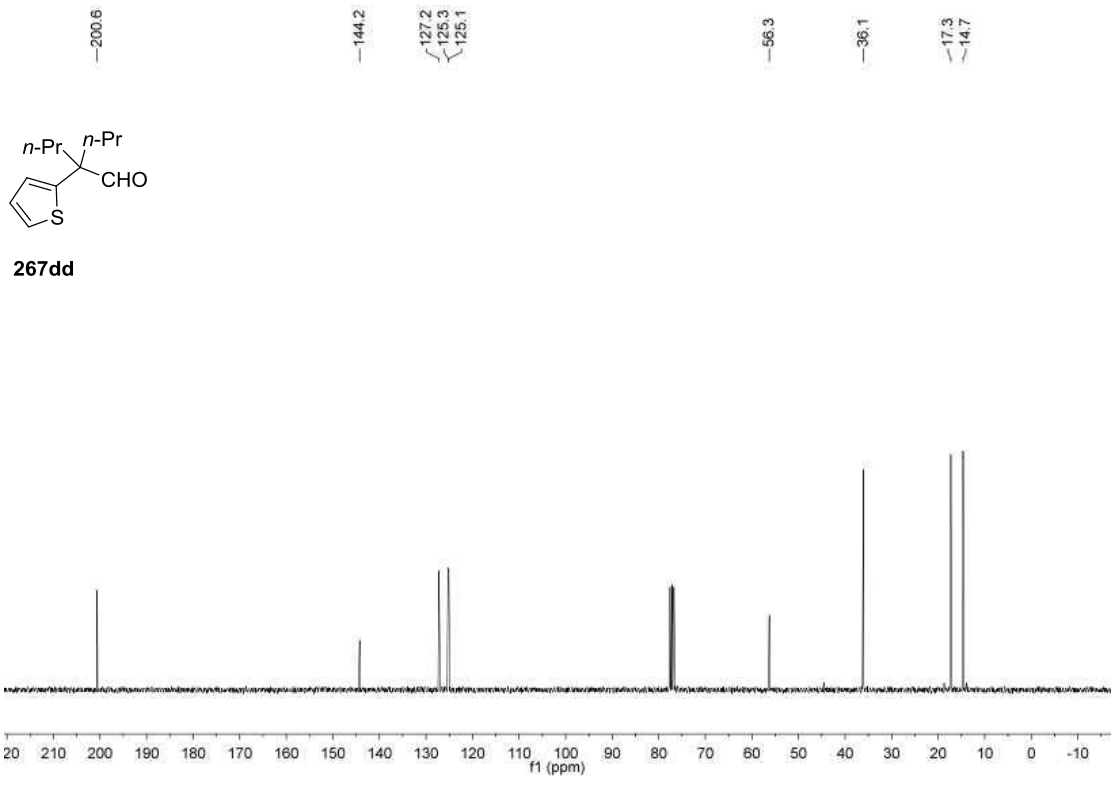
200.6
144.2
127.2
125.3
125.1
56.3
36.1
17.3
14.7
n-Pr
n-Pr
CHO
S
f1 (ppm)

267dd

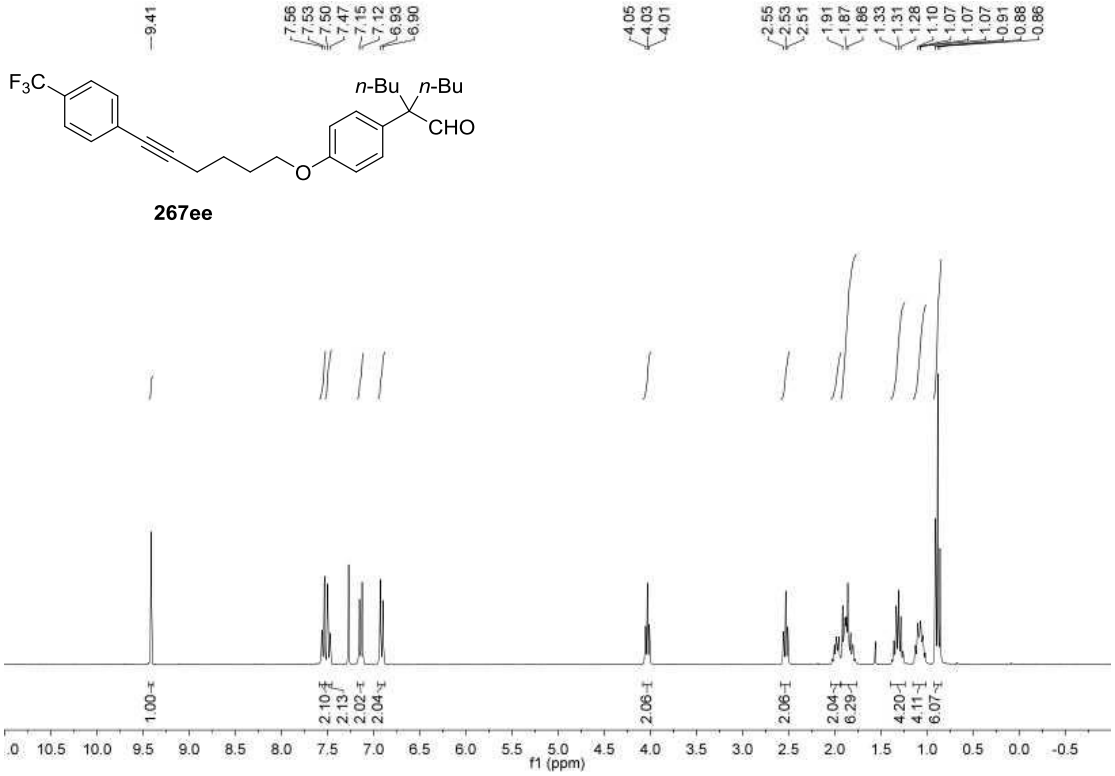
9.41
7.56
7.53
7.50
7.47
7.15
7.12
6.93
6.90
4.05
4.03
4.01
2.55
2.53
2.51
1.91
1.87
1.86
1.33
1.31
1.28
1.10
1.07
1.07
1.07
0.91
0.88
0.86
F3C
n-Bu
n-Bu
CHO
O
1.00
2.10
2.13
2.02
2.04
2.06
2.06
2.04
6.29
4.20
4.11
6.07
f1 (ppm)

267ee

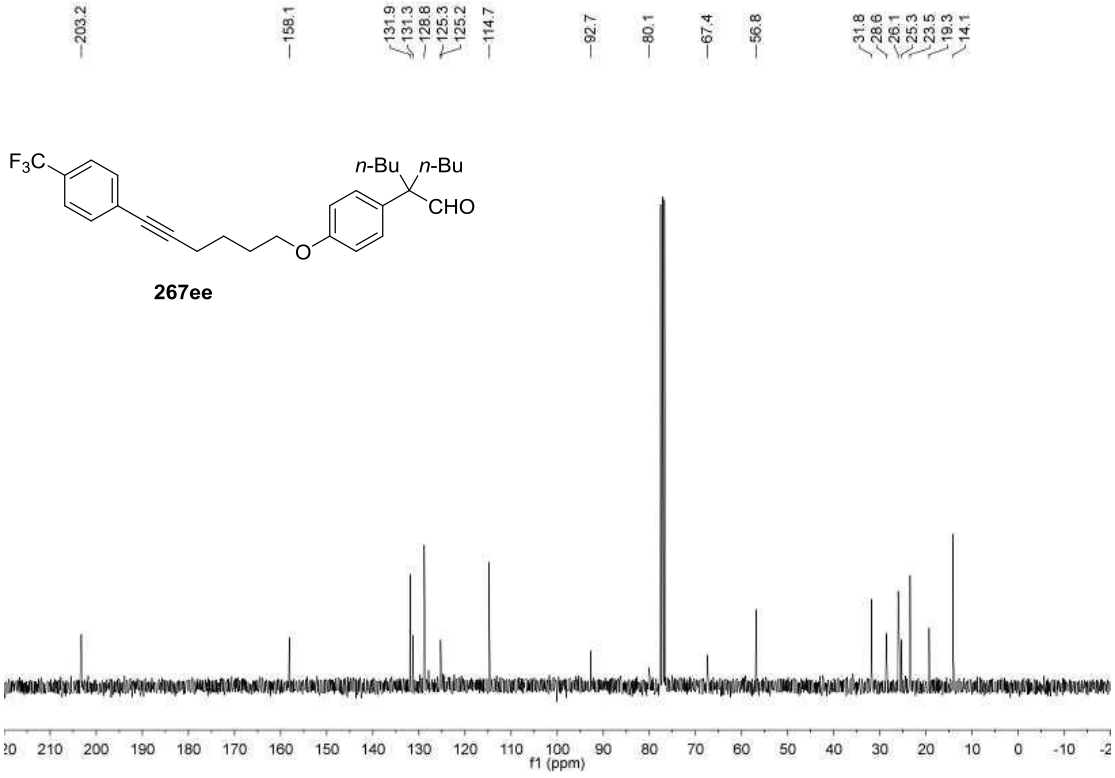
203.2
158.1
131.9
131.3
128.8
125.3
125.2
114.7
92.7
80.1
67.4
56.8
31.8
28.6
26.1
25.3
23.5
19.3
14.1
F3C
n-Bu
n-Bu
CHO
O
f1 (ppm)

267ee

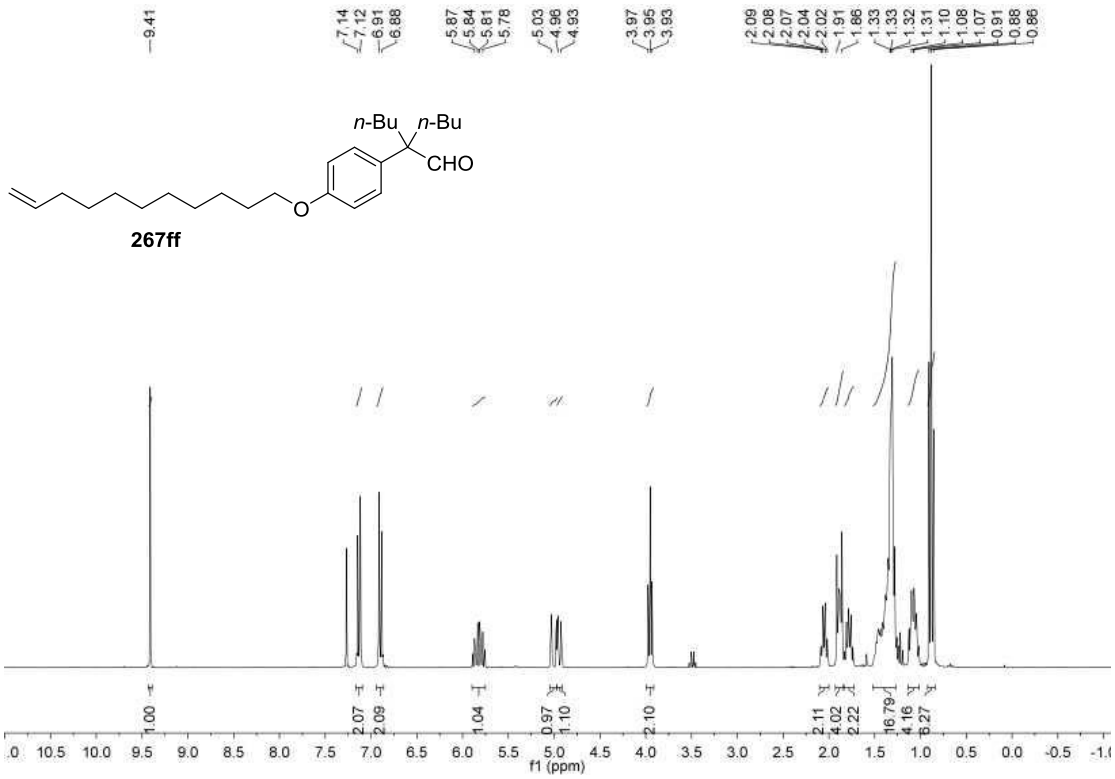
9.41
7.14
7.12
6.91
6.88
5.87
5.84
5.81
5.78
5.03
4.96
4.93
3.97
3.95
3.93
2.09
2.08
2.07
2.04
2.02
1.91
1.86
1.33
1.32
1.31
1.10
1.08
1.07
0.91
0.88
0.86
n-Bu
n-Bu
CHO
O
267ff
1.00
2.07
2.09
1.04
0.97
1.10
2.10
2.11
4.02
2.22
16.79
4.16
6.27
f1 (ppm)

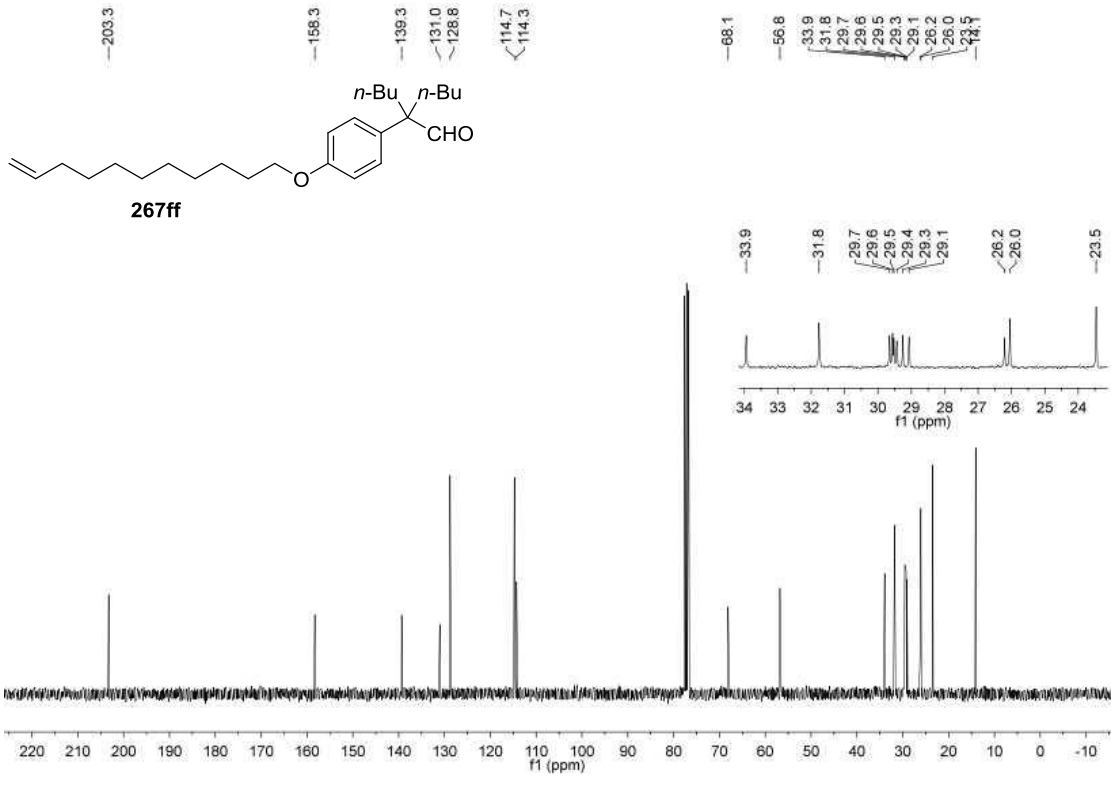
203.3
158.3
139.3
131.0
128.8
114.7
114.3
68.1
56.8
33.9
31.8
29.7
29.6
29.5
29.3
29.1
26.2
26.0
23.5
14.1
n-Bu
n-Bu
CHO
O
267ff
f1 (ppm)
f1 (ppm)

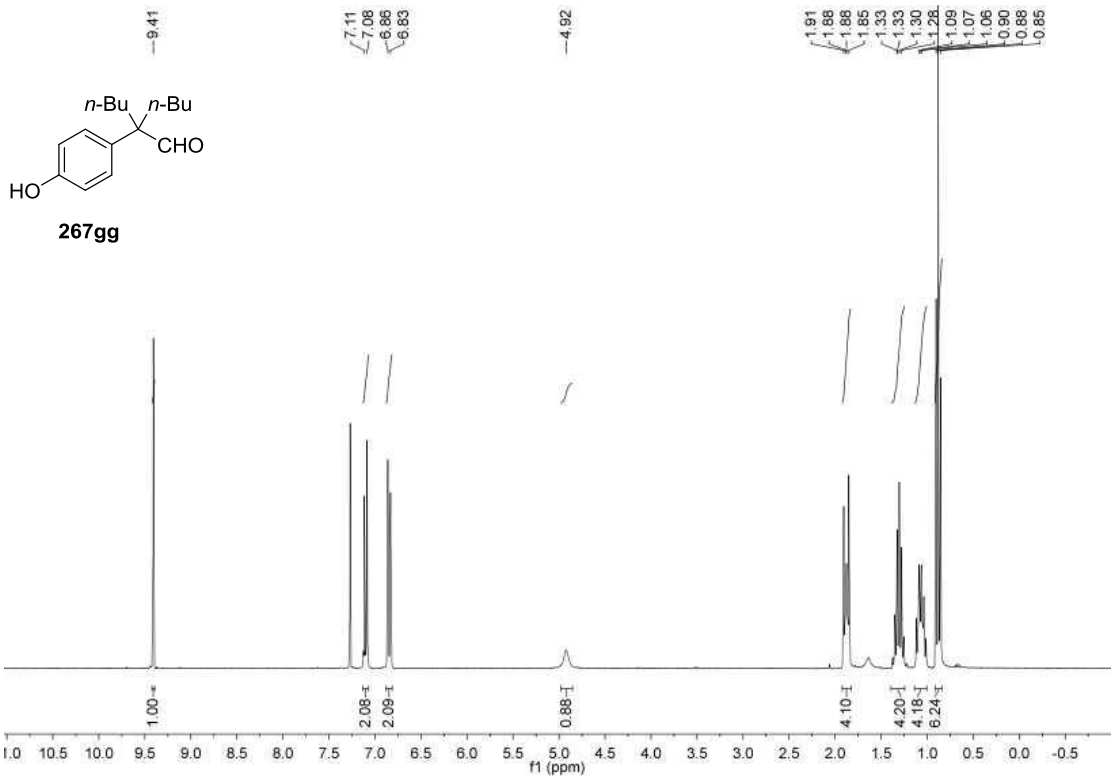
9.41
7.11
7.08
6.86
6.83
4.92
1.91
1.88
1.88
1.85
1.33
1.30
1.28
1.09
1.07
1.06
0.90
0.88
0.85
n-Bu
n-Bu
CHO
HO
267gg
1.00
2.08
2.09
0.88
4.10
4.20
4.18
6.24
f1 (ppm)

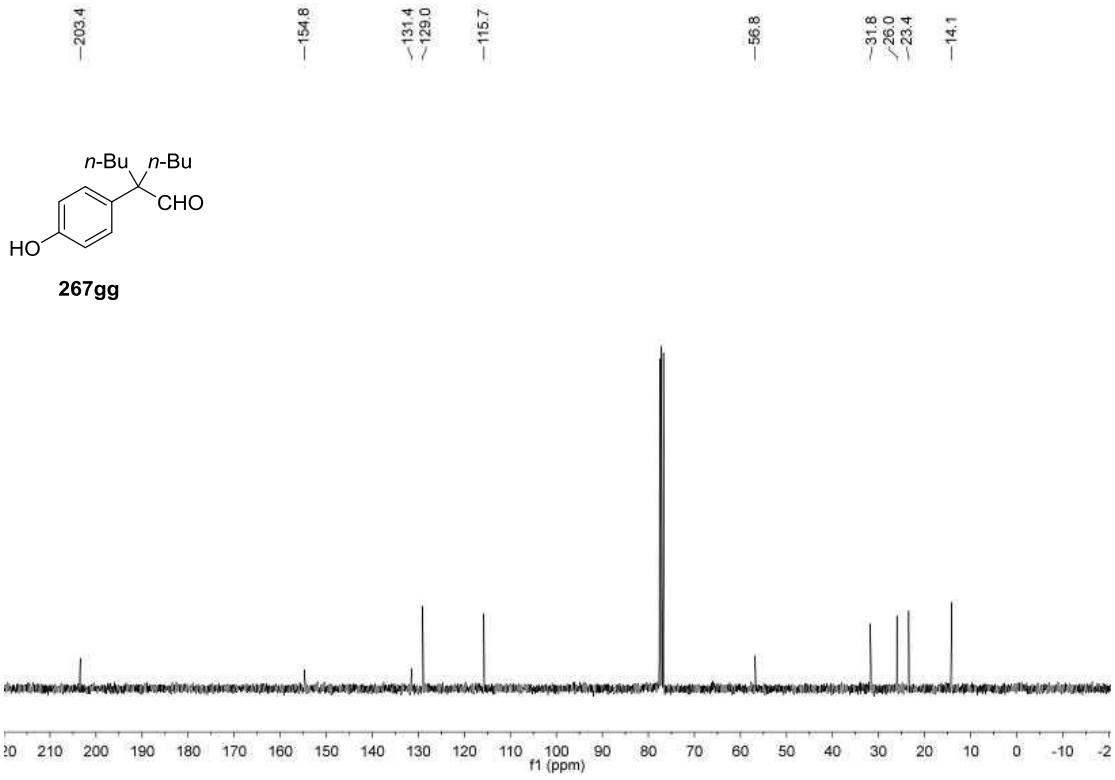
203.4
154.8
131.4
129.0
115.7
56.8
31.8
26.0
23.4
14.1
n-Bu
n-Bu
CHO
HO
267gg
f1 (ppm)

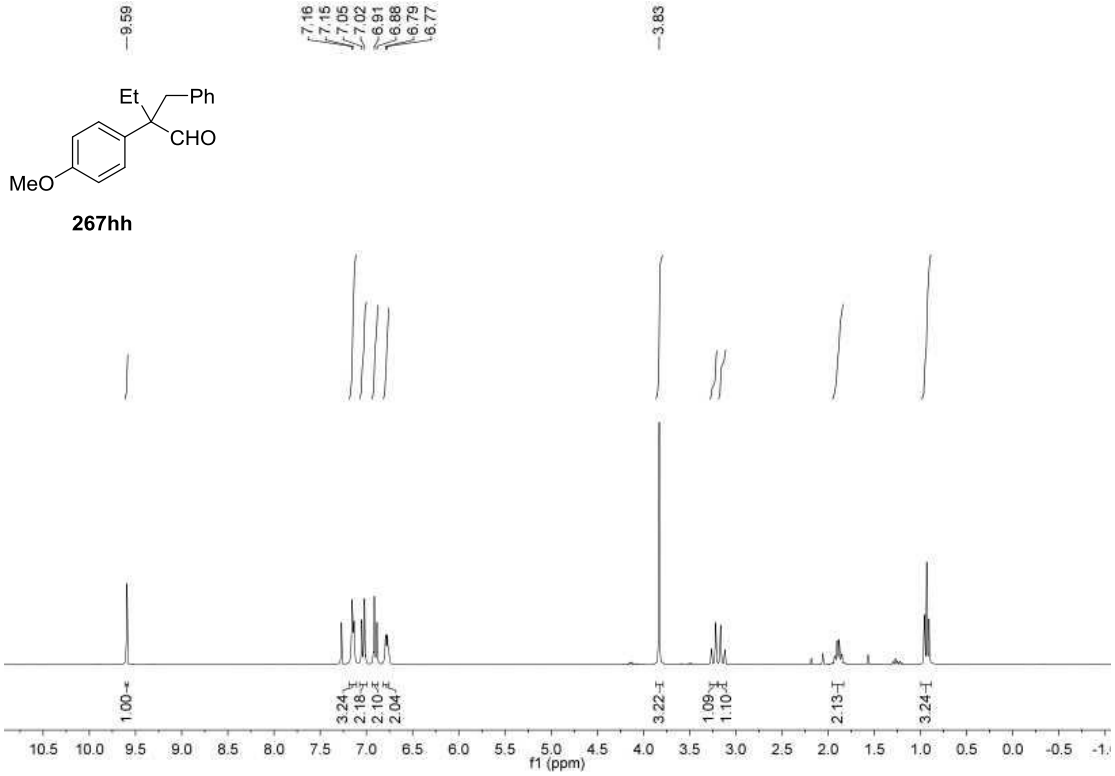
9.59
7.16
7.15
7.05
7.02
6.91
6.88
6.79
6.77
3.83
Et
Ph
CHO
MeO
1.00
3.24
2.18
2.10
2.04
3.22
1.09
1.10
2.13
3.24
f1 (ppm)

267hh

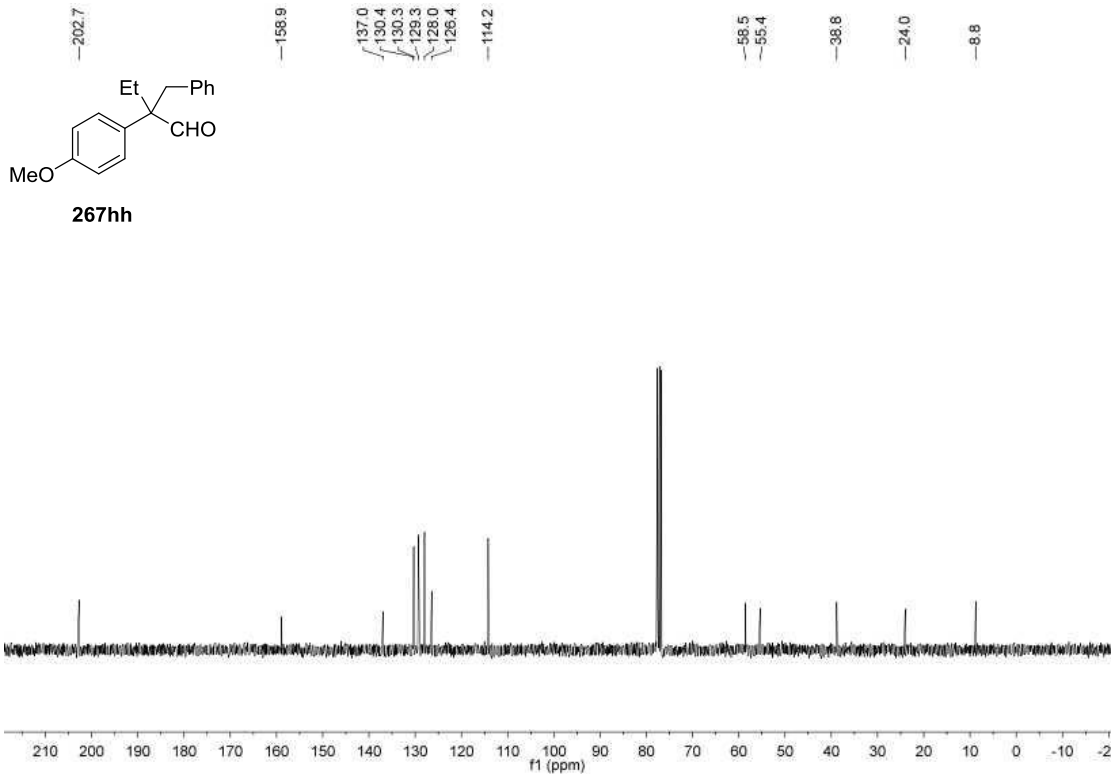
202.7
158.9
137.0
130.4
130.3
129.3
128.0
126.4
114.2
58.5
55.4
38.8
24.0
8.8
Et
Ph
CHO
MeO
f1 (ppm)

267hh

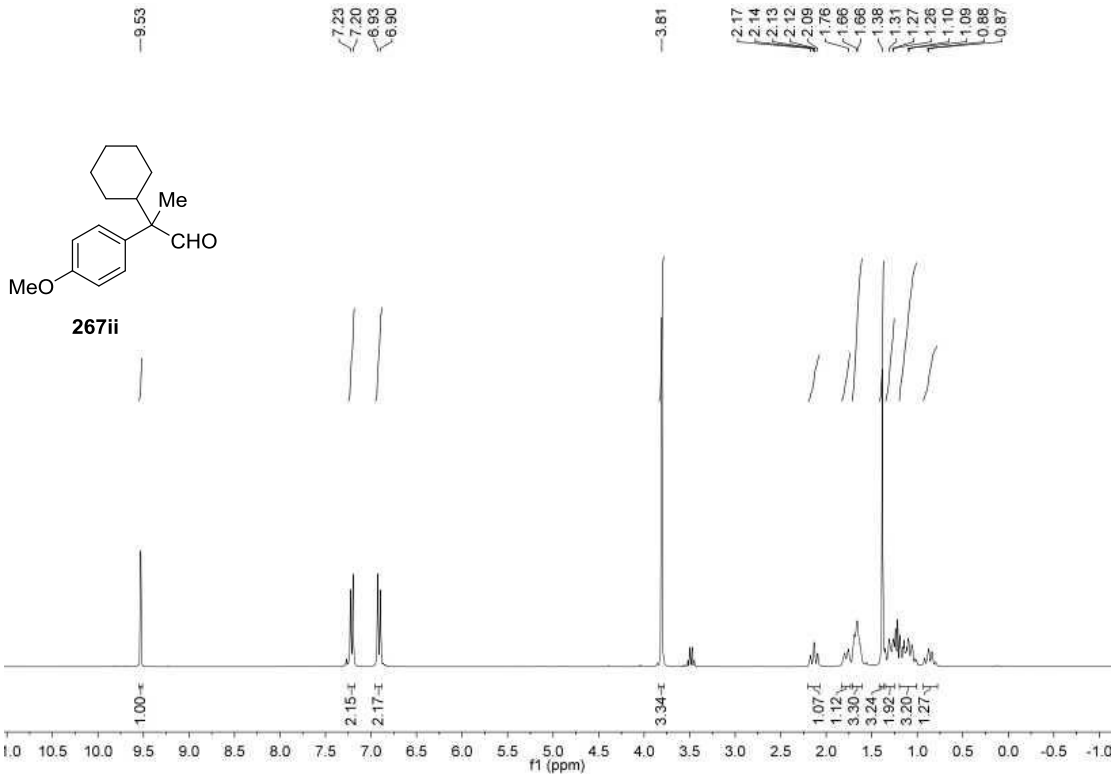
9.53
7.23
7.20
6.93
6.90
3.81
2.17
2.14
2.13
2.12
2.09
1.76
1.66
1.66
1.38
1.31
1.27
1.26
1.10
1.09
0.88
0.87
Me
CHO
MeO
1.00
2.15
2.17
3.34
1.07
1.12
3.30
3.24
1.92
3.20
1.27
f1 (ppm)

267ii

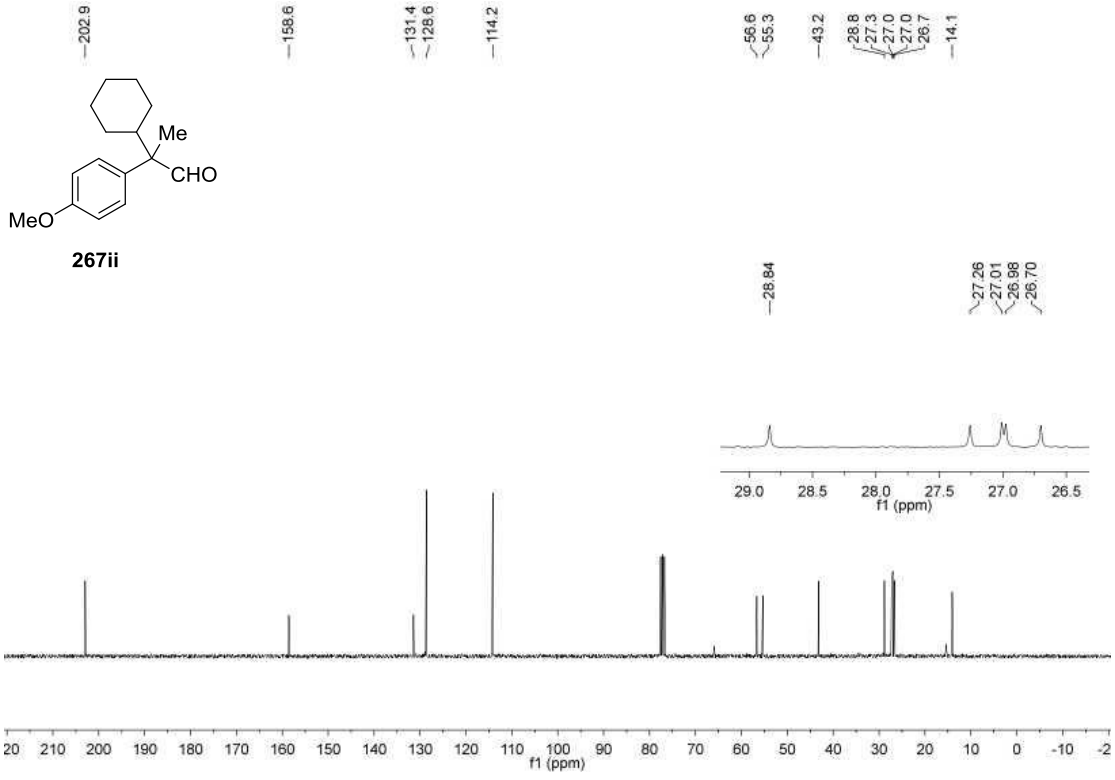
202.9
158.6
131.4
128.6
114.2
56.6
55.3
43.2
28.8
27.3
27.0
27.0
26.7
14.1
Me
CHO
MeO
28.84
27.26
27.01
26.98
26.70
f1 (ppm)

267ii

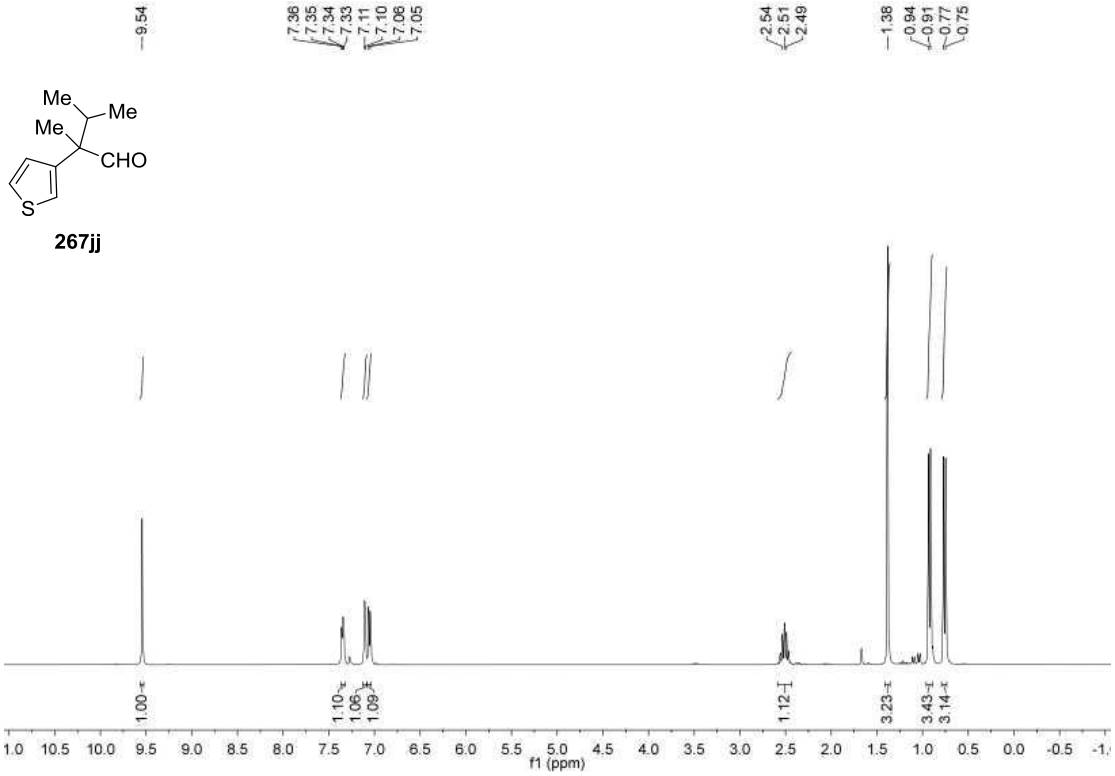
9.54
7.36
7.35
7.34
7.33
7.11
7.10
7.06
7.05
2.54
2.51
2.49
1.38
0.94
0.91
0.77
0.75
Me
Me
Me
CHO
S
1.00
1.10
1.06
1.09
1.12
3.23
3.43
3.14
f1 (ppm)

267jj

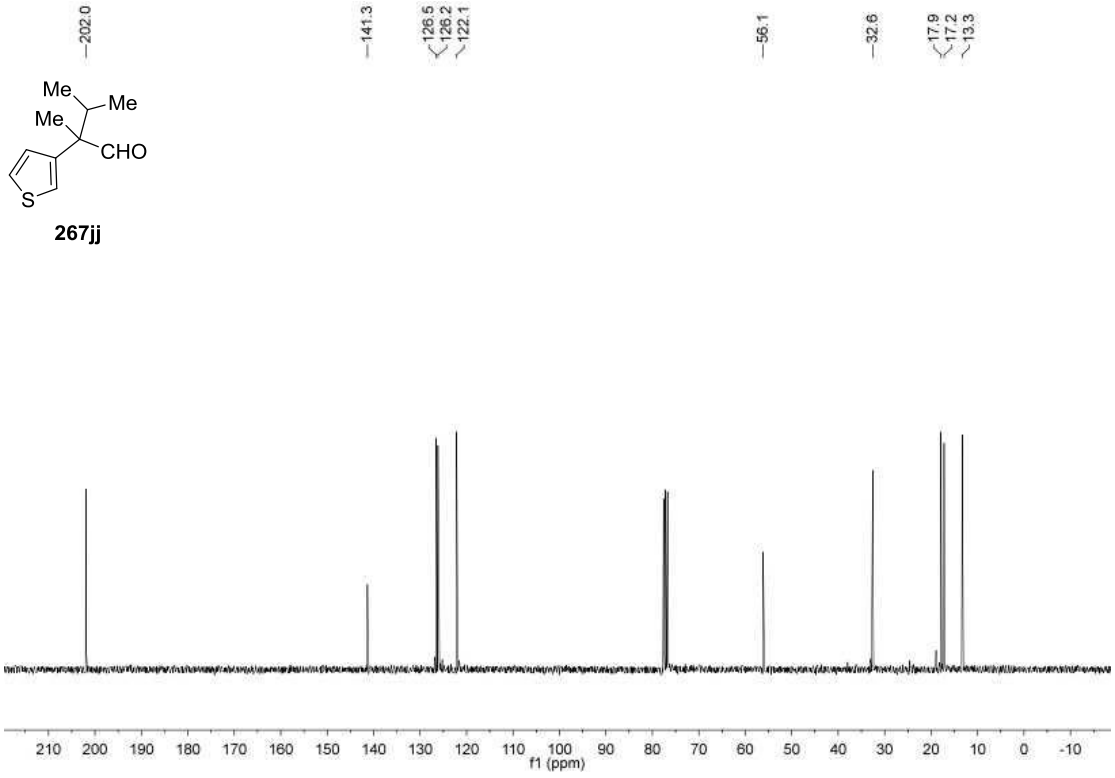
202.0
141.3
126.5
126.2
122.1
56.1
32.6
17.9
17.2
13.3
Me
Me
Me
CHO
S
f1 (ppm)

267jj

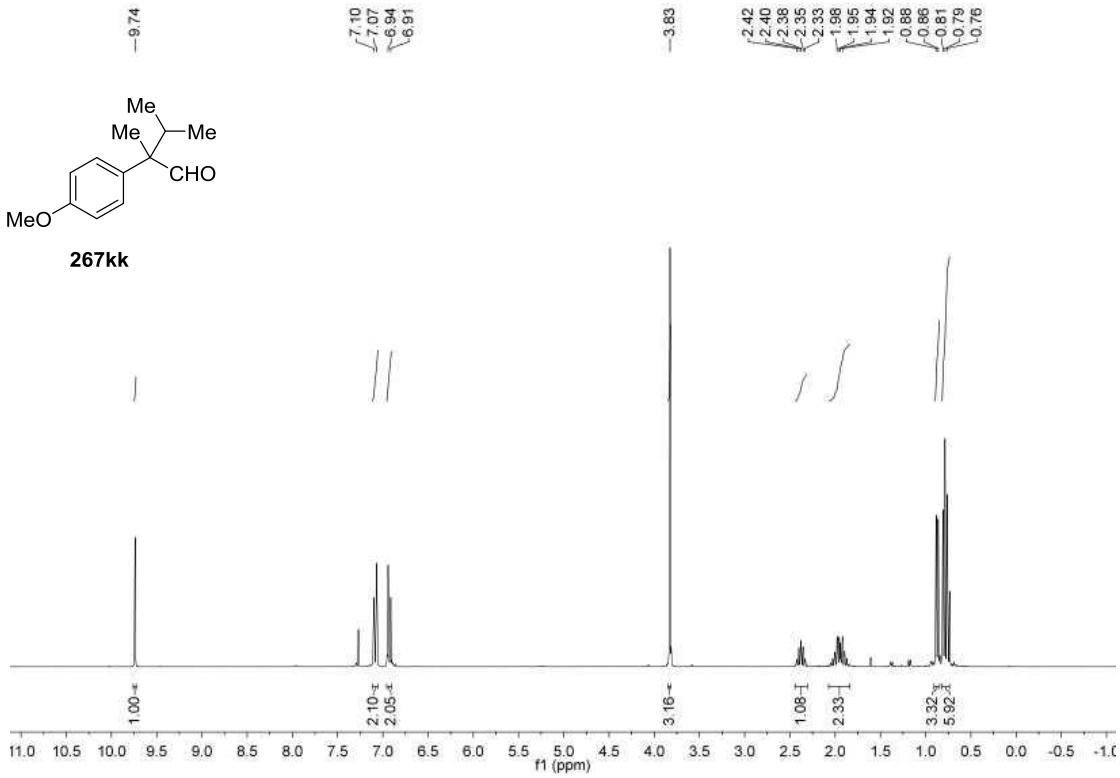
9.74
7.10
7.07
6.94
6.91
3.83
2.42
2.40
2.38
2.35
2.33
1.98
1.95
1.94
1.92
0.88
0.86
0.81
0.79
0.76
Me
Me
Me
CHO
MeO
267kk
1.00
2.10
2.05
3.16
1.08
2.33
3.32
5.92
f1 (ppm)

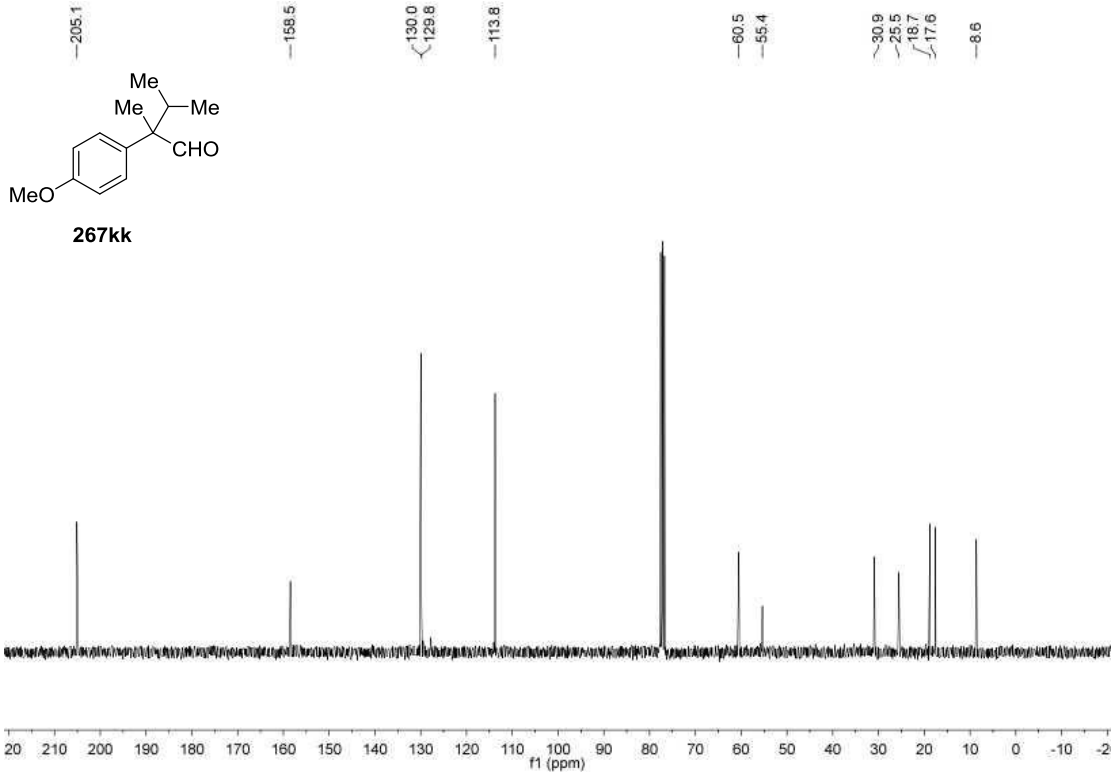
205.1
158.5
130.0
129.8
113.8
60.5
55.4
30.9
25.5
18.7
17.6
8.6
Me
Me
Me
CHO
MeO
267kk
f1 (ppm)

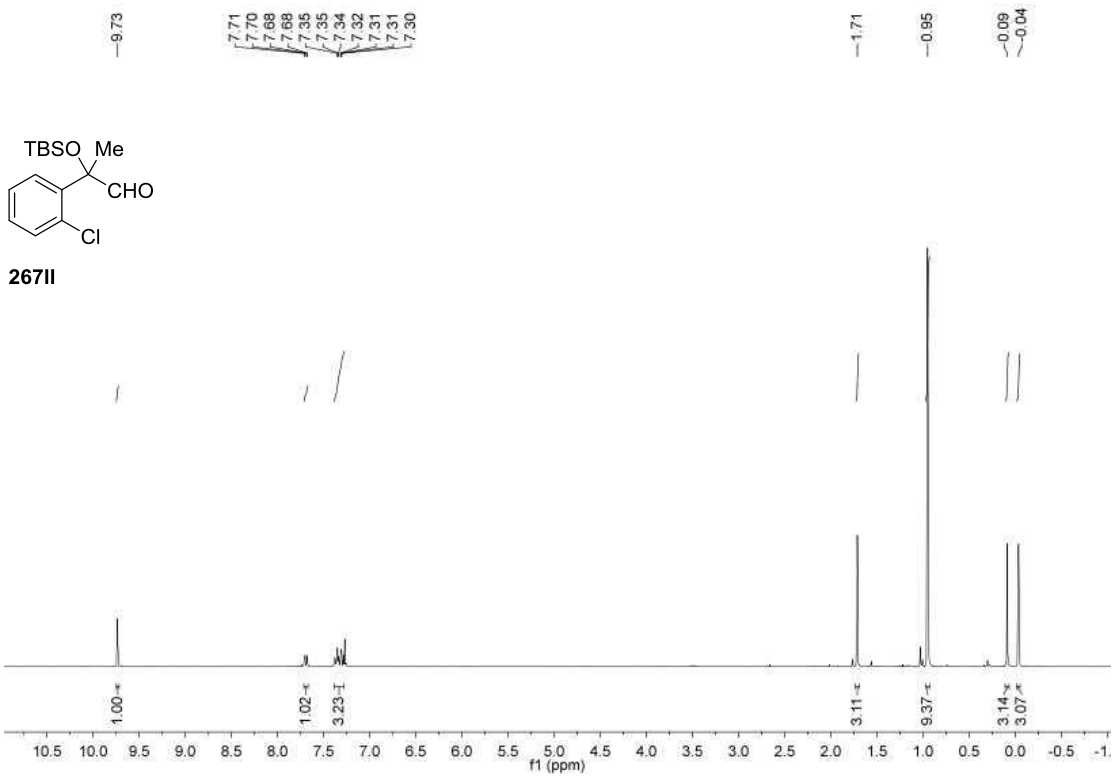
9.73
7.71
7.70
7.68
7.68
7.35
7.35
7.34
7.32
7.31
7.31
7.30
1.71
0.95
0.09
0.04
TBSO
Me
CHO
Cl
1.00
1.02
3.23
3.11
9.37
3.14
3.07
f1 (ppm)

267ll

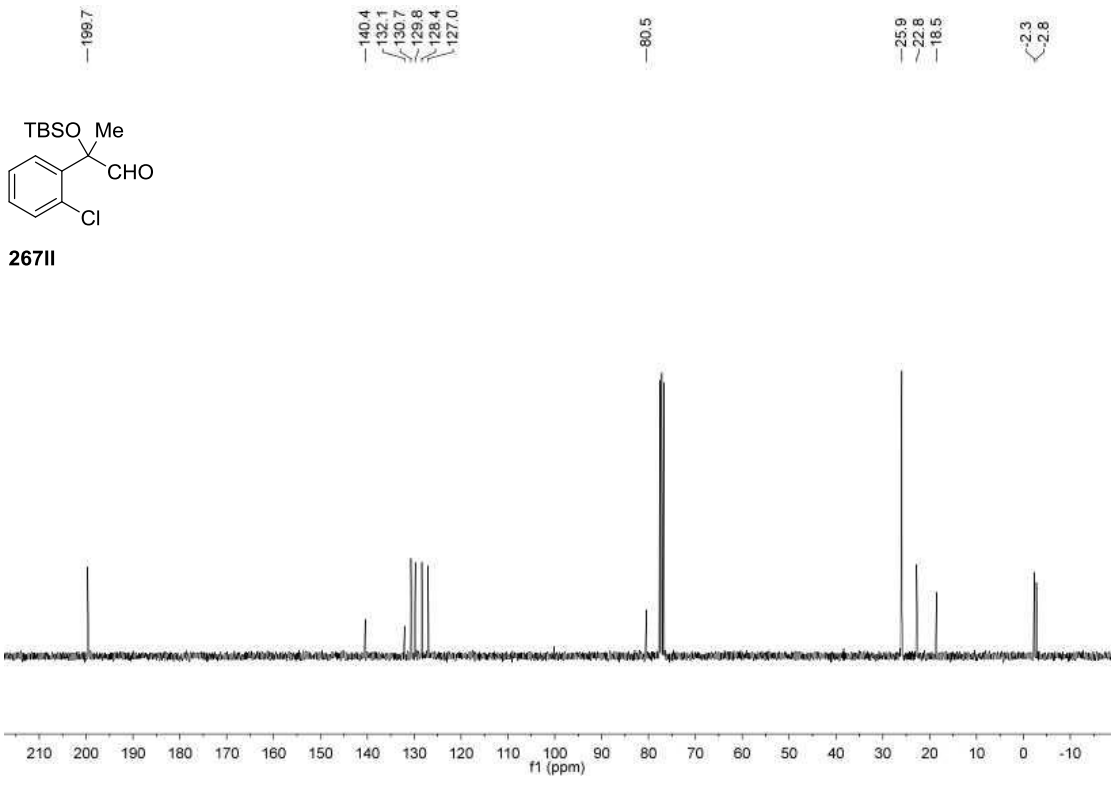
199.7
140.4
132.1
130.7
129.8
128.4
127.0
80.5
25.9
22.8
18.5
-2.3
-2.8
TBSO
Me
CHO
Cl
f1 (ppm)

267ll

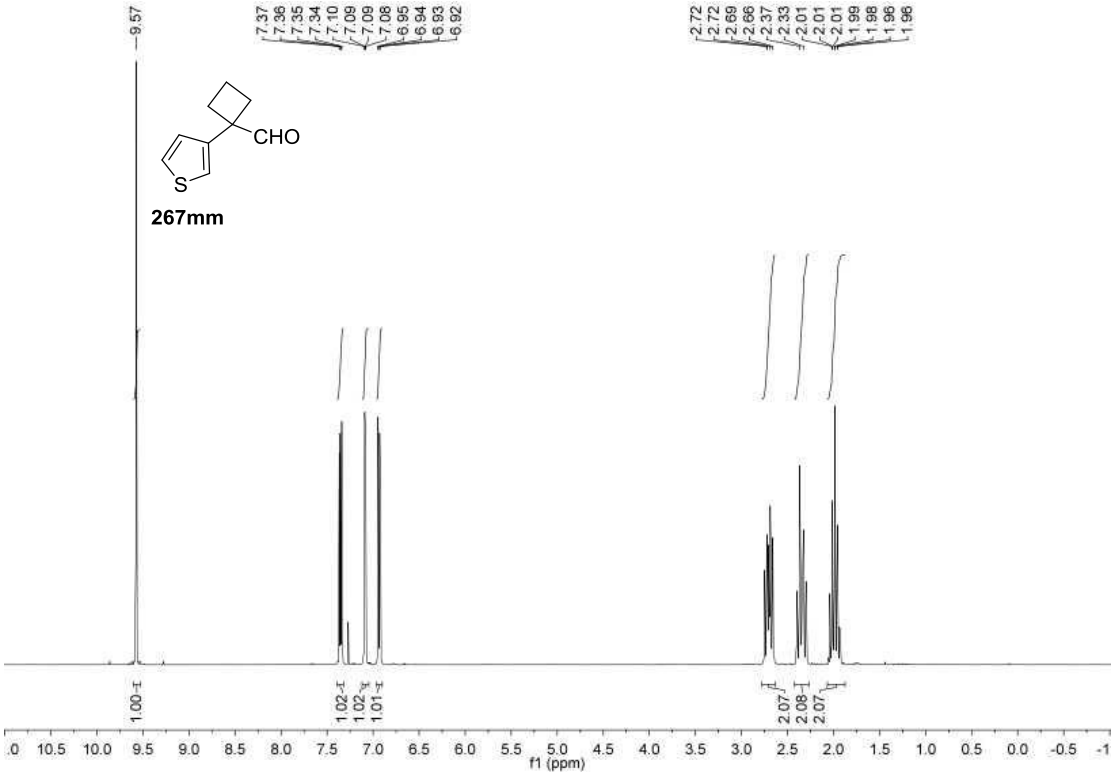
9.57
7.37
7.36
7.35
7.34
7.10
7.09
7.09
7.08
6.95
6.94
6.93
6.92
2.72
2.72
2.69
2.66
2.37
2.33
2.01
2.01
2.01
1.99
1.98
1.96
1.96
CHO
S
267mm
1.00
1.02
1.02
1.01
2.07
2.08
2.07
f1 (ppm)

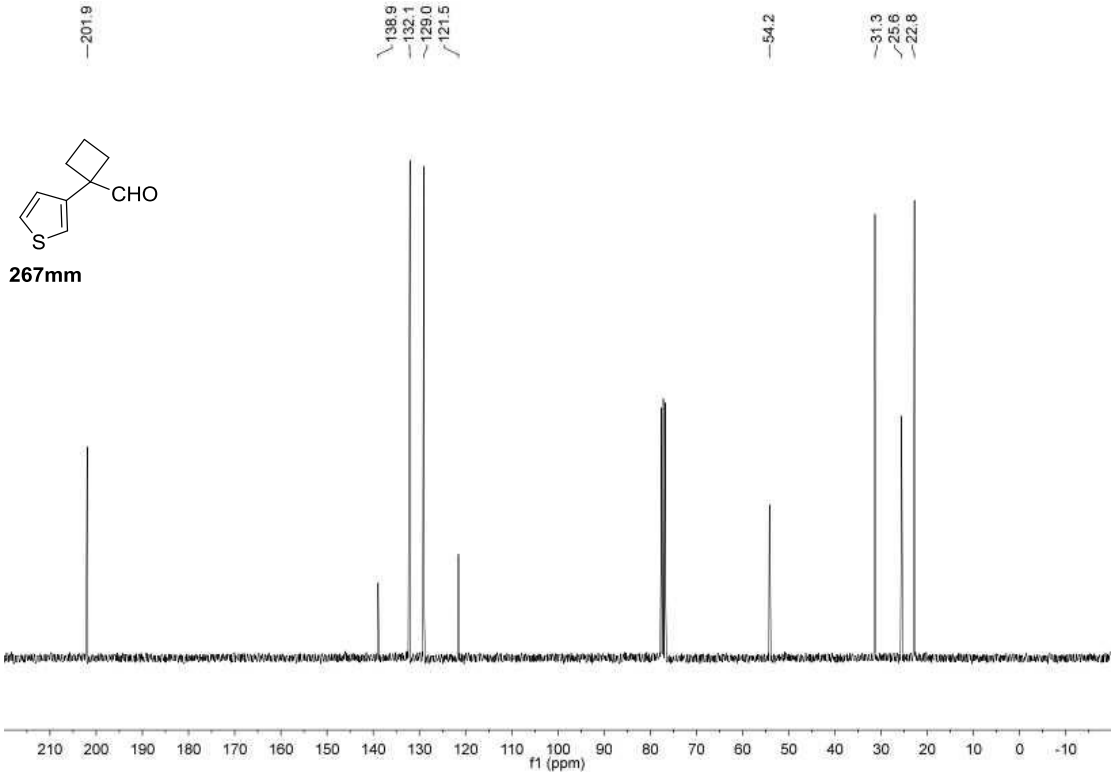
201.9
138.9
132.1
129.0
121.5
54.2
31.3
25.6
22.8
CHO
S
267mm
f1 (ppm)

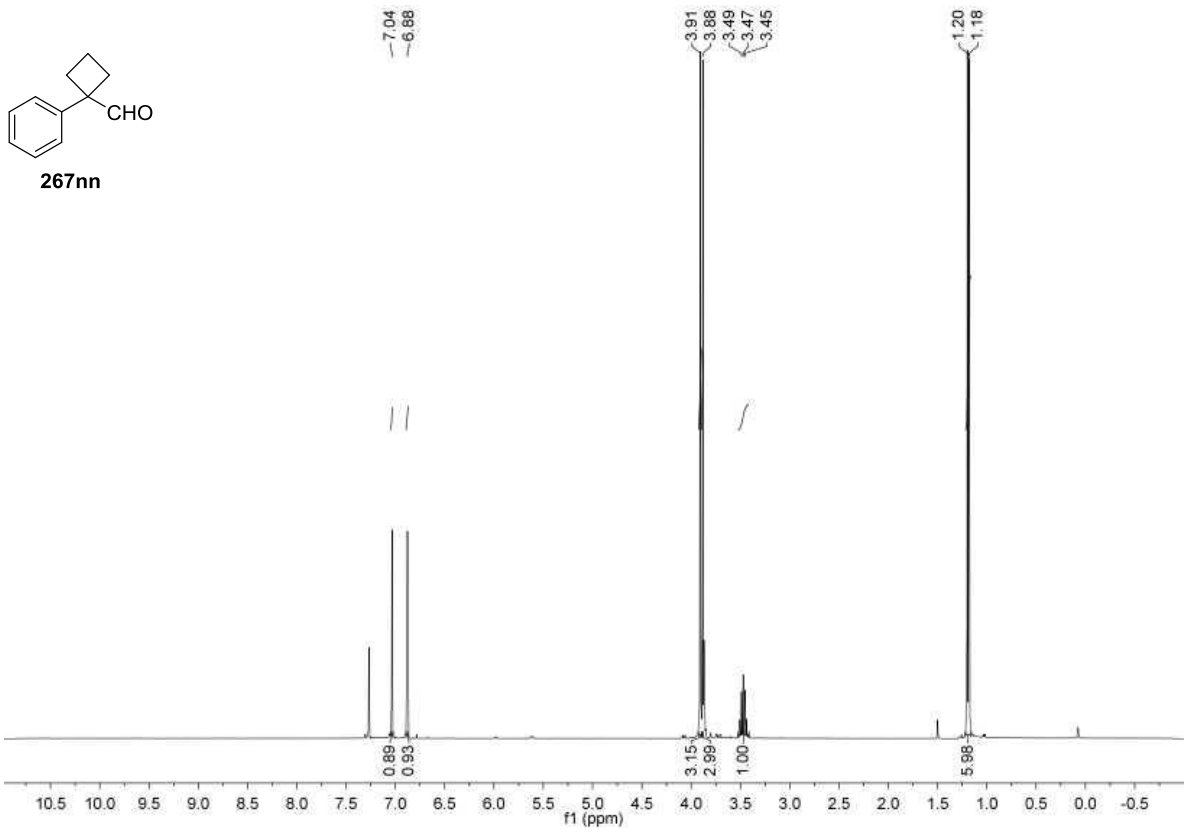
CHO
7.04
6.88
3.91
3.88
3.49
3.47
3.45
1.20
1.18
0.89
0.93
3.15
2.99
1.00
5.98
f1 (ppm)

267nn

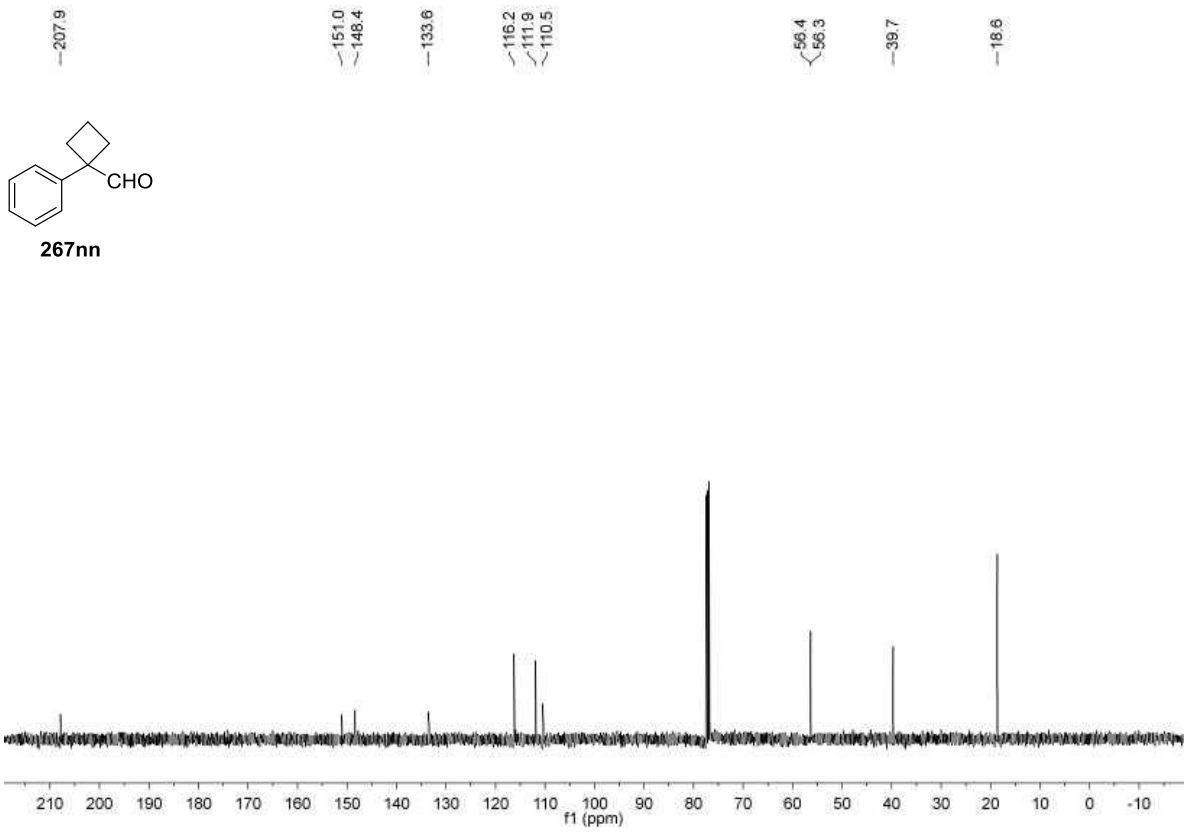
207.9
151.0
148.4
133.6
116.2
111.9
110.5
56.4
56.3
39.7
18.6
CHO
f1 (ppm)

267nn

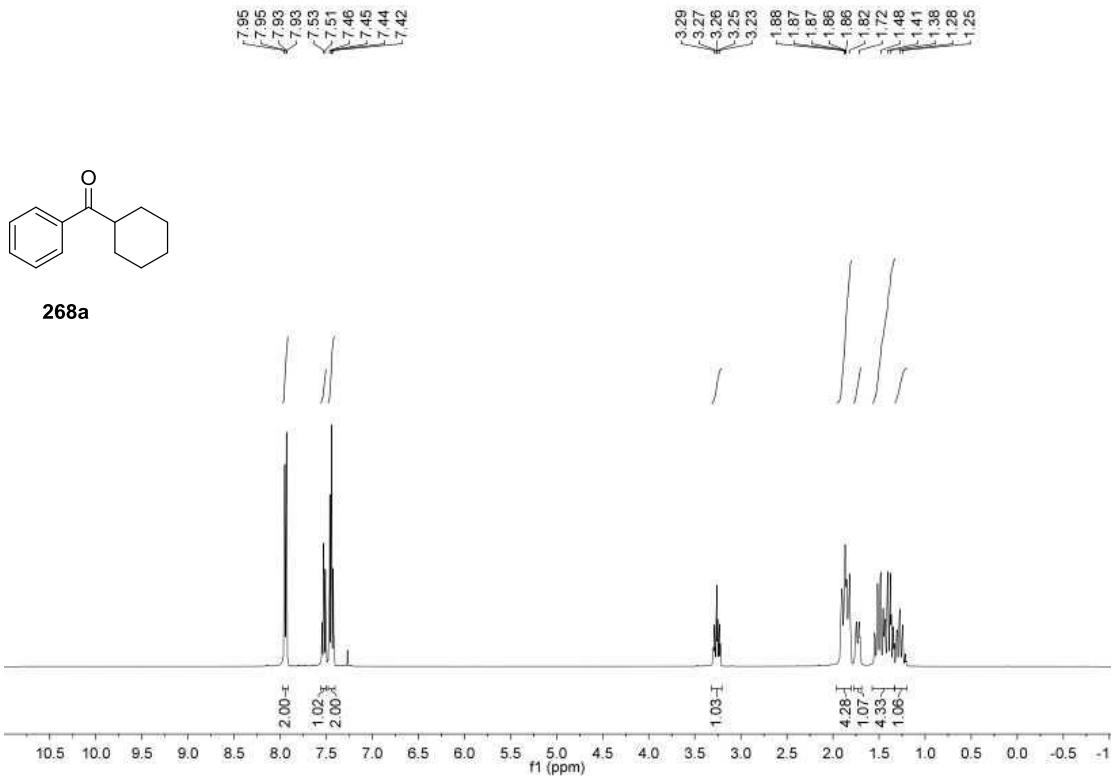
7.95
7.95
7.93
7.93
7.53
7.51
7.46
7.45
7.44
7.42
3.29
3.27
3.26
3.25
3.23
1.88
1.87
1.87
1.86
1.86
1.82
1.72
1.48
1.41
1.38
1.28
1.25
2.00
1.02
2.00
1.03
4.28
1.07
4.33
1.06
f1 (ppm)

268a

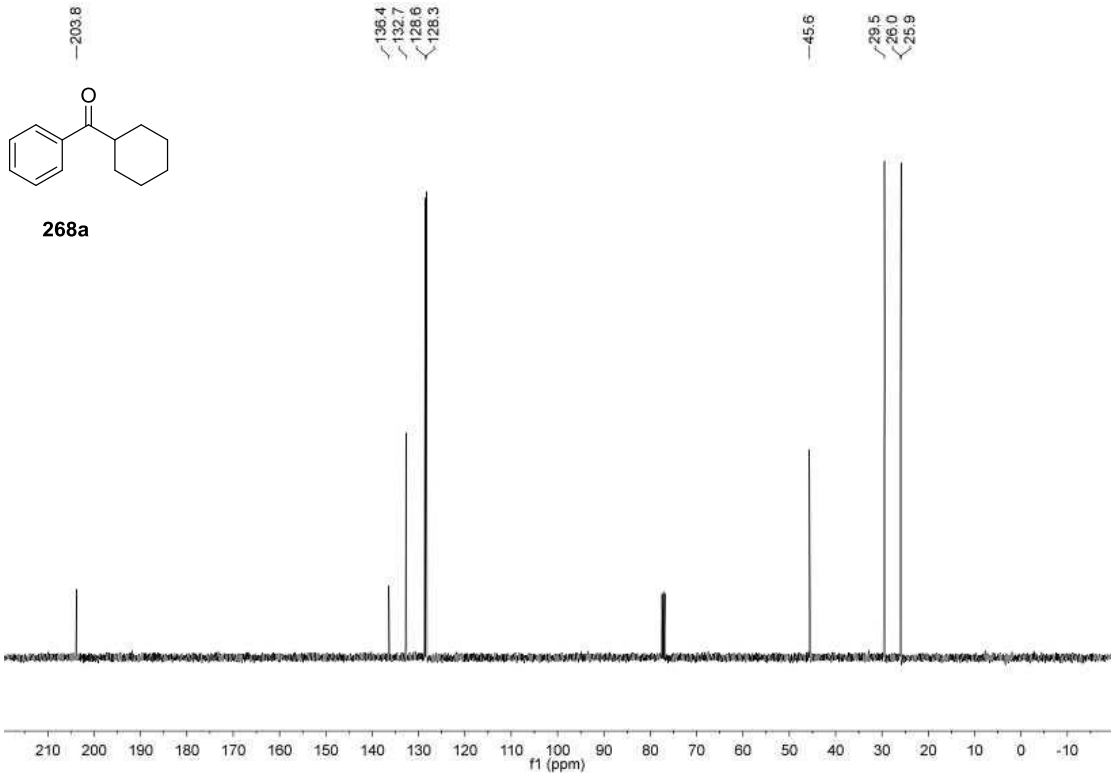
203.8
136.4
132.7
128.6
128.3
45.6
29.5
26.0
25.9
f1 (ppm)

268a

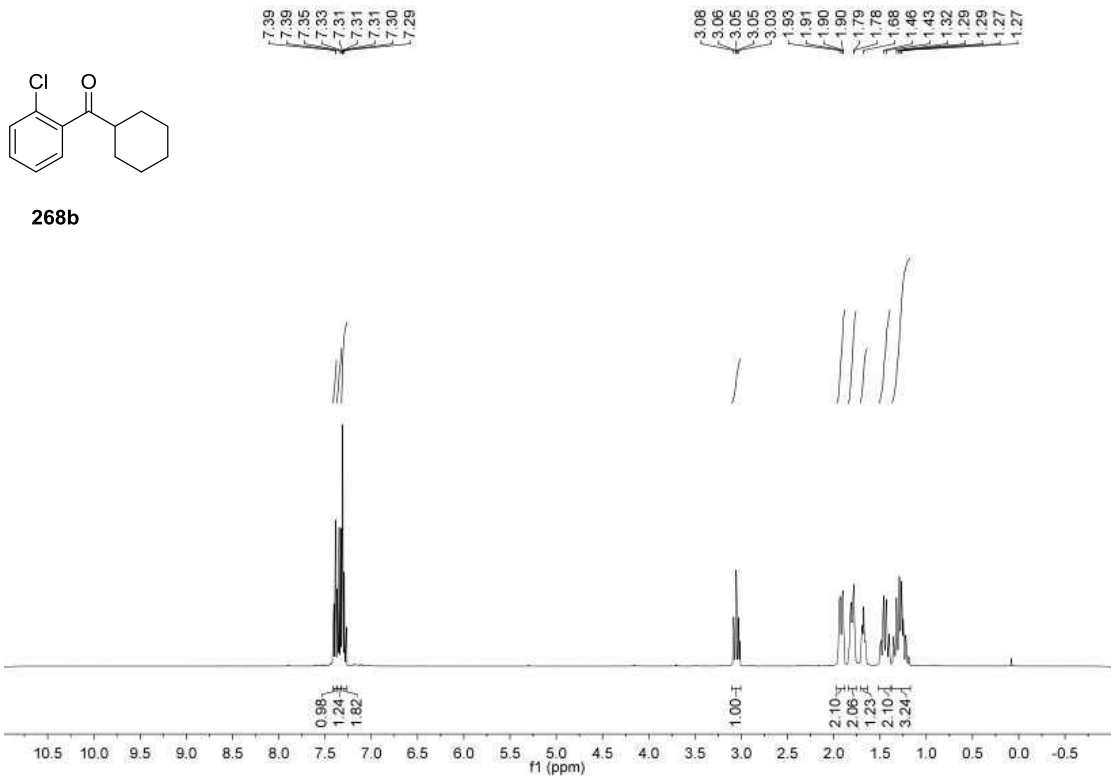
7.39
7.39
7.35
7.33
7.31
7.31
7.31
7.30
7.29
3.08
3.06
3.05
3.05
3.03
1.93
1.91
1.90
1.90
1.79
1.78
1.68
1.46
1.43
1.32
1.29
1.29
1.27
1.27
Cl
O
268b
0.98
1.24
1.82
1.00
2.10
2.06
1.23
2.10
3.24
f1 (ppm)

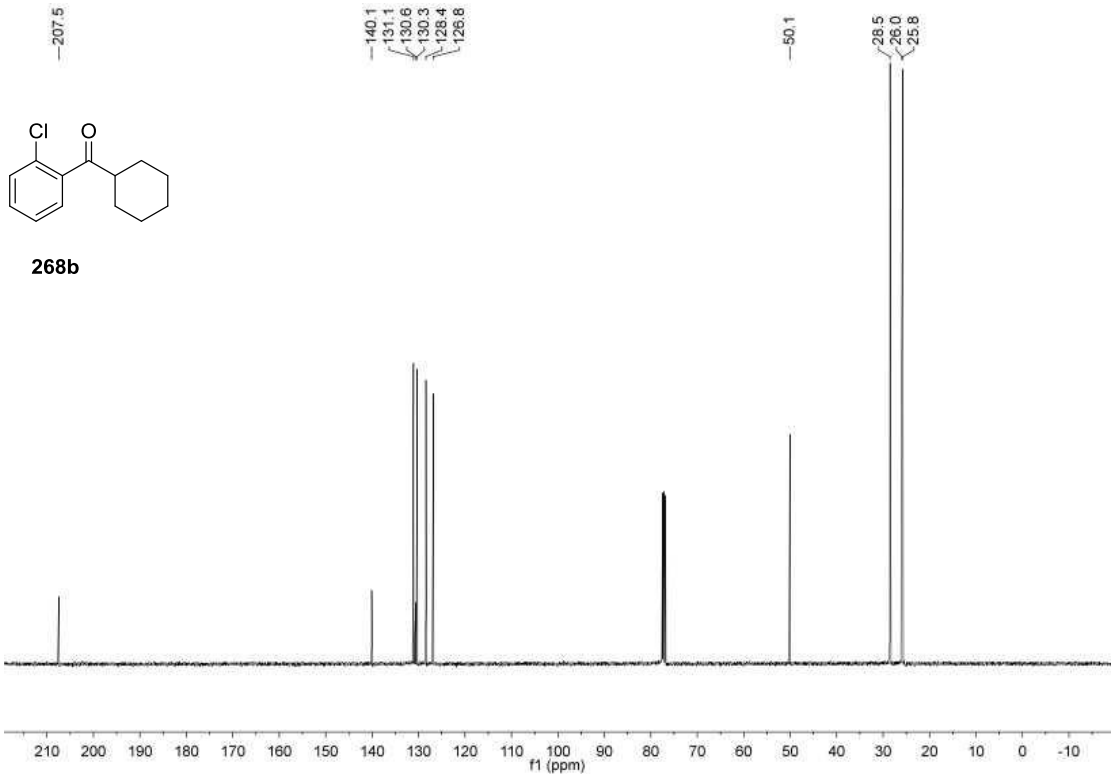
207.5
140.1
131.1
130.6
130.3
128.4
126.8
50.1
28.5
26.0
25.8
Cl
O
268b
f1 (ppm)

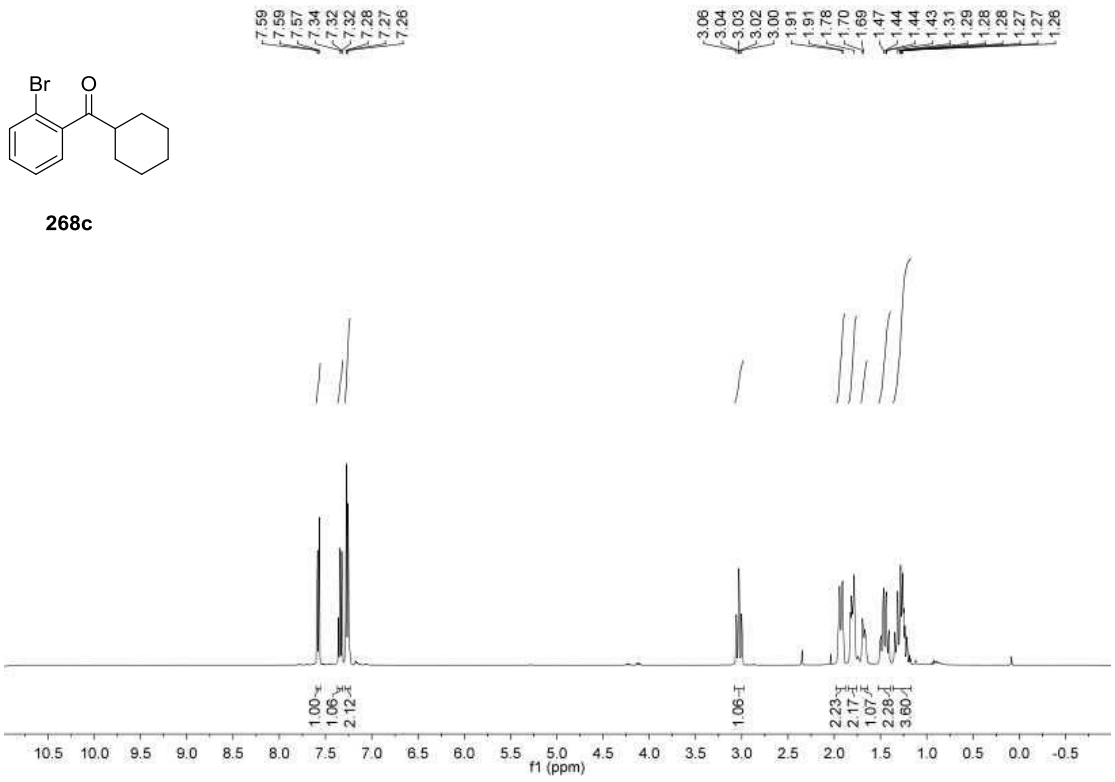
7.59
7.59
7.57
7.34
7.32
7.32
7.28
7.27
7.26
3.06
3.04
3.03
3.02
3.00
1.91
1.91
1.78
1.70
1.69
1.47
1.44
1.44
1.43
1.31
1.29
1.28
1.28
1.27
1.27
1.26
Br
O
1.00
1.06
2.12
1.06
2.23
2.17
1.07
2.28
3.60
f1 (ppm)

268c

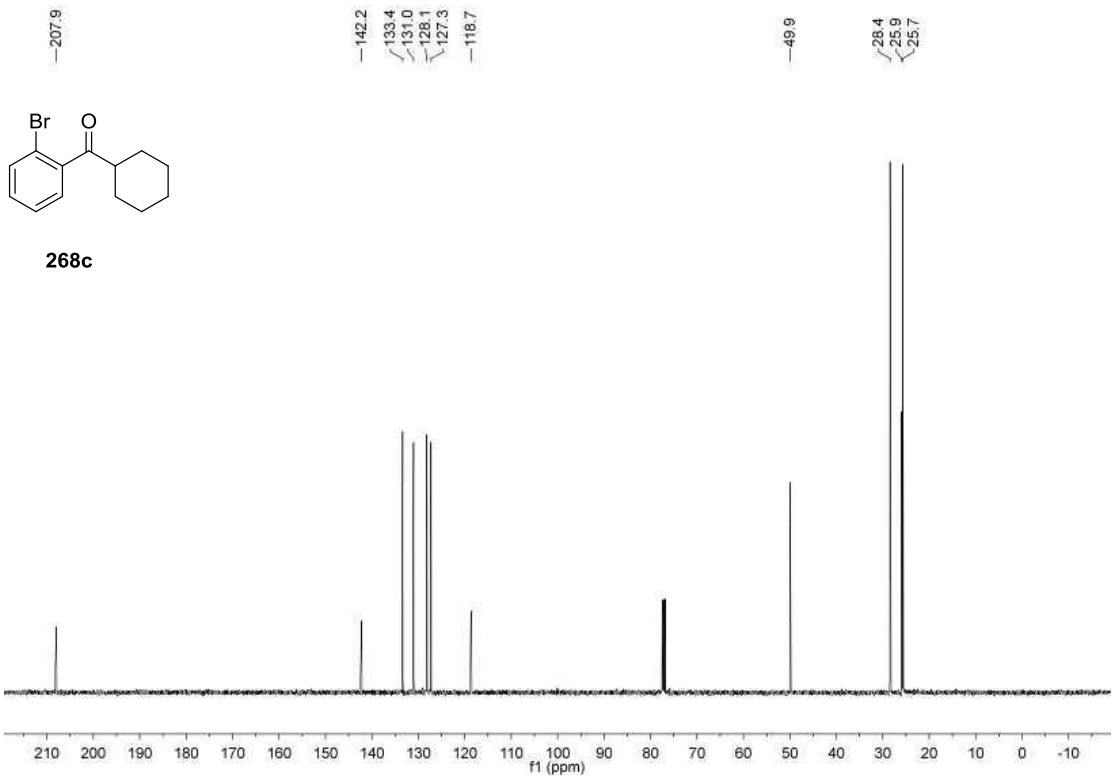
207.9
142.2
133.4
131.0
128.1
127.3
118.7
49.9
28.4
25.9
25.7
Br
O
f1 (ppm)

268c

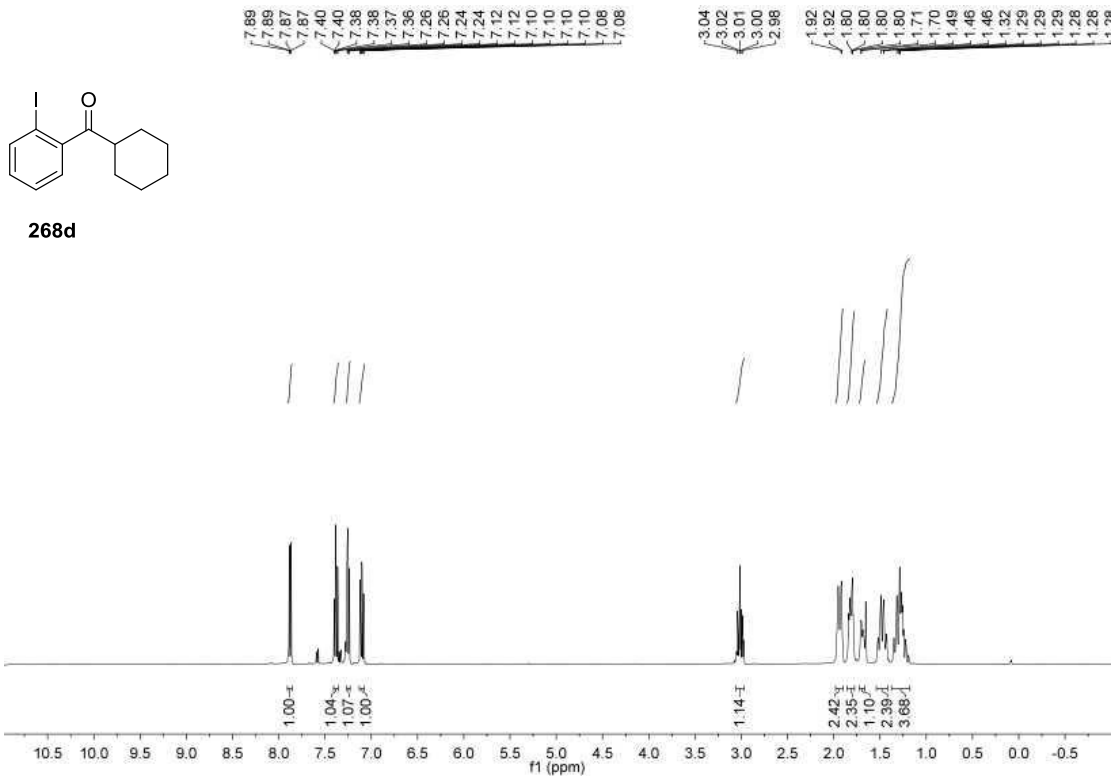
7.89
7.89
7.87
7.87
7.40
7.40
7.38
7.38
7.37
7.36
7.26
7.26
7.24
7.24
7.12
7.12
7.10
7.10
7.10
7.10
7.08
7.08
3.04
3.02
3.01
3.00
2.98
1.92
1.92
1.80
1.80
1.80
1.80
1.71
1.70
1.49
1.46
1.46
1.32
1.29
1.29
1.29
1.28
1.28
I
O
268d
1.00
1.04
1.07
1.00
1.14
2.42
2.35
1.10
2.39
3.68
10.5 10.0 9.5 9.0 8.5 8.0 7.5 7.0 6.5 6.0 5.5 5.0 4.5 4.0 3.5 3.0 2.5 2.0 1.5 1.0 0.5 0.0 -0.5
f1 (ppm)

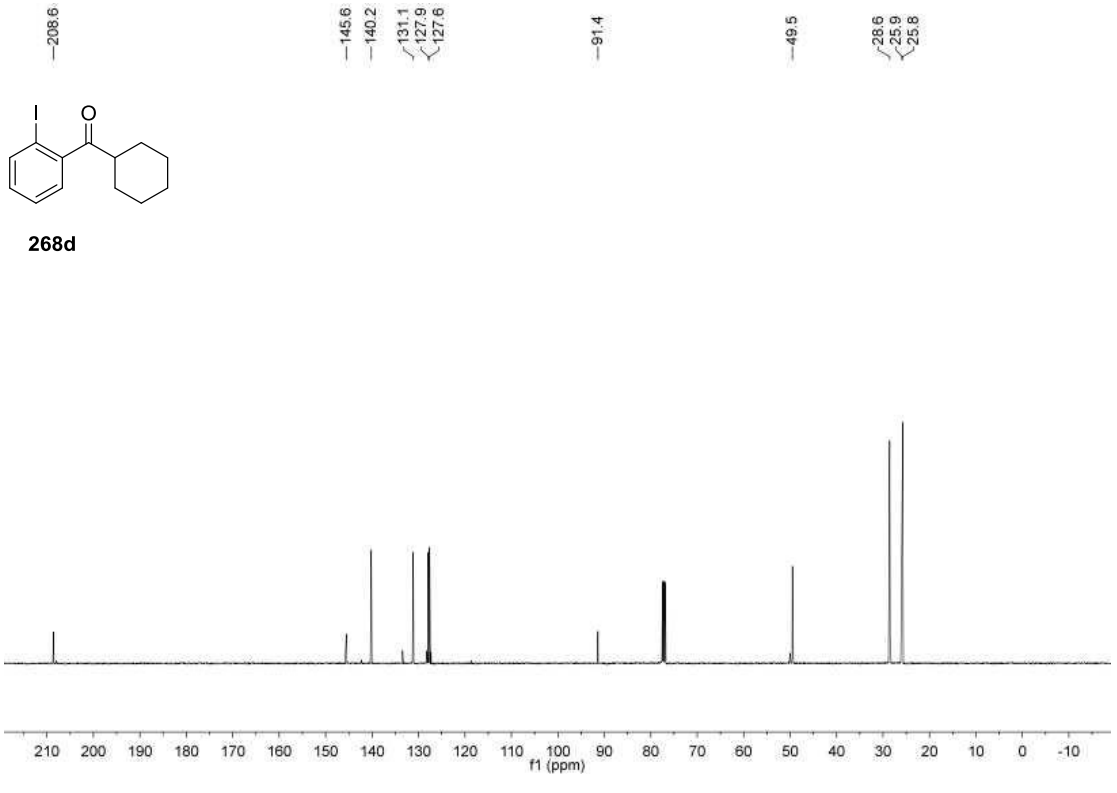
208.6
145.6
140.2
131.1
127.9
127.6
91.4
49.5
28.6
25.9
25.8
I
O
268d
210 200 190 180 170 160 150 140 130 120 110 100 90 80 70 60 50 40 30 20 10 0 -10
f1 (ppm)

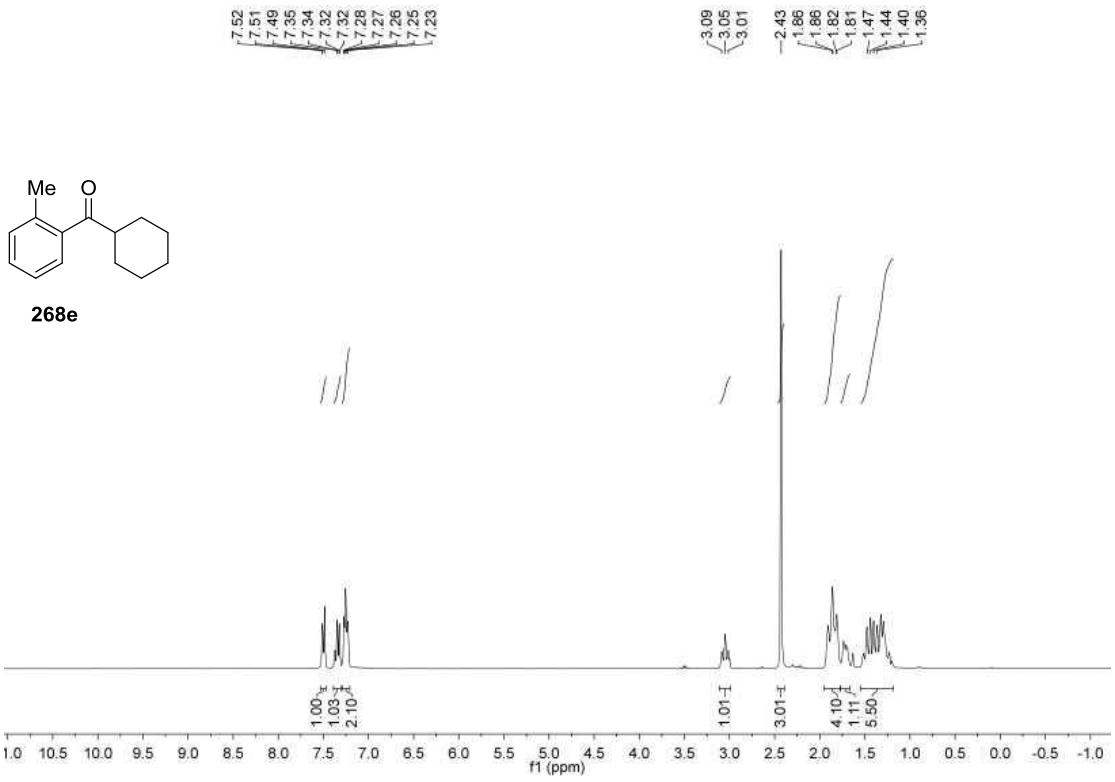
7.52
7.51
7.49
7.35
7.34
7.32
7.32
7.28
7.27
7.26
7.25
7.23
3.09
3.05
3.01
2.43
1.86
1.86
1.82
1.81
1.47
1.44
1.40
1.36
Me
O
1.00
1.03
2.10
1.01
3.01
4.10
1.11
5.50
f1 (ppm)

268e

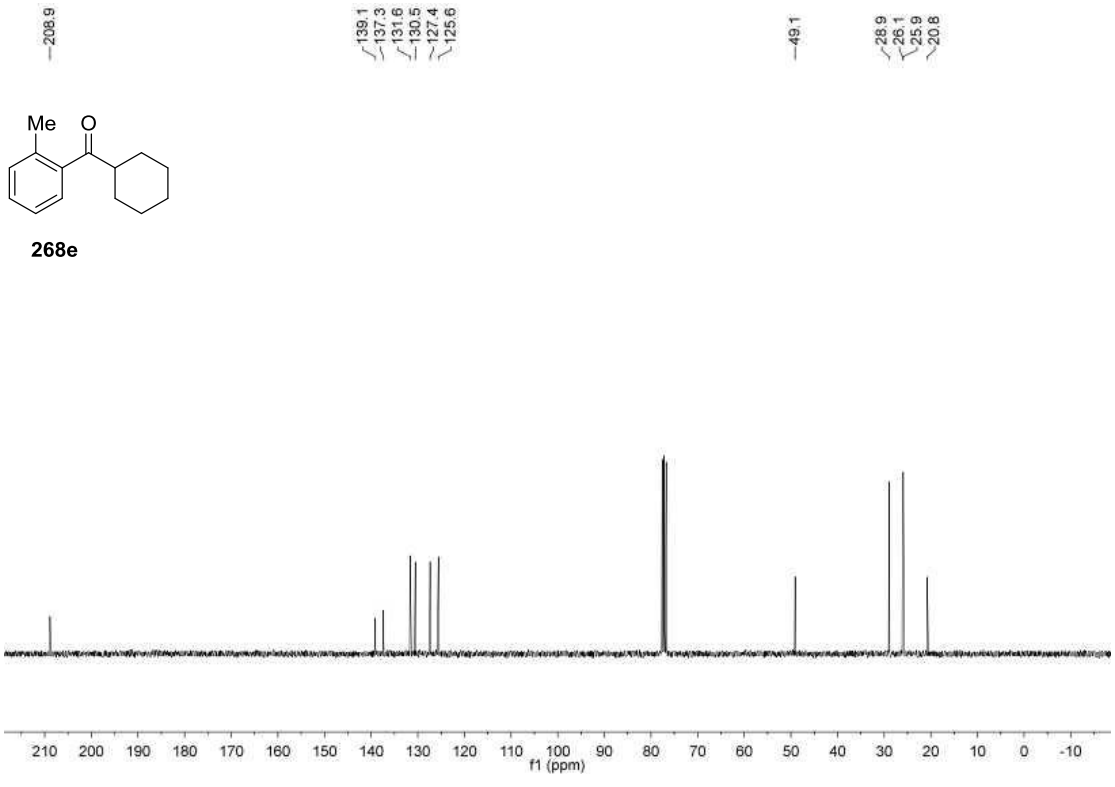
208.9
139.1
137.3
131.6
130.5
127.4
125.6
49.1
28.9
26.1
25.9
20.8
Me
O
f1 (ppm)

268e

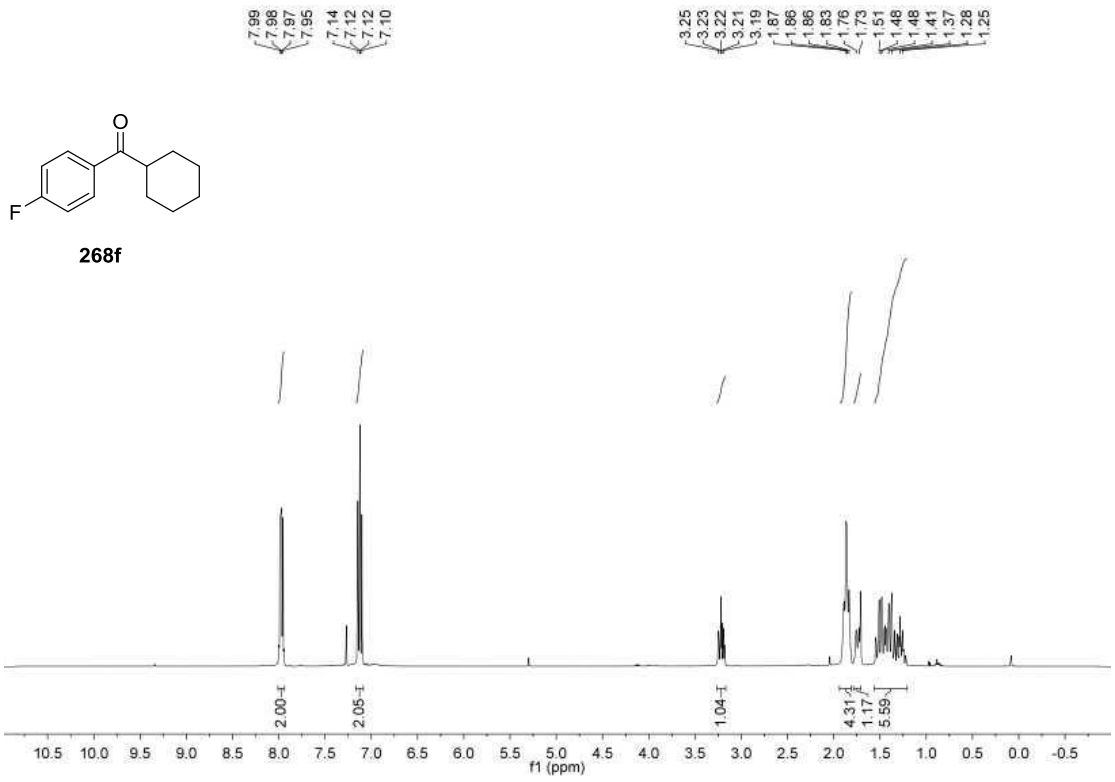
7.99
7.98
7.97
7.95
7.14
7.12
7.12
7.10
3.25
3.23
3.22
3.21
3.19
1.87
1.86
1.86
1.83
1.76
1.73
1.51
1.48
1.48
1.41
1.37
1.28
1.25
O
F
2.00
2.05
1.04
4.31
1.17
5.59
f1 (ppm)

268f

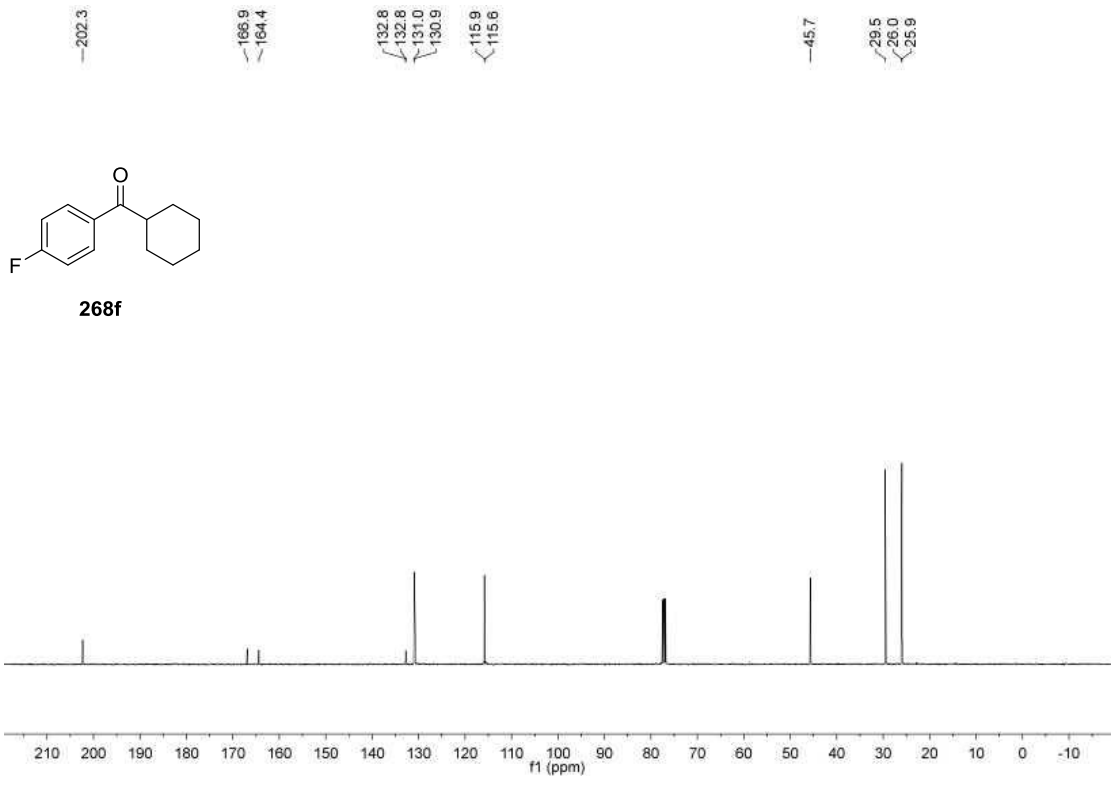
202.3
166.9
164.4
132.8
132.8
131.0
130.9
115.9
115.8
45.7
29.5
26.0
25.9
O
F
f1 (ppm)

268f

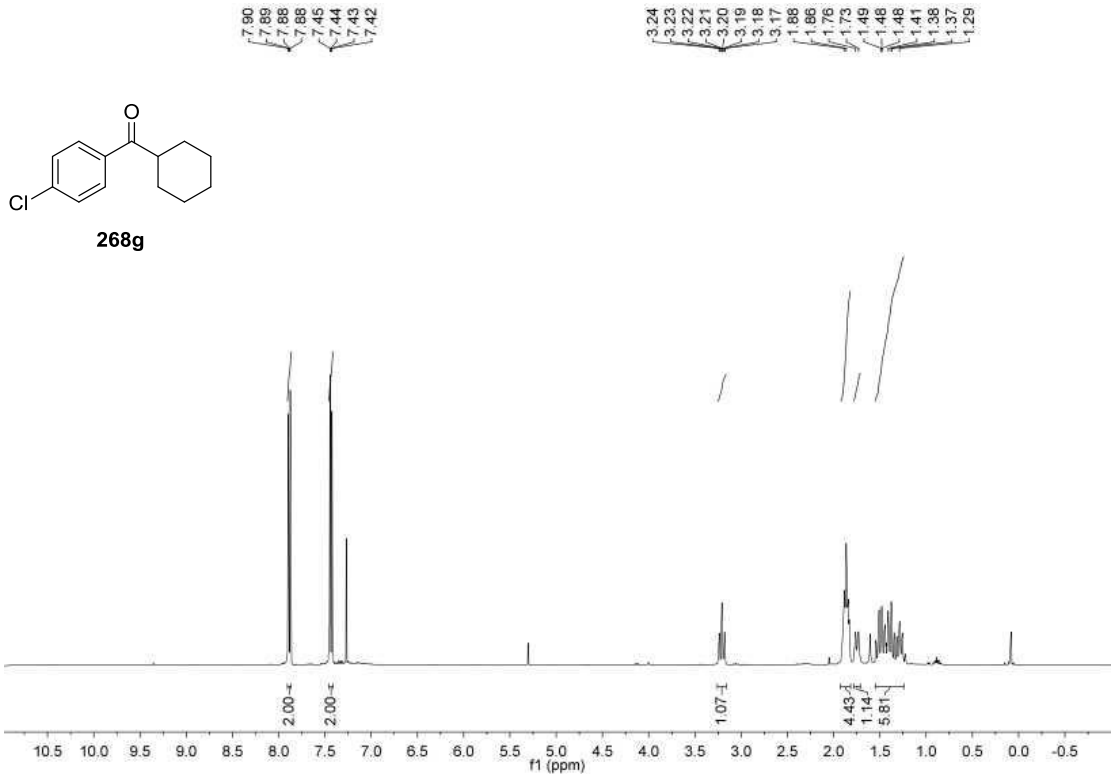
7.90
7.89
7.88
7.88
7.45
7.44
7.43
7.42
3.24
3.23
3.22
3.21
3.20
3.19
3.18
3.17
1.88
1.86
1.76
1.73
1.49
1.48
1.48
1.41
1.38
1.37
1.29
O
Cl
2.00
2.00
1.07
4.43
1.14
5.81
f1 (ppm)

268g

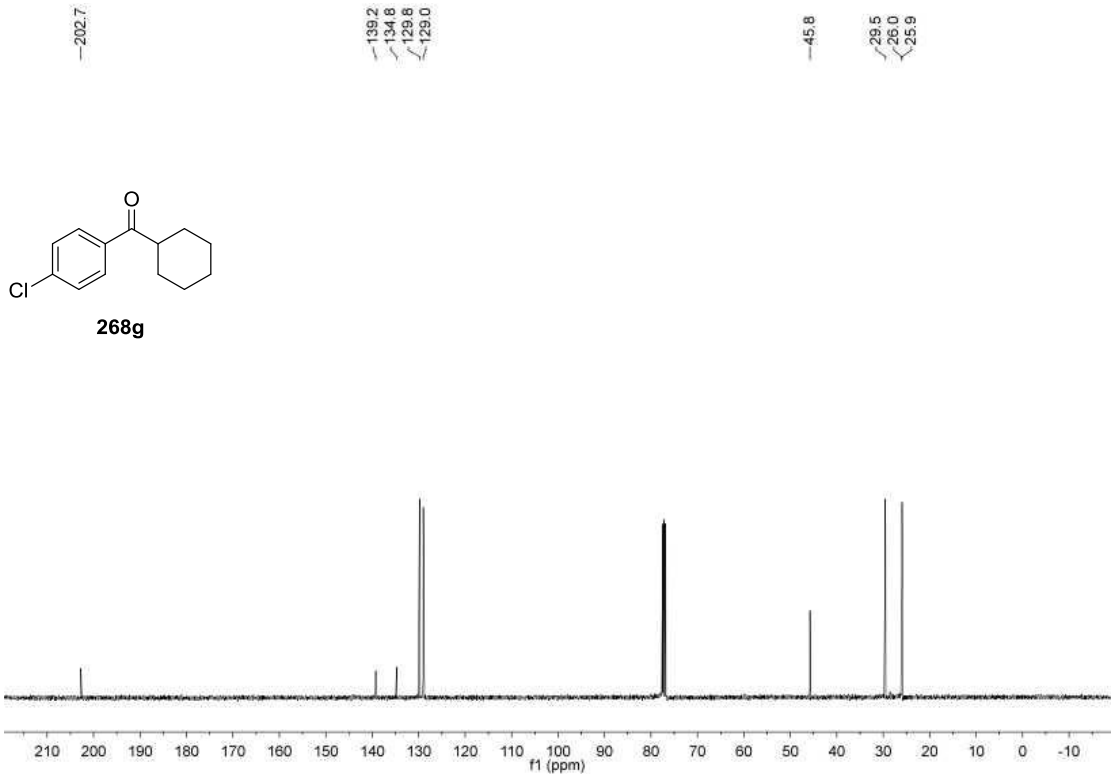
202.7
139.2
134.8
129.8
129.0
45.8
29.5
26.0
25.9
O
Cl
f1 (ppm)

268g

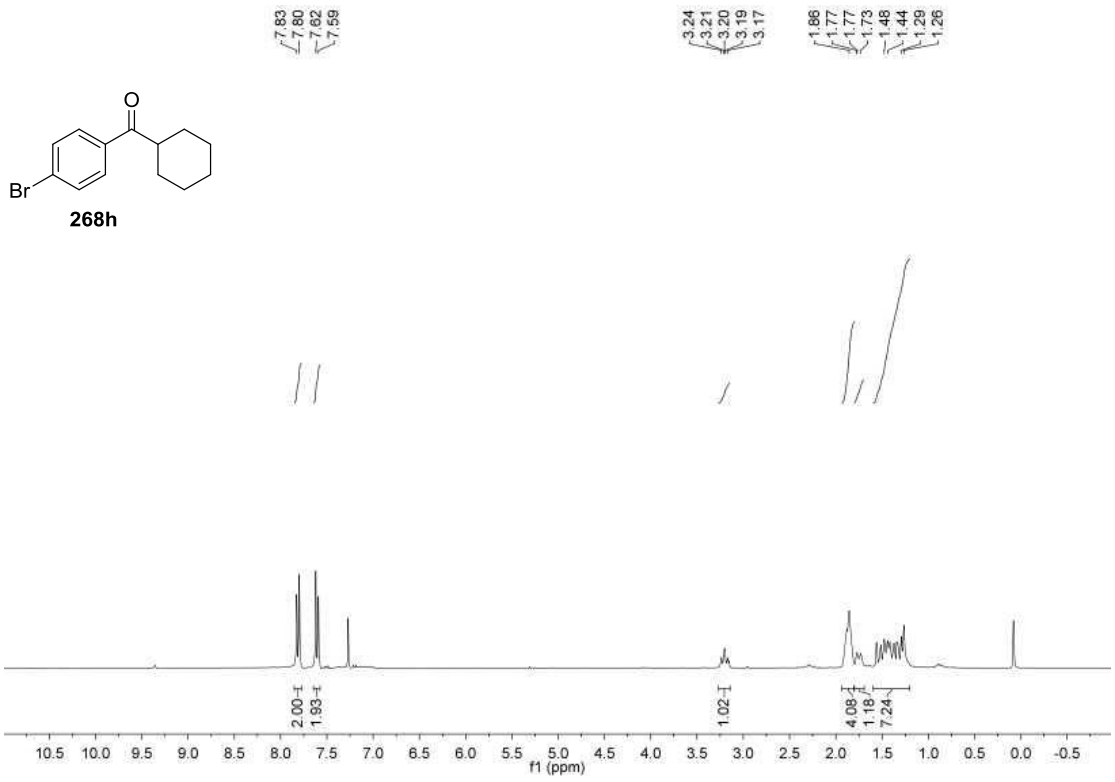
7.83
7.80
7.62
7.59
3.24
3.21
3.20
3.19
3.17
1.86
1.77
1.77
1.73
1.48
1.44
1.29
1.26
O
Br
268h
2.00
1.93
1.02
4.08
1.18
7.24
f1 (ppm)

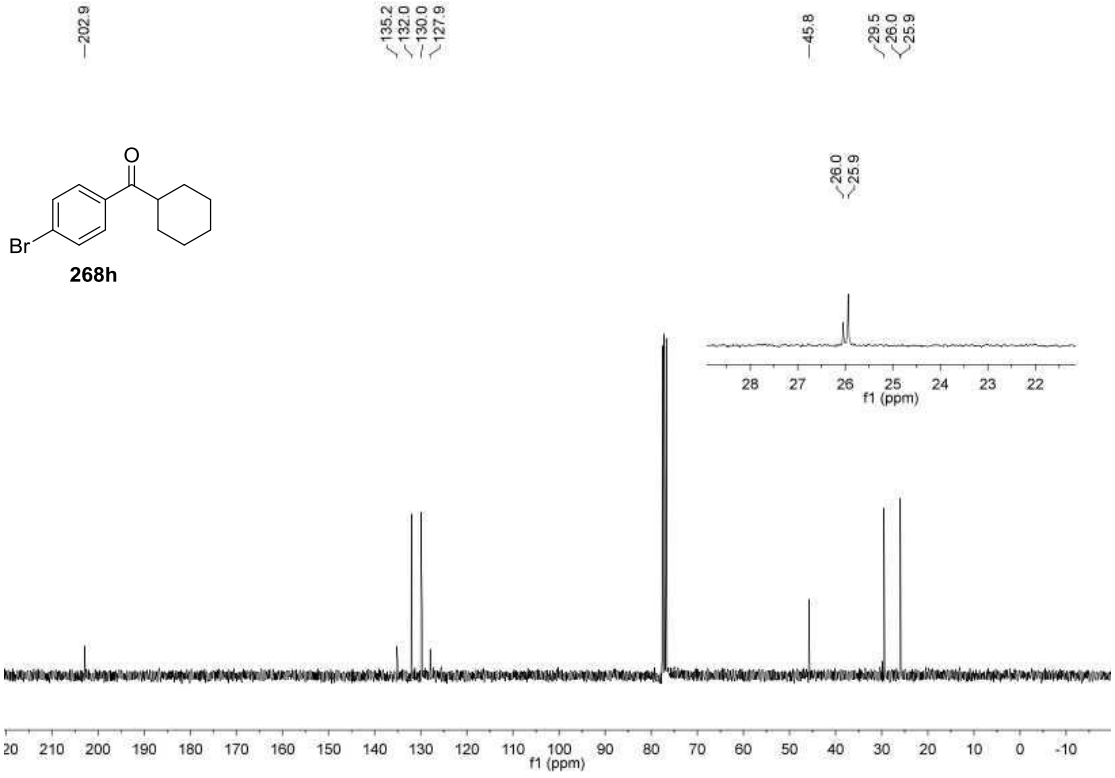
202.9
135.2
132.0
130.0
127.9
45.8
29.5
26.0
25.9
O
Br
268h
f1 (ppm)

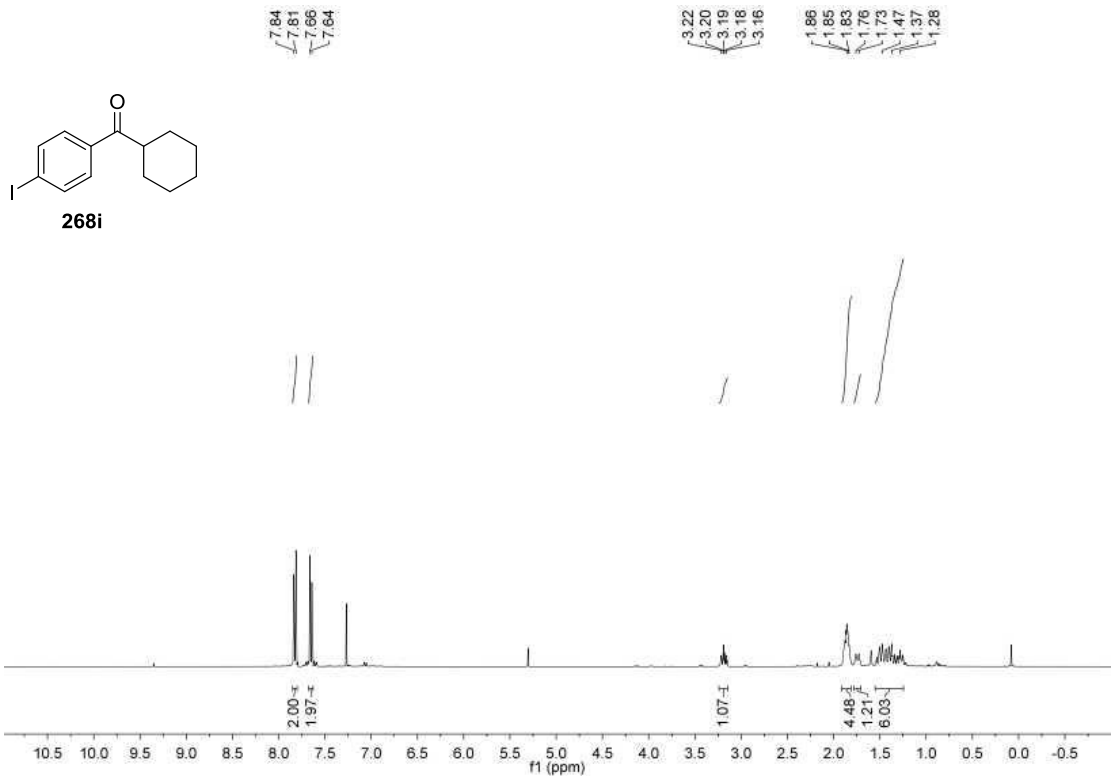
7.84
7.81
7.66
7.64
3.22
3.20
3.19
3.18
3.16
1.86
1.85
1.83
1.76
1.73
1.47
1.37
1.28
O
I
268i
2.00
1.97
1.07
4.48
1.21
6.03
f1 (ppm)

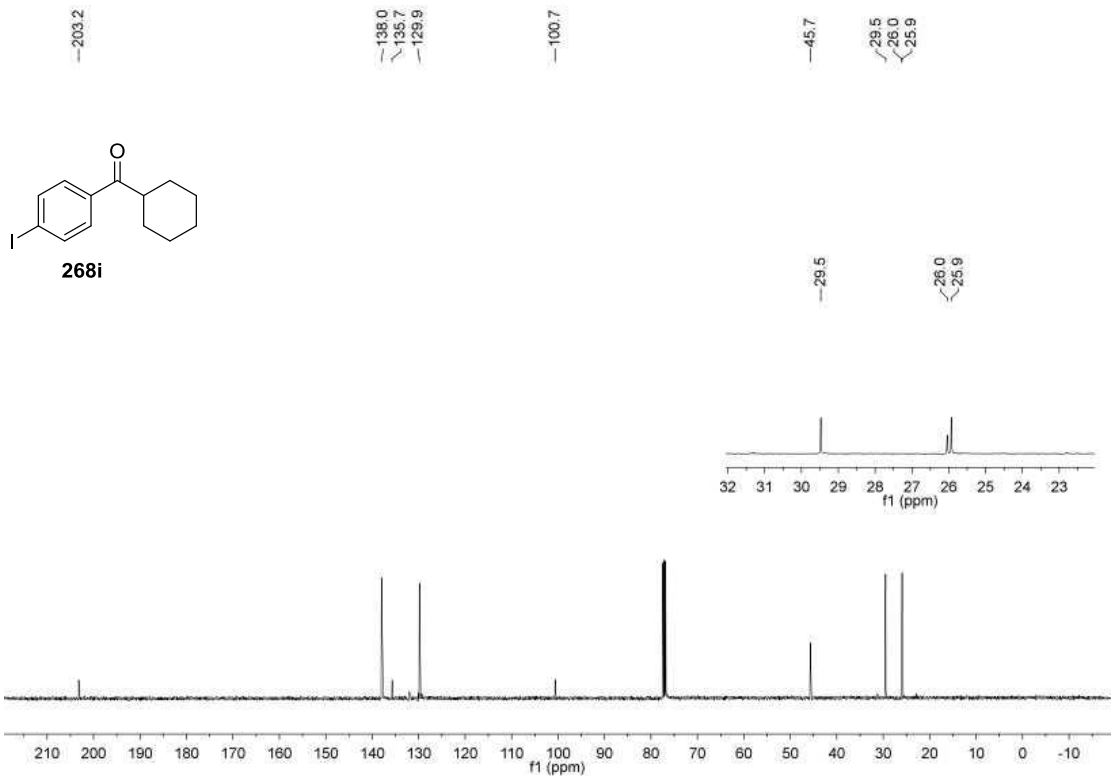
203.2
138.0
135.7
129.9
100.7
45.7
29.5
26.0
25.9
O
I
268i
f1 (ppm)

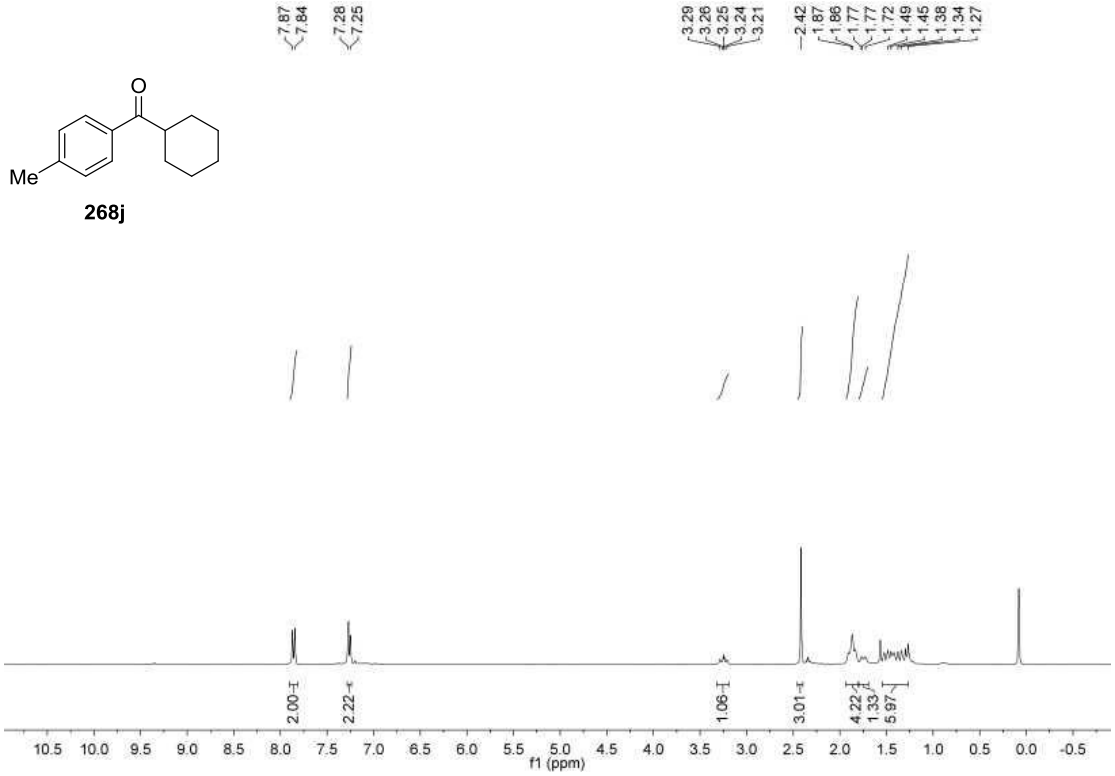
7.87
7.84
7.28
7.25
3.29
3.26
3.25
3.24
3.21
2.42
1.87
1.86
1.77
1.77
1.72
1.49
1.45
1.38
1.34
1.27
O
Me
2.00
2.22
1.06
3.01
4.22
1.33
5.97
10.5 10.0 9.5 9.0 8.5 8.0 7.5 7.0 6.5 6.0 5.5 5.0 4.5 4.0 3.5 3.0 2.5 2.0 1.5 1.0 0.5 0.0 -0.5
f1 (ppm)

268j

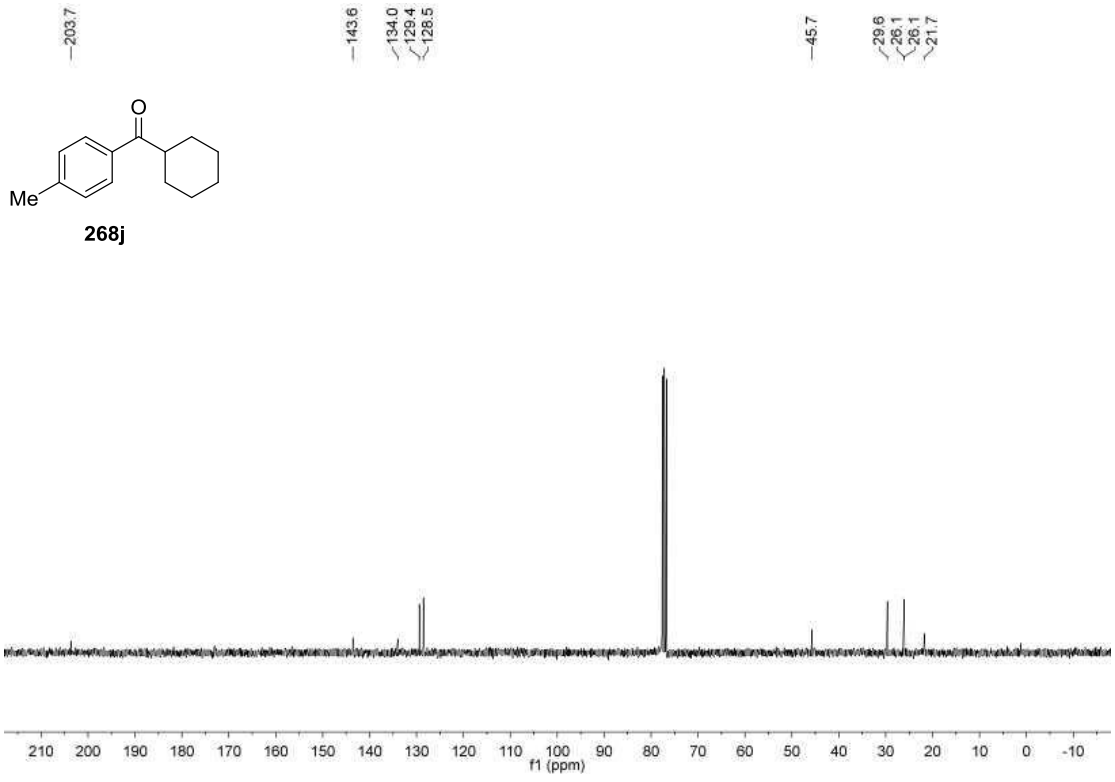
203.7
143.6
134.0
129.4
128.5
45.7
29.6
26.1
26.1
21.7
O
Me
210 200 190 180 170 160 150 140 130 120 110 100 90 80 70 60 50 40 30 20 10 0 -10
f1 (ppm)

268j

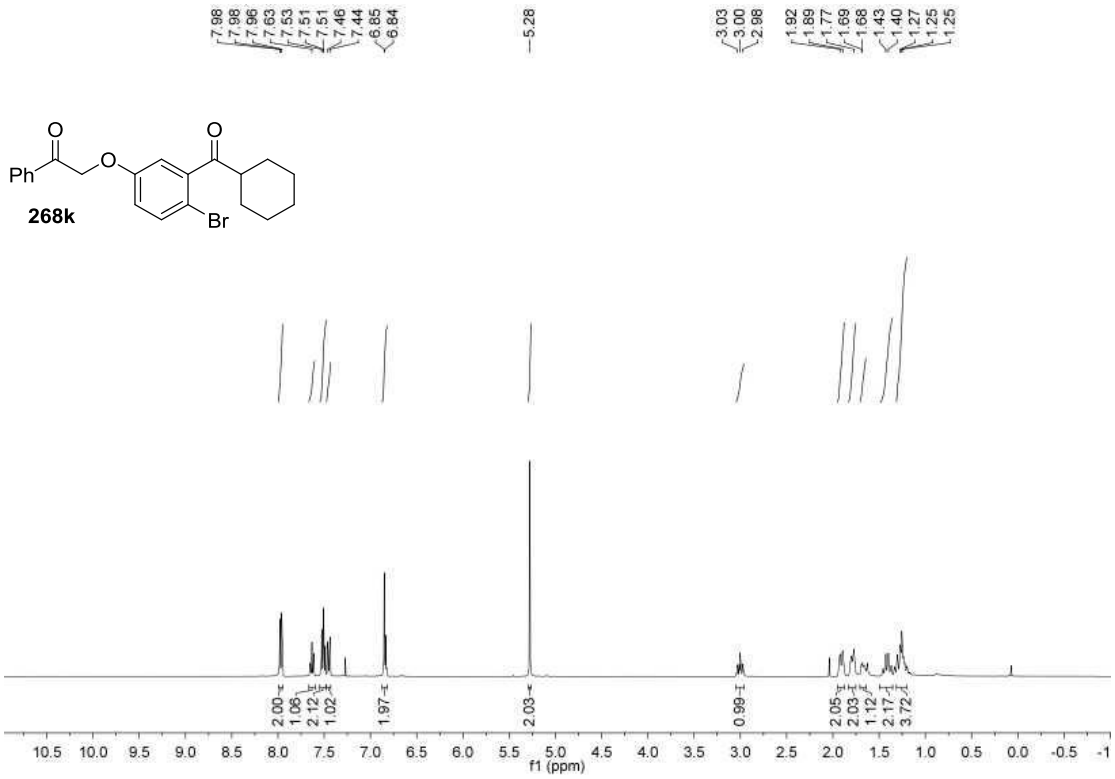
7.98
7.98
7.96
7.96
7.63
7.53
7.51
7.51
7.46
7.44
6.85
6.84
5.28
3.03
3.00
2.98
1.92
1.89
1.77
1.69
1.68
1.43
1.40
1.27
1.25
1.25
Ph
O
O
O
Br
268k
2.00
1.06
2.12
1.02
1.97
2.03
0.99
2.05
2.03
1.12
2.17
3.72
f1 (ppm)

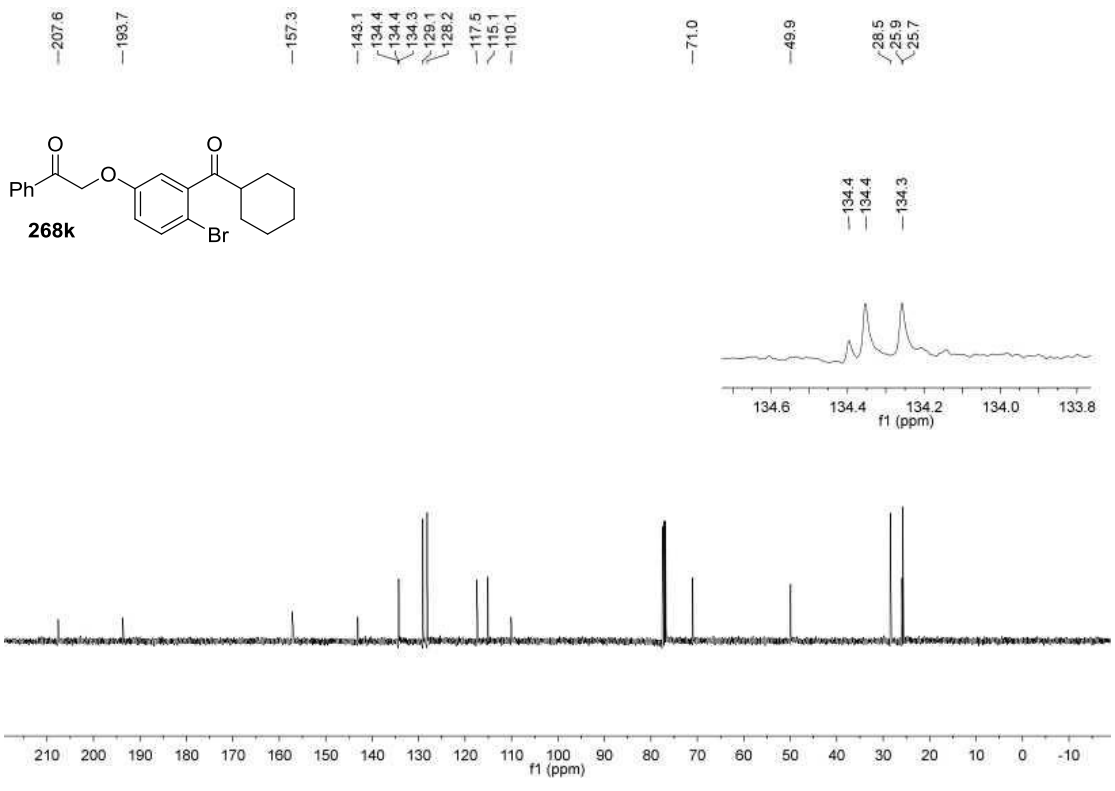
207.6
193.7
157.3
143.1
134.4
134.4
134.3
129.1
128.2
117.5
115.1
110.1
71.0
49.9
28.5
25.9
25.7
Ph
O
O
O
Br
268k
134.4
134.4
134.3
f1 (ppm)
f1 (ppm)

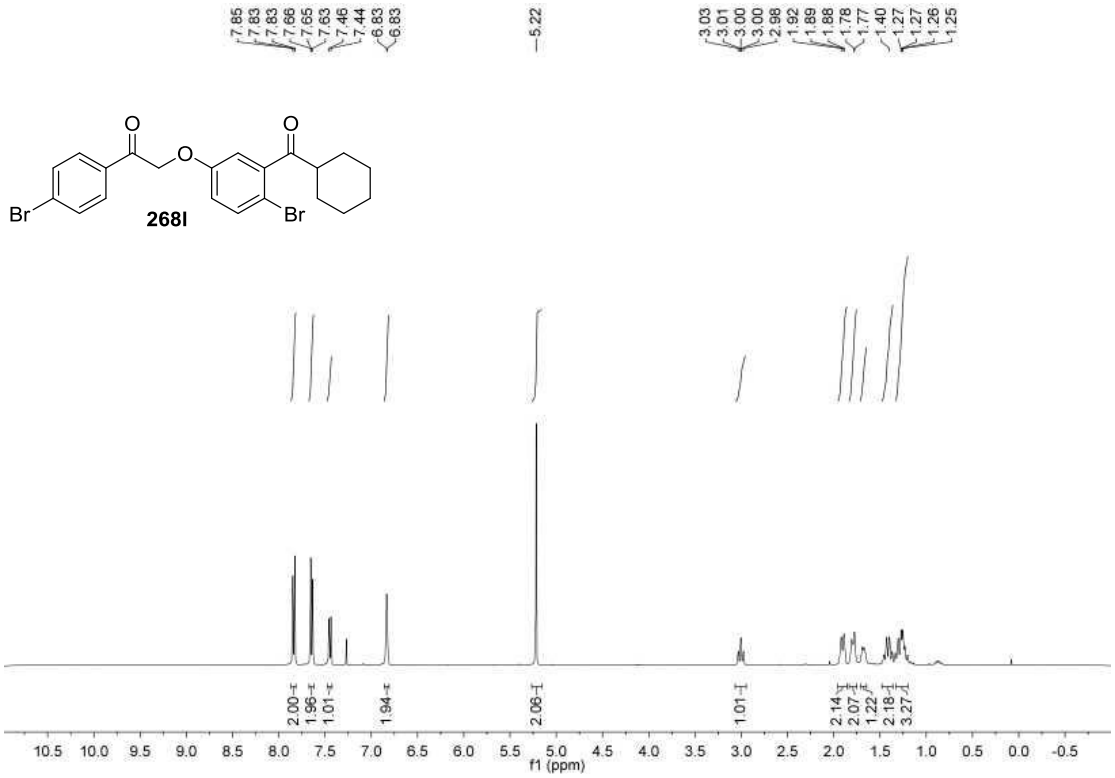
7.85
7.83
7.83
7.66
7.65
7.63
7.46
7.44
6.83
6.83
5.22
3.03
3.01
3.00
3.00
2.98
1.92
1.89
1.88
1.78
1.77
1.40
1.27
1.27
1.26
1.25
O
O
O
Br
Br
2.00
1.96
1.01
1.94
2.06
1.01
2.14
2.07
1.22
2.18
3.27
10.5 10.0 9.5 9.0 8.5 8.0 7.5 7.0 6.5 6.0 5.5 5.0 4.5 4.0 3.5 3.0 2.5 2.0 1.5 1.0 0.5 0.0 -0.5
f1 (ppm)

268l

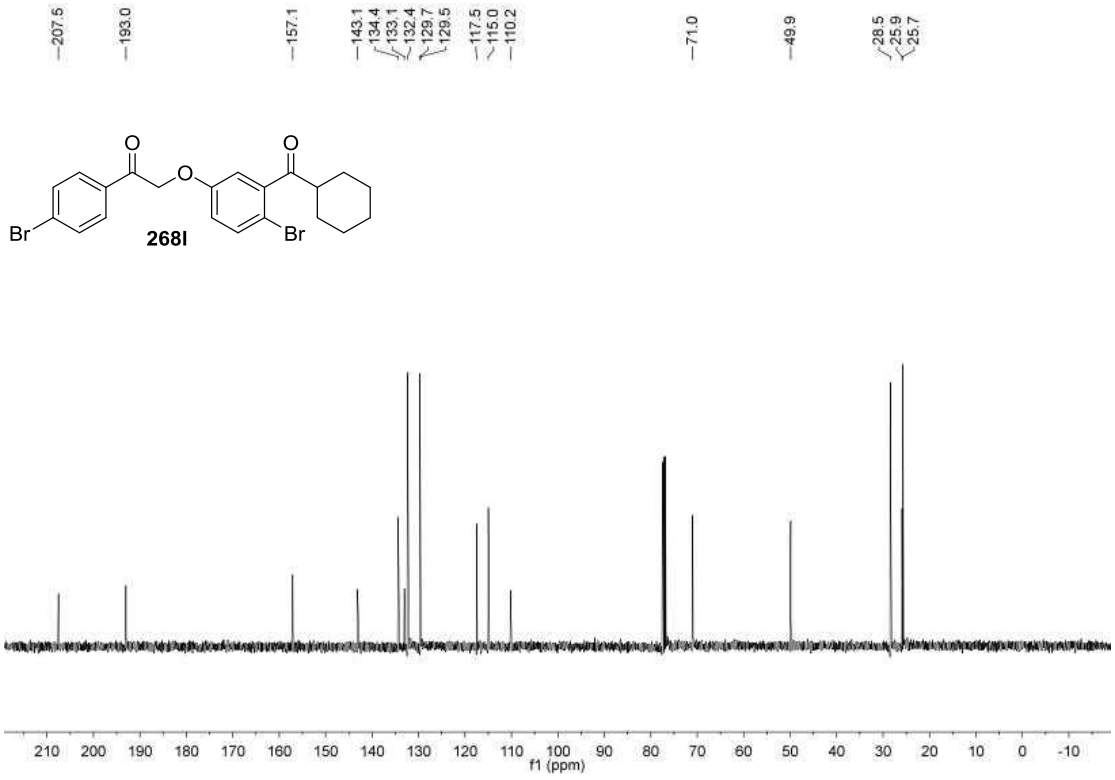
207.6
193.0
157.1
143.1
134.4
133.1
132.4
129.7
129.5
117.5
115.0
110.2
71.0
49.9
28.5
25.9
25.7
O
O
O
Br
Br
210 200 190 180 170 160 150 140 130 120 110 100 90 80 70 60 50 40 30 20 10 0 -10
f1 (ppm)

268l

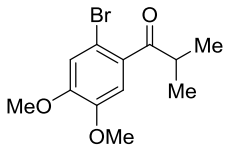
Br
O
Me
Me
MeO
OMe

268r

7.04
6.88
3.91
3.88
3.49
3.47
3.45
1.20
1.18
0.89
0.93
3.15
2.99
1.00
5.98
f1 (ppm)


207.9
151.0
148.4
133.6
116.2
111.9
110.5
56.4
56.3
39.7
18.6

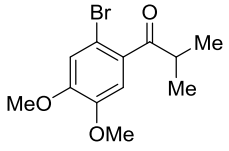
Br
O
Me
Me
MeO
OMe

268r

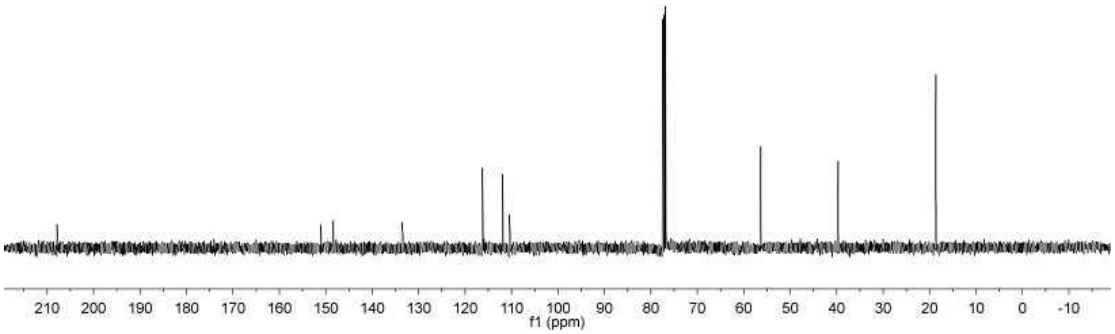
f1 (ppm)

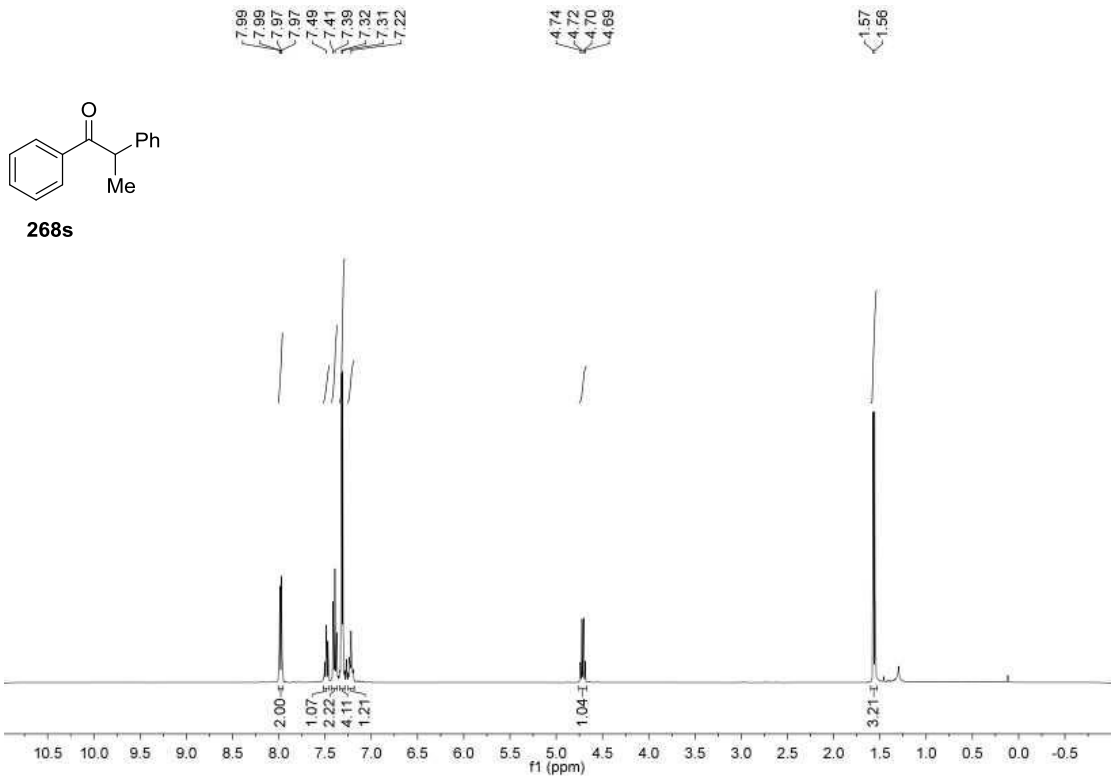
7.99
7.99
7.97
7.97
7.49
7.41
7.39
7.32
7.31
7.22
4.74
4.72
4.70
4.69
1.57
1.56
O
Ph
Me
268s
2.00
1.07
2.22
4.11
1.21
1.04
3.21
f1 (ppm)

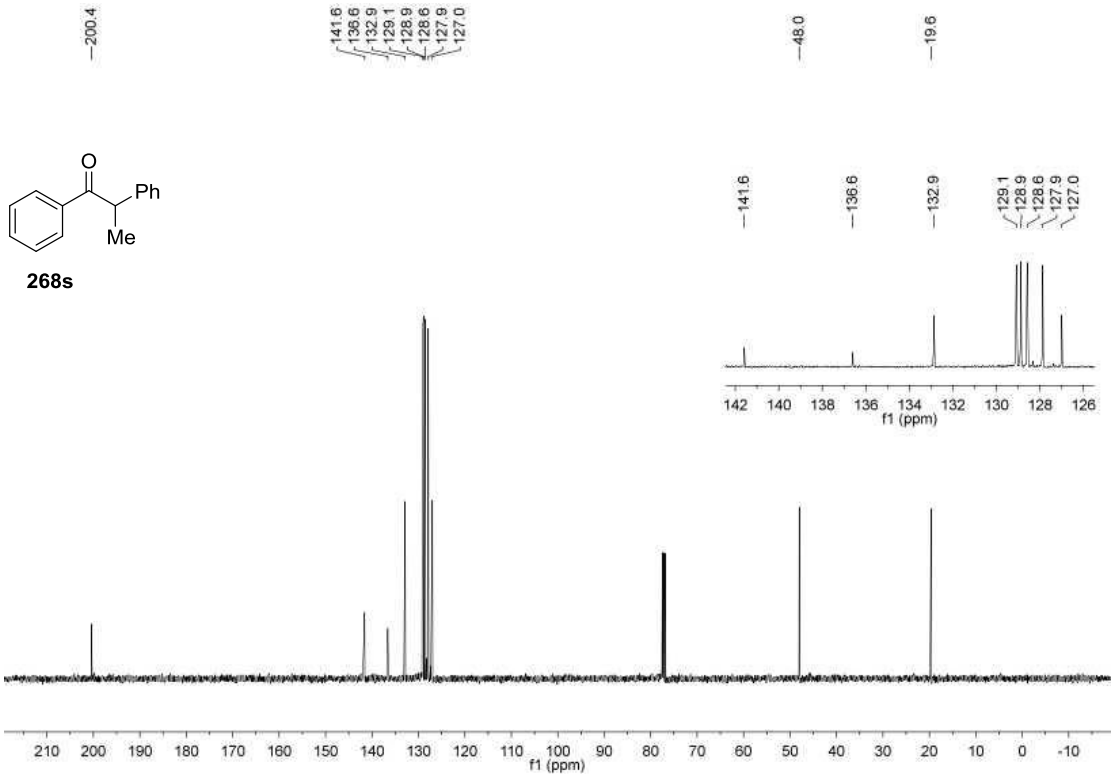
200.4
141.6
136.6
132.9
129.1
128.9
128.6
127.9
127.0
48.0
19.6
O
Ph
Me
268s
f1 (ppm)

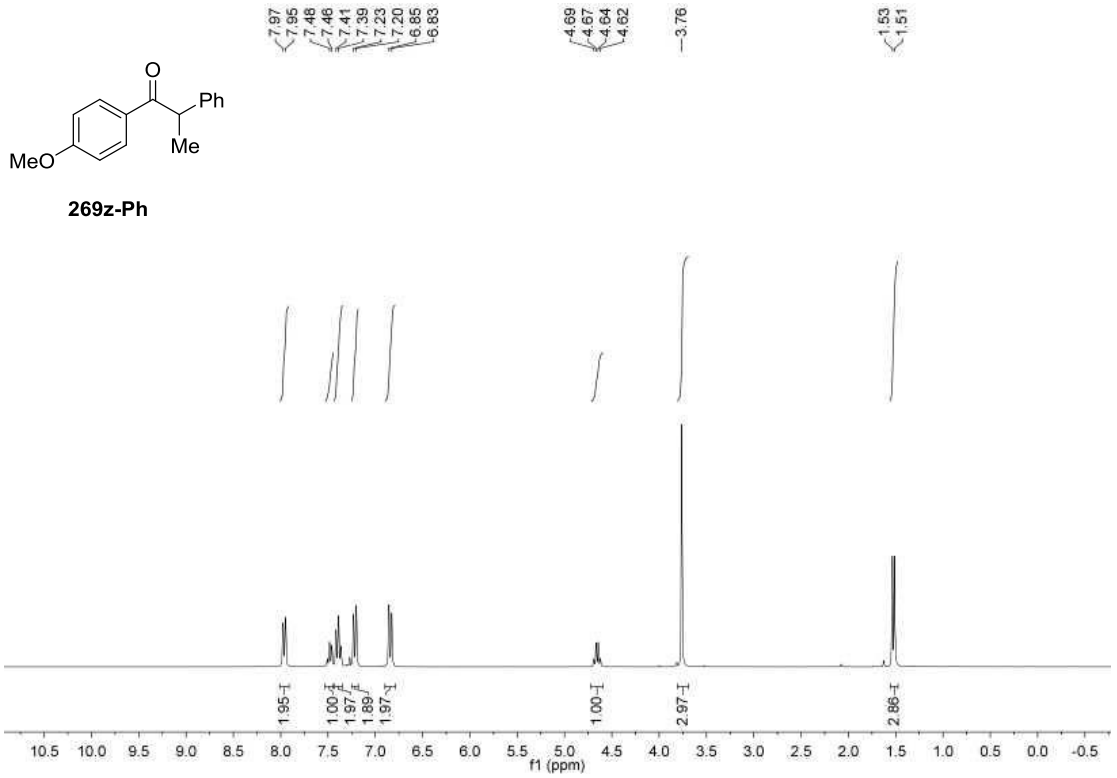

269z-Ph

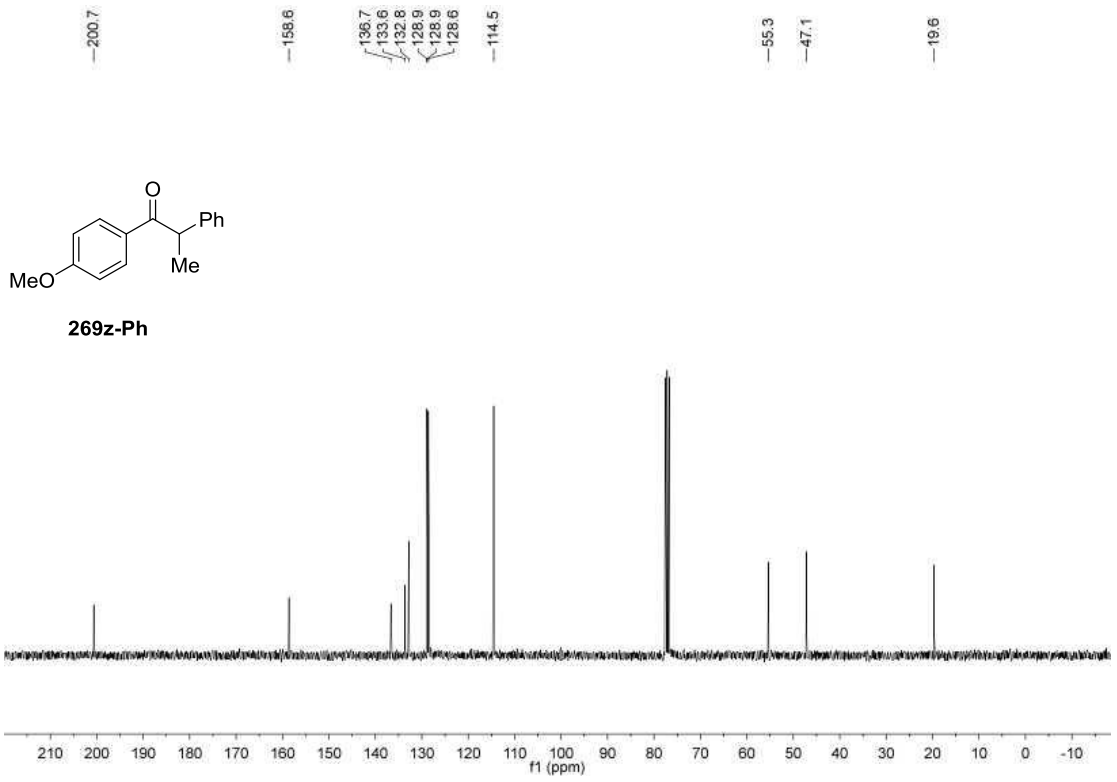

269z-Ph

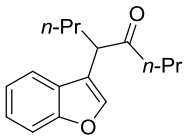
n-Pr
O
n-Pr
O

302aa

7.60
7.55
7.48
7.34
7.34
7.22
7.22
3.85
3.83
3.81
2.43
2.43
2.05
1.87
1.84
1.54
1.33
1.30
0.96
0.93
0.91
0.84
0.82
0.80
1.02
0.97
1.02
1.04
1.13
1.00
2.05
1.10
1.07
2.22
2.39
3.34
3.17
f1 (ppm)


210.2
155.6
142.4
127.1
124.6
122.8
120.2
118.5
111.7
48.7
43.2
33.0
20.9
17.3
14.1
13.7

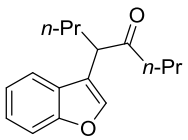
n-Pr
O
n-Pr
O

302aa

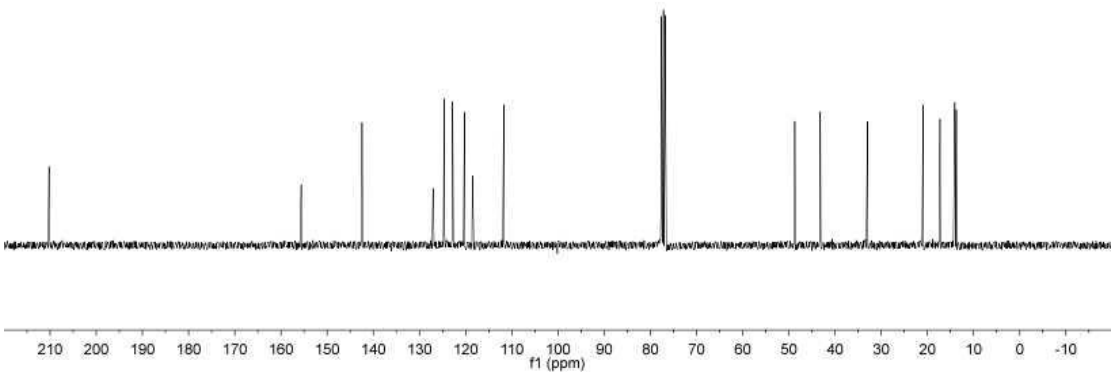
f1 (ppm)

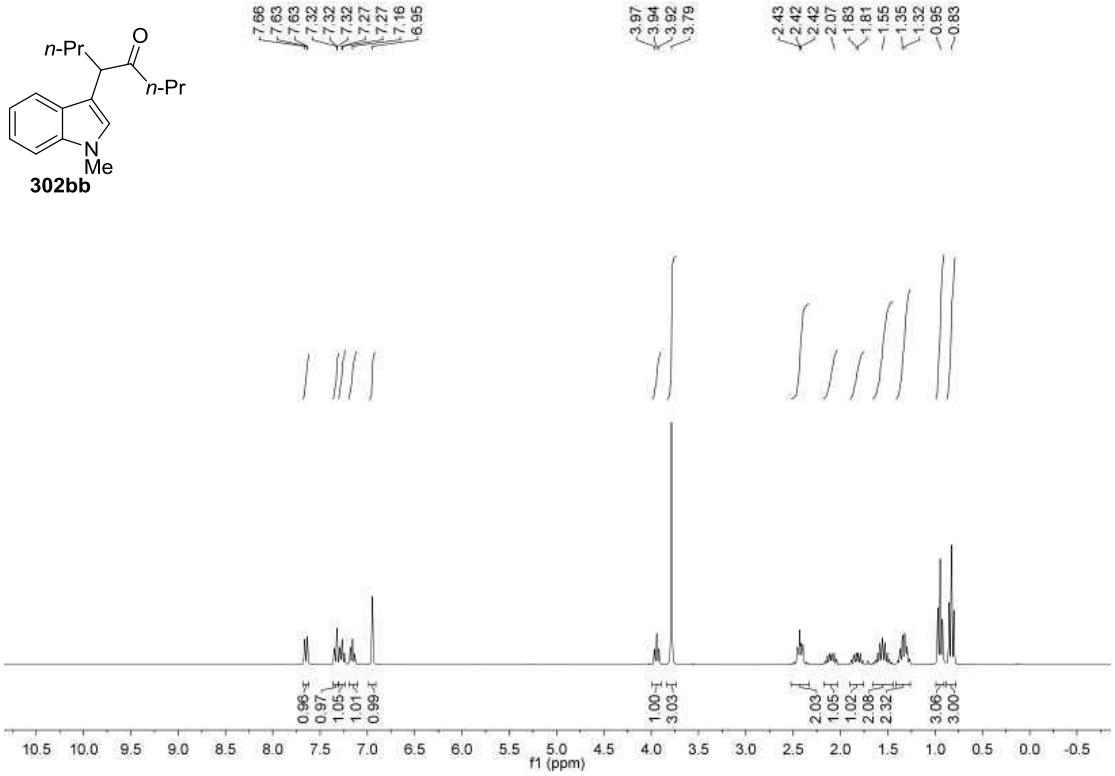
n-Pr
O
n-Pr
N
Me
302bb
7.66
7.63
7.63
7.32
7.32
7.32
7.27
7.27
7.16
6.95
3.97
3.94
3.92
3.79
2.43
2.42
2.42
2.07
1.83
1.81
1.55
1.35
1.32
0.95
0.83
0.96
0.97
1.05
1.01
0.99
1.00
3.03
2.03
1.05
1.02
2.08
2.32
3.06
3.00
f1 (ppm)

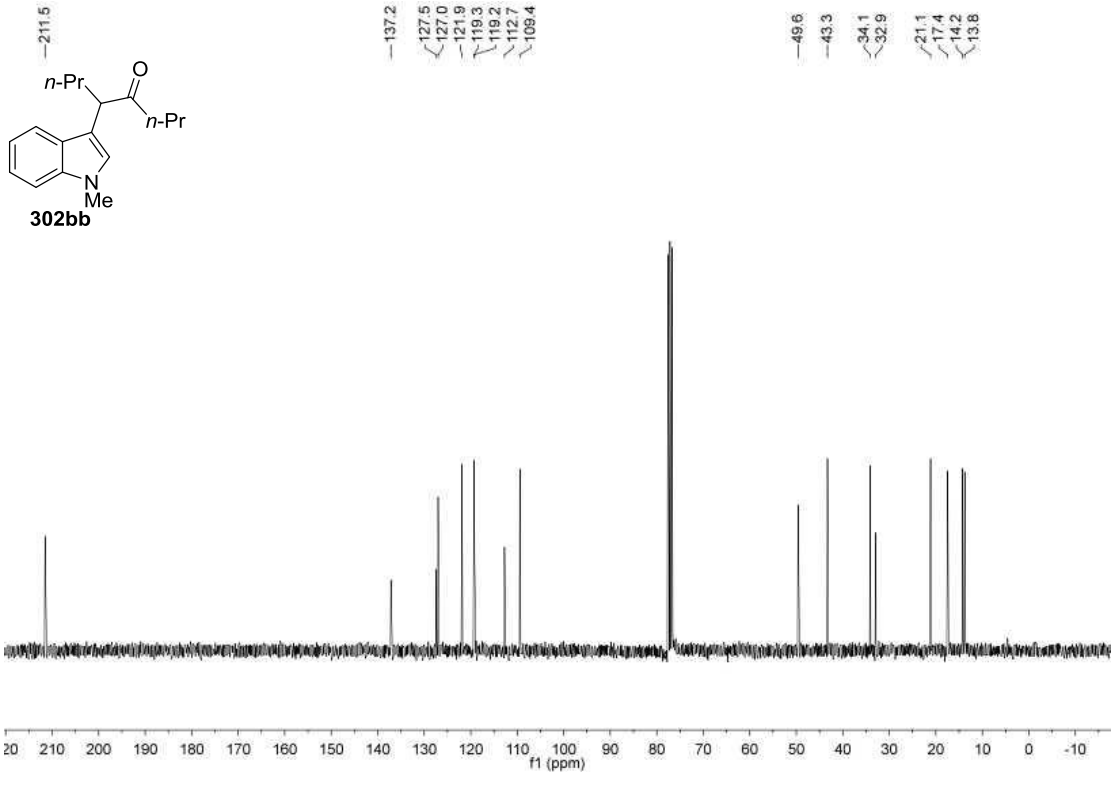
n-Pr
O
n-Pr
N
Me
302bb
211.5
137.2
127.5
127.0
121.9
119.3
119.2
112.7
109.4
49.6
43.3
34.1
32.9
21.1
17.4
14.2
13.8
f1 (ppm)

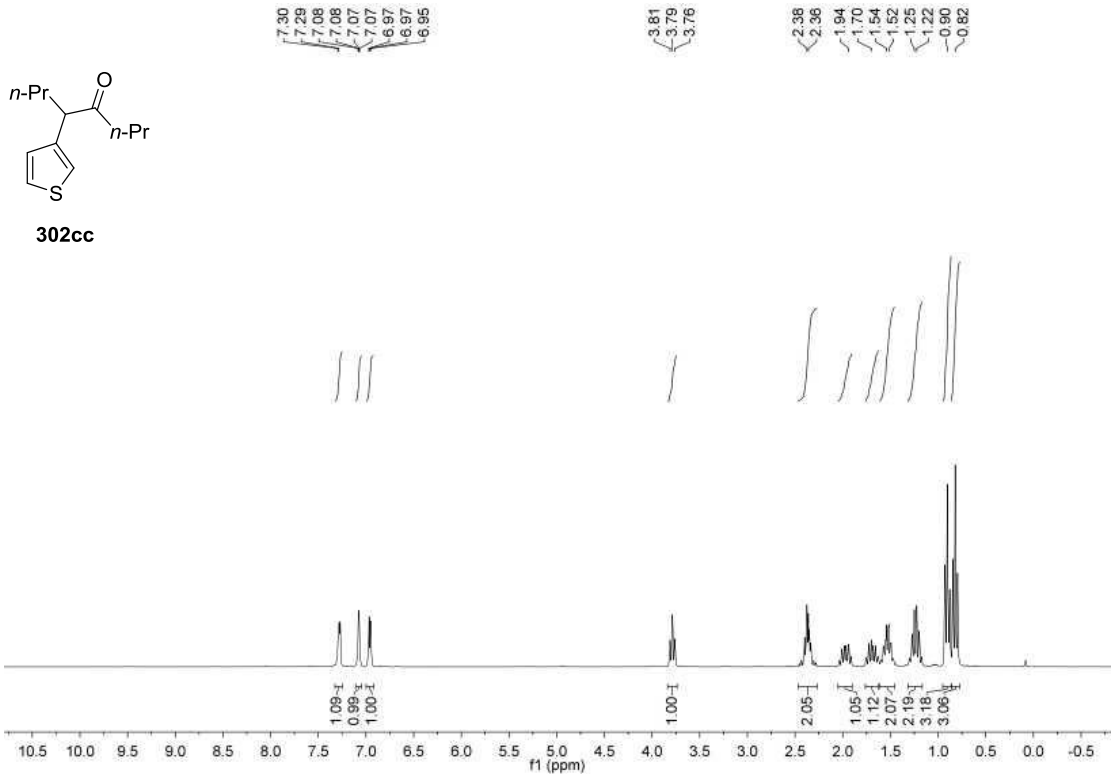
7.30
7.29
7.08
7.08
7.07
7.07
6.97
6.97
6.95
3.81
3.79
3.76
2.38
2.36
1.94
1.70
1.54
1.52
1.25
1.22
0.90
0.82
n-Pr
O
n-Pr
S
1.09
0.99
1.00
1.00
2.05
1.05
1.12
2.07
2.19
3.18
3.06
f1 (ppm)

302cc

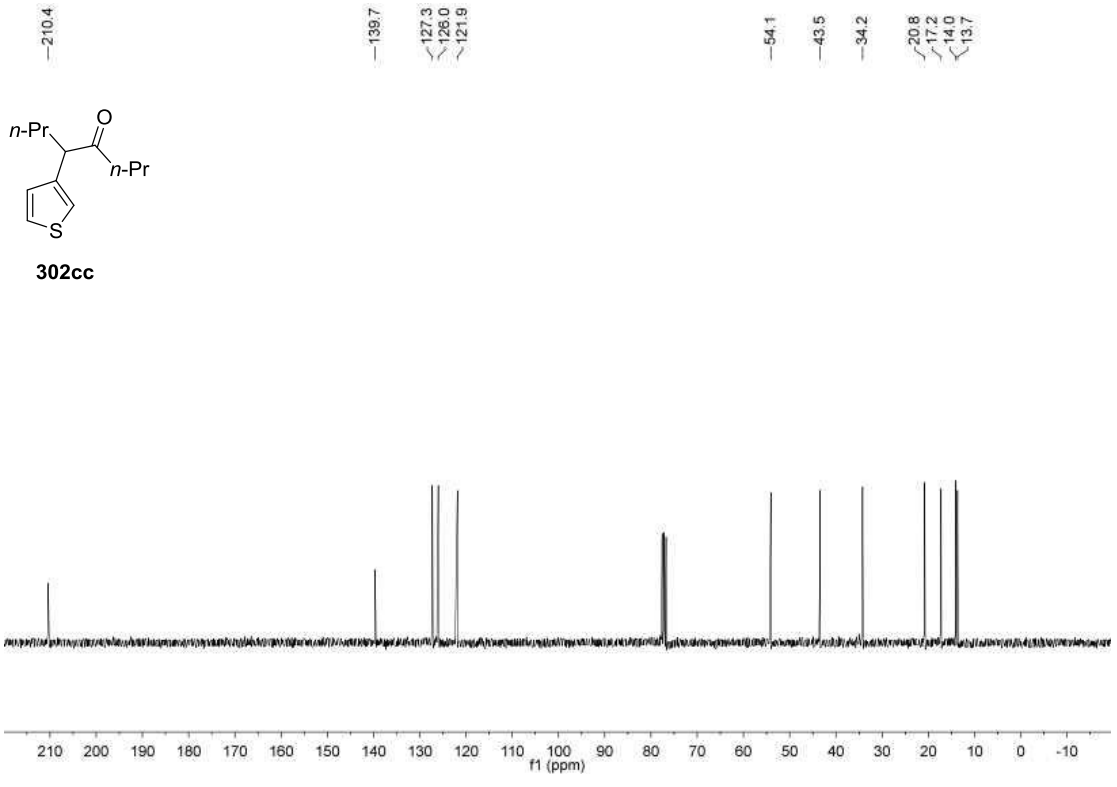
210.4
139.7
127.3
126.0
121.9
54.1
43.5
34.2
20.8
17.2
14.0
13.7
n-Pr
O
n-Pr
S
f1 (ppm)

302cc

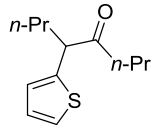
n-Pr
O
n-Pr
S

302dd

6.96
6.89
6.88
6.88
3.95
3.92
3.90
2.45
2.42
2.00
1.98
1.78
1.76
1.56
1.54
1.29
1.27
0.91
0.84
1.00
1.05
1.03
1.02
2.29
1.21
1.24
2.37
2.46
3.61
3.32
f1 (ppm)

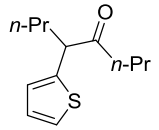
n-Pr
O
n-Pr
S

302dd

209.5
141.9
127.0
125.4
124.7
53.6
43.2
35.5
20.8
17.3
14.0
13.7
f1 (ppm)

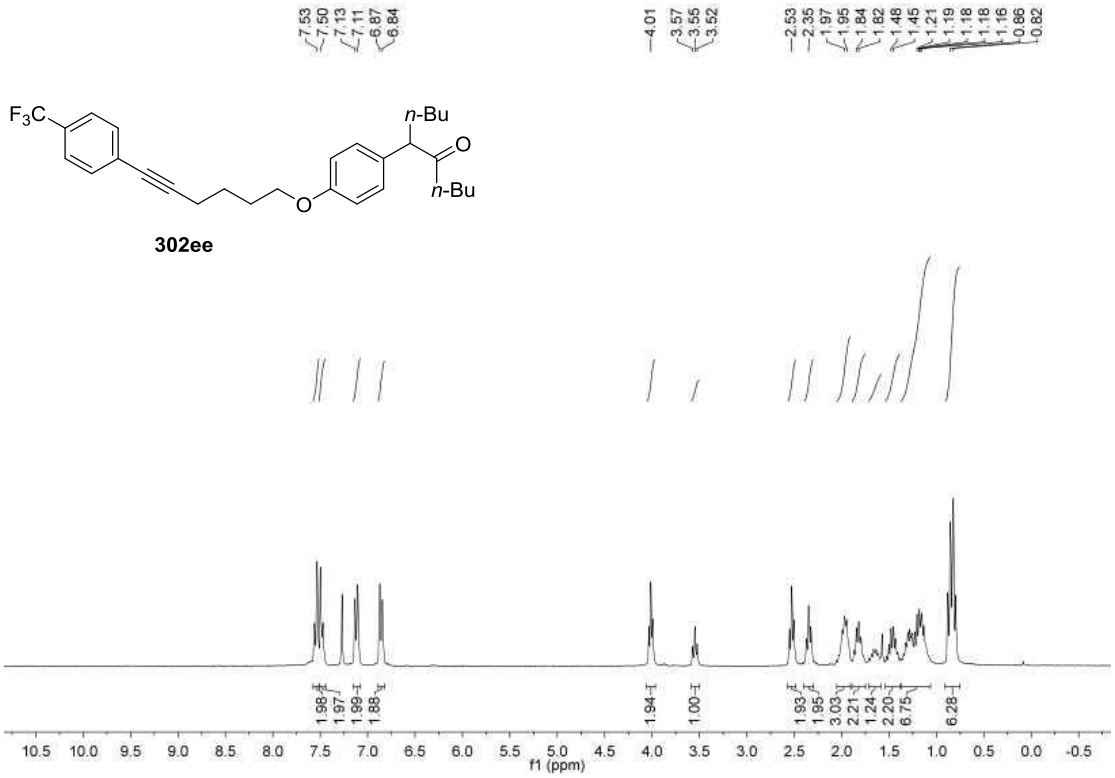
7.53
7.50
7.13
7.11
6.87
6.84
4.01
3.57
3.55
3.52
2.53
2.35
1.97
1.95
1.84
1.82
1.48
1.45
1.21
1.19
1.18
1.16
0.86
0.82
F3C
n-Bu
O
n-Bu
O
302ee
1.98
1.97
1.99
1.88
1.94
1.00
1.93
1.95
3.03
2.21
1.24
2.20
6.75
6.28
10.5 10.0 9.5 9.0 8.5 8.0 7.5 7.0 6.5 6.0 5.5 5.0 4.5 4.0 3.5 3.0 2.5 2.0 1.5 1.0 0.5 0.0 -0.5
f1 (ppm)

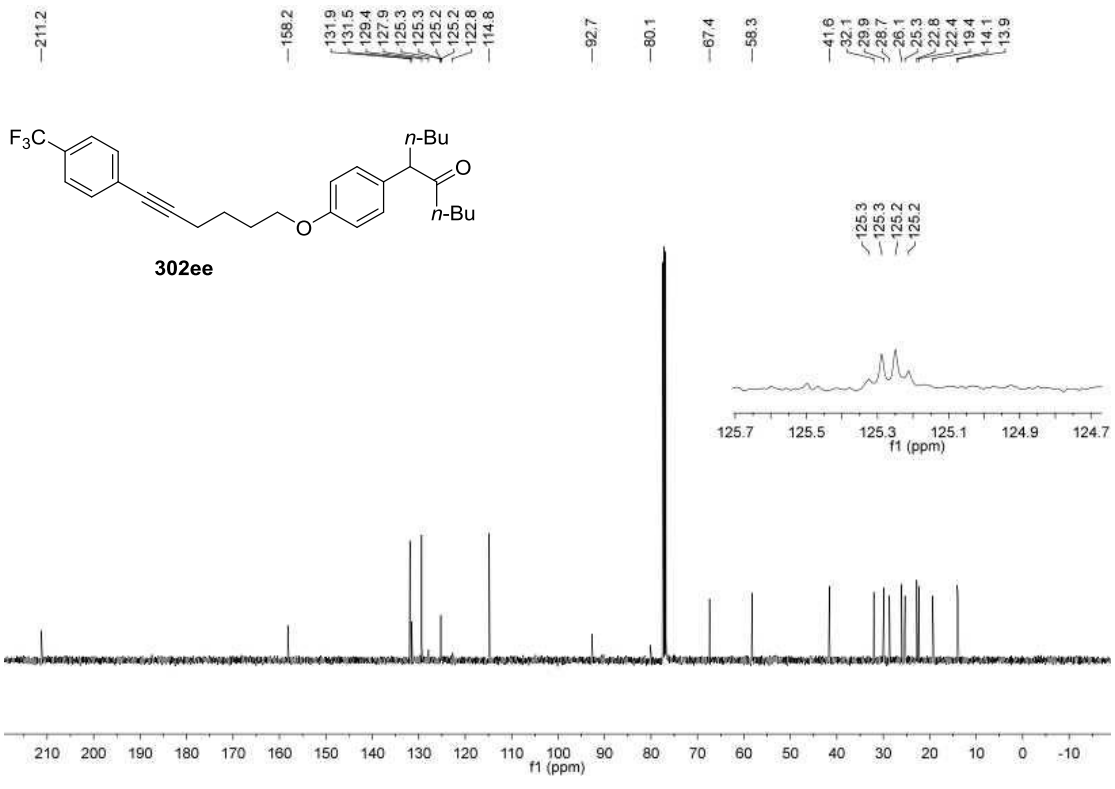
211.2
158.2
131.9
131.5
129.4
127.9
125.3
125.3
125.2
125.2
122.8
114.8
92.7
80.1
67.4
58.3
41.6
32.1
29.9
28.7
26.1
25.3
22.8
22.4
19.4
14.1
13.9
F3C
n-Bu
O
n-Bu
O
302ee
125.3
125.3
125.2
125.2
125.7 125.5 125.3 125.1 124.9 124.7
f1 (ppm)
210 200 190 180 170 160 150 140 130 120 110 100 90 80 70 60 50 40 30 20 10 0 -10
f1 (ppm)

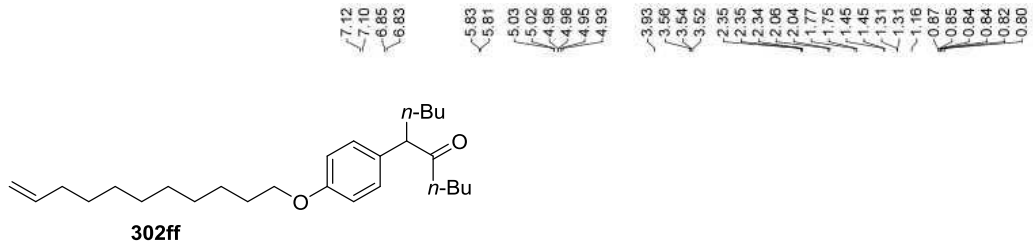
7.12
7.10
6.85
6.83
5.83
5.81
5.03
5.02
4.98
4.98
4.95
4.93
3.93
3.56
3.54
3.52
2.35
2.35
2.34
2.06
2.04
1.77
1.75
1.45
1.45
1.31
1.31
1.16
0.87
0.85
0.84
0.84
0.82
0.80

n-Bu
O
n-Bu
O

302ff

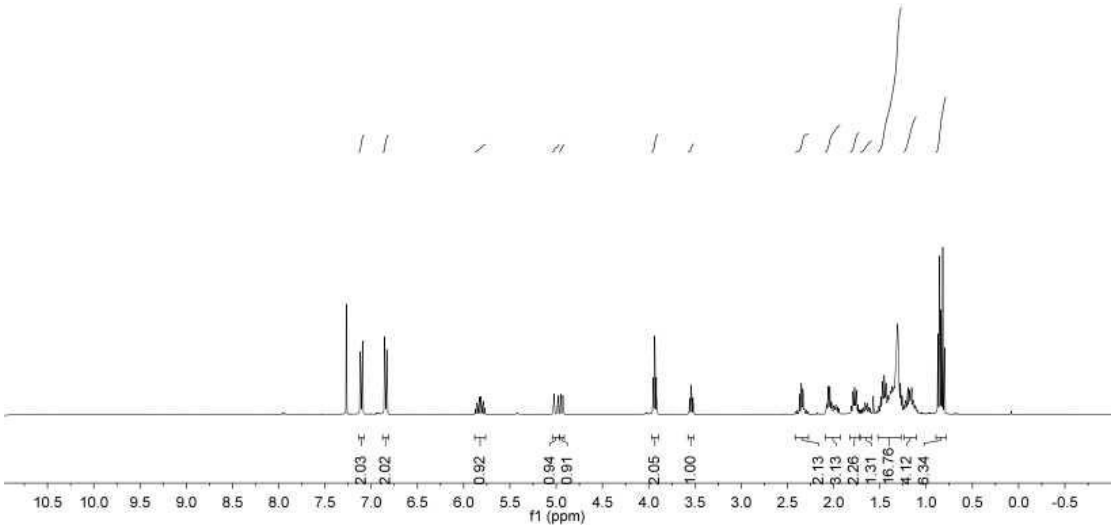
2.03
2.02
0.92
0.94
0.91
2.05
1.00
2.13
3.13
2.26
1.31
16.76
4.12
6.34
10.5 10.0 9.5 9.0 8.5 8.0 7.5 7.0 6.5 6.0 5.5 5.0 4.5 4.0 3.5 3.0 2.5 2.0 1.5 1.0 0.5 0.0 -0.5
f1 (ppm)


211.3
158.4
139.3
131.3
129.3
114.8
114.3
68.1
58.3
41.6
29.6
29.5
29.3
26.1
22.4
14.1
13.9

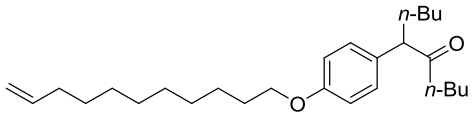
n-Bu
O
n-Bu
O

302ff

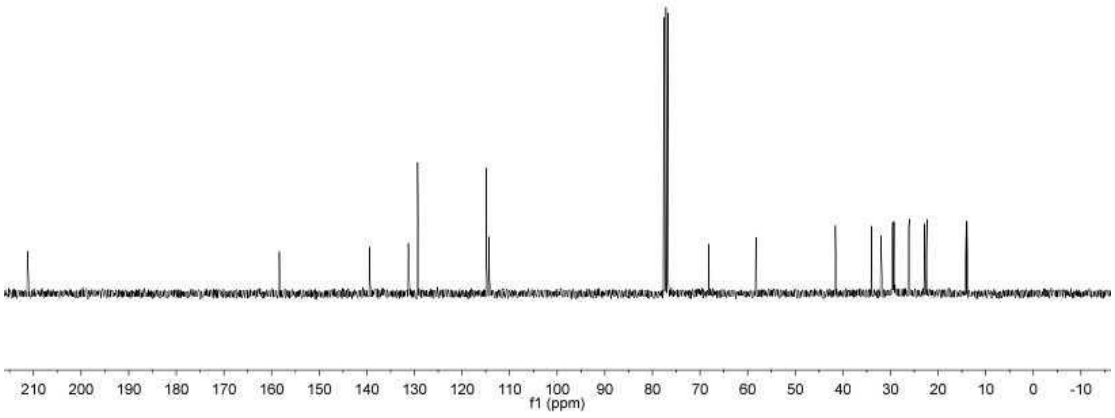
210 200 190 180 170 160 150 140 130 120 110 100 90 80 70 60 50 40 30 20 10 0 -10
f1 (ppm)

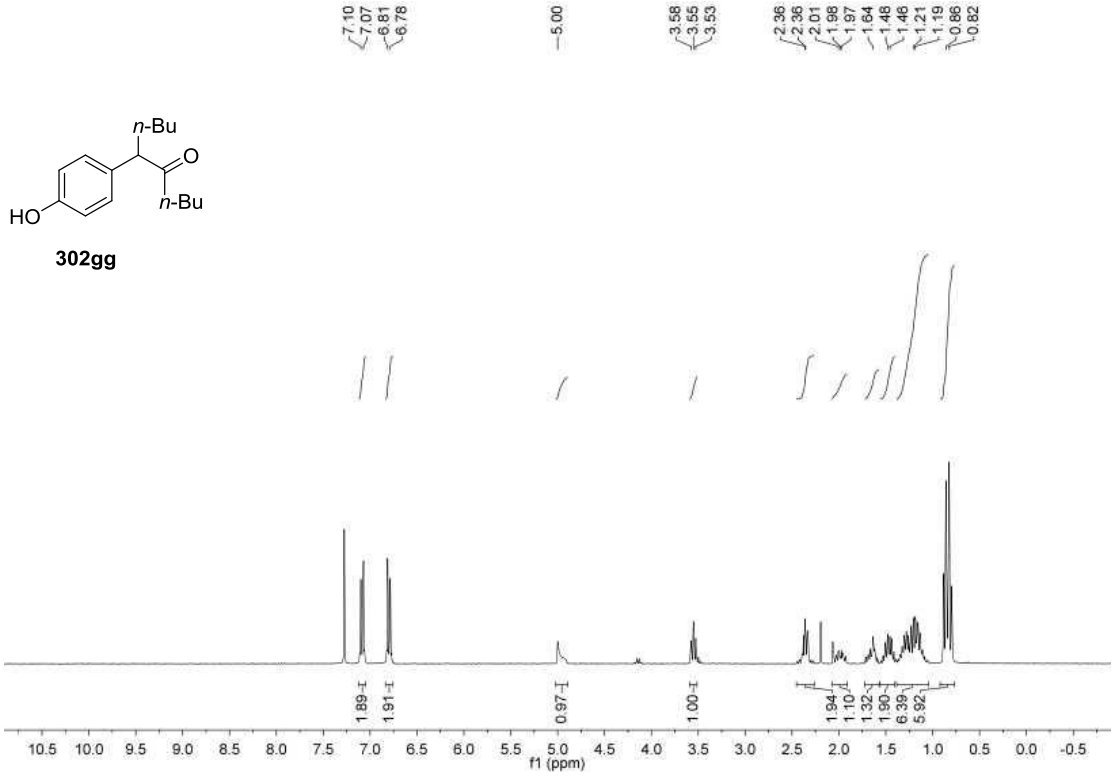
7.10
7.07
6.81
6.78
5.00
3.58
3.55
3.53
2.36
2.36
2.01
1.98
1.97
1.64
1.48
1.46
1.21
1.19
0.86
0.82
n-Bu
O
n-Bu
HO
302gg
1.89
1.91
0.97
1.00
1.94
1.10
1.32
1.90
6.39
5.92
f1 (ppm)

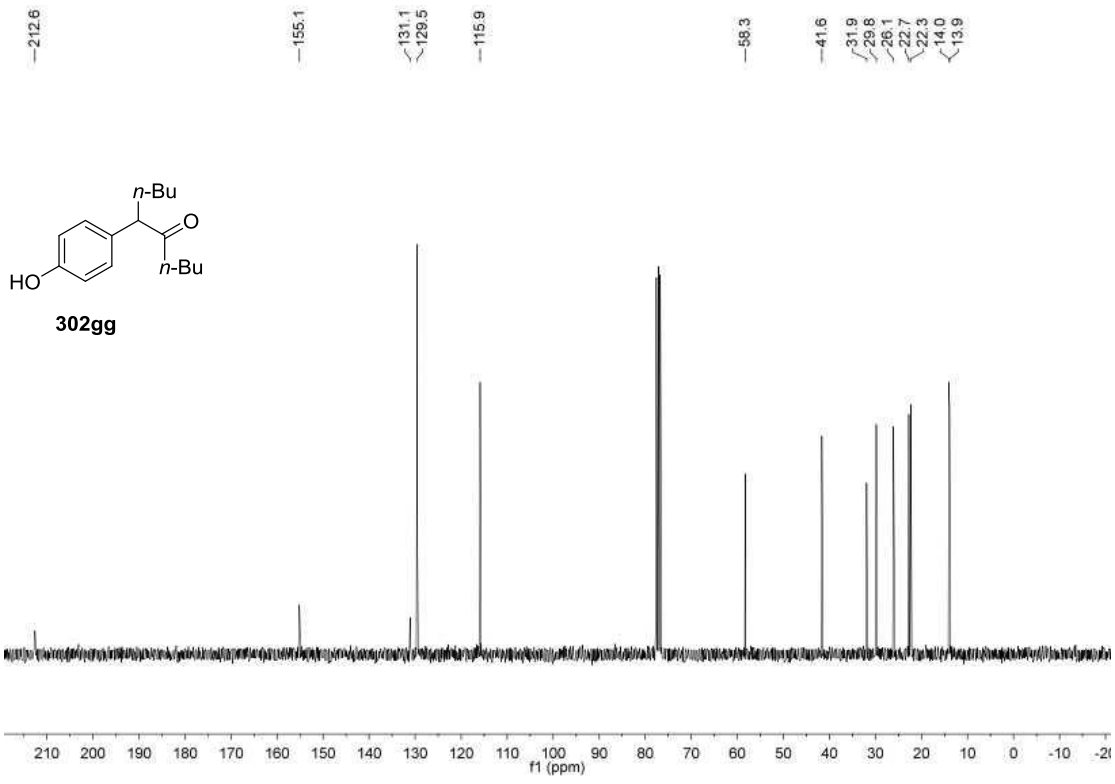
212.6
155.1
131.1
129.5
115.9
58.3
41.6
31.9
29.8
26.1
22.7
22.3
14.0
13.9
n-Bu
O
n-Bu
HO
302gg
f1 (ppm)

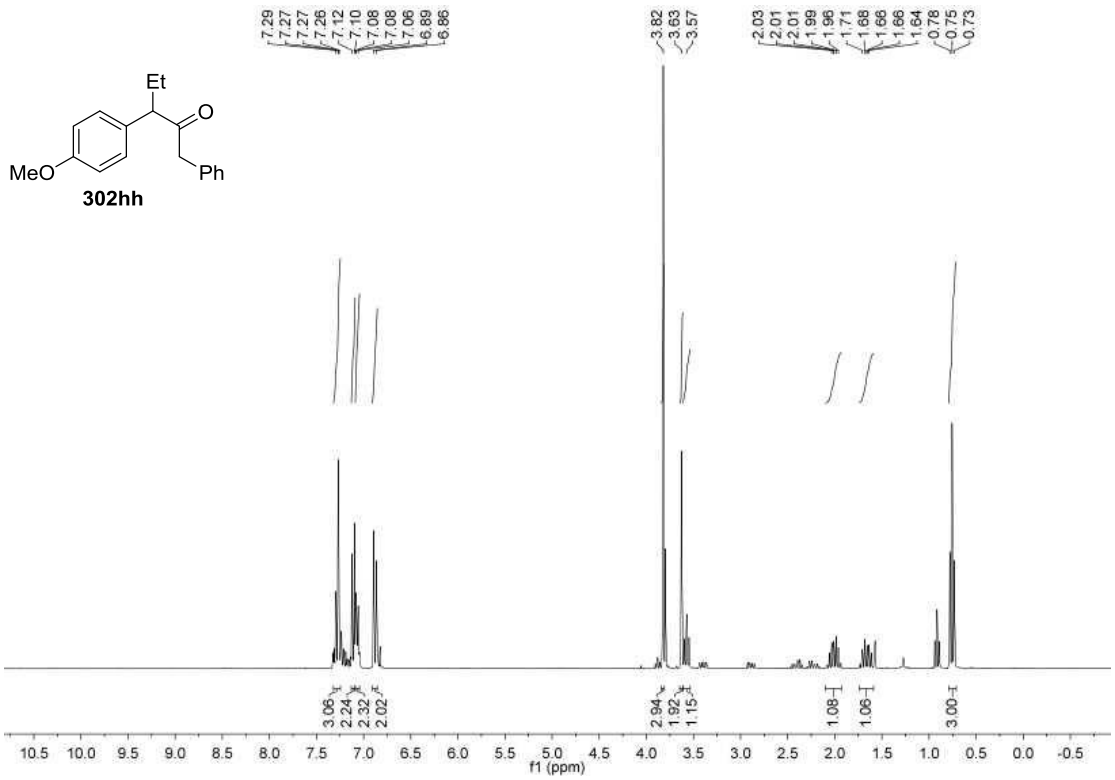
7.29
7.27
7.27
7.26
7.12
7.10
7.08
7.08
7.06
6.89
6.86
3.82
3.63
3.57
2.03
2.01
2.01
1.99
1.96
1.71
1.68
1.66
1.66
1.64
0.78
0.75
0.73
Et
O
MeO
Ph
302hh
3.06
2.24
2.32
2.02
2.94
1.92
1.15
1.08
1.06
3.00
f1 (ppm)

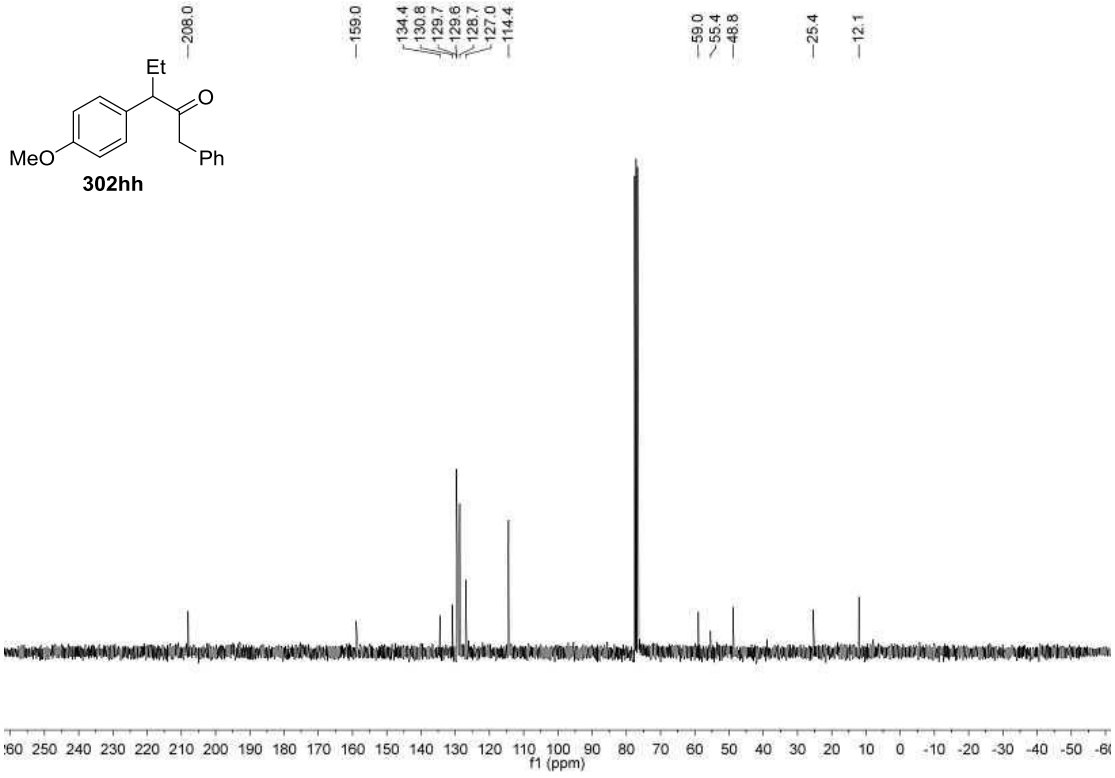
208.0
159.0
134.4
130.8
129.7
129.6
128.7
127.0
114.4
59.0
55.4
48.8
25.4
12.1
Et
O
MeO
Ph
302hh
f1 (ppm)

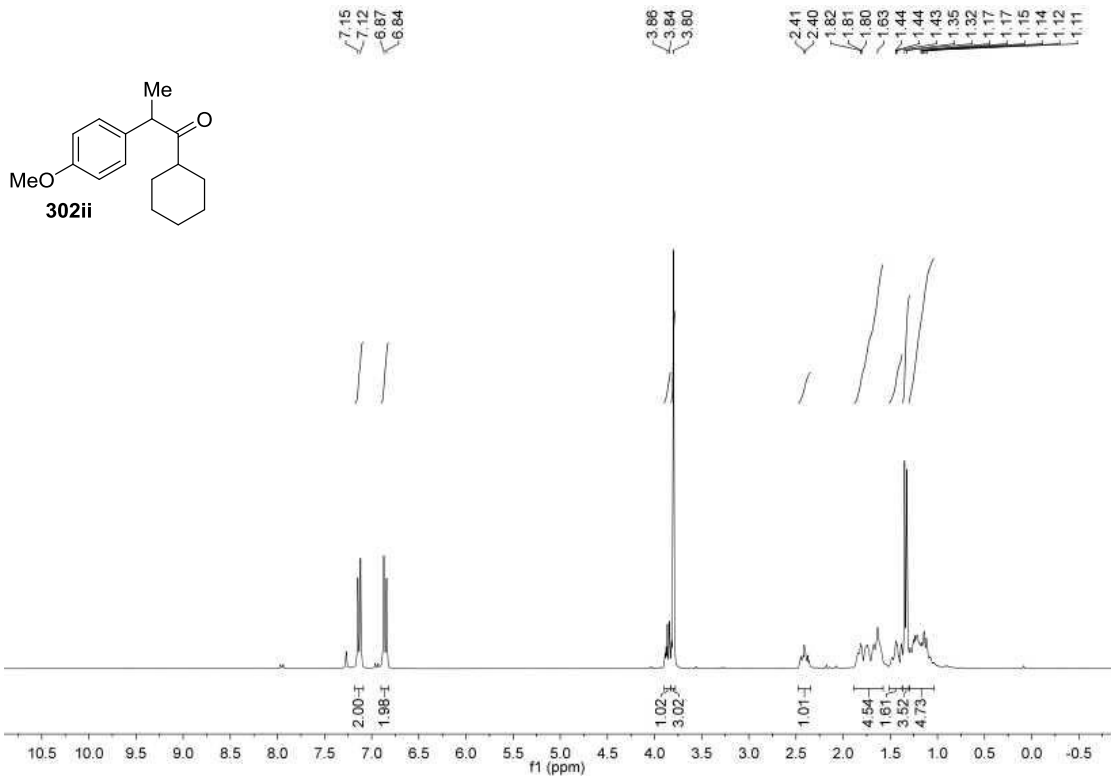
7.15
7.12
6.87
6.84
3.86
3.84
3.80
2.41
2.40
1.82
1.81
1.80
1.63
1.44
1.44
1.43
1.35
1.32
1.17
1.17
1.15
1.14
1.12
1.11
Me
O
MeO
302ii
2.00
1.98
1.02
3.02
1.01
4.54
1.61
3.52
4.73
f1 (ppm)

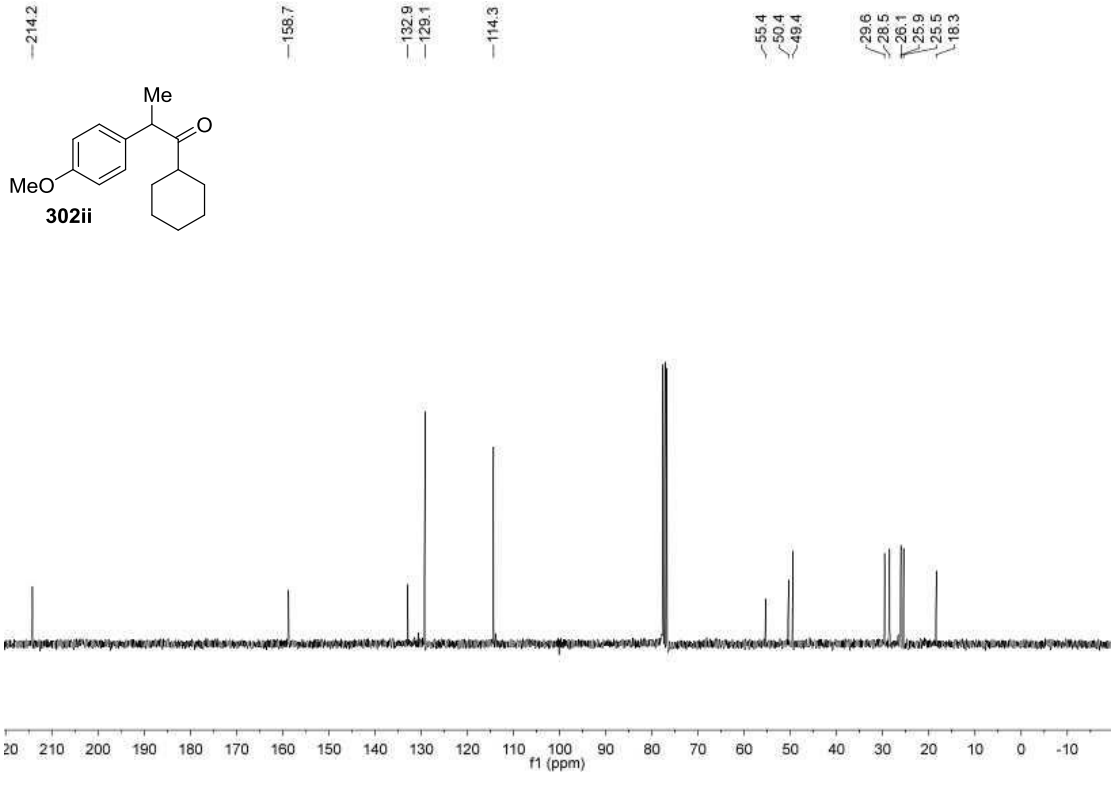
214.2
158.7
132.9
129.1
114.3
55.4
50.4
49.4
29.6
28.5
26.1
25.9
25.5
18.3
Me
O
MeO
302ii
f1 (ppm)

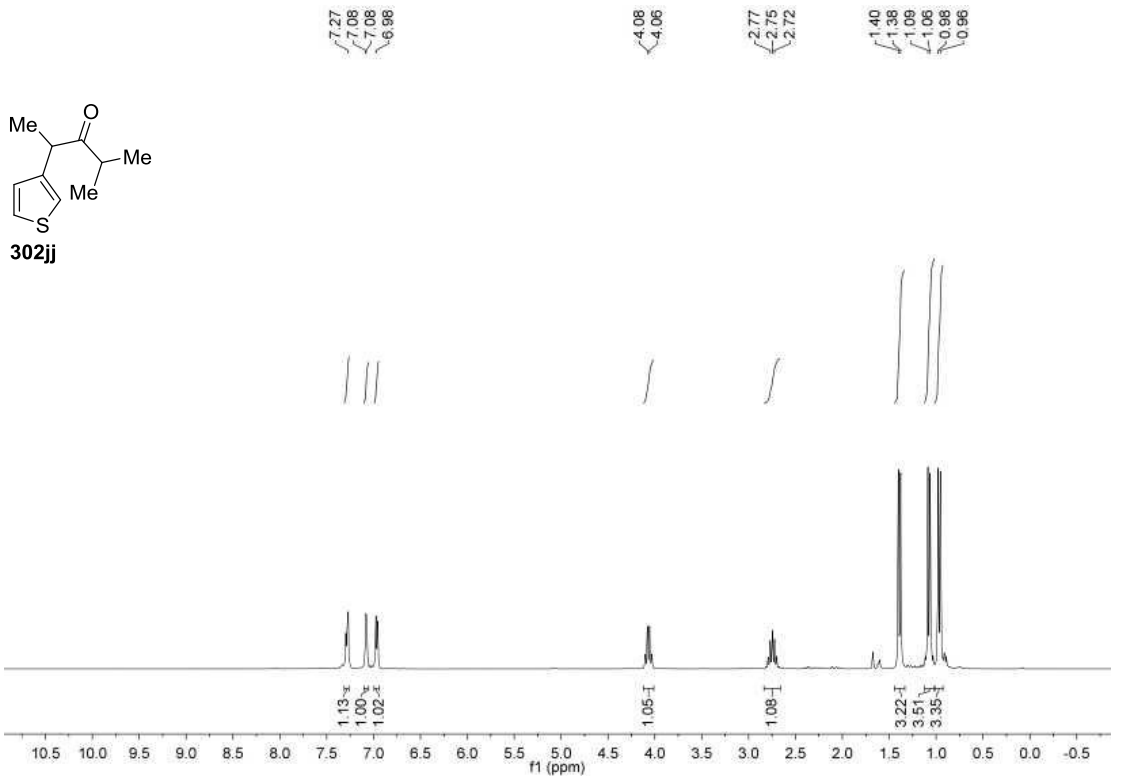
7.27
7.08
7.08
6.98
4.08
4.06
2.77
2.75
2.72
1.40
1.38
1.06
1.06
0.98
0.96
Me
O
Me
Me
S
302jj
1.13
1.00
1.02
1.05
1.08
3.22
3.51
3.35
f1 (ppm)

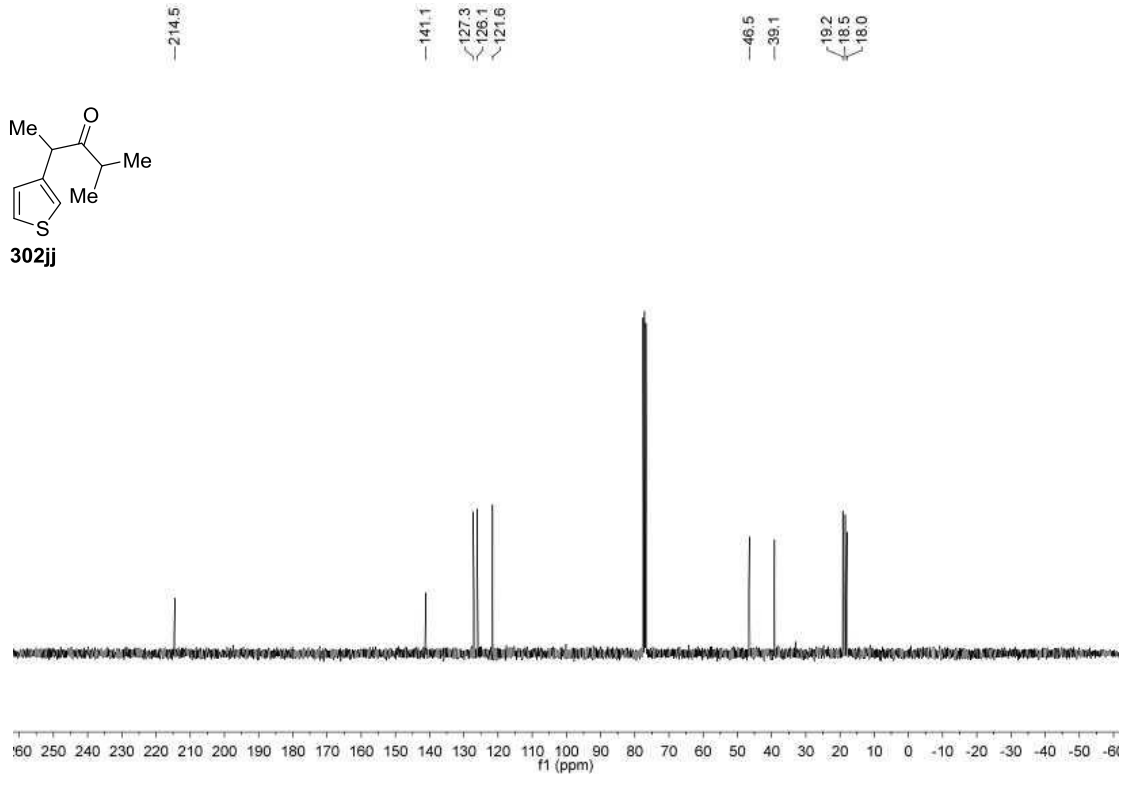
214.5
141.1
127.3
126.1
121.6
46.5
39.1
19.2
18.5
18.0
Me
O
Me
Me
S
302jj
f1 (ppm)

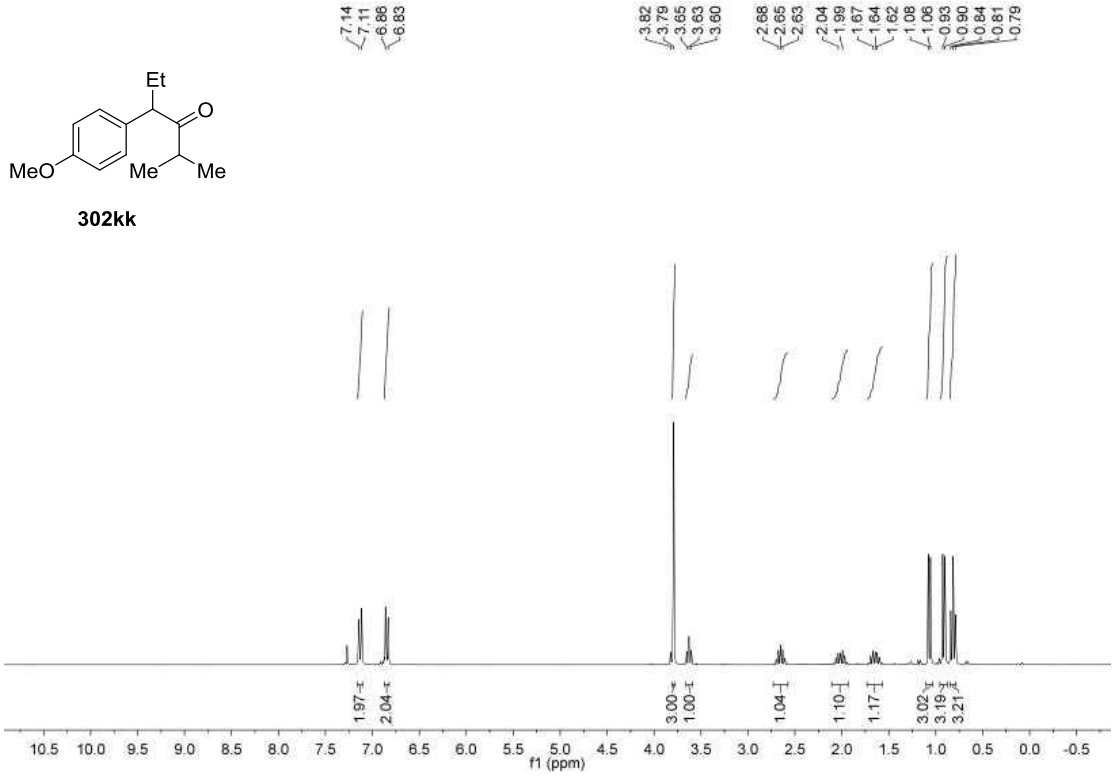
7.14
7.11
6.86
6.83
3.82
3.79
3.65
3.63
3.60
2.68
2.65
2.63
2.04
1.99
1.67
1.64
1.62
1.08
1.06
0.93
0.90
0.84
0.81
0.79
Et
O
MeO
Me
Me
1.97
2.04
3.00
1.00
1.04
1.10
1.17
3.02
3.19
3.21
f1 (ppm)

302kk

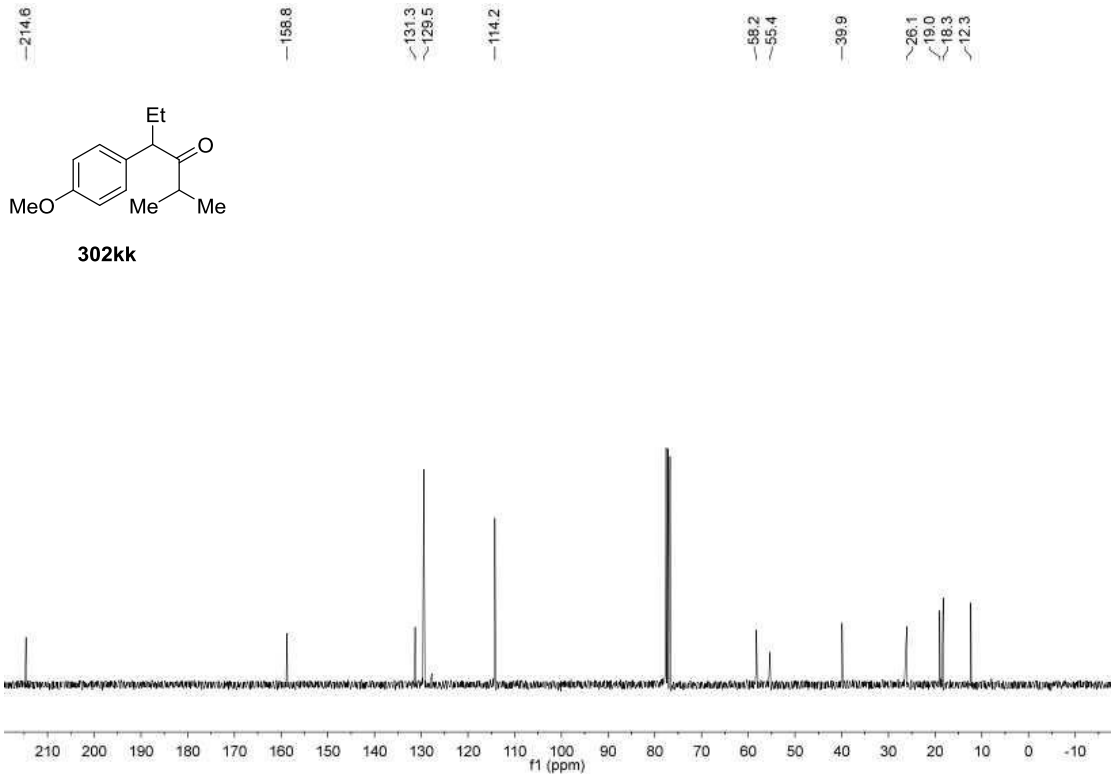
214.6
158.8
131.3
129.5
114.2
58.2
55.4
39.9
26.1
19.0
18.3
12.3
Et
O
MeO
Me
Me
f1 (ppm)

302kk

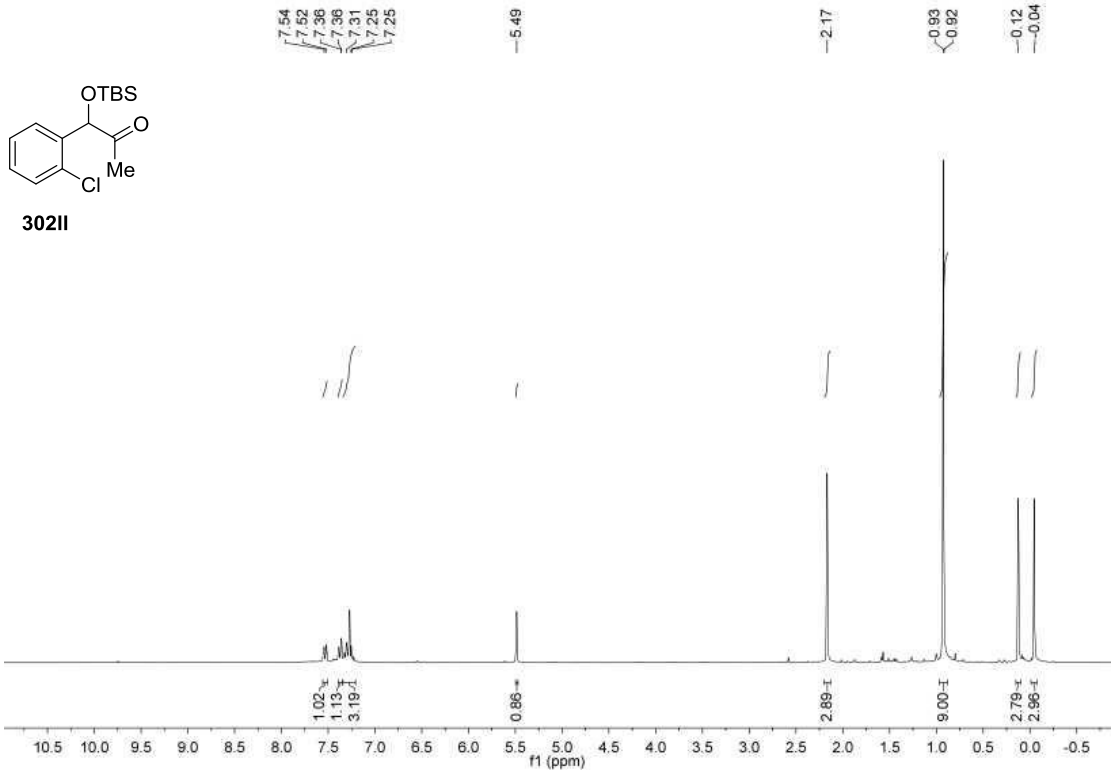
7.54
7.52
7.36
7.36
7.31
7.25
7.25
5.49
2.17
0.93
0.92
0.12
-0.04
OTBS
O
Me
Cl
1.02
1.13
3.19
0.86
2.89
9.00
2.79
2.96
f1 (ppm)

302ll

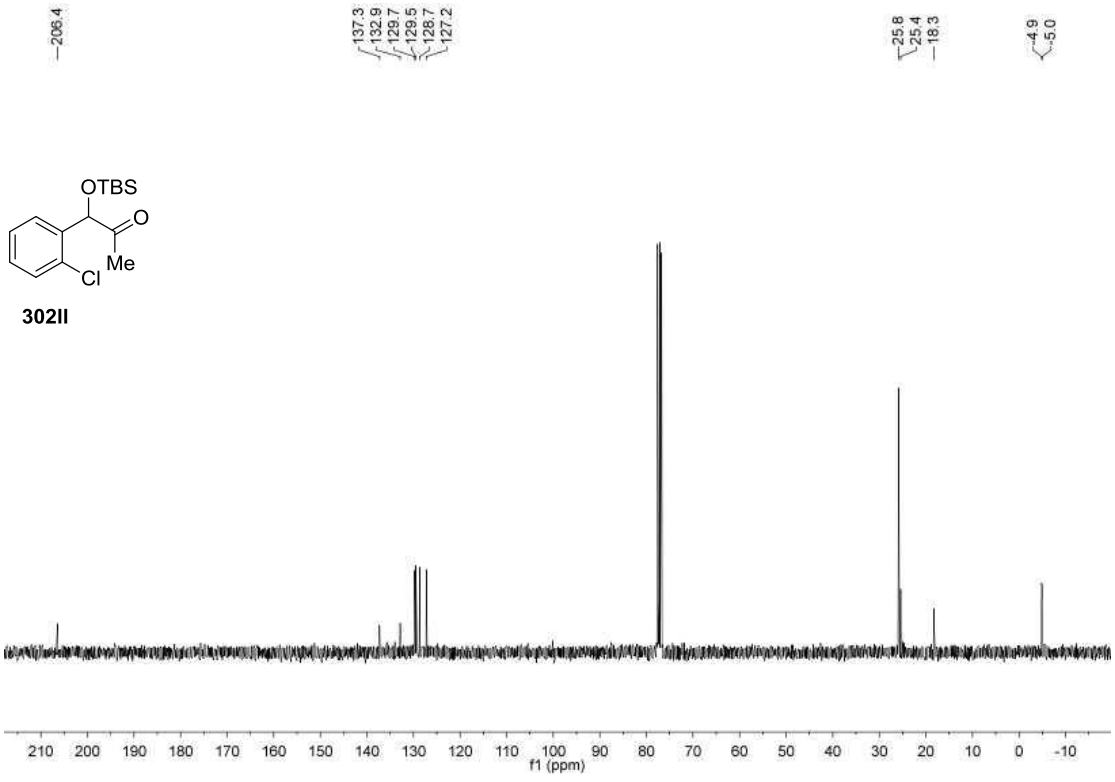
206.4
137.3
132.9
129.7
129.5
128.7
127.2
25.8
25.4
18.3
-4.9
-5.0
OTBS
O
Me
Cl
f1 (ppm)

302ll

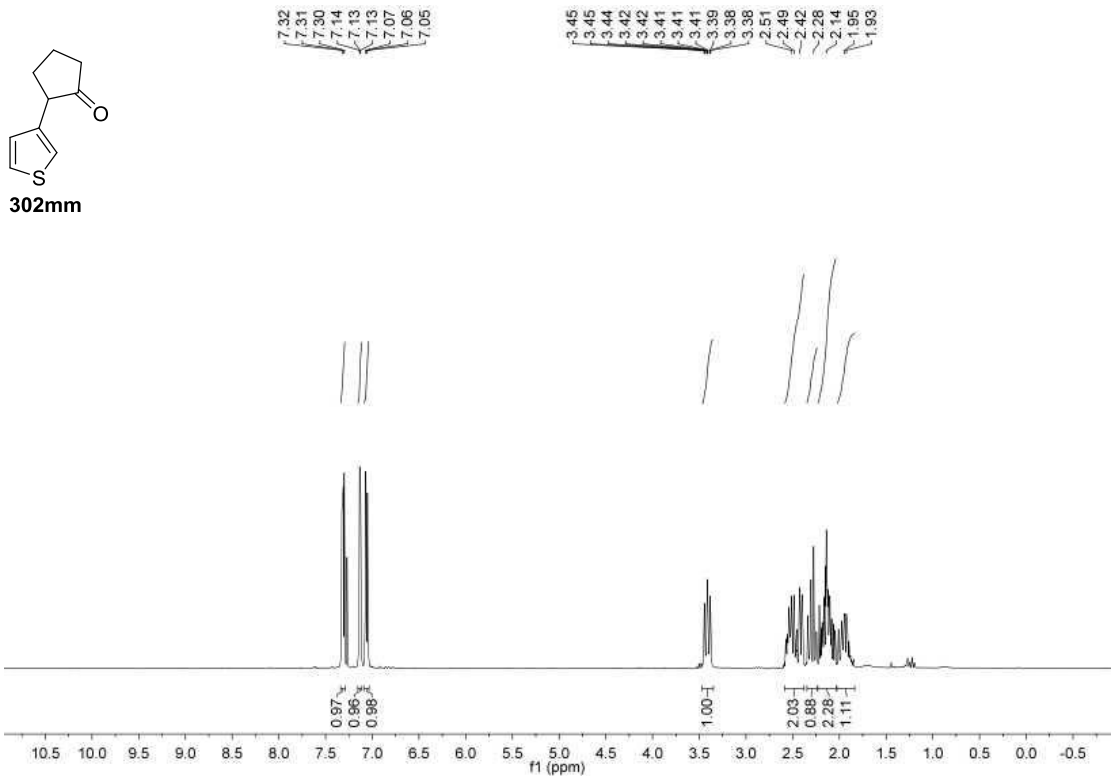
7.32
7.31
7.30
7.14
7.13
7.13
7.07
7.06
7.05
3.45
3.45
3.44
3.42
3.42
3.41
3.41
3.41
3.39
3.38
3.38
2.51
2.49
2.42
2.28
2.14
1.95
1.93
O
S
302mm
0.97
0.96
0.98
1.00
2.03
0.88
2.28
1.11
f1 (ppm)

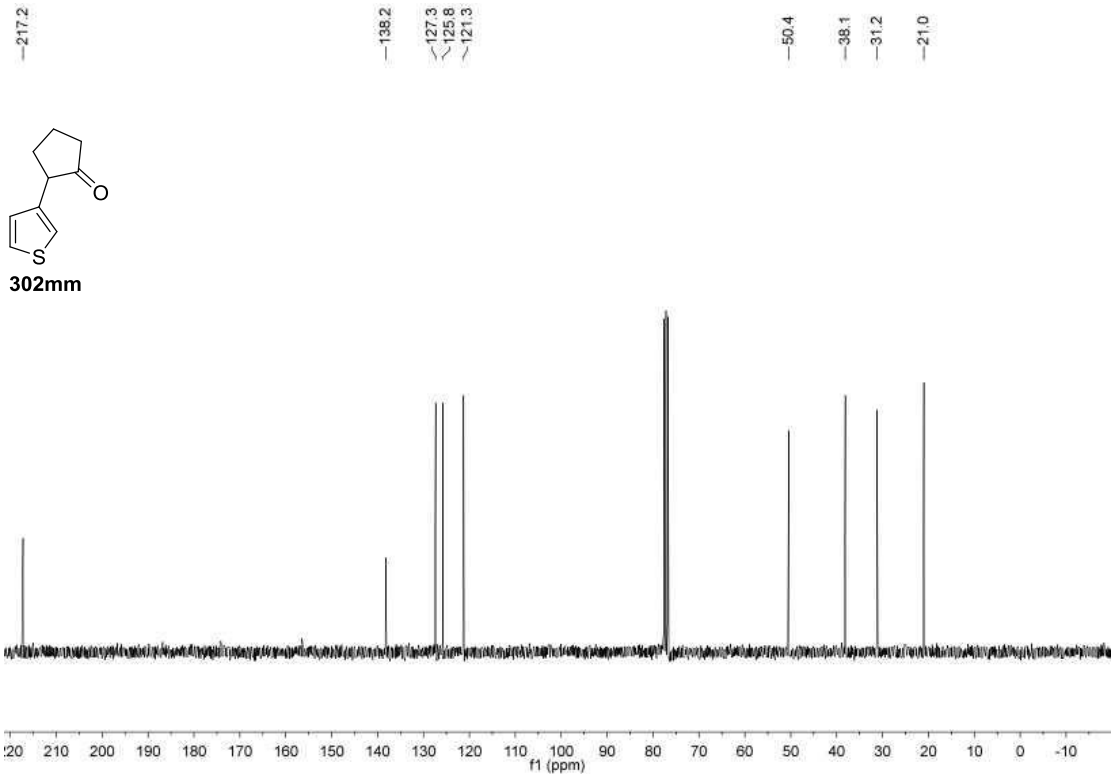
217.2
138.2
127.3
125.8
121.3
50.4
38.1
31.2
21.0
O
S
302mm
f1 (ppm)

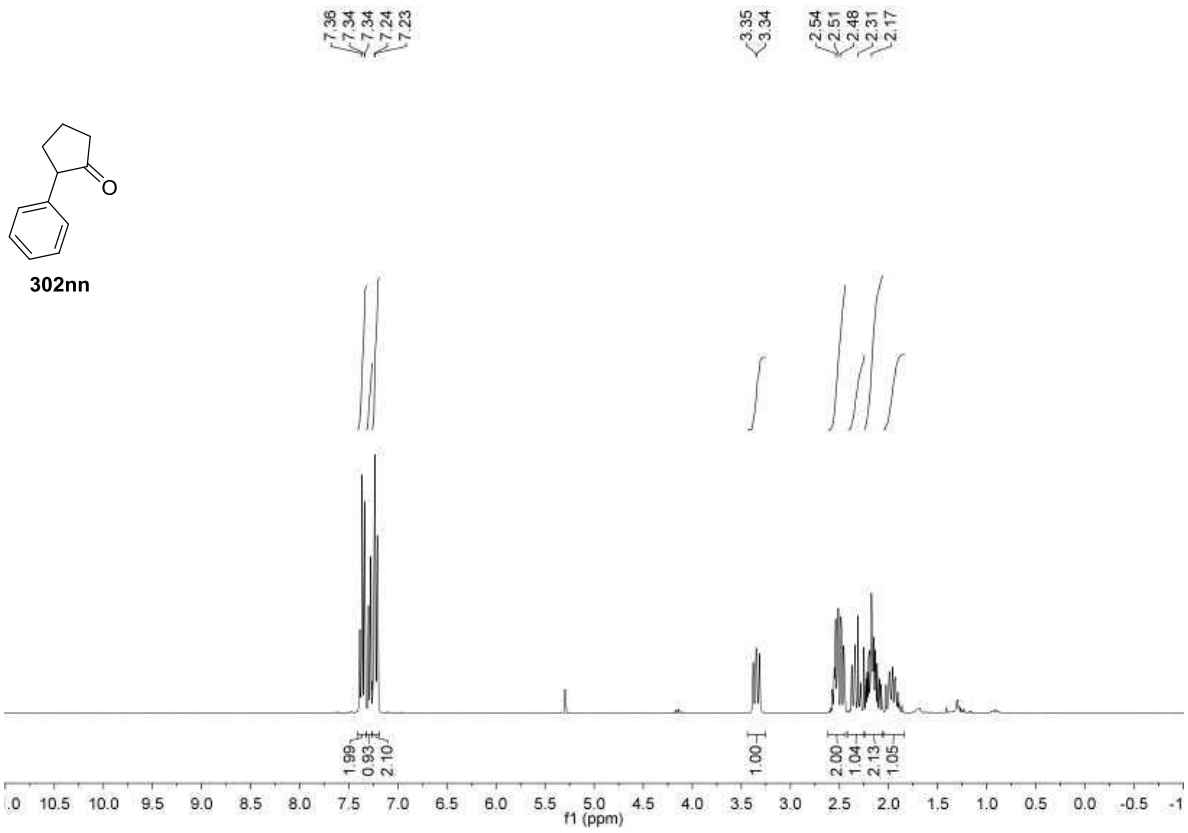

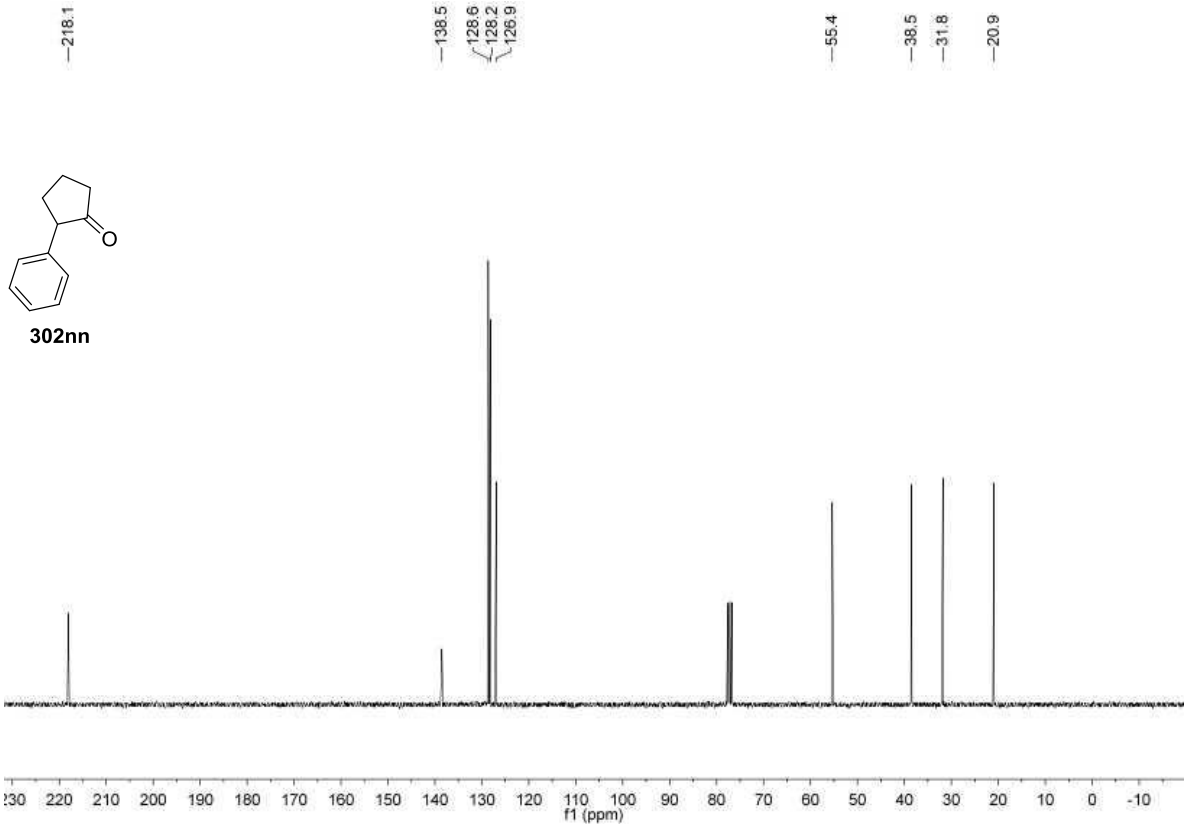

6.3.10. ^{1}H and ^{13}C NMR spectra of compounds for mechanistic studies:

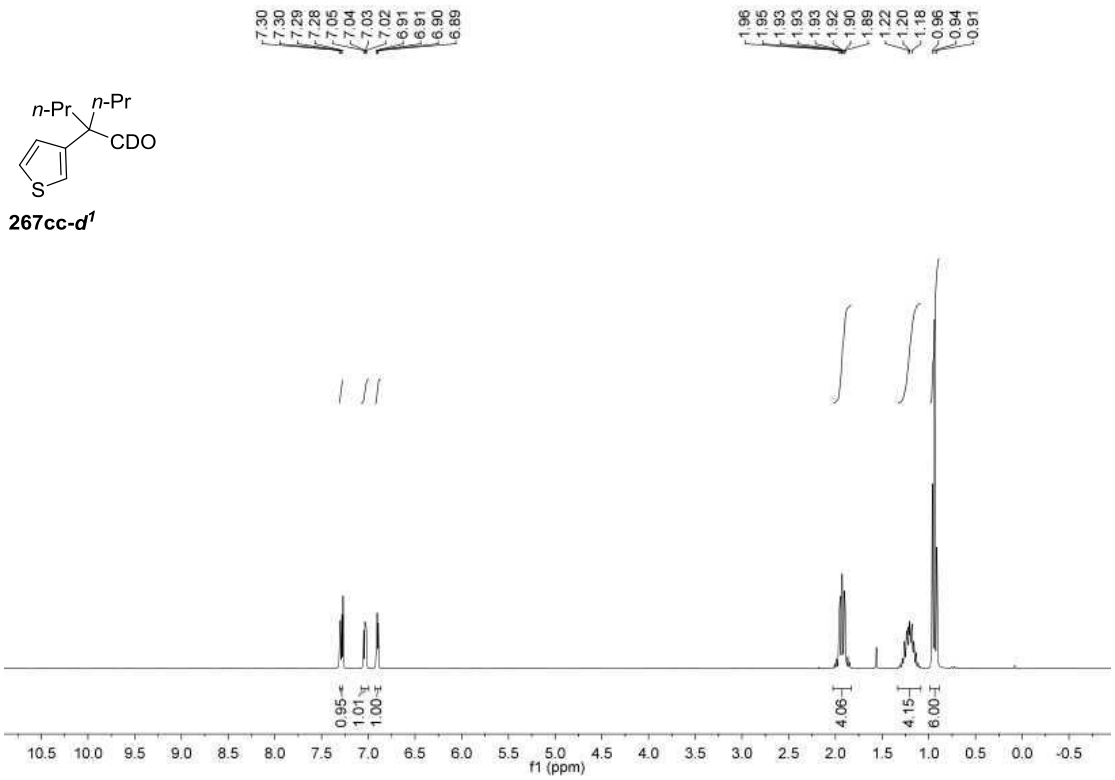

267cc-*d*[1]

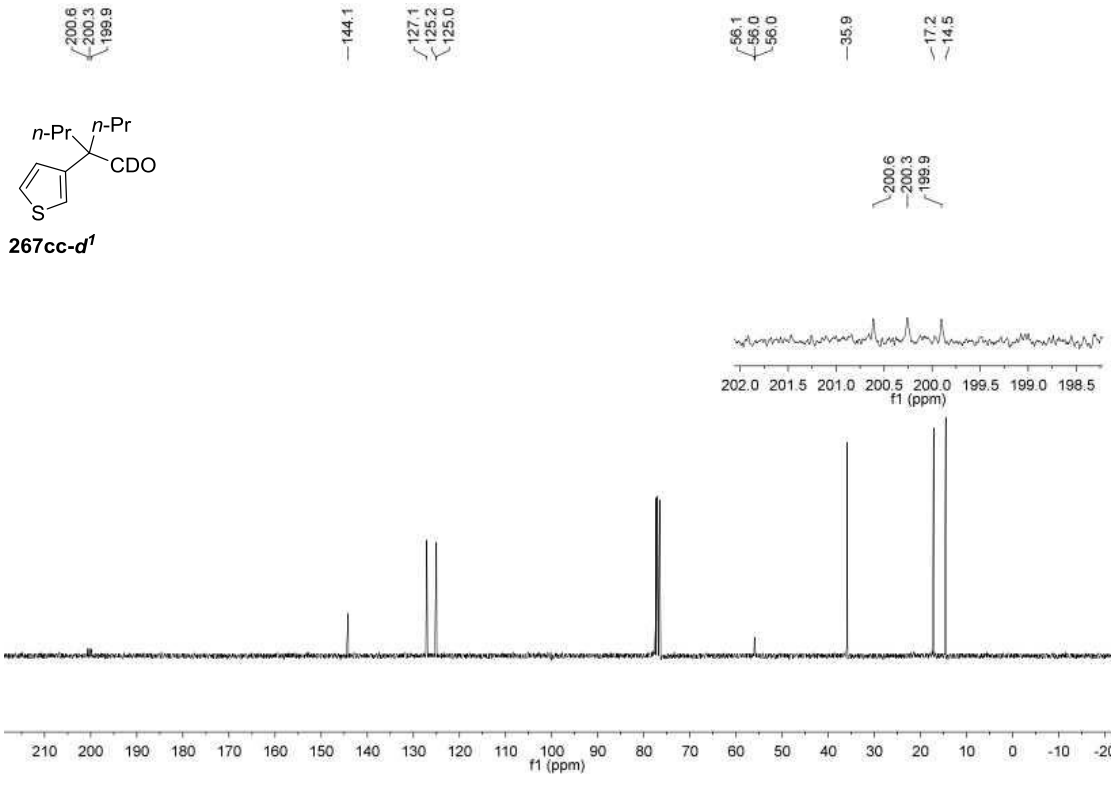

267cc-*d*[1]

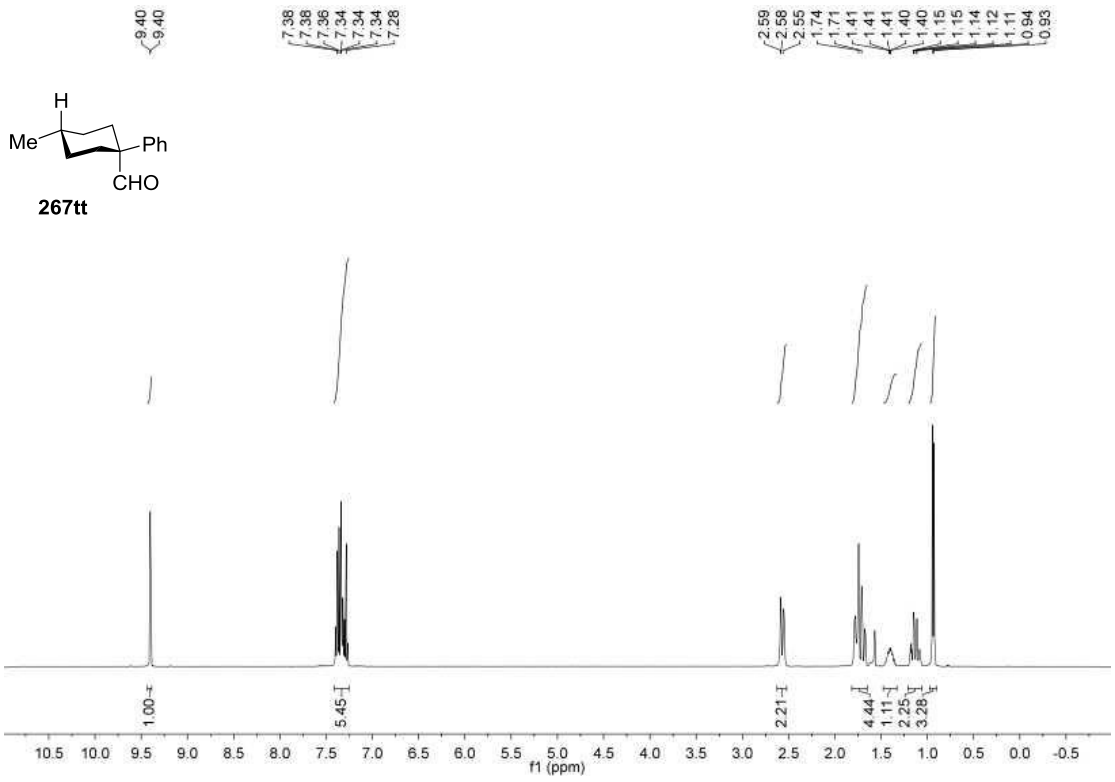
9.40
9.40
7.38
7.38
7.36
7.34
7.34
7.34
7.28
2.59
2.58
2.55
1.74
1.71
1.41
1.41
1.41
1.40
1.40
1.15
1.15
1.14
1.12
1.11
0.94
0.93
H
Me
Ph
CHO
1.00
5.45
2.21
4.44
1.11
2.25
3.28
f1 (ppm)

267tt

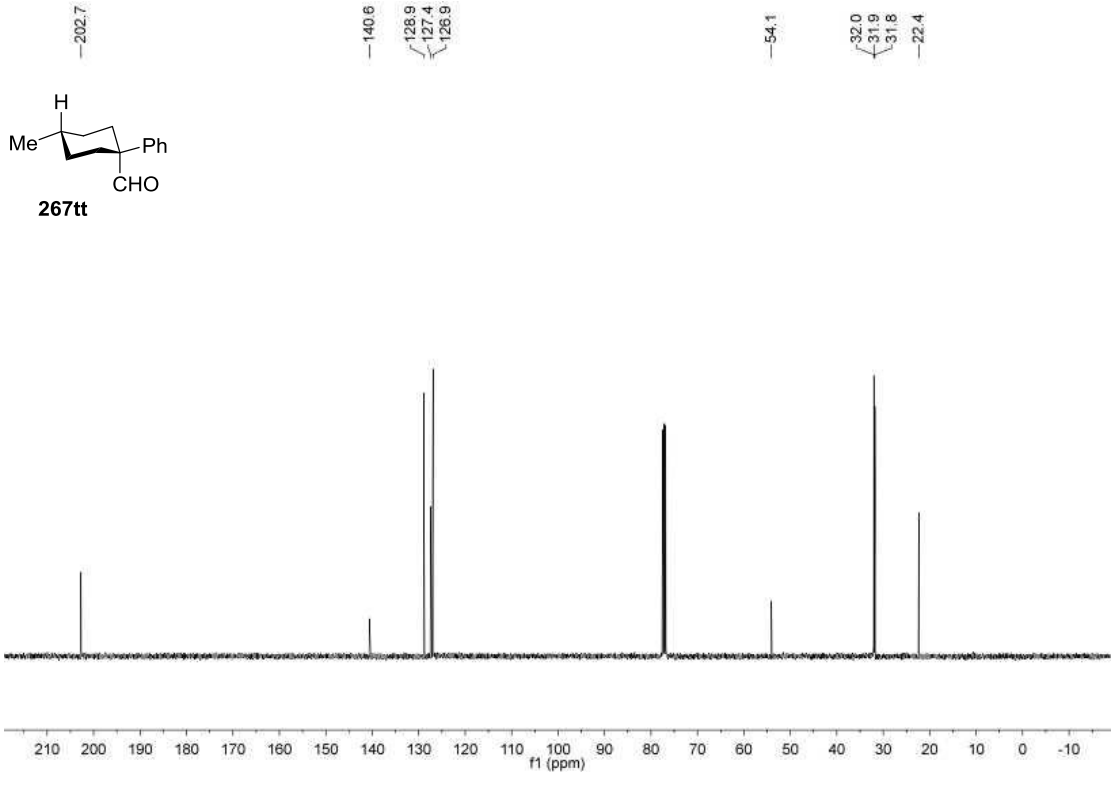
202.7
140.6
128.9
127.4
126.9
54.1
32.0
31.9
31.8
22.4
H
Me
Ph
CHO
f1 (ppm)

267tt

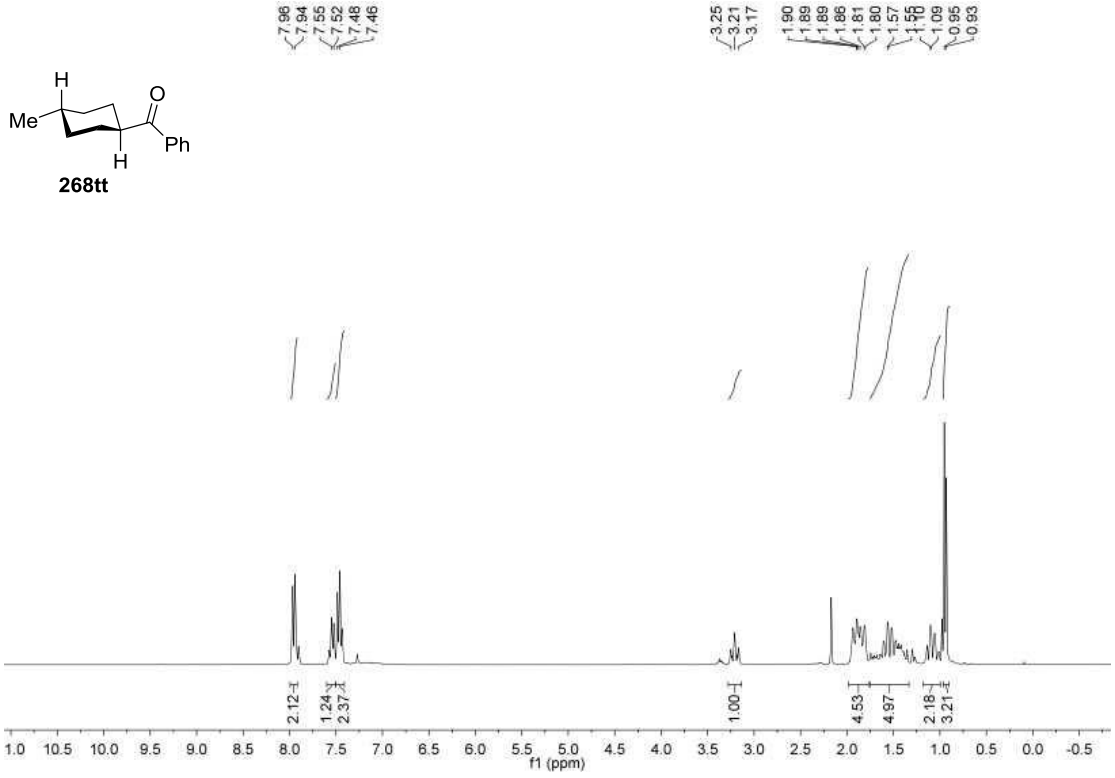
7.96
7.94
7.55
7.52
7.48
7.46
3.25
3.21
3.17
1.90
1.89
1.89
1.86
1.81
1.80
1.57
1.55
1.10
1.09
0.95
0.93
H
Me
O
Ph
H
268tt
2.12
1.24
2.37
1.00
4.53
4.97
2.18
3.21
f1 (ppm)

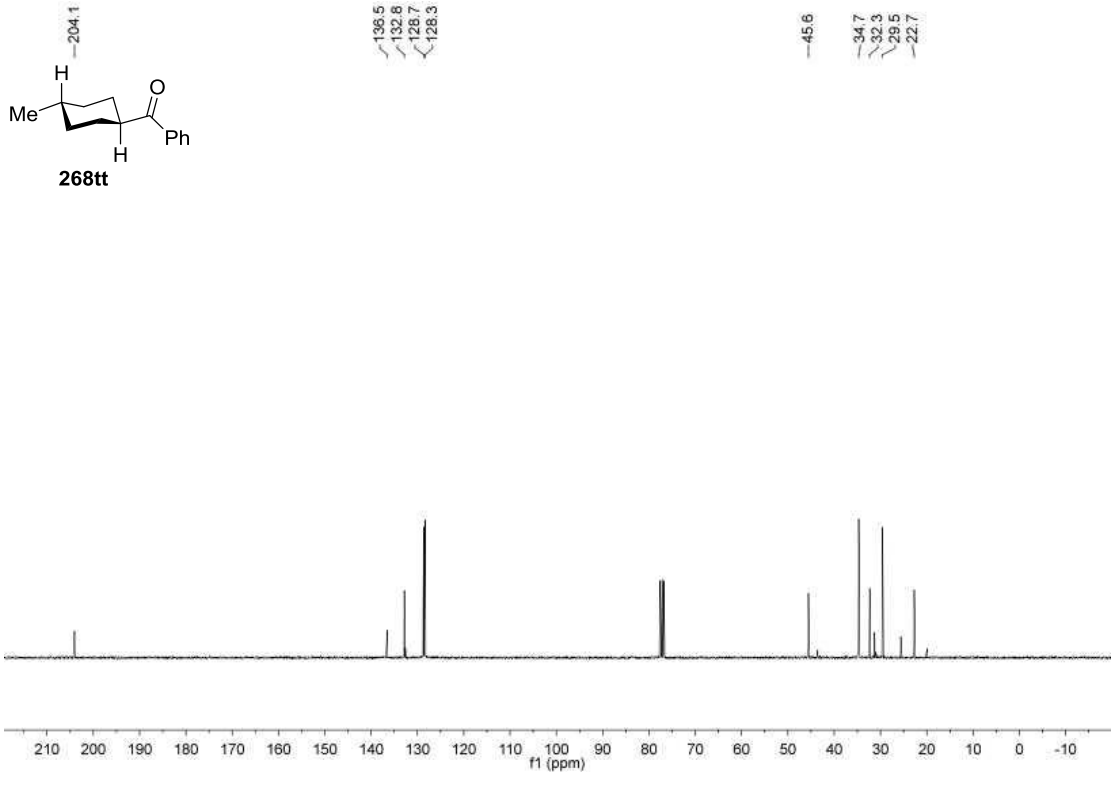
204.1
136.5
132.8
128.7
128.3
45.6
34.7
32.3
29.5
22.7
H
Me
O
Ph
H
268tt
f1 (ppm)